REPAIR OF EARTHQUAKE-DAMAGED REINFORCED CONCRETE STRUCTURES

A Thesis submitted for the degree of Doctor of Philosophy
in the Faculty of Engineering of the University of London
and for the Diploma of Membership of Imperial College

by

Assaad Ibrahim Salama B.Sc., M.Sc.

July 1993

Engineering Seismology and Earthquake
Engineering Section

Civil Engineering Department

Imperial College of Science Technology and Medicine

University of London

BIBL.
LONDN.
UNIV.

To my Father and to the Sacred Memory of my Mother

ABSTRACT

Seismic design using the 'capacity' approach requires a high degree of control on the response and failure mode of RC structures. To advance the design process, individual response parameters, such as stiffness and strength in shear and flexure, as well as ductility, should be appropriately assessed and controlled. The objectives of the present research were to develop techniques for selective repair and strengthening, aimed at the modification of one response parameter without affecting the others. This is applicable to all types of reinforced concrete structures but more specifically to structures exposed to, or damaged by, non-contact explosions and ground born vibrations from blast and earthquakes.

In Part I of the current research, an experimental testing programme was carried out on seventeen reinforced concrete walls of scale 1: 2.5. The models were tested under variable amplitude cyclic loading to simulate severe earthquake strong-motion effect. Vertical steel plates, attached to the cracked zones, proved effective in stiffness reinstatement with no influence on the member strength. Enhancement of the member strength, without affecting its stiffness, was achieved by means of external unbonded reinforcing steel bars attached to the tested model in conjunction with an interaction delay mechanism. External confinement of concrete in maximum compression zones, by means of U-shaped steel plates, increased the member ductility with minimum effect on other response characteristics. Horizontal steel plates were effective in shear strength reinstatement. Epoxy resin injection was also applied to some cracked models, and proved to reinstate the specimen strength at a reduced stiffness.

The results from the testing programme indicated that reinstatement of an individual response parameter can be achieved in practice, thus paving the way towards the developement of a capacity re-design methodology.

Part II deals with the repair of earthquake damaged buildings as a practical application of the selective repair methods tested above. It presents the findings from assessment of structural damage to typical constructions in Erzincan,Turkey after the M_S=6.85, earthquake of March 1992. A non-linear dynamic analysis was carried out on a typical building in order to justify the observed structural damage and to propose schemes for repair and seismic upgrading. Use was made of the newly developed repair techniques to reinstate response characteristics where needed. A comparison between the dynamic response of the building repaired selectively and conventionally was undertaken. This showed a major enhancement in the building response in case of selective intervention.

ACKNOWLEDGEMENTS

I would not have been able to complete this study without the help of my supervisor, Dr. Amr Salah Elnashai. His constant guidance, his encouragement and his ability to impart a small part of his knowledge made producing this thesis an educational as well as a pleasant experience. My gratitude to him is great.

I am also indebted to Professor P. J. Dowling, Head of the Civil Engineering Department, who gave me the chance to pursue my doctoral studies at Imperial College. The assistance of Dr. C. Gabrial of King's College and Dr. Heba Ghabbour of Cairo University in establishing the first contact with Imperial College is greatly acknowledged.

I consider it a privilege to have worked within the Engineering Seismology and Earthquake Engineering Section, and to have been instructed by Professor N. N. Ambraseys, Head of Section.

The partial financial support of the British Council is gratefully acknowledged. Financial support for the experimental work, which was provided by the Science and Engineering Research Council, is also acknowledged.

I am grateful to Eng. Hossam Abou El-Fotouh who gave me the chance to apply some of the findings of the current research to the Souria Building, Cairo and to the Hurgada Paradise Complex, Hurgada, Egypt.

I would like to express my gratitude to Mr. L. J. Tabor, FOSROC Technical Manager, who provided the repair material and assisted me in the concrete repair work throughout the experimental programme. His technical expertise is gratefully acknowledged.

I would like to acknowledge Dr. B. Izzuddin for his infailing support in computer applications and Mr. Clive Hargreaves for his assistance and ability to solve all experimental problems. I would also like to thank Dr. K. Pilakoutas, Dr. A. Elgazouli, Dr. A Madas and Mr. Brian Broderick for their co-oporation during the preparation of this work.

The author would like to extend his thanks to all the technicians of the concrete laboratory for their expert technical support, especially Peter Jellis, Stefan Algar, Robby Wilson, Mike Hobbins, Ken Mitchell and Lee Tooley.

Finally, My deepest gratitude goes to my family, especially my father General Ibrahim Salama who has always encouraged and supported me throughout my education.

TABLE OF CONTENTS

Page

ABSTRACT i

ACKNOWLEDGEMENTS ii

TABLE OF CONTENTS iii

LIST OF FIGURES x

LIST OF TABLES xi

ABBREVIATIONS xii

NOTATIONS xiii

PART I: SELECTIVE REPAIR TECHNIQUES FOR EARTHQUAKE DAMAGED REINFORCED CONCRETE STRUCTURES

1. INTRODUCTION 1
   - 1.1. General 1
   - 1.2. Aspects of Seismic Design 3
   - 1.3. Objectives of the Current Investigation 7
   - 1.4. Organisation of the thesis 9

2. METHODS OF REPAIR AND RETROFITTING 12
   - 2.1. Methods of Crack Repair 12
     - 2.1.1. Epoxy injection 13
     - 2.1.2. Routing and sealing 16
     - 2.1.3. Stitching 16
     - 2.1.4. Additional reinforcement 18
     - 2.1.5. Drilling and plugging 19
     - 2.1.6. Flexible sealing 19

2.1.7. Grouting 20
2.1.8. Drypacking 20
2.1.9. Crack arrest 21
2.1.10. Polymer impregnation 22
2.1.11. Overlays and surface treatments 22
2.1.12. Autogeneous healing 24
2.2. Concrete Jacketing 24
2.3. Addition of Steel Plates and/or Steel Profiles 26
2.4. External Prestressing 27
2.5. Shotcrete Using Ultra Rapid Hardening Cement 27
2.6. Micro-Reinforced Cementatious Composites 28
2.7. Cathodic Protection of Rebars 29

3. REVIEW OF RELATED RESEARCH 35
3.1. Itroduction 35
3.2. Review of Repair Methods 36
3.3. Review of Upgrading Methods 38

4. EXPERIMENTAL PROGRAMME 45
4.1. Introduction 45
4.2. Test Set-Up 46
4.2.1. Loading system 46
4.2.2. Hydraulic power system 47
4.2.3. Electro-hydraulic servo-control 47
4.2.4. Instrumentation 48
4.2.5. Data Acquisition 49
4.3. Loading History 49
4.4. Design of Test Specimens 50
4.5. Construction of Test Specimens 51

5. TEST RESULTS FOR INTACT WALLS 66
5.1. Introduction 66
5.2. Review of Some Previous IC Test Results 67
5.2.1. Model SW4 67
5.2.2. Model SW5 69
5.2.3. Model SW7 70
5.2.4. Model SW9 71

5.3. Observed Behaviour of Tested Models 72
5.3.1. Model SW21 72
5.3.2. Model SW22 75
5.3.3. Model SW23 78
5.3.4. Model SW24 81
5.3.5. Model SW33 83
5.3.6. Model SW35 87

6. REPAIR PHILOSOPHY 104
6.1. Introduction 104
6.2. Selective Repair Techniques 104
6.2.1. Strength-only intervention 104
6.2.2. Stiffness-only intervention 105
6.2.3. Ductility-only intervention 106
6.3. Concrete Integrity Re-Instatement 106
6.3.1. Concrete injection 106
6.3.2. Replacement of damaged concrete 107
6.3.3. Local and surface treatment 108

7. TESTING OF REPAIRED WALLS 111
7.1. Introduction 111
7.2. Observed Behaviour of Models 111
7.2.1. Model SWR4 111
7.2.2. Model SWR5 113
7.2.3. Model SWR7 114
7.2.4. Model SWR9 116
7.2.5. Model SWR21 120
7.2.6. Model SWR22 123
7.2.7. Model SWR24 126
7.2.8. Model SW31 129
7.2.9. Model SW32 134
7.2.10. Model SW34 137
7.2.11. Model SWR35 142

8. ANALYSIS AND DISCUSSION OF TEST RESULTS 163
8.1. general Observations 163
8.2. Comments on Specific Response Parameters 165

8.2.1. Stiffness 165
8.2.2. Strength 166
8.2.3. Hysteresis loops 167
8.2.4. Crack pattern 167
8.2.5. Ductility 168
8.2.6. Failure mode 169
8.3. Comments on Test Results for Repaired Models 170
8.4. Practical Application of Selective Repair Techniques 172

PARTII: APPLICATION OF SELECTIVE ASSESSMENT AND INTERVENTION; THE RECONSTRUCTION OF ERZINCAN (TURKEY).

1. INTRODUCTION 175
1.1. Preamble 175
1.2. General Description 176
1.3. Work Organisation 177

2. COMMENTS ON SEISMIC HAZARD AND VULNERABILITY 178
2.1. Tectonic Setting in North Central Anatolia 178
2.2. A Brief History of Earthquakes in Northeast Turkey 179
2.2.1. Historical records 179
2.2.2. Instrumental data 184
2.3. Description of the 13 March 1992 Erzincan Earthquake 185
2.4. A Note on Earthquake Hazard in Erzincan 186

3. PHILOSOPHY OF INSPECTION 194
3.1. Purpose 194
3.2. Materials 194
3.3. Section Characteristics 195
3.4. Response of RC Members 195
3.5. Sub-assemblages 195
3.6. Overall Structural Features 196
3.6.1. Plan layout 196
3.6.2. Elevation proportion 196
3.6.3. Elevation stiffness and strength distribution 197

3.6.4. Orthogonal framing action 197
3.6.5. Foundation system 197
3.7. Soil Characteristics 197
3.8. The Erzincan Inspection Forms 198
3.9. Results of the Inspection 198
3.9.1. Structural defects 199
3.9.2. Non-structural defects 200
3.10. Discussion 201

4. CRITERIA FOR SEISMIC ANALYSIS AND UPGRADING 203
4.1. Summary of Some Existing Seismic Hazard Studies 203
4.1.1. Commentary 204
4.2. Design Peak Ground Acceleration in Erzincan 205
4.2.1. PGA implicit in the 1975 Turkish code 205
4.2.2. PGA from design earthquakes 206
4.3. Seismic Force Comparison for Prototype Structure 207
4.3.1. Code-based force calculation 207
4.3.2. Forces from the 13 March 1992 Erzincan earthquake 209
4.4. Response Spectral Shapes for Design 210
4.4.1. The Turkish code of 1975 210
4.4.2. The UBC, 1991 211
4.4.3. Spectra based on Newmark and Hall method 211
4.4.4. Spectral shapes from the Erzincan 1992 earthquake 212
4.5. Recommended Earthquake Forces 212

5. REPAIR AND SEISMIC UPGRADING OF A TYPICAL STRUCTURE 215
5.1. Structural System and Description of State of Damage 215
5.1.1. Structural damage 216
5.1.2. Design and construction defects 216
5.1.3. Failure mode 217
5.2. Repair and Upgrading Solutions 218
5.2.1. Case of total column rupture 219
5.2.2. Case of cracked columns 220
5.2.3. Seismic upgrading scheme 220
5.3. Modelling of Upgrading Schemes 220
5.3.1. The analysis software system ADAPTIC and structural models 220

5.3.2. Structural modelling 222
5.4. Behaviour During the 13 March 1992 Earthquake 223
5.5. Seismic Response for Conventionally Repaired Structures 225
5.6. Seismic Response for Selectively Repaired Structure 226
5.7. Concluding Remarks 226

6. CLOSURE 248
6.1. Summary of Conclusions 248
6.1.1. Conclusions related to part I 248
6.1.2. Conclusions related to part II 251
6.2. Proposals for Future Developments 252

REFERENCES 254

APPENDICES 265

Appendix AI: Force-Displacement Test Results 265
AI.1. Force-Displacement for SWR4 265
AI.2. Force-Displacement for SWR5 270
AI.3. Force-Displacement for SWR7 275
AI.4. Force-Displacement for SWR9 280
AI.5. Force-Displacement for SW21 284
AI.6. Force-Displacement for SW22 289
AI.7. Force-Displacement for SW23 294
AI.8. Force-Displacement for SW24 299
AI.9. Force-Displacement for SWR21 302
AI.10. Force-Displacement for SWR22 307
AI.11. Force-Displacement for SWR24 312
AI.12. Force-Displacement for SW31 317
AI.13. Force-Displacement for SW32 321
AI.14. Force-Displacement for SW33 327
AI.15. Force-Displacement for SW34 331
AI.16. Force-Displacement for SW35 335
AI.17. Force-Displacement for SWR35 340

Appendix AII: Force-Steel Strain Test Results 343
AII.1. Force-Steel Strain for SW21 343
AII.2. Force-Steel Strain for SW22 349
AII.3. Force-Steel Strain for SW23 355
AII.4. Force-Steel Strain for SWR9 361
AII 5. Force-Steel Strain for SWR21 364
AII 6. Force-Steel Strain for SWR24 369
AII.7. Force-Steel Strain for SW31 374
AII.8. Force-Steel Strain for SW32 377
AII.9. Force-Steel Strain for SW33 387
AII.10. Force-Steel Strain for SW34 394
AII.11. Force-Steel Strain for SW35 404
AII.12. Force-Steel Strain for SWR35 419

Appendix III: Erzincan Inspection Forms for Typical Building 422

Appendix IV: PLATES 439
Plate 1: Test Set-Up 439
Plate 2: Failure Mode for SW31 440
Plate 3: Details of Interaction Delay Mechanism 440
Plates 4 (a) & (b): Reinforcement Cage for SW31 441
Plate 5: Preparation of Reinforcement Cage for SW34 442
Plate 6: Mr. Tabor (Fosroc Technical Manager) Repairing SW22 442
Plate 7: Casting Model SW34 443
Plate 8: Finishing SW35 443
Plate 9: Strength-Only Intervention, Note Interaction Delay Mechanism 444
Plate 10: Model SWR9, Stiffness-Only Intervention 445
Plate 11: Model SWR21, Note Diagonal Shear Cracks 446
Plate 12: Model SWR24, Note Diagonal Shear Cracks 447
Plate 13: Model SW33, Control Model 448
Plate 14: Model SW32, Ductility-Only Intervention 449
Plate 15: Model SW34, Strength-Only Intervention 450
Plate 16: Model SWR22, Note Shear Failure Mode 451
Pate 17: Typical Shear Failure in Shear Walls, Erzincan, Turkey 452
Plate 18: Typical Shear Failure in Columns, Erzincan, Turkey 452
Plate 19: Column Shear Failure in Typical Building, Erzincan, Turkey 453
Plate 20: Imperial College MSc. Field Mission, Erzincan, Turkey, May 1993 453
Plate 21: The writer Testing RC Walls at IC Lab 454
Plate 22: The Writer Inspecting Typical Damage at Erzincan, Turkey 454

LIST OF FIGURES

PART I Page

Chapter 2: Figures 2.1-2.10 31-34
Chapter 3: Figures 3.1-3.7 42-44
Chapter 4: Figures 4.1-4.8 59-65
Chapter 5: Figures 5.1-5.27 90-103
Chapter 6: Figures 6.1-6.7 109-110
Chapter 7: Figures 7.1-7.33 146-162

PART II

Chapter 2: Figures 2.1-2.6 188-193
Chapter 3: Figures 3.1.(a)-3.1.(b) 202
Chapter 4: Figures 4.1-4.3 213-214
Chapter 5: Figures 5.1-5.24 229-247

LIST OF TABLES

PART I Page

Table 4.1. Summary of Experimental Programme 53
Table 4.2. Reinforcement for Tested Models 55
Table 4.3. Mix Proportion by Weight for Normal Weight Concrete..... 57
Table 4.4. Material Properties of Concrete..... 57
Table 4.5. Steel Reinforcement Properties 58
Table 8.1. Comparison Between Analytical and Experimental Results 173

PART II

Table 4.1 PGA for M_S=7 Earthquake at 12 km Depth 207
Table 4.2 Base Shear Coefficients From the Erzincan Earthquake Spectra for 5% Damping and Structural Period 0.3 seconds 210
Table 4.3. Sample Turkish Code Spectrum 211
Table 4.4 Peak Ground Parameters from 13 March 1992 Earthquake 211
Table 5.1. Comparison of Seismic Response for Intact, Conventionally and Selectively Repaired Frame 228

ABBREVIATIONS

ACI	American Concrete Institution
EC	Eurocode
EQ	Earthquake
ECSP	External Confinement Steel Plates
EUSB	External Unbonded Steel Bar
EUSP	External Unbonded Steel Plate
IC	Imperial College
IDM	Interaction Delay Mechanism
LVDT	Linear Voltage Differential Transducer
MDL	Maximum Displacement Level
NZ	New Zealand Standards
RC	Reinforced Concrete
SW	Shear Wall
SWR	Repaired Shear Wall
UBC	Uniform Building Code

NOTATIONS

$(EI)_e$: Elastic flexural stiffness of the uncracked cross-section

E_S : Young's modulus of steel

g : Acceleration due to gravity

I : Importance factor

L_e : Effective column length

μ : Displacement ductility

M_y : Yield moment

q : Behaviour factor

R_W : Response modification factor

S : Site coeficient for soil characteristics given

T : Fundamental period of vibration, in seconds, of the structure in the direction under consideration

V : Total base shear

v_c : Contribution of the concrete to shear resistance in terms of stresses

W : Total weight of structure

Z : Seismic zone factor

PART I: SELECTIVE REPAIR TECHNIQUES FOR EARTHQUAKE DAMAGED REINFORCED CONCRETE STRUCTURES

CHAPTER 1

1. INTRODUCTION

1.1. General

Earthquakes are some of the most destructive forms of natural hazard. Energy released during fault movement may cause very strong ground shaking, resulting in severe damage to structures and leading to substantial loss of life and property. Seismic risk is the product of seismic hazard and vulnerability, per unit value. Therefore, seismic risk may be high even in areas of low seismicity, as a consequence of the vulnerability of structures. It is the duty of civil engineers to minimise risk by decreasing vulnerability, by building structures, at an acceptable cost, that can withstand strong ground motion with an acceptable damage level (Ambraseys, 1971).

Structural damage in reinforced concrete members may be attributed to incorrect design approach, errors in calculation, inadequate detailing, poor construction practice or a combination of these factors. For many decades, design of new structures has made rapid progress in terms of structural economy and enhanced reliability while rational design of existing damaged and/or weak structures has not undergone the same degree of refinement (Trikha et al, 1991). It is concluded that the development of effective repair and strengthening techniques for existing buildings is at least as important as the development of new designs and construction methods.

The need for the strengthening of structures also arises in cases where existing structures must comply with more recent code requirements or when these structures are to be reassessed for higher loads. This was the case for a number of structures in Japan after the 1978 Miyagiken-oki earthquake, in Mexico City, after the 1985 Mexico earthquake and in Turkey after the 1992 Erzincan earthquake.

In the past thirty years, damage to structures as a result of major earthquakes has led to dramatic developments in earthquake engineering. The result has been the design of

structures with increased ductility and strength against lateral loads. However, many structures still in use have been designed and constructed prior to the development of codes which include such strength and ductility requirements. Many of these structures, designed before 1960, are susceptible to severe damage or collapse in the event of a major earthquake. This was evident from the disastrous results of the 1985 earthquake in Mexico city and the 1992 earthquake in Erzincan (Turkey). Recent research and development in the field of seismic strengthening of structures has decreased the incidence of failure and collapse of structures subjected to major earthquakes. Upgrading the structures by strengthening the weak elements or addition of structural elements has reduced the occurrence of total collapse and the loss of human life (Fintel, 1991).

Structural repair of damaged RC members has been extensively investigated under static loading conditions, while this is not the case for members subjected to dynamic loading conditions. Various methods for structural repair that are commonly applied are based on the addition of new reinforcing steel bars encased in a concrete jacket or the addition of steel plates that are anchored to concrete by means of self-fixing bolts and/or epoxy resin. Such conventional methods will tend to increase the strength and stiffness of the repaired member i.e. simultaneous improvement of both ultimate and serviceability limit states (for primarily flexural members). If the same procedures are applied in the repair of buildings that are extensively damaged by earthquakes, repaired members will pick up more load than that for which they were originally designed, and hence distortion of the earthquake load distribution and violation of the response modification factors that governed the design of the building originally will occur (q factor according to EC8 and R_w factor according to the UBC 91; which is a factor that accounts for energy dissipation capacity and post-elastic resistance of the structure). Moreover, perturbation of the stiffness distribution by repair may cause the building to violate the code regularity requirements, hence full dynamic analysis and re-design will be required (Elnashai, 1992).

The decision to repair and/or strengthen an existing structure depends not only on the field inspection of the damaged structure after an earthquake or on the seismic capacity evaluation of the existing structure, but also on a cost/benefit analysis of the different alternatives of repair and/or strengthening. In the case of Mexico City after the 1985 earthquake, it has been shown that repair and/or strengthening of reinforced concrete buildings is generally more economical than demolition and rebuilding, even in the case of severe structural damage (Bertero, 1992). It was found that some repaired and strengthened reinforced concrete buildings had a final price in the real estate market of about three to four times the overall cost of retrofitting and finishing. However, it must be mentioned that the repair and strengthening costs of foundation, structure and labour

involved in the Mexico City structures might be different from those costs in other countries. The same conclusion was also drawn from the reconstruction programme of Erzincan (Turkey) after the 13 March 1992 earthquake.

Most building codes only address new construction. Also, there is no comprehensive guidance for evaluating the residual strength of a damaged structure and the effectiveness of a given repair method. State-of-the-art methods of repair have largely been developed by experience, engineering judgement and limited experimental evidence. Although experience and engineering judgement are valuable, the effectiveness of repair methods developed in this manner are often not known until after an earthquake. Thus, there is an increasing need for experimental evidence from investigations of various methods of repair in order that the effectiveness of particular schemes may be known before implementation.

1.2. Aspects of Seismic Design

The objectives of earthquake-resistant design are to avoid severe damage under the 'design' earthquake and to avoid total collapse under the 'maximum credible' earthquake. It is the duality of this design premise that renders earthquake-resistant design such a challenging problem. This is because whereas the first requirement demands high structural stiffness, to limit lateral displacements, the second requirement calls for a structure with high ductility and energy absorption capacity (Elnashai and Dowling, 1991).

Design philosophy is a somewhat grandiose term that we use for the fundamental basis of design. It covers the reasons underlying our choice of design loads, and forces, our analytical techniques and design procedures, and our aims for economic and efficient optimisation. The importance of rational design philosophy becomes paramount when seismic considerations dominate design. This is because higher risks of damage under earthquake loadings generally considered more acceptable than under other comparable extreme loads, such as maximum live and wind loads. For example, modern building codes typically specify an intensity of design earthquakes corresponding to a return period of 100 to 500 years for ordinary structures, such as office buildings. The corresponding design forces are generally too high to be resisted within the elastic range of material response, and it is common to design for strength which is a fraction, perhaps as low as 15 to 25%, of that corresponding to elastic response, and to expect the structures to survive an earthquake by large inelastic deformations and energy dissipation corresponding to material distress. The consequence is that the full strength of the

building can be developed while resisting forces resulting from much smaller earthquakes, which occur much more frequently than the design-level earthquake. The annual probability of developing the full strength of the building in seismic response can thus be as high as 1 to 3%. This compares with accepted annual probabilities for achieving ultimate capacity under gravity loads of perhaps 0.01%. It follows that the consequences resulting from the lack of rational seismic design philosophy are likely to be severe (Paulay and Priestley, 1992).

Well-established techniques, used to determine the safe resistance of structures with respect to various static loads, including wind forces, cannot simply be extended and applied to conditions that arise during earthquakes. Although many designers prefer to assess earthquake-induced straining actions in terms of static equivalent loads and forces, it must be appreciated that actual seismic response is dynamic and related primarily to imposed deformation rather than forces. To accommodate large seismically induced deformations, most structures need to be ductile. Thus in the design of structures for earthquake resistance, it is preferable to consider forces generated by earthquake induced displacements rather than traditional loads. Because the magnitudes of the largest seismic-displacement-generated forces in a ductile structure will depend on its capacity or strength, the evaluation of the latter is of importance.

Reinforced concrete structures, being man-made composites with inevitable gross errors, are much more exposed to unforeseen conditions such as seismic loading, than to any other better known loading. The actual trends in seismic design are less deterministic than, say, fifteen years ago. First, a three-fold uncertainty is recognised related to the seismic action (origin, intensity, frequency content); authorities are made more clearly responsible in selecting seismic design 'loads' in a more probabilistic way. Besides, under an 'ultimate' seismic load, limited structural damage is legitimately acceptable; an option which is more economical to the society, resulting in fewer unfair claims against engineers. Second, due to the pronounced elastoplastic behaviour of structures under the design-earthquakes, additional local loading conditions are introduced as better estimators of 'unforeseen' conditions. Third and most important, a basic requirement is introduced related to the energy dissipation capacity throughout the entire structure. As a by-product of this requirement, extensive redistributions of action-effects are feasible without any loss of structural integrity (Derecho, 1989). These trends are also reflected in modern earthquake resistant design codes, especially under the impact of the New Zealand school of thought, and after the publication of such a basic document as the ATC-3 in the USA. Modern codes are more clearly performance oriented than merely a list of seemingly arbitrary rules. The recent draft of the European Code EC8 on Earthquake-Resistant Design adopts this general design philosophy.

The design earthquake is determined from site-specific studies taking into account the (long-term) seismic history of the zone. By specifying the return period of a certain magnitude earthquake, an attenuation relationship, site response to bedrock motion, the lifetime of the structure and an acceptable probability of exceedance for the specified magnitude, a design earthquake is chosen. This may be described in terms of an acceleration time-history, an elastic response spectrum or a uniform risk spectrum (Dorwrick, 1987). A detailed treatment of the definition of seismic design events is an involved activity, and is beyond the scope of this chapter.

As stated above, there are two commonly used procedures for specifying seismic design forces: "The equivalent-static force procedure" and "dynamic analysis". In the equivalent static-force procedure the initial forces are specified as static forces using empirical formulae. The empirical formulae do not explicitly account for the dynamic characteristics of the particular structure being designed or analysed (UBC, 1991). The formulae were, however, developed adequately to represent the dynamic behaviour of what are called regular structures, which have a reasonably uniform distribution of mass and stiffness. For such structures the equivalent-static-force procedure is most often adequate. In this method, a horizontal static force is calculated, taking into account the fundamental period of the structure, its importance, structural system, seismicity of the site, the soil conditions and the total weight of the building. This force, termed 'base shear' is distributed amongst the individual floors; the design is checked, and if necessary modified, for the stresses thus resulting.

Structures that do not fit into this category are termed irregular. Common irregularities include large floor-to-floor variation in mass or centre of mass, and soft stories. Such structures violate the assumptions on which the empirical formulae used in the equivalent-static-force procedures are based. Therefore, its use may lead to erroneous results. In these cases a dynamic analysis can take a number of forms, but should take account of the irregularities of the structure by modelling its dynamic characteristics, including natural frequencies, mode shapes, and damping. This can be achieved by either modal analysis for design purposes or time history analysis for checking existing stuctural design.

Modal spectral analysis can be performed where by changing the equations of motion from the displacements to the mode shapes (generalised displacements), de-coupling of the equations is achieved. This leads to a number of equations which are not simultaneous (Bathe, 1982). The solution of each individual equation yields the response of the system in a specific mode, hence the term 'modal analysis'. Furthermore if only the

maximum response is of interest, use can be made of a 'response spectrum' to obtain the peak response for a mode, or a number of modes.

Time-history analysis using real or artificial earthquake records should be used for structures exhibiting strong non-linear response. In this method, the equations of motion are integrated directly in time, and the response displacements are evaluated at every time increment. Methods of time integration are broadly grouped under explicit and implicit methods.

The choice of earthquake for use in time-history analysis is another very important parameter affecting the obtained results. Real earthquake time-histories are preferable, since they reflect characteristics of actual earthquakes. In the absence of earthquakes recorded at or near the site under consideration, it is recommended to study carefully the seismo-tectonic environment and to choose strong motion accelerograms from similar environments. It is advisable to use three different earthquakes in the analysis of important structures (Bolt, 1989). On the other hand, artificially produced signals are used frequently. These are normally generated from given elastic response spectra, and utilise some assumption regarding the phase distribution to arrive at the transient signal with the same ground motion parameters as the 'original' record.

Earthquake-resistant design of structures may be effected by designing individual members and connections to withstand forces evaluated from structural analysis under the effect of a set of lateral earthquake forces. On the other hand, 'capacity' design concepts adopt a different philosophy, whereby the desired failure mode is identified and the members involved in its development are determined. These key members are detailed with great care to supply sustainable ductility and energy absorption capacity. The rest of the structure is designed for the forces consistent with the ultimate capacity of the key members, hence 'capacity design' (Paulay, 1991).

Modern codes for design against cyclic loads make use of 'capacity design' that utilises a predetermined failure mode to ensure maximum energy absorption and ductile behaviour. In repair or strengthening of an existing structure, if the stiffness or strength distribution is altered significantly, the overall behaviour may deteriorate causing a non-ductile collapse mechanism. Therefore, repair/strengthening of a structure should be conducted with due consideration to two factors, namely:

- The overall building design criterion.
- The required stiffness, strength or ductility re-instatement/enhancement.

The philosophy behind this approach is that failure mode control, required by capacity design principles, dictates a certain behavioural pattern that may be jeopardised by unscrupulous intervention for repair or strengthening. Also, the behaviour factor (q or R_w) of the structure may increase or decrease as the local behaviour of the member is altered. An optimal solution should be sought, leading to a specific criterion for the repair. Buildings designed in accordance with these modern code provisions will be expected to:

- Resist minor earthquakes without damage.
- Resist moderate earthquakes without structural damage but with some non-structural damage.
- Resist major earthquakes without collapse but with structural and non structural damage.

It is evident that it would be uneconomical to design a structure to withstand the greatest likely earthquake without damage. The cost of providing strength to resist very high intensity lateral vibrations must be weighed against the importance of the structure and the probability of the earthquakes. Hence the possibility of damage is accepted, but not loss of life. The code objective is to have structures that will behave elastically under earthquakes which can be expected to occur more than once in the life of the building; the structures, moreover, should be able to survive without collapse the major earthquake that might occur during the life of the building. To avoid collapse during the major earthquake, members must be ductile enough to absorb and dissipate energy by postelastic deformations. The order of ductility involved may be associated with very large permanent deformations. Thus, although the structure should not collapse, the resulting damage might need extensive repair.

1.3. Objectives

Concrete buildings containing RC shear walls have exhibited superior seismic performance in earthquakes of the last thirty years, when compared with rigid frame-type reinforced concrete buildings. While hundreds of frame-type structures collapsed or were severely damaged in past earthquakes, only a few structures containing shear walls collapsed or were heavily damaged. Despite the undeniable observed superiority of structural wall-type concrete structures over concrete frame structures, some codes continued to give preference to concrete ductile frame structures, while placing a substantial penalty on shear walls. This code approach was due to the lack of experimental and analytical background information on shear wall behaviour. This, however, has been rectified in some recent seismic design codes (UBC 91 and

Eurocode8). While a large body of information on shear walls has been accumulated during the 1980's, more experimental and analytical studies are needed to create a solid basis for a rational seismic design approach. The availability of such information would then encourage a wider and more economical utilisation of structural walls for earthquake resistance (Fintel, 1991).

The objectives of the present research are to develop techniques for selective repair and strengthening aimed at the stiffness, strength or ductility of reinforced concrete structural components taking into account the overall structural performance and the criteria used for the original design. This is applicable to all types of RC structures but more specifically to: structures exposed to, or damaged by, non-contact explosions and ground-born vibrations from blast or earthquakes ; structures that were underdesigned for wind effects ; structures that were designed for vertical and wind loads only and due to change in the area seismicity or due to changes in the code regulations they are to be assessed for earthquakes. To achieve such a target, an intensive experimental testing programme was carried out in the concrete laboratory at Imperial College on seventeen RC walls that are designed to fail in some specific failure modes. Walls were then be repaired to re-instate and/or enhance one of the following response characteristics without affecting the others :

- Flexural stiffness.
- Flexural strength.
- Shear strength.
- Shear stiffness.
- Ductility.

Towards the fulfilment of the above objectives, the thesis describes an experimental research programme aimed at verifying the possibility of selective intervension and quantifying the available margins in reinstatement and enhancement of the chosen response parameter.

A total of four walls were over-designed for flexure and under-designed for shear. This was achieved by ensuring that the ultimate flexural capacity exceeded the flexural strength corresponding to its maximum probable shear strength. Shear strength and stiffness re-instatment were designed and applied to damaged walls and re-tested with the minimum possible influence on the flexural strength or stiffness.

Six walls were over-designed for shear and under-designed for flexure. This was achieved by ensuring that the ultimate shear capacity exceeded the shear corresponding to

their maximum probable flexural strength. Flexural stiffness re-instatement was designed and applied for two walls without affecting the flexural strength. Flexural strength enhancement was designed and applied for two other walls without affecting the flexural stiffness. Ductility enhancement was designed and applied to the fifth wall without affecting either its strength or stiffness. The sixth model was tested as a control model.

Seventeen cyclic loading tests were performed within the current experimental programme. Use was made of thirteen concrete wall models. Eight models were tested to damage, repaired and retested. To simulate retrofitting schemes which can be applied to existing structures, three intact models were tested after the enhancement of the flexural strength or ductility.

To emphasise the importance of selective, as opposed to conventional repair, a case study of a typical building in Erzincan (Turkey) was seismically assessed under various repair schemes. The nonlinear dynamic analysis performed on the chosen building showed that conventional repair can lead to disastrous results; and that selective intervention can improve the seismic performance of the building.

1.4. Organisation of the Thesis

Part I of the thesis is concerned with selective repair techniques. After the introductory Chapter 1, various existing methods of repair and retrofitting are reviewed in Chapter 2. Available research work on testing and repair of RC damaged elements subjected to monotonic and cyclic loading is given in Chapter 3. Emphasis is given to investigations of particular relevance to the present research.

Chapter 4 describes the test set-up. This includes loading system, hydraulic power system, electro-hydraulic servo-control system, instrumentation and data acquisition. The section concludes with the design and reinforcement detailing of the test specimens.

The test results for the six intact walls are given in Chapter 5. This includes the loading history, force-displacement hysteresis loops, force-steel strains at various reinforcement elements, crack pattern, energy dissipation capacity and ductility.

Background to the repair philosophy is described in Chapter 6. Newly-developed repair techniques are described and their importance is highlighted. Specific concrete integrity re-instatement schemes that are relevant to the current testing programme are also given. This is followed by a presentation of test results for eleven repaired or enhanced

models in Chapter 7. Attention is paid to the causes and mechanisms of failure, structural deterioration characteristics and the efficiency of the applied repair scheme. A comprehensive comparison with the intact or reference model is also given.

A comprehensive discussion of the test results is given in Chapter 7. This includes the effect of each response parameter on the global model behaviour. An assessment of the effectiveness of the newly-developed repair techniques is also given.

In **Part II** of the thesis, the selective intervention techniques are applied to the real-life solution, the Erzincan (Turkey) earthquake of 13 March 1992. This comprises aspects of hazard as well as vulnerability assessment and risk reduction.

Chapter 2 describes aspects of engineering seismology pertinent to the current work. This includes the tectonic setting in North Central Anatolia, historical and instrumental earthquakes and a short description of the 13 March 1992 event. It also includes a description of the current construction status of the buildings, many of which were in various stages of completion on 13 March, 1992. A summary of observed earthquake damage and defects is furnished. The section concludes with a statement highlighting the serious problems of seismic hazard assessment in the tectonically-active and complex Erzincan region.

Chapter 3 provides background to the inspection policy and inspection forms developed for the fulfilment of this work. The effect of material, section, member, sub-assemblage, structure and site characteristics on seismic performance is used to justify the items comprising the newly-developed inspection forms.

Chapter 4 presents some design criteria for seismic upgrading. This includes a summary of existing seismic hazard studies and comparison of seismic forces for prototype structures. It also includes response spectral shapes for design and concludes with recommended design loads and input ground motion.

Chapter 5 presents the analytical response of a severely damage structure that was repaired and upgraded using two different techniques. The structure is analysed dynamically using the measured acceleration history from the 1992 Erzincan earthquake. The models assembled represented a conventional upgrading method (jacketing) and the new "selective" techniques described, tested and verified in Part I of this thesis. Comprehensive monitoring of several seismic response parameters from the original,

conventionally-upgraded and selectively-retrofitted structure is presented and differences are discussed.

The thesis concludes with Chapter 6 where a summary of Part I and Part II conclusions is given. Finally suggestions for future research and development activities are given.

CHAPTER 2

2. METHODS OF REPAIR AND RETROFITTING

Concrete repair and retrofitting of structures may be associated with the repair of concrete surface, concrete cracks, corroded steel reinforcement, porous concrete, concrete leaking etc. However, the remedy of previous defects might not be sufficient to achieve an acceptable serviceability and ultimate limit states and hence a strengthening scheme might be required. Strengthening of structural members can be achieved by replacing poor quality or defective material and/or by attaching additional load-bearing material. The new load-bearing material may be high quality concrete, reinforcing steel bars, thin steel plates and straps, post-tensioning tendons, or various combination of these materials. The main concern in strengthening is to achieve compatibility and continuity in the structural behaviour between the original material/structure and the new material/repaired structure. An account of the main repair and strengthening techniques that might be used in order to achieve an enhanced structural behaviour will be presented hereafter. This is based on technical publications and recommendations of manufacturers (Fosroc and Sica). It also includes the writer's opinion based on field applications.

2.1. Methods of Crack Repair

Following the evaluation of the cracked structure and the determination of the cause of the cracking, a suitable repair procedure can be selected. Successful repair procedures should take into account the cause of the cracking. For example, if the cracking was primarily due to drying shrinkage, then it is likely that after a period of time the cracks will stabilise. On the other hand, if the cracks are due to a continuing foundation settlement, repair will be of no use until the settlement problem is corrected.

In the following a survey is made of the crack repair methods, including a summary of the characteristics of the cracks that may be repaired with each procedure, the types of structures that have been repaired, and a summary of the procedures that are used.

2.1.1. Epoxy injection

Repair methods for structures with minor damage (i.e. minor cracking with strength of all elements intact) due to earthquake loading have typically focused on repairing bond of reinforcing bars and filling the cracks to reinstate most of the original strength and stiffness of the damaged members. Experimental work in this area has focused on low viscosity epoxy injection (Bertero et al, 1980). This has been a fairly standard practice in the last decade for repairing cracked structural elements.

For large cracks (larger than 4 mm) and regions where concrete has crushed, epoxy injection is inappropriate. Studies on repairing this type of damage have emphasised the removal of the loose concrete and replacement with expansive cement mortar, or other similar material (Kahn, 1980).

Cracks as narrow as 0.05 mm can be bonded by the injection of epoxy. The technique generally consists of drilling holes at close intervals along the cracks, in some cases installing entry ports, and injecting the epoxy under pressure. For massive structures, an alternative procedure consists of drilling a series of holes (usually 22 mm in diameter) that intercept the crack at a number of locations. Typically, holes are spaced at whichever is the shortest, of 200 mm, or at the crack intersection.

Epoxy injection has been successfully used in the repair of cracks in buildings, bridges, dams, and other types of concrete structure. However, unless the crack is dormant (or the cause of cracking is removed, thereby making the crack dormant), it will probably recur, possibly somewhere else in the structure. If the cracks are active and it is desired to seal the crack while allowing continued movement at that location, it is necessary to use a sealant or other material that allows that crack to function as a joint (ACI 224.1R-89).

With the exception of certain specialised epoxies, this technique is not applicable if the cracking is actively leaking and cannot be dried out. While most cracks can be injected, contaminants in the crack (including water) will reduce the effectiveness of the epoxy to structurally repair the crack.

Epoxy injection requires a high degree of skill for satisfactory execution, and application of the technique may be limited by the ambient temperature. The general procedures involved in the epoxy injection are as follows:

i. Clean the cracks. The first step is to clean the cracks that have been contaminated. Oil, grease, dirt, or fine particles of concrete prevent epoxy penetration and bonding. Preferably, contamination should be removed by flushing with water or other specially effective solvent. The solvent is then blown out using compressed air or adequate time is provided for air drying.

ii. Seal the surfaces. Surface cracks should be sealed to keep the epoxy from leaking out before it has gelled. Where the crack face cannot be reached, but where there is backfill, or where a slab-on-grade is being repaired, the backfill material or subbase material is often an adequate seal. A surface can be sealed by brushing an epoxy along the surface of the crack and allowing it to harden. If extremely high injection pressures are needed, the crack should be cut out to a depth of 13 mm and width of about 19 mm in a V-shape, filled with an epoxy, and struck off flush with the surface. If a permanent glossy appearance along the crack is objectionable and high injection is not required, a strippable plastic may be applied along the crack. When the job is completed, the dry filler can be stripped away to expose the gloss-free surface.

iii. Install the entry ports. Three methods are in general use:

- Drilled holes fittings inserted. Historically, this method was the first to be used in conjunction with V-grooving of the cracks. The method entails drilling a hole into the crack, approximately 19 mm in diameter and 13 to 25 mm below the apex of the V-grooved section, into which a fitting such as a pipe nipple or tire valve stem is bonded with an epoxy adhesive. A vacuum chuck and bit are useful in preventing the cracks from being plugged with drilling dust.

- Bonded flush fitting. When the cracks are not V-grooved, a method frequently used to provide an entry port is to bond a fitting flush with the concrete face over the crack. This flush fitting has a hat-like cross section with an opening at the top for the adhesive to enter.

- Interruption in seal. Another system of providing entry is to omit the seal from a portion of the crack. This method can be used when special gasket devices are available that cover the unsealed portion of the crack and allow injection of the adhesive directly into the crack without leaking.

iv. Mix the epoxy. This is done either by batch or continuous methods. In batch mixing, the adhesive components are premixed according to the manufacturer's instructions, usually with the use of a mechanical stirrer, such as a paint and mixing paddle. Care must be taken to mix only the amount of adhesive that can be used prior to commencement of gelling of the material. When the adhesive material begins to gel, its flow characteristics begin to change, and pressure injection becomes more and more difficult. In the continuous mixing system, the two liquid adhesive components pass through metering and driving pumps before passing through an automatic mixing head. The continuous mixing system allows the use of fast setting adhesives that have a short working life.

v. Inject the epoxy. Hydraulic pumps, paint pressure pots, or air-actuated caulking guns can be used. The pressure used for injection must be carefully selected. Increased pressure often does little to accelerate the rate of injection. In fact the use of excessive pressure can propagate the existing cracks, causing additional damage. An average pressure of 10 bars is highly recommended.

If the crack is vertical, the injection process should begin by pumping epoxy into the entry port at the lowest elevation until the epoxy level reaches the entry port above. The lower injection port is then capped, and the process is repeated at successively higher ports until the crack has been completely filled and all ports have been capped.

For horizontal cracks, the injection should proceed from one end of the crack to the other in the same manner. The crack is full if the pressure can be maintained. If the pressure cannot be maintained, the epoxy is still flowing into unfilled portions or leaking out of the crack.

vi. Remove the surface seal. After the injected epoxy has cured, the surface seal should be removed by grinding or other means, as appropriate. Fittings and holes at entry ports should be painted with an epoxy patching compound.

In the specific case of de-laminated bridge decks, epoxy injection can be an effective intermediate term repair procedure. In this case, the first , the second, and sixth steps are omitted. The process is terminated at a specific location when epoxy exits from a crack at some distance from the injection ports. This procedure does not arrest ongoing corrosion.

2.1.2. Routing and sealing

Routing and sealing can be used on cracks that are dormant and of no structural significance. This method involves enlarging the crack along its exposed face and filling and sealing it with suitable joint sealant Fig. 2.1. The routing operation may be omitted, but at some sacrifice in permanence of the repair.

This is the simplest and the most common technique for crack repair. It can be executed with relatively untrained labour (compared with epoxy injection) and is applicable for sealing both fine pattern cracks and larger isolated defects. The method will not be effective on an active crack (for sealing active cracks, refer to section 2.1.6.). Routing and sealing are not applicable for sealing cracks subject to pronounced hydrostatic pressure, except when sealing the pressure face, in which case some reduction in the flow can be obtained.

The routing operation consists of preparing a groove at the surface that is sufficiently large to receive the sealant, using a concrete saw, hand tools, or pneumatic tools. A minimum surface width of 6 mm is desirable. Repairing narrower grooves is difficult. The surfaces of routed joint should be cleaned with an air jet and permitted to dry before placing the sealant.

The purpose of the sealant is to prevent water from reaching the reinforcing steel and hydrostatic pressure from developing within the joint, staining the concrete surface, or causing moisture problems on the far side of the member.

The sealant may be of several materials, depending on how tight or permanent a seal is desired. Epoxy compounds are often used. Hot-poured joint sealants work very well when thorough water tightness of the joint is not required and appearance is not important. Urethanes, which remain flexible through large temperature variations, have been used successfully in cracks up to (19 mm) in width and of considerable depth. There are many commercial products, and the manufacturers should be consulted as to the type and grade most applicable for a specific purpose and condition of exposure.

2.1.3. Stitching

This method involves drilling holes on both sides of the crack and grouting in stitching dogs (U-shaped metal units with short legs) that span the crack (Fig. 2.2). Stitching may be used when tensile strength must be re-established across major cracks. Stitching a

crack tends to stiffen the structure, and the stiffening may be accentuate the overall structural restraint, causing the concrete to crack elsewhere. Therefore, it may be necessary to strengthen the adjacent section using external reinforcement embedded in a suitable overlay.

The stitching procedure consists of drilling holes on both sides of the crack, cleaning the holes, and anchoring the legs of the dogs in the holes, with either a non shrink grout or an epoxy resin-based bonding system. The stitching dogs should be variable in length and orientation or both, and they should be located so that the tension transmitted across the crack is not applied to a single plane within the section but spread over an area.

Spacing of the stitching dogs should be reduced at the ends of cracks. In addition, consideration should be given to drilling a hole at each end of the crack, to blunt it and relieve the concentration of stresses.

Where possible, stitch both sides of the concrete section so that further movement of the structure will not pry or bend the dogs. In bending members, it is possible to stitch one side of the crack only. This should be done on the tension face, where movement is occurring. If the member is in a state of axial tension, the dogs must be placed symmetrically, even if excavation or demolition is required to gain access to opposite sides of the section.

Stitching will not close a crack but can prevent it from propagating further. Where there is a water problem, the crack should be made watertight as well as stitched to protect the dogs from corrosion. This repair should be completed before stitching begins. An exception should be made in the case of active cracks, where the structure must be stabilised before being made watertight, because movement at the crack will break the material within the crack.

The dogs are relatively thin and long and cannot take much compressive force. Accordingly, if there is a tendency for the crack to close as well as to open, the dogs must be stiffened and strengthened by for example, encasement in an overlay.

2.1.4. Additional reinforcement

Two types of reinforcement are in general use:

i. Conventional reinforcement. Cracked reinforced concrete bridge girders have been successfully repaired using epoxy injection and reinforcing bar insertion. This technique consists of sealing the crack, drilling holes (19 mm in diameter) at 45° to the deck surface and crossing the crack plane at approximately 90° Fig. 2.3, filling the hole and crack plane with epoxy pumped under low pressure (342 to 548 KPa), and placing a reinforcing bar into the drilled hole. Typically No. 13 or 16 mm bars are used, extending at least 0.50 m on each side of the crack. The epoxy bonds the bar to the walls of the hole, fills the crack plane, bonds the cracked concrete surfaces back together in one monolithic form, and thus reinforces the section.

A temporary elastic exterior crack sealant is required for a successful repair. Gel-type epoxy crack sealants work very well within their elastic limits. Silicone rubber gap sealants work well and are especially attractive in cold weather or when time is short. The sealant should be applied in a uniform layer approximately 1.6 to 2.4 mm thick and should span the crack by at least 19 mm on each side.

The epoxy used to rebond the crack should have a very low viscosity and a high modulus of elasticity. It should be capable of bonding to concrete in the presence of moisture, and it should be 100 percent reactive (ACI 503R-89).

The reinforcing bars can be spaced to suit the needs of the repair. They can be placed in any desired pattern, depending on the design criteria and the location of the in-place reinforcement.

ii. Prestressing steel. Post-tensioning is often the desirable solution when the major portion of a member must be strengthened or when the cracks that have formed must be closed Fig. 2.4. This technique uses prestressing strands or bars to apply a compressive force. Adequate anchorage must be provided for the prestressing steel, and care is needed so that problem will not merely migrate to another part of the structure. The effects of the tensioning force (including eccentricity) on the stress within the structure should be carefully analysed. For indeterminate structures post-tensioned using this procedure, the effects of secondary moments and induced reactions should be considered.

2.1.5. Drilling and plugging

Drilling and plugging a crack consists of drilling down the length of the crack and grouting it to form a key, Fig. 2.5. This technique is only applicable when cracks run in reasonably straight lines and are accessible at one end. This method is often used to repair cracks in vertical walls.

A hole (typically 50 to 75 mm in diameter) should be drilled, centered on and following the crack. The hole must be large enough to intersect the crack along its full length and provide enough repair material structurally to take the loads exerted on the key. The drilled hole should then be cleaned, made tight, and filled with grout. The grout key prevents transverse movement of the sections of concrete adjacent to the crack. The key will also reduce heavy leakage through the crack and loss of soil from behind a leaking wall.

If water tightness is essential and structural load transfer is not, the drilled hole should be filled with a resilient material of low modulus in lieu of grout. If the keying effect is essential, the resilient material can be placed in a second hole, the first being grouted.

2.1.6. Flexible sealing

Active cracks can be routed out; cleaned by sand-blast, air-water jet, or both; and filled with a suitable field-moulded flexible sealant. As nearly as practical, the sealant reservoir (slot) formed by routing should comply with the requirements for width and shape factor of a joint having equivalent movement. The selection of a suitable sealant and installation method should follow those for equivalent joints.

A bond breaker should be provided at the bottom of the slot to allow the sealant to change shape without a concentration of stress on the bottom, Fig. 2.6. The bond breaker may be polyethylene strip, pressure sensitive tape, or other material which will not bond to the sealant before or during cure. Narrow cracks subject to movement, where aesthetics are not important, may be sealed with a flexible surface seal, Fig 2.7. By using a bond breaker, over the crack, a flexible joint sealant may be troweled over the bond breaker providing an adequate bonding area. This is a very economical procedure and may be used on the interior of a tank, roofs, or other areas not subject to traffic or mechanical abuse.

2.1.7. Grouting

2.1.7.1. Portland cement grouting

Wide cracks, particularly in gravity dams and thick concrete walls, may be repaired by filling the Portland cement grout. The procedure consists of cleaning the concrete along the crack; installing built-up seats (grout nipples) at intervals astride the crack (to provide a pressure tight contact with the injection apparatus); sealing the crack between the seats with a cement paint, sealant, or grout; flushing the crack to clean it and test the seal; and then grouting the whole area. Grout mixtures may contain cement and water or cement plus sand and water, depending on the width of the crack. However, the water-cement ratio should be kept as low as practical to maximise strength and minimise shrinkage. Water reducers or other admixtures may be used to improve the properties of the grout. For small volumes, a manual injection gun may be used; for larger volumes, a pump should be used. After the crack is filled, the pressure should be maintained for several minutes to insure good penetration.

2.1.7.2. Chemical grouting

Chemical grouts consist of solutions of two or more chemicals that combine to form a gel, a solid precipitate, or a foam, as opposed to cement grouts that consist of suspensions of solid particles in a fluid. Cracks in concrete as narrow as 0.05 mm have been filled with chemical grout. The advantages of chemical grouts include their applicability in moist environments (excess moisture available), wide limits of control of gel time, and their application in very fine fractures. Disadvantages are the high degree of skill needed for satisfactory use, their lack of strength, and the requirement that the grout does not dry out of service.

2.1.8. Drypacking

Drypacking is the hand placement of a low water content mortar followed by tamping or ramming of the mortar into place, producing intimate contact between the mortar and the existing concrete. Because of the low water-cement ratio of the material, there is little shrinkage, and the patch remains tight and of good quality with respect to durability, strength, and water-tightness.

Drypack can be used for filling narrow slots cut for the repair of dormant cracks. The use of drypack is not advisable for filling or repairing active cracks. Before a crack may be repaired by drypacking, the portion adjacent to the surface should widened to a slot about 25 mm wide and 25 mm deep. This is most conveniently done with a power-driven sawtooth bit. The slot should be undercut so that the base width is slightly greater than the surface width. After the slot is thoroughly cleaned and dried, a bond coat consisting of cement slurry or equal quantities of cement and fine sand mixed with water to a fluid paste consistency, should be applied. Placing of the dry pack mortar should begin immediately. The mortar consists of one part cement, three parts of sand passing a No.16 (1.18 mm) sieve, and just enough water so that the mortar will stick together when moulded into a ball by hand. If the patch must match the colour of the surrounding concrete, a blend of Portland cement and white cement may be used. Normally, about one-third white cement is adequate, but the precise proportions can only be determined by trial.

To minimise shrinkage in place, the mortar should stand for 1/2 hour after mixing and then be remixed prior to use. It should be placed in layers about 10 mm thick. Each layer should be thoroughly compacted over the entire surface using a blunt stick or hammer, and each layer should be scratched to facilitate bonding with the next layer, There need be no time delays between layers. The mortar may be finished by laying the flat side of a piece of hardwood against it and striking it several times with a hammer. Surface appearance may be improved by a few light strokes with a rag or sponge float. The repair should be cured by using either water or a curing compound. The simplest method of moist curing is to support a strip of folded wet burlap along the length of the crack.

2.1.9. Crack arrest

During construction of massive concrete structures, cracks due to surface cooling or other causes may develop and propagate into new concrete as construction progresses. Such cracks may be arrested by blocking the crack and spreading the tensile stress over a larger area. A piece of bond-breaking membrane or a grid of steel mat may be placed over the crack as concreting continues. A semicircular pipe placed over the crack may also be used Fig 2.8. A description of installation procedures for semicircular pipes used during the construction of a massive concrete structures follows: The semicircular pipe is made by splitting a 200 mm, 16-gauge pipe and bending it to a semicircular section with about a 75-mm flange on each side; the area in the vicinity of the crack is cleaned; the pipe is placed in sections so as to remain centered on the crack; the sections are then welded

together; holes are cut in the top of the pipe to receive grout pipes; and after setting the grout pipes, the installation is covered with concrete placed concentrically over the pipe by hand. The installed grout pipes are used for grouting the crack at a later date, thereby restoring all or a portion of the structural continuity.

2.1.10. Polymer impregnation

Monomer systems can be used for effective repair of cracks. A monomer system is a liquid that consists of small organic molecules capable of combining to form a solid plastic. Monomers have varying degrees of volatility, toxicity, and flammability and do not mix with water. They are very fluid and will soak into dry concrete, filling the cracks, in much the same way as water does.

Monomer systems used for impregnation contain a catalyst or initiator and the basic monomer (or combination of monomers). They may also contain a cross linking agent. When heated, the monomers join together, or polymerise, becoming a tough, strong, durable plastic that greatly enhances a number of concrete properties.

If a cracked concrete surface is dried, flooded with the monomer, and polymerised in place, the cracks will be filled and structurally repaired. However, if the cracks contain moisture, the monomer will not soak into the concrete at each crack face, and consequently, the repair will be unsatisfactory. If a volatile monomer evaporates before polymerisation, it will be ineffective. Polymer impregnation has not been used successfully to repair fine cracks.

Badly fractured beams have been repaired using polymer impregnation by drying the fracture, temporarily encasing it in a watertight (monomer proof) band of sheet metal, soaking the fractures with monomer, and polymerising the monomer. Large voids or broken areas in compression zones can be filled with fine and coarse aggregate before flooding them with the monomer, providing a polymer-concrete repair. This scheme can also be applied as a superficial paint to the cracked surfaces.

2.1.11. Overlays and surface treatments

Cracks in both structural and pavement slabs may be repaired using bonded overlays if the slabs are not subject to movement (note, unbonded overlays can be used to cover, but not necessarily repair, slabs). However, most cracks in slabs are subject to movement caused

by variations in loading, temperature, and moisture. These cracks will reflect through any bonded overlay, negating the overlay insofar as crack repair is concerned. However, slabs with numerous fine cracks caused by drying shrinkage or other one-time occurrences can be effectively repaired by the use of overlays.

Slabs-on-grade in freezing climates should never receive an overlay on surface treatment that is a vapour barrier. An imprevious barrier will cause moisture passing from the subgrade to condense under the barrier, leading to critical saturation of the concrete and rapid disintegration by cycles of freezing and thawing.

Low solid, epoxy resin-based systems have been used to seal the surface of concrete (including very fine cracks). They are suitable for use on surfaces that are not subject to wear. Typically, 17 to 25 percent solvent solutions of epoxy resin systems conforming to ASTM C881 viscosity Grade I, Type I, II, or III are used. The effectiveness of these materials has not been fully established.

Bridge and parking decks and interior slabs may be coated effectively using a heavy coat (1.5 mm +/- 0.25 mm) of epoxy resin. The method will close dormant cracks, even if skid-resistant aggregate is abraded from the surface, since traffic cannot abrade the resin that has penetrated the cracks.

Slabs and decks containing fine dormant cracks can be repaired by applying an overlay of polymer-modified Portland cement concrete mortar. In highway bridge applications a minimum overlay thickness of 38 mm has been used successfully . Polymers suitable for such applications are latexes of styrene butadiene, acrylic, non-reemulsifiable polyvinyl acetate, and certain water-compatible epoxy resin systems. The minimum resin solids should be 15 percent by weight of the Portland cement, with 20 percent by weight of the cement usually being optimum.

Prior to overlay application, the surface should be cleaned to remove laitance, carbonation, or contaminants, such as grease or oil. A bond coat consisting of broomed latex mortar or an epoxy adhesive should be applied immediately before placing the overlay. Since latex normally solidifies rapidly, continuous batching and mixing equipment should be employed. The polymer-modified overlay should be mixed, placed, and finished rapidly (within 15 minutes in warm weather). Disturbing the overlay after the latex begins to solidify will result in cracking of the overlay. Such overlays should be cured for 24 hours.

2.1.12. Autogenous healing

A natural process of crack repair known as "autogenous heating" can occur in concrete in the presence of moisture and absence of tensile stresses. It is a practical application for closing dormant cracks in a moist environment, such a way may be used in mass concrete structures.

Healing occurs through the reaction between calcium hydroxide in the cement paste and carbon dioxide, which is present in the surrounding air and water. Calcium carbonate and calcium hydroxide crystals precipitate, accumulate, and grow within the cracks. The crystals interlace and twine, producing a mechanical bonding effect, which is supplemented by chemical bonding between adjacent crystals and between the crystals and the surfaces of the paste and the aggregate. As a result, some of the tensile strength of the concrete is restored across the cracked section, and the crack may become sealed.

Healing will not occur if the crack is active and is subjected to movement during the healing period. Healing will also not occur if there is a positive flow of water through the crack, which dissolves and washes away the lime deposit, unless the flow of water is so slow that complete evaporation occurs at the exposed face, causing re-deposition of the dissolved salts.

Saturation of the crack and the adjacent concrete with water during the healing process is essential for developing any substantial strength. Submergence of the cracked section is desirable. Alternatively, water may be ponded on the concrete surface so that the crack is saturated. The saturation must be continuous for the entire period of healing. A single cycle of drying and reimmersion will produce a drastic reduction in the amount of healing strength. Healing should be commenced as soon as possible after the crack appears.

2.2. Concrete Jacketing

Concrete jacketing is an example of local strengthening of reinforced concrete walls. The jacket consists of added concrete, longitudinal and transverse reinforcement, around the existing member. While this type of strengthening improves the axial, shear strength and flexural strength of the wall, both stiffness and frequency of the member will be increased. To improve the bond between the old and new concrete, chipping the concrete cover of the original member and roughening its surface would be recommended (Teran et Ruiz, 1992).

In some cases, earthquake loads on reinforced concrete members result in buckled, excessively yielded, or fractured reinforcement. Most researchers investigating repair of this type of damage have recommended repairing the reinforcement by replacement with new steel (Warner, 1977). The damaged concrete has then typically been replaced with new concrete.

In case of shear walls having length greater than 5 m, and in order to avoid separation between old and new concretes, as a result of shrinkage effect, the use of expansive cement concretes is recommended to avoid shrinkage problems. Another alternative would be to apply steel dowels connecting the old to the newly added concrete to ensure the monolithic action of the strengthened section.

Some experimental research using column jacketing has been undertaken at the University of Texas on short columns at two-thirds scale. These columns had shear span to column depths ratio ranging from 1.5 for the unstrengthened specimens to about 1.0 for the strengthened specimens. The results showed that the repaired and strengthened specimens had improved shear and flexural strengths compared with the original specimen. However, the ductility capacities found in these tests were very poor (Jirsa and Stoppenhagen, 87).

Column encasement with rectangular or circular steel sections, steel straps, new closely spaced reinforcing steel ties, or welded wire fabric, together with filling the voids with concrete grout or shotcrete, have all proved successful. Figure 2.9 shows all these methods for increasing shear capacity and/or ductility. In cases were damage is more severe, the longitudinal steel must be replaced, because of buckling or large shear shear distortions of the coloumns and bars (Valluvan et al, 1992).

It is well established that severe seismic loading of columns with small shear span/depth (a/d) ratios and widely spaced transverse reinforcement generally results in shear-dominated failure, leading to structural collapse by the formation of a single storey side sway mechanism. While this can be prevented by increasing column shear capacity, it must be done economically, and without large increases in flexural capacity, which would increase applied shears.Four methods are now available for increasing the shear capacity of a vulnerable column: (1) encase with rectangular or circular steel sections; (2) encase with steel straps; (3) confine it by using welded wire fabric; and (4) confine it by adding spliced ties. A jacket of shotcrete or cement grout is then applied to protect the added steel and make it act integrally with the original column (Jirsa, 1986).

Confinement by encasing the column can increase the shear resistance of the column, but may adversely affect seismic resistance: decreased (a/d) ratio and increased moment capacity make shear-dominated column failure more likely; increased column stiffness decreases the building's fundamental period and increases seismic-induced lateral forces. However, confinement and encasement of the original column is still beneficial; (1) due to increased ductility, column shear performance is adequate even at lower (a/d) ratios; (2) judicious selection and placement of jacket longitudinal steel minimises increases in column flexural capacity; and (3) increased column shear capacity offsets increases in seismic-induced lateral forces.

Strengthening of the existing damaged force-resisting elements has also received some attention. Most of the work in this area has focused on increasing the size and/or improving the ductility of existing members. Some work has been done on repairing shear walls (UNIDO, 1983), but most experimental work has focused on repairing and upgrading the strength and/or ductility of columns. Development of methods for repairing damaged columns in ductile moment-resisting concrete frames is an important task that attracted much research work.

2.3. Addition of Steel Plates and/or Steel Profiles

In some critical cases due to space limitations, occupancy limitations or time factor, the application of a concrete repair scheme might be impossible. A steel strengthening scheme would be the appropriate solution in such a case.

Concrete columns have been reinforced with steel angles at the four corners and tied horizontally by means of steel plates. Such a reinforcing scheme proved to be highly efficient in enhancing the columns shear strength and ductility. The same strengthening scheme might also be applicable by means of vertical steel plates well anchored to the concrete column by means of epoxy resin and mechanical anchors.

According to the experimental work carried out by Tankut and Ersoy (1992), well designed and carefully applied epoxy glued steel plates provided a very successful crack control, leading to a high number of narrow cracks. It was also concluded that the plate thickness did seem to be the desirable way to increase the capacity (Tankut, 1991). Excessive plate thickness led to very undesirable brittle failure of the stress transfer zone (epoxy layer and the concrete layer).

A seismic shear strengthening method for an existing reinforced concrete short column can be achieved by means of steel plates encasing the concrete column. Epoxy injection was applied between the concrete and the steel plates. Columns were tested under axial load and horizontal cyclic loading. Brittle shear failure was avoided and a ductile mode of failure was recorded while, the ultimate flexural capacity was achieved (Yoshimura, 1991).

2.4. External Prestressing

External prestressing is a new technique for strengthening low-rise reinforced concrete structures in Mexico. This strengthening technique consists of the addition of prestressing cables that are post-tensioned to form a bracing system. One end of the diagonal of this bracing is anchored to the top end of the roof column of the structure. Analytical studies have been conducted to evaluate the seismic behaviour of this retrofitting technique. The results of these studies show that this technique produces significant increases in strength and stiffness of the existing structure. However, it must also be mentioned that these studies show that the level of prestress in the cables can significantly modify the stiffness of the structure. Hence, unexpected levels of prestress can produce changes in the dynamic response of the structure not considered in the original retrofitting design. In addition, the prestress in the cables can also produce increases in the axial load of some columns, which can lead to a significant reduction in the ductility capacity of the columns. Strict and periodic control of the level of stresses in the cables must be achieved by field measurements.

From recent research carried out at the university of Austin (Pincheira and Jirsa, 1992), it is concluded that the post-tensioned bracing system can be used for low rise buildings located on both firm and soft soils. However, for medium rise buildings the technique appears to be more appropriate for structures located on firm soils than on soft soils. Bracing schemes for three and ten storey buildings are given in Fig. 2.10.

2.5. Shotcrete Using Ultra Rapid Hardening Cement

Recently, measures to prevent the total failure due to the after shock effect for highly deteriorated concrete structures hit by a major earthquake have been attracting much attention, and a variety of repair and reinforcing methods have been proposed. Dry shotcrete of ultra rapid hardening cement, reinforced with steel fibres is one such method. This method combines the simplicity of shotcrete, the initial strength of ultra rapid

hardening cement, and the reinforcing effect of steel fibres, and has been applied in a wide variety of fields, especially for railway viaducts.

It is well known that workability, resistance to water, acids and chemicals, and the mechanical properties of shotcrete can be greatly improved by adding silica fume. The improvement is mainly attributed to the consistency effect and the micro-filler effect of the silica fume. Similar effects can be expected in shotcrete with ultra rapid hardening cement and steel fibres. It was found experimentally that the optimum substitution percentage was around 10%. The substitution improved the bond strength of joints as well as the bond strength of steel fibres at an early age.

Silica fume substitution also reduced the dust concentrations of shotcrete mortar, provided that the surface moisture content of the fine aggregate was greater than 4%.

2.6. Micro-Reinforced Cementitious Composites

Portland cement based fibrous composites have many construction related applications. Broadly, one can classify these composites as macro-reinforced and micro-reinforced. In the macro-reinforced fibrous cementitious composites, large fibres, usually of steel or polypropylene, greater than 10 mm in length with diameter between 0.1 and 1.0 mm are used. For the volume fractions of fibres that may be efficiently and conveniently incorporated in this category (up to about 2%), the improvements in the tensile strength of the host weak matrix are not significant. The improvements in the toughness and impact strength on the other hand, with steel fibres in particular, are remarkable.

In the micro-reinforced systems, very fine fibres with diameters as small as those of the cement particles (less than 25 Mm) and length less than 10 mm are used. With suitable dispersing and plasticizing agents one can achieve composites with high fibres volume fractions. It has been shown that these composites have significantly improved tensile strength over that of the host matrix, and the toughness improvements are also notable. Some other improvements reported for carbon cement composites, in particular, are: better shrinkage characteristics, improved dimensional stability, better durability, improved impact resistance, and enhanced deformability under bi-axial bending.

For durable repair, the desired characteristics of the repair material include low permeability, high tensile strength, adequate impact resistance, sufficient deformability (ductility), high fracture toughness, low shrinkage, good dimensional stability, and most of all, a strong tensile and shear bond with the base concrete. From experimental

investigations carried out by Banthia it is shown that the micro-reinforced cementitious composites have the material performance characteristics desired for an effective repair.

2.7. Cathodic Protection of Rebars

Cathodic protection is an electrical system designed to stop corrosion by applying electrical current to the affected metal surfaces. Cathodic protection has been used for over 60 years as an effective corrosion protection system in technologies other than building construction. Some deteriorated bridge decks have been restored and protected using this technique. Bridge substructures are also being protected on an experimental basis.

Impressed current cathodic protection uses an external direct current power source to provide the protection current. A rectifier is typically used to feed one or a series of connected anodes. Anodes for impressed current systems may be one of the following: special metal alloys; field-mixed, rigid conductive polymer composites; or manufactured flexible polymer composites.

All anodes corrode or decay with the passage of time. The rate of decay is influenced by anode material chemistry, environmental factors and current flow density. Most manufactures believe that the anode service life exceeds the life of other system components. Cathodic protection systems typically operate at very low pressure levels. Protection of embedded metals is usually achieved at an operating potential of the approximately 1 V (direct current).

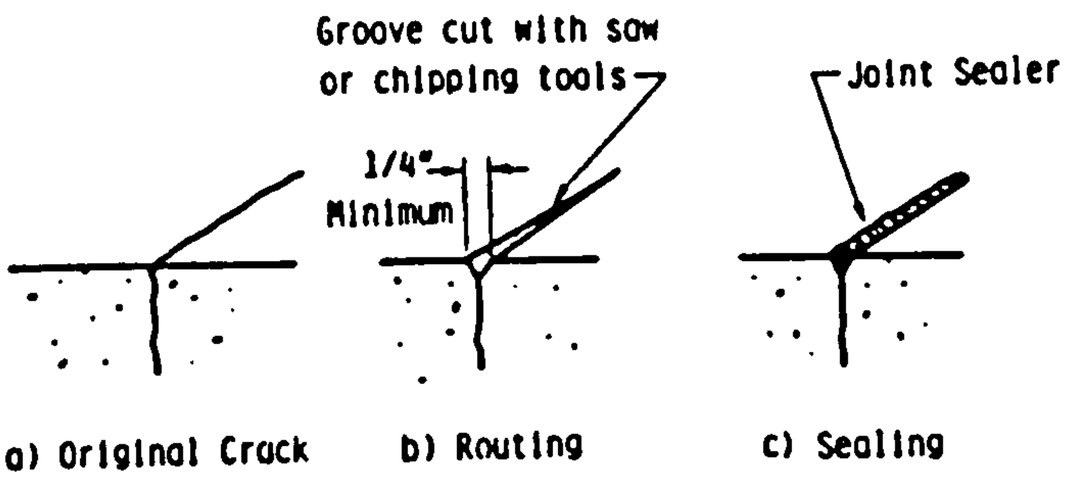
System operation is usually controlled in one of three ways: (1) by applying a constant current, (2) by applying a constant potential, (3) by reference cells or sensors installed in the protected slab. Each control method has certain advantages and disadvantages. The cathodic protection designer determines which control system is best suited to the particular project.

Some cathodic protection systems require a structural system that can support the extra dead load of a conductive layer and asphalt overlay. Frequently, 50 mm of an asphaltic concrete wearing course is used, resulting in an additional 98 kg/m^2 of dead load to the structure. Other cathodic protection uses closely spaced slots cut in the concrete and do not increase the dead load. Another method is to lay conductive strips on the prepared original concrete surface in conjunction with a cementitious overlay. Cathodic protection has been applied to conventionally reinforced concrete floor slabs but not to a post-tensioned or precast floor slab systems. It is possible that prestressing steel might be

embrittled due to the evolution of hydrogen at the steel. The reinforcement network must be electrically continuous for effective system performance. Isolated reinforcement that is not electrically connected to the primary reinforcement network can undergo stray current corrosion.

Cathodic protection systems can be installed on deteriorating concrete floor slabs after appropriate structural repairs have been performed. Cathodic protection is the only current system that can theoretically fully suppress corrosion once it has started. Special steps are needed to insure that possible short-circuit paths between the anodes and reinforcement network are eliminated prior to energising the system.

Although cathodic protection appears to have a place in protecting some parking structures against corrosion, it has not yet achieved widespread use. This system became very common in highly aggressive zones like Abu Dhabi, where the sand and aggregate used in concrete contain high levels of chlorides, so that corrosion starts the day the concrete is placed. There have been reports of concrete damage from corrosion before the construction of a building is completed. Two methods are being used in Abu Dhabi. The first has the conductive coating applied directly to concrete before it receives a coat of plaster. The second is to apply a coat of plaster, then the conductive coating, and finally a decorative cosmetic paint. Bond and performance tests have shown both methods to be acceptable. The systems are powered by controllers that provide low voltage D.C. current to the anode system. The power requirements are minimal and low voltage outputs are safe for the residential units. It was decided that the proper cathodic protection system could extend the life of buildings by at least 25 years, which can be quite an economic solution in case of buildings that have a practical life of ten years only. Nevertheless, before selecting this method to protect a structure, its effect on the specific materials used in a project deserve consideration (Schutt, 1992).



a) Original Crack b) Routing c) Sealing

Fig. 2.1 Repair of Crack by Routing & Sealing

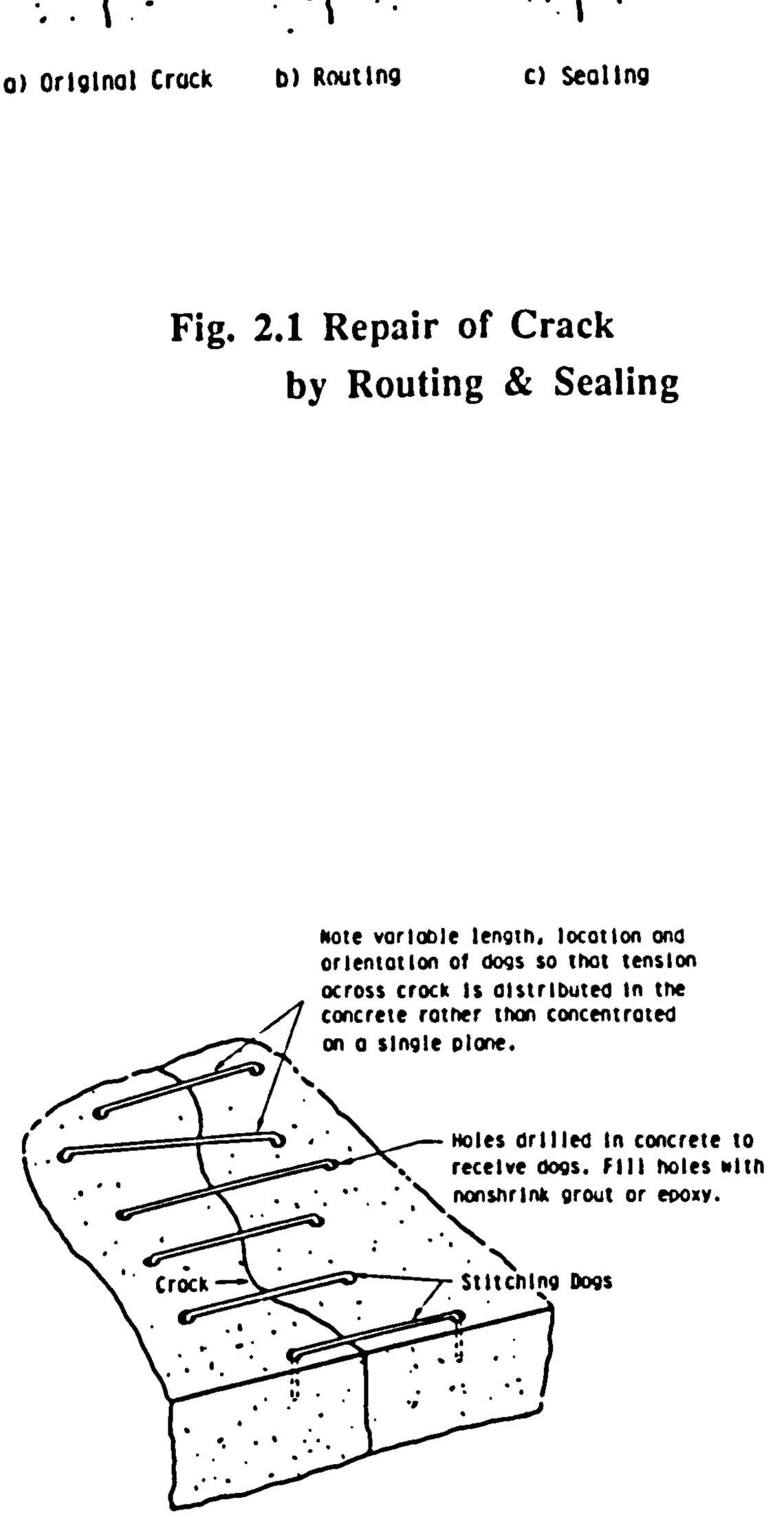
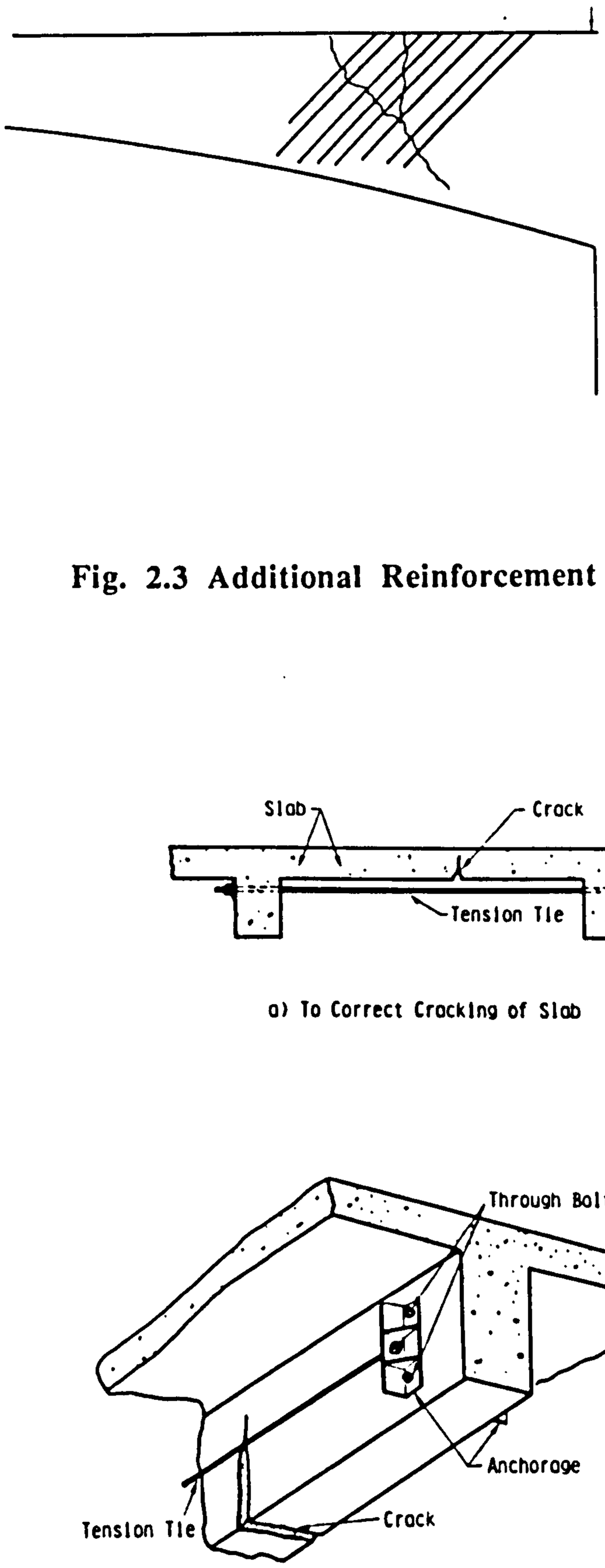


Fig. 2.2 Repair of Crack by Stitching



a) To Correct Cracking of Slab

b) To Correct Cracking of Beam

Fig.2.3 Additional Reinforcement

Fig.2.4 External Prestressing

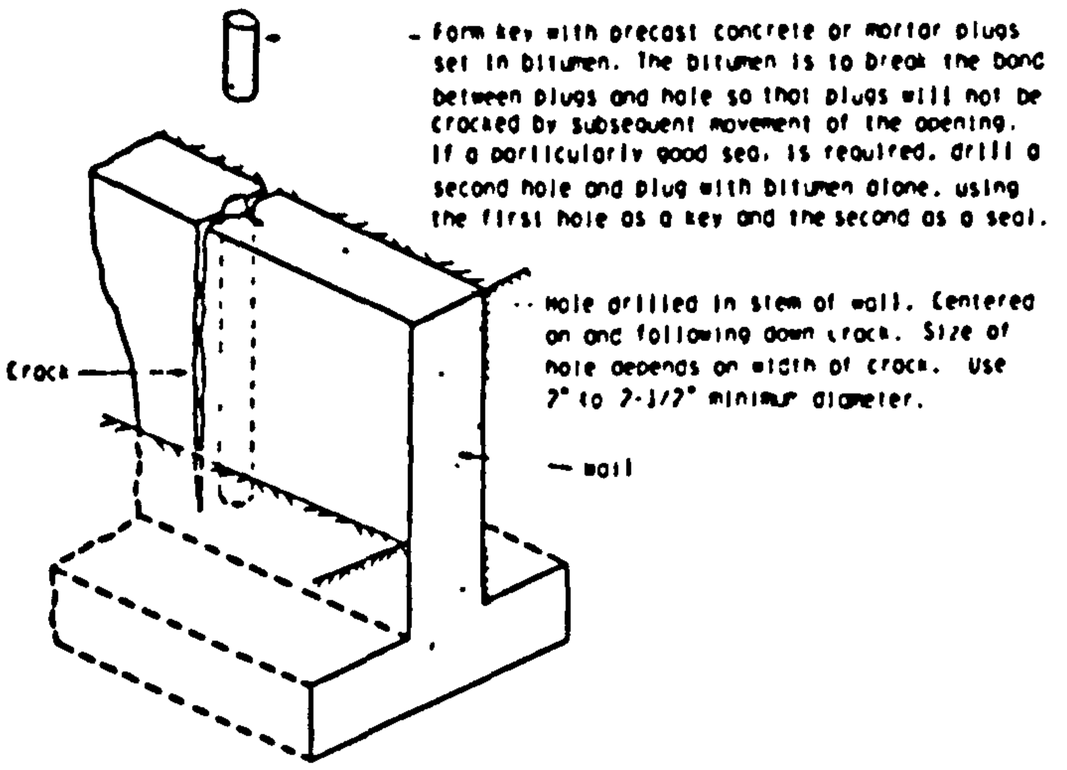


Fig. 2.5 Plugging of Cracks

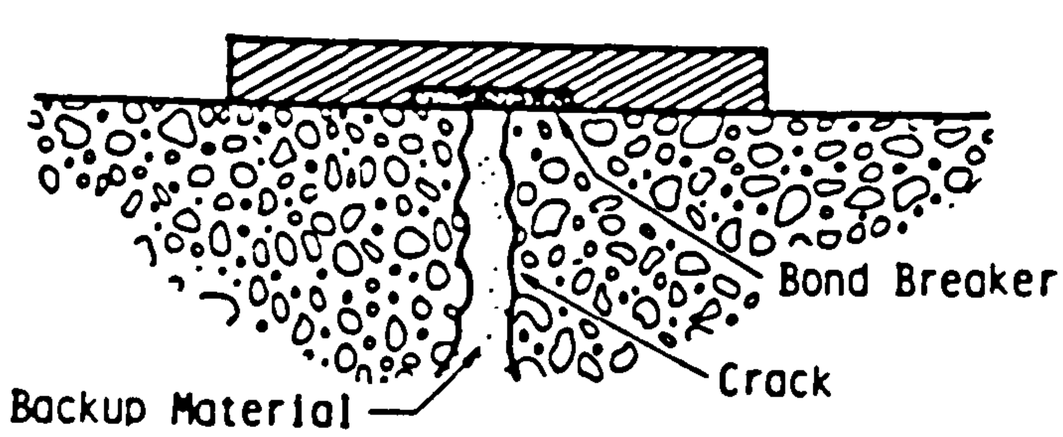


Fig. 2.7 Repair of Crack Using Flexible Surface Seal



Fig. 2.6 Bond Breaker

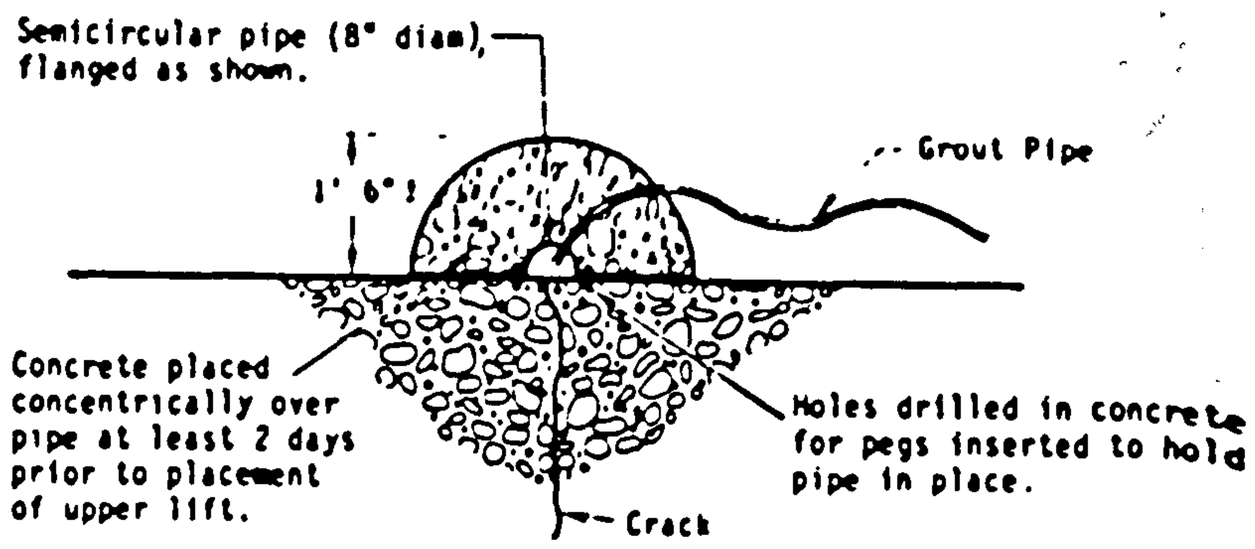
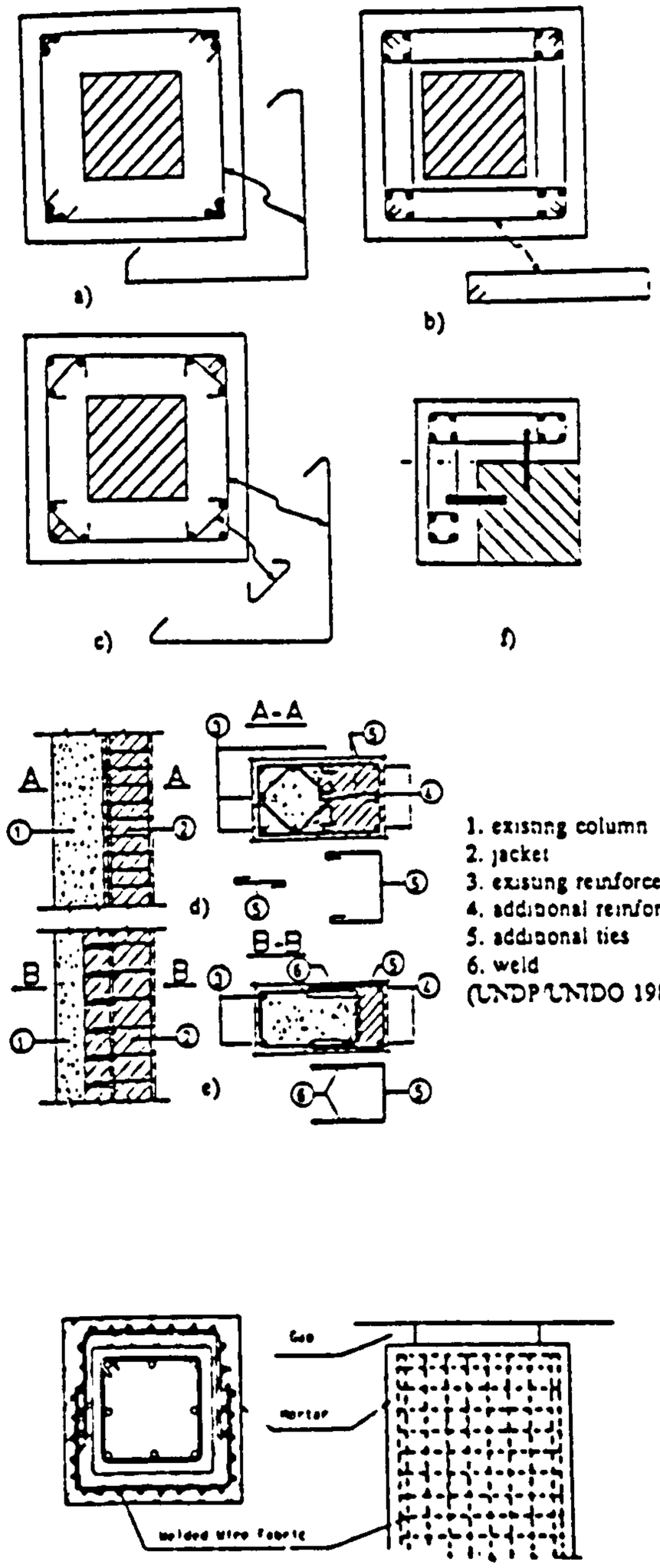
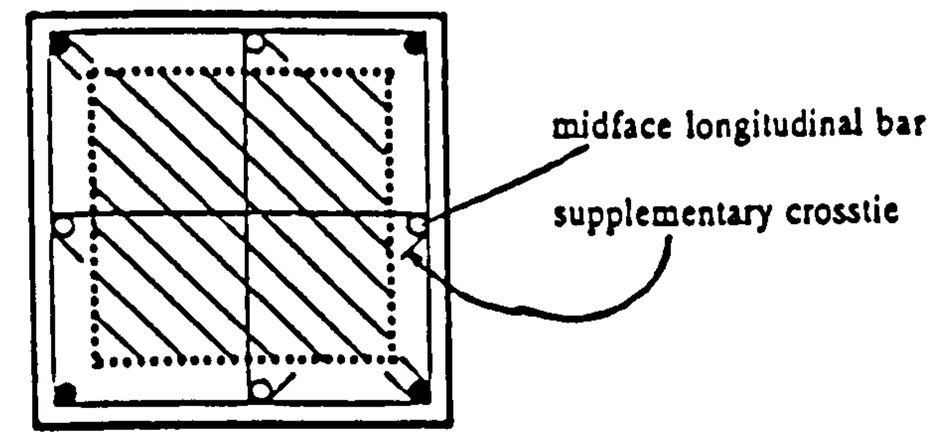
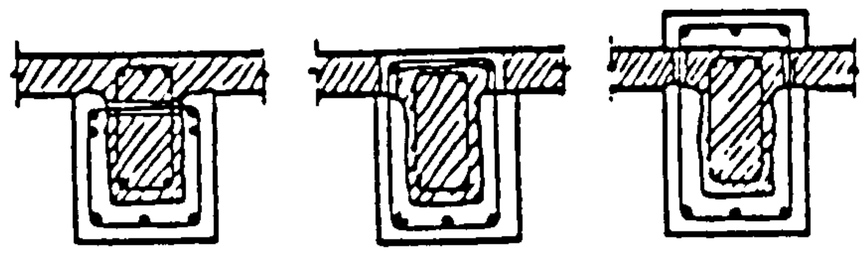
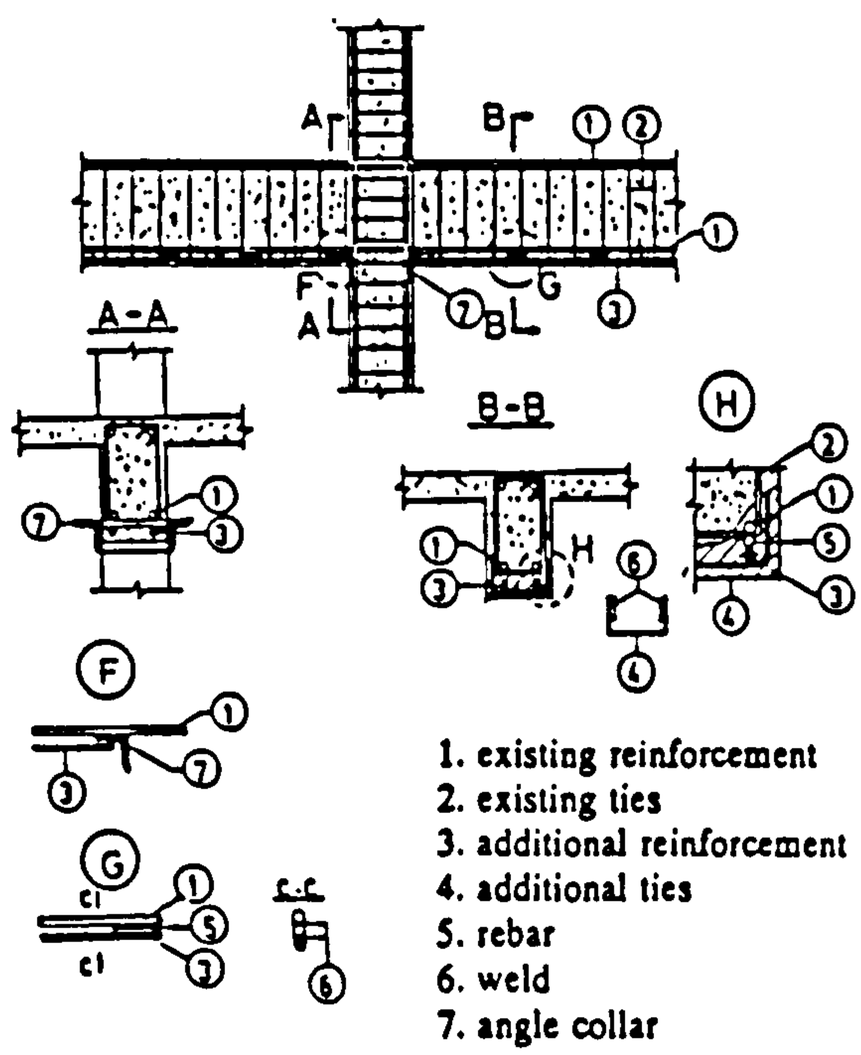


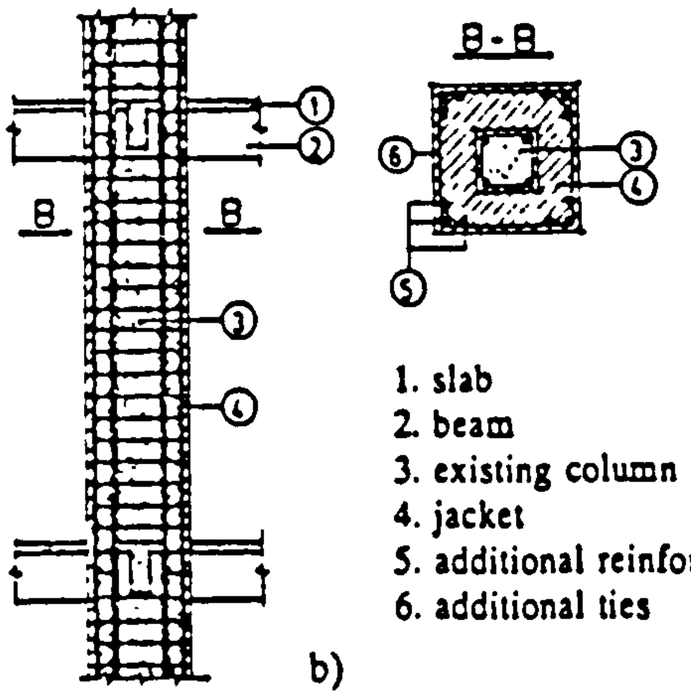
Fig. 2.8 Crack Arrest Method











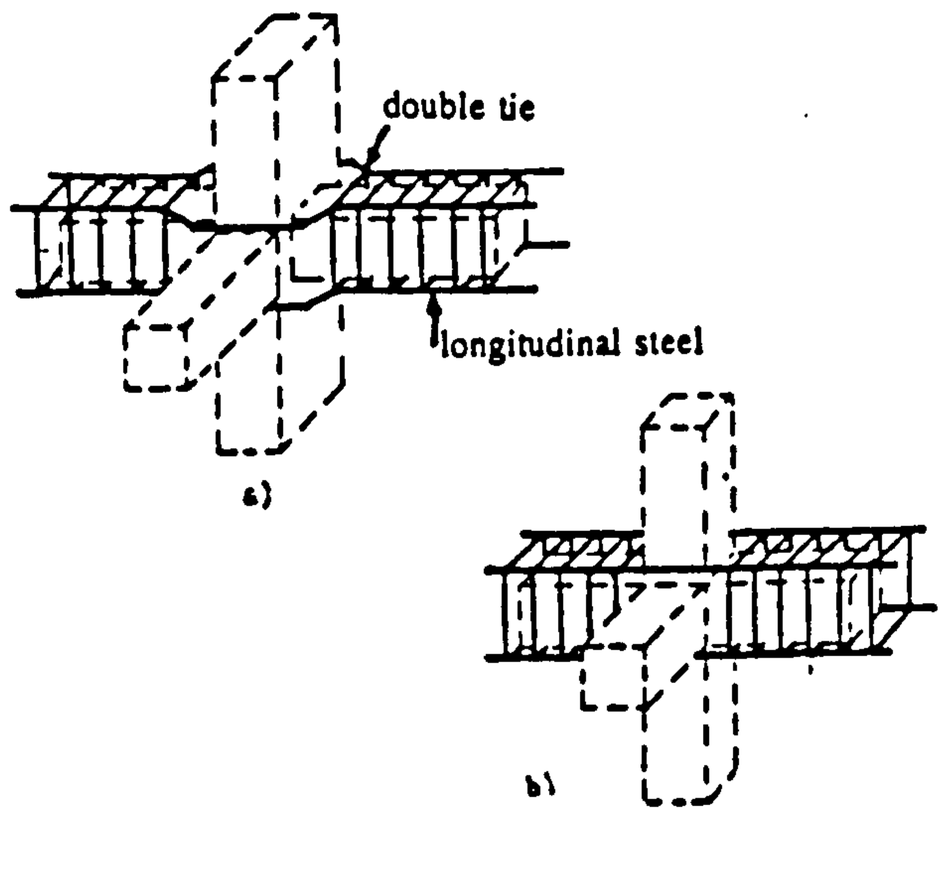


Fig. 2.9 Typical Jacketing Systems

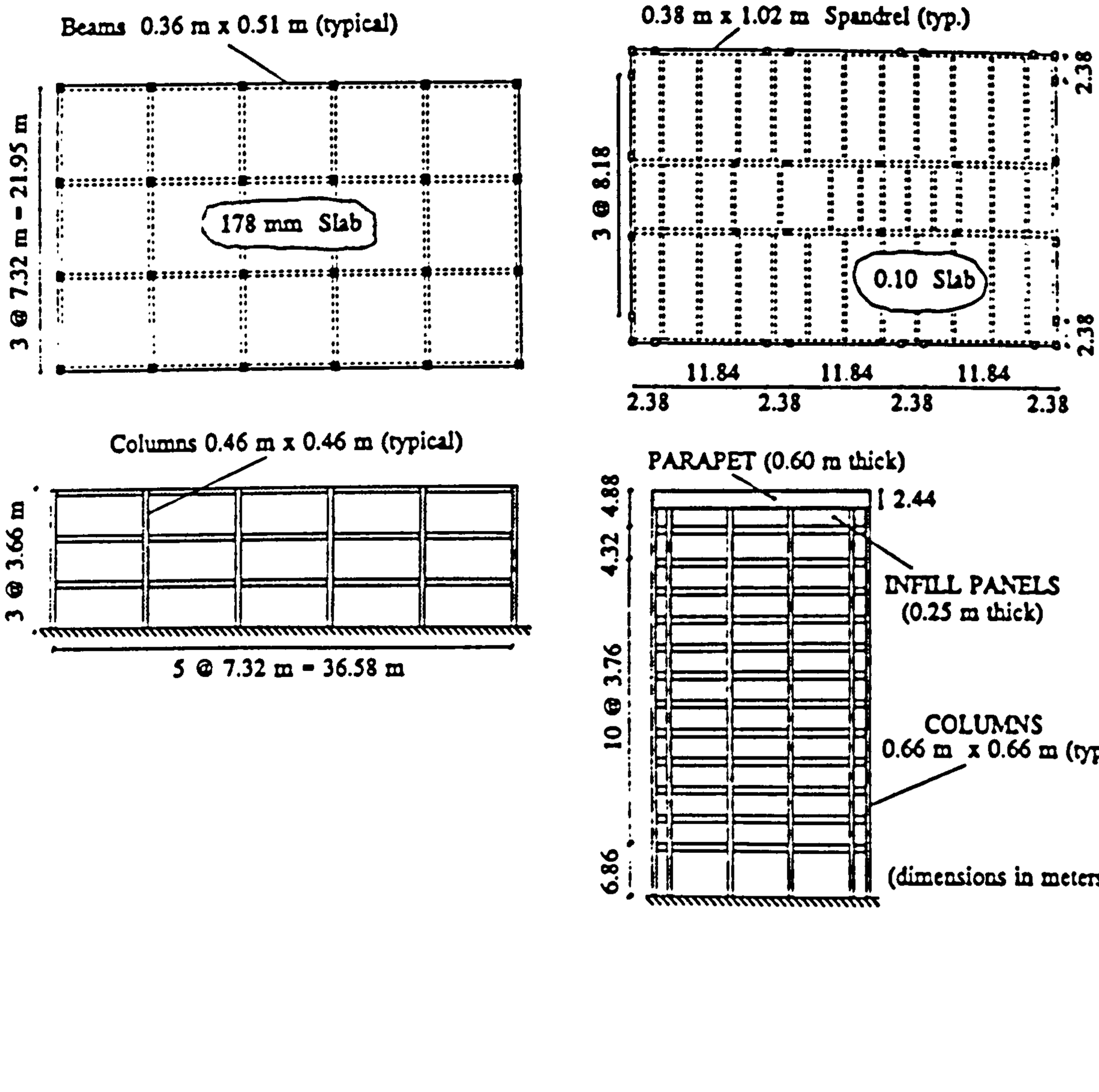


Fig. 2.10 Bracing Schemes for Three and Twelve Storey Buildings

CHAPTER 3

3. REVIEW OF RELATED RESEARCH

3.1. Introduction

Most buildings in many major cities where significant hazard exists, were constructed prior to any specific requirement for earthquake design. Many buildings are therefore prone to damage by earthquake.

Recognition of the need for reinforcement and strengthening of existing buildings to resist seismic forces has continued to increase in recent years. To preserve life and also to safeguard regional economics at risk, it is necessary to provide strengthening to those existing buildings that do not conform to acceptable safety standards under earthquake forces. While compliance with current building codes is not always required, adequate structural safety to meet anticipated forces is needed, based on the probability of earthquakes occurring in the region and affecting the building site. The probability of earthquake occurrence, magnitude, site response intensity, and existing building construction will influence the safety levels which must be met.

In view of the wide variety of terms used, a brief definition is given hereafter:

- Repair: Is the reinstatement of strength and/or stiffness to the structural status before the damaging event.

- Strengthening: Is the increase and/or enhancement of strength or stiffness leading to a higher serviceability and/or ultimate limit state.

- Retrofitting: Is an upgrade of some structural characteristics to conform to new code, regulation or performance criteria.

In the following, a review of literature on aspects of repair and strengthening strictly relevant to the current research is given.

3.2. Review of Repair Methods

Documentation on repair of structures damaged by earthquakes has largely consisted of observation of the repair methods used after an earthquake. Because the repair scheme depends on the cause and extent of damage from a particular earthquake, the method chosen is often dependent on the situation. Unfortunately, a relatively limited amount of experimental research results in respect of repair is available.

Jirsa (1986) tested three short columns in order to evaluate various repair and strengthening techniques. The columns, under constant axial compression, were subjected to reversed cyclic deformations. Two columns were strengthened before testing by adding a 60 mm shotcrete shell whilst the remaining column was repaired after testing. Both strengthened and repaired columns exhibited greater ductility than the original column. Both strengthened columns exhibited similar load-deflection behaviour with stable hysteretic loops for deformations up to 1.5% drift, after which loss of stiffness became apparent. Failure was flexurally dominated. Jacketing, both with or without crossties, resulted in much greater stiffness and strength than that observed for the original, unstrengthened specimen. Inclined cracks developed in both strengthened specimens at drifts in excess of 1%. Supplementary crossties did not significantly increase specimen strength or stiffness in the first cycle to a given drift level, but were beneficial in delaying strength and stiffness deterioration under repeated cycles to drift levels exceeding 2%. The repaired specimen exhibited stable hysteretic behaviour for deformations up to 1.5%, after which it began to lose stiffness under cycling. Failure appeared to be a combination of shear and flexure. This was confirmed by pinching of the hysteresis loops. The repaired specimen had much greater lateral stiffness and strength than the original specimen and slightly less than the strengthened specimens at the first cycle to a given drift level. Inclined cracks were longer, wider, and more numerous in the repaired specimen than in either of the strengthened specimens. The repaired specimen degraded much faster than either of the strengthened specimens under repeated cycles to drift levels exceeding 2%. Some column strengthening schemes are shown in Figs 3.1 and 3.2.

Yoshimura et al (1992) tested short columns under the combined effect of axial load and horizontal cyclic loading. He proposed the use of welded steel tube covering the damaged area only, to reinstate the strength loss. He also showed that the brittle shear failure mode was converted to a flexural ductile one. This method can also be applied for upgrading schemes so as to enhance the seismic response of existing short columns with regard to future seismic events. Fig. 3.4. shows details of the tested

models. The ductile hysteretic response was demonstrated in Fig. 3.3. whereby the brittle shear failure was converted into ductile tension failure.

Strengthening of existing reinforced concrete moment resisting frames often involves the addition of infill walls. The benefit of such strengthening is often limited by failure of splices in existing columns which act as boundary member for the new walls. Valluvan et al (1992) examined different approaches for strengthening column splices. Twelve two-third scale column specimens were constructed with column splice details typical of ordinary moment-resisting frames and were strengthened using a variety of techniques. It was concluded that columns constructed with splices designed for little or no flexure and only axial compression, and comprising part of a frame-wall system, cannot develop tensile yield when subjected to reversed cyclic loads. As a result, the benefit of strengthening RC frames with infill walls is limited by the failure of column splices. Providing continuity in the splice region by welding the bars enabled the columns to yield in tension under reversed cyclic loads. However, it was necessary to add ties to restrain the outward thrust produced by the eccentricity between splices. External reinforcement around the splice region significantly improved confinement and splice strength. The external reinforcement must be grouted in order to permit efficient confinement of concrete. He concluded that continuity and confinement in the splice region significantly improved strength and ductility.

Yamamoto (1992) conducted a study to develop a strengthening method for existing RC columns using FRP (Fibre Reinforced Plastics). Two kinds of test were performed to clarify the effect of FRP strengthening on uniaxial concrete strength and shear-flexural behaviour of existing RC columns. The uniaxial strength of FRP-strengthened concrete increased in proportion to the FRP strengthening ratio. Design equations for the FRP-strengthened concrete columns were obtained. A stress-strain relationship model for FRP-strengthened concrete was also developed. The strength and ductility of these columns were considerably improved. Also, the uniaxial strength was increased three times as much as that of non-strengthened concrete models.

The effect of repair methods for cracked concrete members reinforced with smooth or deformed bars was studied by Tasai (1992). For specimens reinforced with smooth bars, the concrete cover was replaced by epoxy mortar or prepacked concrete mixed resin. This ensured a stiffness enhancement of the repaired members. For specimens reinforced with deformed bars, low viscous epoxy resin was injected into bond splitting cracks along main bars. Bond strength after injection was more than twice that of the original intact member.

Fuse et al (1992) have developed a shear strengthening method for existing RC columns. The addition of tube steel plate and a filler ensured a ductile flexural failure mode. This has replaced the unductile shear failure mode exhibited by the reference model. A practical example was considered whereby this seismic strengthening scheme was applied to an actual building in Japan.

3.3. Review of Seismic Upgrading Methods

One of the main methods for increasing strength is the addition of infill walls within existing frames. This can be accomplished by several techniques. Probably the most common is the replacement of an infill brick wall with an RC one. Kahn et al (1979) performed tests on a series of concrete infill walls. A monolithic wall and an open frame test of the same structure provided the extreme limit cases for the infill wall tests. A full panel precast concrete wall and multiple panel precast wall elements completed their test series, as illustrated in Fig. 3.5. The precast panels were connected only to the beams at top and bottom, without connection to the columns. In fact a space between the columns and the wall edges was maintained to prevent column-to-wall contact. The newly-cast concrete wall had the same maximum capacity as the monolithic wall after taking different concrete strengths into account. Specimen failure initiated by deterioration of the joint between the top of the cast-in-place wall and the bottom of the top beam. Crushing and slipping at this joint resulted in a shear failure of the top of the columns and complete loss of the structure's vertical load carrying capacity. The ductile capacities of these two walls were not high, but the deterioration of the cast-in-place wall was the most rapid.

Infill braces in existing frames are widely used for upgrading purposes in the US and Japan. However, the number of experimental tests incorporating steel or reinforced concrete braces in existing reinforced concrete frames is limited. Hayashi et al (1980) and Sugano and Fujimira (1980) provided some data. Jain (1985) provided an analytical study which concludes that the "X" brace configuration develops better response characteristics than similar "V" braced configuration. The latter researcher noted that the braces substantially increase the column axial forces, and recommends that a dual earthquake resistant structural system is utilised. Much work remains to be done in this field to develop appropriate design recommendations and suggested construction details. Sugano (1981) has provided a useful qualitative comparison of the strengths of various techniques, as shown in Fig. 3.6.

Lee and Goel (1990) have tested the seismic behaviour of steel built-up box-shaped bracing members and their use in reinforced concrete frames. He concluded that the strengthened frames showed excellent hysteretic behaviour under a large number of cyclic deformations up to 3% of storey drift. He also concluded that the hysteresis loops of the strengthened frames were full and stable, with dramatic increase in the energy dissipation capacity. Fustok et al (1991) have tested the steel braces to resist seismic forces in precast concrete structures. He concluded that the added bracing made the drifts more uniform and reduced the ductility demands on columns.

Another important method of increasing strength is the size increase of existing columns. This is one of the most common and efficient methods to increase vertical carrying capacity of the structure. It can be used to increase the shear capacity of the member more than the flexural capacity, thus it can significantly increase the ductility capacity of the column. Sugano (1981) provides some data on various types of column strengthening methods, as shown in Fig. 3.2. The original columns were not ductile and the initial restoring force was lost after a few loading cycles. The maximum strength of the strengthened columns was 25 to 50% larger than the original column and they maintained more than 80% of their maximum strength at a lateral displacement of 0.06 times their length. The original long column had 32% of its strength at this stage of the test and the original short column collapsed. It was noted that this strengthening was more effective for short (high shear) columns. As stated earlier care must be exercised to limit the increase in flexural capacity as the shear capacity is increased.

It is well established that the beam-column connections form a major parameter in the seismic resistance of structures. Strengthening of beam-column connections was studied by Alcocer (1992). Four slab-beam-column joints were constructed and rehabilitated. The specimens were tested under bi-directional cyclic loading. The various parameters tested were: the jacketed elements, level of damage for the original models prior to retrofitting, and the distribution of the reinforcement for the jacket. Test results indicated that stiffness and energy dissipation characteristics were improved for the rehabilitated models.

Bridge failures in the 1971 San Fernando earthquake, the 1987 Whittier earthquake, and the 1989 Loma Prieta earthquake have drawn much attention to the consequences of substandard detailing in bridges constructed before 1970. Some of the problem areas associated with concrete bridge columns are:

i. Inadequate and undependable flexural strength as a result of low seismic design coefficients and the common practice of lapping flexural reinforcement within the potential plastic hinge region.

ii. Inadequate flexural ductility, as a result of insufficient and poorly detailed transverse reinforcement.

iii. Inadequate shear strength, again as result of insufficient and poorly detailed transverse reinforcement, and the use of elastic design methods, which provided lower shear strength than flexural strength in many designs.

Priestly et al (1992) studied various retrofitting schemes to rectify these deficiencies in many of the older bridges in California. Cylindrical steel jacketing of the potential plastic hinge region has been shown to enhance the flexural strength and ductility of flexurally dominated circular columns. A dependable drift ratio exceeding 5% was available. For circular columns with small aspect ratio, brittle shear failure was avoided by encasing the full height of the column with a cylindrical steel jacket. Stable and ductile plastic hinging could be developed, providing a drift ratio in excess of 4%. Elliptical shaped steel jackets were also shown to be effective in enhancing the flexural and shear performance of rectangular columns.

Many older elevated freeways in California were designed considering lateral seismic loads, but the effects of longitudinal bridge response were in some respects ignored. Consideration of longitudinal response has significant impact on outrigger beams, which are used when columns cannot be located directly beneath the superstructure. These outrigger beams were designed for shears and flexure resulting from gravity and lateral loads. However, longitudinal bridge excitation introduces biaxial flexure and shear as well as torsion into these members. In addition to problems carrying torsion, the outrigger-column joint connection is often poorly detailed. Thewalt and Stojadinovic (1992) have carried out an experimental study whereby, three half scale specimens were used to investigate the as-built seismic behaviour of the outrigger beam and joint as well as the behaviour of two retrofitting schemes. The as-built test clearly demonstrated that the outrigger system was deficient in two key areas. First, the essentially unreinforced joint was incapable of developing the strengths of the connected column and beam, especially under cyclic loading. The second problem was that with a repaired joint the out-rigger becomes the weak link susceptible to brittle shear failure. The nature of the joint failure, including crushing of the front of the lower beam steel hooks and peeling off of the straight column bars, influenced the joint retrofit design. The upgrade scheme behaved well, allowing a ten percent lateral drift in the joint closing direction with no noticeable loss in flexural capacity. The torsional retrofitting in

the outrigger worked efficiently. A design level of approximately twice the cracking torsional capacity was also well chosen, in that it limited the maximum longitudinal load that could be taken by the specimen. The longitudinal load must be controlled to avoid flexural failure in the weak direction of the outrigger beam at the point of attachment to the deck. The joint retrofit, consisting primarily of steel and concrete external to the original joint, performed well, transferring the full loads needed to fail the cap and column. The steel retrofitting limited damage to the cap beam and joint area, but drift capacity of the system was dramatically reduced because all damage was now forced to the base of the column, for both lateral and longitudinal loads. Simply detailing the plastic hinge region in the column to retain capacity through larger rotation would have forced the failure to the cap/deck interface through flexure in the weak beam direction, since there was already evidence of bar yielding at this location under the reduced load levels.

In some cases, it is neither possible nor convenient to modify the interior of the existing building for increased earthquake resistance. Supplemental structural framing with increased lateral stiffness can be used to resist the earthquake forces generated in the original building. In implementing these systems it is vital that the connections between the new and the old systems be able to transmit the forces which will be developed. Geometric compatibility and equilibrium of forces become the greatest concerns in designing the supplemental system. A number of examples of successful implementation of exterior strengthening can be noted. Forell (1982) has implemented systems utilising moment frame supplemental structures and braced frame supplemental structures as shown in Fig. 3.8. The selection of supplemental exterior moment frames included considerations for possible future expansion of the building. The new frames were ductile moment frames and their connection to the existing building required modification to the existing exterior longitudinal frames (Hanson, 1986).

The development of a retrofitting strategy to achieve desired displacement levels while maintaining loads requires careful consideration of the complete system. It was found that simply strengthening the weak link was not the best approach, the next weakest link should not be loaded in an undesirable fashion.

Various techniques for increasing the strength and ductility of reinforced concrete members and buildings have been briefly reviewed. Which of these techniques or which combinations are the best for a specific structure can only be determined by the design engineer. The purpose of providing this information is to stimulate the imagination of the structural engineer to consider a number of alternative procedures and to suggest that laboratory data be obtained to substantiate the design assumptions.

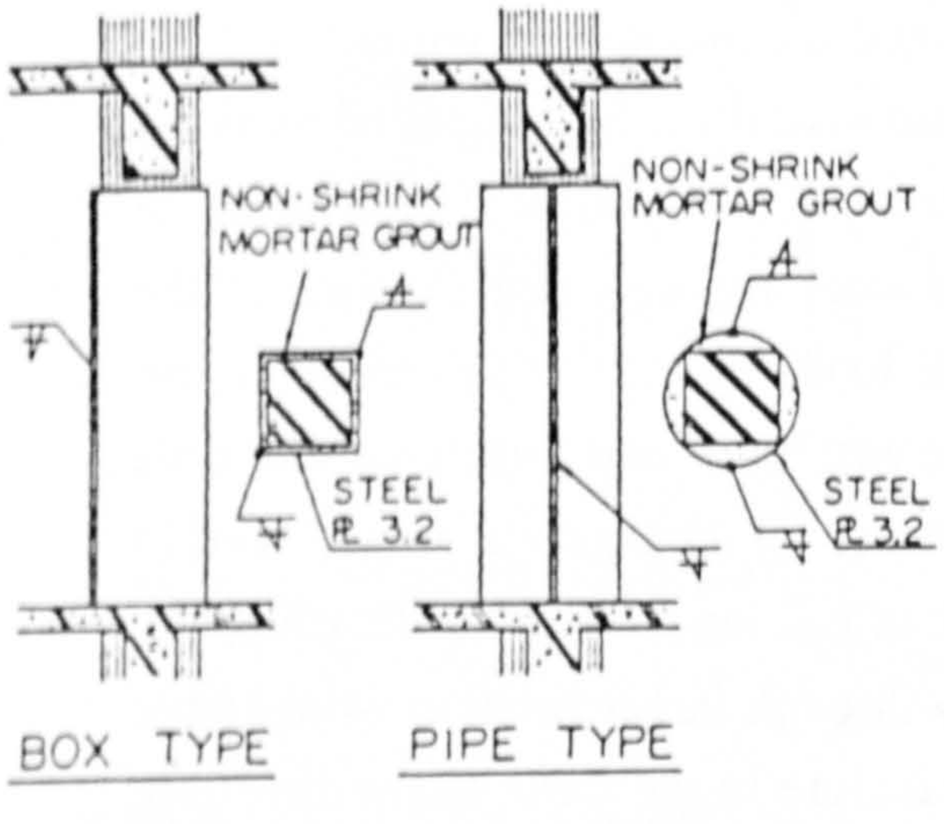


Fig. 3.1 Strengthening Techniques

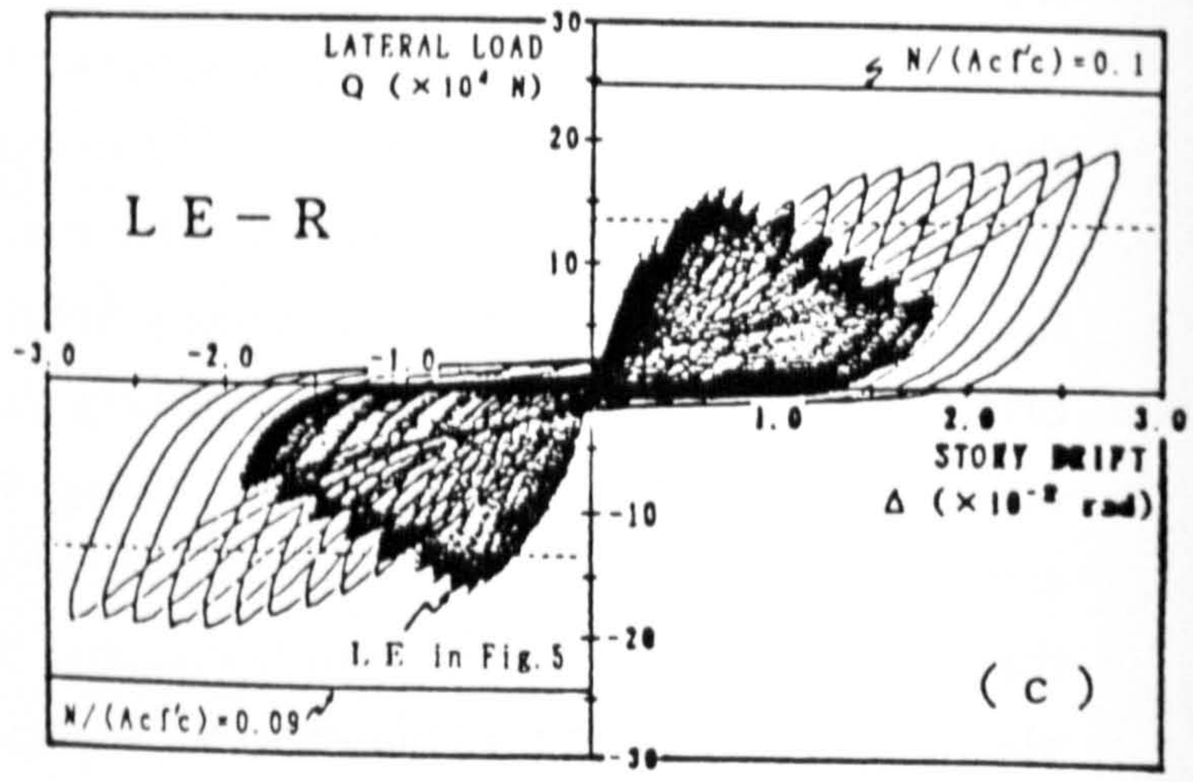


Fig. 3.3 Cyclic Response of Enhanced Columns

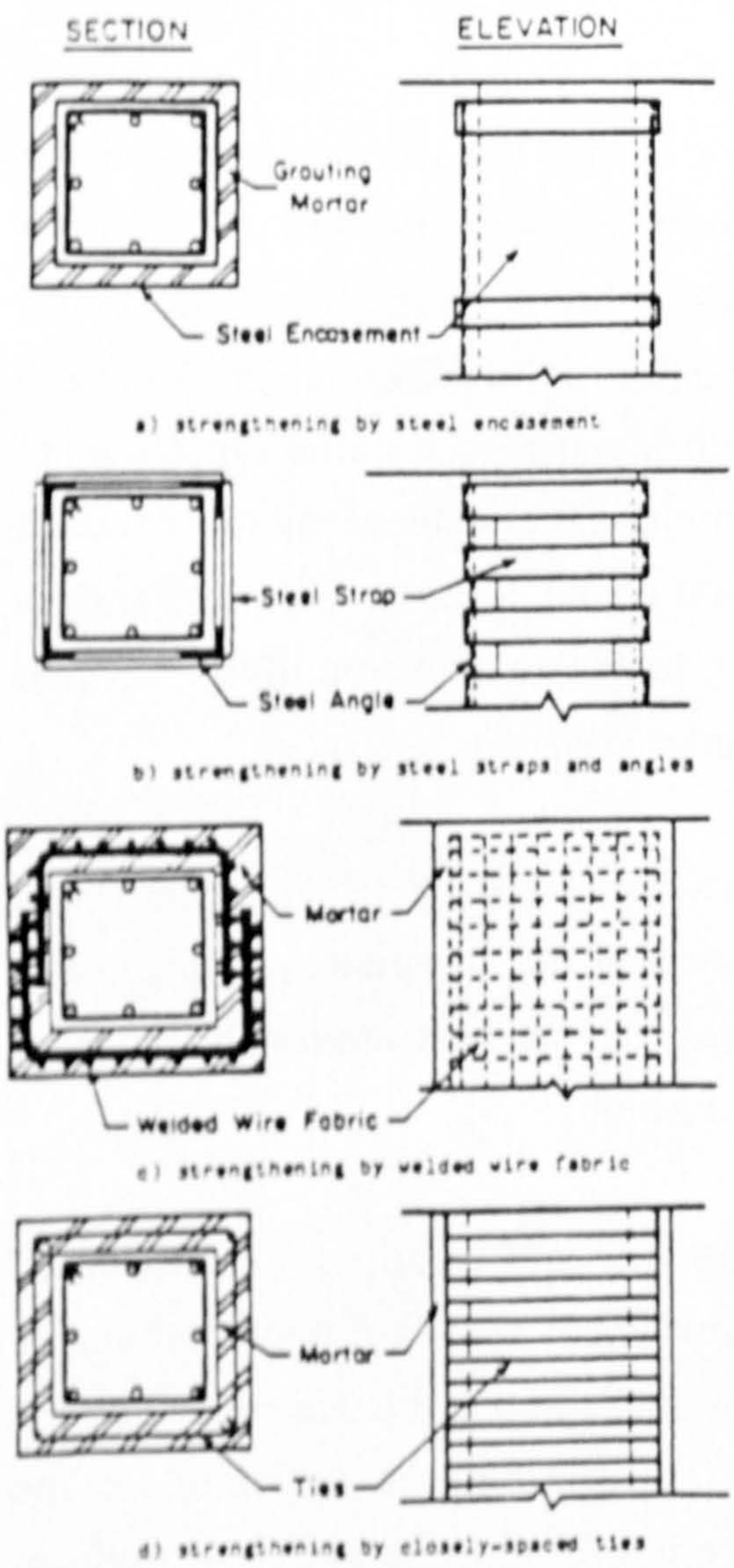


Fig. 3.2. Shear Enhancement for Columns

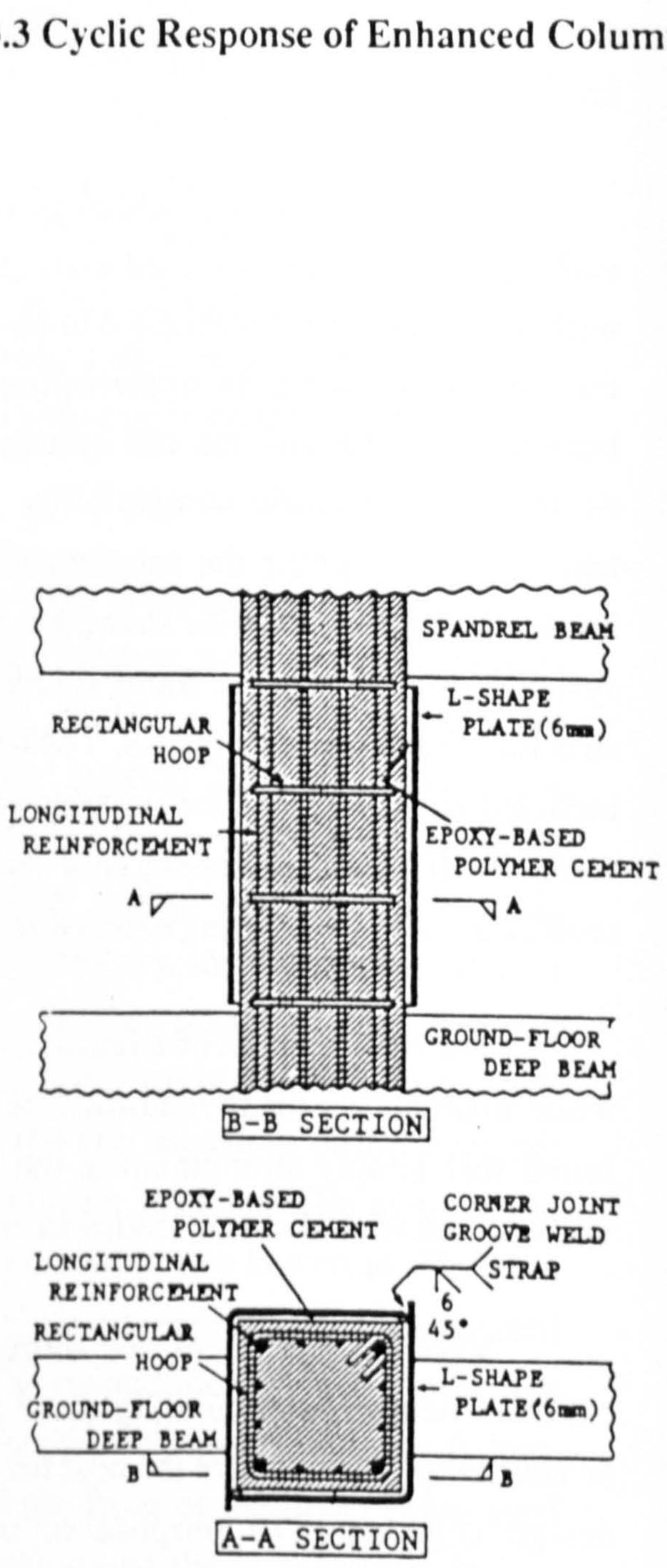


Fig 3.4. Strengthening for Short Columns

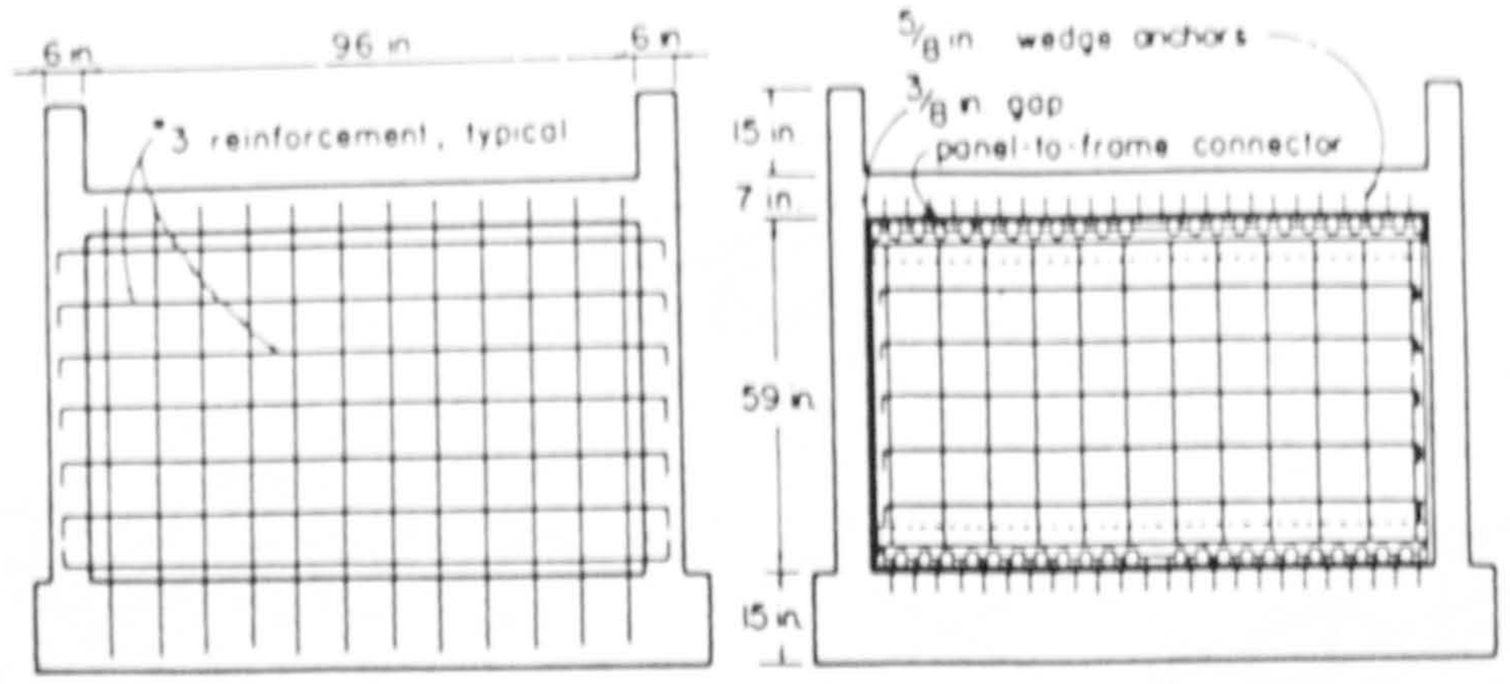


Fig. 3.5. Strengthening by Addition of Shear walls

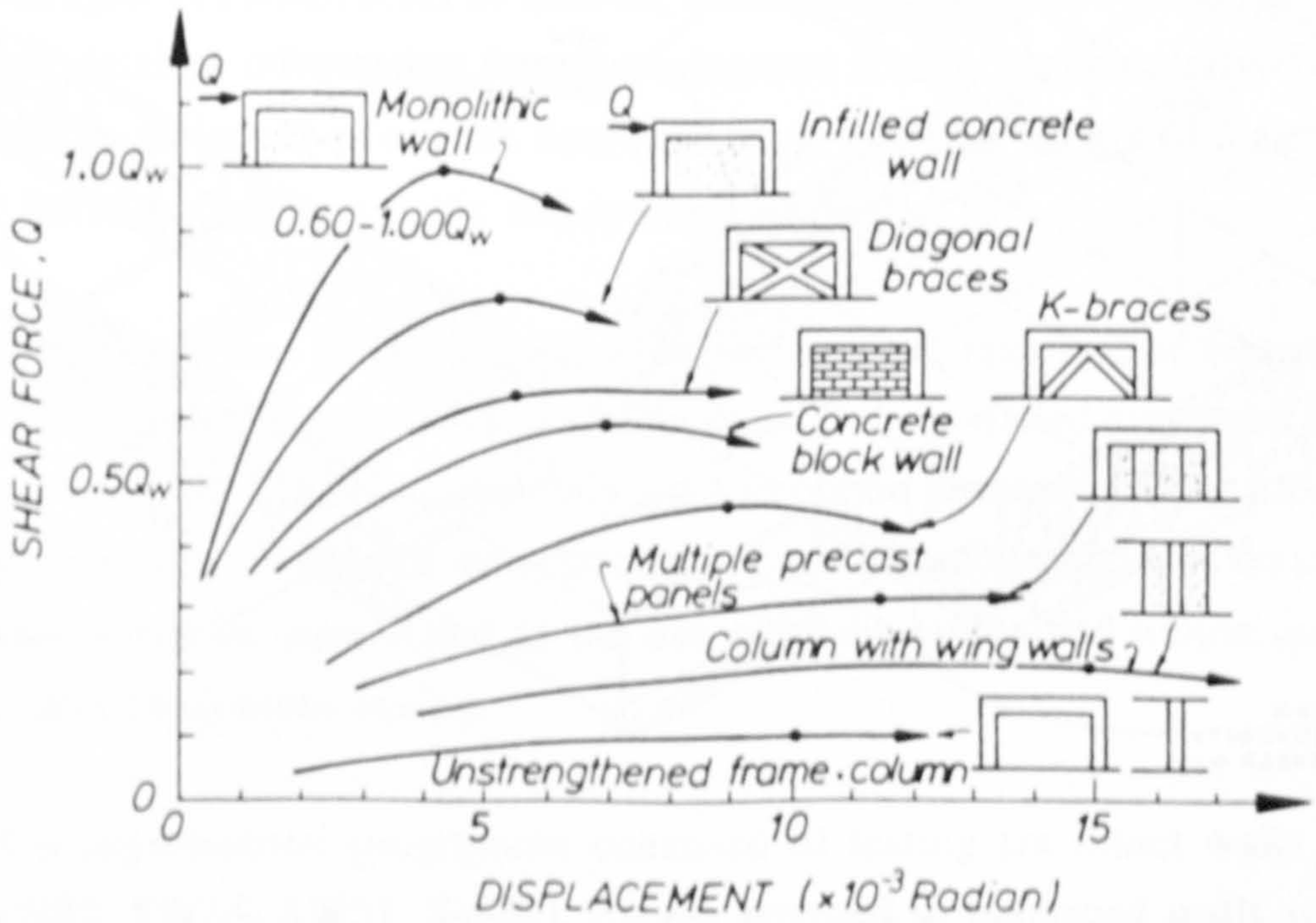


Fig. 3.6. Qualitative Comparison of Various Strengthening Techniques

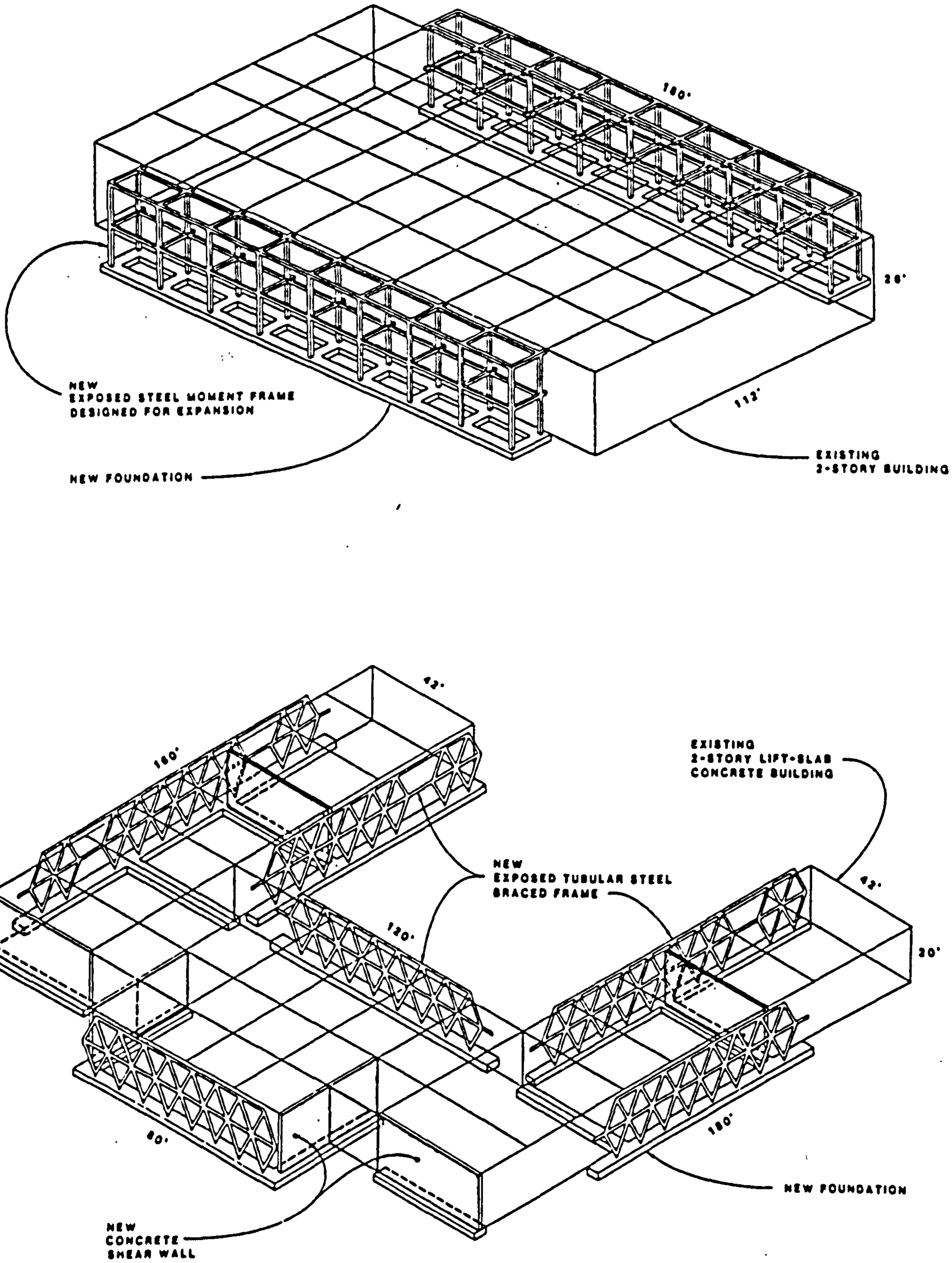


Fig. 3.7 Shematic View of Seismic Bracing

CHAPTER 4

4. EXPERIMENTAL PROGRAMME

4.1. Introduction

In modern sophisticated structural design, great emphasis is placed on the use of advanced analytical techniques. In particular, the proper use of accurate analytical models and methods can be of great assistance in understanding and predicting the response of a structure to a variety of prescribed loadings. Improvements in the availability of computational facilities have enabled extensive analytical investigations of the complex nonlinear behaviour of a variety of structural forms to be performed. The confidence in the results of such analytical procedures is, however, limited to the corresponding confidence in the material and behavioural models used to represent the structure concerned. To ensure that an analytical procedure is sufficiently accurate for application to a particular problem and to assist in the further development of existing models, or the original development of new models, it is necessary to perform a series of experimental investigations.

The aim of structural experimentation is to provide the analyst with information on material properties and their influence on the behaviour of the structural members and assemblages. In certain areas of interest, where theoretical knowledge is especially insufficient, detailed information from experimental results is particularly necessary. Such situations include the complex nonlinear behaviour of a variety of materials and structural forms arising from cyclic and dynamic response.

These conditions certainly exist where the seismic response of a repaired RC structure is under investigation and more specifically, shear walled structures damaged by earthquakes. Test methods commonly used to obtain pertinent information in this area range from simple material tests, through monotonic and cyclic tests on structural members, to dynamic tests found in the use of shake tables and online computer-controlled pseudo-dynamic testing.

This experimental programme consisted of testing six intact walls (SW21, SW22, SW23, SW24, SW33, SW35). Eleven repaired or enhanced walls were also tested within the current programme (SWR4, SWR5, SWR7, SWR9, SWR21, SWR22, SWR24, SW31, SW32, SW34, SWR35). Four of the repaired walls were originally

tested in the previous IC testing programme (SW4, SW5, SW7 and SW9), (Pilakoutas, 1990). Experiments were performed on 1:2.5 scale models. They were tested under cyclic displacement controlled loading. The test set-up and the loading history are described in Sections 4.2 and 4.3, respectively. This was followed by the specimens design and details, construction procedures and material properties in Sections 4.4 and 4.5, respectively.

4.2. Test Set-Up

4.2.1. Loading system

Figure (4.1) shows an elevation of the self-reacting test-rig, the location of the test specimen and the positioning of the dynamic actuator. Also, a general assembly photograph is shown in Appendix AIV. The test-rig comprised of a reaction wall and a guiding steel frame. The reaction wall was assembled from standard concrete blocks. Two columns of three blocks each were embedded on a thin layer of cement grout and were prestressed to the concrete strong floor on the 90 cm x 90 cm grid by means of 50 tonne holding down bolts; ensuring a design capacity of 720 kNm. A yoke of two 300 x 200 mm RHSs were stressed at the correct height on the reaction blocks so as to provide the push and pull capacity of the jack.

The test specimens were post-tensioned to the strong floor through the thick rigid concrete block at the base of the wall (250 x 250 mm), by means of two stiff steel beams (RHSs 300 x 120 x 10 mm) applied at both sides of the wall. These were anchored to the strong floor using four prestressed holding down bolts (38 mm Diam.) carrying 50 tones each. The specimen was then modeled and tested as a vertical cantilever fixed to the strong floor.

The boundary conditions at the top, as shown in Figure 4.1, assume a horizontal load at a constant height. The load had to be applied through a pin so as to eliminate tangential forces due to the extension of the wall. This was achieved by cylindrical rollers made of solid bar and fitted with two circular bearings at their ends. A roller was used at each end of the loading beam. In order to avoid local crushing, a steel spreader plate was fixed at each end of the beam. The front roller was embedded in the collar frame, while the end roller had an adjustable horizontal position through a screw arrangement. The loading collar was free with respect to in-plane horizontal movement, but was restrained from displacing vertically and out-of-plane by a system of flat rollers reacting against two standard laboratory assembly portal frames. With this arrangement

the specimen and the load transferring members were totally encased in a safe way. The horizontal load was applied through the top wall loading beam, which was intended to spread the load in the wall panel. It is inevitable that the beam stiffness will influence the stress distribution locally. However, this would not affect the behaviour of the wall critical zones.

A double-acting hydraulic actuator of 250 kN capacity was used to apply the lateral displacements. No axial load was applied to the walls, since it is usually small in structural shear walls and generally has a favourable effect on their behaviour (Yanez, et al, 1992).

4.2.2. Hydraulic power system

The hydraulic power used by the actuators to impose displacements and loads on the test specimen was provided by two power packs with a combined flow capacity of 460 litres per minute, which were connected to a common ring main complete with start up facility. The hydraulic flow was fed through a 230 litres per minute hydraulic sub-station to the actuator via three hydraulic hoses (pressure , return and drain). A start up pressure of 100 psi and a full operation pressure of 3000 psi was available to the actuator. The force applied by the actuator is developed by the hydraulic pressure acting on the cross-sectional area of the piston (Broderick, 92).

4.2.3. Electro-hydraulic servo-control

Control of the actuator was achieved by means of a servo-controller, which compared the command signal voltage with the displacement transducer voltage output signal. The difference between these two was converted into a current which was fed through a servo valve, causing the actuator to move by directing oil to either end of the actuator piston in proportion to this current. This process was performed in a closed loop, with displacement feedback from the LVDT, until the output displacement signal had reached the command signal. If the actuator had being operated under force control, the feedback signal would have come from the load cell, not the LVDT. It was necessary to set the controller loop gain settings to ensure best performance of the equipment and to avoid an oscillatory approach to the command setting.

The servo-controller used in this experimental programme was an Instron Series 2180 mini-controller which was capable of both force and displacement control. The

selection of appropriate servo-valves was dependent on the actuator amplitude and operating frequency. For large stroke amplitudes and higher operating frequencies, greater capacity was required. For the core of this experiment, a cyclic static test, the size of the servo-valve required is largely governed by the smallest size available. Accordingly, Moog series E760 servo-valves with a capacity of 60 litres per minute were selected for the actuator.

The LVDT was permanently fixed within the actuator, but the load cell had to be independently selected and fitted to the end of the piston by means of male/male couplings. To match the capacities of the actuator, a fatigue resistant load cell with a dynamic rating of 250 kN was selected.

The servo-controller could be used to control the actuator either directly, through its control cabinet, or indirectly by receiving a command from the external source. Similarly, test output could be received through the engineering readout module which is also located in the control cabinet along with the servo-controller, or can be passed to an external device for display and storage. In our case, tests were controlled through the cabinet. The output was passed to a plotter and a data logger for test control and data acquisition.

4.2.4. Instrumentation

In order to obtain the maximum possible information about the wall deformational and rotational behaviour of the tested models under cyclic loading, the models were heavily instrumented. Sixteen linear variable differential transformers (transducers) hereafter refered to as LVDT, were used to record the wall horizontal and vertical deformations at the quarter, mid and full height of the wall. Out-of-plane deformations and base rotation were also recorded. Transducers measuring locations are shown in Fig. 4.2.

Strain of steel reinforcement was measured at 30 locations in order to monitor stages of steel yielding, to plot a strain profile for longitudinal bars, and to plot forces versus strain hysteresis for various reinforcement elements. The strain gauge length was chosen so as to avoid averaging the varying strains of flexural members. However, it is anticipated that due to the large number of cycles, following yield, the local strains may be affected by permanent plastic straining. Different types of electrical strain gauges were used for the different types and diameters of steel reinforcement. All gauges were located facing the centre of the wall so as to avoid damaging them during casting and leveling of the concrete. The deformed bars were ground at the strain gauge locations.

The gauges and wiring were subsequently waterproofed. The gauges were connected to a quarter bridge circuit available with the data logger.

4.2.5. Data Acquisition

Data acquisition was performed through a Hewlett Packard data logging system. Fifty channels were monitored in each loading phase and it was used to scan the channels during the tests. The electrical signals scanned by the logger were sent to a PC that was converting them into engineering units. The test was controlled through a digital display of the applied displacement and the corresponding resisting force. The PC was connected to an X–Y plotter, which plotted the hysteresis loops during the test. These hysteresis loops were used to monitor the horizontal drift and to observe visually the overall wall behaviour while testing.

Data at monitoring points were registered by the PC (30 strain reading and 16 transducer reading). The data were eventually processed and filtered used Excel environment; selective results were plotted using Delta Graph environment. Each test ended with about 300 loading phases (monitoring points) containing around 14000 measurements.

The specimens were painted with a whiting chalk before testing for better crack appearance. A mesh of 120mm grid in both directions was marked to facilitate the crack location. The cracks were marked after each cycle; photographs and slides were taken to keep a record of the crack pattern propagation.

4.3. Loading History

The tests were performed using displacement control loading. It was intended that the applied loading history would represent the extreme conditions experienced during a severe earthquake. During strong shaking, a large number of load reversals is expected at lower displacement levels, decreasing with increased displacement. According to previous tests carried out at Imperial College, insignificant deterioration took place after the second cycle. It was therefore decided that a loading regime of two cycles at each displacement should be followed, up to failure.

This loading regime provided information regarding the load displacement cyclic between the same deformation limits during different sequences of the test.The

BIBL. LONDN. UNIV.

global quasi-static loading histories followed for all the specimens are depicted in Figs. 3.3. and 3.4 showing an increasing displacement amplitude of 2 mm and 3 mm respectively. The failure criterion was the reduction in excess of 30% in the recorded ultimate strength.

4.4. Design of Test Specimens

The tested RC walls were designed to the current US code for the design of reinforced concrete buidings (ACI 318-89). Section analysis was carried out using a nonlinear finite element program (ADAPTIC). Concrete cracking due to cyclic loading was taken into consideration in the section analysis. A multi-surface plasticity model for steel reinforcement was used to predict the actual steel behaviour in the strain hardening region while applying the same loading history as for the tested specimens (Izzuddin et. al, 1989).

For the purpose of the current investigation, use was made of the cubic plastic element with distributed plasticity (section analysis). This was used in conjunction with the passive confinement concrete model developed by Madas and Elnashai (1992). The model takes into account the build-up of confinement with increase in axial stress. Moreover, the section is divided into unconfined (concrete cover), partially confined (middle core) and fully confined areas (boundary elements whenever confined), depending on the geometry of section and confining hoops.

The cubic elastic element assumes a cubic shape function in the chord system, and monitors stresses and strains at various points across two Gaussian sections, allowing the spread of plasticity throughout the cross-section. Each element is defined by two nodes, and the cross-section is divided into a number of monitoring points. The stresses are calculated at each monitoring point and for the two Gaussian sections. The basic characteristic of the element is that it predicts member behaviour based on material stress-strain relationships and large displacements. The accuracy increases by using more elements in the plastic zones of the member and/or by increasing the number of monitoring points in the cross-section.

In static (quasi-static) analysis, use is made of the Newton-Raphson family of iterative procedures, with automatic switching from one option to another according to the number of iterations required for convergence in the last increment. Displacement control was available under proportional loading.

The models under consideration were divided into six elements such that all potentially-critical sections are represented accurately. The analysis was run on a Vax 8600 and a DEC 5000/240 workstation with a mips rating of 42.

In all specimens, the longitudinal reinforcement in the webs was kept identical. This enabled a direct comparison of the behaviour of boundary element reinforcement.

The design shear strength for walls was calculated assuming that the horizontal ties were stressed to 1.25 times the specified yield strength of the steel with a maximum of 415 MPa. This can be explained by the fact that shear detrioration and failure is governed by the concrete shear strain rather than yielding of stirrups, especially when undeformed bars are used. It should be noted that the intermediate longitudinal bars of the wall were considered to be effective in resisting horizontal shear in the middle web by dowel action, provided that a relative slip is expected to occur as a result of a diagonal shear crack i.e.for models failing in shear. Confined concrete in the boundary elements, in the compression side, added to the shear strength. The confining hoops in the boundary elements in the tesion zone also added to the wall strength. This was confirmed experimentally as described in Chapters 5 and 7.

In order to estimate the wall displacement and curvature ductilities, the applied loading consisted of incrementally increasing cyclic displacement as opposed to load control. The later would have recorded the ultimate load without showing the maximum displacement level up to which the ultimate load was sustained.

The computer design involved the same experimentally applied loading scheme prior to the actual model tests. The analytical results, i.e. wall resistance at every deformation level and steel strains, compared well with the obtained experimental results; especially the models dominated by flexural response and failure mode.

A summary of the experimental programme is included in Table 4.1. Typical wall reinforcement for the specimen SW31 is given in Fig. (4.5). Details of reinforcement are given in Figs. 4.6, 4.7 and 4.8.

4.5. Construction of Test Specimens

The concrete used had a 10 mm maximum size aggregate. The design mix is given in Table 4.3 and the cube strength at 28 days for the tested models, f_c, is shown in Table 4.4. The vertical reinforcement in the walls was of deformed steel bars, identified as

HT bars, with measured yield and ultimate strengths given in Table 4.5. As the steel did not have a well-defined yield plateau, the yield strength was defined as the stress at the 0.2% off-set strain. The horizontal reinforcement and hoops in the walls were of plain steel bars, identified as R, bars with a measured yield strength of 380 MPa and ultimate strength of 510 MPa. The concrete cover to the horizontal bars, which were placed outside the vertical bars, was 6 mm to the wall faces and 10 mm to the wall ends.

The moulds were manufactured from 19 mm plywood. Before each casting, the inside of the mould was coated with a releasing agent. Concrete was mixed in the laboratory by using a suitable size concrete mixer. All specimens were cast horizontally in a single monolythic pour. The wet concrete was placed and vibrated in three layers. First the bottom third of the beams, followed by the wall area and the middle third of the beams, and finally the top third of the beams. All models were vibrated on the vibrating table. Control specimens were taken from the same batch while casting the wall. Strict compaction and levelling was imposed on the wall surface, so as to eliminate voids and minimize geometric irregularities.

The specimens were trowel finished one hour after completion of casting and covered with wet hessian and nylon after about four hours. This type of curing was maintained for a week until a control cube was crushed. Control specimens were demolded the day after casting and placed on top of the horizontal wall for identical curing conditions. Curing was stopped on the seventh day unless a weaker strength than expected was recorded. Subsequently, the wall and control specimens were stored under standard laboratory conditions next to the test-rig.

Two 4" x 10" cylinders and six 4" cubes were cast and used as control specimens. At least three of the cubes were tested at the end of each experiment. The cylinders were all tested at the end of the experimental programme (ACI SP-71, 1989).

Table 4.1 Summary of Experimental Programme

Model	Dimensions	Status	Flexural Str. kN	Shear Str. kN	Loading Regime	Repair Objective
SWR4	1200x600x60	Repaired	108	104	Cyclic	Strength
SWR5	1200x600x60	Repaired	132	108.2	Cyclic	Shear Str.
SWR7	1200x600x60	Repaired	132	96.8	Cyclic	Strength
SWR9	1200x600x60	Repaired	88.7/101	128.3	Cyclic	Flex. Stiff.
SW21	1200x600x60	Intact	108	105.4	Cyclic	–
SW22	1200x600x60	Intact	88.7	107.9	Cyclic	–
SW23	1200x600x60	Intact	123	126.3	Cyclic	–
SW24	1200x600x60	Intact	123.4	124.8	Cyclic	–
SWR21	1200x600x60	Repaired	108/119	184.7	Cyclic	Shear Str.
SWR22	1200x600x60	Repaired	88.7/98	119	Cyclic	Stiffness
SWR24	1200x600x60	Repaired	123.4/135	195.6	Cyclic	Shear Str.

Table 4.1 Summary of Experimental Programme (cont.)

Model	Dimensions	Status	Flexural Str. kN	Shear Str. kN	Loading Regime	Repair Objective
SW31	1200x600x60	Enhanced	62	168.8	Cyclic	Flex. Str.
SW32	1200x600x60	Enhanced	62	172.6	Cyclic	Ductility
SW33	1200x600x60	Intact	59	168.8	Cyclic	_
SW34	1200x600x60	Enhanced	62	168.8	Cyclic	Flex. Str.
SW35	1200x600x60	Intact	71	168.8	Cyclic	_
SWR35	1200x600x60	Repaired	71/76	168.8	Cyclic	Flex. Stiff.

Table 4.2. Reinforcement for the Tested Models

MODEL	VERTICAL REINFORCEMENT					SHEAR RFT.		CONFINEMENT RFT.	
	Boundary Element		Web Reinft.		Global Rft.	Rft.	Ratio	Rft.	Ratio
	Area(mm^2)	Ratio (%)	Area(mm^2)	Ratio (%)	Ratio (%)		(%)		(%)
SWR4	904.8	6.283	113.1	0.841	2.823	R4 @ 240	0.175	HT6 @ 120	0.785
SWR5	917.2	12.741	169.6	0.841	3.019	R4 @ 120	0.349	R4 @120	0.349
SWR7	917.2	12.741	169.6	0.841	3.019	HT6 @ 240	0.393	HT6 @ 120	0.785
SWR9	942.5	6.545	113.1	0.841	2.932	R4 @ 70	0.598	R4 @ 70	0.598
SW21	904.8	6.283	113.1	0.841	2.823	R4 @ 100	0.419	R4 @ 20	2.1
SW22	942.5	6.545	113.1	0.841	2.932	R4 @ 100	0.419	R4 @ 33	1.269
SW23	917.3	6.370	113.1	0.841	2.862	R4 @ 60	0.698	R4 @ 60	0.698
SW24	917.3	6.370	113.1	0.841	2.862	R4 @ 75	0.559	R4 @ 15	2.793

Table 4.2. Reinforcement for the Tested Models (cont.)

MODEL	VERTICAL REINFORCEMENT					SHEAR RFT.		CONFINEMENT RFT.	
	Boundary Element		Web Reinft.		Global Rft.	Rft.	Ratio	Rft.	Ratio
	Area(mm^2)	Ratio (%)	Area(mm^2)	Ratio (%)	Ratio (%)		(%)		(%)
SWR24	917.3	6.370	113.1	0.841	2.862	R4 @ 75	.559	R4 @ 15	2.793
SW31	402.1	2.792	113.1	0.841	1.431	R5 @ 60	1.091	R5 @ 30	2.182
SW32	402.1	2.792	113.1	0.841	1.431	R5 @ 60	1.091	–	–
SW33	402.1	2.792	113.1	0.841	1.431	R5 @ 60	1.091	R5 @ 30	2.182
SW34	402.1	2.792	113.1	0.841	1.431	R5 @ 60	1.091	R5 @ 30	2.182
SW35	402.1	2.792	113.1	0.841	1.431	R5 @ 60	1.091	R5 @ 30	2.182
SWR35	402.1	2.792	113.1	0.841	1.431	R5 @ 60	1.091	R5 @ 30	2.182

Table 4.3. Mix Proportion by Weight for Normal Weight Concorete

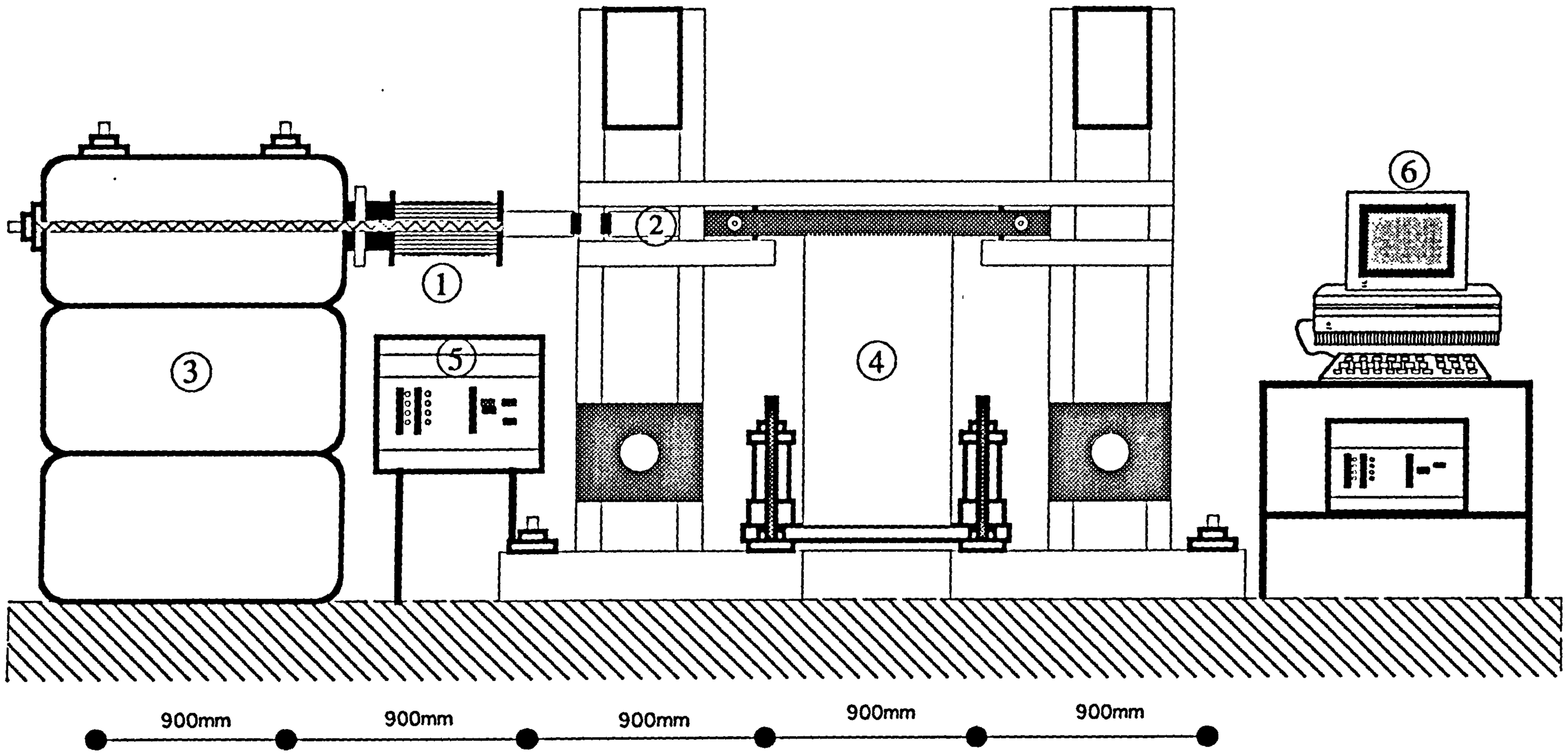
Mix Proportion by Weight	Design Mix Ratio
O. P. Cement	1.00
10 mm Aggregate	2.40
Coarse Sand	1.20
Fine Sand	0.75
Free Water	0.55

Table 4.4. Material Properties of Concrete

Model	Compressive Strength (N/mm^2)
SWR4	49.5
SWR5	47.5
SWR7	45.2
SWR9	53.7
SW21	48.4
SW22	45.1
SW23	47.4
SW24	49.2
SW31	46.4
SW32	48.5
SW33	49.2
SW34	49.4
SW35	48.4

Table 4.5. Steel reinforcement properties

STEEL TYPE	E_{so} N/mm²	f_{sy} N/mm²	E_{sl} N/mm²	f_{su} N/mm²	ε_{ul} Strain x 10^6
4 Round	200,000	400	2600	460	60,000
5 Round	200,000	450	2600	580	52,000
6 Deformed	200,000	545	2200	590	20,000
8 Deformed	200,000	450	3000	660	42,000
10 Deformed	200,000	470	3000	660	42,000
12 Deformed	200,000	460	1300	600	85,000
16 Deformed	205,000	535	1075	590	75,000



1. INSTRON 250 KN HYDRAULIC SERVO-CONTROLLED JACK
2. LOAD CELL
3. CONCRETE REACTION BLOCKS
4. REINFORCED CONCRETE WALL
5. CONTROL UNIT
6. PC + DATA LOGGER

Fig. 4.1. Test Set-up

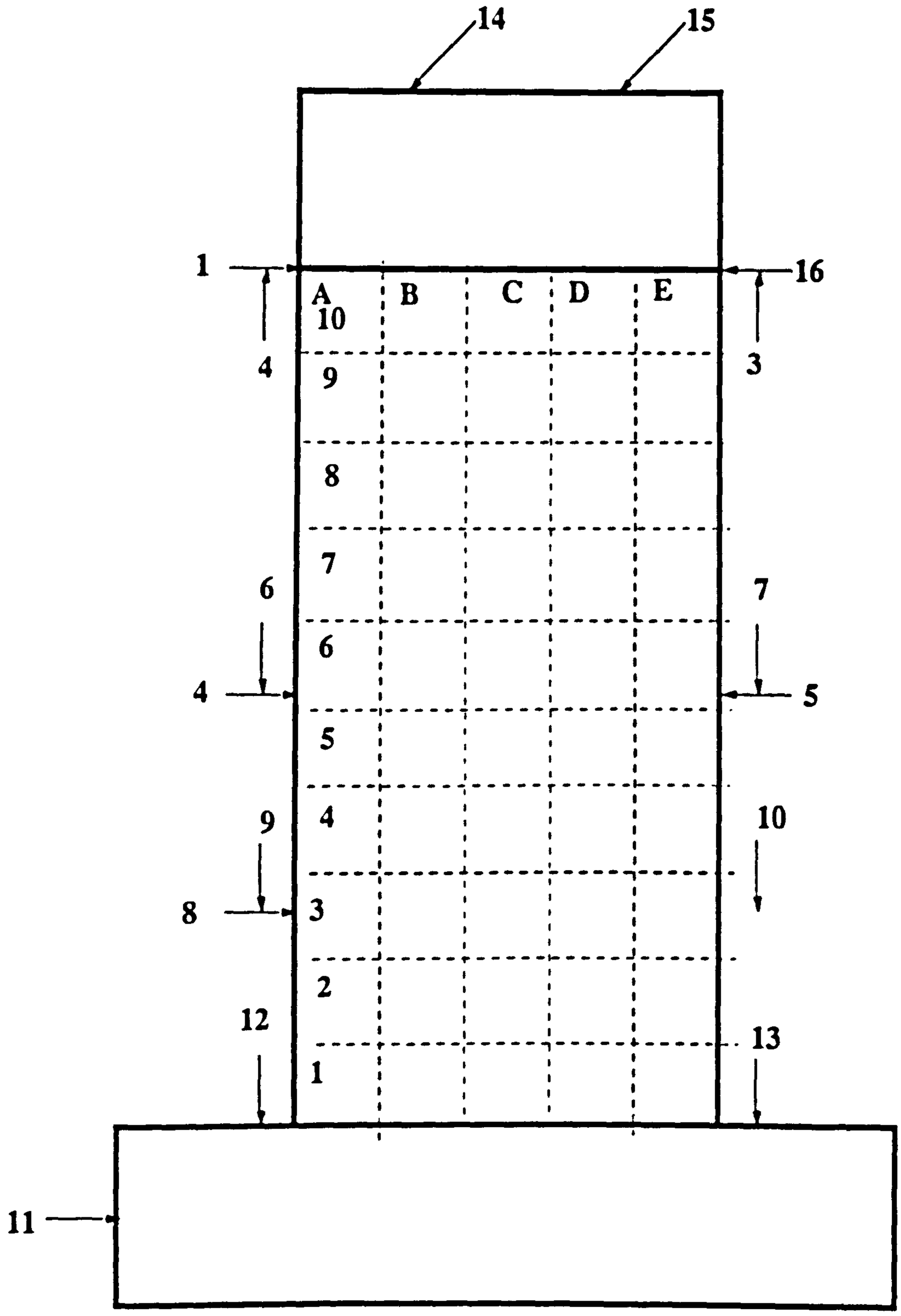


Fig. 4.2 Transducers Reading Ports and Mesh for locating Cracks

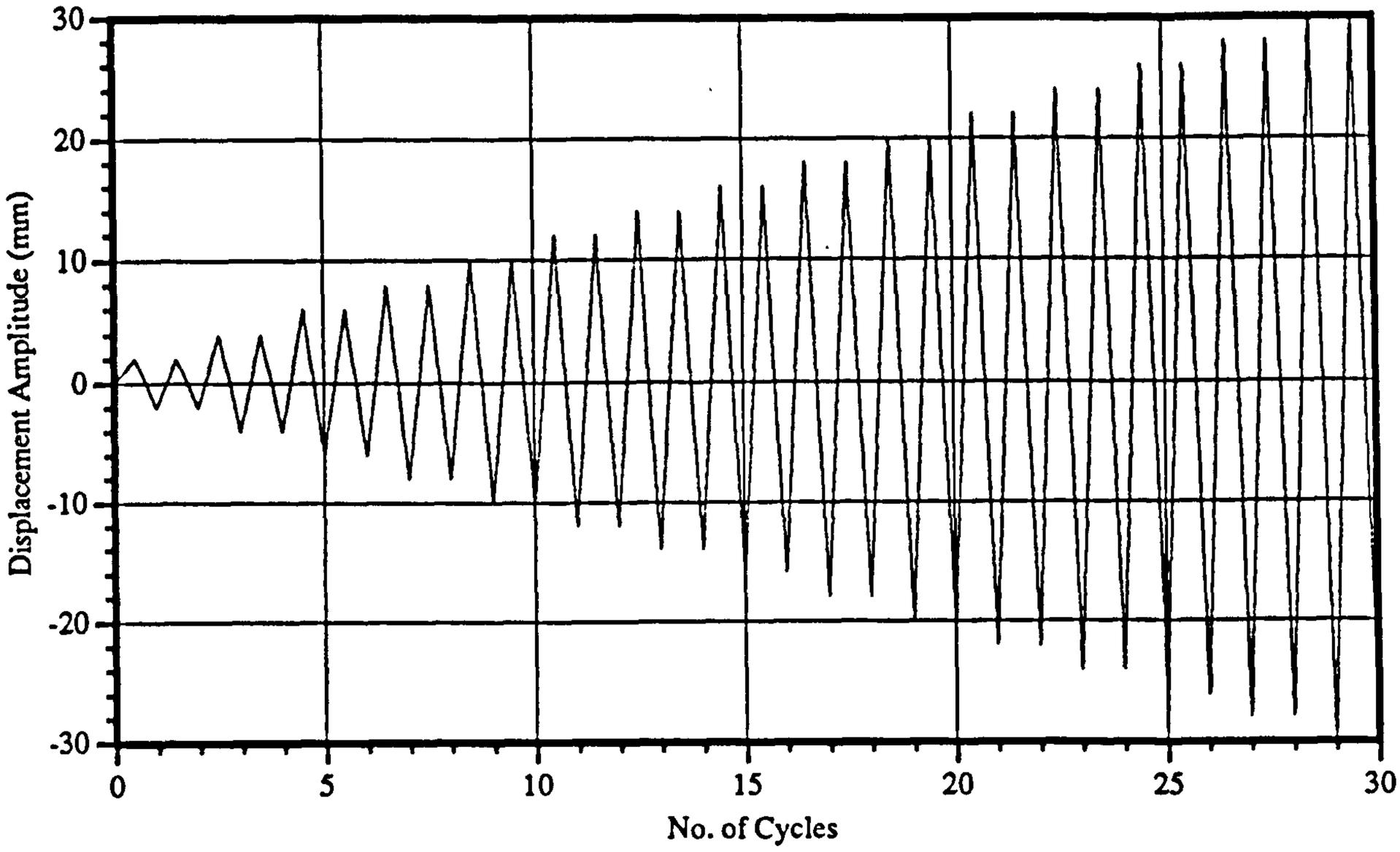


Fig. 4.3. Displacement History 2 mm/step

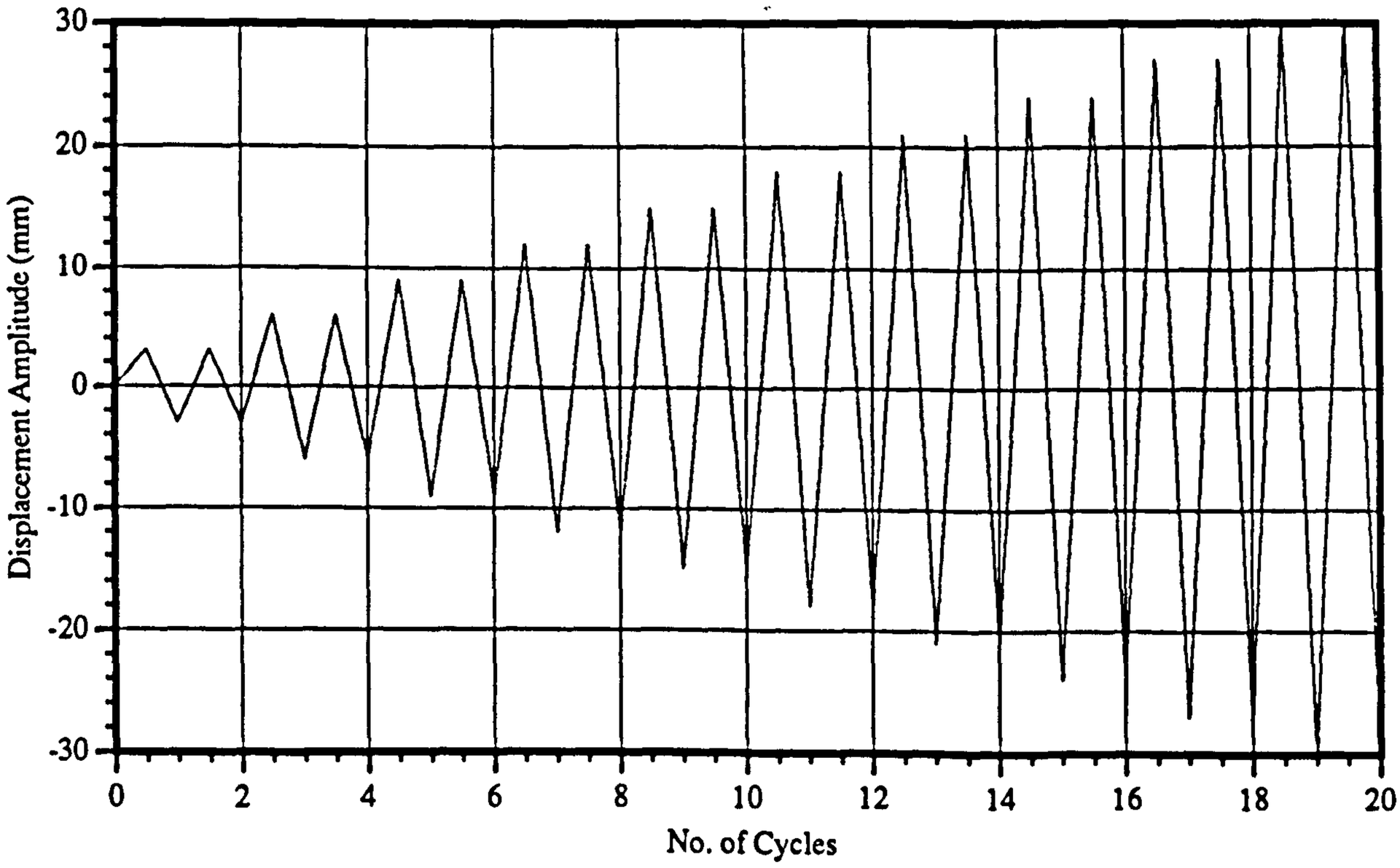


Fig. 4.4.. Displacement History 3 mm/step

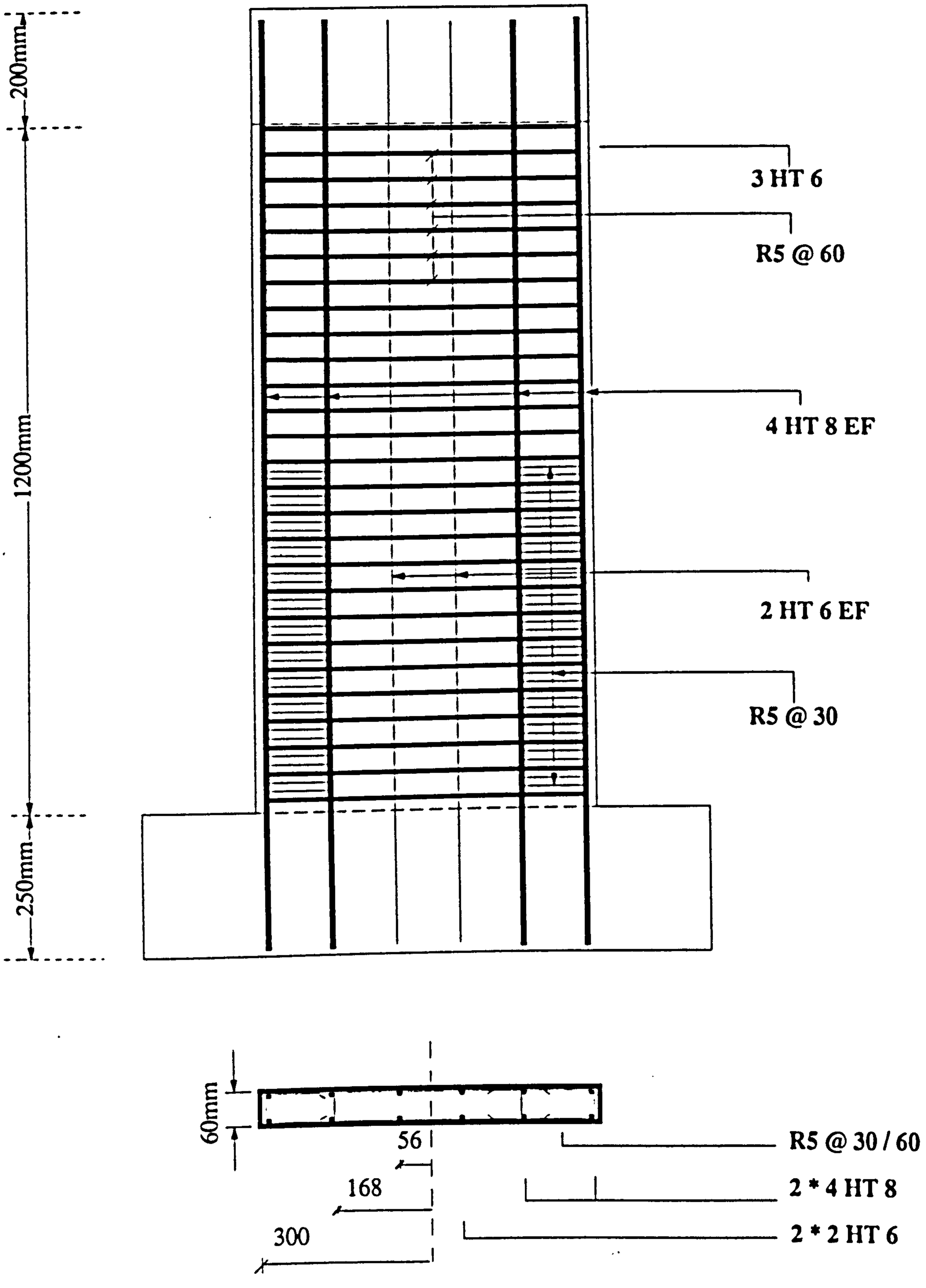


Fig. 4.5. Typical Wall Reinforcement SW31

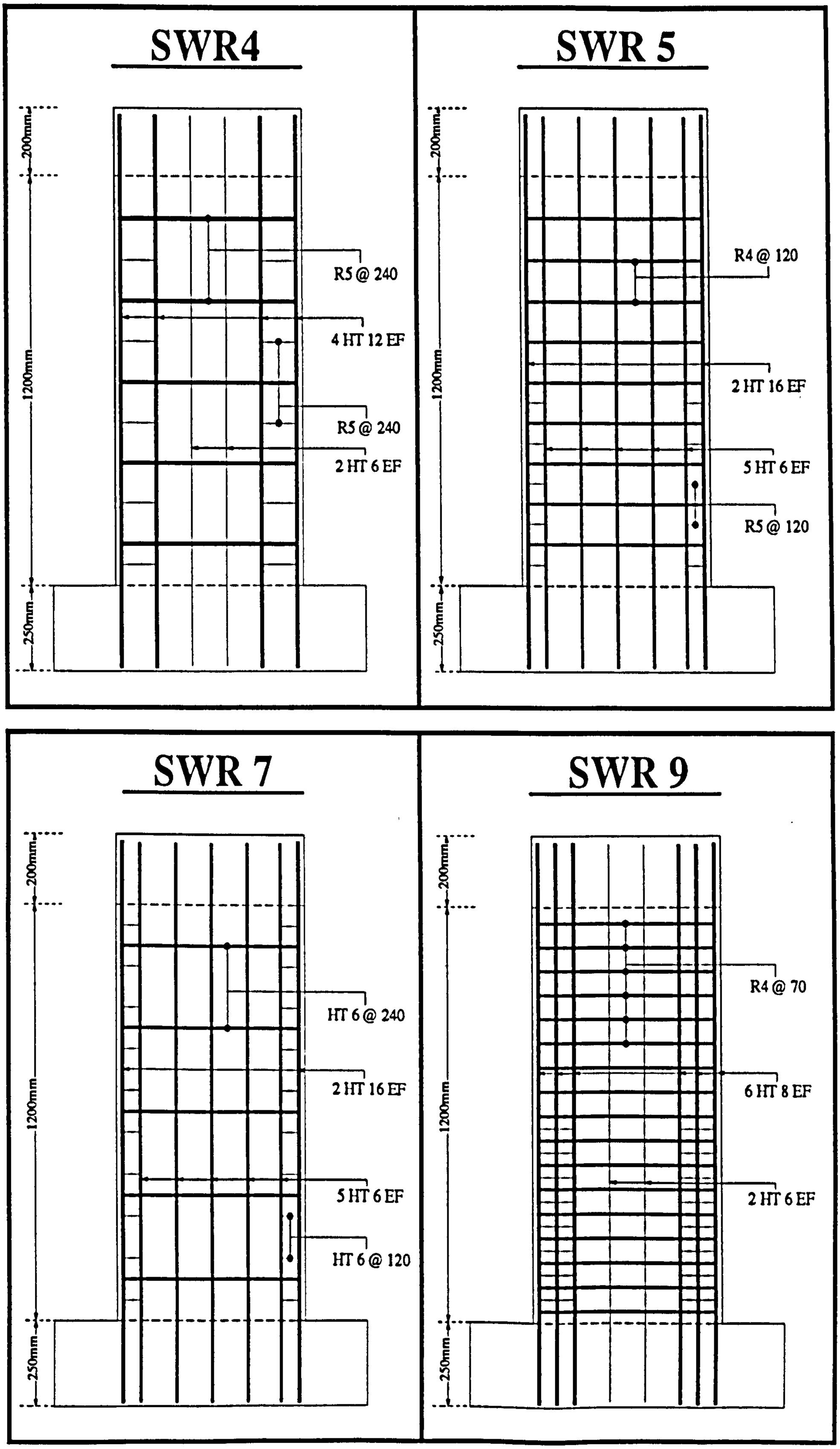


Fig. 4.6. Wall Reinforcement SWR4-SWR5-SWR7-SWR9

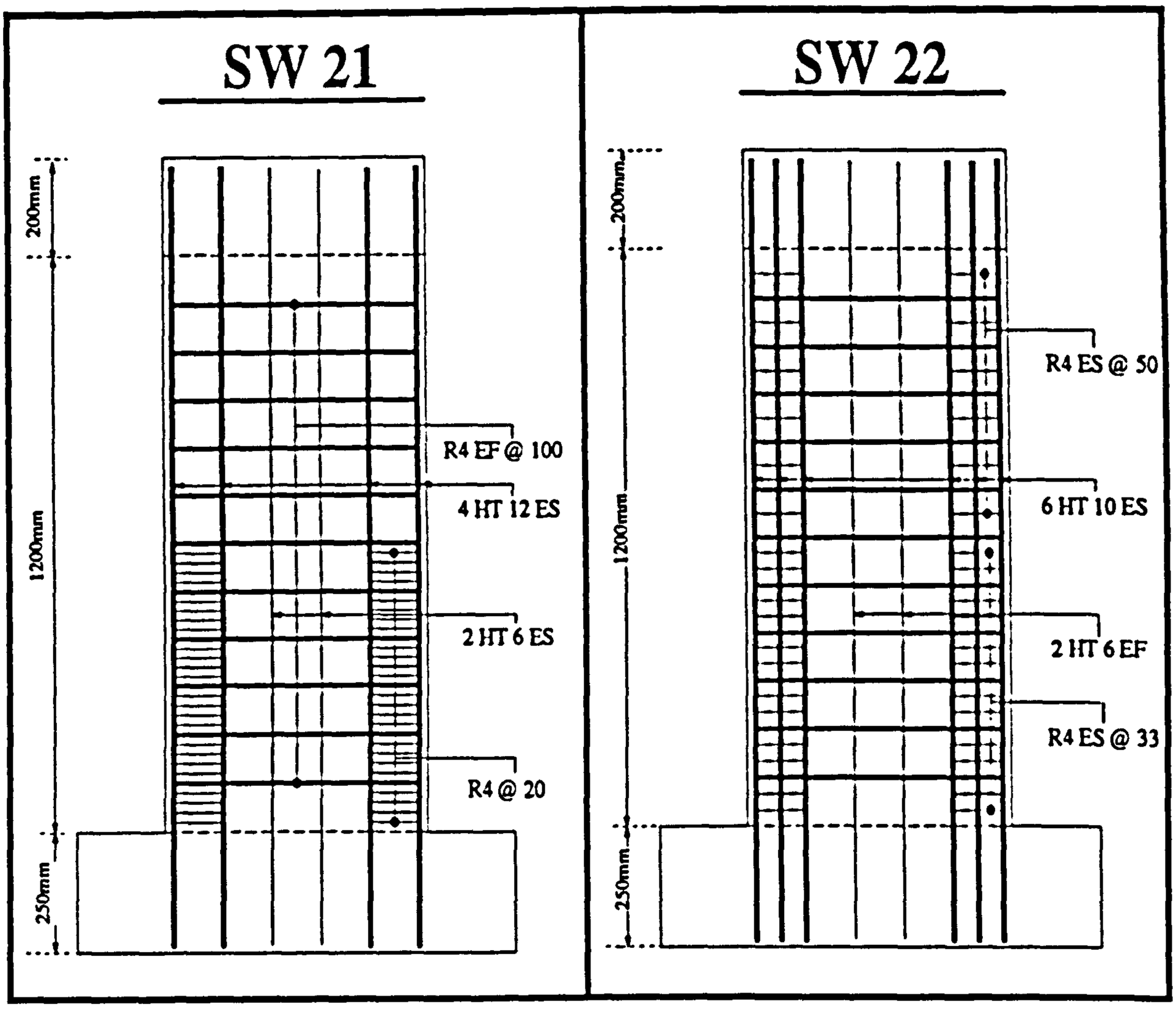


Fig. 4.7. Wall Reinforcement SW21-SW22-SW23-SW24

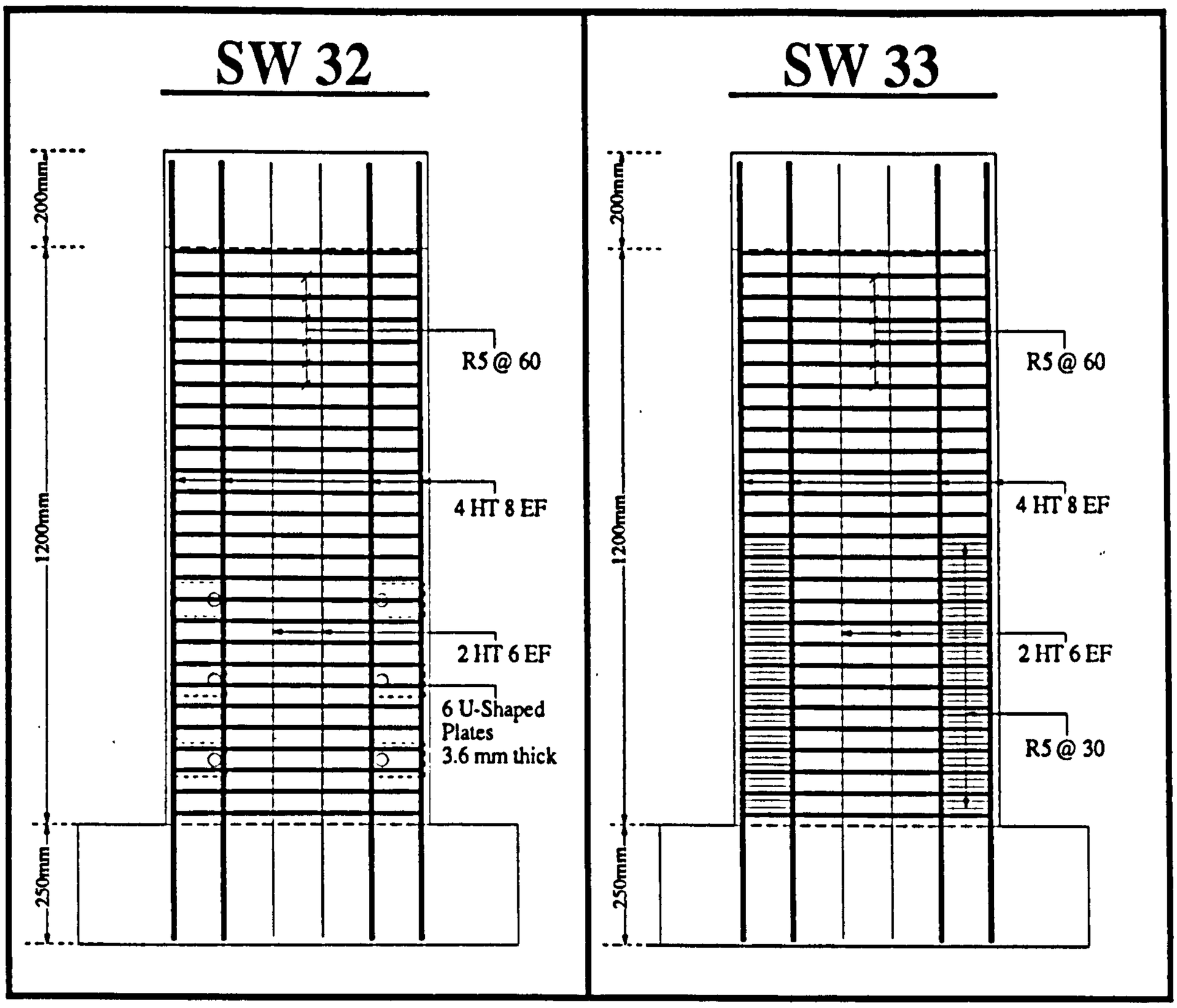


Fig. 4.8. Wall Reinforcement SW32-SW33-SW34-SW35

CHAPTER 5

5. TEST RESULT FOR INTACT WALLS

5.1. Introduction

Six 1: 2.5 scale models were tested under a quasi-static deformation history (SW21, SW22, SW23, SW24, SW33, SW35). The design and details of these specimens, test set-up and deformation history have been discussed in Chapter 4. Four additional models were tested during the previous Imperial College Testing Programme. These are walls SW4, SW5, SW7 and SW9 (Pilakoutas, 1990). They were repaired and retested for the purposes of the current testing programme. To allow for better understanding of the repaired test results described in Chapter 7, a brief description of these tests is included hereafter and therefore, this Chapter focuses on presenting the experimental observations and discussing the test results qualitatively and quantitatively.

For each test, a brief description of the experiment is given. This is followed by a general behaviour of the model including displacement history, details of crack pattern, failure mode and strain in steel reinforcing bars. The Force-Displacement hysteresis curves and Force-Strain in steel curves are included in appendices **AI** and **AII** respectively. Plates showing crack patterns at various maximum displacement levels, hereafter referred to as 'MDL', are included in appendix **AIV**.

An envelope of the hysteresis loops was plotted to give a simpler indication of the wall behaviour than that given by the cyclic plots.

The overall behaviour of each specimen was analysed using the following sources of information:

- A continuous plot of load versus displacement at 16 different locations of the tested wall (hysteresis loops). Measurements were taken at quarter, half and full height of the specimens, as shown in Fig. 4.2. In-plane as well as out-of-plane deformations and rotation at the base were recorded. This would confirm that the assumed boundary conditions are achieved.

– Readings from strain gauges bonded to the reinforcing bars for the newly tested walls. Thirty gauges were attached to the steel bars in the critical wall zones.

– A photographic record of crack pattern development in the tested walls.

5.2. Review of Previous Relevant IC Test Results

The initial phase of testing made use of walls previously-tested at Imperial College (Pilakoutas, 1990). In order that results from re-testing are fully appreciated and to provide a complete record for comparison, the results of intact wall tests are reproduced herein.

5.2.1. Model SW4

The loading programme consisted of incrementally-increasing lateral displacement cycles. Two cycles of displacement were applied at each deformation level with 2 mm increments per new loading phase as shown in Fig. 5.1.

Cracking was observed at 1 mm and before reaching the first MDL (2 mm). The initial wall stiffness calculated at 0.5 mm displacement was 31 kN/mm. The observed stiffness at 2 mm MDL was 19.3 kN/mm (Pilakoutas, 1990).

Cracks propagated from the wall boundaries towards the centres and from the bottom upwards. Near the boundaries, cracks were nearly horizontal while further away they were inclined to the horizontal. The inclination increased along the height. Cracking was apparent up to just above the middle of the wall. By MDL-4, cracks propagated to the entire wall height. At the boundaries, the density of the cracks was rather high; while in the web, the number of main cracks was limited to about three to four on each side. The propagation of these main web cracks towards the opposite side was more in the lower part of the wall. Consequently, intersection of cracks was more frequent in this area. The same pattern of cracking continued until yield.

First yield occurred just before MDL-6. Following yield, cracking became denser and several boundary cracks joined to meet the ends of the web cracks. The number of web cracks increased and so did the apparent inclination of the wall. The latter was due to joining of web cracks originating higher up in the boundaries. By

MDL-16, the lower web cracks had opened up considerably more than all the others. Vertical cracking also appeared near the bottom of the wall at the boundaries, approximately at the position of the main reinforcement. This may indicate that there was spalling of the concrete cover at these locations.

With increasing MDL, the concrete in the lower part of the wall began to show signs of deterioration. At MDL-22, just before failure, the concrete confined by the lowest two hoops in both boundary elements was spalling to a considerable extent. Failure occurred in this area, during cycles at MDL-24, by crushing of the concrete core. An envelope of the force-displacement hysteresis is given in Fig. 5.2. Average stiffness at every displacement level was plotted against displacement and showed steep stiffness degradation with the increase of the displacement level, as shown in Fig. 5.3.

5.2.2. Model SW5

The loading programme consisted of incrementally-increasing lateral displacement cycles. Two cycles of displacement were applied at each deformation level with 2 mm increments per new loading phase up to 8 mm MDL. From 8 mm onward, a single cycle was applied at higher MDLs as shown in Fig. 5.4.

Cracking was observed before reaching the first MDL at 1 mm of displacement. The initial wall stiffness as calculated at 0.5 mm was about 34 kN/mm. The stiffness at MDL-2 was 21.7 kN/mm (Pilakoutas, 1990).

Cracks propagated from the wall boundaries towards the centre and from the bottom upwards. Cracking was apparent up to three quarters of the height of the wall. In the lower half, the frequency of cracks near the boundary was higher than in the web. However, the inclination of these cracks was steeper than for wall SW4. The inclination of the main web cracks was about 30° to the horizontal. By MDL-4 cracks propagated to the whole wall length. In the lower half of the wall, at the boundaries, the density of the cracks increased while in the web the number of main cracks was limited to about four to five in each direction. The inclination of these main web cracks was about 45° in the lower part of the wall. Higher up, the inclination was much steeper up to 60°, indicating the shear nature of these cracks. By MDL-8 the frequency of cracking in the boundaries increased considerably. The main web cracks started joining with cracks originating higher in the boundary than before, and hence increased their apparent inclination. The most precarious crack seemed to be that originating at the top right hand side of the wall. MDL-10 was achieved in one direction at a load of 117.3 kN. Yield level was just achieved in the shear reinforcement, but the flexural reinforcement was just below yield. On attempting to achieve MDL-10 in the reverse direction, abrupt failure occurred at a load of about 110 kN. At this stage two of the main web cracks opened up significantly. However, the crack that caused failure was the lower one, which penetrated the compressive area.

An envelope of the force-displacement hysteresis is given in Fig. 5.5. It shows a sudden drop in strength at 10 mm MDL. Average stiffness at every displacement level was plotted against displacement and showed linear stiffness degradation with the increase of the displacement level as shown in Fig. 5.6.

5.2.3. Model SW7

Displacement control with 2 mm increments per new loading phase as shown in Fig. 5.7, was applied to the tested model.

Shear wall SW7 had most of the main reinforcement concentrated at the boundaries, similar to SW5, but had a higher shear reinforcement percentage, similar to that of wall SW4. The expected flexural strength was higher than that of all other specimens (Pilakoutas, 1990).

Cracking was observed before reaching the first MDL at 1 mm of displacement. The initial wall stiffness as calculated at 0.5 mm was about 33 kN/mm, dropping to 21.3 kN/mm at MDL-2. Cracks initially propagated in a similar manner to wall SW5. Cracking was observed up to three quarters of the height of the wall. In the lower half, the intensity of cracking near the boundary was higher than in the web. By MDL-4, cracks propagated to the whole wall length. In the lower half of the wall, at the boundaries, the density of the cracks increased, while in the web the number of main cracks was limited to about four to five in each direction. The inclination of these main web cracks was less than or equal to 45°, and in general less steep than for SW5. At MDL-8, the extent of cracking at the boundaries increased considerably. The main cracks started joining with cracks originating higher in the boundary, hence increasing their apparent inclination, but not to the extent seen for SW5. Following MDL-8, cracking continued to become denser at the boundaries with an average inclination of more than 45°, unlike for wall SW4 where the boundaries were wider. By MDL-4, the main web cracks were wider than before and seemed to have penetrated the compressive area, at least on the surface (Pilakoutas et al, 1991).

The load capacity peaked at MDL-18, corresponding to a load of 127.3 kN. Following that, the widening of the web cracks increased and there was some loss of strength at MDL-22 by fracturing of a 6 mm reinforcement bar on the LHS virgin cycle. A second bar snapped during the completion of this MDL and the strength was reduced to less than half.

Average stiffness at every displacement level was plotted against displacement and showed gradual stiffness degradation with the increase of the displacement level, as shown in Fig. 5.9. An envelope of the force-displacement hysteresis showing a reasonable ductile behaviour is given in Fig. 5.8.

5.2.4. Model SW9

The applied displacement control loading is presented in Fig. 5.10. It shows that the model was tested cyclically up to 26 mm MDL.

Shear wall SW9 had lateral reinforcement that was designed according to the requirements of the EC2. Cracking was observed before reaching the first MDL after 1 mm of displacement. The initial wall stiffness, as calculated at 0.5 mm, was about 38 kN/mm. The stiffness by MDL-2 was 29.8 kN/mm. By MDL-6 the frequency of cracking in the boundaries had increased considerably. However, a top crack had a shallower angle. After MDL-6, cracking continued to increase in density as observed for previous walls. By MDL-14, the main lower web cracks were wider than before and seemed to be opening faster than the top ones (Pilakoutas, 1990).

The crack pattern until MDL-18 was very well distributed, showing a highly ductile behaviour. Spalling of concrete took place in the web at the criss-crossing of main cracks and was limited to the lower quarter of the wall. The wall survived both cycles at MDL-24 and lost strength during the virgin cycle reverse and at the second cycle RHS MDL-26.

Force-displacement hysteresis loops showed that the model reached its yield strength at 8 mm MDL and sustained same strength level up to 24 mm MDL, achieving a ductility level of 3.0. The wall showed very little reduction in strength level while cycling twice at the same displacement level, which was another proof of the ductile behaviour. Stiffness-displacement curve showed uniform stiffness degradation and the wall was left with a reduced stiffness of 4 kN/mm (nearly 10 % of the initial stiffness).

An envelope of the force-displacement hysteresis, showing high ductile behaviour, is given in Fig. 5.11. Average stiffness at every displacement level was plotted against displacement and showed gradual stiffness degradation with the increase of the displacement level, as shown in Fig. 5.12.

5.3. Observed Behaviour of Tested Models

5.3.1. Model SW21

In order to investigate a mixed flexure-shear type failure, a sensitive shear design was applied for SW21, whereby horizontal steel of ratio only 0.4% was used (R4 @ 100). Design for ductility was provided by means a high hoop reinforcement ratio along the lower mid height (R4 @ 20 - equivalent to a ratio of 2.1%) of the wall edges. The main flexural reinforcement having a ratio of 6.3%, was uniformly distributed in the boundary elements as shown in Fig. 4.6.

5.3.1.1. General observations

The applied loading scheme is shown in Fig. 5.13. Two cycles of displacement were applied at each deformation level with 2mm increments.

The tested wall showed considerable ductility. Horizontal cracks started at 2 mm MDL in the boundary elements. Closely spaced hoops (20 mm) caused the cracks to be narrow and well-distributed. The horizontal cracks progressed into coarsely distributed inclined cracks in the web. Intersecting cracks from opposite loading directions segmented the hinging region into several horizontal layers.

At higher displacement levels, the width of diagonal cracks was increased, associated with an increase in strain for the horizontal steel reinforcement. However, these diagonal cracks were restricted to the area between the boundary elements due to the presence of confining hoops. These proved to be effective in preventing the diagonal crack propagation. Average stiffness at every displacement level was plotted against displacement and showed gradual stiffness degradation with the increase of the displacement level, as shown in Fig. 5.15.

5.3.1.2. Force-displacement hysteresis

The force-displacement hysteresis loops showed mixed flexure-shear performance and failure mode. The wall reached its yield strength (100 kN) at 12 mm MDL and sustained a constant strength level up to 18 mm MDL achieving a displacement ductility level of 1.50. Upon unloading in one direction and reloading in the opposite direction the load

cell met with little initial resistance until the previously-opened cracks were closed, as shown in Fig. AI (21) 1. This can be explained by the fact that the wall stiffness was dictated by the stiffness of compressive reinforcement up to crack closure. An envelope of the force-displacement hysteresis is given in Fig. 5.14.

After the peak flexural strength was recorded, grinding of concrete was inevitable due to sliding of the diagonal cracked surfaces. As crack closure took place, the resistance of the wall was gradually restored. Since the observed pinching of loops was quite noticeable, it is concluded that the wall response was governed by diagonal tension rather than diagonal compression. It has been noticed also that the wall underwent only 4.8 mm vertical extension associated with 21 mm MDL which demonstrates its poor rotational capacity and confirms the shear-dominated behaviour as demonstrated in Figs. AI (21) 2 through 10.

Due to loading and unloading, concrete deterioration took place associated with widening the diagonal cracks. This led to some reduction in the wall strength. The failure was characterised by concrete deterioration in the middle web and spalling of concrete cover in the lower sections of the boundary elements (squares A-1, E-1 shown in Fig. 4.2). The final load cell reading was 70 kN and the zero-load plastic set was 8 mm.

5.3.1.3. Strain gauge readings

Strain gauge plots demonstrated that the outermost reinforcing steel bars reached a yield strain of 2400 microstrains at the first loading stages, as shown in Fig. AII (21) 1. The gauges recorded an average maximum strain of 1100 microstrain and 620 microstrain at quarter and top wall height, respectively, as shown in Figs. AII (21) 6 and 7. Internal boundary element bars sustained up to 840 microstrain, as shown in Figs. AII (21) 4 and 5. This indicated that the full flexural strength of the wall was not achieved. Longitudinal web bars showed a maximum strain of 1050 microstrain, as shown in Figs. AII (21) 2 and 3.

Horizontal steel links were strained up to yield as shown in Figs. AII (21) 9 through 12. They recorded minor strains at the early loading stages up to diagonal crack formation. Very wide diagonal cracks were observed at the yielded locations. They were confined between the two boundary elements due to the dense hoop reinforcement in these elements.

The lower hoop sustained up to 560 microstrain with no sign of concrete deterioration in the boundary elements. Since hysteresis loops showed noticeable strains from both loading sides, as demonstrated in Fig. AII (21) 8, it is concluded that the confining steel hoops added to the shear strength of the wall. This is based on the recorded 400 microstrain when the pertinent boundary member is subjected to tension.

5.3.1.4. Concluding remarks

From the previous experimental investigations, it is concluded that the wall exhibited a shear-dominated deformational behaviour, deterioration and failure mode. The wall achieved 94% of its flexural strength without reaching the designed ductility due to shear failure. If such a wall was to be repaired, reinstating the deteriorated and cracked concrete and improving the shear strength of the wall should be targeted to achieve a higher ductility performance.

5.3.2. Model SW22

In order to investigate a shear failure mode, model SW22 was over-designed for flexure and under-designed for shear, as shown in Table 4.1. The same amount of flexural and horizontal reinforcement was supplied as for SW21. In order to investigate the effect of confinement reinforcement on the global behaviour of the wall, confining steel was reduced at the lower half of the wall from R4 @ 20 to R4 @ 33. Furthermore, it was reduced in the upper half to R4 @ 50.

5.3.2.1. General observations

Incrementally-increasing lateral displacement cycles were applied to the tested model. Two cycles of displacement were applied at each deformation level with 3 mm increments as shown in Fig. 5.16.

Yielding of the outermost longitudinal reinforcement and the formation of the first diagonal tension shear crack in the middle web occurred during the first loading cycle. Diagonal cracks were formed at approximately 40° to the horizontal. It was observed that the diagonal cracks became steeper along the wall height (from 40° to 60°). They were restricted to the area between the boundary elements due to the confining hoops.

Due to the small amount of web reinforcement, diagonal cracks widened instantaneously, and shear reinforcement yielded. The cracks did not close upon the removal of lateral force. This is attributed to the fact that the tensile strength of concrete was larger than the tensile capacity of the web reinforcement provided. In terms of serviceability and damage control, this observation should be viewed as a serious limitation on the use of shear-dominated lightly reinforced walls with restricted displacement ductility capacity.

Two vertical cracks separating the boundary elements from the middle web appeared and joined the diagonal cracks. Once these cracks were formed, a clear truss mechanism was developed which consisted of two relatively stiff boundary elements (chord members) hinging in between a relatively flexible and highly cracked diaphragm (web member).

The computed flexural capacity, based on plane section analysis and taking into consideration the actual confining steel and concrete deterioration due to cyclic loading, was nearly reached during the first cycle of 12 mm MDL (equivalent to 1% drift ratio). At this deformation level, cracks were developed in the boundary elements, where they were somewhat inclined (inclination was reduced with amount of hoop reinforcement). In only a few cases, they extended into diagonal cracks to form a flexure-shear crack pattern.

When the inclined cracked surfaces came in contact under cyclic loading, some grinding of concrete took place. Due to the reduced amount of hoop reinforcement, the stiffness degradation was more pronounced in this case when compared with SW21, where a higher ductile response was recorded. Also, the displacement ductility was reduced from 1.50 in case of SW21 to 1.30 for the current model.

5.3.2.2. Force-displacement hysteresis

Hysteresis loops corresponding to the same deformation level did not reach the previous strength level. However, they did eventually attain the previous capacity at a higher deformation level until the ultimate load was achieved at 12 mm MDL (1% drift). From this stage onwards, previous resistance was not attained even at a higher displacement level. Average stiffness at every displacement level was plotted against displacement and showed constant stiffness degradation with the increase of the displacement level, as shown in Fig. 5.18.

Hysteretic force-deformation relationships recorded during the test indicated that strength decay started at a drift ratio of approximately 1%. Pinching of hysteresis loops, typically observed in shear-dominant response can be noticed from the same hysteresis loops as shown in Fig. AI (22) 1. The wall behaved in a ductile manner up to approximately 0.9 % drift ratio, and showed strength degradation under increasing deformation cycles. Upon unloading in one direction and reloading in the other direction, the load cell met with little initial resistance until the previously-opened cracks were closed, causing stiffness degradation. As crack closure took place, the resistance of the wall element was gradually restored. The initial softening, followed by a gradual build-up of load resistance was reflected in the force-deformation relationship as pinching of loops. Pinching was relatively high since the response was governed by diagonal tension. These curves were followed by a sudden strength loss, contrary to the flexural response, as the web deteriorated under cyclic loading. The envelope of the force-displacement hysteresis is shown in Fig. 5.17.

Under cyclic loading, the previously-observed grinding of concrete took place associated with spalling of concrete cover causing some strength reduction with each loading cycle. The wall eventually failed by concrete deterioration in the web. The final load-cell reading was 60 kN and the zero-load plastic set was 8 mm.

5.3.2.3. Strain gauge readings

Strain gauge plots demonstrated that the outermost reinforcing steel bars attained a yield strain level of 2100 microstrain at the first loading stages, as shown in Fig. AII (22) 1. They recorded an average maximum strain of 900 microstrain and 450 microstrain at quarter and top wall heights respectively, as shown in Figs. AII (22) 7 through 10. Internal boundary element bars sustained up to 1200 microstrain, as shown in Figs. AII (22) 2, 3 and 4. This indicates that the full flexural strength of the wall was not achieved. Longitudinal web bars showed a maximum strain of 400 microstrain as shown in Figs. AII (22) 5 and 6. Their symmetrical behaviour proves their contribution in shear strength by dowel action.

The lower hoop was strained up to 720 microstrain with no sign of concrete deterioration in the boundary elements. From Fig. AII (21) 11, it is concluded that the confining steel hoops added to the shear strength of the wall, since hoops recorded 250 microstrain in the tension cycles of the corresponding boundary elements.

Horizontal steel links sustained up to 1200 microstrain, as shown in Fig. AII (22) 12. They recorded low strain levels at the early loading stages up to the diagonal crack formation. Very wide diagonal cracks were observed at the yielded locations; cracks were confined between the two boundary elements due to the dense hoop reinforcement in these elements. They propagated outwards at top mid height of the wall due to the reduced hoop reinforcing ratio (R4 @ 50).

5.3.2.4. Concluding remarks

It is concluded from the previous test results, that the web horizontal and vertical reinforcement play a vital role in resisting shear loads at post cracking stages. Reducing such steel reinforcement would reduce the wall ductility, accelerate the rate of stiffness degradation and increase the level of concrete deterioration. Also, confining hoops would improve the shear strength of the wall and modify the cracking pattern, and hence the failure mode of the wall. As observed by Elnashai et al (1990), the distribution of the main reinforcement in the boundary element appears to have no effect on the wall behaviour provided that the steel centroid is kept at the same location.

5.3.3. Model SW23

In order to achieve higher ductility and a flexural failure mode, horizontal reinforcement was increased by 50%, reaching a ratio of 0.7% (R4 @ 60) over that provided for SW22. Confinement hoops were applied at a constant rate along the wall height (R4 @ 60) to achieve the same performance. In order to enhance the flexural strength, the main flexural reinforcement (2 HT 16) was concentrated at the wall edges, as shown in Fig. 4.4. Detailed design for model is given in Table. 4.1.

5.3.3.1 General observations

Displacement control cyclic loading was applied to the tested model. Two cycles of displacement were applied at each deformation level with 3 mm increments per new loading phase as shown in Fig. 5.19.

Wall cracking started as horizontal flexural cracks in the boundary elements. Concentration of main flexural reinforcement in the edges (2 HT 16) caused the narrow cracks. The horizontal cracks progressed into coarsely distributed inclined cracks in the web. Due to the presence of confining reinforcement along the total wall height, the major diagonal cracks were restricted to an area between the two boundary elements whereby a vertical crack developed at the intersection of the orthogonal diagonal cracks. The increase in shear resistance at higher displacement levels produced a large number of well-distributed inclined cracks.

After the formation of diagonal cracks, the force in the horizontal reinforcement increased with further widening and propagation of the inclined crack. Further deformation caused a decrease in depth of the compressive zone of the concrete, thereby resulting in crushing of the concrete in compression. This led to spalling and crushing of concrete at 21 mm MDL. The wall eventually failed by web crushing of concrete associated with major deterioration in the boundary elements.

It was observed that the global deformational behaviour of the wall was governed by two relatively rigid boundary elements forming the chord members of a truss connecting in between a relatively stiff web diaphragm. However, the shear resistance was more effective than the SW22 one. This can be easily noticed by comparing the wall extensions at the same displacement level and hence a higher rotational capacity was achieved. Intersection of inclined cracks under reversed cyclic loading resulted in degradation of concrete compressive strength in this region. Also, the

concrete deterioration was much less pronounced than in SW22. This can be justified by the higher web reinforcement ratios.

5.3.3.2. Force-displacement hysteresis

The wall reached its yield strength of 115 kN at 9 mm MDL. The ultimate strength of 125 kN was recorded at 12 mm MDL. The force-displacement hysteresis loops showed that the wall sustained a constant strength level up to 18 mm MDL as shown in Fig. AI (22) 1, achieving a displacement ductility of 2.0. An envelope of the force-displacement hysteresis is given in Fig. 5.20.

The stiffness-displacement curve showed that the stiffness degradation was less pronounced than in the case of SW22, as shown in Fig. (5.21). Rotational capacity was much higher than SW22, as can be concluded from studying Figs. AI (22) 2 through 10. This can be explained by the fact that hysteresis loops for vertical extensions of the wall at various sections showed higher readings. A maximum cyclic extension of 7.2 mm compared with 4.5 mm for SW21 and 4.0 mm for SW22 was recorded. From the force-displacement hysteresis, it is clear that the wall exhibited a higher flexural deformation when compared with both SW21 and SW22.

Energy dissipation capacity was also improved since pinching of loops was reduced allowing larger areas to be enclosed within the hysteresis loops. The analytical flexural strength was achieved with limited displacement ductility due to the light confining steel applied (R4 @ 60). In order to achieve a higher ductility, a higher confining ratio would be applied for SW24.

5.3.3.3. Strain gauge readings

Strain gauge plots demonstrated that the outermost reinforcing steel attained a yield strain level of 2000 microstrain at the first loading stages, as shown in Fig. AII (23) 1. The gauges recorded an average maximum strain of 1400 microstrain and 420 microstrain at mid and top wall height, respectively, as shown in Figs. AII (22) 2 through 4. This allowed the full flexural strength to develop, and the experimental strength matched the analytical one.

The lower hoop sustained up to 2100 microstrain with some signs of concrete deterioration in the boundary elements, as shown in Fig. AII (21) 5 through 9. From the

previous figures, and as the hoops were strained in the tension and compression zones, it may be concluded that the confining steel hoops increased the shear strength of the wall in the tension side of each cycle.

Horizontal steel links were strained up to 1400 microstrain, as shown in Figs. AII (22) 10 through 12. They recorded minor strains at the early loading stages up to diagonal crack formation. Very wide diagonal cracks were observed at the yielded locations. Cracks were restricted to an area between the two boundary elements due to the dense hoop reinforcement at these elements (Madas et al, 1991).

5.3.3.4. Concluding remarks

It may be concluded that the wall ductility can be improved by reducing the expected concrete deterioration due to non ductile-type failure. This can be achieved by increasing the web reinforcement ratio. The concentration of flexural reinforcement in the outermost edges, rather than being uniformly distributed in boundary elements, has a positive effect on both strength and ductility. The hoop reinforcement ratio has a direct effect on wall ductility, its cracking and failure modes.

5.3.4. Model SW24

To obtain a mixed flexure-shear response mode, the model had a balanced shear-to-flexure strength ratio. The flexural reinforcement was applied in the most ductile manner i.e. the main flexural reinforcement was concentrated at wall edges and minimum reinforcement was applied in the middle web associated with heavy confining hoops at the boundary elements up to the mid-wall height (R4 @ 15). In order to limit concrete deterioration, the wall was tested under increased displacement amplitude of cumulative 3 mm/step. The model was cycled twice at each displacement level.

5.3.4.1. General observations

Since the specimen had the same reinforcement as SW23, except for a higher confining steel ratio (four times as much), it was expected to achieve the same strength with higher ductility levels. Unfortunately, due to transportation problems, the specimen was cracked before testing. Nevertheless, the wall achieved its design strength, associated with lower ductility than that achieved by SW23, which had a lower confinement ratio.

Wall cracking was initiated at 2 mm MDL at 45° and was confined to the middle zone between the two boundary elements. After the formation of diagonal cracks, the force in the horizontal reinforcement increased with further widening and propagation of the cracks.

At 15 mm MDL, further diagonal cracks were opened at the top height of the wall originating from the upper wall edge, where no hoops had been provided. It was noticed that the intensity of diagonal cracking in the upper wall edges was much higher than the lower wall edges. This confirms the effectiveness of the confining hoops in shear resistance. As the applied displacement level was increased, concentration of the inclined cracks was observed near the extremes of the web (squares B - 1 and D - 1) in Fig. (4.2).

Upon load reversal, the load cell met with little initial resistance until the previously-opened cracks were closed. The cracked surfaces along diagonal cracks moved relative to each other prior to closure. As crack closure took place, the resistance of the wall element was gradually restored. This initial softening, followed by a gradual build-up of load resistance, was reflected in the force-deformation hysteretic relationship as pinching of loops. Since the observed pinching was relatively low, it is concluded that the wall response was governed by diagonal compression. When the

inclined cracked surfaces came in contact under cyclic loading, some grinding of concrete took place along the cracked surfaces associated with saplling of concrete cover causing strength reduction with each loading cycle. The wall eventually failed by web crushing of concrete in addition to the crushing of the LHS confined concrete core at the boundary element.

5.3.4.2. Force-displacement hysteresis

It is clear from the previous description of test results that the wall behaviour was dominated by diagonal compression in the web and two tension/compression struts represented by boundary members. The force-displacement hysteresis loops showed a non-ductile wall behaviour, since the ultimate strength (105 kN) was achieved at 12 mm MDL and was reduced to 85 kN at 15 mm MDL as shown in Fig. AI (24) 1. Hysteresis loops corresponding to the same displacement level did not reach the same previous strength level and did not even attain the previous capacity at a higher displacement level. The stiffness-displacement curve showed a constant rate of stiffness degradation at a much more pronounced rate than in flexure-dominated response.

5.3.5. Model SW33

Model SW33 is the reference model for the second group of tested walls (SW31 - SW32 - SW34). It had the same reinforcement details as for SW31. The main flexural reinforcement was concentrated in the boundary elements (4 HT 8/BE, equivalent to 2.8% of the boundary element concrete area). Minimum reinforcement (for construction purposes) was applied in the middle web (4 HT 6, equivalent to 0.8%). The model was intended to have a flexural failure mode and hence was over-designed for shear. Shear reinforcement was well above the minimum (R5 @ 60, equivalent to 1.1%). In order to enhance the wall response, confinement steel hoops (R5 @ 30, equivalent to 2.2%) were applied at the lower mid-wall height .

The wall was tested under increased displacement amplitude of cumulative 2 mm/step. The model was cycled twice at the same displacement level. However, this loading scheme was modified during the test as shown in Fig. 5.22. This was due to some mechanical problems, that caused a jump in one direction from 14 to 22 mm MDL. This caused one-sided severe cracking in the wall associated with plastification of steel reinforcement.

5.3.5.1. General observations

Horizontal flexural cracking was observed at 2 mm MDL in the boundary element. Closely spaced hoops (30 mm) caused the cracks to be narrow and well-distributed. The horizontal cracks propagated into coarsely distributed inclined cracks in the web. Intersecting cracks from opposite directions segmented the plastic hinge region into several horizontal layers. At 6 mm MDL, a horizontal crack was observed at the intersection between the wall section and the fixation beam. This was widened up to 2 mm at the highest displacement levels.

The wall reached its yield strength of 50 kN at 6 mm MDL, associated with 2.5 mm vertical extension at the wall edge. The ultimate strength of 57 kN was first recorded at a displacement level of 8 mm and was sustained up to a displacement of 24 mm. At 12 mm MDL, and due to a mechanical problem, the actuator pushed the wall up to 22 mm, causing severe cracking of the model. In order to obtain the maximum possible information from this partially-damaged model, it was decided to proceed from the undamaged side only up to 22 mm MDL. Hence, from 14 mm MDL onward, the model was cycled between 0 and the higher MDL. Also, one cycle only was applied

from that stage onwards. At 22 mm MDL, the wall was cycled again from both sides, as shown in the displacement history as shown in Fig. 5.22.

From 18 mm MDL onward, it was observed that the lowest crack (at the intersection between the wall and the foundation beam) became very wide. This was associated with severe concrete deterioration. Cycling at higher displacement level caused the main reinforcing bars to kink and the wall started to slide horizontally in a rigid body mode typical of a sliding shear failure.

The flexural cracking intensity was noticeably reduced along the wall height. Flexure-shear cracks characterised by horizontal leading to inclined cracks at about 30° were initiated at a much reduced intensity at mid-wall height, (A to E and 5 to 7 in Fig. 4.2). The inclination of cracks was increased along the wall height. This is explained by the fact that flexural stresses are reduced with the wall height. The flexure-shear cracks were clearly observed at higher displacement levels from 16 mm MDL onwards. At the final MDL, a few cracks propagated at the top wall corners with maximum crack width of 0.2 mm (A-9, A-10, E-9, E-10 shown in Fig. 4.2).

The wall eventually failed by sliding shear that was characterised by concrete deterioration at the lowest level associated with 25% strength reduction at 26 mm MDL. Also, the model did not achieve its ultimate design strength because of early concrete deterioration The stiffness-displacement plot shown in Fig. 5.24 confirms the steady state wall behaviour.

5.3.5.2. Force-displacement hysteresis

In order to comment on the ultimate behaviour of the model. The right hand sided hysteresis from 12 to 22 mm loops were mirrored onto the opposite side, as shown in Fig. AI (33) 1. An envelope of the duplicated force-displacement hysteresis, shown in Fig. 5.23, indicate a ductile wall response.

The tested wall showed adequate ductility, achieving a displacement ductility ratio of 4.0. It also showed an extension of 12.5 and 10.5 mm from both left and right sides, respectively, with an average of 11.5 mm net extension as shown in Fig. AI (33) 2. Model response, as tested, confirmed the high ductility as depicted in Figs AI (33) 3, 4, 5, 6, 7 and 8.

Upon cycling at the same displacement level, the wall showed very little stiffness degradation. Upon unloading in one direction and reloading in the opposite direction, a relatively low initial resistance was recorded until the previously-opened cracks were closed. Nevertheless, no pinching in the hysteresis loops was observed. When the cracked surfaces came into contact under cyclic loading at MDLs exceeding 24 mm, some concrete grinding took place, associated with minor strength degradation. This was followed by spalling of the concrete cover.

5.3.5.3. Strain gauge readings

Strain gauge plots showed that the outermost boundary reinforcement yielded at the first loading cycles, as shown in Fig. AII (33) 1, where a maximum strain of 400 microstrains at mid-height of the wall, was recorded. This was shown in Figs. AII (33) 13 and 14.

Internal boundary element reinforcement yielded at the last loading cycles, as shown in Figs. AII (33) 2 and 3. The vertical web reinforcement was strained up to 1500 microstrain only, as depicted from Figs. AII (33) 4 and 5. This indicates that the limited rotational capacity did not allow the wall is ultimate strength to be achieved.

Horizontal ties (links) showed a very low interaction level, as shown in Fig. AII (33) 6 and 7, whereby only 600 microstrain were recorded. This can be attributed to the fact that diagonal shear cracks did not open up and hence truss action did not develop. This also confirms the flexural behaviour of the tested model.

Hoops were extensively strain gauged at various heights in both boundary elements. The lowest hoop showed a minor confining effect confirmed by the gauge reading of only 25 microstrain, as shown in Fig. AII (33) 8. This is due to the fact that sliding shear caused the concrete at the lowest section to deteriorate, and hence hoops were not activated. Higher up, hoops were more active and showed up to 120 microstrain, as depicted from Figs. AII (33) 9, 10, 11 and 12.

5.3.5.4. Concluding remarks

From the test results described above, it may be concluded that while the model behaved in a flexural ductile manner, it failed to achieve its calculated ultimate strength. This can be attributed to the fact that sliding shear did not allow the full development of the flexural capacity. This was confirmed by the fact that the middle web reinforcement did not achieve its yield strength. If sliding shear is to be avoided, increase of the vertical reinforcement at the critical section or the use of diagonal reinforcement is recommended. Alternatively, starter bars may be added with a short length into the wall, in order to prevent such a failure mode.

Among three other models having the same reinforcement, SW33 was the only one that showed clear sliding shear. This can be attributed to the fact that SW31 and SW34 had additional flexural reinforcement interacting at later stages. Moreover, SW32 was reinforced with external U-shaped plates to enhance the confinement effect. These plates protected concrete at the lowest level from deterioration and hence prevented the model from failing in sliding shear. The above mentioned reasons have contributed to reducing the maximum crack width at the lowest section and ensuring a better resistance against sliding shear failure mode. Hence an ultimate strength of 60 kN was recorded in case of SW32, as opposed to 57 kN in the present case.

In view of the area of hysteresis loops, it may be concluded that the energy absorption capacity of an element failing in a pure flexural mode (SW9) is higher than that of an element failing in sliding shear. However, the elements failing in sliding shear showed much better energy absorption capacity than those failing in pure shear.

Since hoop strain-gauge recordings along the wall height did not reduce uniformly, it may be concluded that where cracking took place in the boundary elements, and allowed for local truss action in resisting horizontal shear. This was confirmed by strain gauge readings in the tension cycles. Hoops were also delimiting the diagonal cracks in the middle web to the area between boundary elements where they hoops were concentrated.

5.3.6. Model SW35

In order to prevent the sliding shear failure mode that was observed in SW33, SW35 was reinforced with the same flexural and shear reinforcement in addition to five starter bars penetrating 300 mm into the wall. These were 12 mm in diameter and were positioned at the middle thickness of the wall at mid spacing between the vertical bars, as shown in Fig. 4.8.

In order to simulate light damage to structural elements due to moderately-sized earthquakes, SW35 was cycled up to 14 mm MDL only, so as not to cause severe concrete degradation. Stiffness reinstatement was then targeted for the re-testing phase.

5.3.6.1 General observations

The loading programme consisted of incrementally-increasing lateral displacement cycles. Two cycles of displacement were applied at each deformation level with 2 mm increments, as shown in Fig. 5.25.

Horizontal cracks were observed at 2 mm MDL in the lower bottom third of the tested model. Closely spaced hoops (30 mm) caused the cracks to be narrow and well-distributed. At 4 mm MDL, horizontal cracks propagated throughout the wall height. At 6 mm MDL, horizontal cracks propagated into coarsely distributed inclined cracks in the web. A continuous horizontal crack was clearly noticed at 300 mm from the fixing beam, exactly at the end of the starter bars. It is obvious that the presence of the starter bars completely modified the crack pattern and the wall behaviour in general. Very few cracks were observed in the starter bar area (first 300 mm from bottom beam). They were limited in number as well as in width. Above the starter bars level, more intensive flexural cracks were observed. Their width was also larger than that of the ones below. At the end of the test, neither spalling of concrete cover nor concrete deterioration were observed. Hence, no concrete repair would be needed.

5.3.6.2 Force-displacement hysteresis

The wall reached its yield strength at about 8 mm MDL associated with 2 mm vertical extension as shown in Fig. AI (35) 1, 2 and 3. With the increase of cyclic displacements from 6 mm to 14 mm, the wall displayed a ductile behaviour while a stable resistance of

about (75 kN) was attained. An envelope of the force-displacement hysteresis is given in Fig. 5.26.

The recorded strength was somewhat higher than previous models that had identical reinforcement. This can be attributed to the effect of additional bars, which added to the flexural strength and stiffness of the model. No sliding shear was observed to take place. This was also confirmed from the hysteresis loops, since no pinching was recorded. The enclosed area within the hysteresis loops showed good energy absorption capacity which characterised the efficient ductile failure mode.

Upon cycling at the same displacement level, the model showed negligible stiffness degradation and a negligible drop in strength. When the load was reversed, the wall showed little initial resistance until the previously-opened cracks were closed. As the crack closure took place, the resistance of the wall element was gradually restored. The stiffness-displacement curve shown in Fig. 5.27 confirms the ductile model performance.

5.3.6.3 Strain gauge reading

Strain gauges at the lowest level of the wall showed that the main flexural reinforcement did not yield. The outermost bars showed only 700 microstrain as shown in plots Figs. AII (35) 1, 2 and 4. Internal bars of the boundary elements showed only 300 microstrain as shown in Fig. AII (35) 3. Same internal bars showed 5000 microstrain at quarter of the wall height i.e. at the stoppage of starter bars, as shown in Figs AII (35) 5, 6, 7 and 8. At three quarters of the wall height, recorded strains were again reduced to 800 and 1000 microstrain, as shown in Fig AII (35) 9 and 10, respectively. Vertical web reinforcement showed only 300 microstrain at the lowest level, this was confirmed from plots in Figs AII (35) 11, 12, 13 and 14.

From strain gauge recordings, it is concluded that the flexural critical section for wall reinforcement was shifted from the bottom level up to the section were the starter bars were terminated. This was confirmed by the fact that all bars showed reduced strains at the former level. They reached yield at the upper level. Strains were reduced again higher up the wall.

Horizontal ties showed little interaction, since only 100 and 250 microstrain were recorded in the second and fourth ties, respectively, as shown in Figs AII (35) 25 and 26.

Confining hoops recorded very low strains at the lower level of the walls (28 microstrain). These were increased up the wall height and reached their maximum of 90 microstrain just above the line where starter bars were terminated. This confirms that at lower sections, starter bars were acting in compression as well as in tension. When acting in compression they release the compressed concrete from high compressive stresses, and hence the confining hoops were less activated. Where these bars stopped, higher compressive stresses were carried by concrete and hence hoops had a more pronounced effect. This can be confirmed from plots shown in Figs AII (35) 15, 16, 17, 18, 19, 20, 21, 22 and 23.

5.3.6.4 Concluding remarks

To simulate damage due to a moderate magnitude earthquake, SW35 was tested up to twice the yield displacement (1.1% drift). Neither concrete deterioration nor a drop in strength was observed. The tested model proved the effectiveness of starter bars in preventing sliding failure modes. It also showed that these bars have a beneficial effect on the model strength. At the end of the test, a clear drop in stiffness was recorded (from 24kN/mm down to 6kN/mm). If such a model is to be repaired, stiffness reinstatement would be the target, since it is the only parameter that was affected by testing.

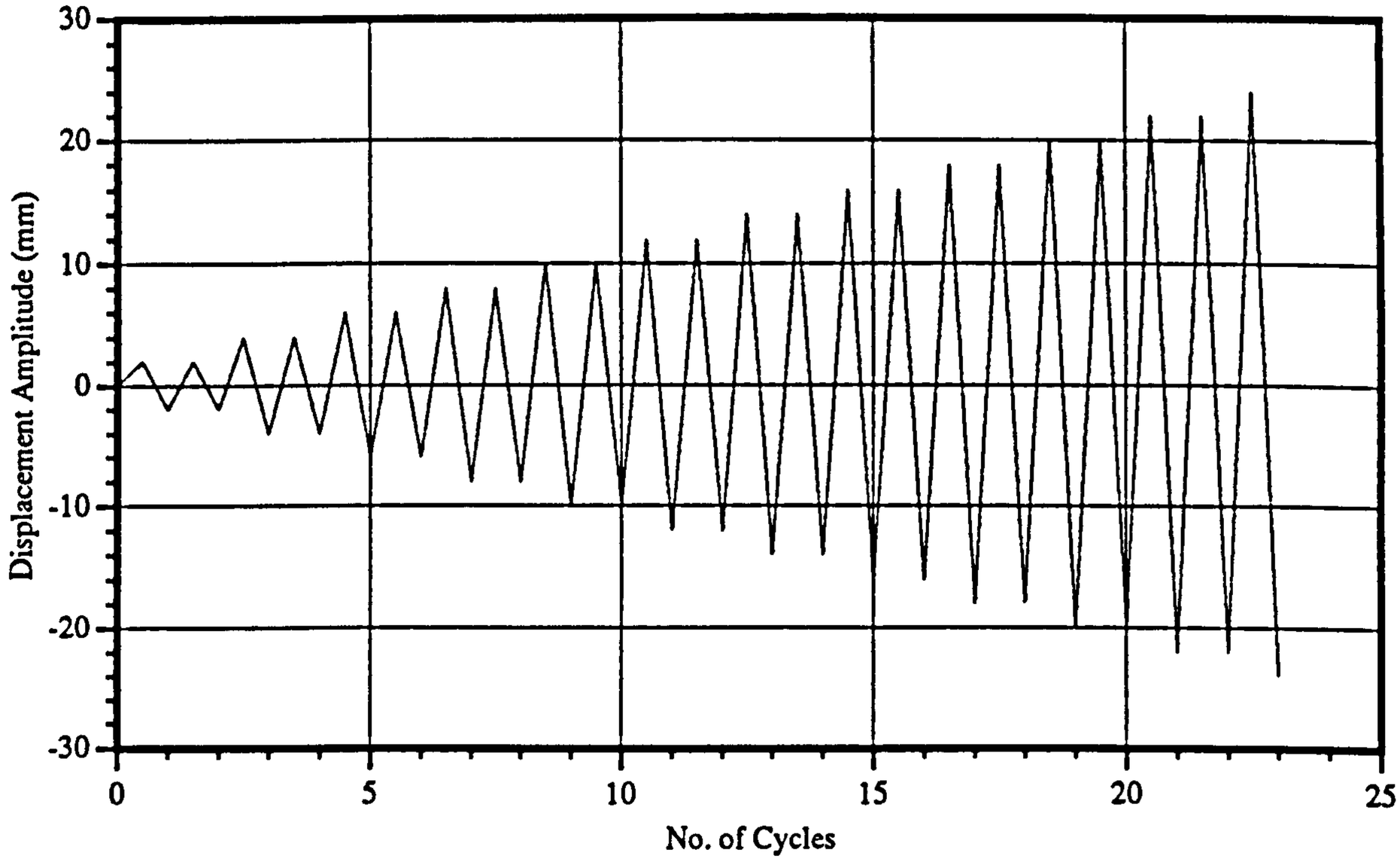


Fig. 5.1 Displacement History for SW4

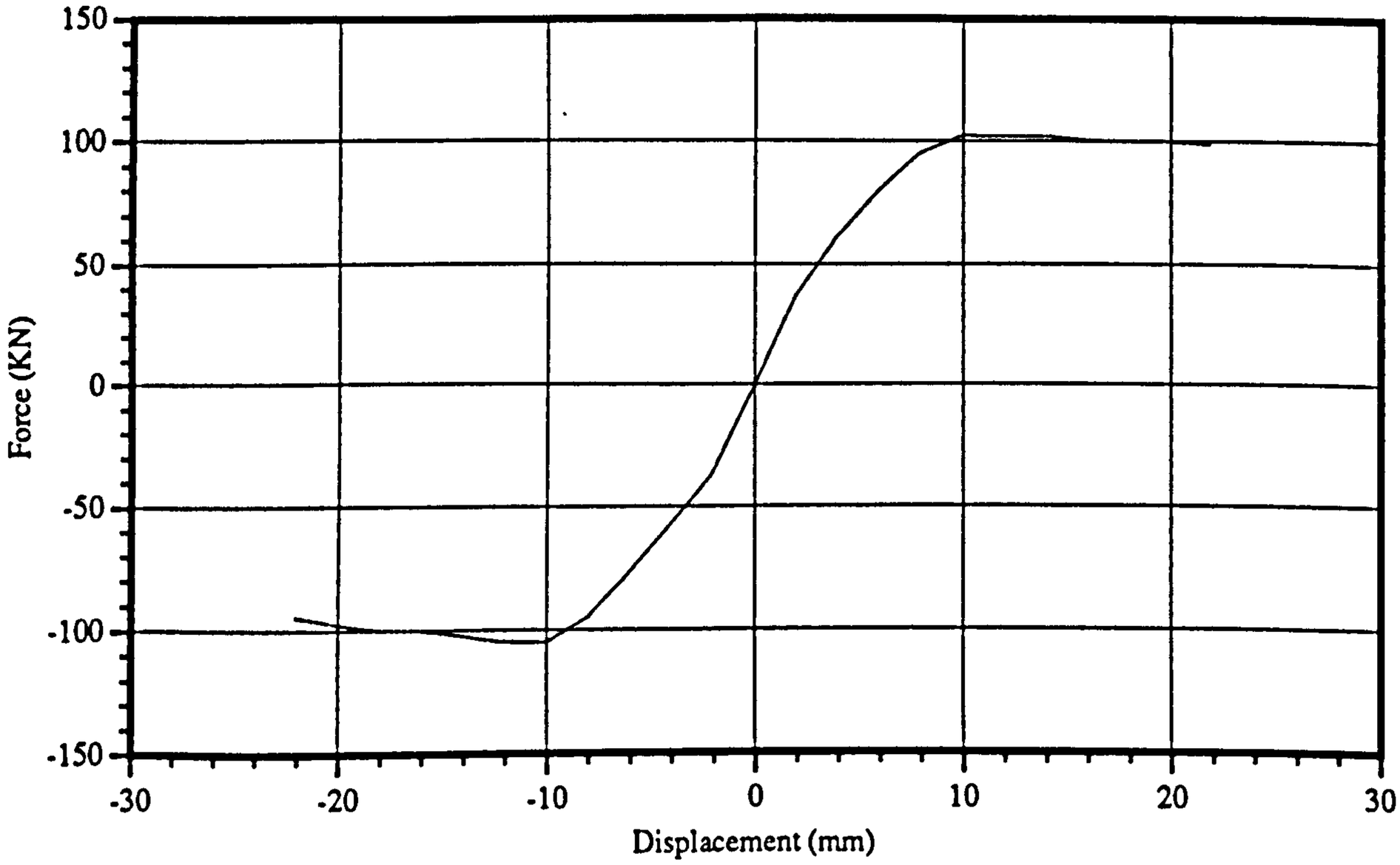


Fig. 5.2 Force-Displacement Hysteresis Envelope for SW4

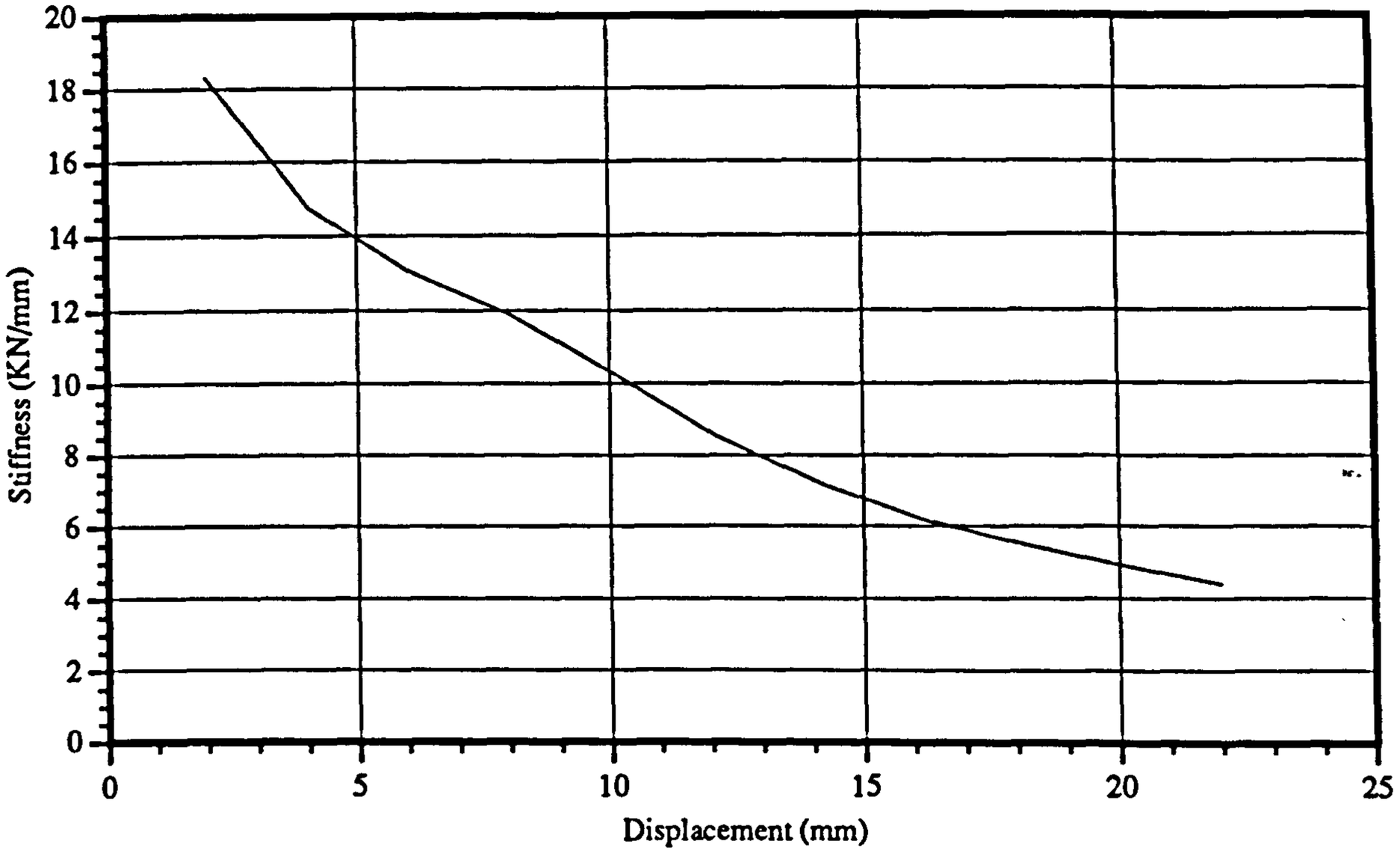


Fig. 5.3 Stiffness-Displacement Plot for SW4

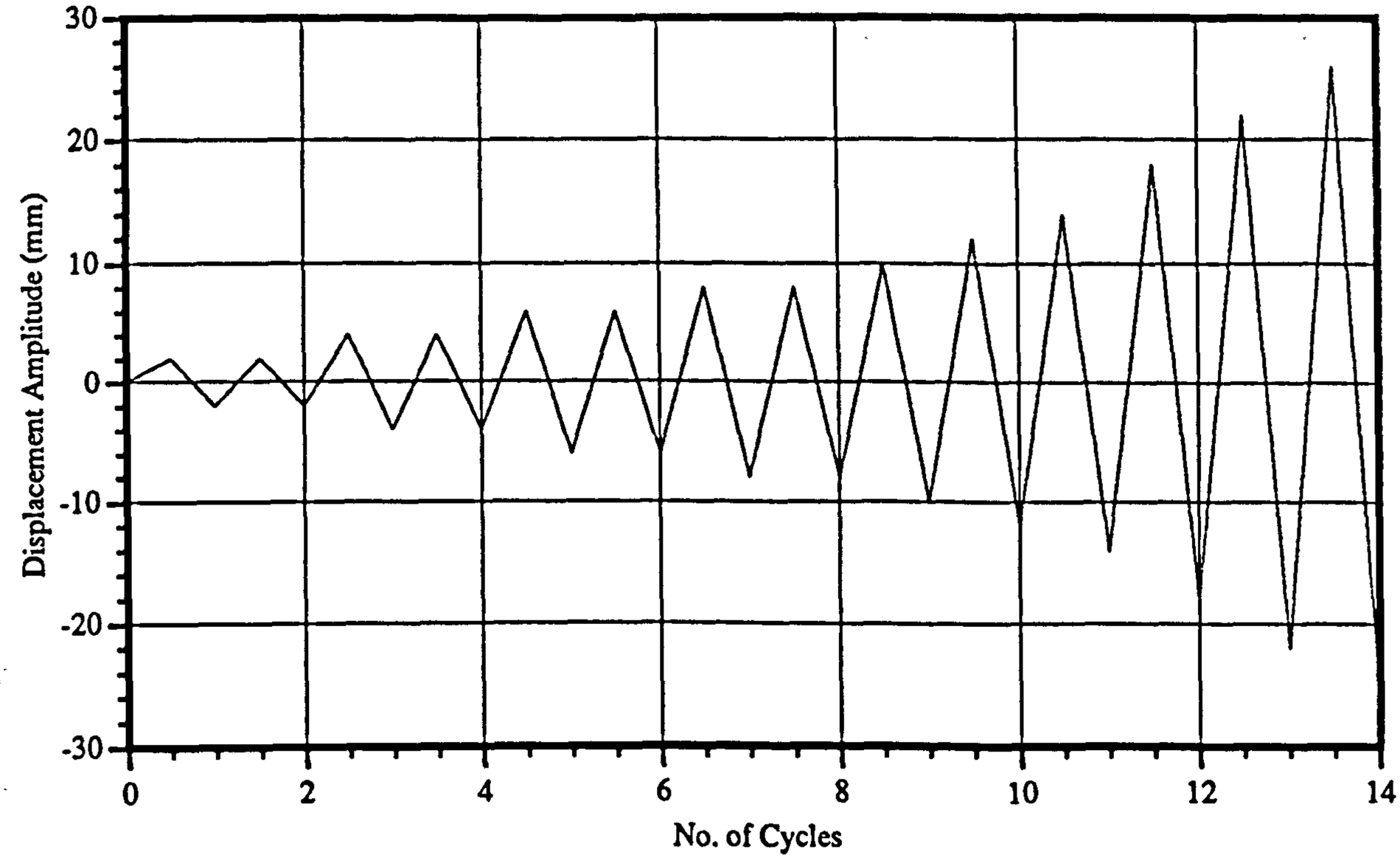


Fig. 5.4 Displacement History for SW5

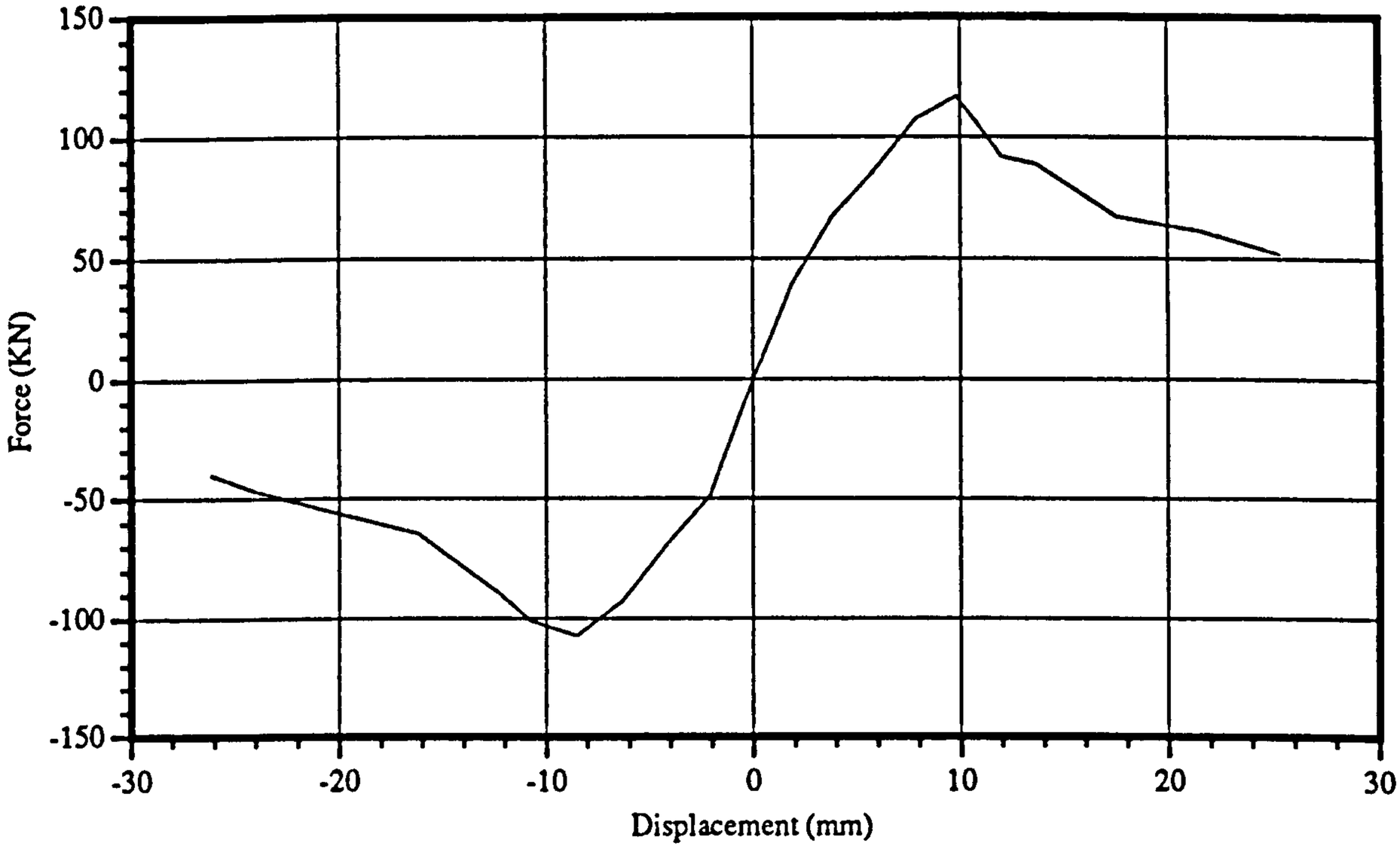


Fig. 5.5 Force-Displacement Hysteresis Envelope for SW5

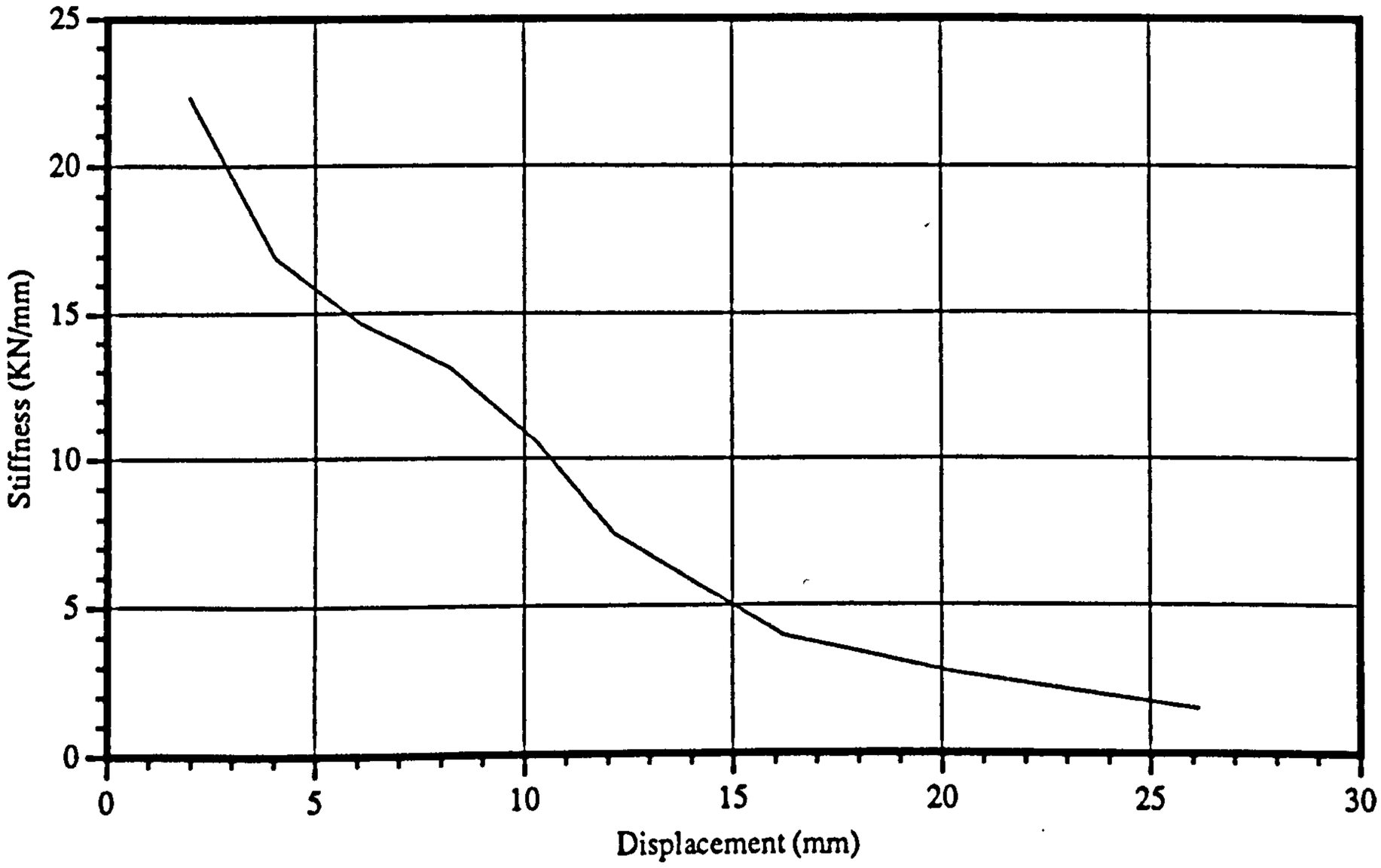


Fig. 5.6 Stiffness-Displacement Plot for SW5

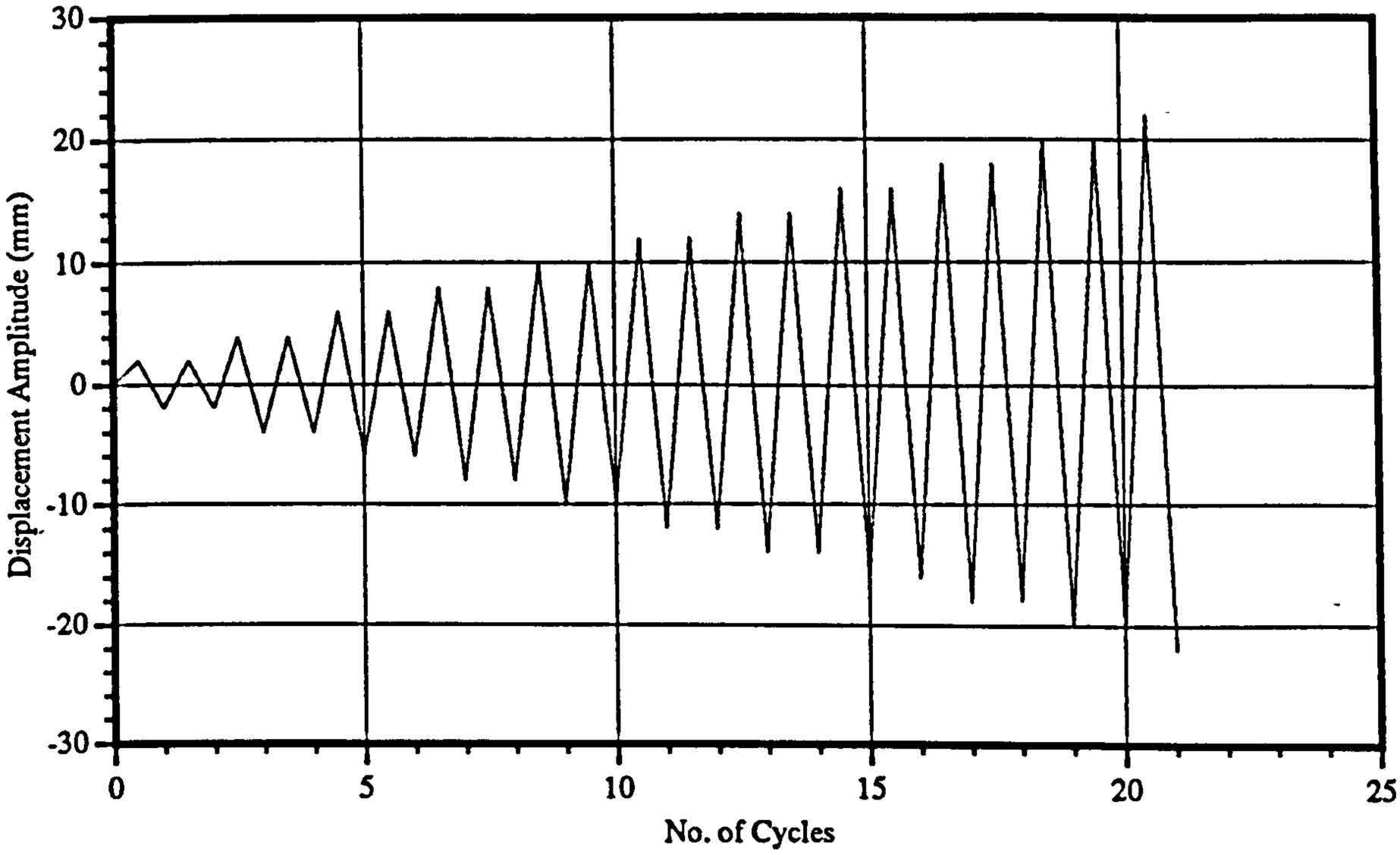


Fig. 5.7 Displacement History for SW7

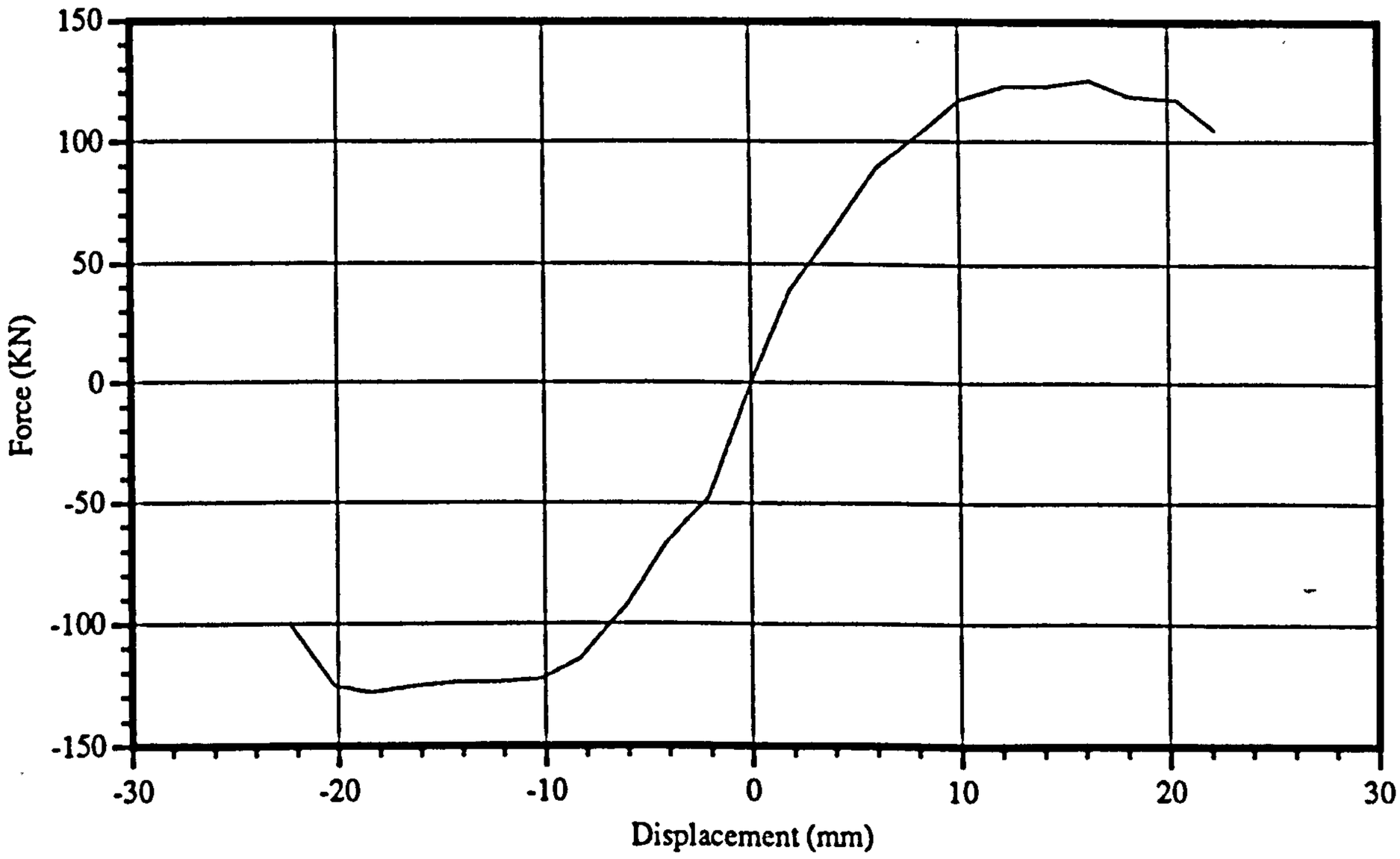


Fig. 5.8 Force-Displacement Hysteresis Envelope for SW7

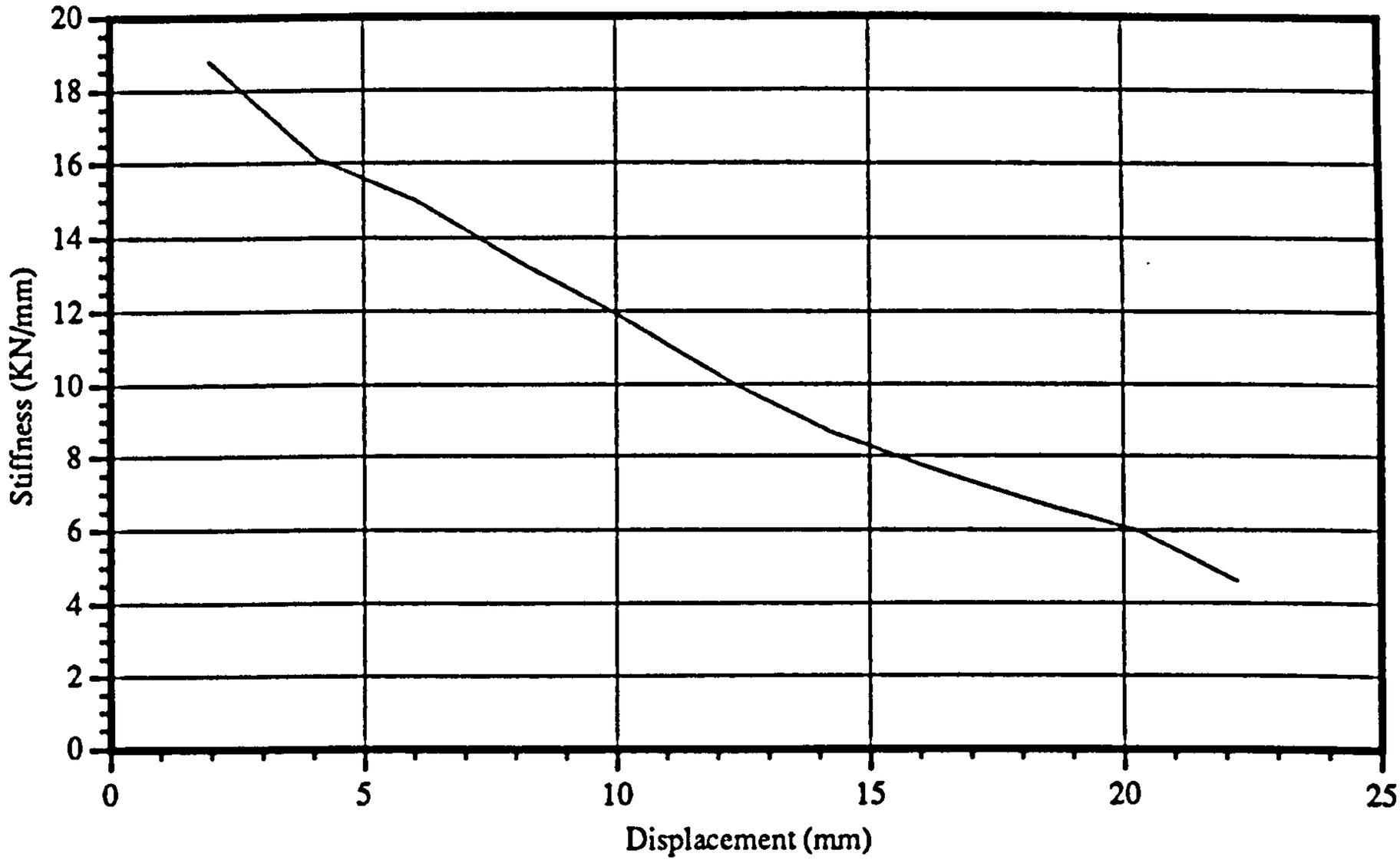


Fig. 5.9 Stiffness-Displacement plot for SW7

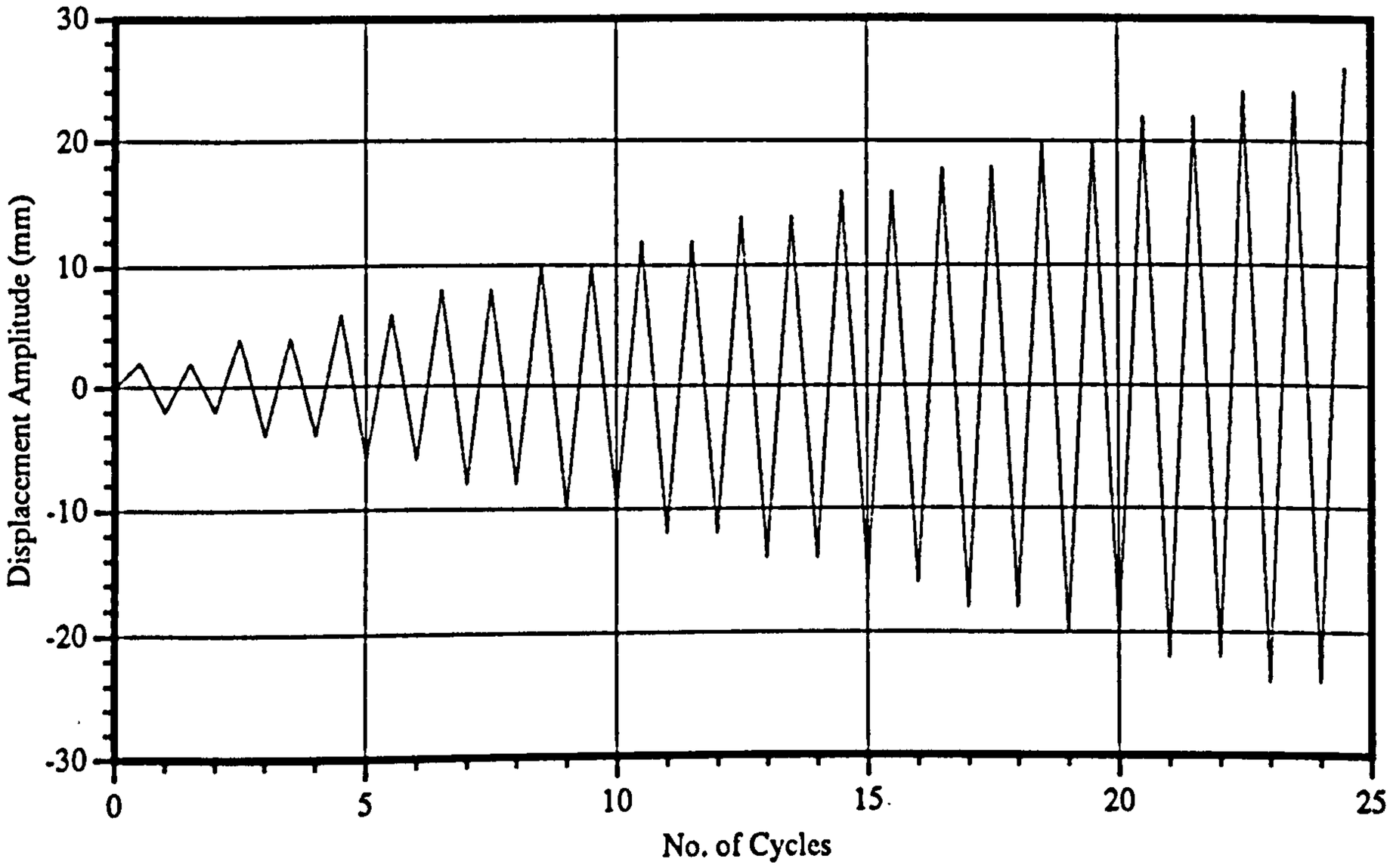


Fig. 5.10 Displacement History for SW9

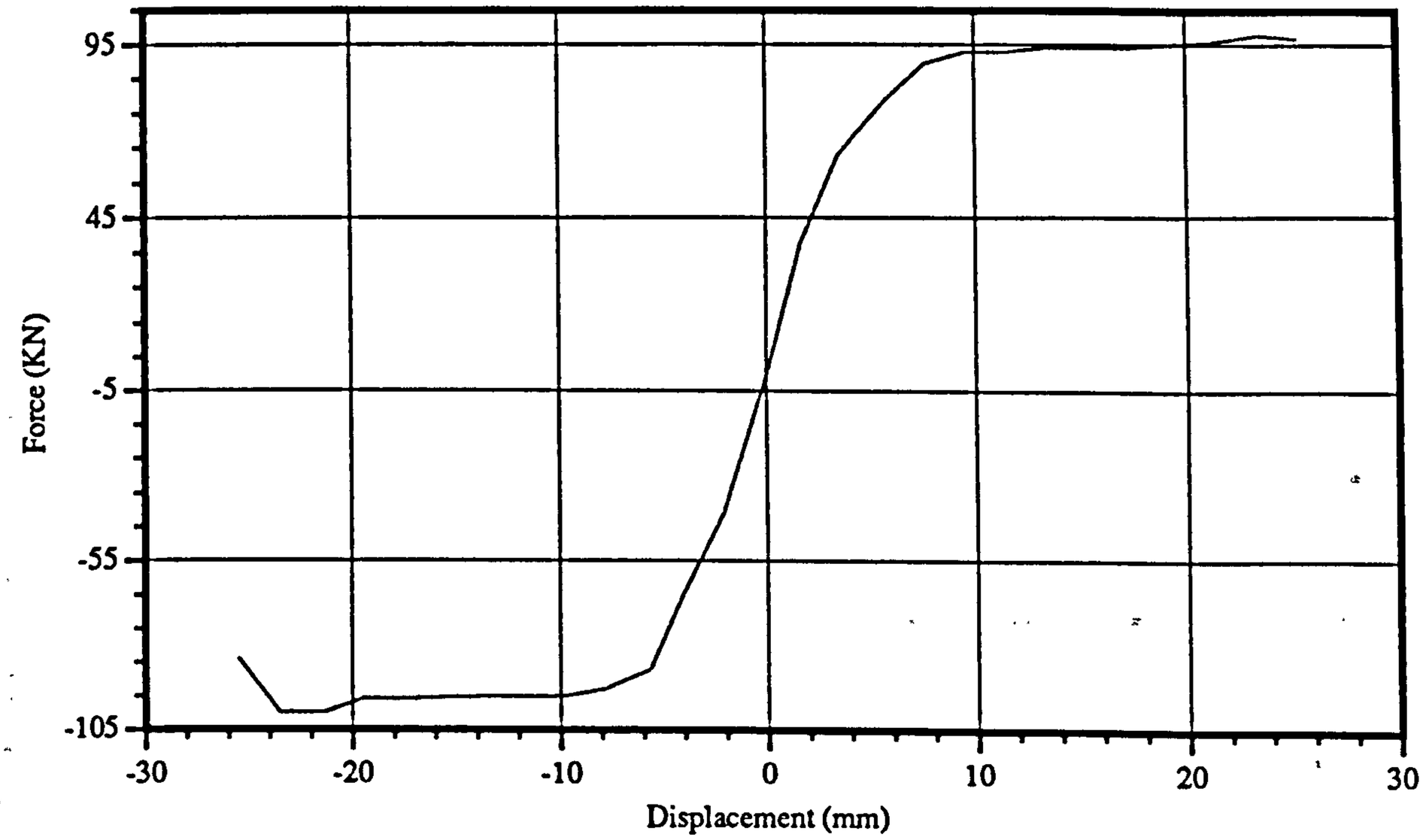


Fig. 5.11 Force-Displacement Hysteresis Envelope for SW9

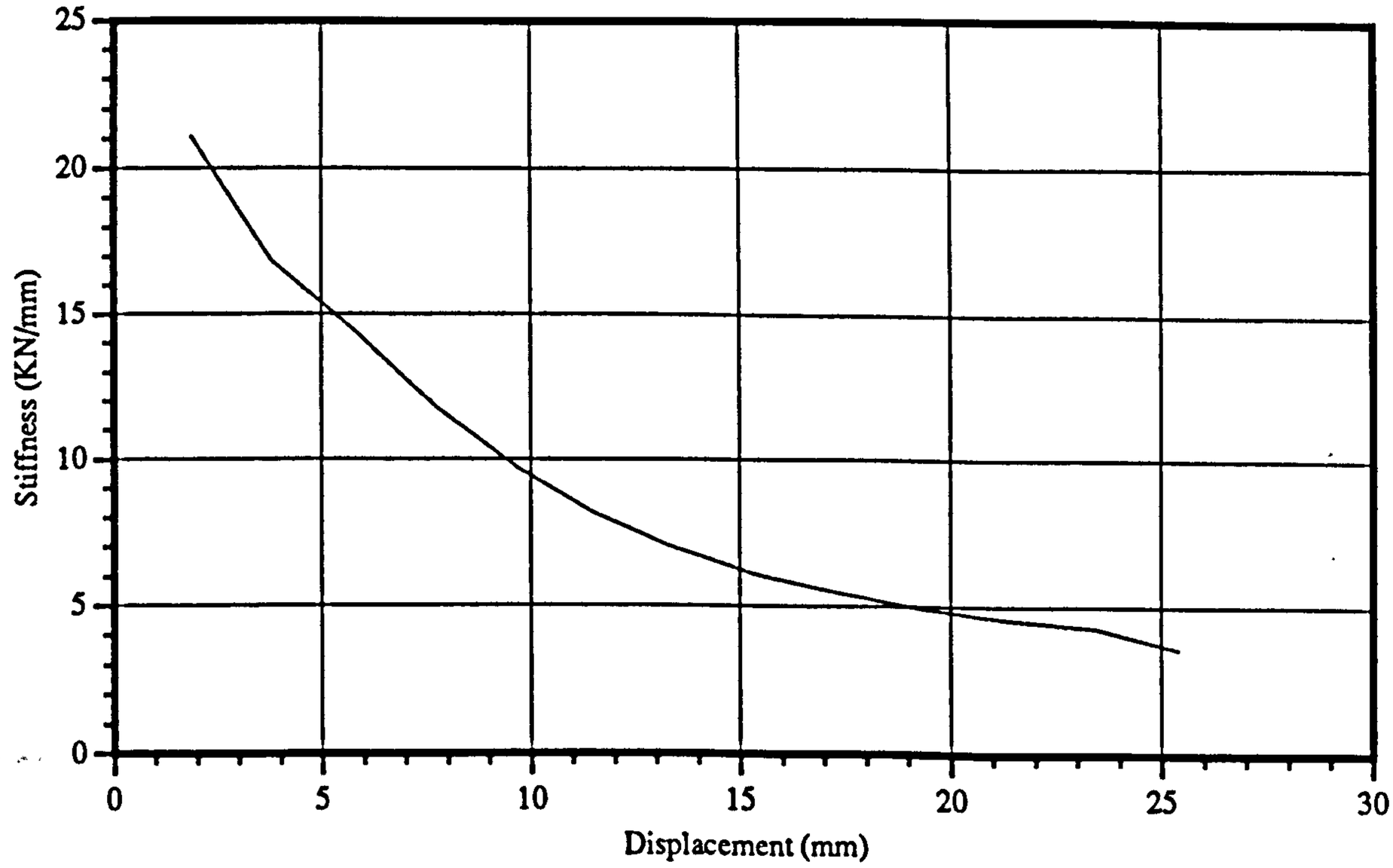


Fig. 5.12 Stiffness-Displacement Plot for SW9

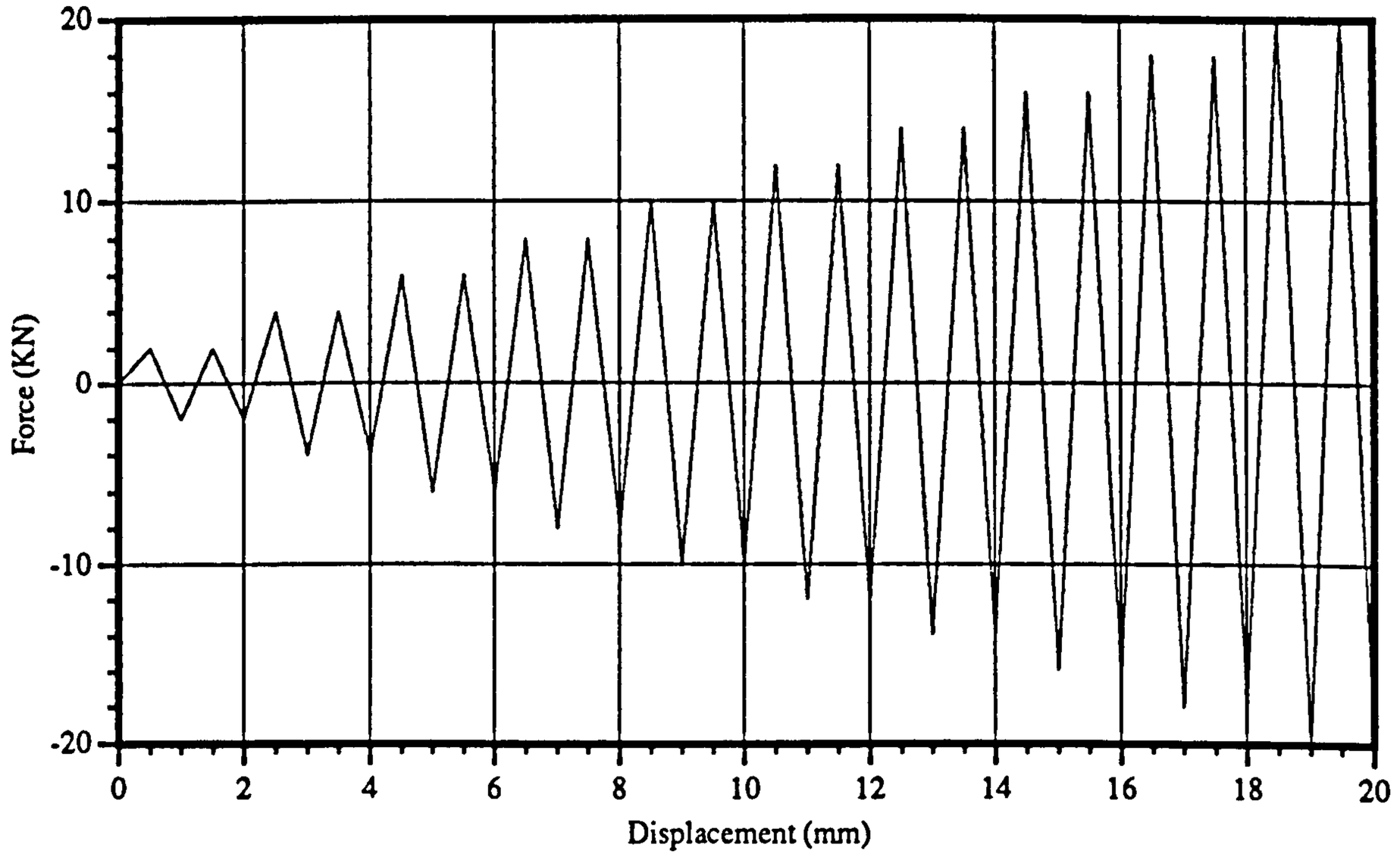


Fig. 5.13 Displacement History for SWR21

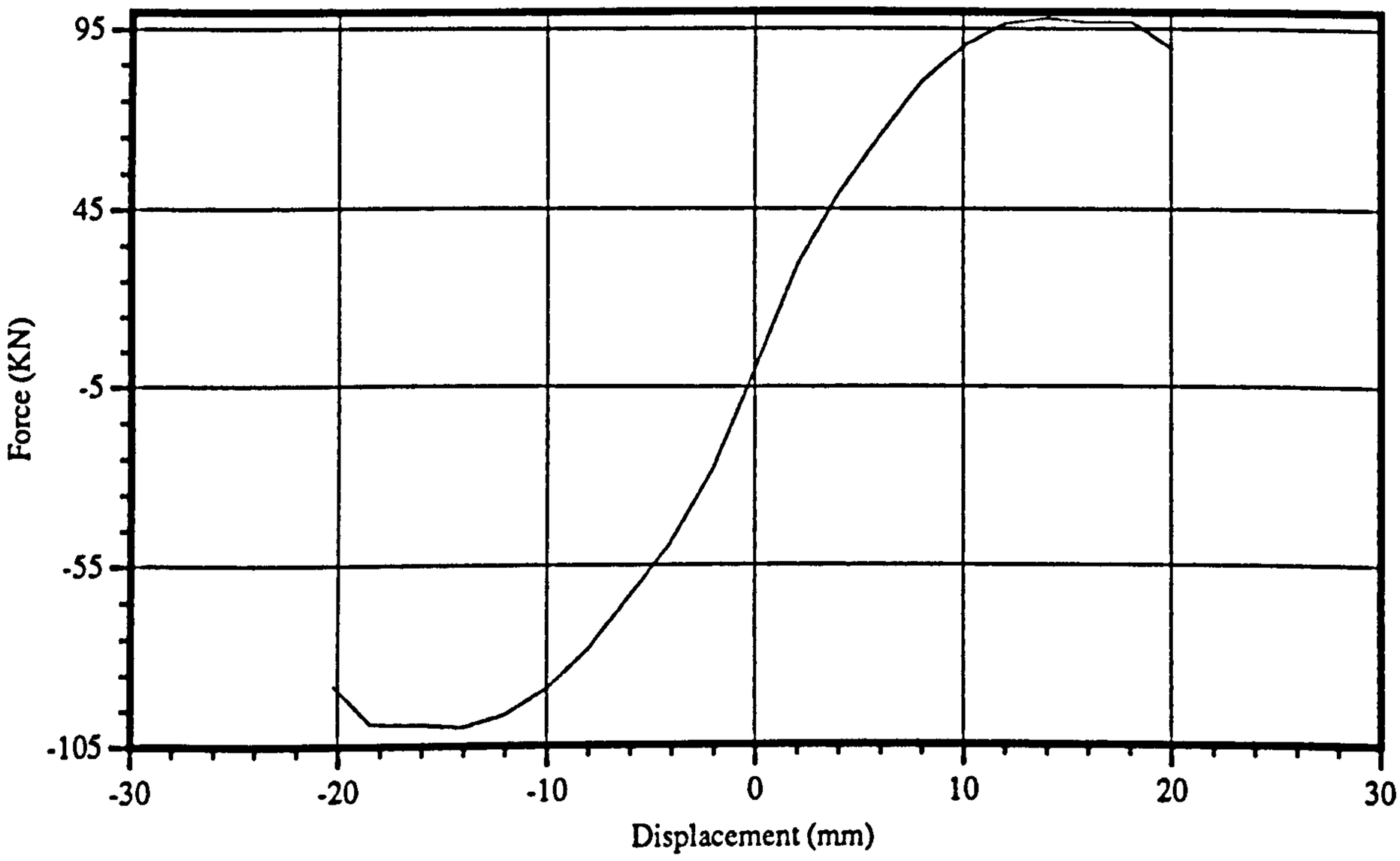


Fig. 5.14 Force-Displacement Hysteresis Envelope for SW21/SWR21

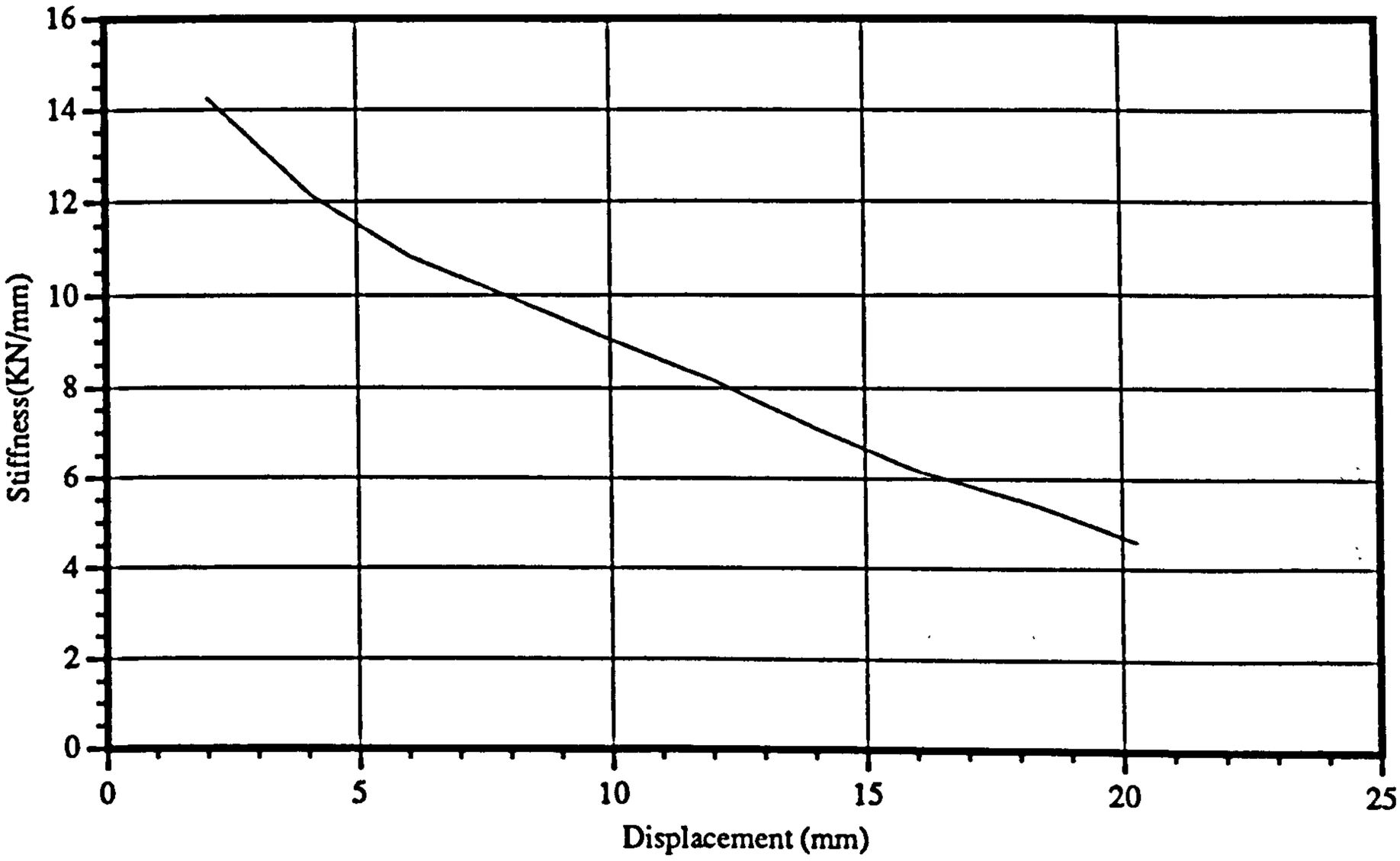


Fig. 5.15 Stiffness-Displacement Plot for SW21

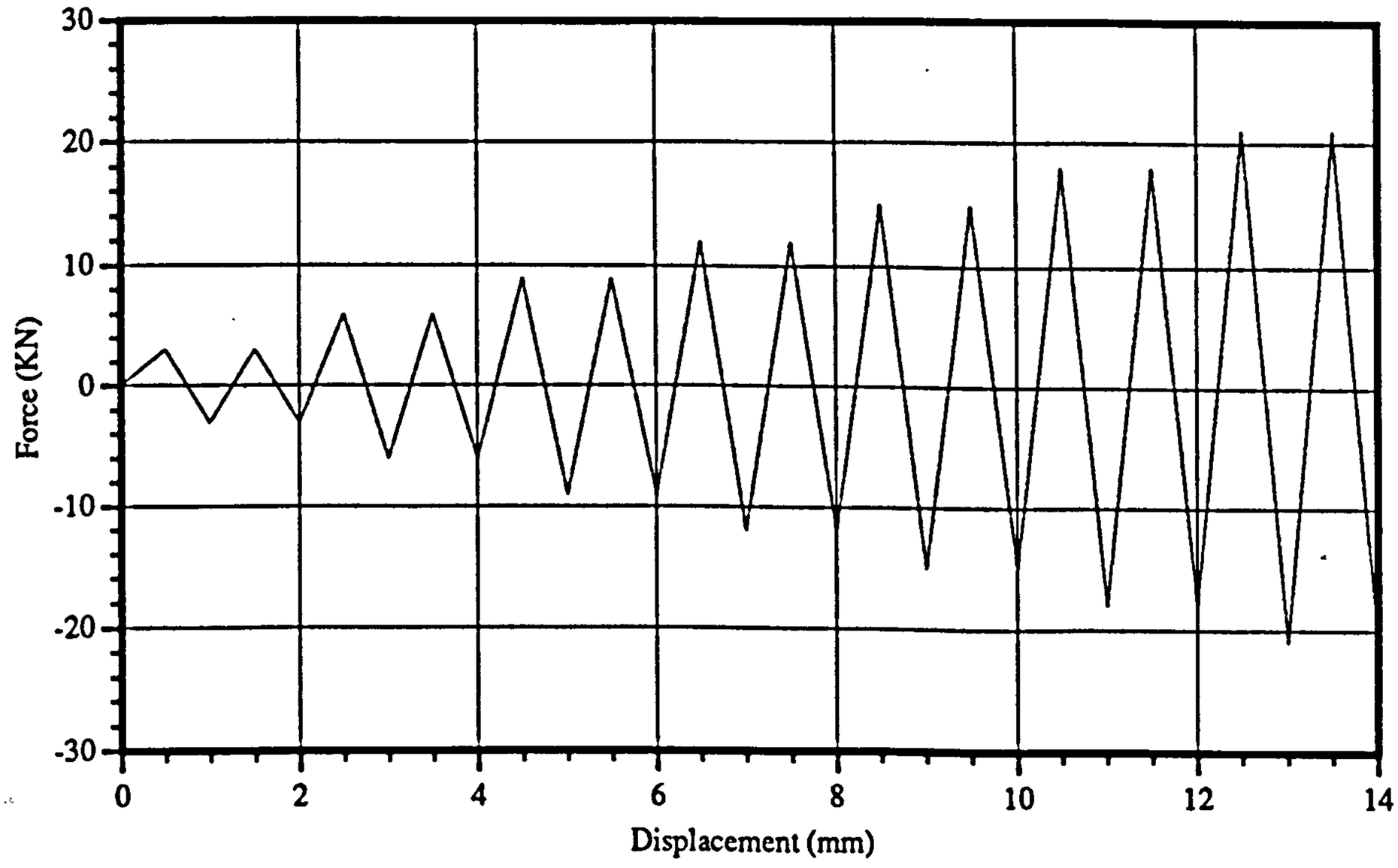


Fig. 5.16 Displacement History for SW22

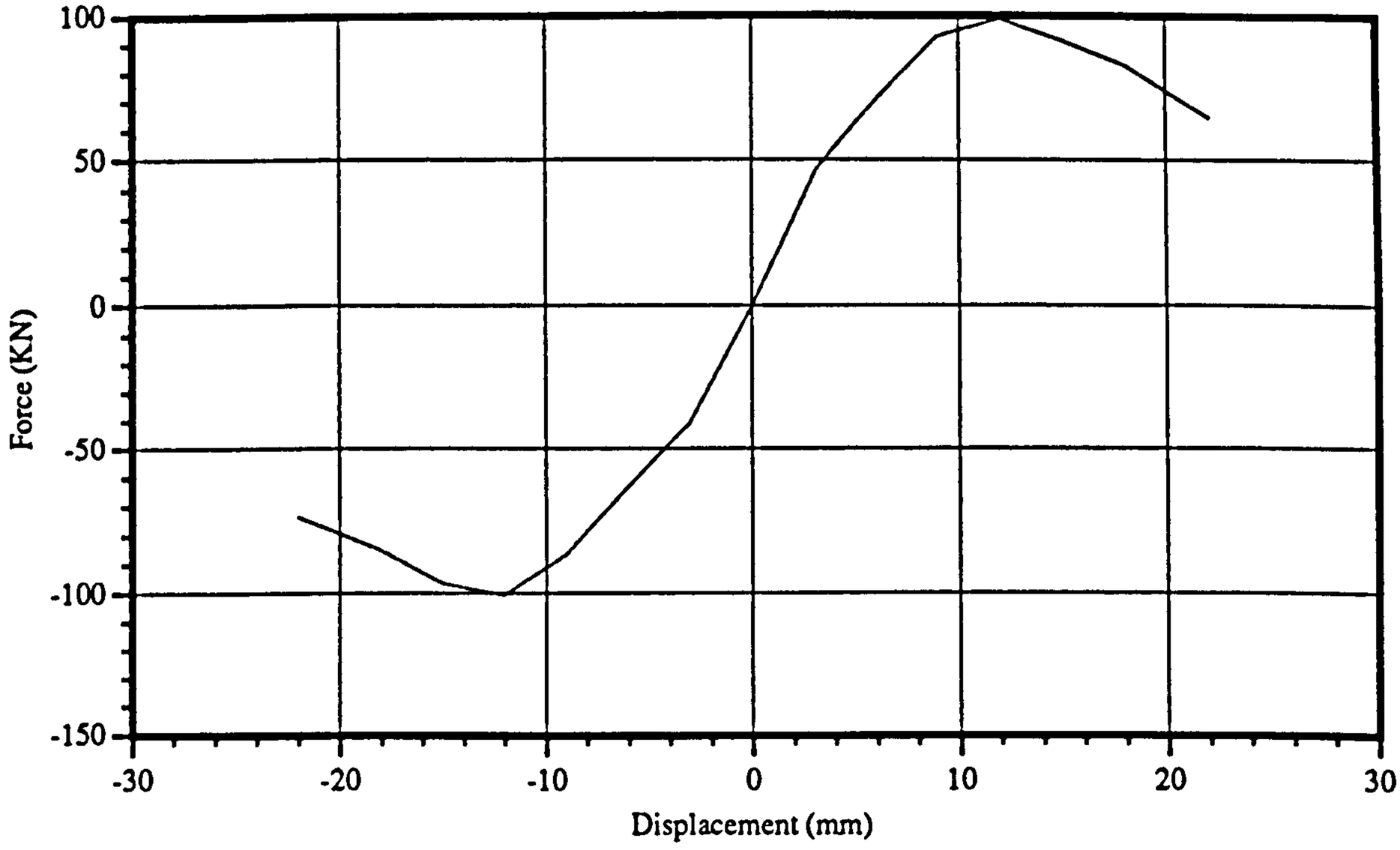


Fig. 5.17 Force-Displacement Hysteresis Envelope for SW22

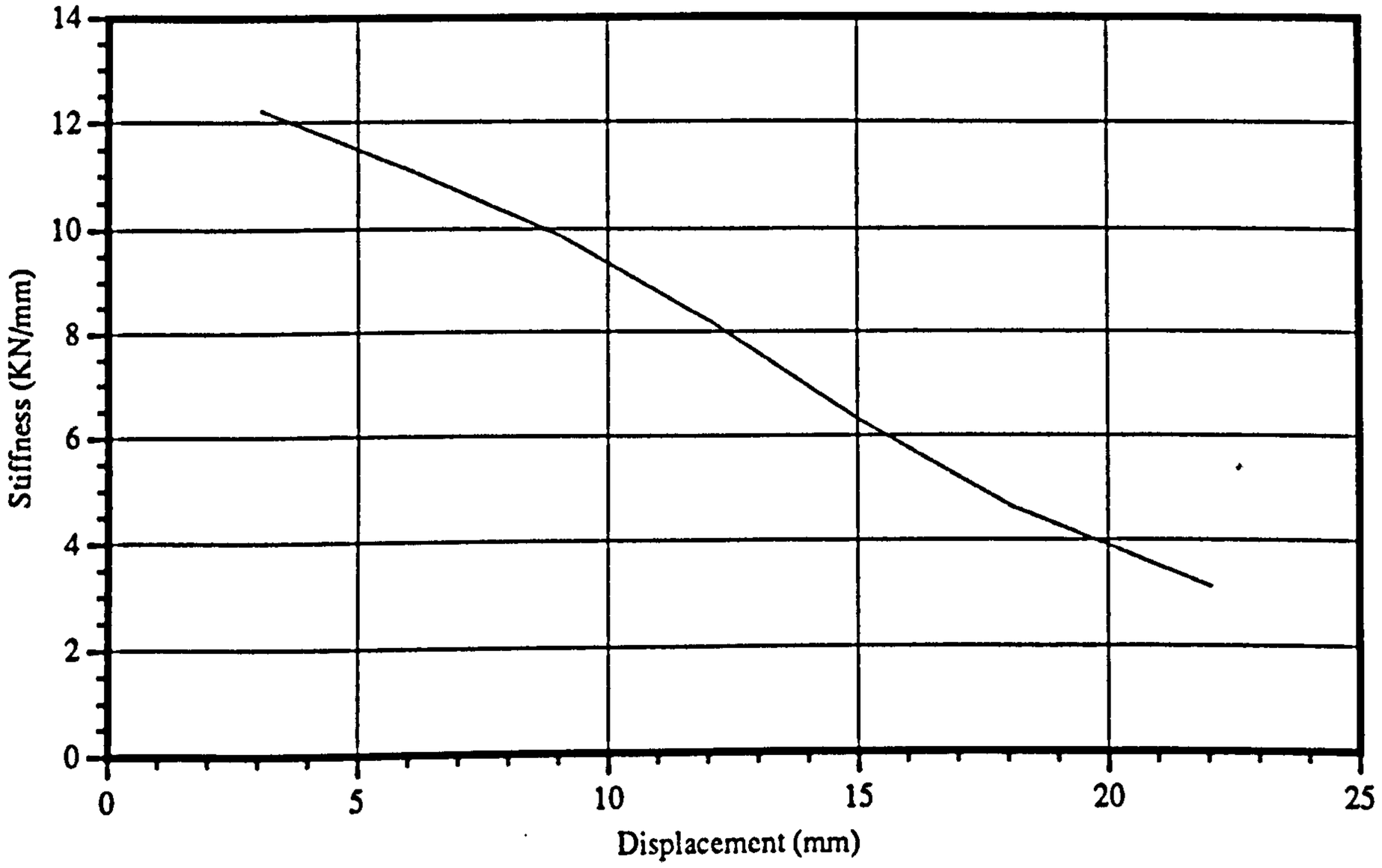


Fig. 5.18 Stiffness-Displacement Plot for SW22

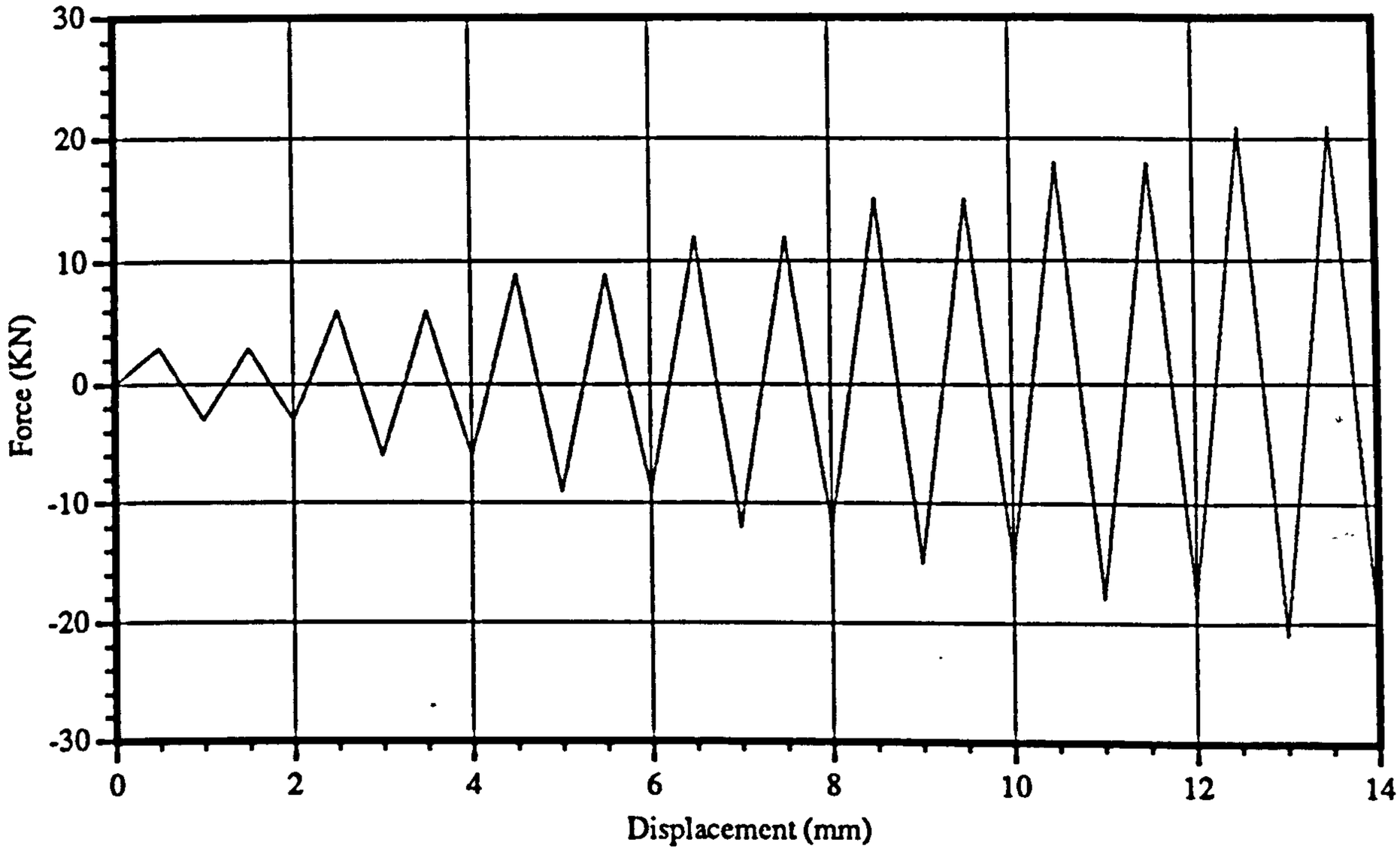


Fig. 5.19 Displacement History for SW23

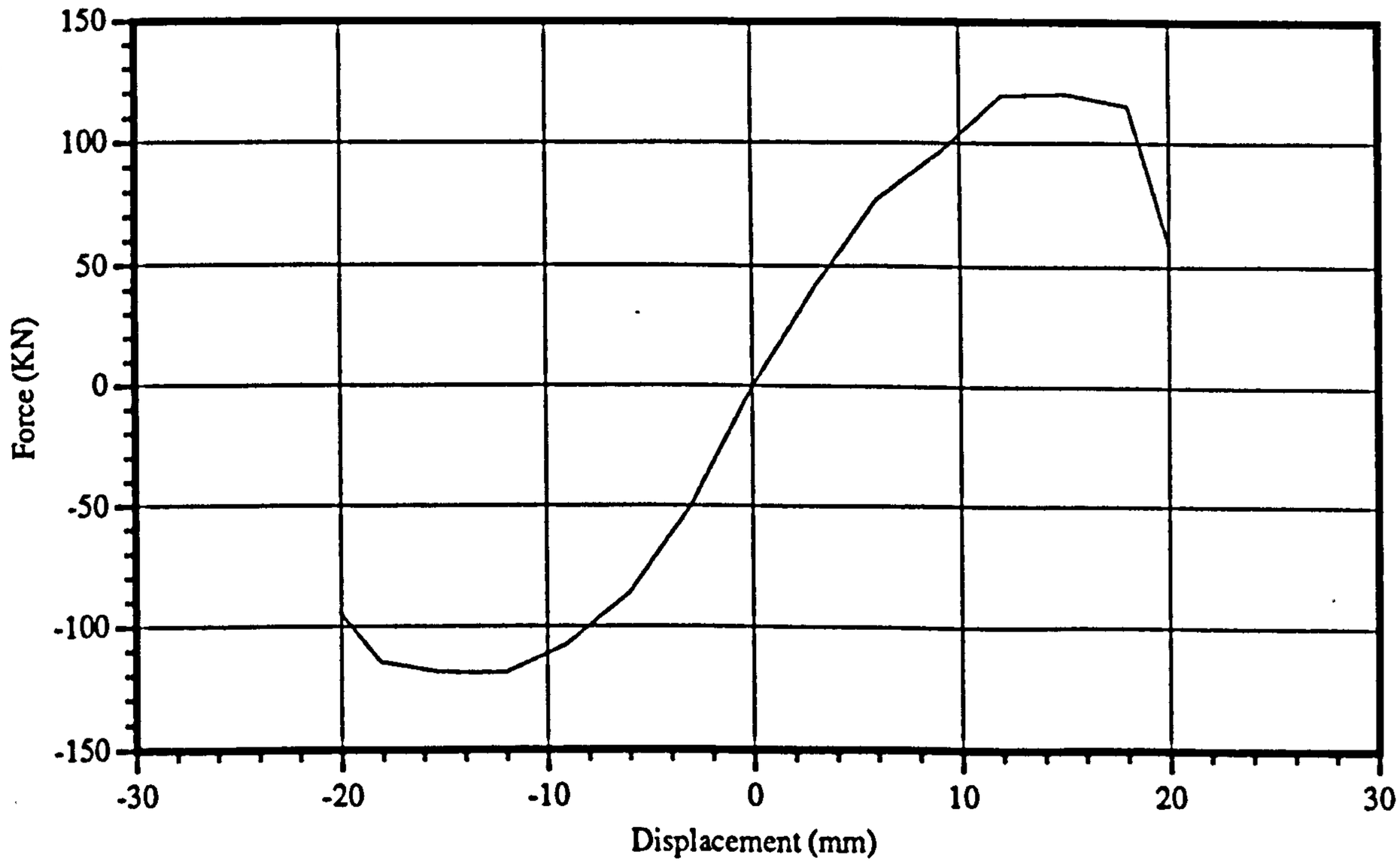


Fig. 5.20 Force-Displacement Hysteresis Envelope for SW23

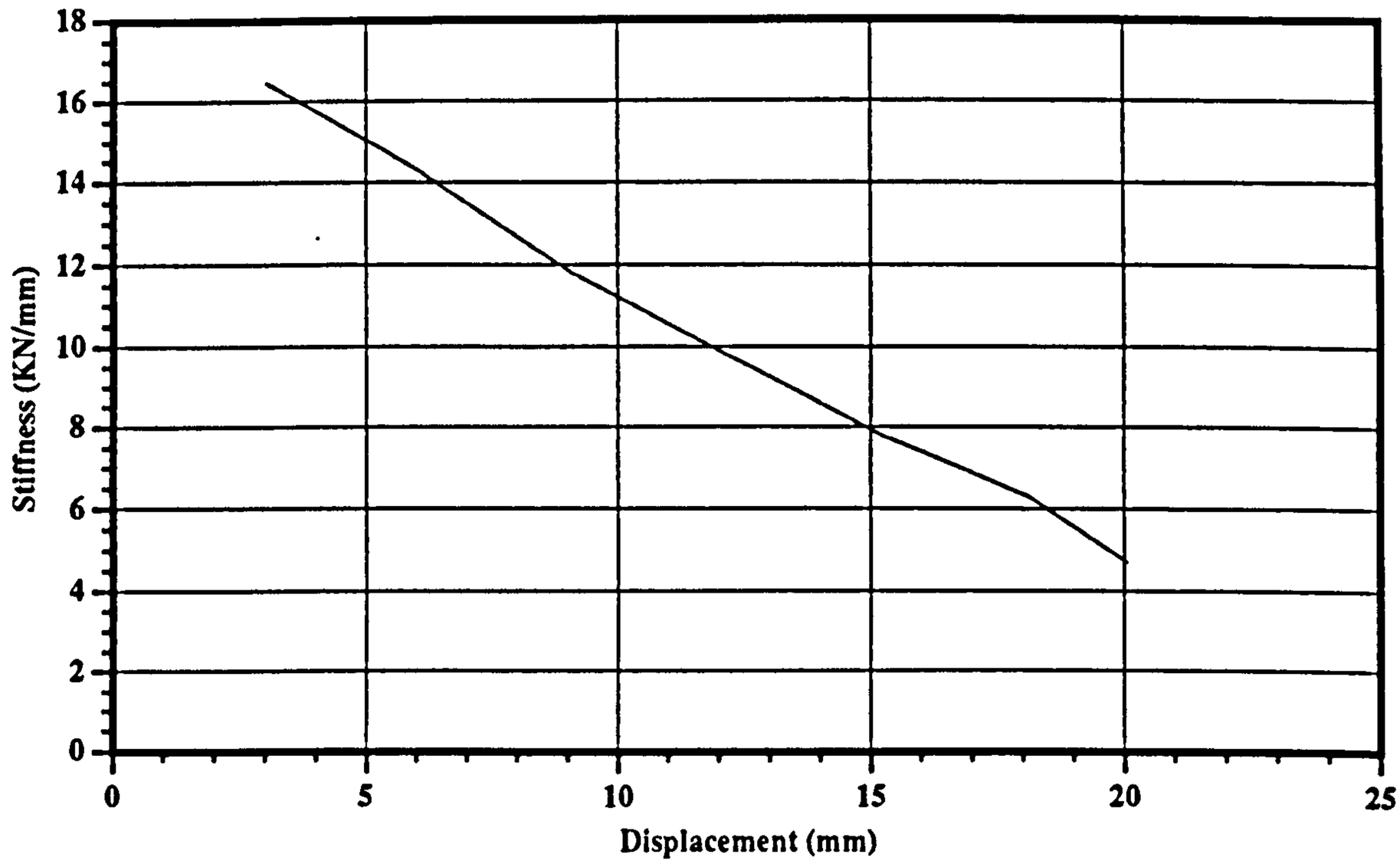


Fig. 5.21 Stiffness-Displacement Plot for SW23

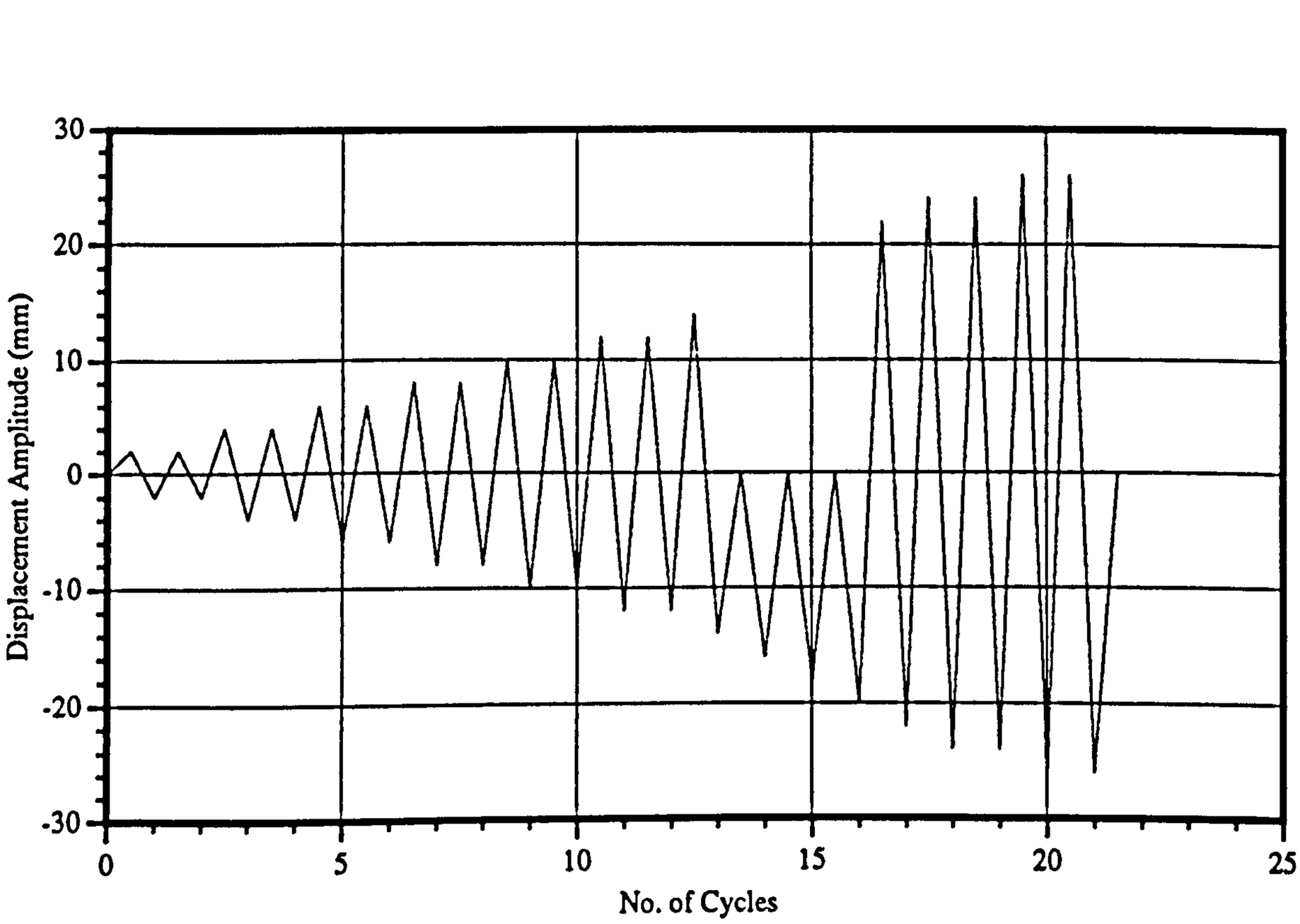


Fig. 5.22 Displacement History for SW33

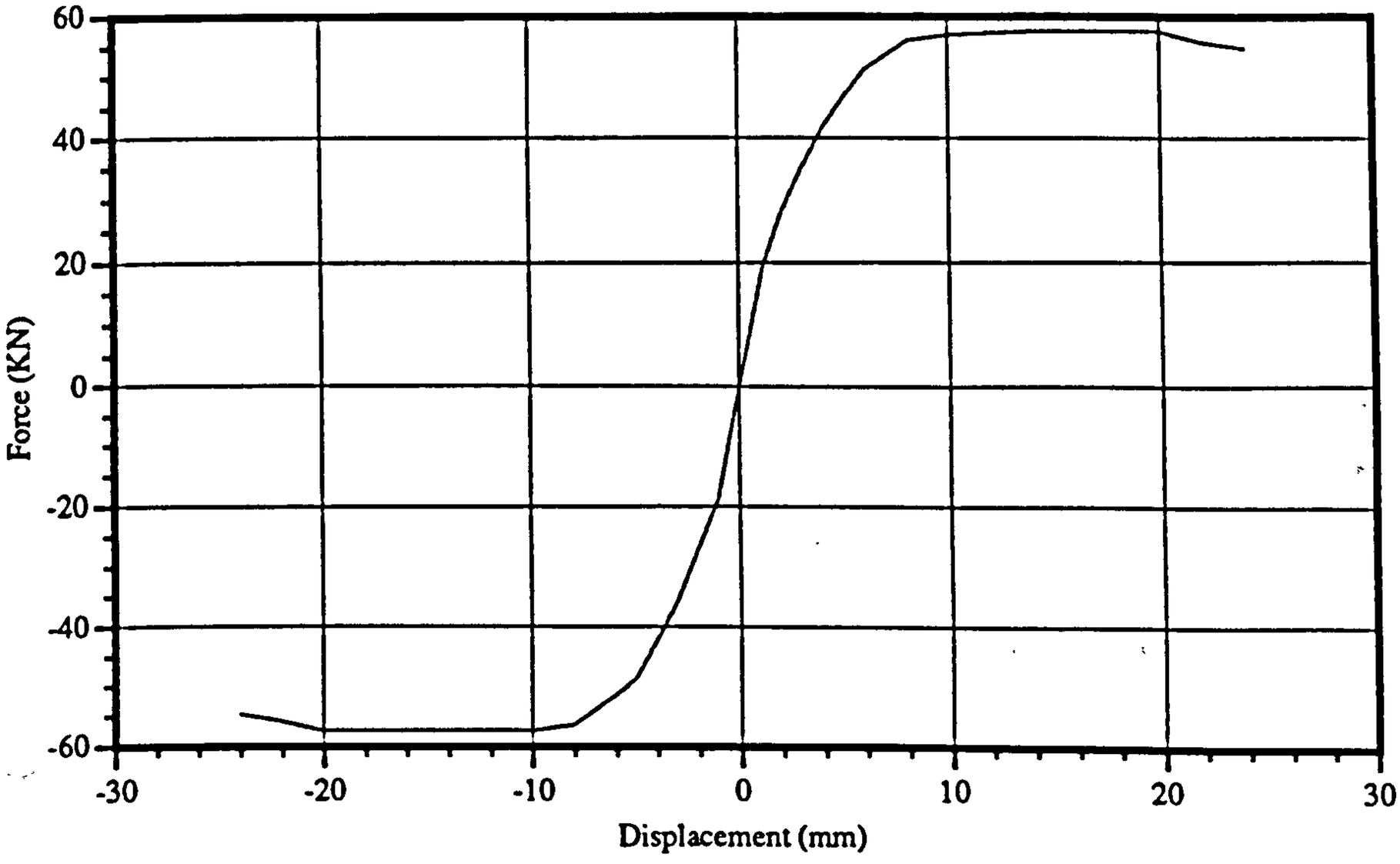


Fig. 5.23 Force-Displacement Hysteresis Envelope for SW33

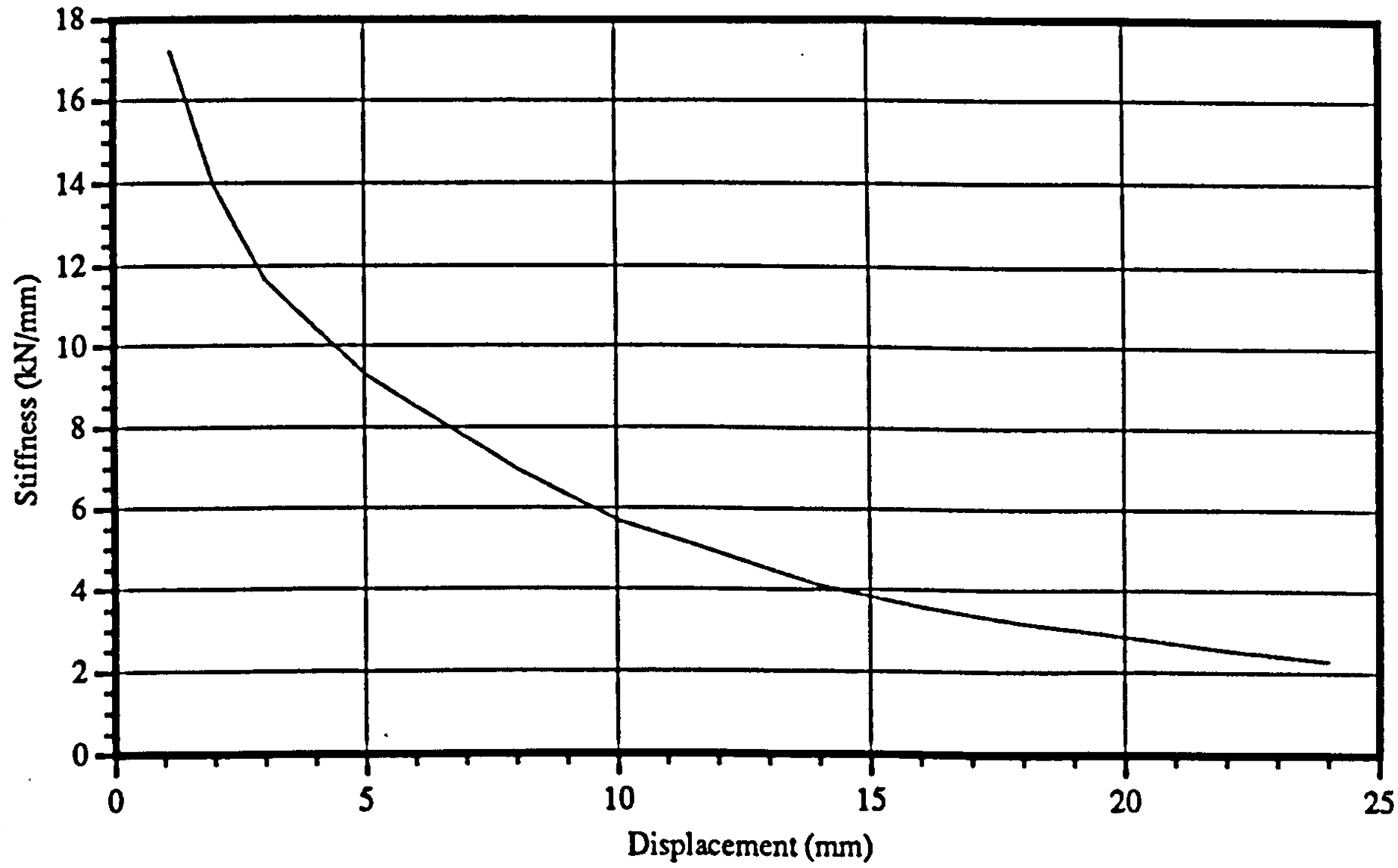


Fig. 5.24 Stiffness-Displacement Plot for SW33

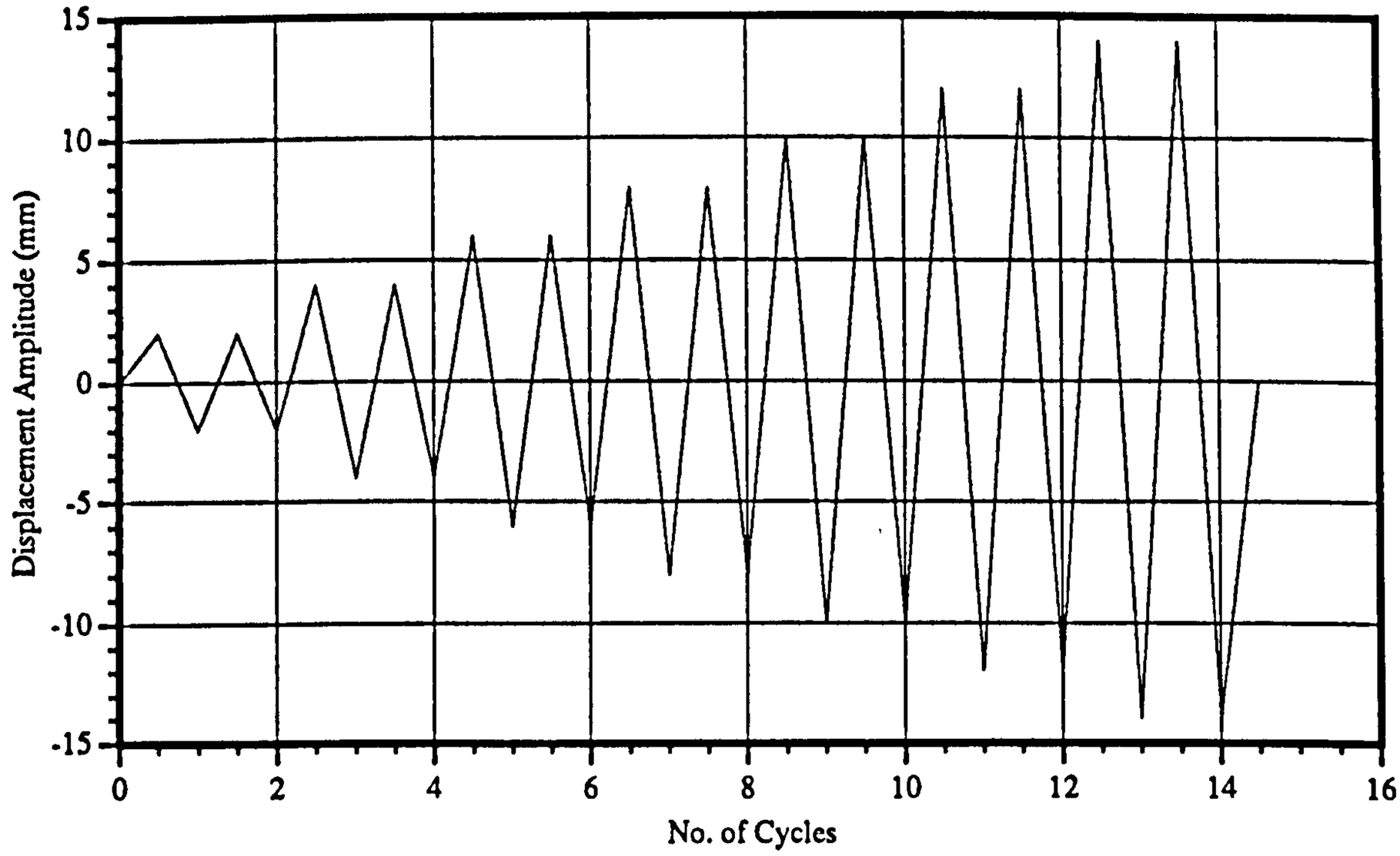


Fig. 5.25 Displacement History for SW35

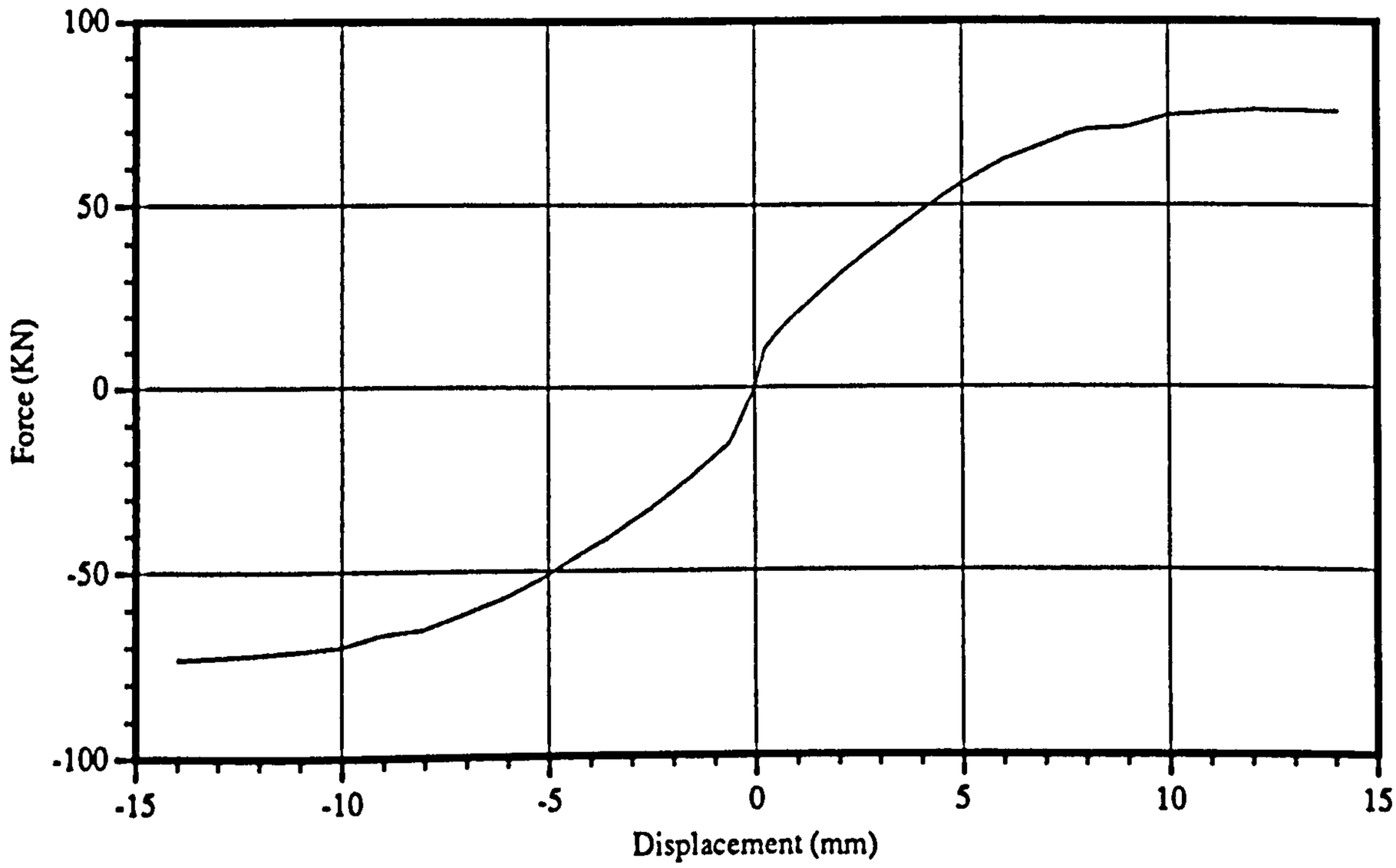


Fig. 5.26 Force-Displacement Hysteresis Envelope for SW35

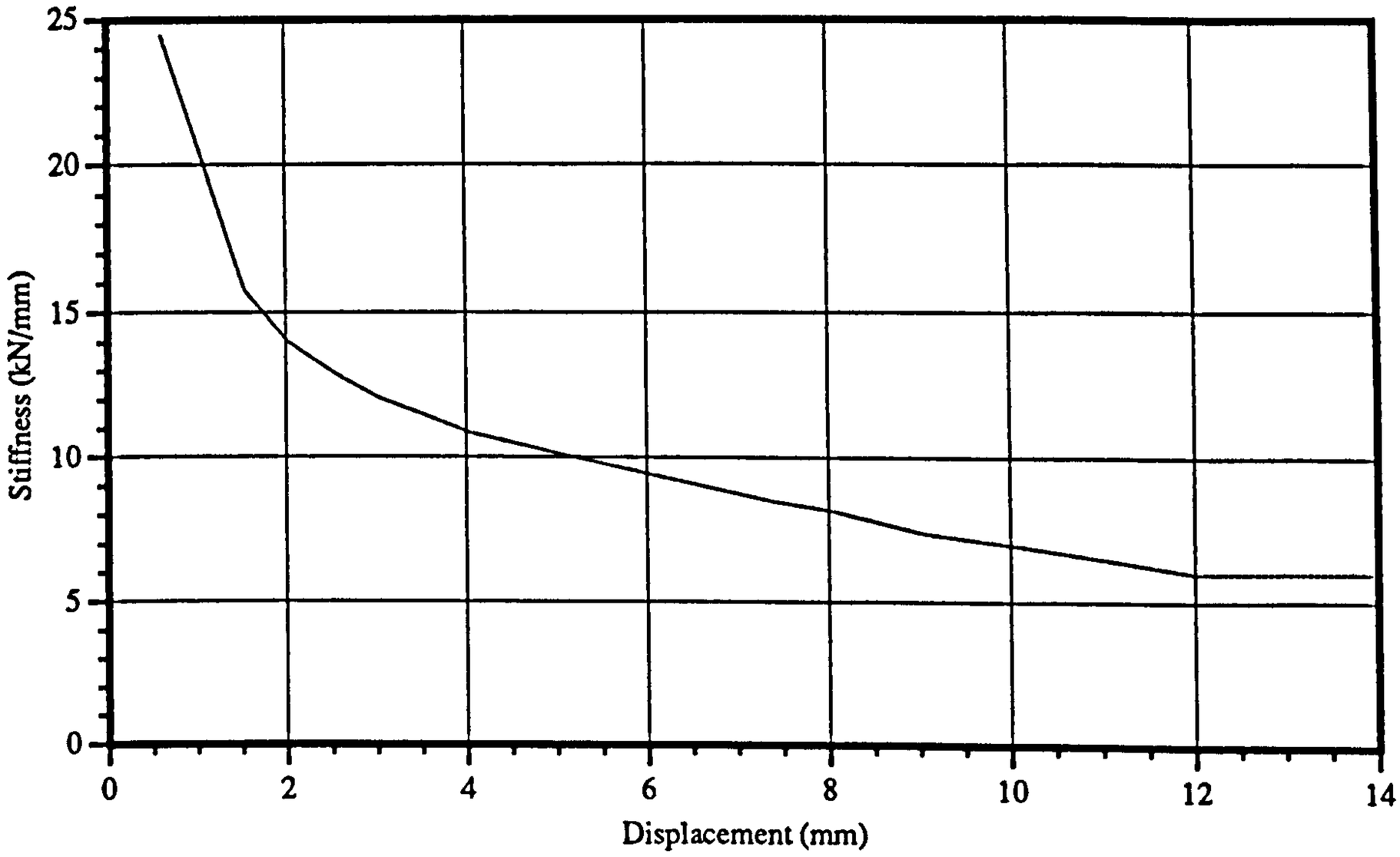


Fig. 5.27 Stiffness-Displacement Plot for SW35

CHAPTER 6

6. REPAIR PHILOSOPHY AND IMPLEMENTATION

6.1. Introduction

Seismic design using the 'capacity' approach requires a high degree of control on the response and failure mode of RC structures. To advance the design process, individual response parameters, such as stiffness and strength in shear and flexure, as well as ductility, should be appropriately assessed and controlled. In this chapter, techniques that lead to the modification of one response parameter without affecting the others are proposed, hence enabling control of the behaviour. Several practical re-design and intervention scenarios are presented and applied to RC wall models tested under cyclic loading.

The research programme entails two approaches:

- Selective Intervention to achieve stiffness, strength or ductility modification by applying one of the techniques mentioned hereafter.
- Concrete integrity re-instatement.

6.2. Selective Repair Techniques

Some novel ideas aimed at selectively affecting a single response parameter with little or no effect on other structural characteristics (Elnashai, 1992) are presented below. These ideas were applied to the previously-tested RC walls after the concrete repair, and to newly designed and constructed walls. These models were retested under cyclic loading and the test results are presented in Chapter 7.

6.2.1. Strength-only intervention

6.2.1.1. Flexural strength

Two schemes were designed and tested, involving the use of additional steel bars or plates, in conjunction with a delay mechanism, to increase the strength without affecting

the stiffness. In the first scheme shown in Fig. 6.1, steel bars are added and a mechanical coupler is used to adjust the tolerance in displacement beyond which the bars take part in the load-carrying process. In the second scheme, shown in Fig 6.2, steel plates are attached to the wall sides by means of Chemical bolts, where the bolts can travel within a groove (slotted hole) before bearing on the steel plate, thus contributing to the flexural capacity of the member. The former scheme was applied to wall SW31, for which test results are presented in section 7.2.8. The latter scheme was applied to wall SW34, for which test results are presented in section 7.2.10.

In practical situations, several other alternatives exist, such as the insertion of steel bars within a plastic duct, with a bar length longer than the distance between the top and bottom slabs. The above schemes are practical, since they are, at worst, as cumbersome as existing jacketing techniques.

6.2.1.2. Shear strength

Two schemes were designed and tested where additional steel plates were glued to the wall using high strength epoxy. In the first scheme, shown in Fig 6.3, wall cracks were not injected, in order to investigate the effect of the steel plates only. This repair procedure was applied to wall SWR21 and test results are shown in section 7.2.5. In the second scheme, the cracks were injected before the application of the horizontal steel plates. This was applied to SWR24 and test results are presented in section 7.2.7.

6.2.2. Stiffness-only intervention

According to the damage level after an earthquake, an increase in stiffness without an increase in strength may be required. This can be effected by one of the two techniques shown in Fig. 6.4 and Fig. 6.5 respectively, amongst others.

The scheme in Fig. 6.5 comprises the addition of closed hoops in the vertical plane spanning the heavily cracked zone (flexural plastic hinge). The hoops are not attached to the foundation beam, hence they do not contribute to the strength of the critical section. The number and location of the vertical hoops dictates the level of stiffness increase.

In the second proposed scheme, shown in Fig. 6.4, a steel plate is glued to the area affected by cracks using epoxy mortars. The plate is attached neither to the loading

nor to the foundation beams, and hence provides no continuous load-transfer mechanism. The location, thickness and width of the steel plate dictates the level of stiffness increase imposed on the RC member, hence control over this response parameter can be exercised.

6.2.3. Ductility-only intervention

This is the simplest application of the selective intervention approach. A hypothetical structural member is deemed satisfactory for both stiffness and strength criteria, but is required to demonstrate extra ductility in order to increase the global behaviour factor. Here, additional stirrups may be added by drilling through the member. Alternatively, steel U-shaped plates may be bolted to the area where additional ductility is required, as shown in Fig. 6.6 and Fig. 6.7 respectively.

To ensure effective interaction between the confining plates and the RC wall, epoxy resin injection was applied between the two surfaces. Also, a high-strength friction grip bolt was used to ensure effective confinement on the open side of the U-shaped steel plate. The application of an initial prestressing force through this bolt by means of a torque control wrench creates an active confinement and hence improves the achieved ductility level.

The application of such techniques will have no effect on the stiffness and strength of the member, since it only affects the confined compressive strength of the concrete. (It is established that the effect of concrete confinement on flexural strength is minimal, especially for low levels of axial load). The use of discontinuous U-shaped profiles is intended to minimize their effect on the stiffness.

6.3. Concrete Integrity Re-instatement

In order to achieve the best performance for the re-instated walls, damaged concrete should be repaired using one or more of the following methods with the object of having concrete performance comparable with the intact state.

6.3.1. Concrete injection

Visible concrete cracks were injected using low viscosity epoxy resin grout following the procedures mentioned in section 2.1.1. Since the epoxy grout cannot penetrate crack

widths less than 0.05 mm, emulsion grout was applied to cracks of width 0.01-0.05 mm. A crack width less than 0.1 mm cannot normally be observed unless crack width lenses are used (FIP, 1991). Such a limitation in repair technology is acceptable, since the basic theory of RC structures is that of cracked materials, even under service loads. Shear wall surfaces were painted with an emulsion paint that penetrated the micro-cracks by capillary action in order to minimize the cracking effect and to ensure a reasonable protection for steel against rusting (CEB, 1985).

6.3.2. Replacement of damaged concrete

Shear walls are primarily horizontal load carrying members. Nevertheless, they carry vertical load due to their own weight and the floor area served, mobilizing 20-30% of the normal strength. Also, under cyclic loading, the wall height increases due to alternating plasticity, thus increasing the axial load. In order to be as practical as possible, concrete replacement should be reduced to the minimum. In practice, when the concrete of a shear wall is heavily damaged, the load that was carried by such a member has to be carried by the adjacent members. The first repair step in such a case is to jack-up the damaged shear wall and the surrounding members, then the to follow steps for concrete replacement mentioned hereafter.

Totally damaged concrete at lower wall edges and middle web, subjected to maximum compressive stresses due to bending and shear actions, respectively, were replaced by a high performance superfluid non-shrink microconcrete. This ensures an enhanced strength of at least 20% above the original concrete.

All damaged, loose, cracked or friable concrete in these areas was removed until sound concrete was reached. The methods used to break-down the concrete ensured that no reinforced steel was loosened or damaged. Mild hammering was applied with the minimum possible angle to the wall so as to induce the minimum dynamic effect and hence minimize micro-crack propagation while removing the damaged concrete. No hammering normal to the plane of wall was allowed (Fosroc, 1991).

Formwork surfaces that were in contact with the repair micro-concrete were treated with suitable mould release agent. Sufficient hydrostatic head or pumping pressure was maintained to ensure that the void was filled completely and no air remained entrapped. Where necessary, provision were made for controllable bleed points to prevent air entrapment and enable the extent of flow of the repair material to be assessed (Ohkubo, 1991).

The repair material used was shrinkage-compensated in both liquid and cured states. It was also pre-packed and factory quality controlled (ACI 223-90).

Even though such a procedure is very simple to apply in laboratory conditions, it is quite costly, risky and time consuming if it is to be applied on actual repair job sites. In practice, we have every interest in keeping the cracked concrete element in its place and trying to rebond it following any of the previously stated repair techniques (Chapter 2). Even with heavily cracked structures, if the fractured concrete is carrying minimum loads, it is ensuring lateral stability against buckling for the main re-bars that are carrying a considerable amount of the vertical loads, and by removing such cracked concrete elements the structure will lose a considerable amount of vertical load carrying capacity.

6.3.3. Local and surface treatment for partially damaged concrete

As in many practical cases, cracking is associated with concrete spalling normally initiated at two intersection cracks. Also, heavily stressed concretes in the unconfined zones (concrete cover) generally spall-off at the first stages of concrete deterioration. Such a deterioration need not entail the replacement of the damaged concrete.

Before injection, a high strength repair mortar can be used to reinstate all types of concrete (i.e. replace cover, fill in the cavities etc.). Where a very large element has spalled off during the initial loading phase, it is recommended that a copper injection nipple be fixed before applying the mortar in order to ensure full penetration of all concrete cavities at a later stage by injecting these locations with epoxy (such a system proved its effectiveness in repairing wall SW22). Such injection ports did consume a considerable amount of grout which confirms that superficial mortar application cannot penetrate deep cavities.

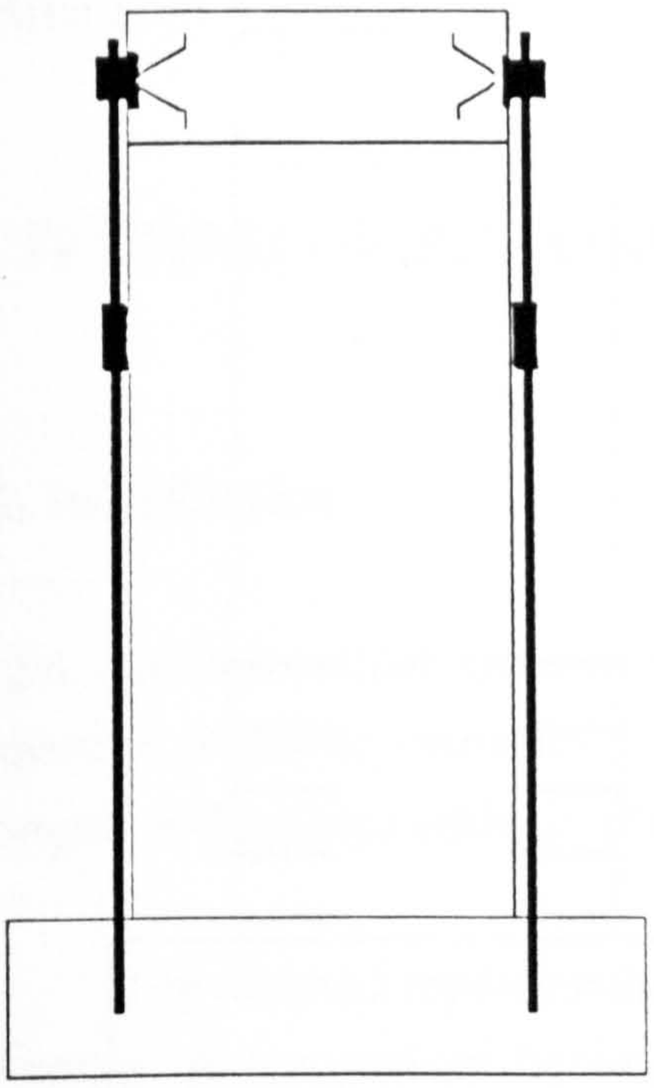


Fig. 6.1 Additional Steel Bars

(Strength-Only)

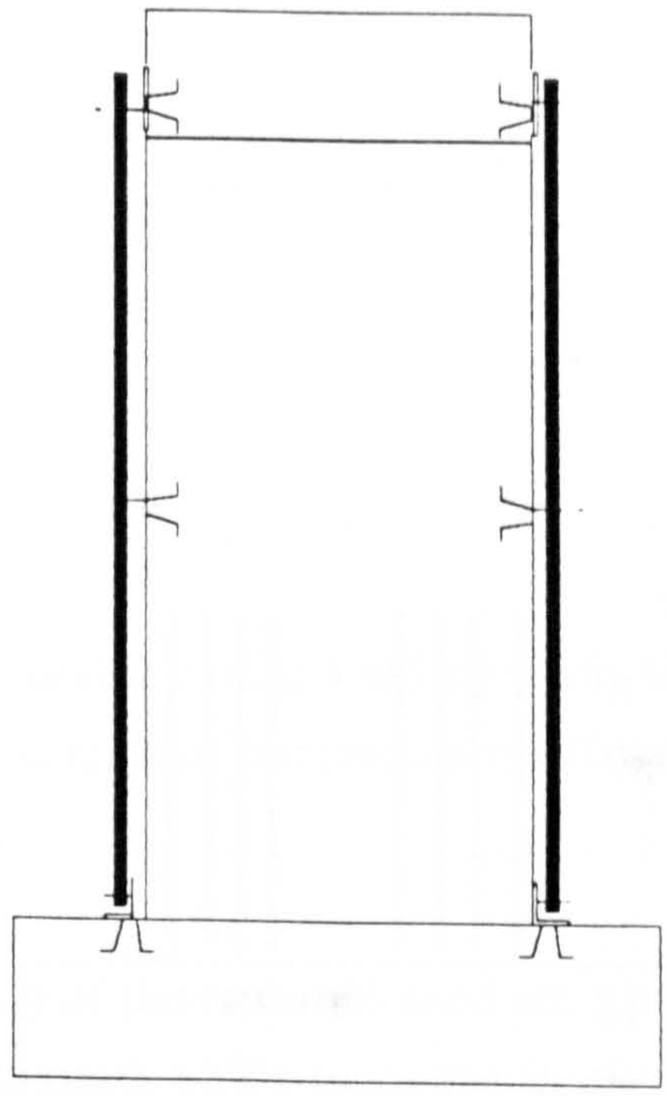


Fig. 6.2 Additional Steel Plates

(Strength-Only)

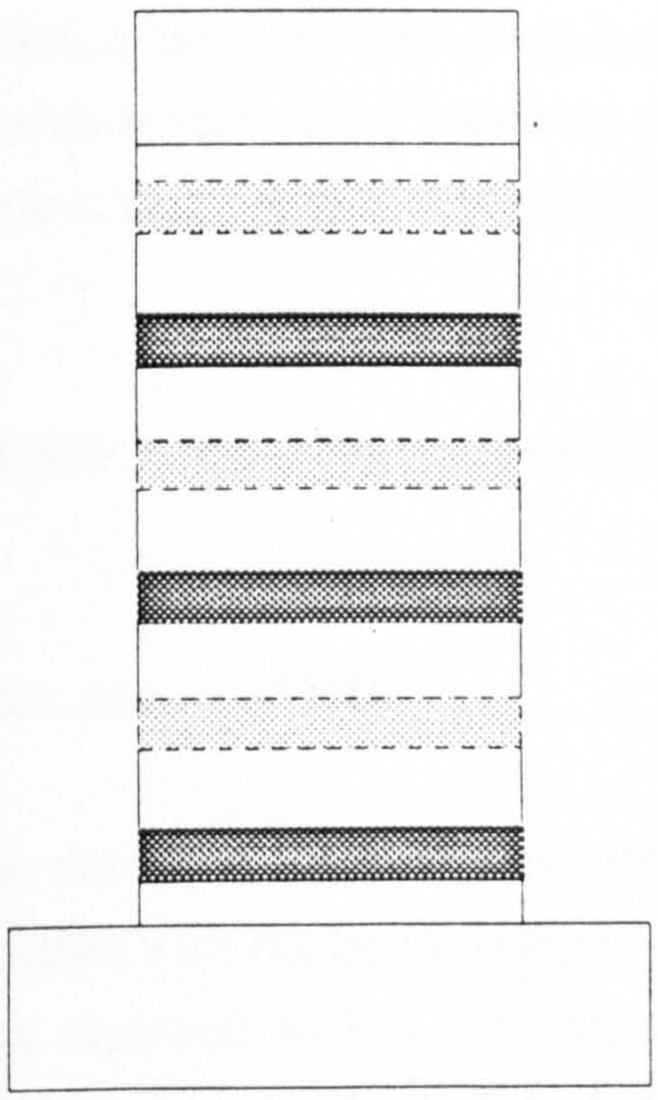


Fig. 6.3 Additional Horizontal Plates

(Shear-Strength)

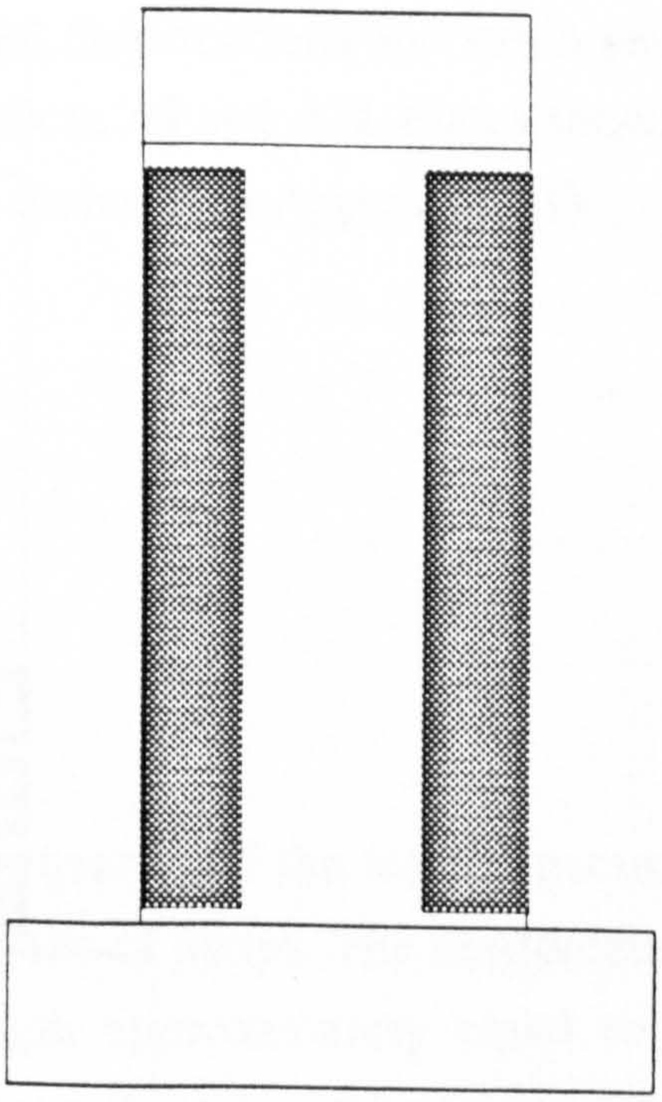


Fig. 6.4 Additional Steel Plates

(Stiffness-Only)

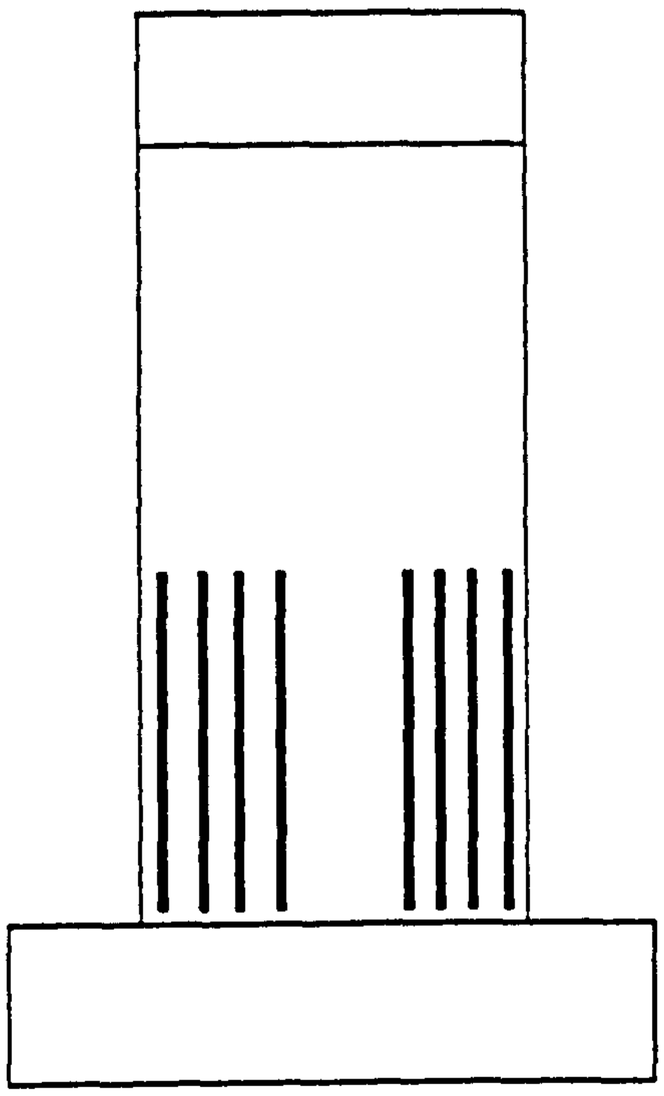


Fig. 6.5 Additional Steel Bars

(Stiffness-Only)

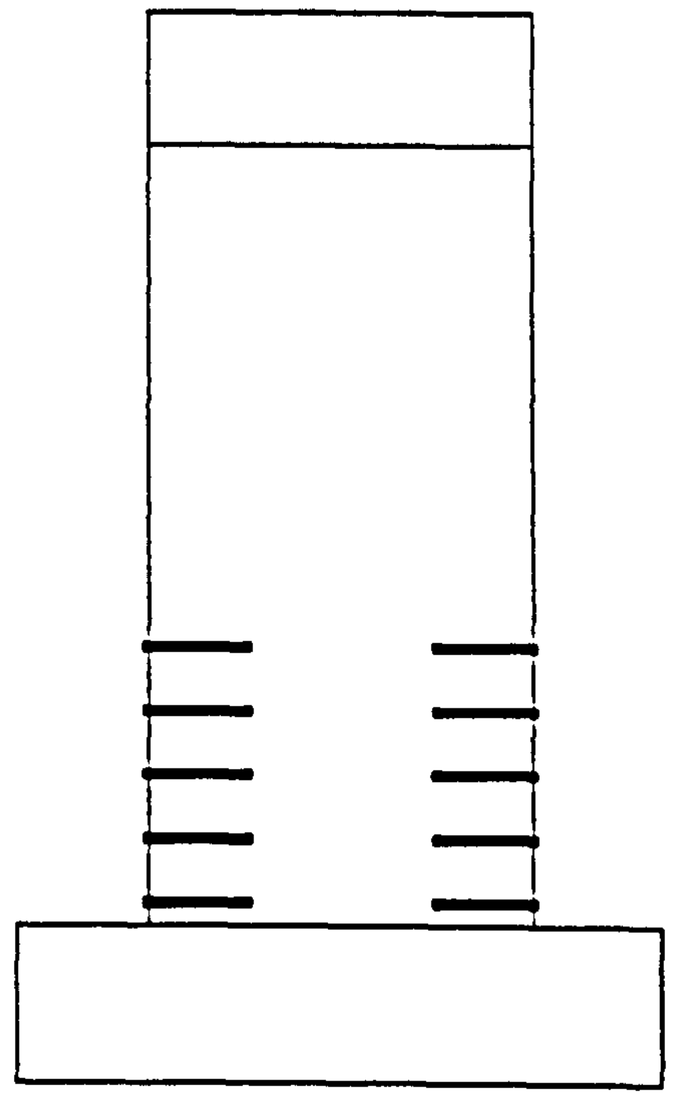


Fig. 6.6 Additional Confining Hoops

(Ductility-Only)

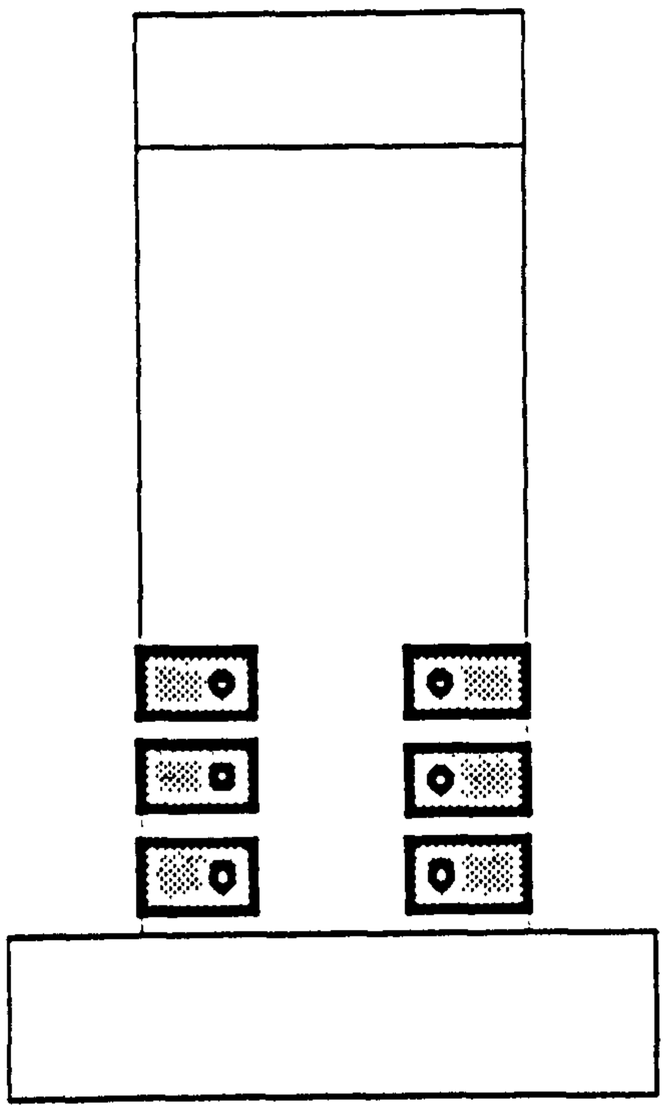


Fig. 6.7 Additional Steel Plates - Confinement

(Ductility-Only)

CHAPTER 7

7. TESTING OF REPAIRED WALLS

7.1. Introduction

Eight repaired and/or strengthened walls were tested under cyclic loading with the objective of either reinstating or enhancing a single response parameter (stiffness, strength or ductility) without affecting the other two.

The adopted repair method and a brief description of the material used are given hereafter. A comparison between the intact and the repaired wall's response is given, highlighting the level of effectiveness of some repair methods and the drawbacks of the others.

In these tests, displacement histories, envelopes of the force-displacement hysteresis loops and stiffness-displacement curves for each model showing the wall response before and after repair are included. A brief description of the wall performance during testing is also given. Detailed wall behaviour; cyclic response at ten different locations measuring horizontal and vertical wall deformations and strain gauge records at up to thirty locations are presented in Appendices **AI** and **AII**. Plates showing the cracking patterns at various displacement levels are included in Appendix **AIV**.

7.2. Observed Behaviour of Models

7.2.1. Model SWR4

The damaged concrete was removed from the bottom quarter of the tested specimen, together with the bottom shear reinforcement and two pairs of hoops. The reinforcement was replaced with 4 mm round bars of yield strength approximately equal to the original, but at a third of the previous spacing. The exposed steel surfaces were treated with a steel reinforcement protection coating and the concrete surfaces with waterproofing polymer adhesive and repair mortar.

A specially manufactured timber shutter was used and concrete of the same composition was recast in the bottom quarter. A super-plasticiser was used so as to reduce the required water content to achieve a good workability. The resulting concrete had a cube strength of 56.7 N/mm^2 at the time of re-testing. Cracks in the remainder of the wall were injected with epoxy resin (Sica, 1992).

The loading scheme is given in Fig. 7.1; the force-displacement hysteresis loop shown in Fig AI (R4) 1 demonstrates that a higher strength as well as displacement ductility were achieved by the repair scheme. An envelope of force-displacement and stiffness-displacement for the intact and repaired walls are shown in Figs. 7.2 and 7.3, respectively.

Some 10% increase of strength was recorded while testing. Since no extra flexural reinforcement was added, the higher strength can be attributed both to the better distribution of confinement as well as to the increased stresses in the flexural reinforcement in tension due to strain-hardening. The higher displacement level achieved can be attributed to better confining steel and concrete quality. Both effects together cause higher strain capacity at the maximum compression zones leading to higher levels of rotational ductility.

A lower initial stiffness was also recorded relative to the intact wall (30% reduction) which can be attributed mostly to the limitations of the epoxy resin injection discussed in detail in section 2.1.1. Nevertheless, a displacement ductility of 2.8 was recorded at the end of the test. The applied repair scheme proved to enhance the flexural and shear capacity as well as the energy dissipation capacity of the wall. Failure occurred by crushing of the web just outside the confined boundary area.

7.2.2. Model SWR5

The initial specimen failed in shear and most of the concrete was severely damaged. Both the shear and hoop reinforcement were opened. Therefore, to prevent shear failure from reoccurring, additional shear reinforcement had to be inserted, hence, concrete from the entire wall (with the exception of the small undamaged concrete triangle at the top) was removed, together with all horizontal reinforcement. New horizontal reinforcement was fixed with double the original steel-to-concrete ratio. A shutter was installed at the back side of the wall which was transported and gunnited vertically on site. The cube strength at the time of re-testing was 46 N/mm^2.

The loading programme consisted of incrementally-increasing lateral displacement cycles. Two cycles of displacement were applied at each deformation level with 3 mm increments as shown in Fig. 7.4. This shows that the repaired model survived a higher number of loading cycles than the intact one The force-displacement hysteresis loop is shown in Fig. AI (R5) 1. To facilitate the comparison between intact and repaired wall behaviour, envelopes of the force-displacement and stiffness-displacement curves are shown in Figs. 7.5 and 7.6 respectively.

The repaired wall showed a more ductile behaviour when compared with the intact wall. It also recorded a 10% increase in strength which is due to the newly-applied shear reinforcement that allowed the wall to achieve its design flexural strength. A ductility level of 1.4 was recorded as opposed to 1.0 for the intact model. Stiffness plots for the repaired model showed a more uniform stiffness degradation.

The repaired wall showed a 10% reduction in stiffness at the initial loading stages. This reduction is attributed to the fact that the gunnited concrete could not ensure a full monolithic action due to the difficulties encountered in penetrating the very small concrete cavities at the interface between old and new concrete. Concrete shrinkage is also considered to have had an effect on stiffness of the tested model. The repaired stiffness was higher than that of the intact wall from the yield level onwards.

7.2.3. Model SWR7

The initial specimen had failed after reaching the ultimate flexural strength through shear deterioration, and the concrete was severely damaged. All the loose concrete up to half height was removed. The shear reinforcement, which was stressed significantly in the initial test and fractured at one point, was replaced with the equivalent amount of 4 mm bars. New special reinforcement was inserted in the web in the vertical direction up to one quarter of the wall height. This reinforcement was not anchored to the beam base, since it was intended to increase the flexural stiffness but not the flexural strength. New concrete was cast vertically in a timber shutter in two layers. The cube strength of the lower layer at the time of re-testing was 46 N/mm^2.

The loading programme consisted of incrementally-increasing lateral displacement cycles. Two cycles of displacement were applied at each deformation level, with 3 mm increments, as shown in Fig. 7.7. The force-displacement hysteresis loop is shown in Fig. AI (R7) 1. To facilitate the comparison between intact and repaired wall behaviour, envelopes of the force-displacement and stiffness-displacement curves are shown in Figs. 7.8 and 7.9, respectively.

Despite the fact that better distributed shear reinforcement was added to the repaired wall, shear failure occurred. The maximum load resisted was 115 kN and failure occurred at 15 mm MDL. This is to be compared with 125 kN for the intact model. The initial stiffness of the specimen was observed to be less than that recorded for the intact model. The effect of the steel devices included in order to enhance stiffness cannot be quantified from a single experiment unless analytical techniques are used. The cause of shear failure cannot be attributed to a reduced contribution from the shear reinforcement since it has been replaced by equivalent reinforcement, which is better attributed.

Repaired wall stiffness showed about 40% reduction when compared with the intact wall stiffness, while the newly-applied concrete recorded a much higher strength. It may be concluded that concrete newly-added will not ensure the initial monolithic action unless special provisions are made. This will result in a much reduced stiffness at the initial stages, reduced flexural strength and limited ductility. To overcome these problems the use of expansive cement concrete, while injecting the interface between the two materials to ensure a direct monolithic action, should be considered. The use of superfluid micro-concrete, used in other models, was shown to reduce these problems of continuity, as discussed in section 7.2.4.

From the test results of SWR5 and SWR7, it may be concluded that the replacement of damaged by newly-cast concrete should be approached with great care. The procedure proved to be fully adequate for strength reinstatement though with some reduction in the stiffness. It is therefore adequate for buildings designed to resist static loads, since stiffness is of very limited importance in such cases. But for buildings subjected to earthquakes or to dynamic loading in general, where stiffness plays an important role in the structure's response, such a system, if applied, would lead to stiffness and strength irregularities leading to code limits violation, and hence a full dynamic analysis and redesign may be necessary (Nian, 1992).

7.2.4. Model SWR9

The intact model SW9, when tested in the previous IC testing programme, exhibited a displacement ductility of 3.0 associated with a ductile failure mode. The failure was characterised by local crushing of concrete in the maximum compression zone. Crack pattern showed a concentration of horizontal flexural cracks at the lower sections of the wall. These reduced in intensity further up the wall height. Flexural-shear cracks characterised by horizontal leading to inclined cracks at 40° were initiated at much reduced intensity in the middle zone of the wall.

7.2.4.1. Repair approach and procedure

One of the research objectives was to achieve stiffness reinstatement without affecting either the wall strength or its ductility. This may be achieved by limiting the number and extent of cracks, as well as reducing crack-face sliding. These objectives were traditionally achieved by epoxy resin injection. However, this system has many practical limitations, as mentioned in section (6.2.2). These were demonstrated experimentally for model SWR22 discussed in section (7.2.6). A new concept was therefore applied in the current research, where steel plates were attached to the cracked wall (by means of high strength epoxy resin) at specific locations. In order not to affect the wall strength, the steel plates were not connected to either the foundation beam or to the top loading beam. Moreover, the dimensions of the plate were reduced to the minimum required to avoid any effects on the deformational behaviour of the wall model. Plate locations were chosen so as to supply the minimum possible strain energy to prevent crack opening.

The applied repair scheme consisted of replacing the crushed concrete by a superfluid micro-concrete (shrinkage compensating) which was poured in a watertight wooden shutter. A pneumatic hammer was employed to roughen the concrete surface and to expose the aggregate, followed by vacuum cleaning to remove the dust and loose particles. Four steel plates of dimensions 1100x160x3.6 mm were attached to the concrete wall (at the wall edges) allowing a 50 mm clearance between the top loading beam, the bottom fixing beam and the steel plates.

To satisfy the code-defined serviceability limit states, since the existing crack width was in excess of that allowed, treatment of exposed cracks was required. A special surface treatment emulsion paint (penetration by capillarity) was used to seal the cracks, thus protecting the steel from corrosion due to moisture migration. (Fosroc, 91).

7.2.4.2. General observations

The wall reached its yield strength of 95 kN at 8 mm MDL, compared to 90 kN for the intact wall specimen. The ultimate strength of 105 kN was first recorded at a displacement level of 14 mm, and was sustained up to a displacement of 26 mm. The observed ultimate strength is in excess of that reached by the intact wall (101kN). This is attributed to the strain-hardening in the main flexural reinforcement. The wall showed a ductile behaviour sustaining a constant strength up to 26 mm MDL and survived the same number of cycles and displacement amplitudes as for the intact wall. A drop in strength occurred at the second cycle of 26 mm displacement amplitude while total failure was observed at 30 mm MDL. This indicates improved performance compared to the original wall, due to the application of high strength superfluid concrete in the maximum compression zones, which achieved a cube strength of 70 MPa compared with 45 MPa for the original concrete mix.

The tested wall showed a lower stiffness up to 4 mm MDL when compared with the intact case. The wall also showed a behaviour comparable with the original wall stiffness at higher MDLs, as shown in Fig. 7.12. With the increase of the displacement amplitude, the original cracks were reopened as a consequence of plate/wall debonding. This was the result of concrete cover failing in shear at the interface between the epoxy mortar and the wall. No newly-developed cracks were noticed during the test, except for the replaced concrete at the lower parts, where new flexural cracks developed following the previous crack pattern. The superfluid concrete showed good interaction with the original concrete; its expansive cement agent proved to be effective, since no shrinkage cracks were noticed. The high strength epoxy was also effective in bonding the two different materials.

7.2.4.3. Force-Displacement Hysteresis

The wall was subjected to a quasi-static cyclic loading according to the displacement history shown in Fig. 7.10. Force-Displacement hysteresis shown in Fig. AI.(R9)1 demonstrated that the wall behaved in a ductile manner at various displacement levels. Also, the wall extension and curvature observed at various levels from Figs. AI (R9) 1 to 10, confirm same observation.

Cycling at the same displacement level the model showed very little stiffness degradation. Upon load reversal, a relatively low initial resistance was recorded until the previously-opened cracks at the debonded steel plate areas were closed. As the crack

closure took place, the resistance of the model was gradually restored. When the cracked surfaces came into contact under cyclic loading at MDLs exceeding 18 mm, some concrete grinding took place, associated with minor strength degradation. This was followed by concrete cover spalling in the maximum compression zones.

Hysteresis loops corresponding to the same deformation level did not reach the previous capacity at MDLs exceeding 18 mm, as long as the compressive strength of the cracked concrete at the boundary edge was not exceeded. As soon as the compressive strength was exceeded, a rapid 30% degradation of strength was recorded at 26 mm MDL, signifying the failure of the model.

An envelope force-deformation curve for both SW9 and SWR9 was plotted in Fig. 7.11 where compatibility of strength and stiffness between the intact and repaired models is manifested.

The repaired wall achieved a displacement ductility level of 3.25 compared with 3.0 for the intact case. This higher ductility level may be attributed to the fact that the replaced concrete at the maximum compression zones had a higher strength level than the original concrete.

7.2.4.4. Strain gauge readings

The external steel plates were gauged at twenty different locations in both the vertical and the horizontal directions. The vertical gauge reading indicated that the plates were activated in the vicinity of flexural cracks and were inactive elsewhere, as demonstrated in Figs. AII.(R9) 1 and 3. This proves the design concept upon which this reinstatement scheme was based. They recorded constant readings along the plate width at the same level, as depicted in Figs AII.(R9) 1 and 2.

The horizontal gauge readings proved that the plates did not affect the wall confinement as shown in Fig. AII.(R9) 4. The splicing plate effect was noticeable even at the upper wall sections where about 70 microstrains where recorded, as depicted in Figs. AII.(R9) 5 and 6. The plates were subjected to a maximum tensile stress of 80 MPa before debonding due to failure of the adhesive. This leads to the conclusion that the use of thin wide plates is preferable to those of narrow geometries.

7.2.4.5. Stiffness re-instatement

It may be concluded that the stiffness degradation of the wall depends mainly on the rate of the wall extension leading to plates debonding. Fig. 7.12. confirms the similarity between the repaired and the intact models with respect to stiffness.

The external plates were only active in tension, while negligible strain readings were recorded in compression. After testing, it was observed that the lower third of the plates were debonded. Steel reinforcement was checked at the end of the test after breaking down the existing concrete at the boundary elements, and was found to be in position with no fracture, bond slippage of stirrups or openings of hoops.

It is hence concluded that the cracked flexural stiffness of structural walls can be fully reinstated, and if requested enhanced, without affecting either strength or ductility. This may be of great importance in the case of existing buildings where tuning the members stiffness can lead to a more regular structure. This would lead to higher allowable behaviour factors according to modern seismic codes which impose strict regularity conditions. Such intervention can be also applied in the case of RC structures damaged by a small magnitude earthquake, which cause a reduction in the stiffness of the structure while having a small effect on the strength. Therefore, in repair of such a structure, reinstatement of stiffness with no effect on strength should be the objective of the intervention scheme.

7.2.5. Model SWR21

Model SW21 was designed to fail in a mixed flexure-shear mode and was intended for a 'shear strength enhancement' repair objective. Diagonal cracks at 45° distributed at a nearly uniform pattern characterised the crack pattern The failure was due to local deterioration of the unconfined concrete (concrete cover) at the intersection of diagonal cracks. The test was stopped at 20 mm MDL (i.e. 1.67% drift) after showing a 20% reduction in strength.

7.2.5.1. Repair approach and procedure

A simple and practical repair scheme for shear strength enhancement was sought for this model. The concrete surface was touched up using high strength mortar. To compensate for the shear strength loss due to cracking of concrete, 6 steel plates 78 x 3.6 mm were attached to the wall by means of high strength epoxy resin. The plates had a lip of 50 mm to prevent end splitting leading to non-ductile behaviour. They were attached to both sides of the wall in a staggered manner, as shown in Fig. 6.3.

To satisfy the code-defined serviceability limit states, since the existing crack width was in excess of that allowed, treatment of exposed cracks was required. A special surface treatment emulsion paint (penetration by capillarity) was used to seal the cracks, thus protecting the steel from corrosion due to moisture migration.

7.2.5.2. General observations

The model was tested under cyclic loading. Two cycles of displacement were applied at each deformation level with 2 mm increments as shown in Fig. 7.13.

The repaired wall showed a 20% reduction in stiffness at the first loading cycle (i.e. 2 mm MDL) as shown in Fig. 7.15. However, the difference between the repaired and intact stiffness was reduced at higher MDLs. They were nearly equal from 6 mm to 14 mm MDL and the repaired wall showed a higher stiffness from 14 mm MDL onwards. This can be explained by the fact that the new stiff wall-plates mechanism was activated at high MDLs where crack arrest took place.

At displacement levels higher than 6 mm, the original cracks were re-opened between the horizontal plates. No newly-developed cracks were noticed during the test, due to the presence of the glued plates.

The failure mode was characterised by the crushing of concrete in the boundary elements, rather than the web, as was the case of the intact wall. This was followed by partial splitting of the first steel strip due to concrete deterioration along the lower wall section.

7.2.4.3. Force-displacement hysteresis

The repaired wall reached its yield strength of 96 kN at 10 mm MDL, compared with 90 kN for the intact wall. This was sustained up to 18 mm MDL. The ultimate strength of 105 kN was in excess of that reached by the intact wall (100 kN). This is attributed to the applied horizontal steel plates which enhanced the wall shear strength and hence allowed the ultimate flexural strength to be developed. The strain-hardening in the main flexural reinforcement also added to the wall strength. Force-Displacement hysteresis demonstrated that the repaired wall achieved higher ductility levels than the intact one, as shown in Fig. AI (R21) 1. A displacement ductility of 1.80 was observed compared with 1.50 for the intact wall.

The vertical displacement readings shown in Figs. AI (R21) 2 and 10, indicate that the wall underwent an extension of 10.5 mm compared with 4.5 mm for the intact wall. This can be attributed to the strain-hardening in the steel reinforcement, in addition to the fact that the shear strengthening allowed the wall to behave in a much more flexural mode. This can be concluded from studying the various vertical and horizontal force-displacement plots.

Upon cycling at the same displacement level, the wall showed very little stiffness degradation and much less than that recorded for the intact wall. This can be attributed to the fact that shear strength was dependent on ductile steel plate behaviour rather than brittle concrete.

Upon load reversal, a relatively low initial resistance was recorded until the previously opened cracks were closed. As the crack closure took place, the resistance of the model was gradually restored. Also, the recorded pinching was less severe than for the intact wall. Hence the energy absorption capacity was improved. When the wide cracked surface came into contact under cyclic loading at MDLs exceeding 18 mm in

one side of the wall and 20 mm in the other side some concrete grinding took place along the cracked surface, associated with strength degradation. This was then followed by concrete cover spalling in the maximum compression zones.

7.2.5.4. Strain gauge readings

The external steel plates were gauged at ten different locations at the third, middle and two thirds of the wall height. The gauge readings proved that the plates were activated in the vicinity of a shear crack and were nearly inactive elsewhere, as indicated in Figs. AII(R21) 1 and 3. Along the lower plate, 200, 70 and 600 microstrain were recorded at the left, middle and right edges, respectively.

The external well-bonded plates showed very little interaction until the original and non-injected cracks reopened due to large imposed displacement levels. At this stage, considerable strain levels were recorded, as depicted in Figs. AII(R21) 4 and 10. Since the hysteresis loops were only one-sided, it is concluded that the steel plates were only active in tension.

7.2.5.5. Shear strength re-instatement

It is concluded from the test results reported herein that the shear strength of RC structural walls can be fully reinstated and, if required, enhanced by bonding external horizontal steel plates to the damaged wall without the need of epoxy injection. Enhancement of the shear strength would prevent brittle shear failure mode and allow the full mobilisation of a ductile flexural mode.

7.2.6. Model SWR22

Severe concrete deterioration was observed for SW22. Its non-ductile shear behaviour associated with severe pinching had induced very wide cracks, concrete spalling and local concrete crushing. A drop of 30% in strength indicated the wall failure.

7.2.6.1. Repair scheme

Epoxy injection was used to repair this model, as discussed in section 6.3.1 Also, treatment for partially damaged concrete was applied according to section 6.3.3.

This repair approach would be important as a temporary measure for heavily damaged reinforced concrete walls and members carrying vertical loads. In practice, a more refined repair scheme should follow at a later stage after a detailed site investigation, damage assessment and structural analysis are carried out.

7.2.6.2. General observations

Wall cracking started as a diagonal crack with 45° inclination at 3 mm MDL parallel to an injected crack line. At 4 mm MDL, three parallel diagonal cracks were clearly noticed. It was noticed that none of the injected cracks opened up. Also, new cracks developed in the vicinity of the original cracks. Due to the concentration of confining hoops at the lower mid-height of the wall in the boundary element (R4 @ 33 in the lower half of the wall, which were reduced to R4 @ 50 in the upper half), the major diagonal cracks were restricted to the area between these elements. Only inclined microcracks were able to develop in the boundary elements. It was also noticed that the intensity of diagonal cracking in the upper wall edges was much higher than in the lower wall edges. This confirmed the effectiveness of the confining steel hoops in shear resistance.

The increase of the applied displacement level produced a large number of well-distributed inclined cracks. It was observed that the global deformational behaviour of the wall was governed by two relatively rigid boundary elements forming the chord members of a truss connecting in between a highly flexible, cracked and deteriorated web element. Upon further increases in the applied displacement level, concentration of inclined cracks was observed near the extremities of the middle web squares B-1 and D-1 shown in Fig. 4.2. Crossing of inclined cracks under reversed cyclic loading resulted

in degradation of concrete compressive strength in this region. This led to spalling and crushing of concrete at 22 mm MDL. The wall eventually failed by web crushing.

It is clear from the above description that the wall behaviour was dominated by diagonal tension limited to the wall middle web and diagonal compression throughout the boundary element and the middle web. An envelope for the hysteresis loops, shown in Fig. 7.17, demonstrates that a 90 % strength reinstatement was achieved by the applied repair scheme associated with a reduced stiffness up to 14 mm MDL. A comparable stiffness with the intact wall at higher displacement levels was recorded, as shown in Fig. 7.18.

Upon load reversal, the wall showed reduced initial resistance until the previously-opened cracks were closed. It also indicated stiffness degradation under cyclic loading. As crack closure took place, the resistance was gradually restored. This initial softening, followed by a gradual build-up of load resistance was reflected in the force deformation hysteretic relationship as pinching of loops. Since the observed pinching was relatively high, it is concluded that the wall response was governed by diagonal tension rather than diagonal compression.

7.2.6.3. Force-displacement hysteresis

The hysteresis loops for the repaired wall had larger areas and hence better energy absorption capacity when compared with the intact wall hysteresis loops, as shown in Fig. AI (R22) 1. When the inclined cracked surfaces came into contact under cyclic loading, some grinding of concrete took place along the cracked surfaces.

Hysteresis loops corresponding to the same deformation level did not reach the previous strength level. Contrary to the flexural response, as the web concrete was deteriorating under cyclic loading, the ultimate strength was followed by a gradual strength loss at higher MDLs, exceeding the yield displacement so long as the diagonal compressive strength of cracked concrete was not exceeded. At this point, a rapid degradation of strength was observed. The failure was characterised by crushing in concrete in the web.

The force-displacement hysteresis loops showed better ductility performance when compared with the original wall. The repaired wall survived five cycles at the maximum strength level, while the original wall survived only one cycle. The repaired wall showed an ultimate strength of 95 kN at 12 mm and this was sustained up to 16

mm MDL compared with 100 kN at 12 mm MDL for the intact wall. The additional observed ductility can be justified by the opening of new narrower cracks due to the efficient closing of the original wide cracks (by epoxy resin injection), in addition to the application of high strength mortar at the locations where original concrete did spall-off, causing rapid reduction in the wall strength.

7.2.5.4. Stiffness re-instatement

Stiffness-displacement curves showed that the repaired wall had a reduced stiffness when compared with the intact wall, as demonstrated in Fig. 7.18. An initial reduction of 30% was recorded. The repaired wall showed a reduced stiffness up to 14 mm MDL. This can be attributed to limitations of the epoxy resin, since it cannot penetrate cracks of less than 0.05 mm width. This can be explained by the fact that the testing of the repaired wall started with a slightly cracked wall manifested in a reduced stiffness.

The assessment of the injected wall stiffness can be only achieved experimentally, since it is highly dependent on the skill of the repair personnel, the viscosity of the applied epoxy, the type of injection nozzle, the injection pressure and the crack width etc. Nevertheless, the repaired wall showed an effective shear strength re-instatement. It also showed a stiffness from 16 mm MDL onwards which is comparable to the intact case. This can be explained by the fact that micro-cracks (where epoxy did not penetrate) have very little contribution to the stiffness at these high displacement levels.

7.2.6.5 Shear strength re-instatement

It may be concluded from the test data reported above that the cyclic wall strength can be partially reinstated by means of epoxy injection associated with surface treatment of the spalled concrete. Moreover, epoxy injection can also improve the capacity of the injected wall to dissipate earthquake energy. Prevention of diagonal tension failure by means of external shear resisting elements would have improved the wall displacement ductility from 1.25 to about 2. Any further improvement in the wall ductility will be limited by web crushing It is also important to note the dependence of the success of epoxy injection on many factors, such as workmanship, viscosity of epoxy etc. Therefore, the degree of stiffness-reinstatement cannot be assumed.

7.2.7. Model SWR24

To satisfy the code-defined serviceability limit states, since the existing crack width was in excess of that allowed, treatment of cracks was required. Cracks were injected using low viscosity high strength epoxy. This would enhance the interface shear resistance along the crack lines and would protect the steel from corrosion. The model was epoxy injected and reinforced with horizontal steel plates to enhance the shear strength. Seven steel plates 78 x 3.6 mm were attached to the model by means of high strength epoxy resin. The plates had a lip of 50 mm to prevent end splitting leading to non-ductile behaviour. They were attached to both sides of the wall in a staggered manner as shown in Fig. 6.3. Hence, a complete repair scheme, as opposed to a selective one, was applied to the model SWR24.

7.2.7.1. General observations

The model was subjected to cyclic loading. Two cycles of displacement were applied at each deformation level with 2 mm increments as shown in Fig. 7.19.

The repaired model showed a stable hysteretic behaviour and a higher energy absorption capacity when compared with the intact model. It recorded 125 kN corresponding to 30 mm displacement as opposed to 110 kN corresponding to 20 mm displacement for the intact wall.

Cracking was first observed at 6 mm MDL at squares 6-B and 6-D, Fig. 4.2. At 8 mm MDL, further cracking was observed at squares 1-D and 1-B. With the increase of displacement level, cracks were propagating towards flatter crack lines and were restricted to the area between horizontal steel straps. Horizontal crack was observed at the lowest section of the wall at 16 mm MDL. At 18 mm MDL, concrete deterioration took place associated with some strength reduction and partial debonding of the first steel plate.

At 20 mm MDL the lowest horizontal crack opened widely. This allowed the reinforcing bars to kink and the wall to slide horizontally in a rigid body mode. With higher MDL, further concrete deterioration took place at the lowest section causing further strength reduction. Maximum concrete deterioration took place in the confined boundary elements. This caused complete debonding of the first horizontal steel strap.

7.2.7.2. Force-displacement hysteresis

The yield and ultimate strengths of the repaired wall were 110 kN (at 8 mm) and 130 kN (at 10 mm). The latter compares to the intact wall ultimate strength of 120 kN (24 mm). This is attributed to the added horizontal steel plates that enhanced the wall shear strength which allowed the ultimate flexural strength to be achieved. Strain-hardening in the main flexural reinforcement also added to the wall strength. An envelope for the force-displacement hysteresis is given in Fig. 7.20. This demonstrates the ductile wall response.

From Force-displacement hysteresis loops shown in Fig. AI. (R24) 1, it is concluded that the repaired model achieved a higher ductility level than the intact model. A displacement ductility of 4 was recorded for SWR24 as opposed to 1.6 for SW24. Energy dissipation capacity from the repaired model was much higher than for the intact case.

Cycling at the same displacement level, the wall showed very little stiffness degradation and much less than was recorded for the intact wall. Also, no strength degradation was observed up to 20 mm MDL. This is a confirmation of higher ductility and could be attributed to the fact that shear strength was dependent on ductile steel plates rather than brittle concrete. The stiffness-displacement curve shown in Fig. 7.21 proves the smooth gradual stiffness degradation.

Upon load reversal, a relatively low initial resistance was recorded until the previously-opened cracks were closed. As the crack closure took place, the resistance of wall element was gradually restored. Also, the recorded pinching was less severe than the intact wall and, hence the energy absorption capacity was improved. When the wide cracked surface came into contact under cyclic loading at MDLs exceeding 20 mm, some concrete grinding took place along the cracked surface associated with strength degradation. This observation was then followed by concrete cover spalling in the maximum compression zones.

7.2.7.3. Strain gauge readings

The external steel plates were gauged at ten different locations at the third, middle and two thirds of the wall height. The gauge readings proved that the plates were activated in the vicinity of a shear crack and were nearly inactive elsewhere as indicated in Figs.

AII(R24) 1 and 2. Along the lower plate, 120 and 200 microstrain were recorded at the middle and left edges respectively.

Following the conventional theory of RC in shear for fully bonded stirrups, the externally well bonded plates showed very little interaction until the original and non-injected cracks reopened due to large imposed displacement levels. At this stage, considerable strain records were recorded, as depicted in Figs. AII(R24) 8, 9 and 10. Since the hysteresis loops were only one sided, it is concluded that the steel plates were only active in tension.

It was noticed that strain recordings were reduced with the wall height. However, higher recordings were observed near to the crack locations irrespective of their height as depicted from Figs. AII (R24) 3, 4, 5 and 6.

7.2.7.4. Shear strength re-instatement

It is concluded from the test results reported herein that the shear strength of RC structural walls can be fully reinstated and, if required, enhanced by bonding external horizontal steel plates to the damaged wall without the need of epoxy injection. Enhancement of the shear strength would prevent brittle shear failure mode and allow the full mobilisation of a ductile flexural mode. Epoxy injection would enhance the shear stiffness, increase the energy absorption capacity and ensure higher durability for the retrofitted structure.

7.2.8. Model SW31

7.2.8.1. Strength enhancement method

To simulate a realistic strength-only intervention scenario, it was intended that model SW31 would have a flexural strength of 90 kN, but was supplied with only 60 kN in the first instance. It was decided to apply External Unbonded Reinforcing Bars (hereafter referred to as 'EURB') to upgrade the strength without affecting the stiffness. The bars were fixed to the foundation beam using high strength epoxy patching mortar and to the top loading beam by means of a steel assembly fixed to the concrete wall. The bars were spliced at their mid height using special couplers that were designed to allow for an initial slack (hereafter referred to as the Interaction Delay Mechanism 'IDM'). The wall was strengthened with 3 EURB of 4 mm diameter on both sides of the wall. The IDM was based on a slack of 3 mm and 4 mm for the central and the side bars, respectively.

The philosophy behind the design of the above a system is that when the wall is loaded horizontally, it undergoes a vertical elongation due to cracking and rotation. If a strengthening scheme is to be designed after the wall has reached its yield strength, a considerable strength enhancement can be achieved without affecting neither the uncracked nor the yield stiffness of the wall. To a lesser extent, the dynamic characteristics of the wall will not be affected.

7.2.8.2. General observations

The loading programme consisted of incrementally-increasing lateral displacement cycles. Two cycles of displacement were applied at each deformation level with 2 mm increments as shown in Fig. 7.22.

Wall cracking started as horizontal flexural cracks in the boundary elements. Closely spaced hoops (30 mm) caused the cracks to be narrow and well-distributed. The horizontal cracks propagated into coarsely distributed inclined cracks in the web. Intersecting cracks from opposite directions segmented the plastic hinge region into several horizontal layers. Because of these horizontal cracks, truss action was not developed to transmit shear. After steel yielding and hence crack widening, shear was transferred primarily by interface friction and dowel action. This shear transfer was adequate to maintain the integrity of the wall until failure occurred due to concrete crushing in the maximum compression zone.

Epoxy grout at the foundation beam showed good performance with no signs of bond failure. Steel reinforcement was checked at the end of the test after breaking down the existing concrete at the maximium compression zones. The hoops as well as the links were found to be in a very good condition which proved that closed links and hoops are indeed justified in such a case.

7.2.8.3. Crack pattern

First cracking was noticed at 1mm MDL at the lowest section of the boundary element i.e. square (A-1) in Fig. 4.2. Horizontal flexural cracks were traced in the lower third of the wall height (A-1 to A-4 and E-1 to E-4) in Fig. 4.2 with maximum crack widths of 1.8 mm while being loaded to MDL higher than 10 mm. These were reduced to 0.6 mm at 0.0 MDL. The relatively wide cracks indicated that the tensile reinforcing steel at the boundary elements yielded at a very early stage. This was confirmed by the strain gauge readings.

The flexural cracking intensity was noticeably reduced along the wall height. Flexure-shear cracks characterised by horizontal leading to inclined cracks at about 30° were initiated at a much reduced intensity at mid-wall height (A to E and 5 to 7) in Fig 4.2. The inclination of cracks was increased along the wall height. These cracks were observed at higher displacement levels from 16 mm MDL onward. At the last MDL, a few cracks propagated at the top wall corners with maximum crack width of 0.2 mm (A-9, A-10, E-9, E-10).

7.2.8.4. Force-displacement hysteresis

The wall reached its yield strength of 56 kN at about 6 mm MDL associated with 2 mm vertical displacement as shown in Fig. AII.(31) 1 and 4. With the increase of cyclic displacements from 6 mm to 10 mm, the wall displayed a ductile behaviour and a stable resistance of about 60 kN was sustained. Meanwhile, the initial uncracked stiffness was reduced from 15 kN/mm to 8 kN/mm at the yield level (thus lending weight to the ACI recommendation of an effective stiffness of 50% of the uncracked stiffness for flexural members, provided that main tensile reinforcement is concentrated in the flexural member edges).

At 10 mm MDL the design vertical slack of 3 mm was consumed by the wall extension allowing the first EURB to contribute to the wall tension reinforcement. This

was manifested by an increase in the wall strength from 60 kN to 65 kN (first recorded cycle by strain gauge 25 logging middle EURB strains). The wall stiffness was further reduced at that stage to 5 kN/mm.

At 14 mm MDL, the remaining two EURB picked-up force, thus causing a further strength increase up to 90 kN. Since the three EURBs started to pick up load at 10 mm MDL at various interacting stages, they were fully interacting at 16 mm MDL. At the IDM stage, and due to the added re-bars, a minor increase in stiffness was observed as shown in Fig. 7.24. The wall showed a second stage of ductile behaviour where the newly achieved strength level of about 90 kN was sustained up to 24 mm MDL.

In order to predict the nonlinear wall behaviour under cyclic loading after being subjected to higher stress levels due to the mobilisation of the EURB, the bars were disconnected at 24 mm MDL to monitor the as-built response of the wall. The wall behaved in a ductile manner; a resistance of 55 kN was sustained (slightly lower than the initially-recorded strength, due to grinding of concrete).

From 24 mm to 28 mm, some increase in crack width was recorded without major concrete deterioration. At that stage, unconfined concrete in the boundary elements (concrete cover) started to spall-off, associated with some strength reduction. Failure of the wall was reached at 30 mm MDL due to deterioration of the confined concrete in the boundary elements and was characterised by a drop in strength of about 40%. The residual strength of the wall was 30 kN on both sides, associated with irrecoverable deformations of 19 mm.

7.2.8.5. Observed ductility

Force-Displacement hysteresis confirmed the ductile wall behaviour at various strength levels, as shown in Figs. AI (31) 1 and 10. It also showed that the wall behaved symmetrically on both sides even at the critical stages of mobilisation of the EURBs at quarter, mid and full height of the wall. A displacement ductility of 4.70 at 60 kN strength level (initial strength) and of 2.40 at 90 kN strength level (enhanced strength) were achieved during testing. An envelope force-deformation curve is shown in Fig. 7.23.

Cycling at the same displacement level showed negligible stiffness degradation and drop in strength, except at the high displacement levels. Upon load reversal, the wall

showed little initial resistance until the previously-opened cracks were closed. As the crack closure took place, the resistance of wall element was gradually restored. This initial softening, followed by gradual build up of load resistance, is reflected in the force deformation hysteretic relationship as 'pinching' of loops. Pinching is generally low and smooth in flexure-type of failures. It is much more abrupt in shear dominated response recorded in other tests. However, the pinching in this case was relatively high due to the release of the elastic energy in the EURB in one side and their interaction on the other side. They were separated by the designed slack that was larger than the wall extension at yield.

7.2.8.6. Strain gauge readings

Strain gauge plots showed that boundary edge reinforcing steels yielded at the very early loading stages i.e. 2 mm to 5 mm MDLs. They displayed a maximum strain of 400 microstrain at mid-height of the wall as shown in Fig. AII.(31) 1.

Horizontal stirrups exhibited a very low interaction level since the recorded strain was only about 300 microstrain at the wall lower level (square 1) shown in Fig. 4.2. This is confirmed from plot AII (31) 2.

As predicted, hoop reinforcement recorded reduced strains with the wall height. This is confirmed from Figs. AII (31) 3 and 4; whereby strains were 235 and 102 for the first and third hoops respectively.

The EURB were only active in tension. They recorded zero strain and hence zero stress until 10 mm MDL (noting that initial yield strength was achieved at 6 mm MDL). They recorded 1800 microstrain at 16 mm MDL as depicted in Figs. AII (31) 5 and 6.

7.2.8.7. Strength enhancement

The seismic flexural strength of structural walls, as confirmed above, can be improved without affecting their stiffness and hence their dynamic characteristics provided that diagonal tension and sliding shear are prevented. In this test, a strength increase of about 50% was achieved without affecting the wall stiffness.

The method can be easily adopted in practice i.e. external unbonded bars can be attached to the lower and upper levels by means of epoxy mortar or self fixing bolts

while having a mechanical coupler allowing for the designed slack to occur along the bar length. The whole assembly should then be protected by means of a concrete jacket that is to be separated from the actual concrete elements by means of 10 mm thick stieropore.

This procedure will ensure that the EURB will have no contribution in the compressive side while ensuring a delayed interaction while acting in the tension side. The concrete jacket will improve the durability of the strengthening system.

7.2.9. Model SW32

To simulate a ductility-only intervention scenario, it was intended that model SW32 would have the highest ductility performance, but was constructed without any special confinement reinforcement in the first instance. This would represent the case of a large percentage of buildings constructed up to the mid-eighties with little or no seismic provisions. Such buildings, comprising a substantial proportion of the existing stock, upon re-assessment, would require a 'ductility-only' intervention.

7.2.9.1 Ductility enhancement method

It was decided to add External Confinement Steel Plates (hereafter referred to as **'ECSP'** to upgrade the wall ductility without affecting neither the wall strength nor its stiffness. These plates were U-shaped. To ensure an effective confining system, the fourth side had to be constrained or continued. This was achieved by tying a high strength grip friction 20 mm diameter bolt through the fourth (opened) side of the plate. An active concrete confinement was ensured when a prestressing force of 20 kN/bolt was applied.

Three U-shaped plates of dimensions 480x120x3.6 mm were fixed to each side of the wall. This ensured that a concrete area of 480x120 mm was confined with each plate. A 20 mm gap was applied between plates to minimise crack-arrest which would disrupt to original stiffness of the member. The **'ECSP'** scheme covered the lower third of the wall.

For ease of construction, a tolerance gap of 2 mm was allowed between the steel plate and the concrete wall. To ensure a monolithic action with the added plates, epoxy injection was allowed between the wall section and plates .

The basic philosophy behind the design of such a system is that when the wall is loaded horizontally, it exerts vertical compressive stresses at the critical zones (wall edges). If the concrete is laterally confined, its ultimate strain as well as stress will be increased. Hence, a higher rotational ductility supply at the critical sections would be achieved.

7.2.9.2. General observations

The loading programme consisted of incrementally-increasing lateral displacement cycles. Two cycles of displacement were applied at each deformation level with 2 mm increments as shown in Fig. 7.25.

Wall cracking started as horizontal flexural cracks in the boundary elements between the **'ECSP'**. These propagated into flexure-shear cracks at about 40°. Cracks were confined between boundary elements at the lower third of the wall and propagated outwards at the upper half of the tested model.

No sign of local failure or incompatibility between the wall and the added scheme was observed. It is therefore concluded that the ECSP design and construction process is adequate. Also epoxy grout was effective in ensuring the interaction of the above-stated scheme at the early loading stages. Furthermore, it limited the flexural cracks in the boundary element whilst relatively wide flexural cracks (1-1.5 mm wide) were observed between the plates.

7.2.9.3. Force-displacement hysteresis

The wall reached its yield (54 kN) strength at about 6 mm MDL associated with 2.6 mm vertical displacement as shown in Fig. AI.(32) 1 and 2. The ultimate strength (62 kN) was reached at 8 mm MDL. With the increase in cyclic displacements from 10 to 22 mm, the wall displayed a ductile behaviour and a stable resistance of about 62 kN was sustained. Meanwhile, the initial stiffness was reduced from 15 kN/mm to 8 kN/mm at the yield displacement.

The wall showed high rotational ductility at various displacement levels. This was confirmed by vertical hysteresis loops showing 8, 8.5 and 9 mm maximum vertical extension at quarter, mid and full wall height, respectively, as shown in Figs. AI.(32) 2, 3, 6, 7, 9 and 10. Hysteresis loops showed large energy absorption capacity as depicted in Figs. AI.(32) 4, 5 and 8. The force-displacement envelope is given in Fig. 7.26 which demonstrates the stable ductile behaviour of the model.

7.2.9.4. Strain gauge readings

Strain gauge plots showed that boundary element external reinforcing bars yielded at 4mm MDL as shown in Fig. AII.(32) 1. Internal boundary element steel yielded at 6 mm

MDL as shown in Figs. AII.(32) 4, 7 and 8. Web reinforcing steel was also observed to yield as shown in Figs. AII.(32) 5 and 6. This confirmed the high rotational ductility acquired due to the added **'ECSP'**.

The confining steel plates **'ECSP'** prevented the initiation of diagonal cracks at the wall edges. It also delimited the truss action in resisting shearing forces at the lower third of the wall. Hence, only very low interaction from horizontal links was recorded at the bottom third of the wall; only 400 microstrain were recorded as indicated in Fig. AII.(32) 7. At 500 mm from the foundation beam, where **'ECSP'** stopped, horizontal links showed lower interaction level whereby 150 microstrain were recorded as shown in Fig. AII.(32) 10. At the top wall height, strain in links was again reduced to 40 microstrain as shown in Fig. AII.(32) 12.

The **'ECSP'** proved to be extremely effective in confining the concrete in compression, as confirmed in the above performance criteria. This was justified by strain recordings at various sides of these plates. From the strain gauge plots shown in Figs. AII (321) 13, 14, 15, 16, 17, 18, 19 and 20, it may be concluded that the short-sided plate (60 mm) recorded higher strains than the longitudinal side of the plates. This confirms the need of closely spaced ties in the confined zones. Also, it highlights the importance of closed hoops 135º keys.

7.2.9.5. Ductility enhancement

It is concluded from the test results reported above that the curvature and displacement ductility supply of shear walls could be improved without affecting their strength or stiffness. In this test, a displacement ductility of 4 was achieved while no confinement reinforcement was provided in the first intense. This is confirmed from the stiffness-displacement plot for SW32/SW33 shown in Fig. 7.27.

The method can be easily adopted in practice whereby steel plates can be attached to the wall corners by means of high strength grip friction bolts. The clearance gap between the two surfaces may be filled with non-shrink grout to ensure good monolithic action. This ductility enhancement scheme was applied to a twelve storey height building in Cairo (Souria building, 1992). Alternatively, external hoops may be provided at the wall edges after drilling holes in the concrete wall to allow for continuity of steel reinforcement. This was observed in practice in various sites. Due to financial and time constraints, testing this scheme was not possible.

7.2.10. Model SW34

7.2.10.1. Strength enhancement method

To simulate a realistic strength-only intervention scenario, it was intended that model SW34 would have a flexural strength of 85 KN, but was supplied with only 55 kN in the first instance. It was decided to apply **E**xternal **U**nbonded **S**teel **P**lates (hereafter referred to as **'EUSP'**) to upgrade the strength without affecting the stiffness. The 1200x60x5 mm plate was connected to the wall through a cleat angle at the soffit of the plate, which was attached to the foundation beam through 3 chemical bolts 12 mm in diameter. The plates were also attached to the top loading beam by an assembly of steel angles and gusset plates as shown in Fig. 6.2. Self-fixing mechanical bolts 16 mm diameter were used at the top connection. To allow for an initial slack (hereafter referred to as the **I**nteraction **D**elay **M**echanism **'IDM'**), slotted holes were added to the connecting gusset plates. This allowed for 3 mm slack at the top of the steel plate

The philosophy behind the design of such a system is that when the wall is loaded horizontally, it undergoes a vertical elongation due to the wall cracking and rotation. If a strengthening scheme is selected to contribute after the wall has reached its yield strength, a considerable strength enhancement can be achieved without affecting neither the uncracked nor the yield stiffness of the wall. To a lesser extent, the dynamic characteristics of the wall will be affected.

7.2.10.2. General observations

Cyclic loading was applied to the tested model. Two cycles of displacement were applied at each deformation level with 2 mm increments as shown in Fig. 7.28.

Wall cracking started as horizontal flexural cracks in the boundary elements. Closely spaced hoops (30 mm) caused the cracks to be narrow and well-distributed. The horizontal cracks propagated into coarsely distributed inclined cracks in the web. Intersecting cracks from opposite directions segmented the plastic hinge region into several horizontal layers. Because of these horizontal cracks, truss action was not developed to transmit shear. After steel yielding and hence crack widening, shear was transferred primarily by interface friction and dowel action. This shear transfer was adequate to maintain the integrity of the wall until failure occurred due to concrete crushing in the maximum compression zone.

Self fixing mechanical bolt attachments at the top loading beam were properly designed and did not show any distress. Also, chemical bolts at the foundation beam showed a good performance with no signs of bond failure. Steel reinforcement was checked at the end of the test after breaking down the existing concrete at the maximum compression zones. The hoops as well as the links were found in a very good condition which proved that closed links and hoops are justified in case where high ductility supply is needed.

7.2.10.3. Crack pattern

First cracking was noticed at 1.5 mm MDL at the lowest section of the boundary element, i.e. square (A-1) in Fig. 4.2. Horizontal flexural cracks were traced in the lower third of the wall height (A-1 to A-4 and E-1 to E-4) in Fig. 4.2 with maximum crack widths of 2.2 mm while being loaded to MDL higher than 10 mm at the soffit of the wall. The cracks were reduced to 0.6 mm at 0.0 MDL. The relatively wide cracks indicated that the tensile reinforcing steel at the boundary elements yielded at a very early stage. This was confirmed by the strain gauge readings.

The flexural cracking intensity was noticeably reduced along the wall height. Flexure-shear cracks characterised by horizontal leading to inclined cracks at about 25°, to the horizontal, were initiated at a much reduced intensity at mid-wall height (A to E and 5 to 7) in Fig 4.2. The inclination of cracks was increased along the wall height. These cracks were observed at higher displacement levels from 16 mm MDL onwards. At the last MDL, a few cracks propagated at the top wall corners with maximum crack width of 0.2 mm (A-9, A-10, E-9, E-10).

7.2.10.4. Force-displacement hysteresis

The wall reached its yield strength at about 6 mm MDL associated with 2.7 mm vertical displacement as shown in Fig. AII.(34).1, 2 and 3. With the increase in cyclic displacements from 6 mm to 8 mm, the wall displayed a ductile behaviour and a stable resistance of about 60 kN was obtained. Meanwhile, the initial stiffness was reduced from 15 kN/mm to 8 kN/mm at the yield level.

At 8 mm MDL the design vertical slack of 3 mm was consumed by the wall extension allowing the EUSP to contribute to the wall tension reinforcement. This was manifested by an increase in the wall strength from 60 kN to 70 kN (first recorded cycle

by strain gauge 25 logging middle EUSP strains). The wall initial stiffness was further reduced at that stage to 5 kN/mm.

At 12 mm MDL, further strength increase up to 80 kN was recorded. Since the three EUSPs started to pick up load at 8 mm MDL, they were fully interacting at 12 mm MDL. At the IDM stage, and due to the added steel plates, a minor increase in stiffness was observed as shown in Fig. 7.30. The wall showed a second stage of ductile behaviour where the newly-achieved strength level of about 80 kN was sustained up to 26 mm MDL. An envelope of force-displacement hysteresis is given in Fig 7.29. This would represent the wall response under monotonic loading until the onset of strength decay.

Failure of the wall was reached at the second cycle of 26 mm MDL due to deterioration of the confined concrete in the boundary elements and was characterised by a drop in strength of about 20%. The residual strength was 60 kN on both sides, associated with an irrecoverable displacement of 17 mm.

7.2.10.5. Observed ductility

Force-Displacement hysteresis showed the ductile wall behaviour at various strength levels as shown in Figs. AI (31) 1 and 10. It also showed that the wall behaved symmetrically on both sides even at the critical stages of mobilisation of the EURBs at quarter, mid and full height of the wall. A displacement ductility of 4.70 at 60 kN strength level (initial strength) and of 2.40 at 90 kN strength level (enhanced strength) were achieved during testing. A single line force-deformation curve provides an envelope for the hysteresis loops. This curve would also simulate approximately the wall behaviour under monotonic loading up to the onset of strength decay, as depicted in Fig. 7.32.

Cycling at the same displacement level for such a ductile system showed negligible stiffness degradation and negligible drop in strength except at the ultimate displacement levels. Upon load reversal, the wall showed little initial resistance until the previously-opened cracks were closed. As the crack closure took place, the resistance of the wall element was gradually restored. This initial softening, followed by gradual build-up of load resistance, is reflected in the force-deformation hysteretic as 'pinching' of the loops, which is generally low and smooth in flexure-dominated response. It is much more abrupt in shear-dominated response, as was observed and recorded in other tests. Nevertheless, the pinching in this case was relatively high due to the release of the

elasto-plastic strain energy in the EUSP in one side and their interaction on the other side. The wall-EUSP were separated by the designed slack that was larger than the wall extension at yield.

When opposing sides of cracks came into contact under cyclic loading at MDLs exceeding 24 mm, some grinding of concrete took place associated with minor strength degradation. .This was then followed by concrete cover spalling. Hysteresis loops corresponding to the same deformation level did not reach the previous capacity at a higher deformation levels, so long as the axial compressive strength of the cracked concrete at the boundary edge was not exceeded. At this point, a rapid degradation of strength decay was clear at 26 mm MDL

7.2.10.6. Strain gauge readings

Strain gauge plots showed that boundary edge reinforcing steels yielded at the very early loading stages i.e. 2 mm to 5 mm MDLs as shown in Figs. AII.(31).1, 2, 11 and 12. They showed a maximum strain of 450 Microstrain at mid-height of the wall as shown in Fig. AII.(31) 22. Internal boundary element reinforcement also yielded at early stages as depicted from Figs AII.(31) 3, 4, 9 and 10. Web reinforcement have also yielded as confirmed in Figs AII.(31) 5, 6, 7 and 8.

Horizontal stirrups showed a very low interaction level since the maximum recorded strain was only about 250 microstrain at the wall low level (square 2) as shown in Fig. AII.(34).13, 14 and 15.

Hoop reinforcement at the lowest level (square 1), Fig. 4.2, showed a high level of confinement. About 150 microstrain were recorded Fig AII.(34) 16. Hence, concrete started to deteriorate and then crushed due to loss of effective confinement. However, the hoops at one third of the wall height recorded low strain and hence low confining stress as depicted in Figs. AII (34) 18 and 24: a maximum of 80 microstrain was recorded. It can be concluded from strain gauge readings that the shear reinforcement could have been reduced without affecting the wall behaviour and its ductility.

The EUSP were only active in tension. They recorded zero strain and hence zero stress until 10 mm MDL (noting that initial yield strength was achieved at 6 mm MDL). They recorded 1800 microstrain at 12 mm MDL as observed in Figs. AII (34) 19 and 20. One sided force-strain hyteresis were recorded (tension side only) for each of them

(only 10 microstrain was recorded in the compression side which reflected the buckling load of these EURBs and which is practically negligible).

7.2.10.7. Strength enhancement

It is concluded from the test that the flexural strength of shear walls can be improved without affecting their stiffness and hence their dynamic characteristics, provided that diagonal tension and sliding shear failures are prevented. In this test, a strength increase of about 50% was achieved. This is confirmed from the stiffness-displacement plot for SW33/SW34 shown in Fig. 7.30. In practice, a device for general interaction would be needed (such as a spring mechanism) to avoid the application of an impact force upon loading the EURPs.

The method can be easily adopted in practice i.e. external unbonded steel plates and/or profiles can be attached to the lower and upper levels by means of self fixing bolts while having slotted holes allowing for the designed slack to occur along the any of the connections. The whole assembly should then be protected by means of an efficient anti-corrosive paint, epoxy type of material or equivalent. This procedure will ensure that the EUSP will have no contribution on the compressive side but ensure a delayed interaction while acting on the tension side.

7.2.11 Model SWR35

The intact model SW35 exhibited a displacement ductility of 2.0. It was cycled up to 14 mm MDL only. The model was reinforced with five starter bars 12 mm in diameter to prevent shear sliding failure and showed extensive flexural cracking above the top line of starter bars. The cracks were reduced in intensity further up the wall height. The wall showed no sign of concrete deterioration or spalling of concrete cover.

7.2.11.1. Repair approach and procedure

The stiffness of the model was targeted as the objective of the intervention, with the intention of not affecting neither the strength nor the ductility, hence representing a stiffness-only scheme. This may be achieved by delimiting the number and extent of cracks as well as reducing the crack-face sliding. This objective is conventionally achieved by epoxy resin injection. However, this system has many practical limitations as mentioned in section (6.2.2). These were demonstrated experimentally for model SWR22 discussed in section (7.2.6).

As for model SWR9, a new concept was applied whereby steel plates were attached to the cracked wall (by means of high strength epoxy resin) at specific locations. In order not to affect the wall strength, the steel plates were neither connected to the foundation beam nor to the top loading beam. Moreover, the dimensions were reduced so as to avoid any effects on the deformational behaviour of the wall model. Plate locations were chosen so as to supply the minimum possible strain energy to prevent crack opening. The main difference between this model and SWR9 is that the former had the maximum crack intensity at the quarter of the wall height and was cycled up to 14 mm MDL only i.e. 1.1% drift, while the later had the maximum crack intensity at the lower level of the wall and was subjected to severe concrete deterioration when tested up to a maximum displacement level of 26 mm, i.e. 2.1% drift.

The applied repair scheme consisted of attaching four steel plates onto the concrete wall. No epoxy resin injection was applied. To achieve such a repair scheme, a pneumatic hammer was employed to roughen the concrete surface and to expose the aggregate, followed by vacuum cleaning to remove all dust and loose particles. Four steel plates of dimensions 1100x19x3.6 mm were attached to the concrete wall (at the wall edges) allowing for 50 mm clearance between the top loading beam, the bottom fixing beam and the steel plates.

To satisfy the code-defined serviceability limit states, since the existing crack width was in excess of that allowed, treatment of exposed cracks was required. A special surface treatment emulsion paint (penetrating by capillarity) was used to seal the cracks, thus protecting the steel from corrosion due to moisture migration.

7.2.11.2. General observations

The model was subjected to cyclic loading with controlled displacement. Two cycles of displacement were applied at each deformation level with 2 mm increment per step as shown in Fig. 7.31.

The wall reached its yield strength of 70 kN at 6 mm MDL. This was sustained up to a displacement level of 18 mm. The wall showed a ductile behaviour sustaining a constant strength up to 18 mm MDL, and survived a higher number of cycles and displacement amplitudes compared to the intact wall. A drop in strength occurred at the first cycle of 20 mm displacement amplitude while further drop in strength took place at higher displacement levels.

The tested wall showed lower stiffness up to 4 mm MDL, when compared with the intact wall behaviour. It showed comparable behaviour with the original wall stiffness at higher MDLs, as shown in Fig. 7.33. With the increase of displacement amplitude, the original cracks were reopened as a consequence of plate/wall debonding. This was the result of concrete cover failing in shear at the interface between the epoxy mortar and the wall.

With every increment of displacement level, plate-concrete debonding took place. This was confirmed by a clear strength reduction in the second cycle at the same displacement level.

Concrete deterioration took place from 16 mm MDL onwards, causing a drop in strength at the second cycle of the same MDL. At 20 mm MDL, severe concrete deterioration took place leading to a 25% drop in strength.

7.2.11.3. Crack pattern

No newly developed cracks were observed up to 10 mm MDL and the lowest squares [A-1 to E-1] were totally uncracked. Also, no newly-developed cracks were observed in the lowest 30 cm due to the presence of the additional starter bars.

The observed crack pattern consisted mainly of diagonal cracks confined between the two steel plates. The highest intensity of cracks associated with the largest crack width was observed in squares [C-3, C-4], just above the line of the starter bars.

7.2.11.4. Force-displacement hysteresis

Force-displacement hysteresis shown in Fig AI (R35) 1 demonstrated that the wall behaved in a ductile manner with stable hysteresis loops up to 18 mm MDL. However, its displacement ductility was reduced to 3.0 instead of 4.0 for SWR9. This can be attributed to the fact that starter bars caused over-stiffening of the first quarter of the wall height. No cracks were observed in this area. Also no horizontal drift was recorded and hence the effective deformable wall height was reduced to 90 cm. In view of effective heights of both SWR9 and SWR35, (120 and 90 cm respectively), it is concluded that the wall showed the same rotational ductility capacity as SWR9. However, the reduced effective wall height led to a reduced displacement ductility. An envelope for the force-displacement hysteresis was given in Fig. 7.32.

7.2.11.5. Strain gauge readings

The external steel plates were gauged at sixteen locations along the wall height; recording strains in the vertical direction. These showed that the highest strain readings were in the vicinity of the line of starter bars, where 150 microstrain were recorded, as shown in Figs AII (R35) 5.

Below the above-mentioned critical line, a maximum of 100 microstrain was recorded as depicted in Figs AII (R35) 1 and 2. These were reduced further up the wall height down to 40 microstrain as depicted in Figs AII (R35) 3 and 4.

The outermost flexural reinforcement were strained up to 700 microstrain at the lowest section of the wall. Internal boundary element reinforcement were strained up to 320 microstrain only. This is attributed to the presence of starter bars and confirms that

the maximum critical section for main flexural reinforcement was shifted upwards by the end of starter bars as shown in Figs AII (R35) 7 and 8.

The lower hoops recorded only 30 microstrain. The lower ties showed also low level of interaction whereby only 60 microstrain were recorded. This was confirmed by the fact that no diagonal cracks were observed in the lower third of the wall, where additional starter bars were provided.

7.2.11.6. Stiffness reinstatement

It is concluded that the stiffness degradation of the repaired wall depends mainly on the rate of the wall extension leading to plates debonding. A compatible stiffness-displacement behaviour for the intact and repaired wall was achieved, as may be confirmed by Fig. 7.33.

After testing, it was observed that the lower third of the plates were debonded. Steel reinforcement was checked at the end of the test after breaking down the existing concrete at the boundary elements and was found to be fracture free, no bond slippage of stirrups or opening in hoops was observed.

It is hence concluded that the cracked flexural stiffness of shear walls can be fully reinstated, and if requested enhanced, without affecting either strength or ductility. This may be of great importance in the case of exiting buildings where tuning the members stiffness can lead to a more regular structure. This would lead to higher allowable behaviour factors according to modern seismic codes which impose strict regularity conditions. Such intervention can be also applied in the case of RC structures damaged by a small magnitude earthquakes, which cause a reduction in the stiffness of the structure while having a small effect on the strength. Therefore, in repair of such a structure, reinstatement of stiffness with no effect on strength should be the objective of the intervention scheme.

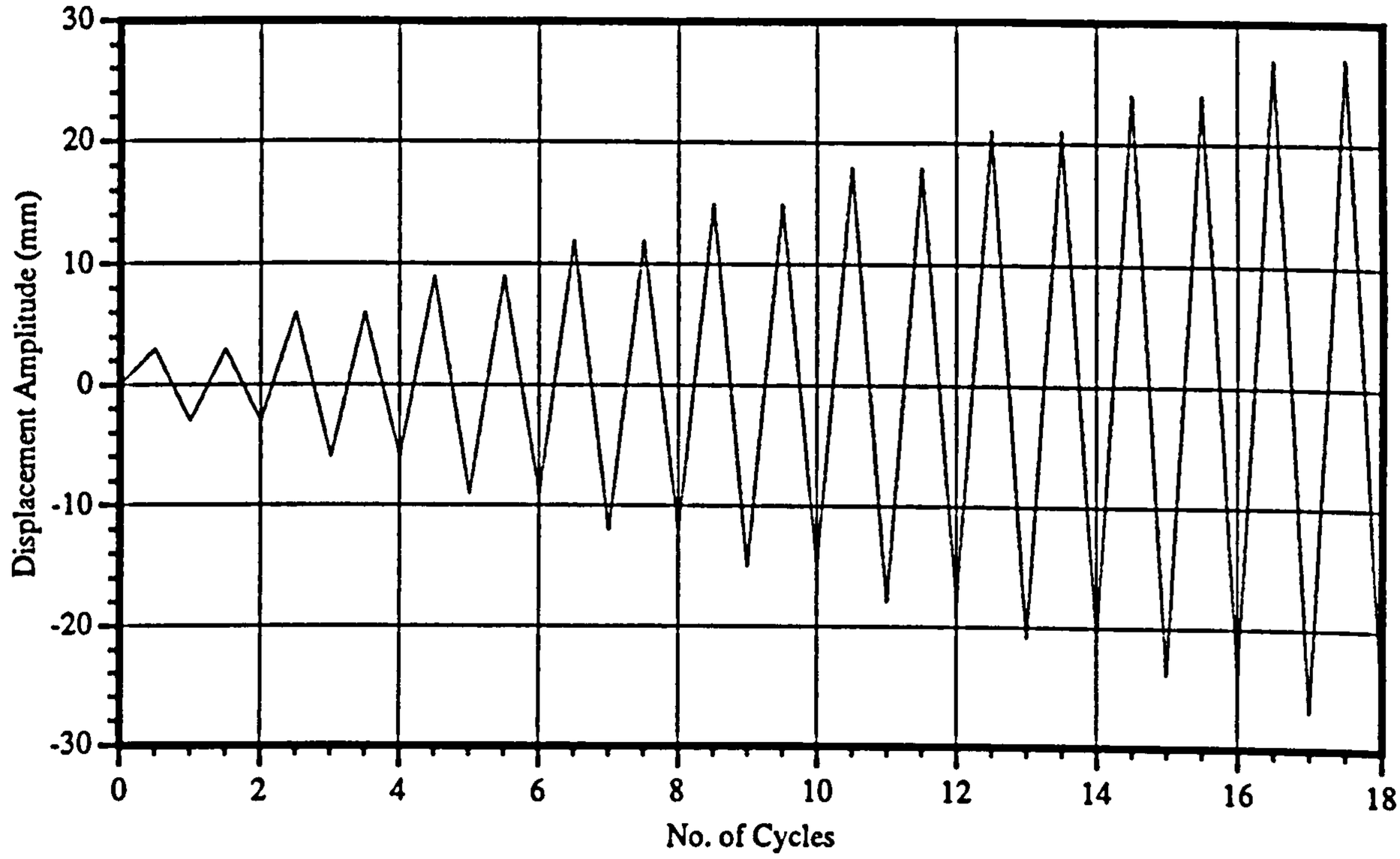


Fig. 7.1 Displacement History for SWR4

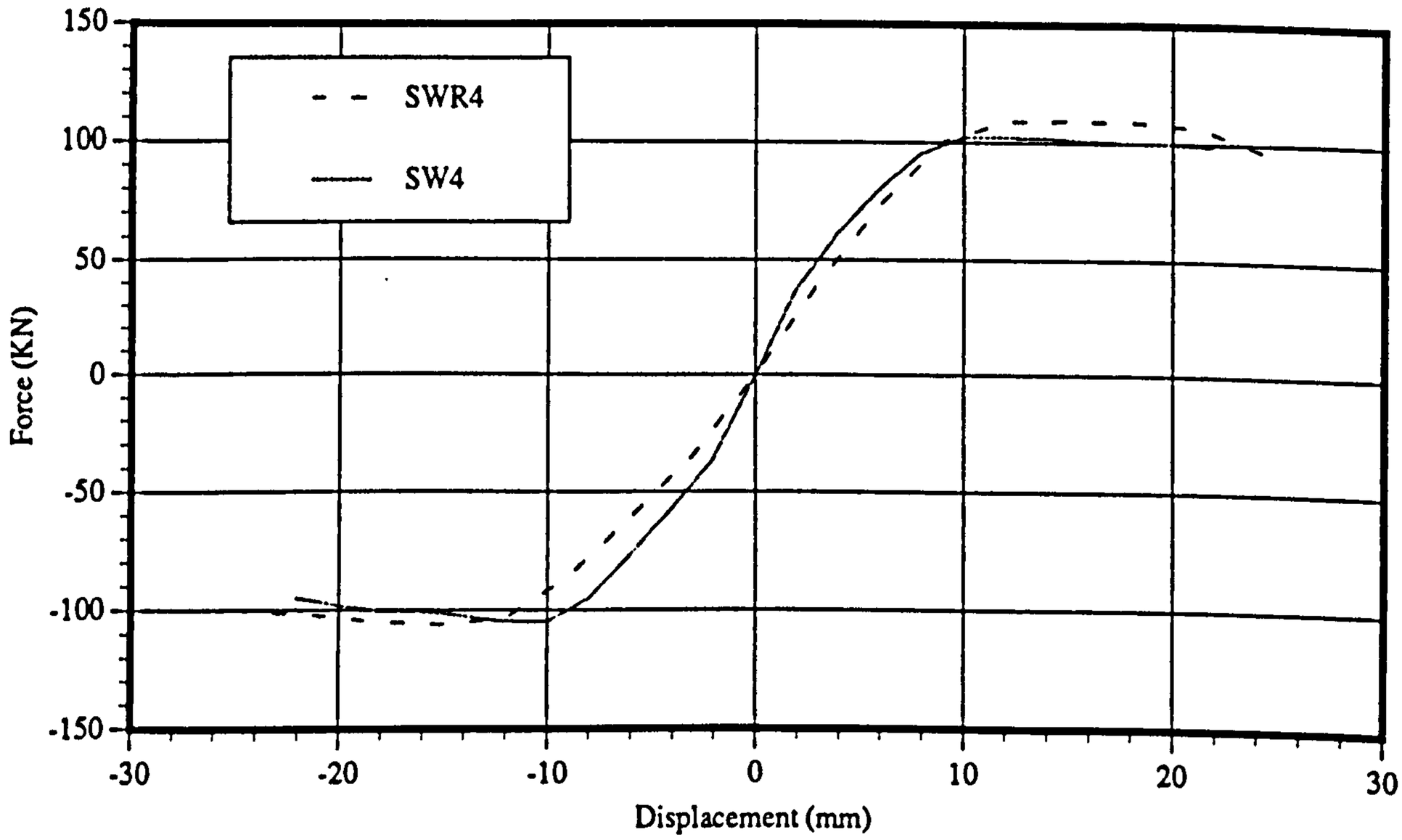


Fig. 7.2 Force-Displacement Hysteresis Envelope for SW4/SWR4

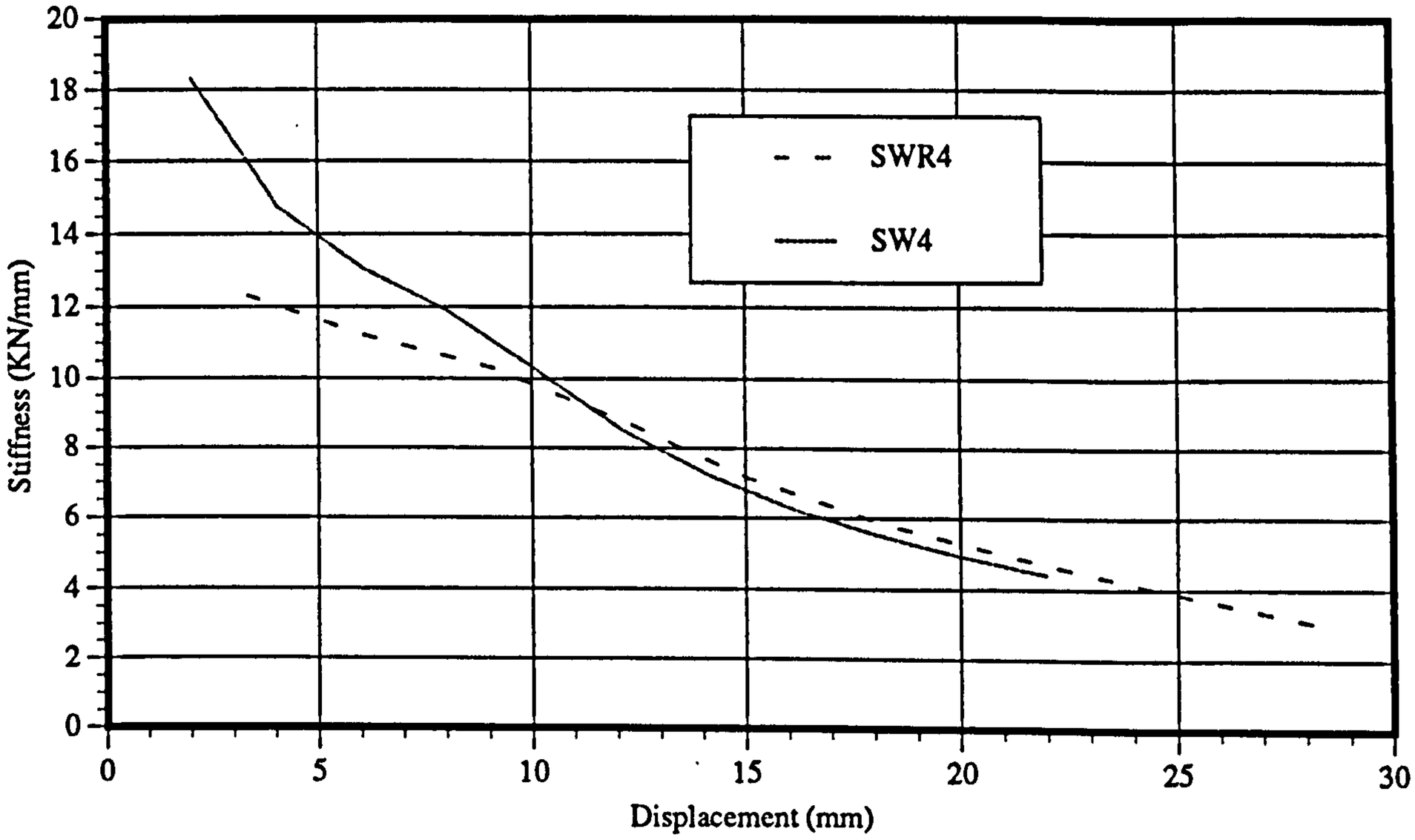


Fig. 7.3 Stiffness-Displacement for SW4/SWR4

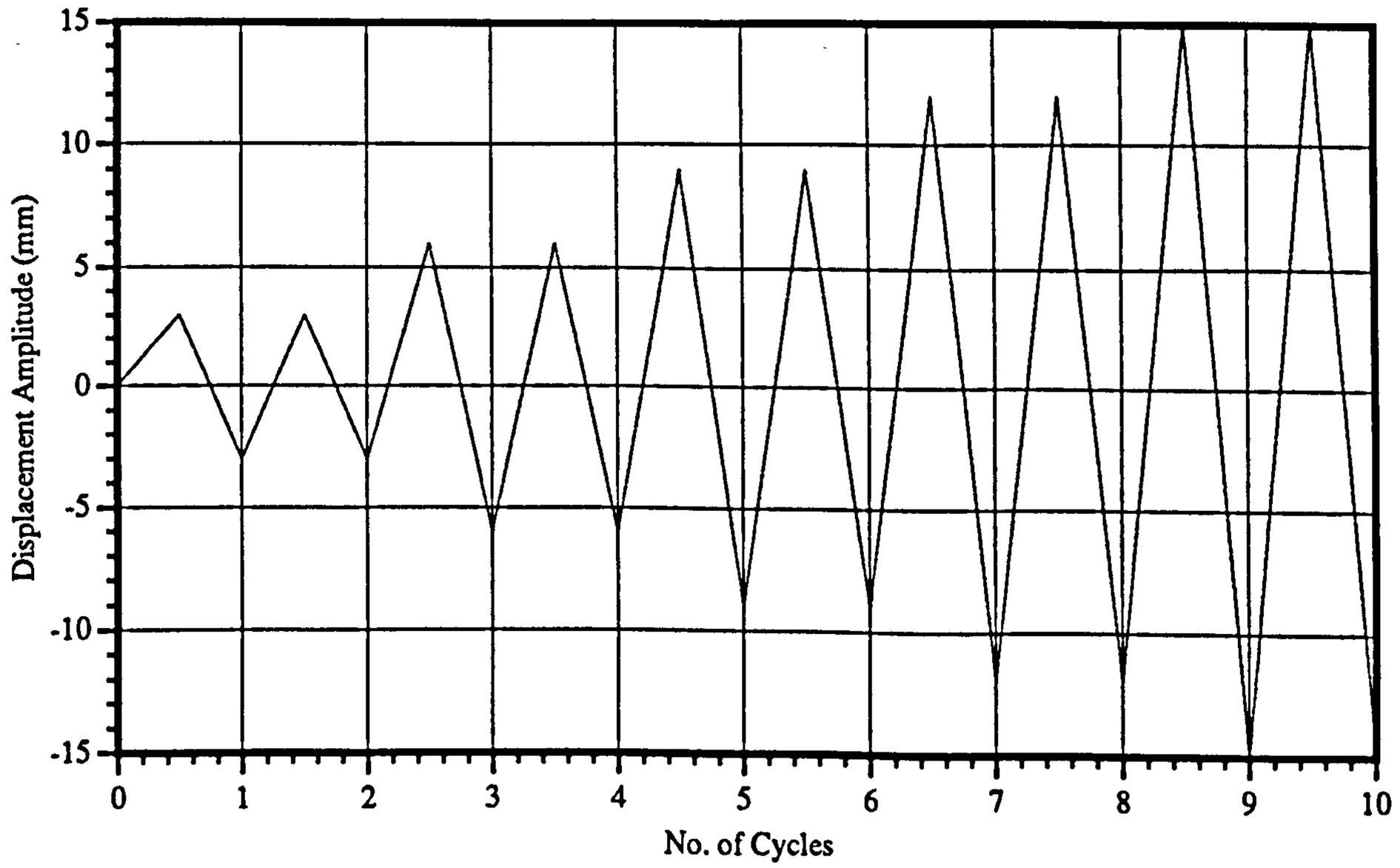


Fig. 7.4 Displacement History for SWR5

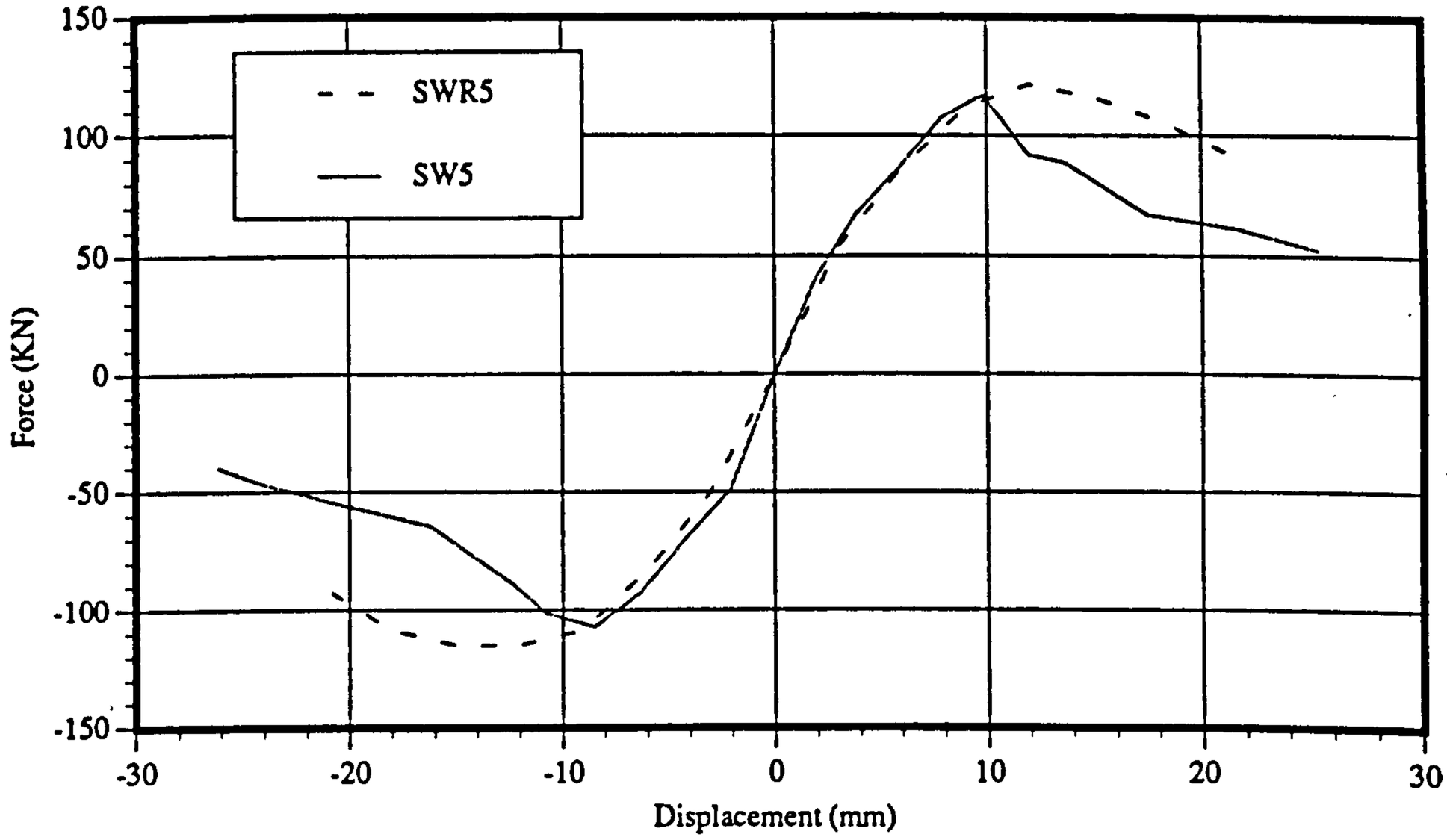


Fig. 7.5 Force-Displacement Hysteresis Envelope for SW5/SWR5

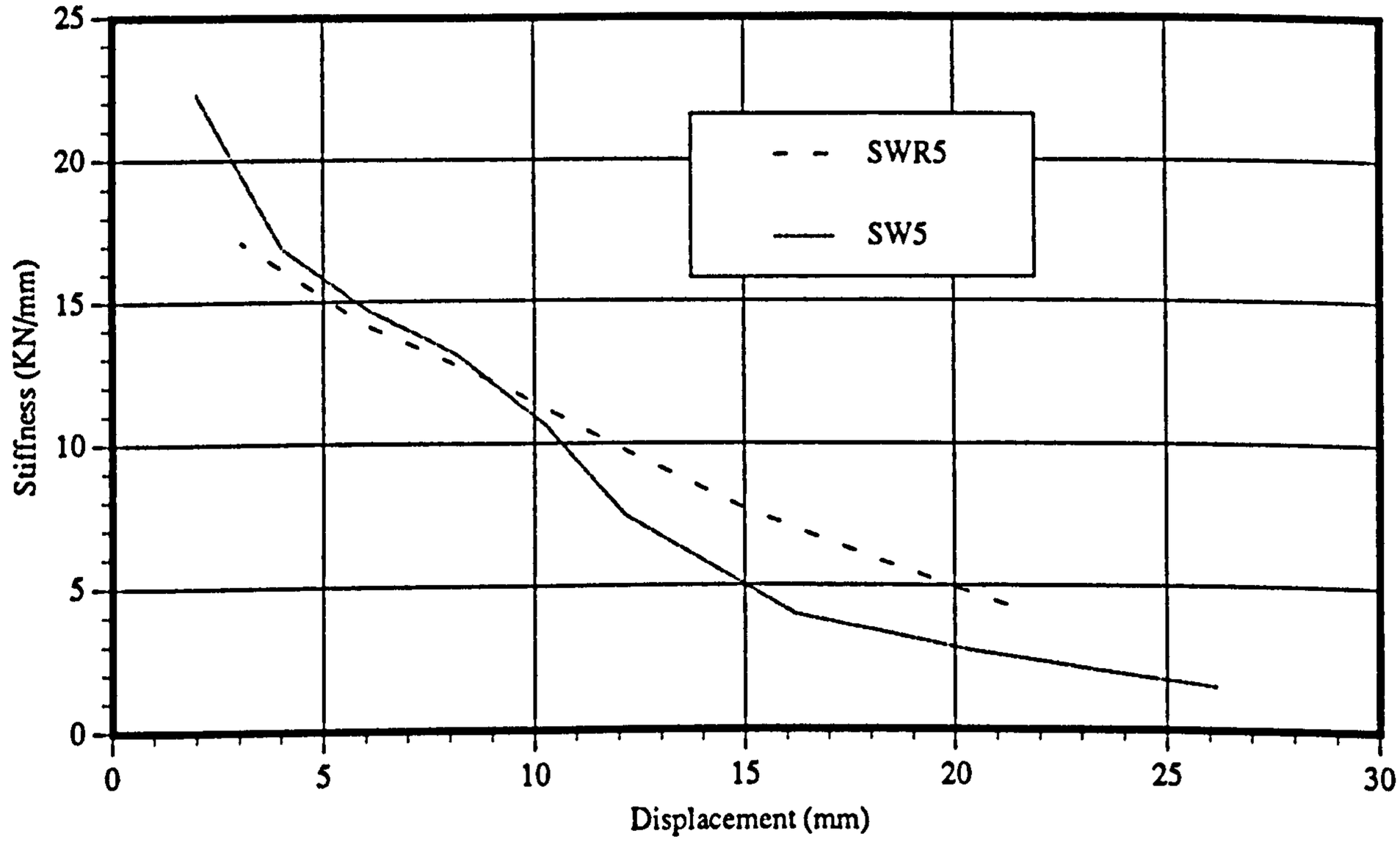


Fig. 7.6 Stiffness-Displacement Plot for SW5/SWR5

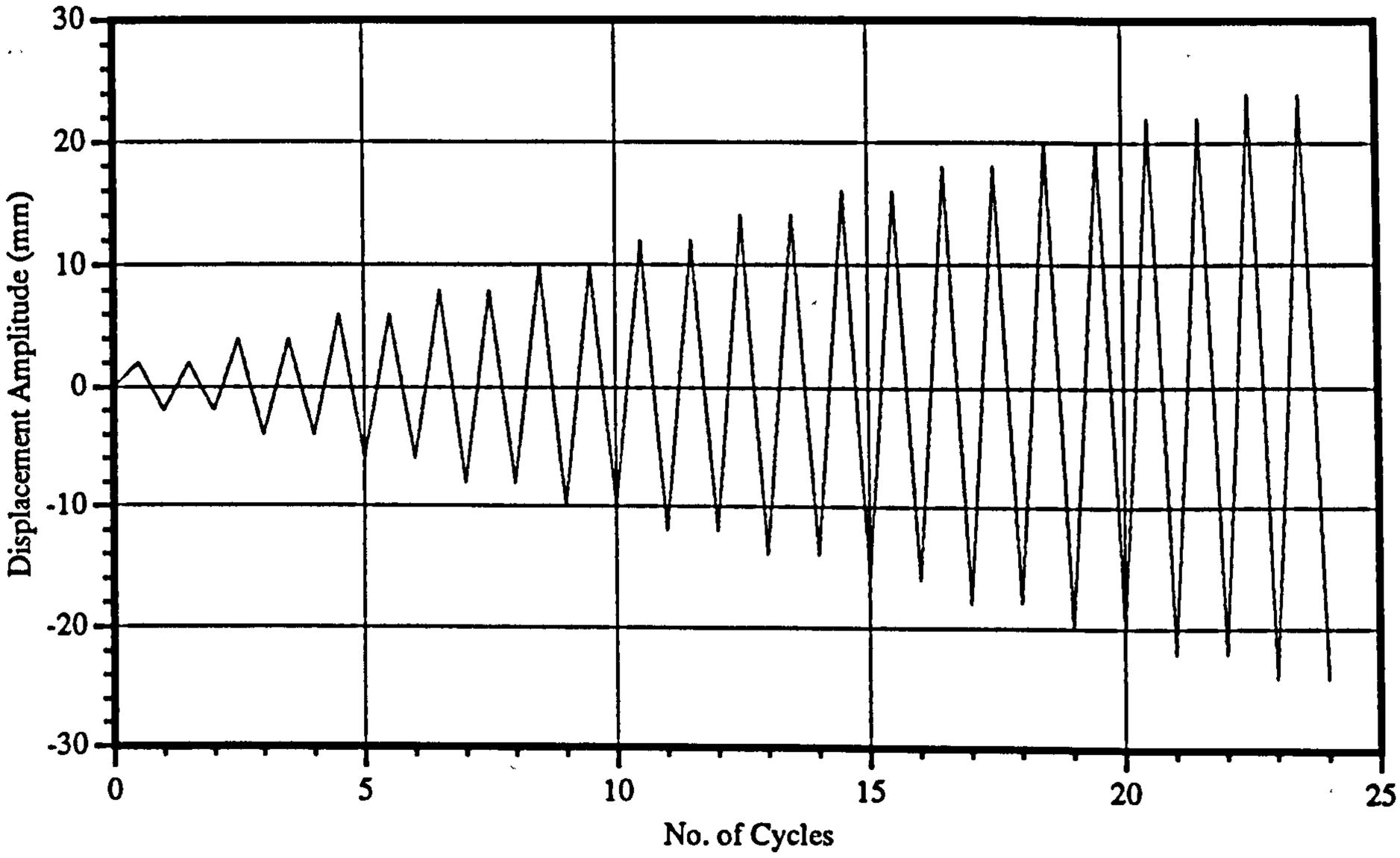


Fig. 7.7 Displacement History for SWR7

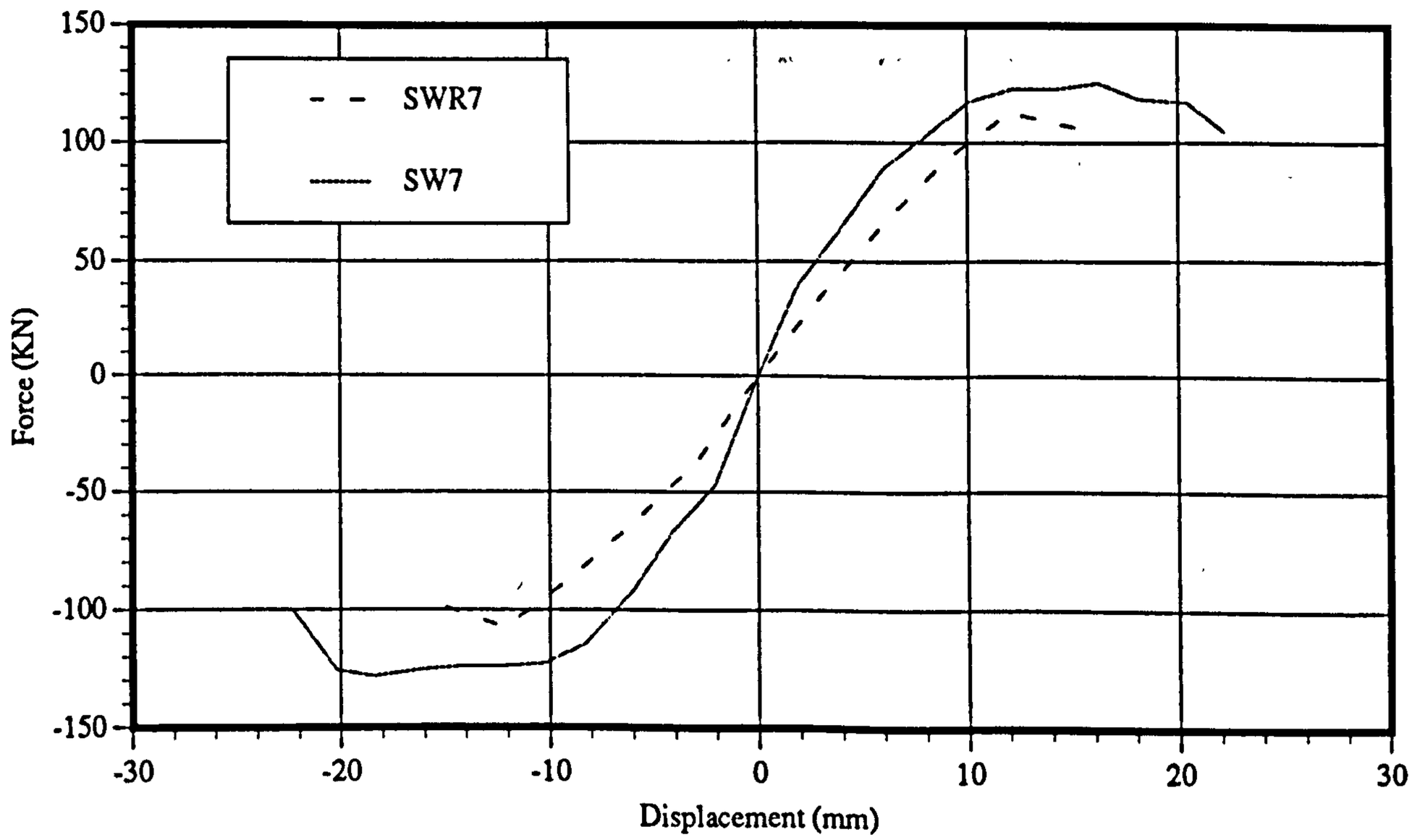


Fig. 7.8 Force-Displacement Hysteresis Envelope for SW7/SWR7

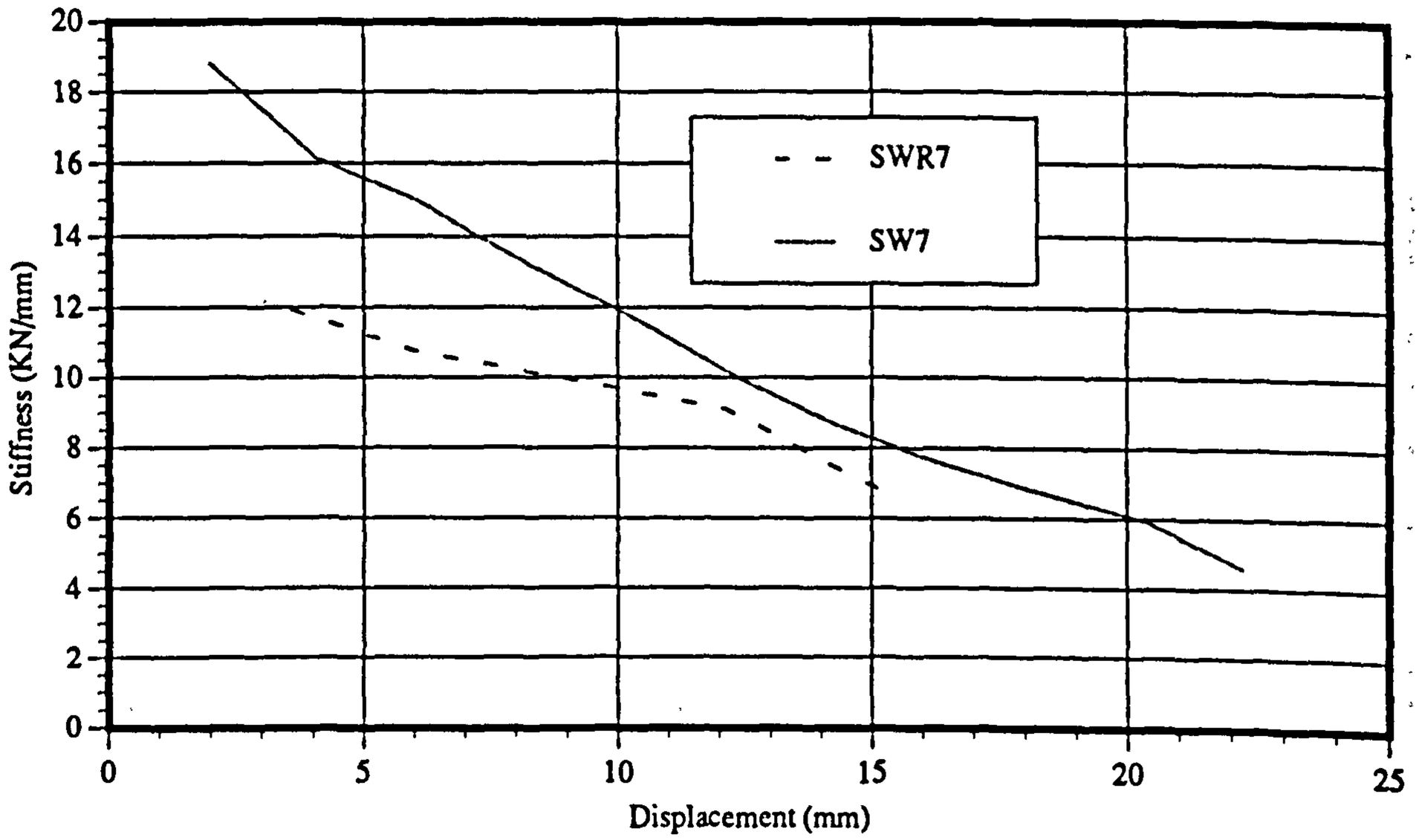


Fig. 7.9 Stiffness-Displacement Plot for SW7/SWR7

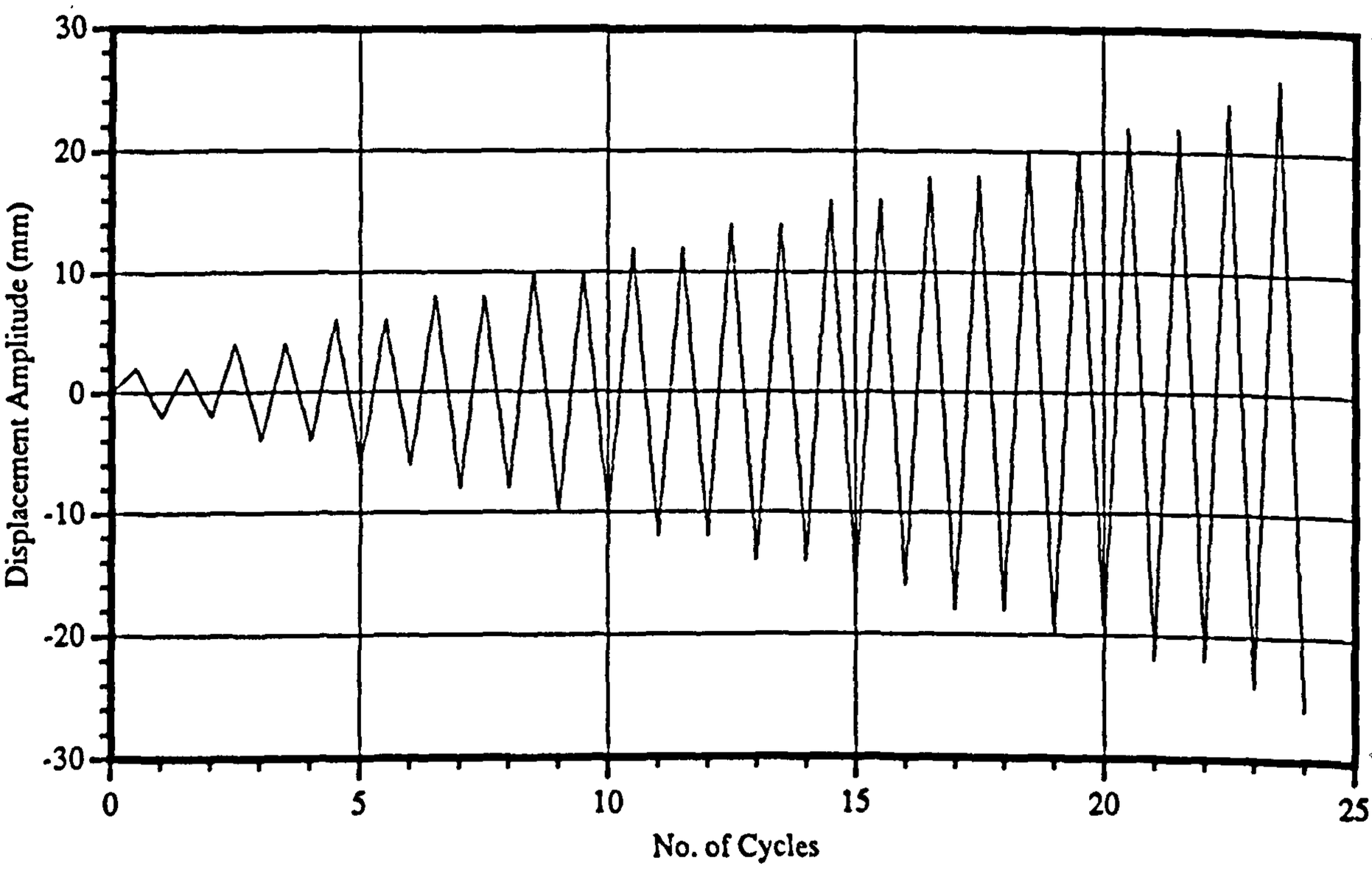


Fig. 7.10 Displacement History for SWR9

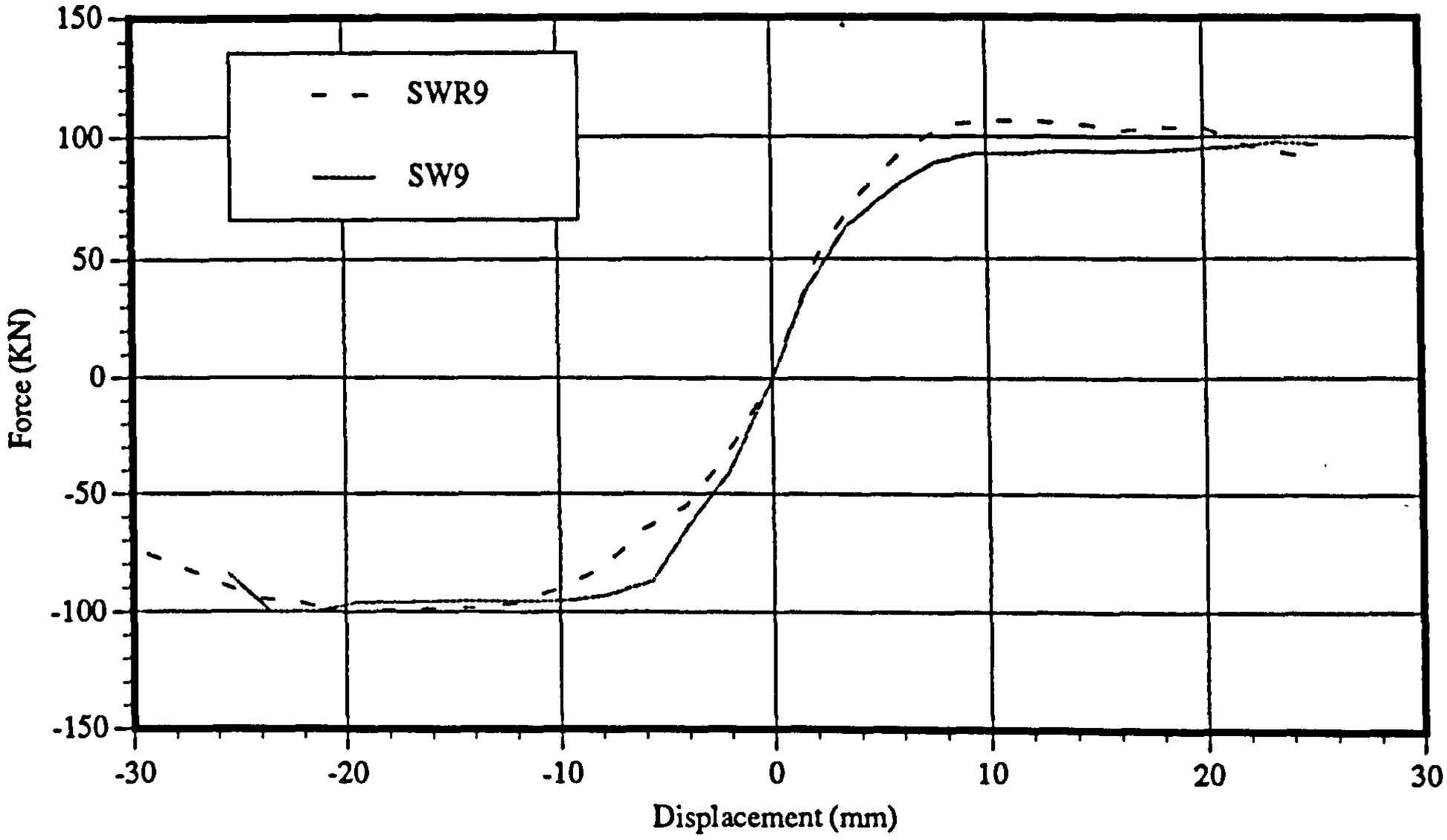


Fig. 7.11 Force-Displacement Hysteresis Envelope for SW9/SWR9

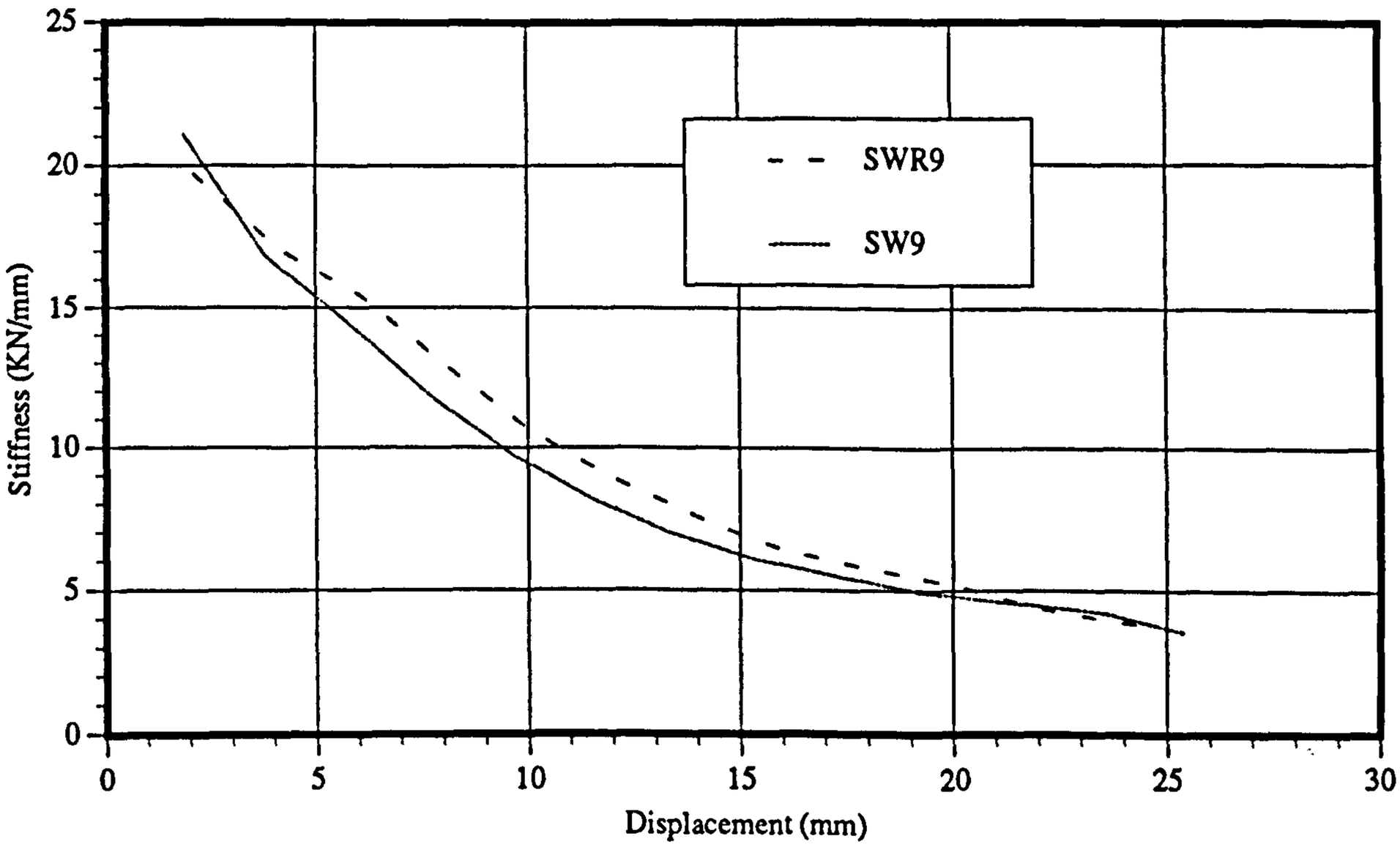


Fig. 7.12 Stiffness-Displacement Plot for SW9/SWR9

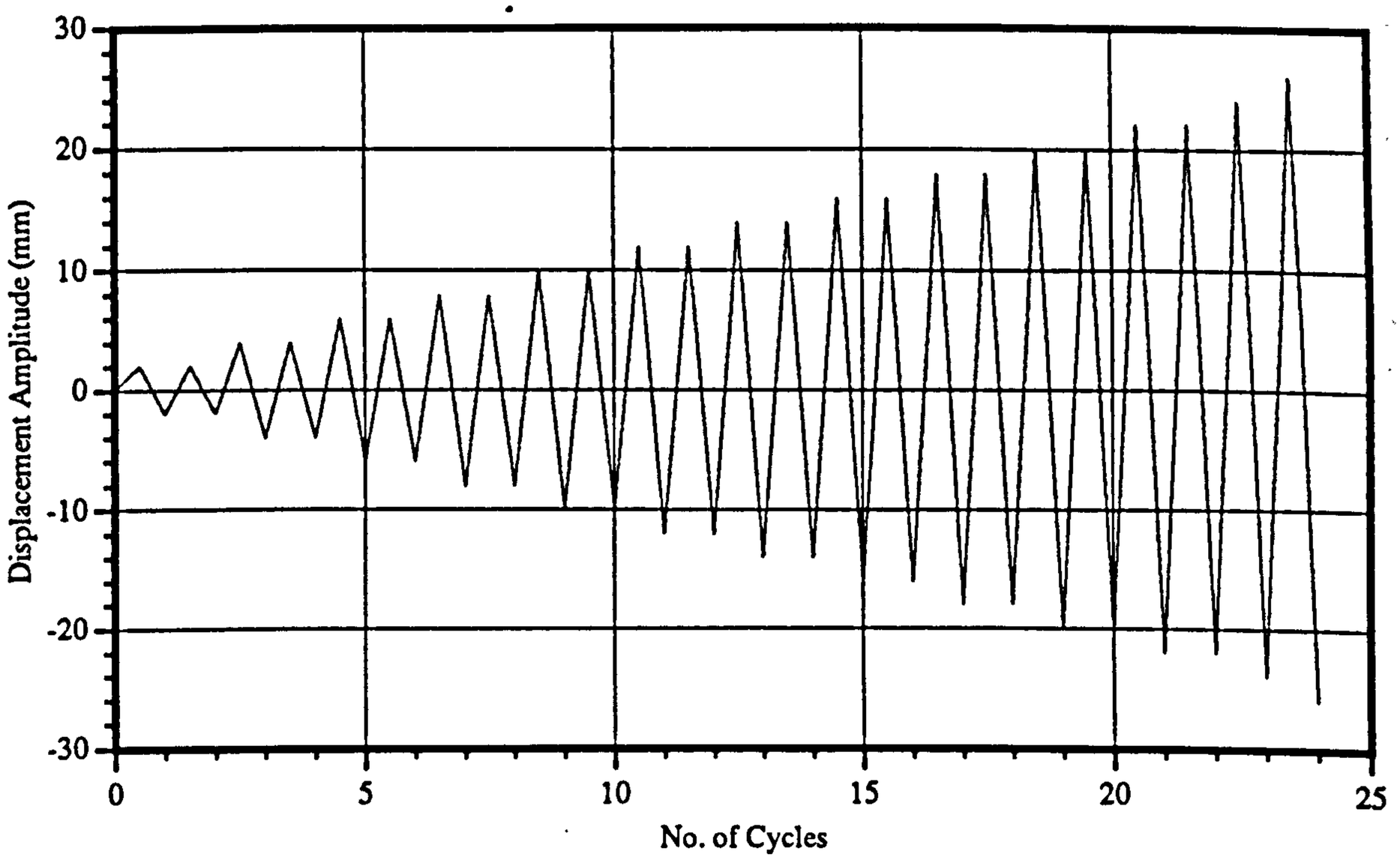


Fig. 7.13 Displacement History for SWR21

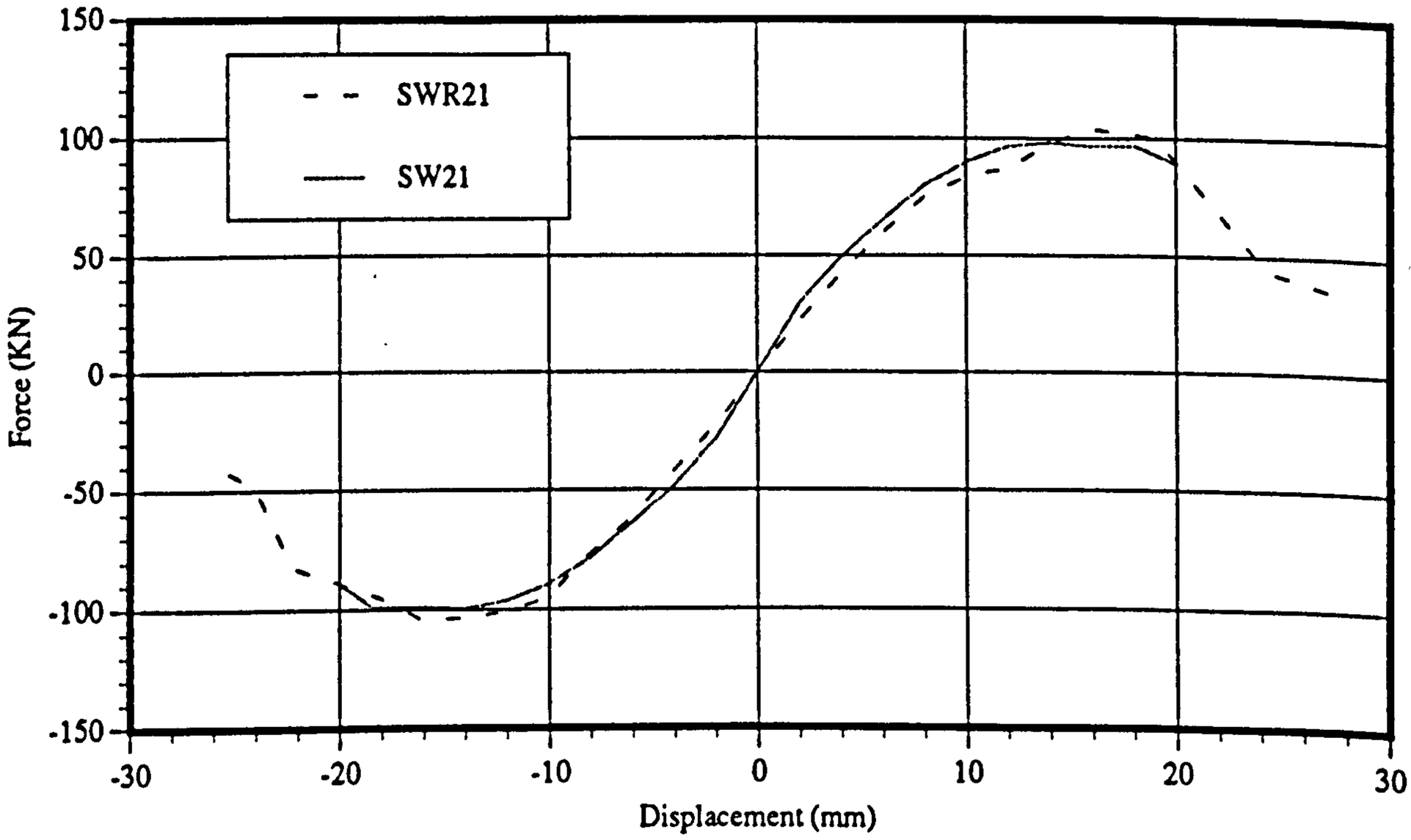


Fig. 7.14 Force-Displacement Hysteresis Envelope for SW21/SWR21

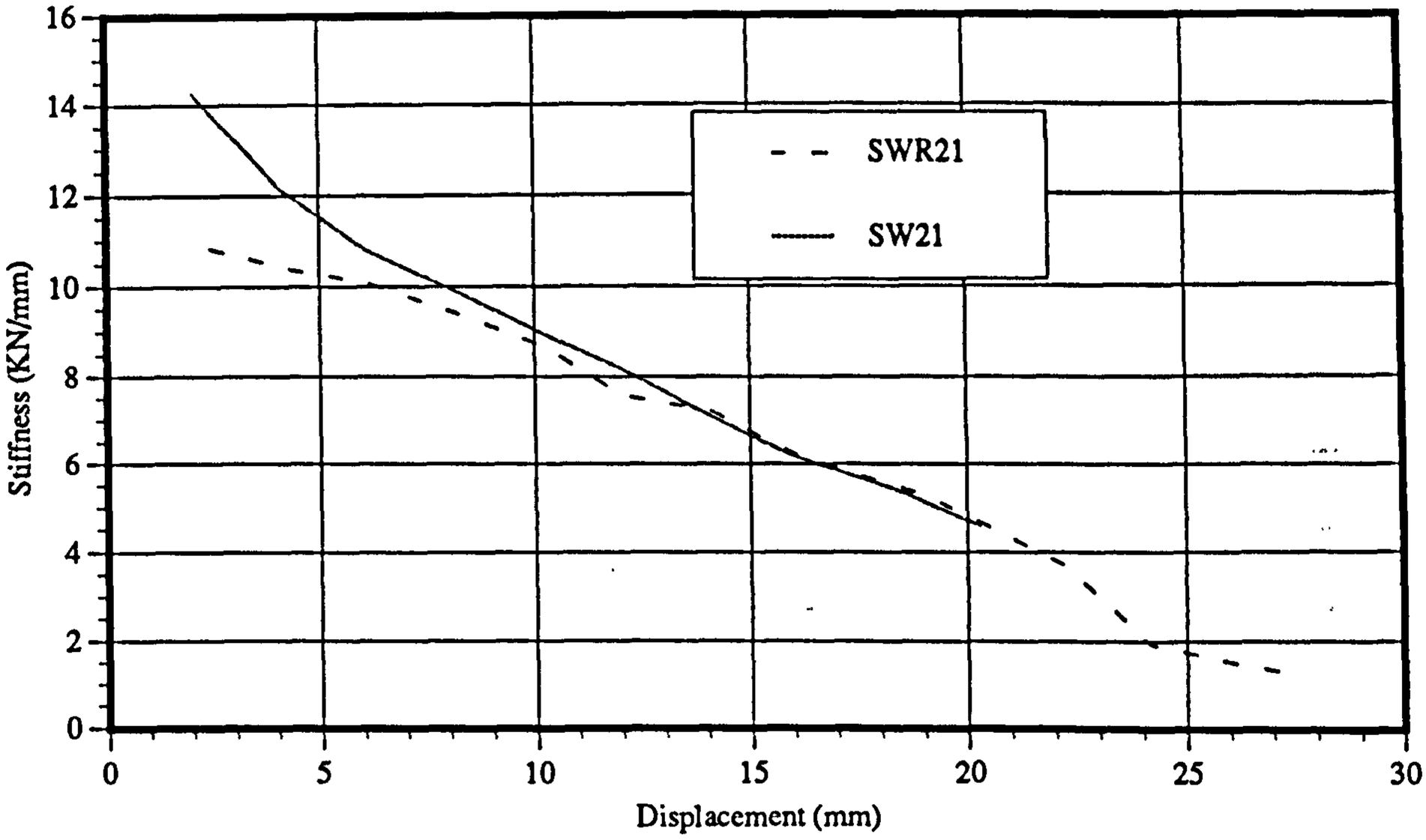


Fig. 7.15 Stiffness-Displacement Plot for SW21/SWR21

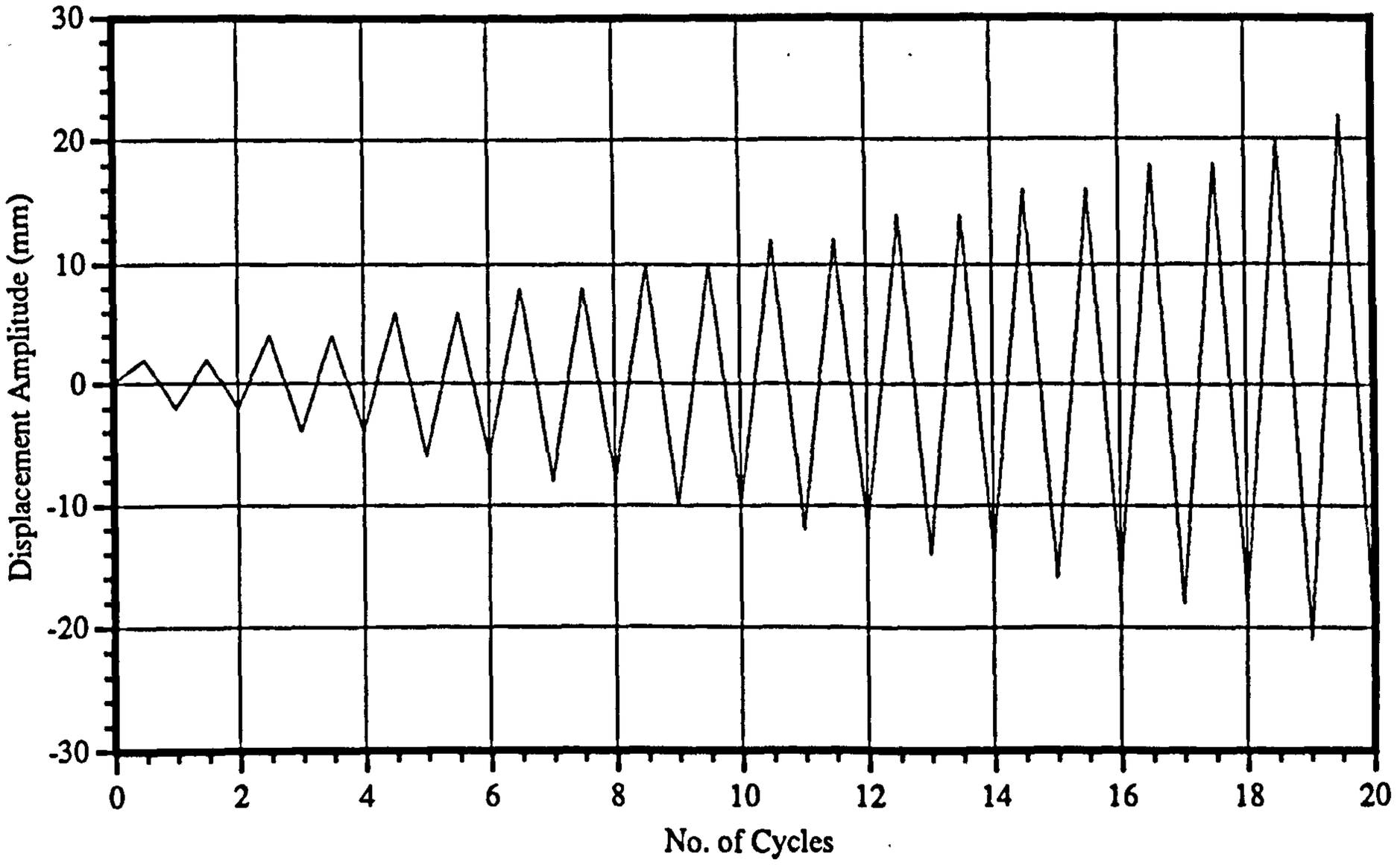


Fig. 7.16 Displacement History for SWR22

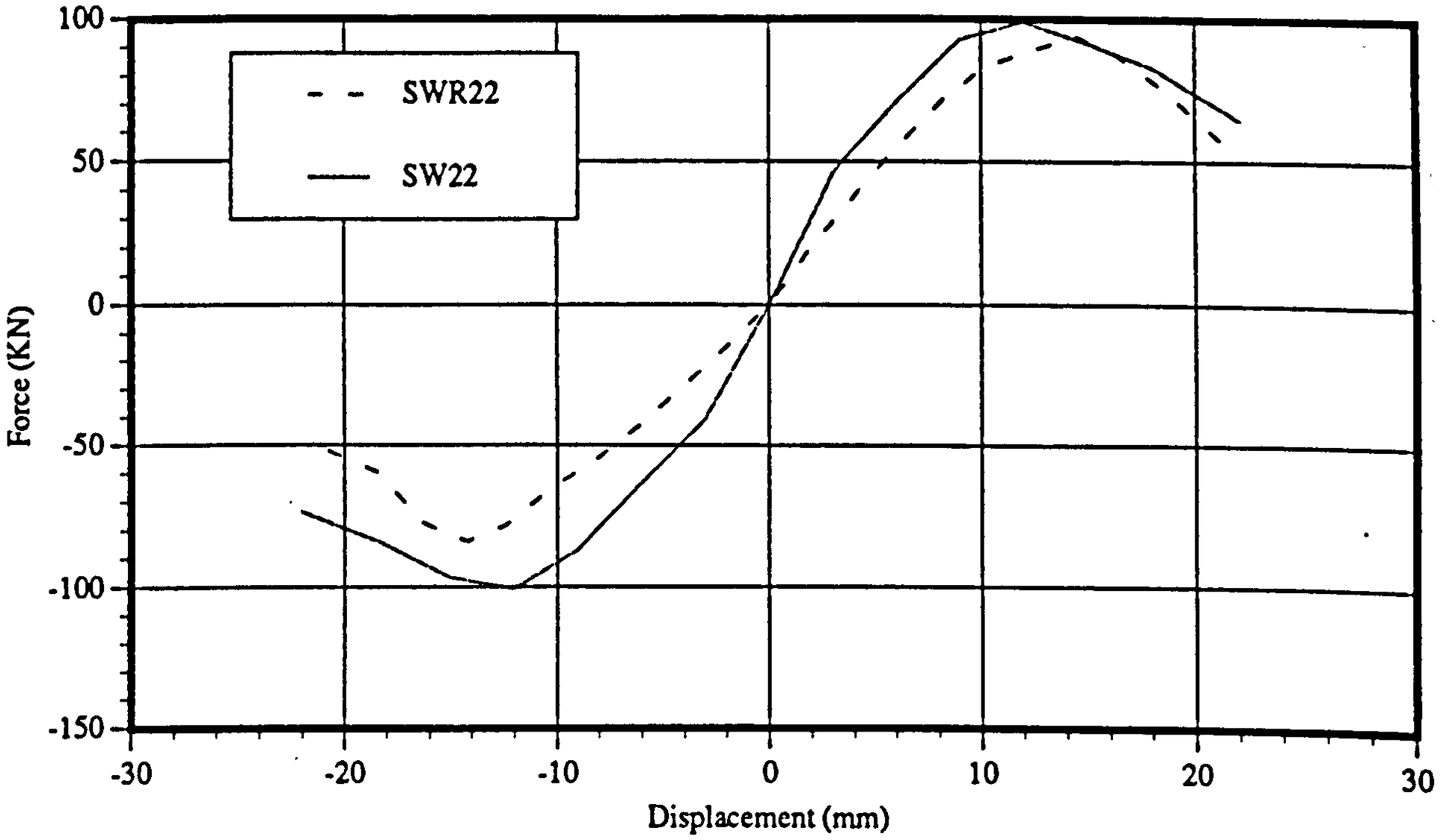


Fig. 7.17 Force-Displacement Hysteresis Envelope for SW22/SWR22

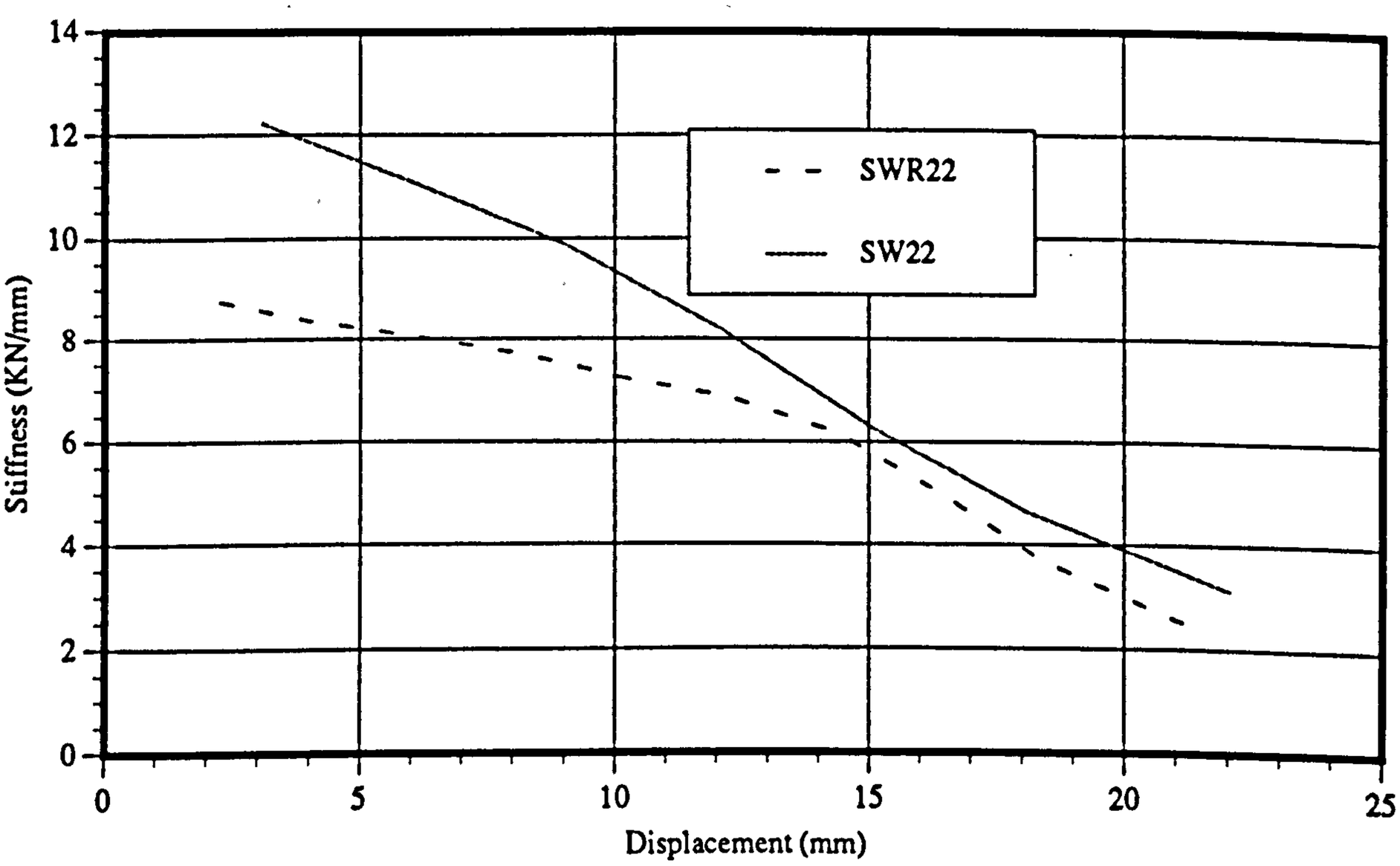


Fig. 7.18 Stiffness-Displacement Plot for SW22/SWR22

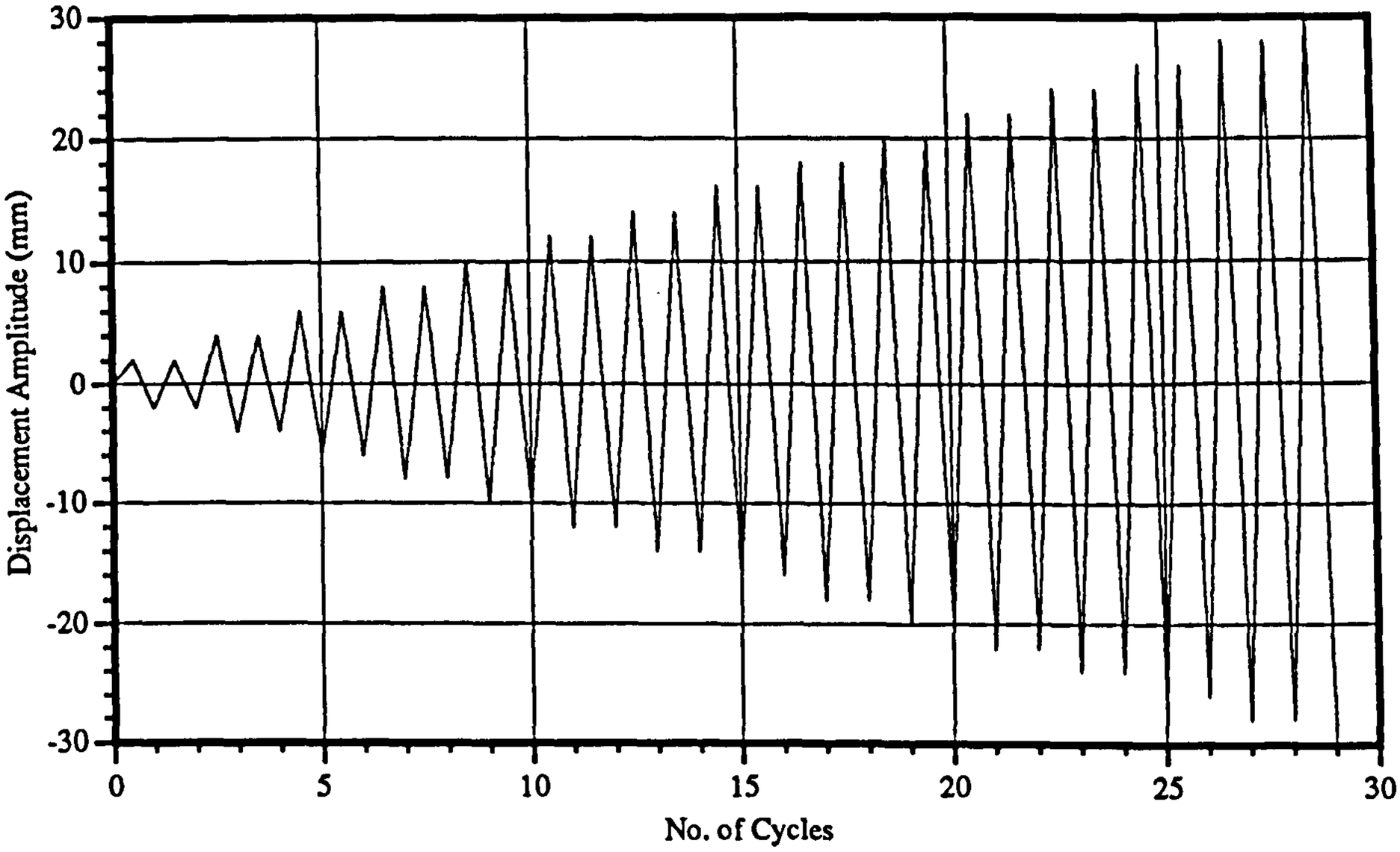


Fig. 7.19 Displacement History for SWR24

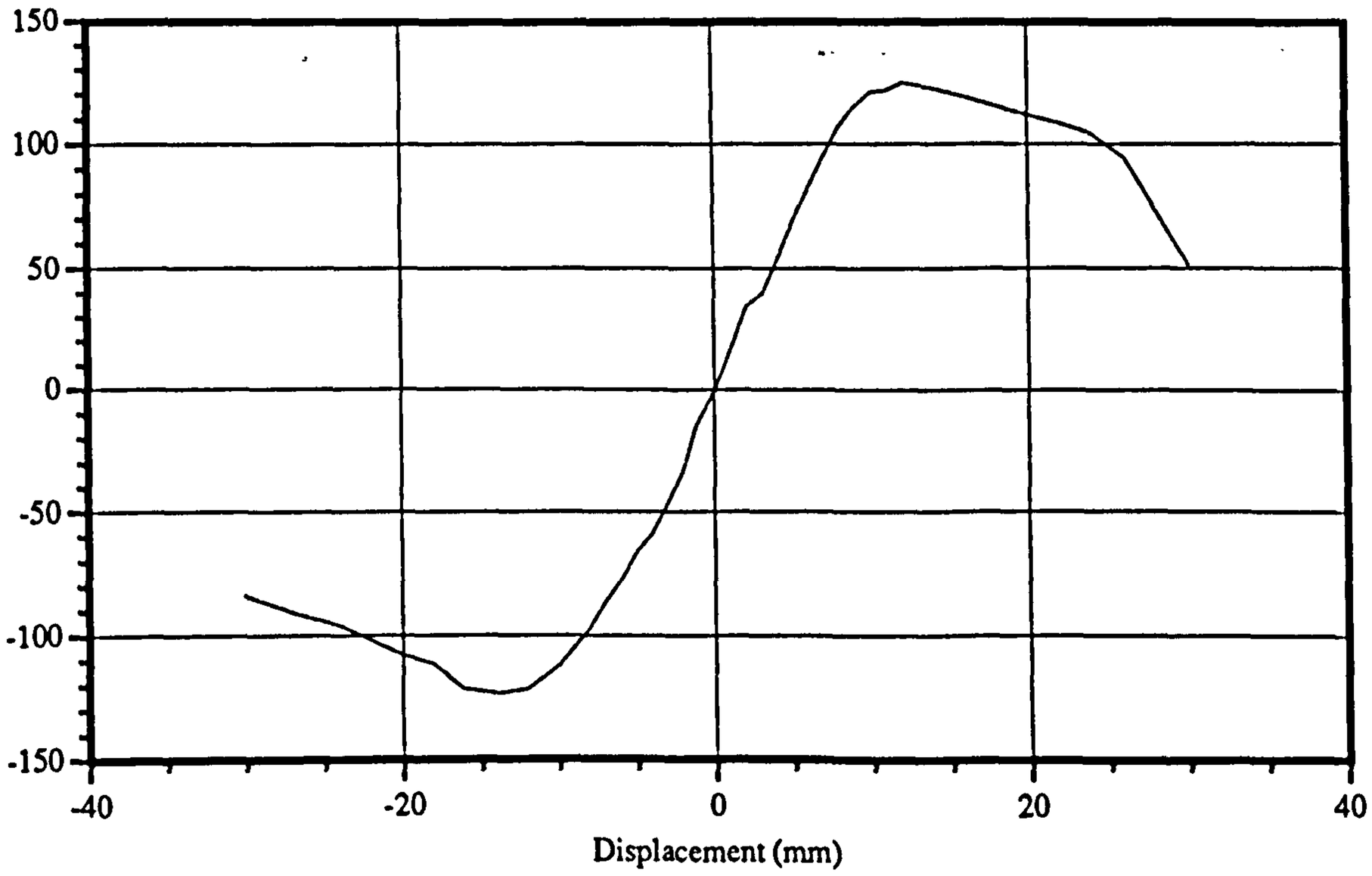


Fig. 7.20 Force-Displacement Hysteresis Envelope for SWR24

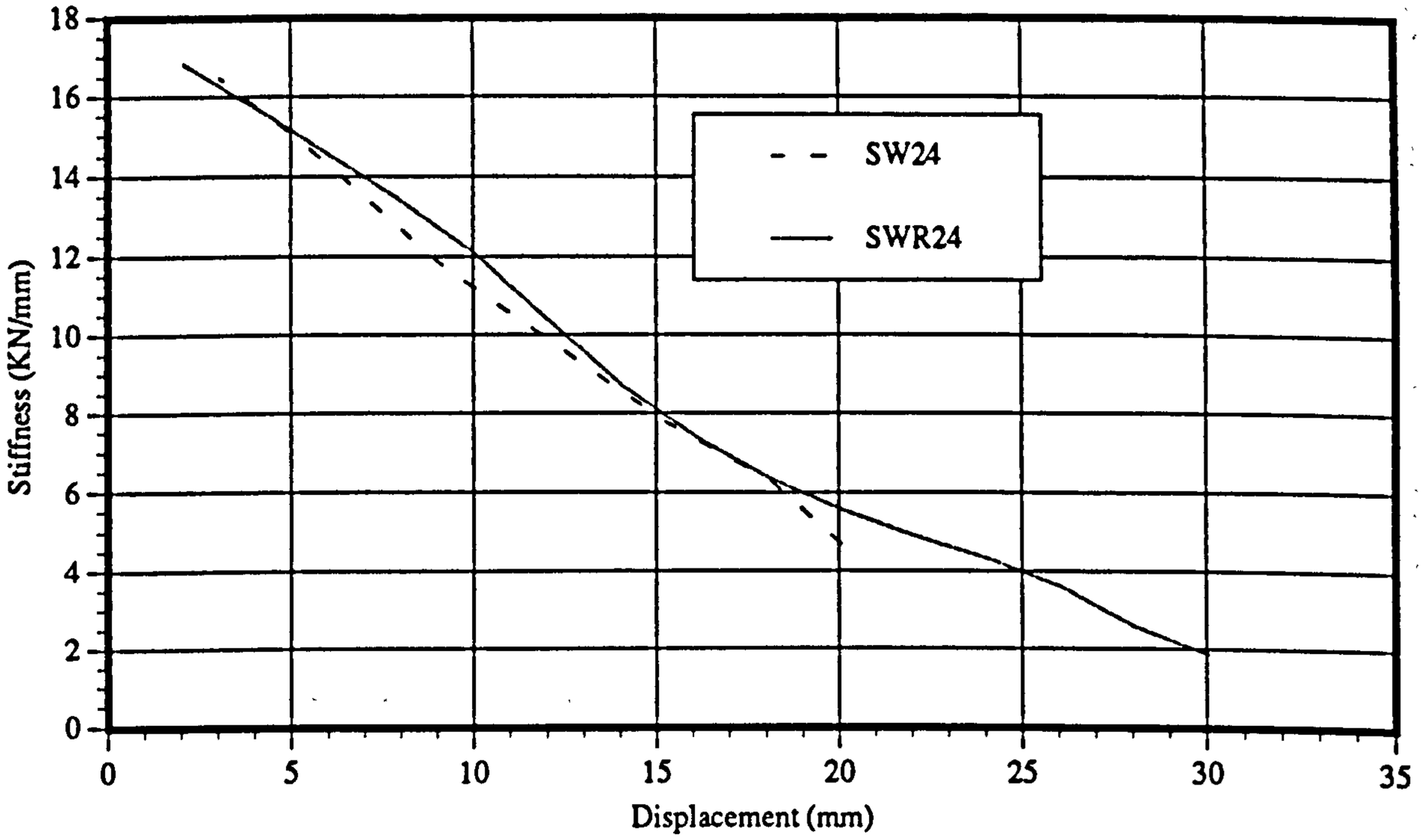


Fig. 7.21 Stiffness-Displacement Plot for SW24/SWR24

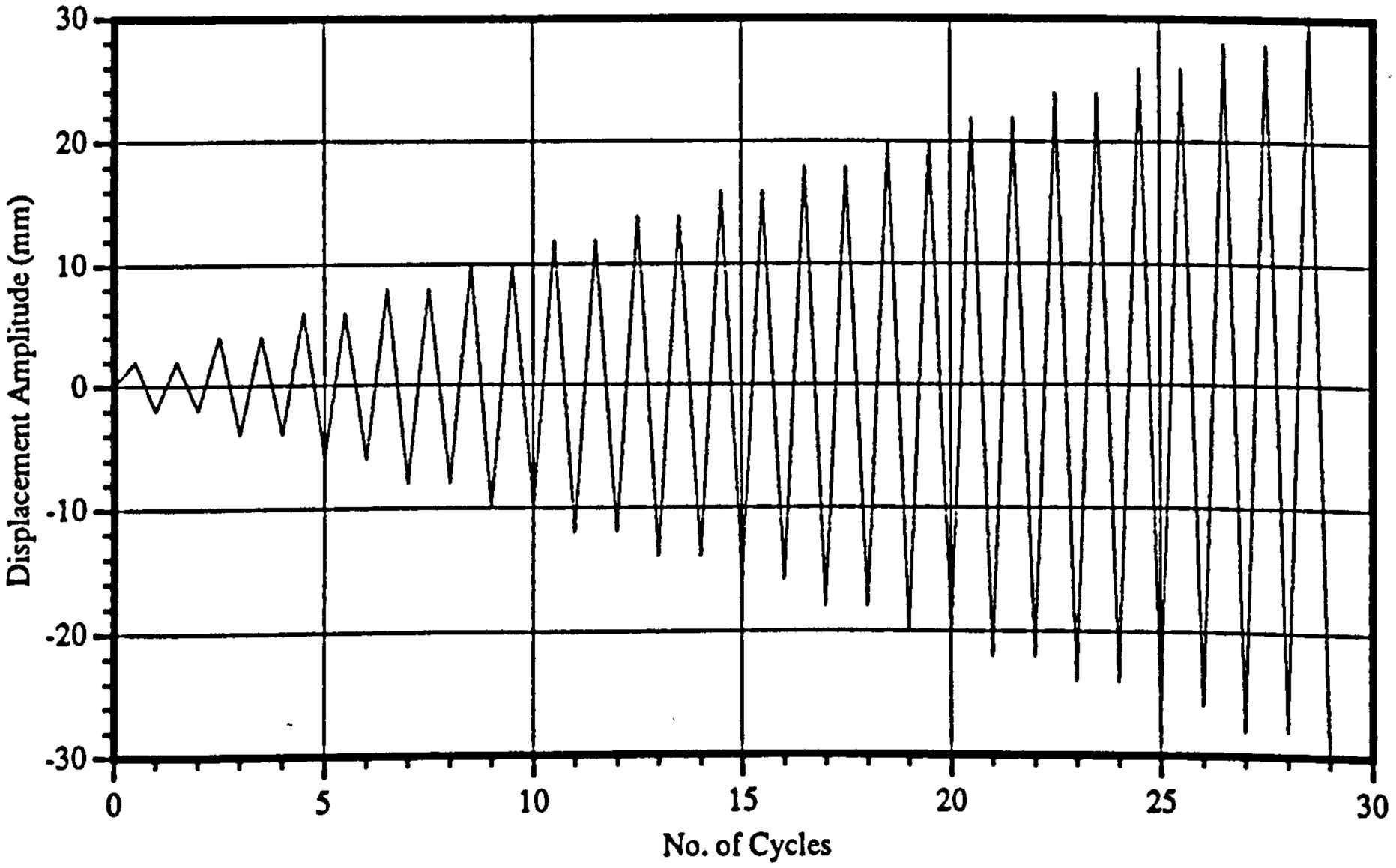


Fig. 7.22 Displacement History for SW31

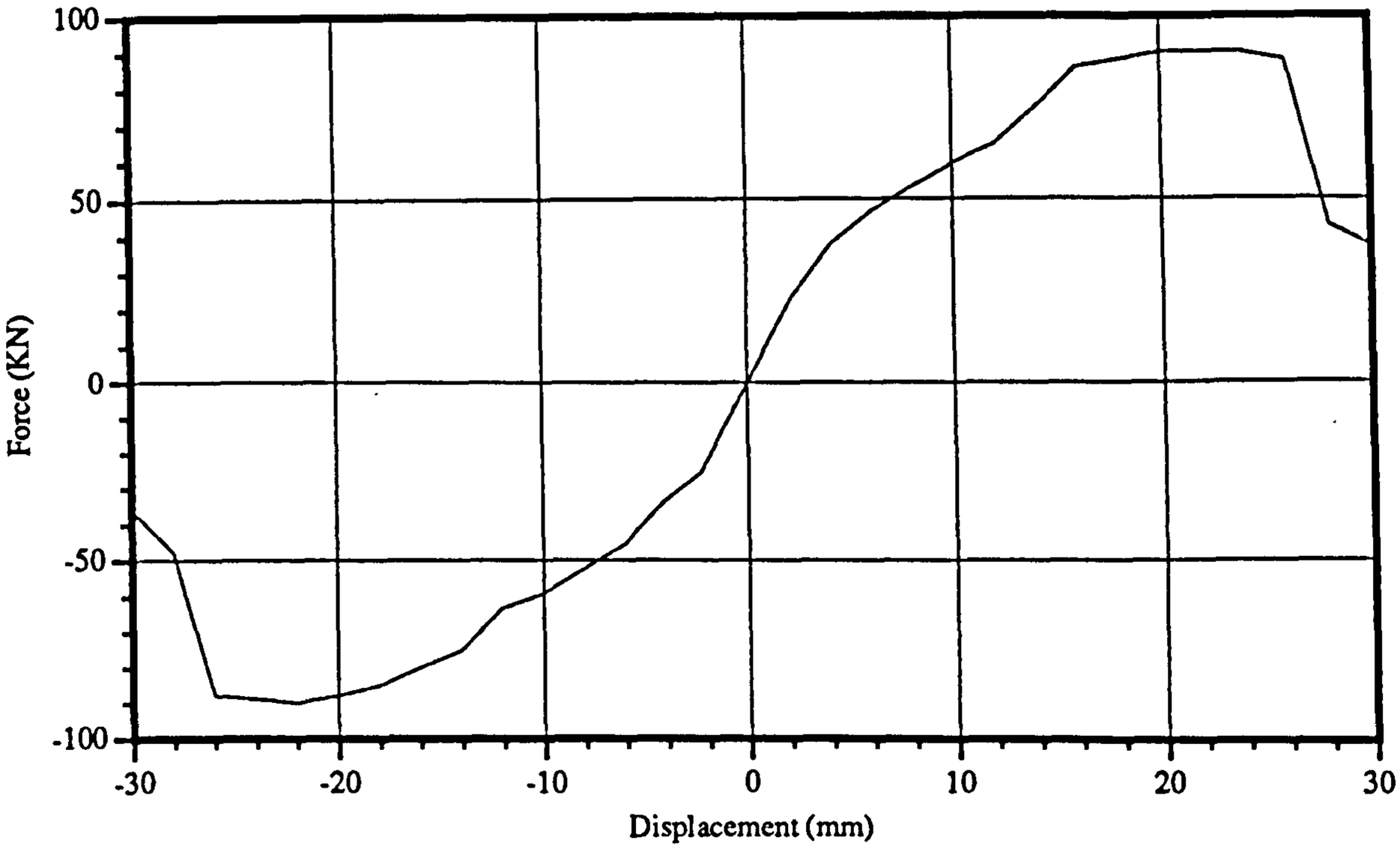


Fig. 7.23 Force-Displacement Hysteresis Envelope for SW31

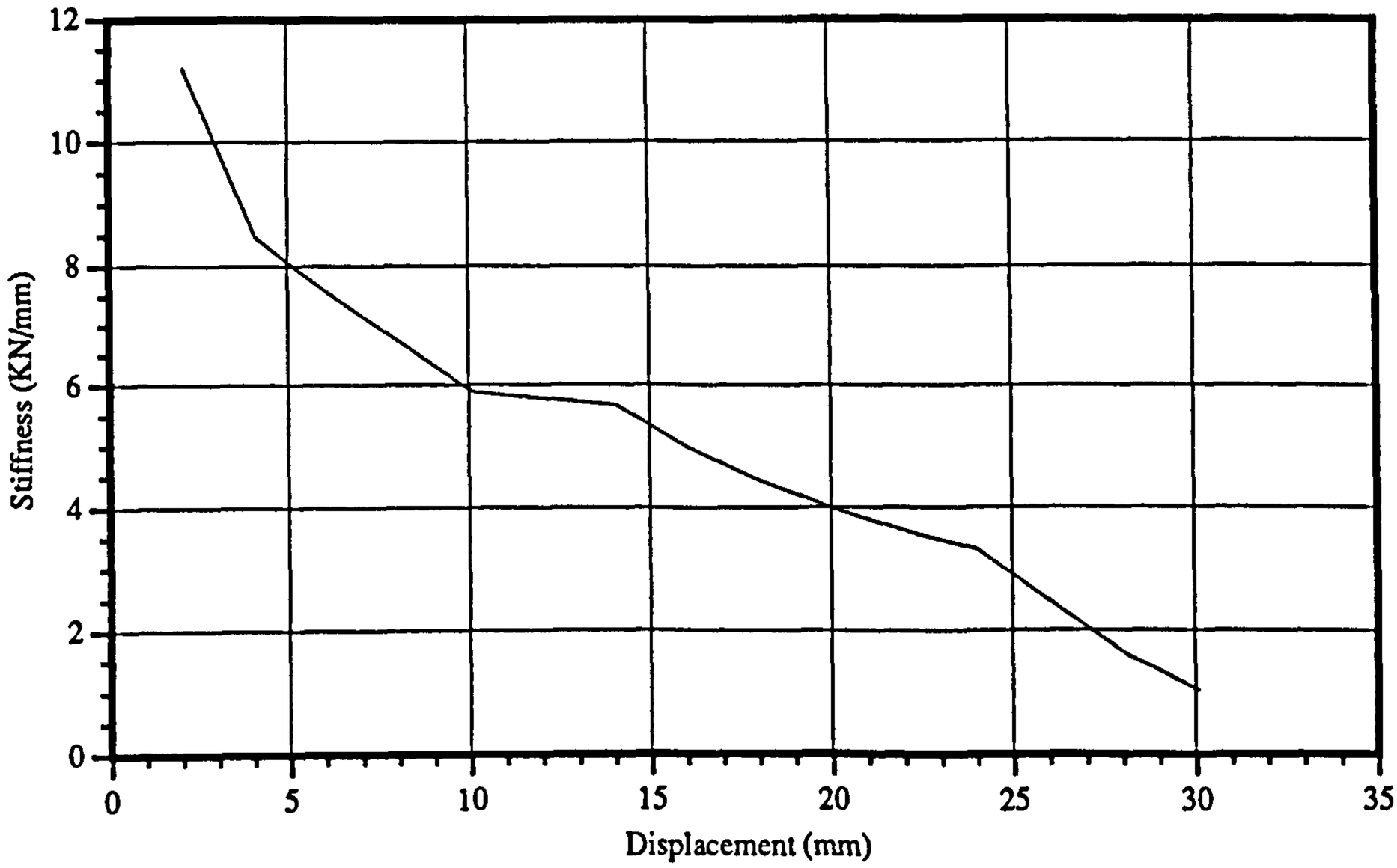


Fig. 7.24 Stiffness-Displacement Plot for SW31

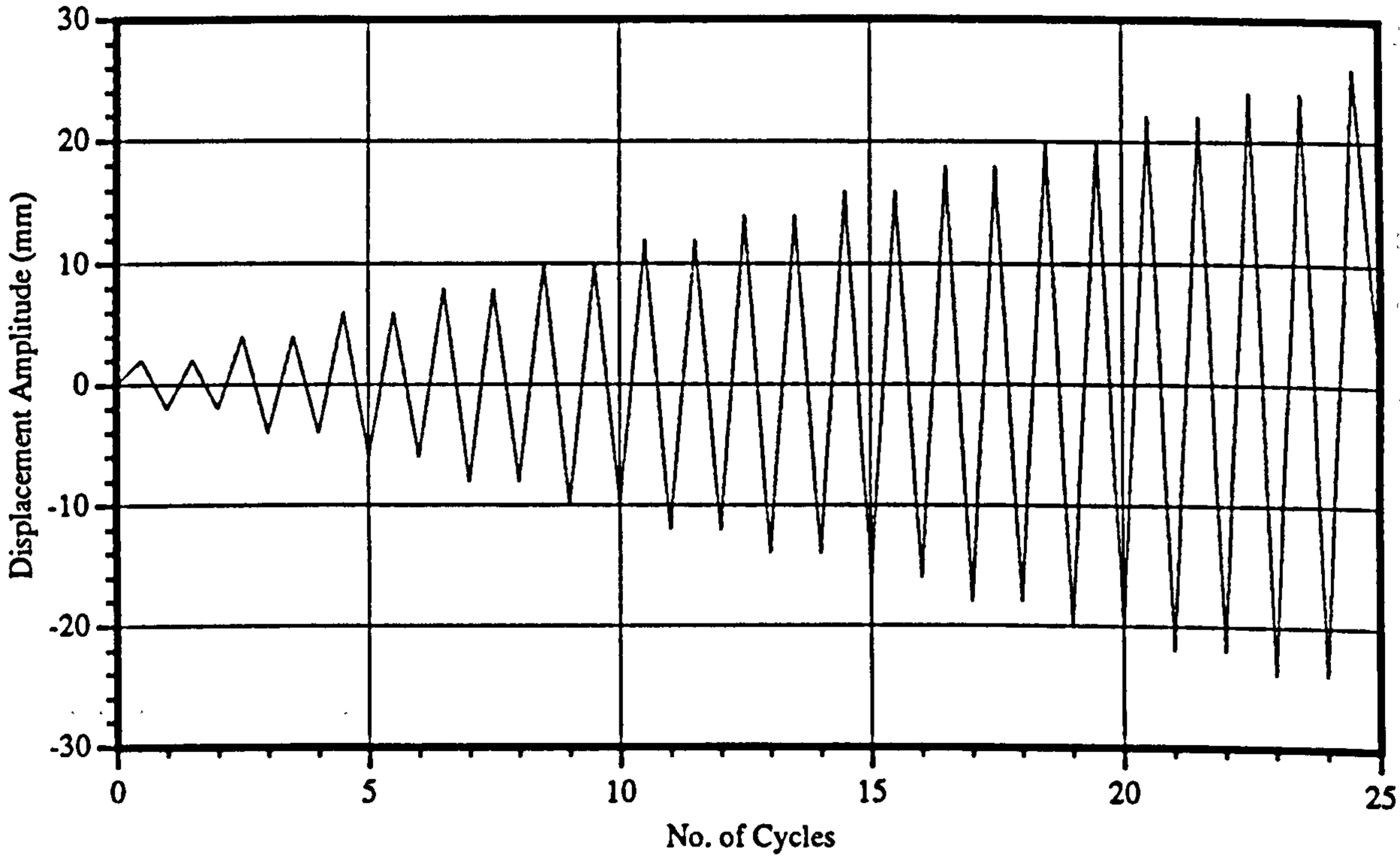


Fig. 7.25 Displacement History for SW32

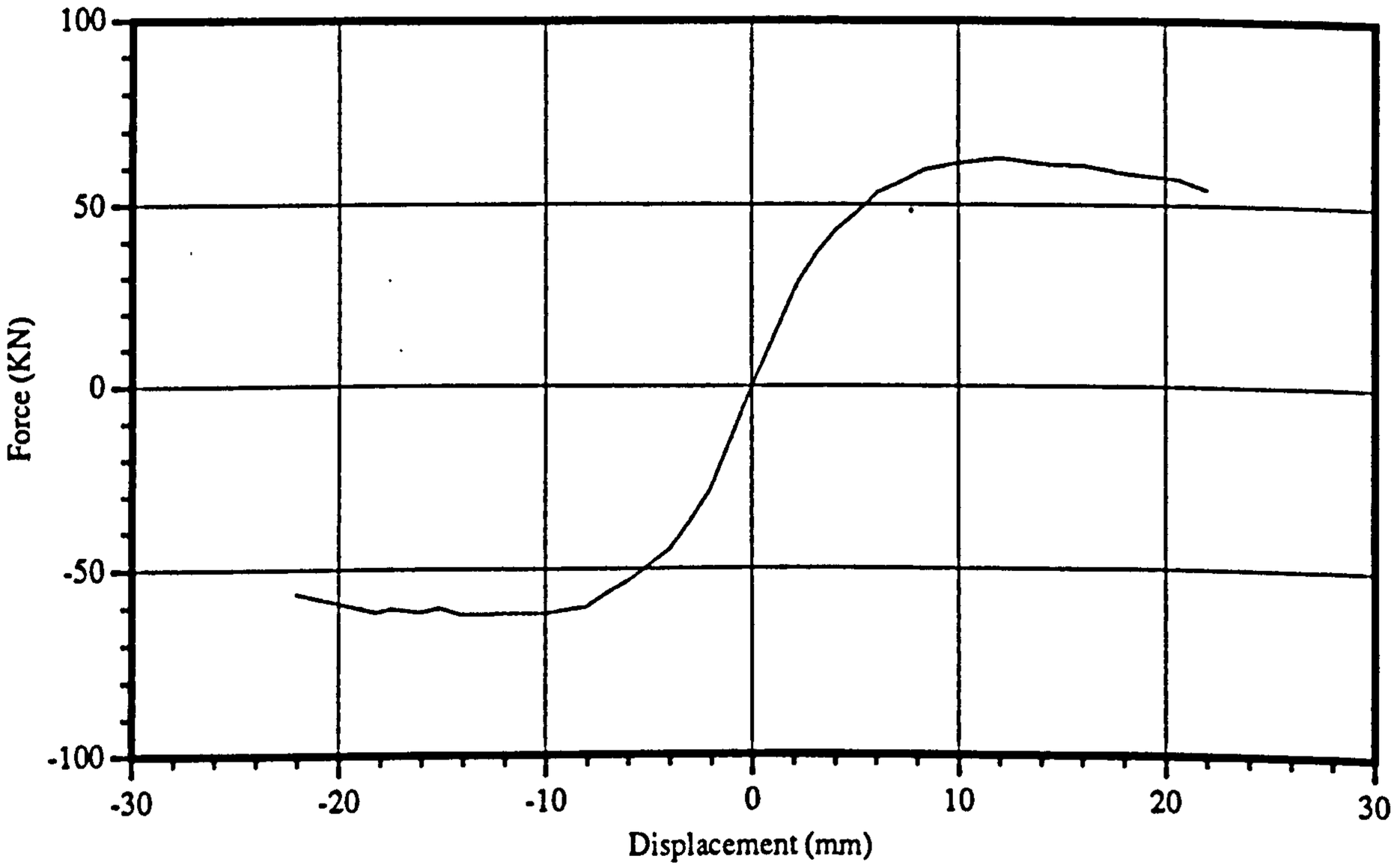


Fig. 7.26 Force-Displacement Hysteresis Envelope for SW32

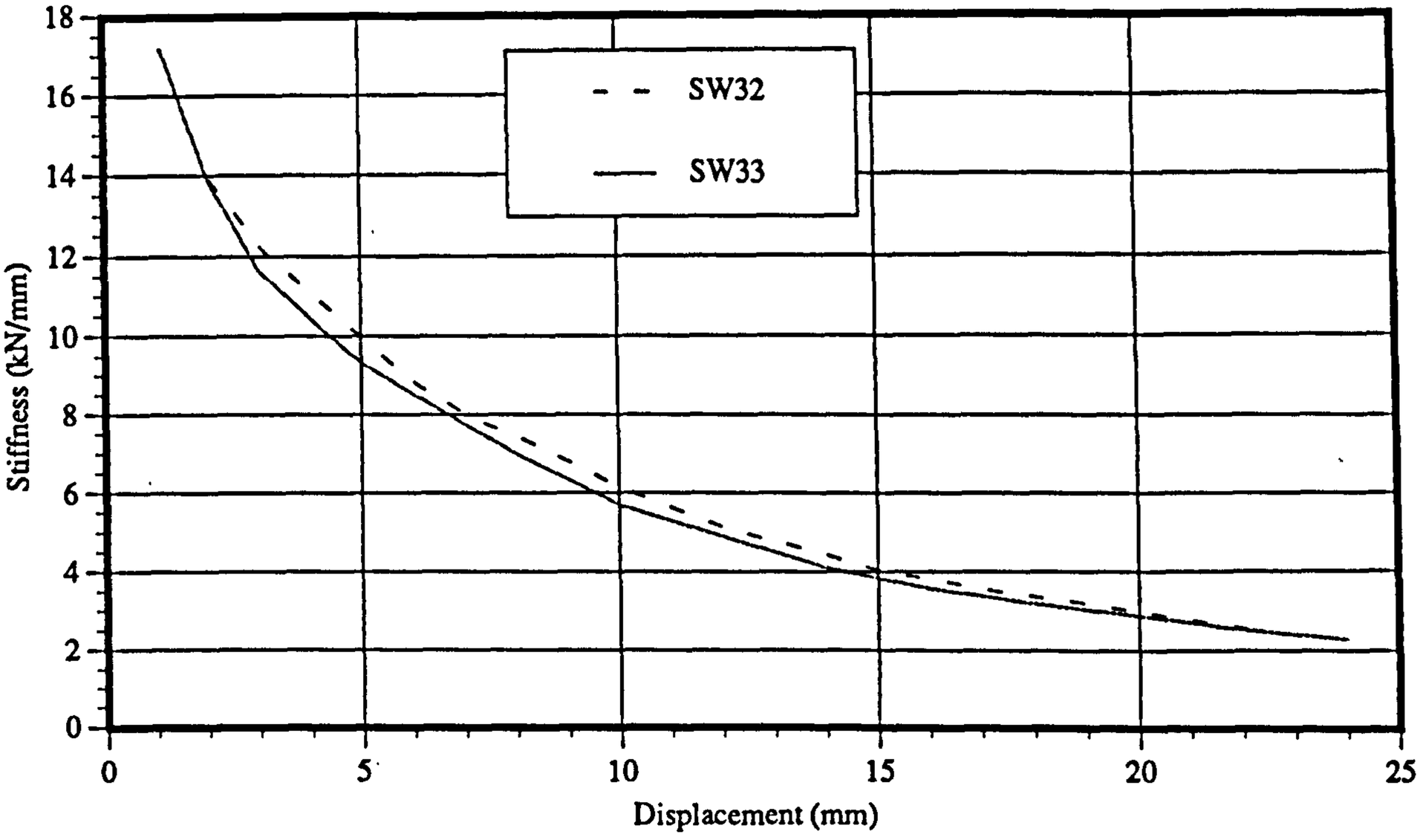


Fig. 7.27 Stiffness-Displacement Plot for SW32/SW33

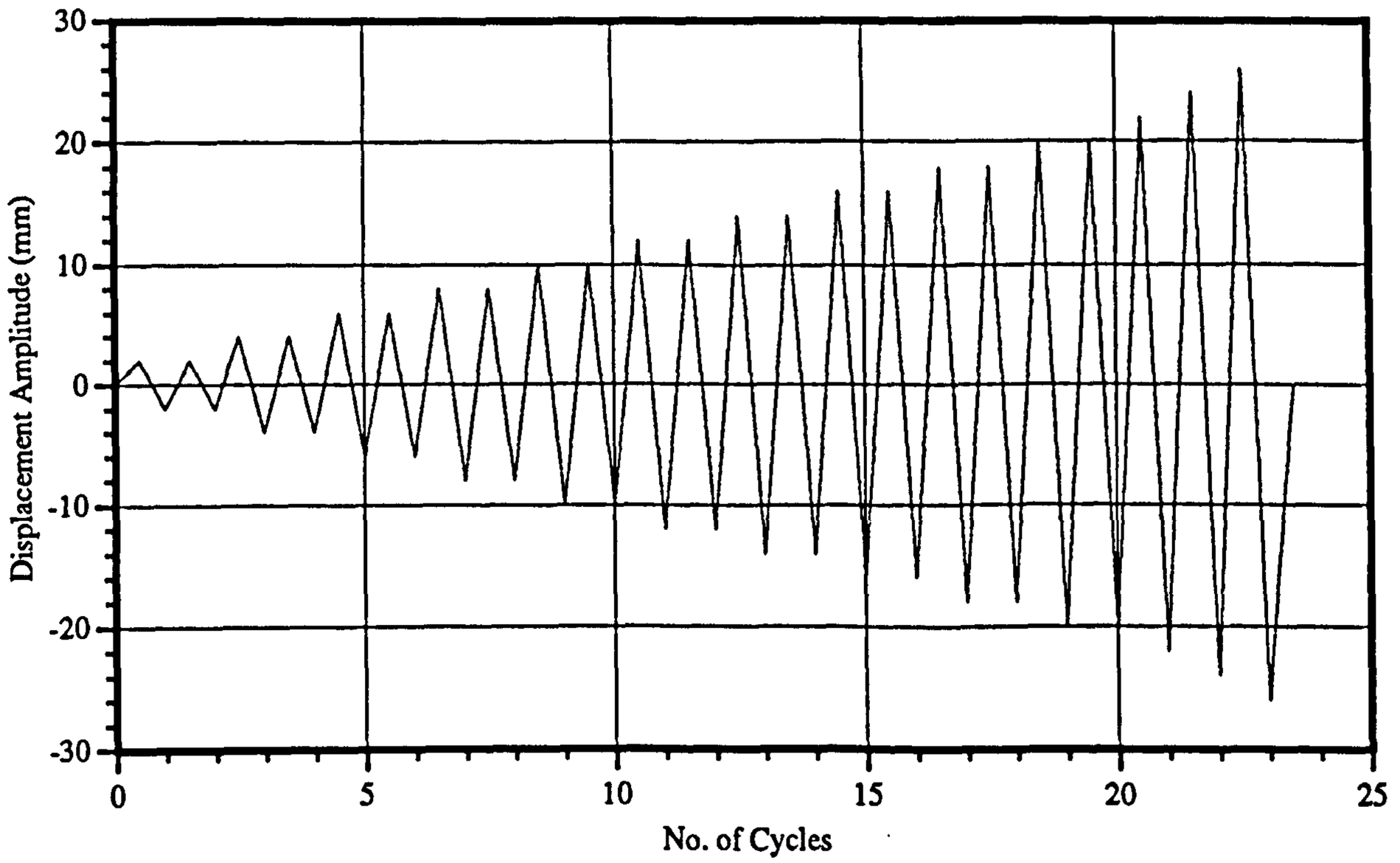


Fig. 7.28 Displacement History for SW34

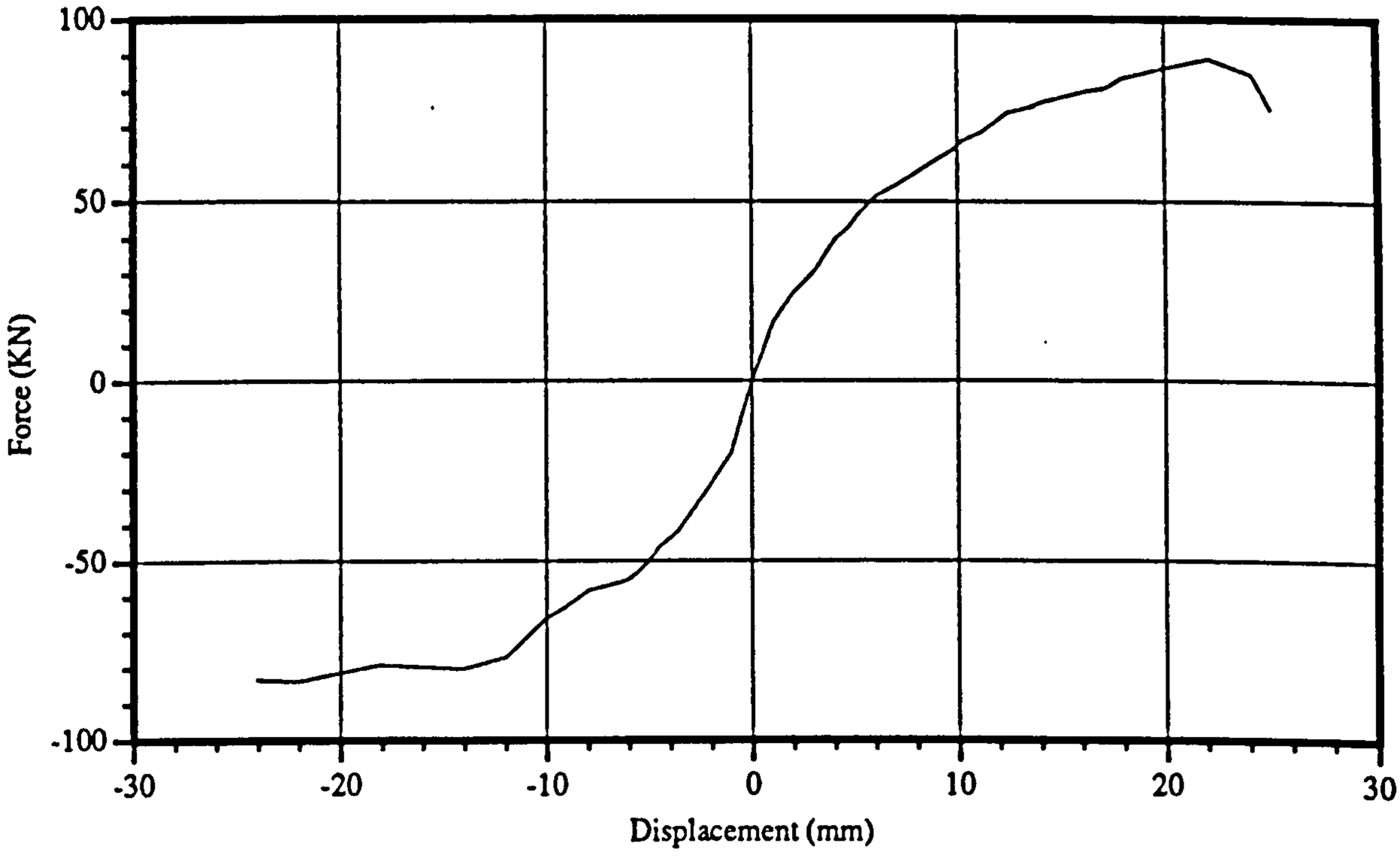


Fig. 7.29 Force-Displacement Hysteresis Envelope for SW34

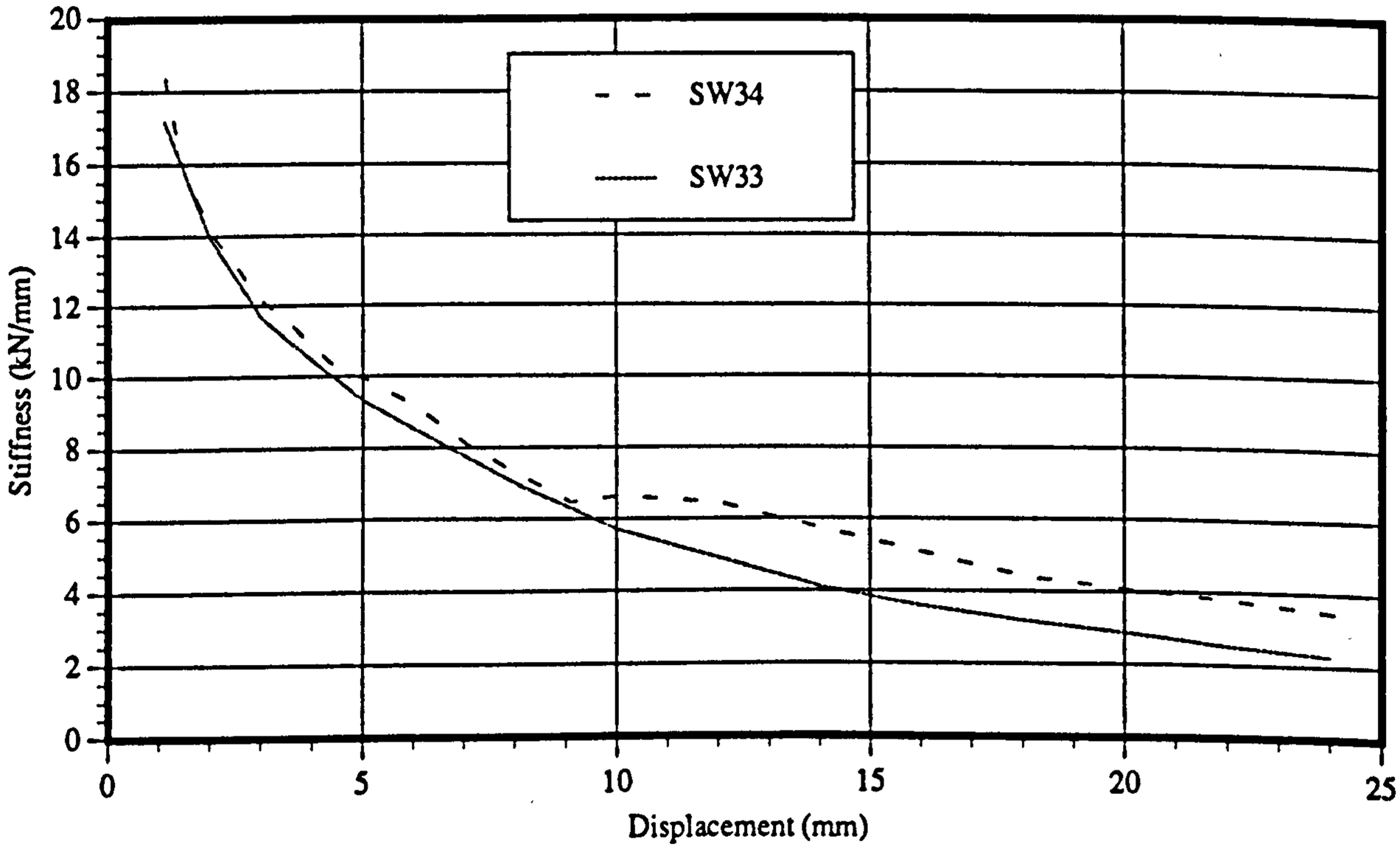


Fig. 7.30 Stiffness-Displacement Plot for SW34

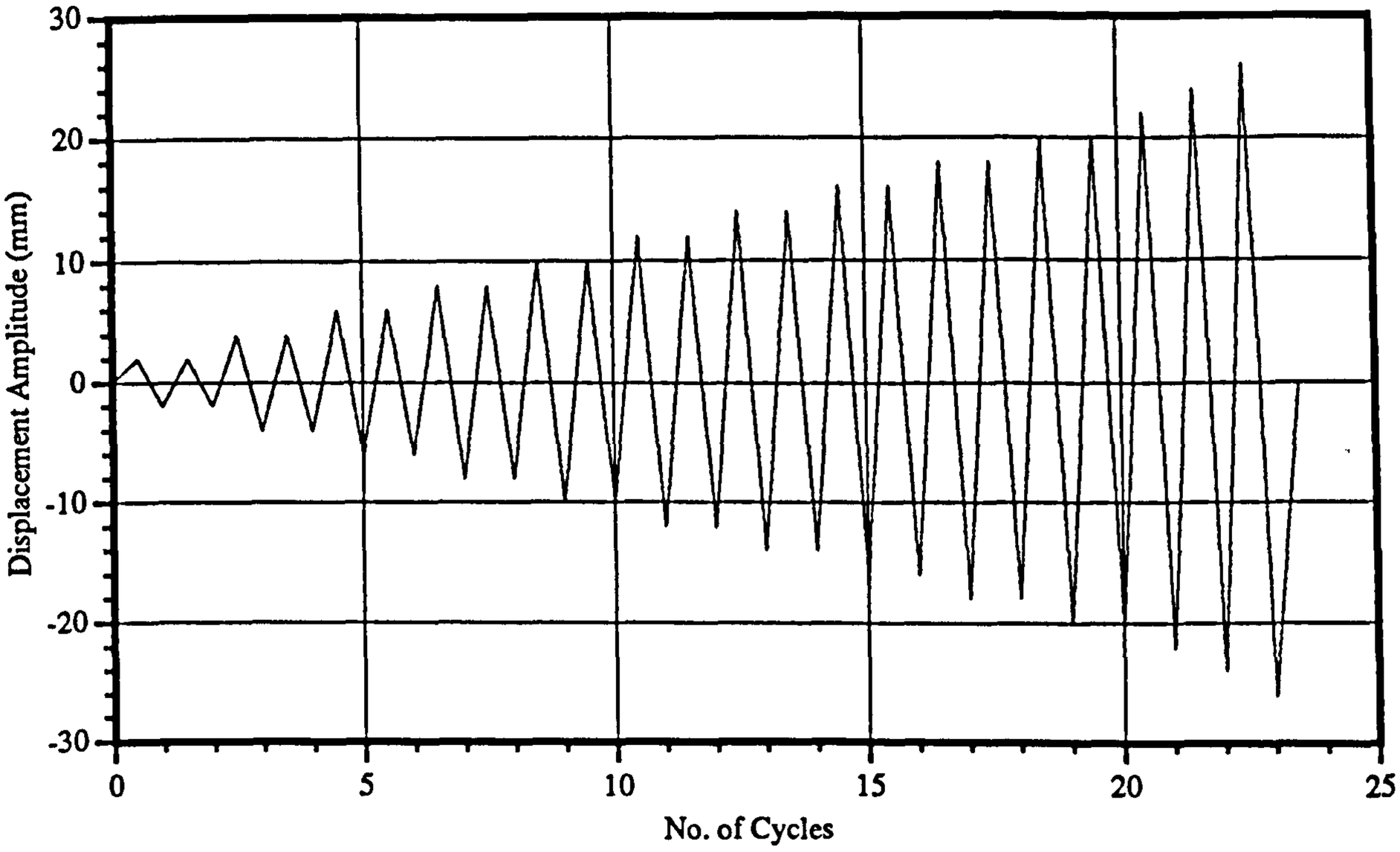


Fig. 7.31 Displacement History for SWR35

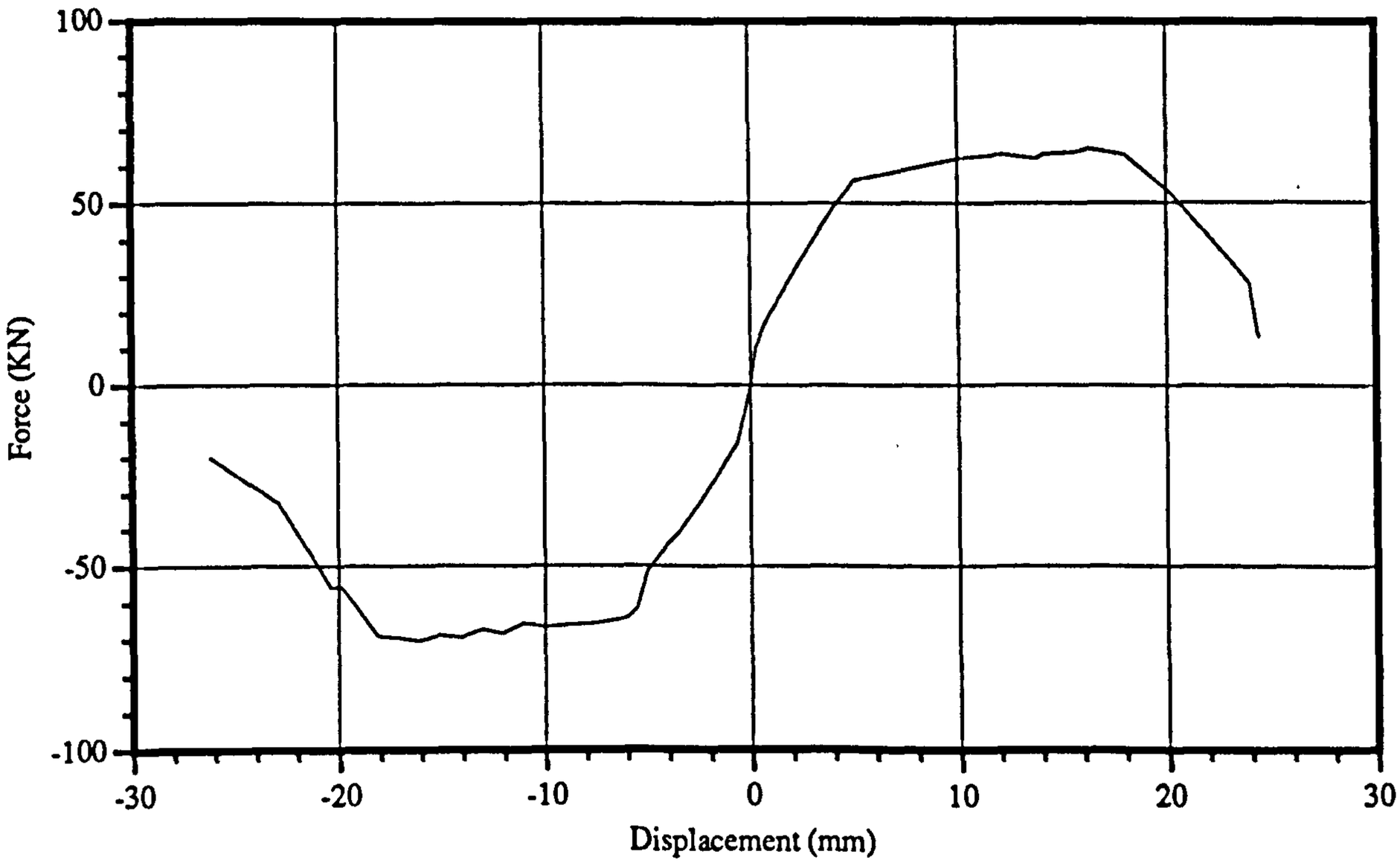


Fig. 7.32 Force-Displacement Hysteresis Envelope for SWR35

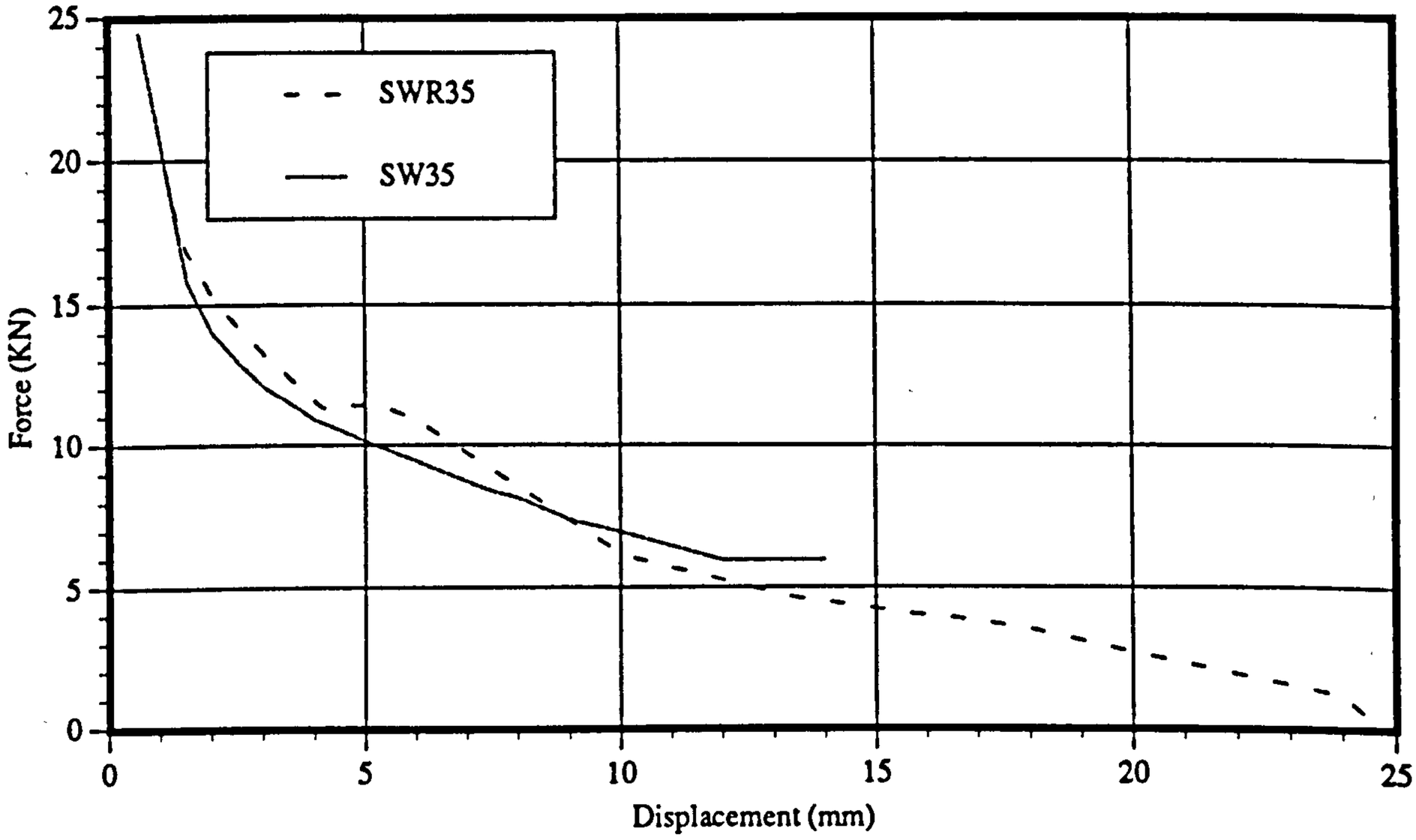


Fig. 7.33 Stiffness-Displacement Plot for SW35/SWR35

CHAPTER 8

8. ANALYSIS AND DISCUSSION OF TEST RESULTS

8.1. General Observations

In general, the observed behaviour of all the tested walls followed the same general pattern. After the application of the first displacement level, flexural cracking occurred at the base of the wall, starting at the extreme fibre in tension. With increasing displacement, the flexural cracking continued to spread at a slight inclination towards the compression zone at the base of the wall. As the imposed displacement was increased, diagonal shear cracking occurred. This diagonal cracking produced a sudden change in strains in the web reinforcement, especially in horizontal reinforcement. All specimens displayed yielding of the longitudinal reinforcement in the boundary elements and were able to resist lateral loads greater than the yield load, except for SW5 which failed in a brittle shear mode. The tests were concluded after the lateral resistance of the walls had decreased by 30% of the maximum strength.

It was observed that at large inelastic cyclic displacements, the shear resistance provided by the diagonal concrete compression force path diminished, while that by a truss mechanism formed by the wall web reinforcement became dominant. This is due to the concrete deterioration near the shear cracks. The observation was reinforced by low strain readings in the horizontal reinforcement at these stages. It may be concluded that the horizontal reinforcement ratio is ineffective unless a drift ratio of at least 1% is reached.

Specimens SW21 and SW22 contained 0.004 horizontal web reinforcement, noting that the minimum specified in the ACI code is 0.0025. After the formation of diagonal cracks, the force in the horizontal reinforcement increased with further widening and propagation of the inclined crack. Increased displacement caused the horizontal web reinforcement to yield. Further deformation caused a decrease in depth of the compressive zone of the concrete, thereby resulting in crushing of the concrete in compression. In general, specimens subjected to high shear stresses lost load capacity by web crushing. Also, a significant increase in the amount of horizontal reinforcement had only a small effect on ductility prior to web crushing.

There is no advantage in using large amounts of horizontal reinforcement, because neither the lateral strength nor the deformation capacity increase significantly with the amount of horizontal web reinforcement. Nevertheless, the observed mode of failure depends to a great extent on the amount of web reinforcement.

Because all the reinforcement in the tension boundary element of the wall does not yield simultaneously, a unique definition for the yield displacement of the specimens does not exist. A definition based on the yield of one or more layers is subjective. The mean drift ratio is defined as the maximum displacement during stable loading cycles divided by the height of the wall. All walls withstood a mean drift of more than 1% without an appreciable loss of lateral strength. The population of the test specimens was almost equally divided between walls that failed during a loading cycle to a new maximum displacement level and walls that failed during cycles to a previously achieved displacement.

An increase in the ductility of the walls which failed in flexure was observed, with an increase in the amount of confinement reinforcement in the boundary elements. The influence was negligible for walls that failed in shear. However, the lateral strength of walls that failed in shear was observed to increase with an increase in the amount of confinement reinforcement in the boundary element (SW21/SW22).

The ductility of the walls appeared to be sensitive to the number of loading cycles and the applied displacement amplitudes. The deformation capacity of the walls was observed to decrease with an increase in the number of load reversals beyond yield for all modes of failure.

The mean drift sustained by the test specimens subjected to cyclic loading did not appear to be sensitive to the observed mode of failure. However, the ductility of walls that failed in shear tended to be less than the ductility of walls that failed in flexure. Values of displacement ductility ranged from 1.60 to 4.0 for walls that failed in flexure and from 1.0 to 1.5 for walls that failed in shear.

As expected, flexural failure was observed in the specimens with small amounts of longitudinal reinforcement in the boundary elements associated with a high ratio of horizontal reinforcement. Shear failure was observed in specimens with higher longitudinal reinforcement associated with lower ratios of horizontal steel. However, a quantitative statement relating the observed mode of failure to the amount of reinforcement in the boundary elements cannot be made due to the limited number of the available test data.

Coupling of shear distortions and rotations suggests that an analytical model for shear stiffness should be related to the flexural stiffness and level of rotations. With additional test data, it may be possible to formulate a set of rules by which an instantaneous 'effective' shear stiffness can be determined from the instantaneous rotation, vertical load, and previous rotation history. This could then be used in time-history dynamic analysis to evaluate the effects of shear yielding and shear stiffness degradation on the response of wall-frame structures.

8.2. Comments on Specific Response Parameters

A qualitative analysis of stiffness, strength, hysteresis loops, crack patterns, ductility, and failure modes for the intact and repaired walls is presented hereafter. The objective is to study all criteria affecting wall behaviour for each of the proposed selective interventions in order to investigate the practical implications and applicability of the proposed techniques.

8.2.1. Stiffness

Various approaches for stiffness reinstatement were designed and tested in the current research, such as vertical steel plates, horizontal steel plates and epoxy injection. The first scheme proved to be the most effective. The yield stiffness (design stiffness) was fully reinstated and stiffness degradation was compatible with the intact wall (SW9/SWR9).

The response of the epoxy injected and horizontal steel plated walls resembled the intact wall stiffness-displacement curves at nearly twice the yield displacement. Repaired and intact walls showed comparable behaviour from that displacement level onward. Also, the intact wall strength was fully reinstated (SW21/SWR21 and SW22/SWR22).

Due to the ductile performance of the walls which had a flexural failure mode, it was observed that their stiffness degradation was much less pronounced than in those walls which displayed a shear failure mode.

8.2.2. Strength

When design for strength is required, reliance must be placed on a flexural response quantified by the attainable maximum curvature ductility. As a general rule, limitations on maximum curvature are set by the strain capacity of concrete in compression, as was observed while testing SW23. When required, this strain capacity can be adequately increased by suitable confinement of the compressed concrete. This was observed while testing (SWR9 and SW31).

Shear mechanisms are not considered to be suitable for energy dissipation in seismic environments. For this reason, an elastic shear response is desirable. The seismic repair strategy adopted should aim to prevent shear failure. Considerations supporting this approach include:

– While a diagonal tension failure in a web reinforced member may be ductile, the mechanism cannot be used for effective energy dissipation under reversed cyclic shear. Transverse shear reinforcement (stirrups) can contribute to shear strength only in tension. This was observed while testing (SW22).

– Upon shear reversal, a new compression field needs to develop. This is only possible if diagonal cracks, which, as a result of extensive previous yielding of shear reinforcement, close. In the process of crack closure, greatly reduced shear resistance is offered by the structure, resulting in a pinched hysteretic response, such as that exhibited by SW21.

In order to prevent the shear failure mode exhibited by the intact wall SW21, the retrofitting scheme was designed for shear strength. This was readily achieved by the application of capacity design philosophy, whereby the dependable shear strength of the retrofitted wall was made 25% higher than the shear force associated with the flexural over-strength developed at the base of the wall. Hence, the undesirable effect of shear was minimized and significant ductility was developed as a result of yielding of the vertical reinforcement.

A comparison between analytical and experimental results is given in table 8.1 whereby the nominal strength predicted by the previously-mentioned analytical tools, described in section 4.4, resulted in acceptably accurate deformation and strength predictions.

8.2.3. Hysteresis loops

The shape of the hysteresis loops for the force-displacement relationships varies according to the loading level as shown in appendix AI. The flexural displacement loops have smaller residual displacement and hence have wider shapes, associated with higher dissipation capacity, not only after cracking, but also after yielding.

All tested walls possessed substantial inelastic rotational capacity under load reversal. In general, ductility decreased as the maximum level of shear stress increased. It was noticed that horizontal reinforcement designed to remain elastic at a shear force corresponding to the maximum moment capacity decreased the rate of deterioration of the compression fields. This allowed larger rotations to occur prior to web crushing.

Alternate tensile yielding of the reinforcing steel caused 'growth' of the hinging region. When a specimen was loaded beyond yield in one direction and then unloaded, permanent deformations remained in the steel (plastic strain). The specimen was then loaded in the opposite direction, only the reinforcement was effective in resisting the moment prior to crack closure. This steel section had a lower stiffness than the composite concrete and steel section. Finally, the cracks closed at higher rotation levels, the combined steel-concrete section became effective and the stiffness increased. This observation was more pronounced in the case of non-injected repaired walls. While this transition between two stiffnesses had little effect on the force-displacement hysteresis loops for walls which failed in flexure, it caused pinching of the loops and significantly affected the shear resistance of those walls which failed in shear, leading to shear failure.

8.2.4. Crack pattern

In general, the observed behaviour of the repaired and/or enhanced walls followed the same crack pattern as for the intact walls. At the first MDLs, flexural cracking occurred at the base of the wall starting at the extreme fibre in tension. With increasing applied displacement, and hence wall resistance, the flexural cracks continued to spread at a slight inclination towards the compression zone at the base of the wall. As the displacement was increased, diagonal shear cracking occurred. This diagonal cracking produced a sudden change in the strains in the web reinforcement.

Confinement hoops, wherever available, caused the flexural cracks to be narrow and well-distributed. For walls that exhibited shear failure, these hoops limited the

propagation of diagonal cracks into the boundary elements. They also caused a vertical crack separating the stiff boundary elements from the flexible web diaphragm.

The ratio of flexural-to-shear reinforcement determined the cracking pattern. Light flexural reinforcement was associated with moderate shear reinforcement and led to the propagation of flexural cracks throughout the wall height. Slight crack inclination along the wall height was noticed. This was observed in walls SWR9, SW31, SW32, SW33, SW34 and SWR35. On the other hand, relatively heavy flexural reinforcement associated with light shear reinforcement, caused the propagation of diagonal cracks.

The energy absorption of the wall was manifested by cracks opening and propagating either in flexure or in shear. Cyclic loading, for flexural of crack patterns, caused opening and closing of cracks with insignificant strength and stiffness loss. However, for shear crack patterns, sliding at the crack-face occurred prior to crack closure. This was associated with some grinding of the concrete, leading to a decrease in both strength and stiffness. Therefore, the strength and stiffness degradation was more pronounced for shear response, as compared to flexural response.

8.2.5. Ductility

For members that failed originally in shear, epoxy injection did not lead to higher ductility (SWR22). On the other hand, specimen SWR21 which was retrofitted using horizontal steel plates, showed higher ductility. For practical cases, if both schemes are applied concurently, a much higher ductility level can be achieved. This was confirmed from testing SWR24. The same performance was achieved in the case of SWR5 after the addition of horizontal shear reinforcement to prevent the original brittle failure mode.

For members that failed originally in flexure, the addition of steel plates and/or replacement of damaged concrete by higher strength concrete also led to higher ductility when compared with the intact wall (SW9/SWR9).

For model SW31, where IDM was attached to the external unbonded bars, two ductility levels, 4.20 and 2.20, were achieved at both the original and the enhanced strength levels, respectively. A 50% enhancement in strength without affecting the wall stiffness was achieved. Energy dissipation capacity was also enhanced due to yielding of the external unbonded reinforcing bars.

8.2.6. Failure modes

8.2.6.1. Flexural failure mode

This failure mode was observed for models SWR9, SW31, SW32, SW33, SW34 and SW35. Although no fracture in the main reinforcement was reported, yield was reached at early loading stages, followed by a very clear flexural cracking pattern. Such a mode was characterised by large force-displacement hysteresis loops, indicating high energy dissipation capacity.

8.2.6.2. Flexure-shear failure mode

When a structural wall fails by shear due to wide inclined cracks or web crushing after the yielding of flexural reinforcement, it is said to have failed in a flexure-shear mode. Due to rapidly developed shear deformation after yielding, failure takes place before the flexural deformation capacity is achieved. Strictly speaking, this may be refered to as a member that achieved its ultimate flexural strength capacity at a limited deformational capacity due to shear deterioration at the post yield stage. Thus, the ductility ratio decreases to a great extent. There were two different cases in this category:

i. Sliding shear failure

When a large part of the shear strength of a slender wall depends on the shear reinforcement, diagonal cracks are arrested by the high reinforcement ratio. Flexural cracks increase in width in the lower parts of the wall. With stress concentrations at the bottom part of the wall due to the principal stresses arising from the bending and shear straining mechanisms, concrete starts to deteriorate. With an increase in supplied energy or by increasing the controlled displacement level, crushing of the web concrete will develop, associated with bending of vertical reinforcement (kinking), pinching of the hyteresis loops and great reduction in the energy dissipation capacity. This was observed in model SW33.

ii. Shear along inclined cracks

This failure takes place soon after the yielding of flexural reinforcement by the formation of a significant inclined crack rather than the crushing of the web concrete. The deformational capacity in such a case will be much lower than in the sliding shear case. Such brittle failure mode is undesirable and should be avoided.

The above failure mode was observed in models SW21, SW22 and SW24. These models did achieve the theoretical flexural yield load experimentally but failed to achieve the designed ductility levels for which the confining reinforcement was provided. The repair objective for models SWR21 and SWR24 was to achieve a more ductile failure mode through enhancing the shear strength. This was achieved by means of external steel plates without injecting the cracks for model SWR21 and with crack injection for model SWR24. A major improvement in the hysteretic behaviour was noticed while testing the two repaired models.

8.2.6.3. Shear failure mode

When a wall is over-designed for flexure, this failure takes place. It is characterized by a sudden brittle type of failure. The ultimate flexural strength is not achieved and the energy absorption capacity is positively reduced. This is the worst type of failure that can occur to a wall. If this wall happened to be an external wall, failure may produce structural collapse.

This failure mode was observed for model SW5 in the previous IC testing programme. The repair scheme comprised the addition of shear reinforcement to the damaged model before retesting. The repaired model achieved its ultimate flexural strength with a limited ductility ratio and a poor energy dissipation capacity.

8.3. Comments on Test Results for Repaired Models

From the previous experimental investigations, the following conclusions are drawn.

- The use of expansive cement or superfluid micro-concrete is highly recommended for the replacement of damaged concrete within a repair strategy.

– The use of epoxy injection in repairing cracked members has the effect of reinstating the member strength at a reduced stiffness level.

– A highly-effective stiffness reinstatement scheme, with no effect on the member strength, can be achieved using vertical steel plates. These plates should partially cover the cracked zones. This may be of great importance in the case of exiting buildings where tuning the members stiffness can lead to a more regular structure. This would lead to higher allowable behaviour factors according to modern seismic codes which impose strict regularity conditions. Such intervention can be also applied in the case of RC structures damaged by a small magnitude earthquakes, which cause a reduction in the stiffness of the structure while having a small effect on the strength

– Horizontal steel plates, attached to the damaged model by means of epoxy mortar, proved to be effective in shear strength reinstatement without the need of crack injection. Enhancement of the shear strength would prevent brittle shear failure mode and allow the full mobilisation of a ductile flexural mode. However, the epoxy injection would increase the energy absorption capacity.

– It is feasible to increase the strength of the member without affecting its stiffness by adding an interaction delay mechanism to the externally-supplied reinforcing reinforcement bars. Alternatively, steel plates with slotted holes have proven to achieve same target. The seismic flexural strength of structural walls can be improved without affecting their stiffness and hence their dynamic characteristics provided that diagonal tension and sliding shear are prevented. A strength increase of about 50% was achieved without affecting the wall stiffness.

– It is feasible to increase the ductility of a member, and hence the structure, by adding external confining plates. This can be achieved without affecting neither stiffness nor strength. In the current testing programme, a displacement ductility of 4 was achieved while no confinement reinforcement was provided in the first intense.

It is to be noted that the testing programme was not intended to be comprehensive. It was aimed at demonstrating the practicality of selective intervention to affect a specific response characteristic with little or no effect on others. Towards this end, the tests are considered to have achieved their objectives.

8.4. Practical Application of Selective Repair Techniques

The application of the stiffness-only reinstatement scheme in practical design would necessitate further investigations of the various influencing parameters namely: location, width, height and thickness of the steel plates. Pealing and shear failure of the bonding epoxy should be investigated further. Also, the effect of the above scheme on the deformational behaviour of the retrofitted element, especially the plastic hinge length, should be assessed and compared with the intact case.

The strength-only scheme seems straight-forward from the analytical point of view. Nevertheless, a detailed study that would cover bars location, number and diameter is required. Moreover, a definition of displacement ductility of the retrofitted member is needed, since the load-displacement plot exhibits two yield points. Also, protection of the EURB to ensure the required durability and practical slacks with simple procedures to achieve them should be investigated further. Finally, a mechanism that enables the gradual participation of the EURB in the flexural response would be preferable to the system tested in this thesis.

For the ductility-only intervention scheme, a parametric study that would cover the number of plates, their location, thickness and width should be performed. The wall-plates connection integrity should be carefully studied in order to ensure monolithic action.

The above studies would lead to design expression that enable repair engineers to arrive at the required intervention characteristics given the percentage increase in stiffness, strength or ductility.

Table 8.1 Comparison between analytical and experimental results

Model	Analytical Results		Experimental Strength (kN)	Displacement Ductility	Failure Mode
	Flex. Str. (kN)	Shear Str. (kN)			
SWR4	108	135	125	2.8	Flexure
SWR5	132	142	130	2.0	Flexure-Shear
SWR7	132	140	115	1.7	Shear
SWR9	101	128.3	105	3.25	Flexure
SW21	108	105.4	102.3	1.5	Flexure-Shear
SW22	112	107.9	105	1.3	Flexure-Shear
SW23	123	126.3	120.2	2.0	Flexure-Shear
SW24	126.4	124.8	125	1.6	Flexure-Shear
SWR21	119	184.7	105	1.8	Flexure-Shear
SWR22	125	119	95	1.6	Flexure-Shear

Table 8.1 Comparison between analytical and experimental results (cont.)

Model	Analytical Results		Experimental Strength (kN)	Displacement Ductility	Failure Mode
	Flex. Str. (kN)	Shear Str. (kN)			
SWR24	126.4	159.6	130	4.00	Flexure
SW31	62	168.8	90	4.20	Flexure
SW32	62	172.6	62	4.00	Flexure
SW33	59	168.8	57	4.20	Flexure
SW34	62	168.8	80	4.20	Flexure
SW35	62	168.8	75	2.70	Flexure
SWR35	62	168.8	78	3.30	Flexure

PART II: APPLICATION OF SELECTIVE ASSESSMENT AND INTERVENTION; THE RECONSTRUCTION OF ERZINCAN (TURKEY)

CHAPTER 1

1. INTRODUCTION

1.1. Preamble

The Anatolian region of Turkey has frequently been affected by large earthquakes on a regular basis over the past several hundred years. It is in order to attempt to alleviate the social, cultural and economical effects of such disasters that the study of seismology and earthquake engineering receives world-wide attention.

The complex nature of the causative processes of earthquakes and their interaction with the constructed environment make such study a difficult and challenging task. In particular, in order to gain a fuller understanding of the field, there arises the constant need for new information relating to the manifestation of earthquake effects. Post-earthquake reconnaissance offers the most viable mechanism for acquiring such information. To this end, engineering seismology and earthquake engineering researchers at Imperial College have undertaken many field missions to the site of major seismic events over the past few decades. The latest such field mission to Erzincan in Turkey, continuing a policy of seeking to learn the lessons of significant earthquakes, forms the basis of this research (Ambraseys et al, 1992). The writer contributed to the Earthquake Field Training Units (EFTU) mission to Erzincan in August 1992. This resulted in comprehensive report on aspects of engineering seismology as well as structural earthquake engineering observations and conclusions. Due to the large number of partially-damaged RC structures in the area affected by the March 1992 event, it was considered of great value to contemplate the application of the selective intervention techniques discussed in Part I of the thesis to damaged buildings in Erzincan. It was fortuitous that the writer's supervisor, Dr. Elnashai, was involved in the "Reconstruction of Erzincan" project managed by the Turkish Ministry of Reconstruction Re-settlement and funded by the world Bank. This gave the writer the chance to spend more than two

weeks working in Erzincan on this project. A follow-up (third) mission was organised, when the writer re-visited Erzincan for one week in May 1993.

1.2. General Description

The town of Erzincan in North-Eastern Anatolia was struck by a magnitude (M_S) 6.8 earthquake at 19h19m on the 13th of March, 1992. The source of the earthquake was located at an epicentral distance of 6km from Erzincan and at a depth of approximately 10km. The town of Erzincan had experienced several major documented earthquakes in the past, most recently in 1939 when more than 23,000 people perished and initial fears were that the March 13th event had produced a similar death toll. Although these fears proved unfounded, much devastation did occur, with 541 people losing their lives, nearly 4000 others suffering injury and total damage to property and infrastructure in the region being estimated at over £250 million.

Field observations in August 1992 illustrated the extent of structural damage experienced in Erzincan. Acceleration response spectra derived from the main shock accelerograms show that horizontal acceleration responses as high as 1.5g were experienced by moderately damped structures of natural period 0.3-0.5 seconds. The frequency content of the ground motions imposed the most severe loading conditions on those structures of over three storeys in height which were mostly of reinforced concrete construction. Many structures, especially in the commercial centre, suffered complete collapse, while others, including hospitals, were so severely damaged that they were demolished soon afterwards. A great number of buildings however, particularly in the residential sector, suffered only partial damage, leaving them suitable for repair and allowing investigators to study the causes of structural damage.

The causes of poor seismic performance may be attributed to both design and construction defects. The provisions of the current Turkish earthquake resistant design codes are shown to be inadequate in catering for an event of this magnitude, while typical design layouts and detailing are deficient in ensuring a ductile building response. In addition, the poor quality of construction displayed in a large number of reinforced concrete buildings, reduced their capability to resist the effects of the earthquake. Investigations of the non-linear response of structural systems to the particular ground motions recorded at Erzincan, show that exceptionally large ductility demands were imposed on structures of fundamental natural period between 0.3 and 0.5 seconds whose strength capacity was less than one-third of the maximum load imposed by the earthquake. Field observations and evaluations of a series of partially-damaged large

buildings in Erzincan show that these conditions would have led to the observed failure of many structures in the town.

Most multi-unit housing in Erzincan is of generally similar construction-three to five storey buildings, cast-in-place concrete floors and concrete frames. The latter usually have hollow clay brick masonry infill. Most apartment buildings have basements which are usually about one-half storey below grade. The basement concrete frames usually have concrete block infill instead of hollow brick.

The concrete frames in the housing units are of "non-ductile" (brittle) construction, in that their detailing is not consistent with modern concepts of seismic resistance and seismic energy absorption requirements. This type of construction (non-ductile concrete frames with masonry infill) was proven to be very vulnerable to seismically-induced damage in many past earthquakes world-wide.

1.3. Work Organisation

This part of the thesis concerns the application of the concept of selective intervention on an RC frame typical of the building stock in Erzincan. A non-linear dynamic analysis was carried out in order to investigate and verify the observed structural damage. Use was made of the previously-developed selective repair techniques described in Part I. A comparison between the dynamic response of the building repaired selectively and conventionally is undertaken. This showed a major enhancement in the building response in the case where selective repair techniques were applied.

CHAPTER 2

2. COMMENTS ON SEISMIC HAZARD AND VULNERABILITY

2.1. Tectonic Setting in North Central Anatolia

Erzican is located near the junction of two major fault zones which are the result of the compression of Arabia against Eurasia, and only a few kilometres south of the main North Anatolian fault break. This is a major tectonic lineament where large earthquakes have ruptured its whole 1000 km length from about 30°E to its junction with the East Anatolian Fault 41°E. As a result of this compression, central Turkey west of Erzincan moves westwards as a block relative to Eurasia along the North and East Anatolian faults, while the region east of Erzincan moves eastwards along less well defined faults. (See Fig. 2.1). Several faults branching off these lineaments occur outside these major zones, visible on satellite images or marked on the geological map of Turkey as linear Quaternary depressions. It is difficult, however, to relate any recent seismicity to these splay faults.

Figure 2.2 summarises the tectonic activity in this part of Turkey in terms of fault mobility. Slip vectors are marked by arrows whose length is proportional to velocity. The right-lateral strike-slip rate on the North Anatolian Fault is about 3.0 cm/yr, while the rate of the East Anatolian fault, which is left-lateral, is less, Jackson & McKenzie (1984). The motion on the North Anatolian Fault at this rate has easily been accommodated by the seismicity of this century, with a reasonably uniform strain release along the fault. Thus the average moment rate is about 2.3×10^{26} dyn.cm.yr^{-1} and can account for the observed slip on the North Anatolian Fault, Jackson & McKenzie (1988). It is obvious, therefore, that the tectonic elements around Erzincan have a very high seismic potential.

On a local scale, this high earthquake potential is characterized by relatively infrequent major events associated with a relatively low activity background. The long-term seismicity demonstrates that periods of relative quiescence lasting 100 to 150 years in certain segments of the major faults in the Erzincan region can follow large earthquakes, such as those described below, and that some portions of the faults creep asesmically, perhaps by as much as a centimetre per year, Ambraseys (1970). However, the long-term record of the Anatolian Fault Zone, in which Erzincan is located, suggests that earthquakes with M_S between 6.0 and 7.2 are more common in periods of relative quiescence than previously thought.

An elaborate description of the origin of the complex geological features of the Erzincan Basin is given by Barka and Gülen (1989).

2.2. A brief History of Earthquakes in Northeast Turkey

In the following, a summary of the historical and instrumental seismicity of the Erzincan region is given, after Ambraseys et al (1992).

2.2.1. Historical records

Erzincan has been affected by large earthquakes associated with the North and East Anatolian fault zones, and its earthquake history is relatively well documented. In what follows we summarise the effects of the largest earthquakes in Erzincan. Much of this information has been extracted from Armenian sources, supplemented for the later period by Ottoman documents. As to the casualty and damage figures in these documents, they are too high. Such few official records as exist all deal with relatively smaller numbers. What we know of population, logistics and food supply all points to smaller numbers and one should often divide the chroniclers' figures by five. But reliable damage statistics simply do not exist, even for the first half of the 20th century.

1236

An earthquake in Erzincan caused the collapse of Armenian churches and considerable damage to the walls of the city.

1254 Oct. 11

A destructive earthquake in the North Anatolian zone associated with extensive faulting. In Erzincan 10,000 people were killed and damage extended to the west in the Su ƒehri area and beyond. The earthquake chiefly affected country areas rather than the few larger towns of the region, most of them already ruined by the Mongol invasion a year earlier. According to Armenian sources the damaging effects of the earthquake extended to Sivas and many villages in that district were totally destroyed, the loss of life being variously estimated, between 15,000 and 56,000. The earthquake was felt as far as Azerbaijan, 400 km away.

1281

An earthquake in Erzincan which caused no damage.

1287 May 6

This was a destructive earthquake in eastern Anatolia which also affected Erzincan, but details about the damage to the town are lacking.

1290

Another earthquake in eastern Anatolia, probably the largest of a series during that period. The earthquake was reported from Erzincan where there was no damage. Elsewhere in Eastern Anatolia, however, there was great loss of life.

1345

An earthquake was felt in Erzincan which should have been the result of a large, distant earthquake. It caused considerable damage but no loss of life.

1356

A series of earthquake shocks, seven to eight a day, were felt in Erzincan from an epicentral area well to the south of the town.

1374 Dec. 8

A damaging earthquake in Erzincan as a result of which many houses in the region and the walls of the town collapsed. This was probably a local shock of considerable magnitude, as its damaging effects did not extend very far.

1419 Mar. 26

A destructive earthquake in Erzincan which caused great loss of life in its district. The shock affected a comparatively large area and its numerous aftershocks obliged the survivors to flee the town for many weeks.

1433

Repeated shock originating from an epicentre well to the southeast of the town caused

considerable concern in Erzincan but apparently no damage to the town.

1457 Apr. 23

This was a destructive earthquake centring to the southeast of the town. The walls and most of the houses in Erzincan were overthrown and 12,000 people perished in the immediate vicinity of the town. The destruction extended to Kigi and its district. The shock caused great concern in Bitlis and it was reported from as far as Mardin.

1477

This, apparently, was a large earthquake originating from the central part of the North Anatolian fault zone. Its destructive effects extended from Tasova, through the district of Amasya to near Erzincan, a tract of land which was totally destroyed. Erzincan suffered considerable damage but details are lacking.

1482 Nov.

The earthquake of 1477 was followed by another destructive shock which this time involved Erzincan. With the exception of a few buildings the whole city collapsed and 10,000 people died under the ruins. Another 20,000 people were killed in 20 villages and towns of its district. This apparently was a catastrophic event. The town was abandoned and left in ruins for many years after the event; its walls were left in ruins. Eventually it was rebuilt with low rise houses for fear of another earthquake.

1535

A violent earthquake in Erzincan and in the whole country destroyed a number of houses and monasteries to the west of the town. Many other buildings were ruined and many people lost their lives.

1575 Nov. 5

An earthquake in Erzincan which was followed by aftershocks for four months obliged the people to live in the open. This was the result of an earthquake with an epicentre in the region of Bingöl.

1579

A major earthquake in the Northern Anatolian Fault zone caused extensive damage in the regions of Çorum, Amasya, which extended to the region of Erzincan where it caused heavy loss of life. Although information about damage to the town itself is lacking, we know that many of the Armenian settlements in this region were obliterated.

1583 June 17

This was another destructive earthquake in Eastern Anatolia. Preceded by a foreshock, the main shock almost totally destroyed Erzincan; 15,000 people were killed in the kaza and 5,000 were buried in the ruins of the town, some of whom survived. The loss was so great that the survivors were excused from taxation for a number of years.

1601

This earthquake centred southeast of Erzincan in the districts of Tercan and Turuperan where it caused great destruction. In Erzincan a number of houses were destroyed but with no great loss of life.

1666 Nov. 24

A destructive earthquake in northern Anatolia close to Erzincan destroyed the greater part of the town. Most of the mosques and churches, including public buildings and a part of the walls of the town collapsed, killing 1500 people. The shock was violent in Erzurum but there is no evidence of damage.

1668 Aug. 17

On 17 August, there followed another violent earthquake, stronger than any that had gone before, which affected a very large part of northern Anatolia. This, in fact, was one of the largest earthquakes associated with the Anatolian Fault Zone. It affected the region from Çankìrì in the west to Erzincan in the east. Damage in Erzincan was serious but details are lacking, except that it took many years for the trade in the town to come back to normal.

1712

An earthquake occurred this year in Erzurum. It is not know whether it caused any damage.

1784 Jul. 18

A major erathquake in Eastern Anatolia. It affected a large area extending from Erzincan to Muƒ and including the districts of Muƒ and Kigi. Erzincan was almost totally destroyed and the loss of life exceeded 10,000. The destruction extended to the districts of Tercan, Kigi and Tarom. In the district of Kigi alone 1500 were killed and villages along the Elmalì Dere were totally destroyed. Erzincan was left in ruins for a number of years and nothing remained of its historic buildings, but gradually it was rebuilt on a more regular plan than before.

1939 Dec. 26

Between 1784 and 1938 many earthquakes were felt in Erzincan, causing very little or no damage. None of them was either large or centered close to the town.

The destructive shock of 1939 involved the Northern Anatolian fault zone and in many respects it was a major event similar to the earthquake of 1668. This was a multiple earthquake with a surface wave magnitude of 7.8, preceded on the 21st of November by a damaging foreshock of magnitude 5.7 near Tercan. The earthquake was associated with a well-defined 250 km long, righ-lateral surface rupture which extended from near Amasya to Refaiye west of Erzincan. It is probable that this rupture extended for anthoher 100 km eastwards towards Erzincan, but the field evidence for this is not clear. The slip on average was about 350 cm with maximum values approaching 450 cm.

According to the official Red Cross report the earthquake killed in all 23,149 people, out of which 10,088 perished in the vilayet of Erzincan, and 3,576 were injured. The shock destroyed 6,601 houses, and damaged a further 605 beyond repair, chiefly one and two storey masonry constructions. Erzincan, being an important military station, was always well built. At the time of the earthquake, of about 16,000 inhabitants, the town lost 80% of its population and Erzincan itself was reduced to ruins. The last remnants of the historical remains in the central district of Erzincan were completely eradicated in the earthquake. Almost the only buildings to escape were the two barracks, situated on the mountainside away from the low-lying part of the valley in which the town lies. Fires, broke out in many parts of the town, and failure of the water supply system due to excessive deformations of the ground, added to the destruction. Torrential rains and floods followed on the 30th and 31st of December. These caused further casualties and damage to houses and communications. We have been unable to find any published information describing the effects of this earthquake in Erzincan and surrounding districts. Much of the damage survey carried out after the earthquake did not extend much east of Refaiye. Snow-drifts and sub-zero temperatures hindered relief work, and many of the

villages, whose ruins disappeared under the snow, were not cleared before the Red Cross left the country later in the spring of 1940. From unpublished reports it appears that much of the damage in the west part of the epicentral area was due chiefly to old and poorly built adobe, brick and stone masonry buildings and houses, whilst better built cast-in-situ reinforced concrete public buildings of recent construction escaped with some heavy damage but without collapsing. However, in the east part of the epicentral area, including the region of Erzincan, there was practically complete destruction of all types of buildings, old and new, including the very few of reinforced concrete, chiefly government buildings.

The shock was widely felt, from Albania to the Caucasus and from Malta to Cyprus. It was followed by relatively few and weak aftershocks. After the earthquake Erzincan was relocated; plans were drawn up laying out a new town with wide regular streets and low-rise houses, not exceeding two storeys, a restriction relaxed in the decades that followed. Drainage and irrigation have been carried out to diminish marsh land and improve cultivation.

1941 Nov.12

An earthquake of magnitude 5.9 centering between Kemah and Erzincan caused new damage in Erzincan, where a number of newly built houses, including the railway station, were ruined with the loss of 15 lives.

Earthquake shocks originating in Eastern Anatolia during this century were frequently felt in Erzincan, some of them causing panic and occasionally damage.

2.2.2. Instrumental data

There are many erathquake catalogues for Turkey i.e. Pìnar and Lahn (1952), Ergin et al (1967,1971), Ocal (1968), Alsan et al (1975), Ayhan et al (1983). They are of different accuracy and completeness, particulary before 1960.

Instrumentally-recorded epicentres, as reported by various seismological agencies during the period 1898-1992 have variable degrees of accuracy. The epicentral locations of events before the mid 1960s of all magnitudes calculated routinely have large errors, as do smaller events after that period. Alsan et al (1975) and Dewey (1976) recalculated epicentral positions and assessed focal depth using the phases reported in ISS/ISC.

The determination of focal depth in the region is however difficult, particularly before the installation of local seismographic stations. Surface wave magnitudes for the larger events $M_S > 5.8$ have been assessed only recently by reference to original long-period seismograms or station bulletins, Ambraseys (1988)

Figure 2.3 shows the recalculated distribution of earthquakes with $M_S > 6.0$ in Turkey during the period 1899-1986. A list of re-assessed instrumental and macroseismic characteristics of crustal events with $M_S > 5.8$ in the region was given by Ambraseys et al (1992).

2.3. Description of the 13 March 1992 Erzincan Earthquake

The main shock of the earthquake was recorded by three SMA-1 accelerographs at epicentral distances of 6, 70 and 71 kilometre. The closest of these, located in the centre of Erzincan, is of great interest on account of its near-field nature and the fact that it should reflect closely the ground motions experienced by the majority of affected structures in the town. Here, peak ground accelerations of 0.495 g and 0.399 g were recorded in the East-West and North-South directions respectively, while the peak ground velocity was estimated at 109 cm/sec. Figure 2.4 depicts the stronger E-W component of the earthquake record (Ambraseys et al, 1992). Considerable aftershock activity continued for some time after March 13th with the most significant of these ($M_S = 5.8$) occuring at an epicentral distance of 24 km from Erzincan on March the 15th. Extensive monitoring of the aftershock activity and the teleseismic study of the earthquake suggest that the main shock was a complex multiple event that involved not only the North Anatolian Faulty in the immediate vicinity of Erzincan, but also other conjugate faults in and off the Erzincan basin.

Investigation of the recorded ground motions (Ambraseys et al, 1992) revealed the large amplitude and quasi-periodic nature of the ground displacement, a feature which is particulary noticable in the North-South direction and which may be due to coherence effects. In addition, 70% of the energy flux was associated with two closely spaced pulses which occured 2 seconds after the beginning of the motion, while in all, nearly 60% of the total energy flux was in the North-South direction. These observations are consistent with near-field motion from a medium magnitude earthquake. There occurs also an apparent truncation of the peak ground acceleration pulse for almost 0.4 seconds; a feature which may be associated with the failure of a soil layer at the site of the accelerograph.

The above summary is based on extracts from the work of Ambraseys et al

(1992). However, literature on the 13 March 1992 Erzincan earthquake abound. A comprehensive report was published by Bosphorus University (1992) including contributions covering seismological, geotechnical and structural aspects as well as post-earthquake disaster response and mitigation. Moreover, Gülkan (1992) has undertaken an in-depth study of the earthquake in conjunction with the "Learning from Earthquakes" project of the EERI. The report gives valuable information on the seismology and geotechnics of the Erzincan region and strong motion data analysis, and concludes with recommendations for the mitigation of future losses.

2.4. A Note on Earthquake Hazard in Erzincan

The seismic record of the region of Erzincan shows that in the last 800 years the town has been destroyed completely on at least four different occasions and that it has been heavily damaged with great loss of life an equal number of times. In fact there are very few old towns in the world like Erzincan, in which nothing remains of their historical heritage in terms of monuments and old buildings, because of the high, persisting seismic activity of the region in which they are situated.

It is perhaps significant that the long-term seismic record of the region of Erzincan also shows extended periods of relative quiescence, such as the one between 1784 and 1939, a well-documented period of 155 years, during which activity was subdued. Referring to this period, we notice that in assessing hazard it is simply not possible to ignore the chance that all of our records may be for a quiescent period in the seismicity of the region. This is one of the possibilities that must be born in mind in making the judgemental decision in assessing long-term activity, and this is the principal reason why statistics alone cannot quickly and simply answer the hazard-evaluation question in Erzincan.

Some of these early events in this part of Anatolia were truly major, associated with large scale surface breaks of the Anatolian fault zone which converge from the the west, southwest and northeast on the site on which the town is built. The well established slip rate of 3 cm/yr of the close-by North Anatolian fault leaves little doubt about its enormous damaging potential. Therefore, the statistical assessment of the hazard from the seismicity of the last few decades alone is not adequate to define an appropriate basis for design.

Many studies exist, where attempts have been made to derive design input motion parameters using techiques for completion of earthquake catalogues where gaps

are observed. Use was made of a number of statistical assumptions, leading to varying results. The question still remains as to whether peak ground accelerations can be reliably predicted in the vicinity of an active and complex fault system such as that close to Erzincan.

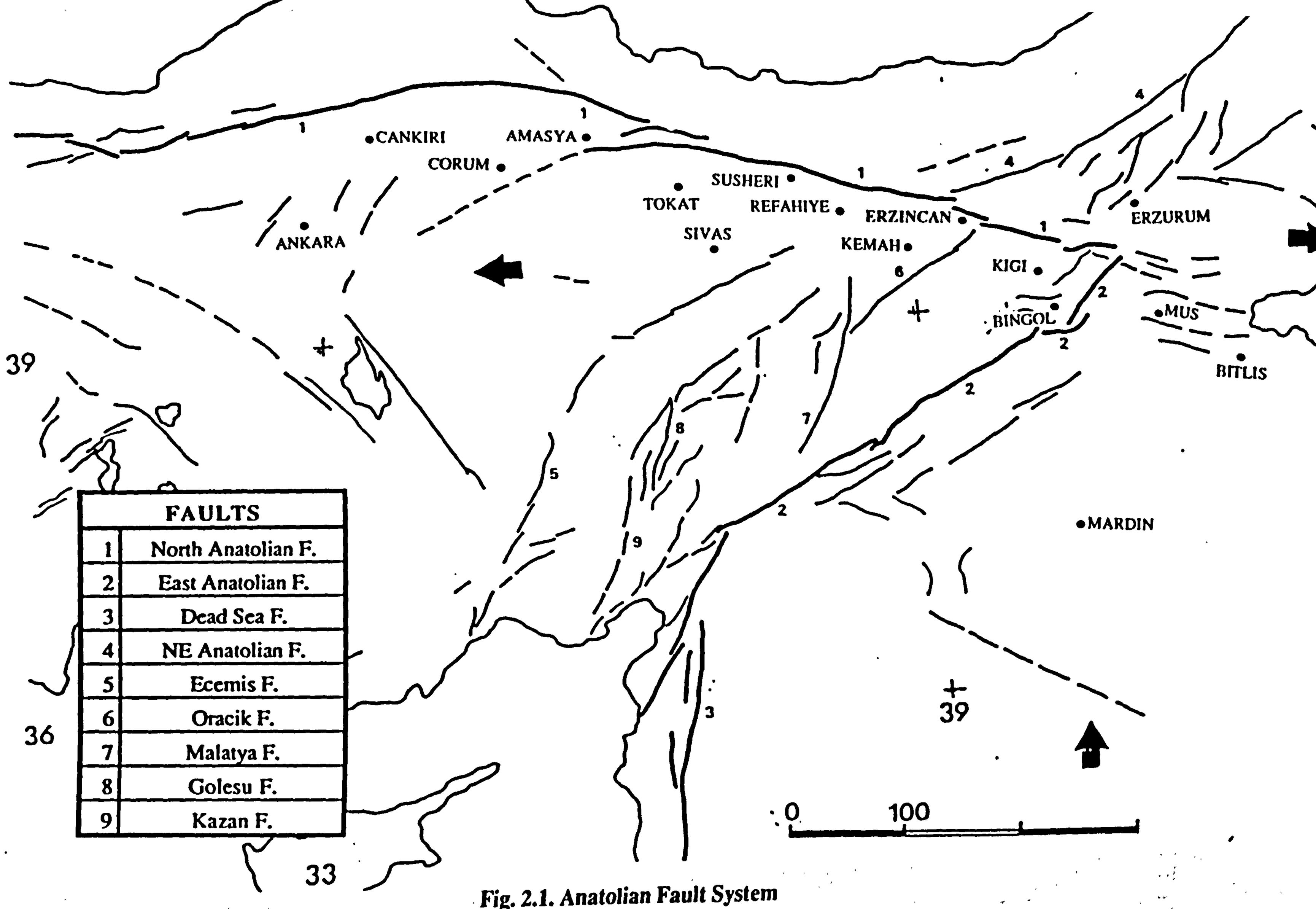


Fig. 2.1. Anatolian Fault System

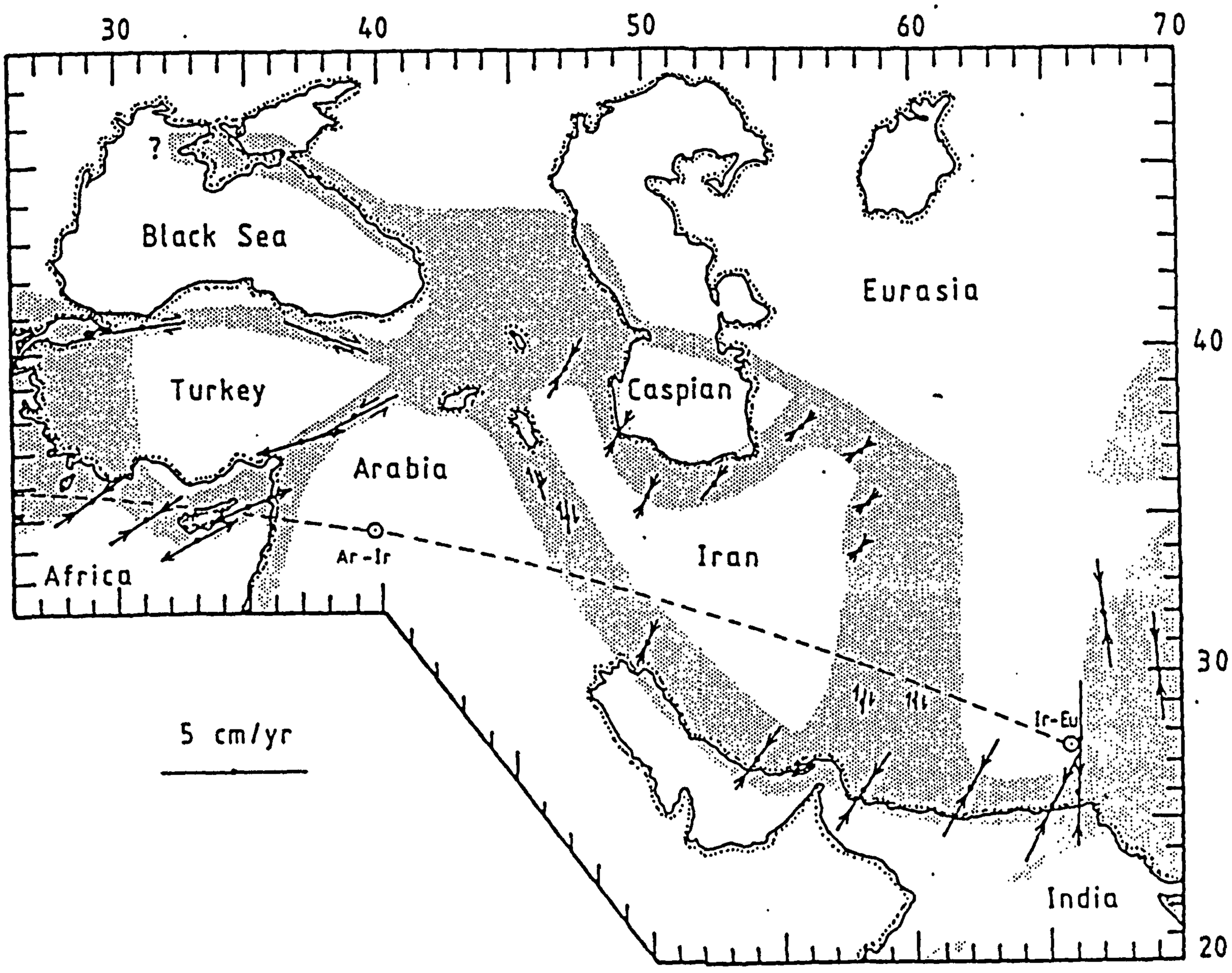


Fig. 2.2. Regional Tectonic Activity

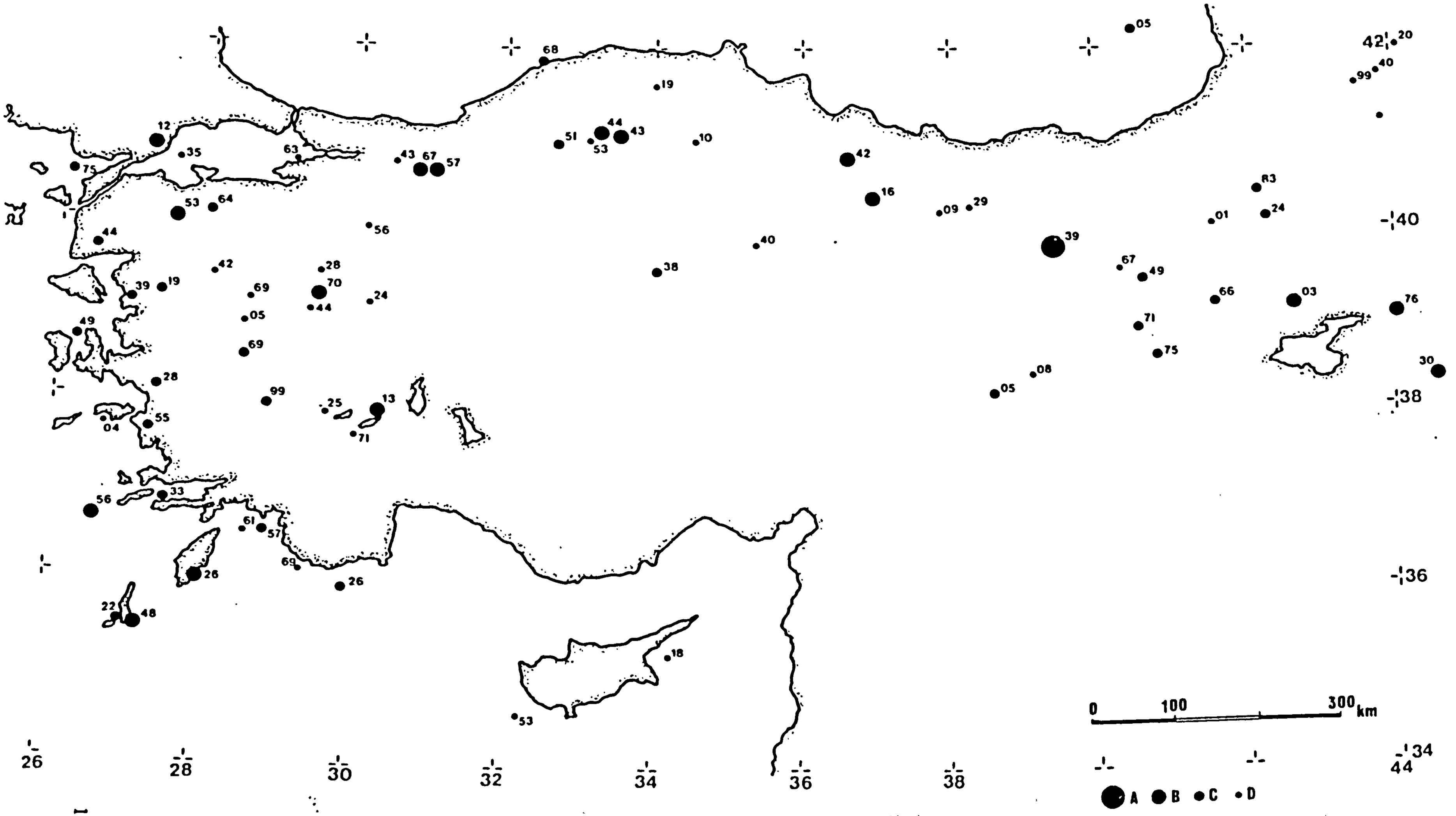


Fig. 2.3. Distribution of Earthquakes in Turkey, $M_S > 6$

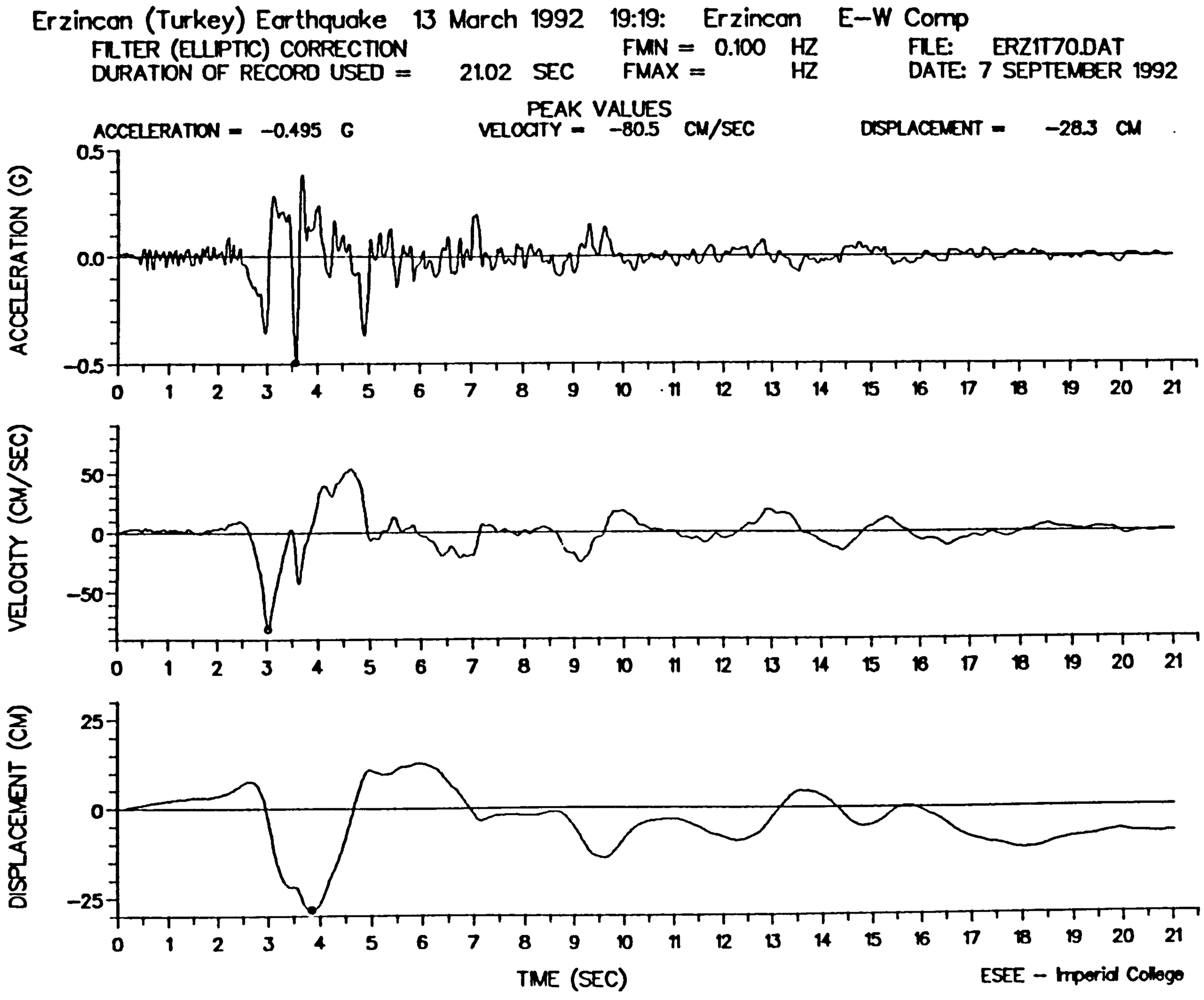


Fig. 2.4. Erzincan Earthquake (13 March 1992); Main Shock, E-W Component, Corrected by ESEE (Ambraseys et al, 1992)

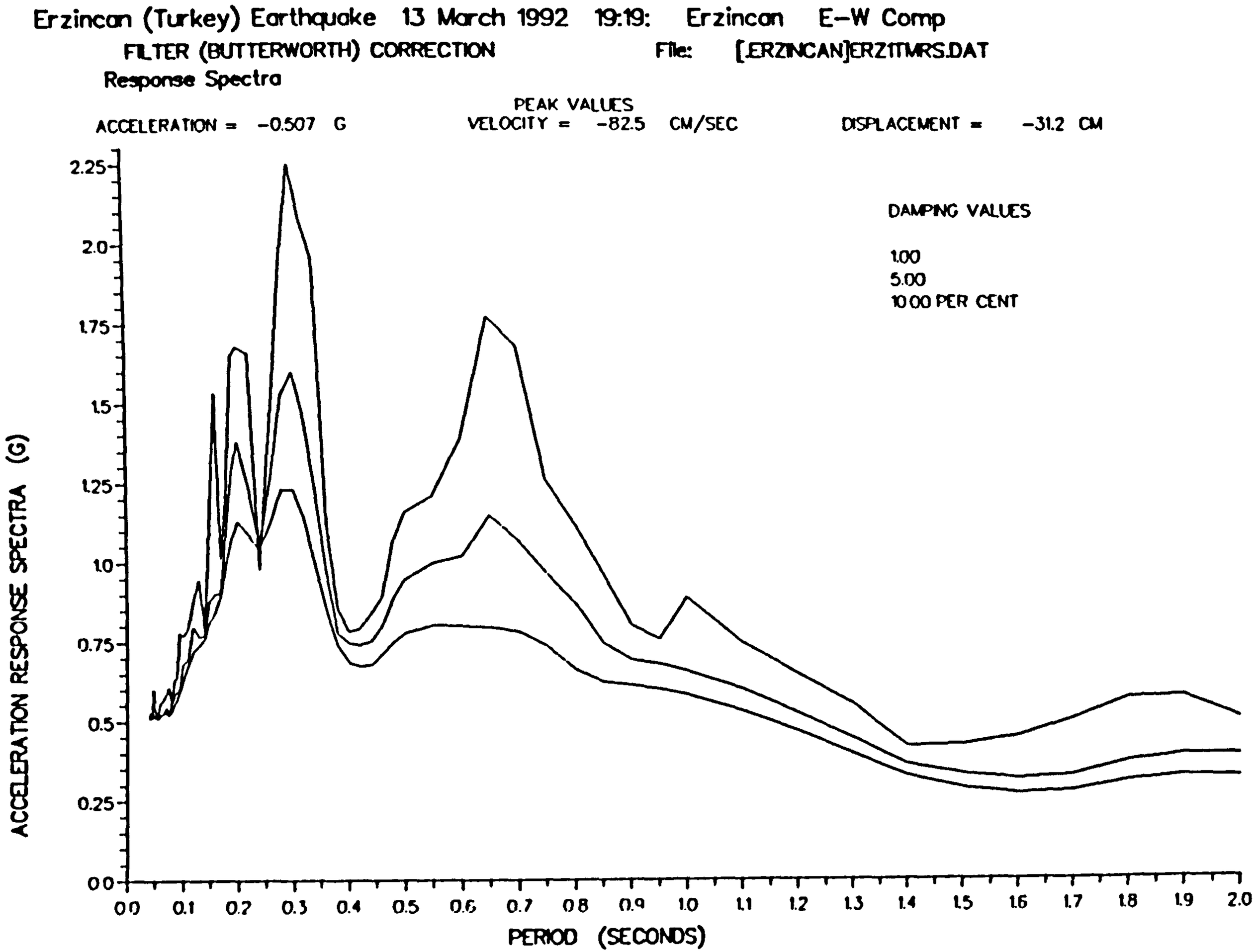


Figure 2.5. Acceleration Response Spectra for Erzincan Earthquake (13 March 1992); Main Shock, E-W Component (Ambraseys et al, 1992)

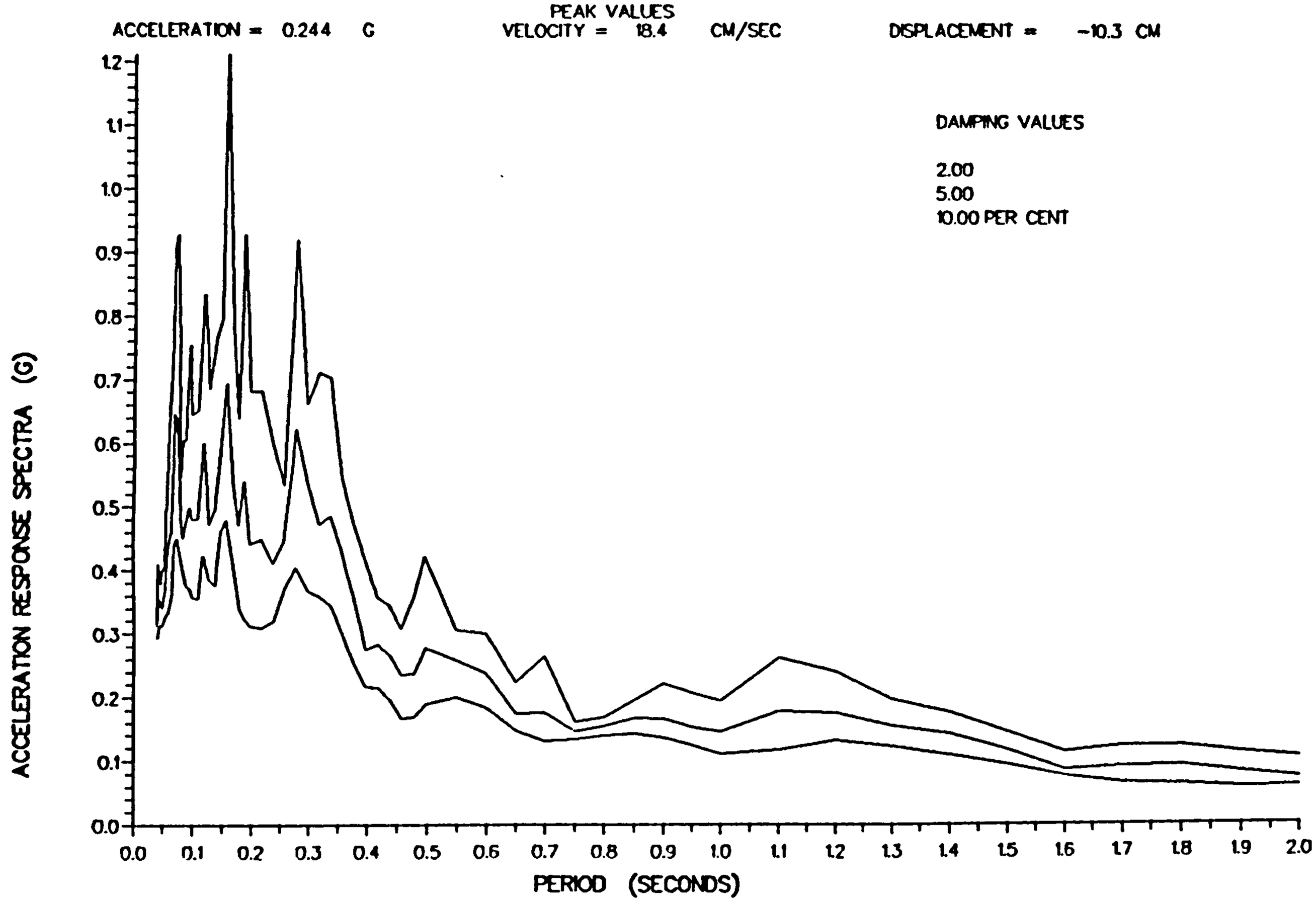


Figure 2.6. Acceleration Response Spectra for Erzincan Earthquake (13 March 1992); Main Shock, N-S Component (Ambraseys et al, 1992)

CHAPTER 3

3. PHILOSOPHY OF INSPECTION

3.1. Purpose

Several aspects of earthquake vulnerability and field reconnaissance were take into consideration in the planning stage of the inspection effort. It was considered essential to collect all information needed, or likely to be needed, in order that follow-up site visits could be eliminated or minimised. Also, it was decided not to utilise existing inspection forms, such as those in ATC20, but to modify them specifically for Erzincan. Based on the previous experience of members of the inspection teams, the repetitively-observed features leading to inferior seismic resistance were listed. These were included in the inspection forms alongside more conventional items included in existing forms. The forms were intended to be as comprehensive, yet as simple-to-use as possible, so that any chosen vulnerability assessment technique may be readily applied using the collected data. In subsequent sections, the background to the Erzincan Inspection Forms is given on a hierarchical basis.

3.2. Materials

This is one of the most important items of seismic vulnerability assessment, since the remedy of such a problem is difficult. From a concrete strength viewpoint, the presence of low strength concrete would indicate that even the static design gravity load carrying capacity could be below normally-accepted standards. With regard to the flexural capacity, the effect of the compressive strength is less pronounced, since the steel yield normally governs. (In some cases, the priority of detailed assessment of the structure was somewhat downgraded when the concrete strength was deemed wholly unacceptable).

In terms of seismic resistance, the yield strength of the steel plays a most significant role. On the one hand, the yield strength should not be lower than that used for designs, otherwise "capacity" problems may result. On the other hand, it can be shown that the curvature ductility supply drops for an increase in yield strength. Hence, increase as well as decrease in yield strength are viewed as negative seismic performance features. Also, the deformations, or lack of them, on bars are important,

since plain bars have an inferior bond behaviour leading to shortening of the plastic hinge length, and inadequate resistance to pullout. This, for a given curvature ductility, causes a reduction in the displacement (or rotation) ductility.

3.3. Section Characteristics

Detailing, at the section level, is of great significance to the integrity and ductility of the member, and hence the structure. The adequacy of the cover ensures that early buckling of longitudinal reinforcement does not occur. Also, stirrup detailing is very important to ensure that confinement is available after several cycles of inelastic load reversals. The 90° stirrup link is inadequate for seismic resistance. The 135° stirrup extension is required for medium ductility. Fully overlapping or welded stirrups are necessary for high ductility structures.

3.4. Response of RC Members

The slenderness ratios of members govern their susceptibility to buckling under high axial loading with transverse motion. Hence column dimension in section and elevation should be recorded. In the inelastic range, the ductility of the member, for a given curvature ductility, is a function of the plastic hinge length. Closely-spaced stirrups in the plastic hinge zone are essential for ductile response. The dissipative length is normally taken as about 0.2L, where L is the total length of the column. The spacing of stirrups along the length is hence an important parameter to monitor.

3.5. Sub-Assemblages

Structural analysis is undertaken assuming rigid connection behaviour. Opening of beam-column connections would influence the distribution of internal forces, since the location of points of contraflexure will vary. Therefore, the integrity of beam-column connections is essential to the adequacy of the building's performance. Observed patterns of damage of beam-column connections confirms that the two main failure modes are panel zone shear failure and cracking in the vicinity of beam sophit. Hence, information on the reinforcement in and around the beam-column connection is sought in the inspection effort.

Another most important sub-assemblage response aspect is the ratio between beam and column capacities. Hinging at the extremities of beams is a stable energy dissipation mechanism that does not lead to a global mode of failure. Therefore, a column overstrength factor is commonly recommended in earthquake resistance codes. The inspection procedure should take account of this feature.

Alignment of members framing into connections is important, since non-alignment leads to unaccounted actions. In elevation, beams of different depths framing into two opposite sides of a connection cause local moments on column heads as well as high local shear. This may cause shear cracking between the centre lines of the beams. In plan, non-alignment causes a torque to be applied on the column, leading to near-spiral cracks.

3.6. Overall Structural Features

The overall structural configuration has a profound effect on the seismic performance of structures. Some of the salient features which were used to construct the Erzincan inspection forms are discussed below.

3.6.1. Plan layout

The earthquake inertia load is applied at the centre of mass and is resisted at the centre of rigidity. If the two centres do not coincide due to irregularities in mass and /or stiffness this has the effect of causing torsional motion of the structure leading to additional torque-induced column shear forces, especially at columns distant from the centre of motion.

Another important aspect of plan configuration is the presence of re-entrant corners. This not only complicates the dynamic response but causes a nonuniform distribution of ductility demand, increasing at the edges of the outer wings.

3.6.2. Elevation proportion

The elevation aspect ratio of a building has implications on the ultimate rocking column load due to overturning. Where the structure has a height significantly larger than four times the plan base dimension the resultant of seismic forces is applied at a high point,

causing large overturning moments. This may overload columns in compression and in parallel lead to uplift and excessive in the limit, instability.

3.6.3. Elevation stiffness and strength distribution

Stiffness and strength may not necessarily be proportionally related, where the transverse system is comprised of frames and walls. Regular distribution of both in the longitudinal direction ensures uniform ductility demand and close correlation between the force distribution used in codes and that actually experienced by the structure. Commonly-observed damage has been attributed to soft storey behaviour and concentrated cracking has often been correlated with abrupt changes in stiffness and strength. The inspection forms aim to record abrupt stiffness changes in excess of, say, 20%. No attempt has been made to assess strength distribution irregularities since no walls are used in the existing building inventory.

3.6.4. Orthogonal framing action

Unlike wind loads, earthquake induced loads have no pre-determinable prevailing direction. Therefore, adequate framing action should be provided in both directions, in the absence of RC walls. The inspection forms include an item to record such deficiency by identifying beams that are likely to have no moment connection with the column. These are normally beams of depth shallower than beams in the orthogonal direction.

3.6.5. Foundation system

Under earthquake loading relative movement, horizontally or vertically, causes distress to the super-structure. Therefore, tying of footings in two orthogonal directions by ground beams is important when the foundations are on soft soil. Otherwise the use of strip footings or raft foundation would be beneficial.

3.7. Soil Characteristics

Site characteristics and amplification have been identified in many earthquakes as some of the most important parameters affecting structural damage. For example,

amplifications of up to 3.0 were observed in northern San Francisco (Marina District) during the Loma Prieta earthquake of 17 October 1989.

The depth of deposits to bed rock, alongside the constitution of the deposits, dictates the site periods. These have been observed to be reflected in high amplifications, such as in the Emerville (Oazkland) record, where large magnifications corresponding to a period of 1.8 seconds were observed.

The presence of a near-surface water table is also of great significance. Under sustained excitations, liquefaction of saturated and partially saturated granular soils may result, especially in the near-field. This will lead to large permanent ground displacement.

The average shear wave velocity of the site is significant in two respects, namely site period calculations and the influence of asynchronous motion. This latter effect may lead to net static extension or compression of horizontal structural members. The inspection forms include items covering the above effect, so as to permit further assessment. This, however, was not considered in the analysis of the typical building.

3.8. The Erzincan Inspection Forms

A thorough review of inspection forms used by several earthquakes reconnaissance groups from several countries was conducted. The forms for the analysed building are provided in Appendix AIII. Their effectiveness has been proven in the field, where a large number of buildings under consideration (one thousand, four hundred and fourty) were inspected within a very tight schedule allowed. The results of the inspection are summarised in section 3.9 below.

A novel feature of the forms is the extent to which structural configuration parameters, ductility-based detailing and capacity design concepts are added. Also, the short itemised commentary has proven valuable in the field in minimising non-uniformity.

3.9. Results of the Inspection

Initially the primary task of the inspection was to find and record damage, flaws and deficiencies caused by the March 1992 earthquake. However, in the pursuit of this

information many other defects unrelated to earthquake effects were found which were too significant to overlook. Hence, "observed damage and defects" refer not only to earthquake-induced damage but also to inherent, as-built deficiencies.

The information recorded included all of the basic information needed for a proper identification of the building along with an assessment of the degree of structural completion, the general condition of the structure and a detailed, representative accounting of the type, location, size and extent of damage and defects observed. In addition a geotechnical evaluation was undertaken by a qualified geotechnical engineer. Also, for some buildings, samples of concrete and reinforcing steel were taken, for later testing and evaluation. The adapted inspection policy and the utilised inspection forms where coincident with the philosophy of inspection briefed in section five.

The observed damage could be attributed to both design and construction defects. It is worth noting that the standard of construction in Erzincan was observed to be very poor; and as had been reported by other parties, and that poor structural designs, often flouting even basic earthquake-resistant principles, were at least as responsible for the observed failures. However, it is also probably the case that the most blatant examples of poor construction practice were to be found in those buildings which suffered complete or partial collapse during the earthquake and were therefore not available for comparative investigation. Many of the most commonly observed features of poor construction practice, such as low quality concrete and inadequate reinforcement detailing, would have been prevented by proper supervision and inspection. As such construction supervision was evidently not a common occurrence, designs assuming high levels of global and local ductility were unsuitable for application to the region. Amongst various construction deficiencies, we can state the following:

3.9.1. Structural defects

Some of the observed structural defects are stated hereafter:

- Low concrete strength; high water/cement ratio. An average of 12 N/mm^2 was recorded for private housing and 220 N/mm^2 for governmental buildings.
- Poor concrete consistency; rock pockets, significant variability in degree of consolidation, evidence of bleeding, cold jointing and improper mixing, placement and consolidation.

– Poor concrete form work; no proper control of cross-sectional dimension, member spacing, plumpness, poor vertical and horizontal alignments. Acceptable tolerences were largely exceeded.
– Poor reinforcement; smooth undeformed bars.
– Poor positioning of reinforcement; bar cover varies form 0 to 7.5 cm or more. Column ties and beam stirrup spacing are erratic and too widely spaced. Tie detailing did not include seismic hook into column core. Hence, ties opened up at various locations associated with concrete cover spalling.
– Inappropriate design; low reinforcing steel percentage in columns and beams. Most of the building stock had aseismic design forces of 10 - 13% of the vertical load with no special reinforcement provisions for ductility. These were found to be much less than the earthquake induced forces.
– Absence of sufficient stirrups in beams, absence of sufficient column ties and at the beam-column connections. Inadequate shear walls or moment resisting frames for modern seismic design.
– No consideration of in-fill wall interaction with structural frame.
– Poor anchorage of reinforcement, inadequate hook or embedment length to develop bars ultimate capacity, inadequate cover to develop sufficient bond. Particularly, since smooth (undeformed) rebar was used.
– Voids in concrete made by embedded conduits or concrete removed to provide pipe support access to beam bottom reinforcenment often in critical locations.
– Cracks; horizontal, vertical, diagonal, partially or completely penetrating structural member.
– Crushing and spalling of concrete in columns and beams.

A summary of the distribution of damage in the city is given in Fig. 3.1.

3.9.2. Non-structural defects

Some of the observed non-structural defects are listed hereafter:

– Cracking or failure of masonry joints.
– Cracking of masonry.
– Separation of masonry.
– Masonry falling out.
– Absence of reinforcement in masonry.
– Absence of connections of masonry to frame.

– Design deficiency.

In many cases, it was clearly observable that the masonry infill panels provided a significant reserve strength to the structure beyond that included for by the structural design. These panels contributed to the individual storey shear resistances by acting in a manner similar to that of a bracing strut, while the increased flexural strength served to reduce the horizontal displacements and ductility demand in the structural frame. Consequent damage to the masonry panels was evidenced by shear cracking, often in an x-pattern, and the jamming of the wall panels between the elements of the structural frame. Inspection of the ground displacement response derived from integration of the accelerogram recorded at Erzincan Meteorological Station indicates that only one displacement cycle of large amplitude occurred during the earthquake. Thus, the cyclic deterioration and degradation of the structural and non-structural elements was not as a significant feature as it might have been during a longer period of strong motion including multiple arrivals of strong waves. In such a case the ability of the masonry infill panels to continue to resist a substantial proportion of the lateral loading would be more in question. The behaviour of partially-constructed buildings which possessed infill walls in some but not all locations was illustrative in this regard, as concentration of damage often occured in the open frames or storeys with the completed areas surviving relatively unharmed.

3.10. Discussion

A key element in this part of the work was the collection, then utilisation, of information on the buildings under consideration. From a 'collection' viewpoint, the Erzincan forms are adequately comprehensive, based on modern seismic design practice and user-friendly. Their hierarchical structure enabled the optimization of the inspection effort. In this respect in cases where, for example, material quality was deemed wholly unacceptable, much less effort than normal was allocated to other aspects of the inspection, hence more worthy structures were prioritised.

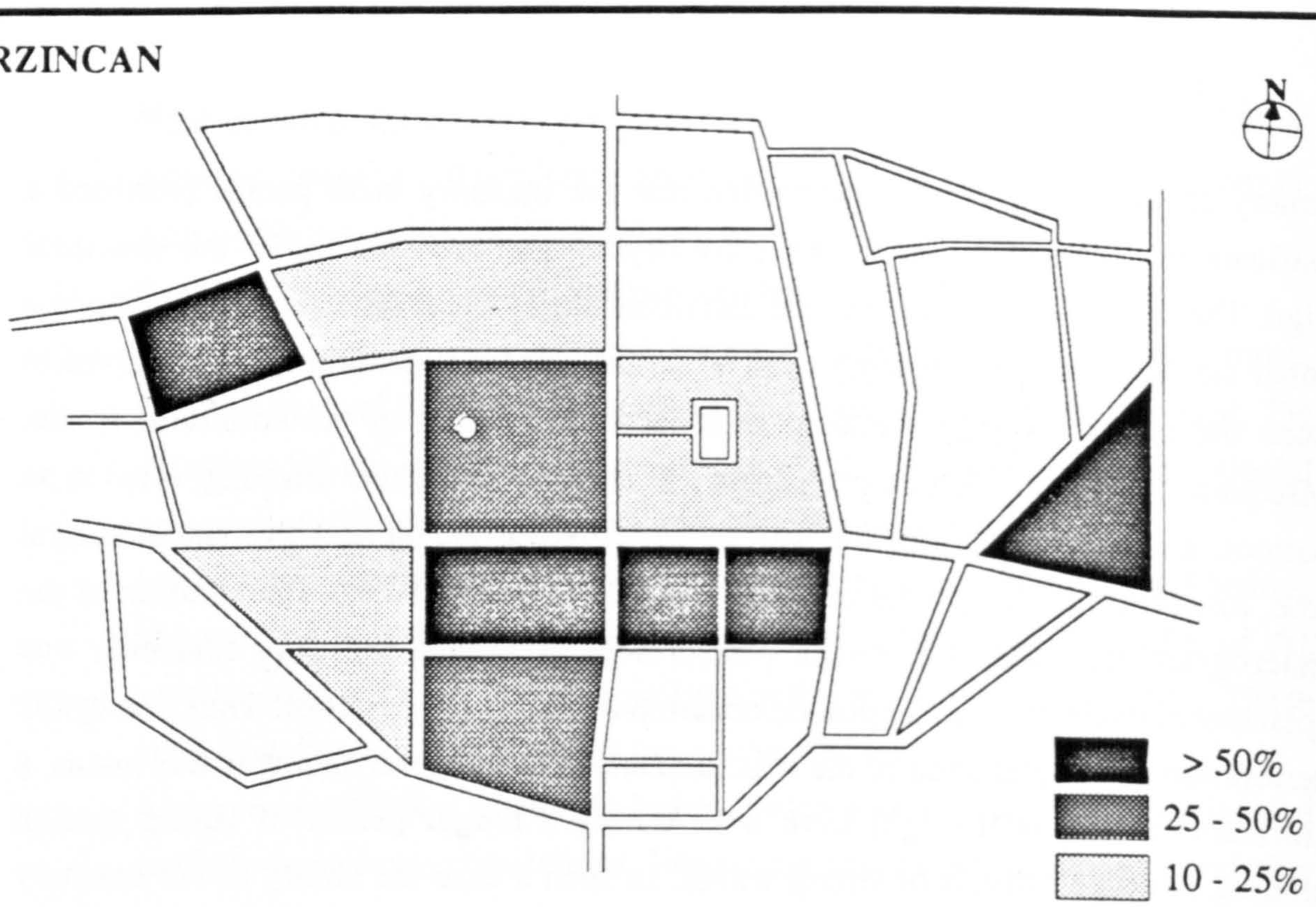


Fig. 3.1. (a) Distribution of Collapsed, Demolished or Heavily Damaged Buildings (by percentage)

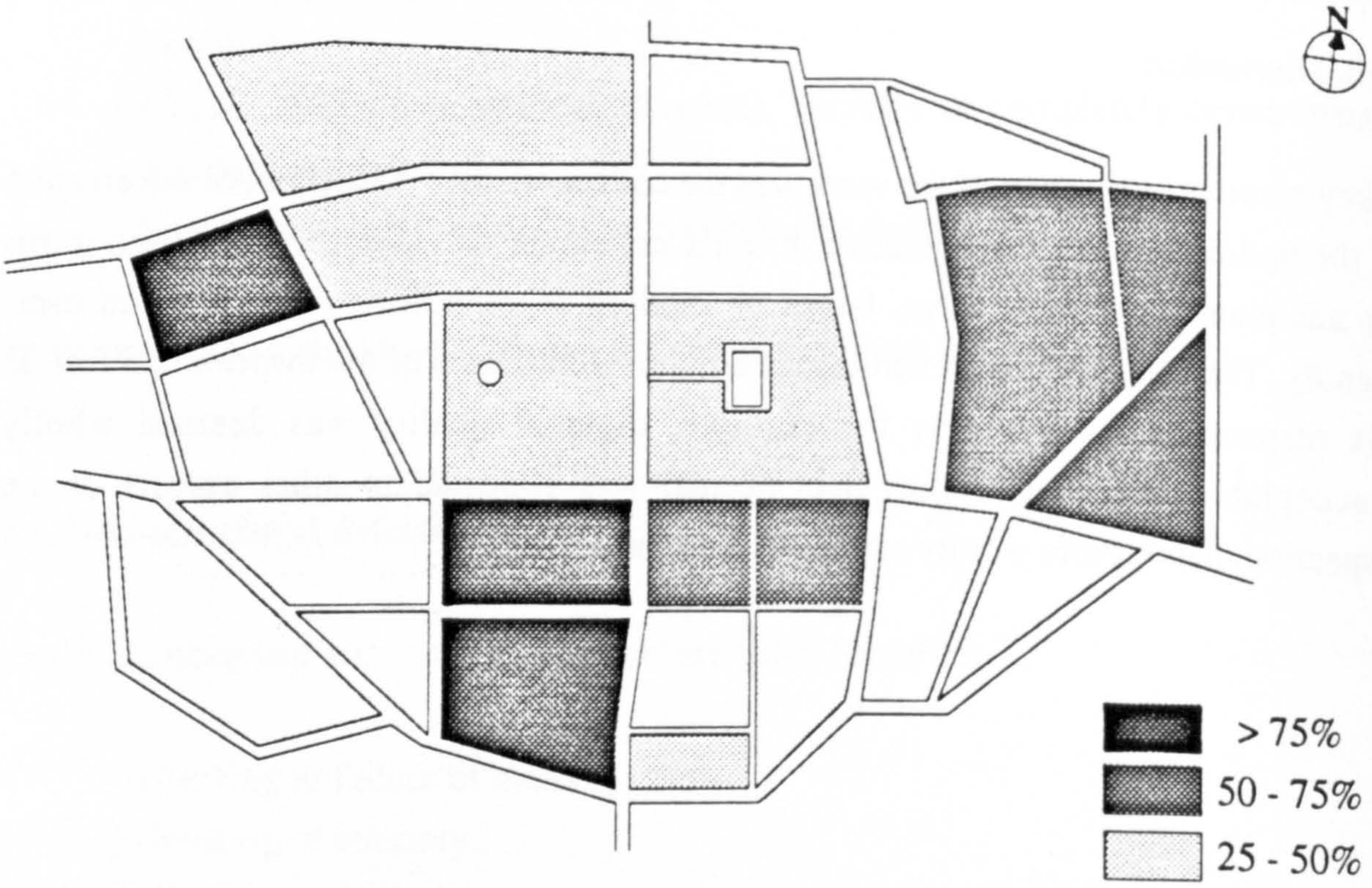


Fig. 3.1.(b)Distribution of Damaged Buildings (by percentage)

(Ambraseys et al, 1992)

CHAPTER 4

4. CRITERIA FOR SEISMIC ANALYSIS AND UPGRADING

4.1. Summary of Some Existing Seismic Hazard Studies

Seismic hazard in Northern Turkey has been extensively studied by several researchers (Ambrasseys, 1988). These studies covered statistical methods, varying from the widely-used Gutenberg - Richter cumulative frequency distribution to the more elaborate Gunble extreme value analysis. In the following, abrief description of three studies on seismic hazard in Anatolia, this is not a comprehensive review and is intended to demonstrate possible approaches to evaluate seismic hazard in a complex tectonic environment of relatively high seismicity where insufficient data exists.

A study was conducted by Gürpìnar et al (1979), using magnitude-frequency, intensity-magnitude and intensity-distance relationships as well as magnitude-fault rupture length equations. Regression analysis using two parameters was undertaken, resulting in three relationship between intensity and d1, d2 and d3, defined as iso-seismal distance parallel to fault from macroseismic epicentre, transverse distance and average distance, respectively.

Use was made of the widely-used Gutenberg - Richter cumulative frequency distribution applied to the 30°E - 42°E sector of the North Anatolian fault. The authors report, quite rightly, that the data are incomplete, biased towards large magnitude (by the selection of the largest reported magnitude from various stations) and by the lack of early data. This is compensated for by employing statistical methods for "filling the gaps" through assuming a Poisson distribution of data based on the relatively more complete time-spans and magnitude range. The error in the estimate of the mean rate of occurrence of each magnitude group is then minimized. The resulting recurrence relationship is given by:

$$\log N = 4.62 - 0.80\ M \qquad (4.1)$$

The authors used the above relationship to draw expected intensity maps for different return periods using Cornell's method. It was agreed that this gives more reliable results than the Gumble III model. The essential design step of deriving ground motion parameters from intensities was not addressed in the study. Based on this study,

intensity in Erzincan is about X for a 475 year return period and about XI for a 10,000 year return period. No recommendation was made on a relationship to obtain ground parameters from the assigned intensities.

The values given above contrast with those quoted by Yarar et al (1980). The authors of the study gave intensity maps for 200 and 500 years return period that would correspond to intensity 7.5 and 8.0 respectively. The latter figure should compare with the intenity X given in the study by Gürpìnar et al (1979). This may be due to differences in assumptions used in the study, not fully discussed in the available references. In the study by Yarar et al, iso-peak ground acceleration contours were drawn. These give a rock peak ground acceleration in Erzincan of 0.3-0.4 g and 0.4-0.5 g for return periods of 200 and 500 years, respectively.

An over view of seismic hazard assessment studies in Turkey was compiled by Erdik et al (1988). Reference is made to a study by Erdik et al (1985), where the peak ground acceleration zoning map was proposed. These give a value of about 0.5 g for Erzincan for a 10% probability of exceedance in 50 years, which is suitable for residential buildings (although a 20% probability of exceedance is sometimes acceptable, thus warranting a reduction in peak ground acceleration).

Based on a Gumble III distribution of extreme values (justified on the ground of the high curvature of the frequency magnitude relationship), Burton et al (1983) derived magnitude contours for Turkey. With a return period of 75 years, earthquake magnitudes have been contoured, giving a maximum earthquake in Erzincan of 7.0 to 7.25 (m_S) with, based on the maximum strain-energy release, a magnitude of about 7.5 to 7.75 (m_S).

Erdik et al (185) conducted a seismic hazard study for the Electric Power Authority for Turkey. Intensity maps were derived for Turkey for return periods of 225, 475 and 10,000 years. Moreover, peak ground acceleration contours for the same return periods were derived. This gives PGA values for Erzincan between 40% and 60% of the gravitational acceleration (on rock). It is, however, important to note that these are maximum predictions from a study undertaken with important structures (nuclear power plants) in mind.

4.1.1. Commentary

There is a wide variety of design parameters under earthquake conditions derived for Erzincan. This is due to the large number of ingredients and assumptions needed for

seismic hazard assessment, some of which are :

- The status of earthquake catalogues.
- Method used to complete gaps in catalogues, if required.
- Attenuation relationships utilized.
- Source model(s) used.
- Nature of the magnitude frequency relationship.
- Selected return period and acceptable probability of exceedance.

From the studies cited above, the design earthquake in Erzincan would be in the range of m_S = 7.0 to 7.25 (Burton et al, 1983) the peak ground acceleration for a 10 % probability of exceedance is about 0.5 g (Erdik et al, 1985) and the MSK intensity of VIII to X for a return period of about 500 years (Yarar et al, 1980; Gürpìnar et al, 1979).

It should be noted, however, that major assumptions are involved in the derivation of the above values. The fact still remains that in the past, there have been prolonged periods of quiesence, such as between 1794 and 1939; a well-documented period of 155 years during which seismic activity was subdued. Therefore, it might be that our short observation period is during a relatively quiescent period, hence statistics done cannot provide a satisfactory answer to hazard assessment problems in Erzincan. This must be augmented by sound engineering judgement based on considerations of the relative safety and economy of a particular site and project.

4.2. Design Peak Ground Accelerations in Erzincan

In the following sub-sections several studies are used and approaches presented for the investigation of the range of peak ground accelerations for design of engineering structures in Erzincan. This is intended to provide criteria for assessment of the "demand", having established the "supply" from the inpection work.

4.2.1. PGA Implicit in the 1975 Turkish Code

The Turkish Code entitled "Specifications for Structures to be Built in Disaster Areas" was issued by the Ministry of Reconstruction and Resettlement in July 1975. The Code does not give explicitly the anchor PGA, nor are any of the parameters used readily identifiable as a PGA. Below, an attempt is made to evaluate the implicit PGA in the code, based on the writer's experience and reasonable assumption.

The base shear equation is given by:

$$F = C_0 K S I W \qquad (4.2)$$

where:
- C_o is the seismic zone coefficient (0.03 to 0.1)
- K is the structural type coefficeint (0.6 to 3.0)
- S is the dynamic coefficent for the structure (0.2 to 1.0)
- I is the building importance coefficient (1.0 to 1.5)

If a short period structure is assumed to be founded on a site such that the spectral coefficient is maximum and responding elastically (no force reduction for ductility), then the base shear to weight ratio will be given as follows (for highest seismicity and high importance).

$$C = 0.1g \times 2.0 \times 1.0 \times 1.5 = 0.3\ g \qquad (4.3)$$

Assuming an average spectral magnification factor of 2.5, the implicit peak ground acceleration (PGA) in the highest zone of seismicity according to the 1975 Turkish code is 0.12g (unless we assume that there is an implicit ductility factor of about 4.0 used to arrive at the range of C_o of 0.03 to 0.1) This is surprisingly low, compared to an implicit PGA in UBC of 0.55g, calculated as follows.

$$V/W = 0.4g \times 1.25 \times 2.75(max) / 1 = 1.38\ g \qquad (4.4)$$

$$PGA = 1.38g / 2.5 = 0.55\ g \qquad (4.5)$$

It is to be noted that the above has no implication on the safety and economy of designs to the Turkish Code and to the UBC; it only serves as an indication of the process of calibration which each code undergoes. For specific buildings, the two codes may give results closer than those implied by the crude calculation carried out above. However, there is value in the above calculations; if a peak ground acceleration of 0.5g was to be used in the Turkish Code, the implication would be that elastic forces should be increased by a factor of about 2.7, strictly speaking. Other base shear coefficients, however, are used to calibrate the results to known acceptable values. It is, therefore, appropriate to attempt to use PGA values for Turkish code scaling purposes.

4.2.2. PGA from design earthquakes

Attention is focused on the study by Burton et al (1983), where a maximum earthquake

of magnitude m_S = 7.0 to 7.25 has been proposed. Form the study by Gürpìnar et al (1979), the North Anatolian earthquakes have depths of not more than 20 km (crustal) with an average of about 12 km, based on 8 previous earthquake depth estimates. If the conservative depth of 12 km in considered, the following table may be constructed for the peak ground acceleration for various epicentral distances. This is based on the attenuation relationship of Ambraseys and Bommer (1991). This relationship was derived from shallow Eurasian earthquakes and has given good comparisons with the acceleration recorded for the 13 March 1992 Erzincan earthquake (Ambraseys et al, 1991).

Distance to Fault trace (Km)	0	3	5	10	12	15	20
PGA (g) 50% Exceedance	0.38	0.36	0.35	0.35	0.26	0.23	0.18
PGA (g) 16% Exceedance	0.69	0.66	0.63	0.52	0.47	0.42	0.34

Table 4.1. : PGA for Ms = 7.0 Earthquake at 12 Km Depth

The choice of a magnitude 7.0 is deterministic, since, as discussed above, statistics only cannot be relied upon under the circumstances prevalent in Erzincan. It is to be noted that a magnitude 7.2 (m_S) will have a probability of exceedance during the 50 years life time of the structure of about 50%, according to the 75 year return period derived by Burton et al (1983). A magnitude m_S = 7.0 earthquake, according to the same study, will have a probability of being exceeded of about 57 %.

4.3. Seismic Force Comparison for Prototype Structure

4.3.1. Code-based force calculations

In this section, earthquake induced forces are calculated from the existing version of the Turkish Code (1975) and the UBC 1991. Additionally, an attempt is made to evaluate probable forces imposed on structures by the 13 March 1992 earthquake in Erzincan.

It was necessary to make certain assumptions regarding peak ground acceleration, structural characteristics and soil conditions. These should have been viewed as "indicative" and are subject to alteration at a later stage. The following was assumed:

Structural period consistent with a shear wall structure of four storeys (height 40 ft) founded on deep alluvium. The site was in the highest seismic zone and was of ordinary importance. The response modification factor (R_W in UBC and K in the Turkish Code) is for a shear wall structure where the walls provide the total resistance to transverse loading.

The Turkish Code (1975) gives the following :

$$V/W = C = C_0KSI \qquad (4.6)$$

where C_0 : seismic zone coefficient
K : structural type coeficient
S : spectral coefficient
I : building importance coefficient

For the prototype structure, the following values are fixed :

C_0 : 0.1 (highest zone coefficient)
K : 1.33 (building with box system)
S : 1.0 (maximum value)
I : 1.0 (ordinary importance)

Therefore,

$$V/W = 0.1 \times 1.33 \times 1.0 \times 1.0 = 0.133 \qquad (4.7)$$

Hence the structure should be designed for a transverse force of 13.3% of the appropriate vertical weight.

The same parameters are used for the UBC 1991 code where the base shear equation is given as follows :

$$V/W = ZIC / R_W \qquad \text{and } C = 1.25S / T^{2/3} \qquad (4.8)$$

where : Z : zone factor
I : importance factor
R_W : response modification factor
S : site coefficient
T : structural period

For the structure under consideration, the following values are used :

Z	=	0.4	(highest seismicity)
I	=	1.0	(ordinary importance)
R_W	=	6.0	(building frame inter shear walls)
S	=	1.2	(deep dense or stiff soil)
T	=	0.3	(40ft high shear wall structure)

Noting that the maximum value of C is 2.75, the base shear coefficient is given as :

$$V/M = 0.4g \times 1.0 \times 2.75 / 6.0 = 0.18g \qquad (4.9)$$

Therefore the structure should be designed for a lateral force equal to 18% of the appropriate vertical load. This is about 38% over the Turkish Code base shear of 0.13g. Also, UBC loads are working loads while Turkish seismic loads are supposed to be ultimate loads. Hence, another 40% difference exists between the two codes.

Other possible options, such as using UBC with an increased zone factor to reflect the predicted PGA in Erzincan may be explored. Also, the use of the Erzincan spectra may be explored. Sample calculations are given as follows.

The UBC (1991) used with a zone factor of 0.5 (instead of 0.4), gives a base shear of 23% of the weight. Use of the Erzincan spectra, on the other hand, would require some major decisions regarding the level of structural ductility. Therefore,the treatment below would have been viewed as preliminary.

4.3.2. Forces from the 13 March 1992 Erzincan earthquake

The elastic spectra from the Erzincan earthquake are shown in Figs 2.5 and 2.6. Herein, it was again assumed that the structure has a period of 0.3 seconds (3.3 Hz). No ground amplification is applied, since the spectra reflect actual site response characteristics. It is argued herein that the near-field record from the Erzincan earthquake is indeed representative of local site conditions, since the very deep alluvial deposits in the Erzincan basin are of a constant depth throughout the Town. Conversely, the predominance of the E-W component, with exceptionally high peak ground acceleration and velocity, may not be a true representative feature, since the complex fault system comprising the North, Northeast and East Anatolian faults may generate different directionality effects. It would, therefore, be very conservative to use the E-W spectrum

alone. Finally, for a structure of period 0.3 seconds, the scaling of the elastic spectrum should be performed by dividing by $(2\mu - 1)^{0.5}$ and not μ since it lies in the "velocity-sensitive" zone of the spectrum. Table 4.2. is constructed to give an indication of base shear coefficients resulting from the Erzincan earthquake.

Response	Elastic	$\mu = 2$	$\mu = 4$	$\mu = 6$
C (E - W)	1.52	0.87	0.57	0.45
C (N - S)	0.52	0.30	0.19	0.15
C (average)	1.02	0.58	0.38	0.30

Table 4.2.: Base Shear Coefficients From the Erzincan Earthquake Spectra for 5% Damping and Structural Period 0.3 seconds for the Shown Ductility Ratios.

The decision regarding whether to choose the E-W, N-S or the average is, as demonstrated in Table 4.2, of great significance for the ensuing design.

4.4. Response Spectral Shapes For Design

In the case of modal spectral analysis, there is a need for the spectral shape to be defined. Herein, there are several options; the Turkish Code spectrum, the UBC spectrum, a Newmark-Hall spectrum and spectral shapes representative of the recent earthquake. The procedure for defining each is given below.

4.4.1. The Turkish Code of 1975

The code does not give an elastic (or indeed a design) spectrum. However, the parameter S is period - dependent, and hence can be used to plot a design spectrum. This is performed for a specific set of all other parameters. Below is an example for parameters used in section 4, but changing the structural period T. The design spectrum can be plotted from values given in Table 4.3 below.

Period (seconds)	0.1	0.5	1.0	1.5	1.6	1.7	1.8	1.9	2.0
Spectral ordinate	0.13	0.13	0.13	0.12	0.11	0.1	0.09	0.08	0.08

Table 4.3: Sample Turkish Code Spectrum for C_0=0.1 , K=1.33, T_0=1.2, I=1

For an elastic spectrum, a corner period T_1 will have to be assumed. This may be taken as that used by UBC or any other well-respected seismic code.

4.4.2. The UBC, 1991

The UBC gives an elastic spectrum for various types of soil, normalized by the peak ground acceleration. This is shown in Fig. 4.1.

4.4.3. Spectra based on Newmark and Hall method

Newmark and Hall gave spectral amplification factors given the peak ground parameters. Here there is a choice, since no predictions of peak ground velocity and displacement are available for Erzincan. Use can be made of the peak parameters from the 13 March earthquake, but a decision is needed as to whether to use the E-W, N-S or average ground parameters. Herein, it is assumed that the average is used.

Peak values	a (g)	v (cm/sec)	d (cm)
N - S	0.39	109	35
E - W	0.5	85	28
Average	0.44	95	31

Table 4.4: Peak Ground Parameters from 13 March 1992 Earthquake

For a 5 % damping and 84 percentile, the spectral amplification factors recommended by Newmark and Hall are 2.6 for acceleration, 1.9 for velocity and 1.4 for displacement. Using these values, the spectral ordinates for the Erzincan earthquake would be (average of the two components) 1.14 g, 180 cm /sec and 51 cm. These values can be used on a

tripartite plot to arrive at an elastic spectrum. It is noted that the 8 to 33 Hz modification should be applied as depicted from Fig. 4.2.

4.4.4. Spectral shapes from Erzincan 1992 earthquake

As opposed to using the peak ground parameters from the Erzincan earthquake to plot an elastic spectrum based on the Newmark and Hall amplification factors, we may "smooth" the spectra from the actual event. This is highly subjective, but is nevertheless explored herein. Either of the two shown normalized 5% damping elastic spectral shapes shown may be used, with the appropriate scaling to the desired peak ground acceleration. The judgemental, subjective basis of the spectral shapes are shown in Fig. 4.3.

4.5. Recommended Earthquake Forces

With due regard to the above sub-sections, where various options for PGA selection and spectral shapes, it is herewith recommended that the strong-motion data from the Erzincan 13 March 1992 earthquake are used for analysis and re-design. This is based on the fact that the peak ground accelerations measured for the 1992 event are not vastly different to those obtained from the above-reviewed hazard studies. Moreover, the homogeneity of the soil condition in the Erzincan basin implies that future earthquakes are likely to exhibit strong-motion characteristics similar to those measured for the 1992 earthquake.

It is, however, to be noted that this recommendation is subjective. It serves the purpose of the current investigation, where the objective is to assess the variation in seismic response parameters for the re-designed building as a function of the repair approach used.

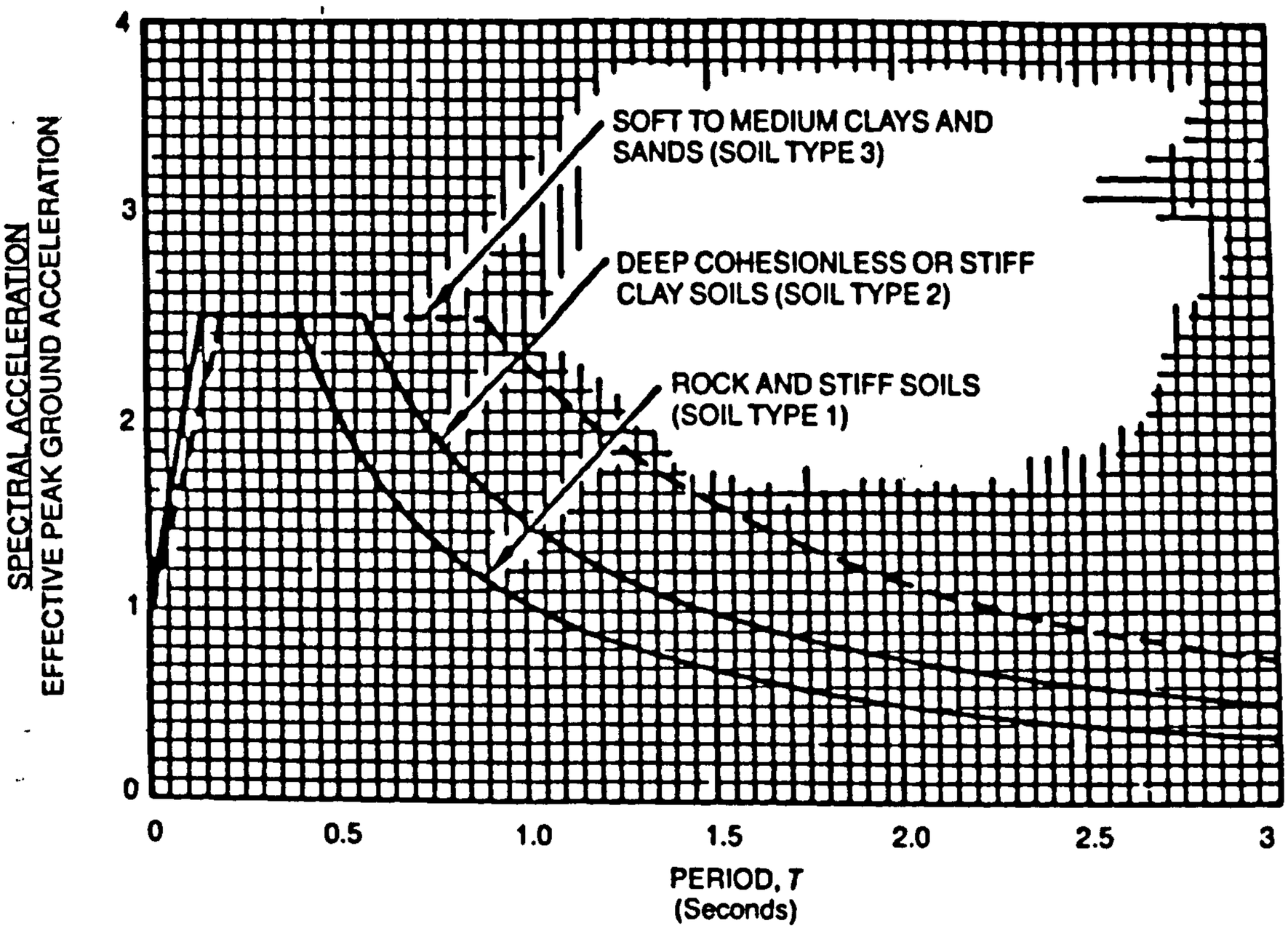


Fig. 4.1 Normalized Response Spectral Shapes, UBC-91

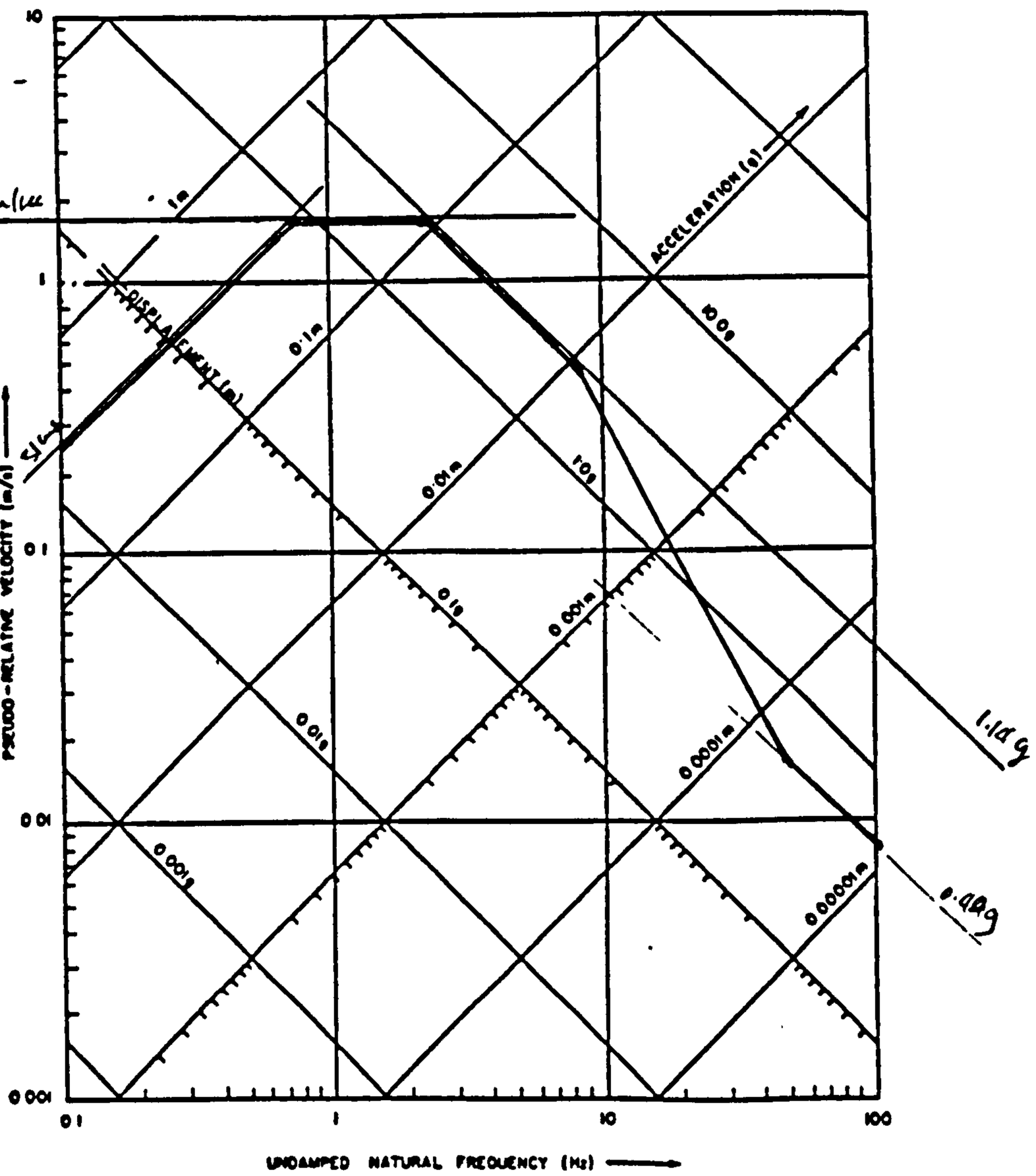


Fig. 4.2. Response Spectra from Newmark and Hall

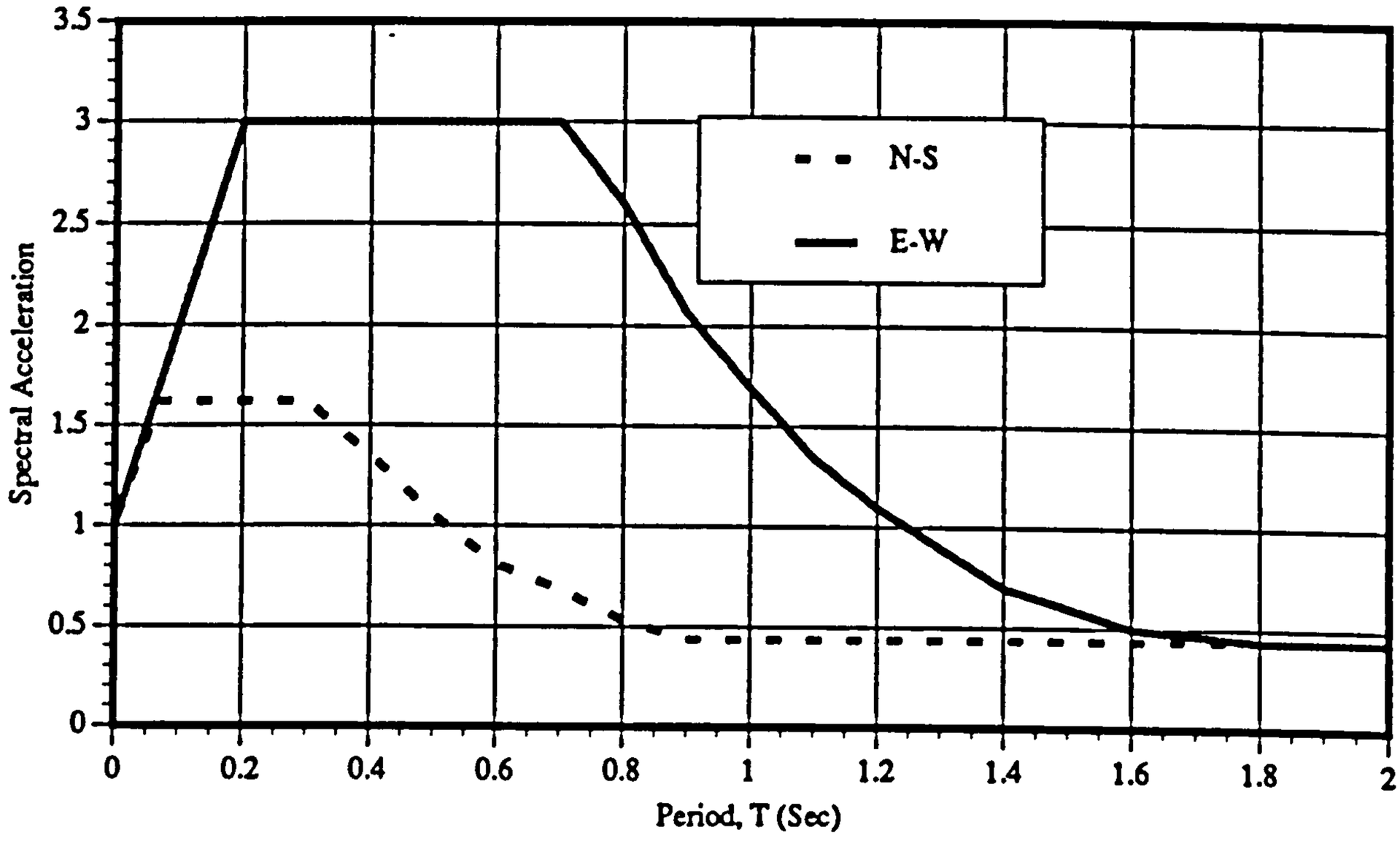


Fig. 4.3. Spectral Shapes from Erzincan 1992 Earthquake

CHAPTER 5

5. REPAIR AND SEISMIC UPGRADING OF A TYPICAL STRUCTURE

In order to investigate the effect of the previously-described selective repair techniques, a typical reinforced concrete framed structure representative of the building stock in Erzincan was studied under seismic loading conditions. After a brief description of the structural system, the observed structural damage is briefly discussed and inspection results are given. This is followed by a time history non-linear dynamic analysis. The loading conditions imposed upon the structure can be identified from the accelerograms recorded in the town's Meteorological Station. These records reveal peak ground accelerations of the order of 0.5g and a strong motion duration in excess of 10 seconds. The meteorological station lies at ten kilometres from the construction site and hence the importance of such analysis is emphasised.

Use was made of some of the previously developed repair and upgrading techniques. The upgraded building response is compared with the building repaired with one of the conventional methods adopted in similar buildings.

5.1. Structural system and Description of State of Damage

The structural system consists of reinforced concrete frames in both longitudinal (20.00 m) and short (10.00 m) directions, measured in the E-W and N-S respectively, as shown in Fig. 5.1. The short direction frames showed poor frame continuity, only the exterior frames were aligned.

The concrete cores taken from columns and beams at various levels showed a characteristic concrete strength of about 15 MPa. The tested steel samples taken from top storey columns gave a yield strength of 300 MPa associated with a ductility of 12. At the time of the earthquake, the building had a basement and four storeys complete with infill partitions. However, exterior walls for the basement had not been built, and hence a soft storey existed.

The building was designed to the Turkish code of 1975. Modern reinforced concrete design and detailing schemes were not observed either in the design drawings or in the reinforcement details of the damaged members. Floor beams were reinforced with straight and bent bars. This ensured a reasonable reinforcement ratio at the upper

fibre (negative moment critical sections) and much lower ratios at the bottom fibre of the continuous beams. Such an arrangement of reinforcement allowed for very poor frame action and wide cracks were observed at various beam-column connections. This was confirmed analytically as will be described hereafter. Details of the reinforcement of main sections are shown in Figs 5.10. and 5.11.

5.1.1. Structural damage

i. Basement Level: Failure of two columns due to shear; concrete cracking in three other columns. Beam hinging associated with cracking at the beam-column connections at various locations. It was observed that beam cracks were wider at the soffit of the beams; the crack width was reduced along the beam depth. The distribution of column damage is shown in Fig. 5.1. Cracks were also observed in the grade beams at the mid-spans and at footing edges. No damage to the isolated footings was observed. Foundation design is presented in Fig. 5.2.

ii. Ground Level: Beam hinging was observed at various locations. This was characterised by wide vertical cracks at the face of columns. Some flexural cracks at the mid-spans of beams were also recorded. The observed cracks were as wide as 2 mm. Severe non-structural damage was also observed in brick walls.

iii. First, Second and Third Floors: Only non-structural damage was observed at these levels. This reduced farther up the height of the building.

Details of inspection results are given in appendix AIII.

5.1.2. Design and construction defects

After inspecting the damaged structure and the structural design drawings, the following weaknesses in the system are noteworthy:

i. Inadequate strength in both directions, since the earthquake-induced forces were much higher than the building strength, and hence structural failure would have been expected. This can be observed from the shear and flexure demand on the columns as depicted from Table 5.1. Also the steel strain/time plots show plastification of various joints. A sample of these curves is given in Fig. 5.18.

ii. Stiffness and strength irregularities due to the soft storey created at the basement level. No partitions were built and no special provision to regularise the strength and stiffness was provided.

iii. Low level of structural redundancy. This would lead to poor framing action while resisting earthquake loads. Accordingly, the structure had a low behaviour factor. The observed non-alignment in the structural system would also lead to torsional effects on some columns.

iv. The concept of weak beam-strong column was not adopted, some beams were much stiffer than the connected columns, leading to shear failure in columns.

v. Poor reinforcement detailing for columns, beams and beam-column connections associated with a poor level of construction.

vi. The use of smooth bars throughout the building. This led to local bond failures and gave rise to reduced strength and stiffness.

vii. It was observed that columns were designed only for flexure and axial force. No special shear reinforcement was provided in any of the damaged columns. Shear reinforcement in columns was restricted to the absolute minimum. There was no concentration of ties at the column extremities and ties were not observed at the beam-column connections. Accordingly, failure of columns was observed at these locations.

viii. Splicing of the main column reinforcement at the floor level. According to modern seismic codes and for such a highly seismic area, steel splicing should take place at the mid-storey height to avoid stress concentration at the potential critical sections.

ix. The relatively high flexibility of the structure initiated severe secondary order effects. This led to higher strength demand and local failure in some columns.

5.1.3. Failure mode

The building was subjected to a peak ground acceleration of 0.5g in the longitudinal (E-W) direction and 0.4g in the short (N-S) direction. The shear and flexural strength supply were much lower than the demand as depicted from Table 5.1. The vertical load carrying capacity was severely hindered due to column failures; even though, the

building did not collapse. The load was transferred from the damaged columns to the nearest intact ones. Structural damage was concentrated along the longitudinal axis B , shown in Fig. 5.1, which possessed a higher stiffness than the three other frames together.

In order to design a repair and upgrading scheme that would lead to improved response in future earthquakes, a non-linear dynamic analysis was performed on the existing building before and after repair. The frame along axis B was chosen as a representative planar structure because of the observed concentration of damage and relatively high stiffness. The applied input motion was the Erzincan 13 March 1992 E-W component of a duration of 21 seconds and PGA of 0.5g.

The response parameters used to characterise the seismic behaviour of the frames are the followings:

- Inter-storey drift.
- Plastic hinge formation and distribution.
- Rotation of critical sections.

These response parameters are considered adequate, though not comprehensive, for the progress of this analysis.

5.2. Repair and Upgrading Solutions

In order to reinstate the original strength and stiffness of the building, two approaches may be followed:

i. Conventional approach.
ii. Selective intervention approach.

The conventional approach calls for epoxy injection of the cracks for stiffness reinstatement and concrete jacketing of the damaged columns for strength reinstatement. This approach was observed to be adopted in various repaired buildings in Erzincan. The column jackets were 200 mm thick and were reinforced with 2% steel reinforcement ratio, along with a high percentage of steel ties to insure good confinement and hence high ductility.

The selective approach consists of stiffness reinstatement mainly using steel plates attached to the cracked elements, shear strengthening of columns to avoid the

observed shear failures and flexural strength enhancement using additional reinforcement along with Interaction-Delay-Mechanism. The philosophy of these new repair schemes have been comprehensively described in section 6.2.1. of Part I of this thesis. In the following, a brief description of the selective repair methods relative to each state of damage is given.

5.2.1. Case of total column rupture

For the totally disintegrated columns, there is a need for strength reinstatement. This can be achieved by the addition of a partial steel collar 20 mm thick around the damaged area according to the following steps:

- Prop-up the area of the damaged column and the surrounding columns at least for the lower two storeys .
- Remove the cracked concrete cover around the core of each damaged column.
- Surround the damaged area with a steel jacket (20 mm thick). This should have a clearance of 5 mm with the concrete column.
- After sealing the bottom of the steel jacket with an inorganic sealer and piercing it with an aluminium tube through it, place round coarse aggregate into the clearance between the tube and concrete core. The maximum size of the coarse aggregate should not exceed 10 mm in diameter, as shown in Fig. 5.5.
- Seal the top of the steel jacket after burying the aluminium exhaust pipes.
- Inject an epoxy-based polymer cement under pressure from the bottom pipe.
- Allow for curing of the polymer cement (about two weeks) and cut off the top and bottom sealers.

This scheme has already been tested under vertical and cyclic loading and proved extremely efficient in converting the brittle failure mode into a ductile one (Yoshimura et al, 1992). Hence, a strength-only reinstatement was achieved without the increase of stiffness, as would have been the case if column jacketing was employed.

5.2.2. Case of cracked columns

The observed column cracks were mainly due to shear overstressing. This would cause shear strength and stiffness reduction. Use is made of horizontal steel plates attached to the cracked elements by means of high strength epoxy mortar. These proved effective in reinstating shear stiffness (SWR21-SWR24). The enhancement of the shear strength

would also lead to the attainment of the full flexural capacity, hence a ductile failure mode is brought into the picture.

5.2.3. Seismic upgrading scheme

In order to upgrade the seismic resistance of the structure, both shear and flexural strength should be increased. Shear strength upgrading, for the required elements only, can be achieved by adding horizontal steel plates as described in section 6.2.2 of Part I. Plates 100x5 mm spaced by 30 mm were implemented from both sides of columns.

Care should be taken, when the flexural strength is targeted, not to violate the stiffness regularity so as not to penalise other members, as described in section 6.5. This can be achieved by the addition of new reinforcing bars, along with an interaction delay mechanism, as previously described in section 6.2.1. of part I. The flexural strengthening scheme was based on the addition of 6 bars of 32 mm diameter on both edges of columns located at the intersection of axes B with 2 and 5. These were applied to the lower two storeys only where high strength demands were anticipated. They were attached to the structure at the foundation and floor levels only. Mechanical connectors were applied at the mid storey heights to ensure an 'Interaction Delay Mechanism', with a design slack of 2 mm. These bars are protected by means of concrete encasement, fully separated from the original concrete with foam material.

Alternatively, the same objectives can be achieved using high yield and low elastic modulus material [hbg AKZO or equivalent]. This has a yield value of 1200 MPa at a third of the E value of steel. This material is already in use as prestressing strands for special structures.

5.3. Modelling of Upgrading Schemes

5.3.1. The analysis software system ADAPTIC and structural models

ADAPTIC is an advanced frame package developed at Imperial College (Izzuddin and Elnashai, 1989), based on concepts of adaptive mesh refinement, automatic solution strategy and automatic time-step and load-step adjustment. The program is suited to plane and space frame analysis under static proportional/non-proportional loading as well as dynamic loading, including independent support motion. The program has been extensively verified by comparison to commercially-available packages. It was demonstrated that ADAPTIC combines economy and accuracy, but more significantly

robustness. This latter features renders the program especially suited to collapse analysis where the point of genuine structural failure is essential for the use of the results.

For the purpose of the current investigation, use was made of the cubic plastic element with distributed plasticity (section analysis). This was used in conjunction with the uniaxial constant confinement concrete model. Moreover, the section is divided into unconfined, partially confined and fully confined areas, depending on the geometry of section and confinement hoops.

The cubic element assumes a cubic shape function in the chord system, and monitors stresses and strains at various points across two Gaussian sections, allowing the spread of plasticity throughout the cross-section. Each element is defined by two nodes, and the cross-section is divided into a number of monitoring points. The stresses are calculated at each monitoring point and for the two Gaussian sections. The basic characteristic of the element is that it predicts member behaviour based on material stress-strain relationships and large displacements. The accuracy increases by using more elements in the plastic zones of the member and/or by increasing the number of monitoring points in the cross-section.

A bilinear kinematic hardening steel plasticity model was utilised for the reinforcing bars. This was shown to compare well with more elaborate constitutive characterisations, such as the multi-surface plasticity model (Elnashai and Izzuddin, 1993) for global analysis purposes. Explicit description of rectangular and flanged sections was used, so as to account for the varying stiffness and strength of the beam section when subjected to alternating moments.

Comprehensive dynamic analysis capabilities are also implemented in ADAPTIC. Separate non-structural elements are used to calculate inertia and damping forces. Direct integration using the unconditionally-stable Newmark method is used, with automatic time-step adjustment. The forcing functions may be load or displacement time histories. Independent support motion is also possible, using displacements, velocities or accelerations. The solution procedure used is iterative and can be full or modified Newton-Raphson or a combination of both. Automatic switching from one strategy to the other is also included.

In dynamic analysis, the choice of time step for integration is of significance; ADAPTIC employs an automatic procedure for the choice and updating of the integration time-step to achieve optimum accuracy and efficiency.

5.3.2. Structural modelling

The frame under consideration was divided into a number of elements such that all potentially-critical sections were accurately represented. This resulted in about 240 elements, as shown in Figs 5.8, 5.9, 5.10 and 5.11. The analysis was run on a DEC 5000/240 workstation with a mips rating of 42.9.

The proposed model is intended to represent the basic phenomenon of delayed interaction from the added steel reinforcement through a reliable and sufficiently accurate approach. This was implemented within the nonlinear analysis program ADAPTIC. The computer modelling of the building was based on two important aspects, namely:

i. The model should represent the actual structural behaviour as closely as possible.
ii. The number of joints and members should be minimised to improve the efficiency of the analysis in order to reduce the CPU time, without sacrificing accuracy.

To this end the computer models were developed, as presented in the following sub-sections.

5.3.2.1. Strength-only intervention

i. The main concrete element, either shear wall or column, was idealised using either the rectangular concrete column section, or the flexural wall section.

ii. The uniaxial constant confinement concrete model was employed; along with multisurface cyclic plasticity model, for steel reinforcement.

iii. Steel required for flexural strength increase was added to the original sections. This was fixed to a fictitious foundation beam and to the top of the strengthened element through a stiff horizontal member, as depicted in Fig. 5.6.

iv. To allow for the structural gap between the initial and full-interaction stages, use was made of the trilinear asymmetric elasto-plastic joint element. A one-sided loading curve (tension only) was specified. This was intended to allow the designed structural gap to be modelled. Hence, a strength increase without affecting the stiffness was achieved analytically.

v. The model was used to predict the analytical response of the tested shear wall SW31. The model was designed for 85 kN but was supplied with a strength of 60 kN only at the first instance. The analytical model showed good agreement with the tested behaviour of SW31 and SW33 (enhanced and reference models, respectively). Fig. 5.6 shows the analytical response compared with the tested response shown in Fig. AI (31).1.

vi. From the above results, it is concluded that it is possible to model the previously-developed strength-only intervention analytically. This has the advantage of increasing the member strength without affecting its elastic dynamic characteristics.

5.3.2.1. Stiffness-only intervention

As observed experimentally and confirmed by strain gauge readings, the steel plates attached to a cracked concrete element were only activated near the cracks. To achieve a realistic model for such behaviour, the steel plates were not connected to the foundation beam, but were connected to the wall through top and bottom horizontal stiff beams as depicted in Fig. 5.7. The envisaged model was tested by comparison to walls SW9 and SWR9. The analytical response was observed to be in good agreement with the test results shown in Fig. AI (R9).1.

5.4. Behaviour During the 13 March Earthquake

For the above mensioned typical structure described in section 5.1 of Part II, concentrated (lumped) mass elements were employed at the beam-column connections. The eigenvalue analysis performed with ADAPTIC for the frame on axis B yielded an estimate of the natural frequency of vibration for the structure corresponding to a period of 0.32 seconds. This value indicated that the structure possessed a relatively high stiffness. A period of 0.4 to 0.5 seconds would have been expected for a typical five storey structure. However in the short direction, the building exhibited significantly lower stiffness and hence a longer period of 0.55 seconds.

Acceleration response spectra derived from the acceleration records and shown in Figs. 2.4 and 2.5 indicate that horizontal acceleration response as high as 1.5g in the East-West direction and 0.8g in the North-South direction were experienced for structures with damping levels of 5% of critical. These spectra also reveal the long-period nature of the ground motion, with highest response in the E-W direction being

experienced by structures of period 0.3-0.7 seconds. The magnitude of response in the N-S direction is almost as great for structures of natural periods as high as 2 seconds as it is for those of 0.5 seconds. This explains why major structural damage was observed in the longitudinal direction of the building, while much less damage was observed in the short direction.

The nonlinear time-history dynamic analysis performed on the five bay, five storey frame on axis B showed that substantial energy dissipation through inelastic deformations in the nonlinear range was exhibited by the frame elements at various beam and column sections. The formation of plastic hinges was characterised by steel yielding at both extreme fibres. An example of the steel strain plots versus time is given in Fig. 5.18.

Due to the poor reinforcement ratio and detailing at the beam-column connections, it was found that for most beams between axes 1-3 and 4-6, top and bottom steel yielded. Hence, beam hinging is attributed mainly to low reinforcement ratios (less than the minimum specified by the codes) rather than good seismic design (weak-beam strong column) and proper detailing.

The dynamic analysis of the intact frame showed that inelastic deformations reduce with the increase in height above the base. However, the frame was sufficiently stressed to cause plastic hinges right up to the top of the frame. These analytical findings were confirmed by field observations whereby cracks as wide as 3 mm were observed at the first level, while only micro-cracks (0.3 mm) were observed at the top level.

Column hinging took place at the connection between the foundations and columns at sections 1, 22, 85, 106. This was confirmed by field observations where horizontal micro-cracks associated with spalling of the unconfined concrete were recorded. Shear in columns was plotted versus axial force. It was found that the seismic shear strength demand was in excess of the supplied shear strength, especially at minimum axial load instances (in some exceptional cases, columns were subjected to axial tension). This led to shear failure in two columns. Also, shear cracking was observed in four other columns, as depicted in Fig. 5.1. The plastic hinge formations are shown in Fig. 5.12.

Interstorey drifts were as high as 44 mm (H/68) at the basement level, reducing to 12 mm at the top storey. The big difference between these two values prooves that the structural system was not effective. Also, these values were in excess of those specified by most seismic codes. It is emphasised that the frame was originally very stiff, as concluded from the short period obtained from the eigenvalue analysis mentioned

previously. From the above, it may be concluded that to satisfy the code-defined drift limit for such a highly seismic area, shear walls should have been supplied to reduce the drift.

5.5. Seismic Response for Conventionally Repaired Structure

To predict the dynamic response of repaired structures in case of a future seismic event, the damaged columns at the basement were rehabilitated with a 20 cm concrete jacket. Since cracks are normally epoxy injected, a 20% reduction in stiffness was assigned to the repaired structure to account for the non-injectable micro-cracks. A higher concrete quality was assigned to the concrete designed for the jacket (30 MPa). This repair scheme was extensively used for the repair of various damaged structures, including the military hospital of Erzincan after the 1983, M_S=5.4 earthquake.

The eigenvalue analysis performed with ADAPTIC for the frame on axis B, yielded the natural frequency of vibration for the structure giving a period of 0.29 seconds. This reflects the effect of strengthening on the shortening of the structural period. Hence, an increase in the seismic induced forces should be anticipated.

The dynamic analysis showed no failure or yielding in the repaired level. Also, the strength demand on floor beams was reduced when compared with the intact frame response. However, the strength demand on the level just above the repaired one was nearly doubled for the columns on axes 2, 5, 1 and 6 especially for the first floor columns as briefed in Table 5.1. This led to plastic hinge formations at sections 5, 9, 26 and 31 as depicted in Fig.5.12. Also, large displacement and curvature ductility demands were imposed on this particular level. Curvature ductility demands in excess of 15 were recorded for the above critical sections. These high strength and ductility demands could not be sustained by the existing structure and a total failure of the structure would be expected.

This analytical observation was confirmed by the failure of the military hospital in Erzincan (eight storey building) during the 1992 earthquake. The building was repaired after the 1983 earthquake with column jacketing to the basement level and the cracks were epoxy injected. The collapse of this hospital caused many casualties.

The maximum building drift was 120 mm as opposed to 135 mm for the intact structure. While the interstorey drifts were reduced for the repaired level, they were increased for the other four storeys, as shown in Table 5.1.

Due to severe irregularity of strength and stiffness, plastic hinges in beams were not spread throughout the frame height. Hence, energy dissipation was concentrated in a limited number of plastic hinges imposing high ductility demands and leading to a probable structural failure. The plastic hinge formations for both intact and repaired structures are shown in Figs 5.12 and 5.13.

5.6. Seismic Response for Selectively Repaired structure

To improve the dynamic response of the structure, use was made of the selective repair techniques developed in Part I of this thesis. Stiffness reinstatement was achieved by means of steel plates. Shear strength enhancement for the damaged columns was achieved by means of steel collars added to the columns at the top. Increase of flexural strength was achieved by the provision of steel bars along with the interaction delay mechanism. The plastic hinge formation pattern is judged to be more effective than both the intact and conventionally repaired frames. This is confirmed from Fig.5.14.

Computer modelling of the above scheme was discussed in section 5.2. The eigenvalue analysis yielded results similar to the original frame. The dynamic analysis showed lower total drifts. The interstorey drift became more regular and the plastic hinge formation became less intense especially for columns. Strains in steel members were also reduced and the collapse mechanism observed previously was totally avoided.

The added steel members were activated at about three seconds from the start of shaking. They acted in tension only, thus reducing strength demand on other members of the frame. A comparison of seismic response parameters for the intact, conventionally-repaired and selectively-repaired frames is given in table 5.1.

The table confirms the potential benefit of selective repair/retrofitting techniques in tuning the response of RC frames to seismic excitations. The columns showing the percentage increase/decrease in response parameters for conventional and selective interventions confirm that the latter is comprehensively superior to the former.

5.7. Concluding Remarks

Conventional repair methods are difficult to control in so far as the level of reinstatement or enhancement of stiffness, strength and ductility is concerned. On the other hand, selective techniques are, philosophically, in harmony with capacity design

principles and provide tools for the development, in parallel, of a capacity redesign philosophy.

From the analytical results, it is clear that the structure selectively repaired had better seismic response than the conventionally repaired one. Moreover, the latter may experience a total collapse with a future seismic event. A brief commentary on these results is given hereafter:

– Inter storey drift was totally disturbed by the column jacketing: it was reduced from 43.8 mm to 6.8 mm at the first level column and was increased for all the unprepared floor with percentages varying from 4% at the second level up to 52% at the third level. Whist for selectively repaired frame, inter storey drift was uniformly reduced.

– Plastic hinges at the foundation level were avoided in both repair cases.

– The seismic induced forces (base shear) was increased in case of jacketed columns by 21%. An increase of only 4% was observed in case of the selectively repaired frame.

– Strength and curvature ductility demands at second level columns were increased due to column jacketing. This would lead to a premature failure at that level in case of a future seismic event. Also, concrete has attained its crushing strain and stress at the same critical sections.

– Plastic hinges in beams was more intense in case of CRF as depicted from Figs. 5.12, 5.13. They were concentrated in a limited number of plastic hinges. This is attributed to poor lower reinforcement ratio and detailing rather than proper seismic design. Selective repair ensured better distribution of plastic hinges spread throughout the repaired frame. No plastic hinges in columns were observed as depicted in Fig. 5.14.

The results shown above, though not comprehensive, indicate clearly the potential benefit of controlled intervention to optimise seismic response. Improvements of 30% in inter-storey drift control, 200% in curvature ductility demand and 60% in strength demand have been achieved via the application of selective repair techniques in lieu of conventional intervention schemes. Also, interstorey drift became more uniform, whist a noticeable reduction was observed at the lower two levels, higher ones were noticed at the higher levels, hence leading to a more uniform strength and ductility demands.

Table 5.1. Comparison of Seismic Response for Intact, Conventionally and Selectively Repaired Frame.

Characteristics	Intact Frame	Convent. Rep. Fr.	Selective Rep. Fr.	Selective Rep./Cov.R
(a) Period (Sec)	0.329	0.283	0.325	1.148
(b) Total Drift (mm)	135	125	120	0.96
Inter- Storey Drift level 1.	43.8	6.8	22	3.235
Inter- Storey Drift level 2.	39.6	41.2	32	0.777
Inter- Storey Drift level 3.	27	39.4	33	0.837
Inter- Storey Drift level 4.	23.7	36.2	31	0.856
Inter- Storey Drift level 5.	15.8	23.6	29	1.228
(c) Strength Demand (kNm)				
Element 1	4.4e+2	1.3e+3	3.9e+2	0.3
Element 21	8.5e+2	2.4e+3	7.2e+2	0.3
Element 5	2.6e+2	5.2e+2	1.6e+2	0.3
Element 25	6.4e+2	9.8e+2	4.2e+2	0.428
Element 217	4.7e+2	2.7e+2	2.6e+2	0.962
(d) BaseShear (kN)/Frame	17.6e+2	21.2e+2	18.8e+2	0.886
Element 1	4.8e+2	3.9e+2	1.9e+2	0.487
Element 22	3.7e+2	6.4e+2	7.2e+2	1.125
(e) Steel Strain				
Element 1	0.016	0.0007	0.0013	1.857
Element 4	0.001	0.0003	0.00058	1.933
Element 5	0.0014	0.034	0.0011	0.032
Element 21	0.022	0.0003	0.0012	4
Element 24	0.00048	0.0002	0.0007	3.5
Element 25	0.0021	0.036	0.001	0.027
Element 121	0.0018	0.003	0.0021	0.7
Element 126	0.0013	0.0016	0.0028	1.75
Element 127	0.0015	0.0018	0.0019	1.056
Element 145	0.0023	0.013	0.0026	0.20
Element 169	0.012	0.018	0.022	1.222
Element 175	0.008	0.018	0.014	0.778
Element 193	0.014	0.02	0.031	1.55
Element 198	0.013	0.013	0.028	2.153
Element 217	0.016	0.011	0.036	32.727
Element 222	0.013	0.0012	0.034	28.333

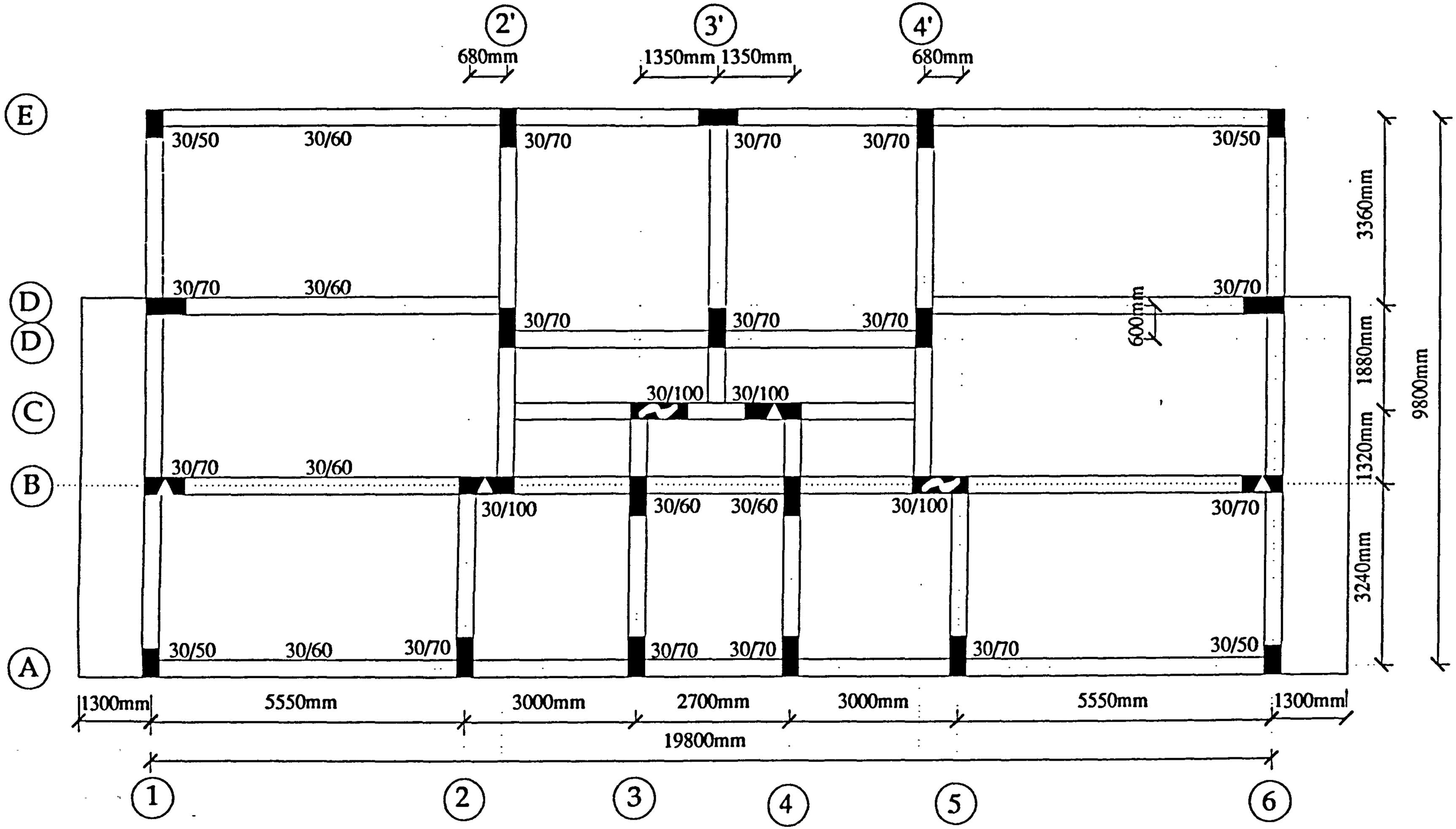
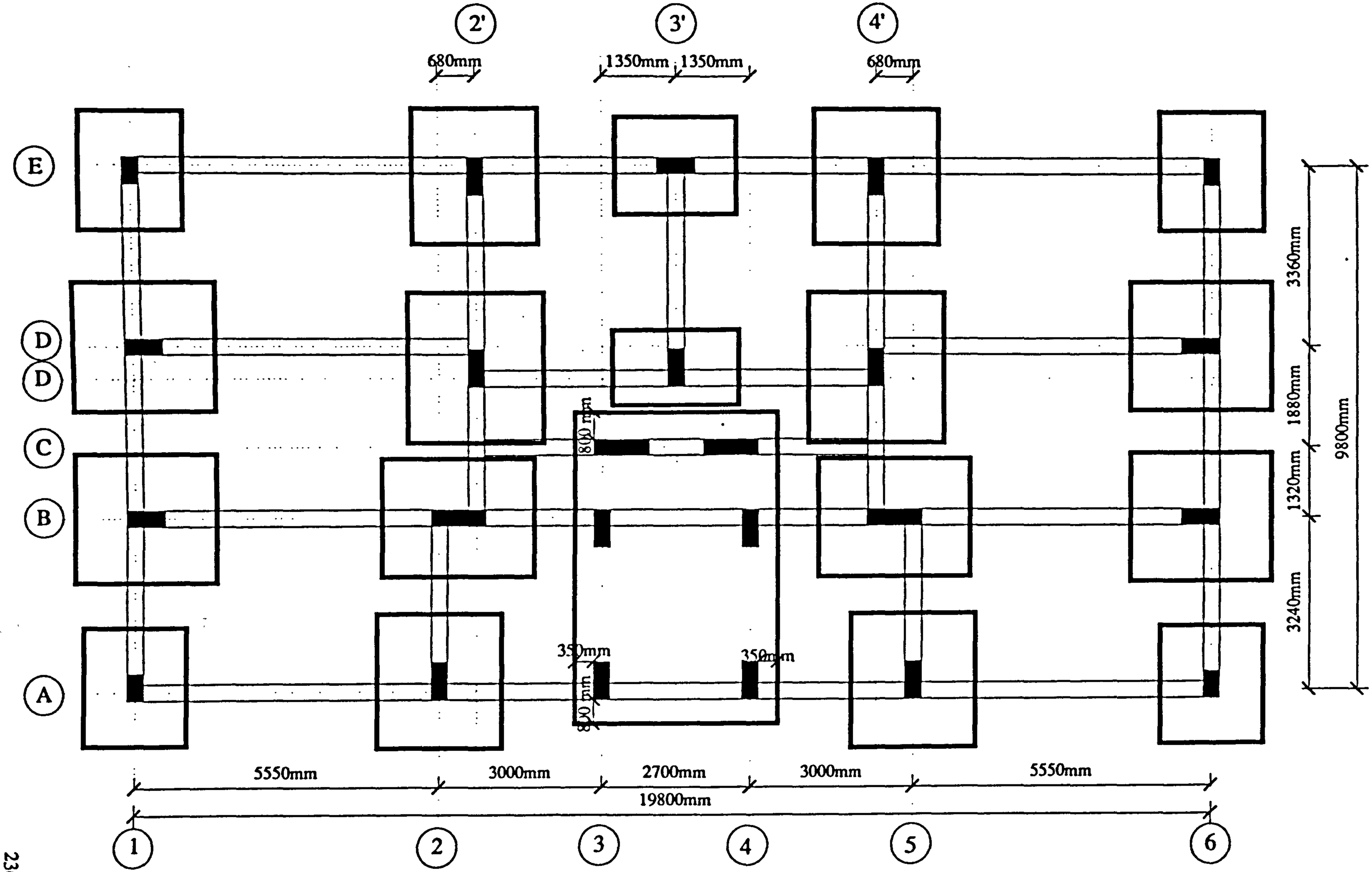


Fig. 5.1. Damage to Columns for Typical Building - Erzincan Turkey



5.2. Foundations for Typical Building - Erzincan Turkey

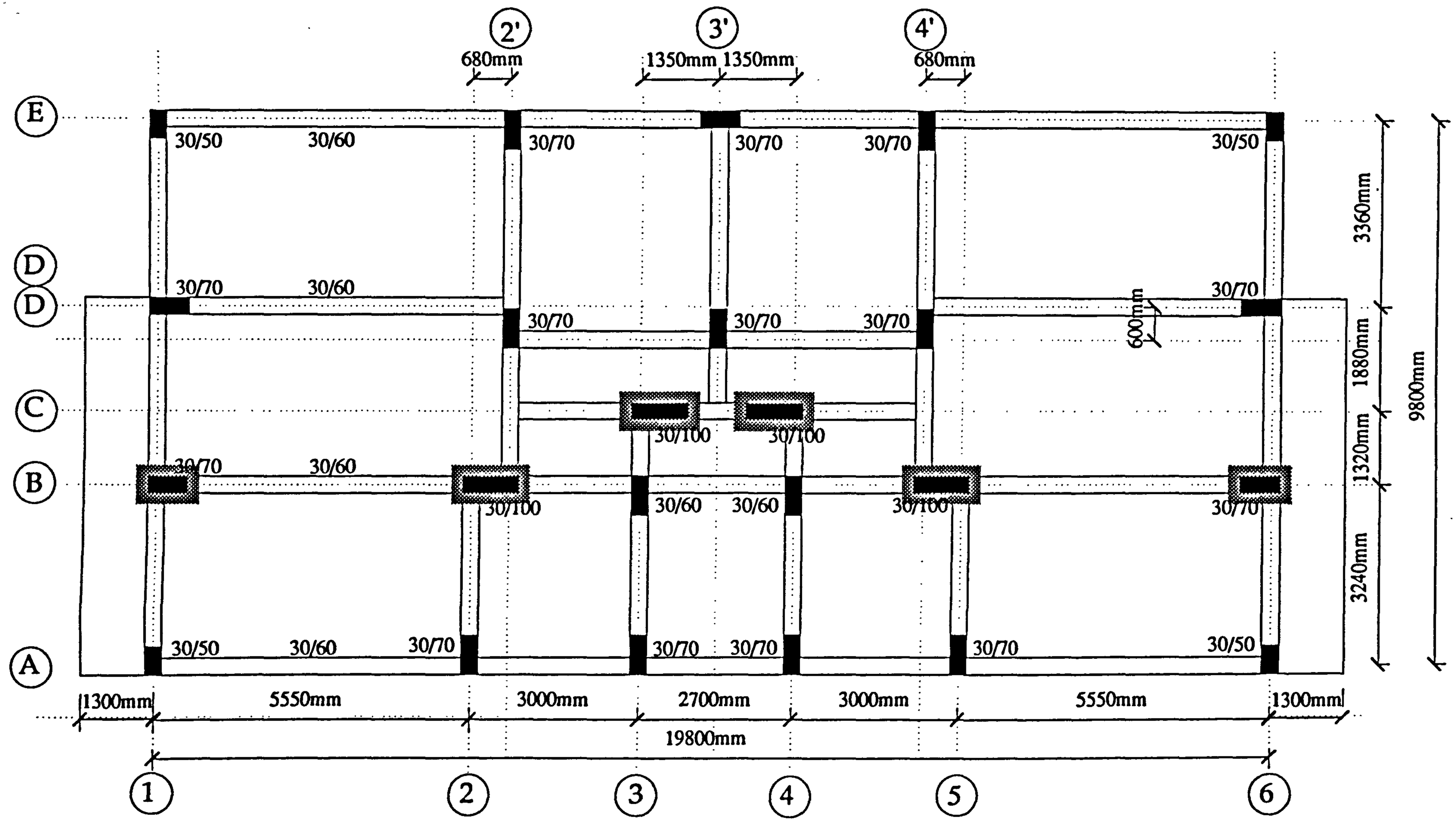


Fig. 5.3. Conventional Repair for Damaged Building - Erzincan Turkey

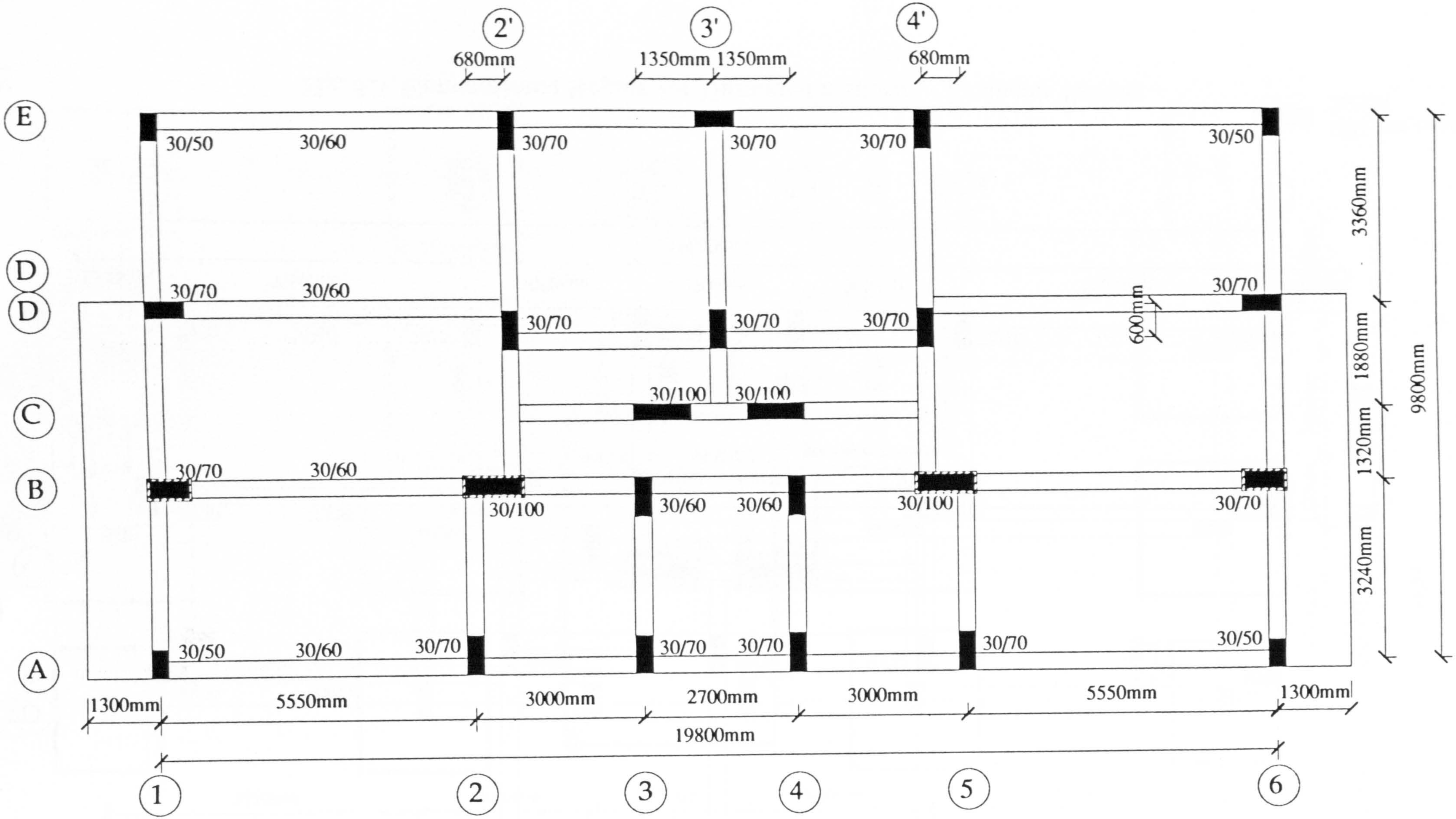


Fig. 5.4. Selective Repair for Damaged Building - Erzincan Turkey

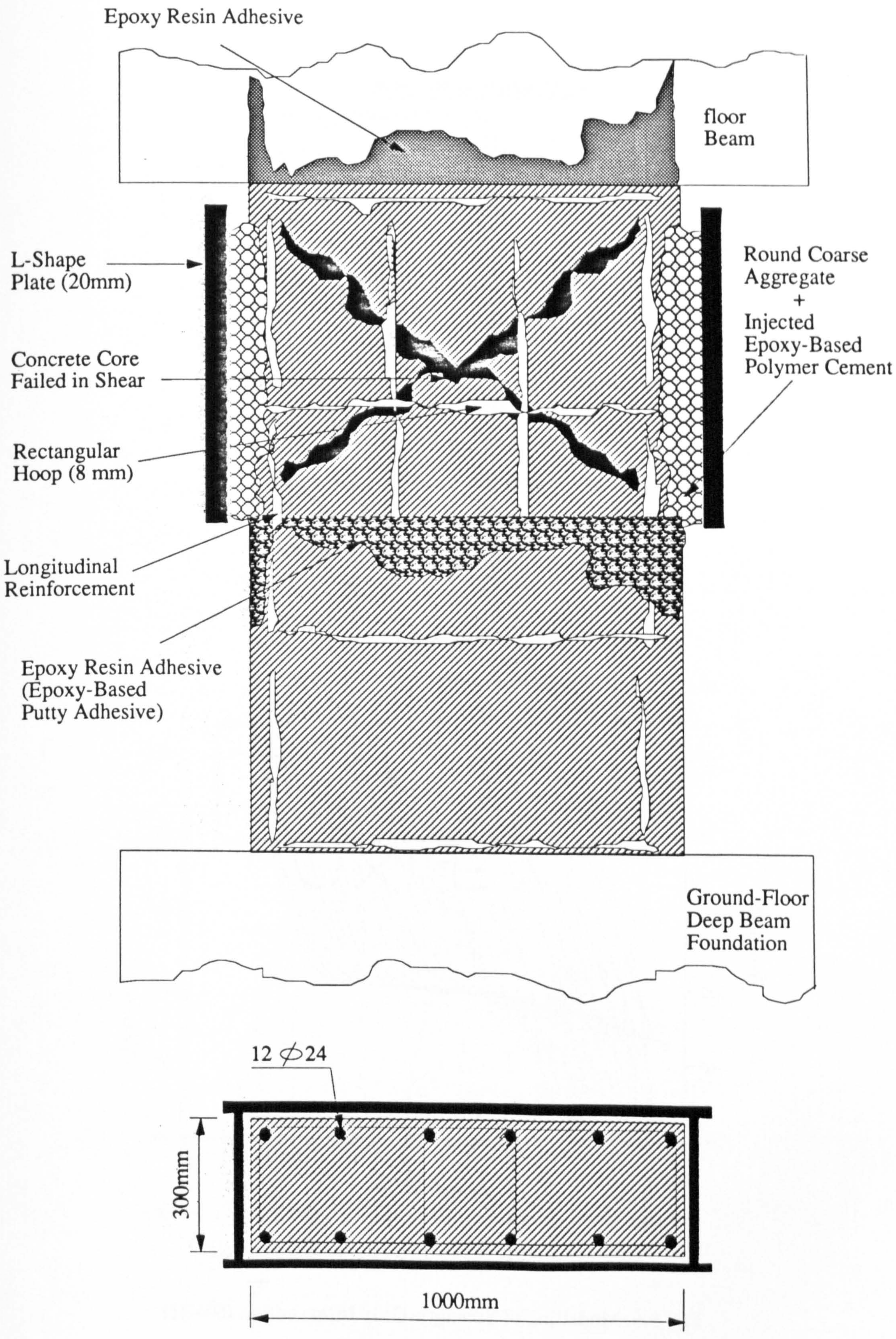
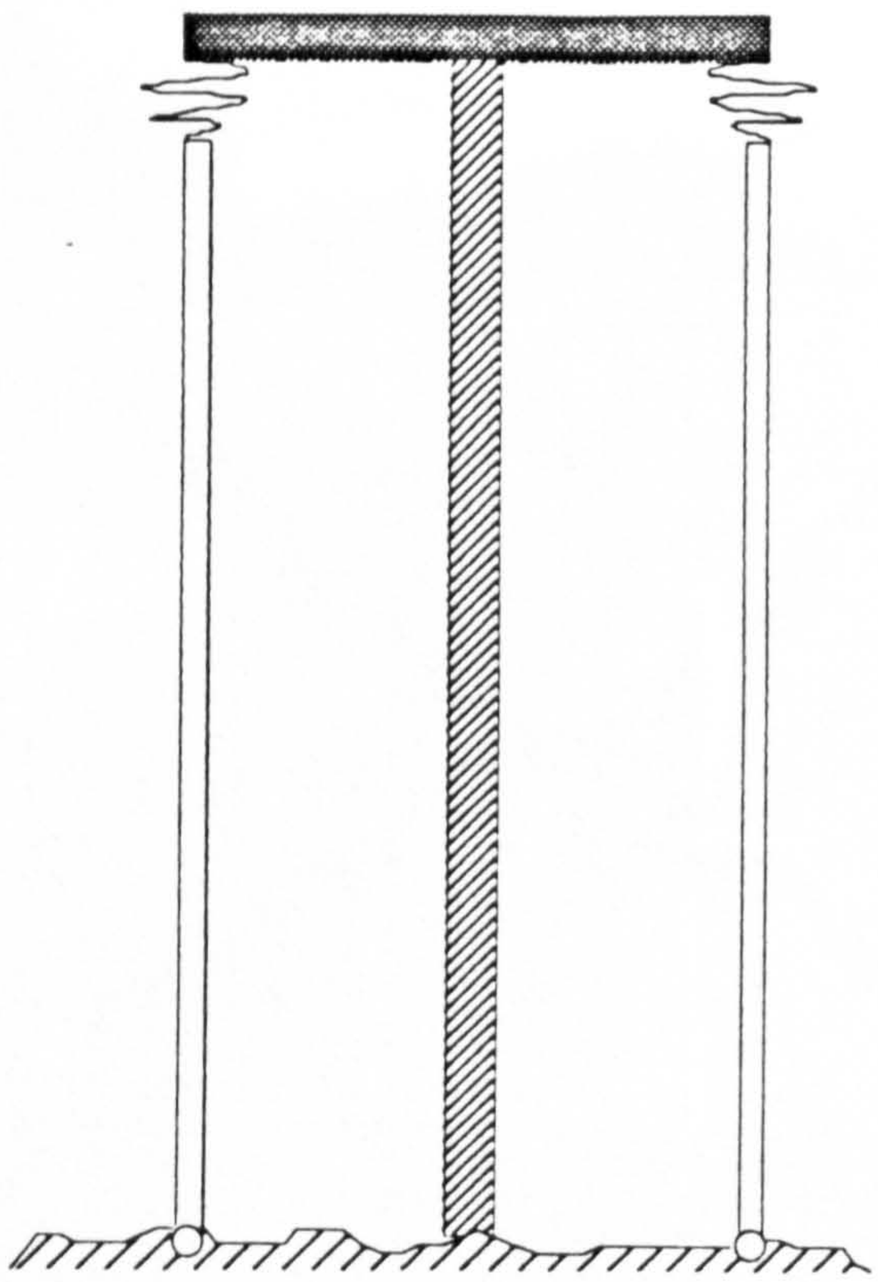


Fig. 5.5. Details for Selective Repair



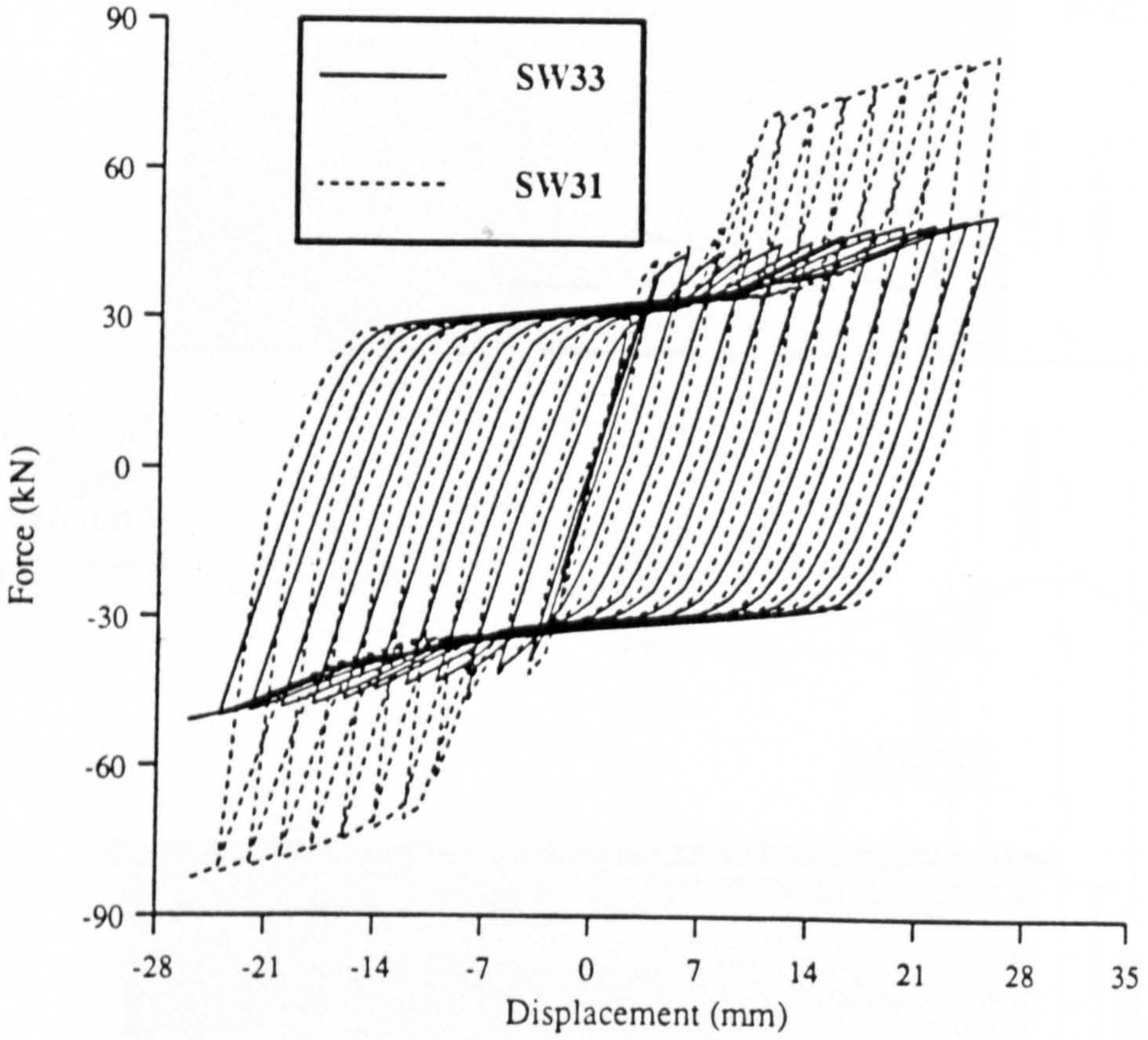
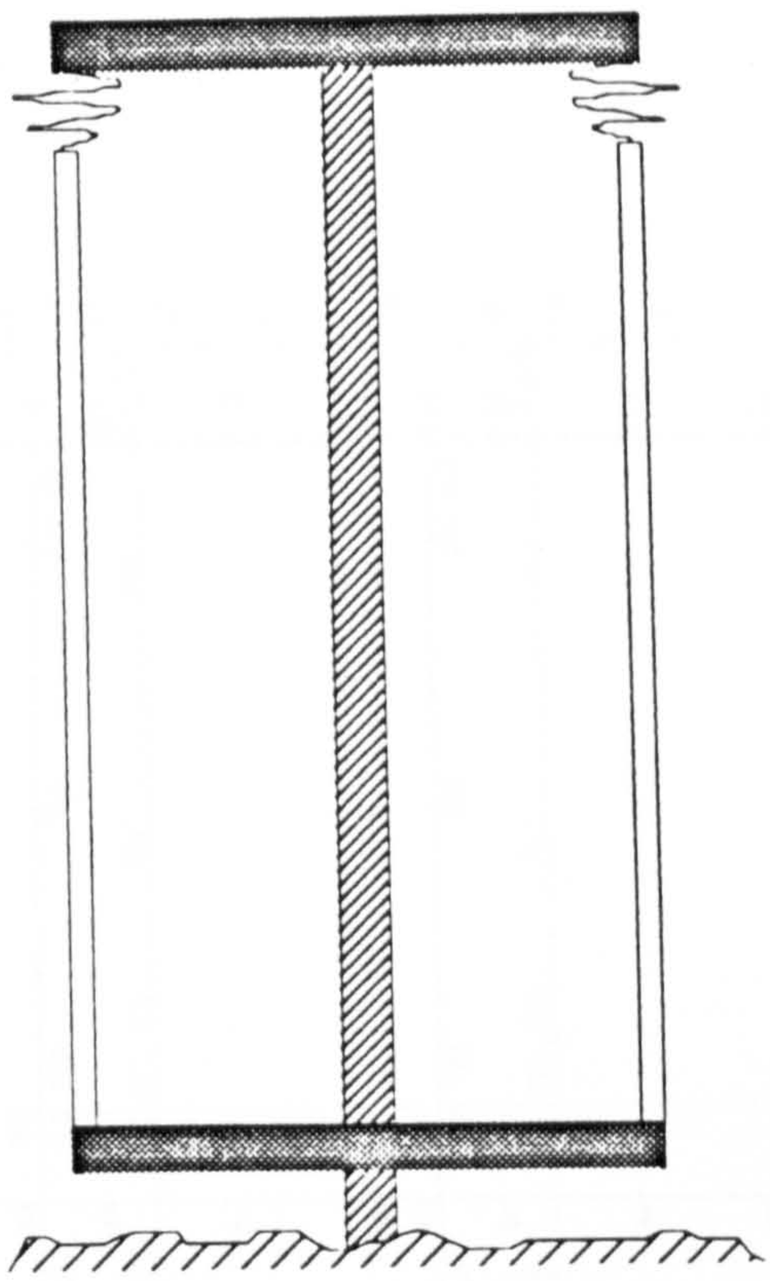


Fig. 5.6. Modelling of Strength-Only Intervention (SW31)



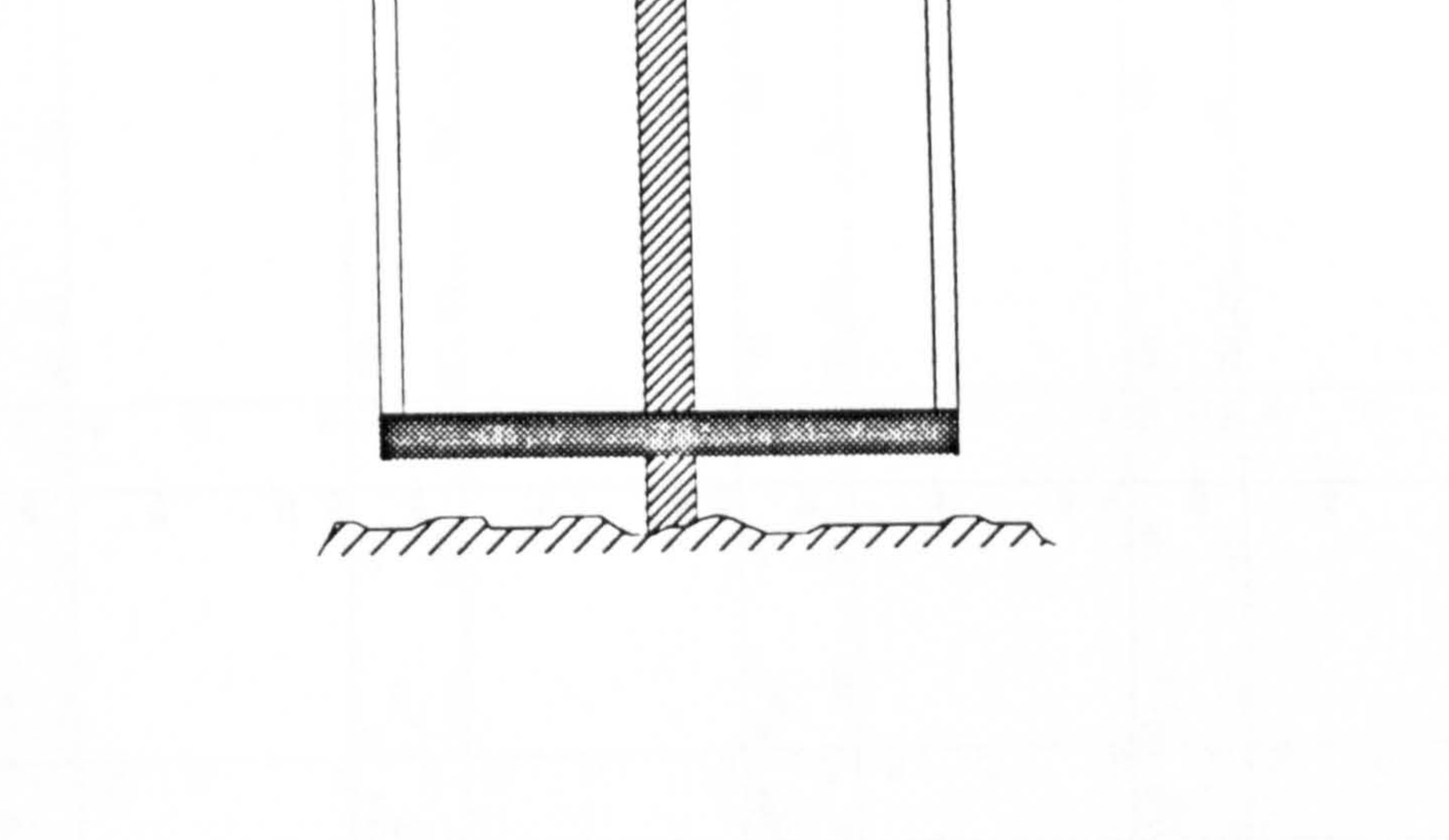


Fig. 5.7. Modelling of Stiffness-Only Intervention (SW9/SWR9)

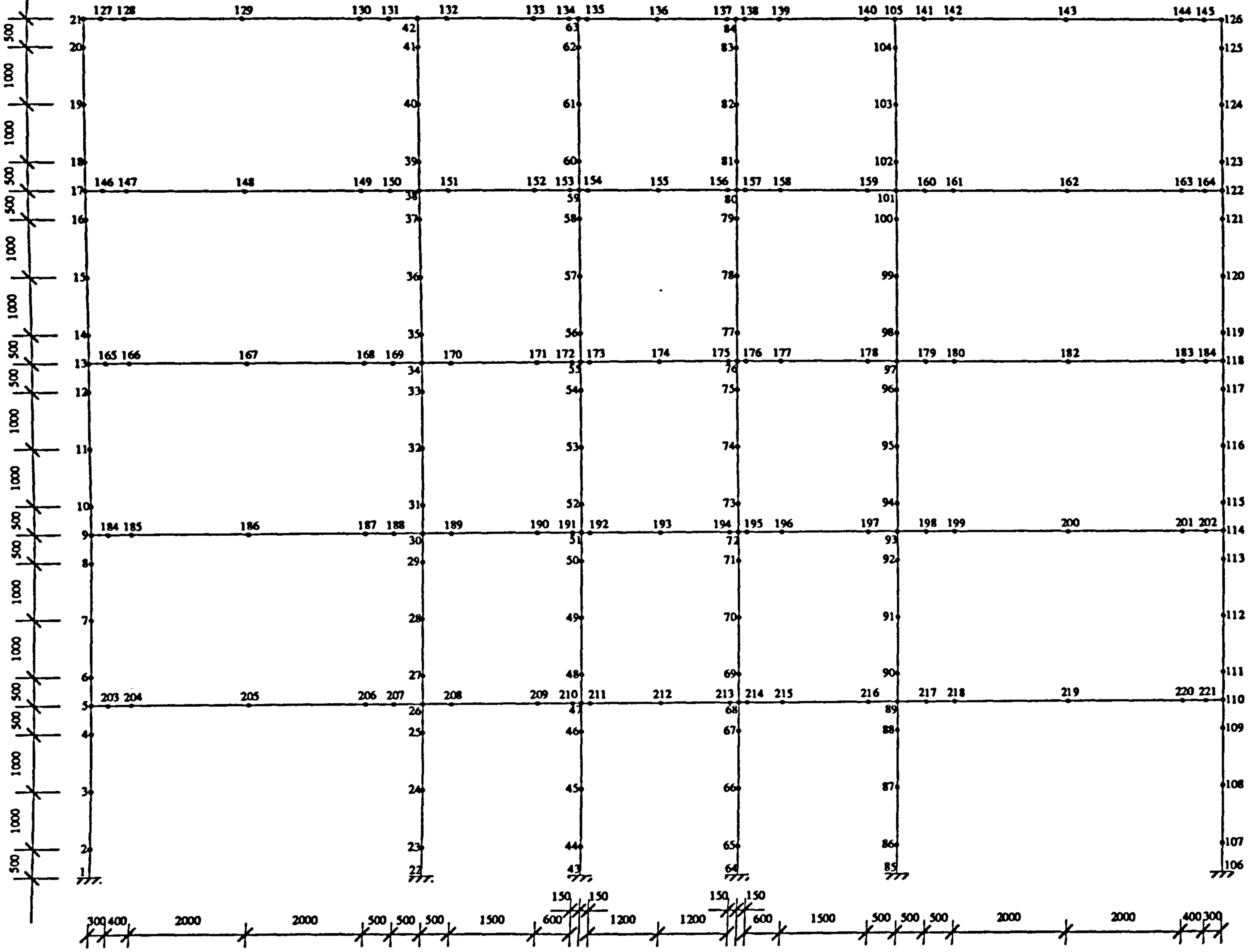


Fig. 5.8. Node Numbering

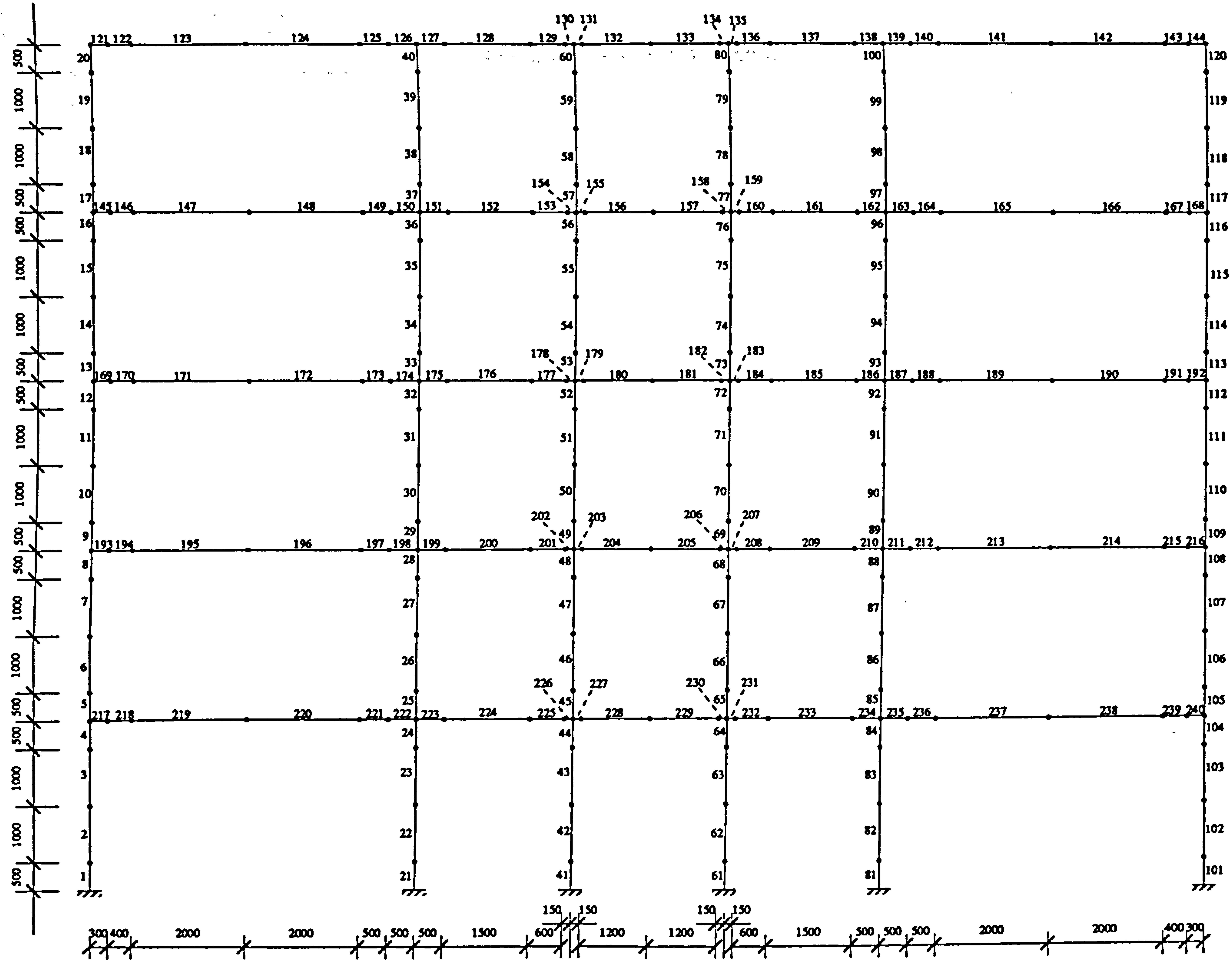


Fig. 5.9. Element Numbering

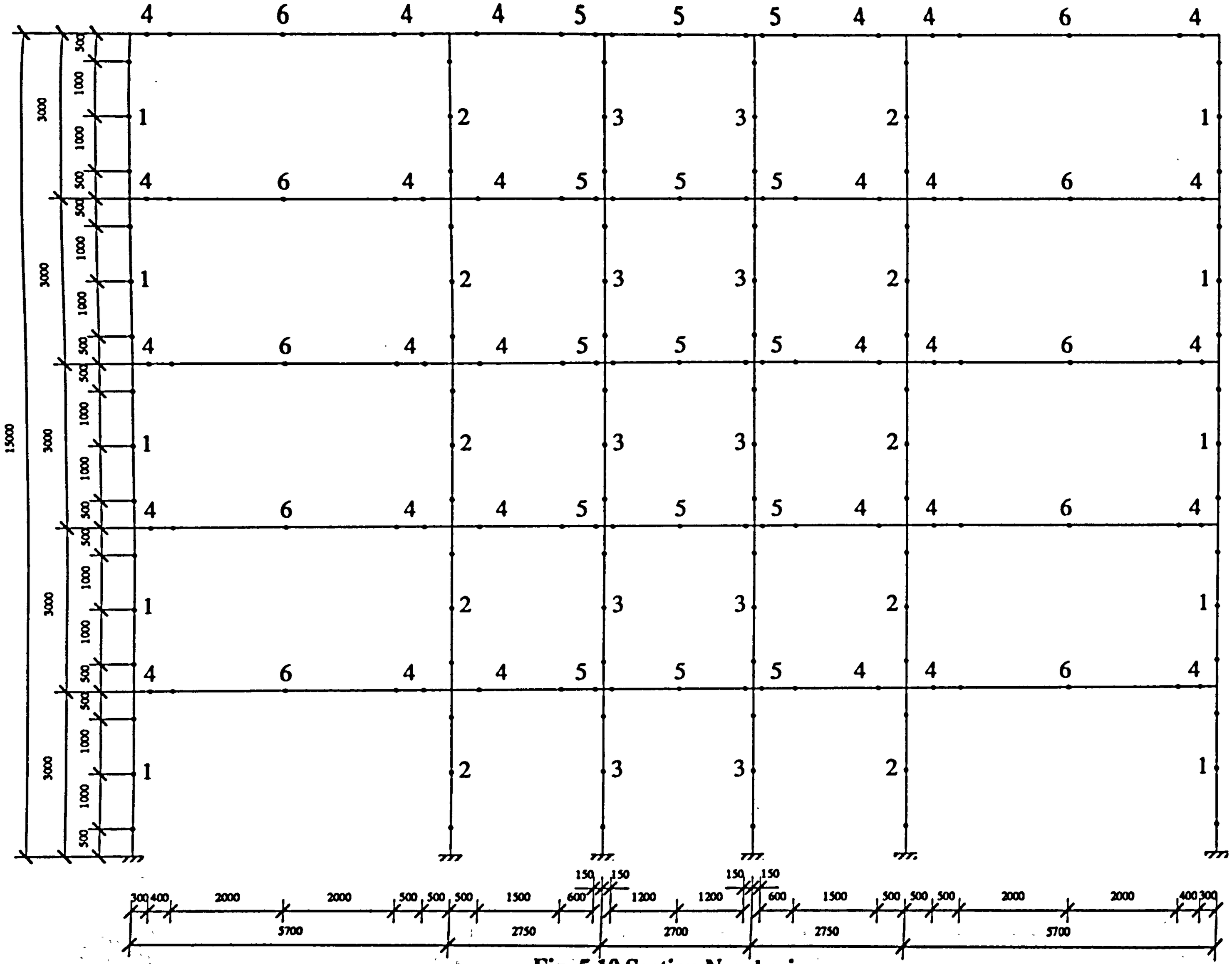


Fig. 5.10 Section Numbering

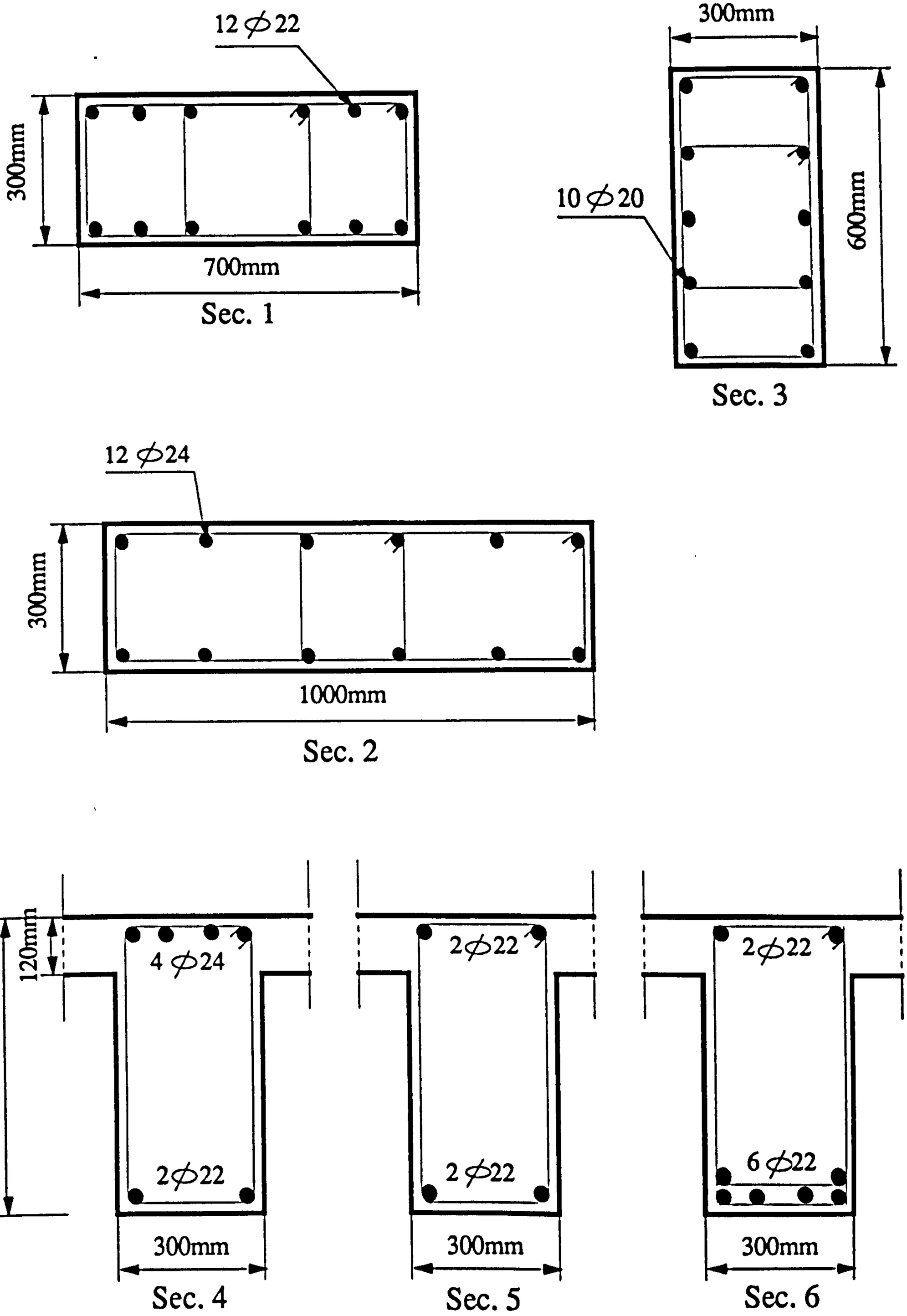


Fig. 5.11. Reinforcement for RC Sections

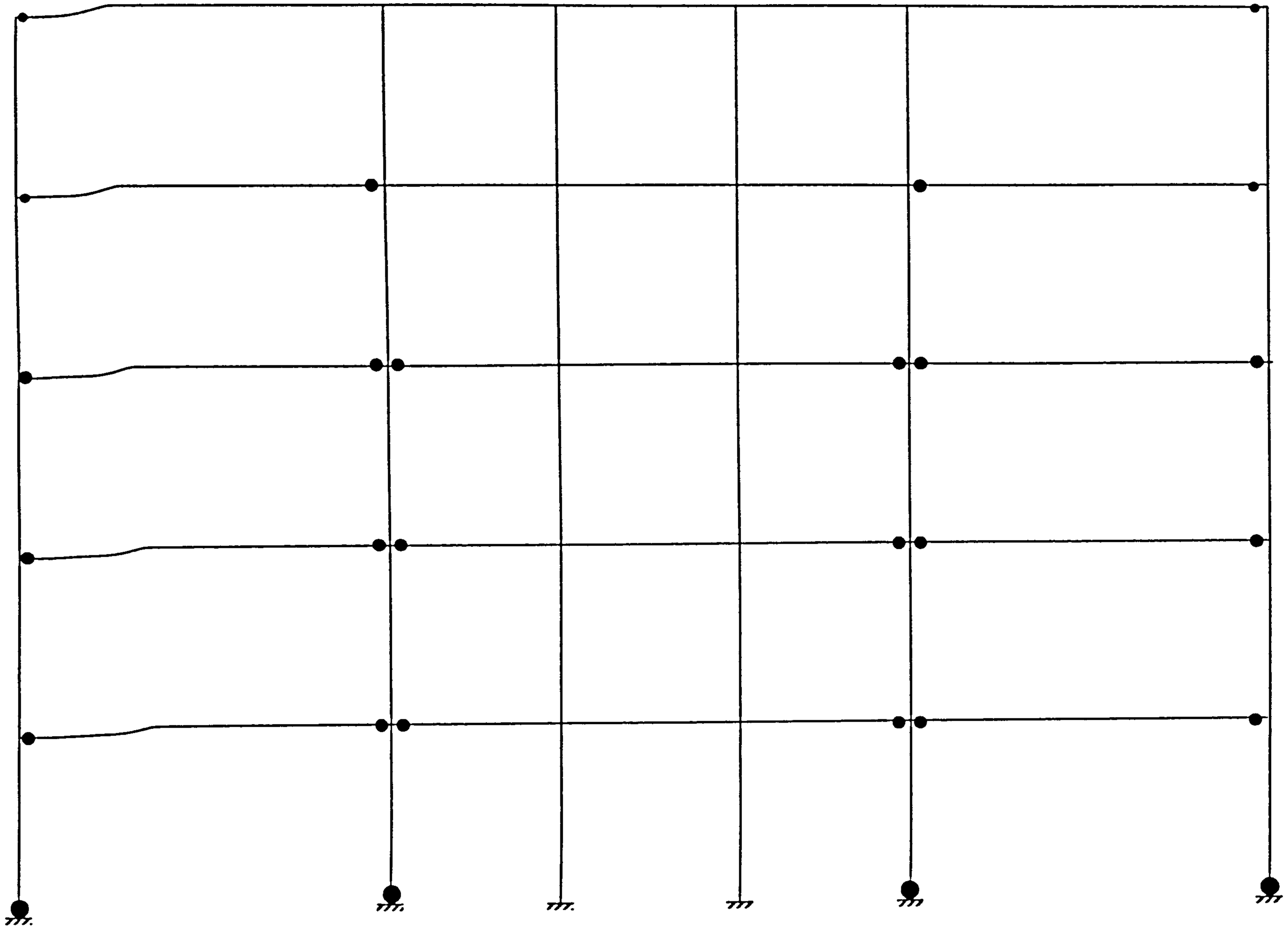


Fig. 5.12. Plastic Hinge Formation for Intact Frame

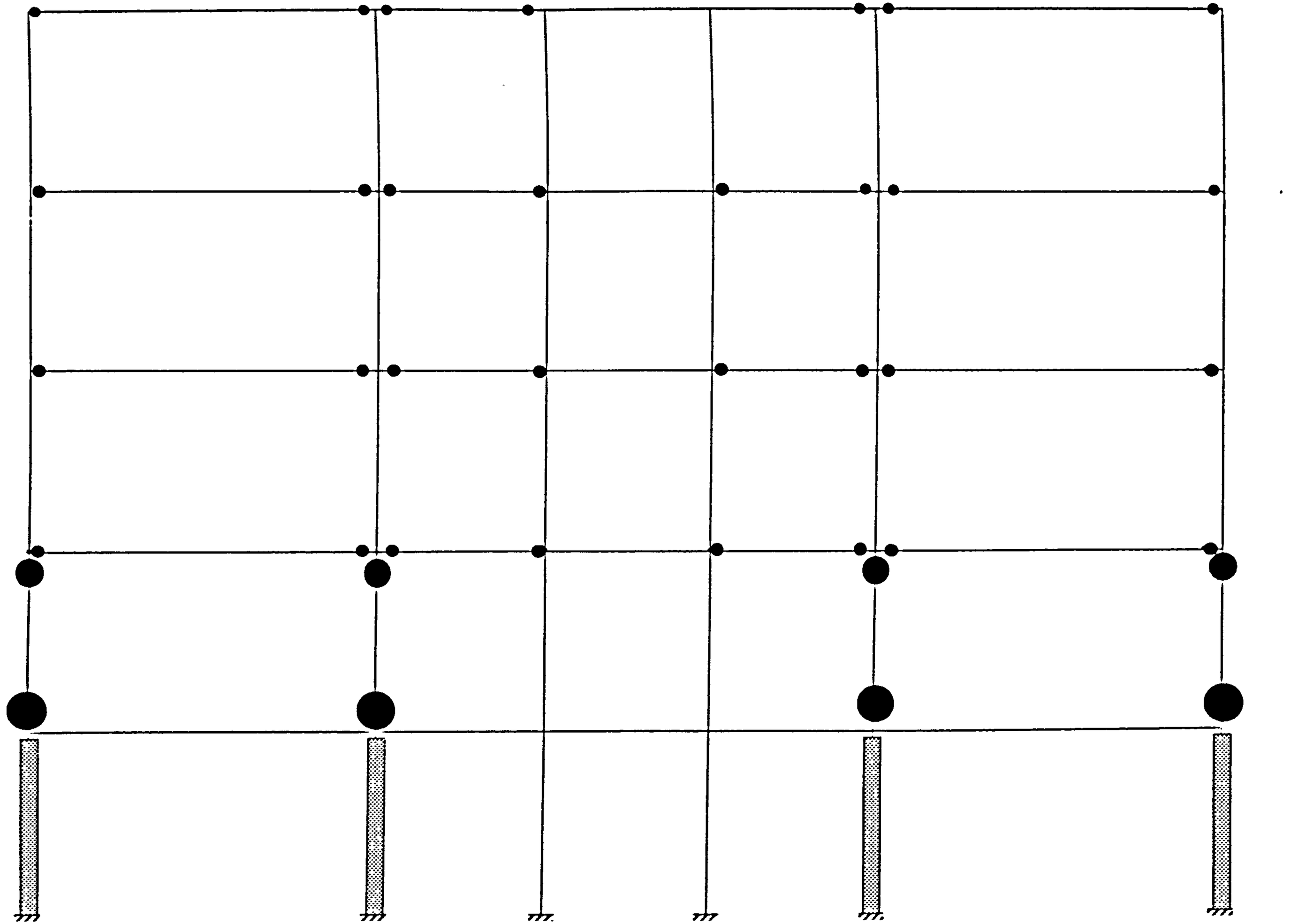


Fig. 5.13. Plastic Hinge Formation for Conventionally Repaired Frame

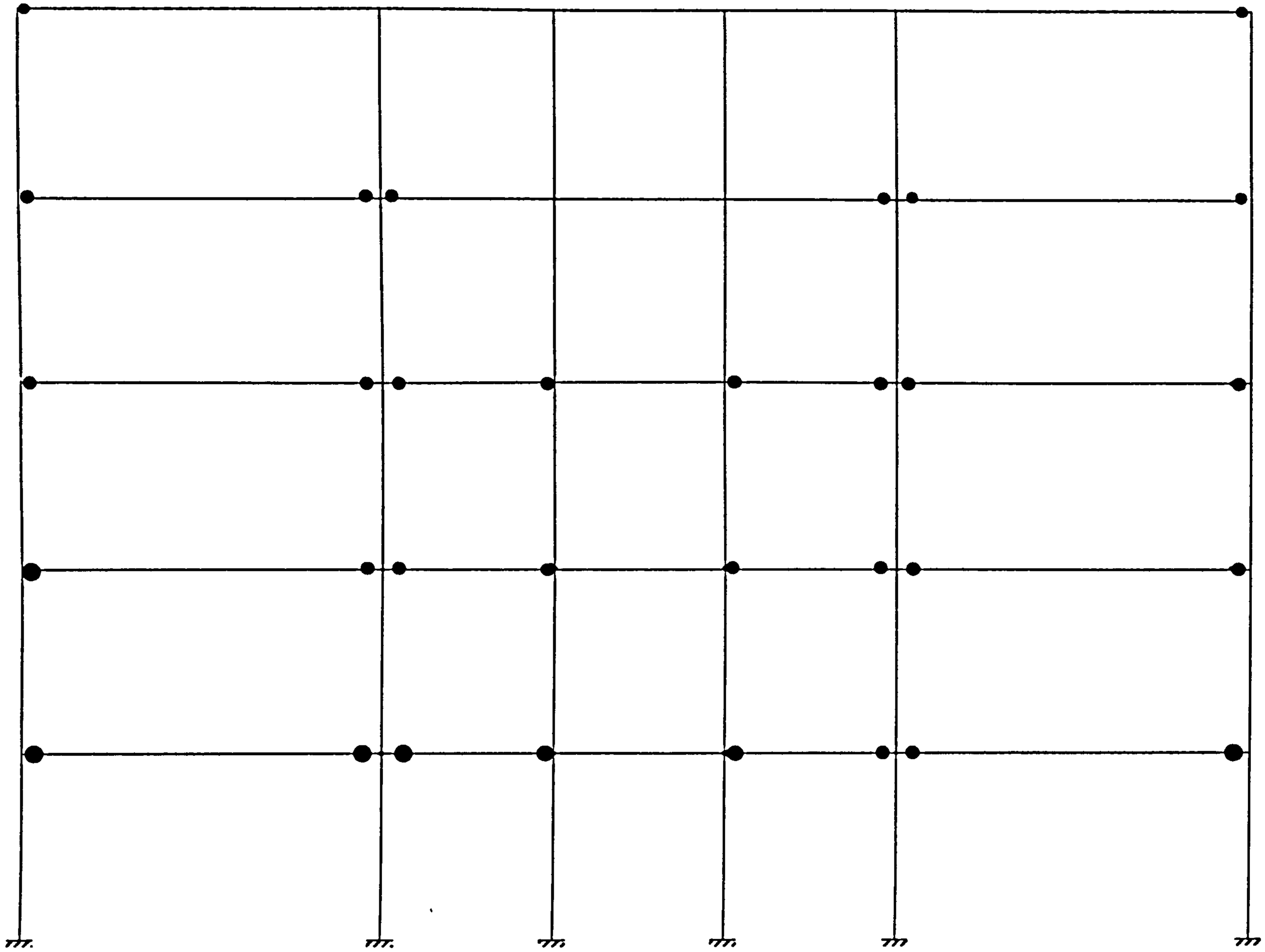


Fig. 5.14. Plastic Hinge Formation for Selectively Repaired Frame

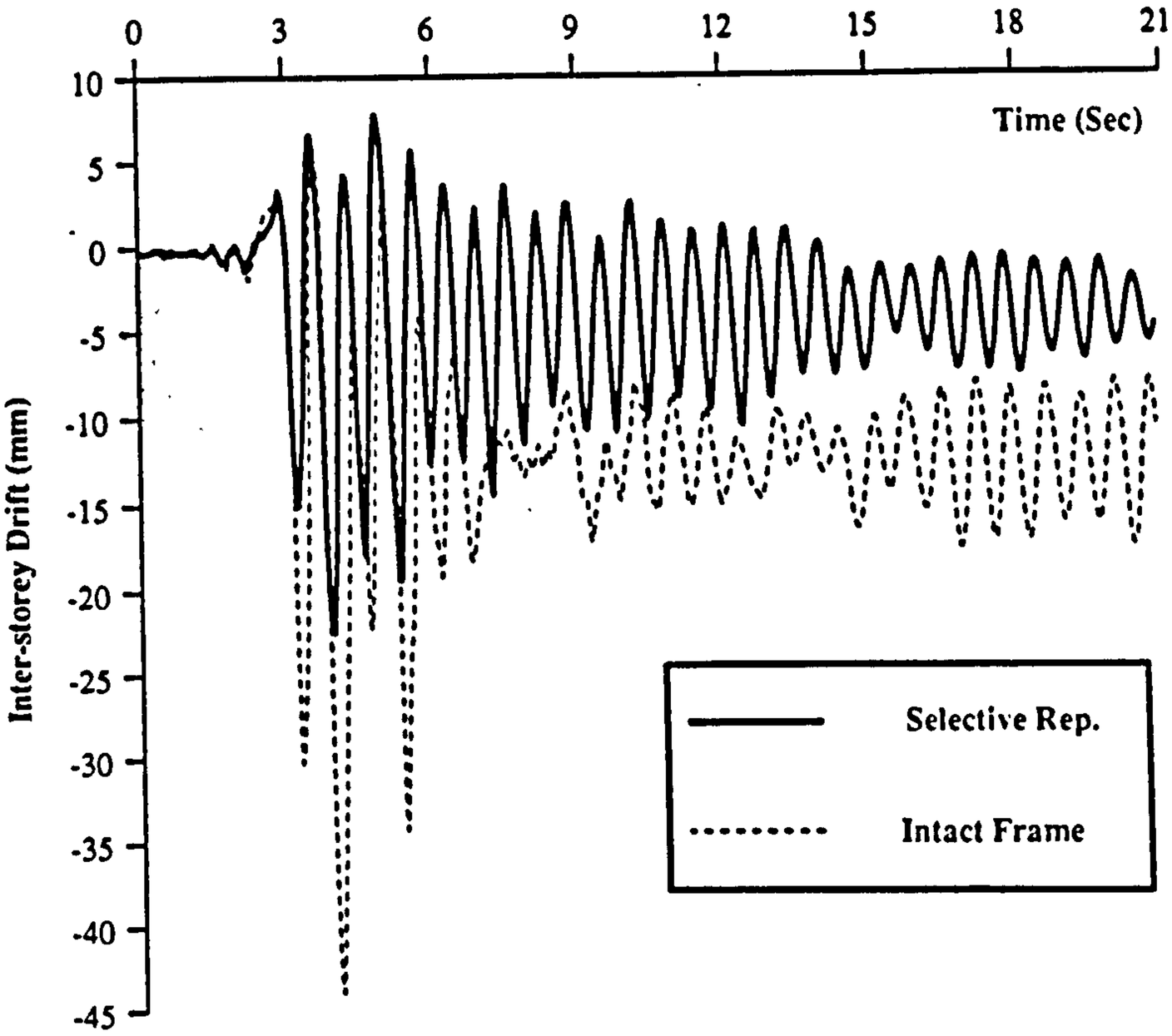


Fig. 5.15. Inter-storey Drift for Selectively-Repaired Frame, level 1.

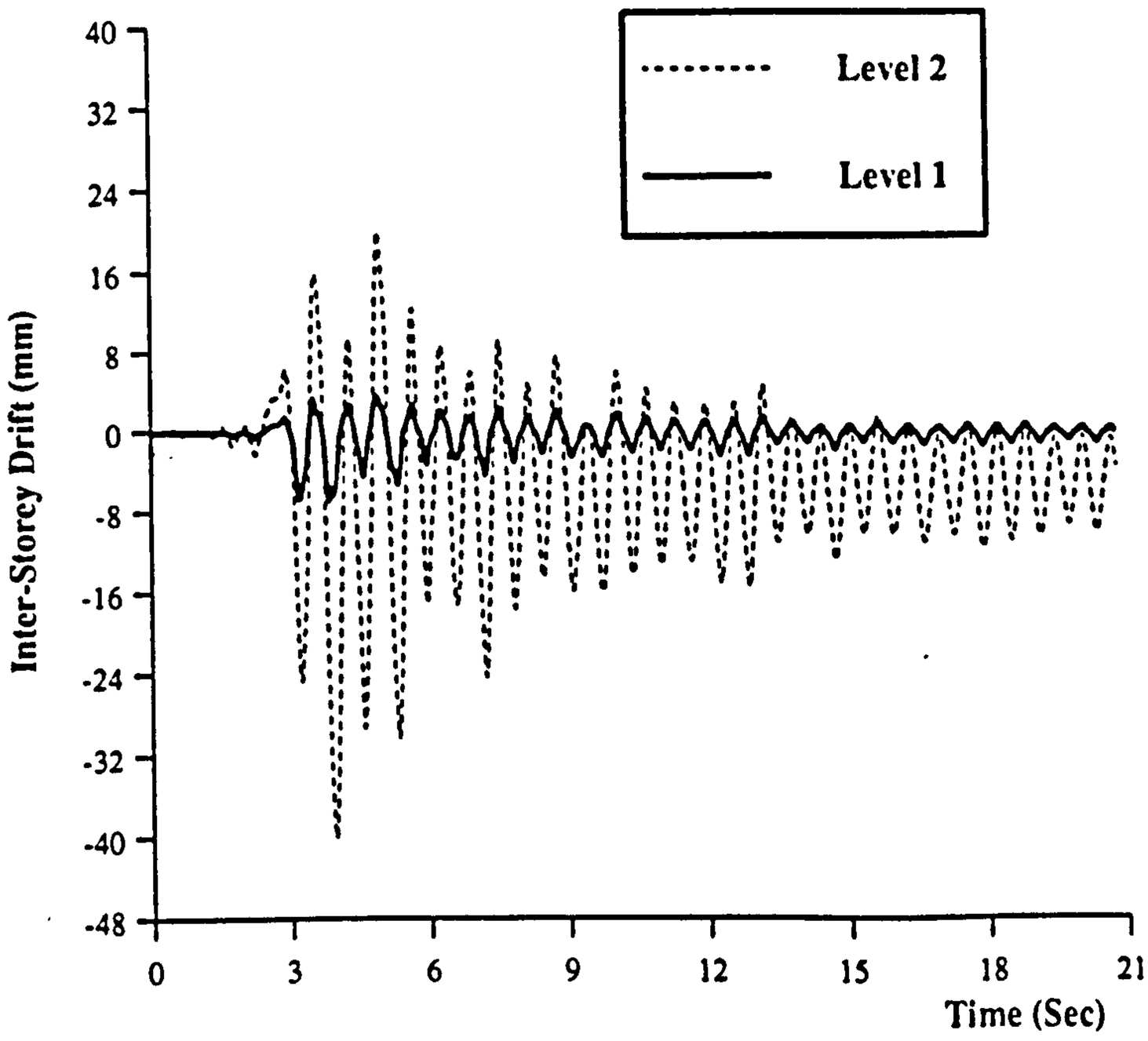


Fig. 5.16. Inter-storey-Drift for Conventionally-Repaired Frame, levels 1 and 2.

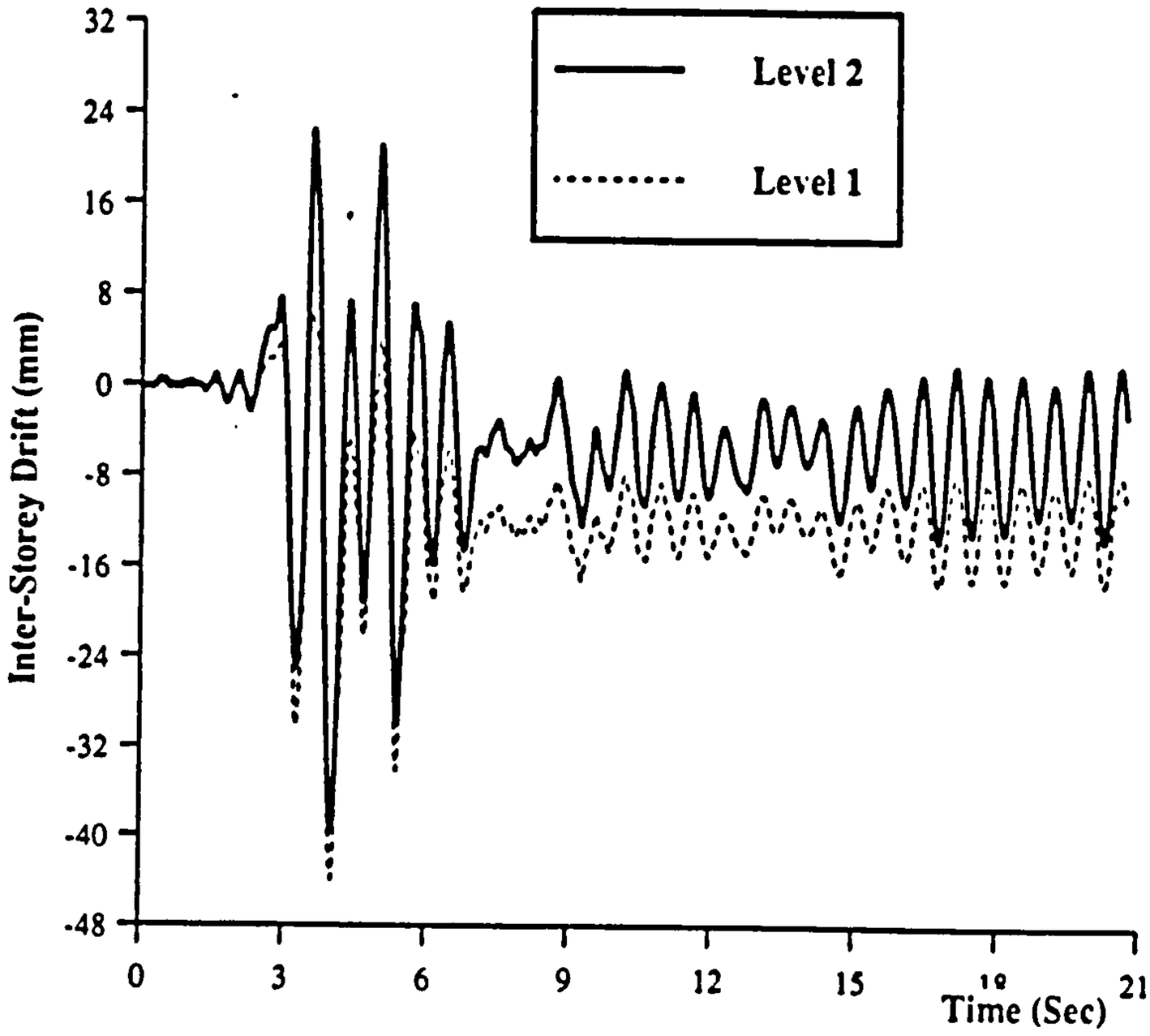


Fig. 5.17. Inter-storey-Drift for Intact Frame, levels 1 and 2

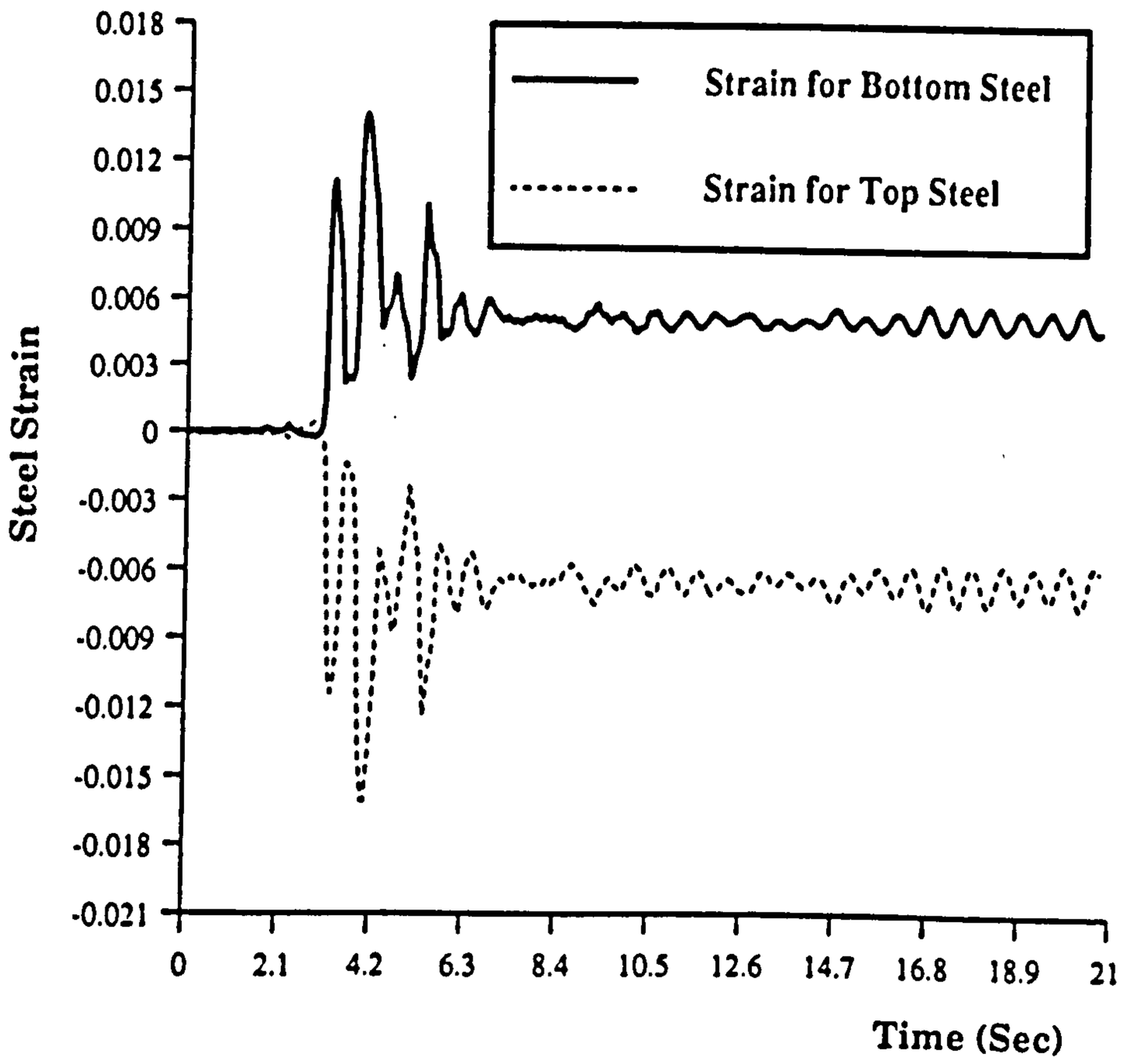


Fig. 5.18. Strain in Main Steel, Column-Foundation Section, Intact Frame (Elm 1)

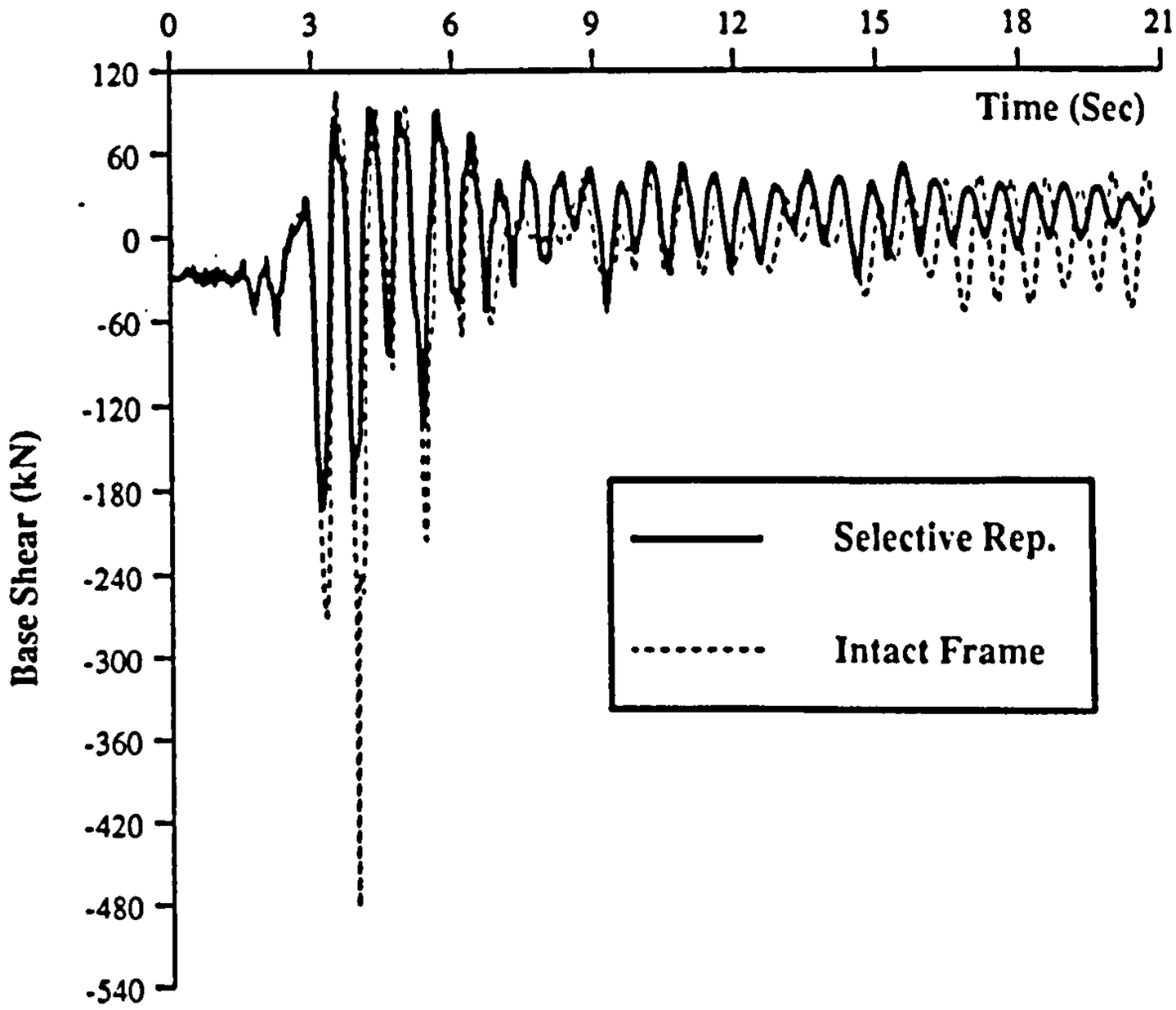


Fig. 5.19. Base Shear, Exterior Column (1) for Intact/Selectively-Repaired Frame

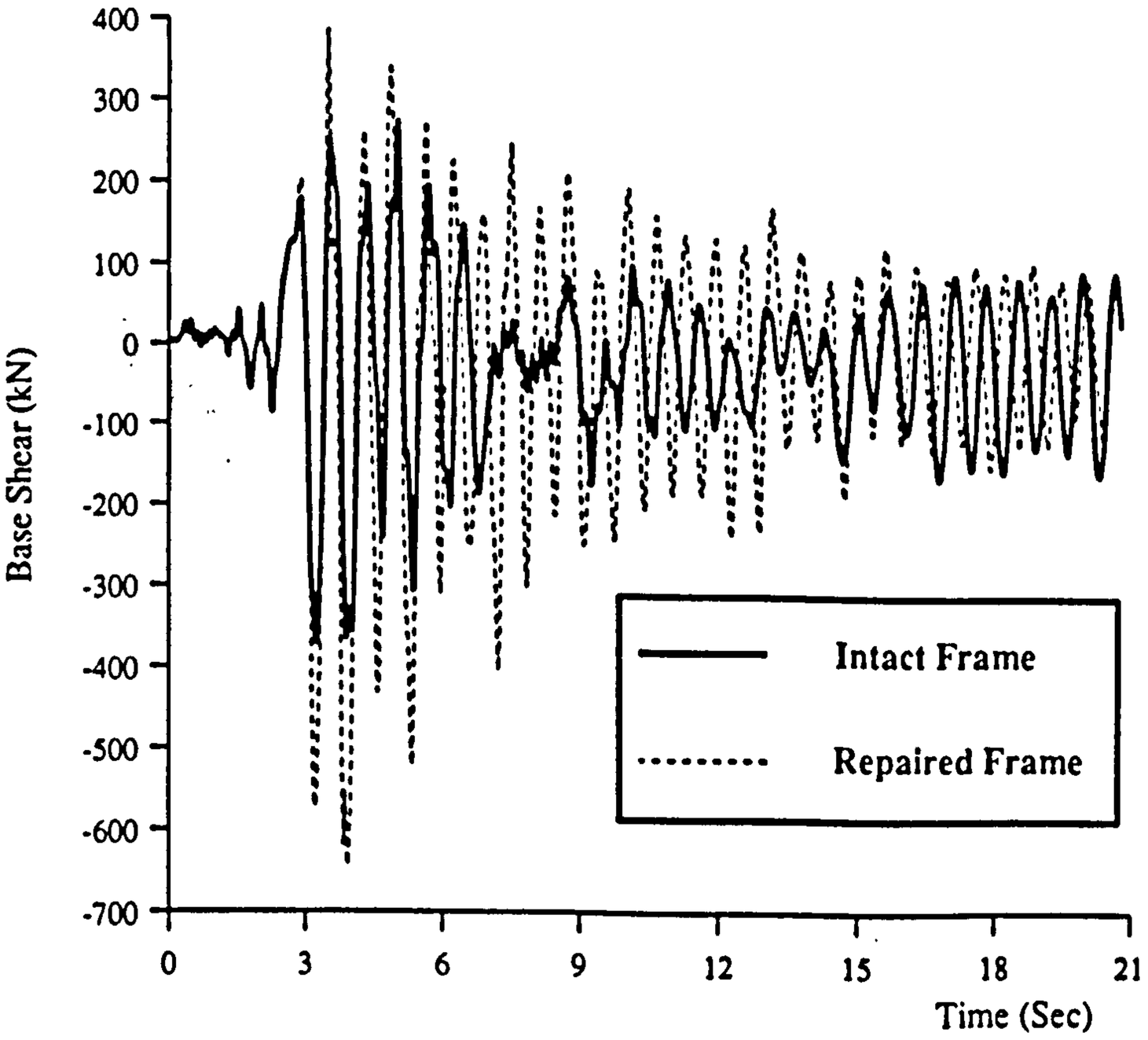


Fig. 5.20. Base Shear, Interior Column (21) for Intact/Conventionally-Repaired Frame

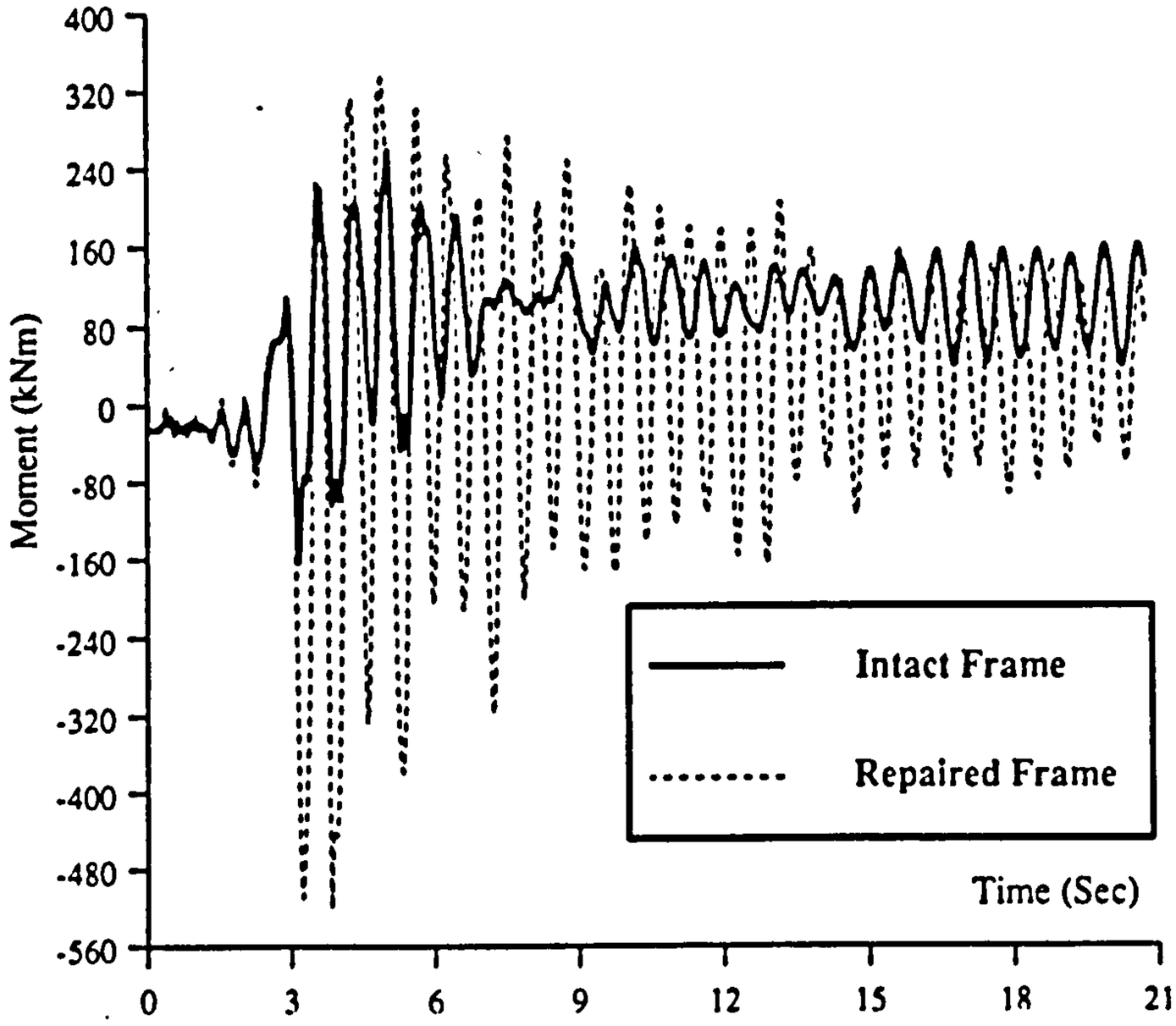


Fig. 5.21. Strength-Demand for Conv. Repair at Second level Exterior Column (5)

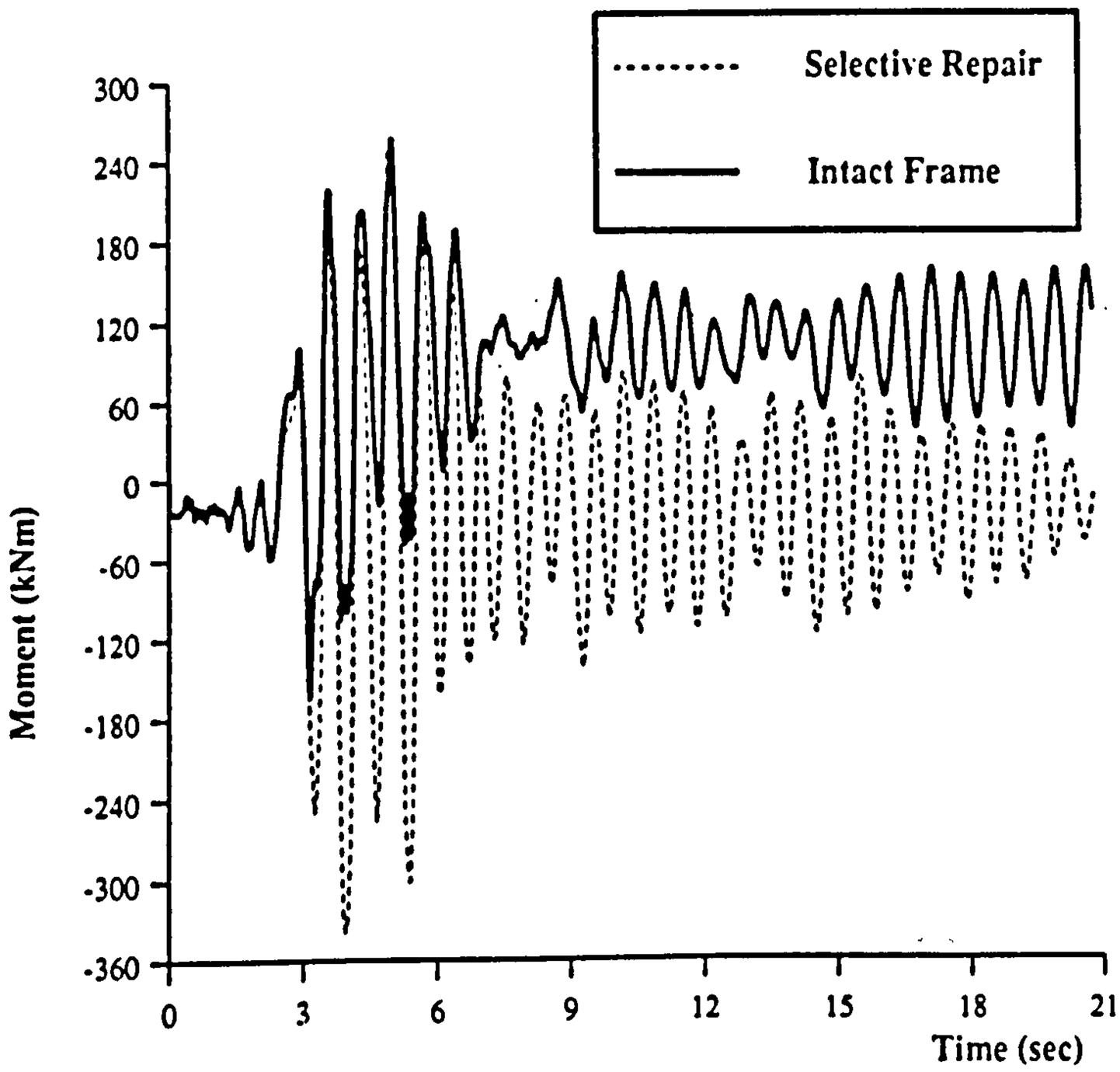


Fig. 5.23. Strength-Demand for Selective Repair at First level Exterior Column (5)

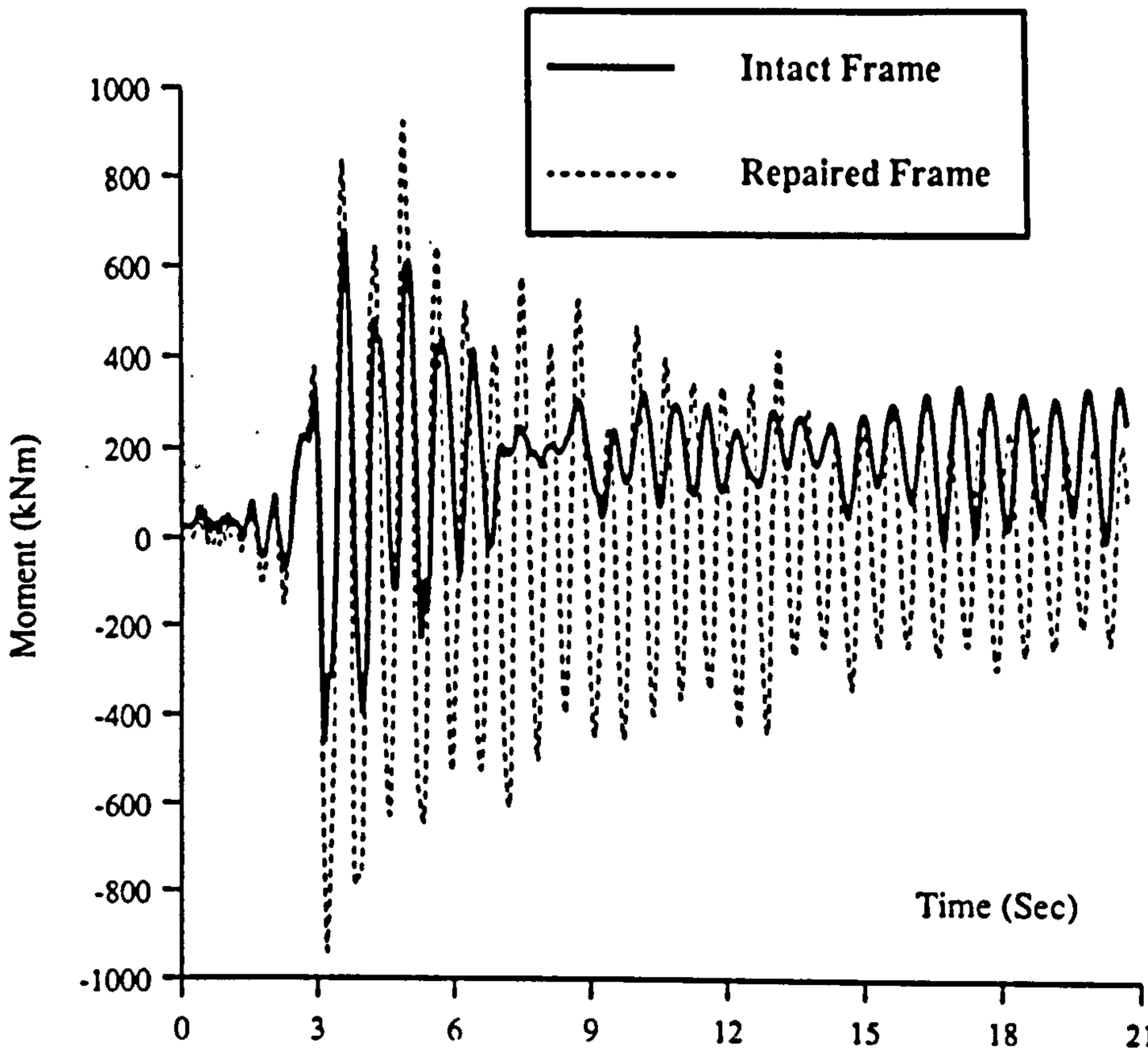


Fig. 5.22. Strength-Demand for Conv. Repair at Second level Interior Column (25)

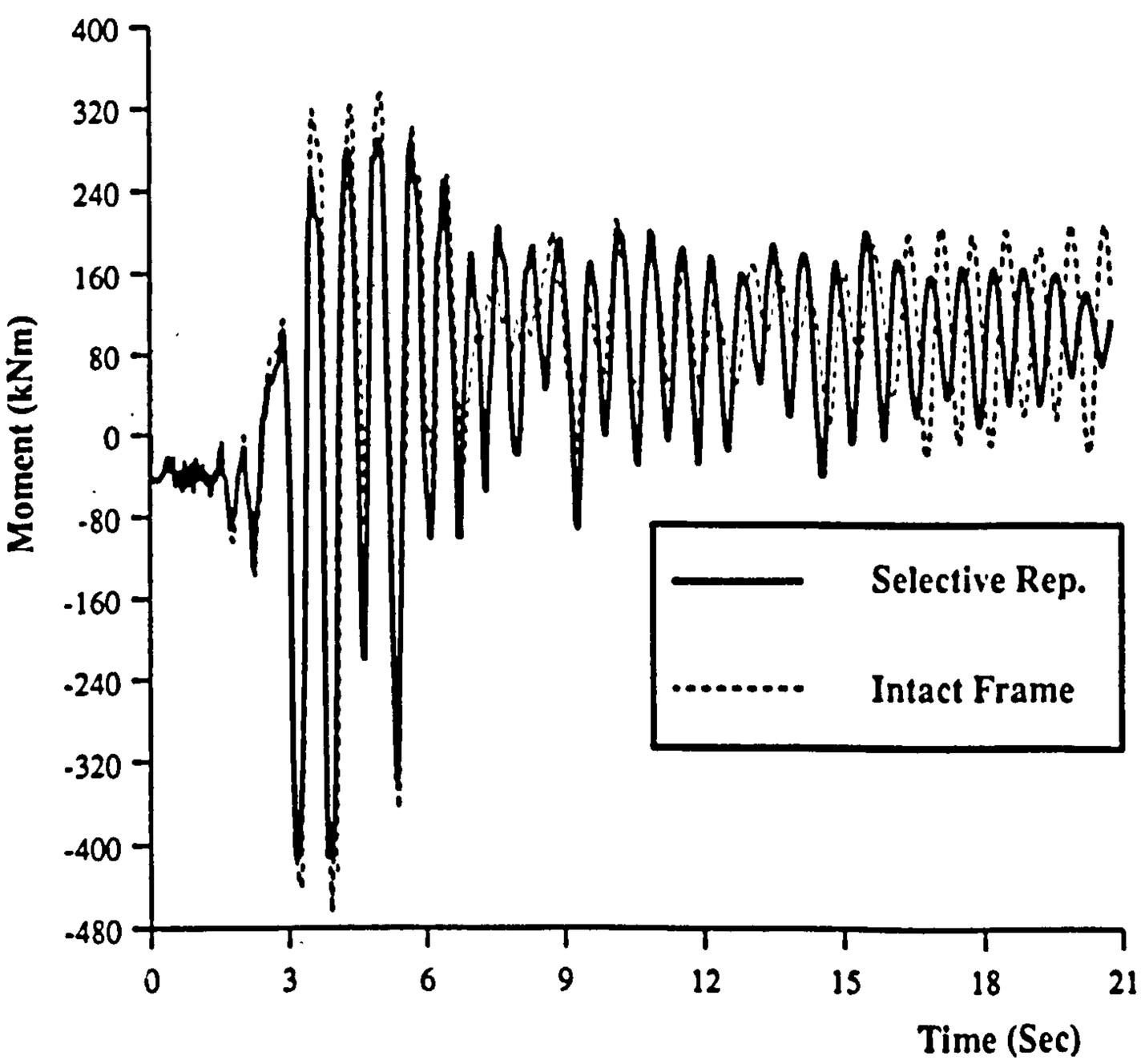


Fig. 5.24. Strength-Demand for Selective Repair at First level Interior Column (5)

CHAPTER 6

6. CLOSURE

6.1. Summary of Conclusions

A summary of the general conclusions based on the results given in this research is presented hereafter. Specific conclusions were discussed in the process of presentation of the work, and for the sake of compactness, are not repeated here .

6.1.1. Conclusions related to Part I

Capacity re-design is needed to re-tune the balance of the damaged structures not designed for a ductile failure mode. Hence, the individual response parameters, such as stiffness, strength and ductility, should be appropriately assessed and controlled. In case where an upgrade of the seismic performance is needed, the increase of ductility-only may be the most economical solution. The need of stiffness-only reinstatement may arise in cases when slight damage occurs in a building hit by a medium size earthquake, causing structural cracks only, leading to some loss in stiffness. In case of total rupture of main structural elements, a strength-only reinstatement must be targeted. Conventional repairs by jacketing the damaged members may lead to stiffness and strength irregularities. This may lead to higher strength and ductility demands at the floor above as demonstrated clearly in Chapter 5 of Part II.

- A total of seventeen isolated RC wall models were tested to scale 1 : 2.5. To simulate degradation under earthquake loading, the models were subjected to a displacement-controlled severe cyclic loading regime.

- The yield and ultimate moments were estimated accurately by section analysis using the nonlinear FE program ADAPTIC. Shear strength was also estimated based on the resistance of the horizontal reinforcement in truss action, the vertical web reinforcement in dowel action, concrete in compression above the neutral axis and the horizontal confining hoops.

– It was concluded that the transverse load was resisted in the early stages by concrete in compression. At about 1% drift, the load resisted by concrete was reduced significantly and the web reinforcement was activated.

– The lateral strength of walls that failed in shear was observed to increase with an increase in the amount of confinement reinforcement in the boundary elements.

– Since hoops were stressed in the tension sides of each cycle, it is concluded that the observed enhancement in shear strength is due to the confining steel hoops in both boundary elements.

– The ductile behaviour of walls is associated with wall extension. This tends to increase the vertical applied load on such a ductile member, which in turn will improve the wall strength in shear and will reduce its curvature ductility.

– Base wall rotations accounted for less than 1% of the total horizontal displacement at ultimate conditions. Hence, the analytical assumption of full fixity at the base was achieved experimentally.

– To investigate the effectiveness of a simple and inexpensive repair method, the damaged concrete for (SW4 and SW5) was replaced by superfluid and gunnite concrete, respectively. Also, additional shear reinforcement was added to the repaired walls. The specimens showed enhanced ductility and seismic performance.

– A stiffness reinstatement scheme was designed and applied for a heavily-cracked model (SW9) and a moderately-cracked model (SW35). Vertical steel plates were attached to the specimen using high strength epoxy. The effectiveness of such a system was proven experimentally. A full yield stiffness reinstatement was achieved without affecting either the wall strength or its ductility.

– A shear strength reinstatement scheme was applied to model (SW22), whereby the cracked wall was injected with epoxy in conjunction with surface treatment for the spalled concrete. A satisfactory seismic performance was observed from the repaired wall.

– In order to achieve a simpler shear reinstatement scheme, a different procedure was employed whereby horizontal steel plates were attached to model (SW21) by means of high strength epoxy mortar. No epoxy injection was applied. Shear strength was reinstated, associated with a reduction in stiffness. Also, a higher ductility level was observed. The same repair scheme was also applied to (SW24) after the injection of the cracks with epoxy. The repaired model confirmed the previous observations with better energy absorption capacity.

– To simulate a realistic strength-only intervention scenario, external unbonded reinforcing steel bars were attached to the tested model (SW31). The bars were spliced and jointed at their mid-height by means of special couplers that were designed to allow for an initial designed slack. In order not to affect the wall dynamic behaviour based on the yield stiffness, the slack was made equal to the wall vertical extension at yield. This flexural strength enhancement scheme added 50% strength to the tested model. It also added to the energy absorption capacity through yielding of the external bars. This was observed from the enlarged force-displacement hysteresis loops. The same objective was also achieved for (SW34). The model was equipped with external steel plates with slotted holes, with a slot clearance equal to the wall extension at yield.

– Ductility-only intervention was achieved for model (SW32). External U-shaped steel plates were added to the model. The open side of the U-shape was closed by means of a high strength grip friction bolt. Epoxy injection was applied between the steel plate and the concrete wall to ensure monolithic action. This scheme proved effective in providing an external confinement device for the concrete in compression. Hence, the model ductility was enhanced and compared well with the initially detailed elements for high confinement.

– From the tests described in Part I, it was concluded that intervention aimed at affecting a single response parameter with little or no effect on others, can be achieved in practice. This would provide tools for engineers undertaking seismic repair and upgrading to re-tune the structural performance and to suite a desired response and failure mode.

6.1.1. Conclusions related to Part II

– The Erzincan earthquake of the 13th of March 1992 was a complex multiple event that involved not only the North Anatolian Fault, but also other conjugate faults in North-East Anatolia. The main shock was of a magnitude $m_S = 6.8$ and was located at an epicentral distance of 6km from the centre of the town of Erzincan. The source had a depth of approximately 10km.

– The main shock of the earthquake was recorded by 3 SMA-1 type accelerographs at epicentral distances of 6, 70 and 71 kilometres. Peak ground accelerations of 0.495g and 0.399g were experienced in the E-W and N-S directions respectively, while the peak ground velocity, experienced in the N-S direction, was 109cm/sec.

– A wide array of damage was observed, from minor cracking in plaster with little or no structural damage, to extreme structural damage and even total collapse. Indeed the most overwhelming and unacceptable fact was that these structures, apart from any earthquake induced damage, were critically lacking in material strength, appropriate design and satisfactory construction technique. In particular, the low concrete quality, the use of smooth (undeformed) reinforcing steel and gross inadequacy of confinement in critical elements made it impossible to assign any quantifiable capacity for seismic resistance to the existing construction.

– It is important to distinguish between method of inspection (data collection) and the method of utilising the collected information to assess the status of seismic resistance of a building. In section 2 of this report, the philosophy of inspection was discussed and the background of the inspection forms used was highlighted.

– The level of expected seismic event along the design criteria for upgrade was discussed. The expected future peak ground acceleration may not be much larger than the ones caused by the 13 March 1992 earthquake. Therefore, the need for structural enhancement must encompass not only increased strength and balanced stiffness but adequate and reliable ductility.

– A nonlinear dynamic analysis performed on a typical structure in Erzincan showed that substantial energy dissipation through inelastic deformations in the nonlinear range was exhibited by the structural elements at various beam and

column sections. The formation of plastic hinges was characterised by steel yielding at both extreme fibres. A comparison between the flexure and shear strengths supply and demand have shown that the latter were higher. This explains the state of damage observed on site and reported herein.

– The damaged structure was repaired by the addition of a 20cm concrete jacket to the damaged columns (conventional repair method). The dynamic analysis performed on the repaired structure showed that excessive curvature ductility and flexural strength demands, on the level above the repaired one, would be expected. The strength demand at that particular level increased by 80% when compared with the intact frame. This would lead to a probable mechanism and total collapse in case of a future seismic event. This was also confirmed by the failure of the military hospital in Erzincan (eight storey building). The building was repaired with the same approach after the 1983 earthquake.

– The same structure was repaired selectively using some of the novel techniques developed in the current research. Strength-only intervention was applied for repair and enhancement of the seismic performance. The applied scheme reduced the strength demand on the members penalised by the conventional repair by some 70%. Interstorey drifts were reduced by 50% on average and became more uniform. Plastic hinge formation was spread in a more regular pattern throughout the building height and ensured a better energy dissipation capacity.

The significance and potential benefit from selective repair has been demonstrated by the reduction in strength demand and interstorey drifts. The regularisation of the latter, along with better plastic hinges distribution without a noticeable increase in the base shear.

6.2. Proposals for Future Developments

Based on the research findings from this thesis, there are two developments that assume immediate importance. Firstly, quantitative guidelines are needed for the assessment of the effect of conventional repair techniques on 'capacity design' parameters, such as energy absorption capacity and failure mode. This will enable engineers to determine whether conventional intervention schemes are adequate and what is the likely effect of the intervention on the original design concept. To achieve the above objective, systematic parametric studies are required to relate the level and location of stiffness,

strength or ductility enhancement to the overall behaviour factor. This is especially significant for dual frame/wall systems, where the wall shear and flexural strength play roles that are of changing importance along the response path.

The second immediate requirement is the development of preliminary design guidelines for the novel intervention techniques tested in this thesis. On the stiffness-only side, simple expressions are needed to relate the location, width and thickness of the bonded steel plates on the percentage stiffness reinstatement. Moreover, a rational definition of ductility for the strength-only scheme (where two yield levels are observed) is required, alongside rules to allow decoupling of the effect of flexural overstrength and shear resistance. Finally, design expressions for shear strength enhancement by horizontal bonded steel plates is sought. These objectives should be addressed through a desk study of all the available and future experimental results followed by the application of simple mechanics principles to derive the required expression.

REFERENCES

ACI 223-90 (1990). Standard Practice for the Use of Shrinkage-Compensating Concrete, *American Concrete Institute*, Detroit 33 pp.

ACI 224R-89 (1989). Control of Cracking in Concrete Structures, *American Concrete Institute*, Detroit, 43 pp.

ACI 224.1R-89 (1989). Causes, Evaluation, and Repair of Cracks in Concrete Structures, *American Concrete Institute*, Detroit, 20 pp.

ACI 340.4R-91 (1991). Design Handbook, Vol. 2, Columns, *American Concrete Institute*, Detroit, 242 pp.

ACI 426R-74 (1980). The Shear Strength of Reinforced Concrete Members, *American Concrete Institute*, Detroit, 111 pp.

ACI 503R-89 (1989). Use of Epoxy Compounds with Concrete, *American Concrete Institute*, Detroit, 33 pp.

ACI Committee 318 (1989). Building Code Requirement for Reinforced Concrete ACI 318-89, *American Concrete Institute*, Detroit, 353 pp.

ACI CSM 8-85 (1985). Structural Repair - Corrosion Damage and Control, *American Concrete Institute*, Detroit, 233 pp.

ACI SCM 13-86 (1986). Back-to-the-Basics Repair of Concrete, *American Concrete Institute*, Detroit, 147 pp.

ACI SCM 16-87 (1987). Repair and Rehabilitation of Concrete Structures, *American Concrete Institute*, Detroit, 185 pp.

ACI SCM 21-89 (1989). Repairs of Concrete Structures - Assessments, Methods and Risks, *American Concrete Institute*, Detroit, 514 pp.

ACI SP-71 (1989). ASTM Standards in ACI 301 and 318. *American Concrete Institute*, Detroit, 180 pp.

Alcocer, S.M. (1992). Rehabilitation of RC frame connections using jacketing. *Tenth World Conference on Earthquake Engineering*, vol. 9, Balkema. pp. 5235-40.

Alsan, E., Tezican, L. and Bath, M. (1975). An earthquake catalogue for Turkey for the interval 1913-1970. *Publ. Seism. Inst*, Uppsala, no. 7.75.

Ambraseys, N.N. (1970). Some characteristics features of the North Anatolian Fault Zone, *Tectonophysics*, vol. 9, pp. 143-165.

Ambraseys, N.N. (1988). Engineering seismology. *International Journal of Earthquake Engineering and Strctural Dynamics* vol. 17, pp. 17-70.

Ambraseys, N.N., Elnashai, A.S., Broderick, B.M, Salama, A.I. and Soliman, M.M. The Erzincan Earthquake of 13 March 1992, *Engineering Seismology and Earthquake Engineering Sect. Report No 92/11, Imperial College*, London, UK, 128 pp.

Ambraseys, N.N. (1971). Value of historical records of earthquakes. *Nature*, 232 (5310), pp. 375-379.

Ambraseys, N.N. and Bommer, J. (1991). The attenuation of ground accelerations in Europe, *International Journal of Earthquake Engineering and Strctural Dynamics*, vol.20, pp. 1179-1202.

Ammann, W.J. (1992). Fastening system under seismic loading conditions. *Tenth World Conference on Earthquake Engineering*, vol. 9, Balkema. pp. 5247-52.

Ayhan, E., Alsan, E. et al (1983). Turkiye ve dolaylari deprem Katalogue 1881-1980, *Bogazici Univ. Publ.*, Istambul.

Barka, A. and Gulen, L. (1989). Complex evaluation of the Erzincan basin, *Journ. Struct. Geol.*, vol. 11, pp. 275-283.

Bathe, K.J. (1982). *Finite Element Procedures in Engineering Analysis*, Prentice Hall.

Bertero, V.V., Cowel, A and Popov, E. (1980). Repair of Bond in R/C structures by epoxy injection, *Proceedings of the first Seminar on Repair and Retrofit of Structures*, Ann Arbor, Michigan, Vol. 1, pp. 234-240.

Bertero, V.V. (1992). Seismic upgrading of existing structures. *Tenth World Conference on Earthquake Engineering*, vol. 9, Balkema. pp. 5101-106.

Bertero, V.V. and Brakken, S. (1981). Effect of the infils in Seismic Resistant Building, *Proceeding of the Second Seminar on Repair and Retrofit of Structures*, Ann Arbor, Michigan, Vol. 2, pp. 377-419.

Bolt, B.A. (1989). Chapter 1 The Nature of Earthquake Ground Motion, *The Seismic Design Handbook*, Reinhold, pp.1-31.

Bosphorus University (1992). March 13, 1992 (Ms = 6.8) Erzincan Erarthquake; A preliminary Reconnaisance Report, *Bosphorus University Press*, May.

Broderick, B.M. (1992). Experimental and Analytical Studies in the Seismic Response of Composite Frames. *Eng. Seismology and Earthquake Engineering Report. Imperial College*. 137 pp.

Burton, P.W., McGonigle, R., Makropoulos, K.C., Ucer, S.B. (1983). Seismic risk in Turkey, the Aegean and eastern Mediterranean: The occurrence of large magnitude earthquakes. *Geophys. J. R.*, pp. 476-501.

CAN3-A23.3-M84 (1989). Design of Concrete Structures for Buildings. *Canadian Standards Association,* Ontario, 223 pp.

Cardenes, A.E., Russell H.G., and Corley (1980). Strength of low-rise Structural Walls. *ACI SP-63, Reinforced Concrete Structures Subjected to Wind and Earthquake forces*, American Concrete Institute, Detroit, pp. 221-74.

CEB Manual, (1985). Cracking and Deformations. *Comite Euro-International du Beton*. Ecole Polytechnique federale de Lausanne, 62 pp.

Cheung, P.C., Pauly, T. and Park, R. (1991). Mechanisms of Slab Contributions in Beam-Column Subassemblages. *ACI SP-123, Design of Beam-Column joints for Seismic Resistance*, American Concrete Institute, Detroit, pp. 259-91.

Cheung, P.C., Pauly, T. and Park, R. (1991). New Zealand Tests on Full-Scale Reinforced Concrete Beam-Column-Slab subassemblages designed for Earthquake Resistance. *ACI SP-123, Design of Beam-Column joints for Seismic Resistance*, American Concrete Institute, Detroit, pp. 1-38.

Collins, M.P. (1991). The Response of Reinforced Concrete Elements Subjected to Shear. *Concrete Shear in Earthquake*, Elsevier Applied Science, pp. 13-23.

Crainic, L. and Postelnicu, T. (1992). Strengthening of an Earthquake-Damaged Building, *Structural Engineering International*, pp.194-98.

Derecho, A.T. (1989). Chapter 9 Seismic Design of Reinforced Concrete Structures, *The Seismic Design Handbook*, Reinhold, pp. 238-74.

Dewey, J.W. (1976). Seismicity of Northen Anatolia, *Bull. Seism. Soc. Amer. vol. 66*, pp. 843-868.

Dowrick, D.J. (1987). *Earthquake Resistant Design for Engineers and Architects*, John Wiley, 540 pp.

EC2, Eurocode No.2 (1984): Common Unified Rules for Concrete Structures, Report EUR 8848 DE, EN, FR, Industrial Processes, Building and Civil Engineering, *Commission of the European Communities*, 340 pp.

EC8, Eurocode No.8 (1988): Structures in Seismic Regions - Design, Part 1, General and Building, Report EUR 12266 EN, Industrial Processes, Building and Civil Engineering, *Commission of the European Communities*, 240 pp.

Erdik, M., Doyuran, V., Akkas, N. and Gulkan, P. (1985). A probabilistic Assessment of the Seismic Hazard in Turkey, *Tectonophysics*, 117, pp. 295-344.

Elnashai, A.S. (1992). Effect of Member Characteristics on the Response of RC Structures. *Tenth World Conference on Earthquake Engineering*, vol. 6, Balkema. pp. 3275-80.

Elnashai, A.S. and Agbabian, M.S., *Evaluation of US and European Practice in Seismic Design of R/C Structures*, Submitted to Earthquake Spectra.

Elnashai, A.S. and Pilakoutas K. (1992). Interpretation of Testing Results for RC Panels, *ACI Structural Journal*, Accepted for publication August 1992.

Elnashai, A.S. and Dowling, P.J. (1991). Chapter 2 Seismic design of steel structures, *Structures subjected to dynamic loading - Stability and Strength series*, Elsevier, pp. 27-76.

Elnashai, A.S., Izzuddin, B.A. and Dowling, P.J. (1989). Efficient Large Displacement Elastoplastic Dynamic Analysis of Structures, *Journal of European Earthquake Engineering* , No 3, pp. 32-41.

Elnashai, A.S., Pilakoutas, K. and Ambraseys, N.N. (1990). Experimental Behaviour of Reinforced Concrete Walls Under Earthquake loading, *International Journal of Earthquake Engineering and Structural Dynamics,* Vol 19, No 3, pp. 389-407.

Ergin, K., Guclu, U. and Uz, Z. (1967). A catalogue of earthquakes of Turkey and the surrounding area (1100 to 1964). *Istanbul Technical University*, Publication No. 24.

Ergin, K., Guclu, U. and Akasay, G. (1971). A catalogue of earthquakes of Turkey and the surrounding area (1965-1970). *Istanbul Technical University*, Publication No. 29.

Fang, E. (1991). Failure modes of RC tall shear walls. *Concrete Shear in Earthquake*, Elsevier Applied Science, pp. 125-33.

Fenwick, R.C. (1991). The behaviour of plastic hinge zones in seismic resistant concrete structures. *Earthquake, Blast and Impact*, Elsevier Applied Science, pp. 221-230.

Fintel, M. (1991). Need for shear walls in concrete buildings for seismic resistance. *Concrete Shear in Earthquake*, Elsevier Applied Science. pp. 34-42.

FIP, (1991). Repair and Strengthening of Concrete Structures, *FIP Commission on Practical Construction*, 37 pp.

Forel, F. (1982). Seismic Strengthening of Existing Buildings. *Proceedings of the third Seminar on Repair and Retrofit of structures*, US/Japan Cooperative Earthquake Research Program, Department of Civil Engineering, University of Michgan.

Fosroc (1991). *Concrete Repair and Protection. User's Manual.* UM2387, 285 pp.

Fuse, T., Okuta, K., Hiramatsu, K., Ozawa, T., and Nara, N. (1992). Cyclic loading tests of reinforced concrete column strengthened with steel tube. *Tenth World Conference on Earthquake Engineering*, vol. 9, Balkema. pp. 5227-33.

Fustok, M., Goel, S.C. and Wight, J.K. (1991). Use of Steel Braces To Resist Seismic Forces in Precast Concrete Structures. *Research Report UMCE 91-13, Ann Arbor*, Michigan 48109, 229 pp.

Gulkan, P. (1992). A Preliminary Field Reconnaissance Report on the Erzincan Earthquake of 13 March 1992, *Learning from Earthquake Series.*, 45 pp.

Gupinar, A., Erdik, M., Oner, M. and Yucemen, S. (1979). Seismic risk analysis of Northen Anatolia based on intensity attenuation. Proceeding of the Second National Conference on Earthquake Engineering, Stanford, pp. 72-81.

Hanson (1986). Strengthening of Reinforced Concrete in Buildings. ACI SCM 14-86. *Seismic Design of Existing Structures*. American Concrete Institute, Detroit, 21pp.

Hayashi, Toshio, Hideakira Niwa and Masashi Fukuhara, (1980). The Strengthening Methods of Existing Reinforced Concrete Buildings., *Seventh world conference on Earthquake Engineering Istambul, Turkey.*

Izzuddin, B.A., Elnashai, A.S. and Dowling, P.J. (1990). Large displacement nonlinear dynamic analysis of space frames. *European Conference on Structural Dynamics*. Balkema pp. 491-96.

Izzuddin, B.A. and Elnashai, A.S. (1989). ADAPTIC, A program for Static and Dynamic Analysis of Structures by Adaptive Mesh Refinement; User manual. *Engineering Seismology and Earthquake Engineering Report ESEE/89-7,* 82 pp.

Jackson, J., McKenzie, D. (1984). *Active tectonics of the Alpine-Himalayan belt between Turkey and Pakistan*, Geoph. Journ. R. astr. Soc., vol. 77 pp. 185-264.

Jain, A. K., (1985). Seismic response of RC Frames with Steel Braces, J*ournal of Structural Engineering*, ASCE, Vol. III, No. 10, pp. 2130-2148.

Jirsa, J.O. (1986). Strengthening Existing Structures. ACI SCM 14-86. *Seismic Design of Existing Structures*. American Concrete Institute, Detroit, 46 pp.

Jirsa, J.O. and Stoppenhagen, D.R. (1987). Seismic Repair of a Reinforced Concrete Frame Using Encased Columns. *Phil M. Ferguson Structural Engineering Laboratory,* PMFSEL Report No, 87-2, 120 pp.

Kahn, L.F, (1980). Strengthening Existing RC Columns for Earthquake Resistance, *Proceedings of the seventh World Conference on Earthquake Engineering*, Istambul, Turkey, Vol. 4, Part 1, pp. 327-334.

Kahn, L.F, Lawrence, F. and Robert, D. Hanson, (1979). Infilled Walls for Earthquake Strengthening, *Journal of Structural Division,* ASCE, Vol. 105, No. ST2, pp. 283-296.

Kline, T. (1991). Crack Repair: An Engineer's Perspective. *Concrete International*, Vol. 13 No. 6. American Concrete Institute, Detroit, pp. 47-49

Lanca, S.I. (1992). Reinforced Concrete Shear Walls Stressed by Horizontal Loads. *Tenth World Conference on Earthquake Engineering*, vol. 6, Balkema. pp. 3241-44.

Lee, H. and Goel, S.C. (1990). Seismic Behaviour of Steel Built-up Box-Shaped Bracing Members and their use in Strengthening Reinforced Concrete Frames. *Research Report UMCE 90-7, Ann Arbor*, Michigan 48109, 285 pp.

Lopes, M.S. (1991). Seismic Behaviour of RC Walls with low Shear Ratio, *PhD Thesis, Engineering Seismology and Earthquake Engineering Section*, Imperial College, London, 439 pp.

Machida, A. and Mutsuyoshi, H. (1991). Evaluation of Ductility of RC Members and Influence of Ductility on Inelastic Response Behaviour of RC Frame Structures. *Concrete Shear in Earthquake*, Elsevier Applied Science, pp. 355-64.

Madas, P. and Elnashai, A.S. (1991). A new Passive Confinement Model for Concrete Subjected to Variable Amplitude Cyclic Loading, Imperial College, *Eng. Seismology and Earthquake Eng. Research Report No. ESEE 91/2*, 56 pp.

Nakashi, T., Toda, T. and Makita, T. (1992). Experimental study on deformation capacity of reinforced concrete shear walls. *Tenth World Conference on Earthquake Engineering*, vol. 6, Balkema. pp. 3231-36.

Nian, D.X. (1992). Inelastic Response and Effective Design of Asymmetric Buildings under strong Earthquake Loading, *PhD Thesis, University College*, London.

NZS 3101 Part 1 (1982). Code of Practice for the Design of Concrete Structures, *Standards Association of New Zealand*, Wellington, 127 pp.

NZS 3101 Part 2 (1982). Commentary on the Design of Concrete Structures, *Standard Association of New Zealand*, Wellington, 156 pp.

NZS 4203 (1984). Code of Practice for general Structural Design and loadings for buildings, *Standards Association of New Zealand*, Wellington, 100 pp.

Ocal, N. (1968). Turkiyenin sismisitesi ve zelzele cograyasi, *Publ. Istanb. Kandili Rasathn.*, no. 8, Istambul.

Oesterle, R.G., Fiorato, A.E., Aristizabal-Ochoa, J.D. and Corley, W.G. Hysteretic Response of Reinforced Concrete Structural Walls. *ACI SP-63, Reinforced Concrete Structures Subjected to Wind and Earthquake Forces*. American Concrete Institute. pp. 243-74.

Ohkubo, M. (1991). Current Japanese System on Seismic Capacity and Retrofit Techniques for existing Reinforced Concrete Buildings and Post-Earthquake Damage Inspection and Restoration Techniques. *University of California*, San Diego, La Jolla, California.

Park, R. and Paulay, T. (1975). *Reinforced Concrete Structures*, John Wiley and sons, New York, 769 pp.

Paulay, T. (1991). Experimental Studies in New Zealand of Seismic Shear Effects, *Concrete Shear in Earthquake*, Elservier Applied Science, pp. 24-33.

Paulay, T. (1991). Seismic Design Strategies for Shear Resistance in Reinforced Concrete Structures, *Concrete Shear in Earthquake*, Elsevier Applied Science, pp. 397-418.

Paulay, T. and Priestly, M.J.N. (1992). *Seismic Design of Reinforced Concrete and Masonry Buildings*. John Wiley and sons, New York, 744 pp.

PCA-UBC (1992). Design of Concrete Buildings for Earthquake and Wind Forces. *Portland Cement Association and the International Conference of Building Officials*, 425 pp.

Pilakoutas, K. (1990). Earthquake-Resistant Design of RC Walls, *PhD Thesis, Engineering Seismology and Earthquake Engineering Section, Imperial College*, London, 360 pp.

Pilakoutas, K. and Elnashai, A.S. (1991). Seismic design of ductile RC members. *Earthquake, Blast and Impact*, Elsevier Applied Science, pp. 510-520.

Pinar, N. and Lahn, E. (1952). Turkiye depremleri izahli Katalogu, *Publ. Yapi ve Imar Isleri Reilsl.*, vol. 6, nr. 36, Ankara.

Pincheira, J.A. and Jirsa, J.O. (1992). Post-tensioned bracing for seismic retrofit of RC frames. *Tenth World Conference on Earthquake Engineering*, vol. 9, Balkema. pp. 5199-204.

Priestley, M.J.N, Seible, F. and Chai, Y.H. (1992). Seismic retrofit of bridge columns using steel jackets. *Tenth World Conference on Earthquake Engineering*, vol. 9, Balkema. pp. 5285-90.

Proceedings of the First Seminar on Repair and Retrofit of structures, (1980). *US/Japan Cooperative Earthquake Research Program*, Dept. of Civil Engineering, University of Michigan.

Proceedings of the Third Seminar on Repair and Retrofit of Structures, (1982). *US/Japan Cooporative Earthquake Research Program*, Dept. of Civil Engineering, University of Michigan.

Saatcioglu, M. (1991). Hysteretic Shear Response of low-Rise Walls. *Concrete Shear in Earthquake*, Elsevier Applied Science. pp. 105-114.

Schutt, W.R. (1992). Cathodic Protection of New High-Rise Buildings in Abu Dhabi. *Concrete International*, American Concrete Institute, Detroit, pp. 45-47.

Sica (1992). *Concrete Repair. Technical Information.* 250 pp.

Sugano, S. (1981). Seismic Strengthening of Existing Reinforced Concrete Buildings in Japan, *Bulletin of the New Zealand National Society for Earthquake Engineering*, vol. 14, No. 4.

Sugano, S. and Fujimura, M. (1980). Aseismic Strengthening of existing Reinforced Concrete Buildings, *Seventh world conference on Earthquake Engineering* Istanbul, Turkey.

Tankut, A.T. and Ersoy, U. (1992). Behaviour of Repaired/Strengthened Reinforced Concrete Structural Members. *ACI SP-128 Evaluation and Rehabilitation of Concrete Structures and Innovations in Design.* American Concrete Institute, Detroit, 1504 pp.

Tasai, A. (1992). Effective repair with resin for bond failure of RC members. *Tenth World Conference on Earthquake Engineering*, vol. 9, Balkema. pp. 5211-16.

Tassios, T.P. (1991). Chapter 4 Seismic Design of Concrete Structures, *Structures subjected to dynamic loading - Stability and Strength series*, Elsevier, pp. 115-65.

Teran, A. and Ruiz, J. (1992). Reinforced concrete jacketing of existing structures. *Tenth World Conference on Earthquake Engineering*, vol. 9, Balkema. pp. 5101-106.

Thewalt, C.R. and Stojadinovic B.I. (1992). Behaviour and retrofit of bridge outrigger beams. *Tenth World Conference on Earthquake Engineering*, vol. 9, Balkema. pp. 5291-96.

Trikha, D.N., Jain, S.C.and Hali, S.K. (1991). Repair and Strengthening of Damaged Concrete Beams. *Concrete International* Vol. 13 No. 6. American Concrete Institute, Detroit, pp. 53-59.

UBC 91 (1991). Uniform Building Code, *International Conference of Building Officials*, Whittier, California, 1050 pp.

United Nations Industrial Development Organisation (1983). Repair and Strengthening of Reinforced Concrete, Stone and Brick Masonary Buildings, Building *Construction Under Seismic Conditions in the Balkan Region*, Vienna, Vol. 5.

Valluvan, R., Kreger, M.E. and Jirsa, J.O. (1992). Strengthening of column splices in infilled shear walls. *Tenth World Conference on Earthquake Engineering*, vol. 9, Balkema. pp. 5121-26.

Valluvan, R., Kreger, M.E. and Jirsa, J.O. (1992). Strengthening of column splices in infilled shear walls. *Tenth World Conference on Earthquake Engineering*, vol. 9, Balkema. pp. 5121-26.

Warner, J. (1977). Methods for repairing and retrofitting (Strengthening) Existing Buildings, Workshop on Earthquake-Resistant Reinforced Concrete Building Construction. University of California, Berkely, Vol. II, pp. 789-819.

Wood, S.L. (1991). Observed Behaviour of Slender Reinforced Concrete walls Subjected to Cyclic Loading. *ACI SP-127, Earthquake-Resistant Concrete Structures Inelastic Response and Design*. American Concrete Institute, Detroit pp.453-78.

Yamamoto, T. (1992). FRP strengthening of RC columns for seismic retrofitting. *Tenth World Conference on Earthquake Engineering*, vol. 9, Balkema. pp. 5205-10.

Yanez, F.V., Park, R. and Paulay, T. (1992). Seismic behaviour of walls with irregular openings. *Tenth World Conference on Earthquake Engineering*, vol. 6, Balkema. pp. 3303-308.

Yoshimura, K., Kikuchio, K. and Kuroki, M. (1992). Seismic Shear Strengthening Method for existing Reinforced Concrete Short Columns. *ACI SP-128, Evaluation and Rehabilitation of Concrete Structures and Innovations in Design*. American Concrete Institute, Detroit, 1504 pp.

Zuhua, L., Kreger, M.E. and Jirsa, J.O. (1991). Evaluation of Slab-Beam-Column Connections Subjected to Bi-directional Loading, *ACI SP-123, Design of Beam-Column Joints for seismic resistance*. American Concrete Institute, Detroit, pp. 39-77.

Appendix AI: Force-Displacement Test Results

AI.1 : Force Displacement for SWR4

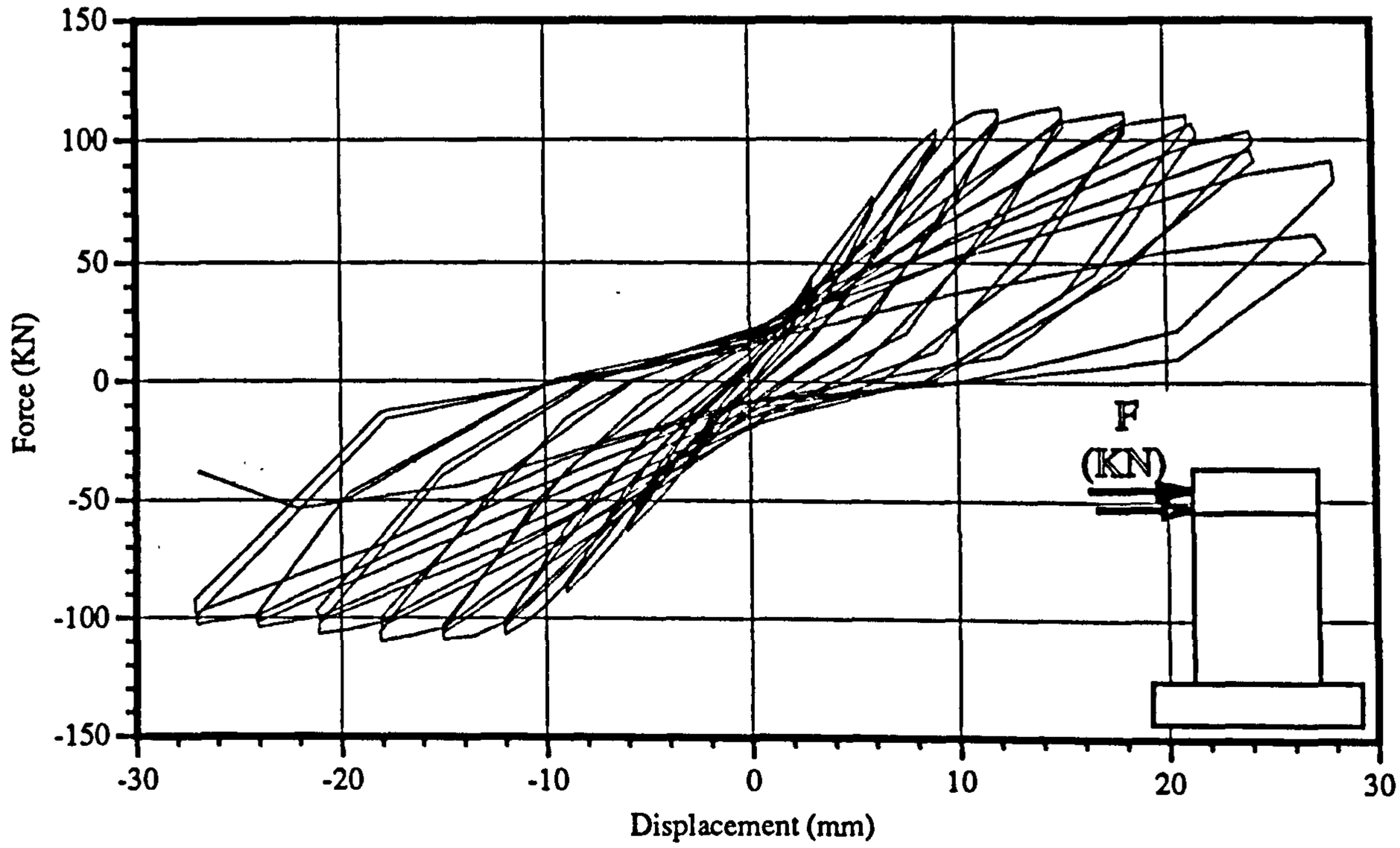


Fig. AI. (R4) 1 Force - Displacement for SWR4 at Node 1

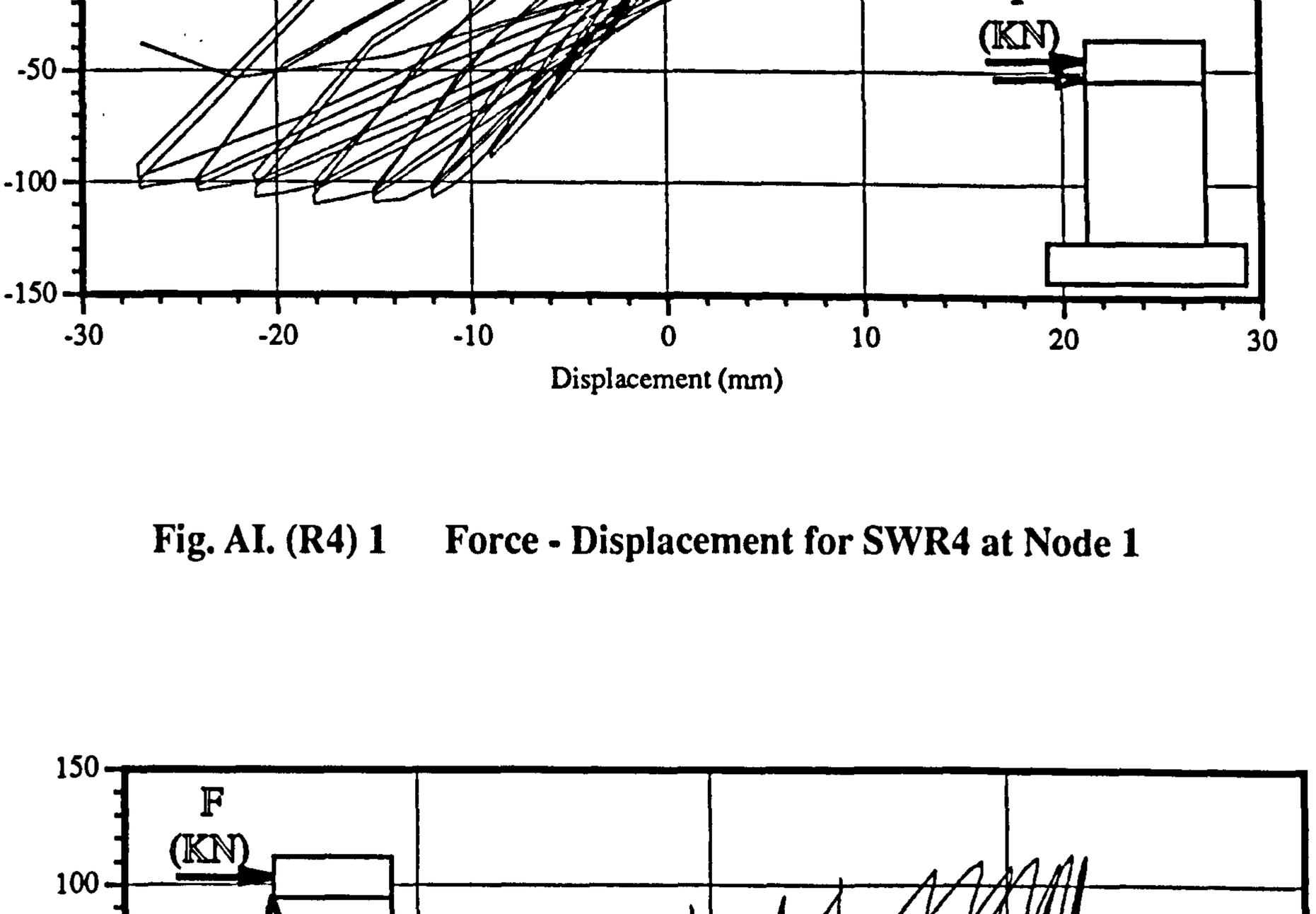


Fig. AI. (R4) 2 Force - Displacement for SWR4 at Node 2

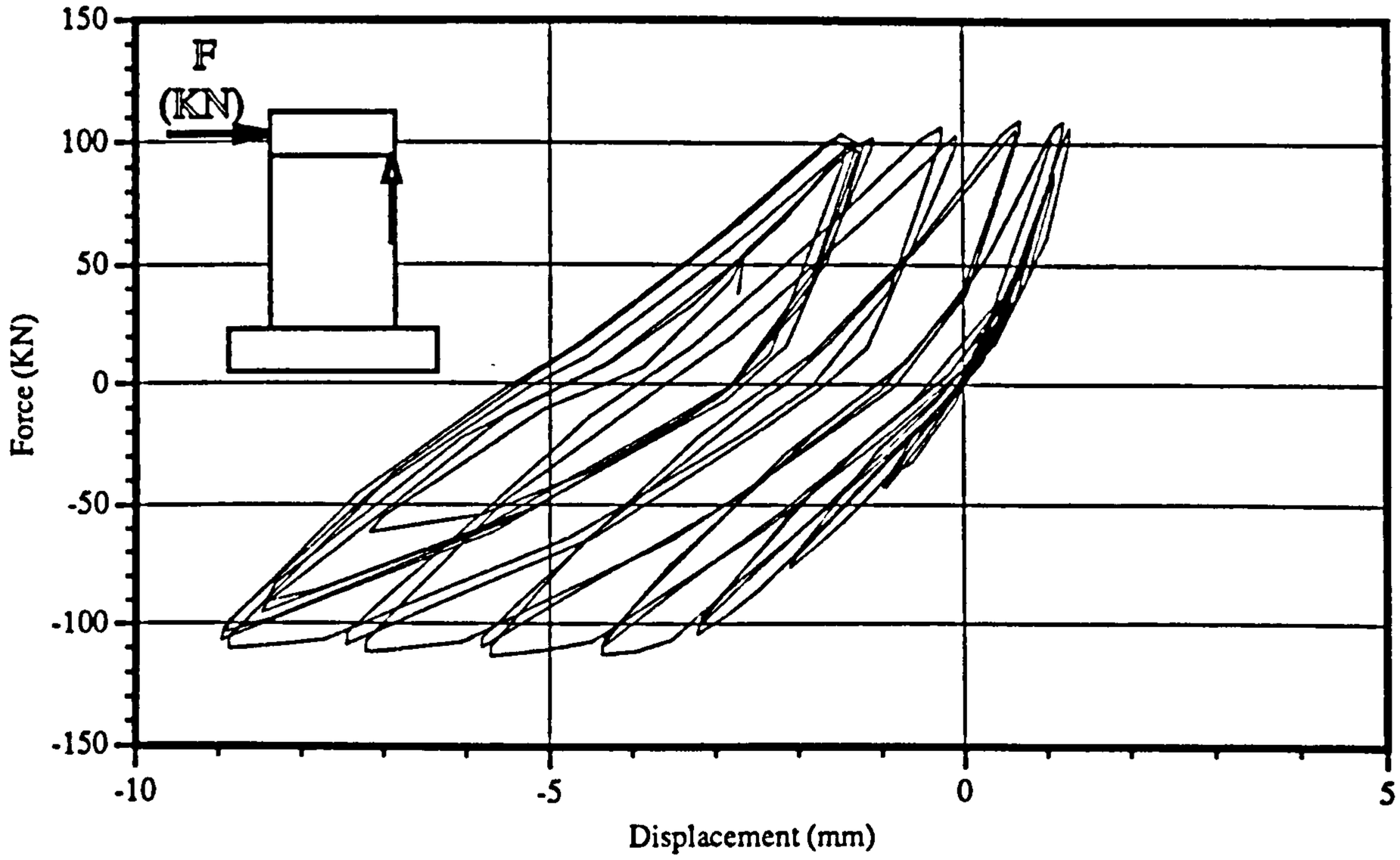


Fig. AI. (R4) 3 Force - Displacement for SWR4 at Node 3

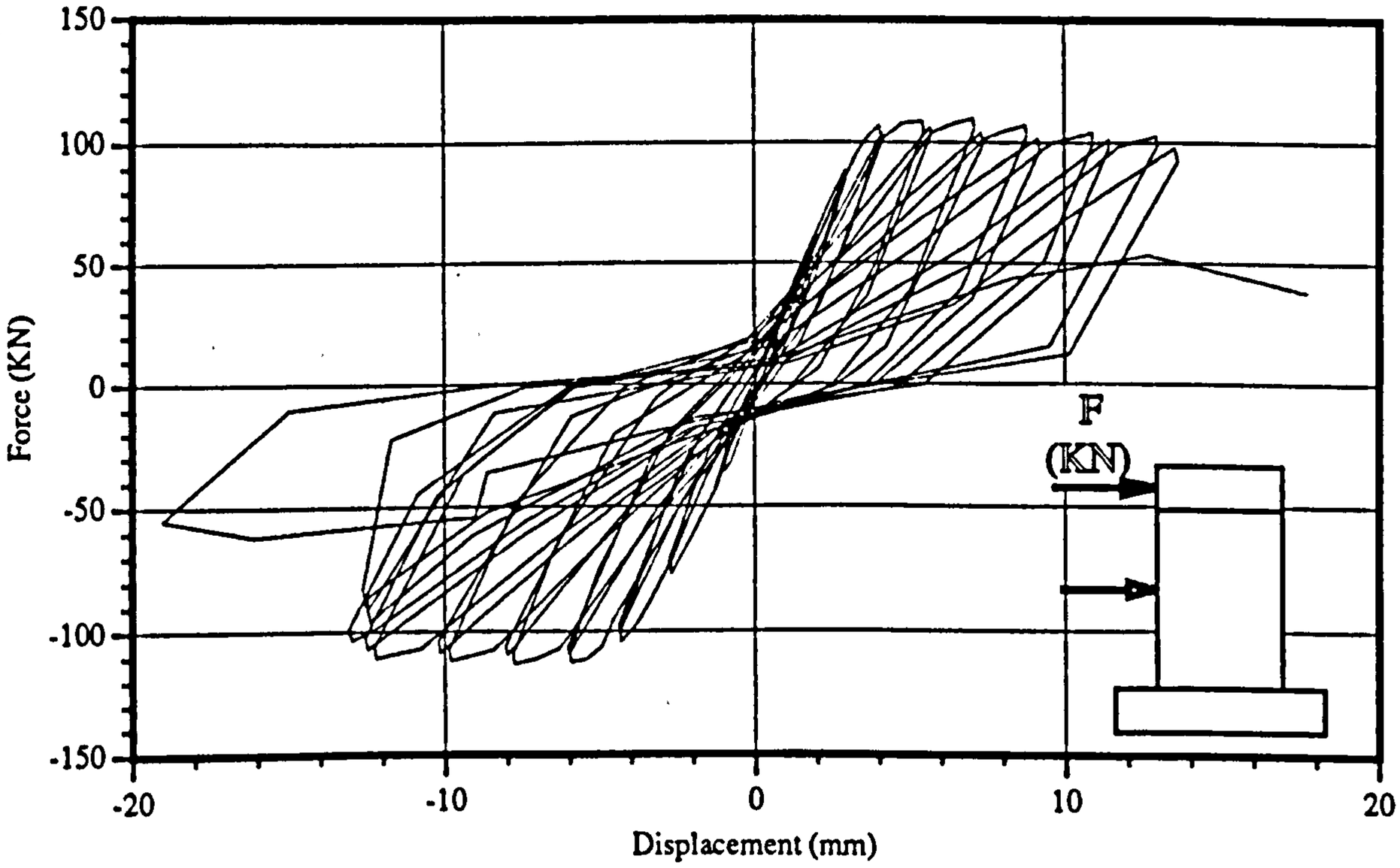


Fig. AI. (R4) 4 Force - Displacement for SWR4 at Node 4

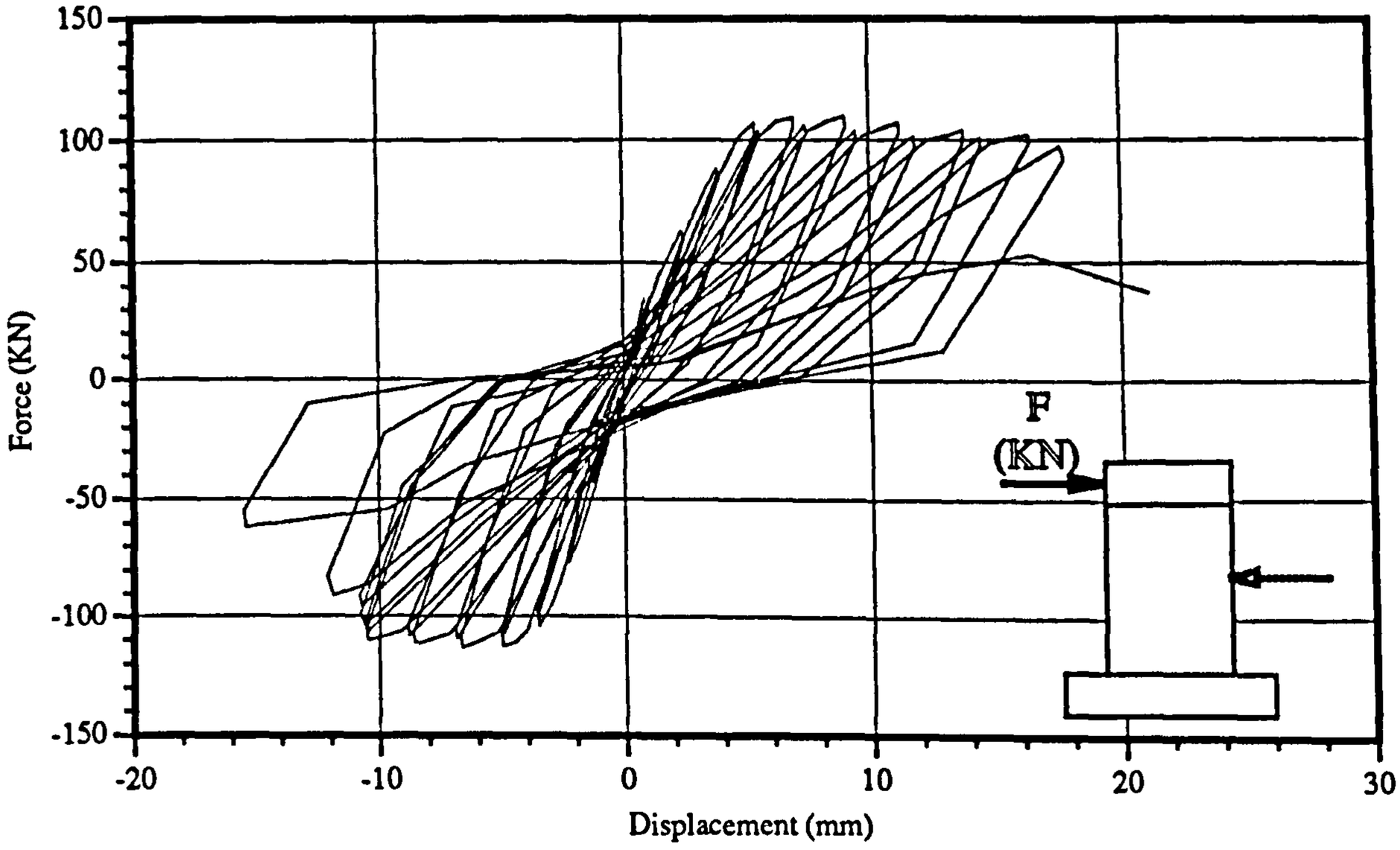


Fig. AI. (R4) 5 Force - Displacement for SWR4 at Node 5

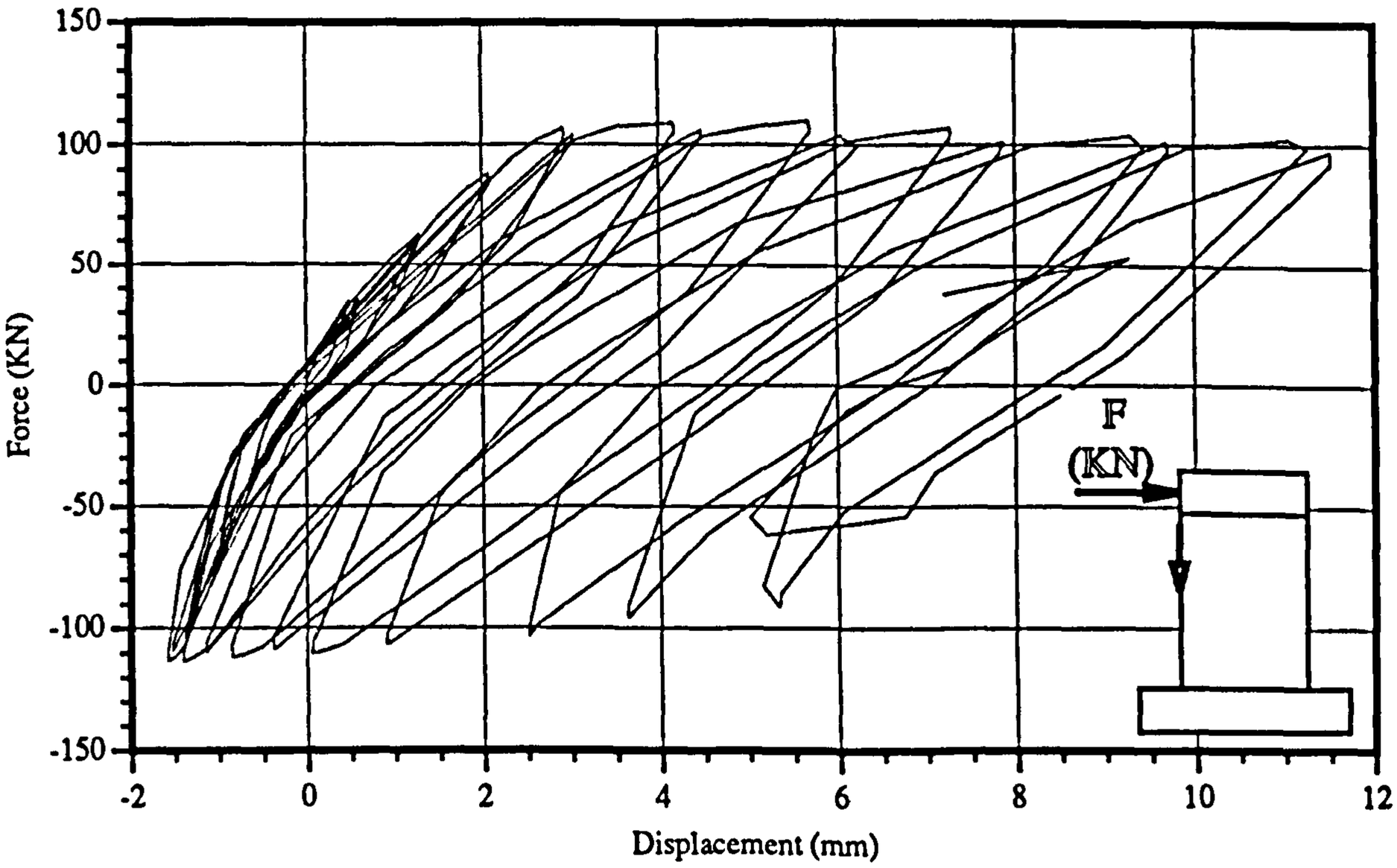


Fig. AI. (R4) 6 Force - Displacement for SWR4 at Node 6

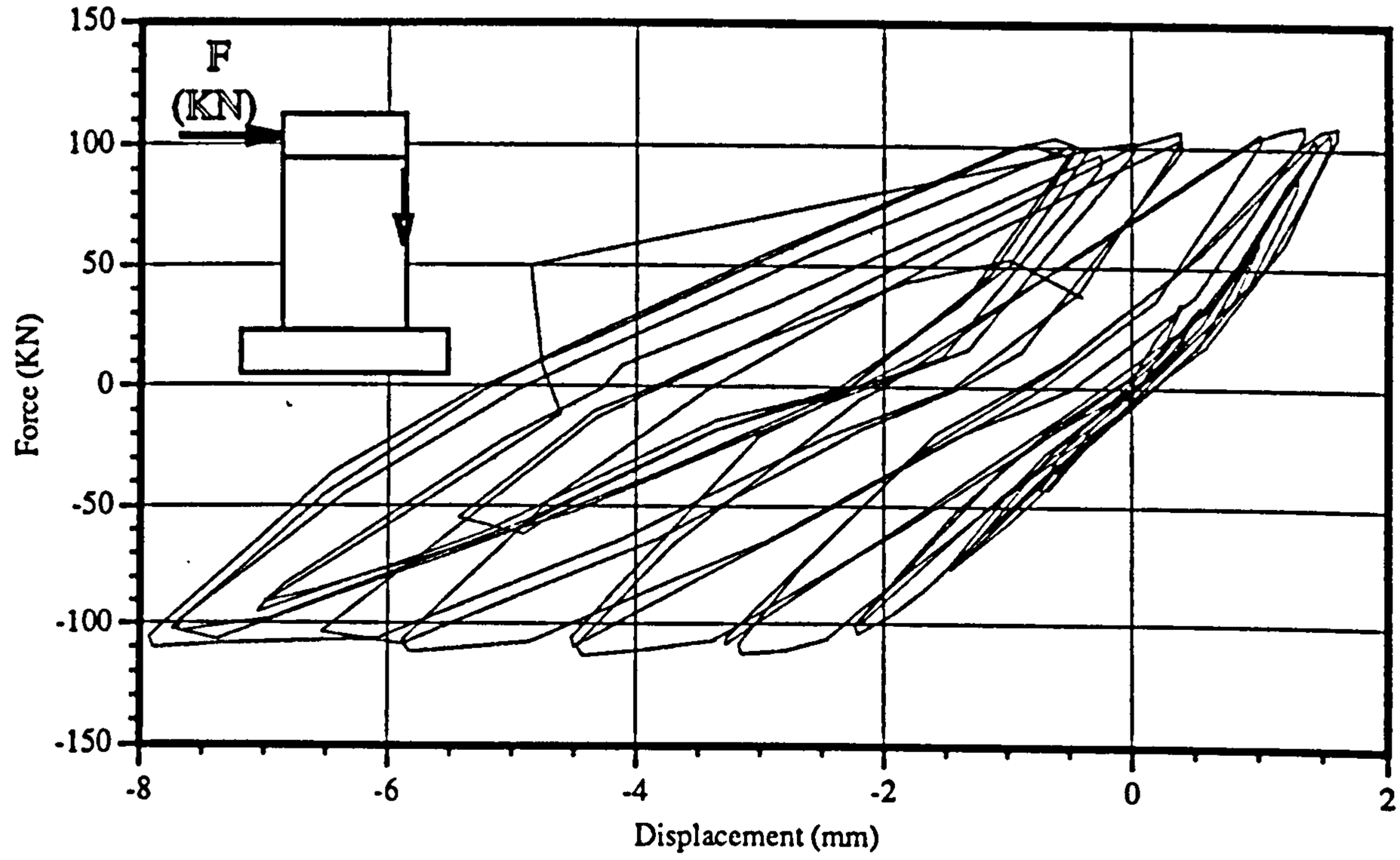


Fig. AI. (R4) 7 Force - Displacement for SWR4 at Node 7

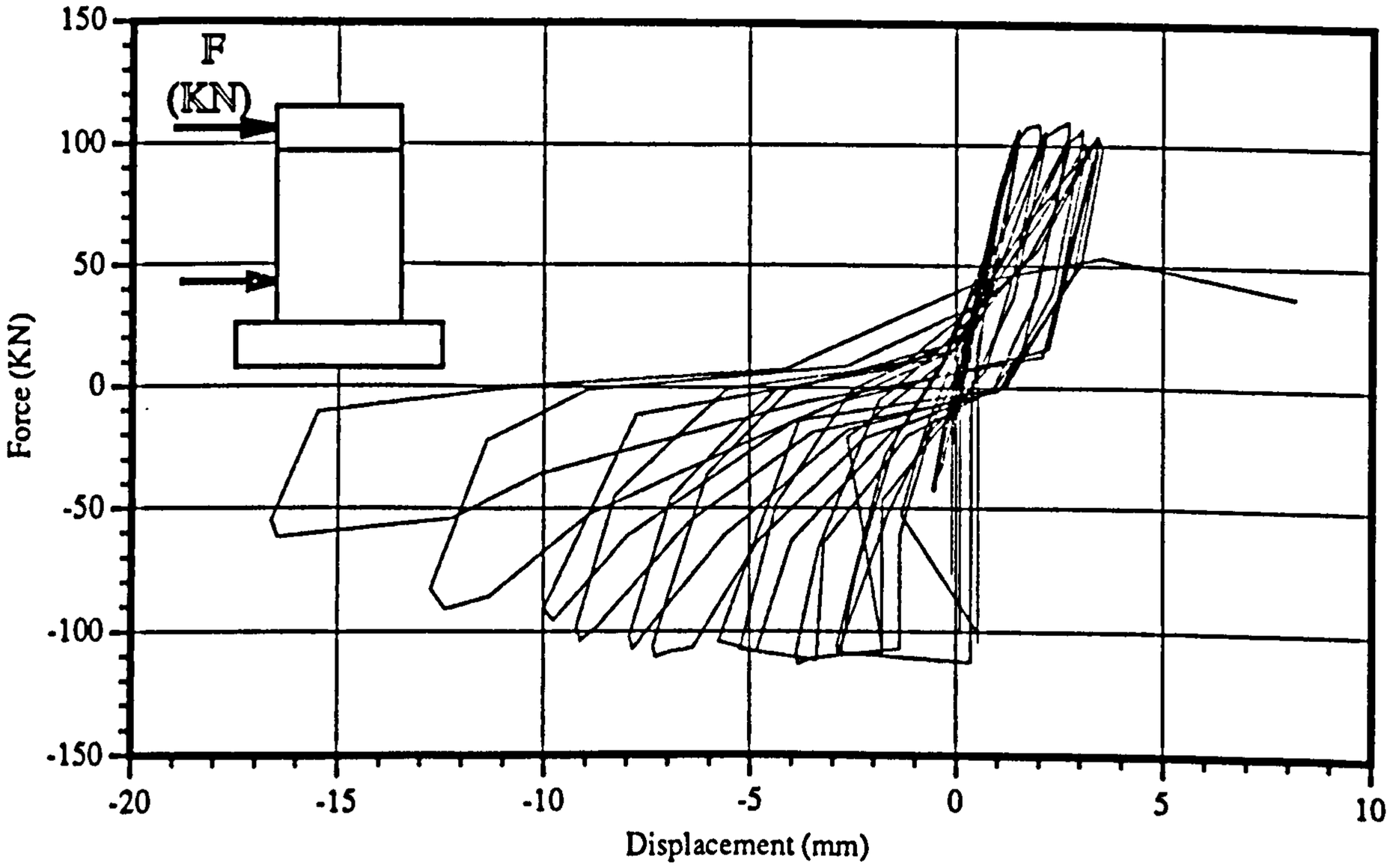


Fig. AI. (R4) 8 Force - Displacement for SWR4 at Node 8

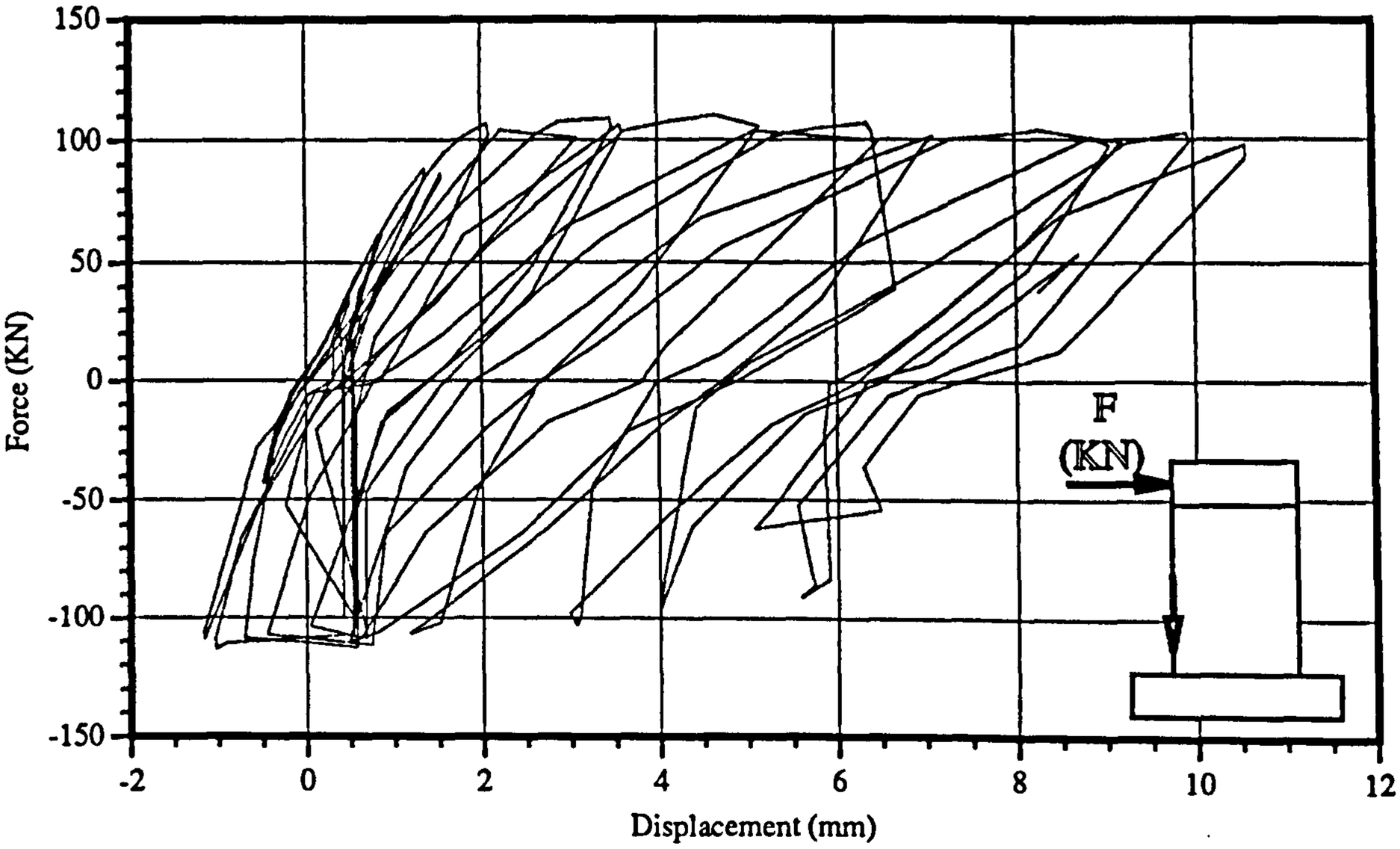


Fig. AI. (R4) 9 Force - Displacement for SWR4 at Node 9

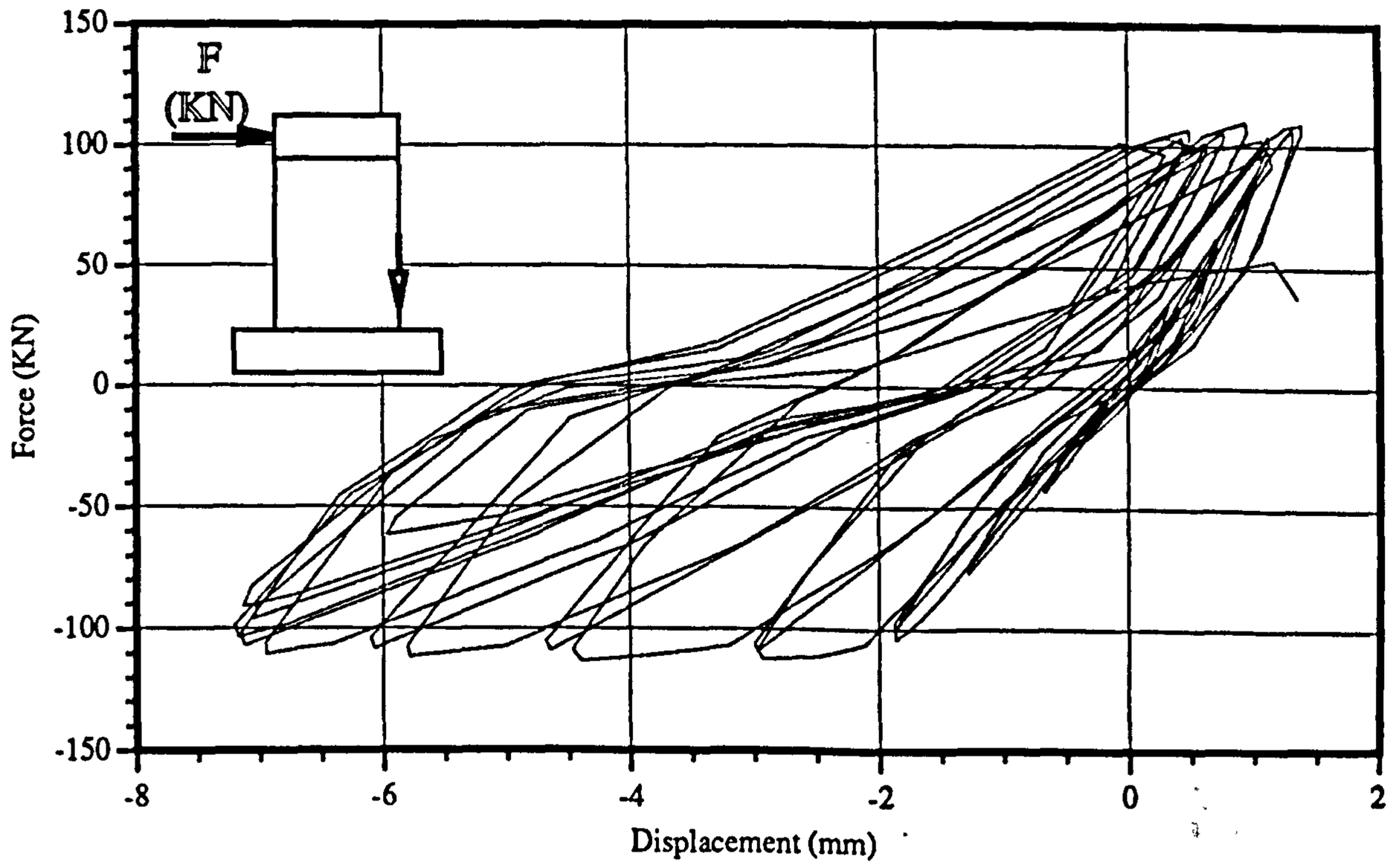


Fig. AI. (R4) 10 Force - Displacement for SWR4 at Node 10

AI.2 : Force Displacement for SWR5

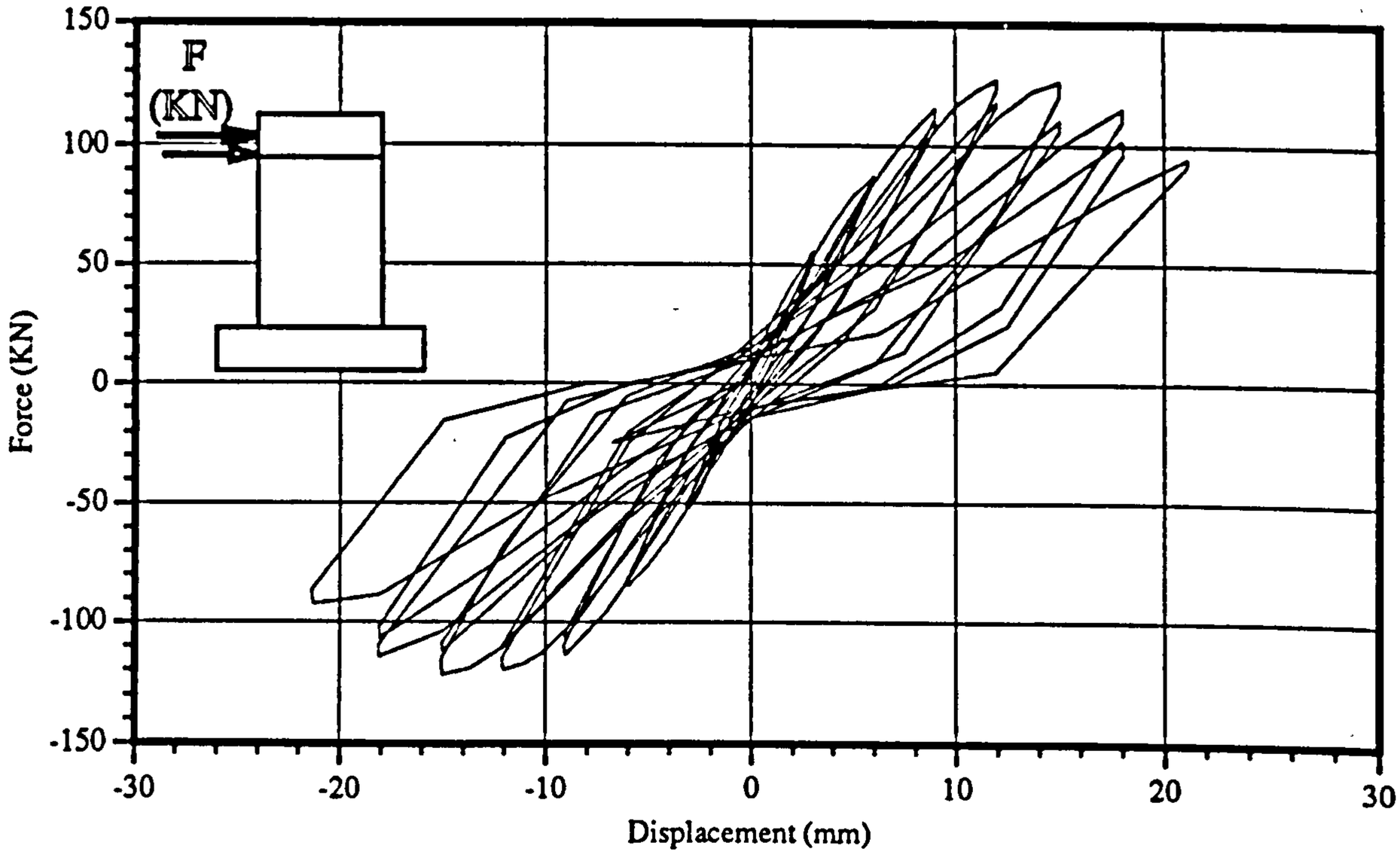


Fig. AI. (R5) 1 Force - Displacement for SWR5 at Node 1

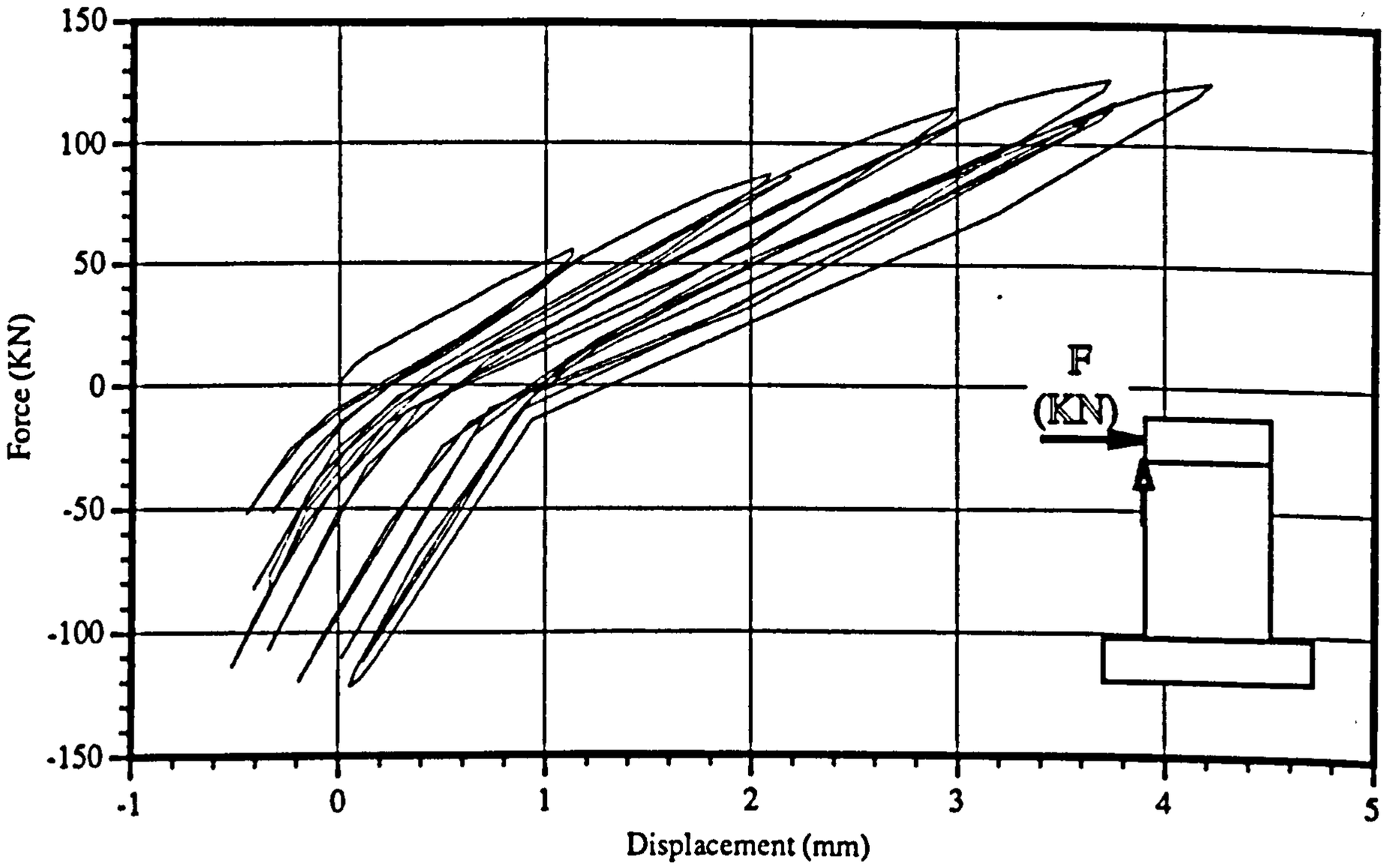


Fig. AI. (R5) 2 Force - Displacement for SWR5 at Node 2

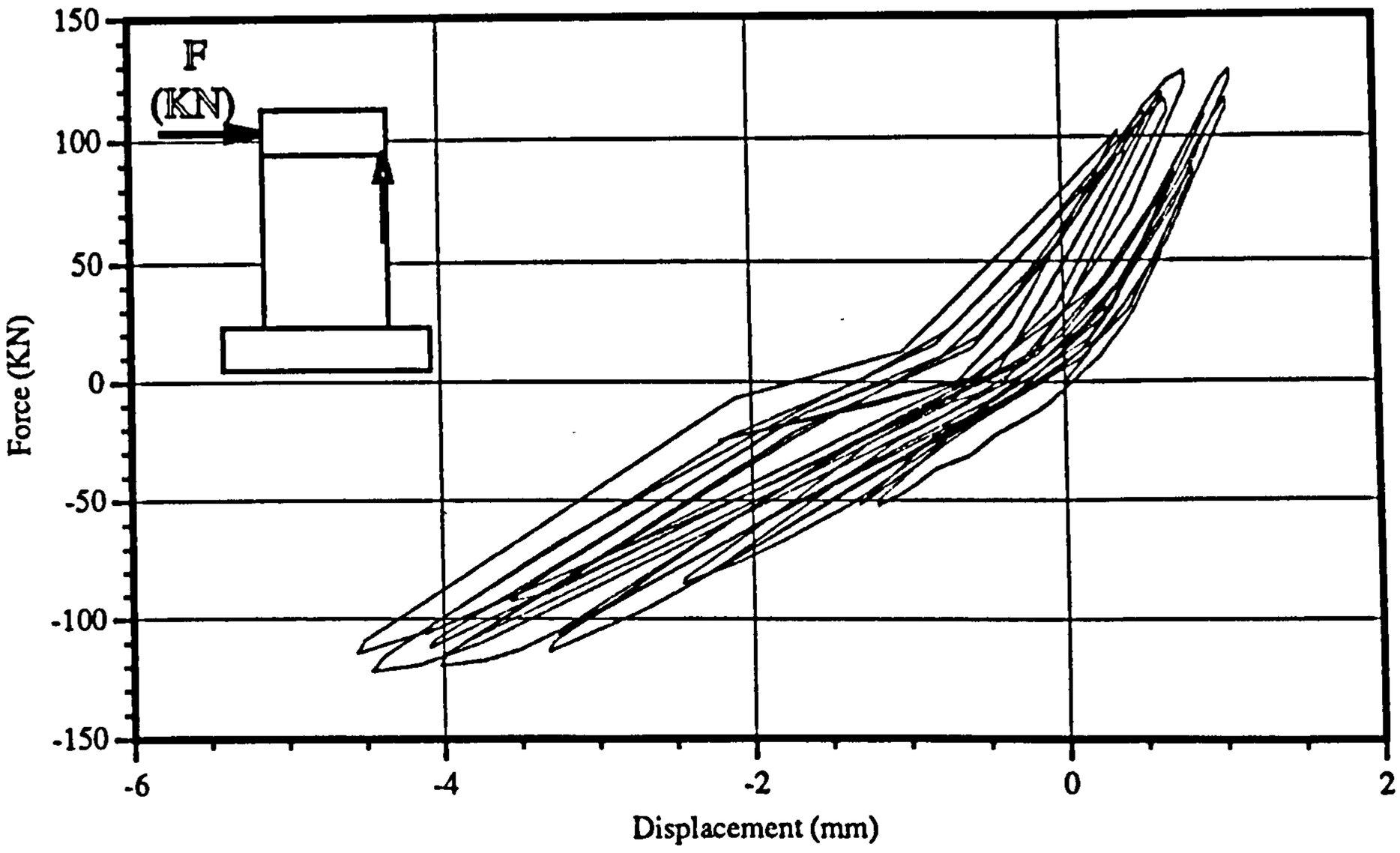


Fig. AI. (R5) 3 Force - Displacement for SWR5 at Node 3

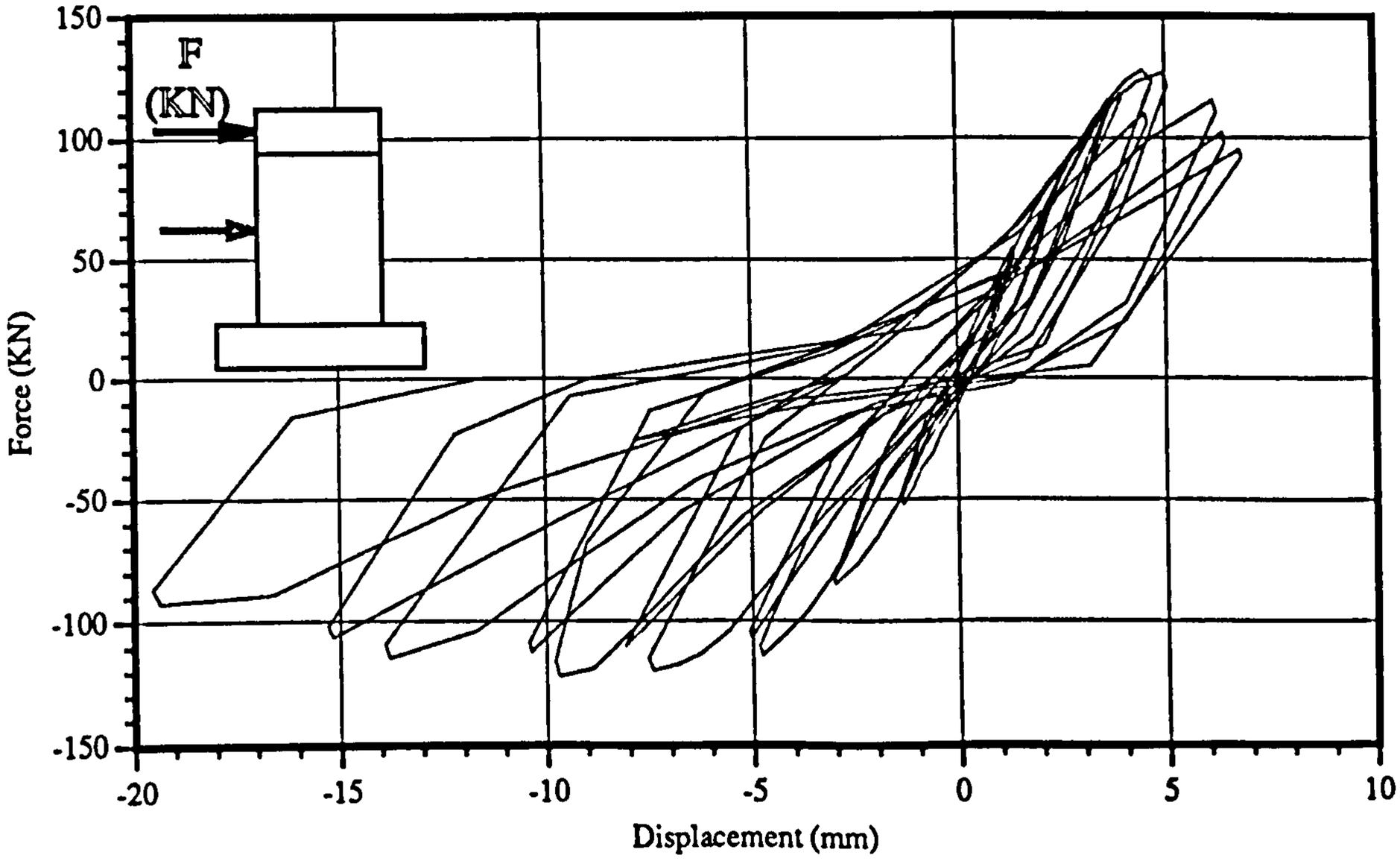


Fig. AI. (R5) 4 Force - Displacement for SWR5 at Node 4

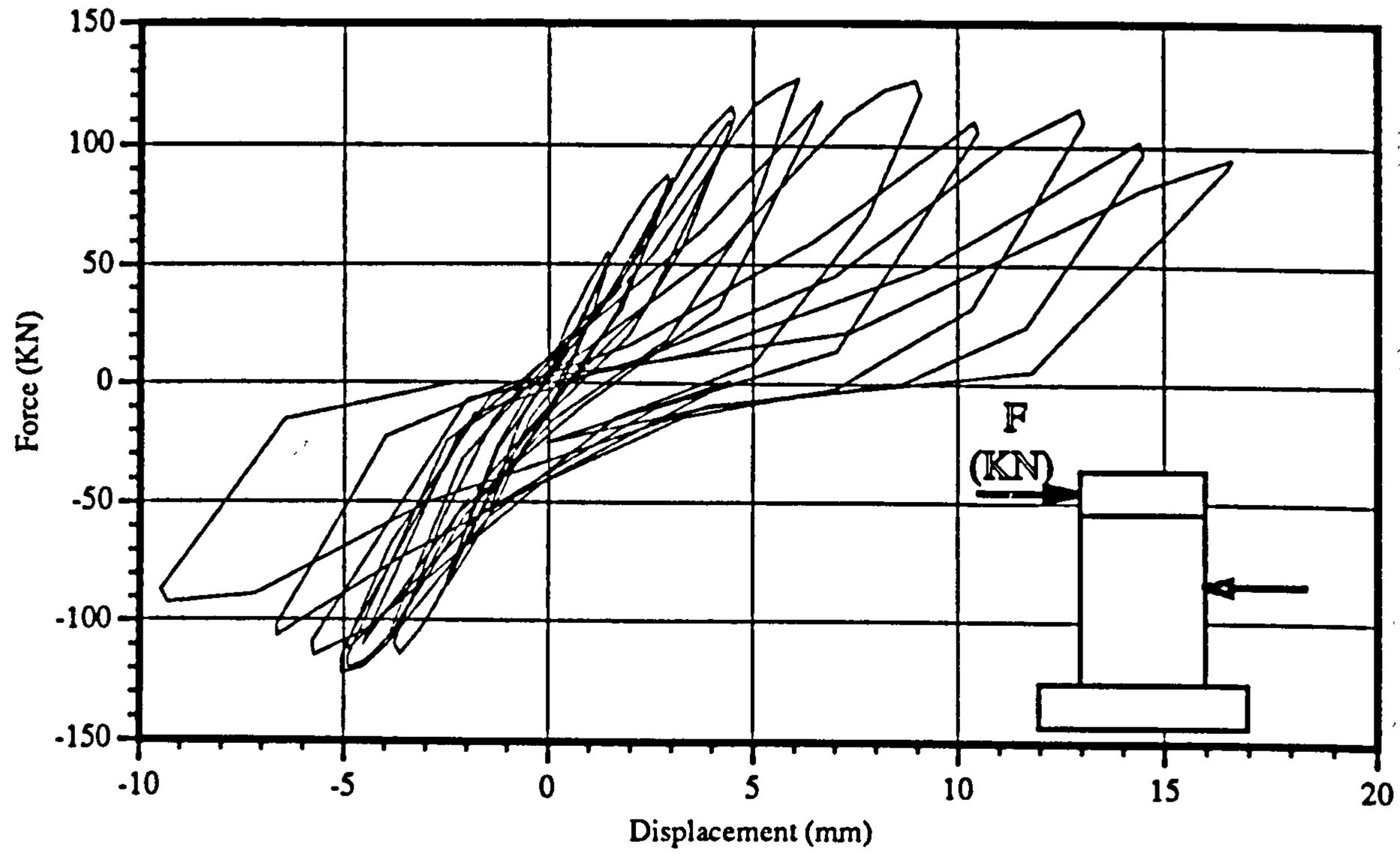


Fig. AI. (R5) 5 Force - Displacement for SWR5 at Node 5

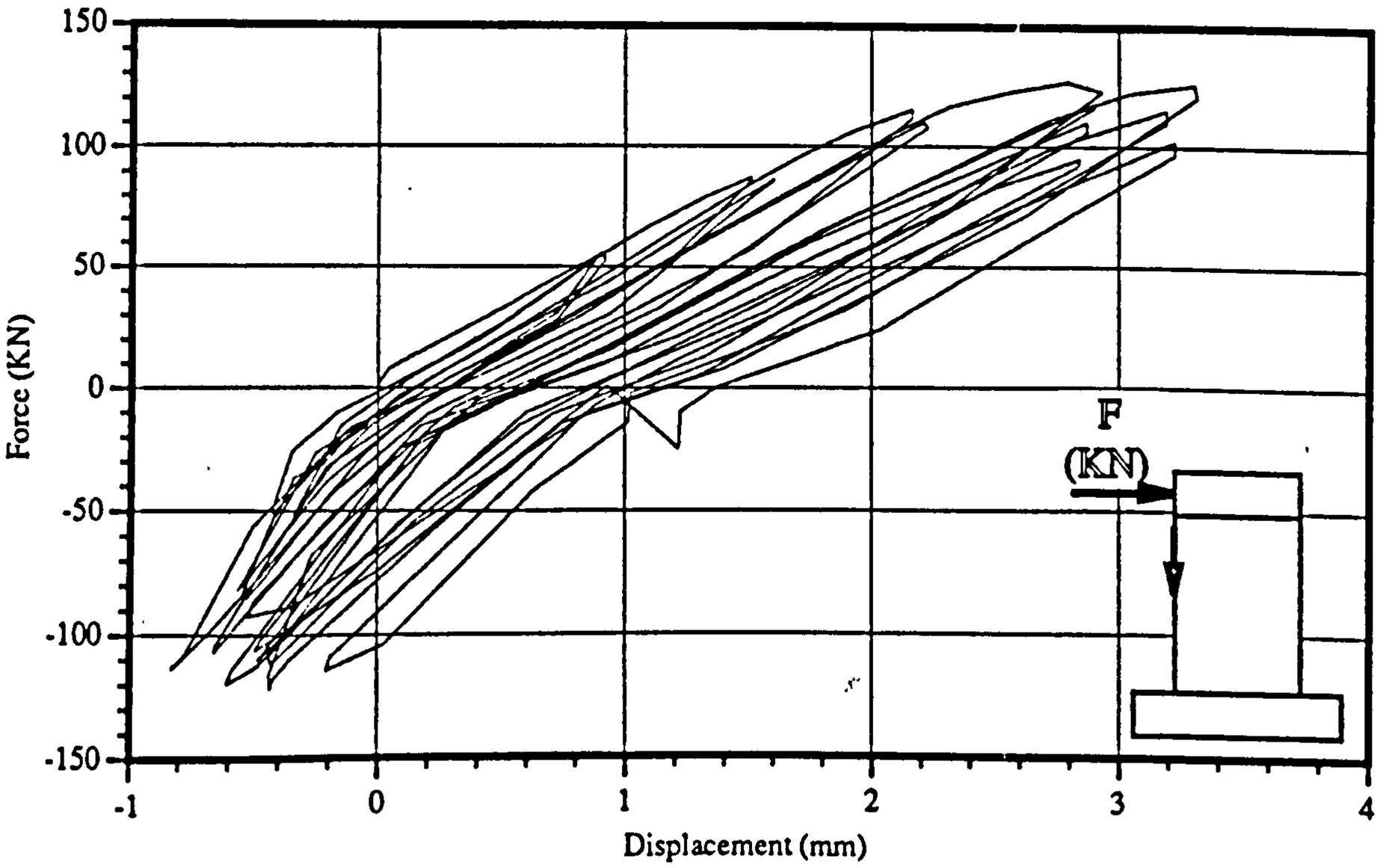


Fig. AI. (R5) 6 Force - Displacement for SWR5 at Node 6

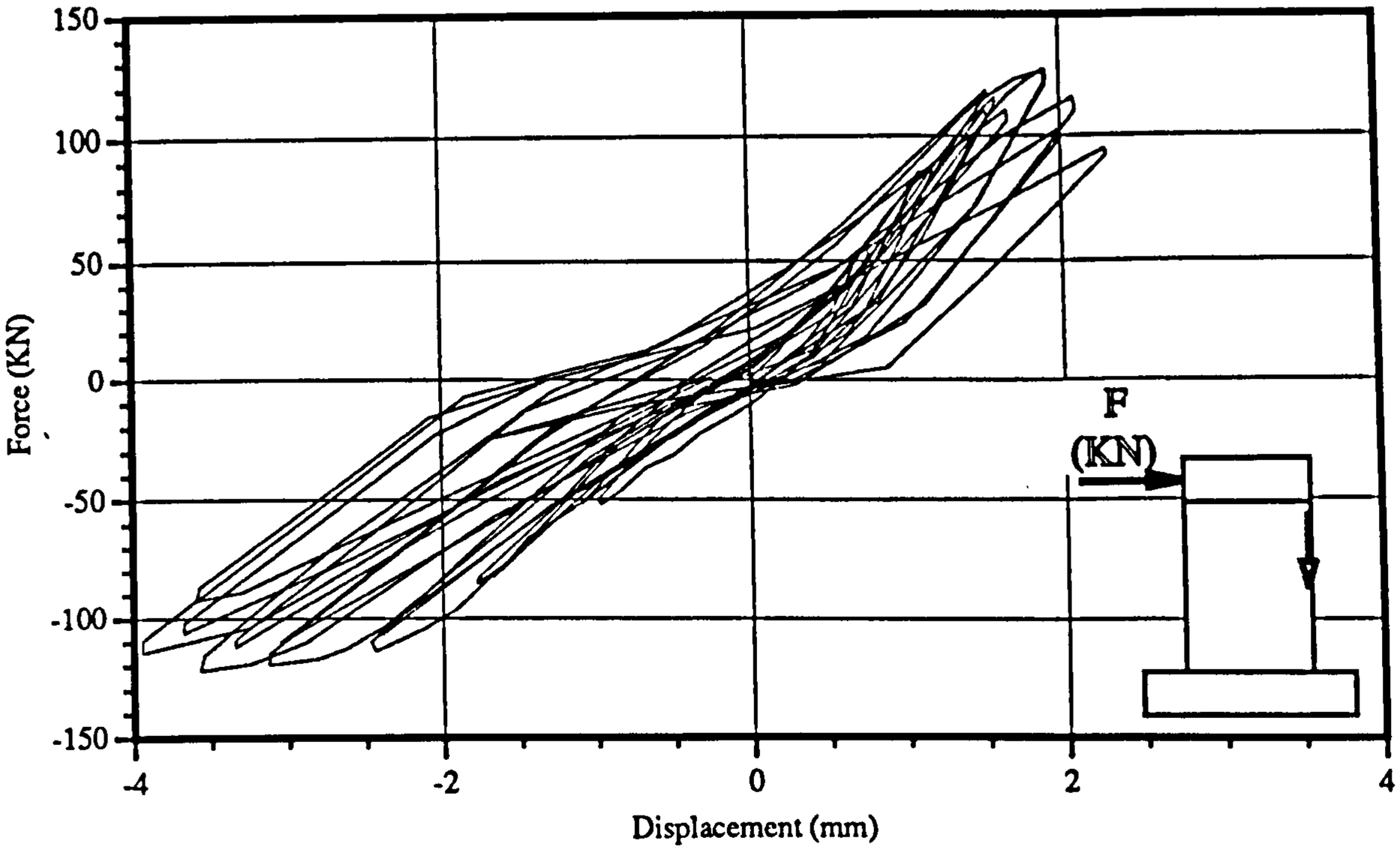


Fig. AI. (R5) 7 Force - Displacement for SWR5 at Node 7

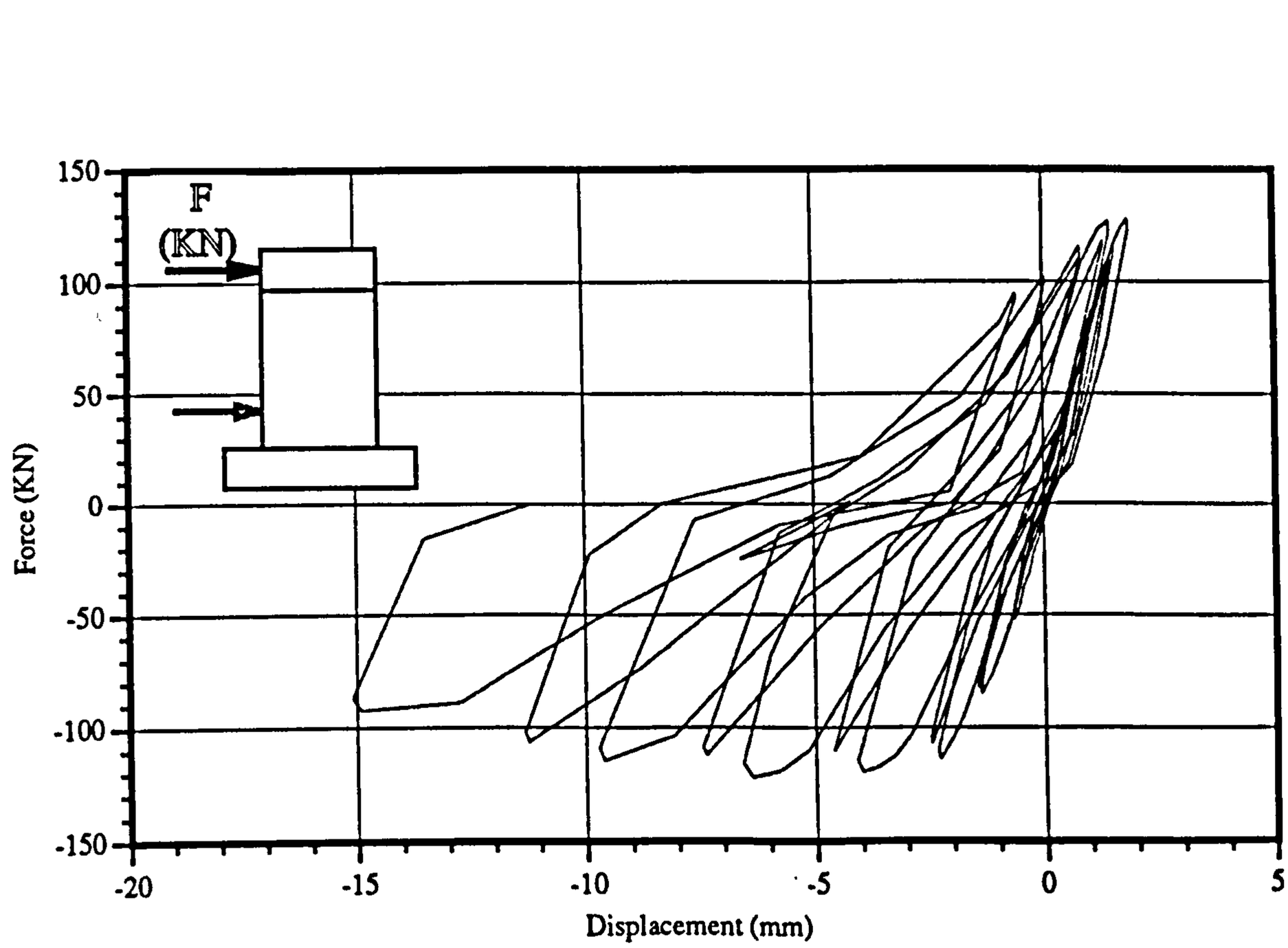


Fig. AI. (R5) 8 Force - Displacement for SWR5 at Node 8

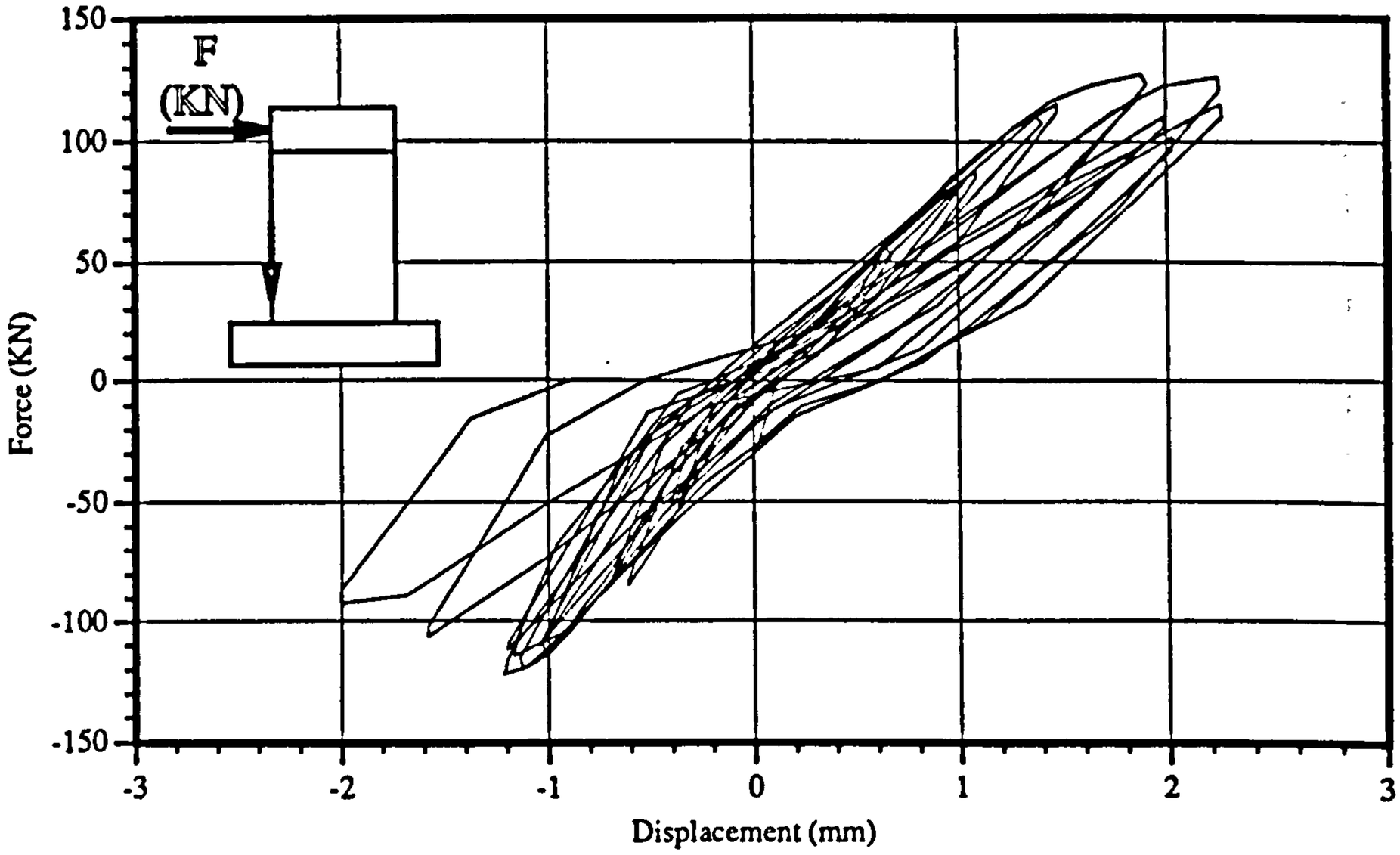


Fig. AI. (R5) 9 Force - Displacement for SWR5 at Node 9

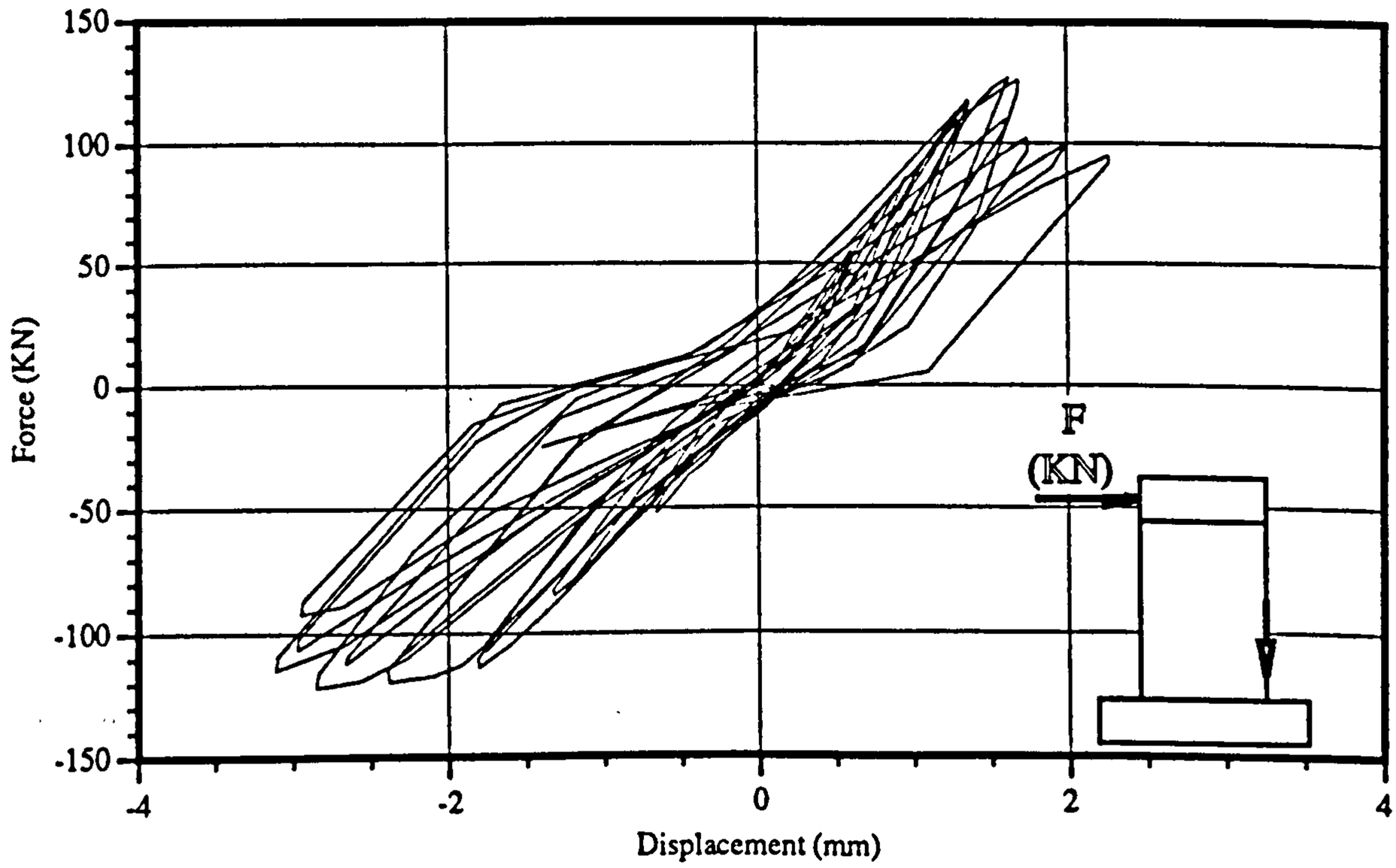


Fig. AI. (R5) 10 Force - Displacement for SWR5 at Node 10

AI.3 : Force Displacement for SWR7

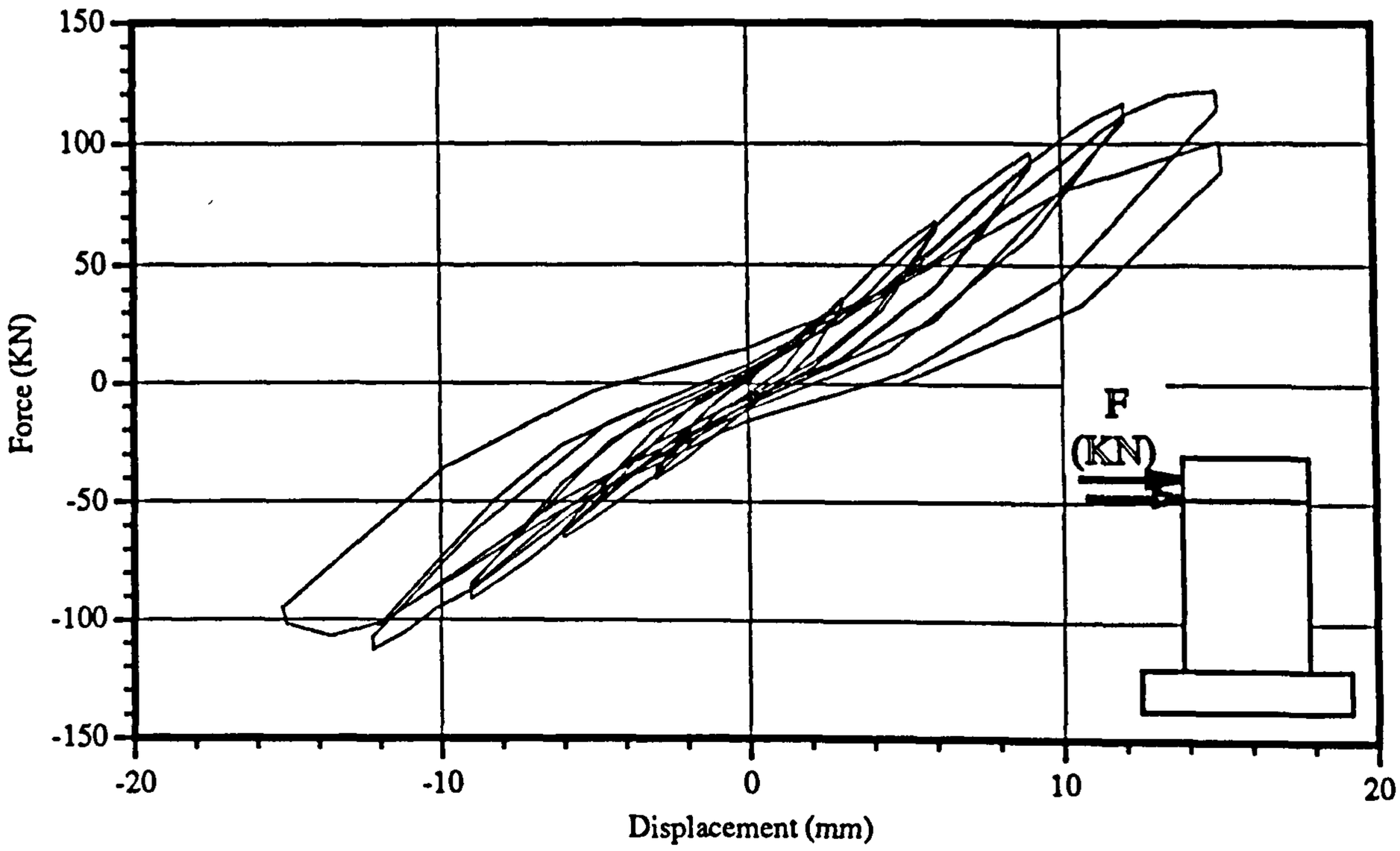


Fig. AI. (R7) 1 Force - Displacement for SWR7 at Node 1

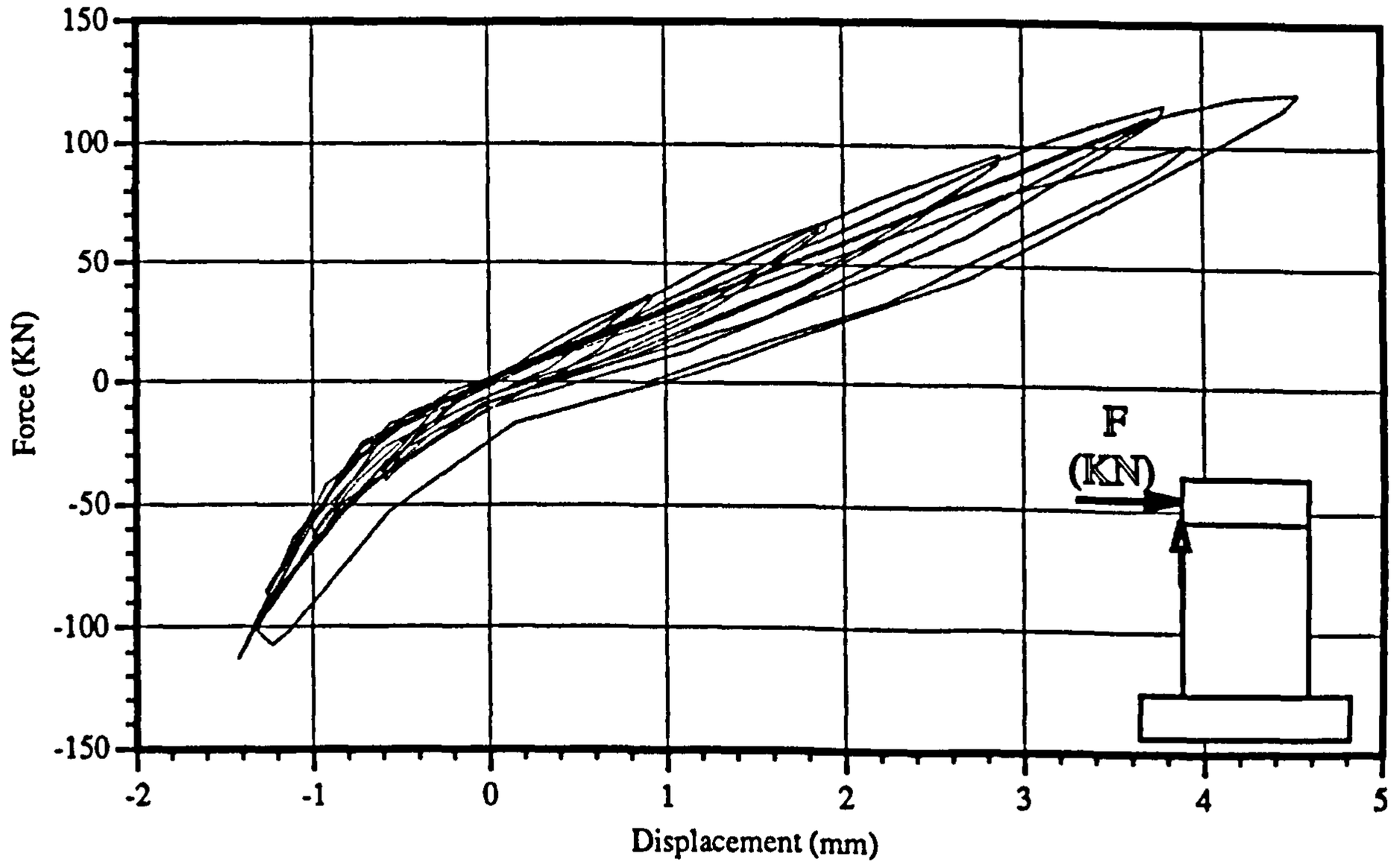


Fig. AI. (R7) 2 Force - Displacement for SWR7 at Node 2

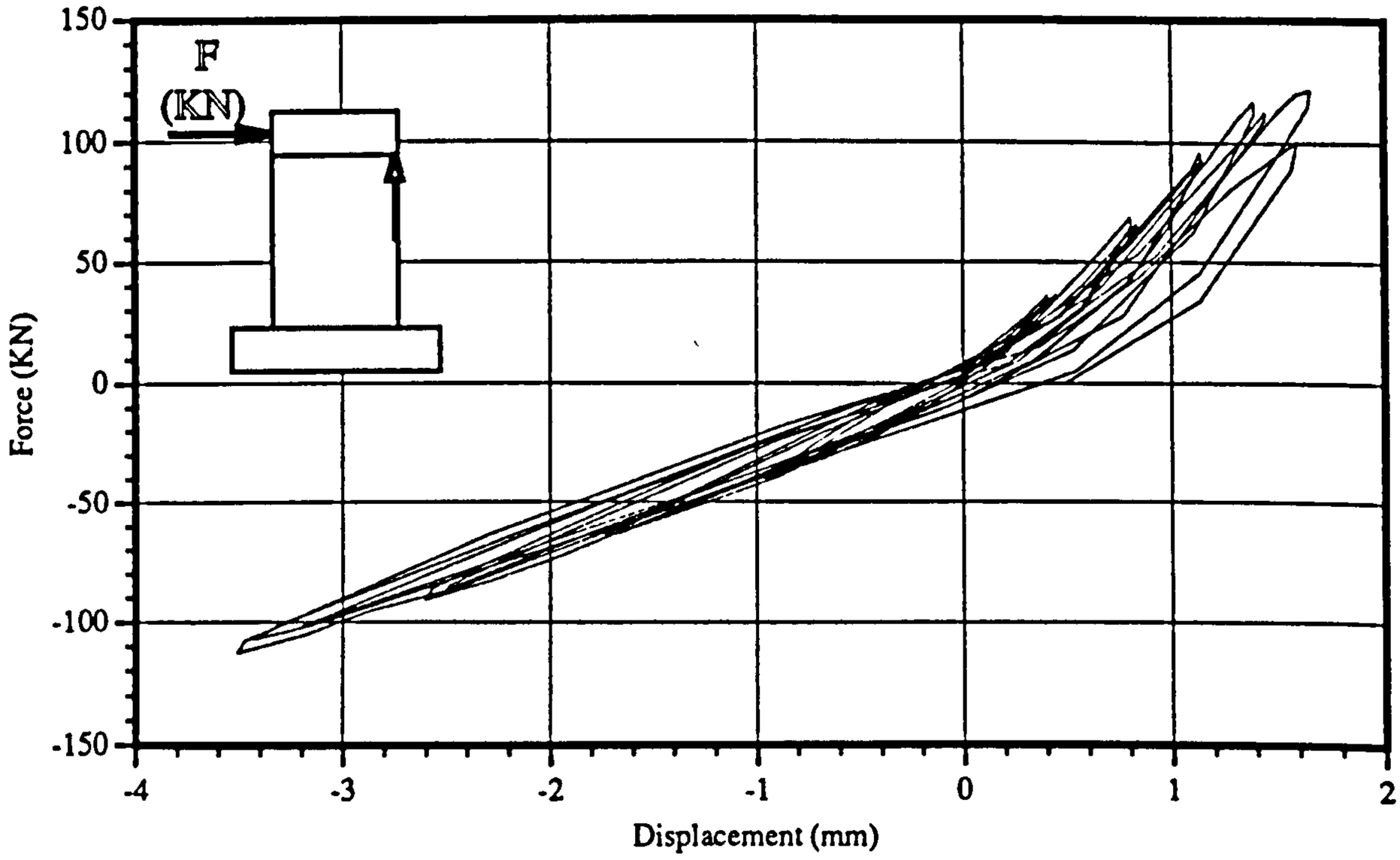


Fig. AI. (R7) 3 Force - Displacement for SWR7 at Node 3

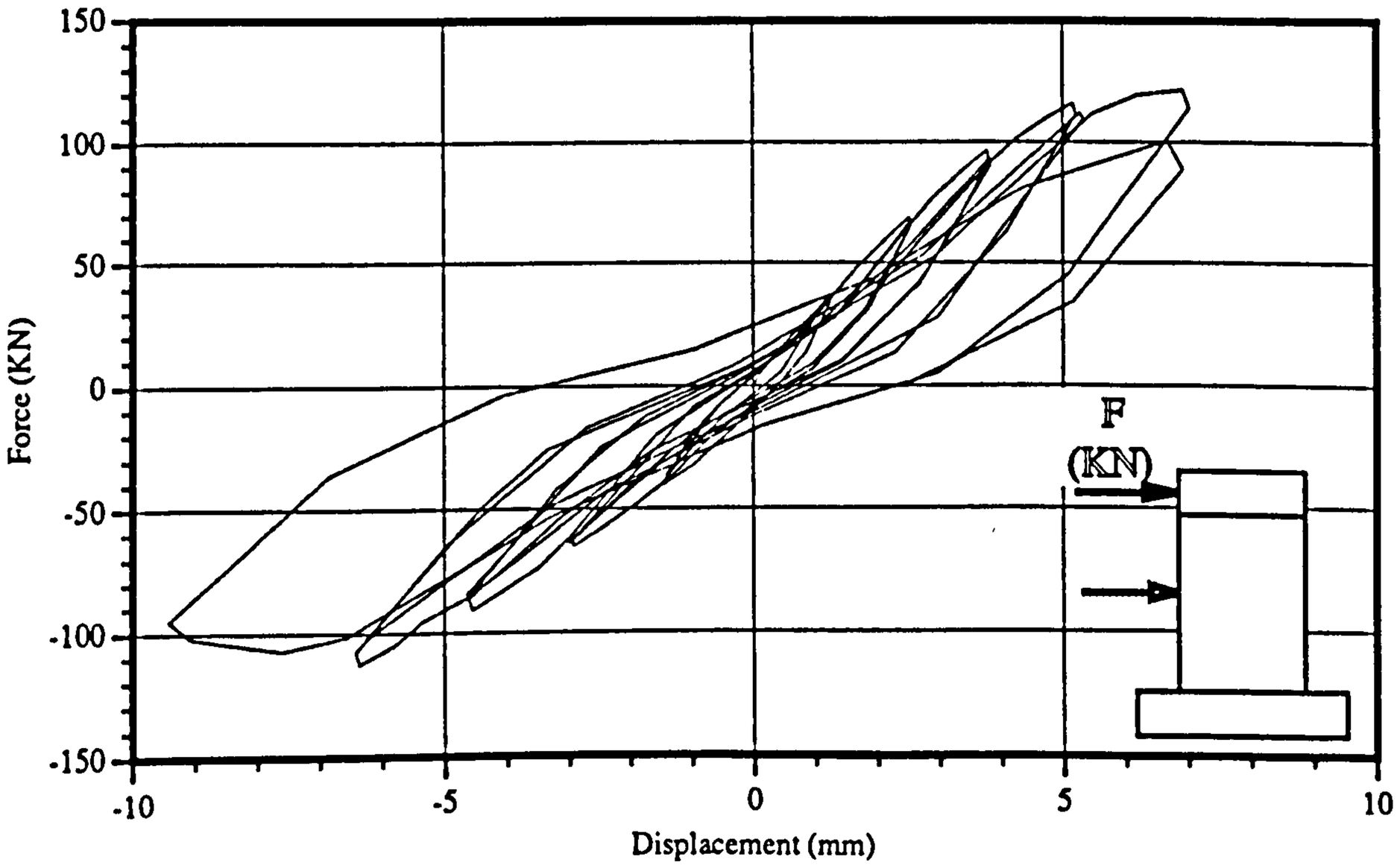


Fig. AI. (R7) 4 Force - Displacement for SWR7 at Node 4

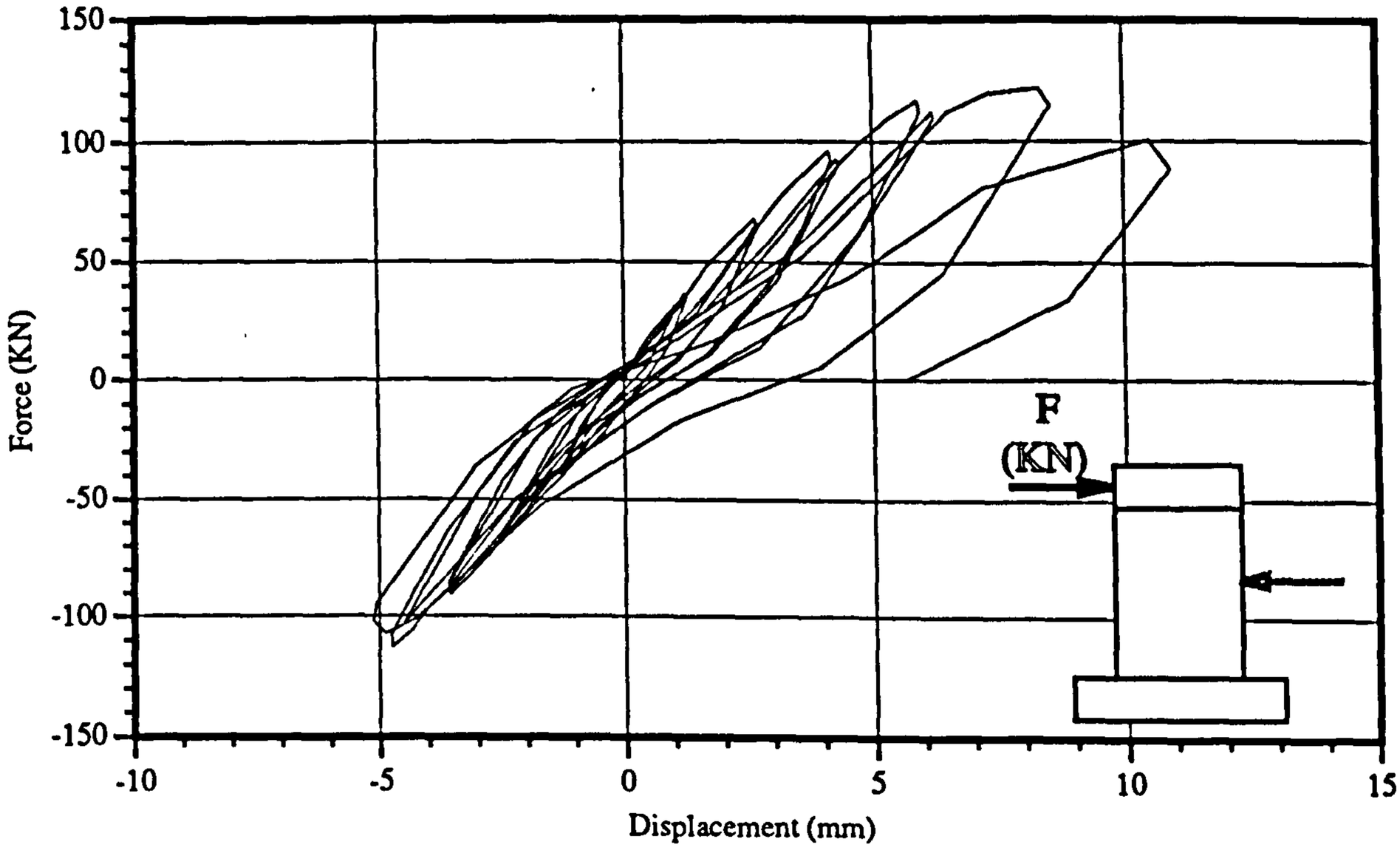


Fig. AI. (R7) 5 Force - Displacement for SWR7 at Node 5

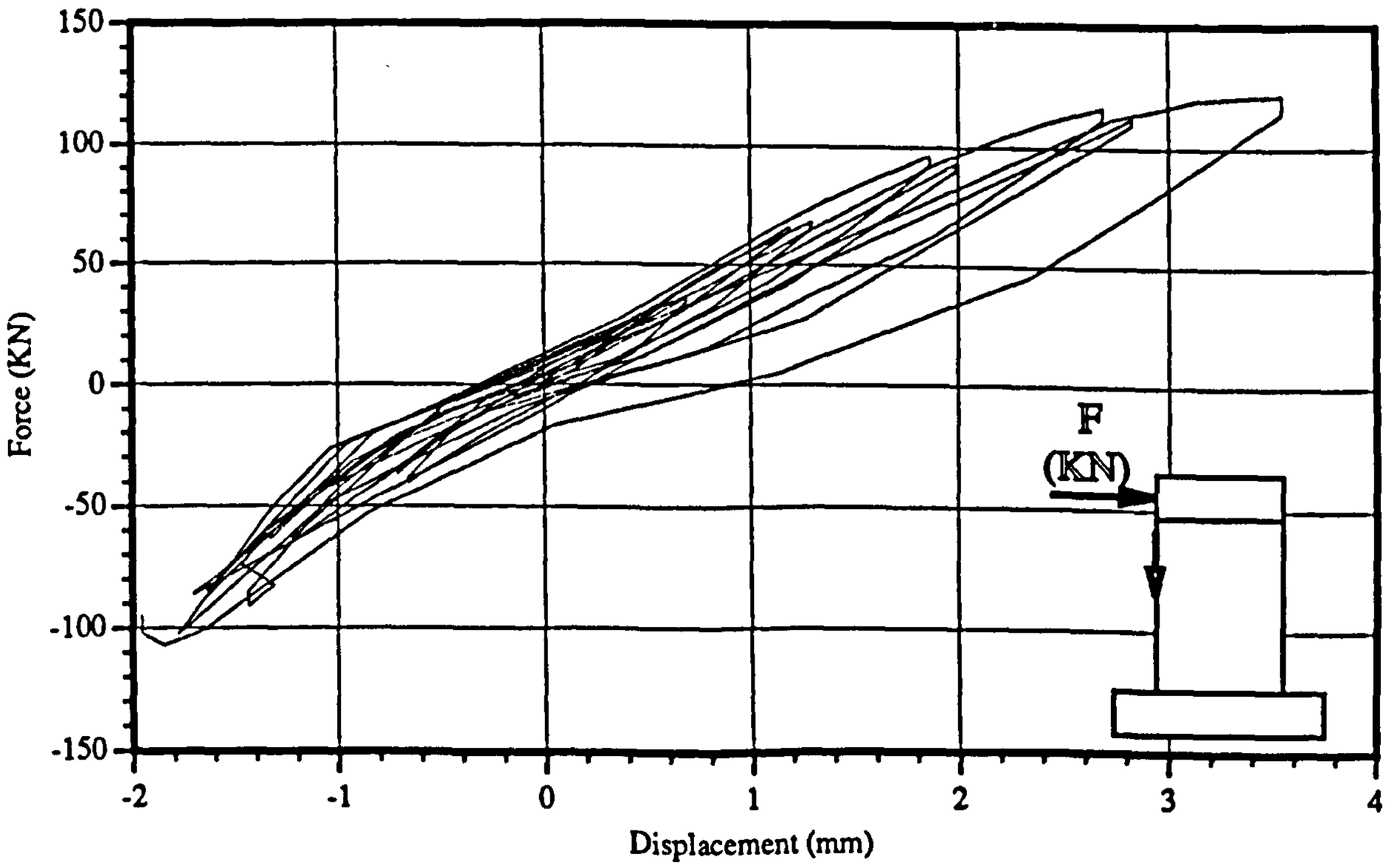


Fig. AI. (R7) 6 Force - Displacement for SWR7 at Node 6

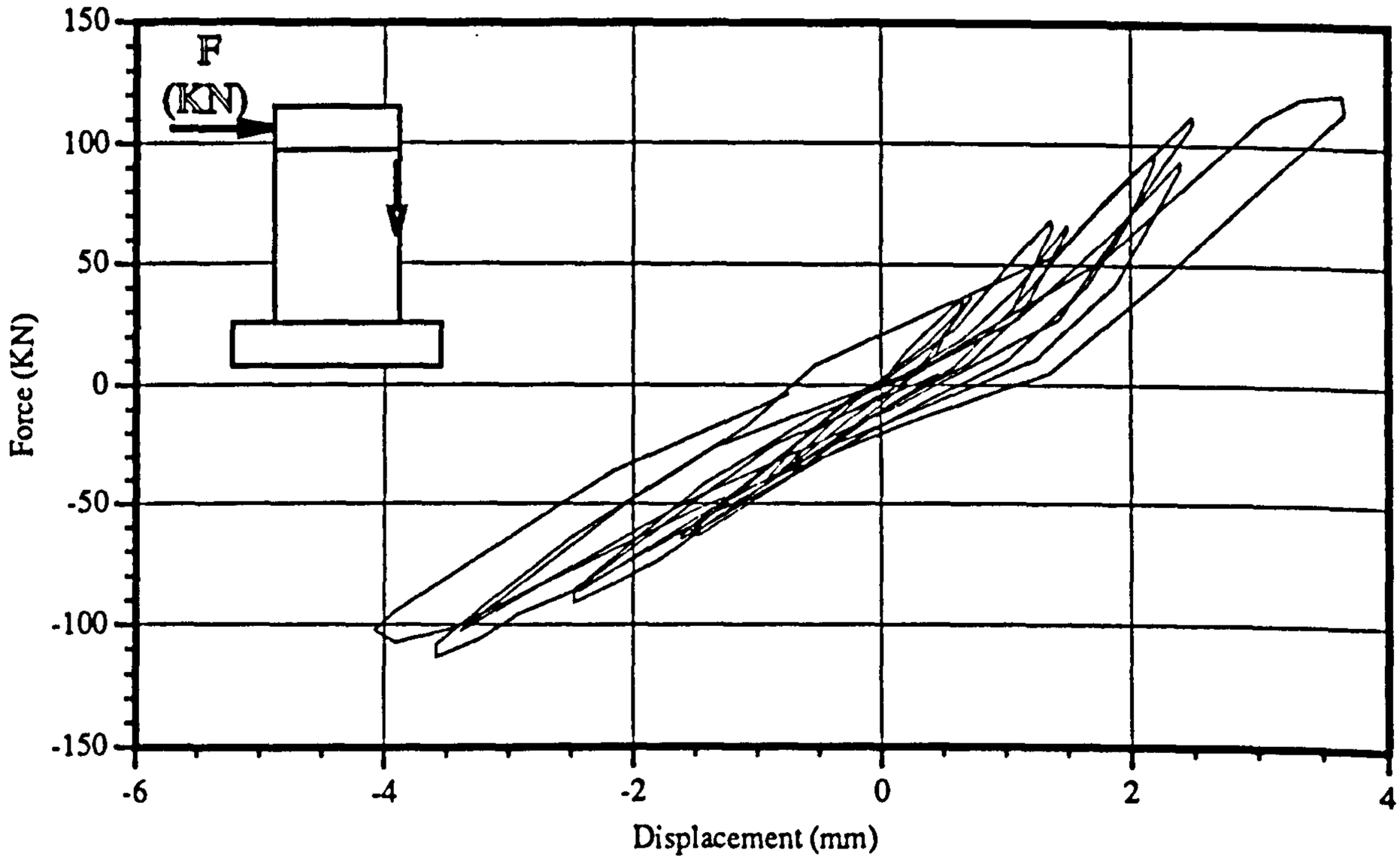


Fig. AI. (R7) 7 Force - Displacement for SWR7 at Node 7

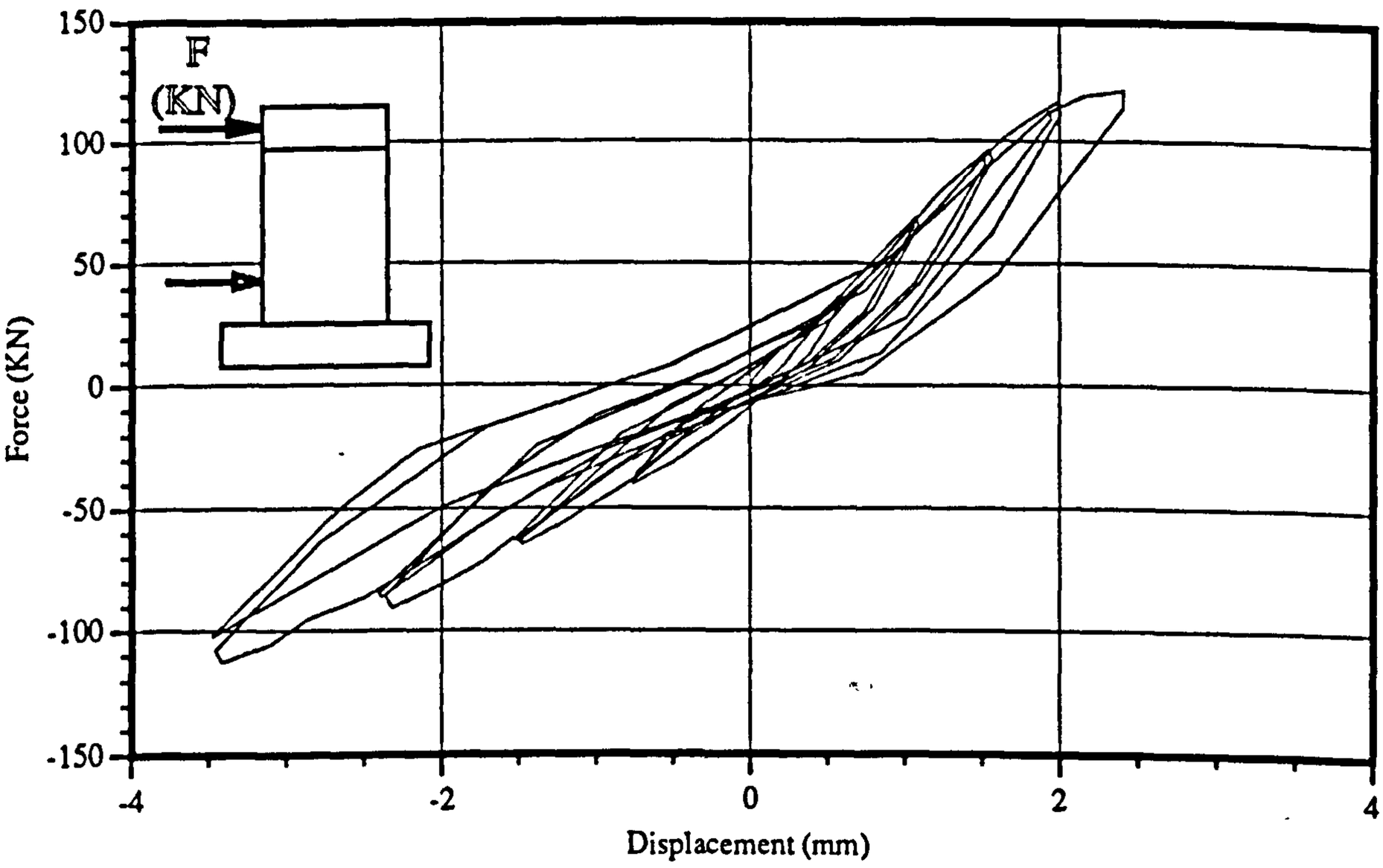


Fig. AI. (R7) 8 Force - Displacement for SWR7 at Node 8

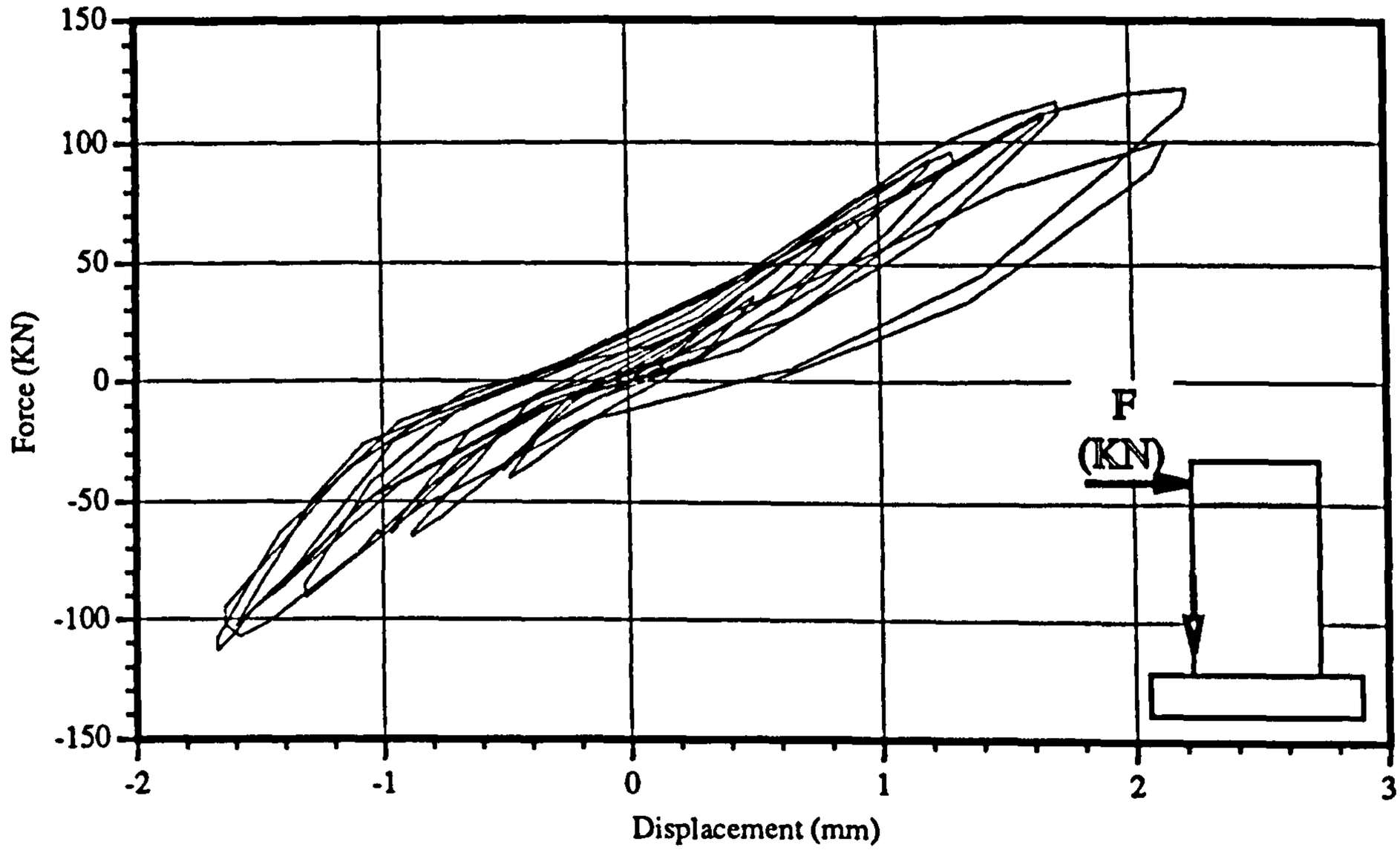


Fig. AI. (R7) 9 Force - Displacement for SWR7 at Node 9

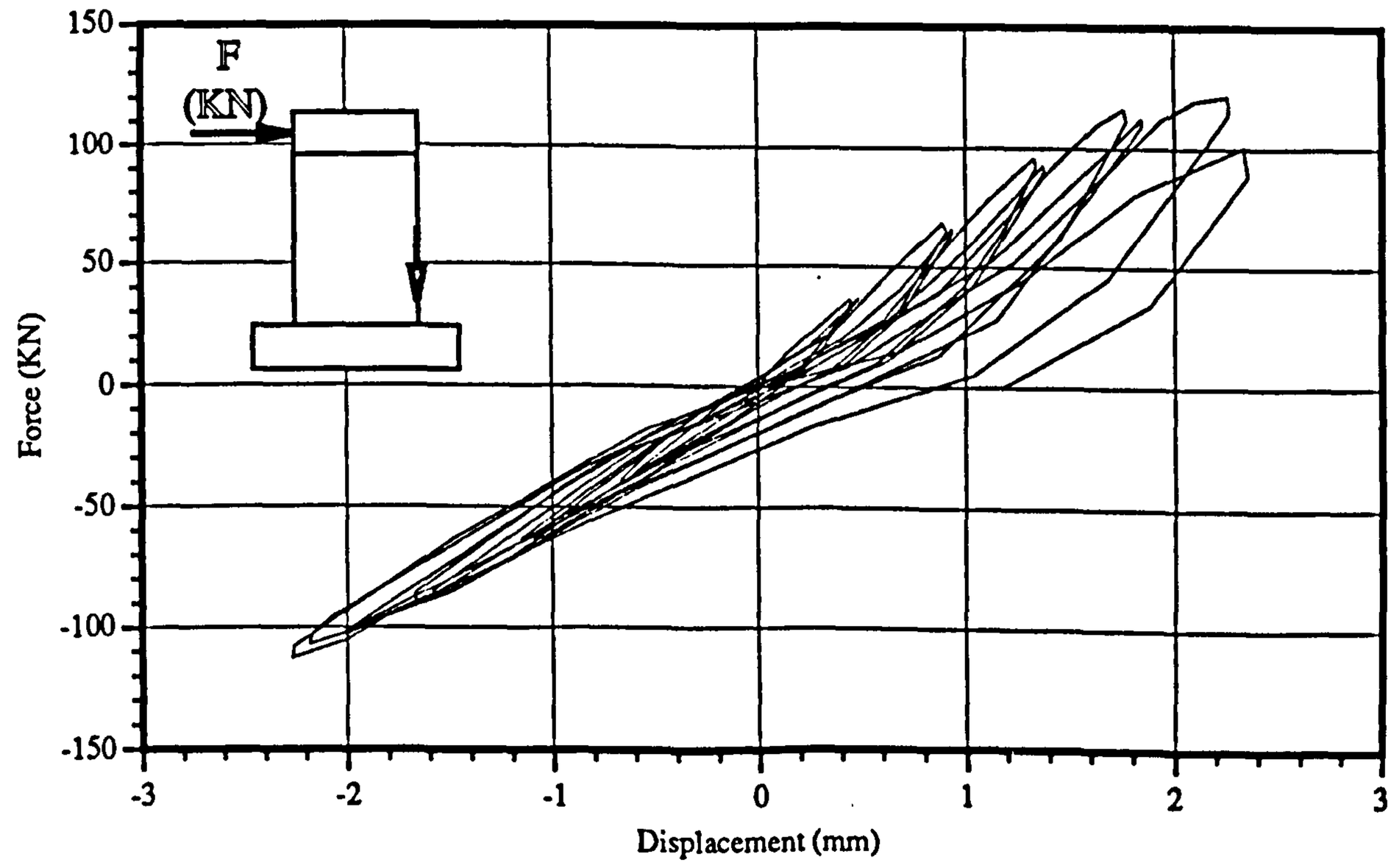


Fig. AI. (R7) 10 Force - Displacement for SWR7 at Node 10

AI.4 : Force Displacement for SWR9

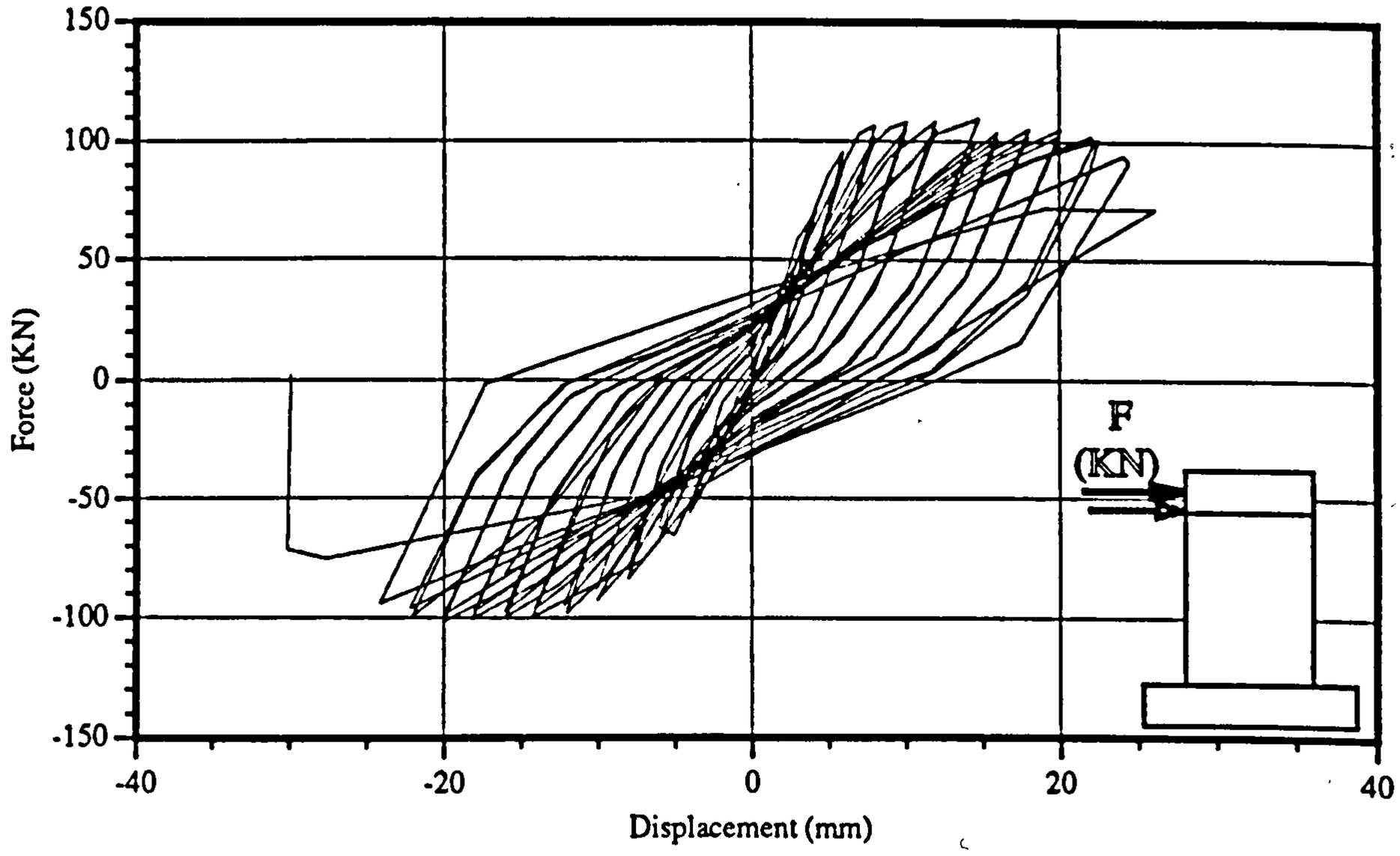


Fig. AI. (R9) 1 Force - Displacement for SWR9 at Node 1

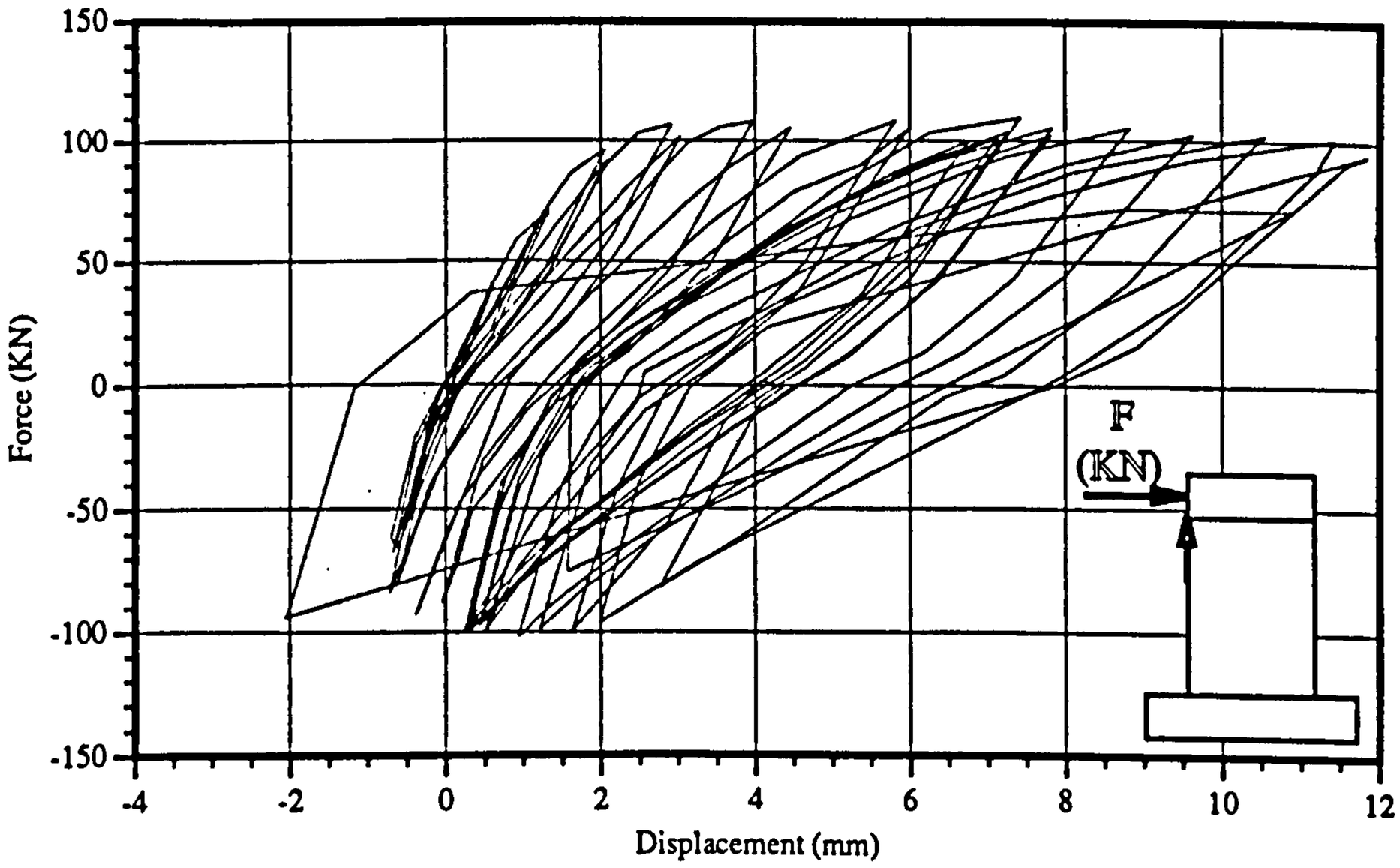


Fig. AI. (R9) 2 Force - Displacement for SWR9 at Node 2

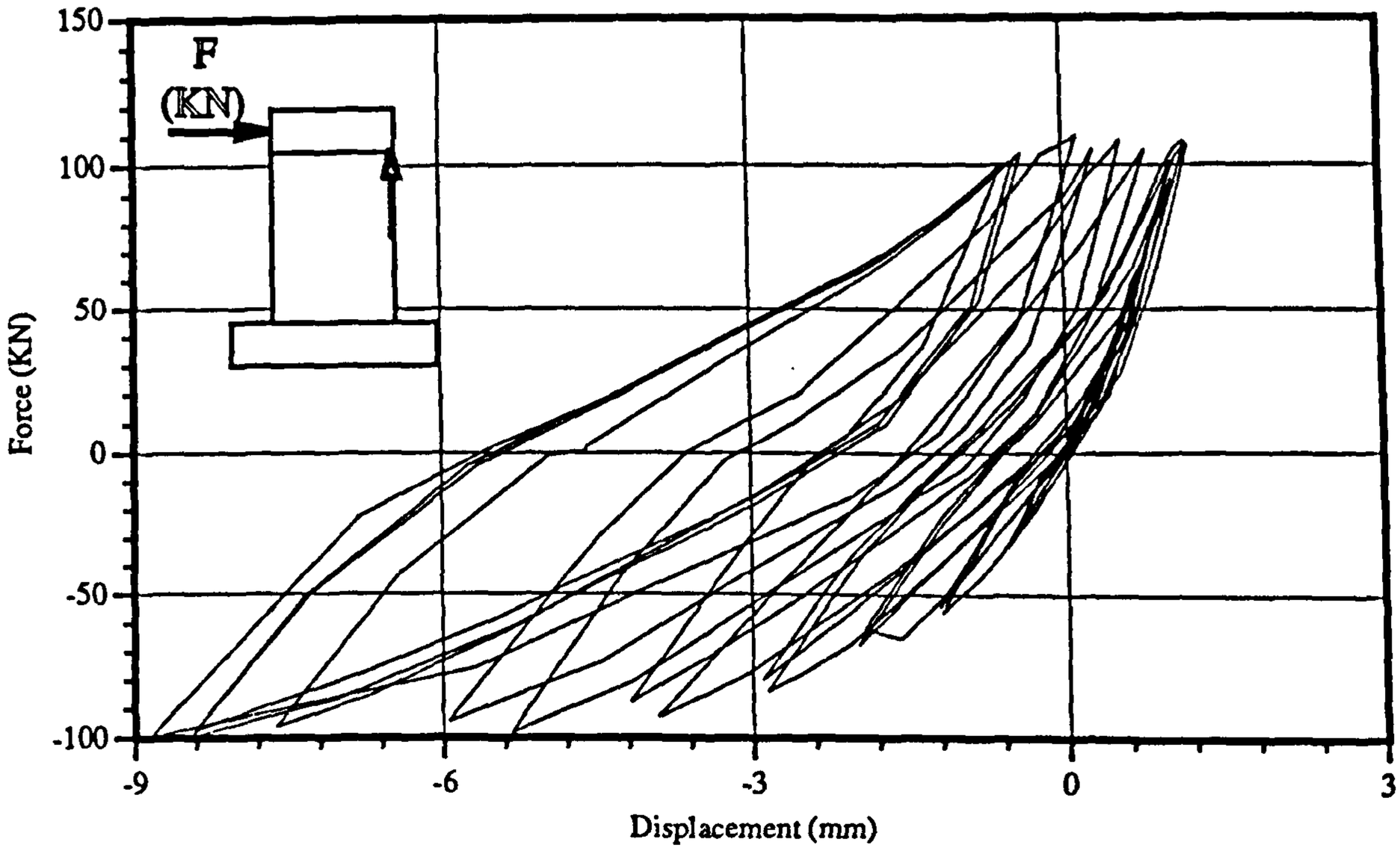


Fig. AI. (R9) 3 Force - Displacement for SWR9 at Node 3

Fig. AI. (R9) 4 Force - Displacement for SWR9 at Node 6

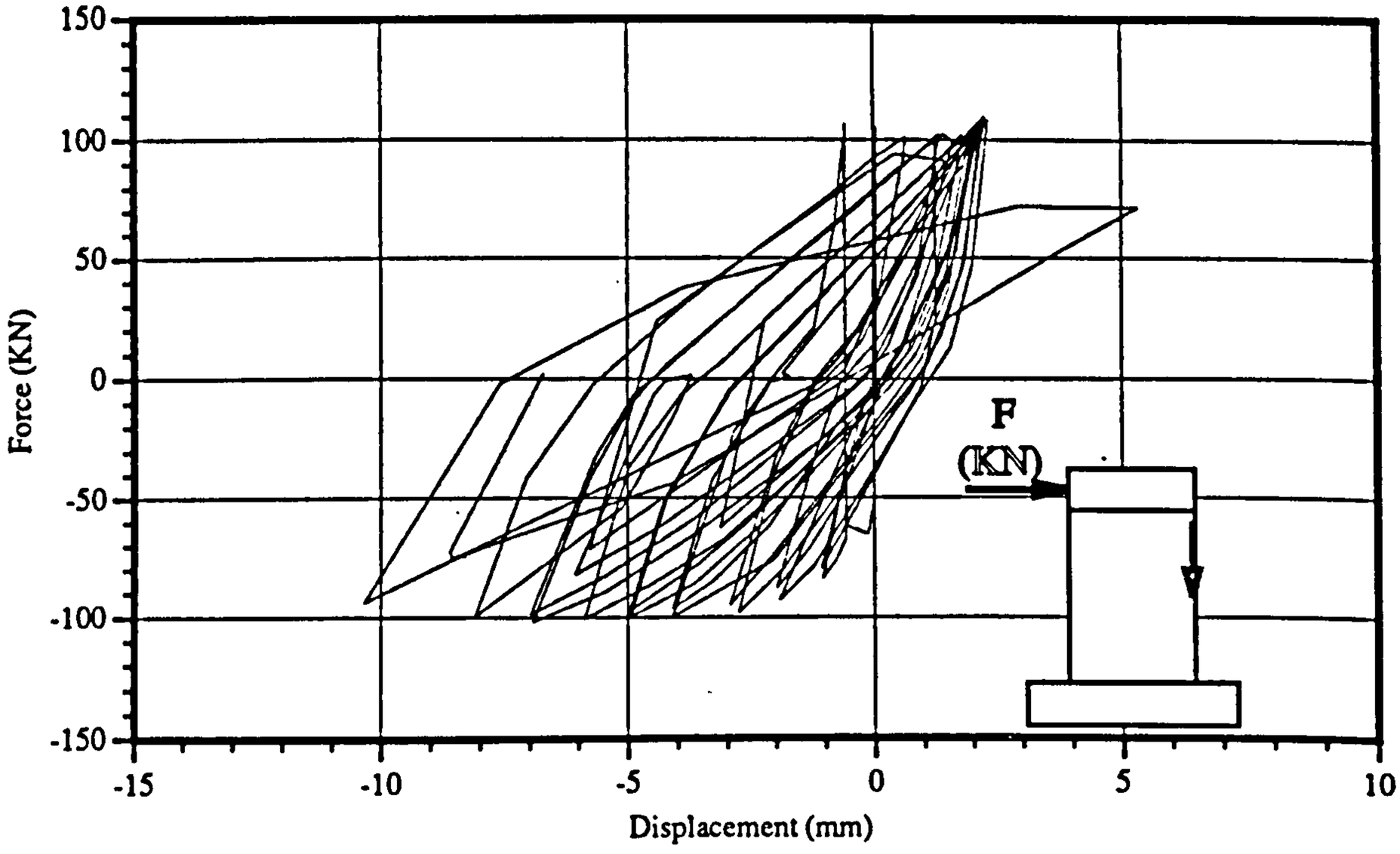


Fig. AI. (R9) 7 Force - Displacement for SWR9 at Node 7

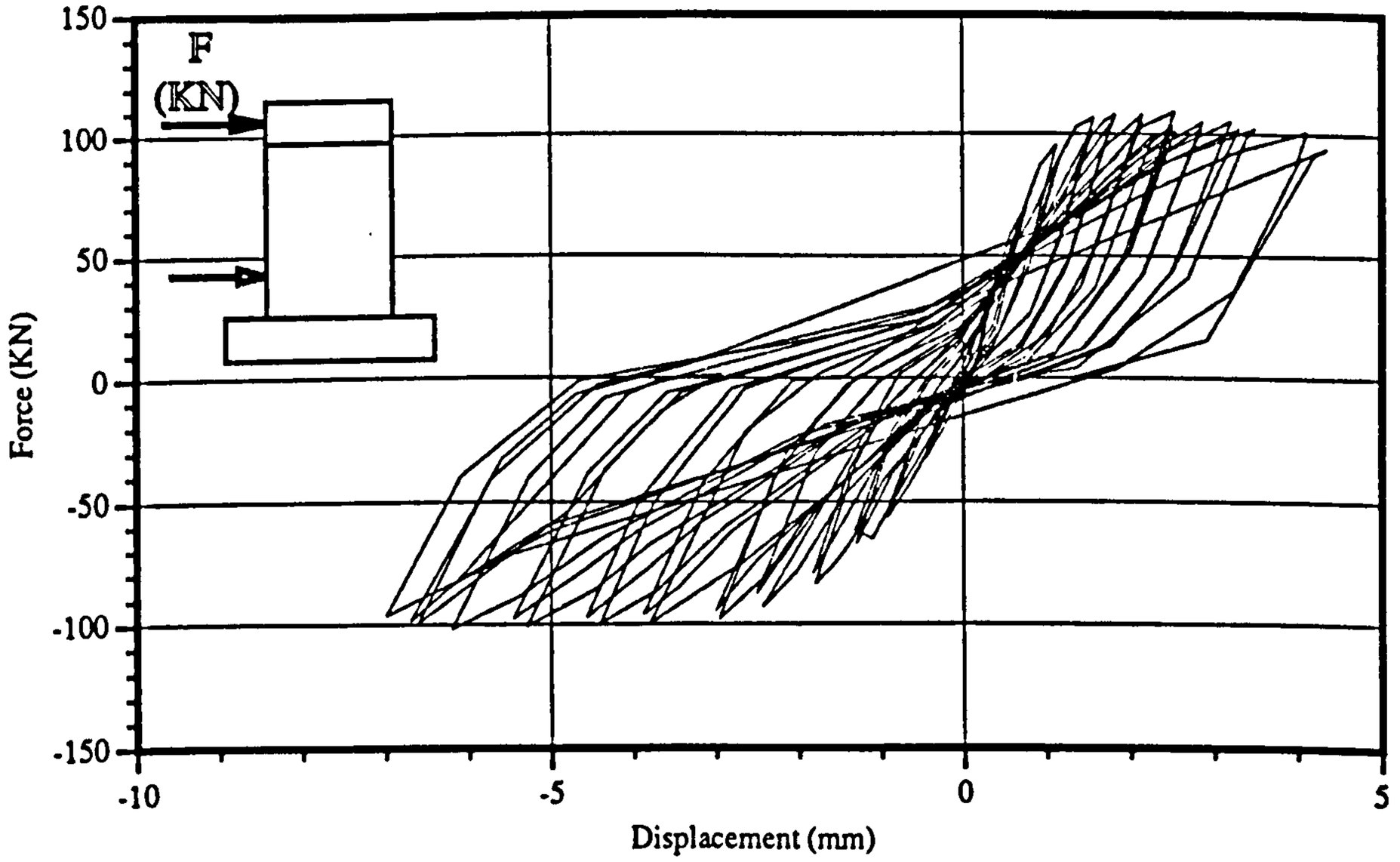


Fig. AI. (R9) 8 Force - Displacement for SWR9 at Node 8

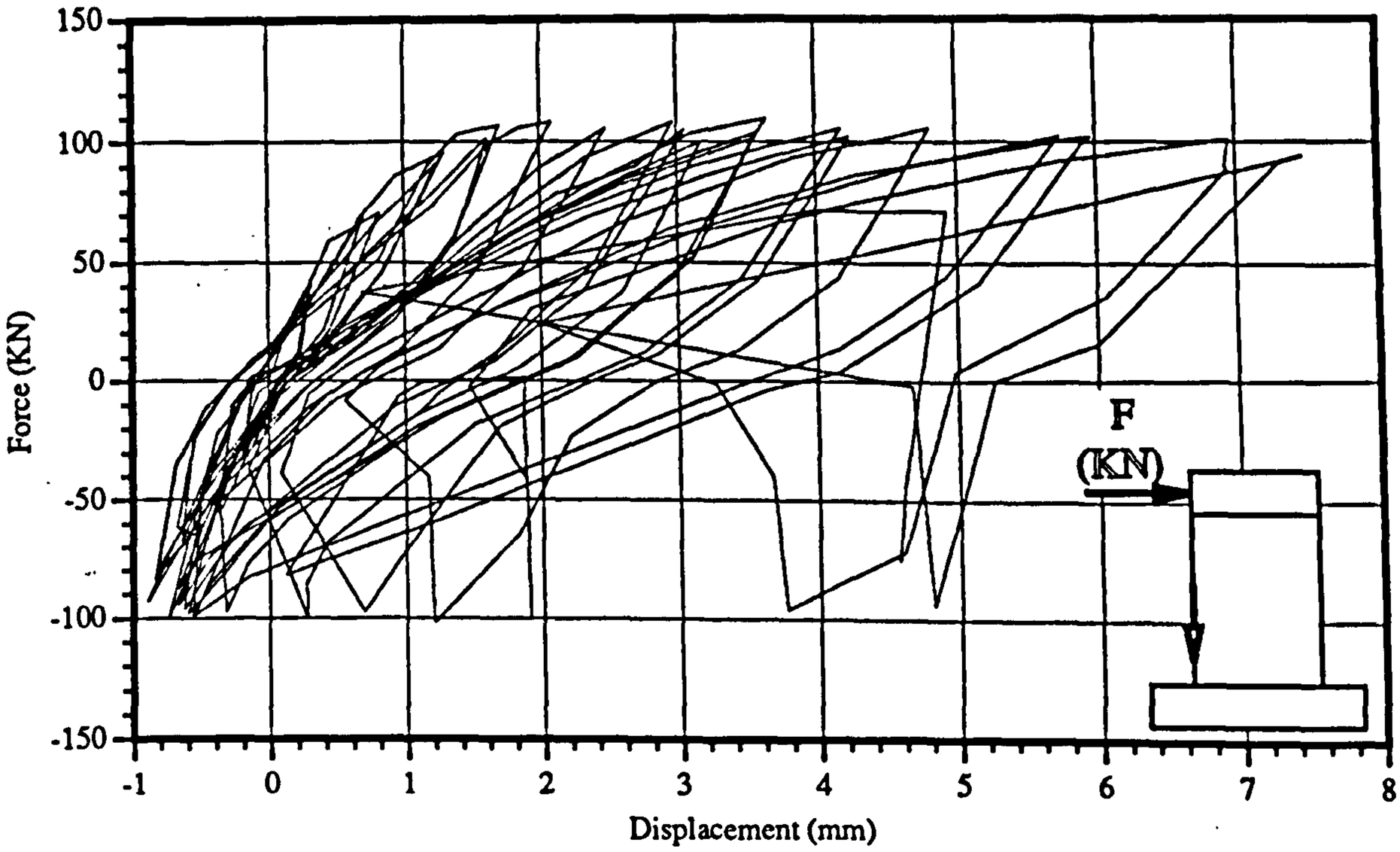


Fig. AI. (R9) 9 Force - Displacement for SWR9 at Node 9

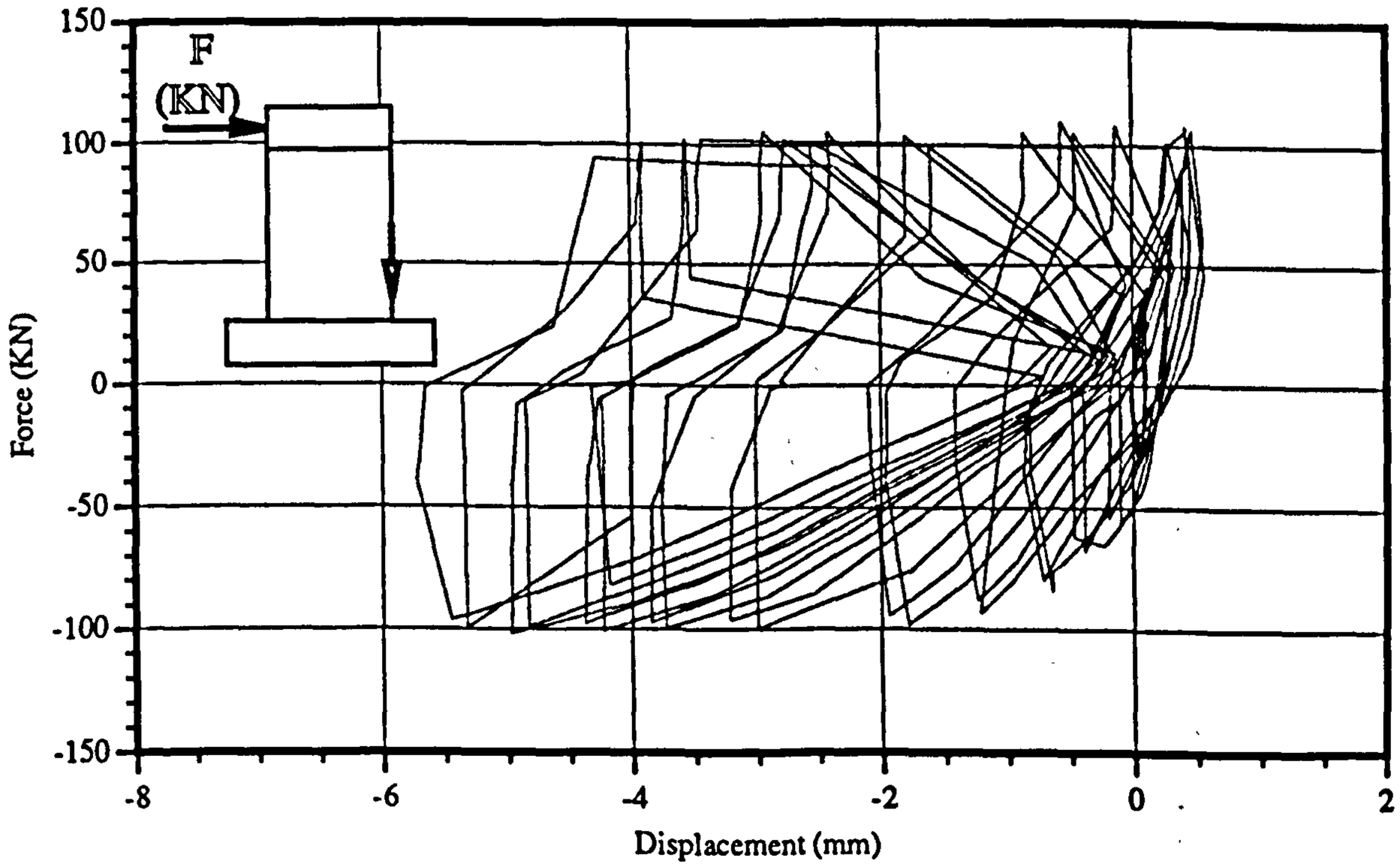


Fig. AI. (R9) 10 Force - Displacement for SWR9 at Node 10

AI.5 : Force Displacement for SW21

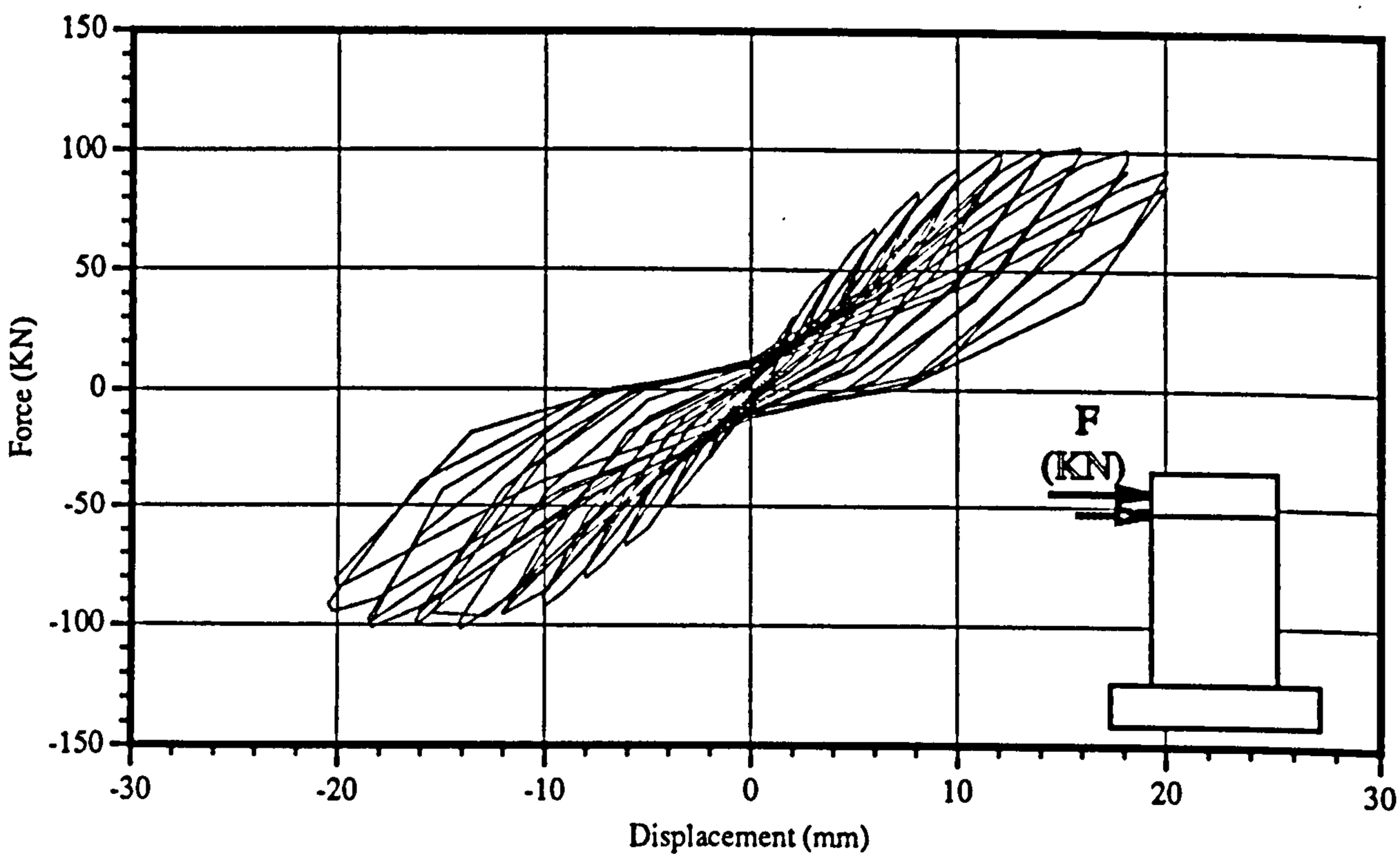


Fig. AI. (21) 1 Force - Displacement for SW21 at Node 1

Fig. AI. (21) 2 Force - Displacement for SW21 at Node 2

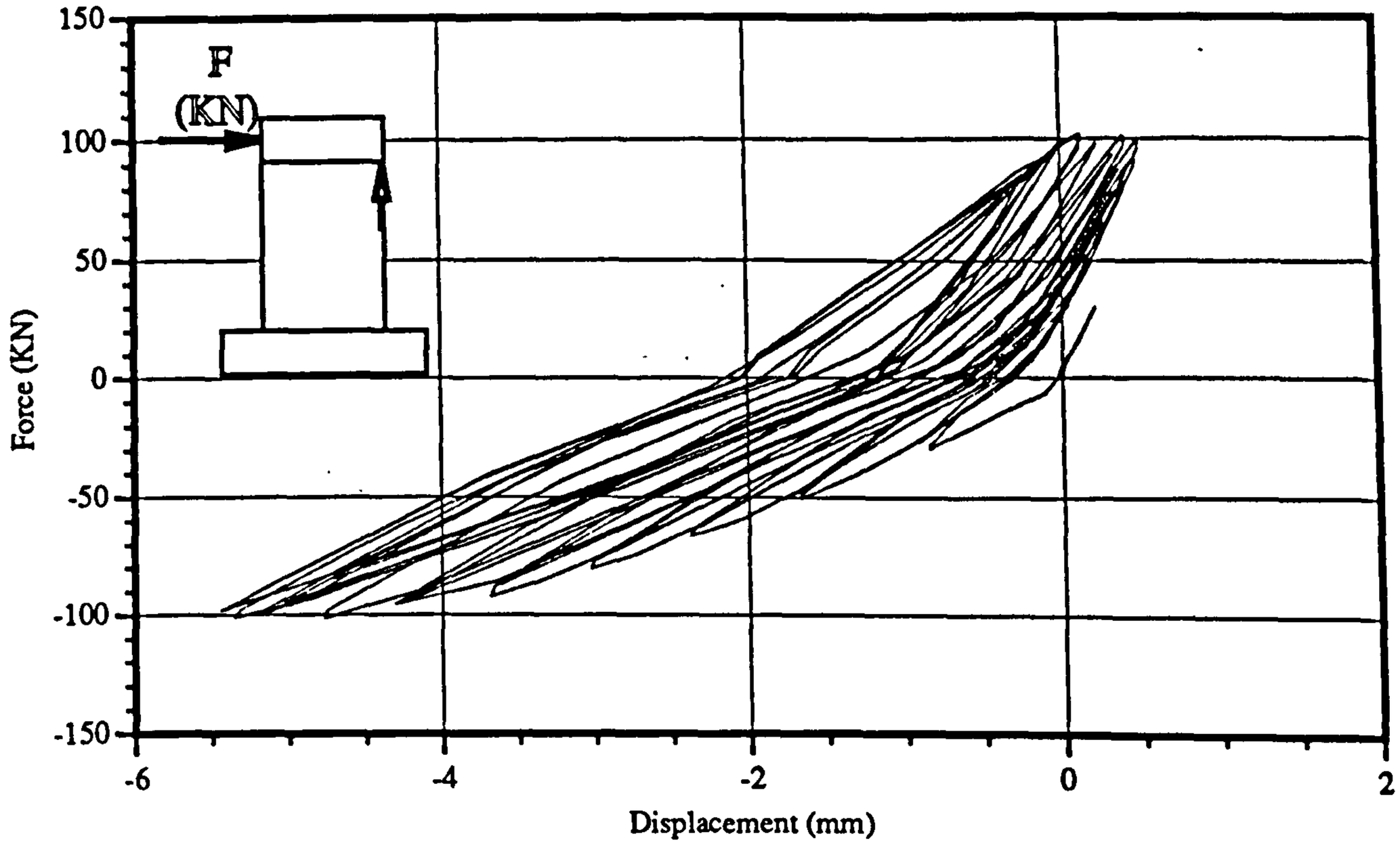


Fig. AI. (21) 3 Force - Displacement for SW21 at Node 3

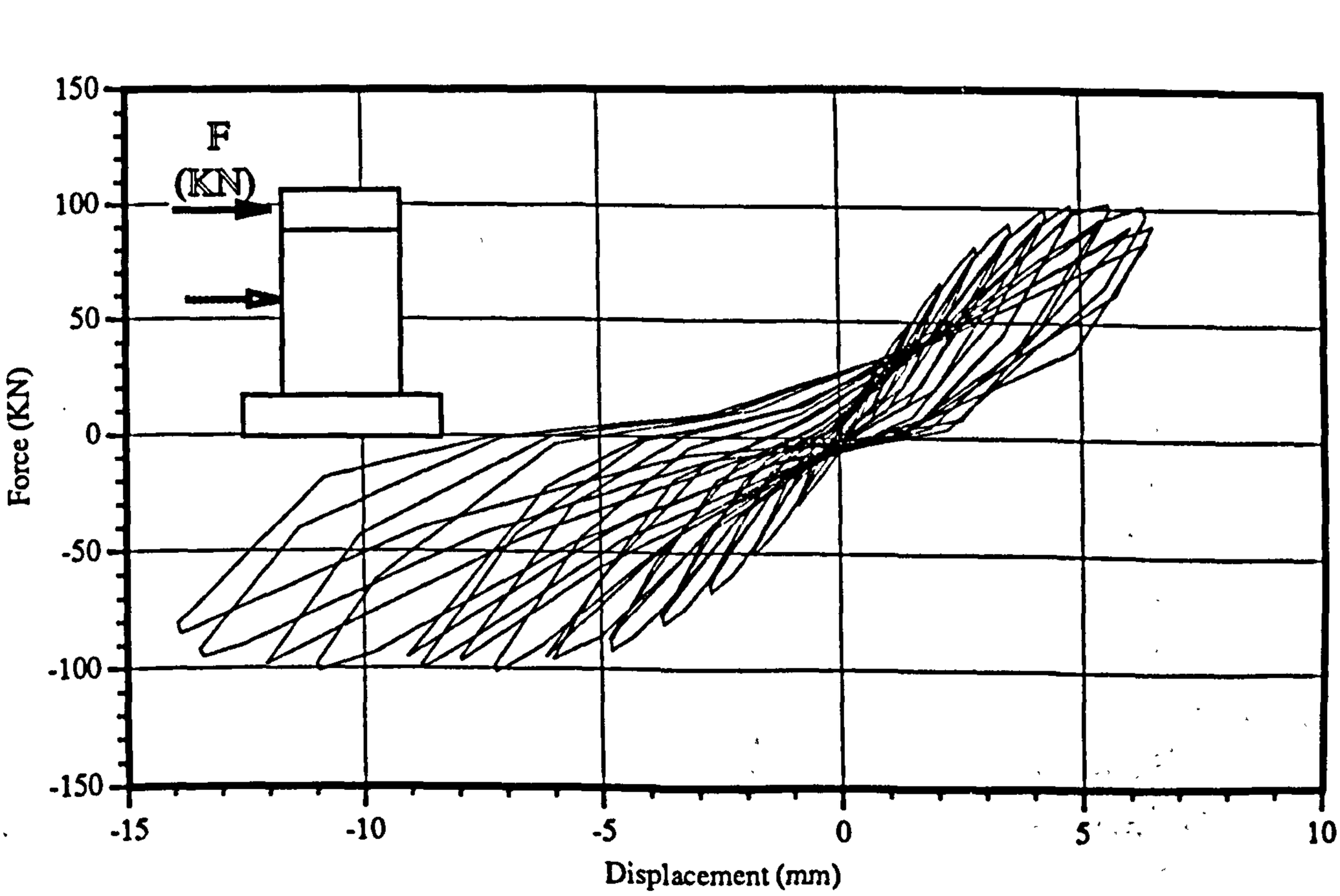


Fig. AI. (21) 4 Force - Displacement for SW21 at Node 4

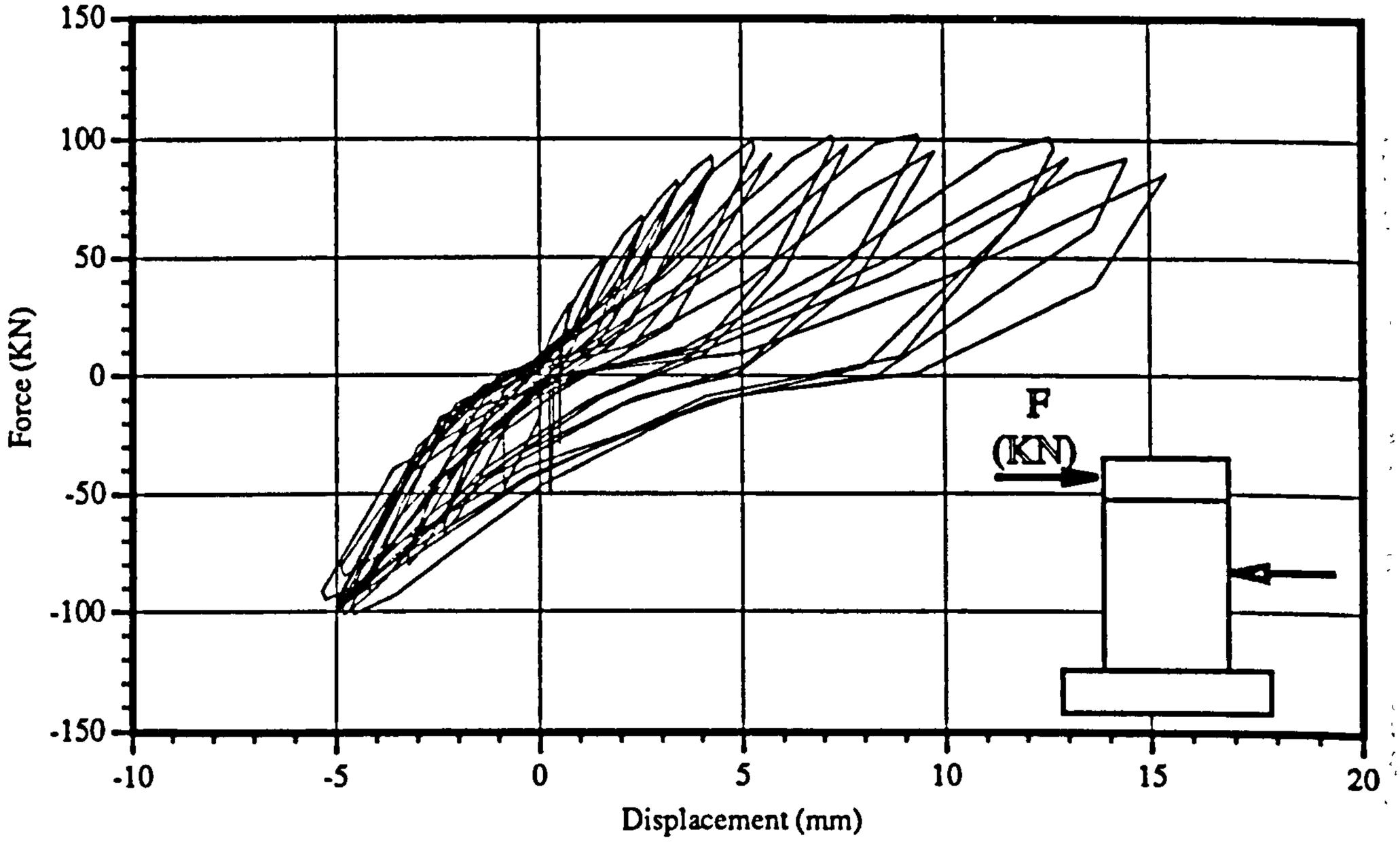


Fig. AI. (21) 5 Force - Displacement for SW21 at Node 5

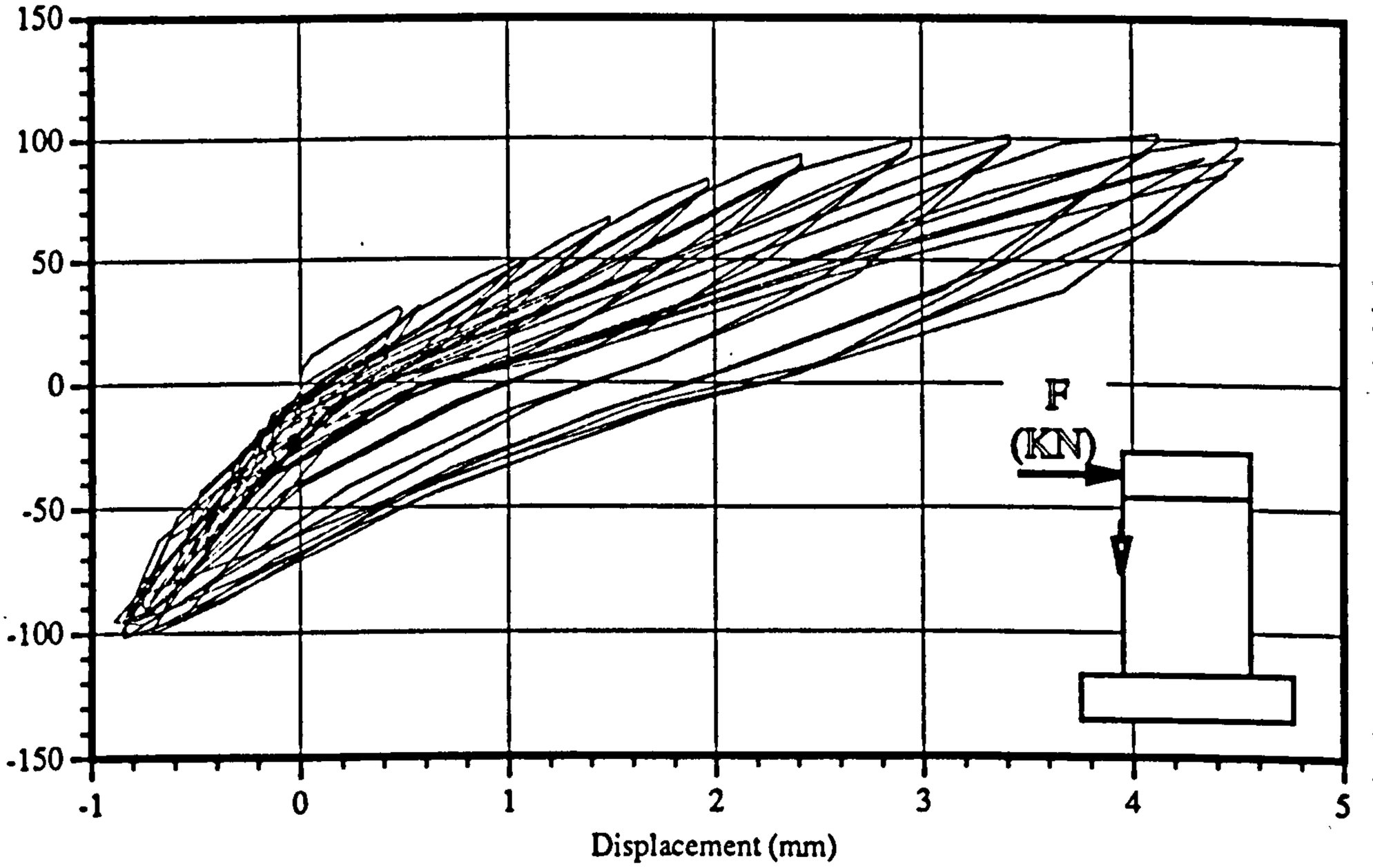


Fig. AI. (21) 6 Force - Displacement for SW21 at Node 6

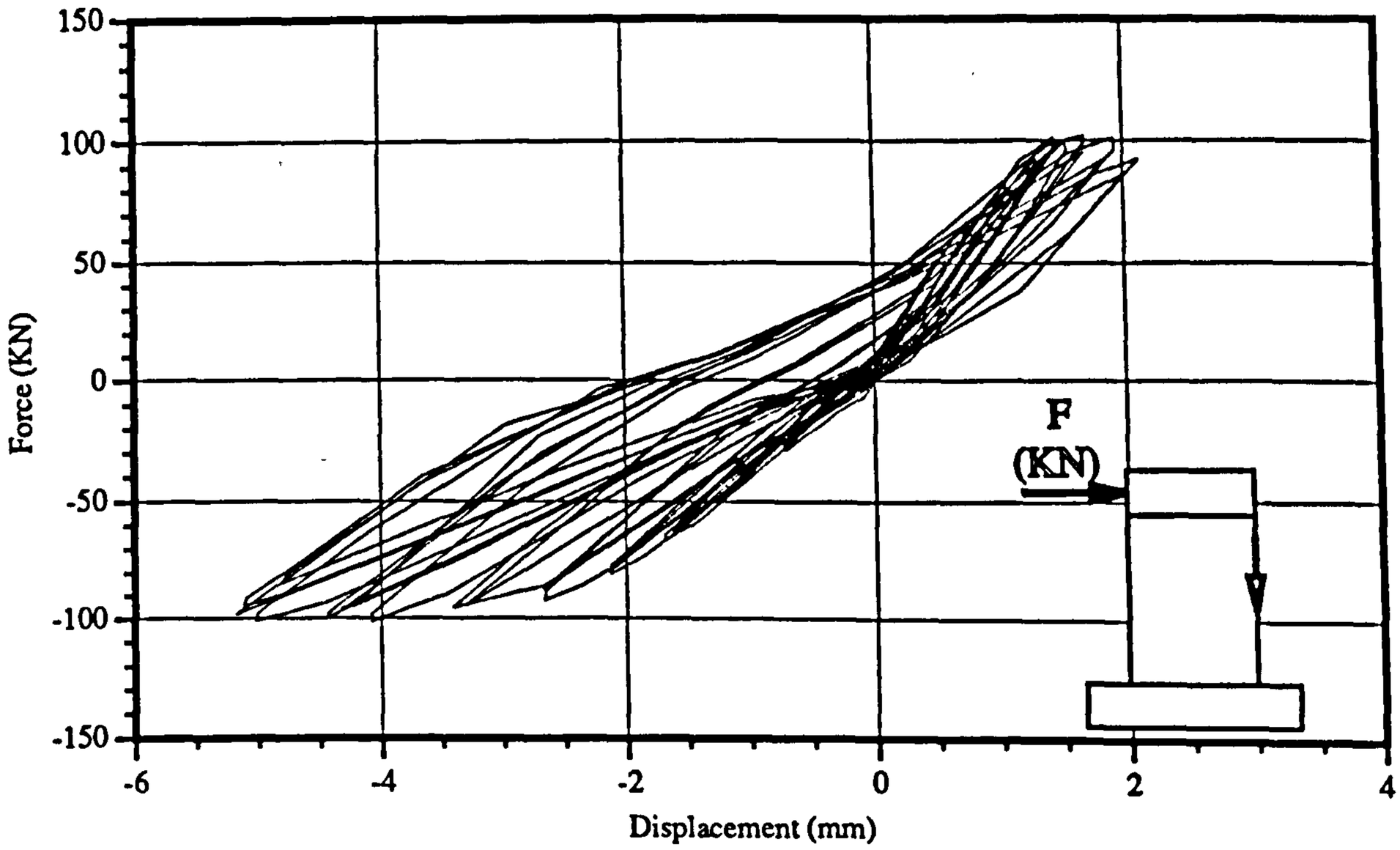


Fig. AI. (21) 7 Force - Displacement for SW21 at Node 7

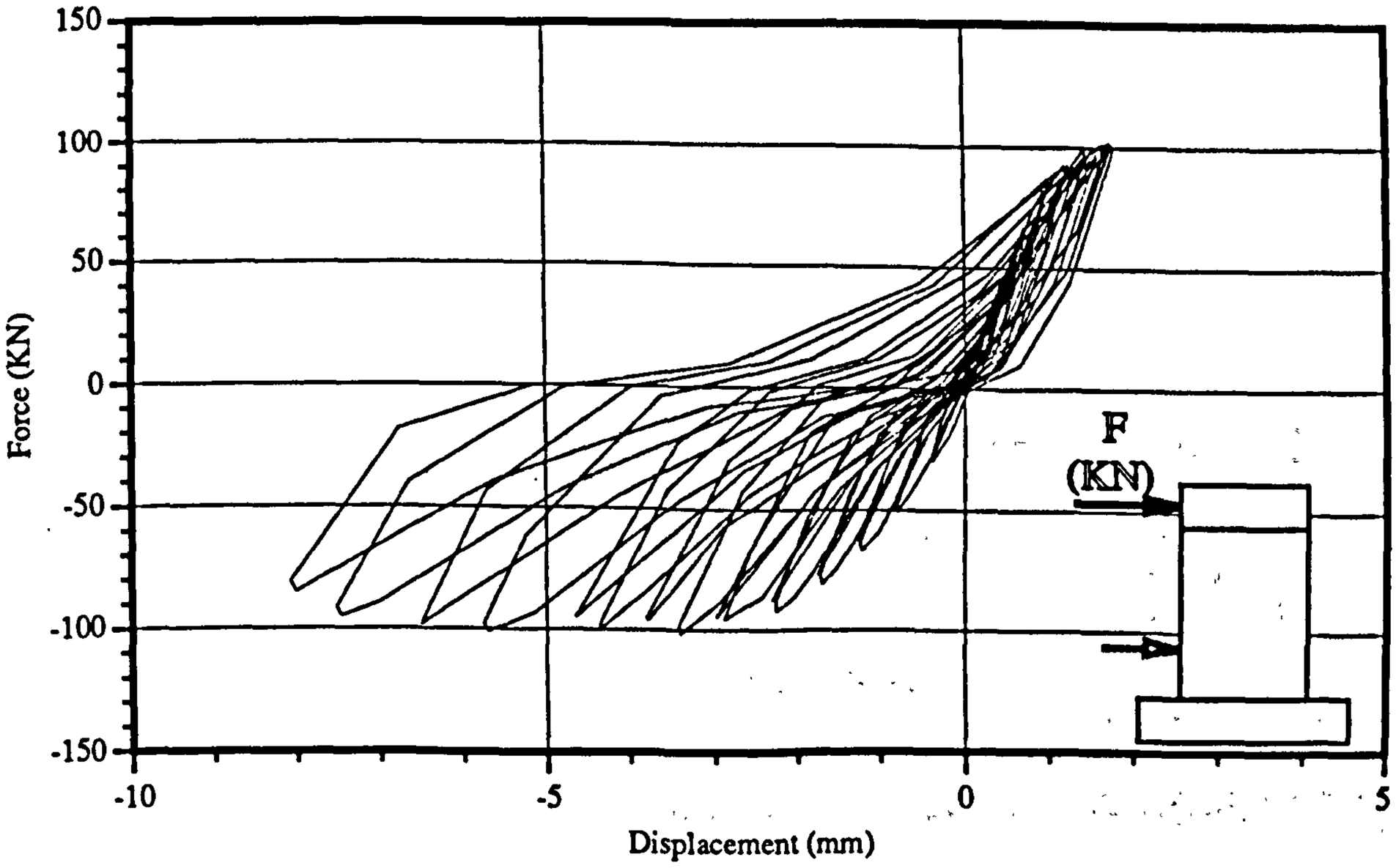


Fig. AI. (21) 8 Force - Displacement for SW21 at Node 8

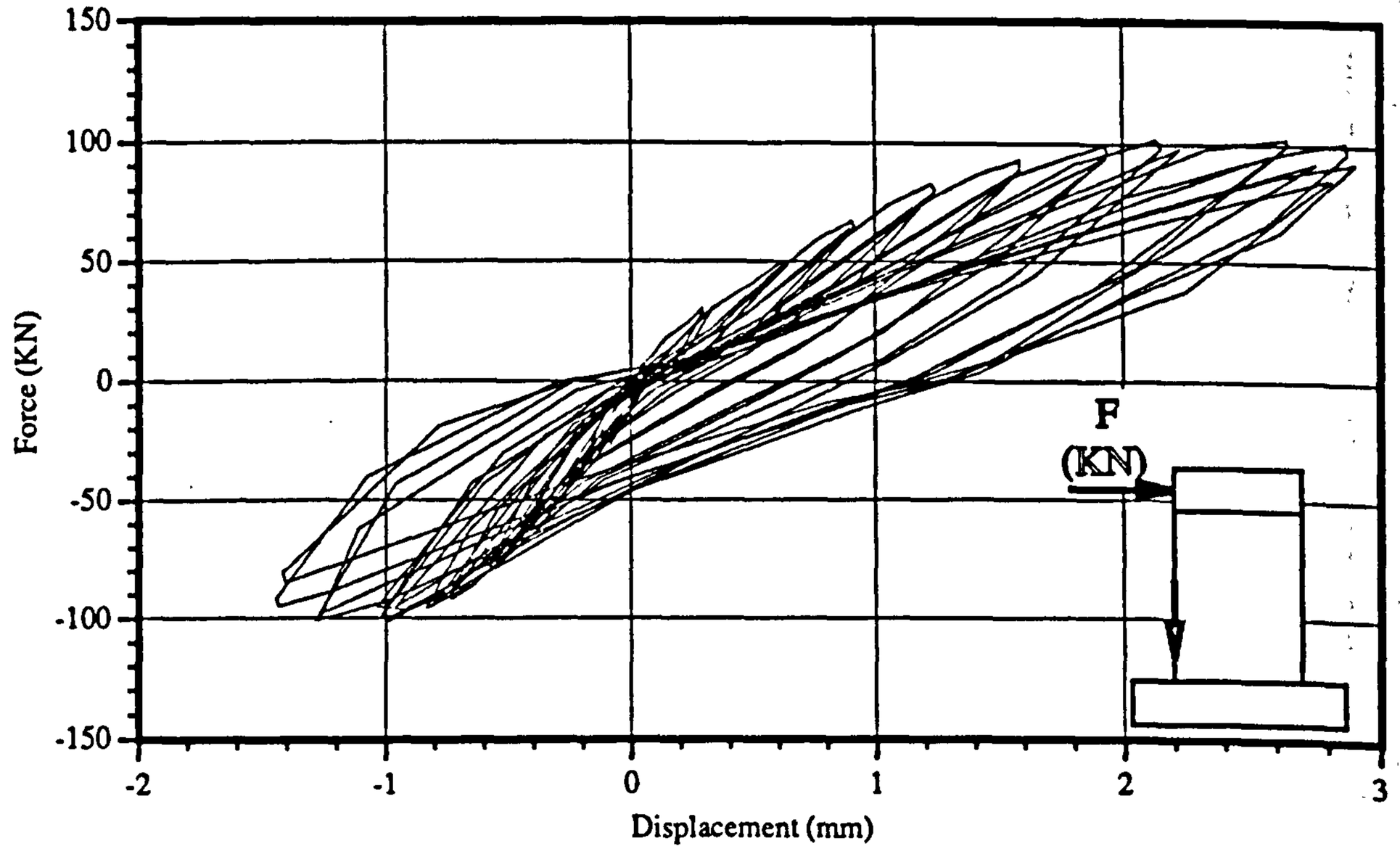


Fig. AI. (21) 9 Force - Displacement for SW21 at Node 9

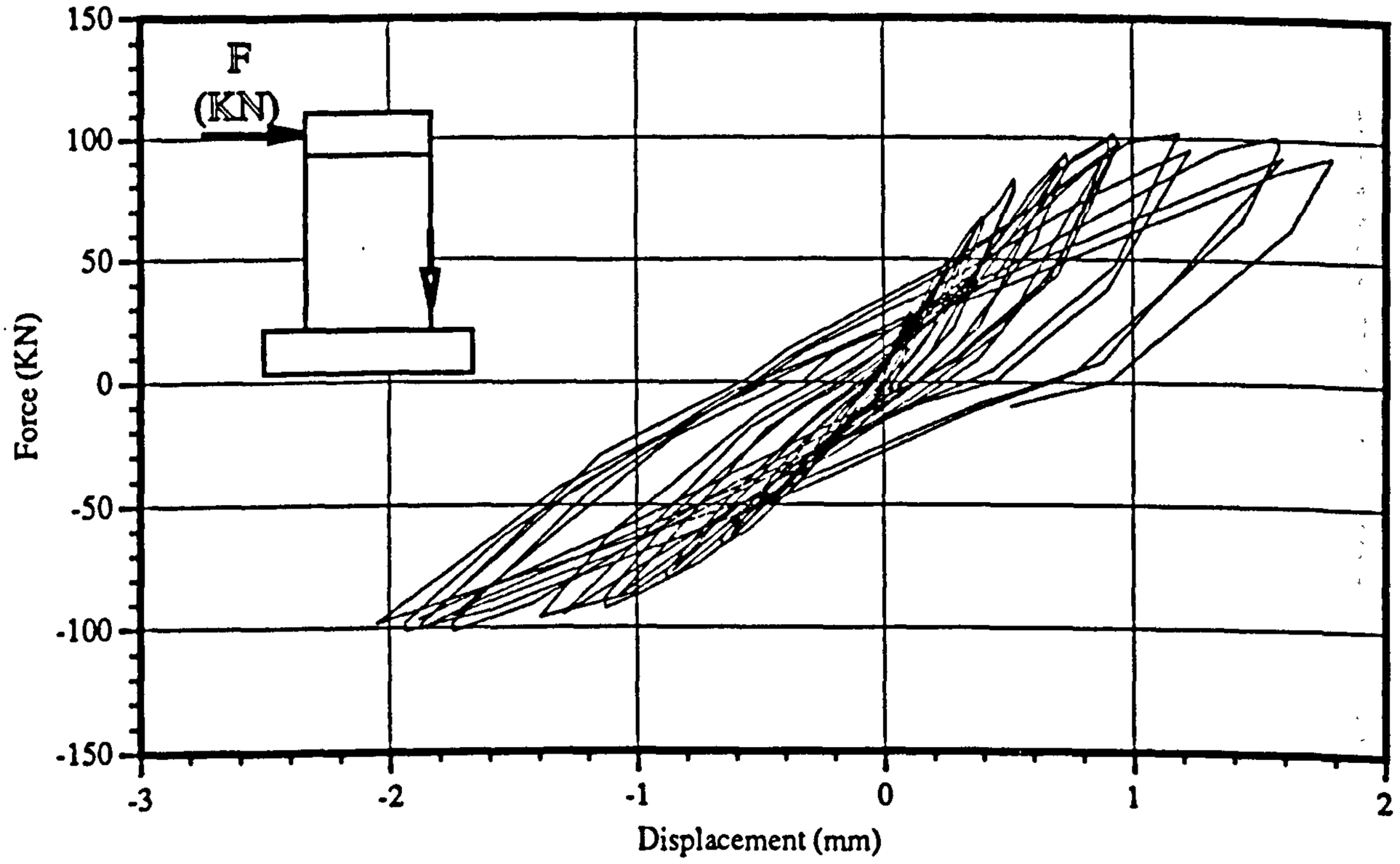


Fig. AI. (21) 10 Force - Displacement for SW21 at Node 10

AI.6 : Force Displacement for SW22

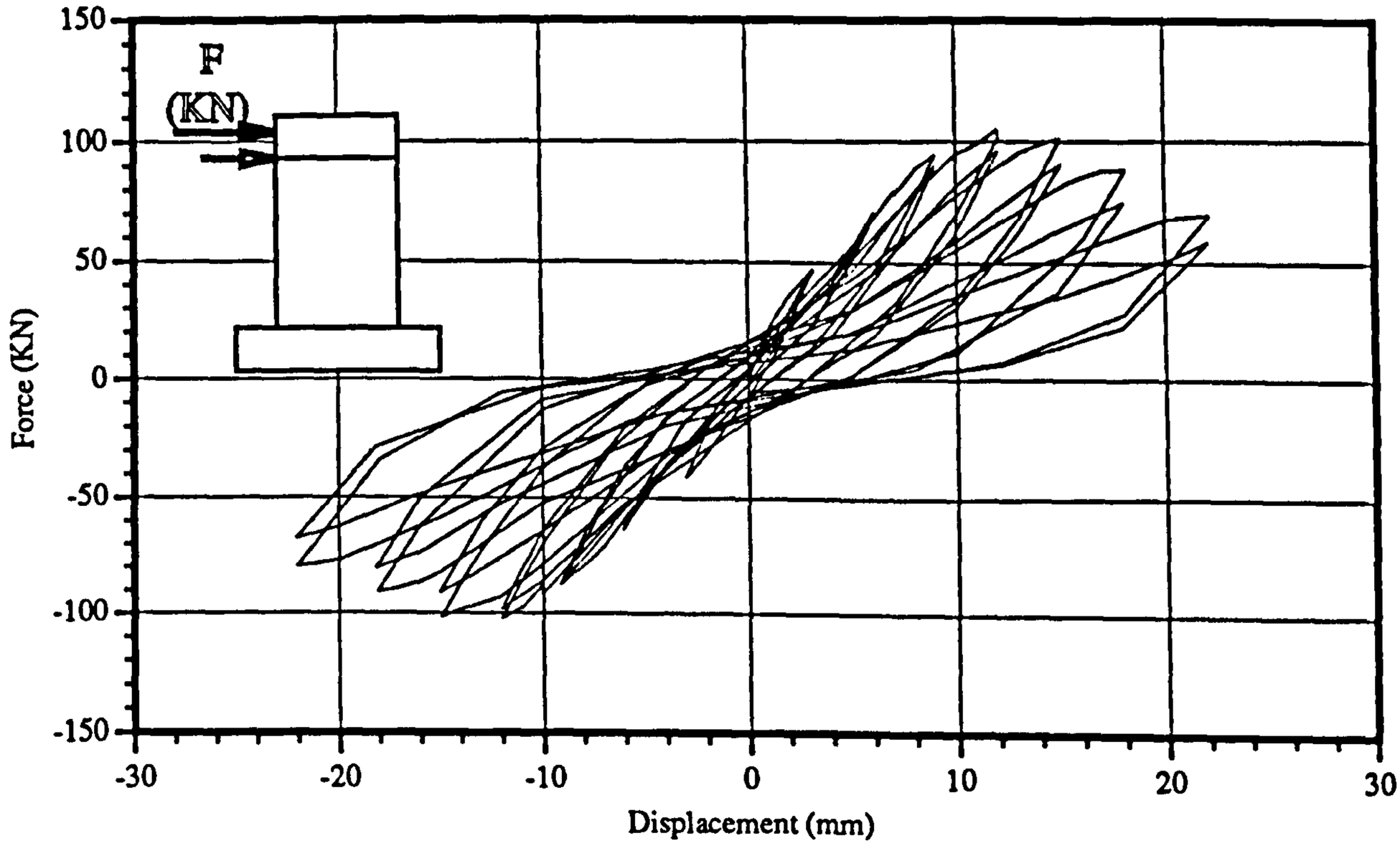


Fig. AI. (22) 1 Force - Displacement for SW22 at Node 1

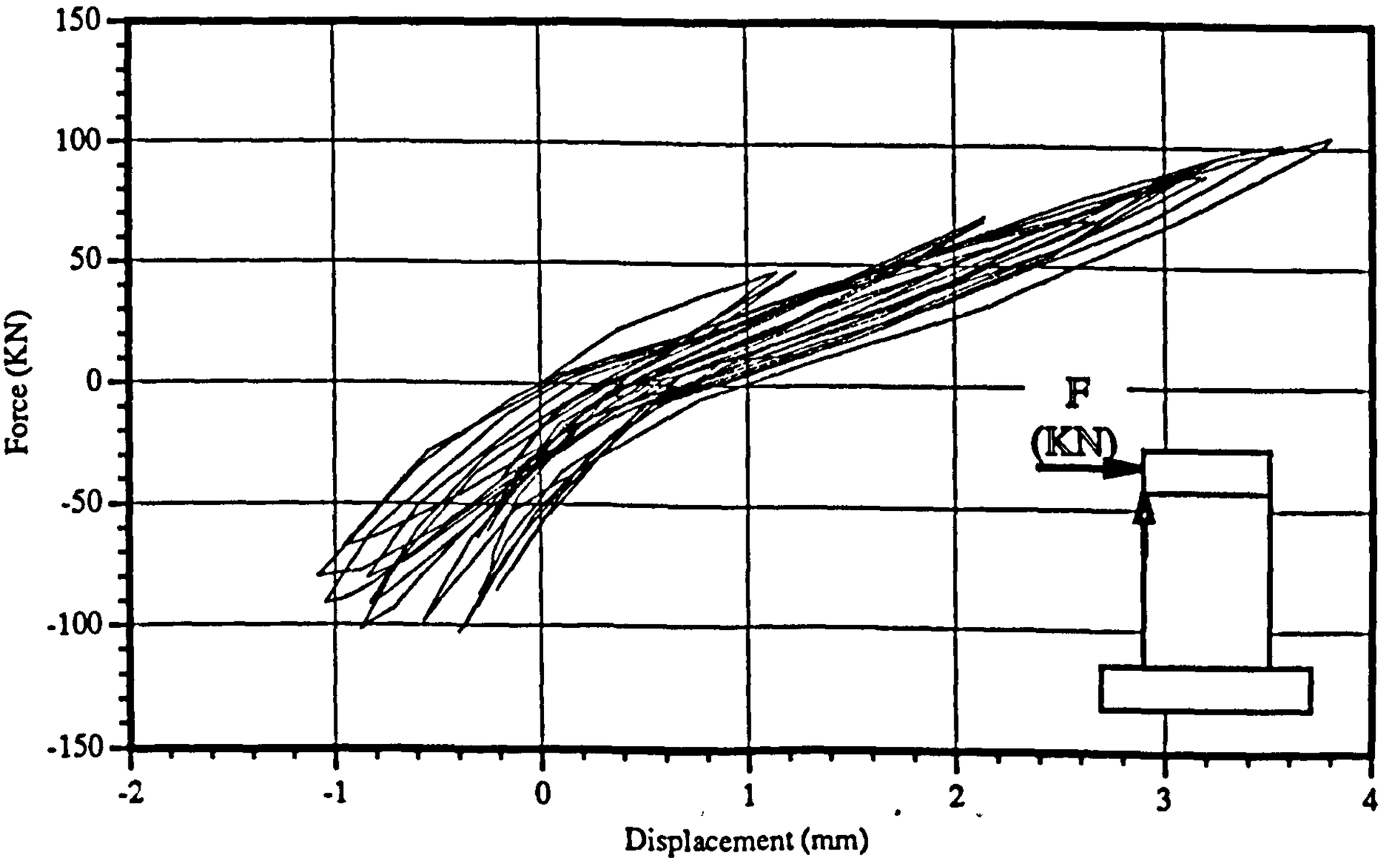


Fig. AI. (22) 2 Force - Displacement for SW22 at Node 2

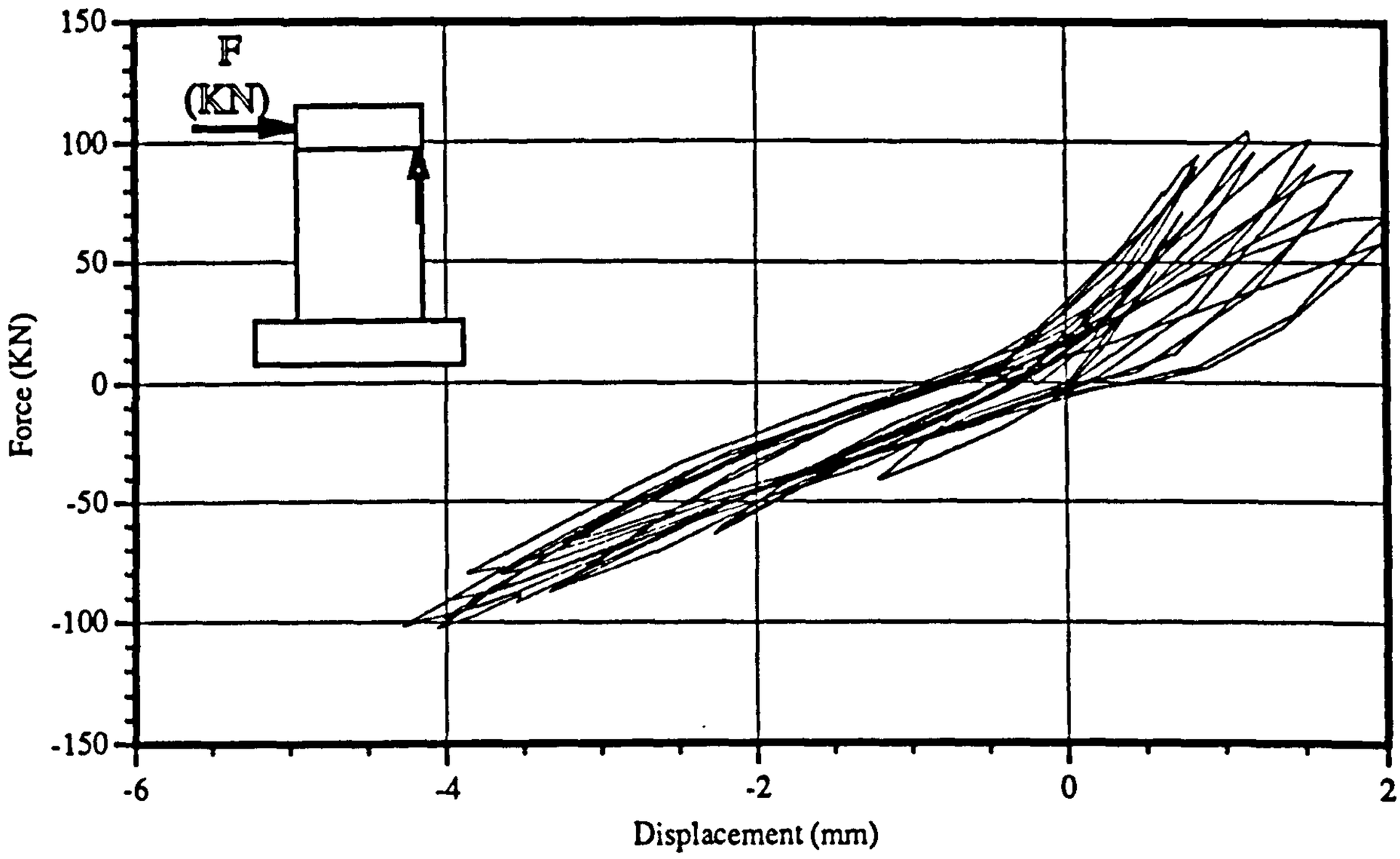


Fig. AI. (22) 3 Force - Displacement for SW22 at Node 3

Fig. AI. (22) 4 Force - Displacement for SW22 at Node 4

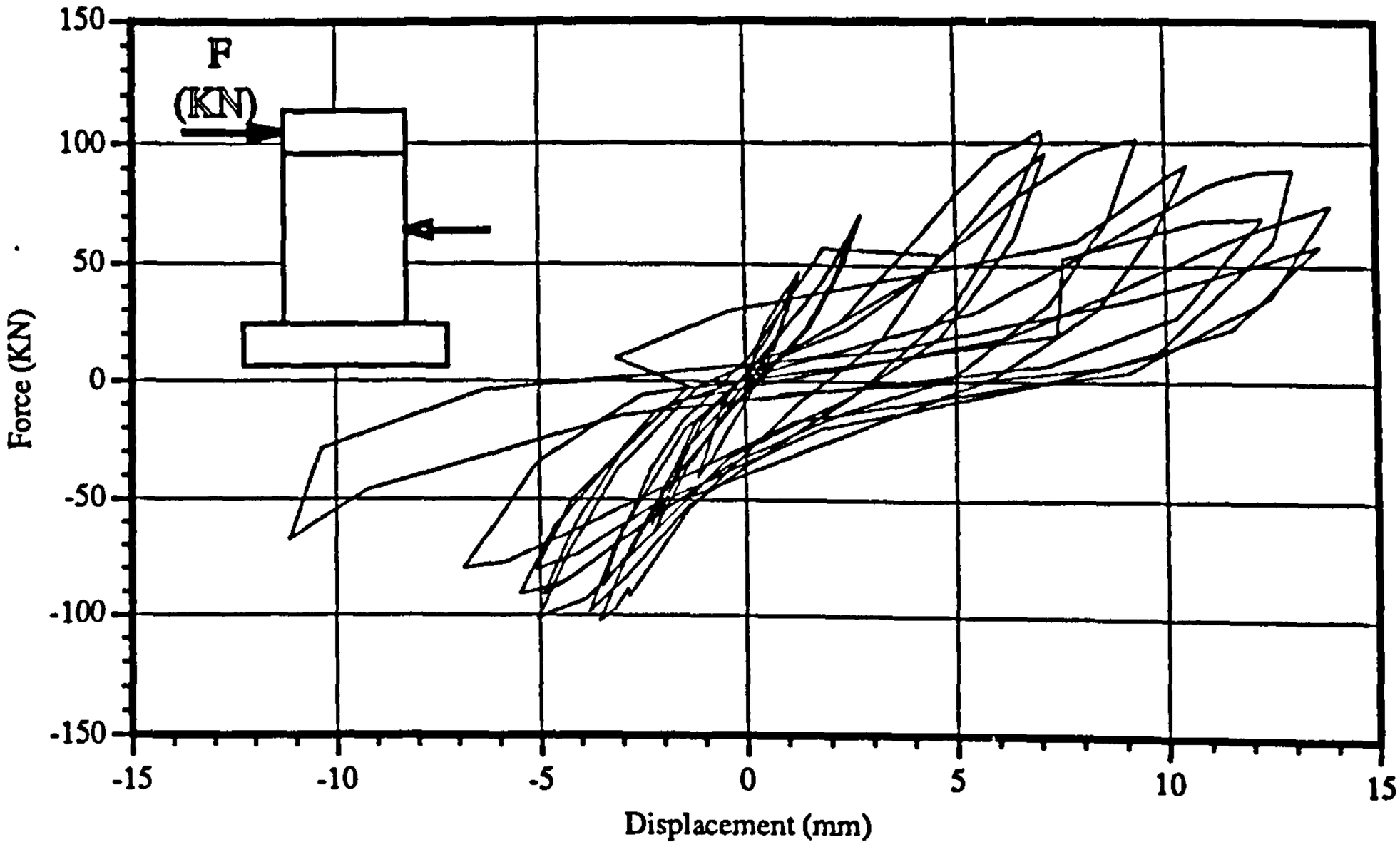


Fig. AI. (22) 5 Force - Displacement for SW22 at Node 5

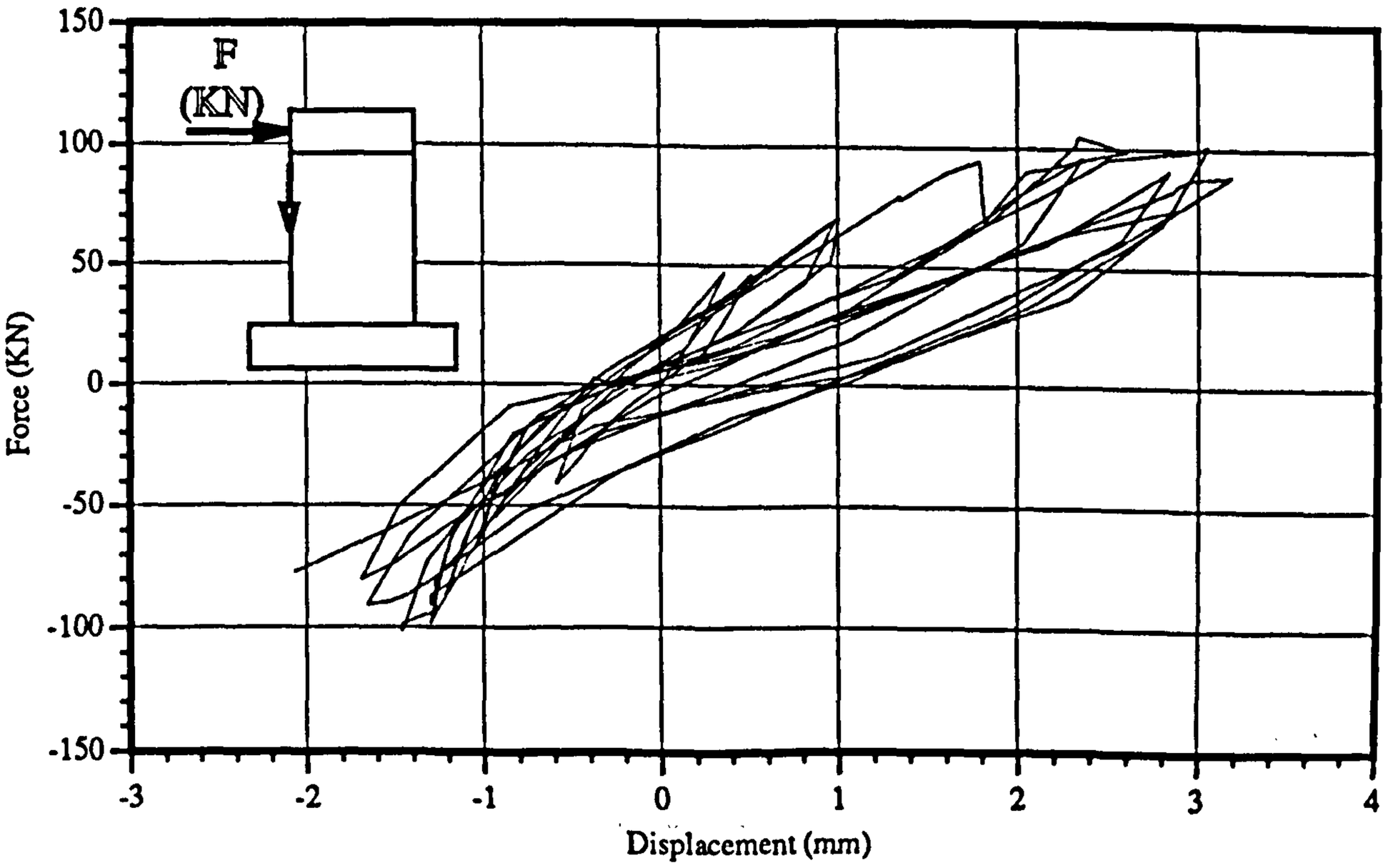


Fig. AI. (22) 6 Force - Displacement for SW22 at Node 6

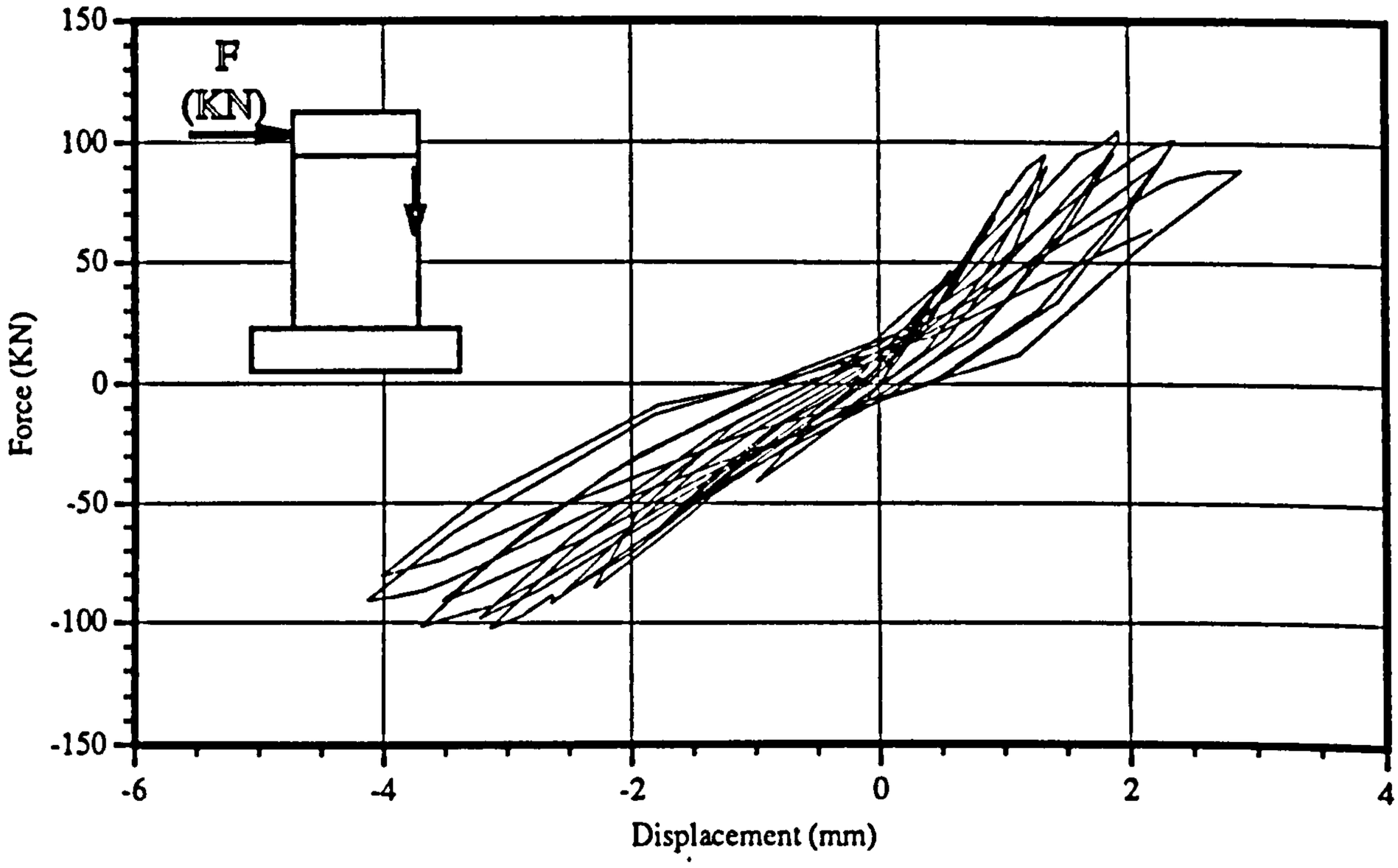


Fig. AI. (22) 7 Force - Displacement for SW22 at Node 7

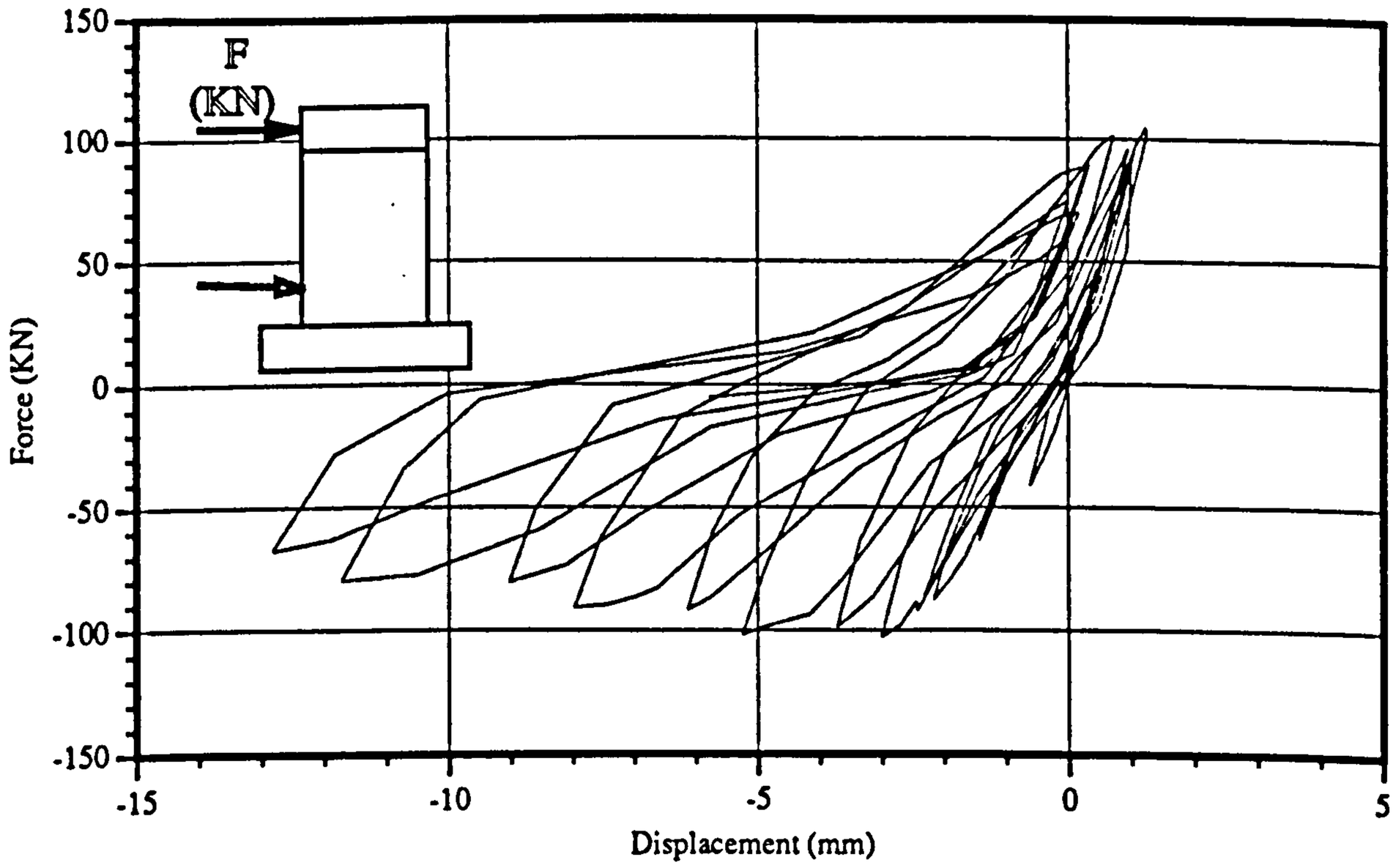


Fig. AI. (22) 8 Force - Displacement for SW22 at Node 8

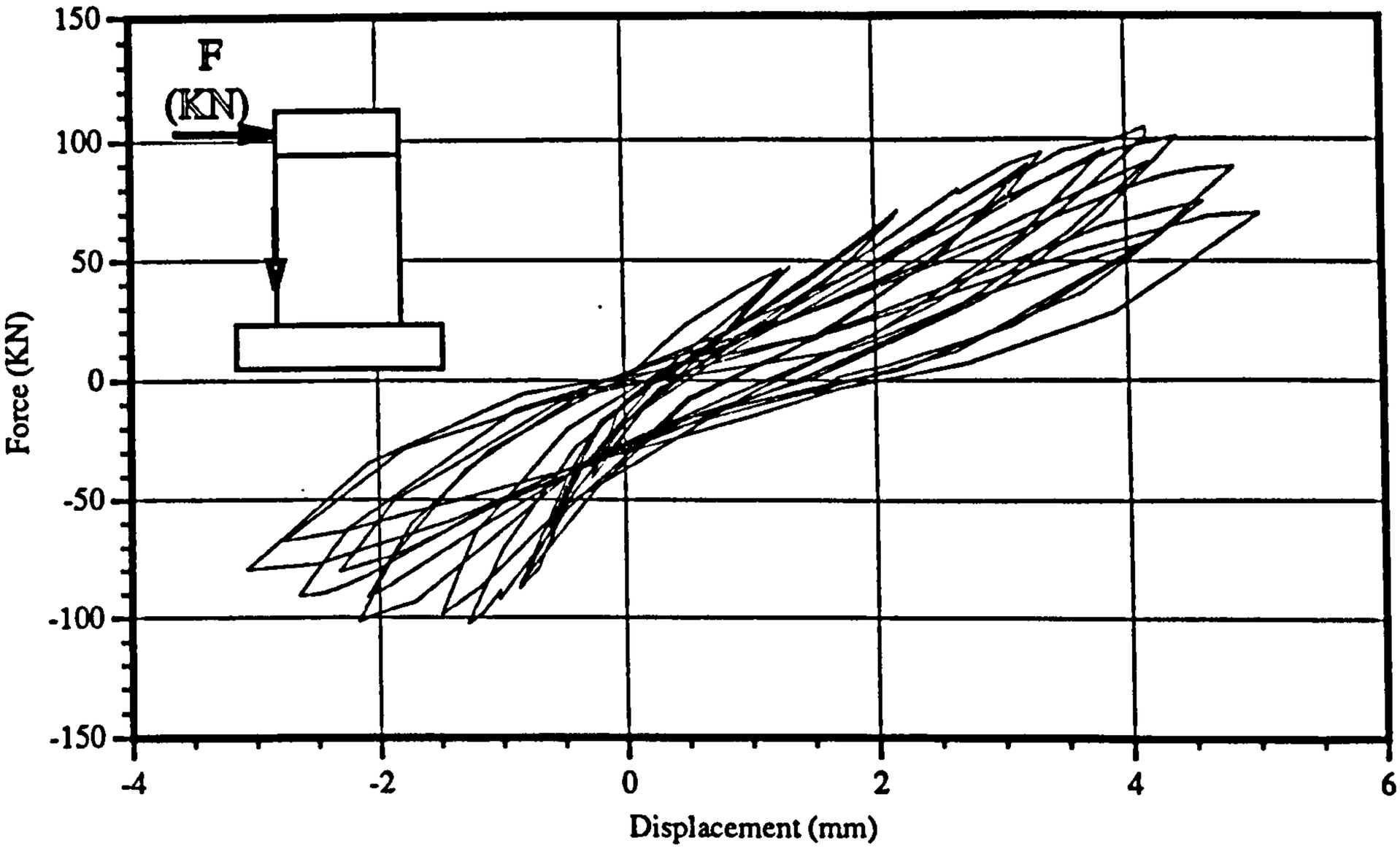


Fig. AI. (22) 9 Force - Displacement for SW22 at Node 9

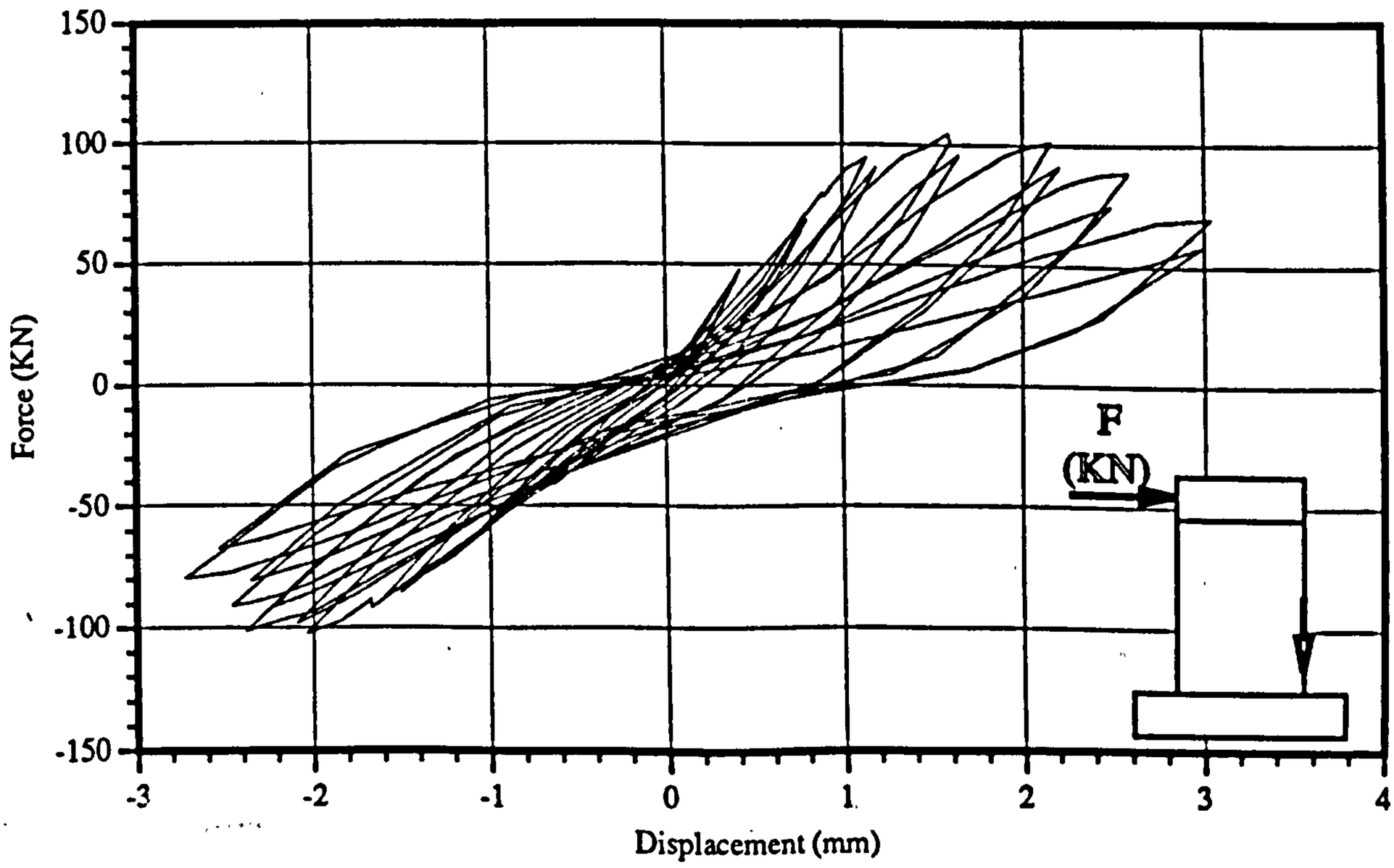


Fig. AI. (22) 10 Force - Displacement for SW22 at Node 10

AI.7 : Force Displacement for SW23

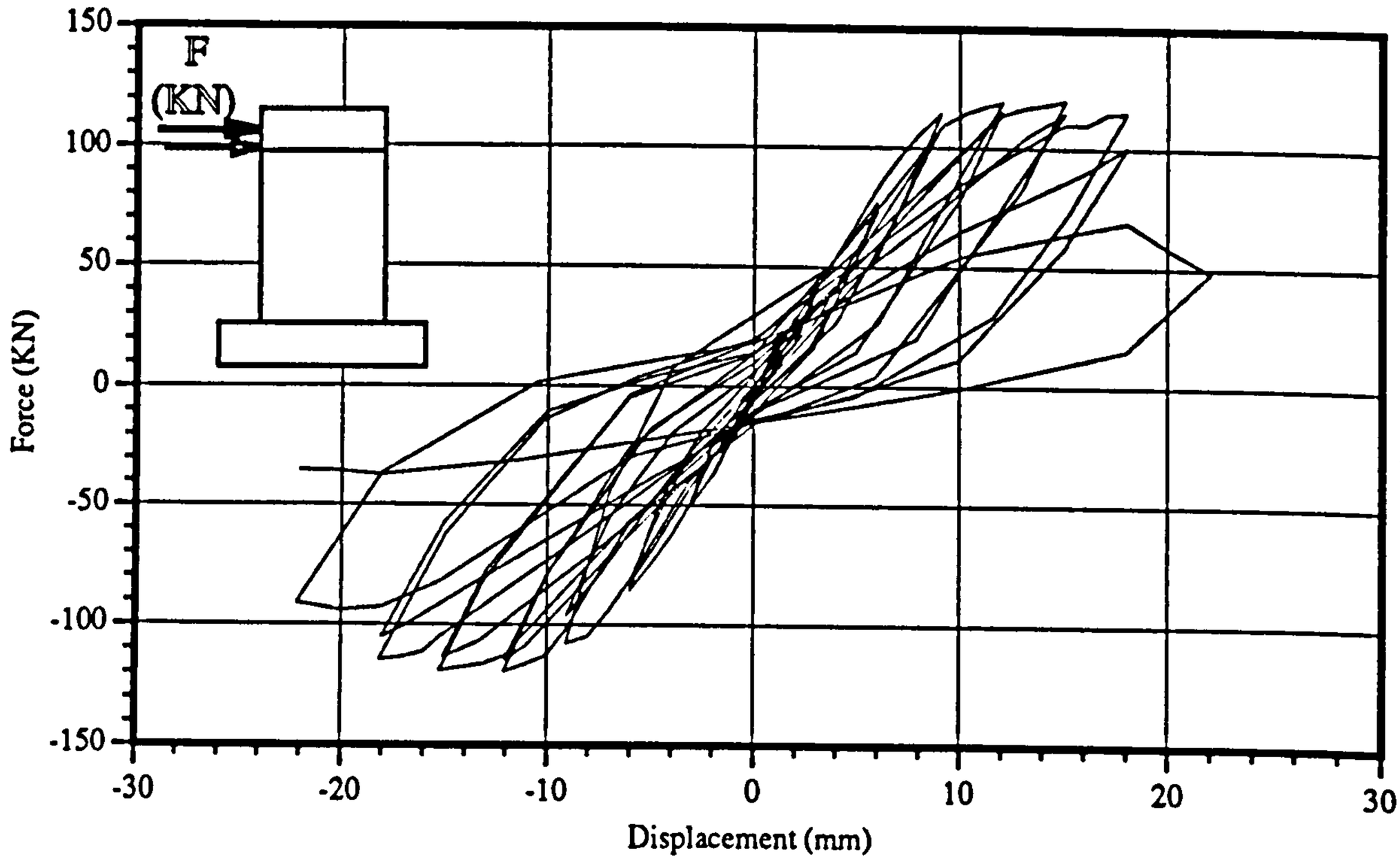


Fig. AI. (23) 1 Force - Displacement for SW23 at Node 1

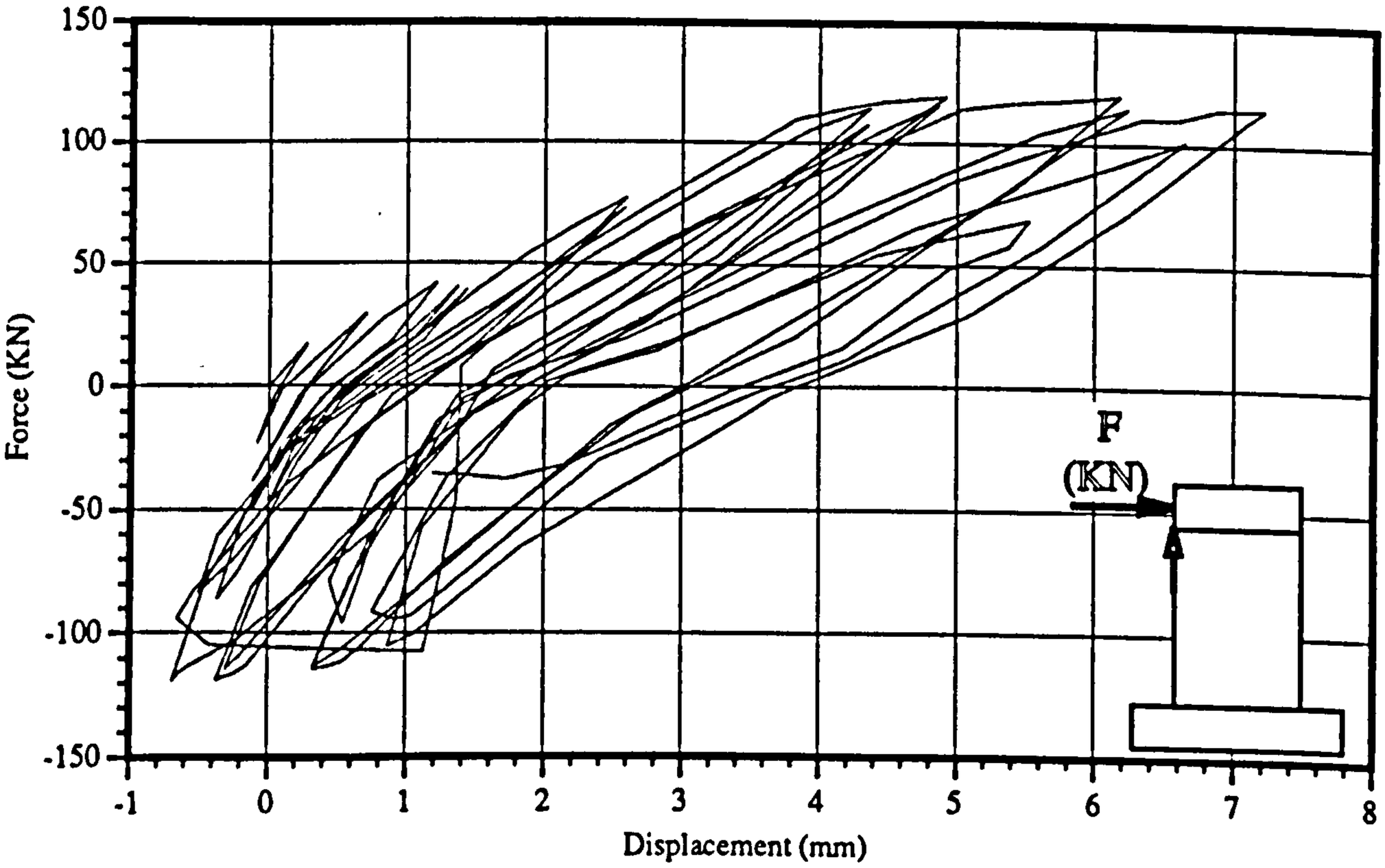


Fig. AI. (23) 2 Force - Displacement for SW23 at Node 2



Fig. AI. (23) 3 Force - Displacement for SW23 at Node 3

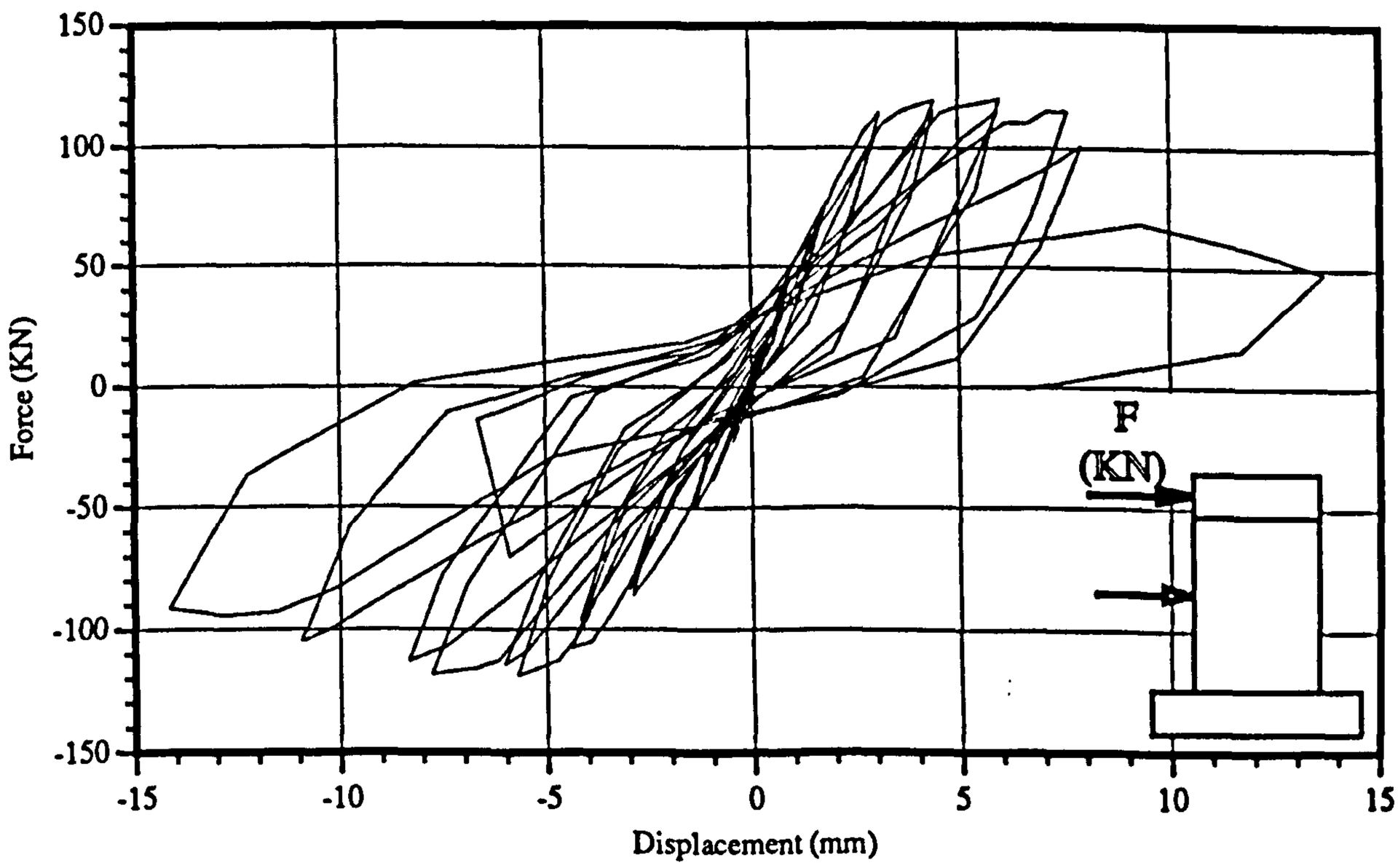


Fig. AI. (23) 4 Force - Displacement for SW23 at Node 4

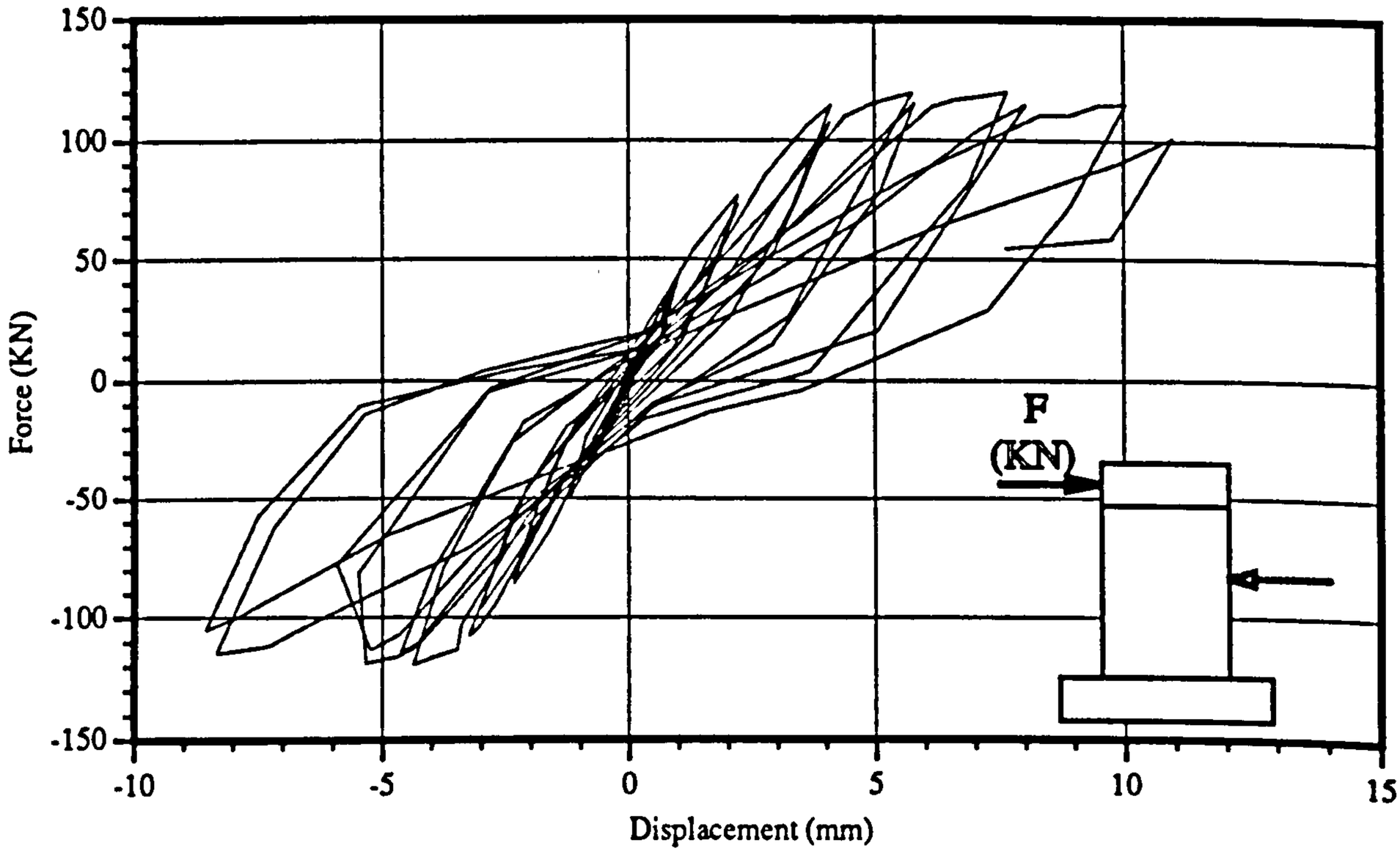


Fig. AI. (23) 5 Force - Displacement for SW23 at Node 5

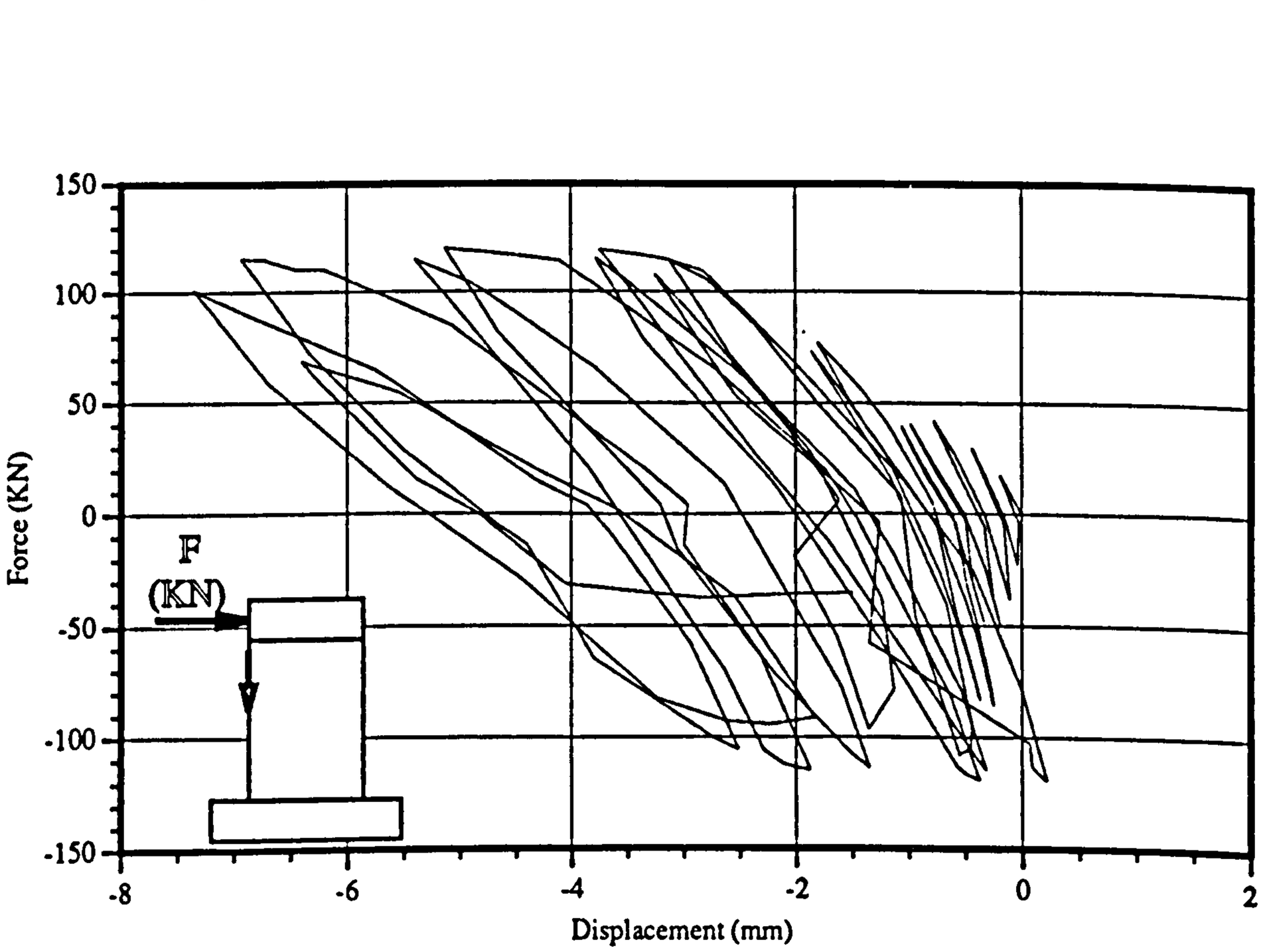


Fig. AI. (23) 6 Force - Displacement for SW23 at Node 6

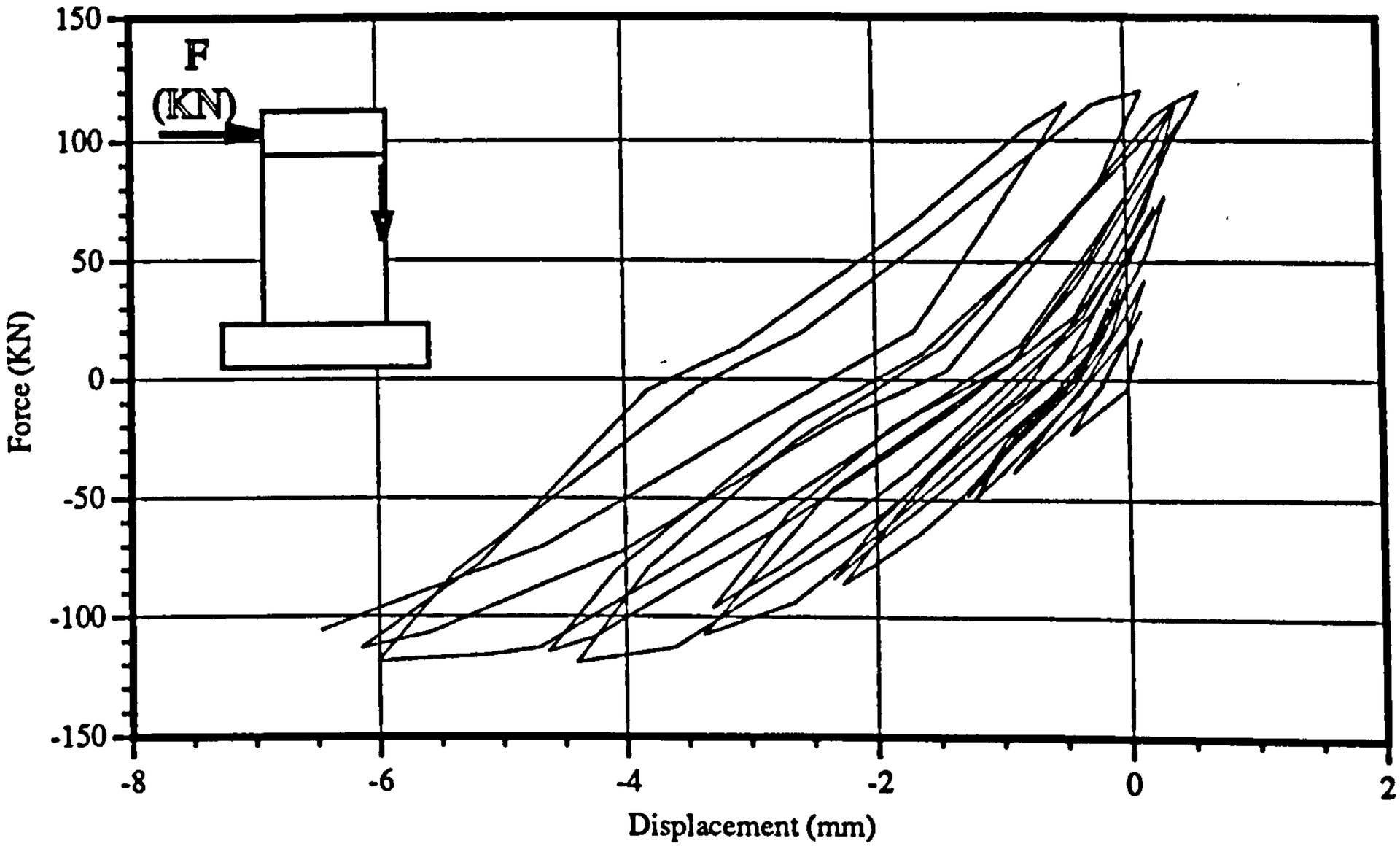


Fig. AI. (23) 7 Force - Displacement for SW23 at Node 7

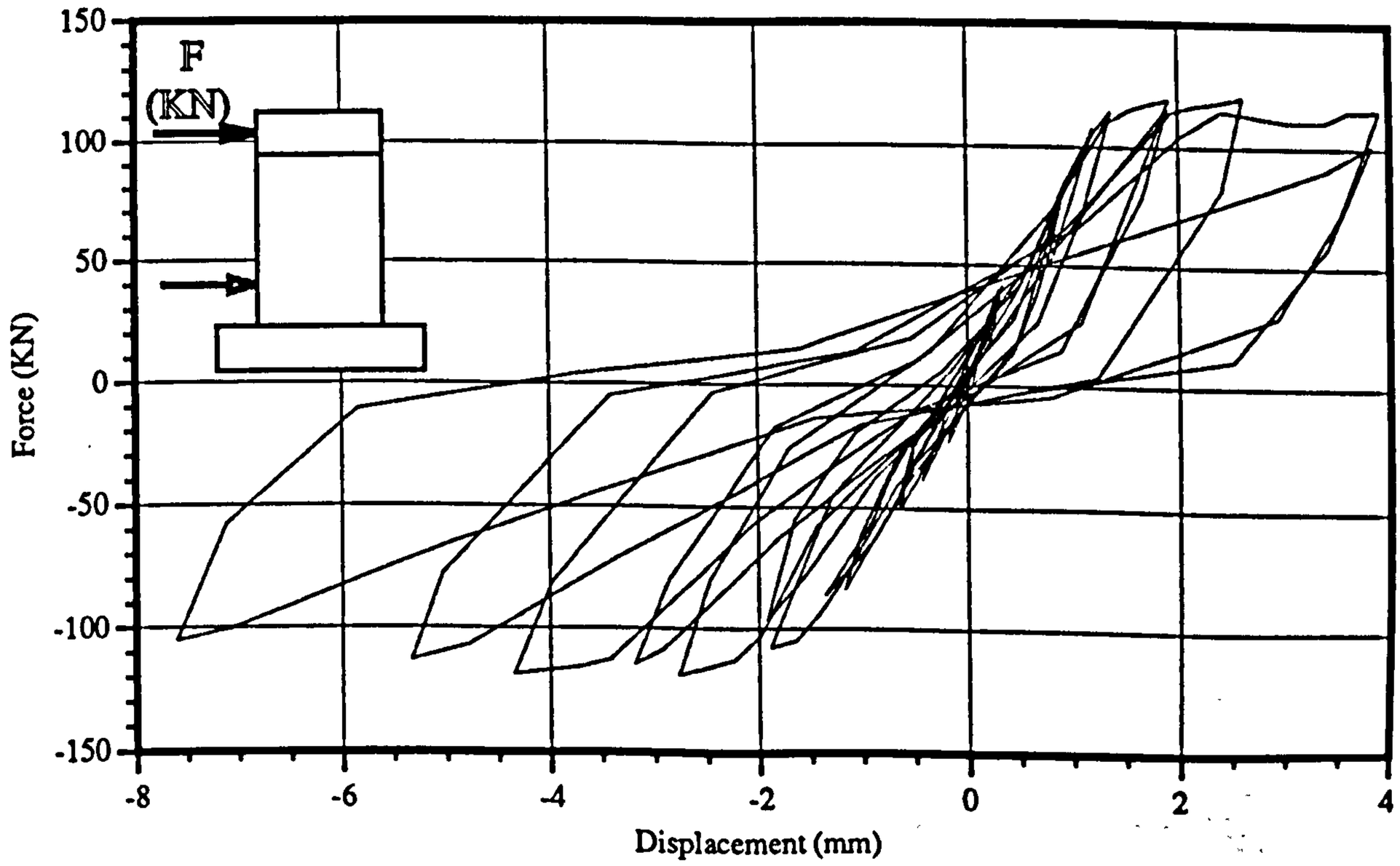


Fig. AI. (23) 8 Force - Displacement for SW23 at Node 8

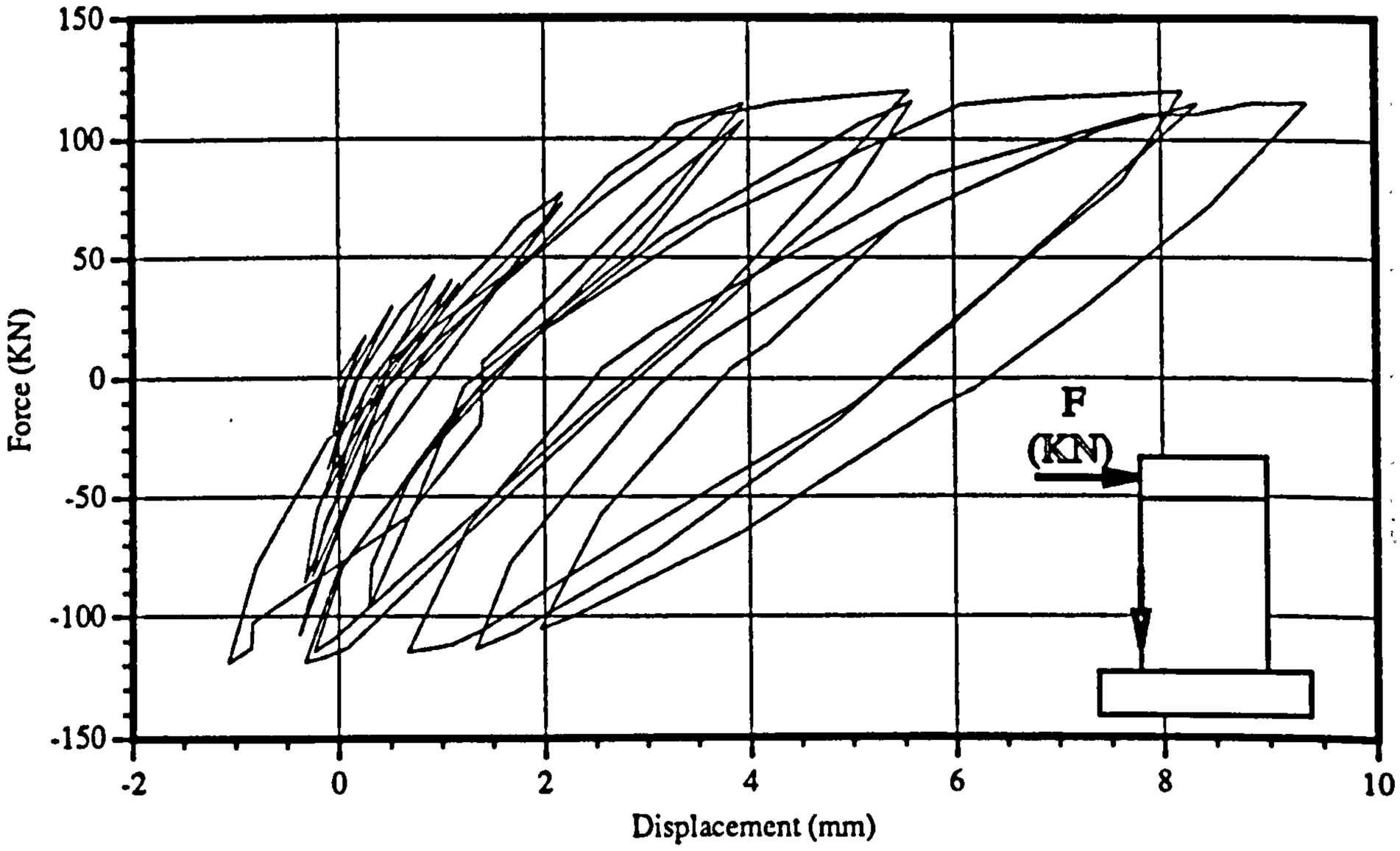


Fig. AI. (23) 9 Force - Displacement for SW23 at Node 9

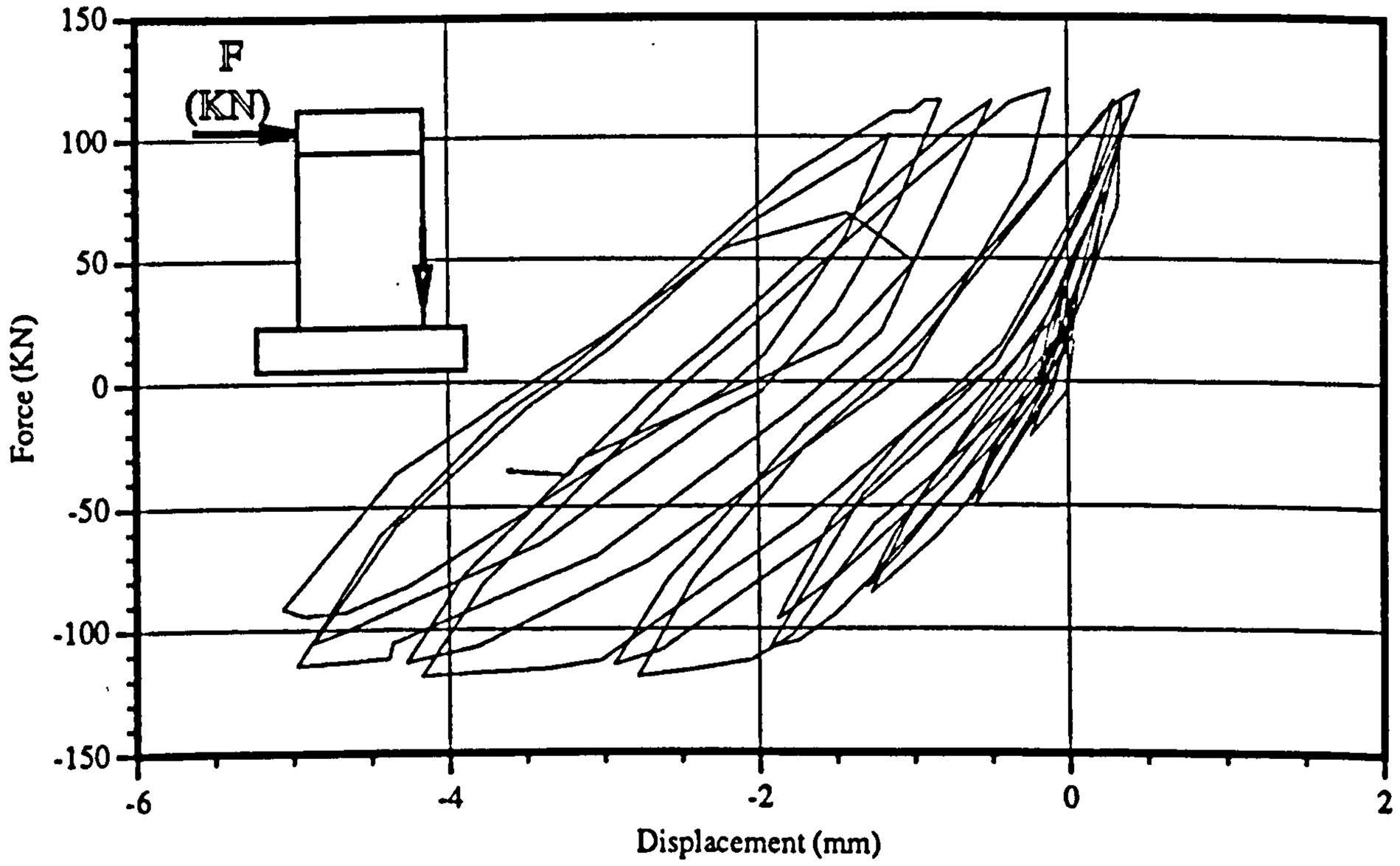


Fig. AI. (23) 10 Force - Displacement for SW23 at Node 10

AI.8 : Force Displacement For SW24

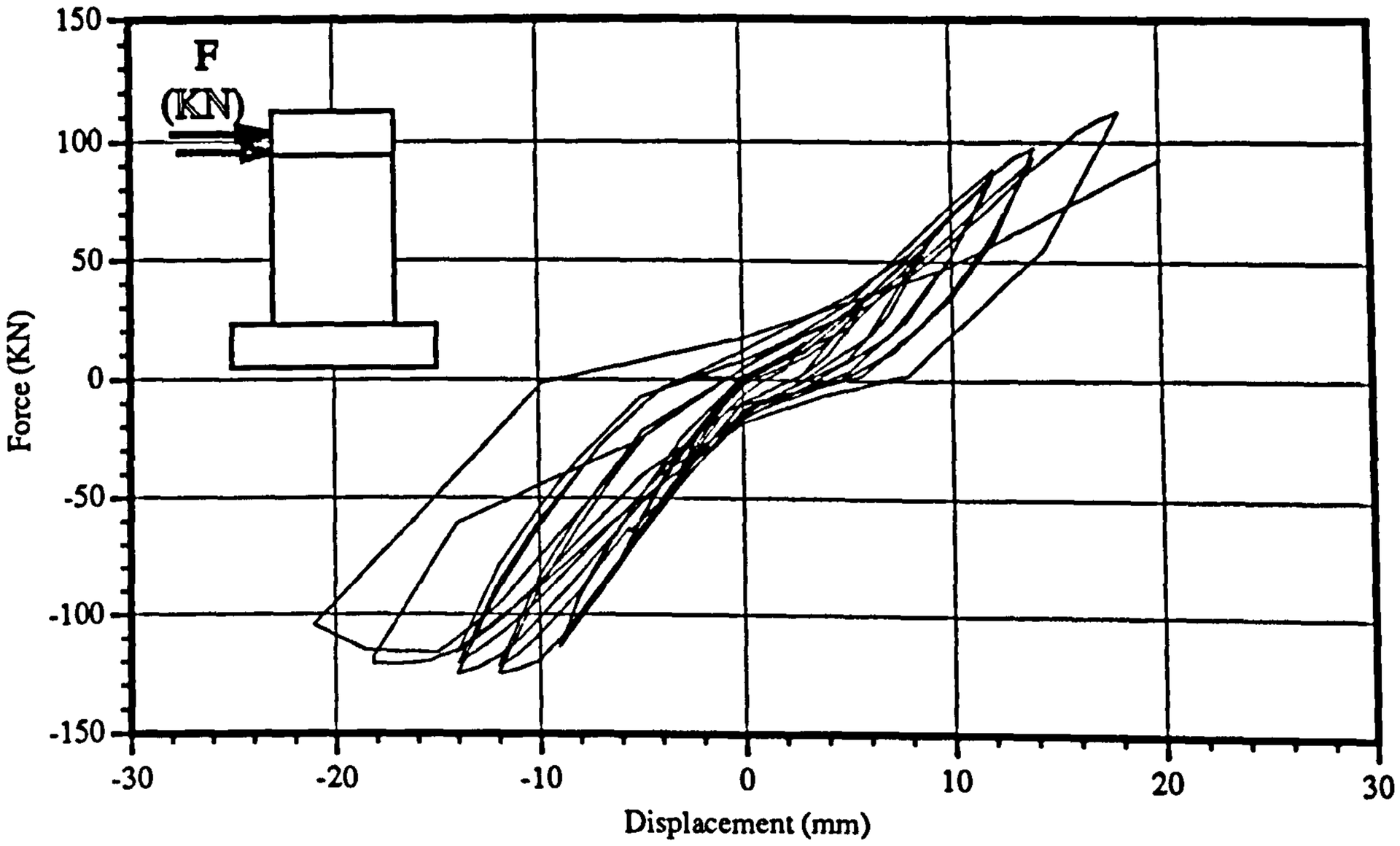


Fig. AI. (24) 1 Force - Displacement for SW24 at Node 1

Fig. AI. (24) 2 Force - Displacement for SW24 at Node 2

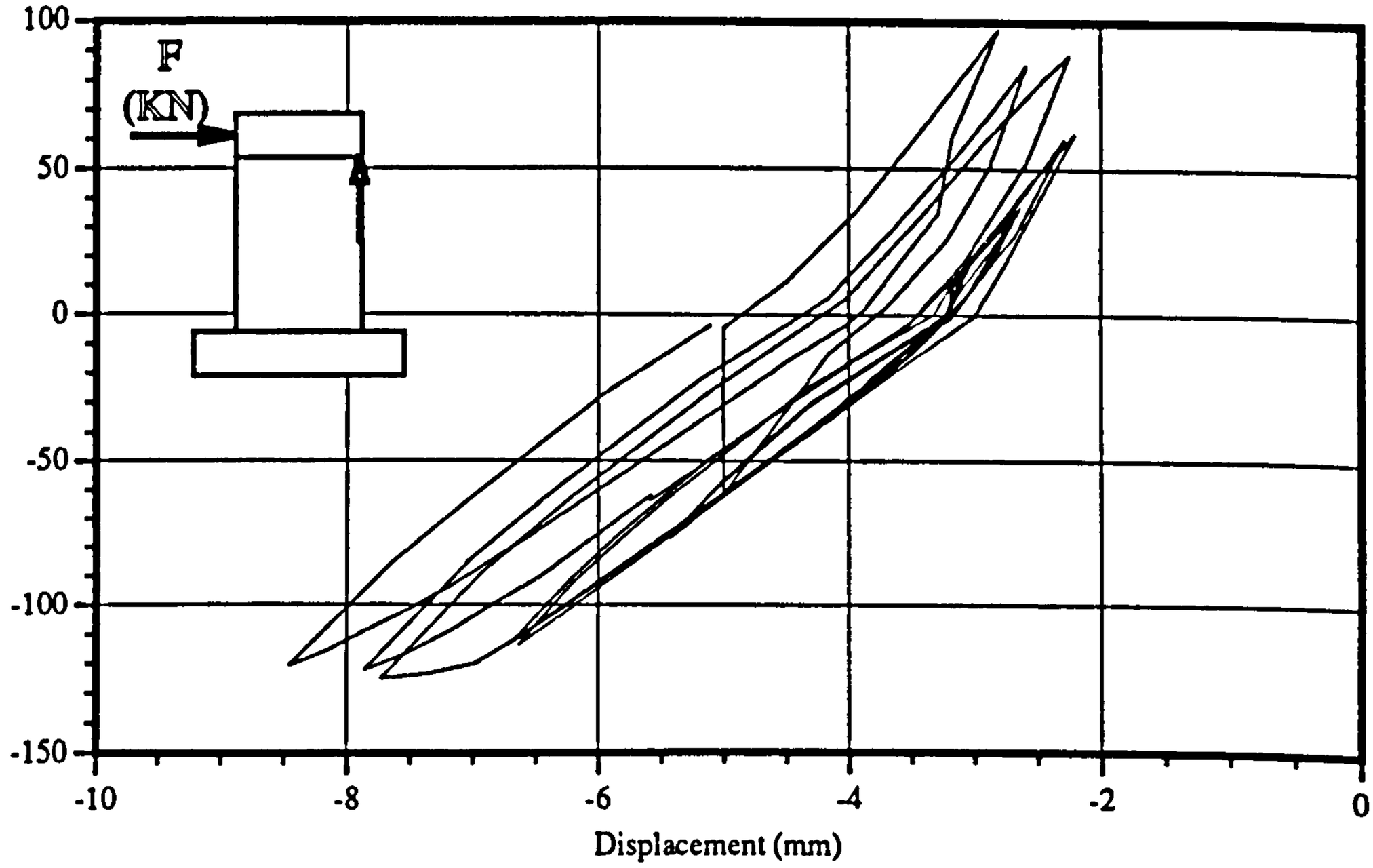


Fig. AI. (24) 3 Force - Displacement for SW24 at Node 3

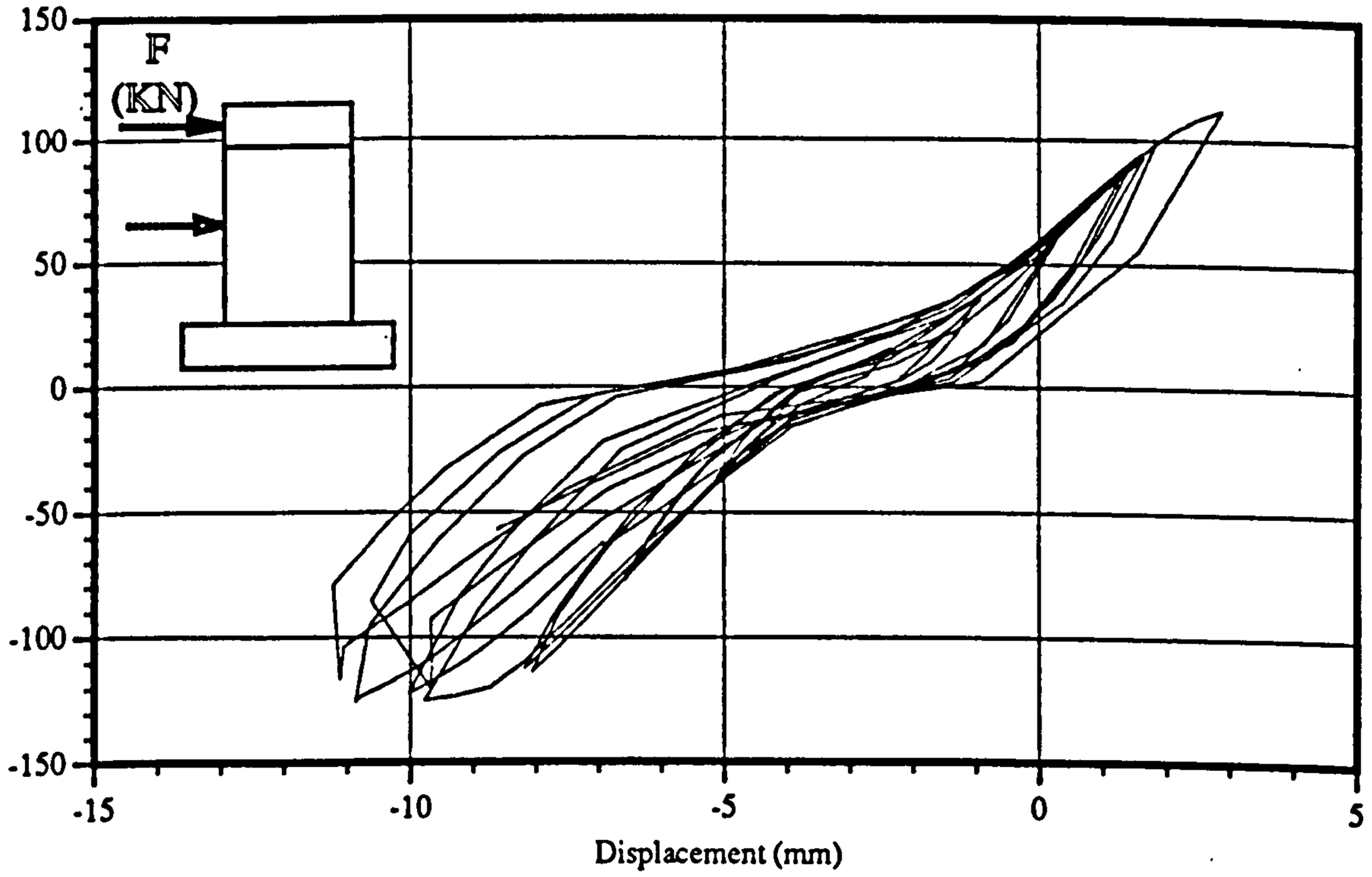


Fig. AI. (24) 4 Force - Displacement for SW24 at Node 4

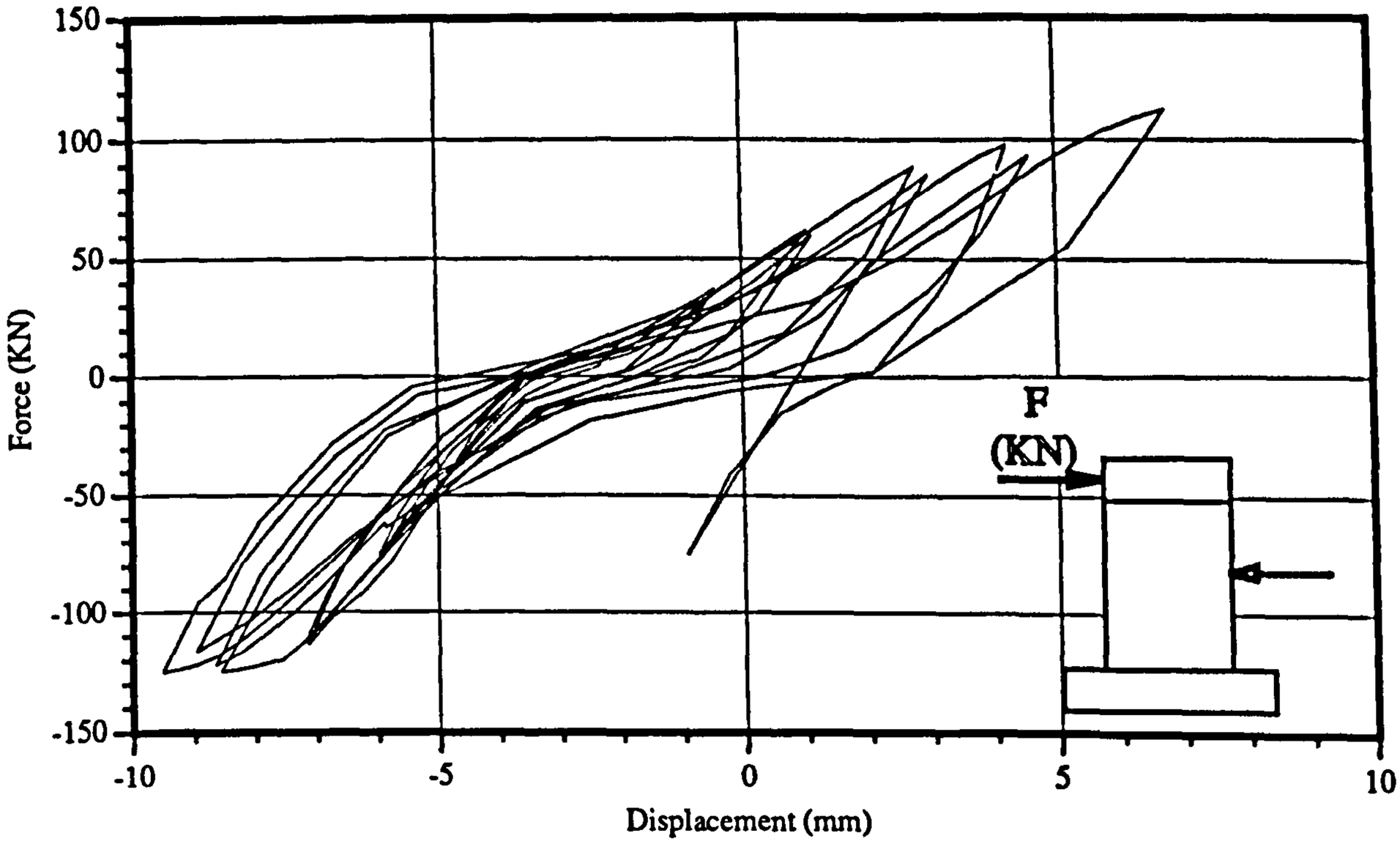


Fig. AI. (24) 5 Force - Displacement for SW24 at Node 5

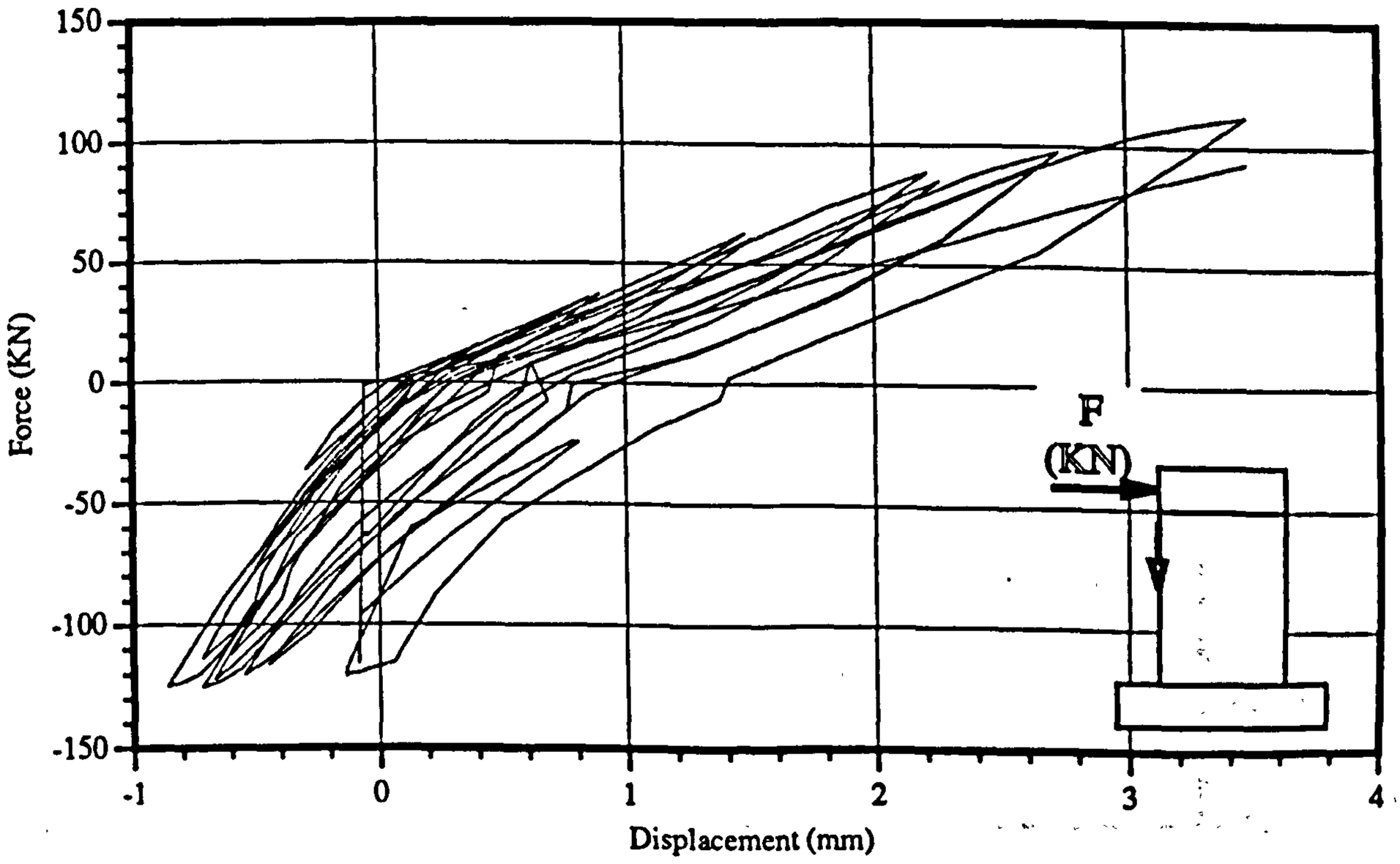


Fig. AI. (24) 6 Force - Displacement for SW24 at Node 6

AI.9 : Force Displacement for SWR21

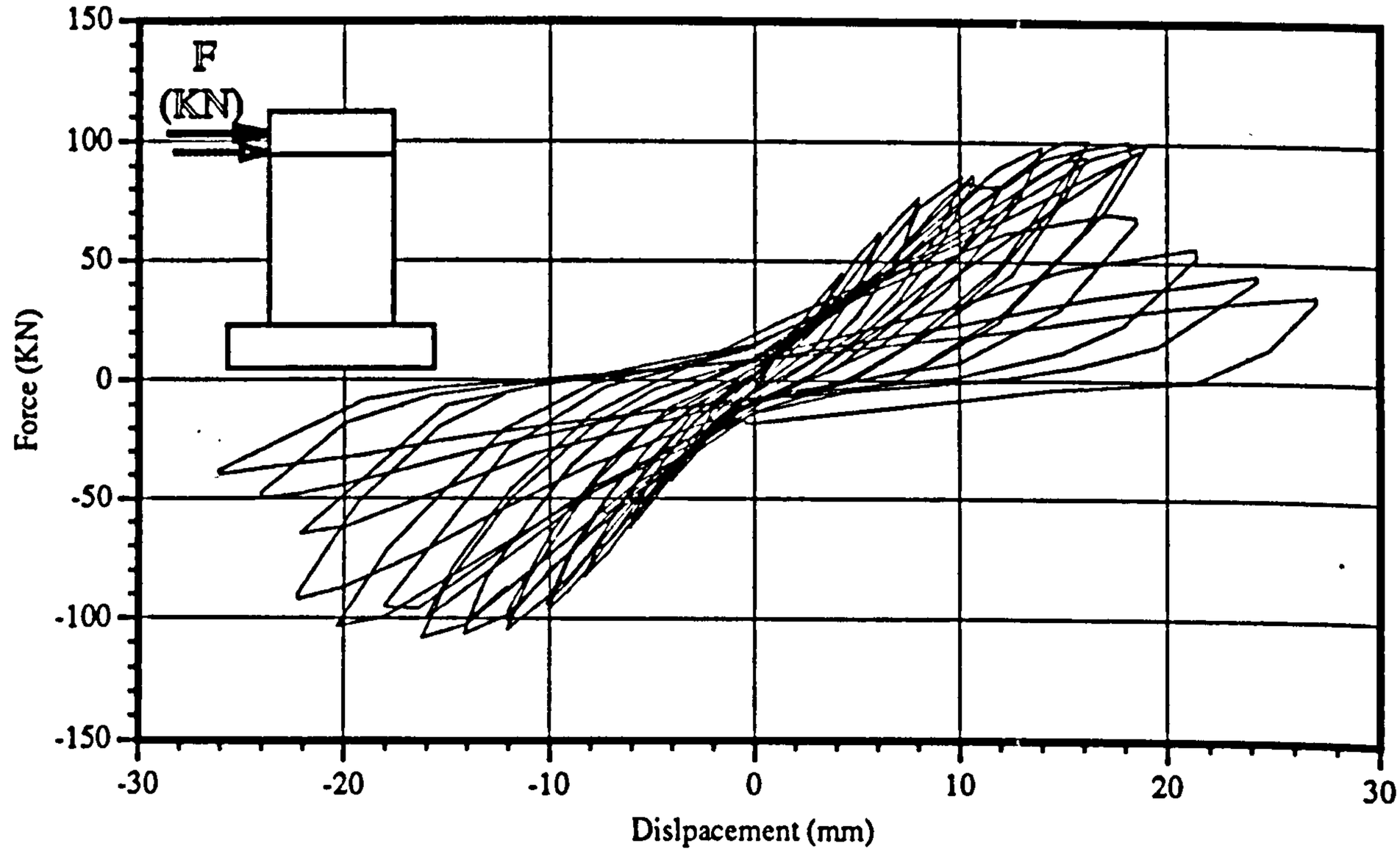


Fig. AI. (R21) 1 Force - Displacement for SWR21 at Node 1

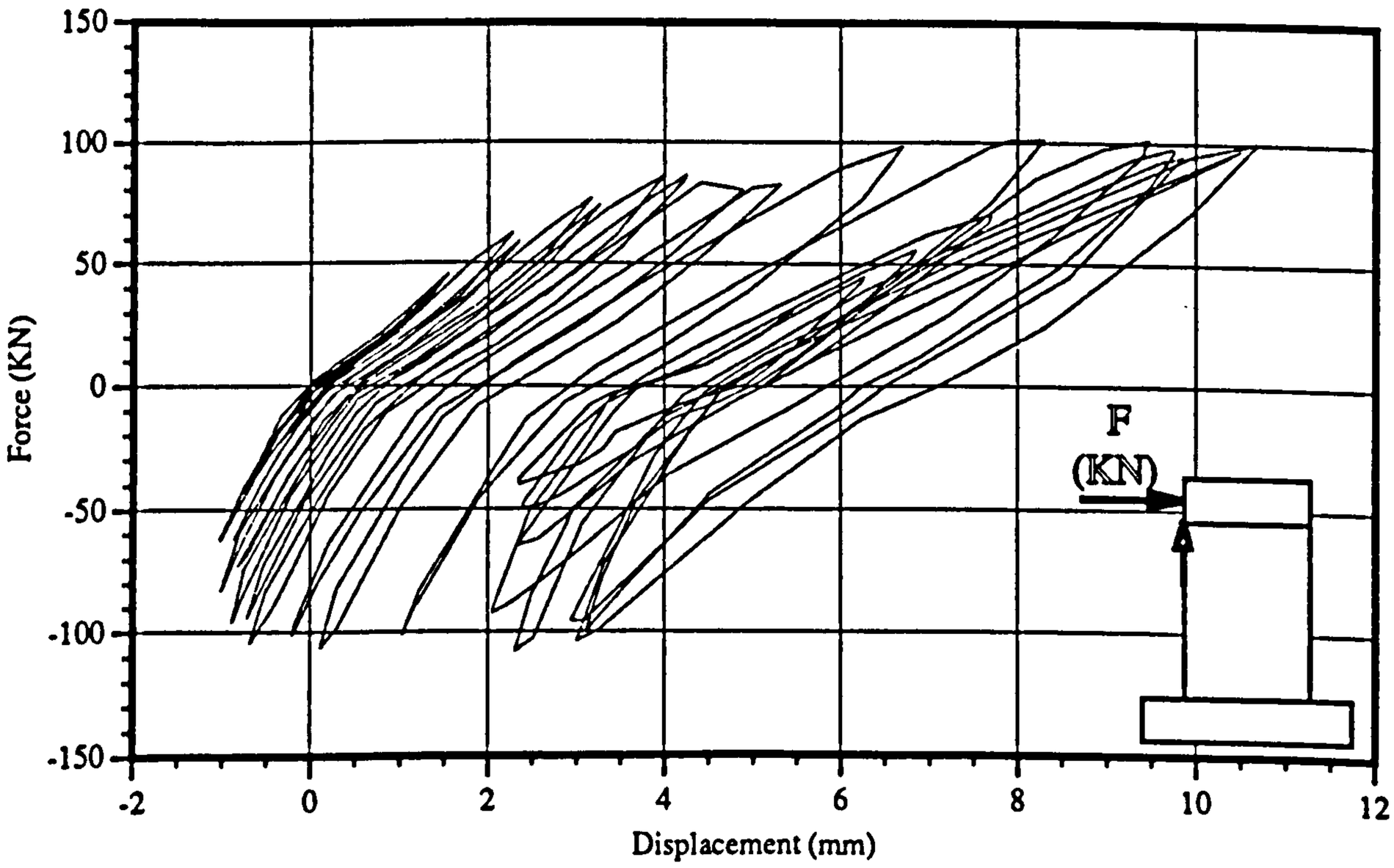


Fig. AI. (R21) 2 Force - Displacement for SWR21 at Node 2

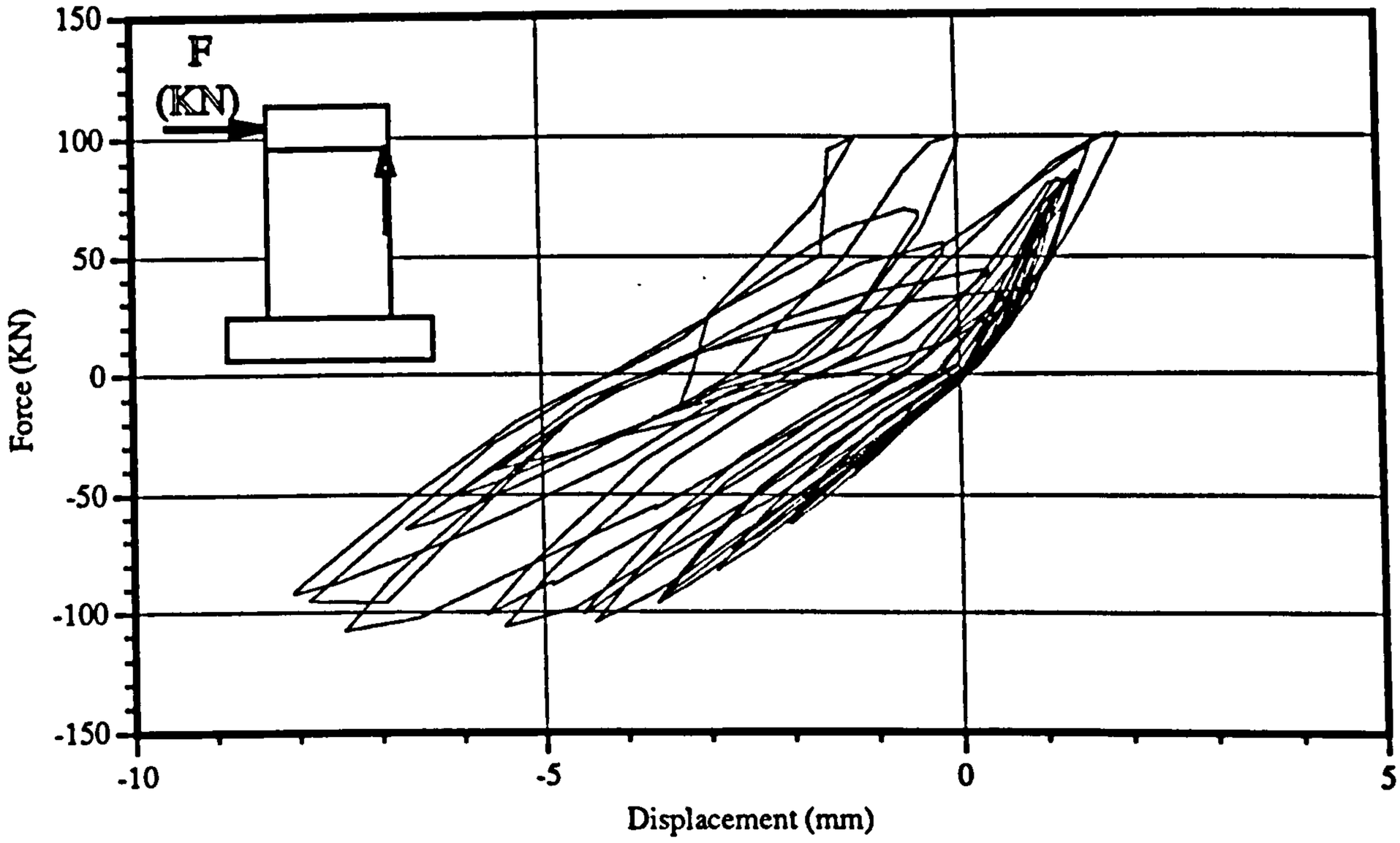


Fig. AI. (R21) 3 Force - Displacement for SWR21 at Node 3

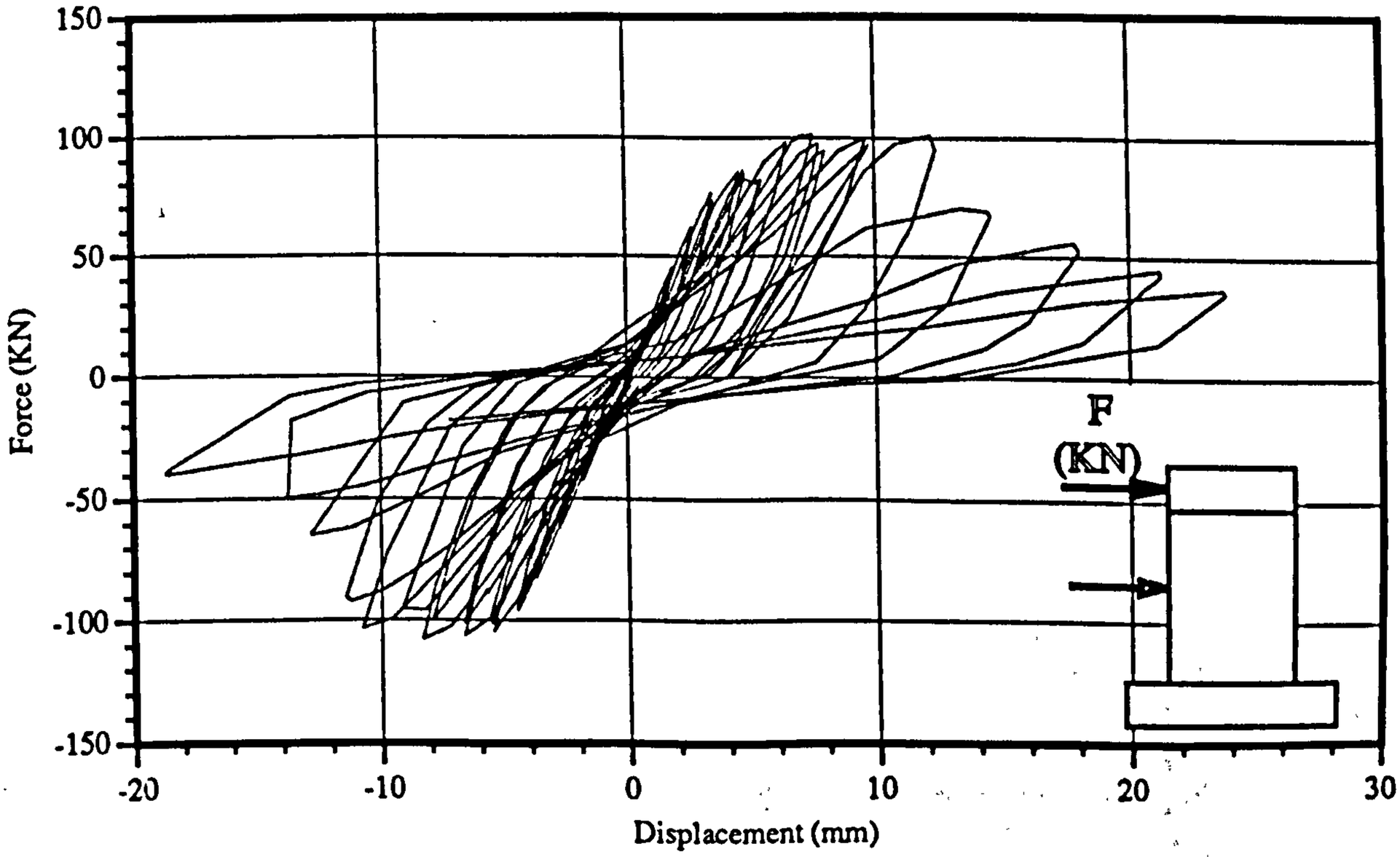


Fig. AI. (R21) 4 Force - Displacement for SWR21 at Node 4

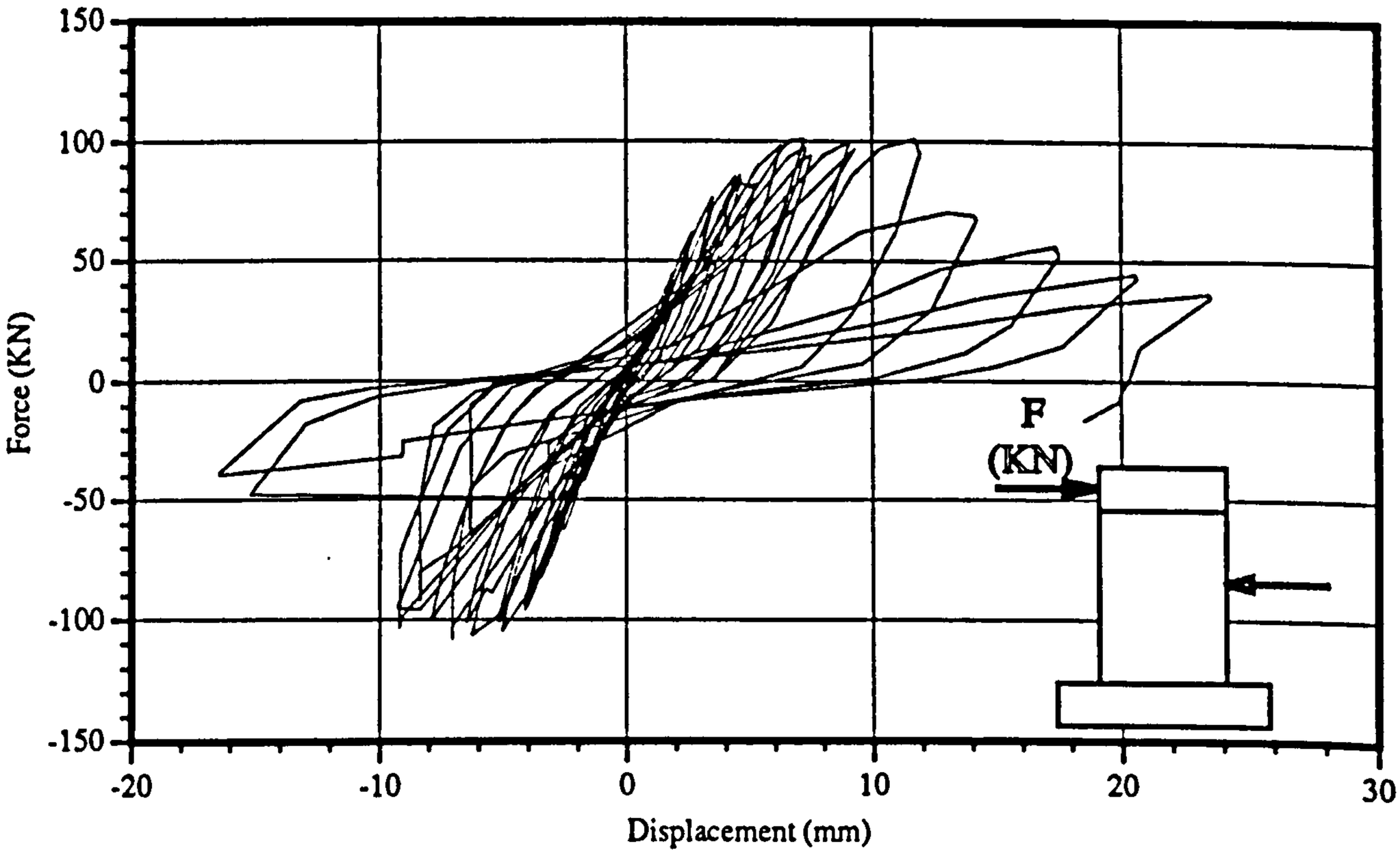


Fig. AI. (R21) 5 Force - Displacement for SWR21 at Node 5

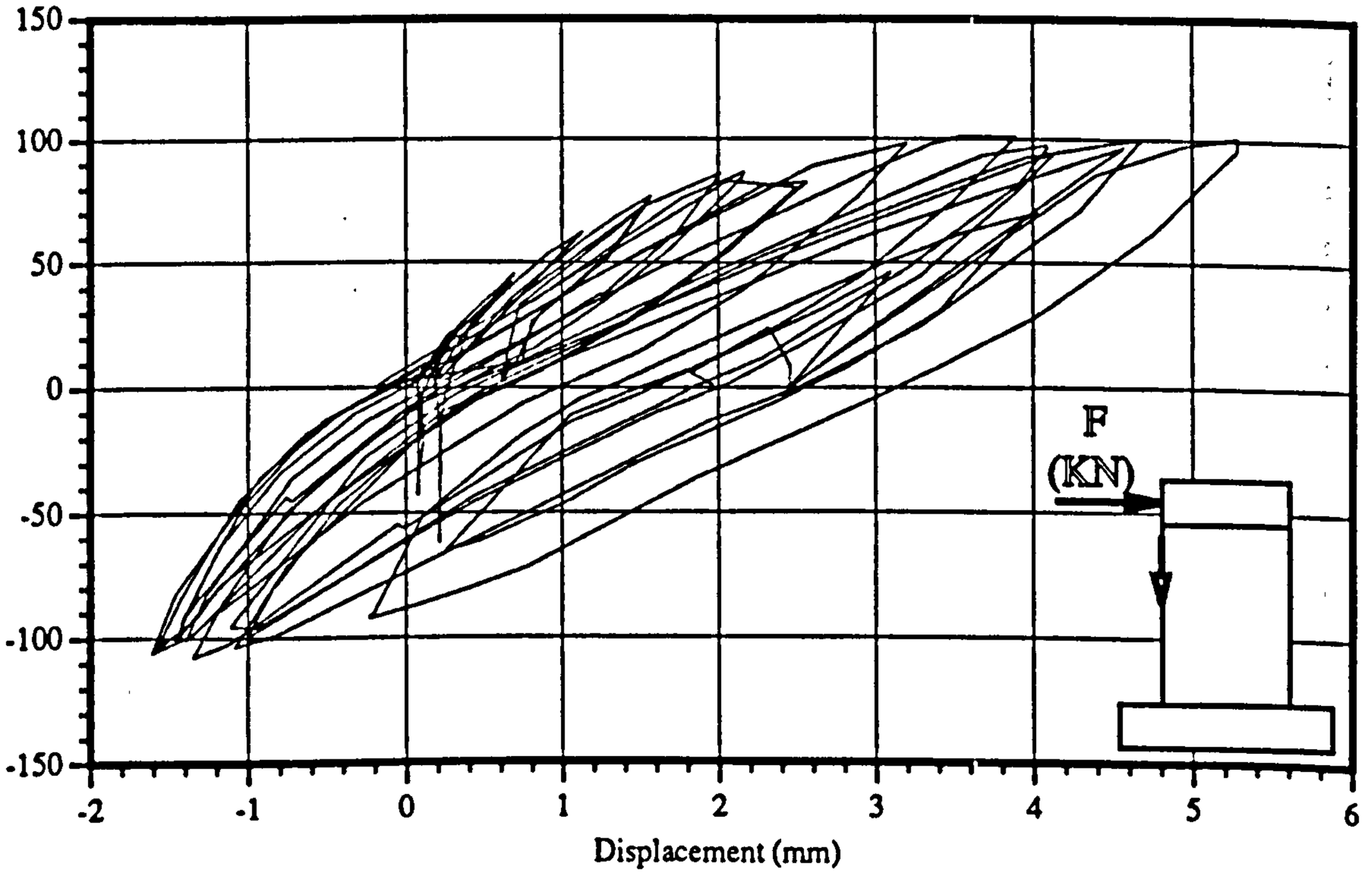


Fig. AI. (R21) 6 Force - Displacement for SWR21 at Node 6

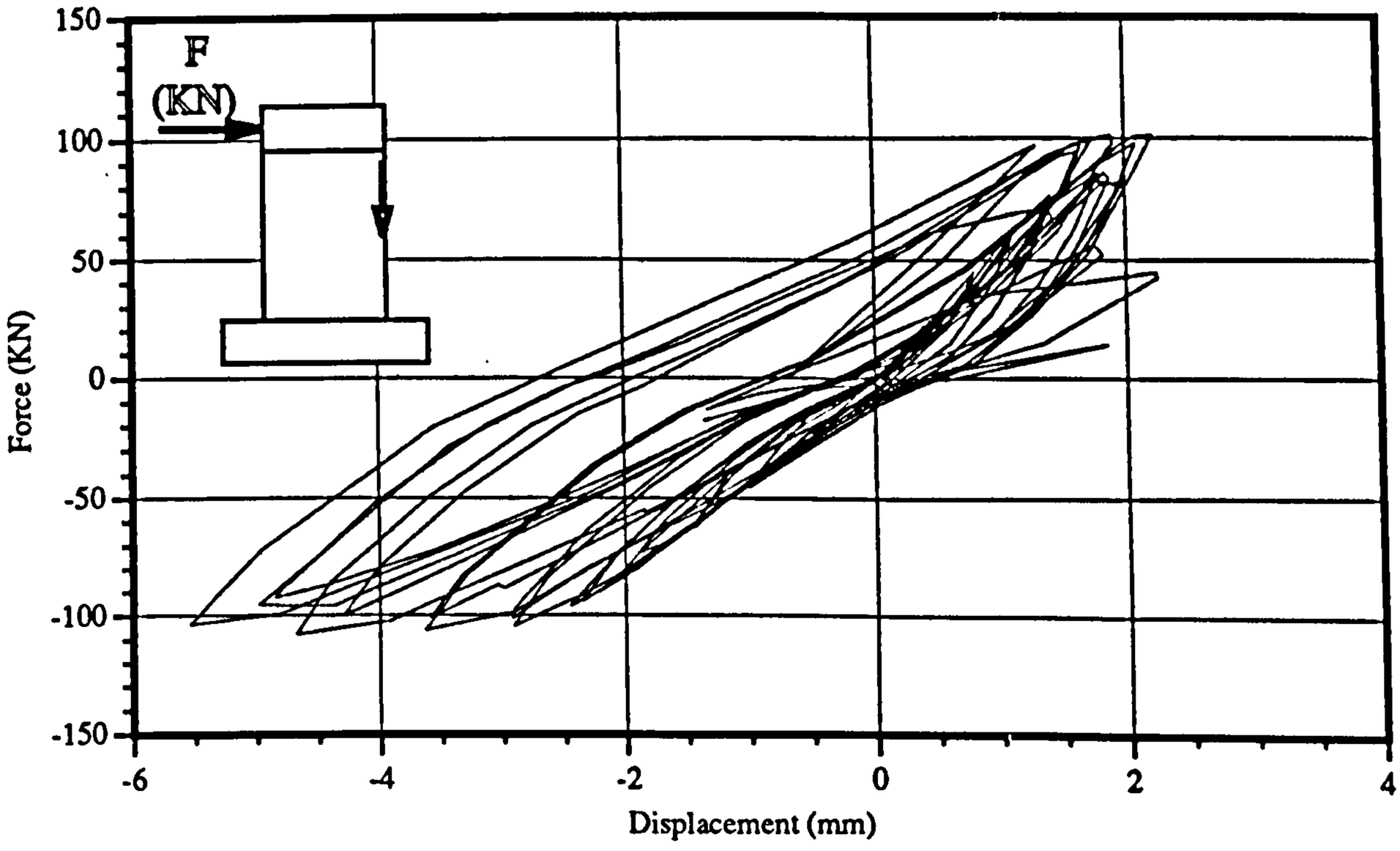


Fig. AI. (R21) 7 Force - Displacement for SWR21 at Node 7

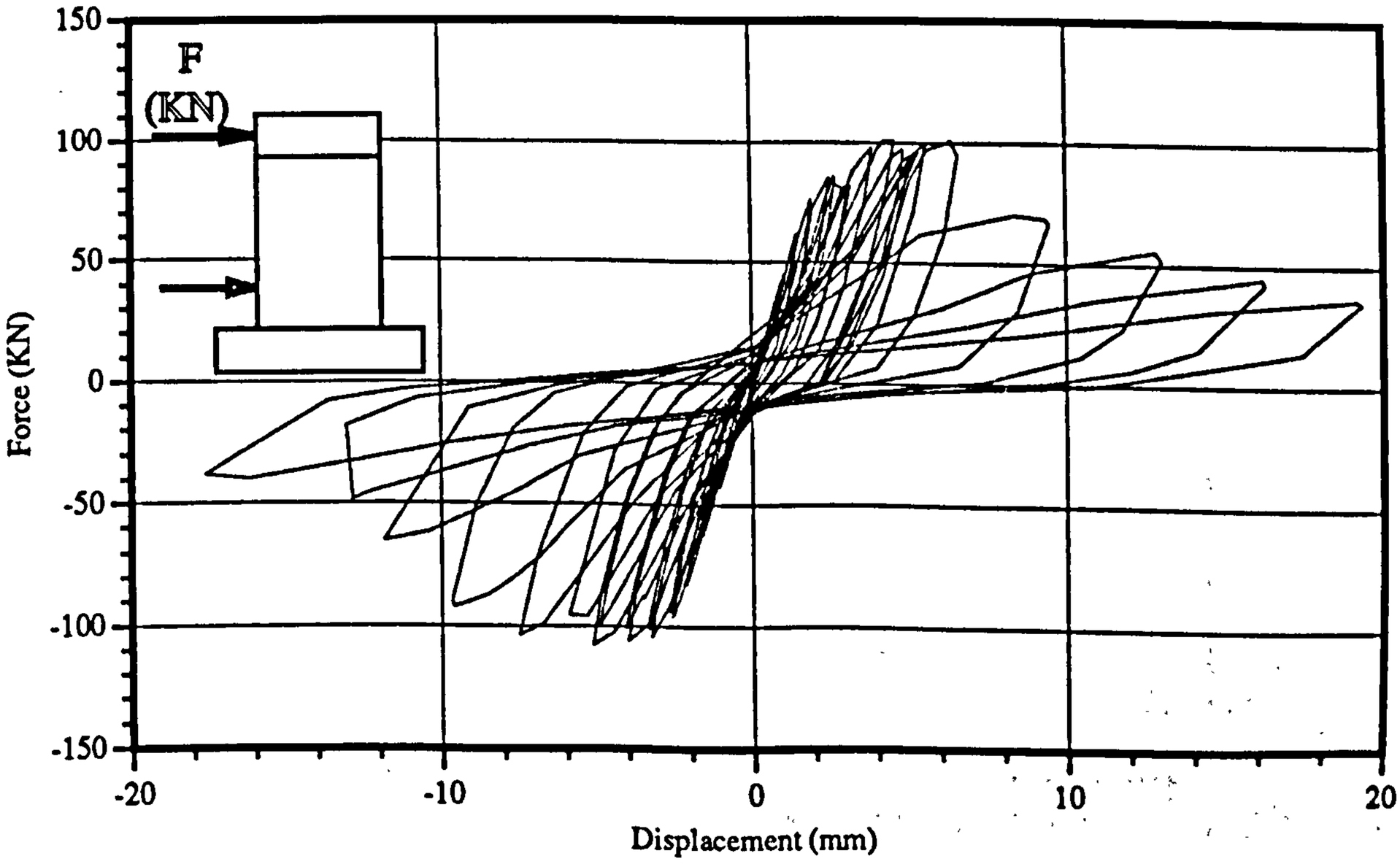


Fig. AI. (R21) 8 Force - Displacement for SWR21 at Node 8

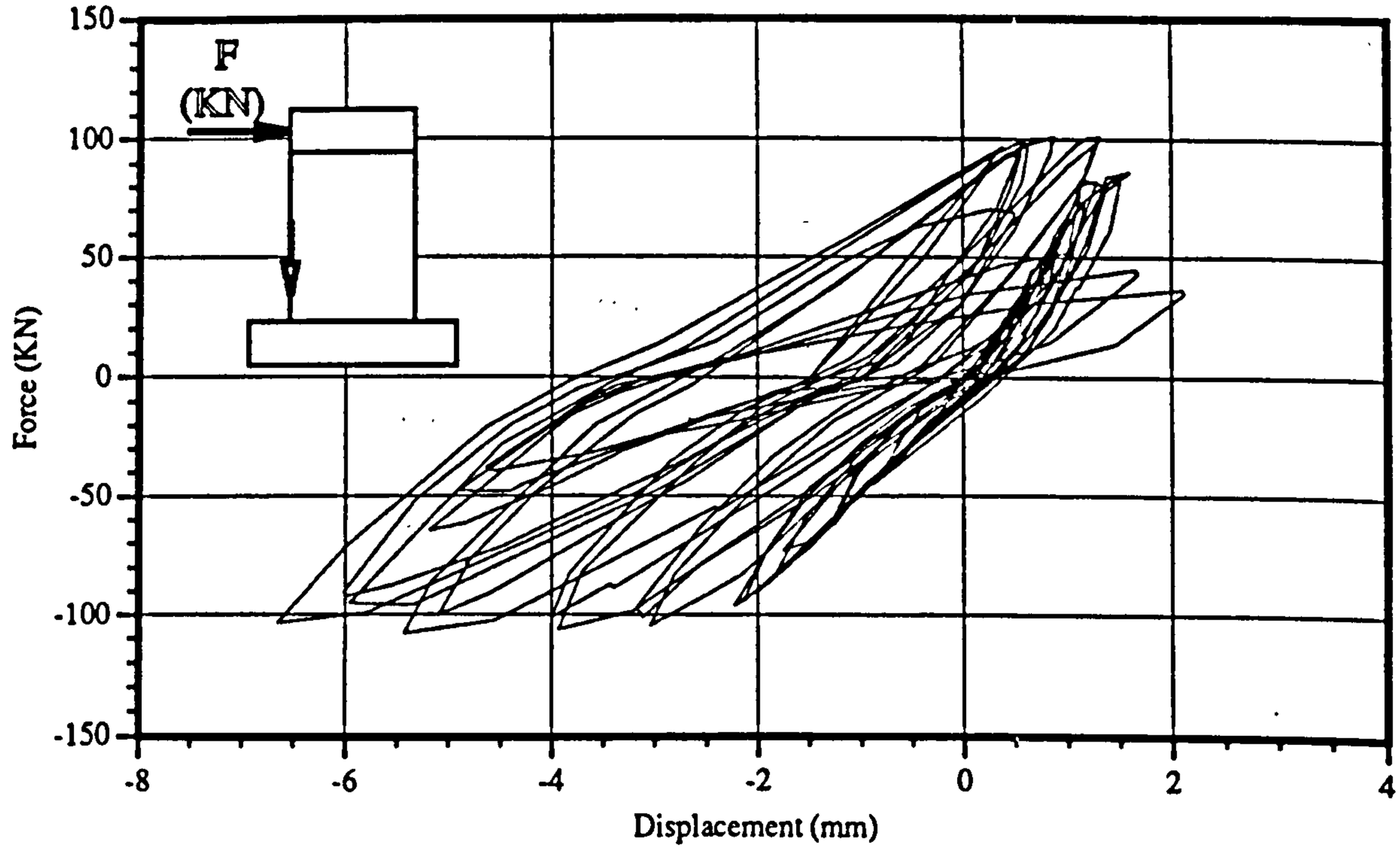


Fig. AI. (R21) 9 Force - Displacement for SWR21 at Node 9

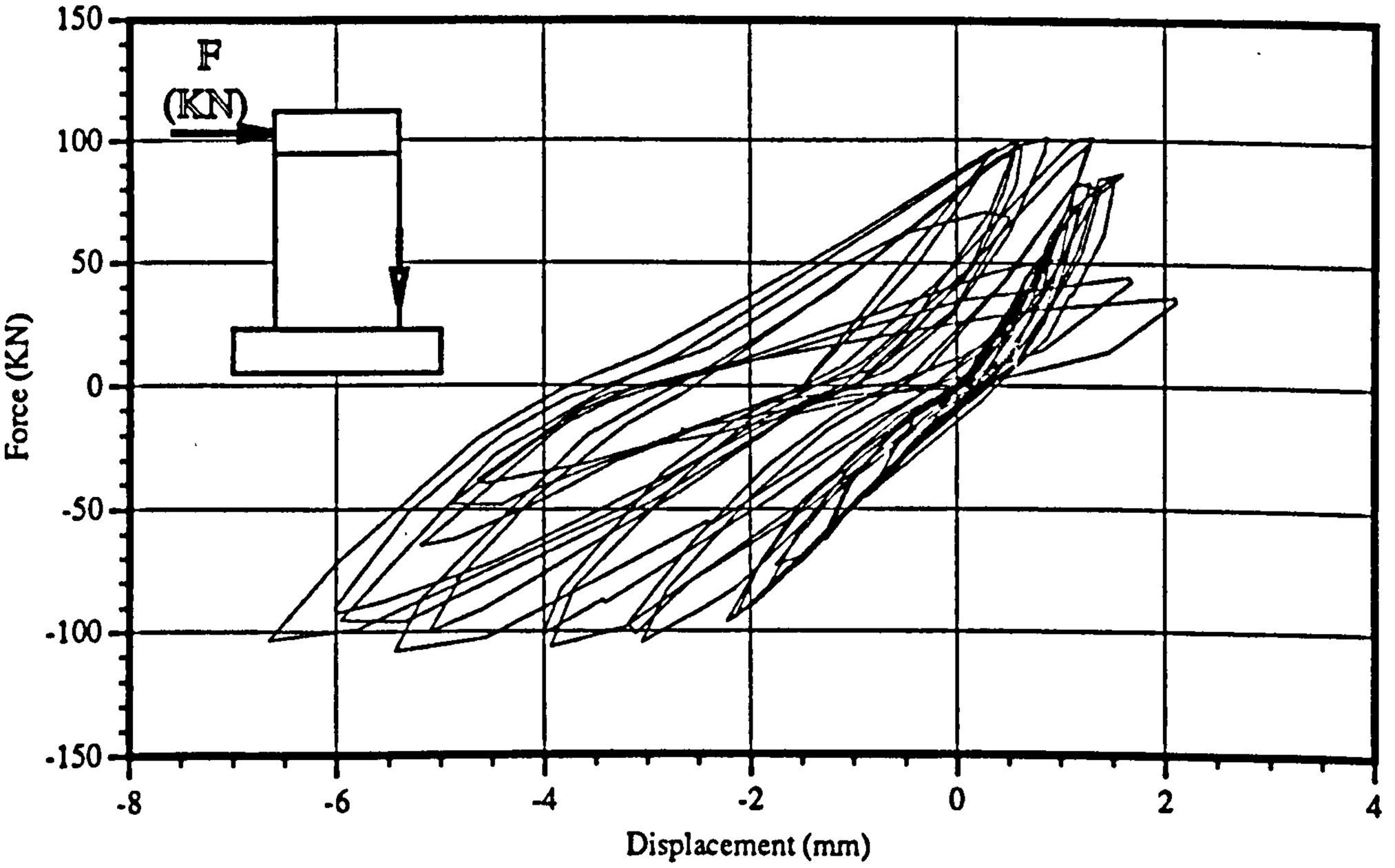


Fig. AI. (R21) 10 Force - Displacement for SWR21 at Node 10

AI.10 : Force Displacement for SWR22

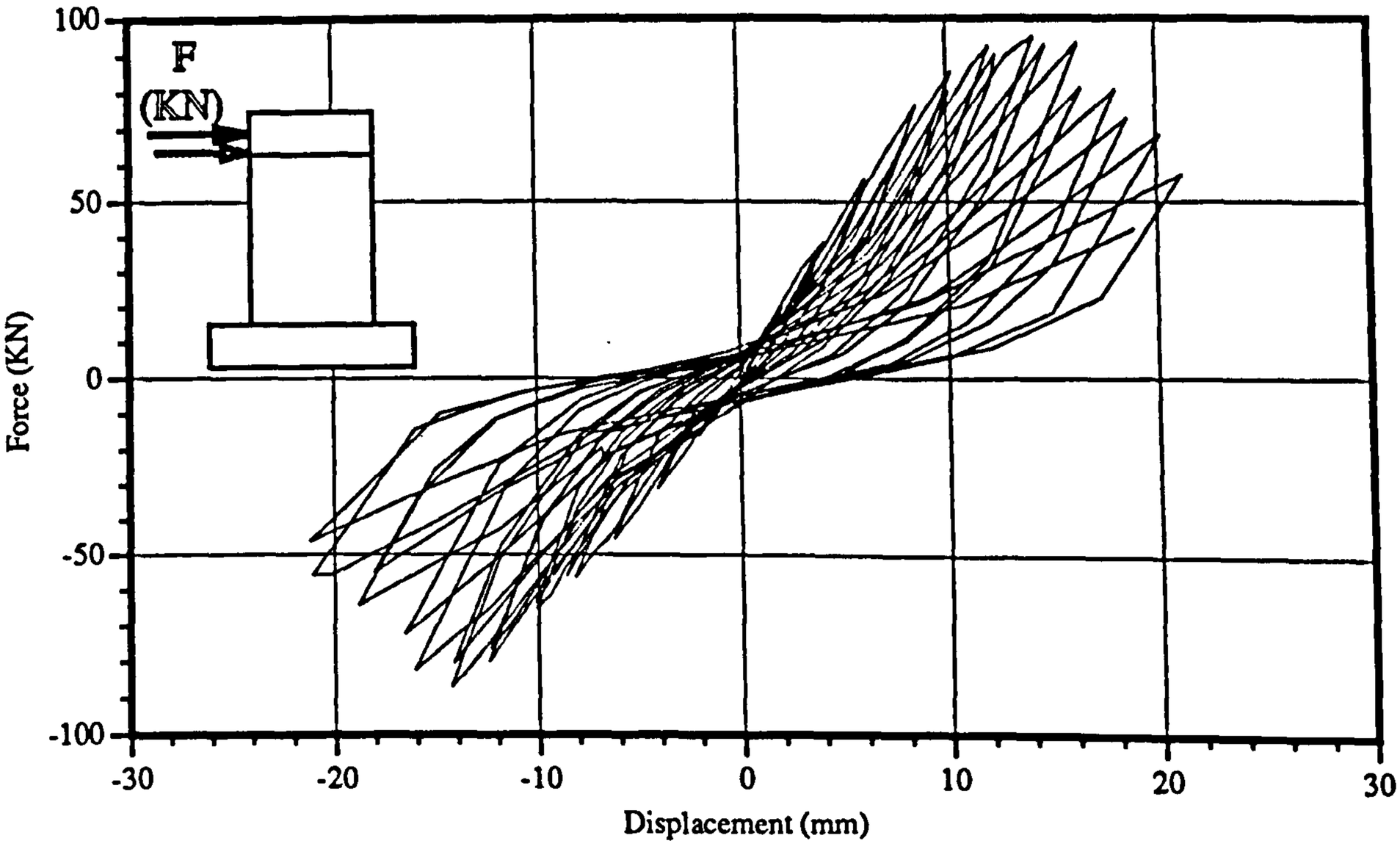


Fig. AI. (R22) 1 Force - Displacement for SWR22 at Node 1

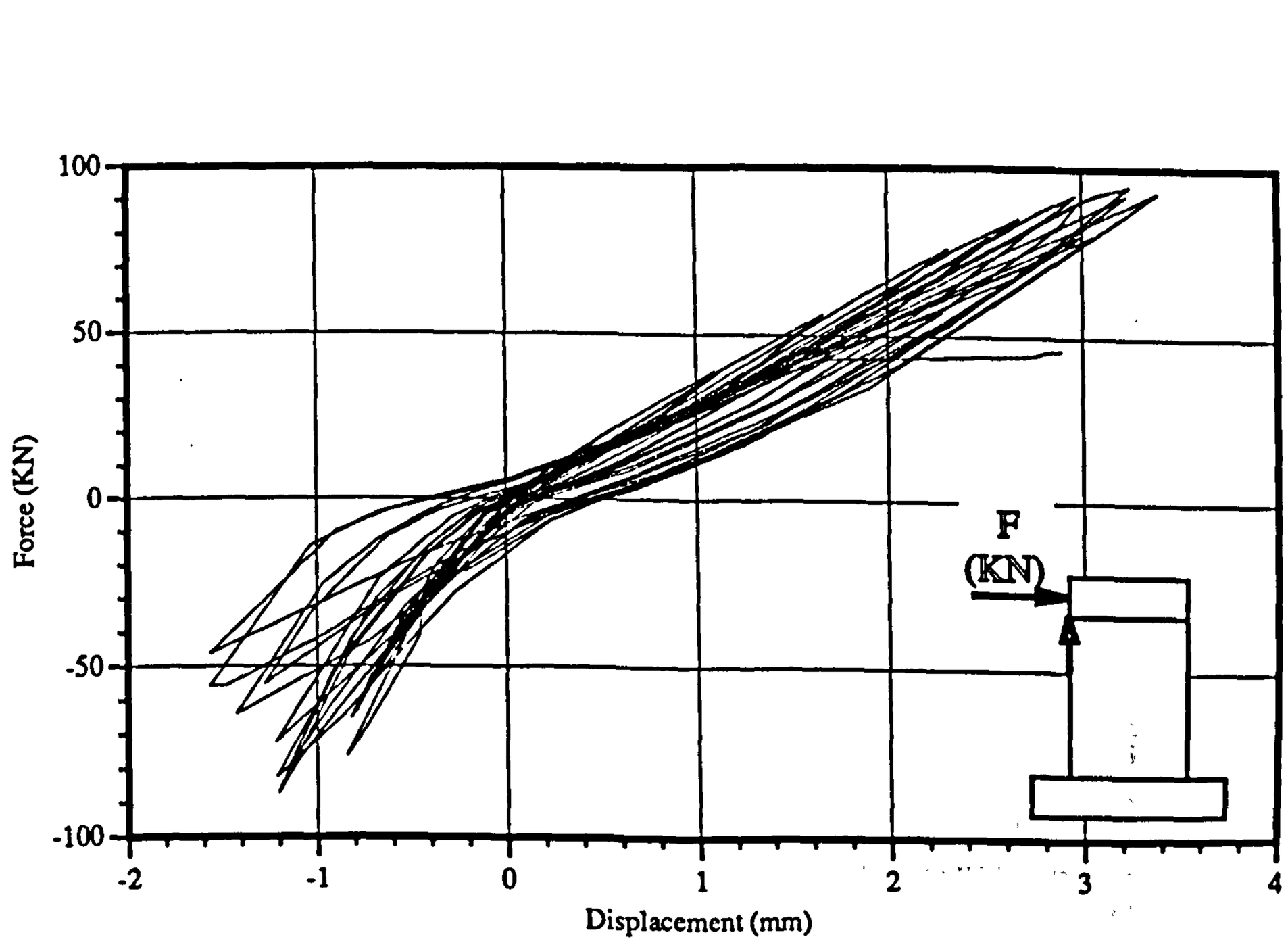


Fig. AI. (R22) 2 Force - Displacement for SWR22 at Node 2

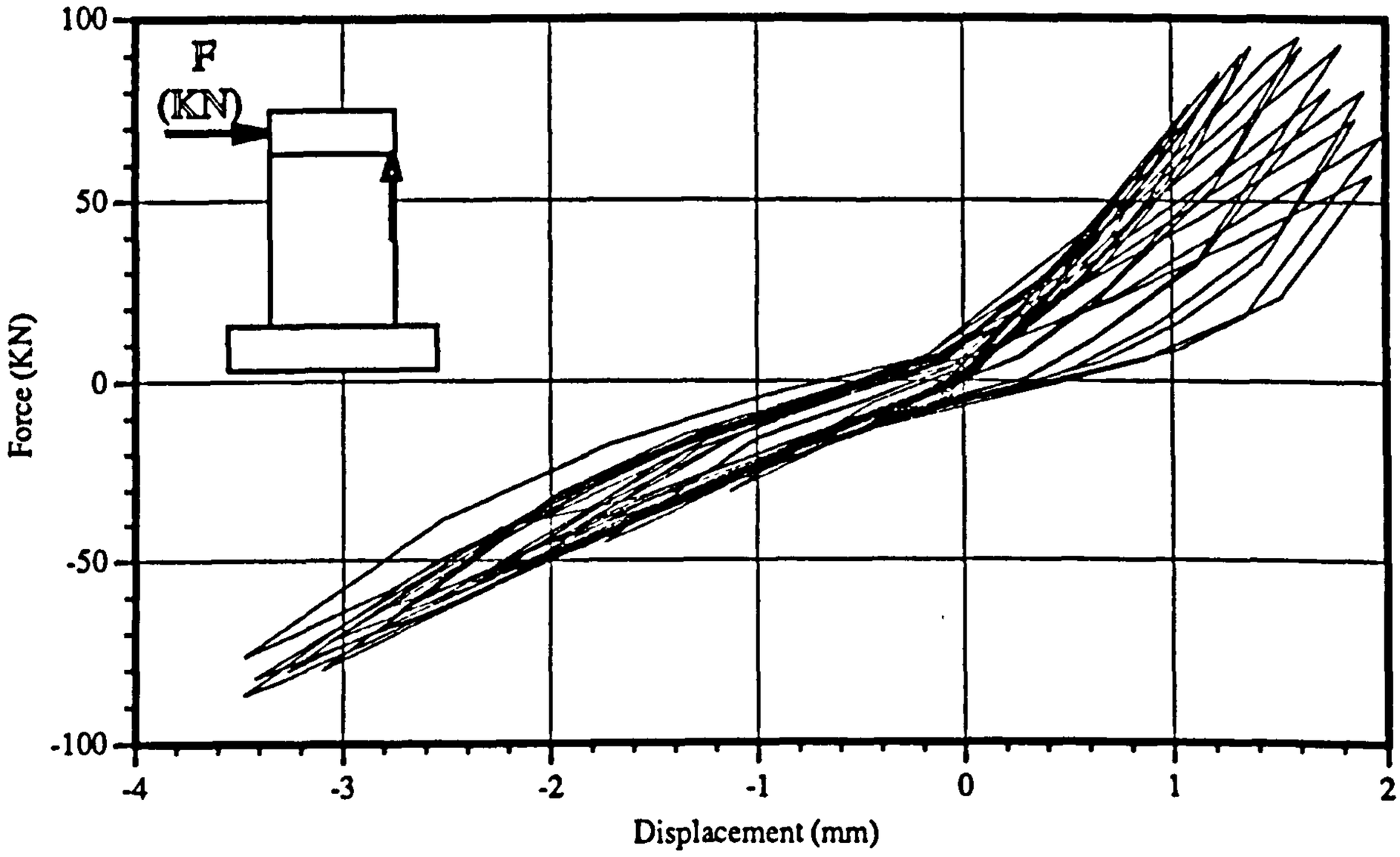


Fig. AI. (R22) 3 Force - Displacement for SWR22 at Node 3

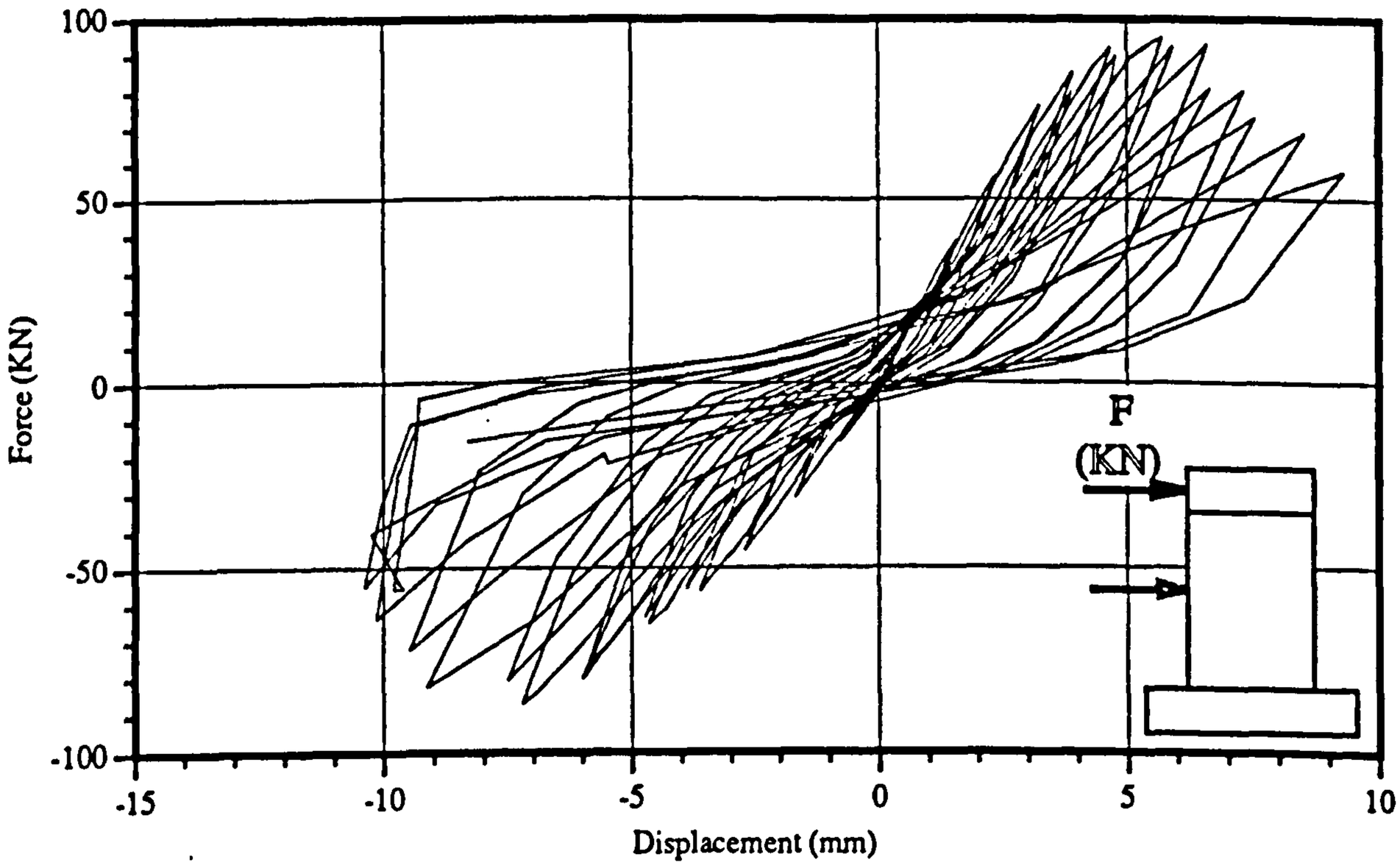


Fig. AI. (R22) 4 Force - Displacement for SWR22 at Node 4

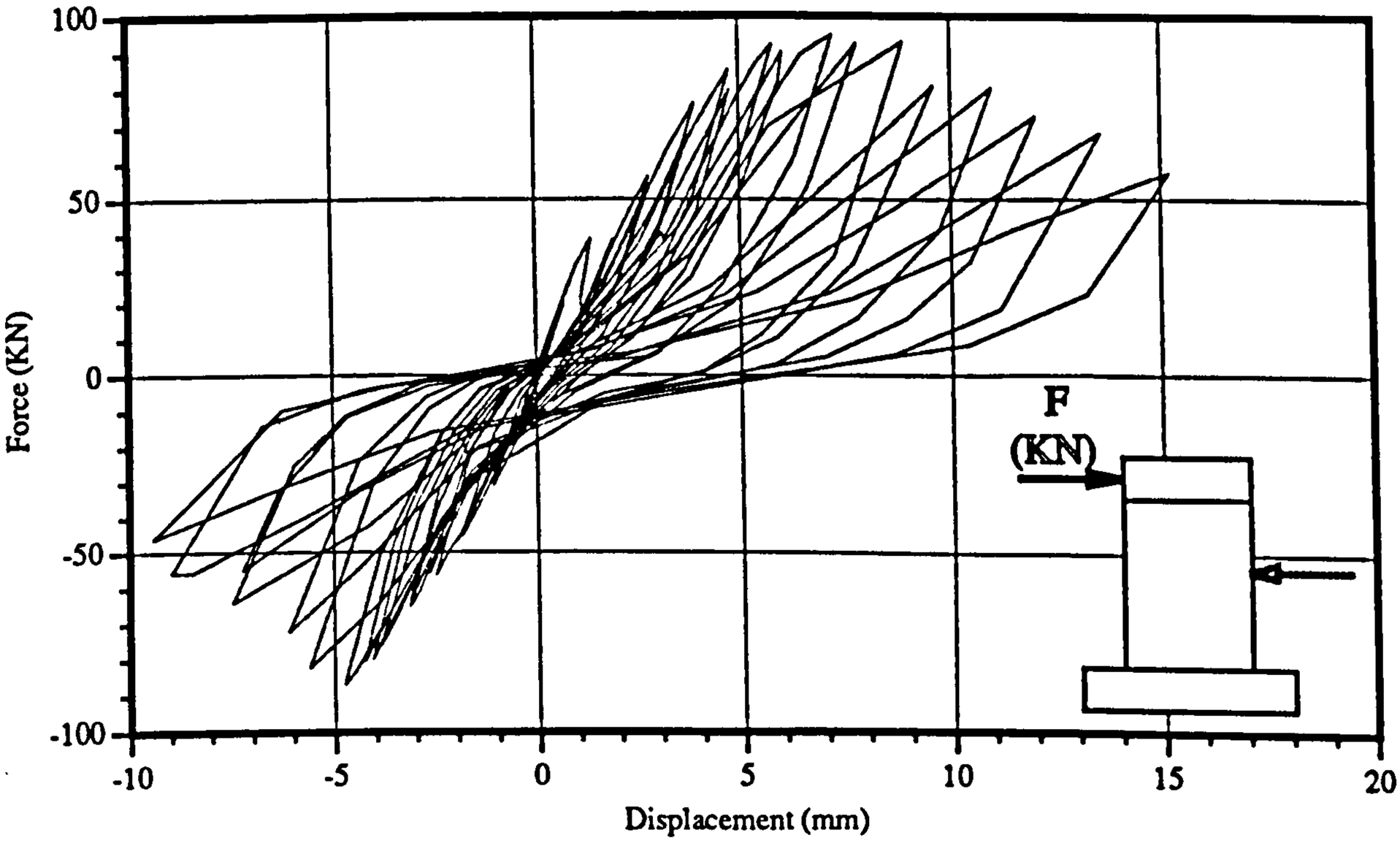


Fig. AI. (R22) 5 Force - Displacement for SWR22 at Node 5

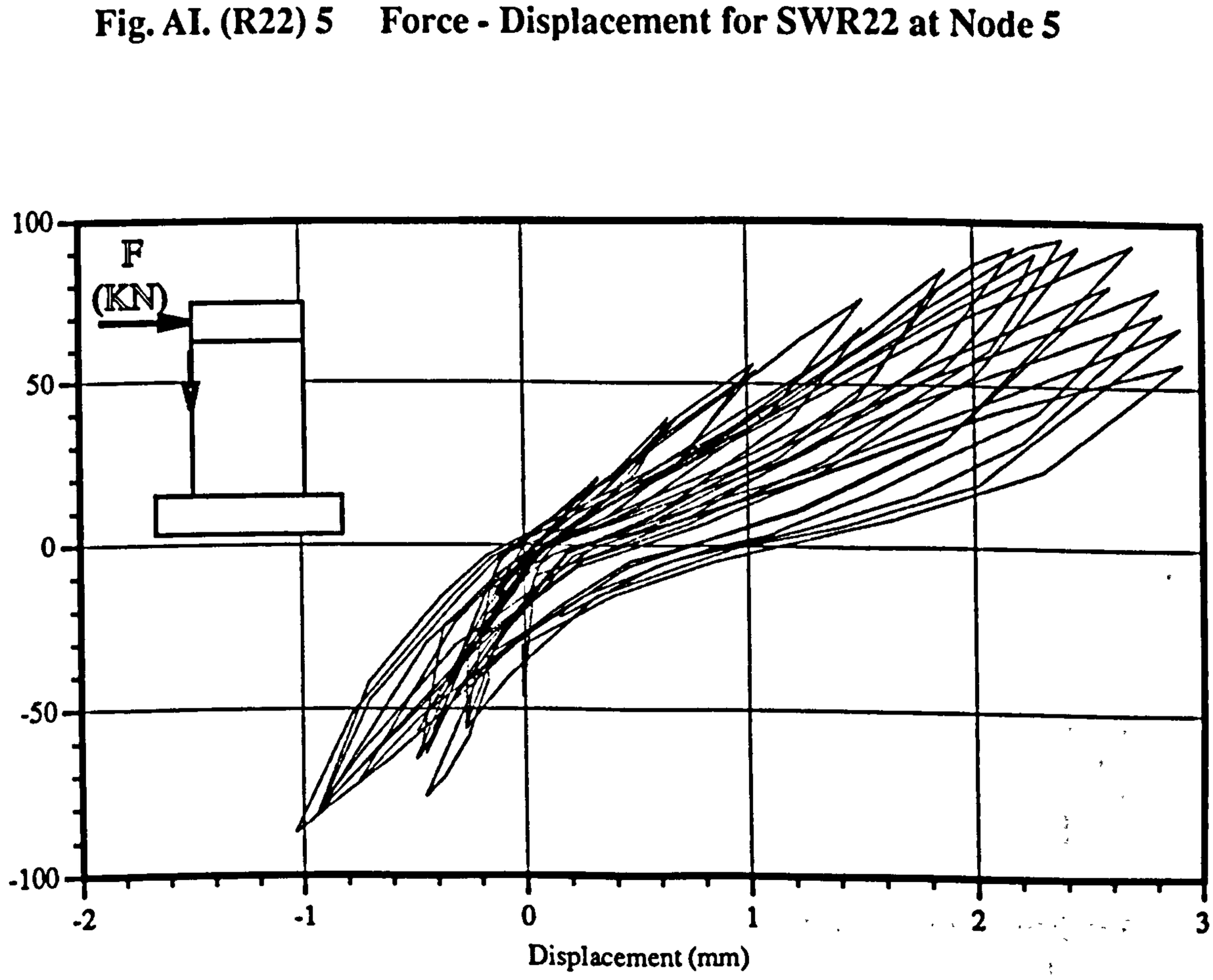


Fig. AI. (R22) 6 Force - Displacement for SWR22 at Node 6

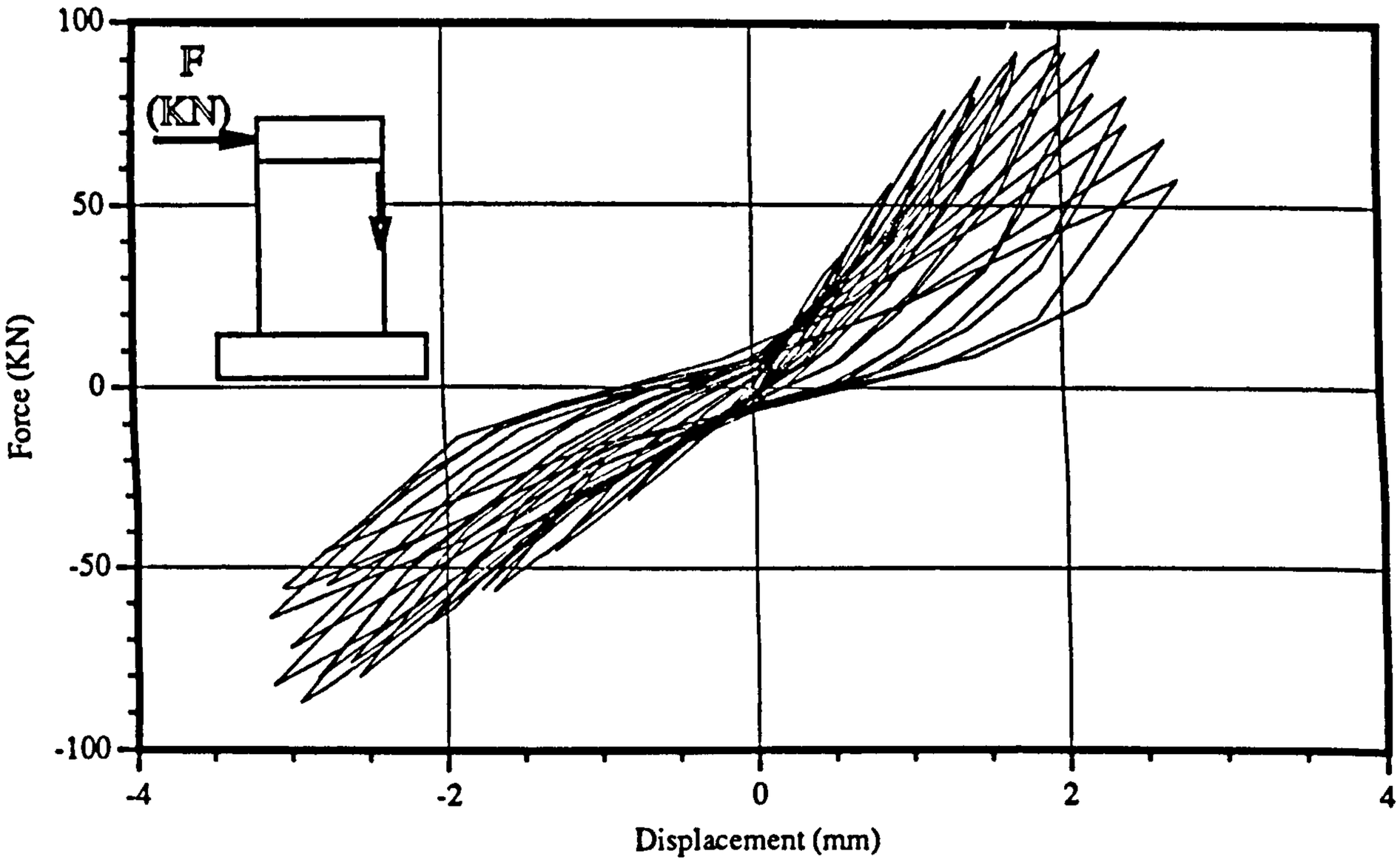


Fig. AI. (R22) 7 Force - Displacement for SWR22 at Node 7

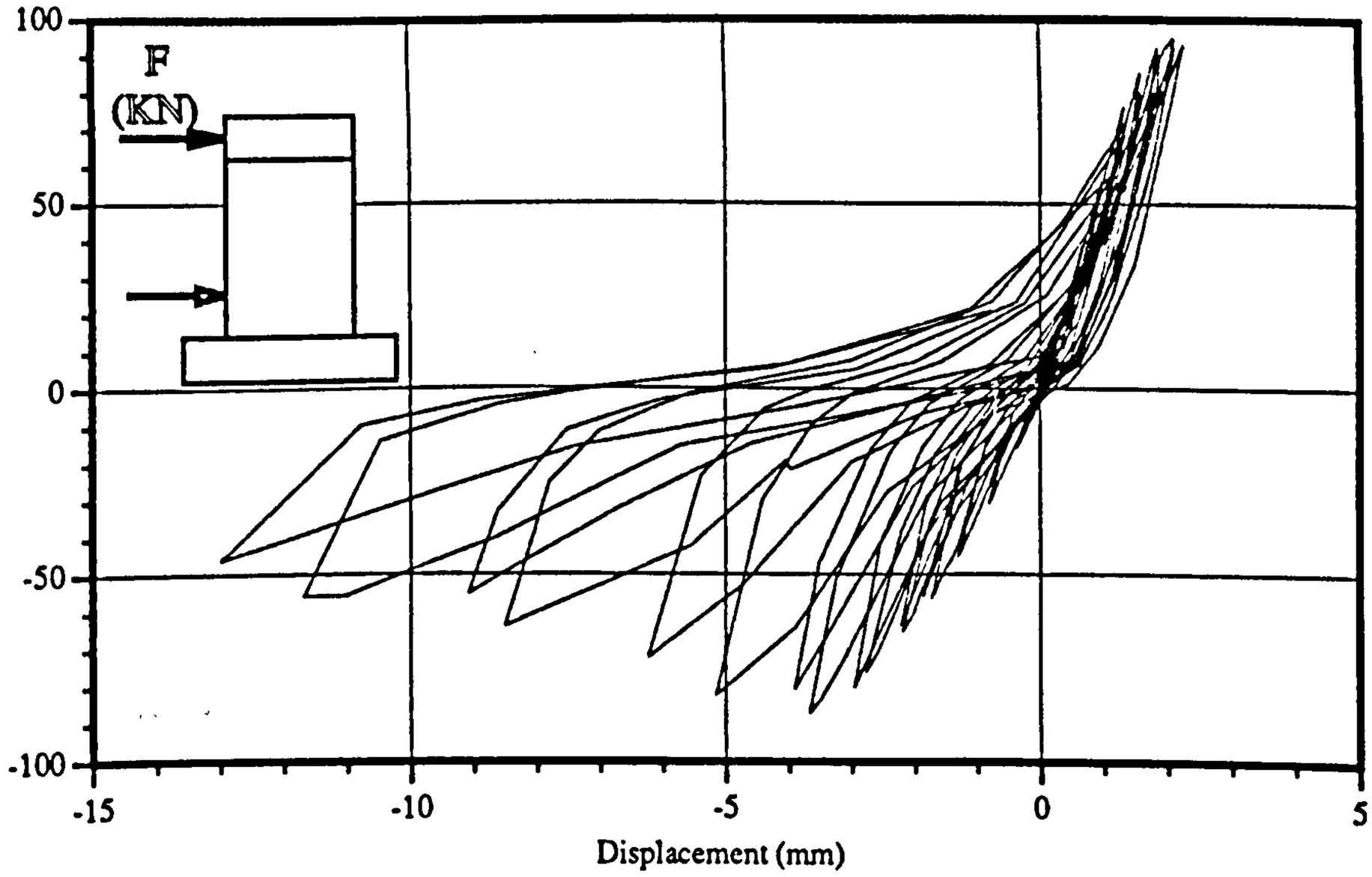


Fig. AI. (R22) 8 Force - Displacement for SWR22 at Node 8

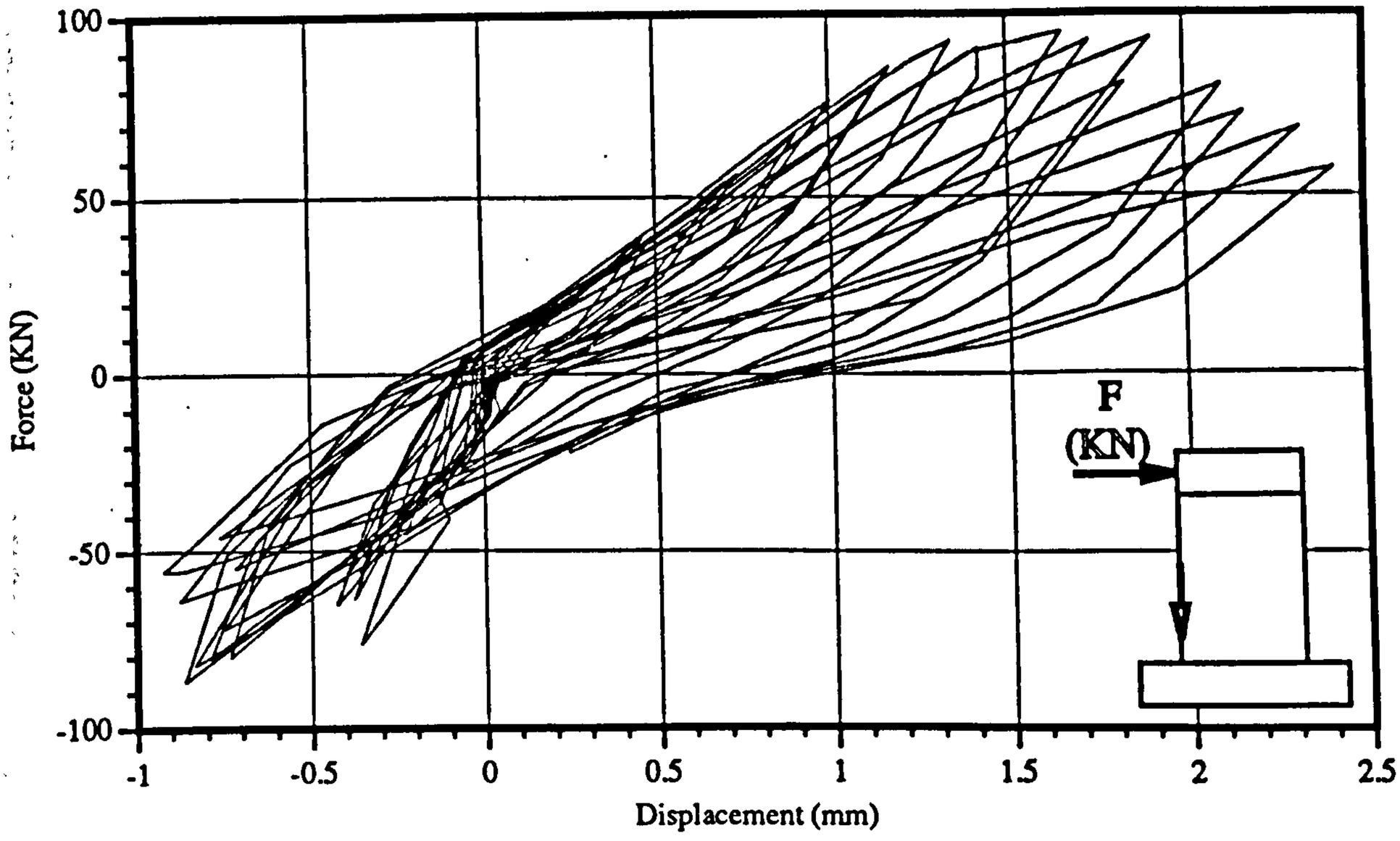


Fig. AI. (R22) 9 Force - Displacement for SWR22 at Node 9

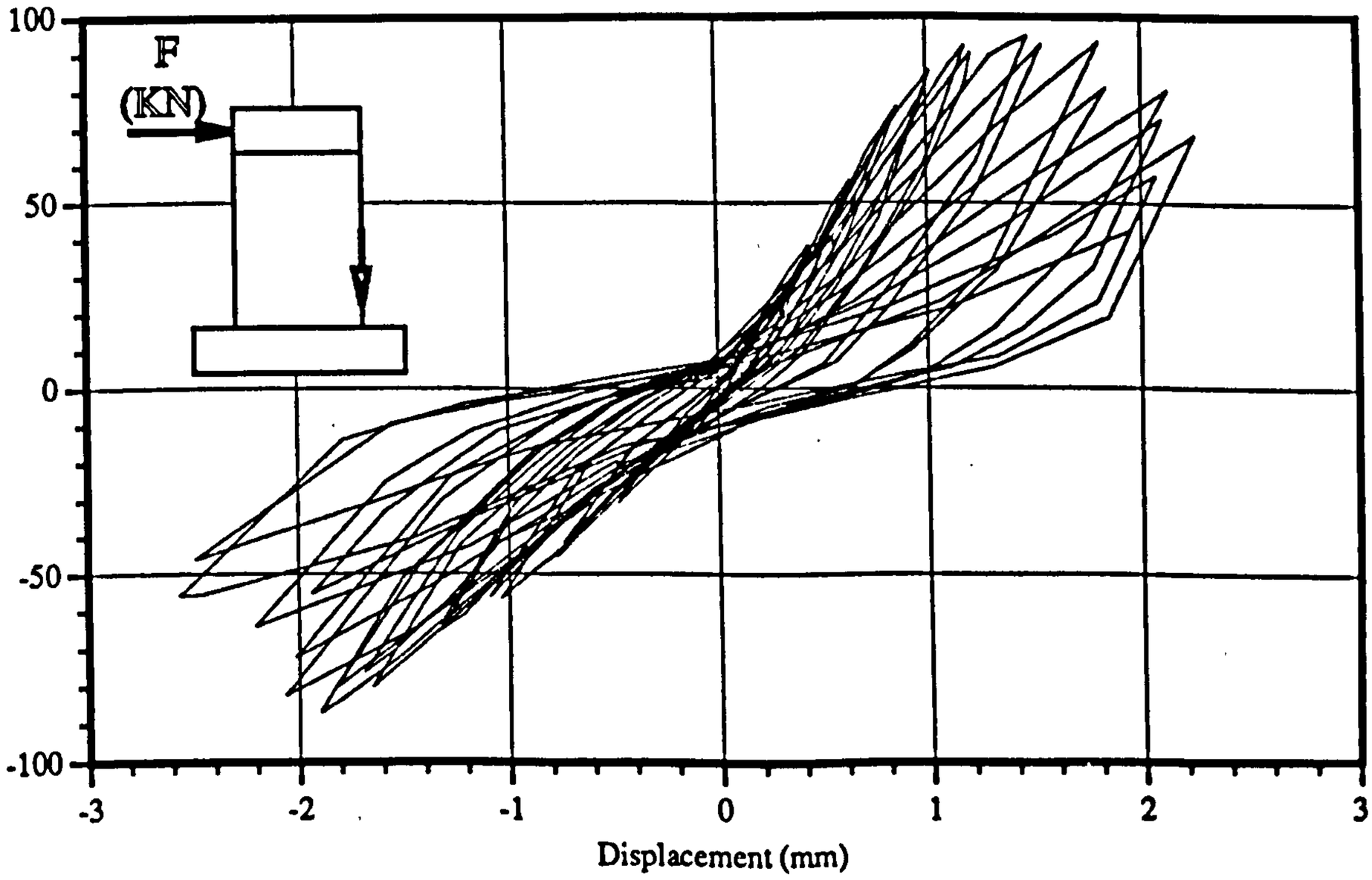


Fig. AI. (R22) 10 Force - Displacement for SWR22 at Node 10

AI.11. : Force Displacement for SWR24

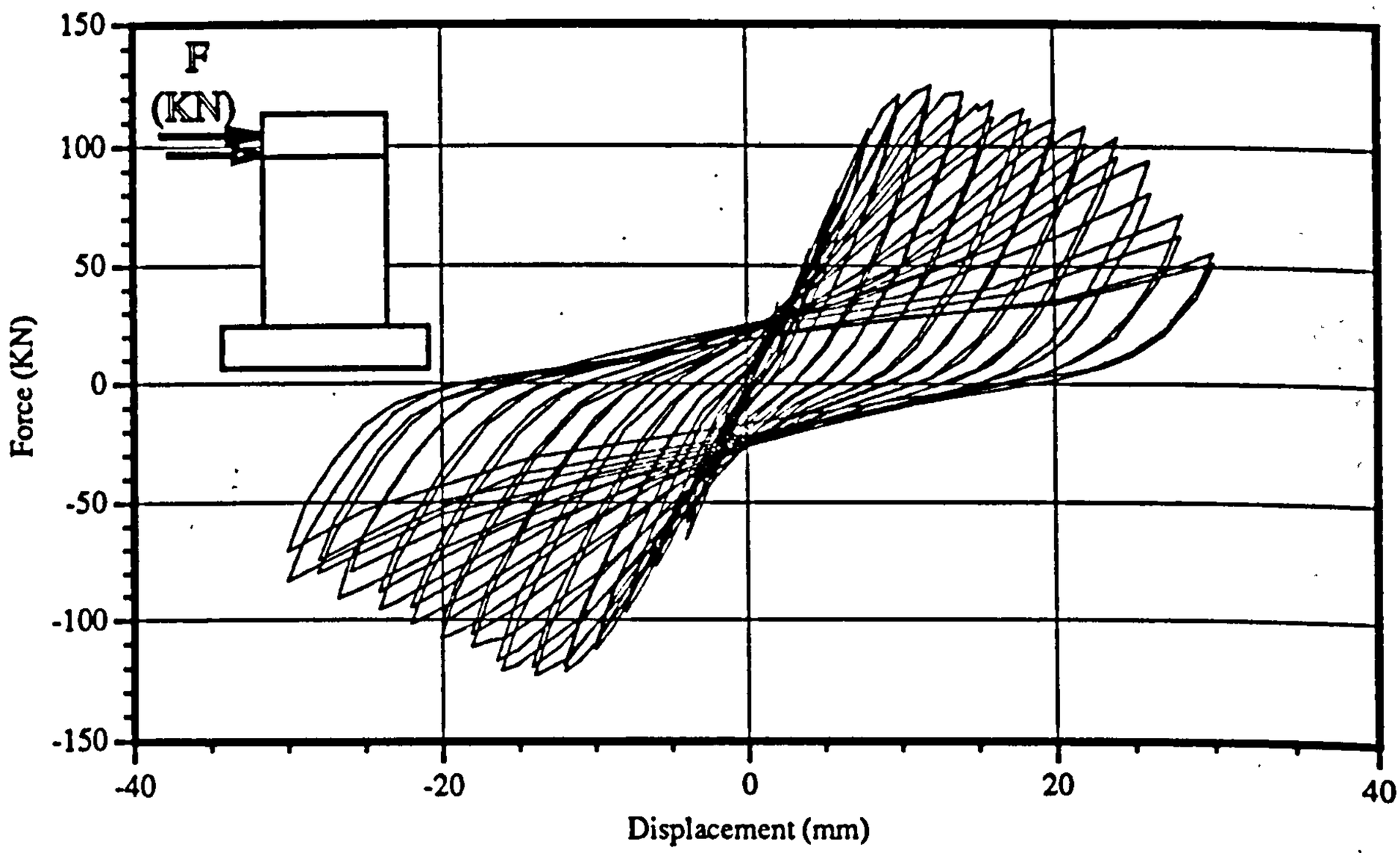


Fig. AI. (R24) 1 Force - Displacement for SWR24 at Node 1

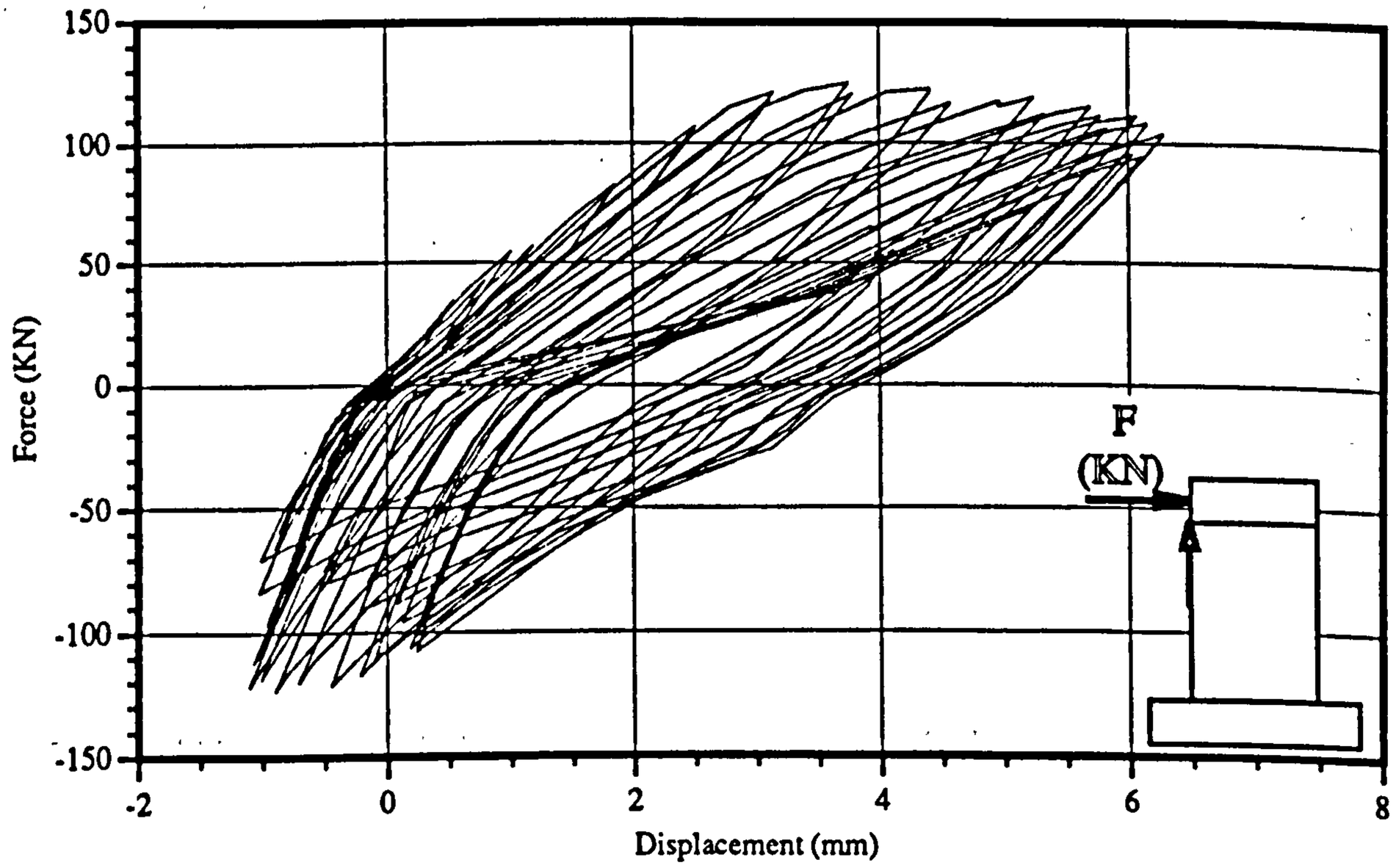


Fig. AI. (R24) 2 Force - Displacement for SWR24 at Node 2

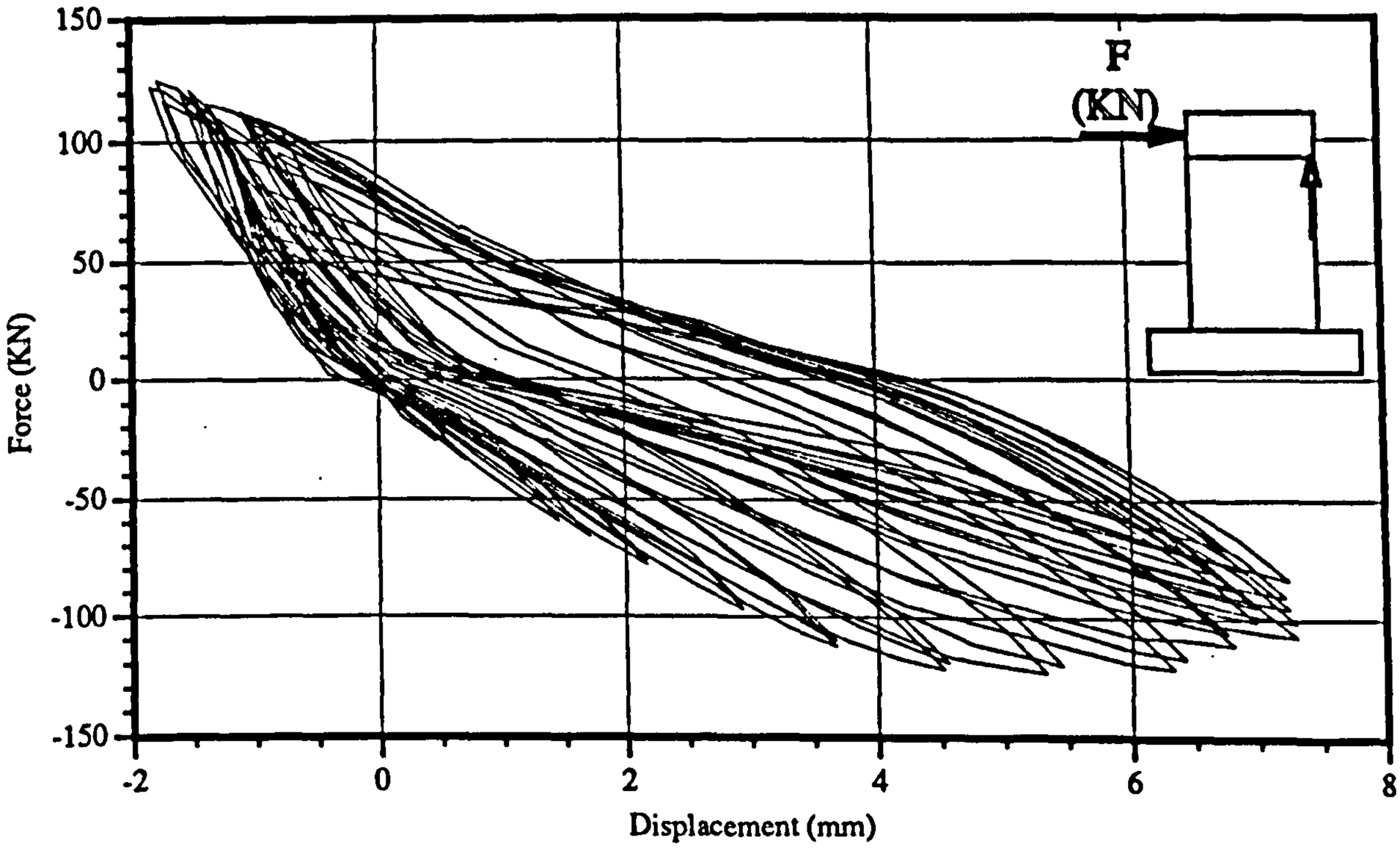


Fig. AI. (R24) 3 Force - Displacement for SWR24 at Node 3

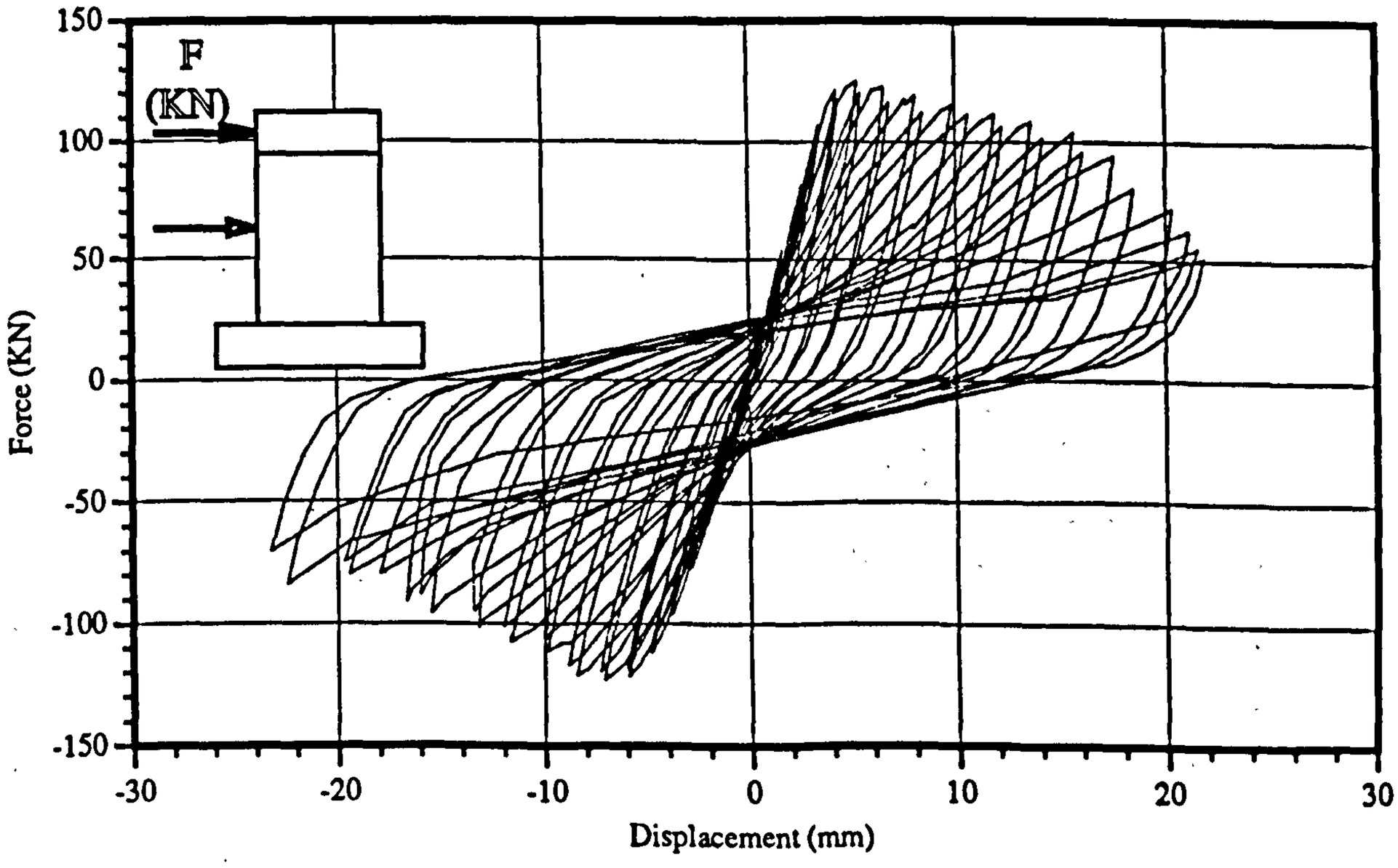


Fig. AI. (R24) 4 Force - Displacement for SWR24 at Node 4

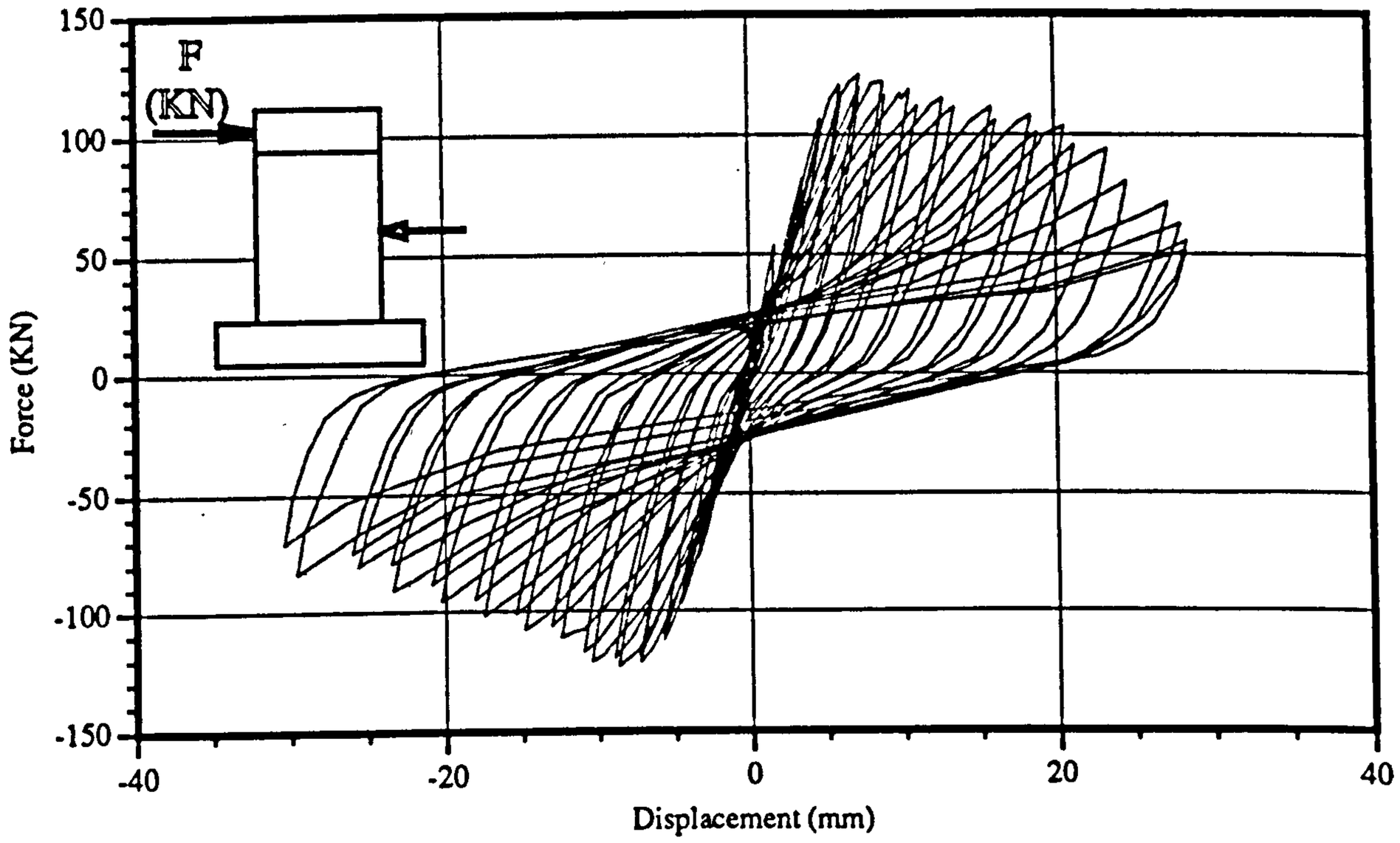


Fig. AI. (R24) 5 Force - Displacement for SWR24 at Node 5

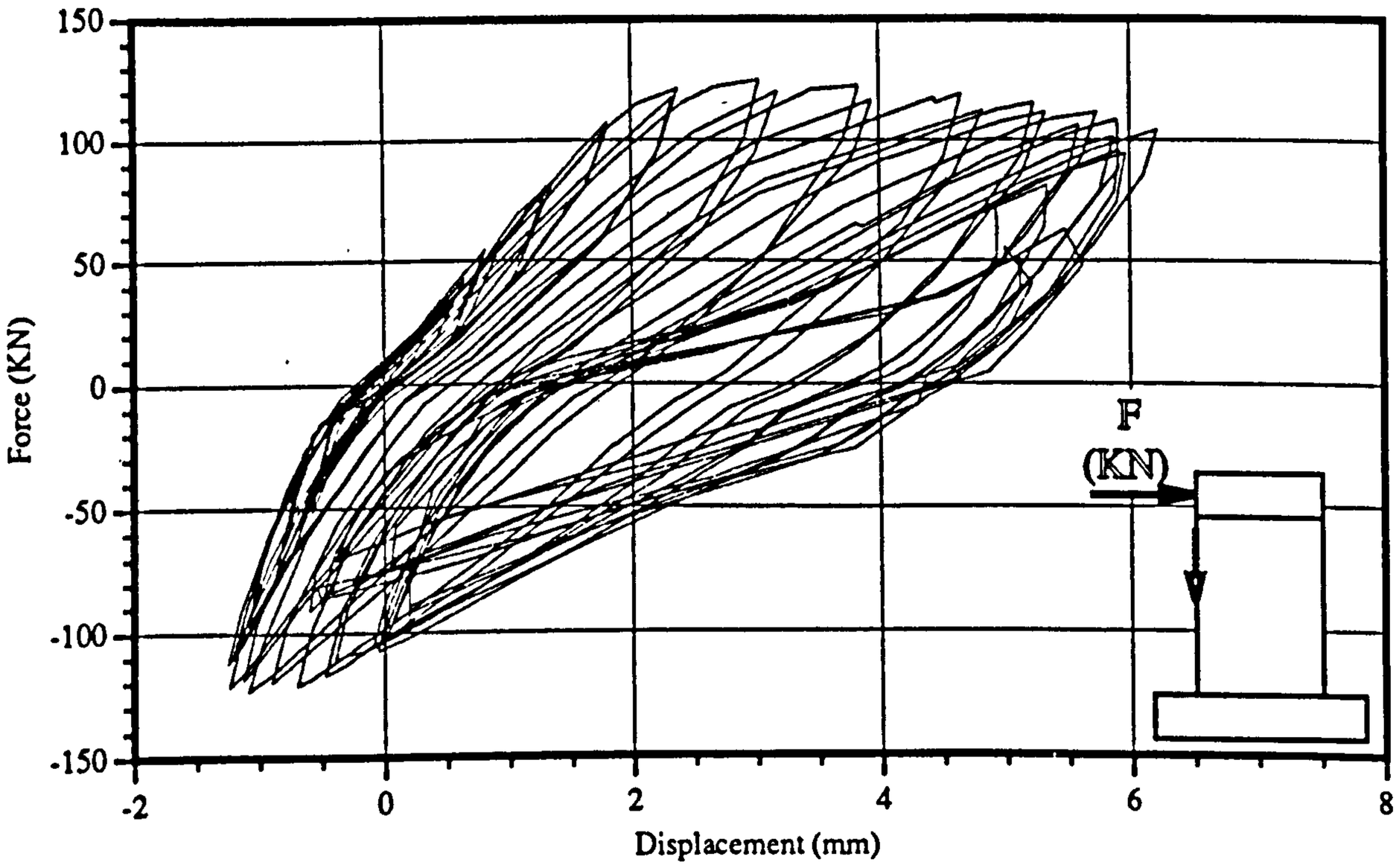


Fig. AI. (R24) 6 Force - Displacement for SWR24 at Node 6

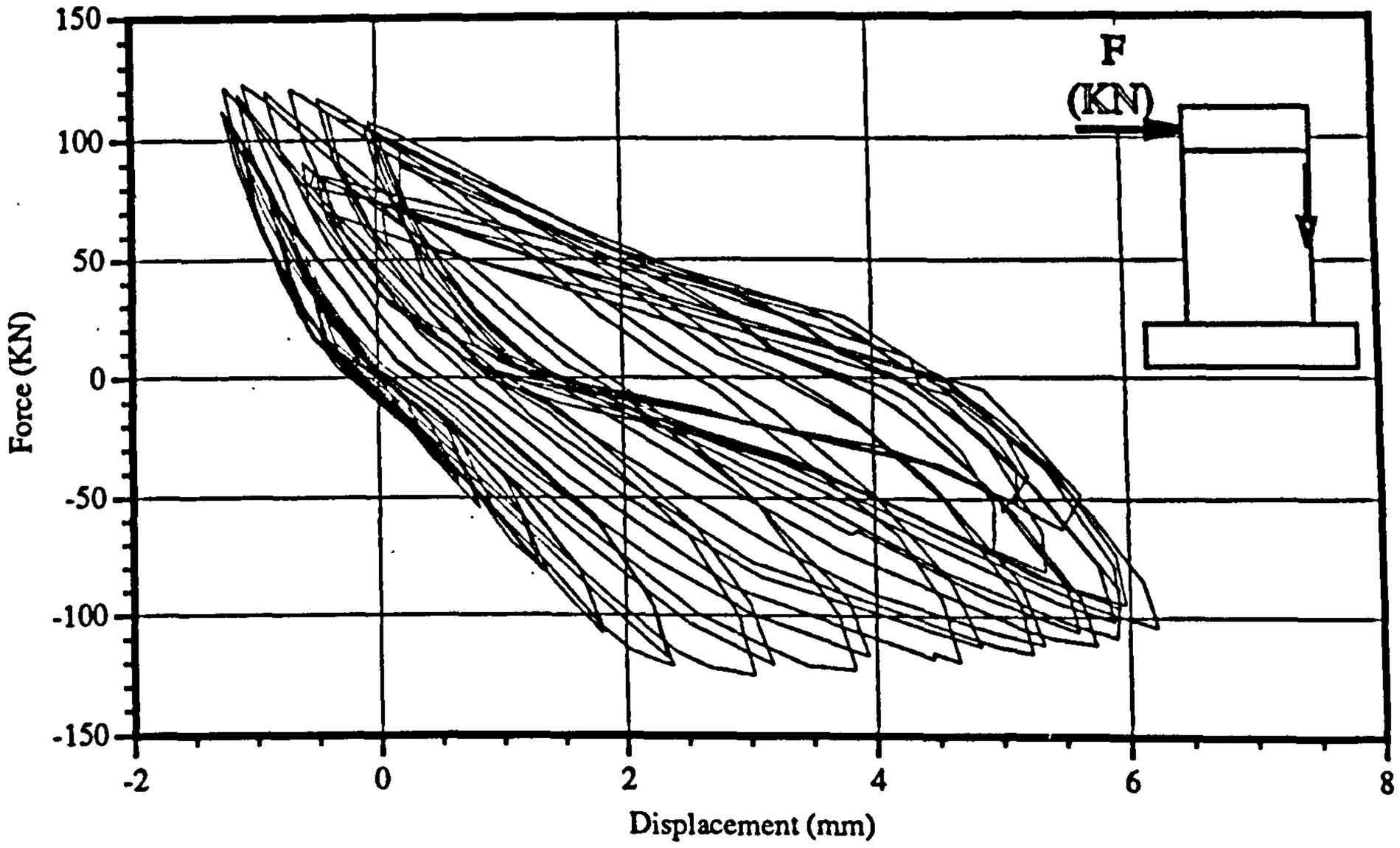


Fig. AI. (R24) 7 Force - Displacement for SWR24 at Node 7

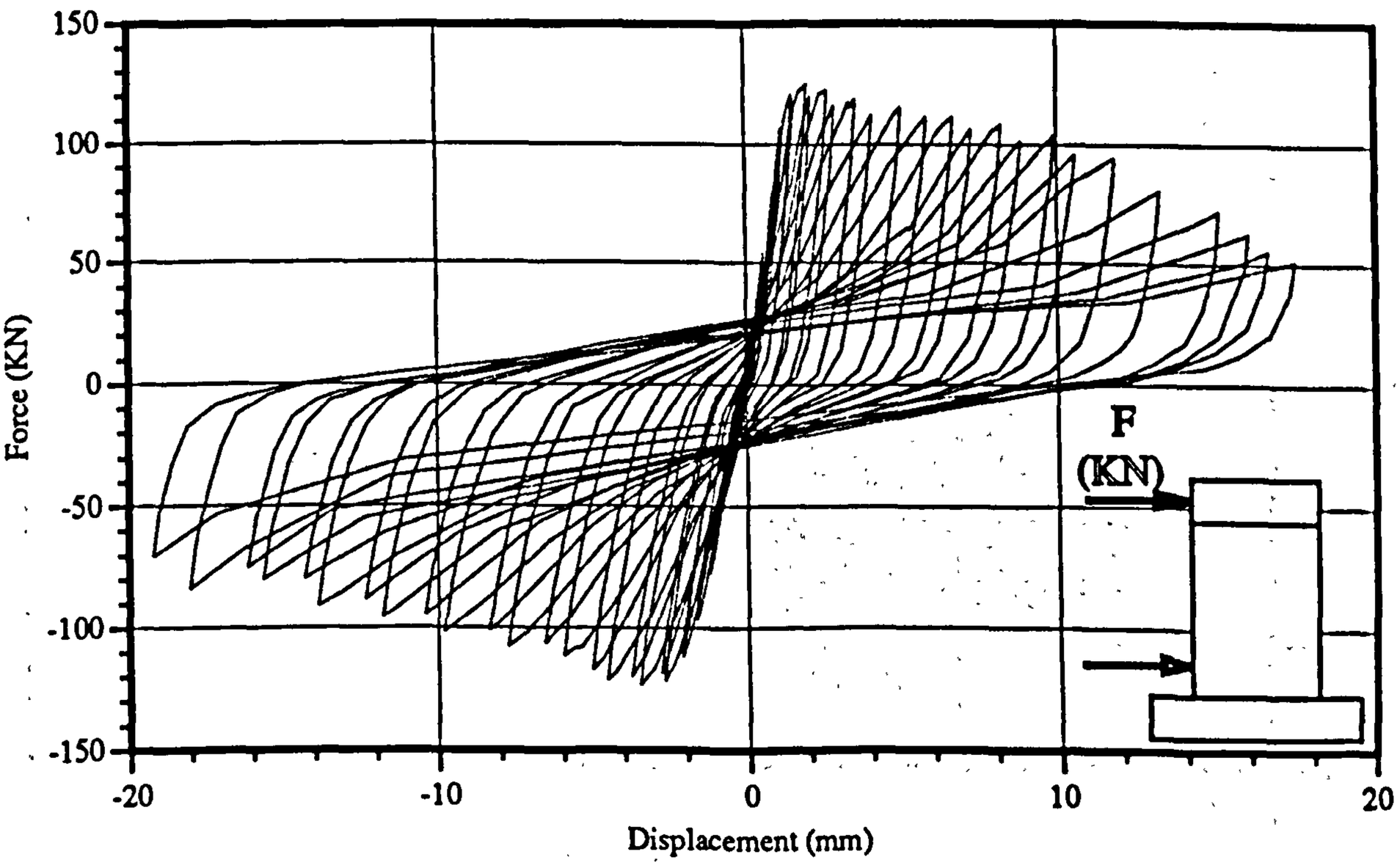


Fig. AI. (R24) 8 Force - Displacement for SWR24 at Node 8

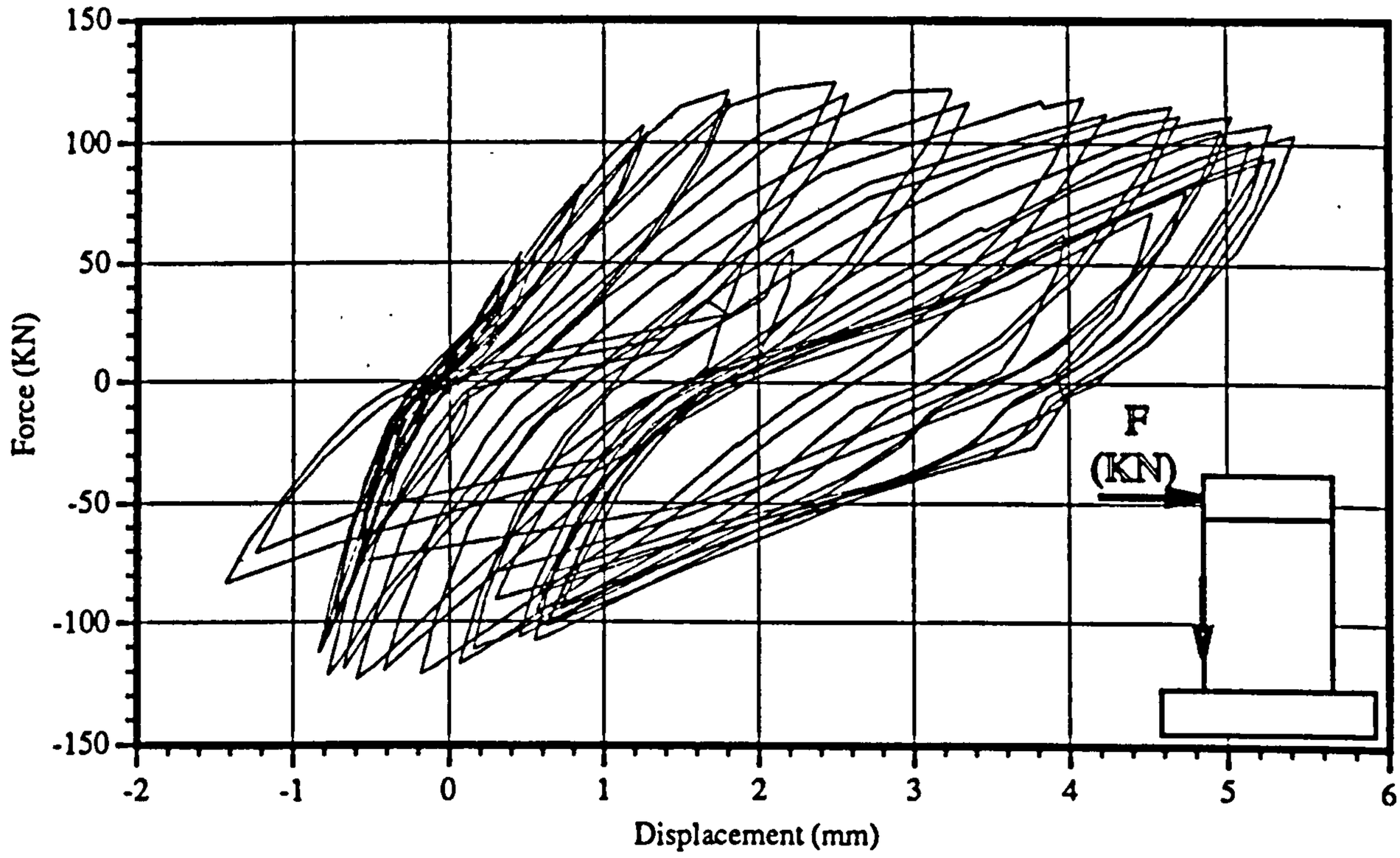


Fig. AI. (R24) 9 Force - Displacement for SWR24 at Node 9

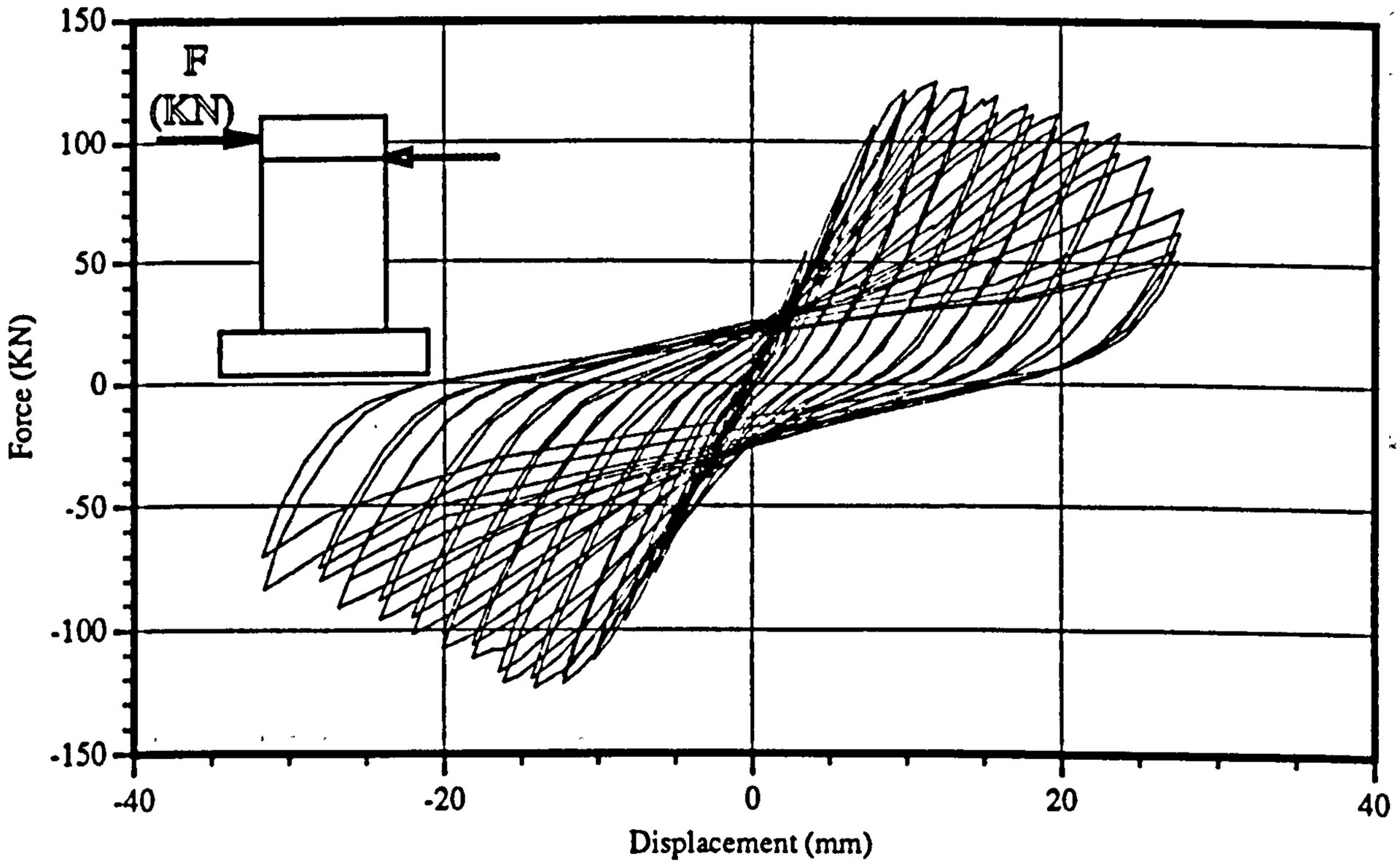


Fig. AI. (R24) 16 Force - Displacement for SWR24 at Node 16

AI.12 : Force Displacement for SW31

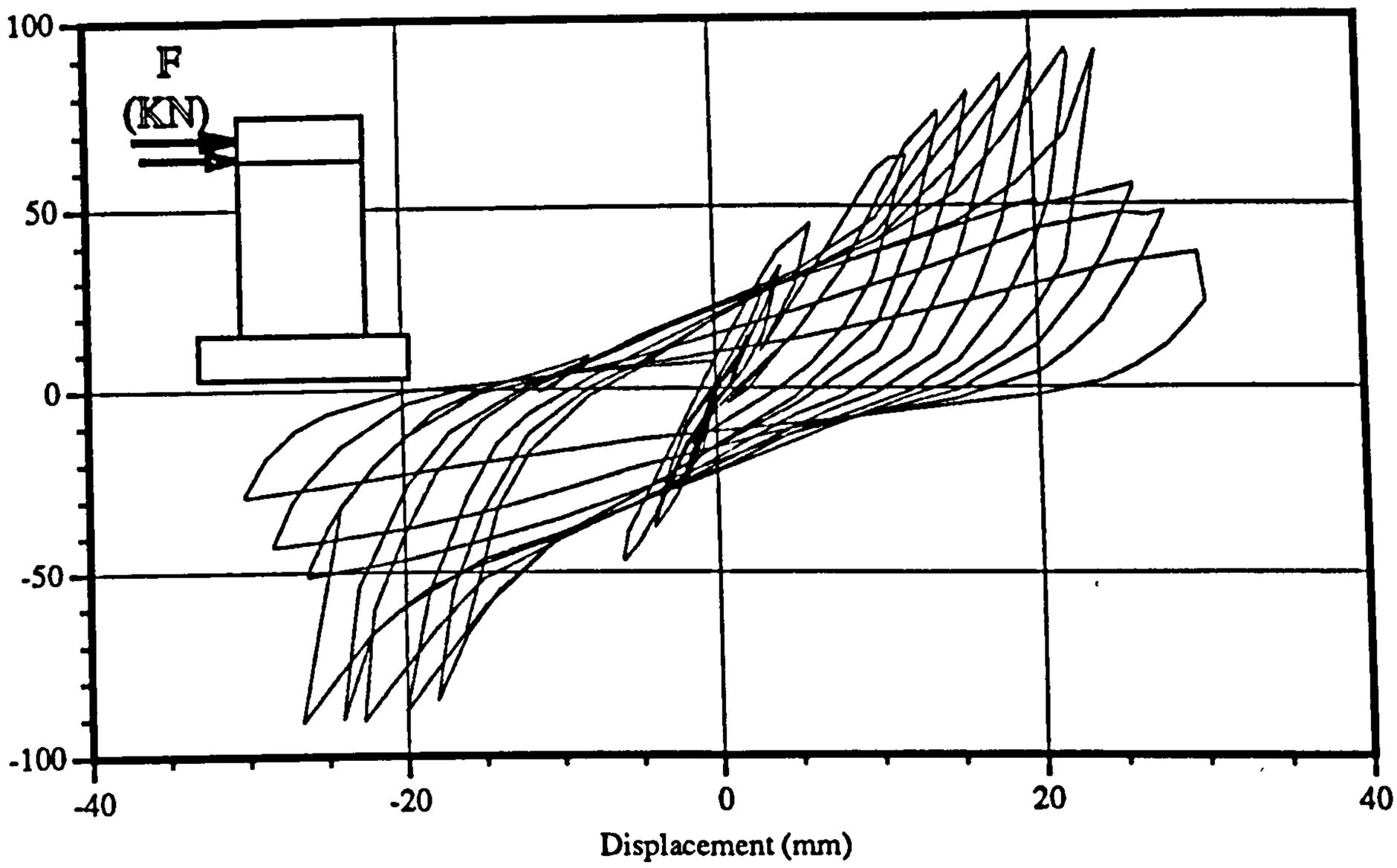


Fig. AI. (31) 1 Force - Displacement for SW31 at Node 1

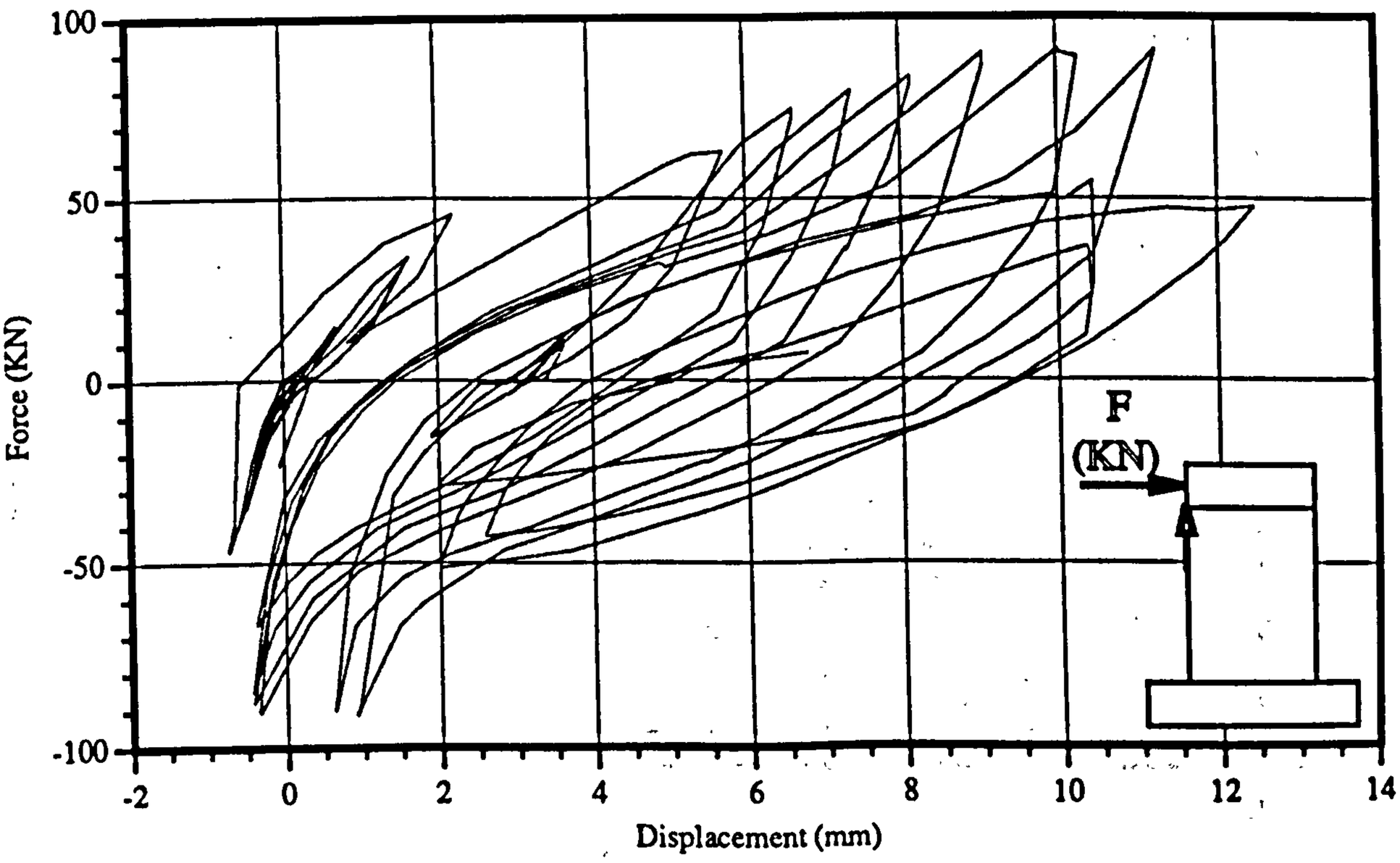


Fig. AI. (31) 2 Force - Displacement for SW31 at Node 2

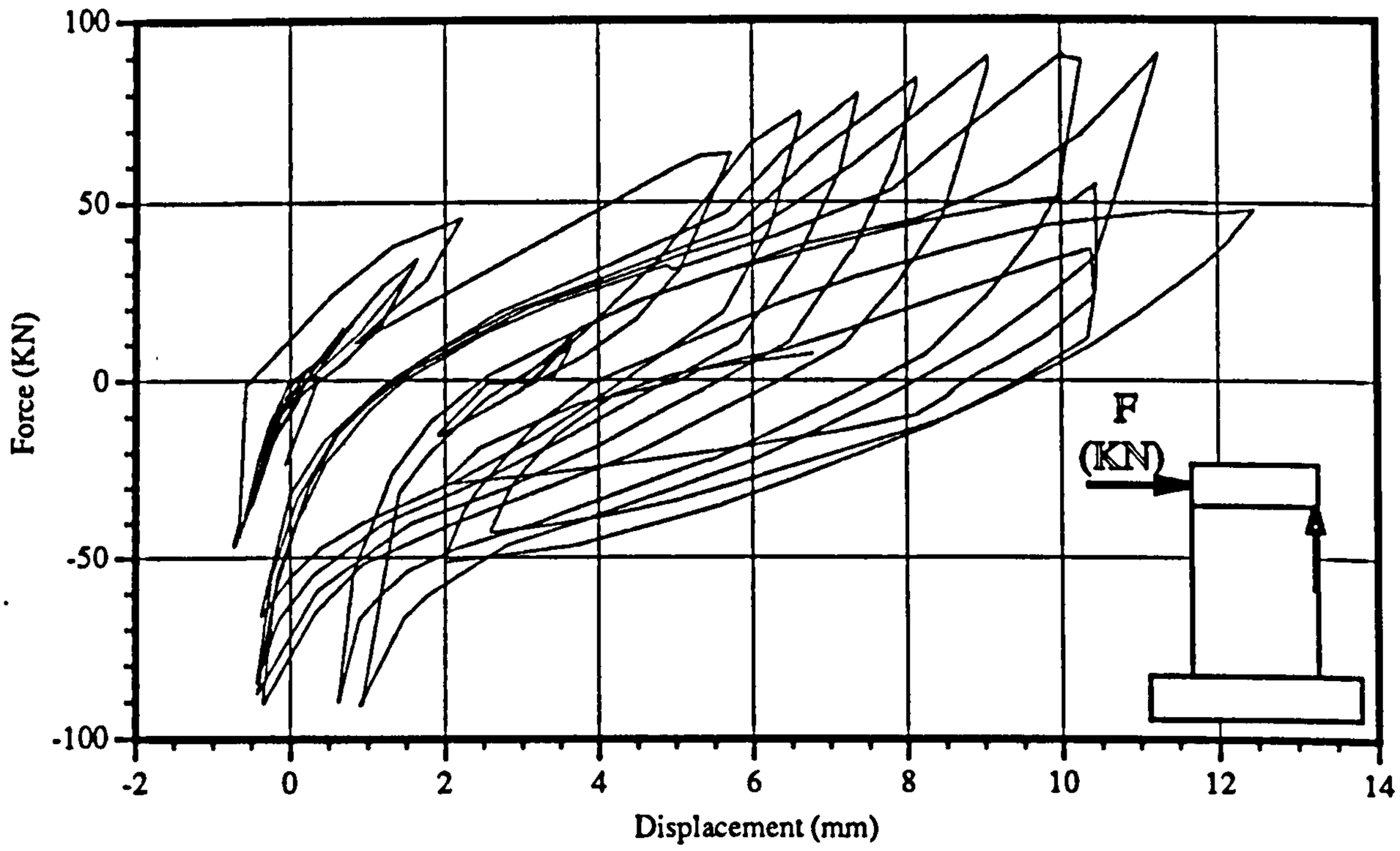


Fig. AI. (31) 3 Force - Displacement for SW31 at Node 3

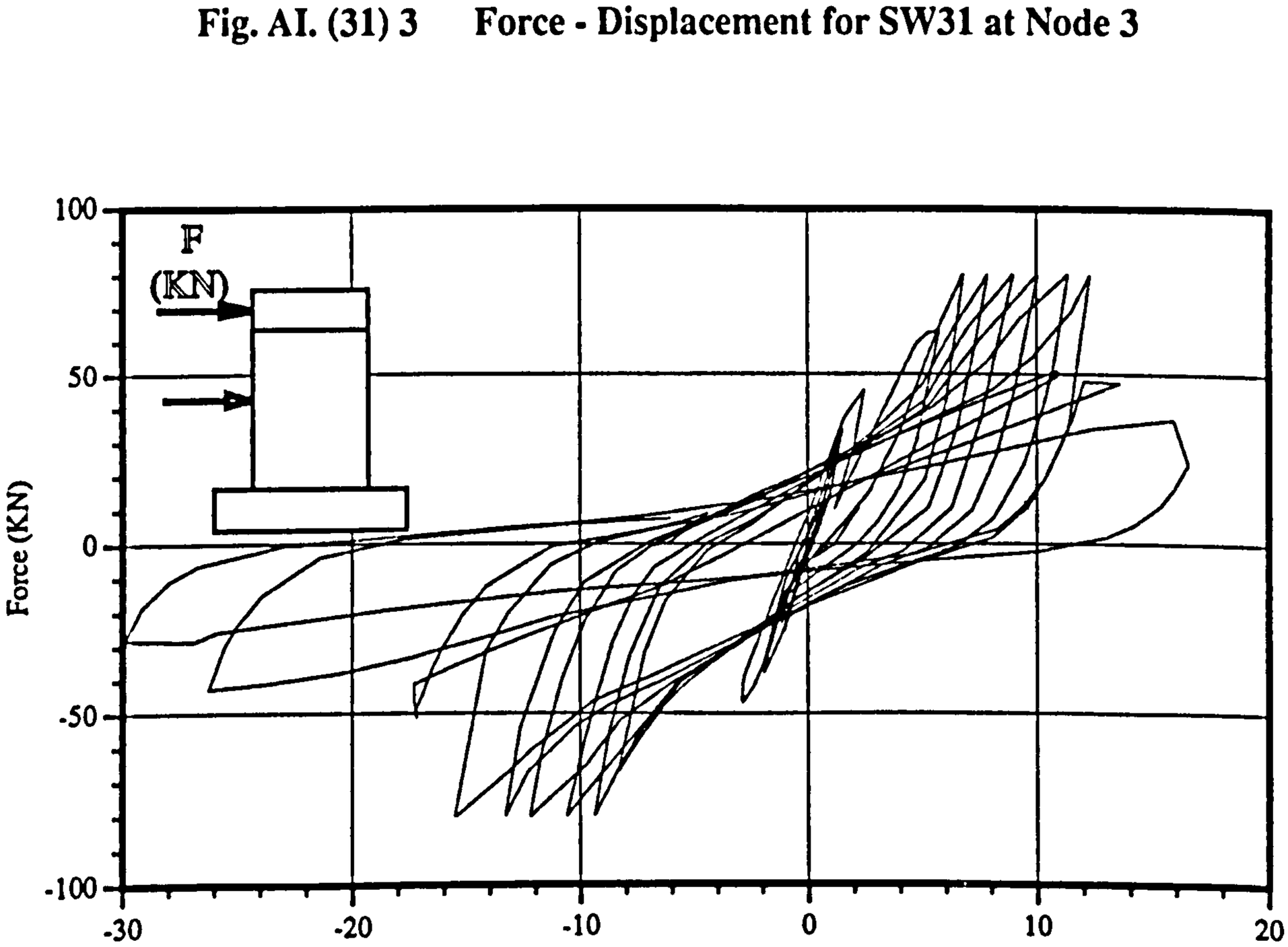


Fig. AI. (31) 4 Force - Displacement for SW31 at Node 4

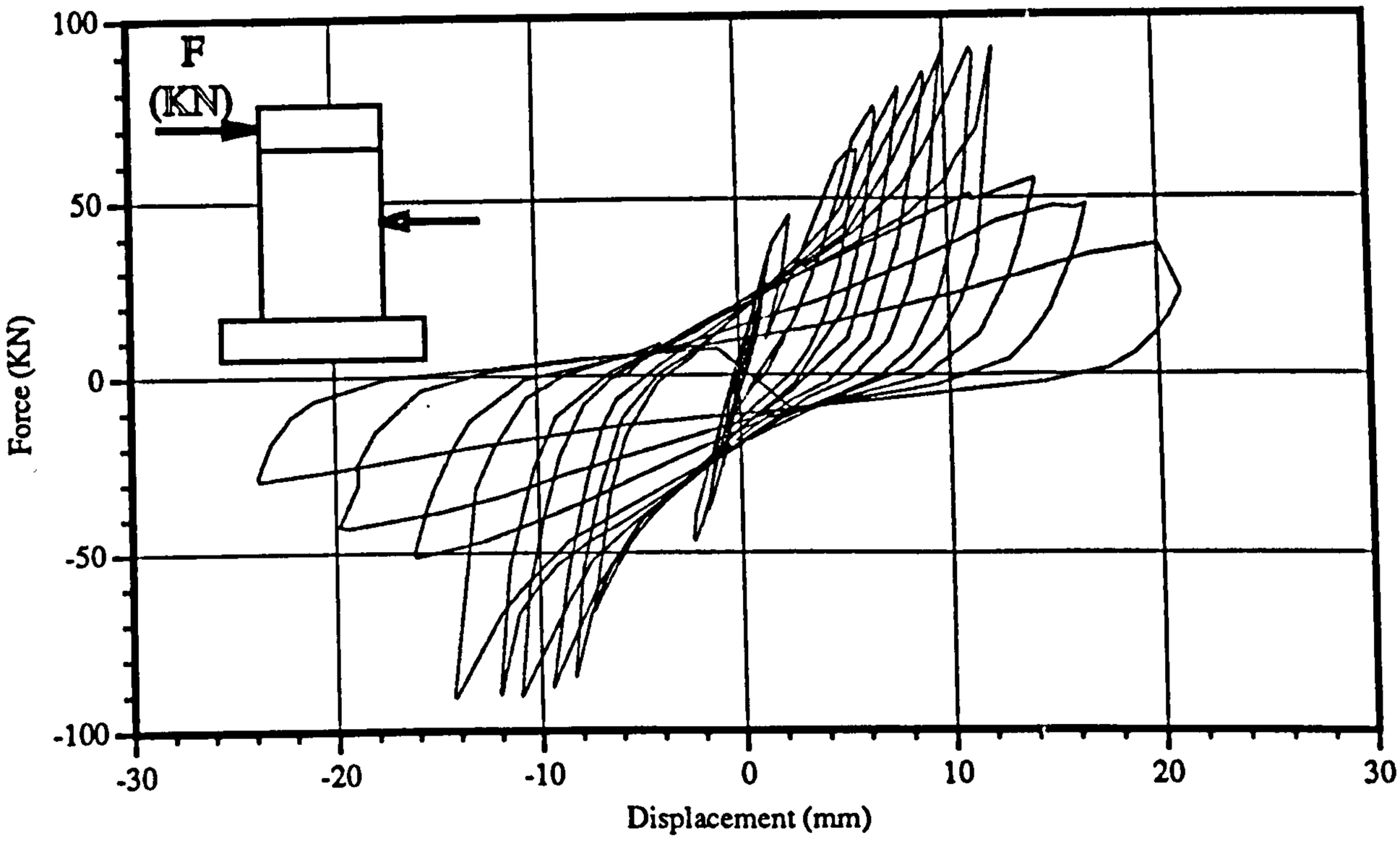


Fig. AI. (31) 5 Force - Displacement for SW31 at Node 5

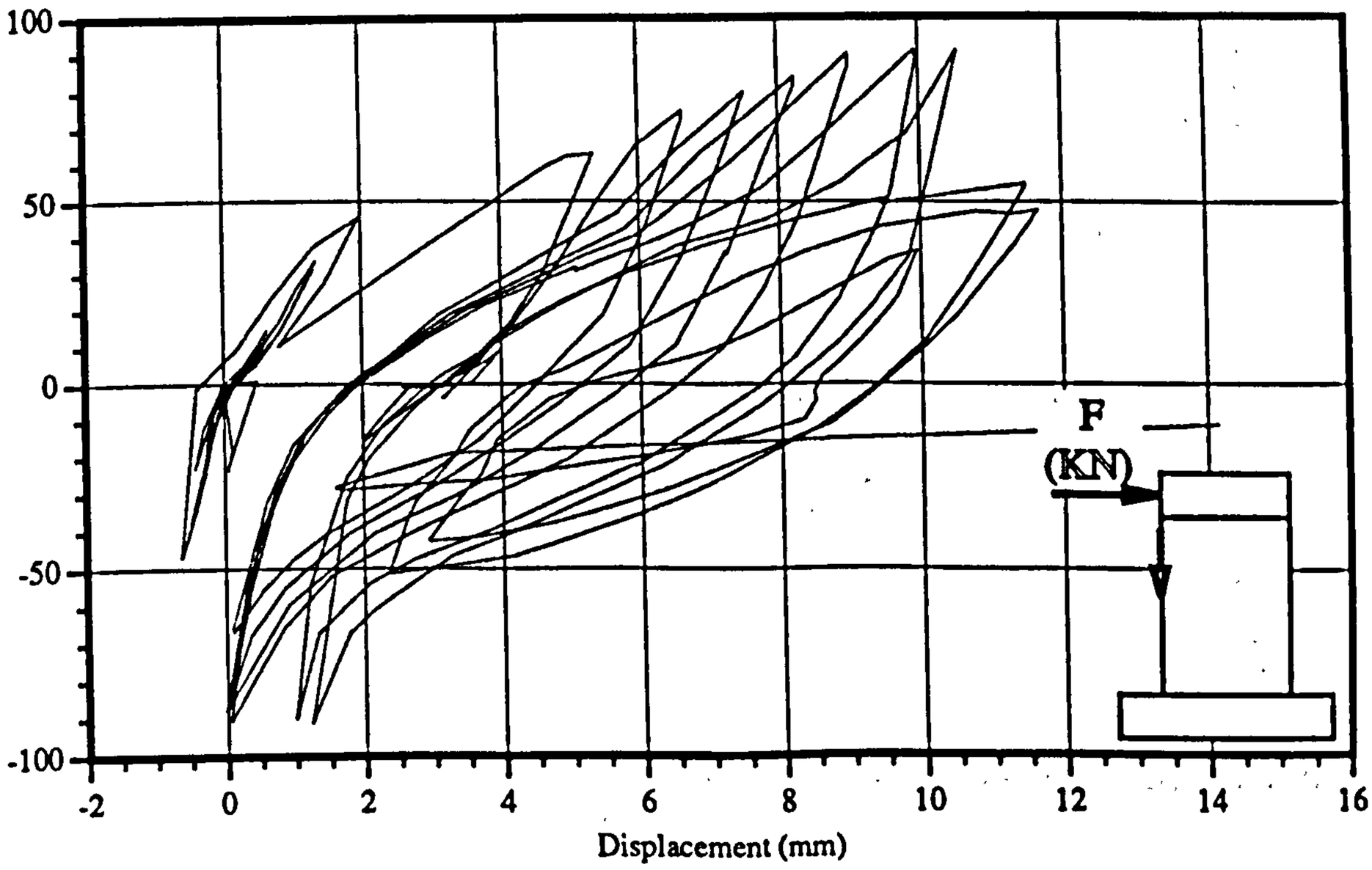


Fig. AI. (31) 6 Force - Displacement for SW31 at Node 6

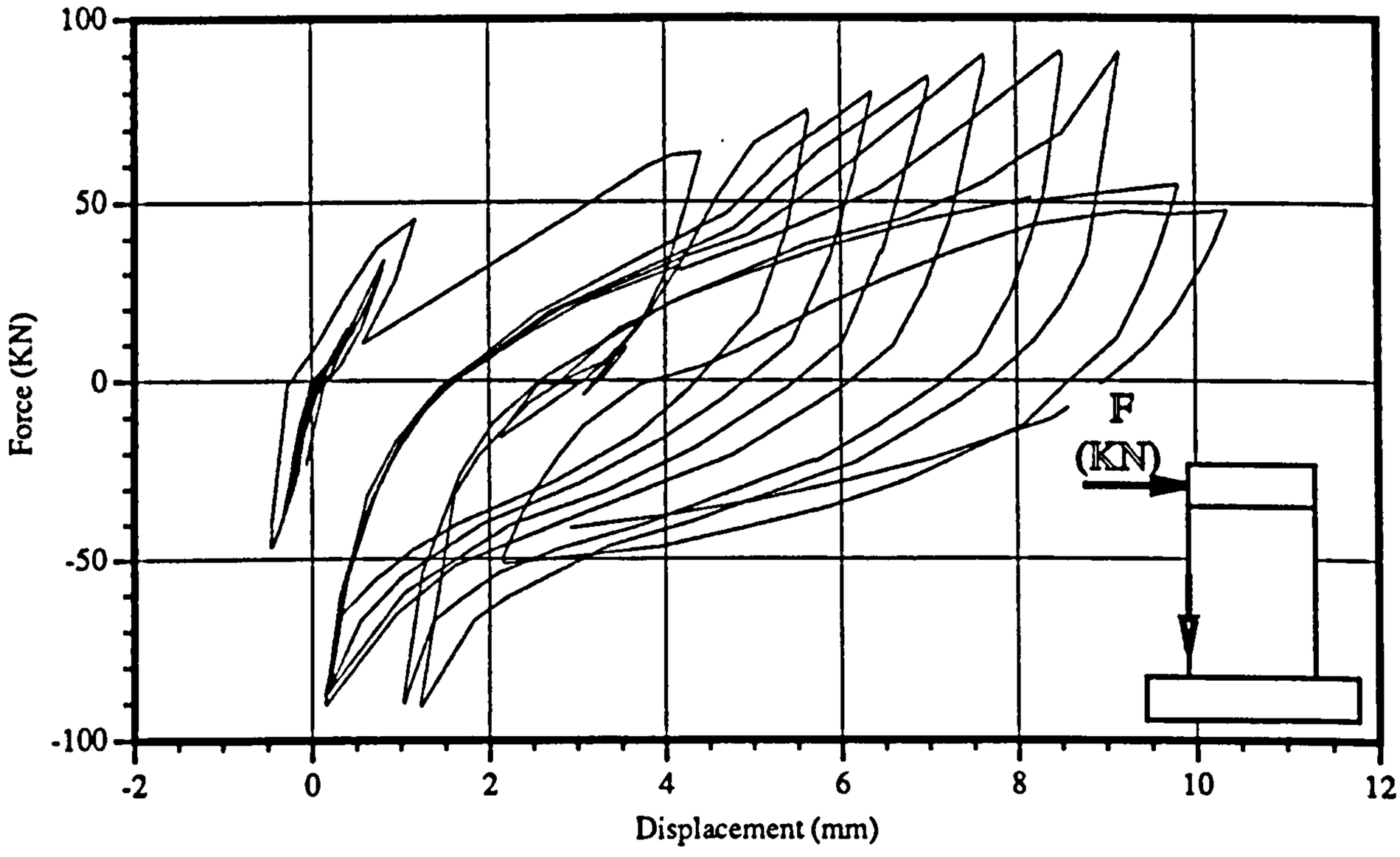


Fig. AI. (31) 9 Force - Displacement for SW31 at Node 9

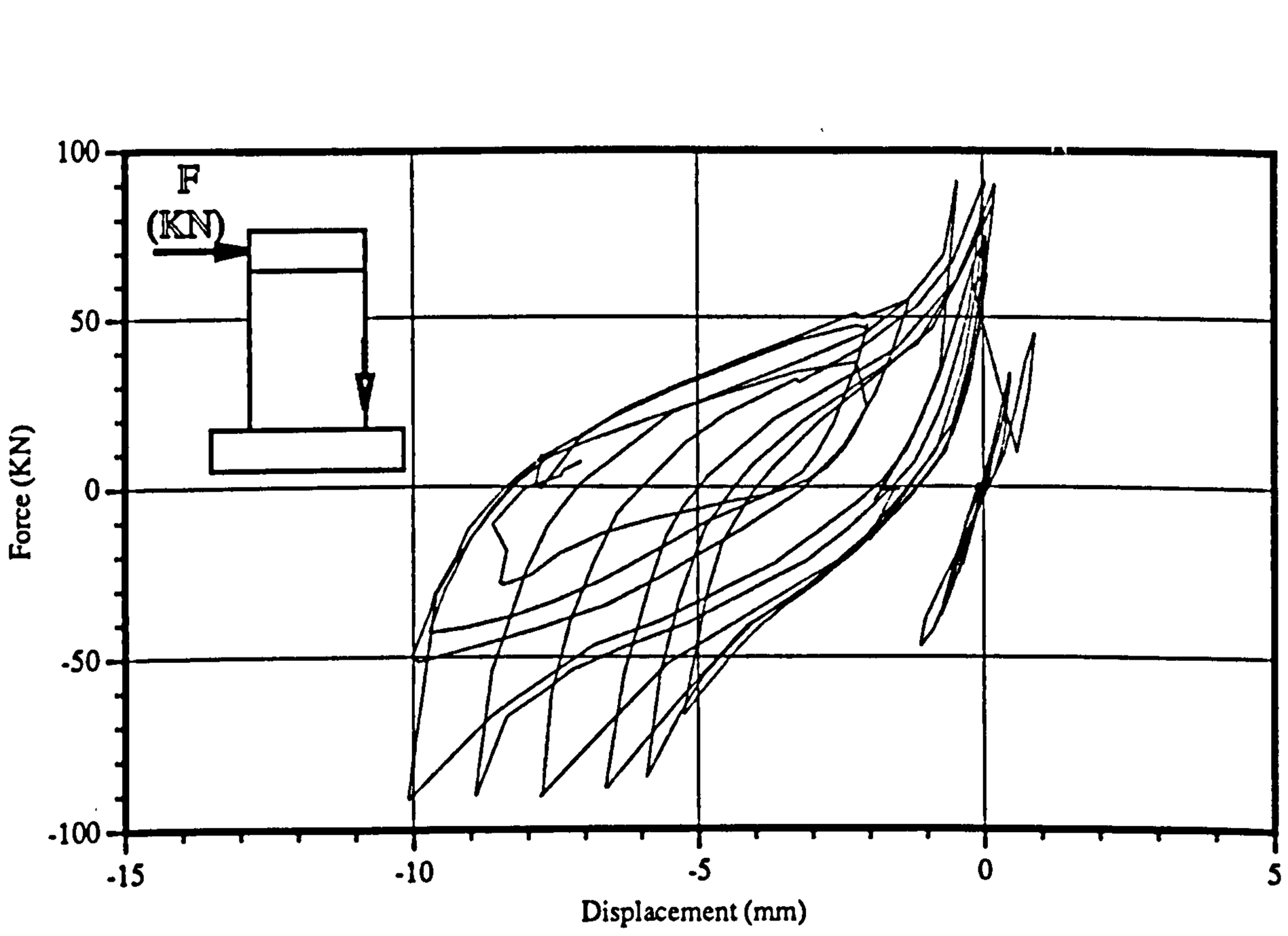


Fig. AI. (31) 10 Force - Displacement for SW31 at Node 10

AI.13. : Force Displacement for SW32

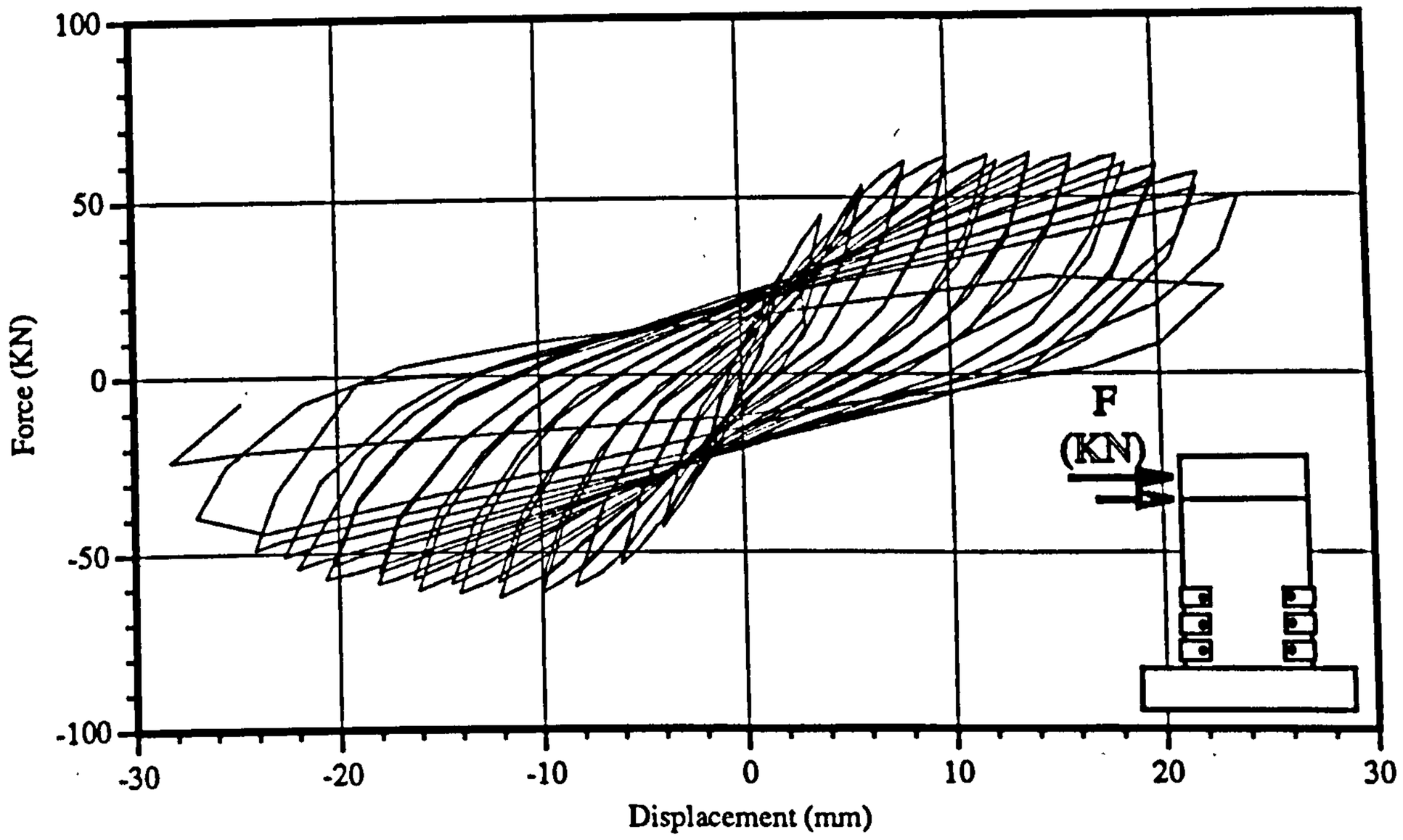


Fig. AI. (32) 1 Force - Displacement for SW32 at Node 1

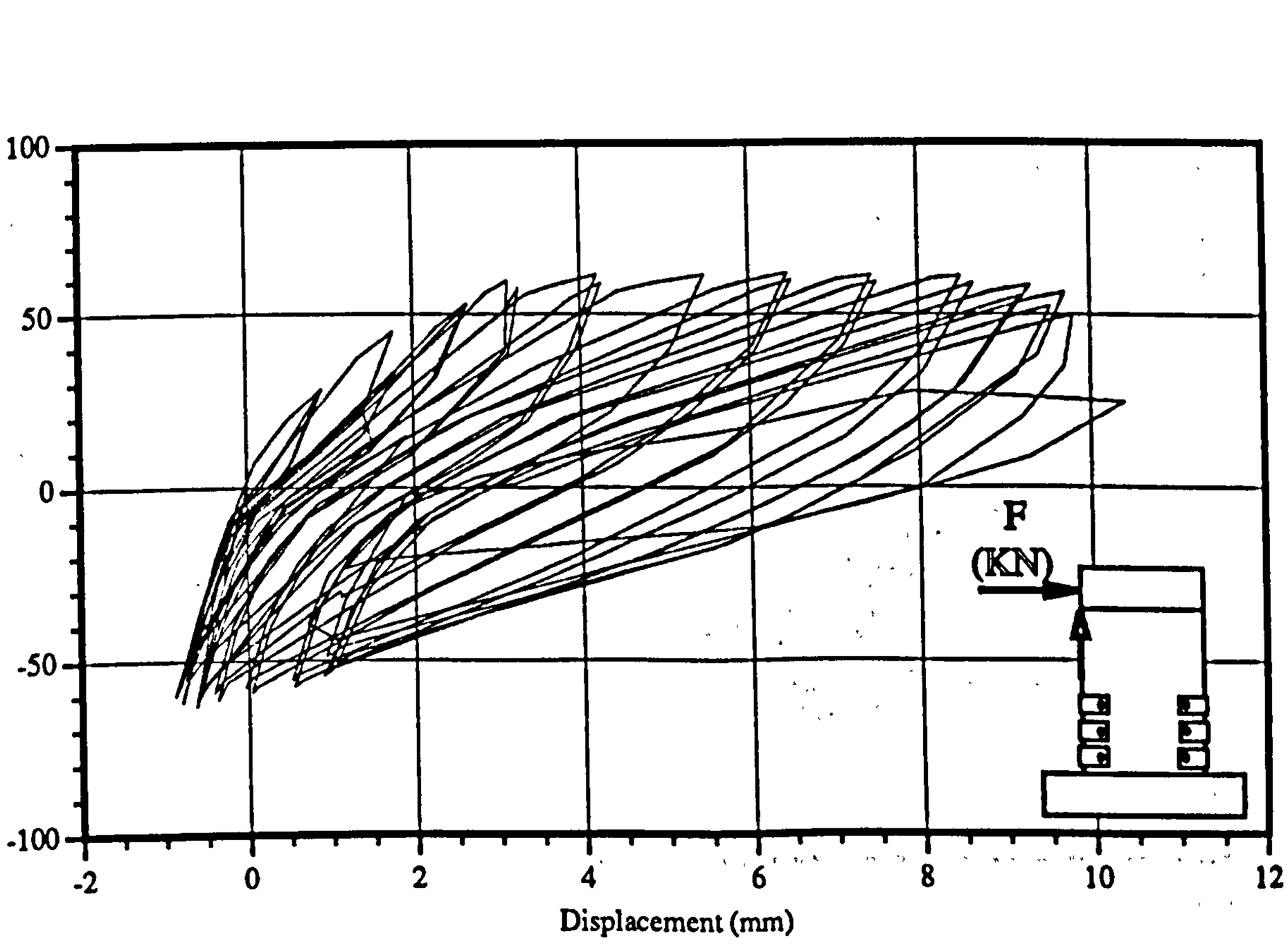


Fig. AI. (32) 2 Force - Displacement for SW32 at Node 2

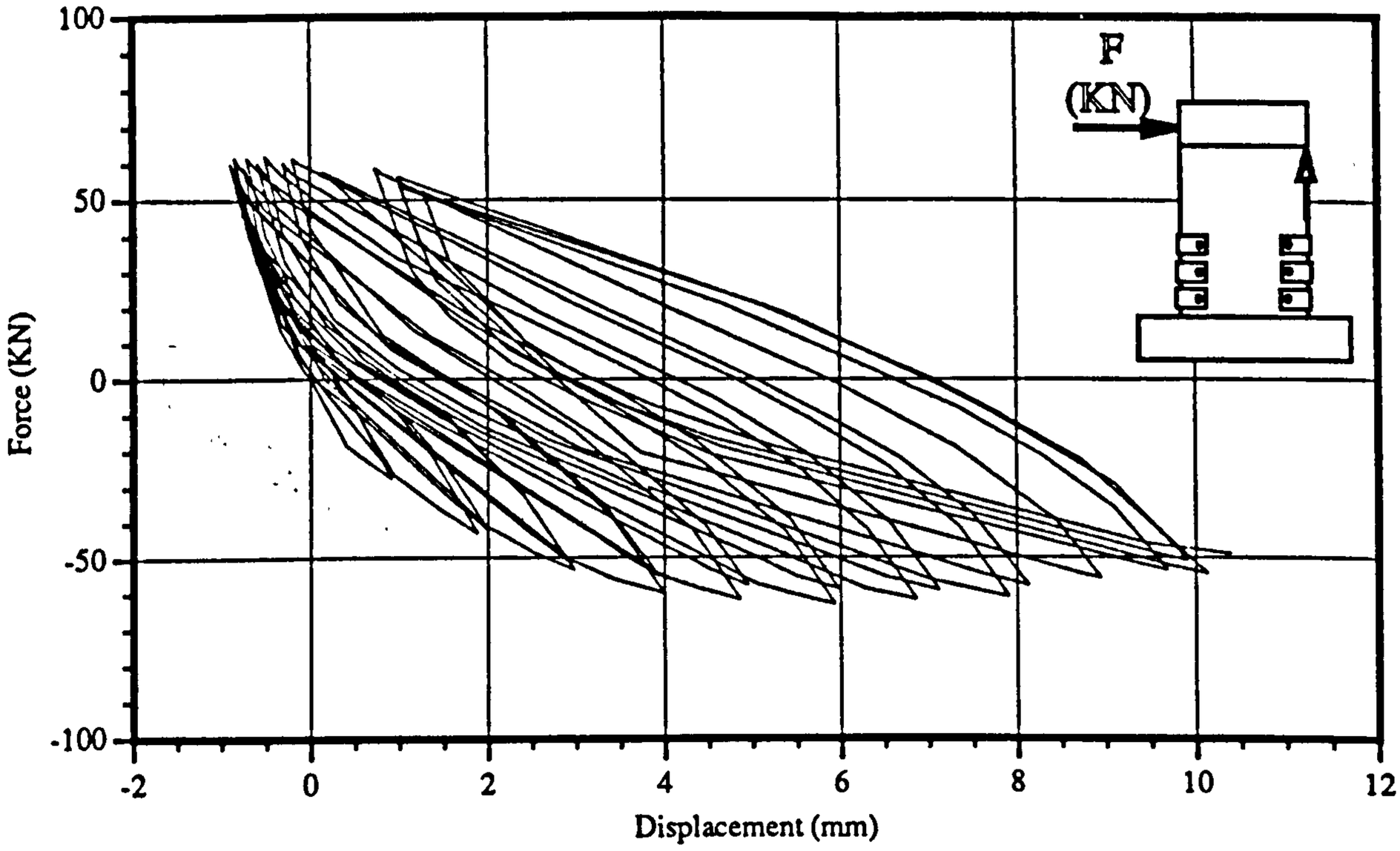


Fig. AI. (32) 3 Force - Displacement for SW32 at Node 3

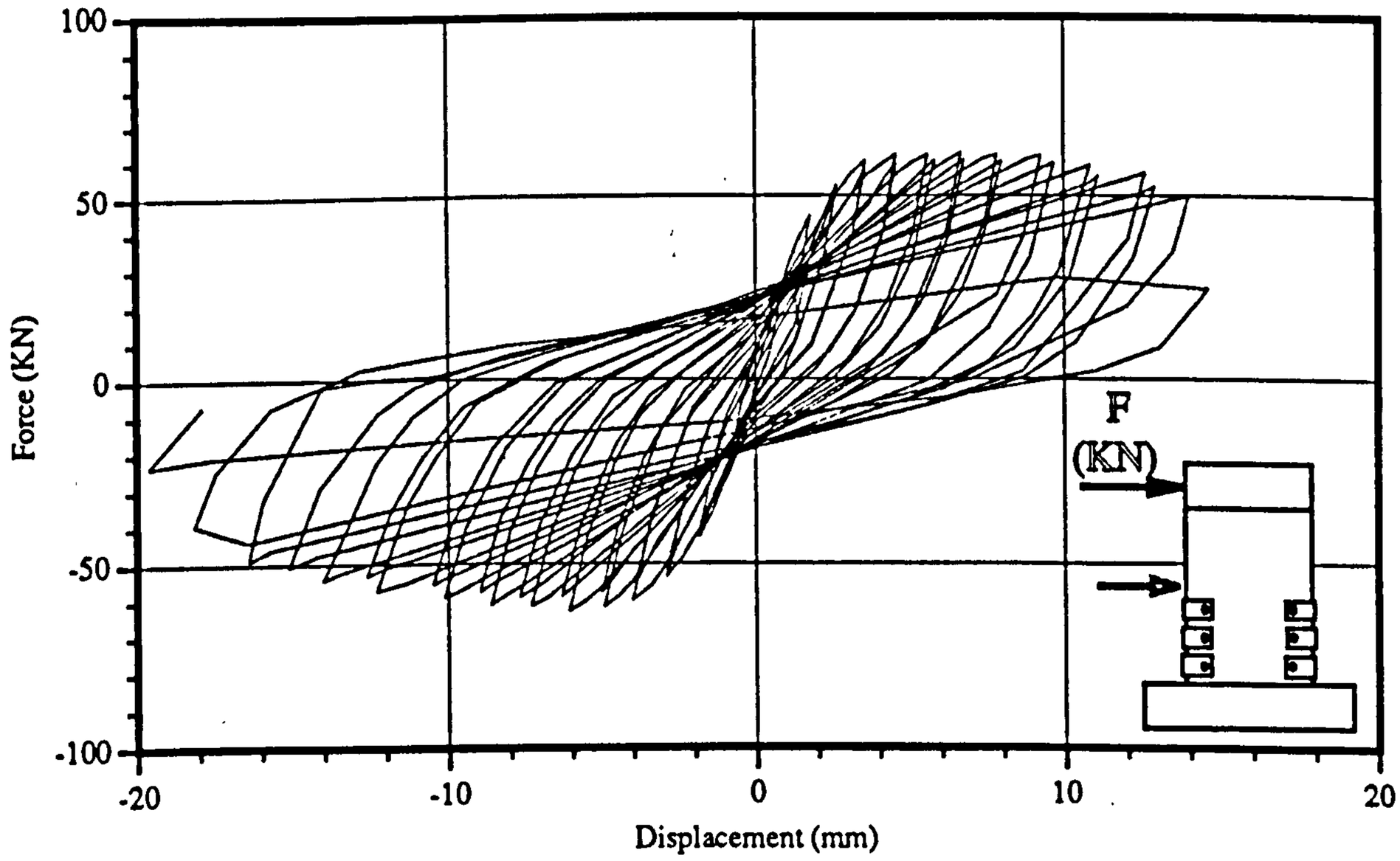


Fig. AI. (32) 4 Force - Displacement for SW32 at Node 4

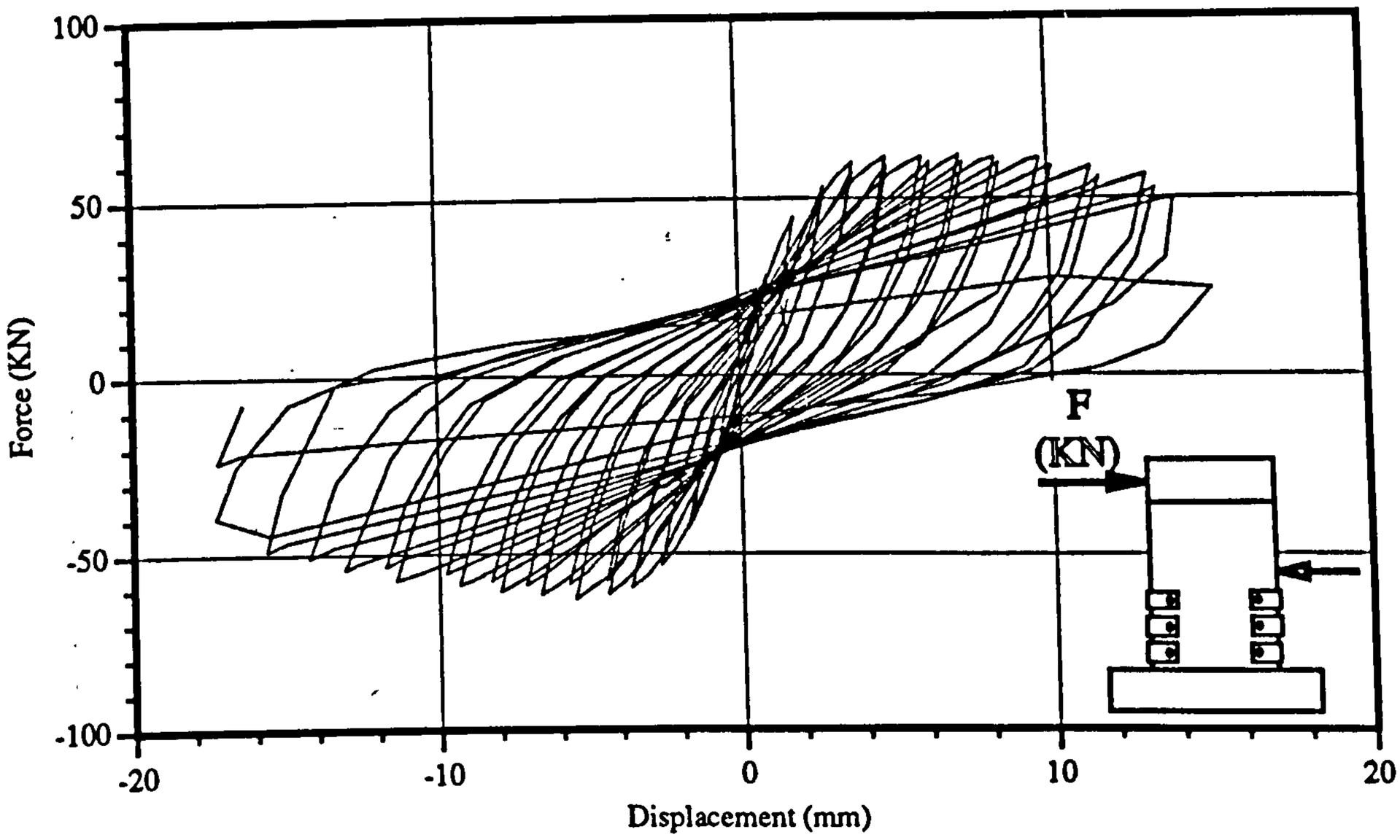


Fig. AI. (32) 5 Force - Displacement for SW32 at Node 5

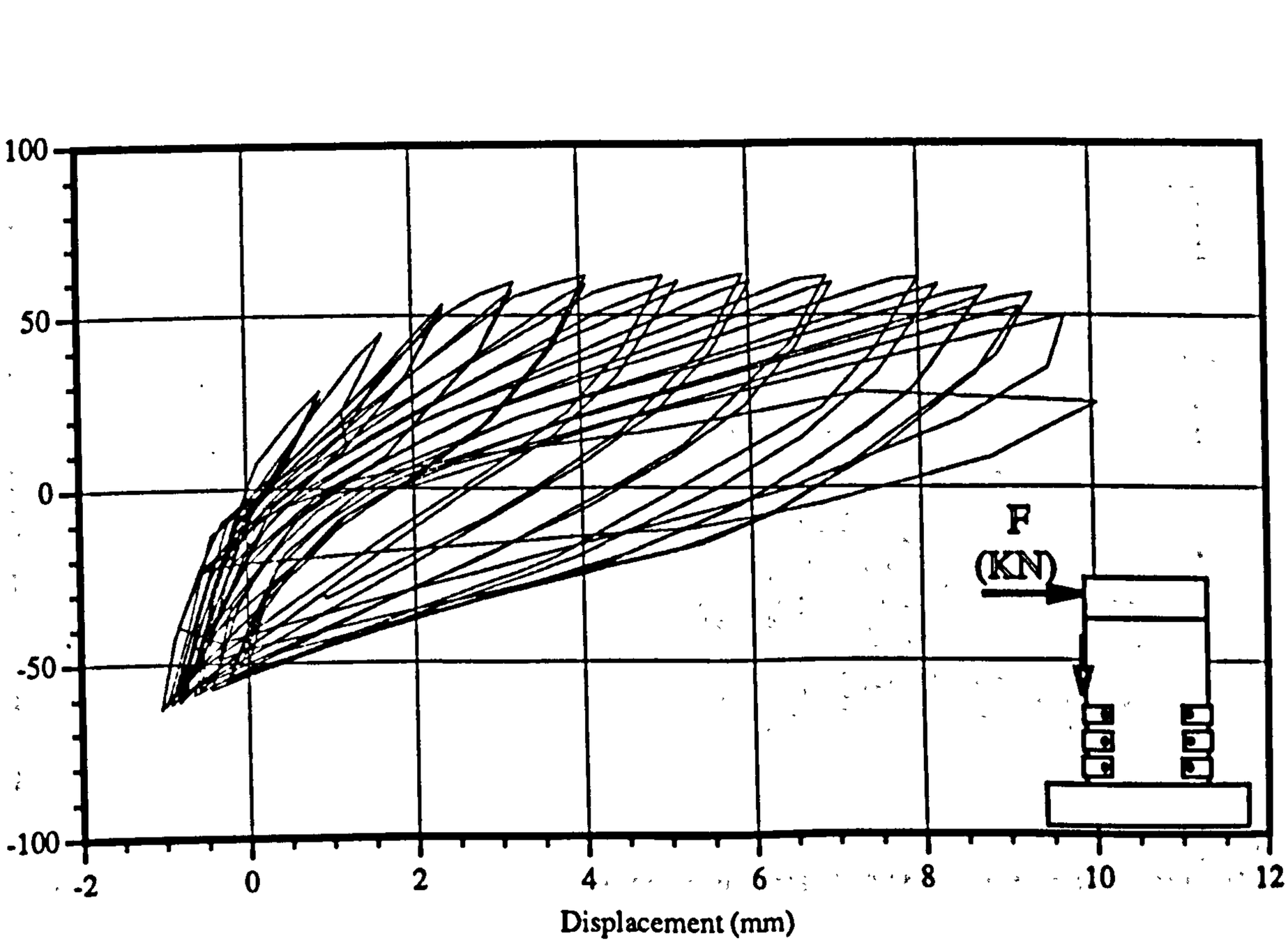


Fig. AI. (32) 6 Force - Displacement for SW32 at Node 6

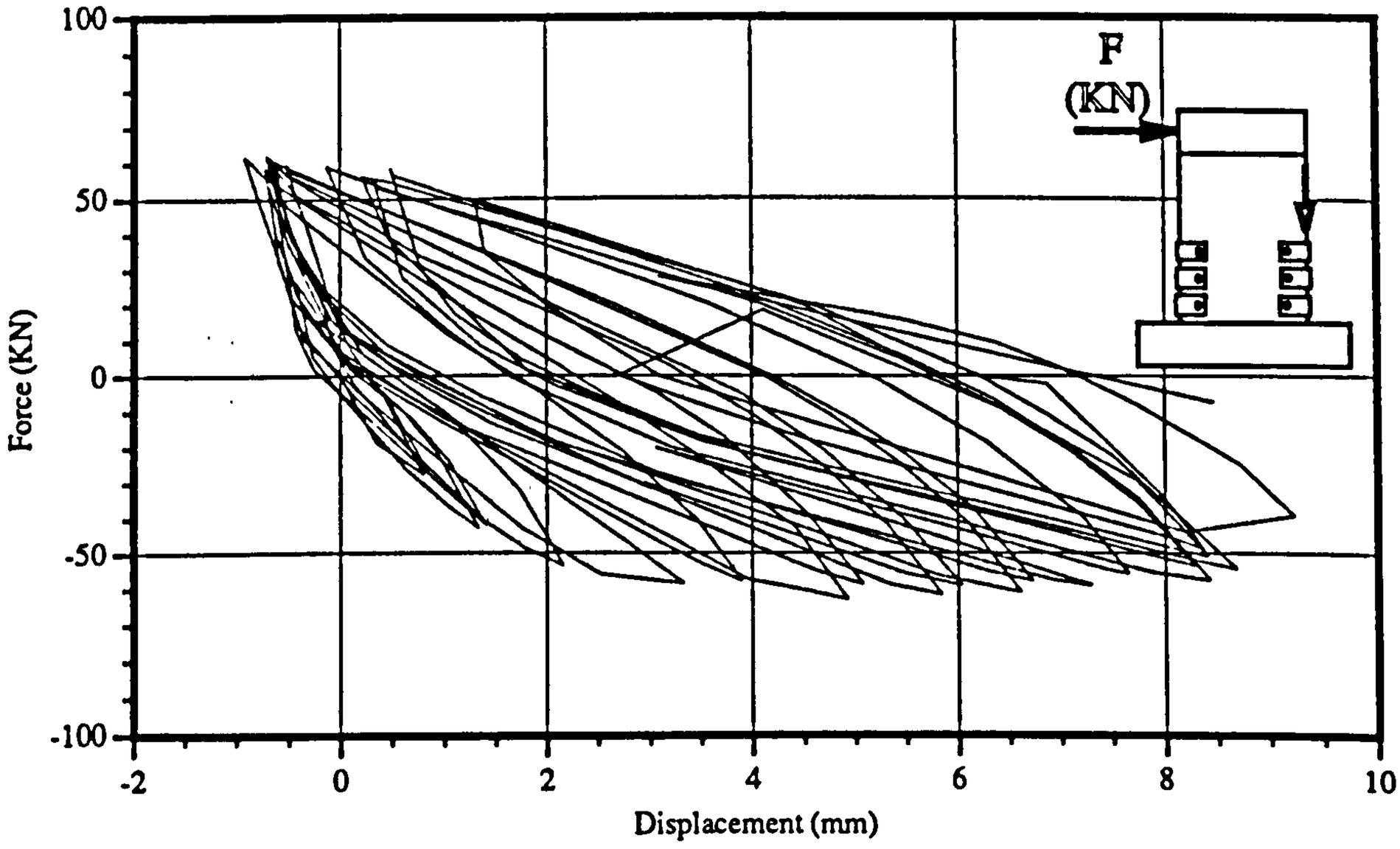


Fig. AI. (32) 7 Force - Displacement for SW32 at Node 7

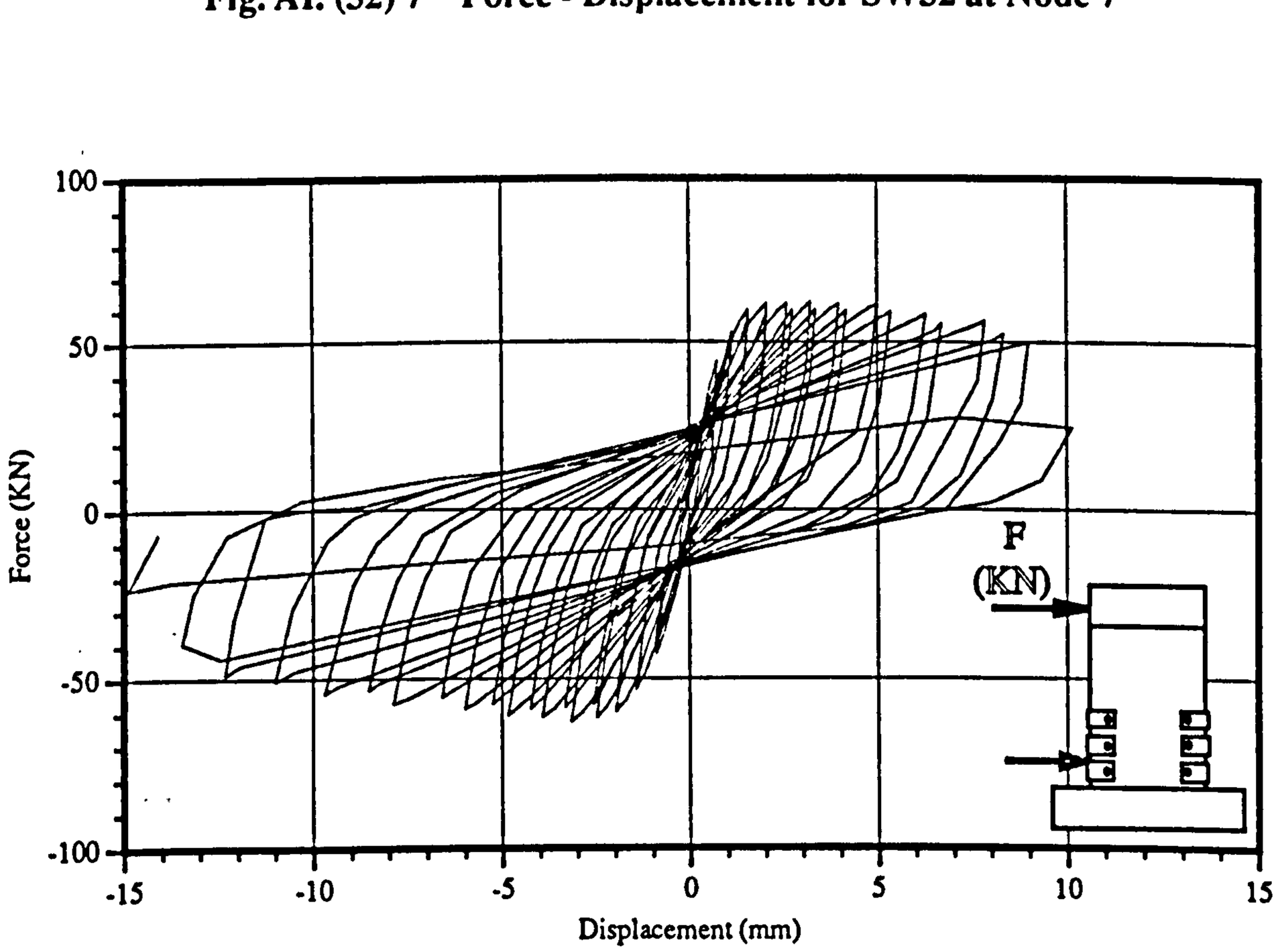


Fig. AI. (32) 8 Force - Displacement for SW32 at Node 8

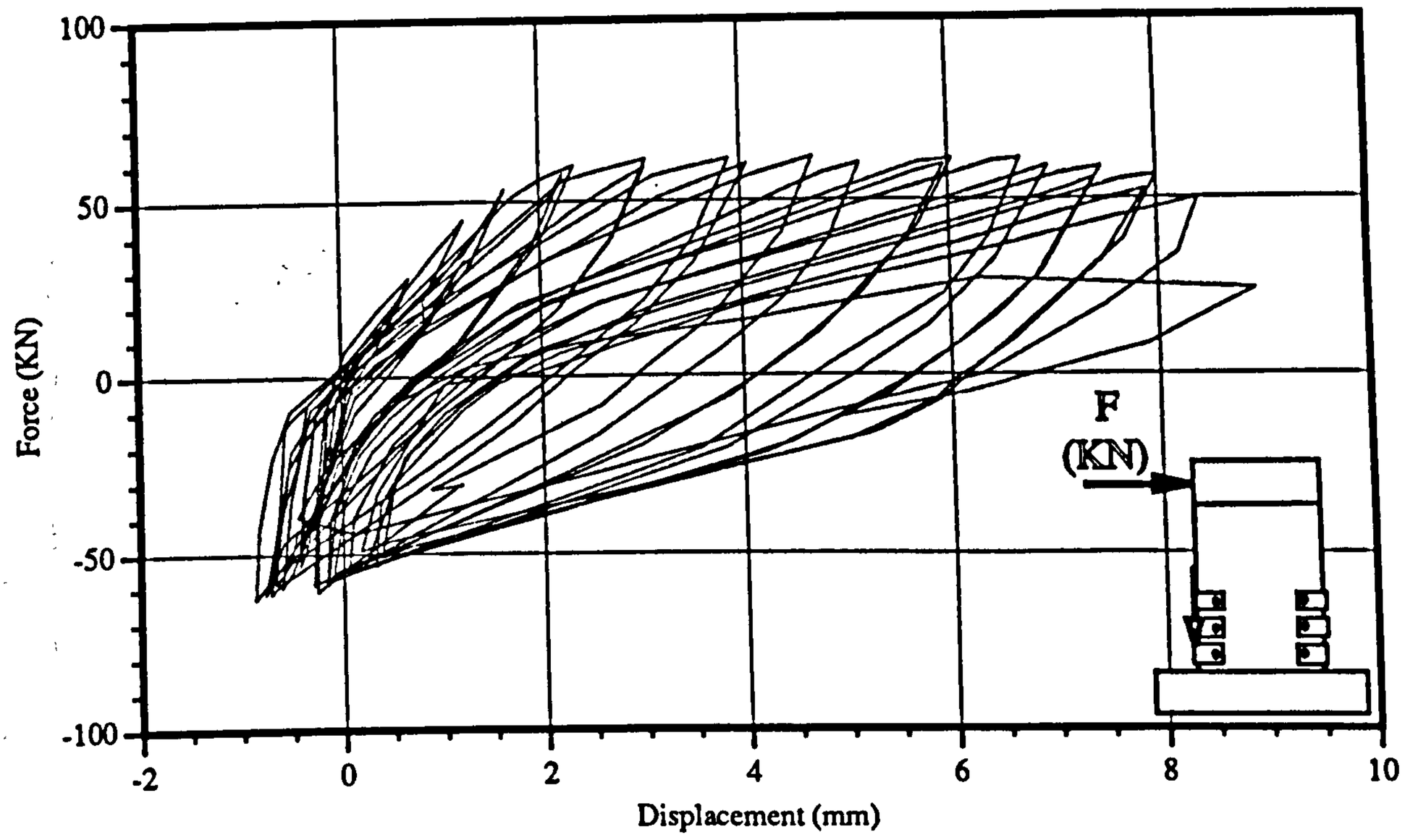


Fig. AI. (32) 9 Force - Displacement for SW32 at Node 9

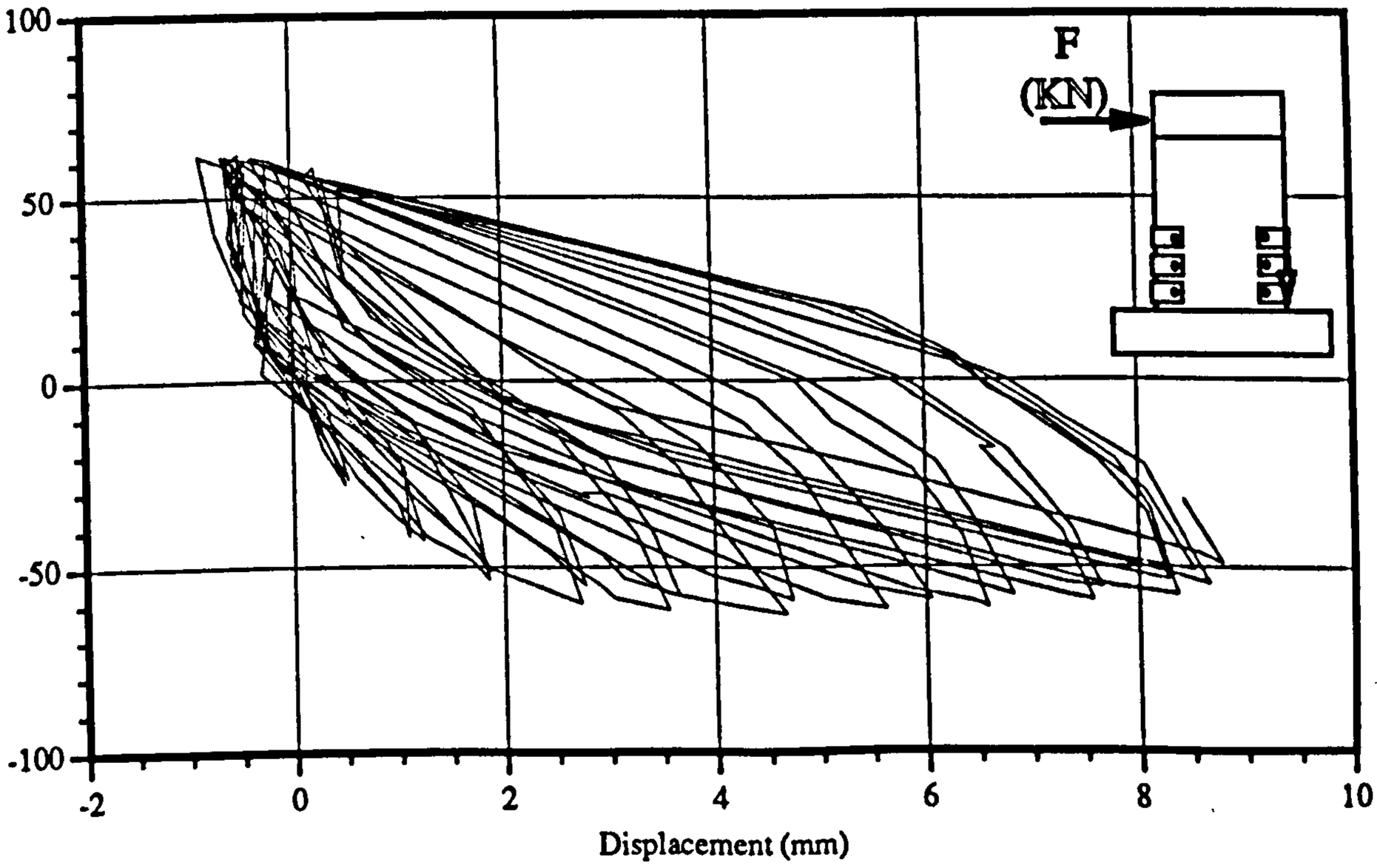


Fig. AI. (32) 10 Force - Displacement for SW32 at Node 10

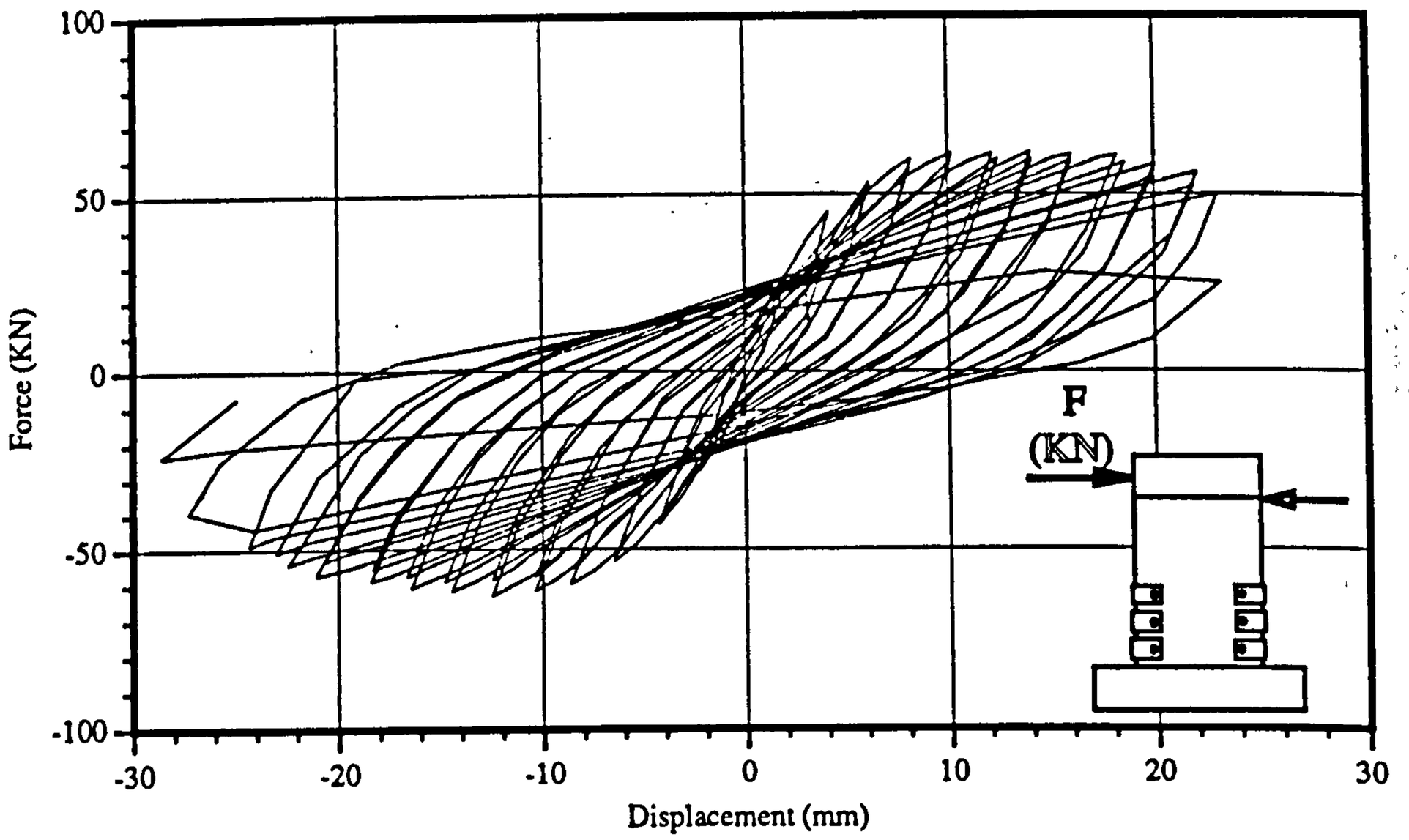


Fig. AI. (32) 16 Force - Displacement for SW32 at Node 16

AI.14. : Force Displacement for SW33

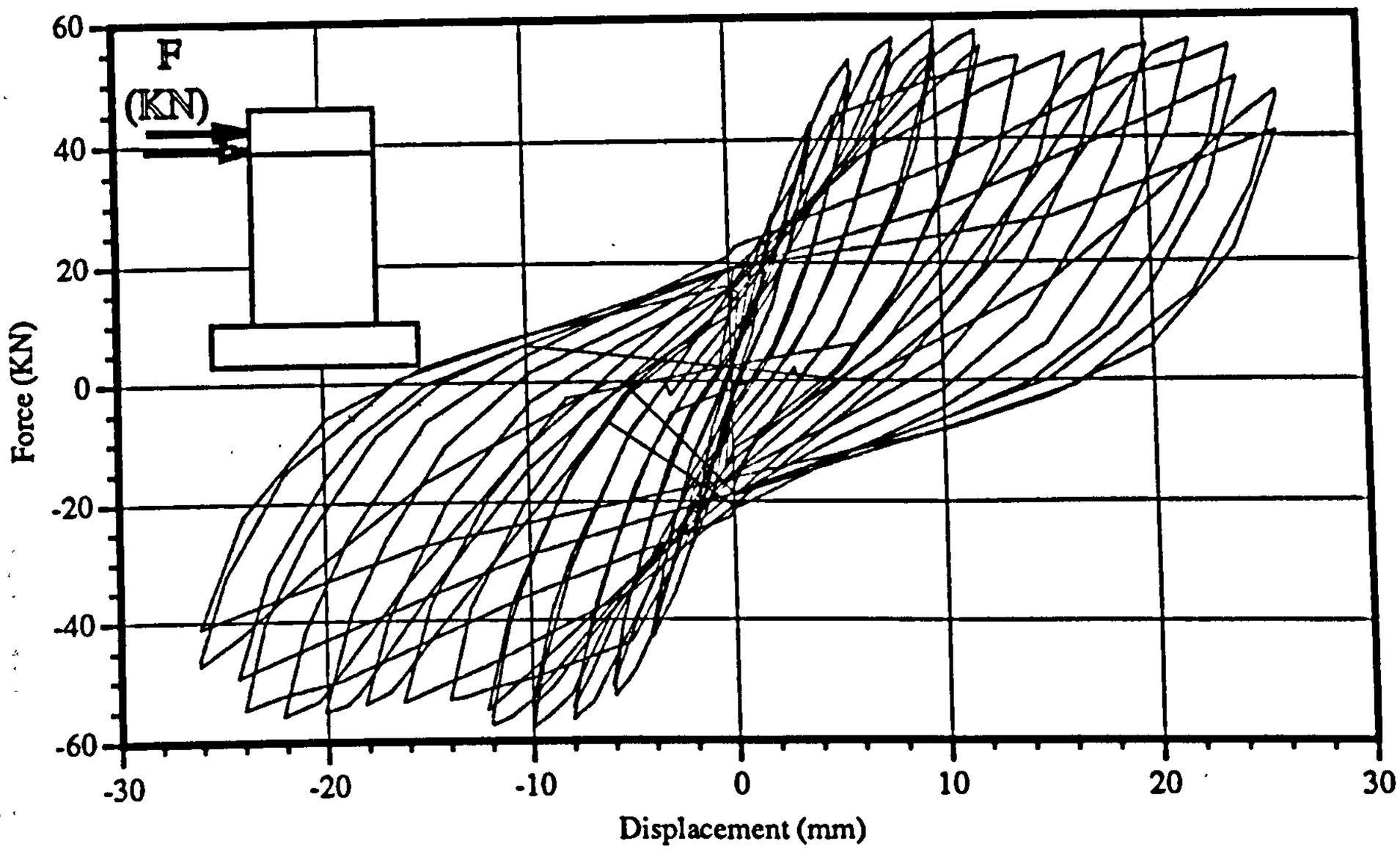


Fig. AI. (33) 1 Force - Displacement for SW33 at Node 1

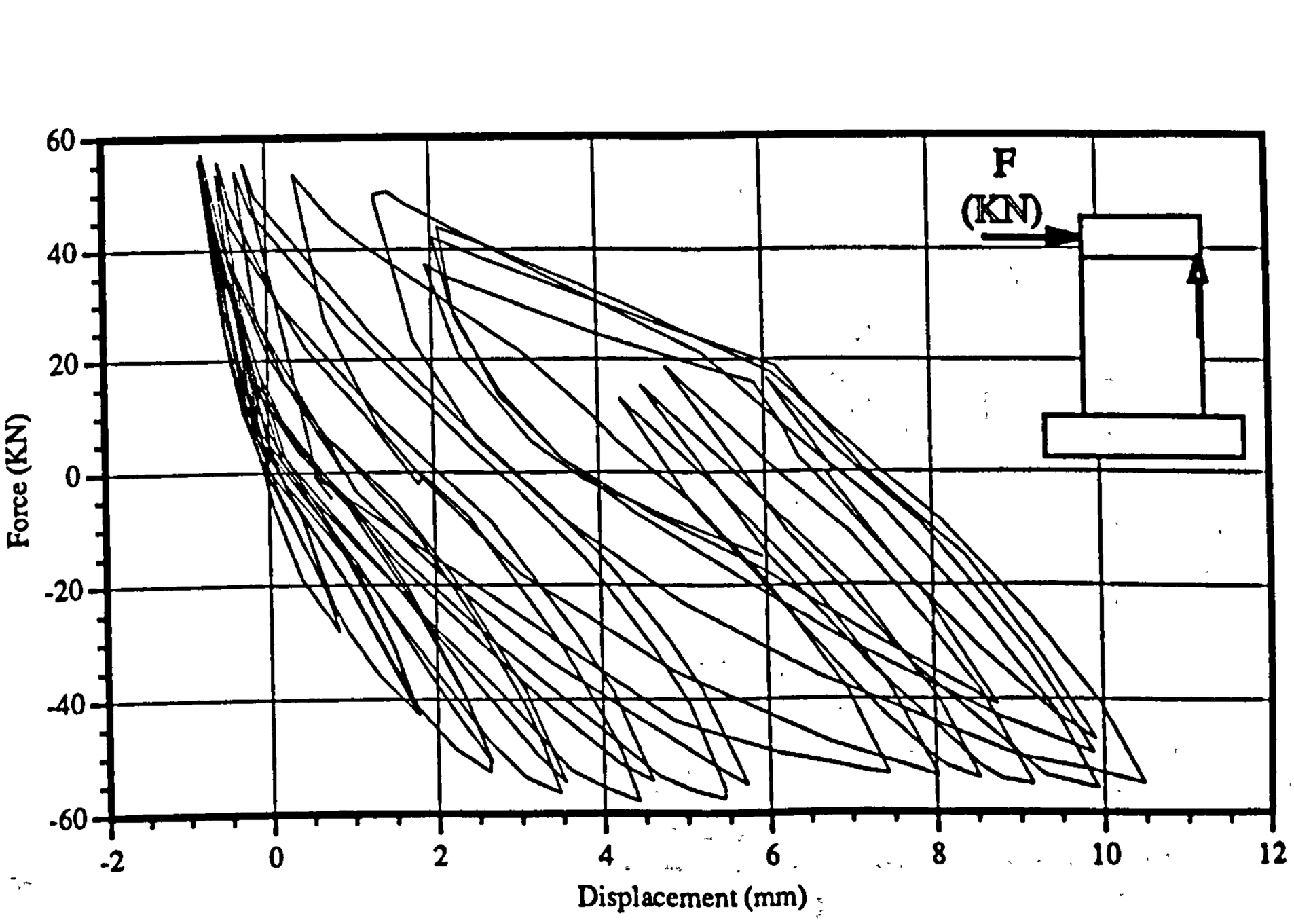


Fig. AI. (33) 3 Force - Displacement for SW33 at Node 3

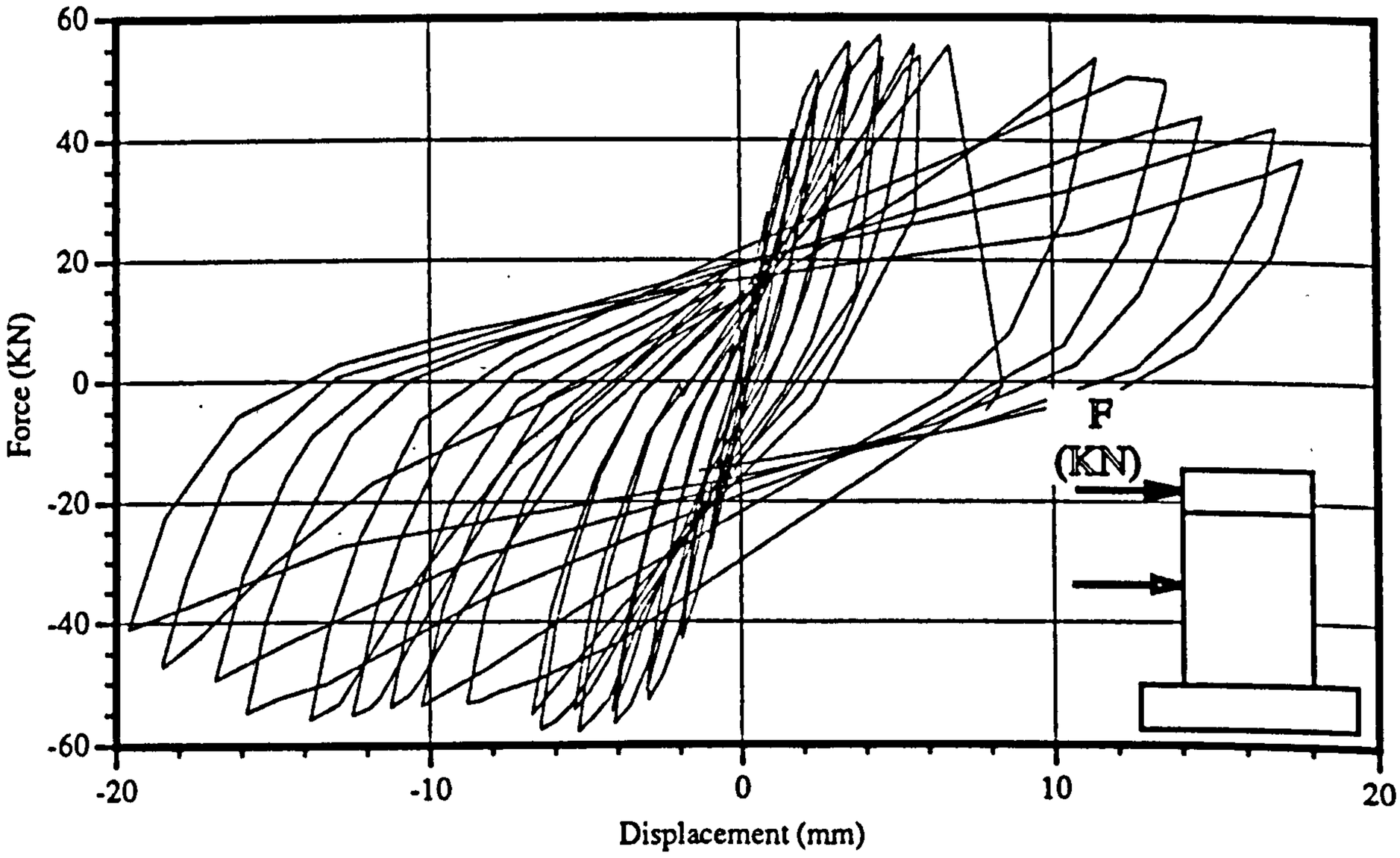


Fig. AI. (33) 4 Force - Displacement for SW33 at Node 4

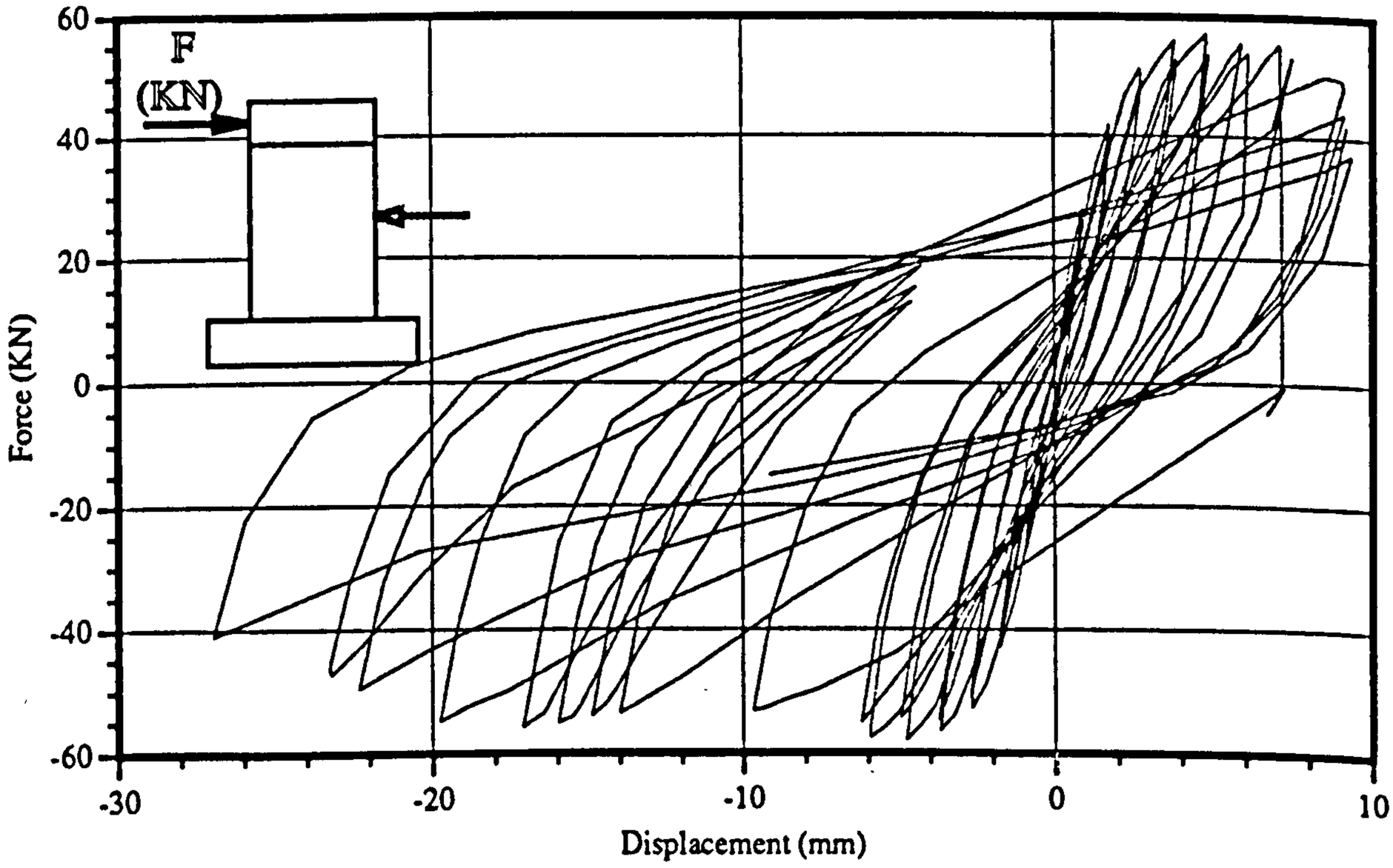


Fig. AI. (33) 5 Force - Displacement for SW33 at Node 5

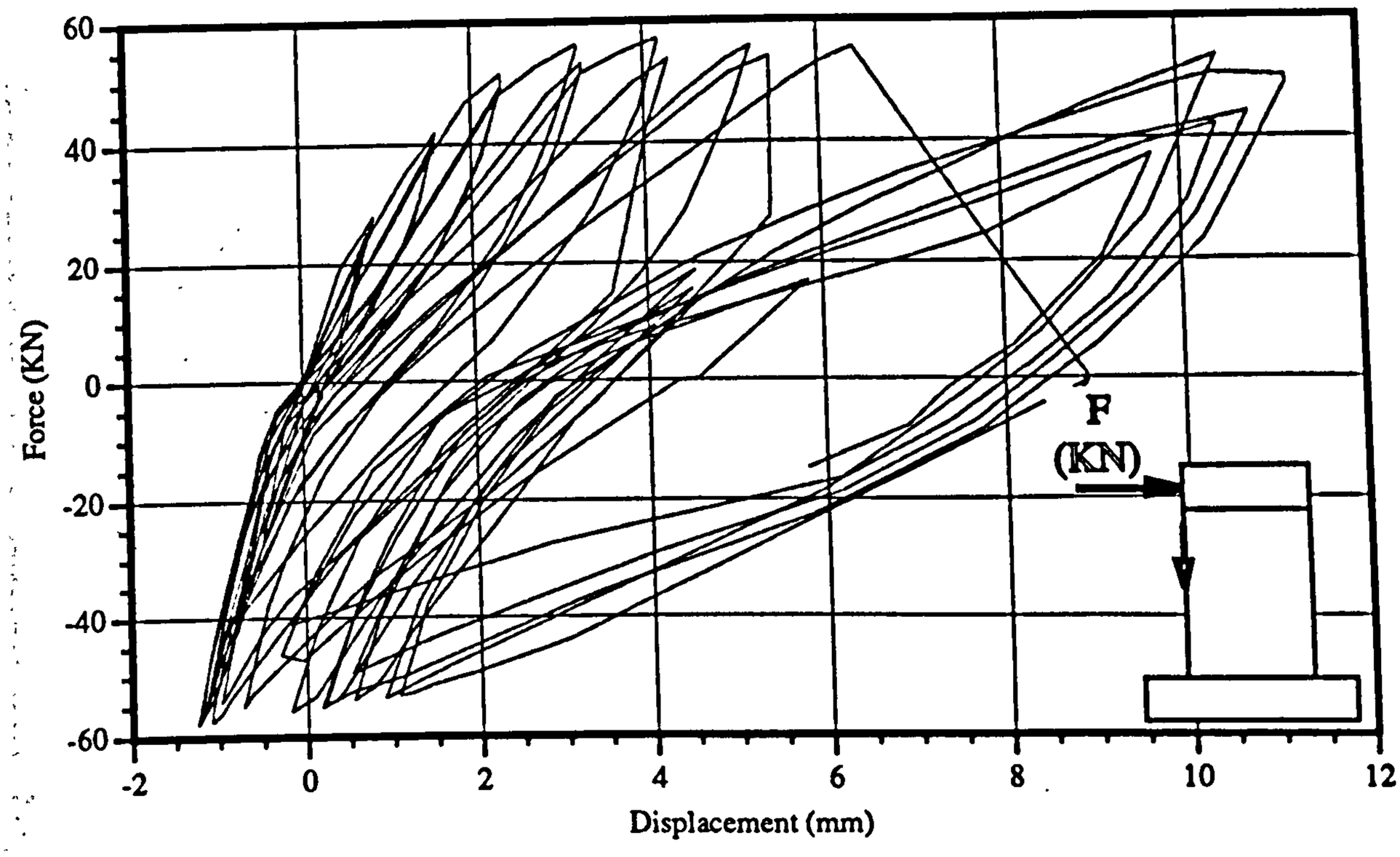


Fig. AI. (33) 6 Force - Displacement for SW33 at Node 6

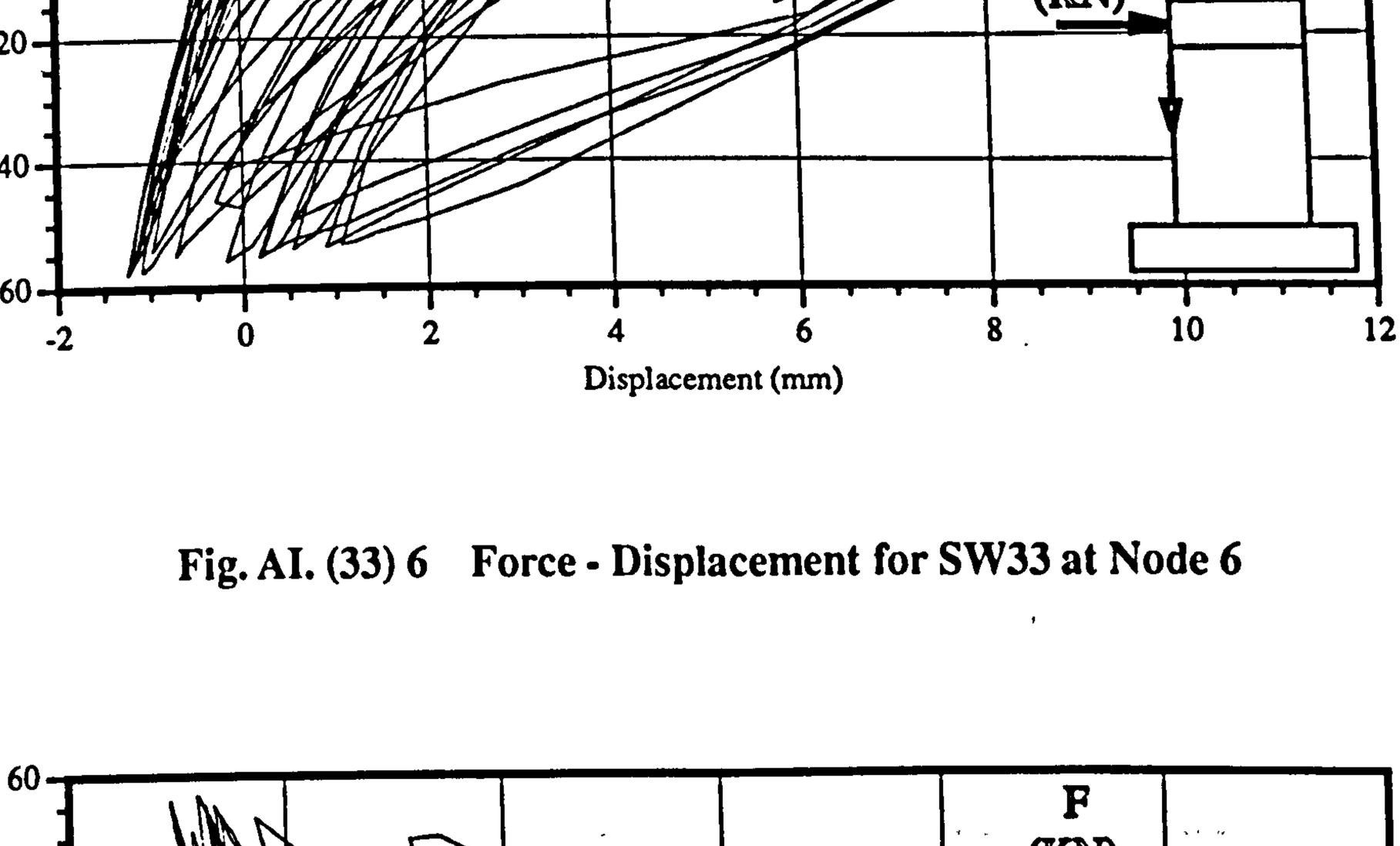


Fig. AI. (33) 7 Force - Displacement for SW33 at Node 7

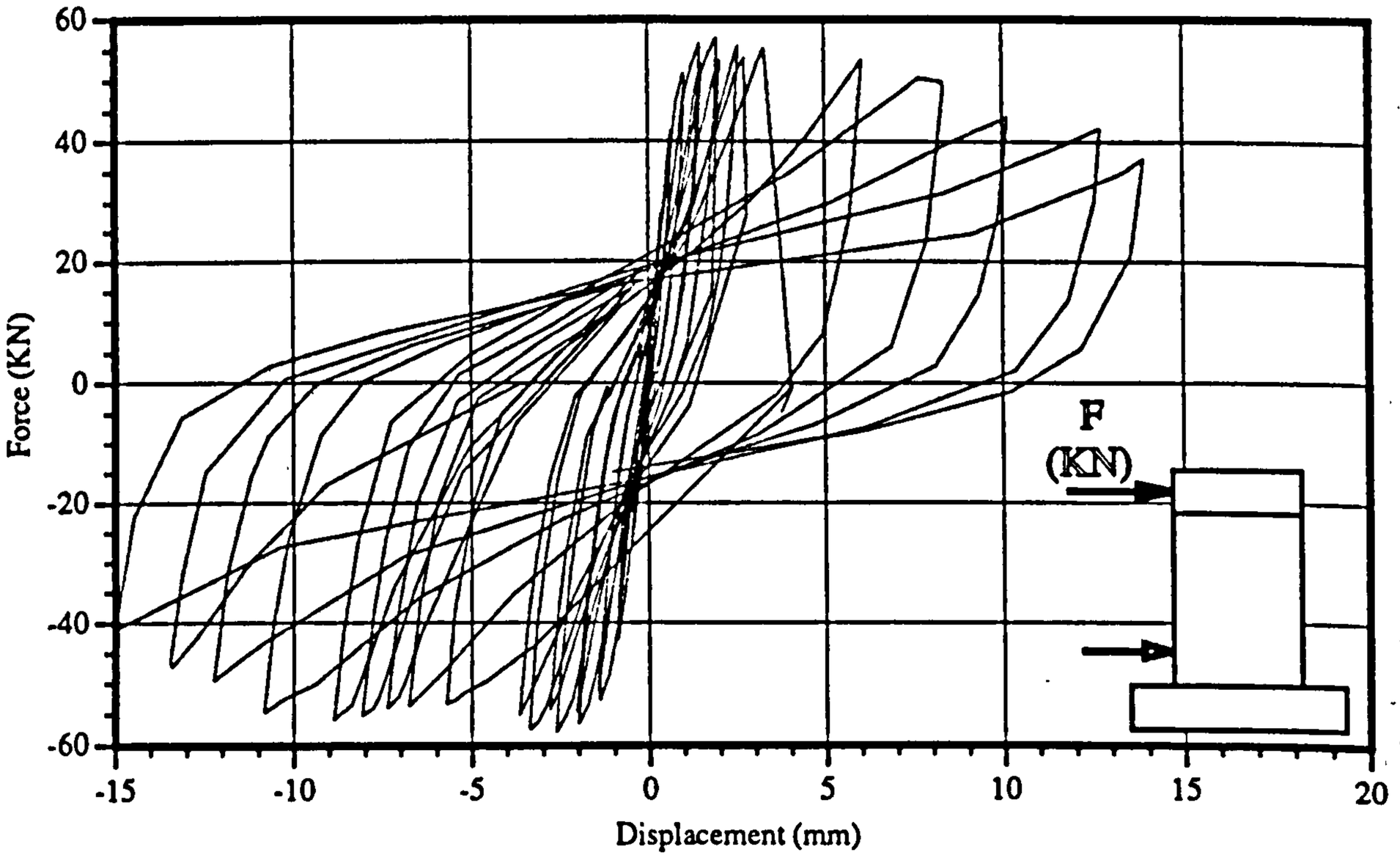


Fig. AI. (33) 8 Force - Displacement for SW33 at Node 8

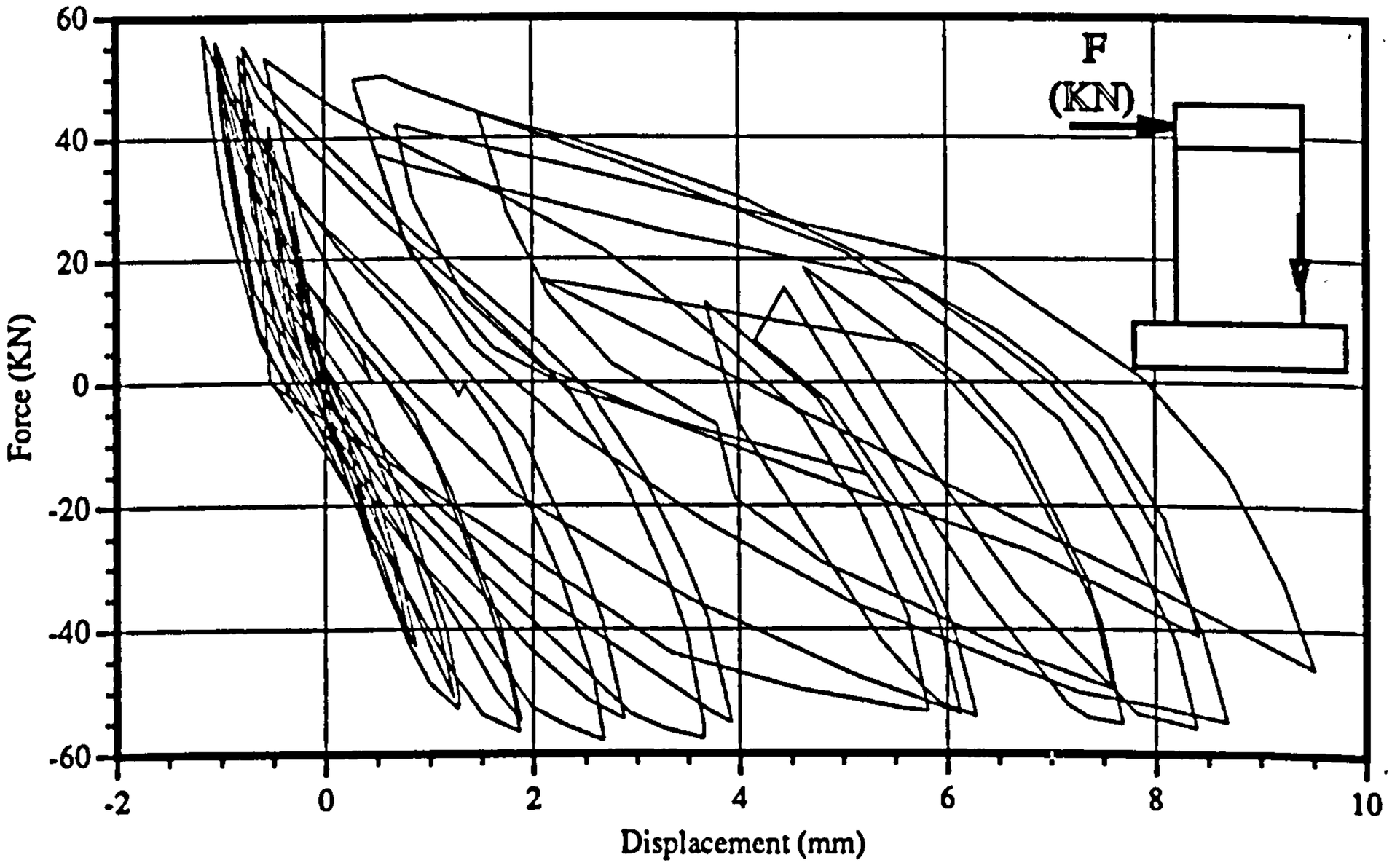


Fig. AI. (33) 10 Force - Displacement for SW33 at Node 10

AI.15. : Force Displacement for SW34

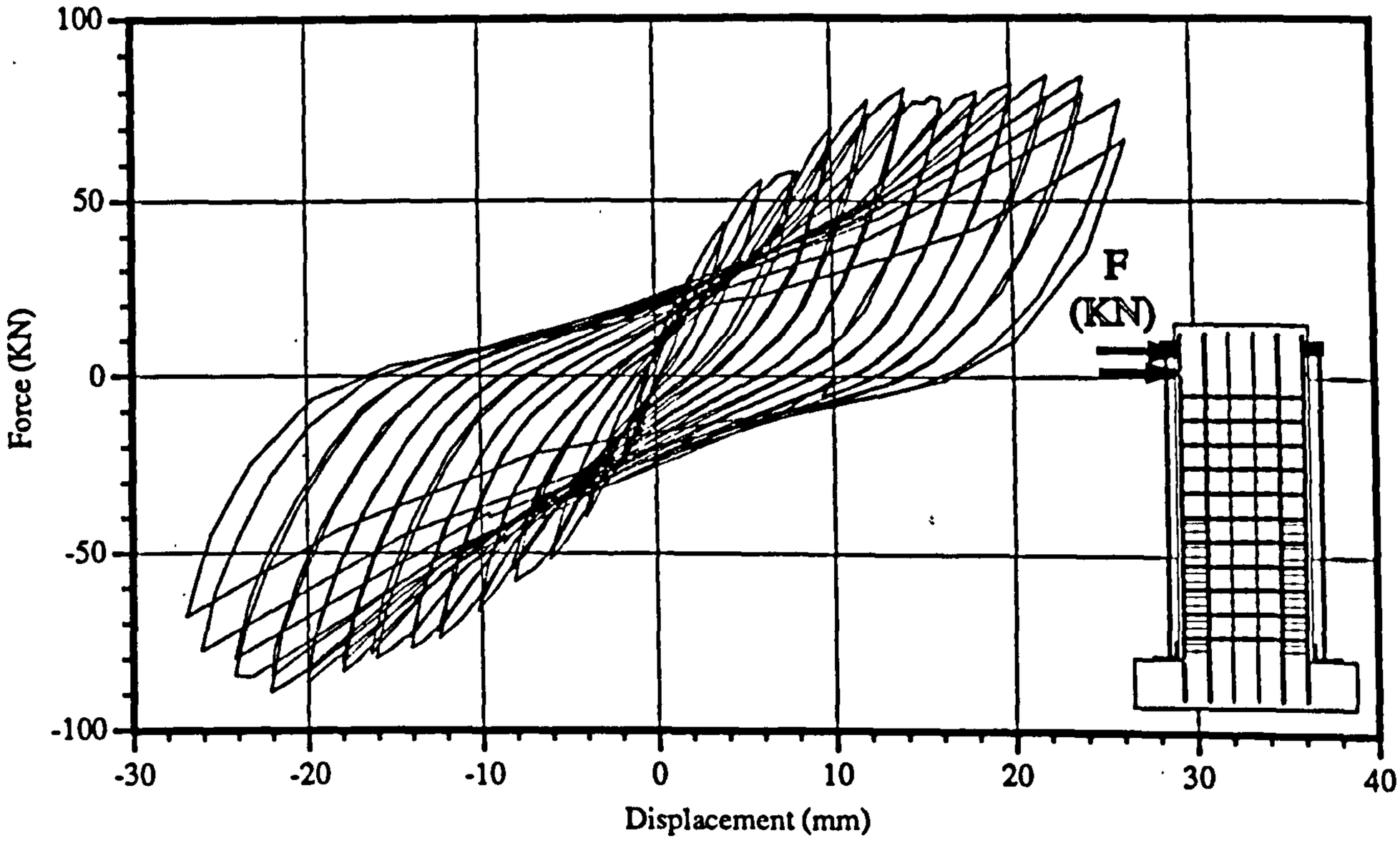


Fig. AI. (34) 1 Force - Displacement for SW34 at Node 1

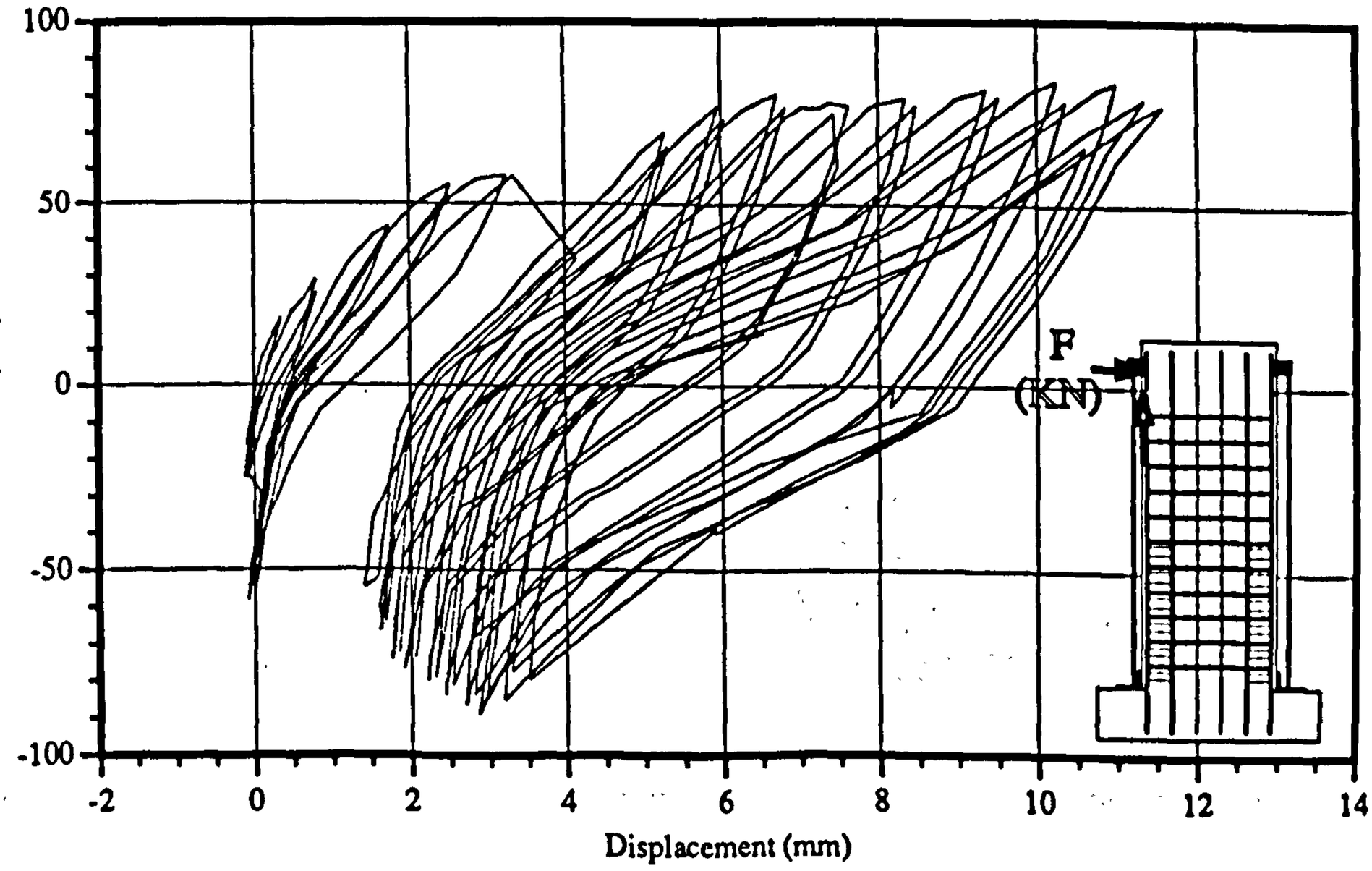


Fig. AI. (34) 2 Force - Displacement for SW34 at Node 2

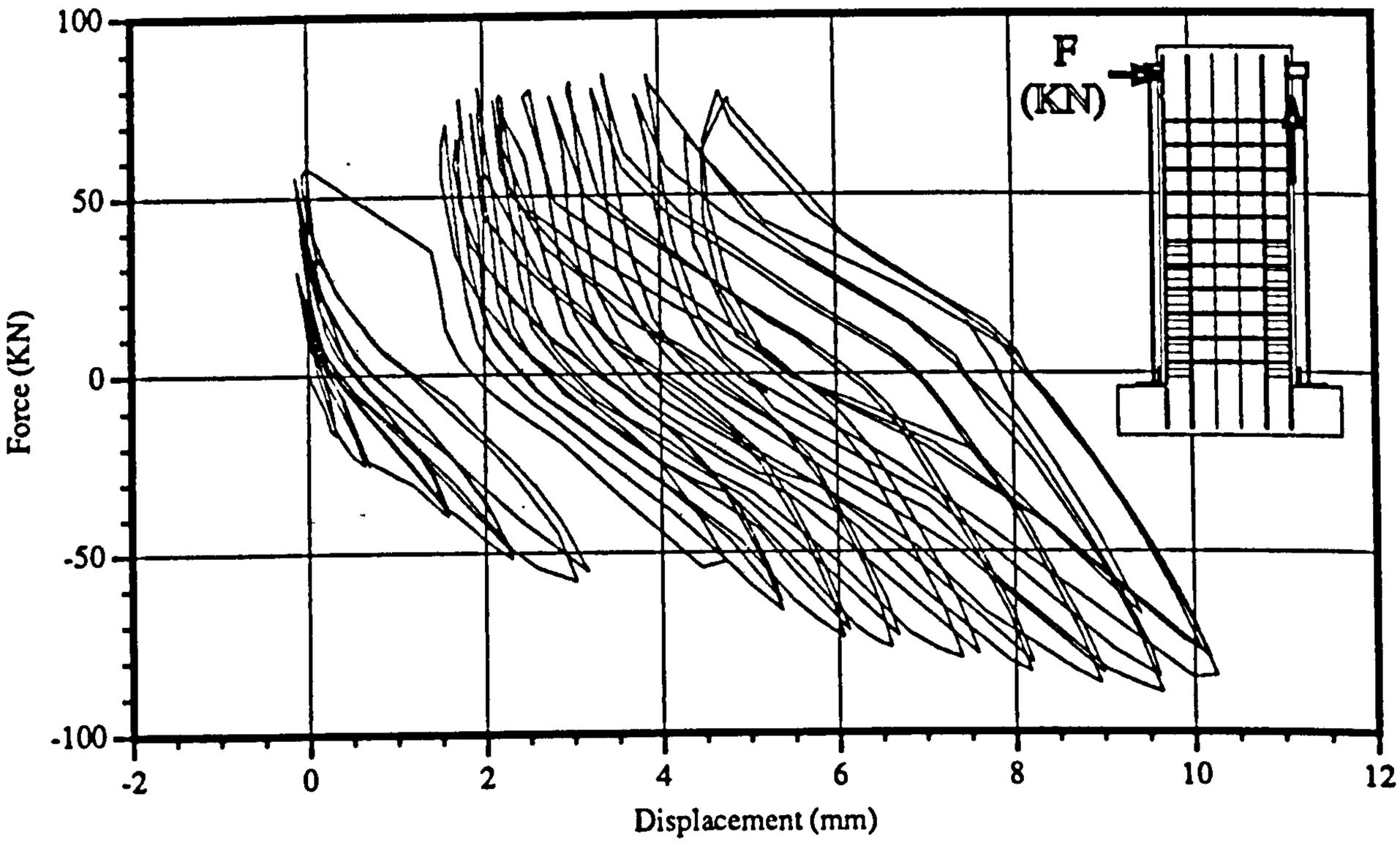


Fig. AI. (34) 3 Force - Displacement for SW34 at Node 3

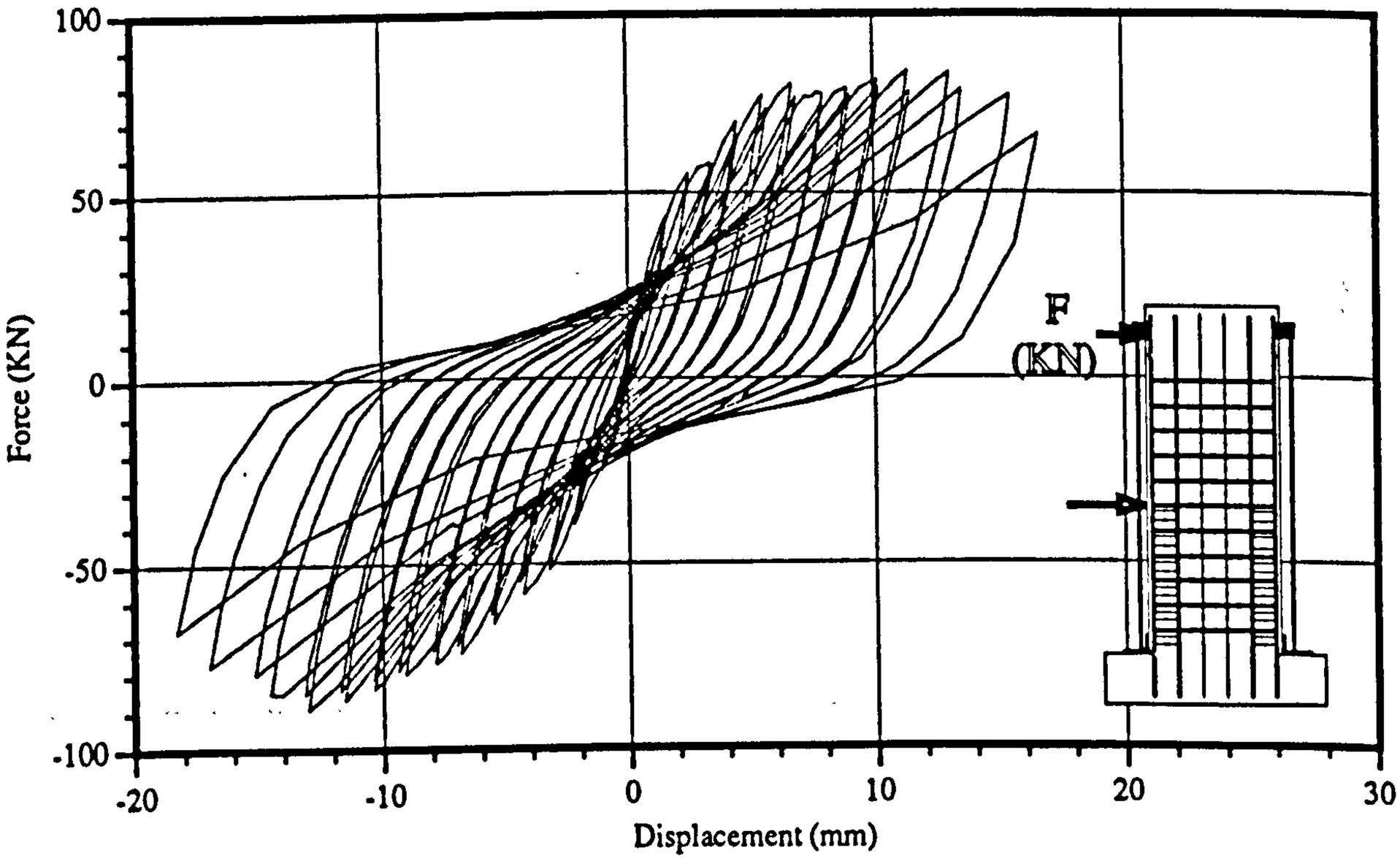


Fig. AI. (34) 4 Force - Displacement for SW34 at Node 4

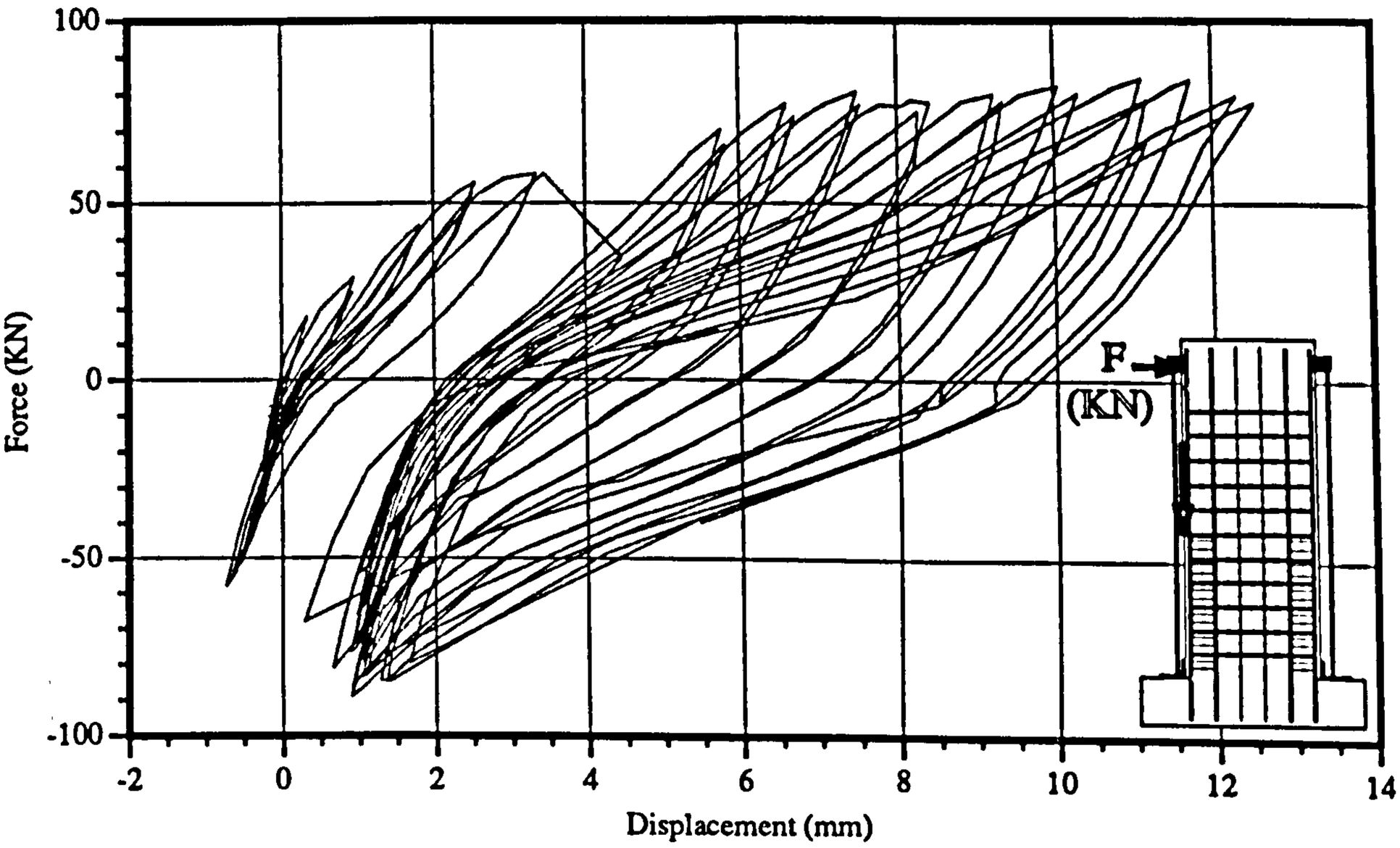


Fig. AI. (34) 6 Force - Displacement for SW34 at Node 6

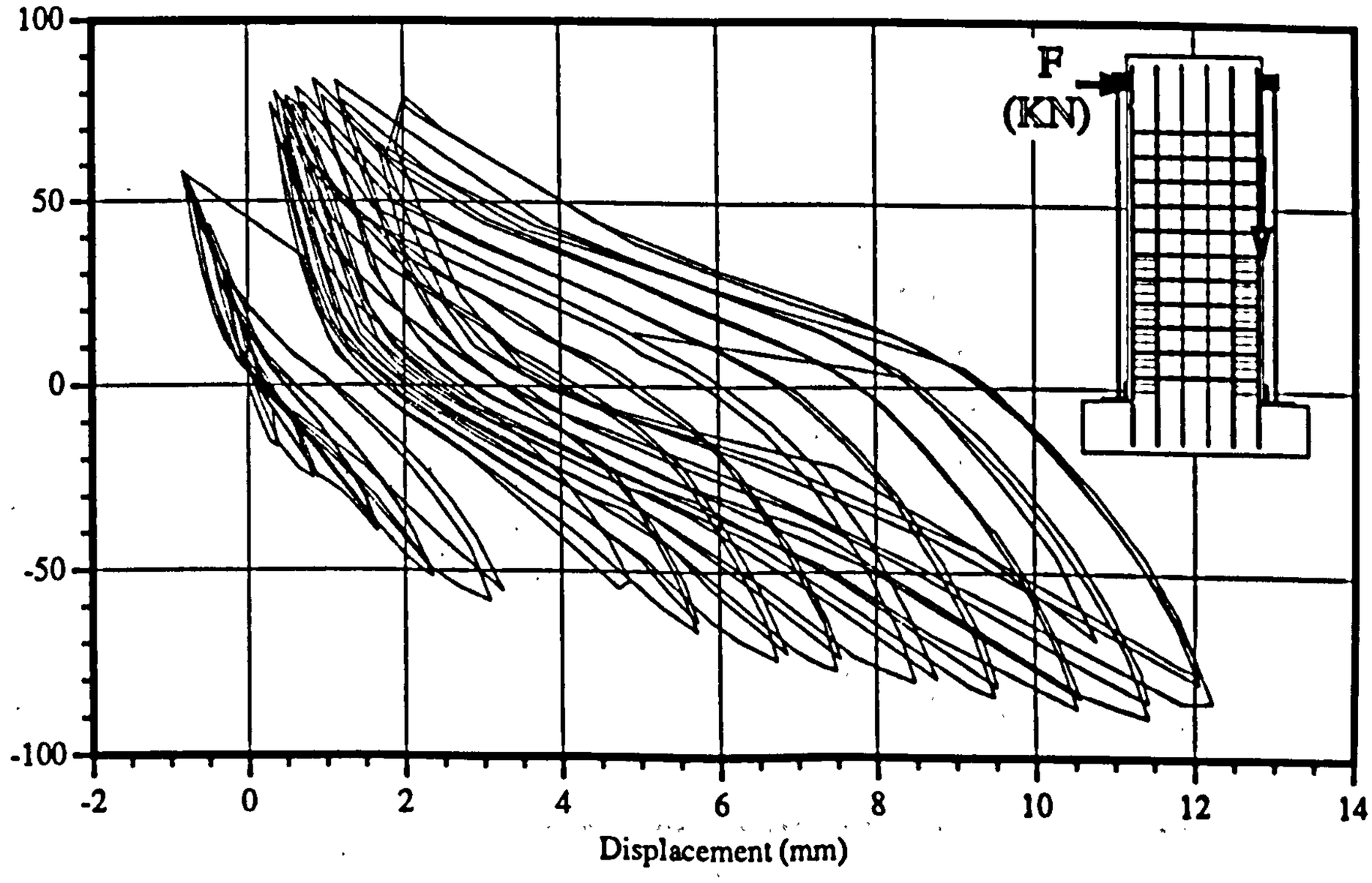


Fig. AI. (34) 7 Force - Displacement for SW34 at Node 7

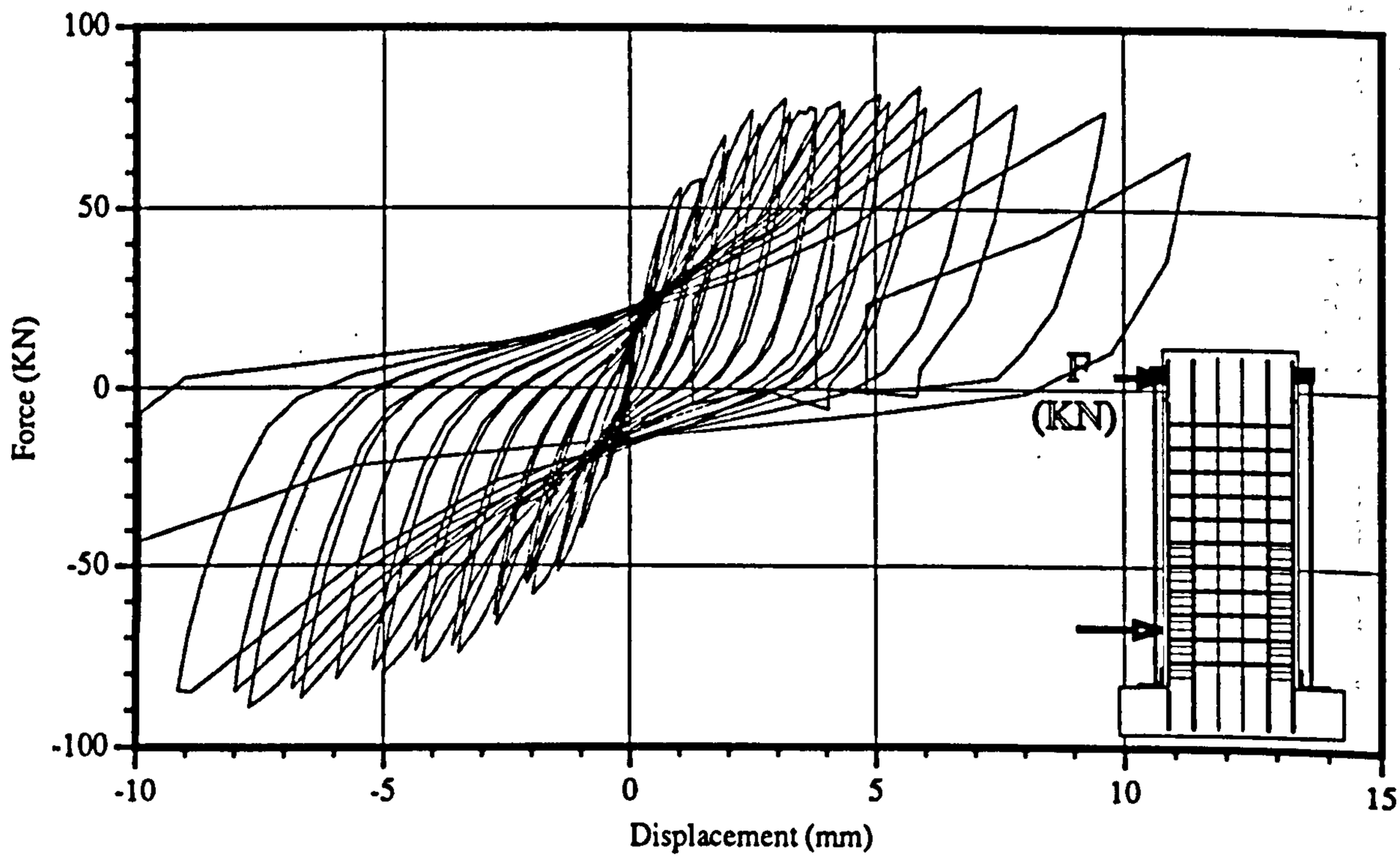


Fig. AI. (34) 8 Force - Displacement for SW34 at Node 8

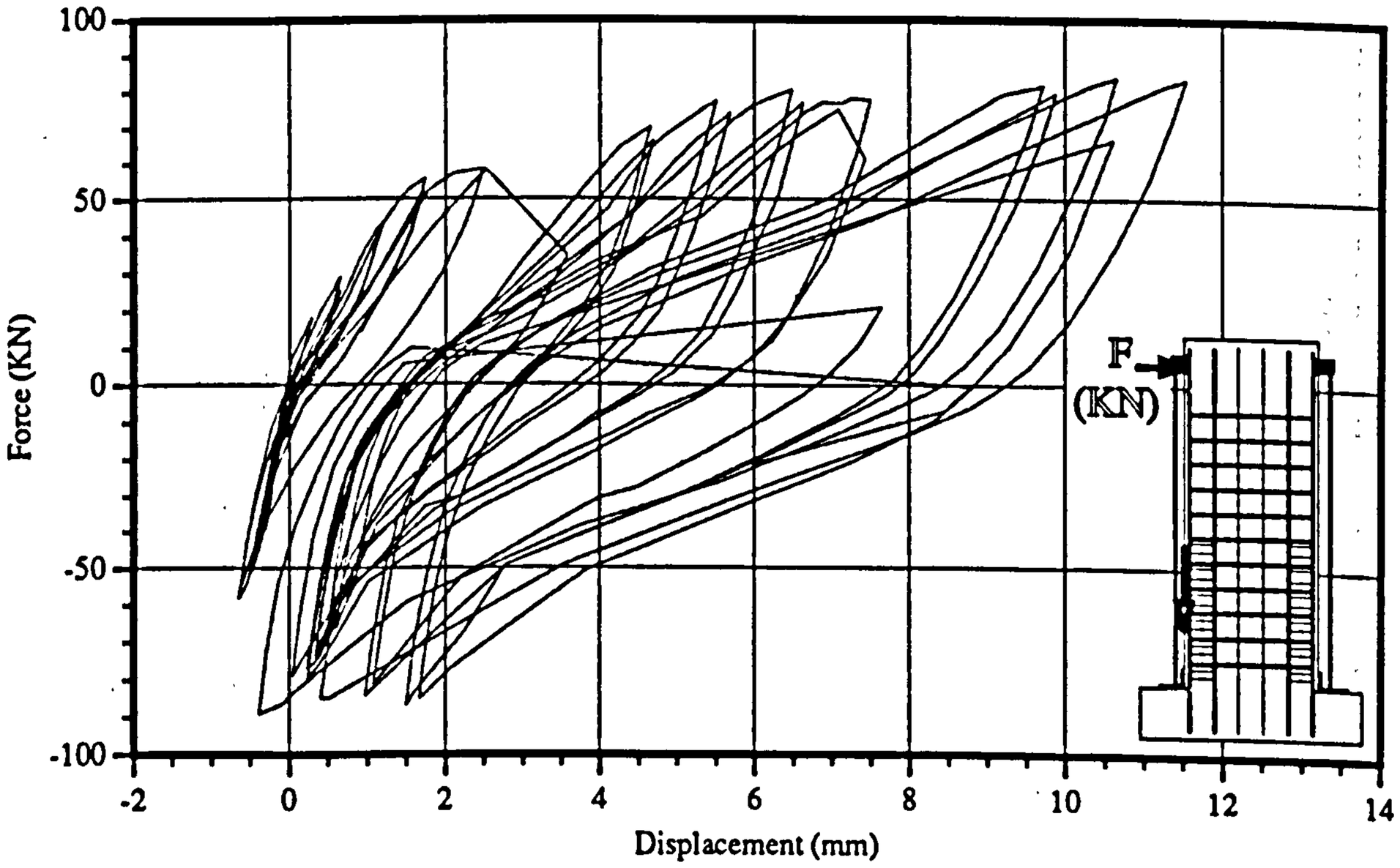


Fig. AI. (34) 9 Force - Displacement for SW34 at Node 9

AI.16. : Force Displacement for SW35

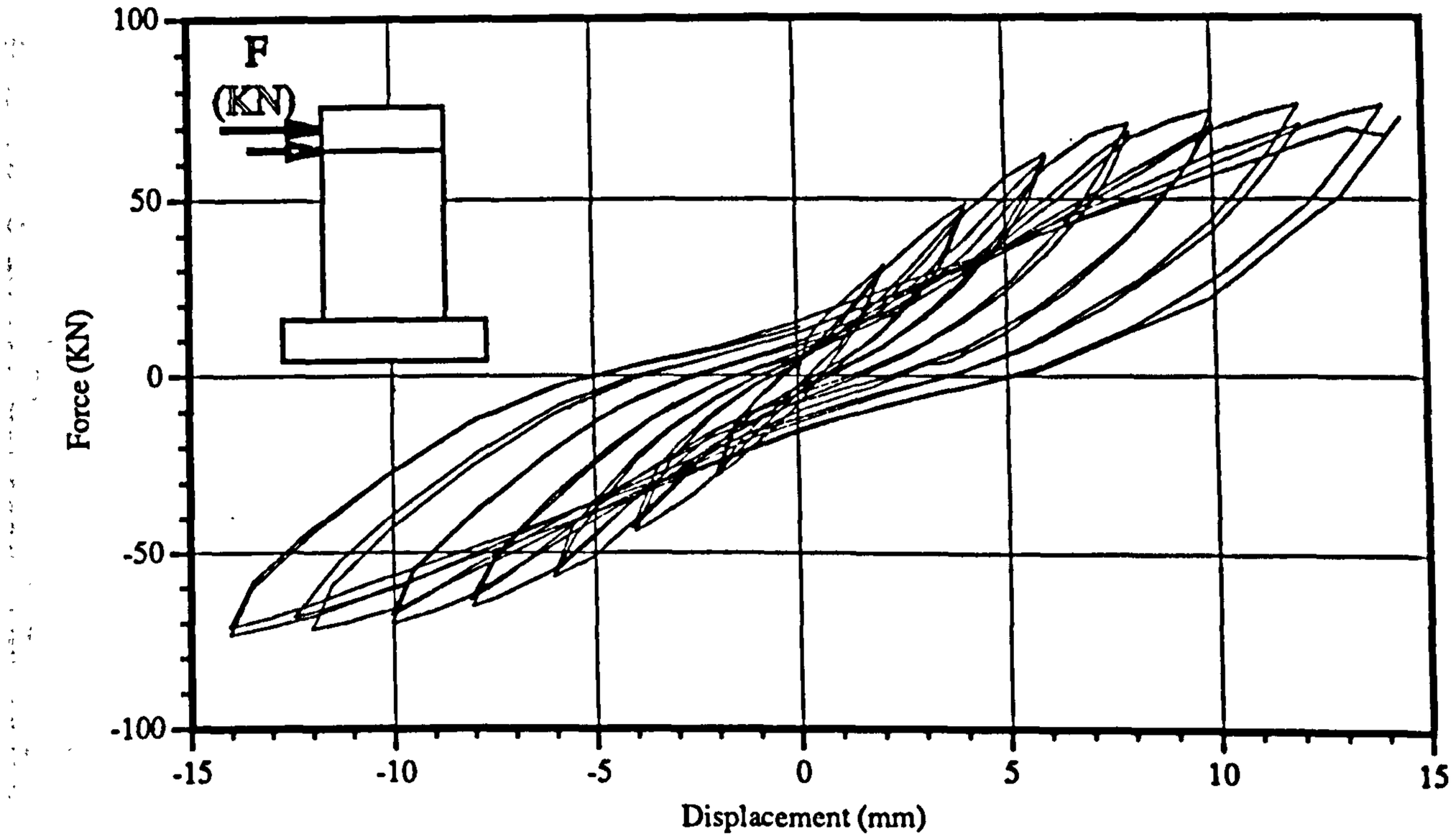


Fig. AI. (35) 1 Force - Displacement for SW35 at Node 1

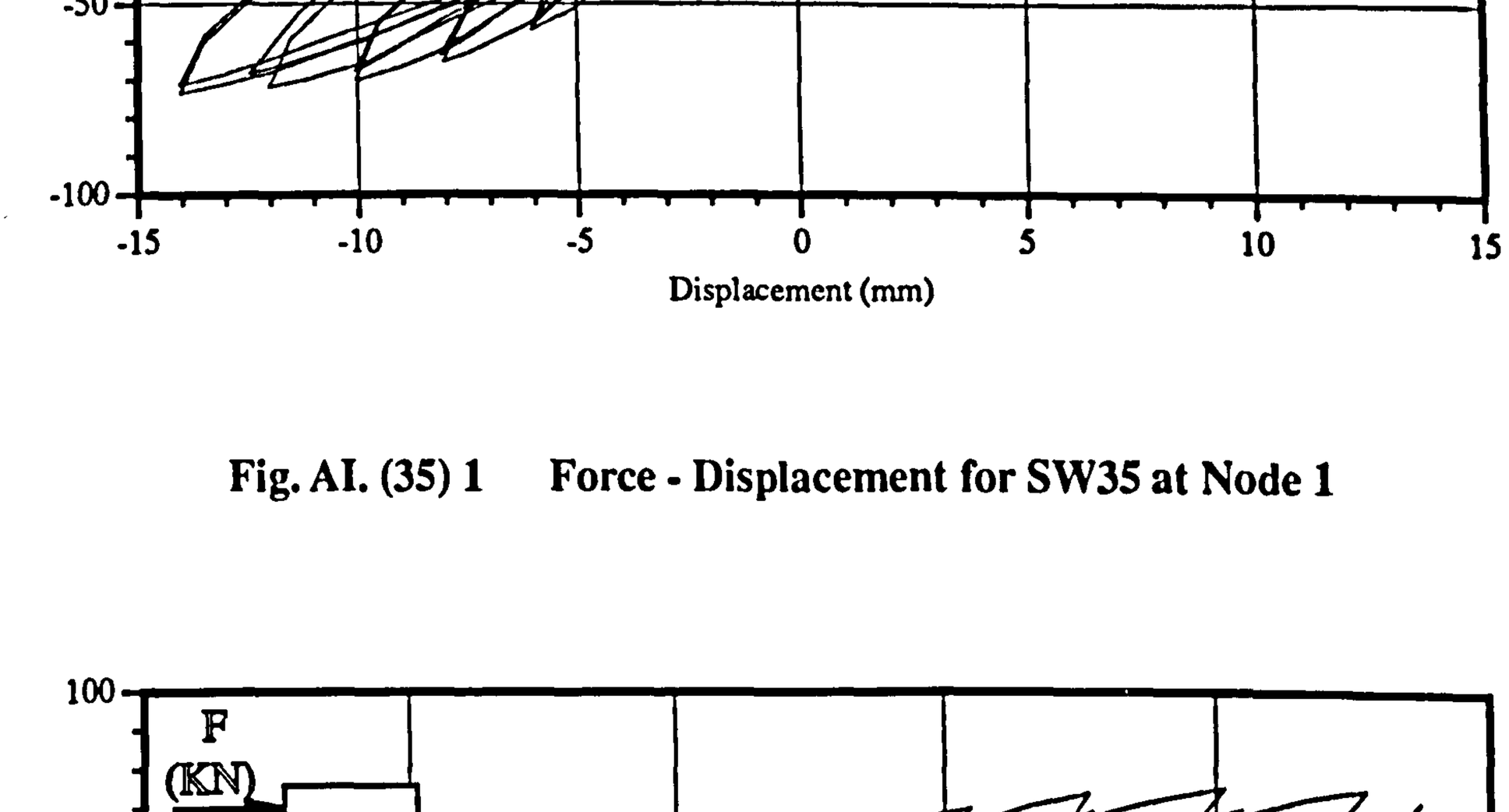


Fig. AI. (35) 2 Force - Displacement for SW35 at Node 2

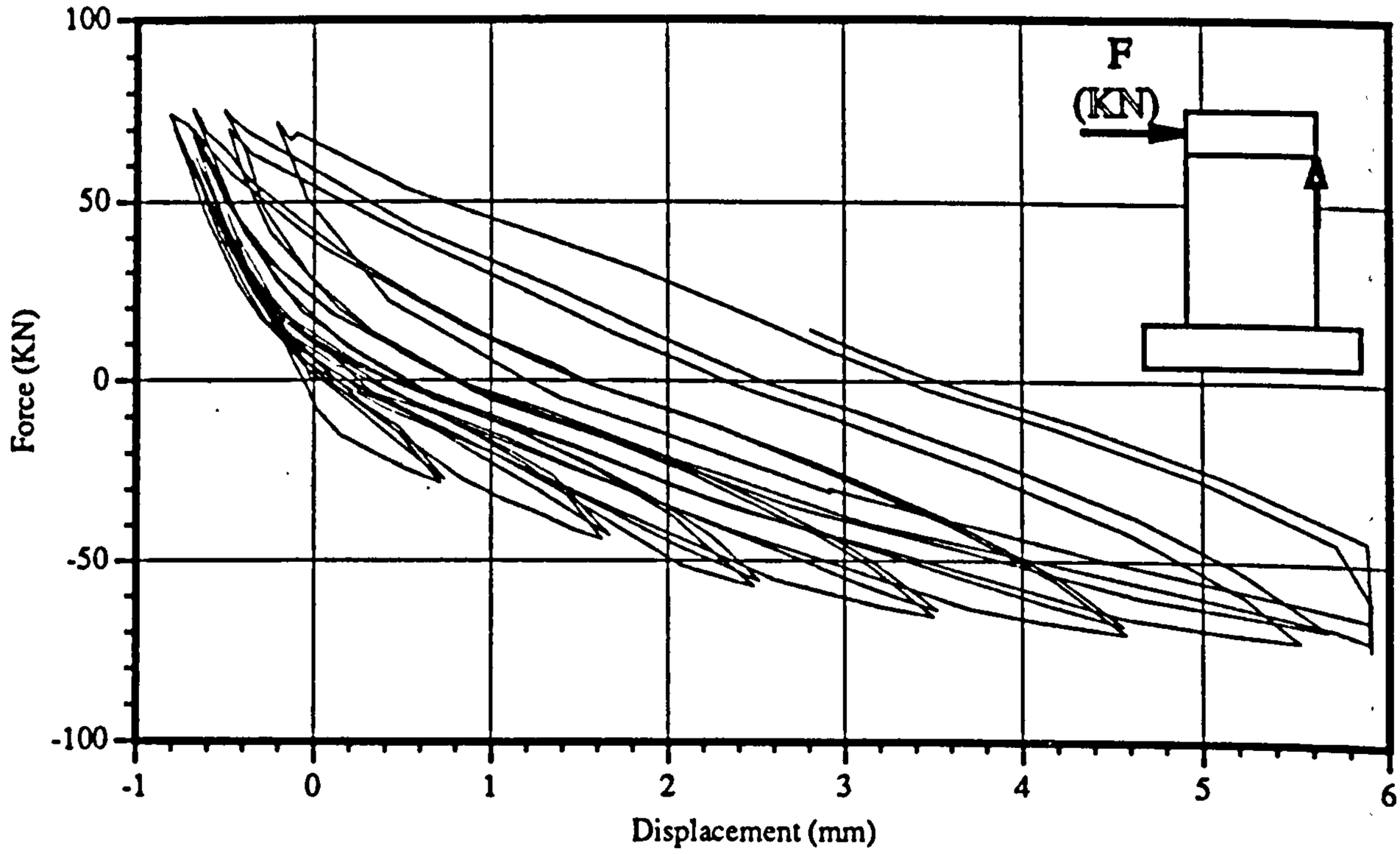


Fig. AI. (35) 3 Force - Displacement for SW35 at Node 3

Fig. AI. (35) 4 Force - Displacement for SW35 at Node 4

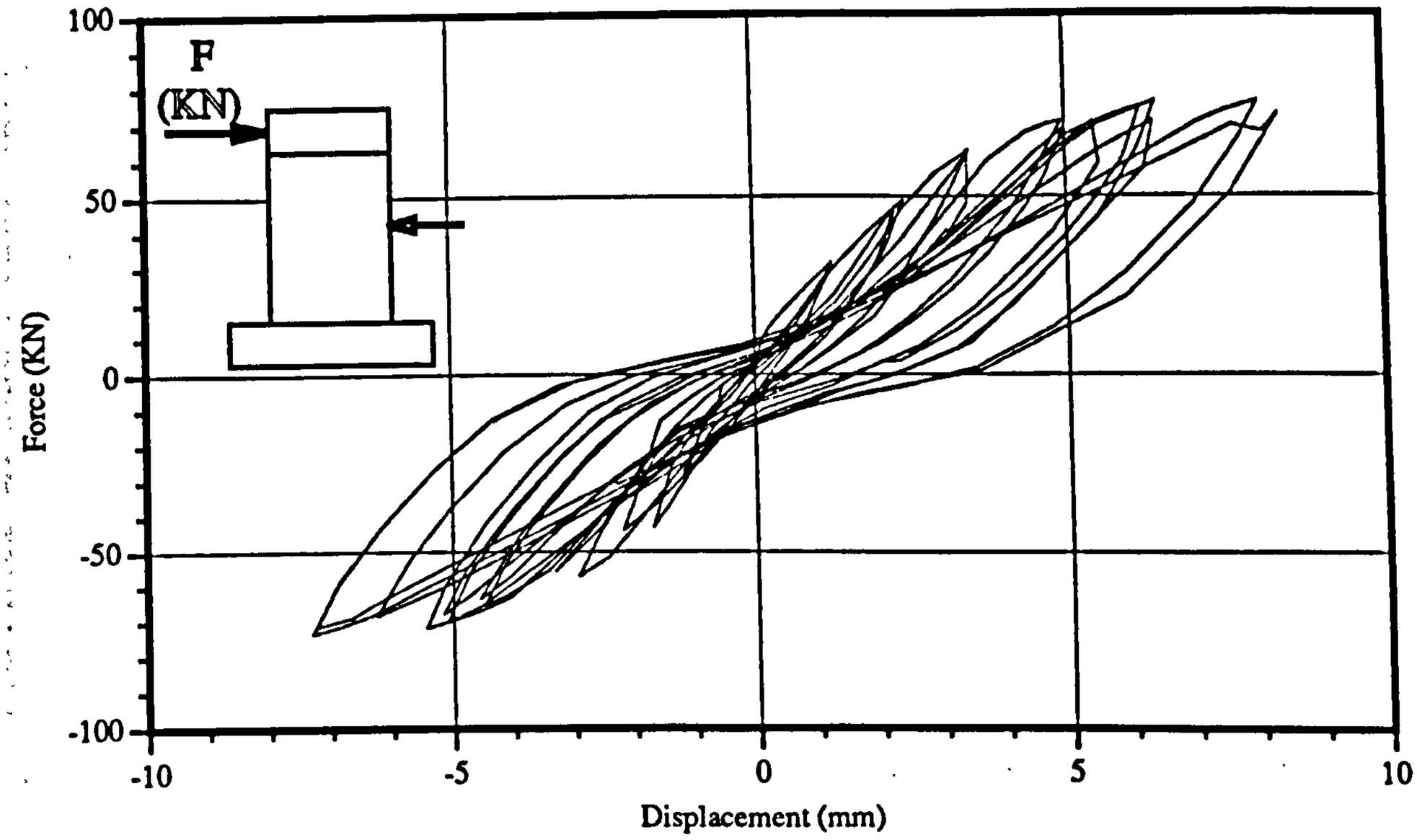


Fig. AI. (35) 5 Force - Displacement for SW35 at Node 5

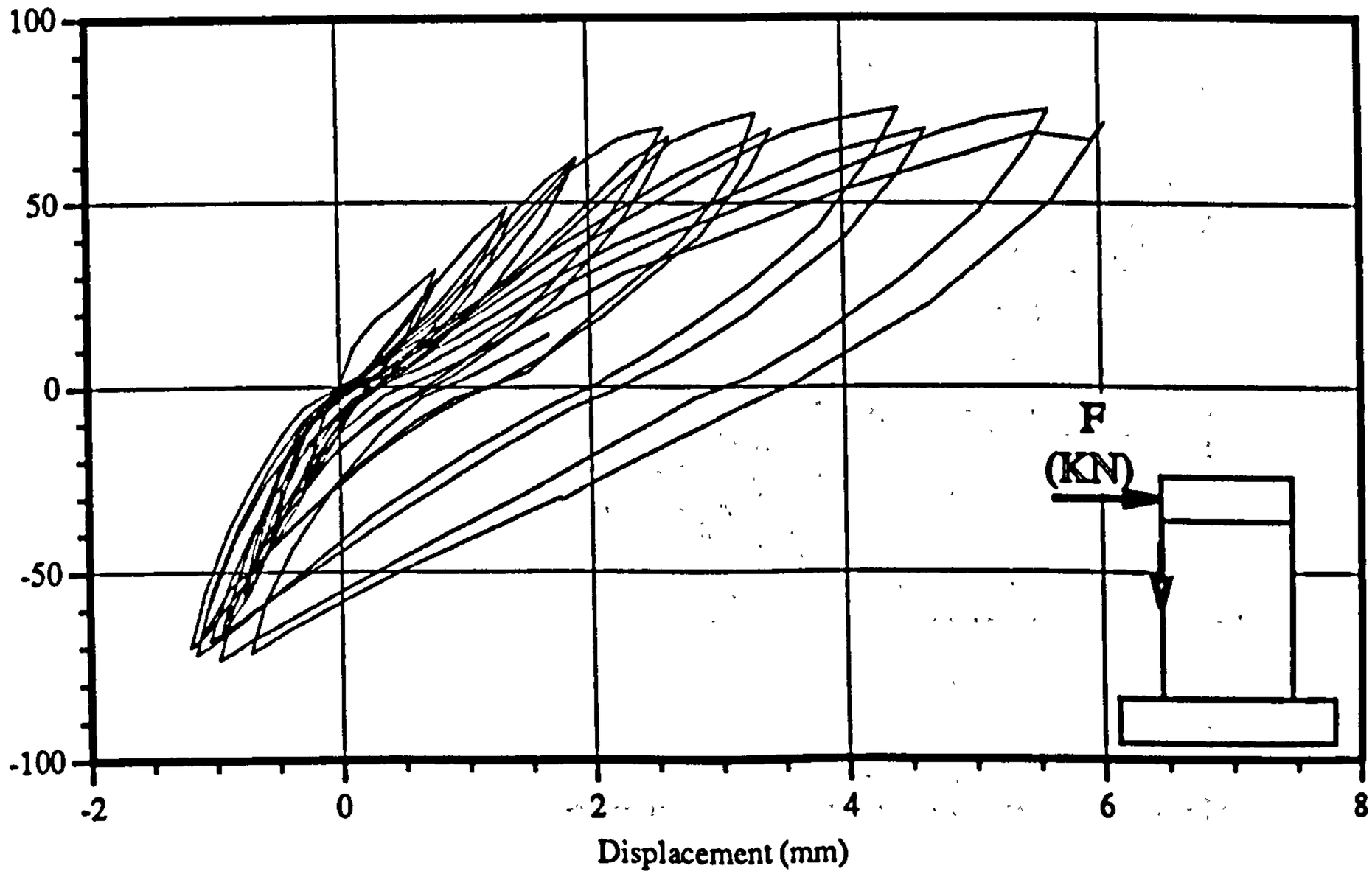


Fig. AI. (35) 6 Force - Displacement for SW35 at Node 6

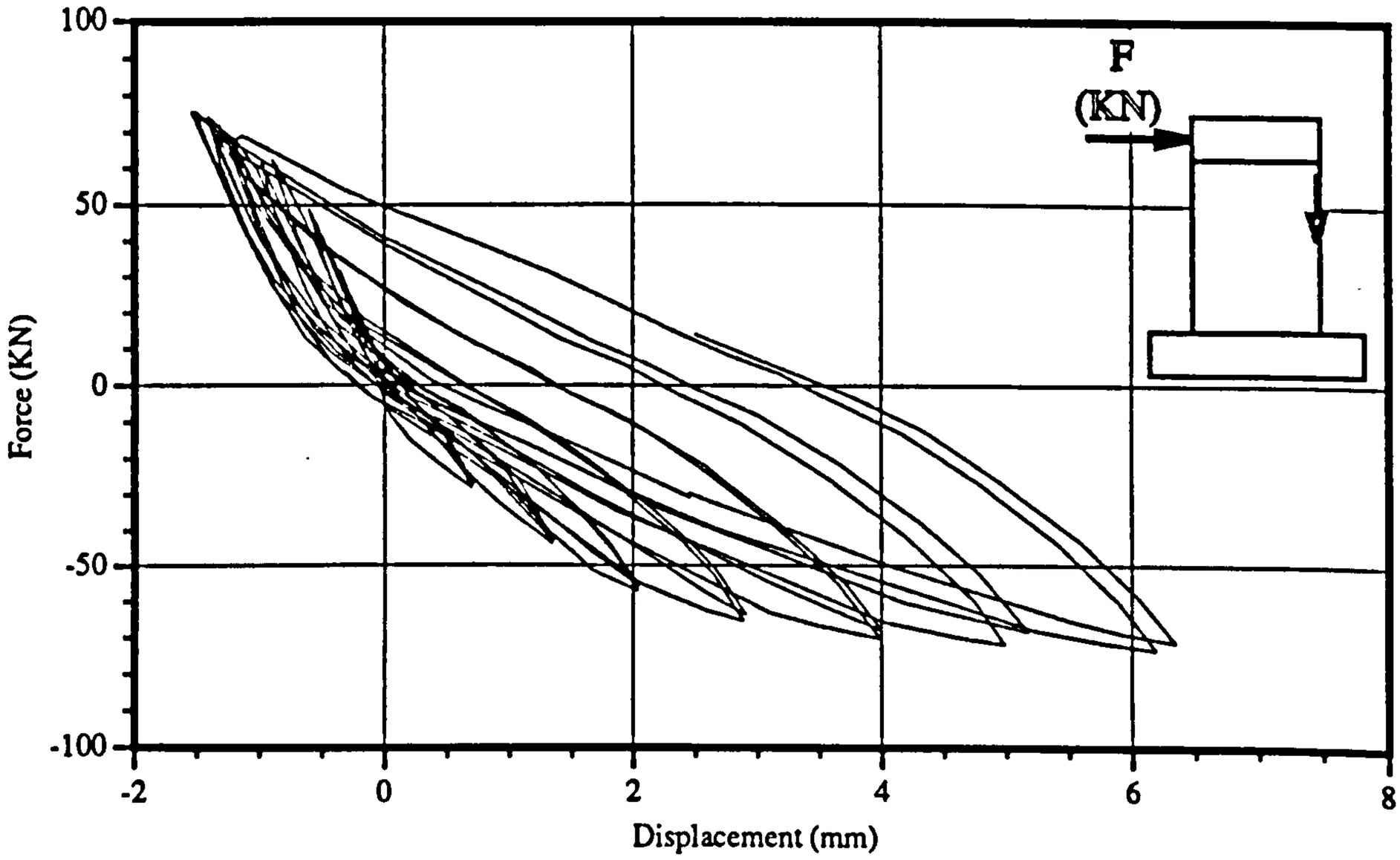


Fig. AI. (35) 7 Force - Displacement for SW35 at Node 7

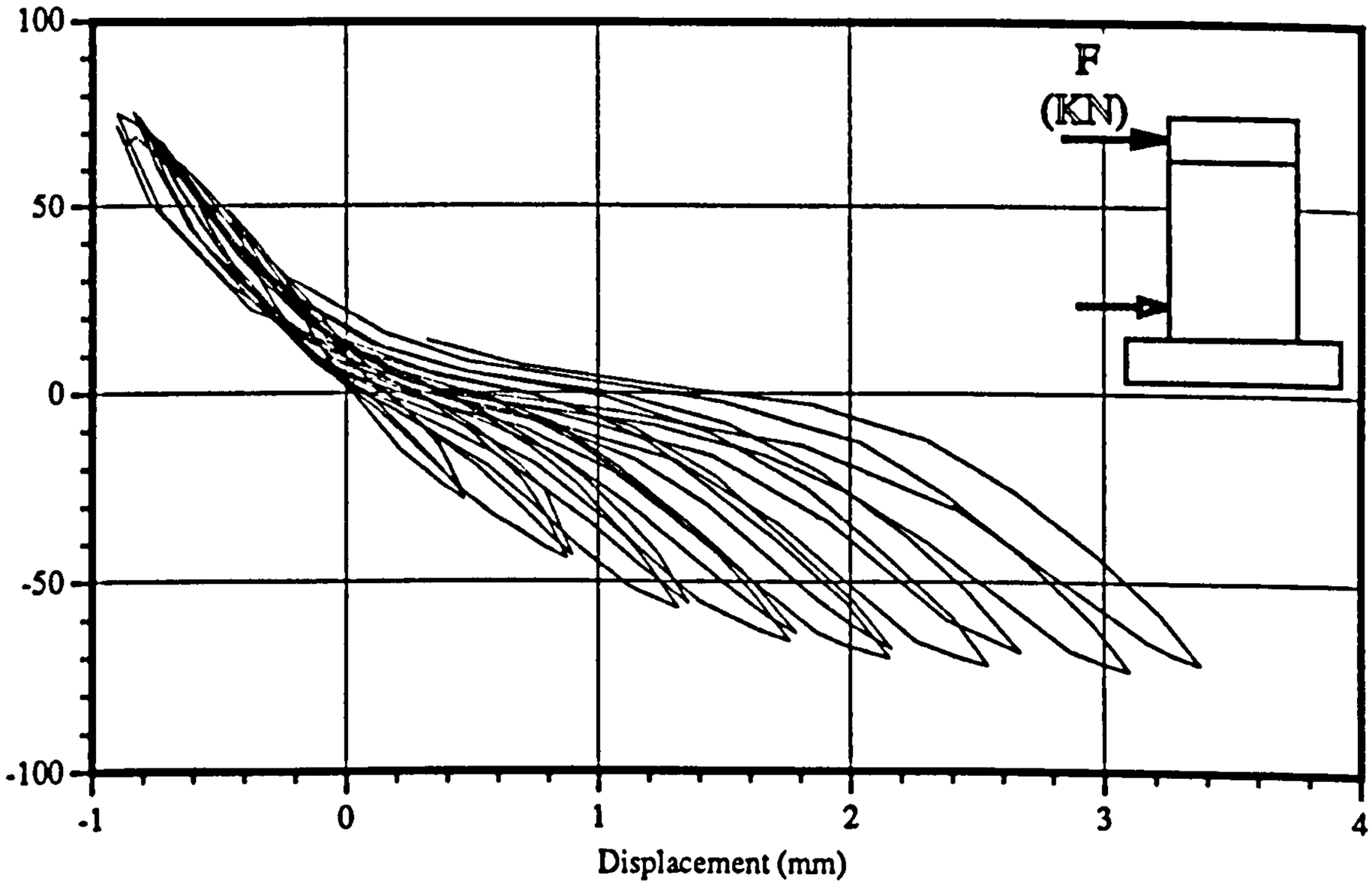


Fig. AI. (35) 8 Force - Displacement for SW35 at Node 8

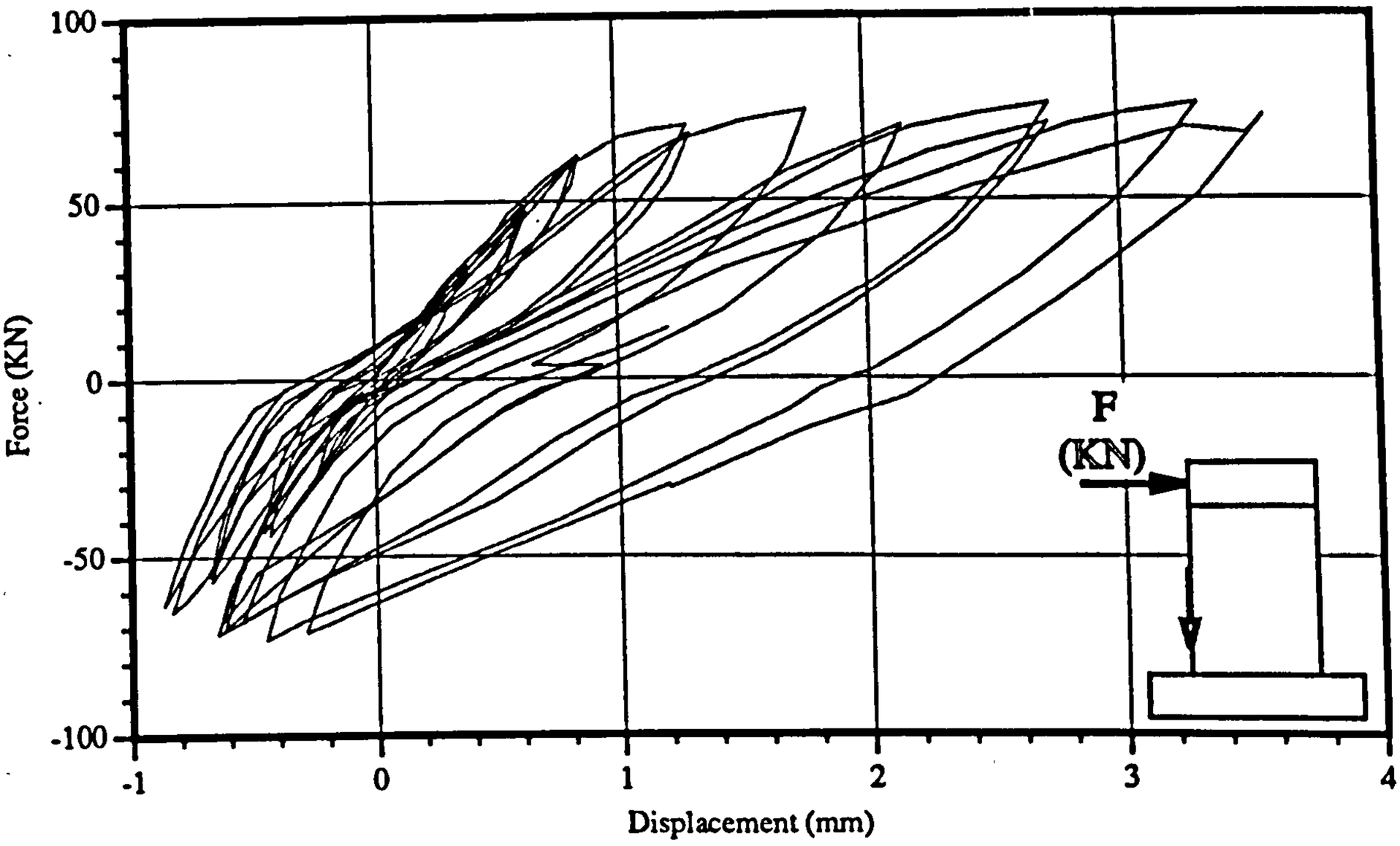


Fig. AI. (35) 9 Force - Displacement for SW35 at Node 9

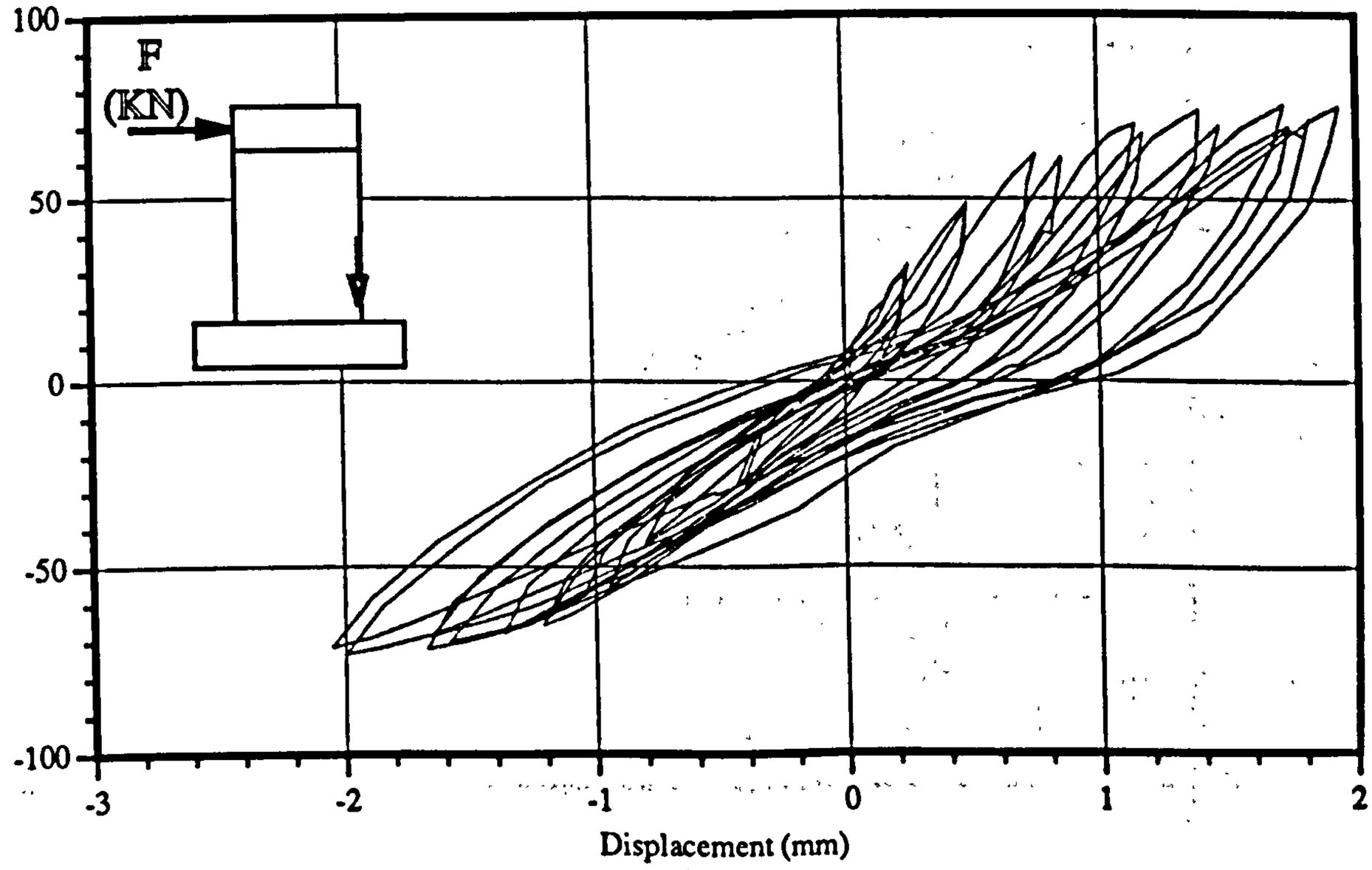


Fig. AI. (35) 10 Force - Displacement for SW35 at Node 10

AI.17. : Force Displacement for SWR35

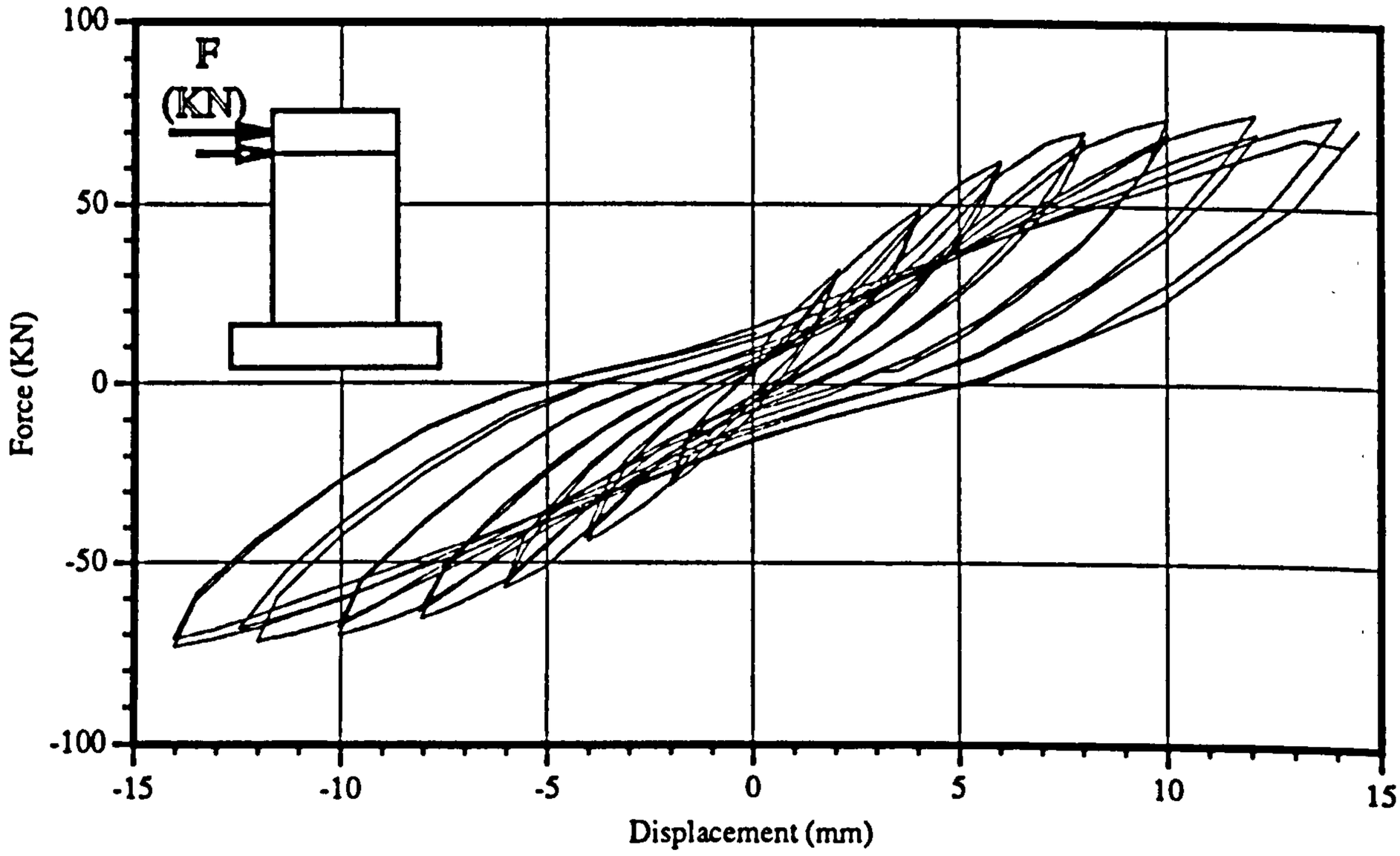


Fig. AI. (R35) 1 Force - Displacement for SWR35 at Node 1

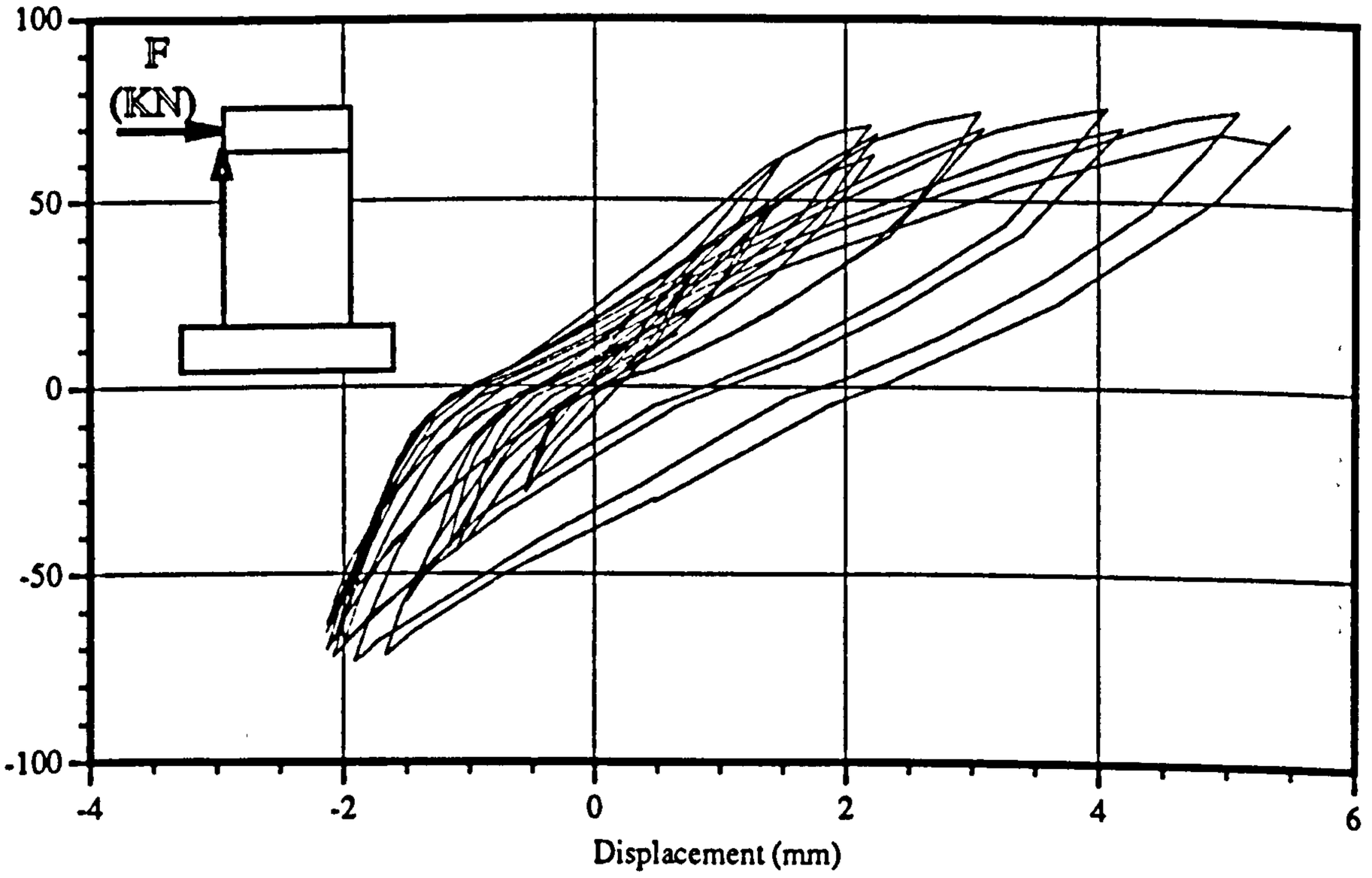


Fig. AI. (R35) 2 Force - Displacement for SWR35 at Node 2



Fig. AI. (R35) 3 Force - Displacement for SWR35 at Node 3

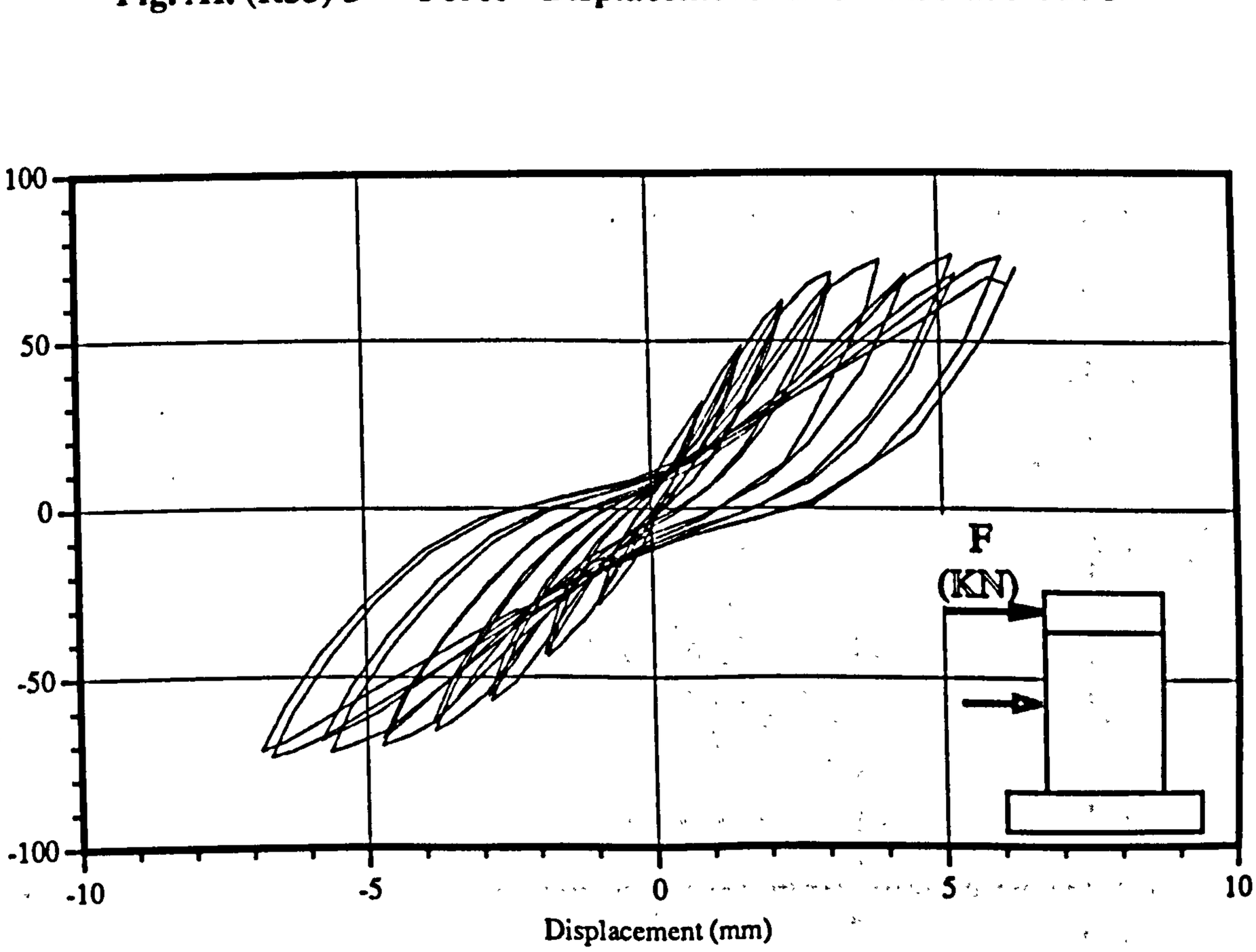


Fig. AI. (R35) 4 Force - Displacement for SWR35 at Node 4

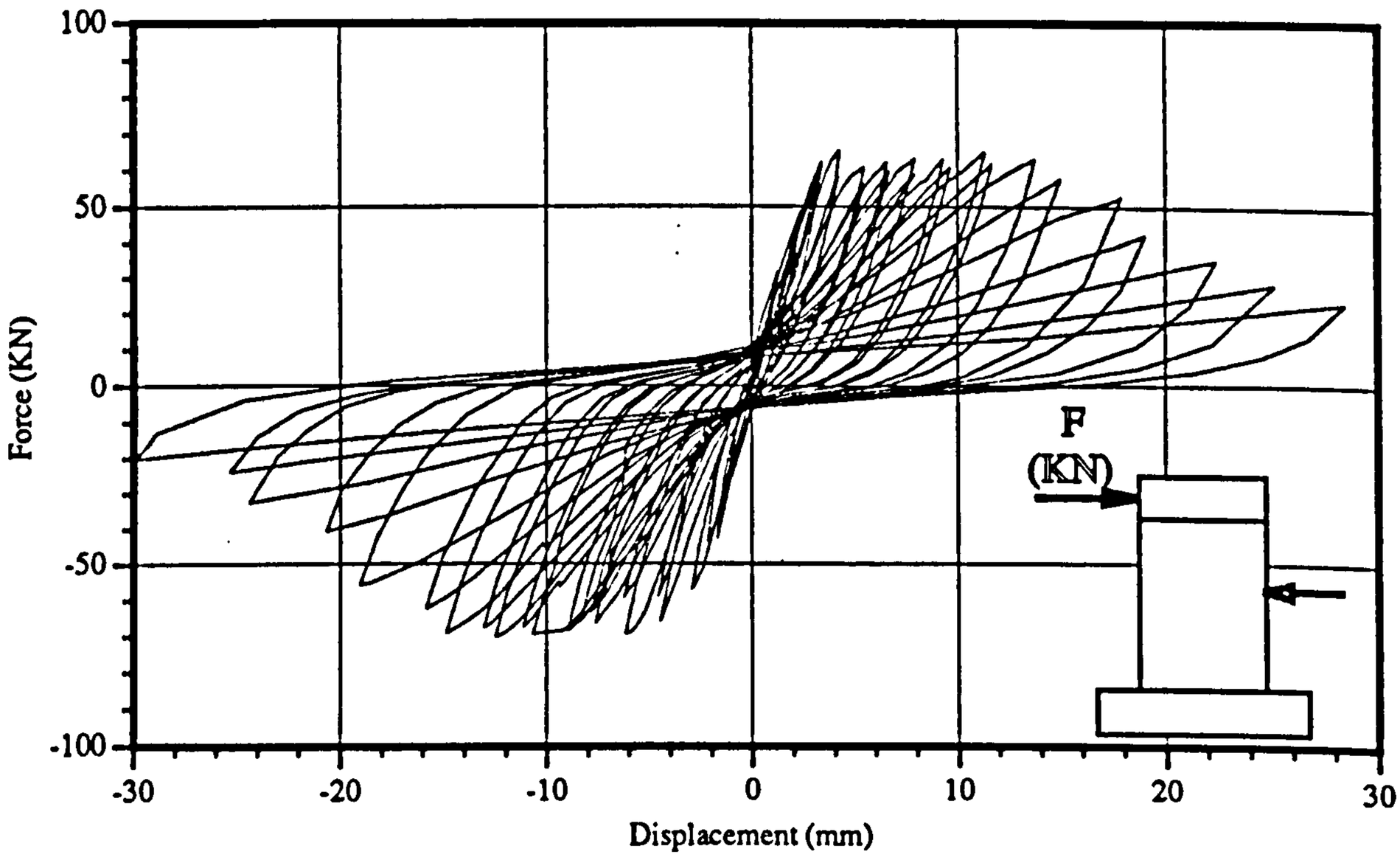


Fig. AI. (R35) 5 Force - Displacement for SWR35 at Node 5

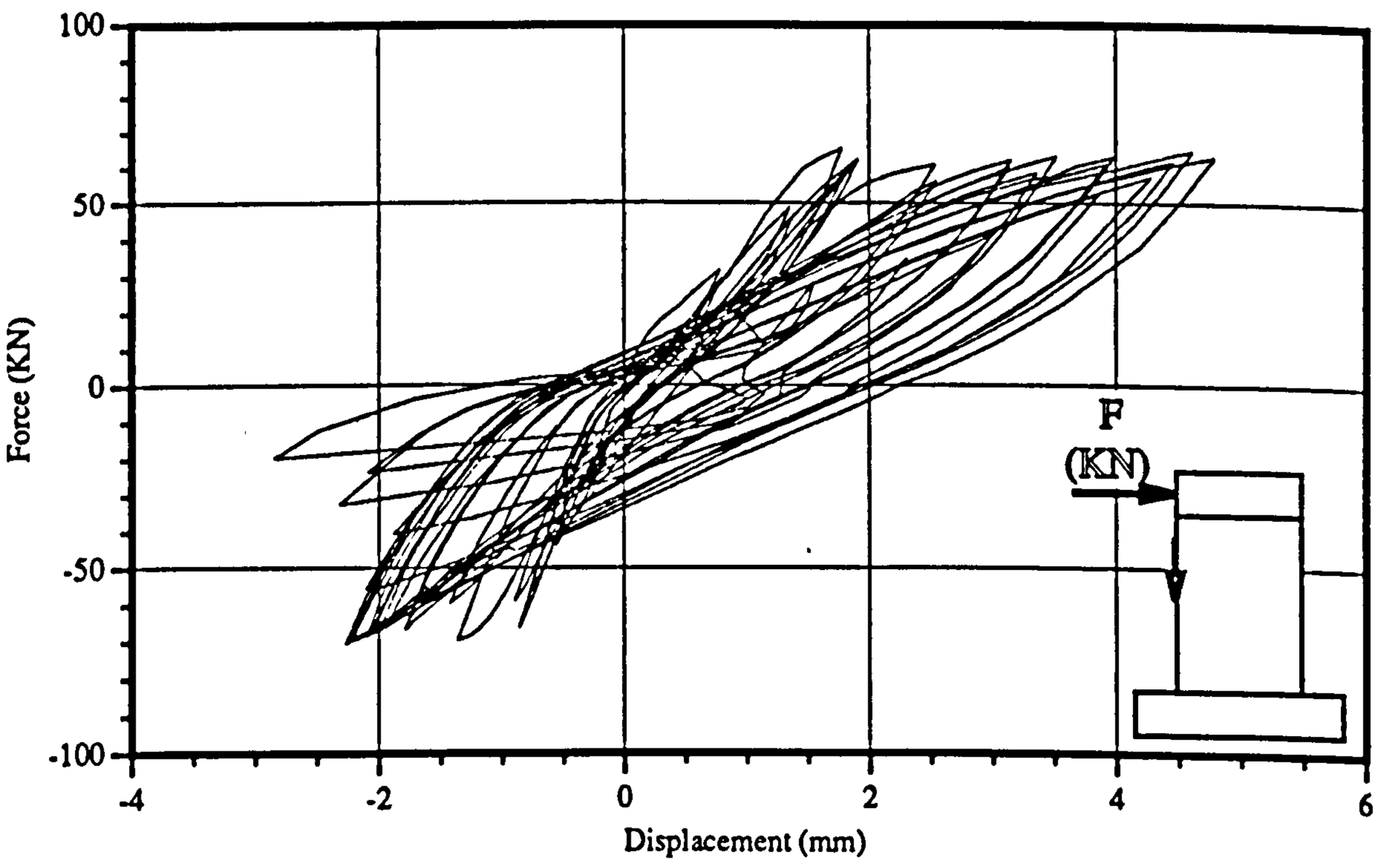


Fig. AI. (R35) 6 Force - Displacement for SWR35 at Node 6

Appendix AII: Force-Steel Strain Test Results

AII.1 : Force-Steel Strain for SW21

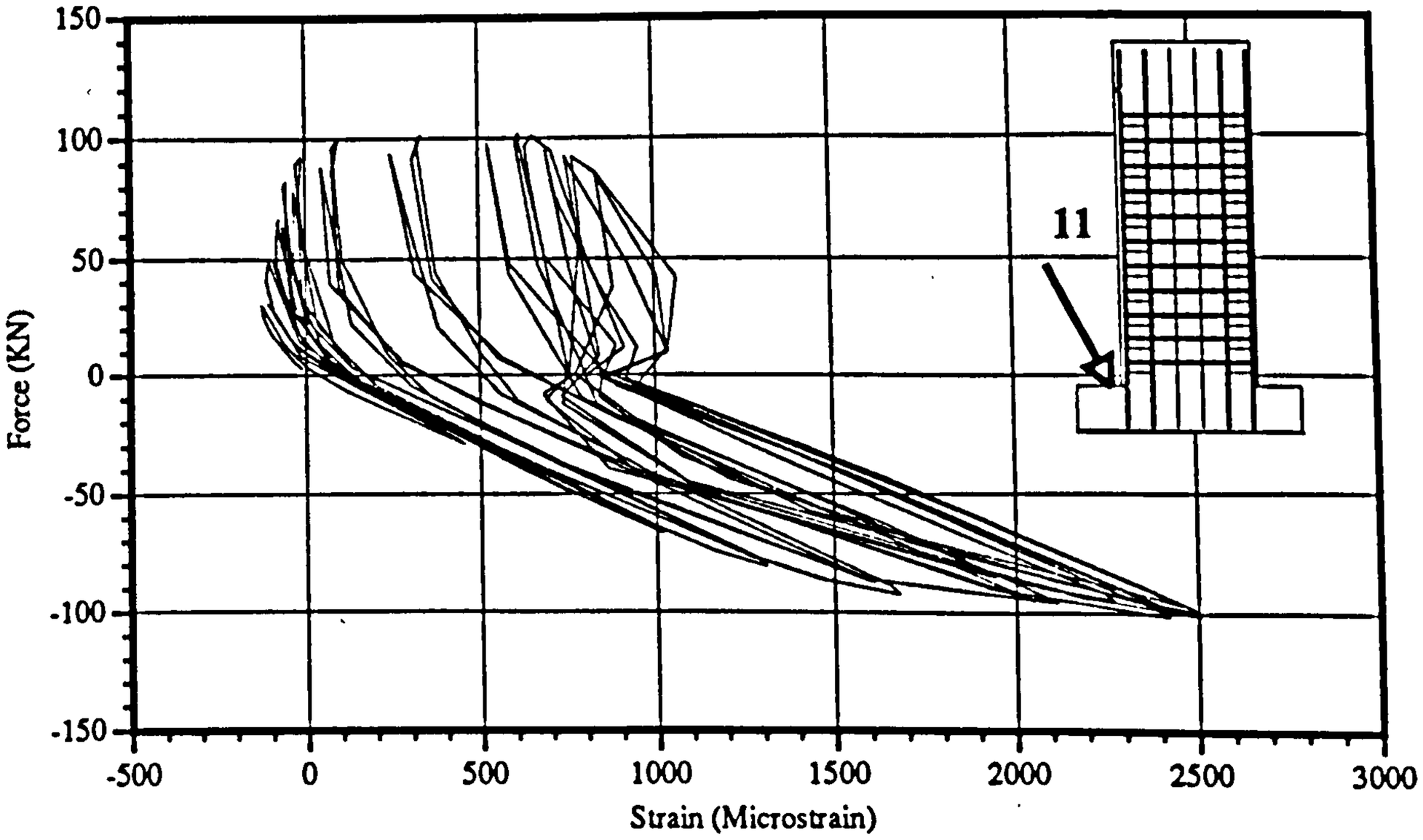


Fig. AII (21) 1 Force - Steel Strain for SW21 at Node 11

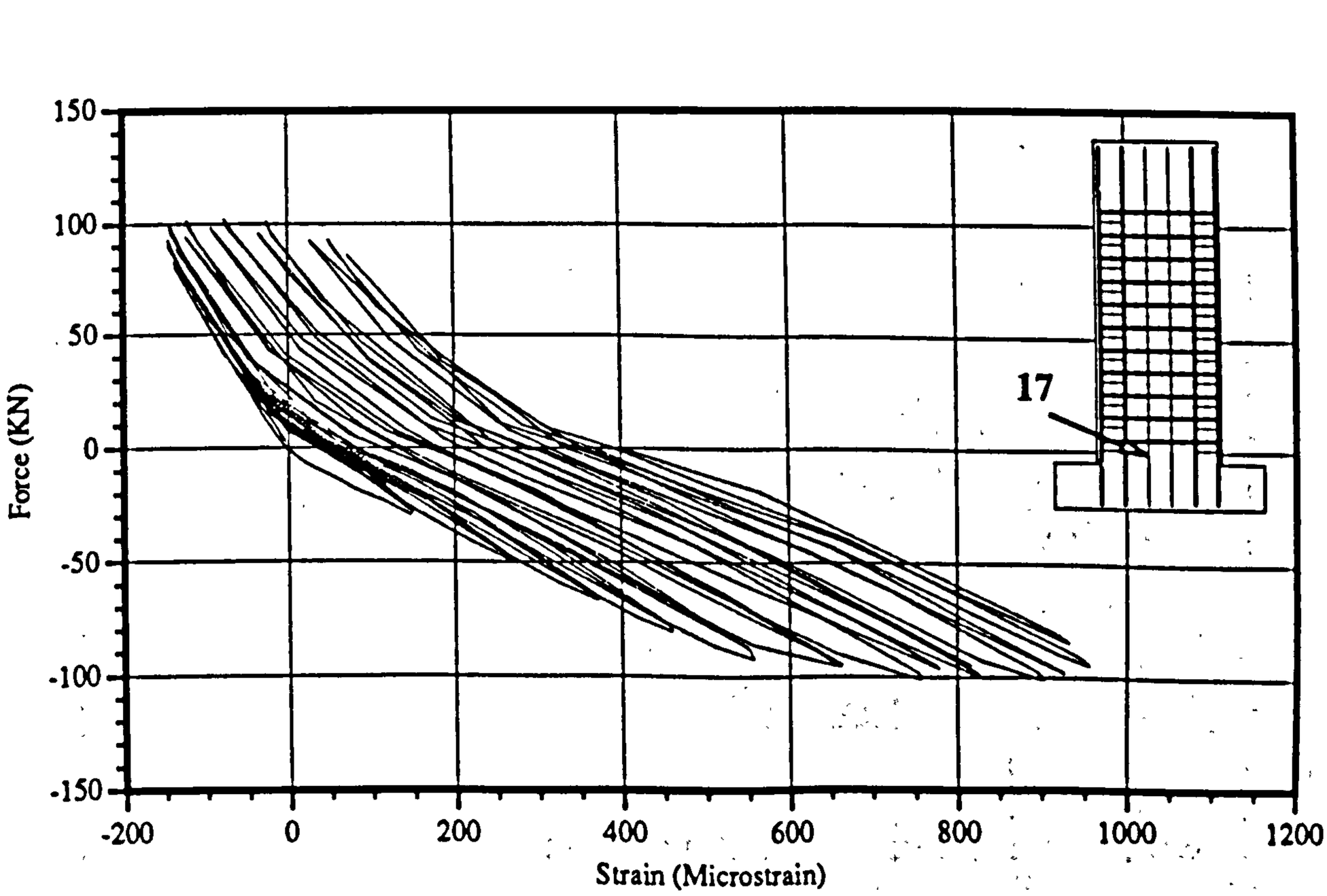


Fig. AII (21) 2 Force - Steel Strain for SW21 at Node 17

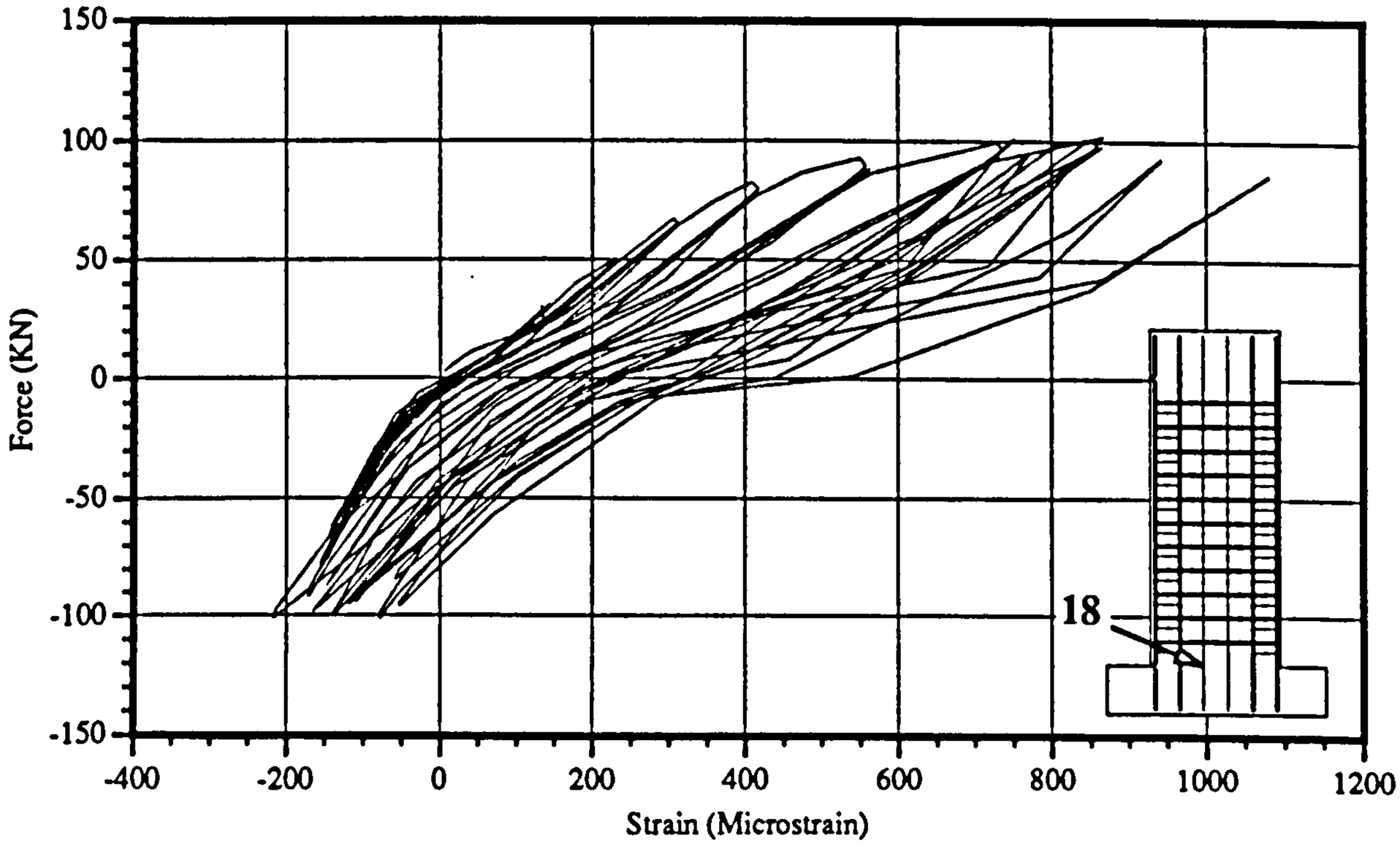


Fig. AII (21) 3 Force - Steel Strain for SW21 at Node 18

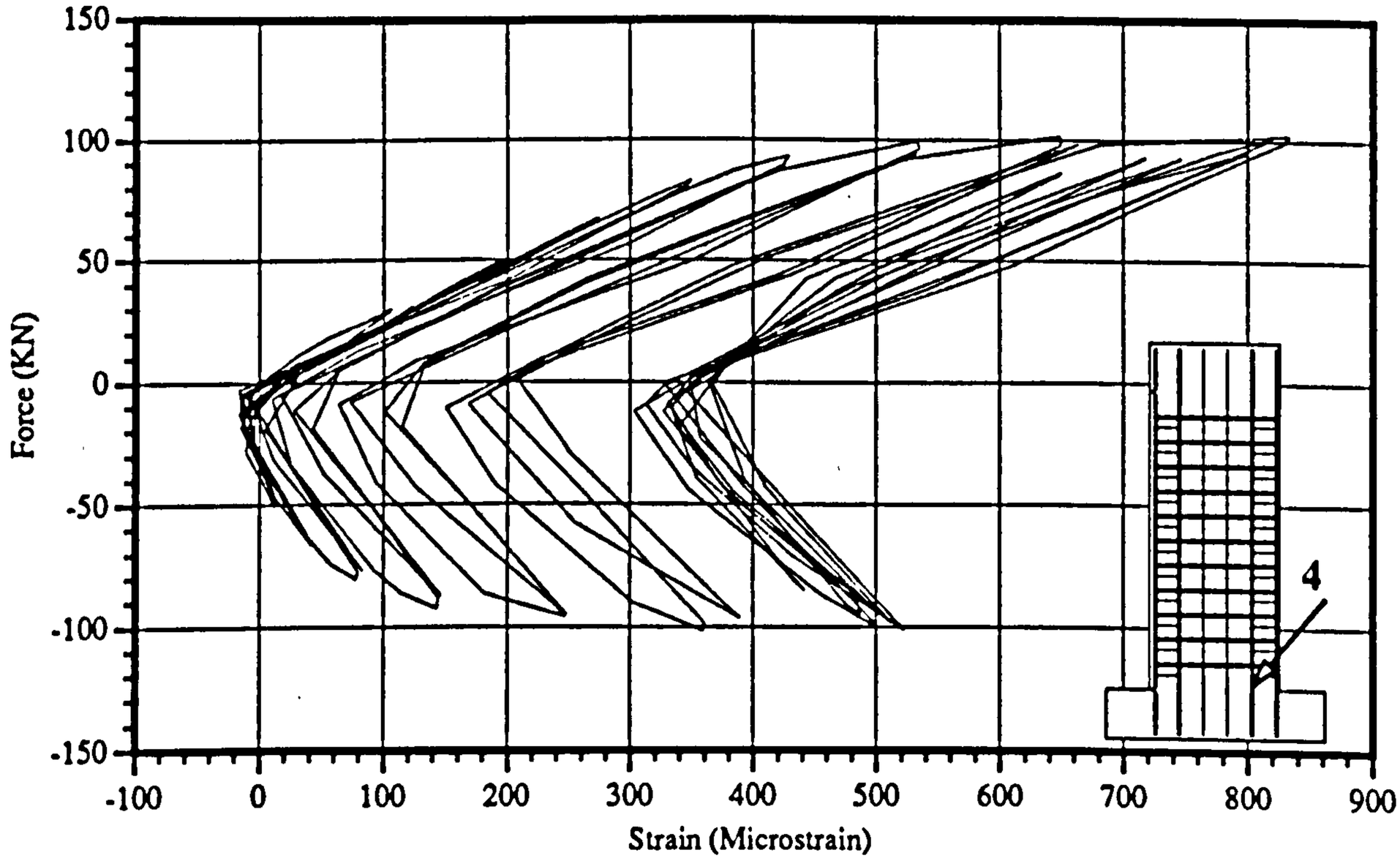


Fig. AII (21) 4 Force - Steel Strain for SW21 at Node 4

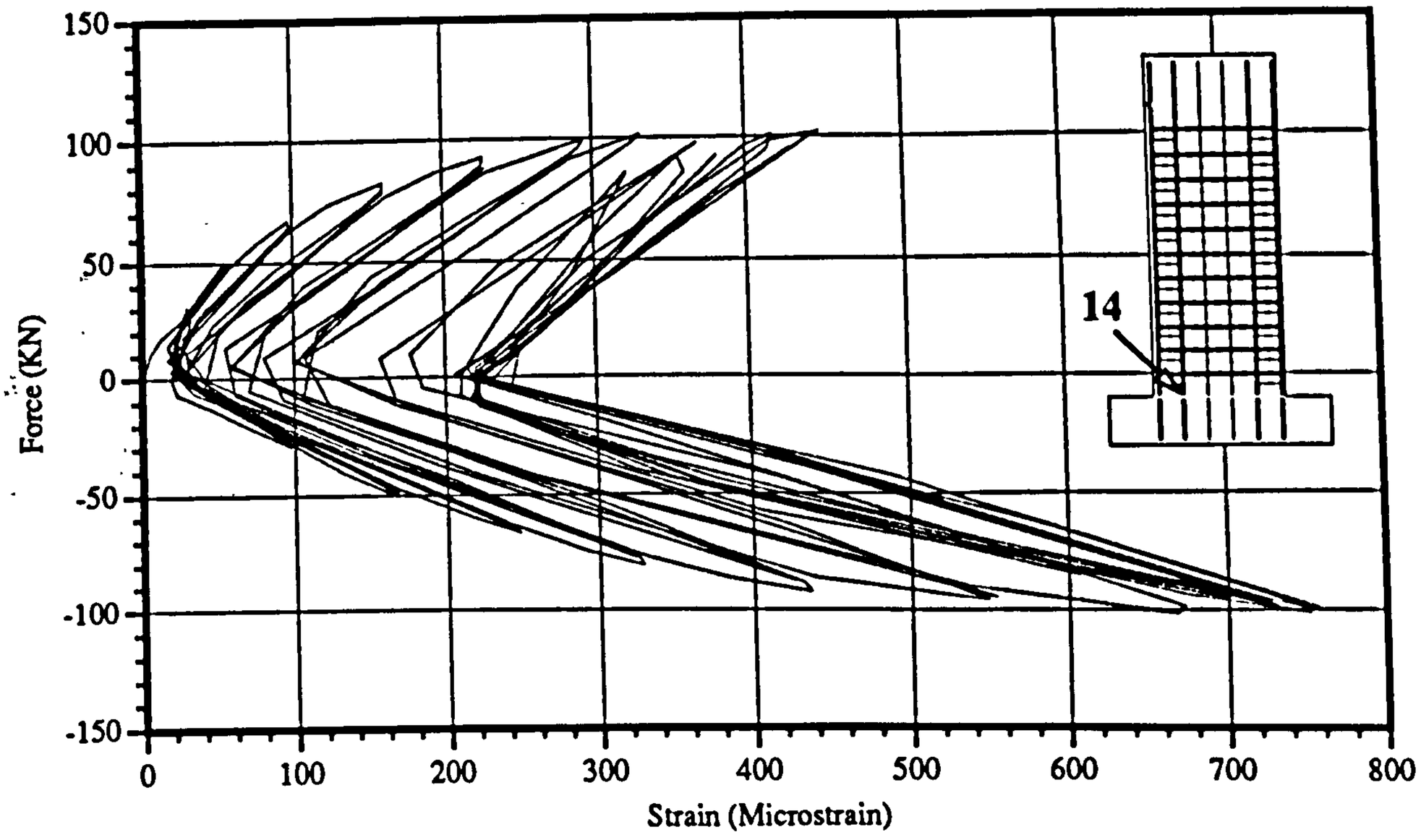


Fig. AII (21) 5 Force - Steel Strain for SW21 at Node 14

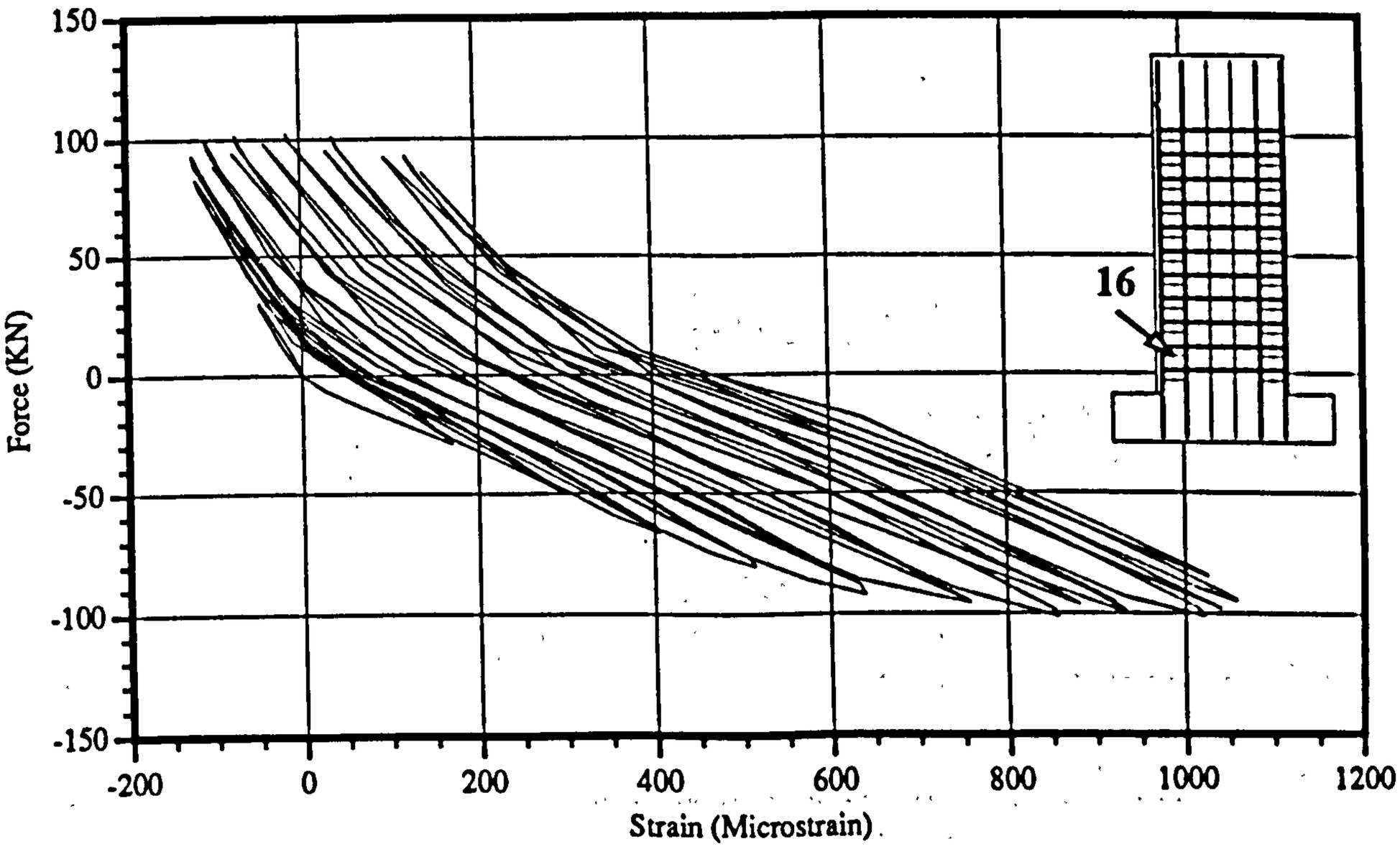


Fig. AII (21) 6 Force - Steel Strain for SW21 at Node 16

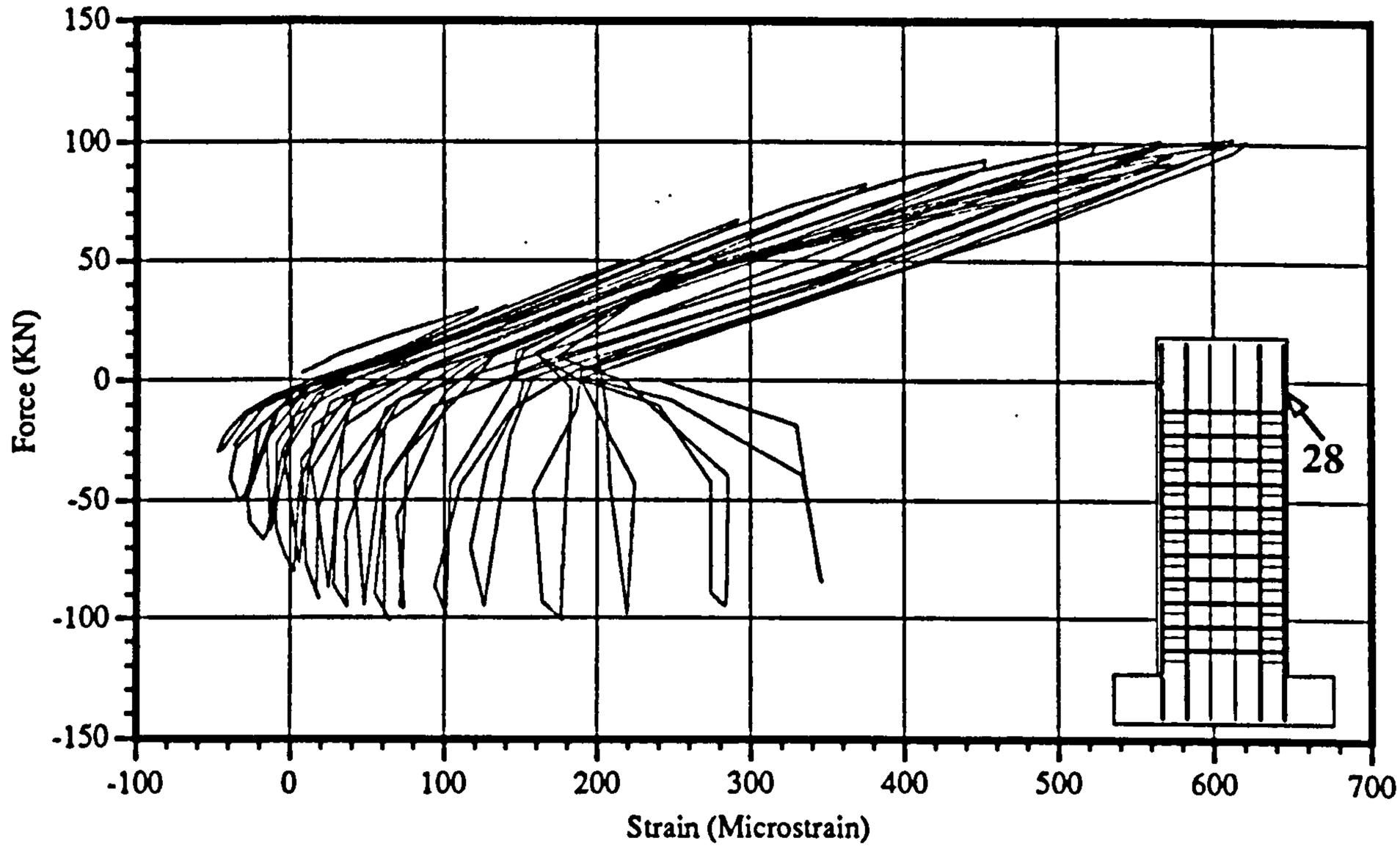


Fig. AII (21) 7 Force - Steel Strain for SW21 at Node 28

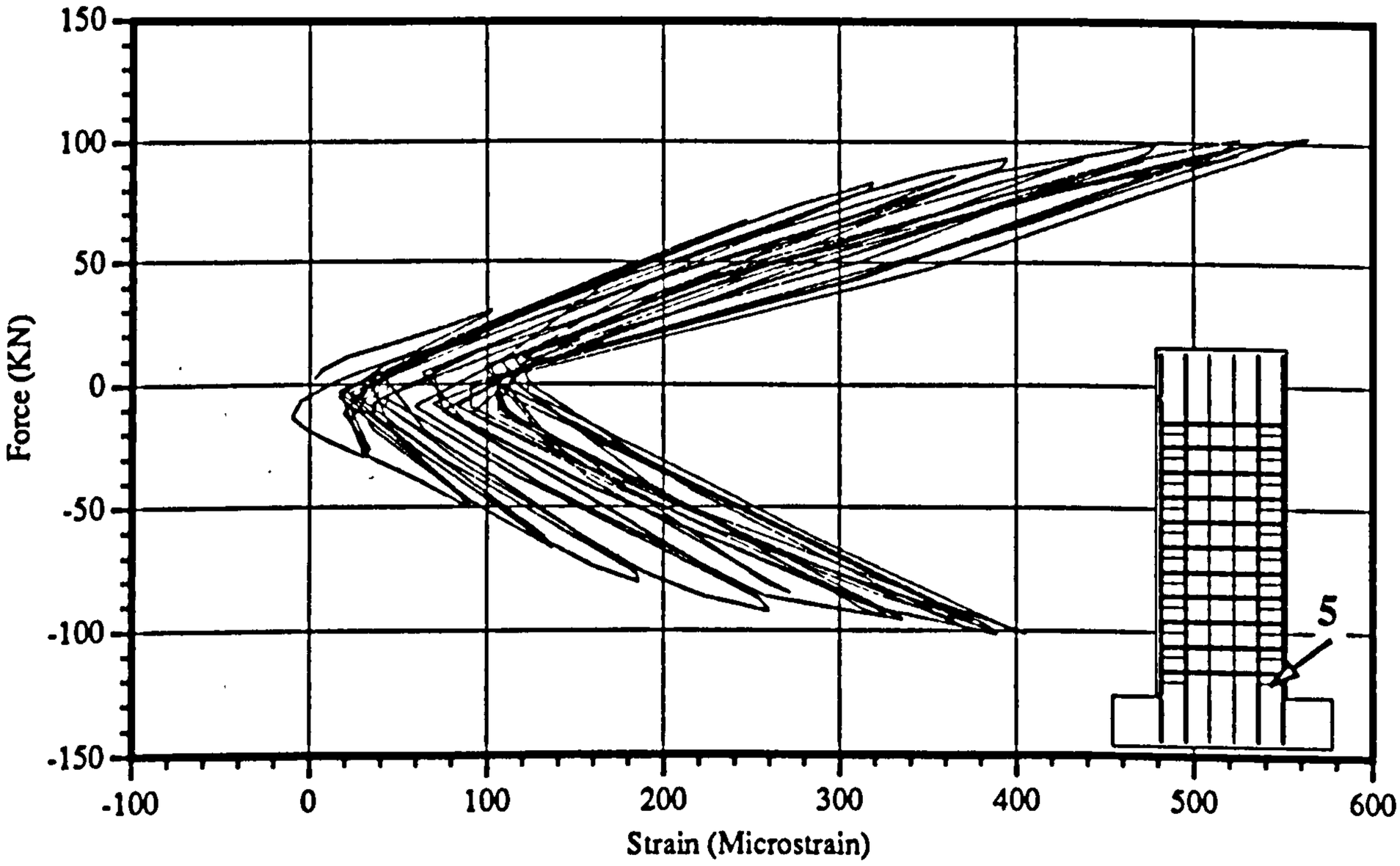


Fig. AII (21) 8 Force - Steel Strain for SW21 at Node 5

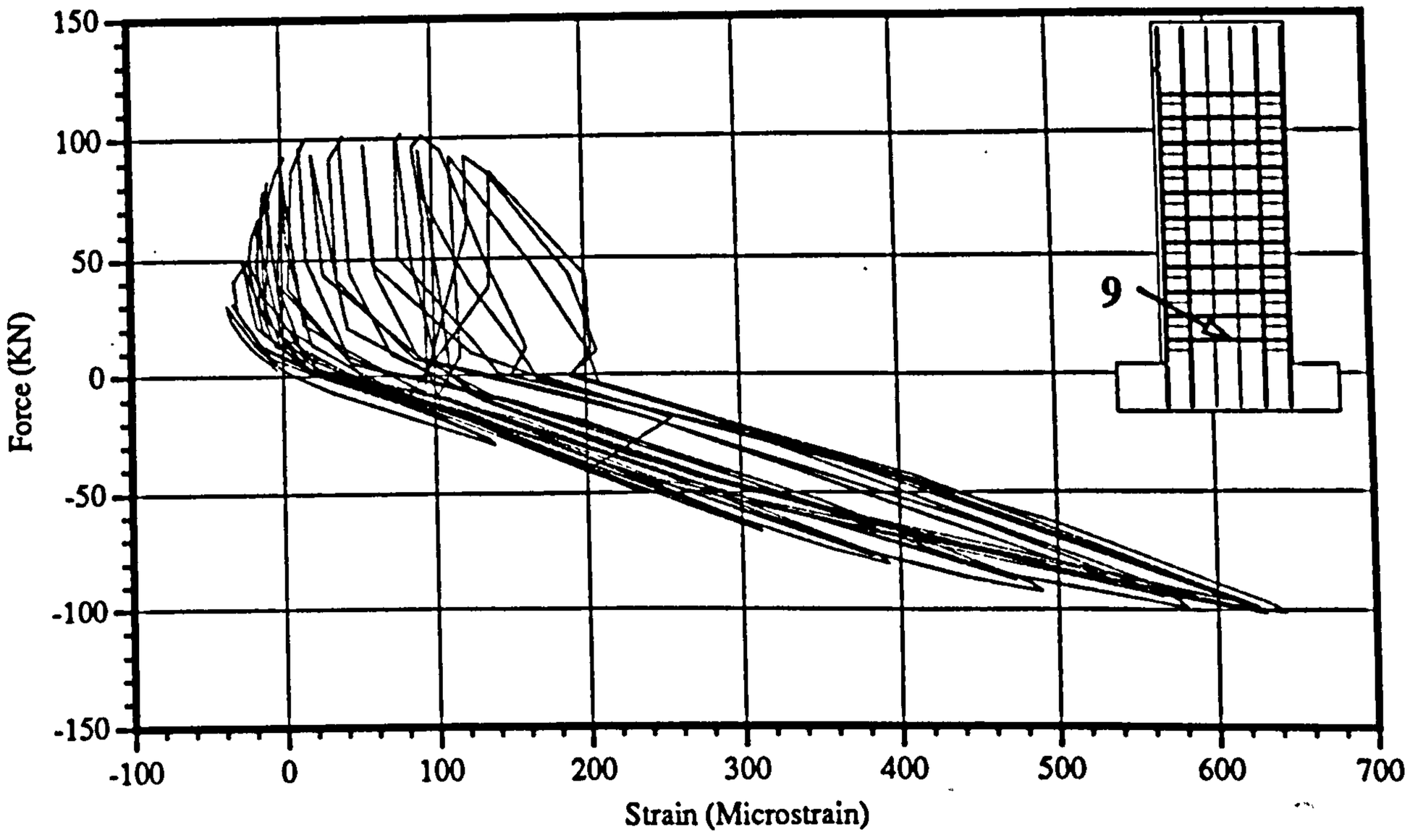


Fig. AII (21) 9 Force - Steel Strain for SW21 at Node 9

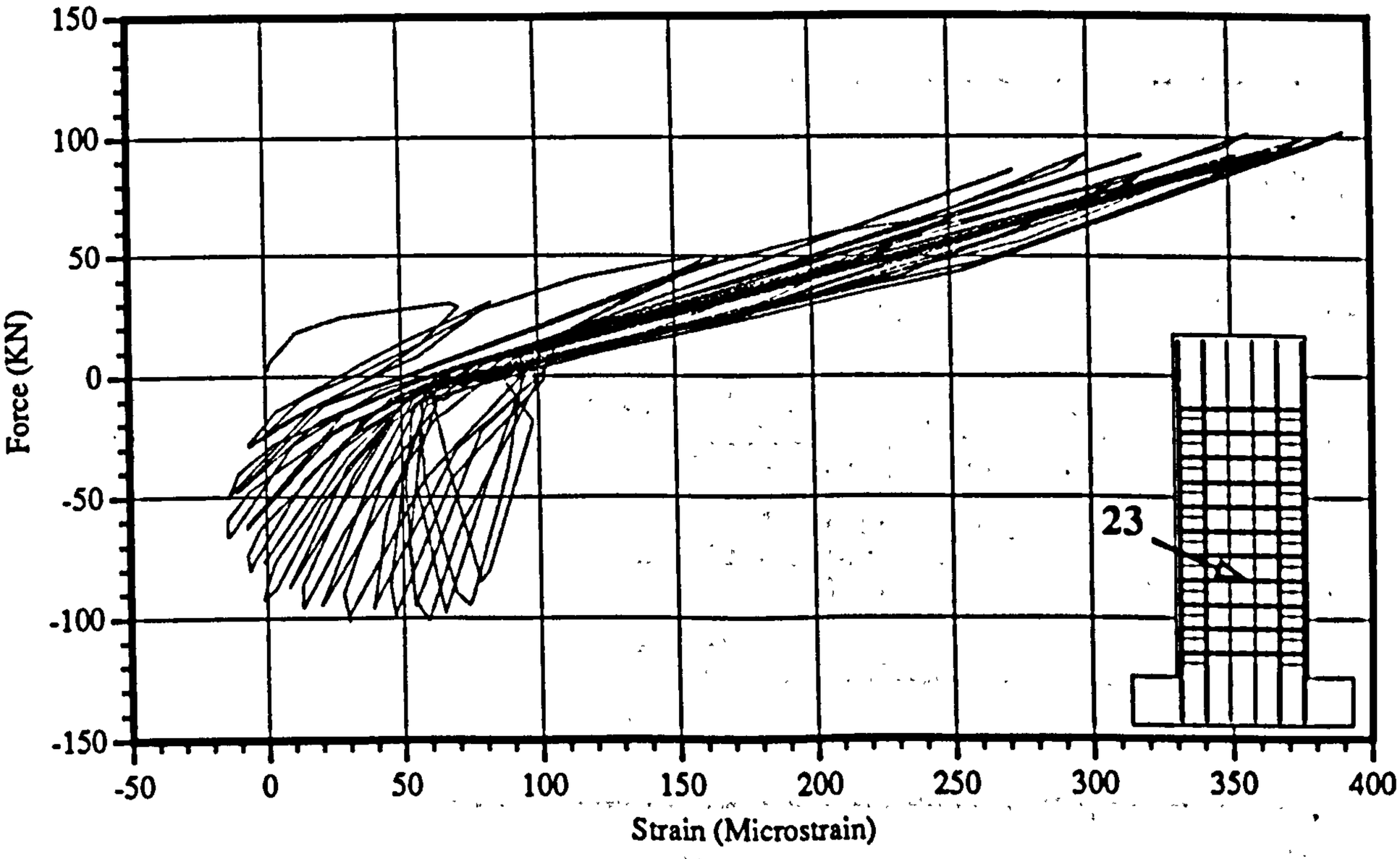


Fig. AII (21) 10 Force - Steel Strain for SW21 at Node 23

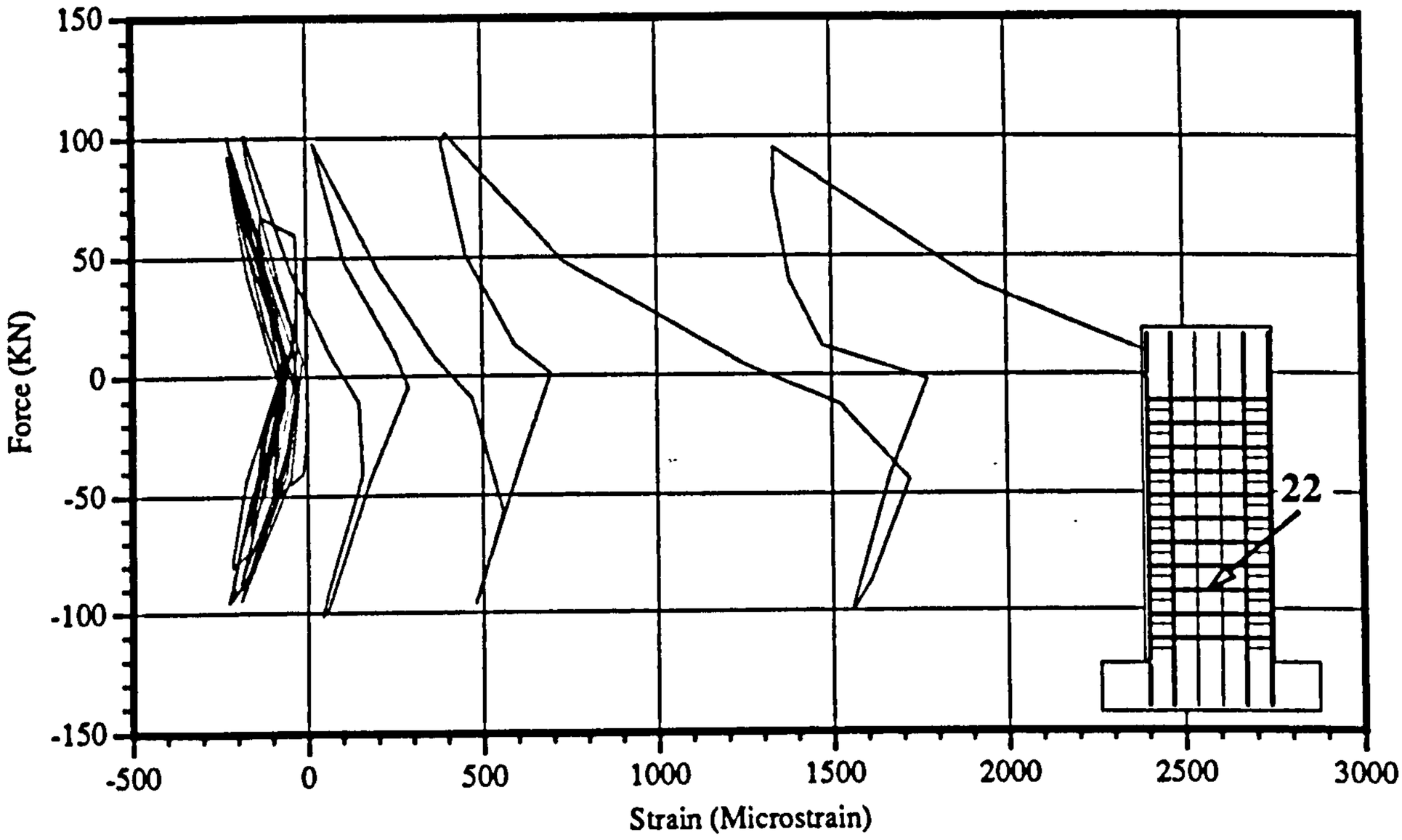


Fig. AII (21) 11 Force - Steel Strain for SW21 at Node 22

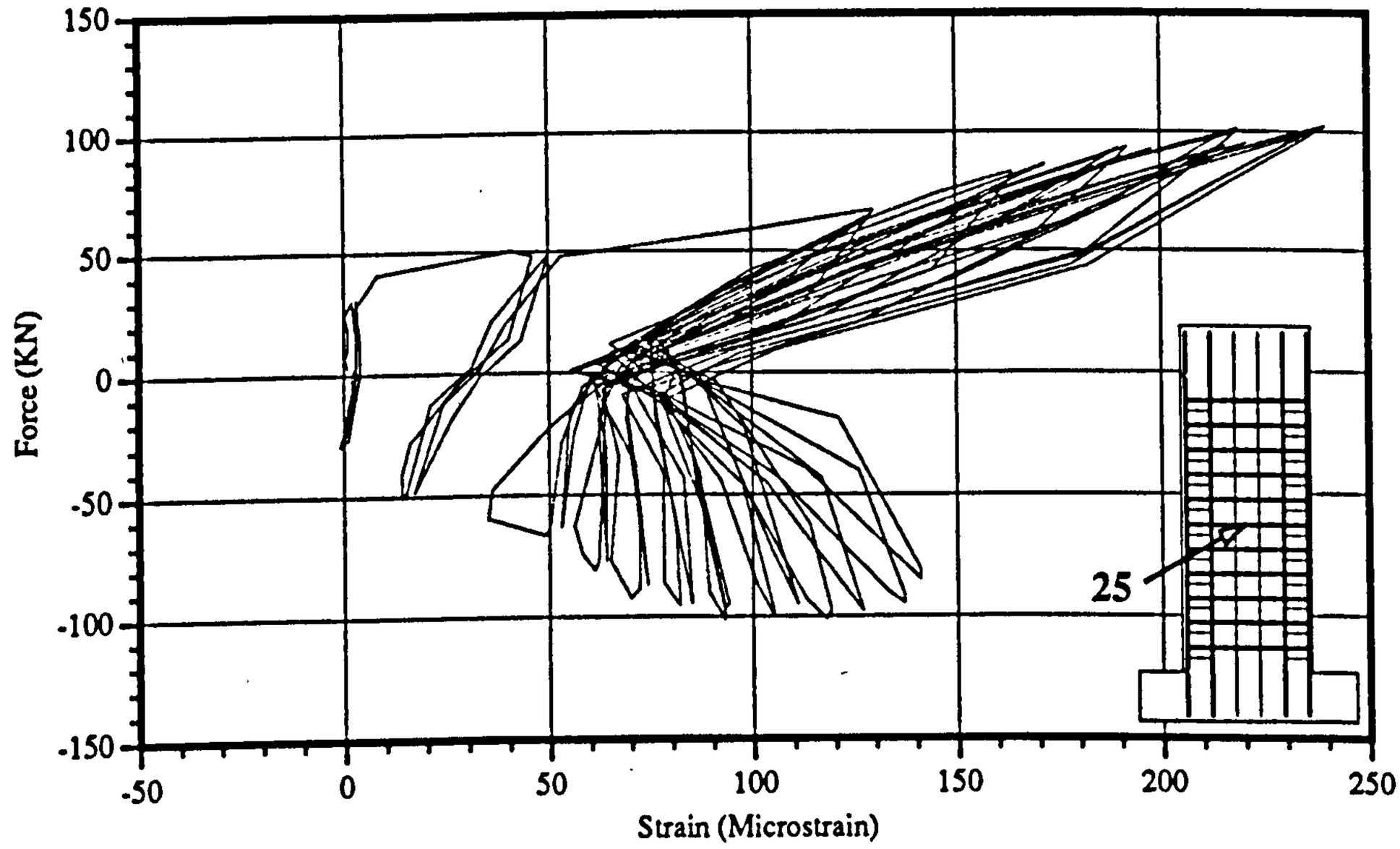


Fig. AII (21) 12 Force - Steel Strain for SW21 at Node 25

AII.2 : Force-Steel Strain for SW22

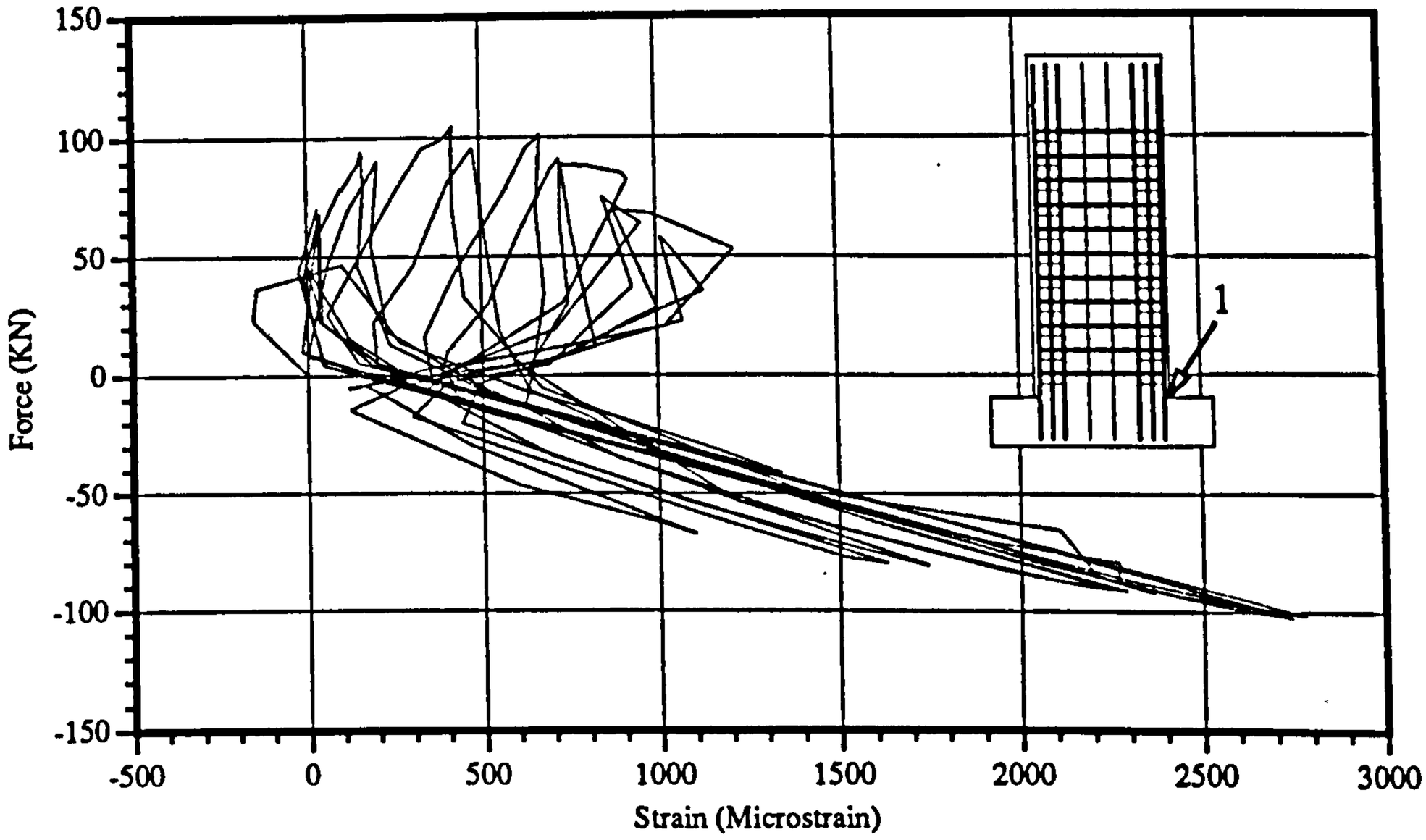


Fig. AII (22) 1 Force - Steel Strain for SW22 at Node 1

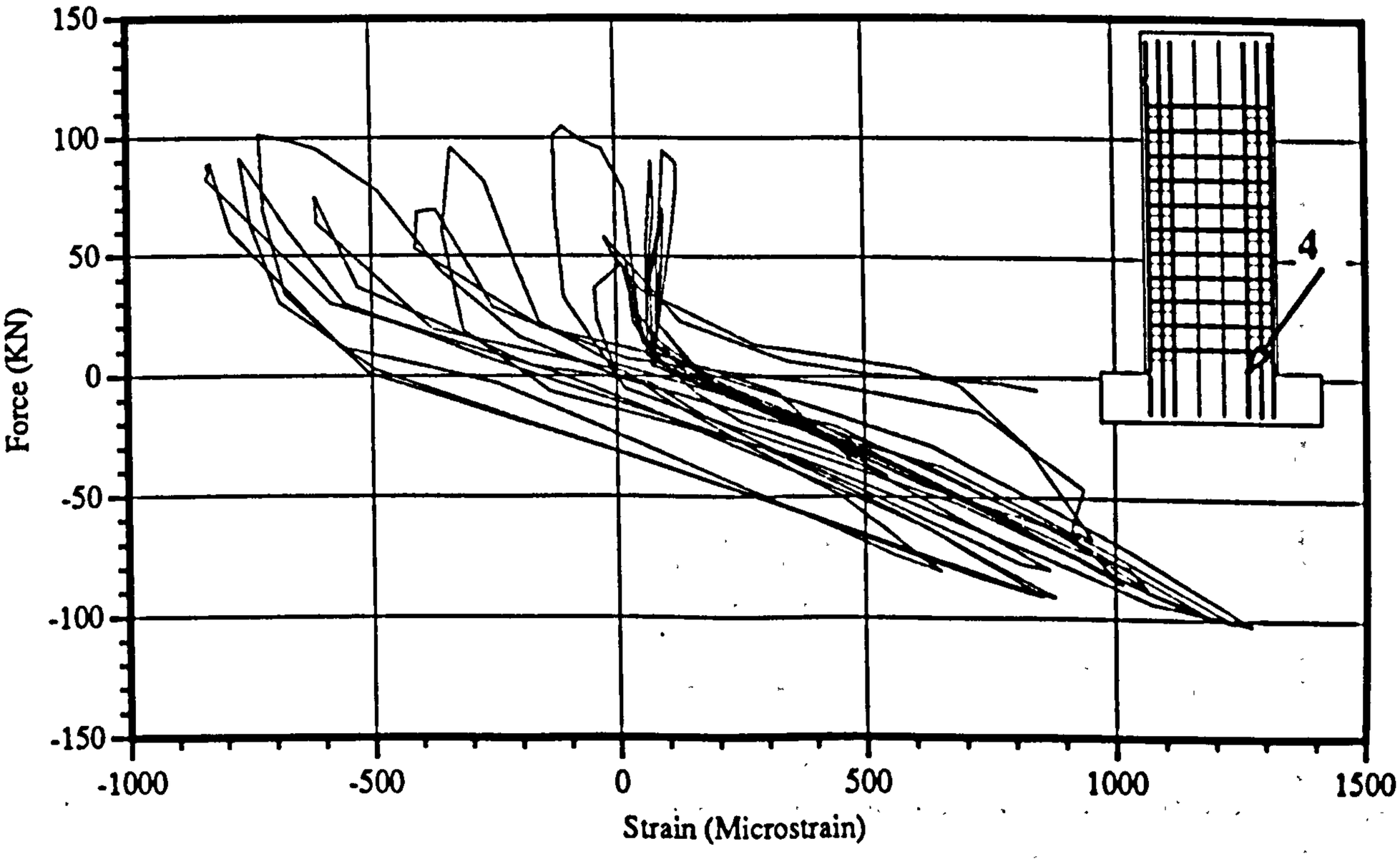


Fig. AII (22) 2 Force - Steel Strain for SW22 at Node 4

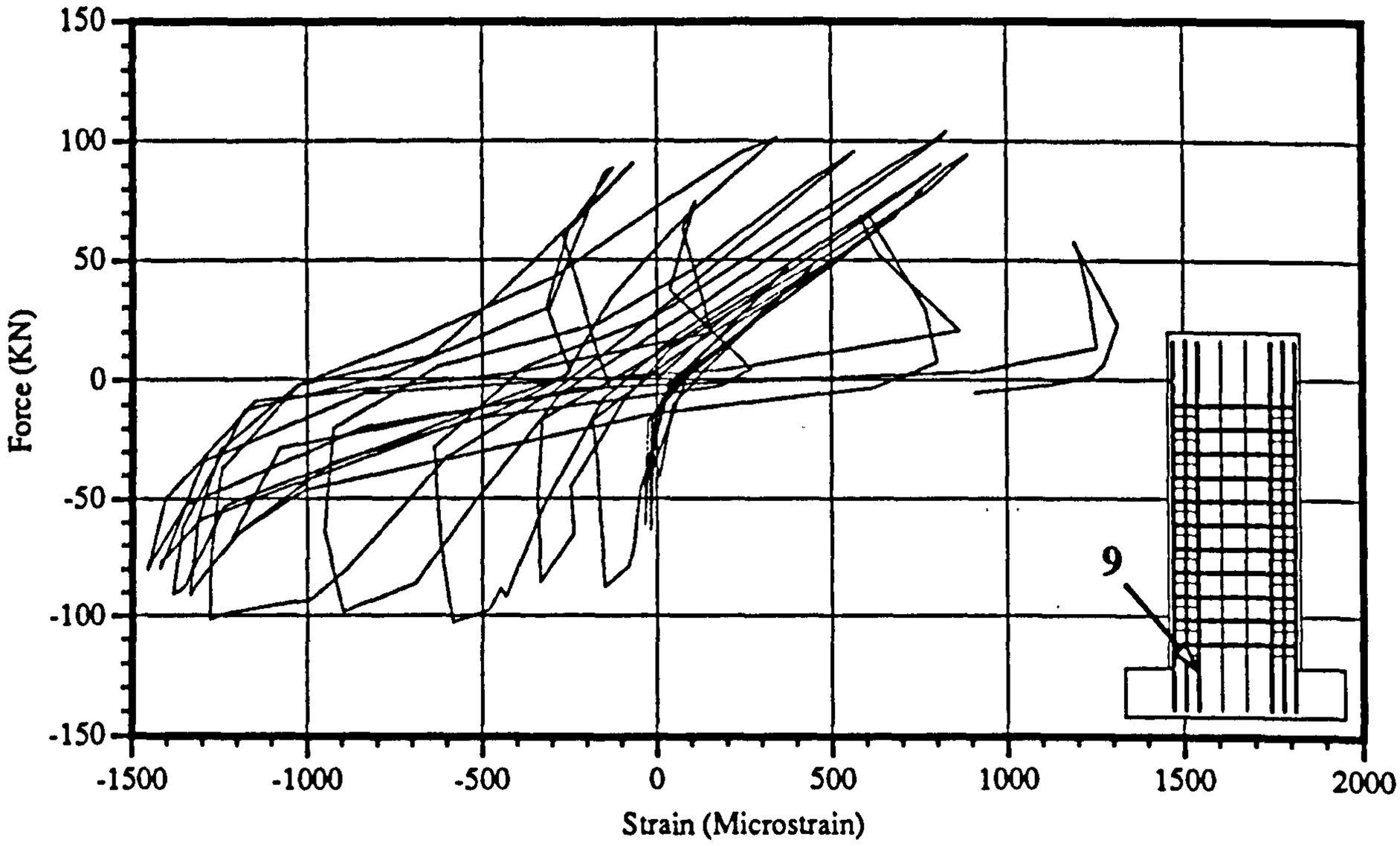


Fig. AII (22) 3 Force - Steel Strain for SW22 at Node 9

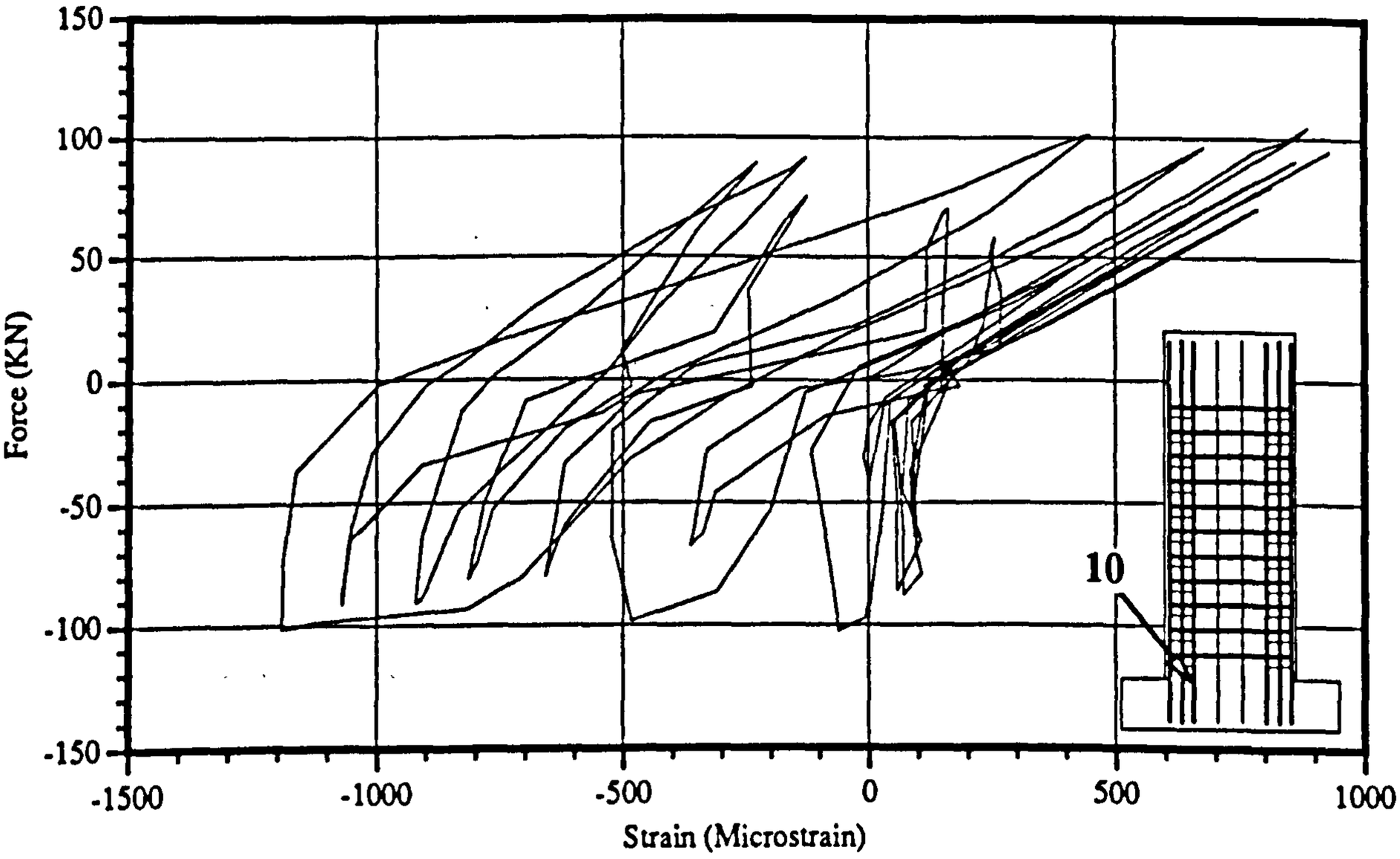


Fig. AII (22) 4 Force - Steel Strain for SW22 at Node 9

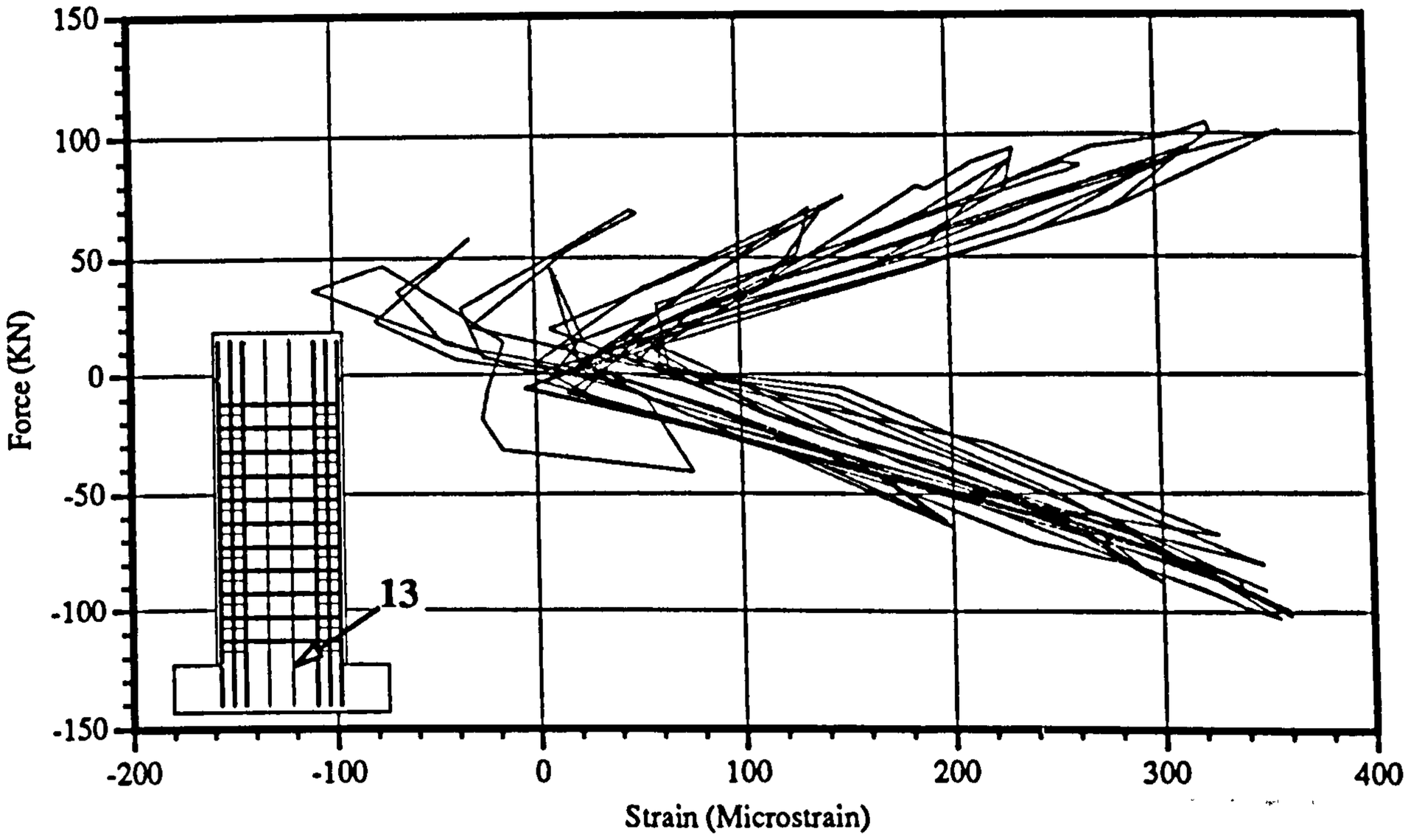


Fig. AII (22) 5 Force - Steel Strain for SW22 at Node 13

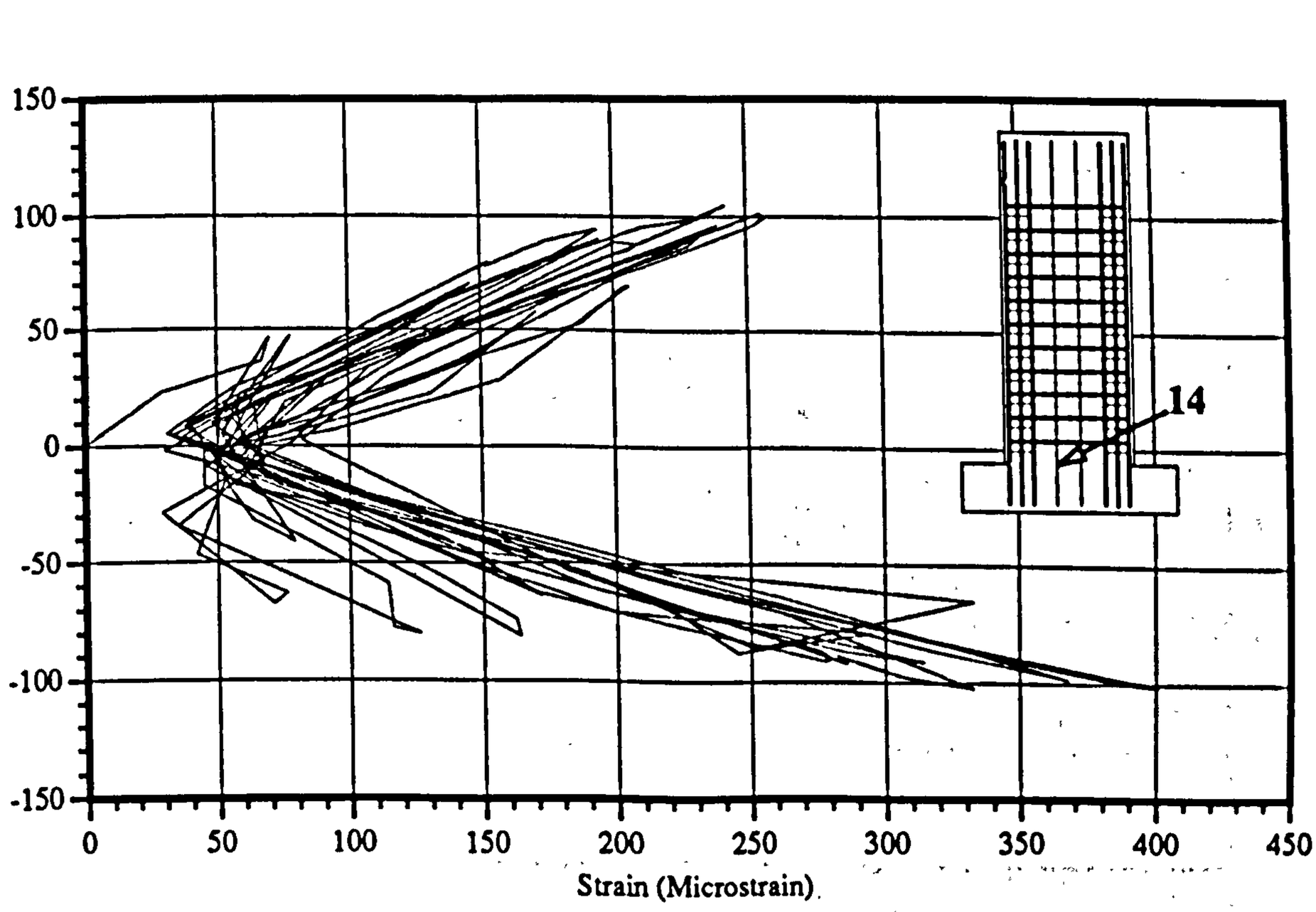


Fig. AII (22) 6 Force - Steel Strain for SW22 at Node 14

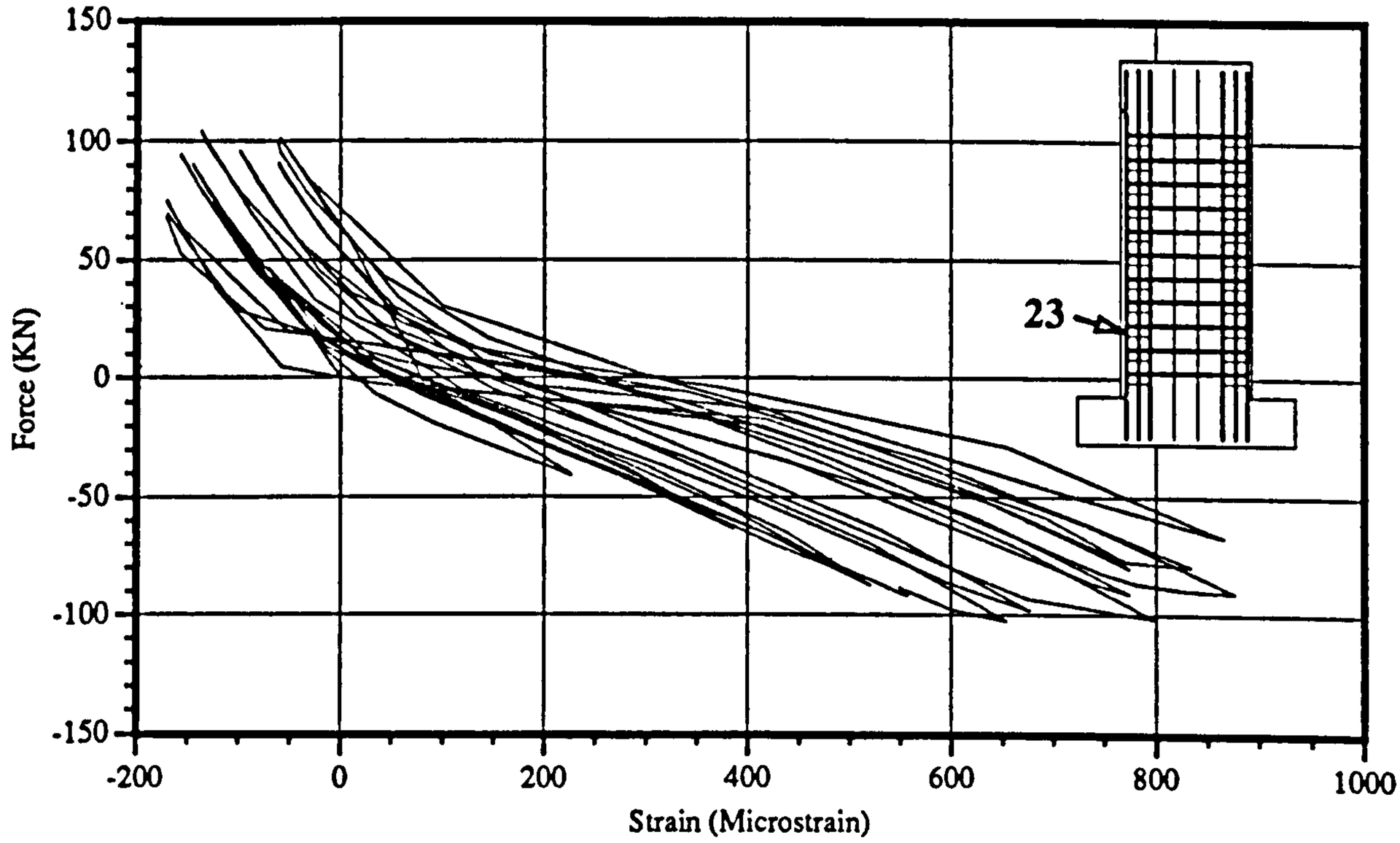


Fig. AII (22) 7 Force - Steel Strain for SW22 at Node 23

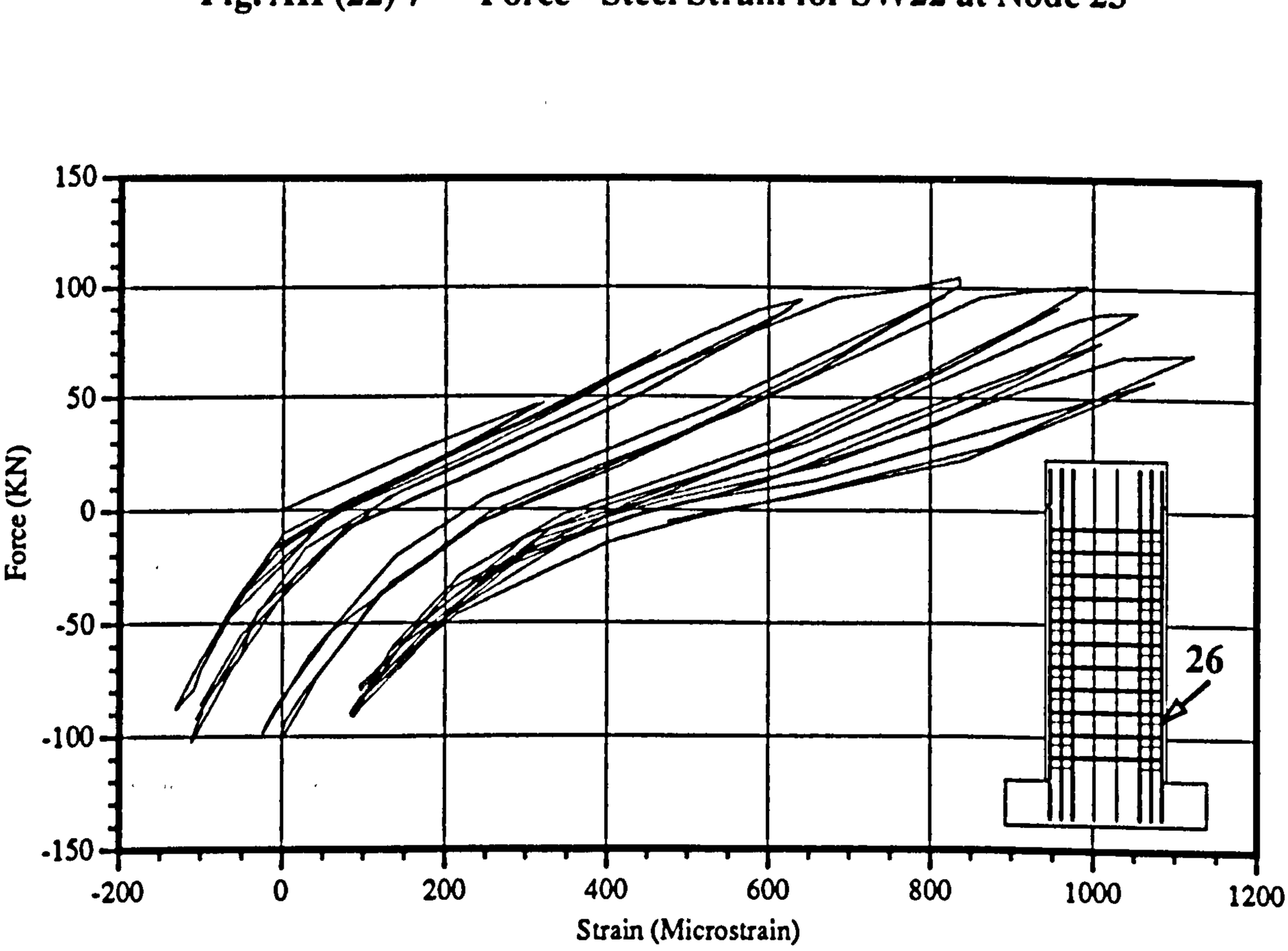


Fig. AII (22) 8 Force - Steel Strain for SW22 at Node 26

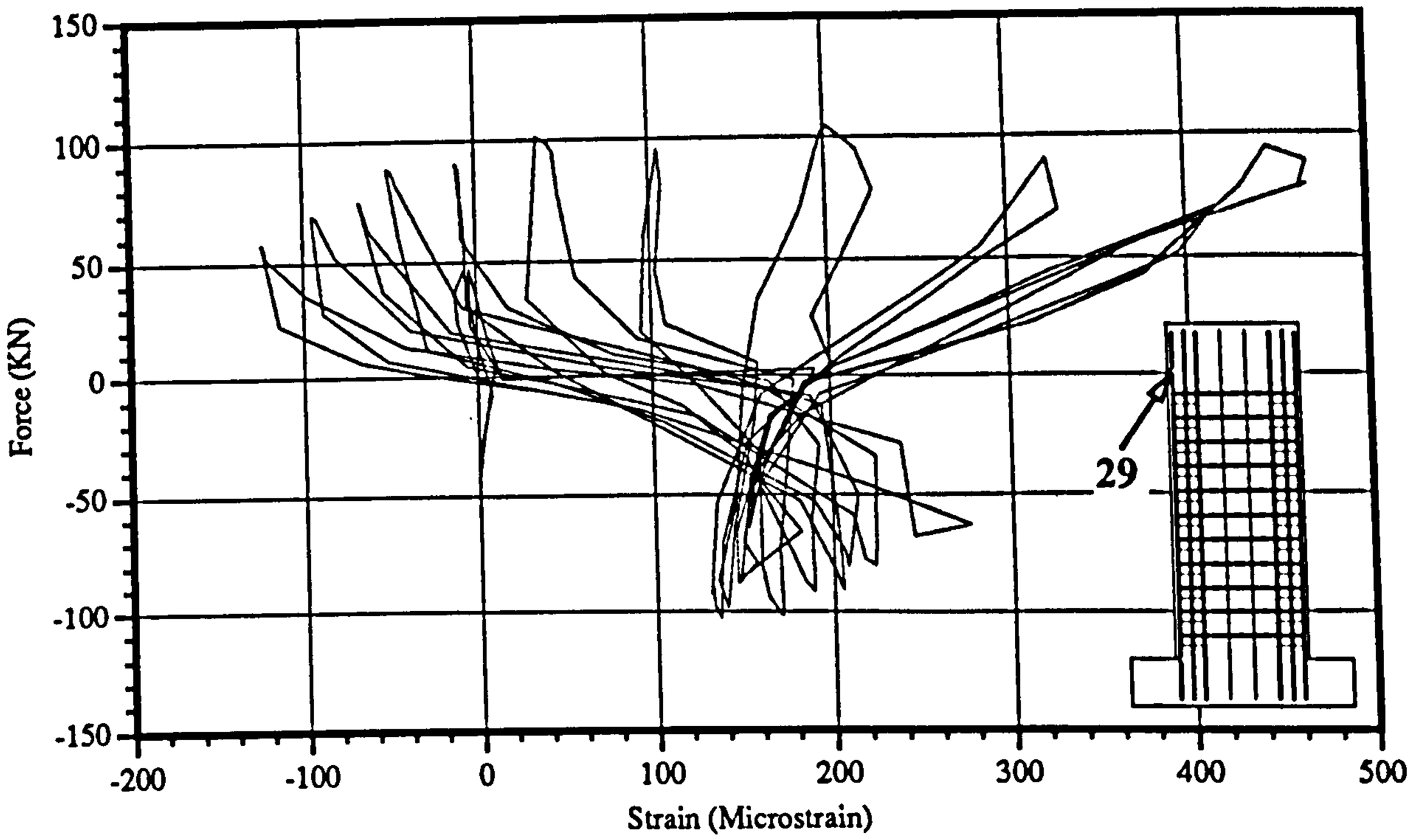


Fig. AII (22) 9 Force - Steel Strain for SW22 at Node 29

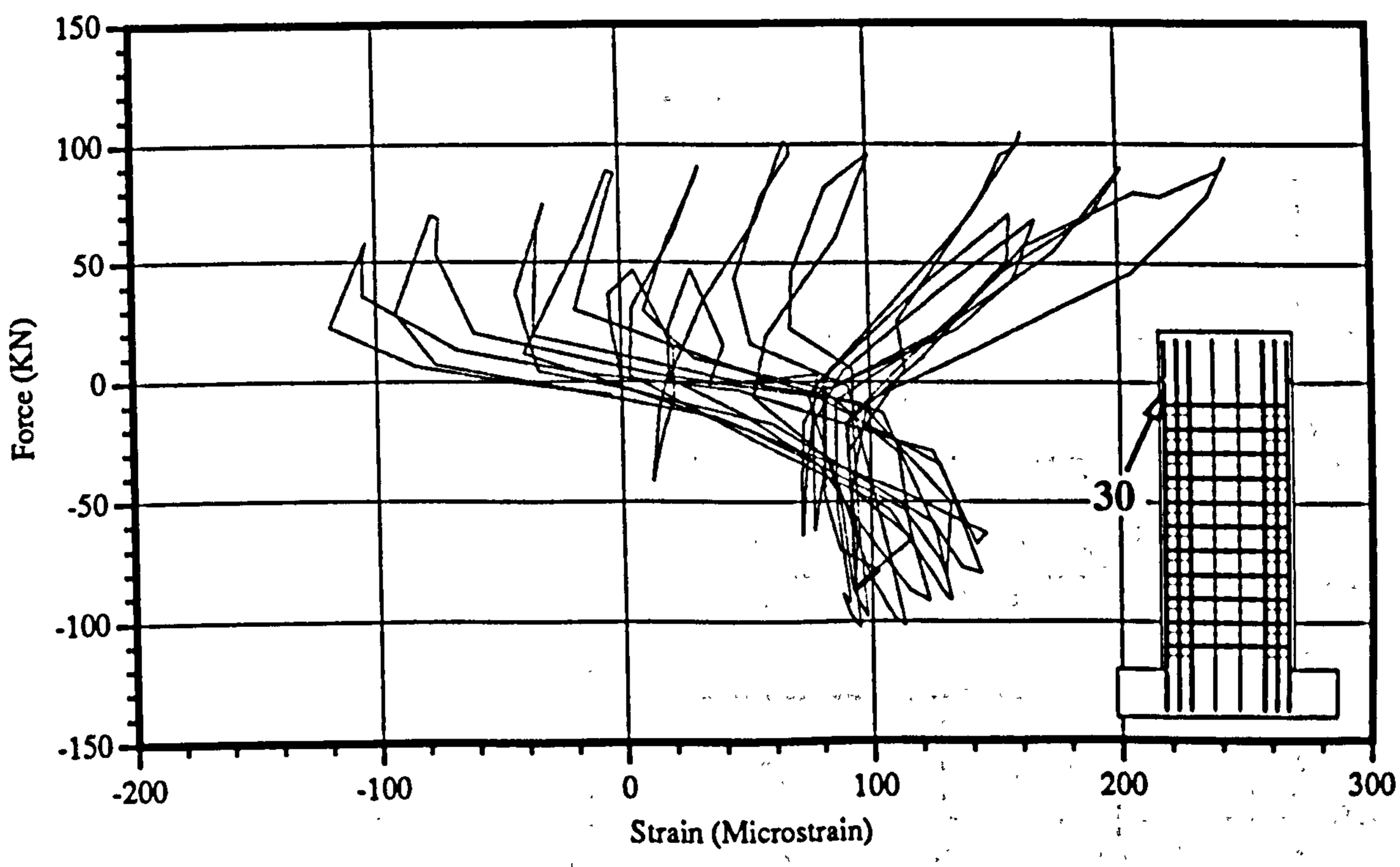


Fig. AII (22) 10 Force - Steel Strain for SW22 at Node 30

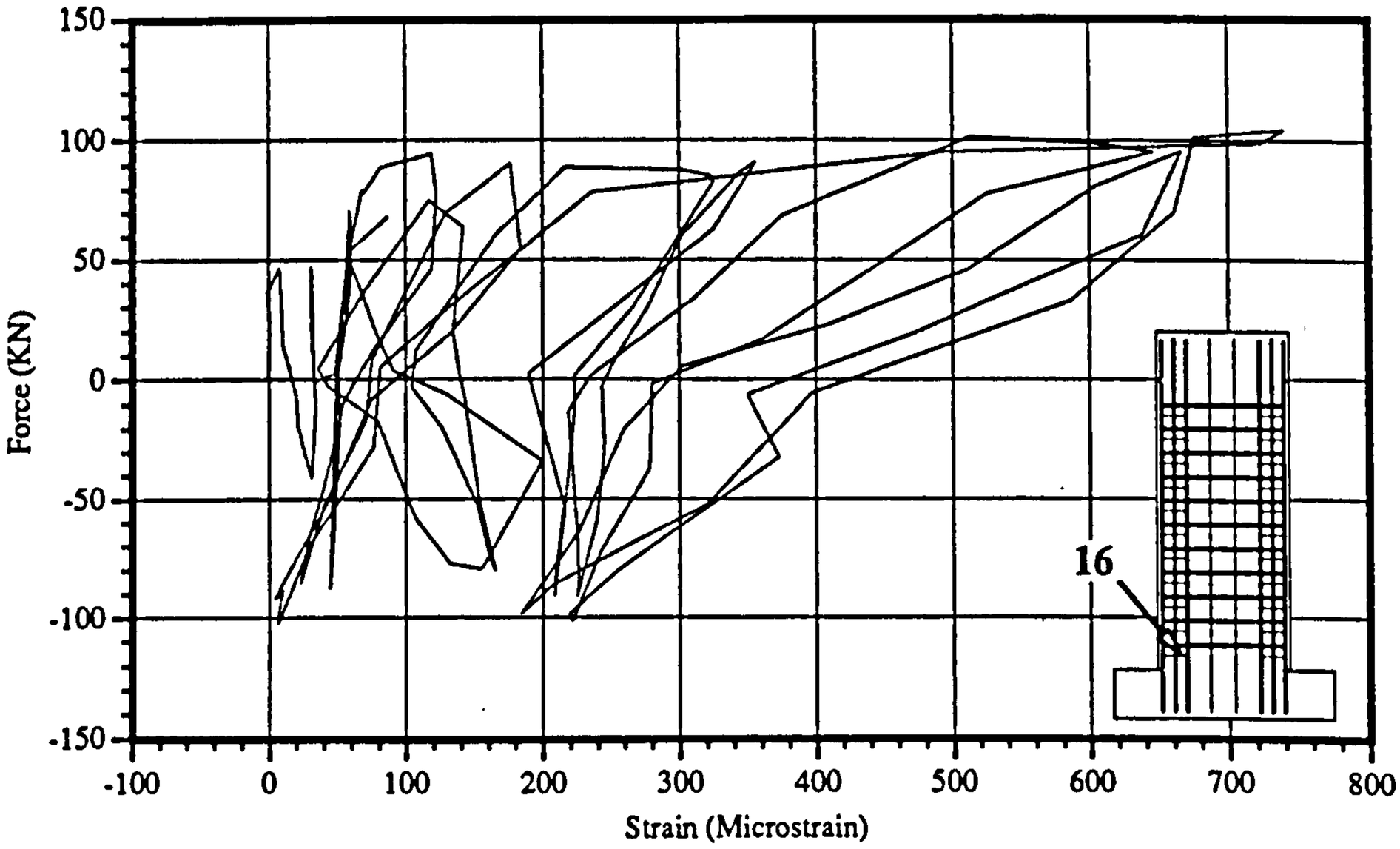


Fig. AII (22) 11 Force - Steel Strain for SW22 at Node 16

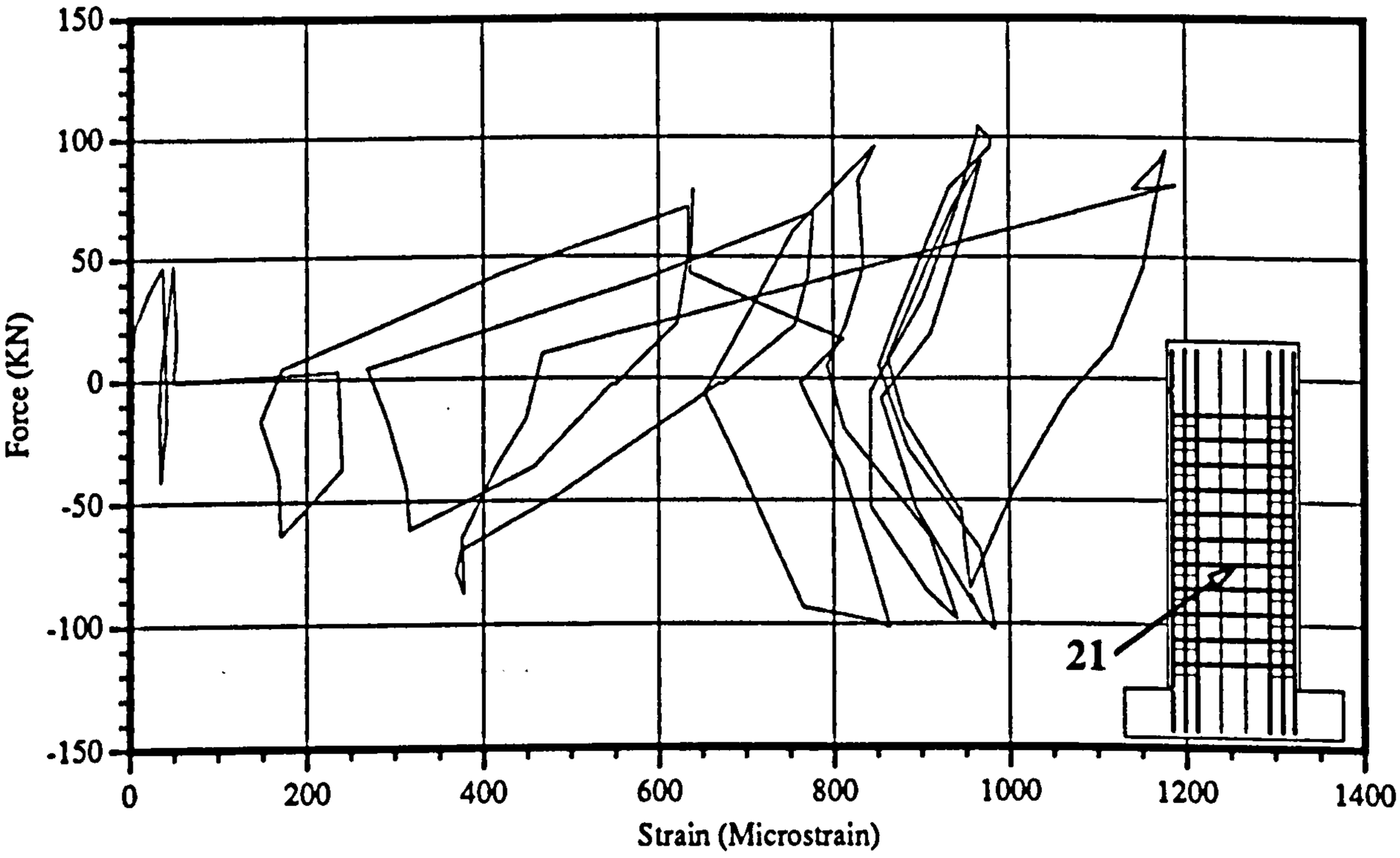


Fig. AII (22) 12 Force - Steel Strain for SW22 at Node 21

AII.3 : Force-Steel Strain for SW23

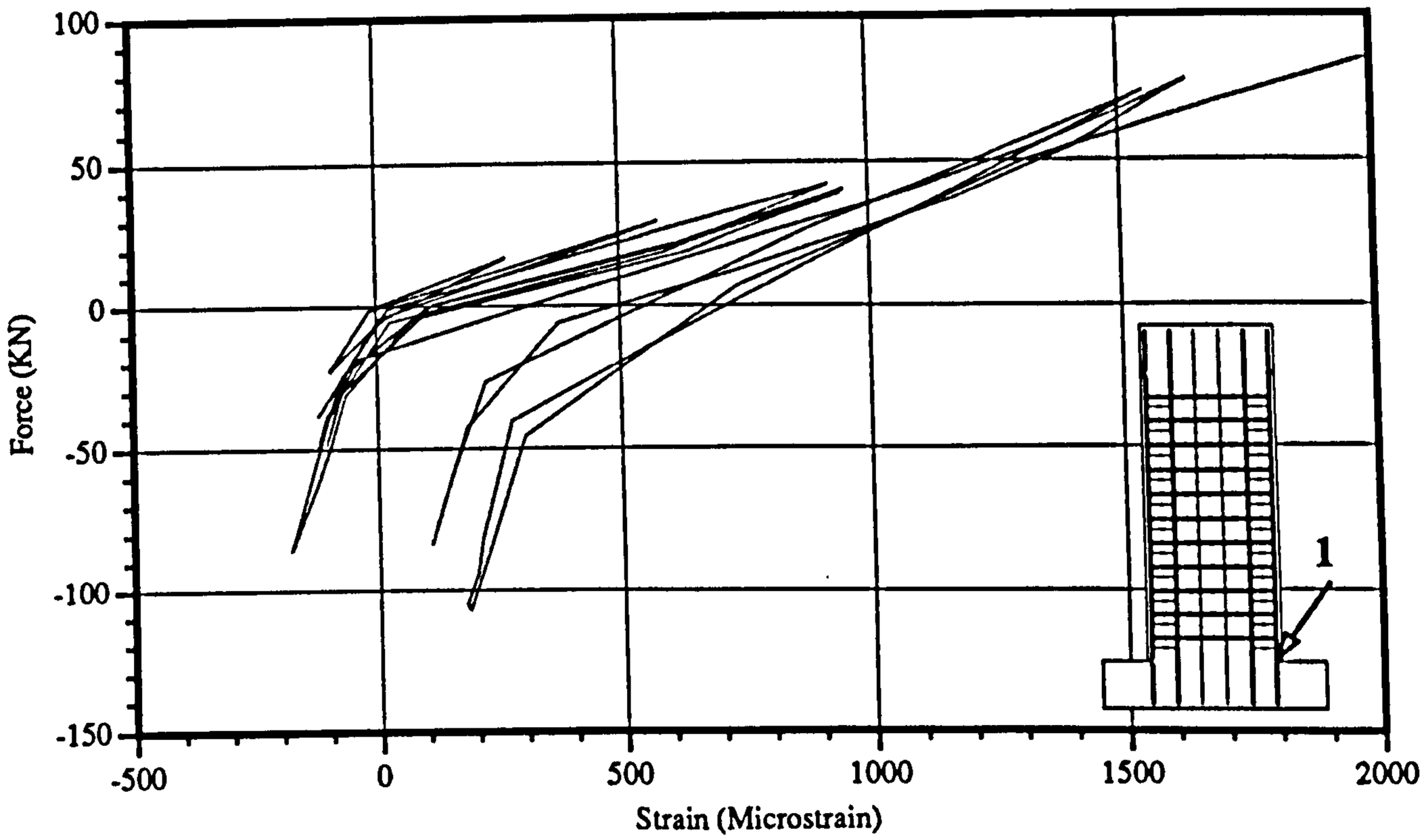


Fig. AII (23) 1 Force - Steel Strain for SW23 at Node 1

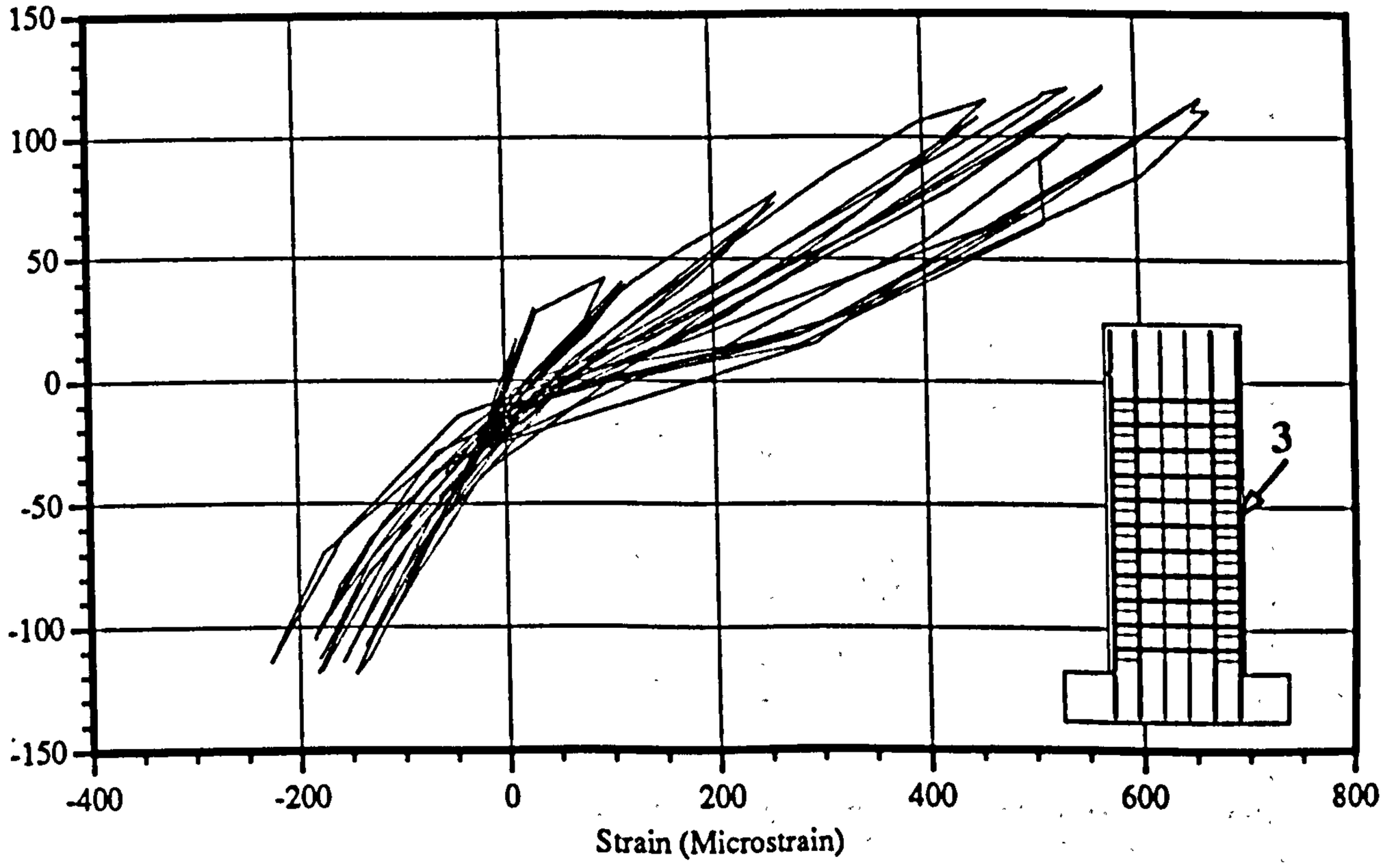


Fig. AII (23) 2 Force - Steel Strain for SW23 at Node 3

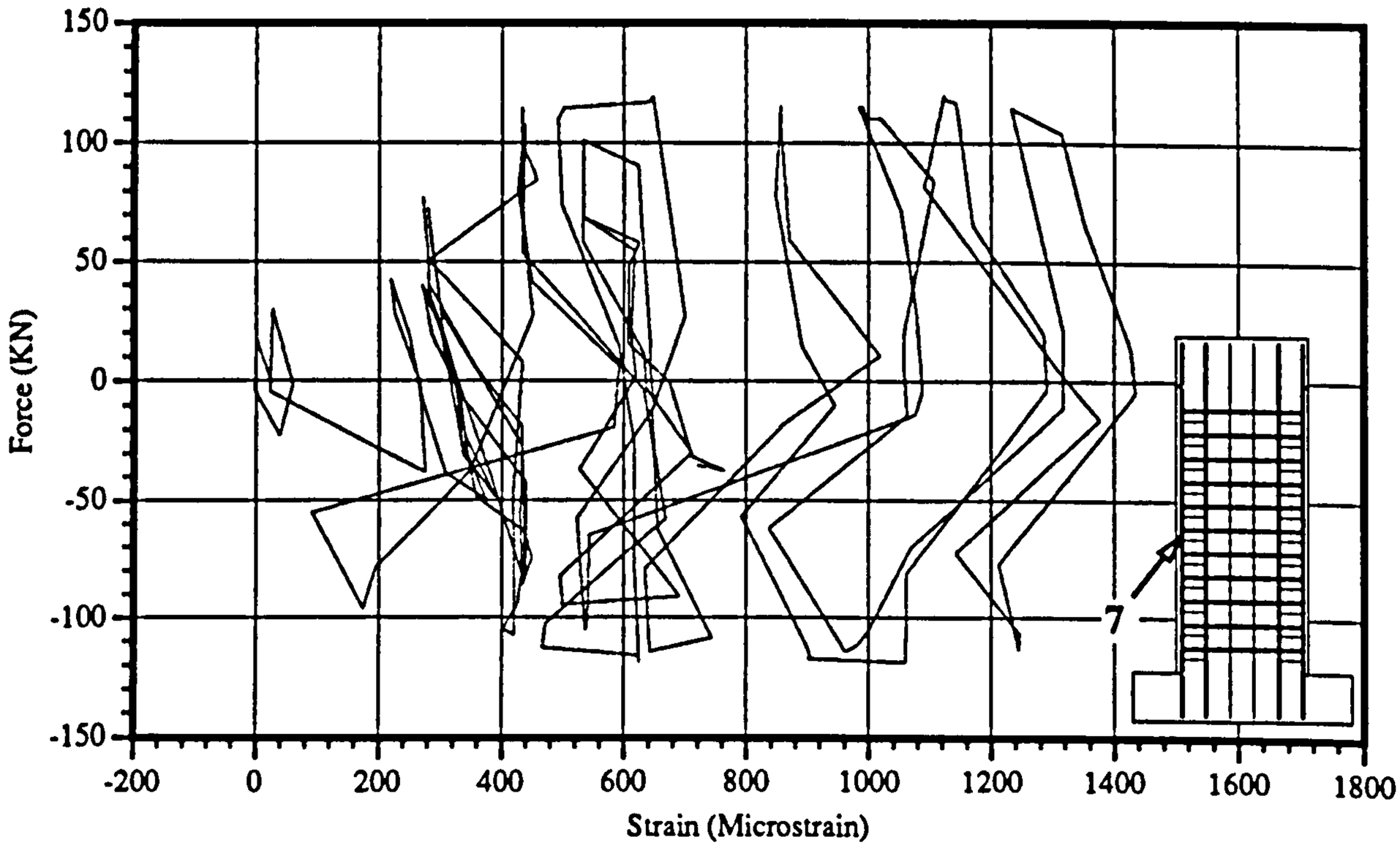


Fig. AII (23) 3 Force - Steel Strain for SW23 at Node 7

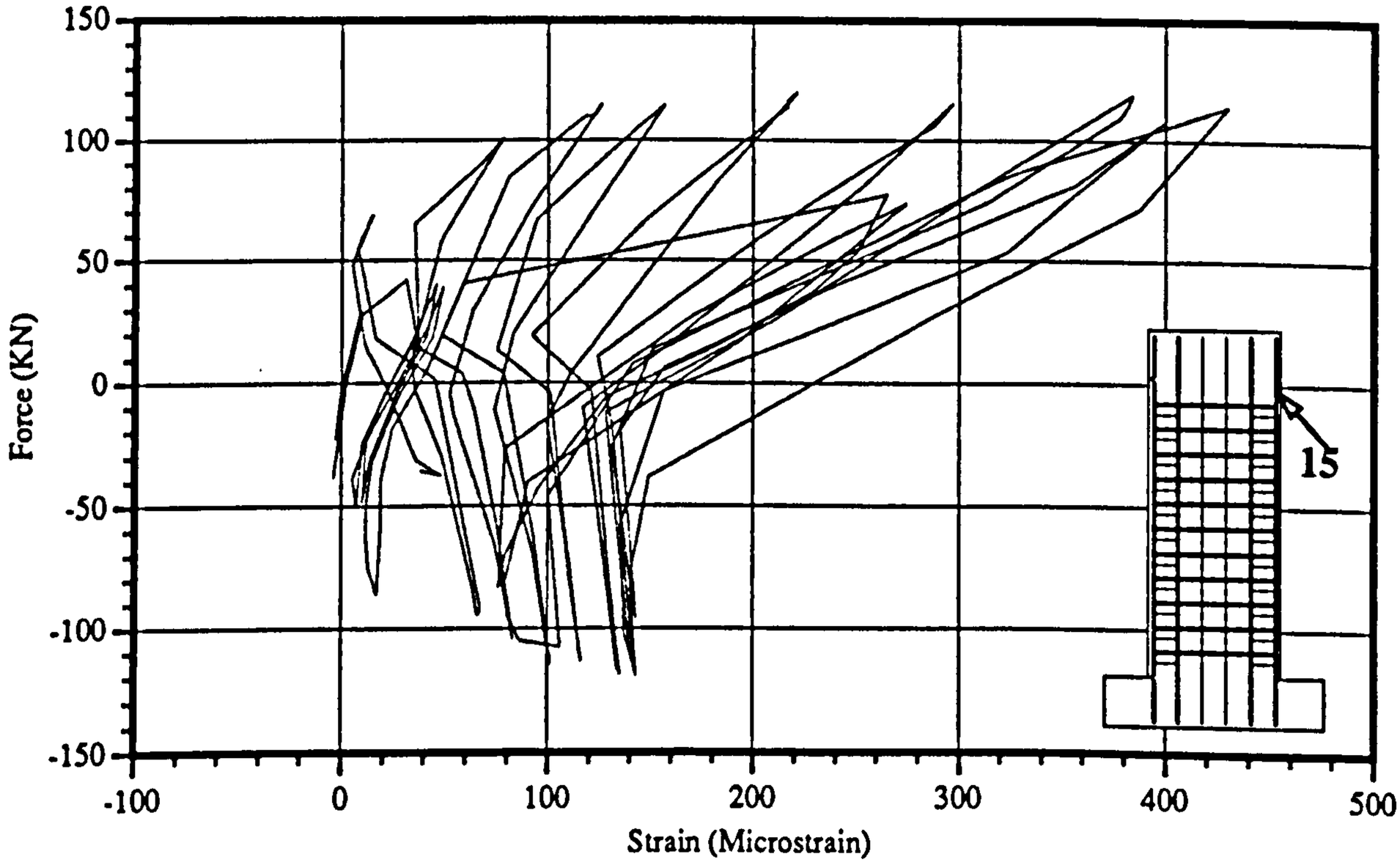


Fig. AII (23) 4 Force - Steel Strain for SW23 at Node 15

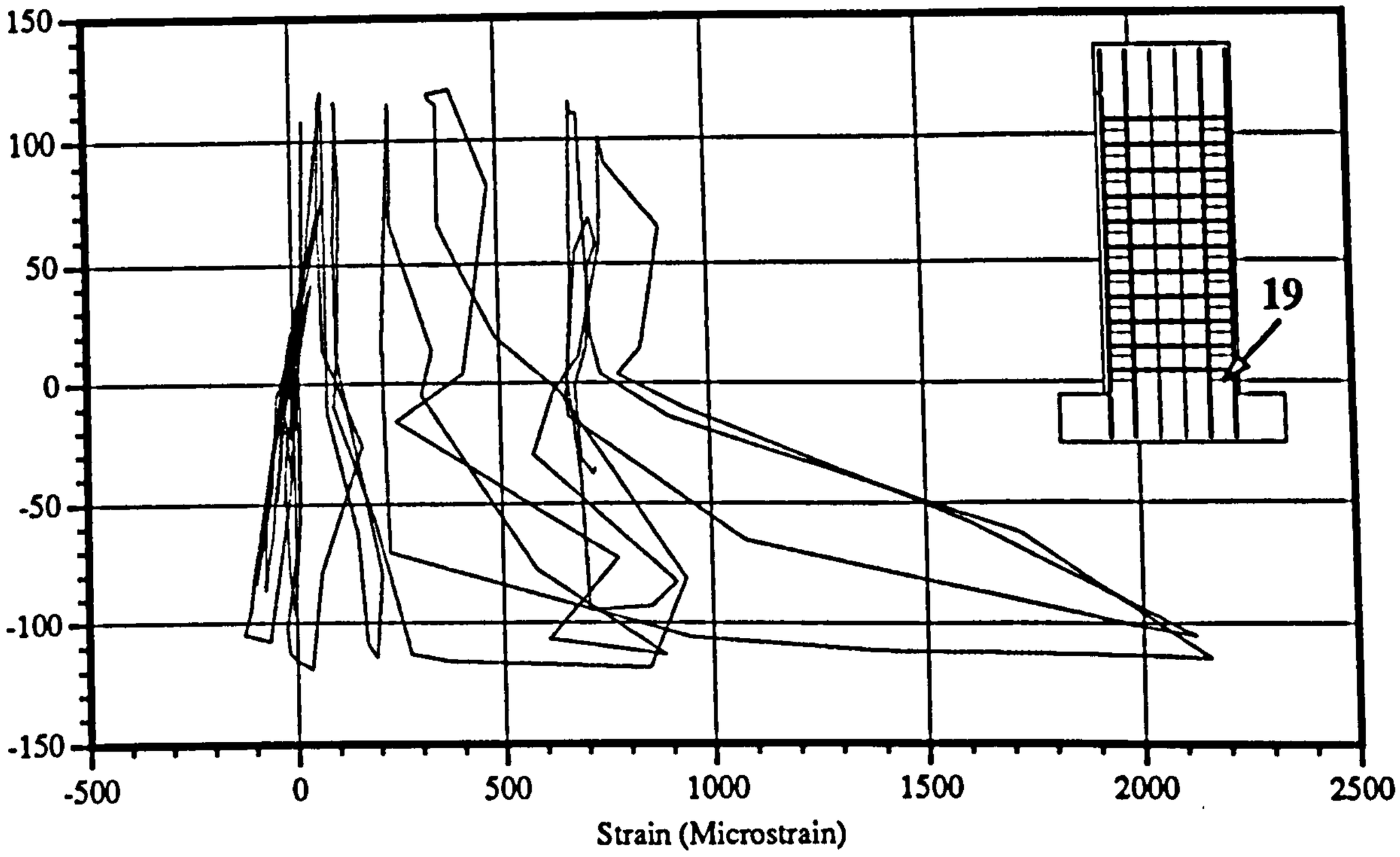


Fig. AII (23) 5 Force - Steel Strain for SW23 at Node 19

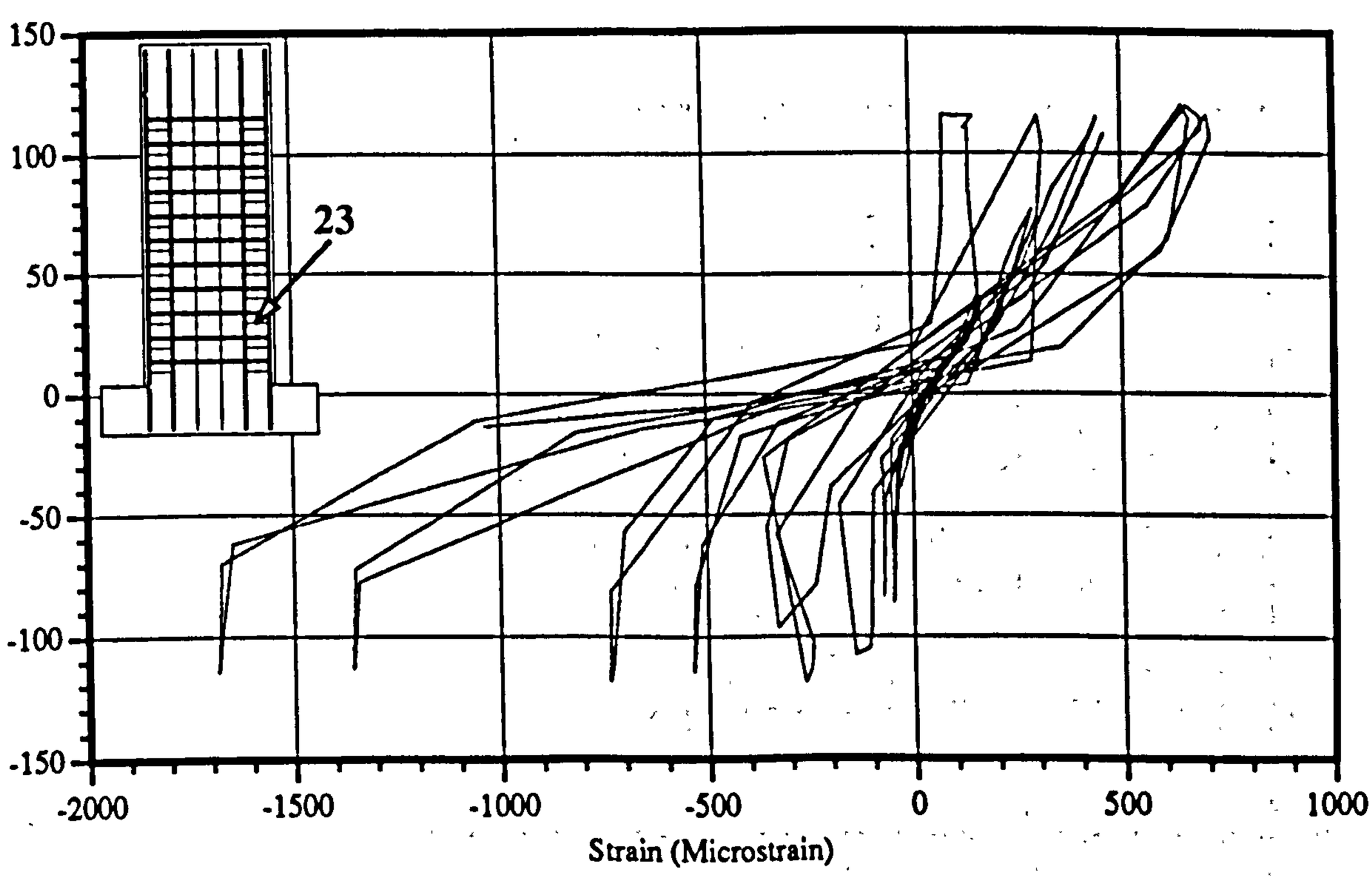


Fig. AII (23) 6 Force - Steel Strain for SW23 at Node 23

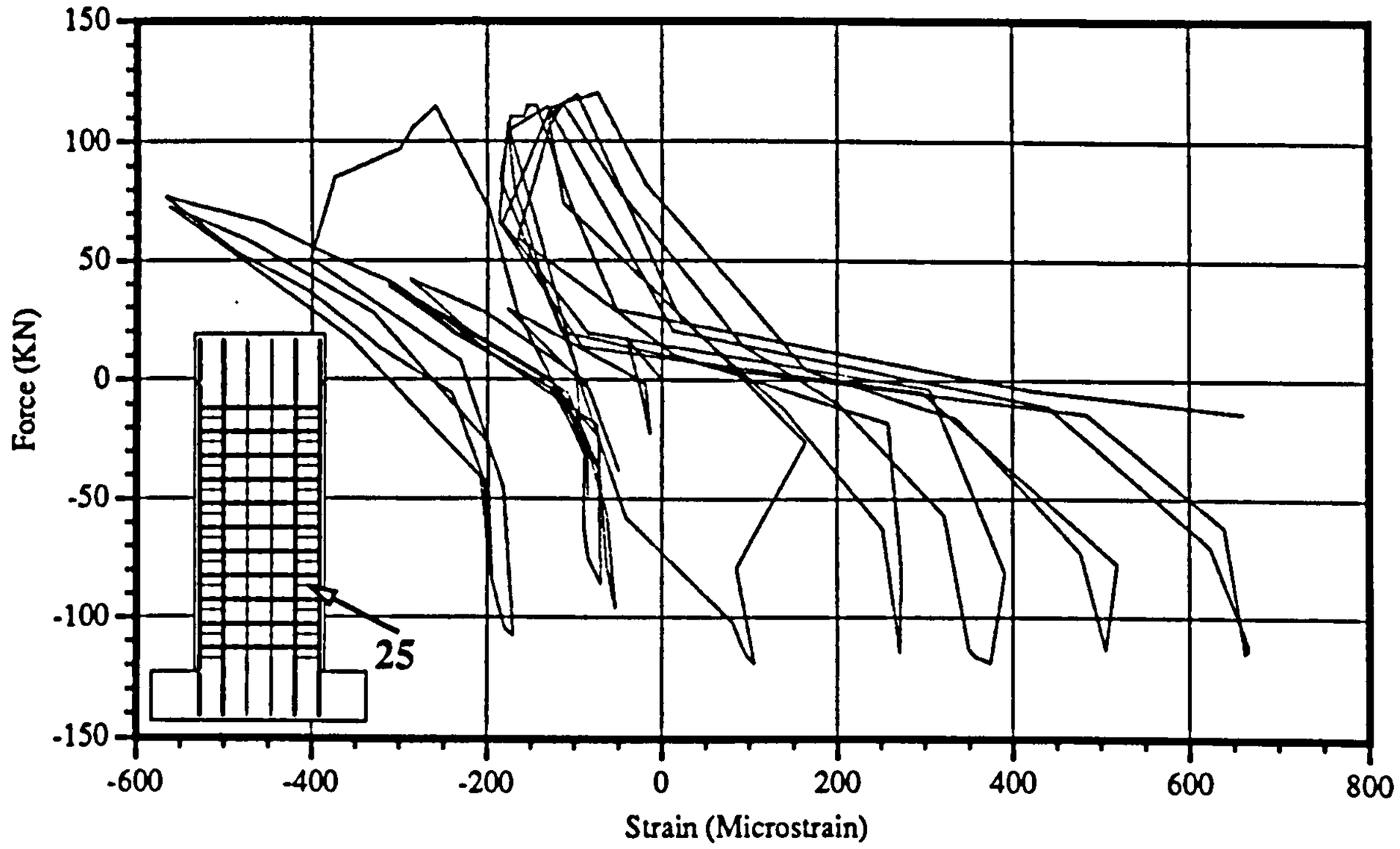


Fig. AII (23) 7 Force - Steel Strain for SW23 at Node 25

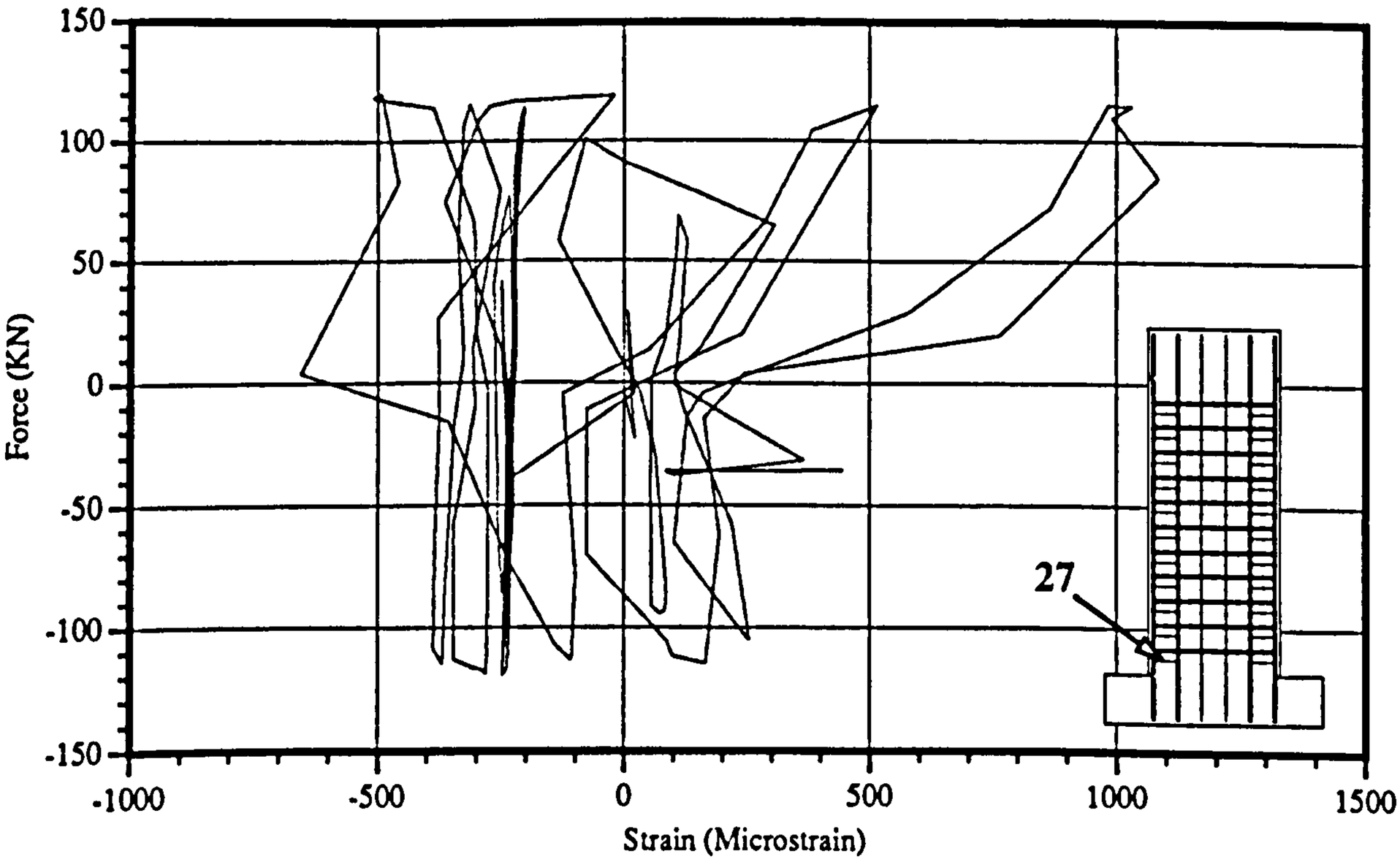


Fig. AII (23) 8 Force - Steel Strain for SW23 at Node 27

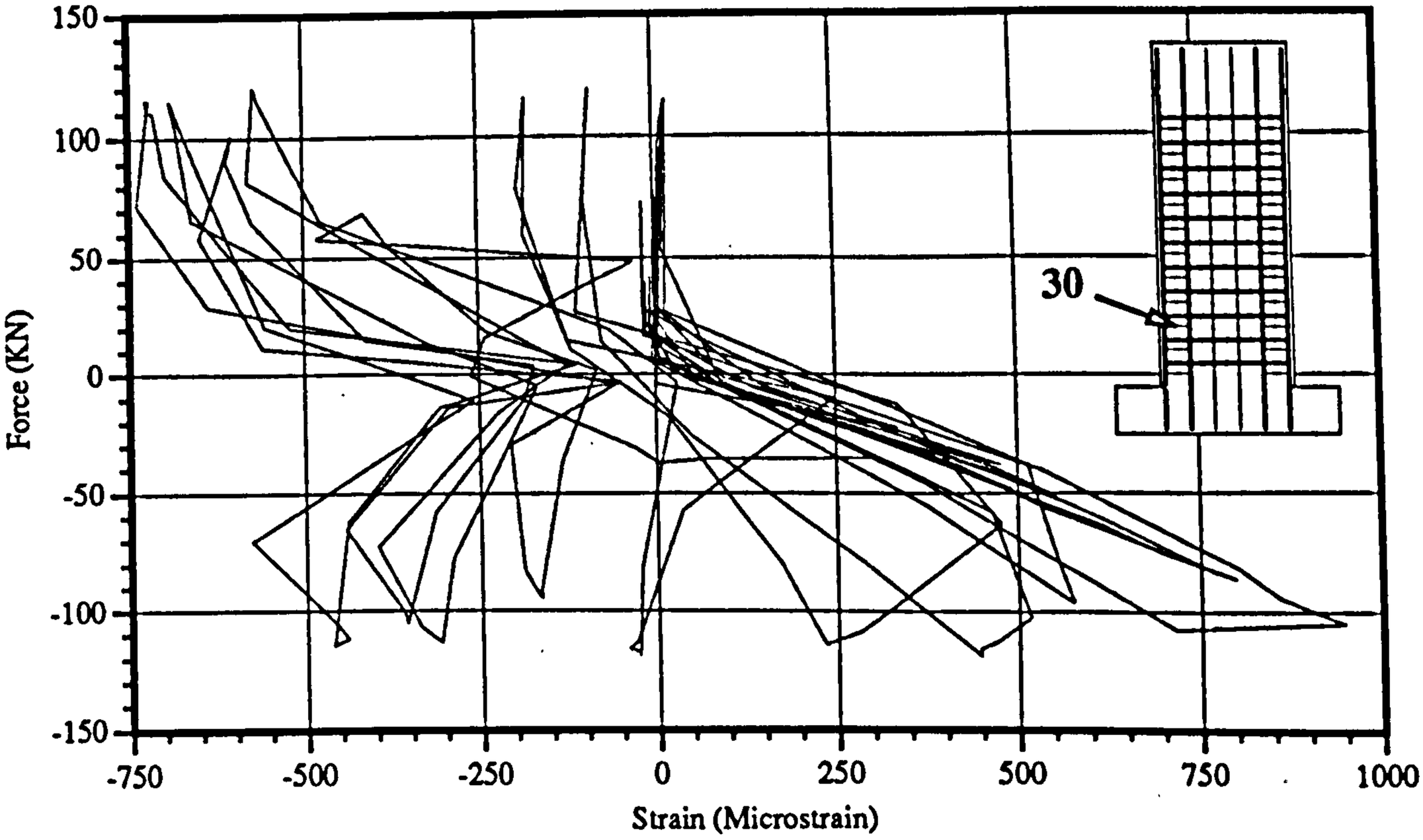


Fig. AII (23) 9 Force - Steel Strain for SW23 at Node 30

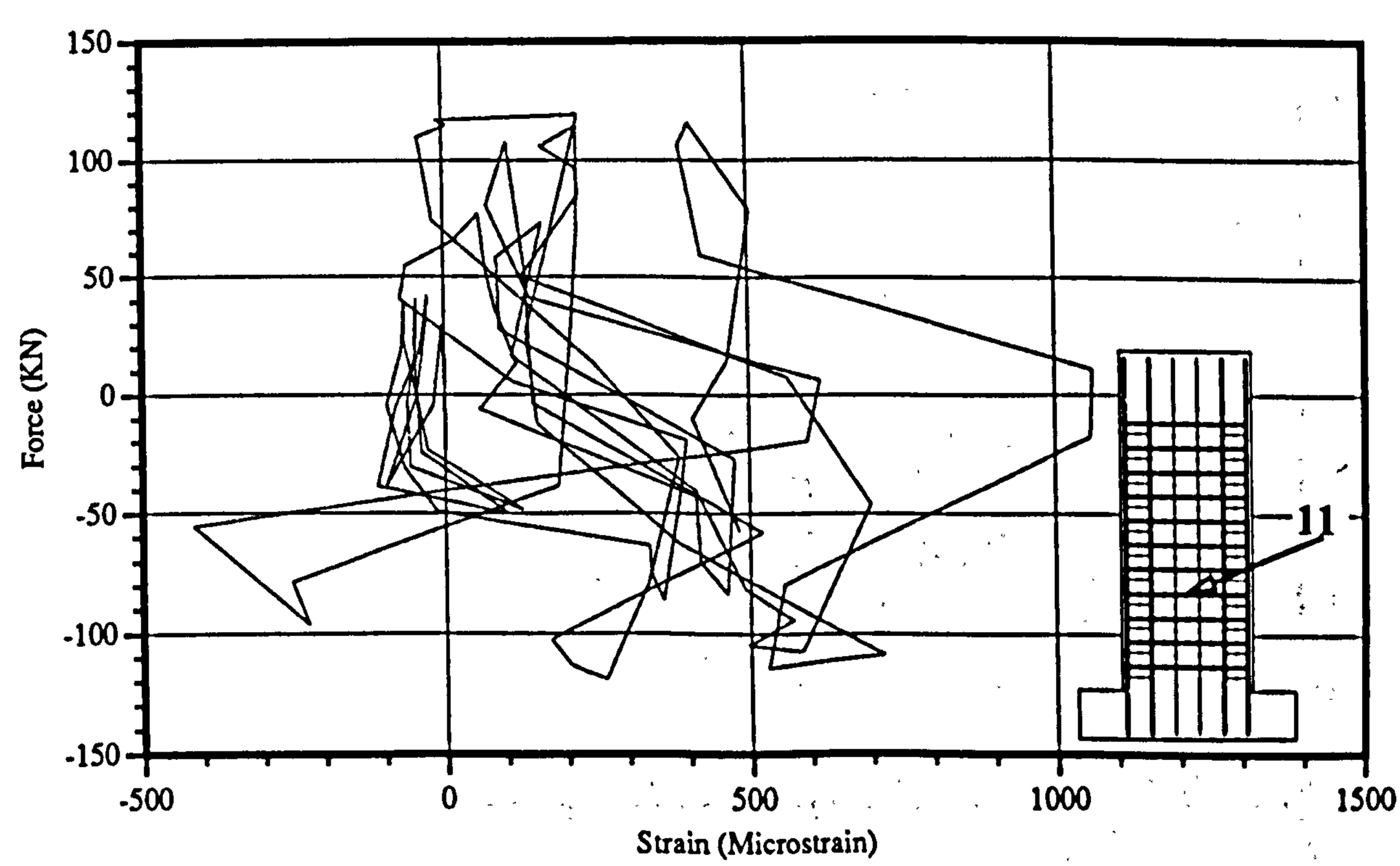


Fig. AII (23) 10 Force - Steel Strain for SW23 at Node 11

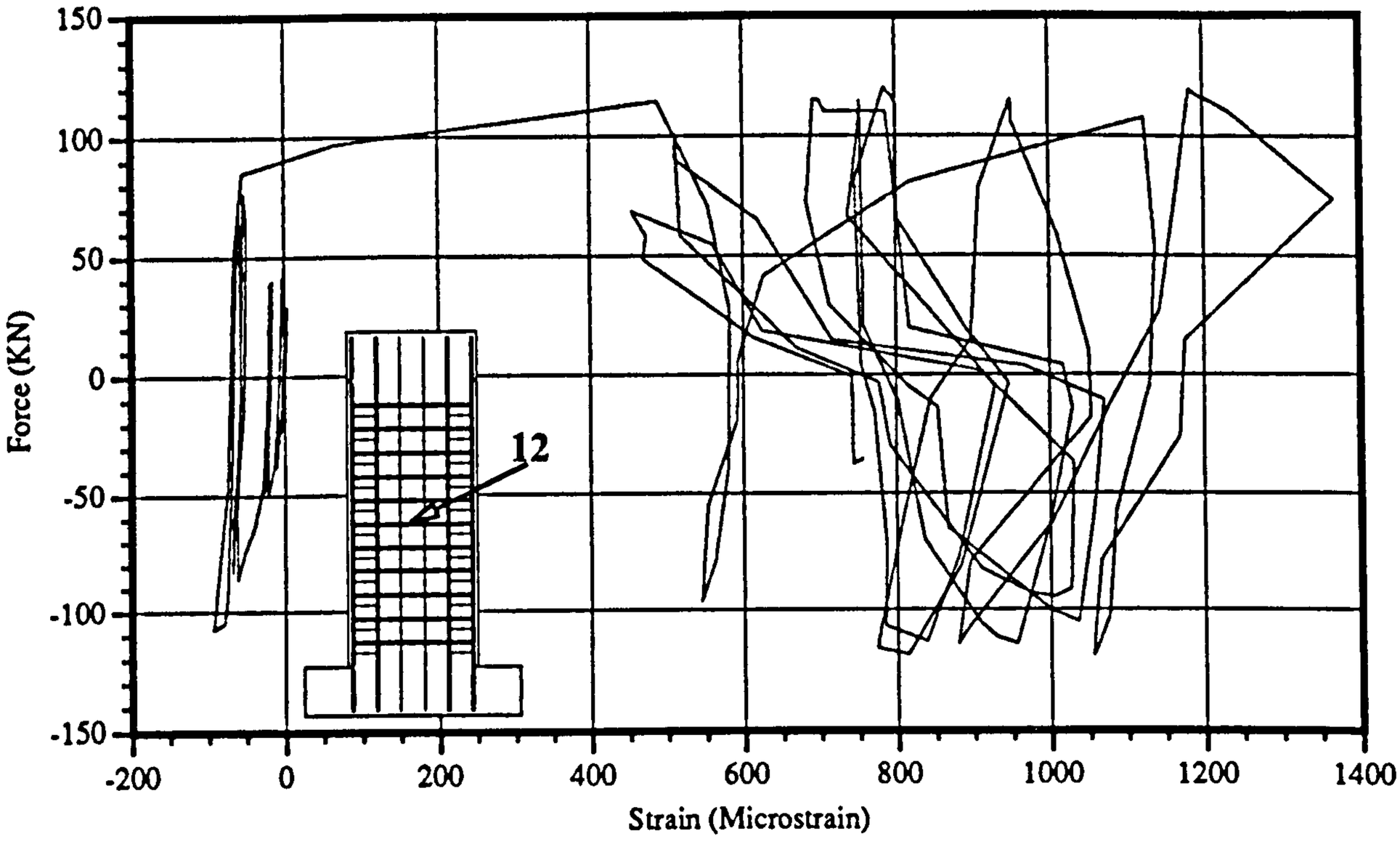


Fig. AII (23) 11 Force - Steel Strain for SW23 at Node 12

Fig. AII (23) 12 Force - Steel Strain for SW23 at Node 14

AII. 4 Force-Steel Strain for SWR9

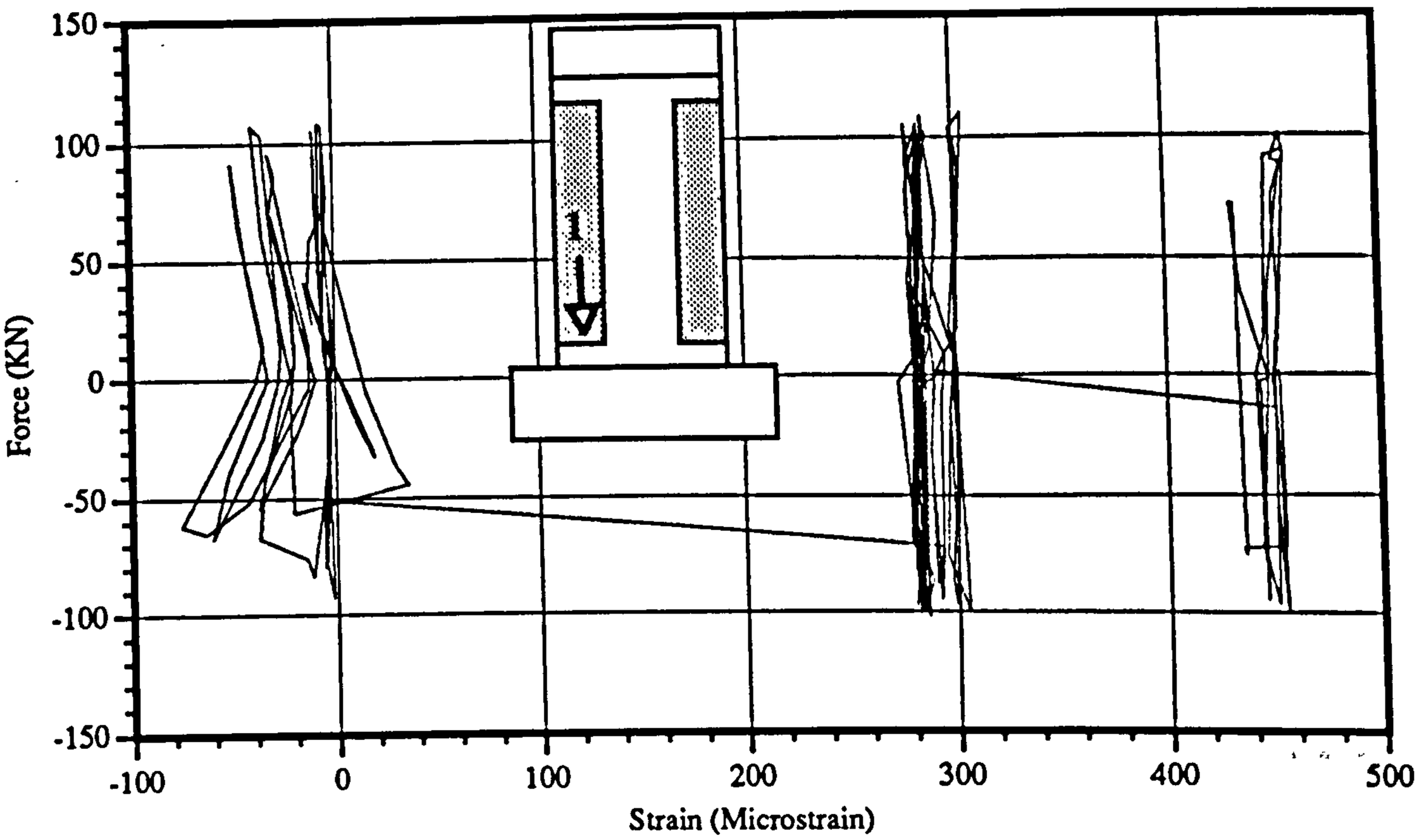


Fig. AII (R9) 1 Force - Steel Strain for SWR9 at Node 1

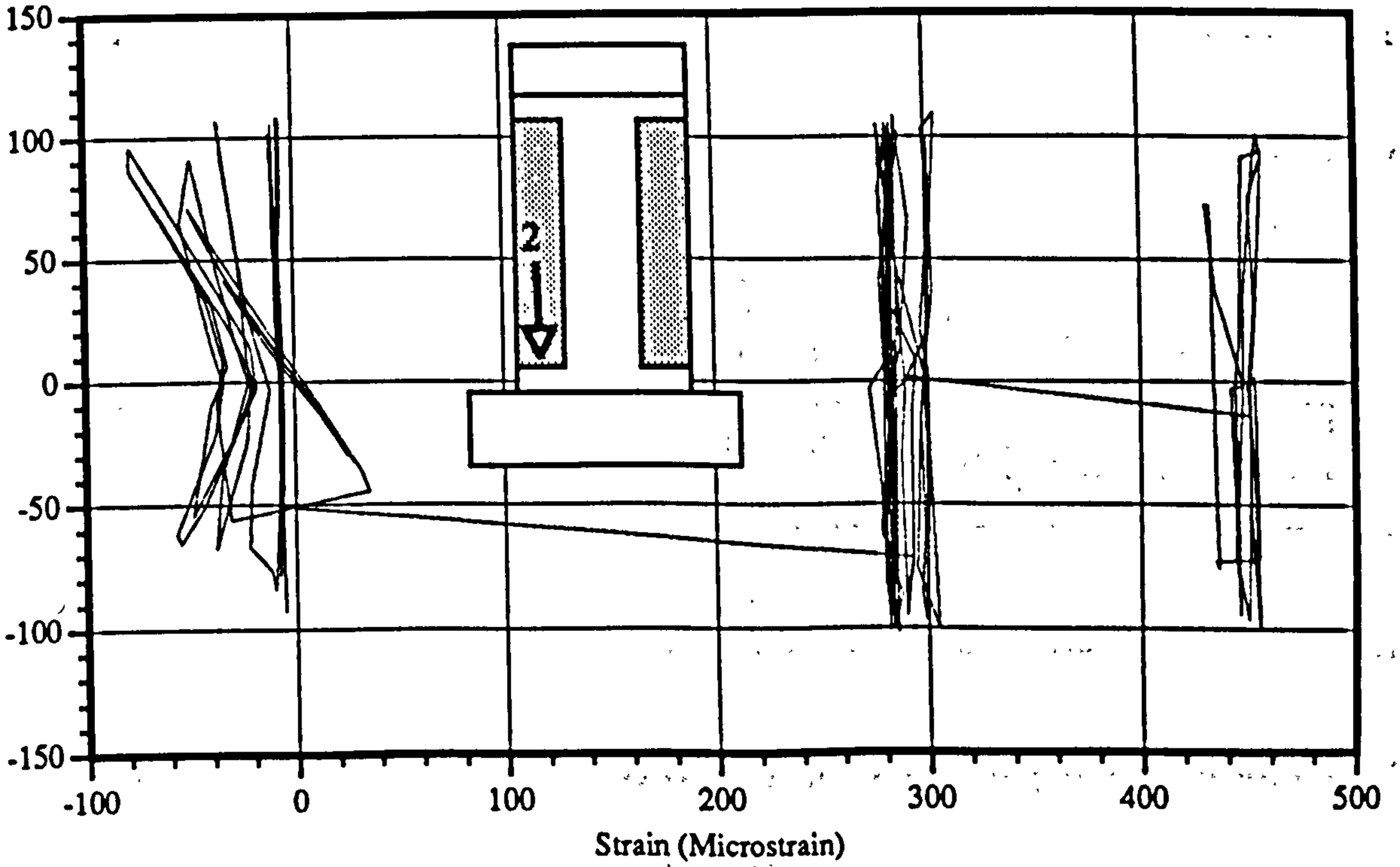


Fig. AII (R9) 2 Force - Steel Strain for SWR9 at Node 2

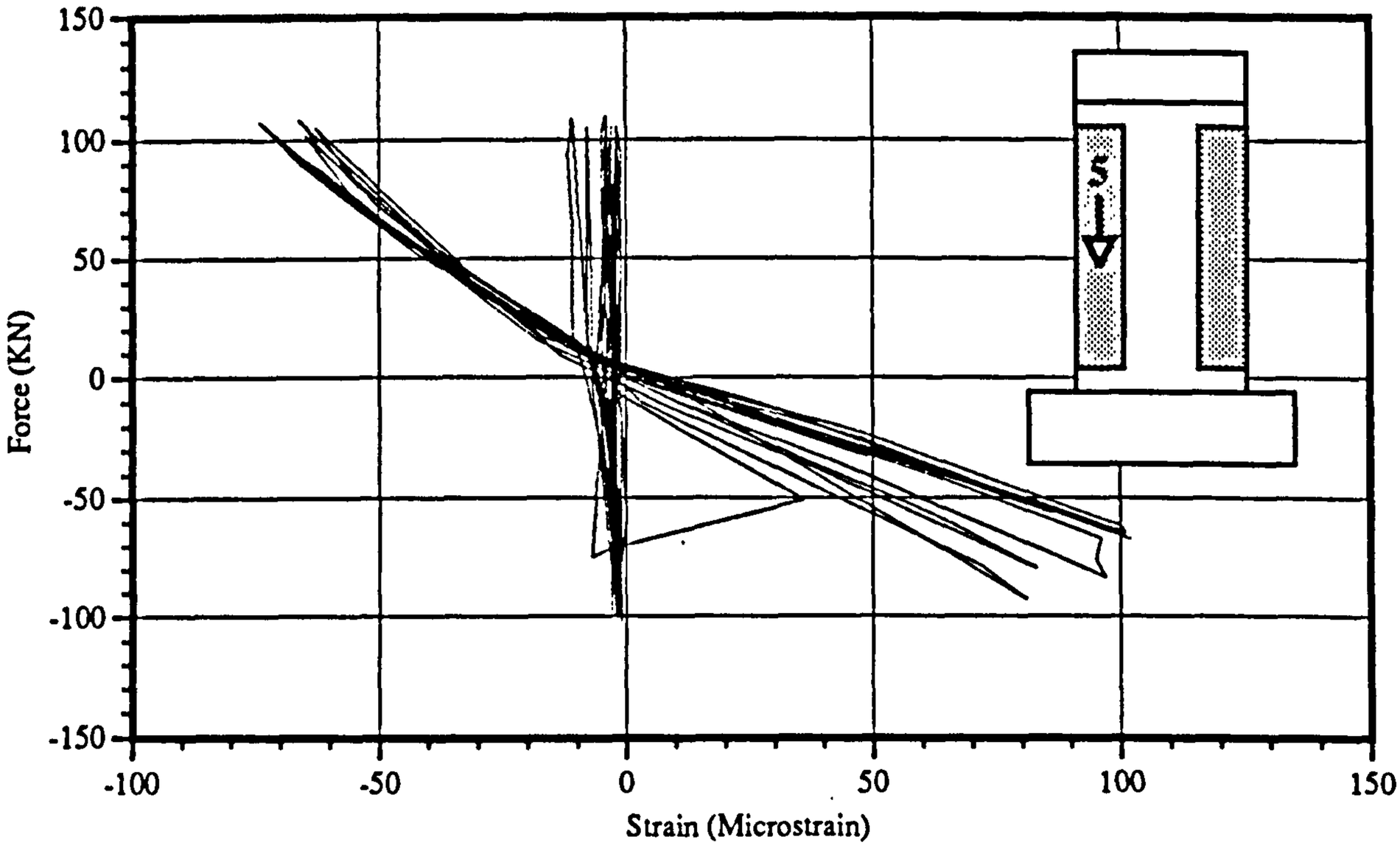


Fig. AII (R9) 3 Force - Steel Strain for SWR9 at Node 5

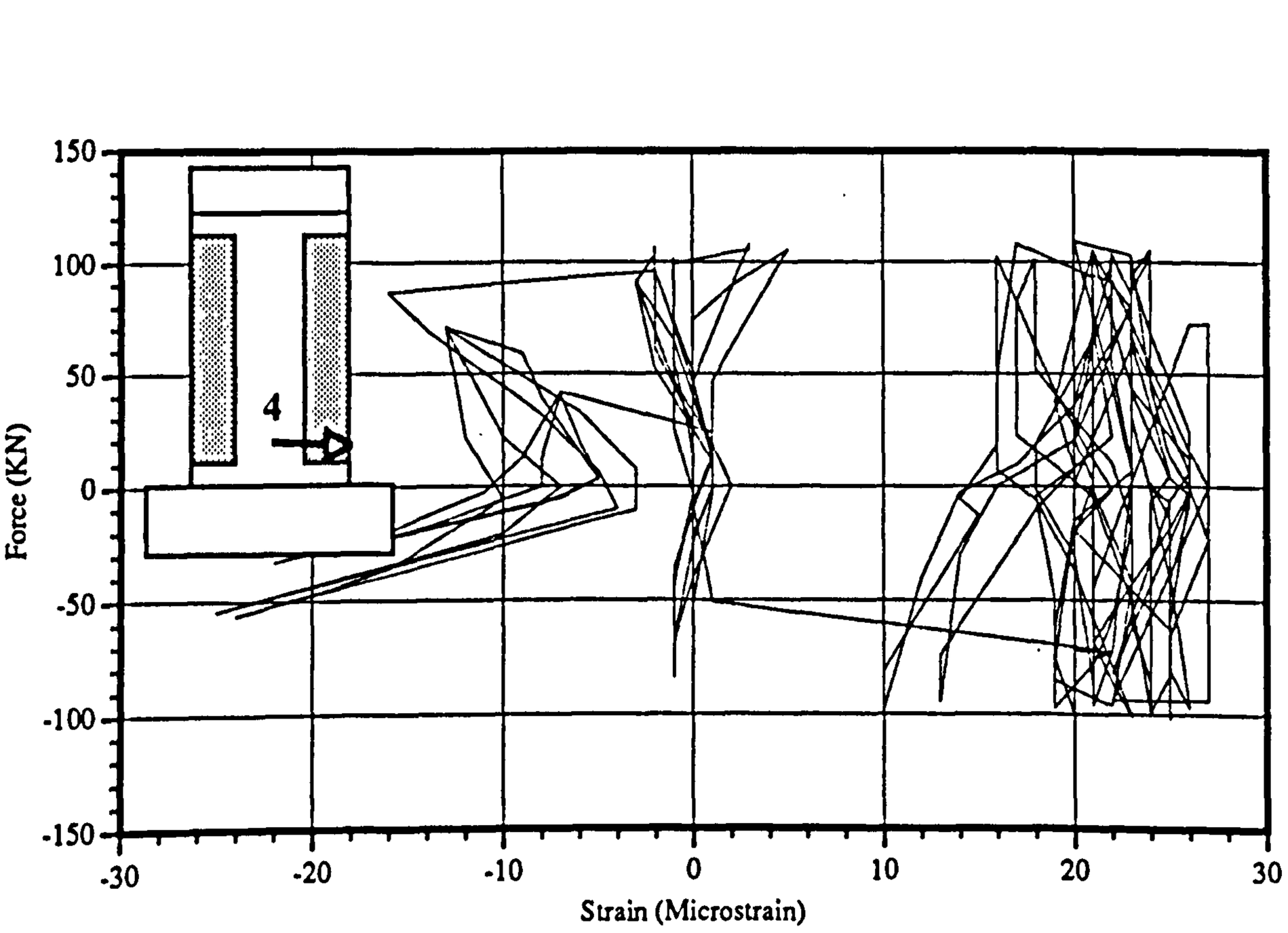


Fig. AII (R9) 4 Force - Steel Strain for SWR9 at Node 4

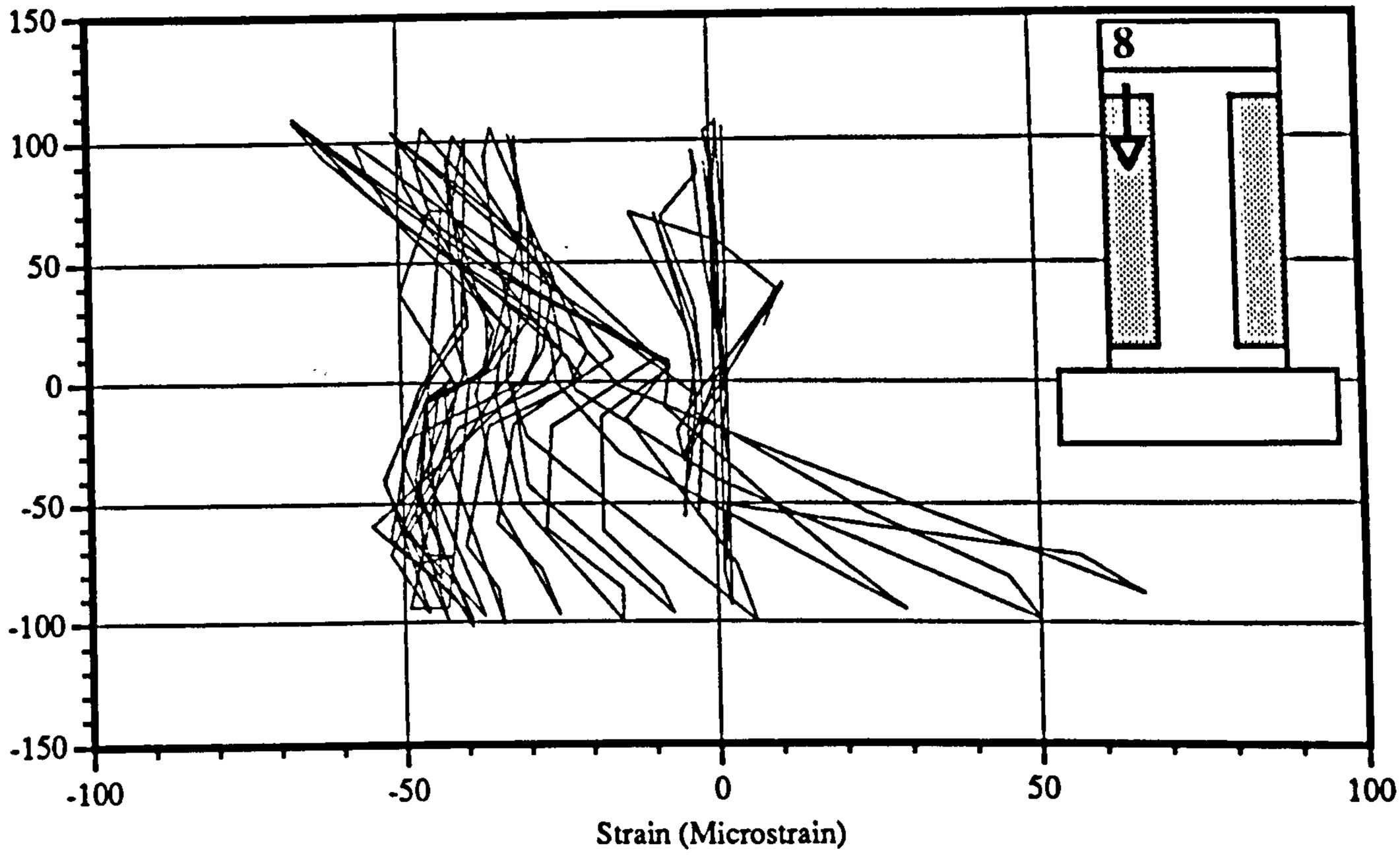


Fig. AII (R9) 5 Force - Steel Strain for SWR9 at Node 8

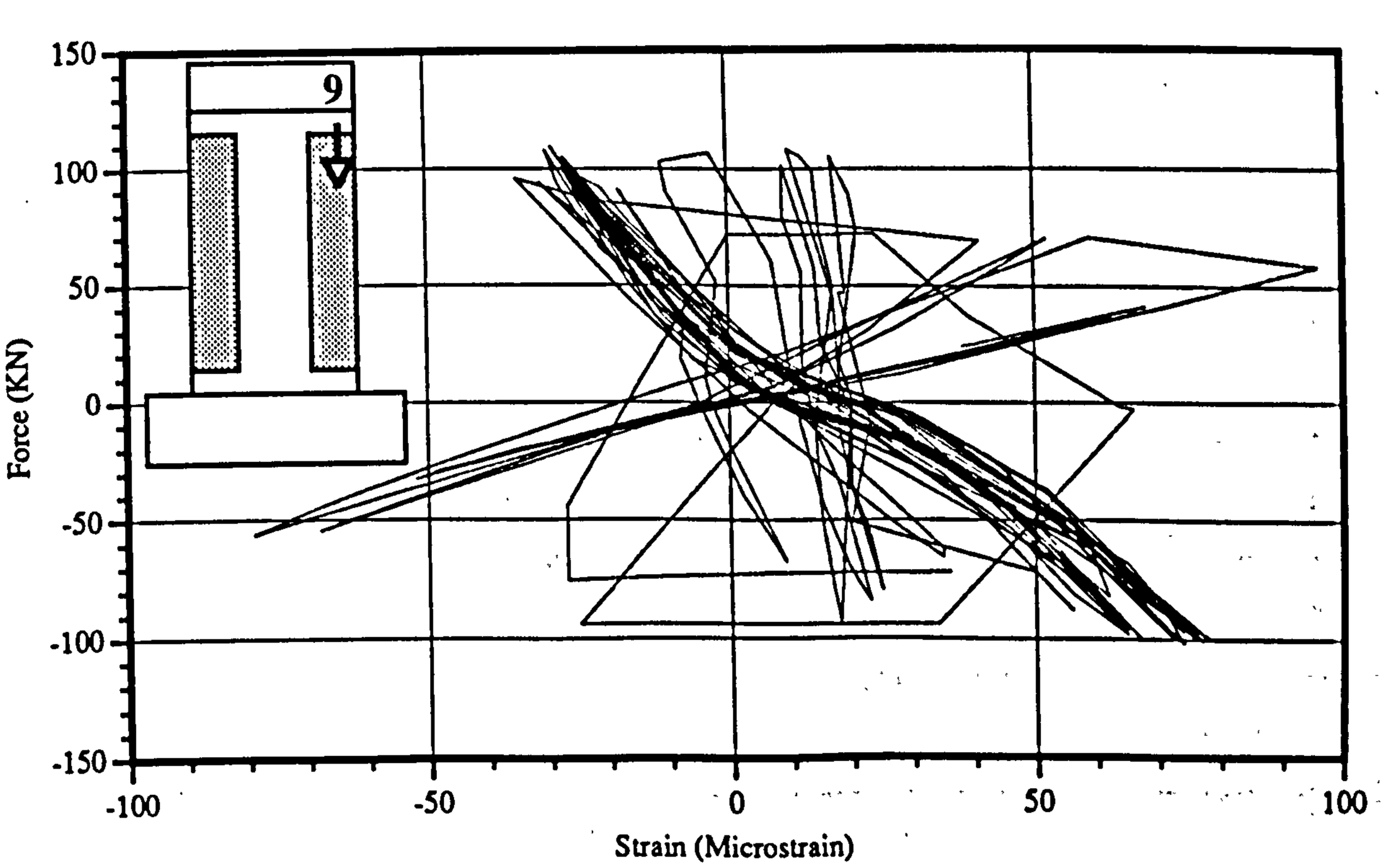


Fig. AII (R9) 6 Force - Steel Strain for SWR9 at Node 9

AII.5 : Force-Steel Strain for SWR21

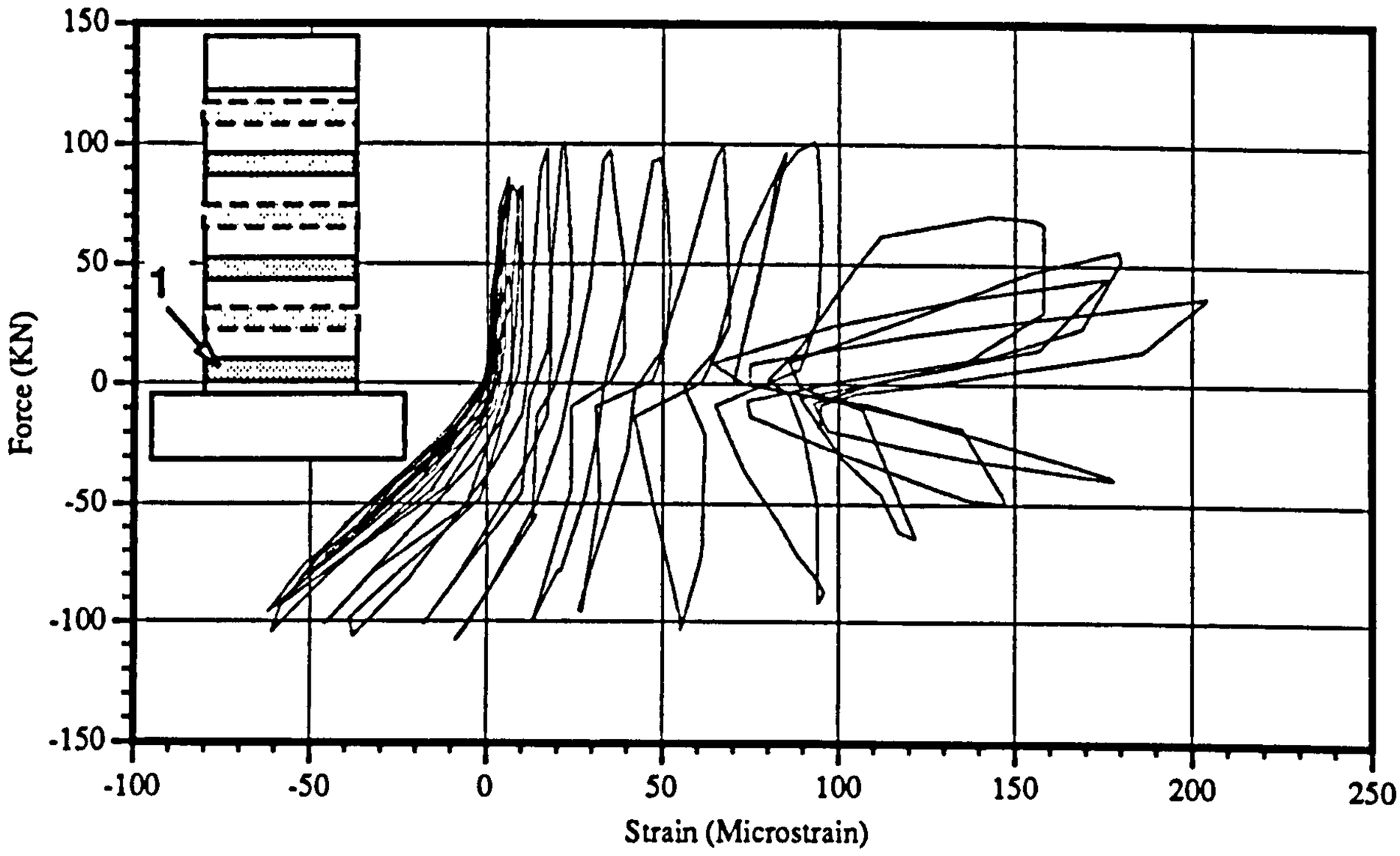


Fig. AII (R21) 1 Force - Steel Strain for SWR21 at Node 1

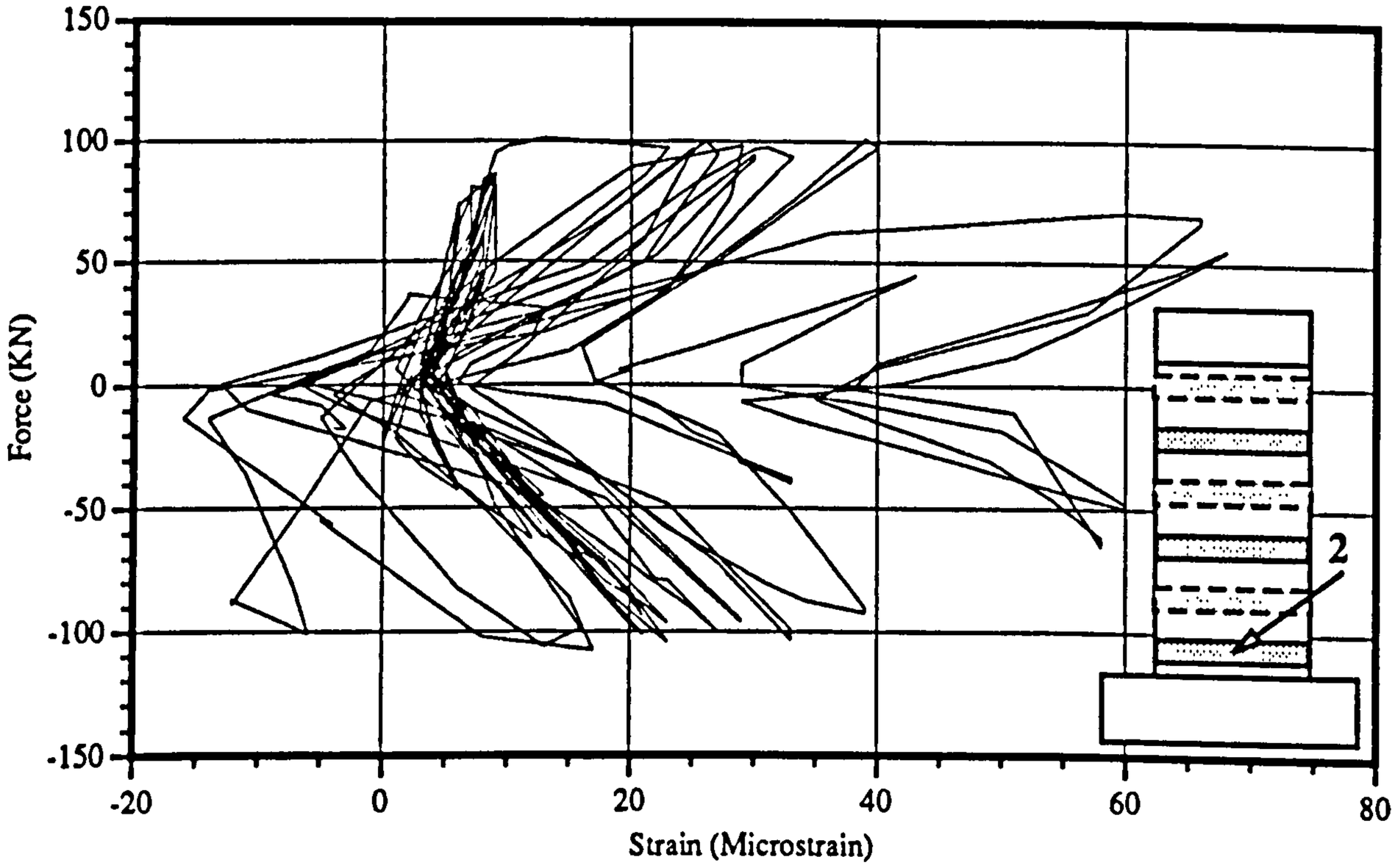


Fig. AII (R21) 2 Force - Steel Strain for SWR21 at Node 2

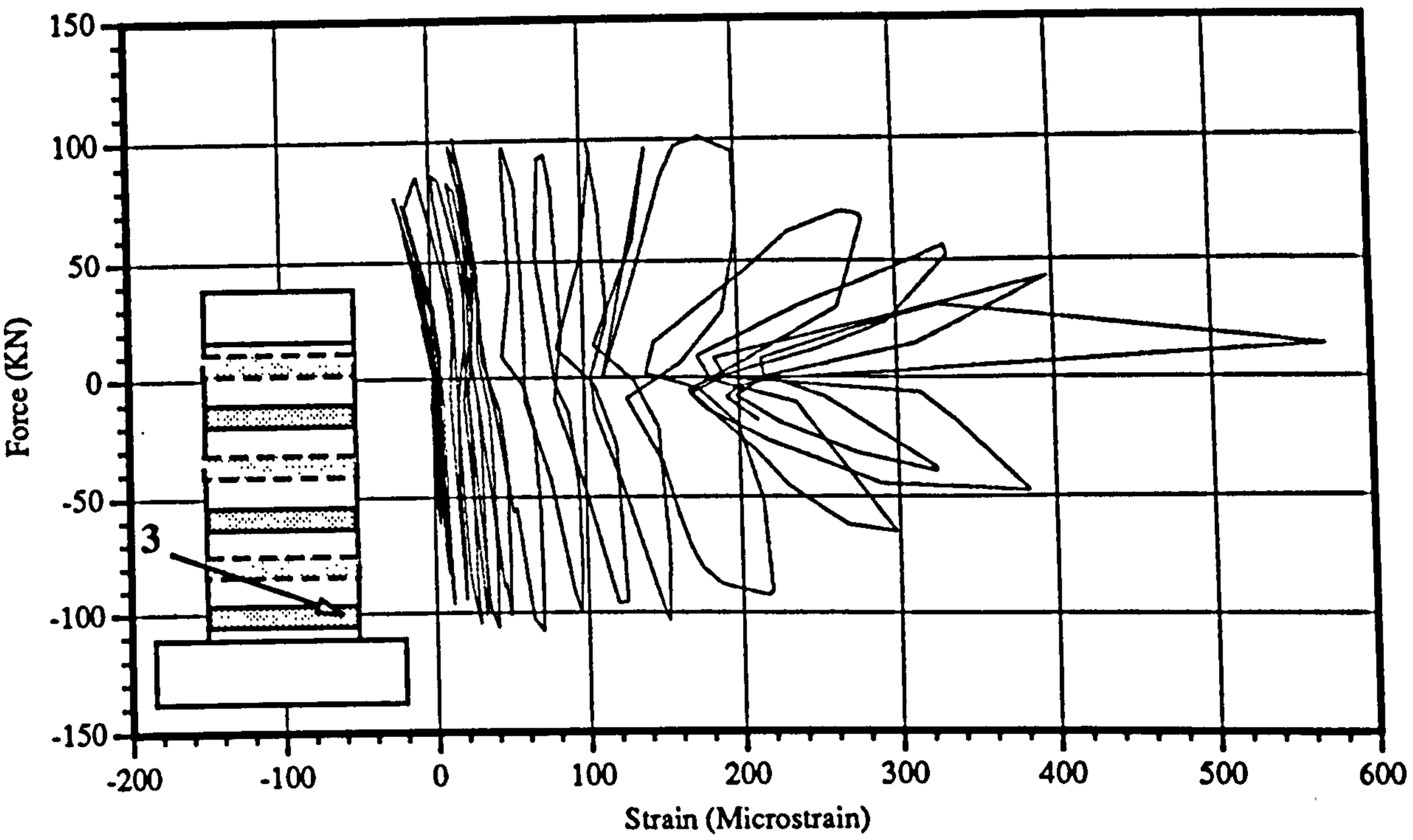


Fig. AII (R21) 3 Force - Steel Strain for SWR21 at Node 3

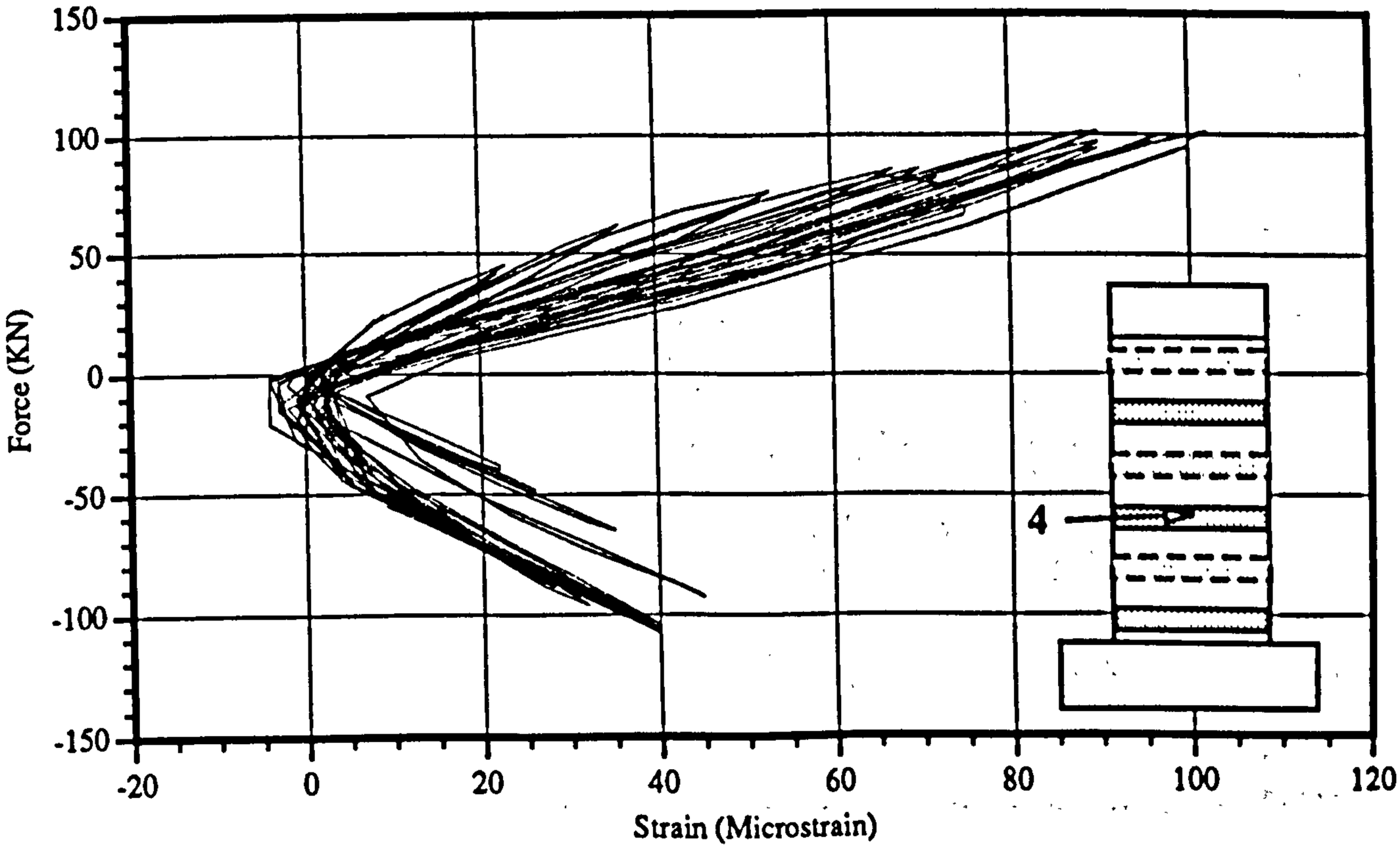


Fig. AII (R21) 4 Force - Steel Strain for SWR21 at Node 4

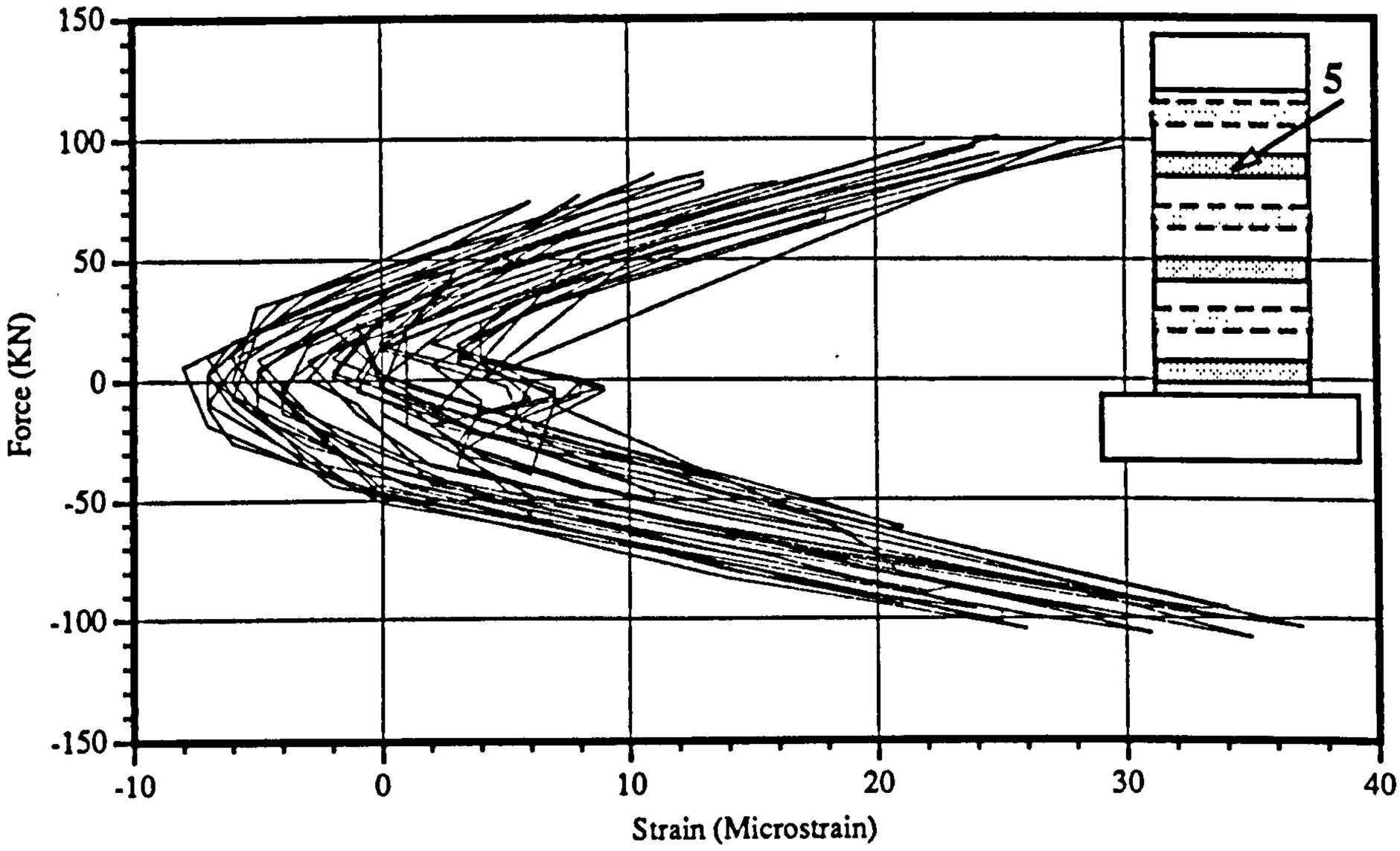


Fig. AII (R21) 5 Force - Steel Strain for SWR21 at Node 5

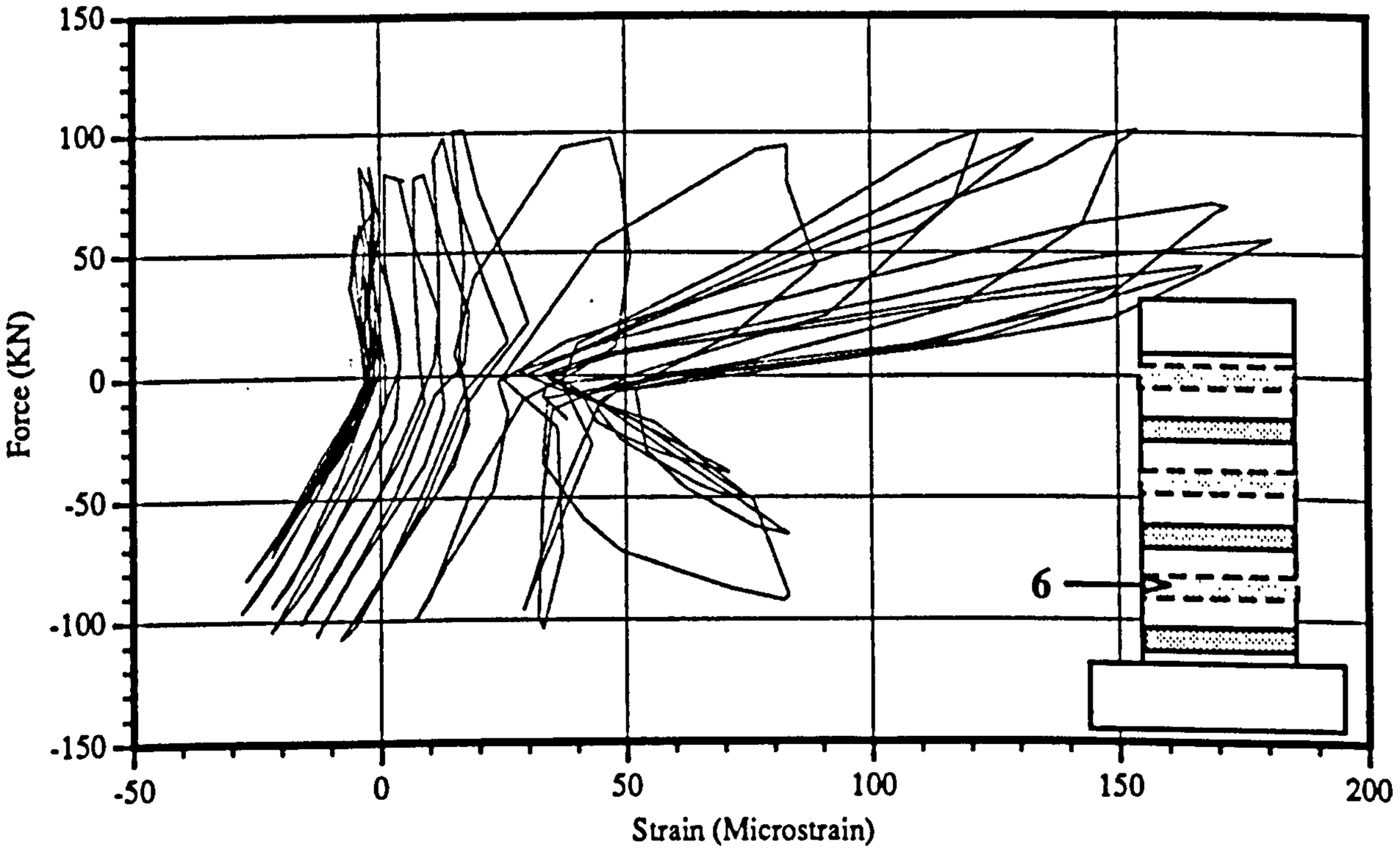


Fig. AII (R21) 6 Force - Steel Strain for SWR21 at Node 6

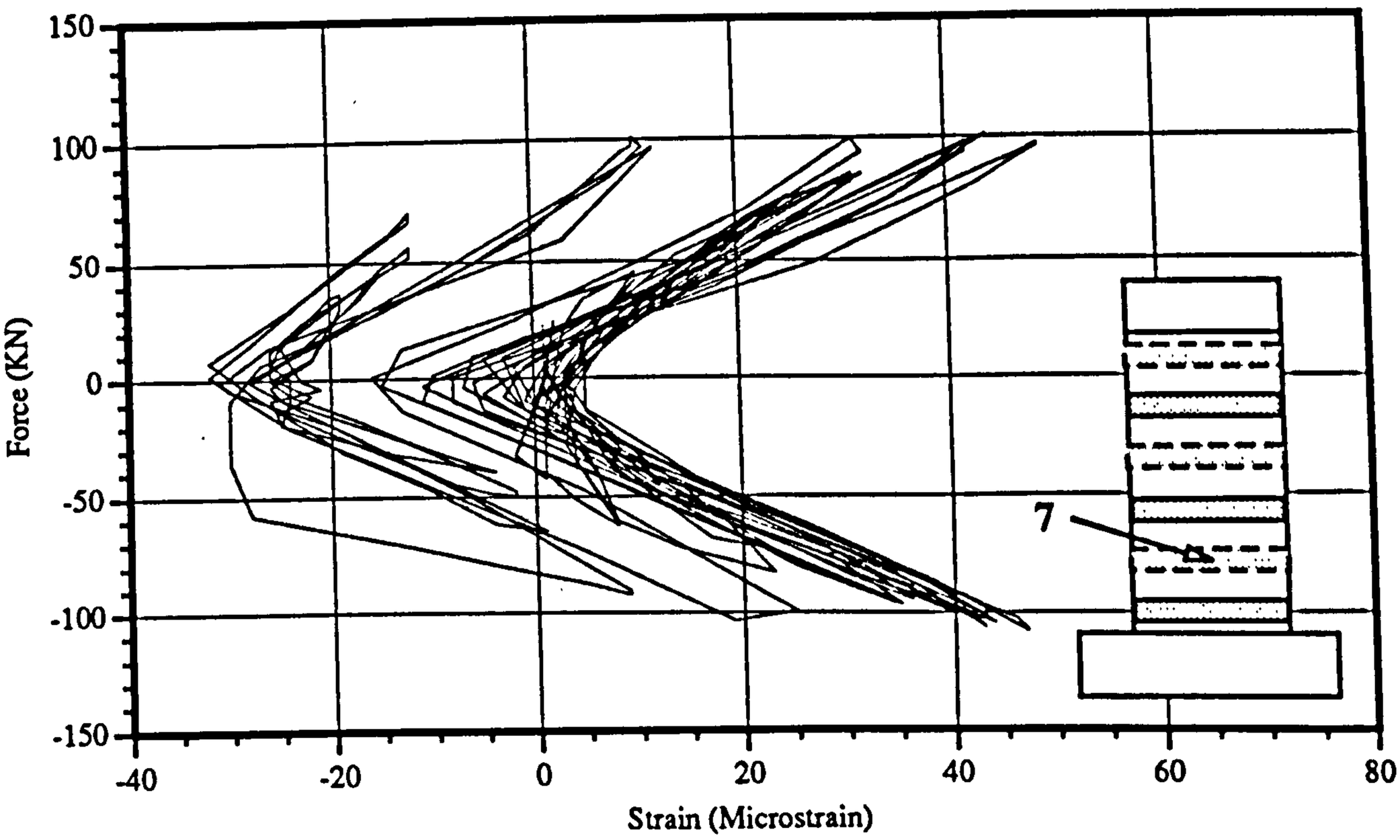


Fig. AII (R21) 7 Force - Steel Strain for SWR21 at Node 7

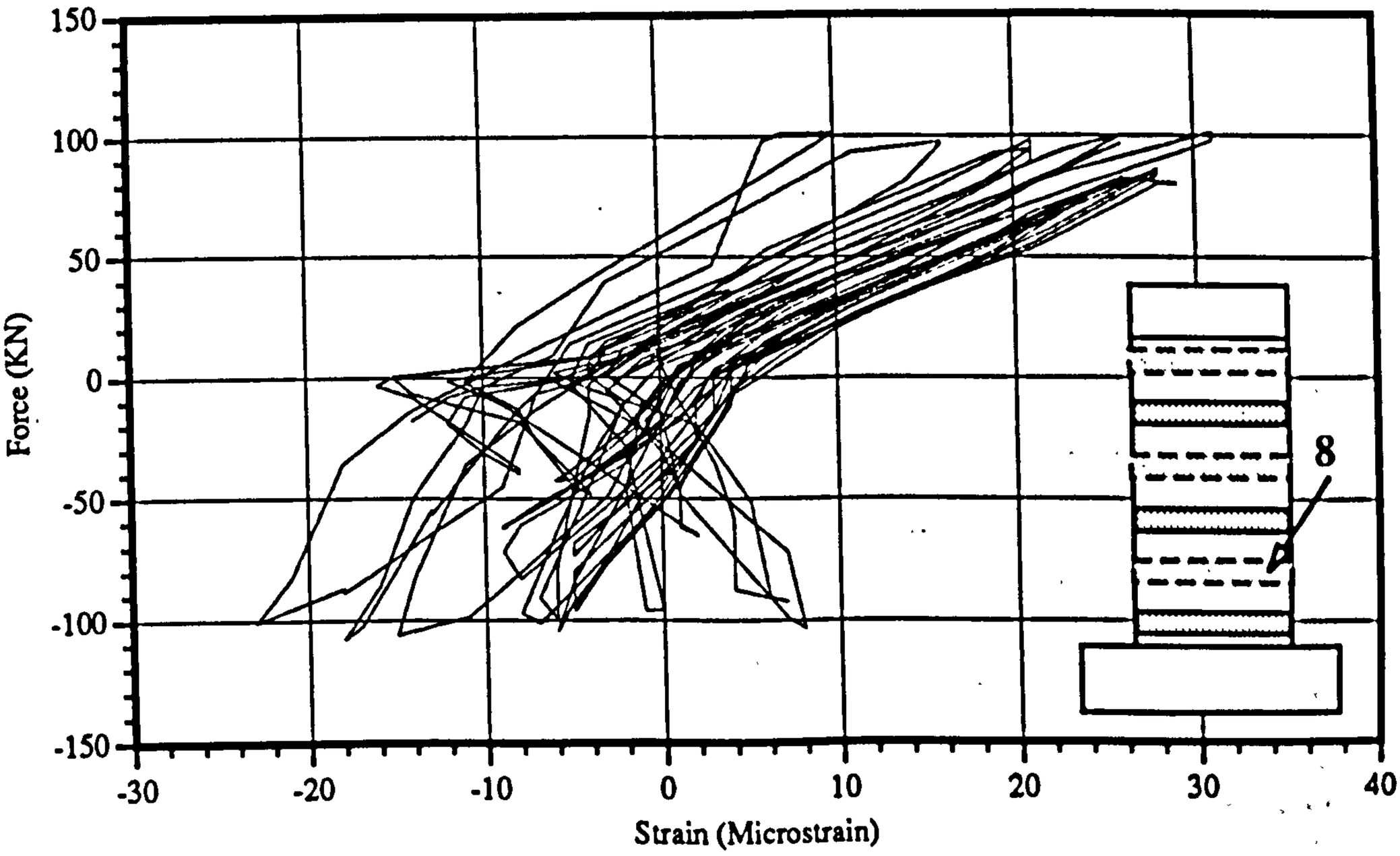


Fig. AII (R21) 8 Force - Steel Strain for SWR21 at Node 8

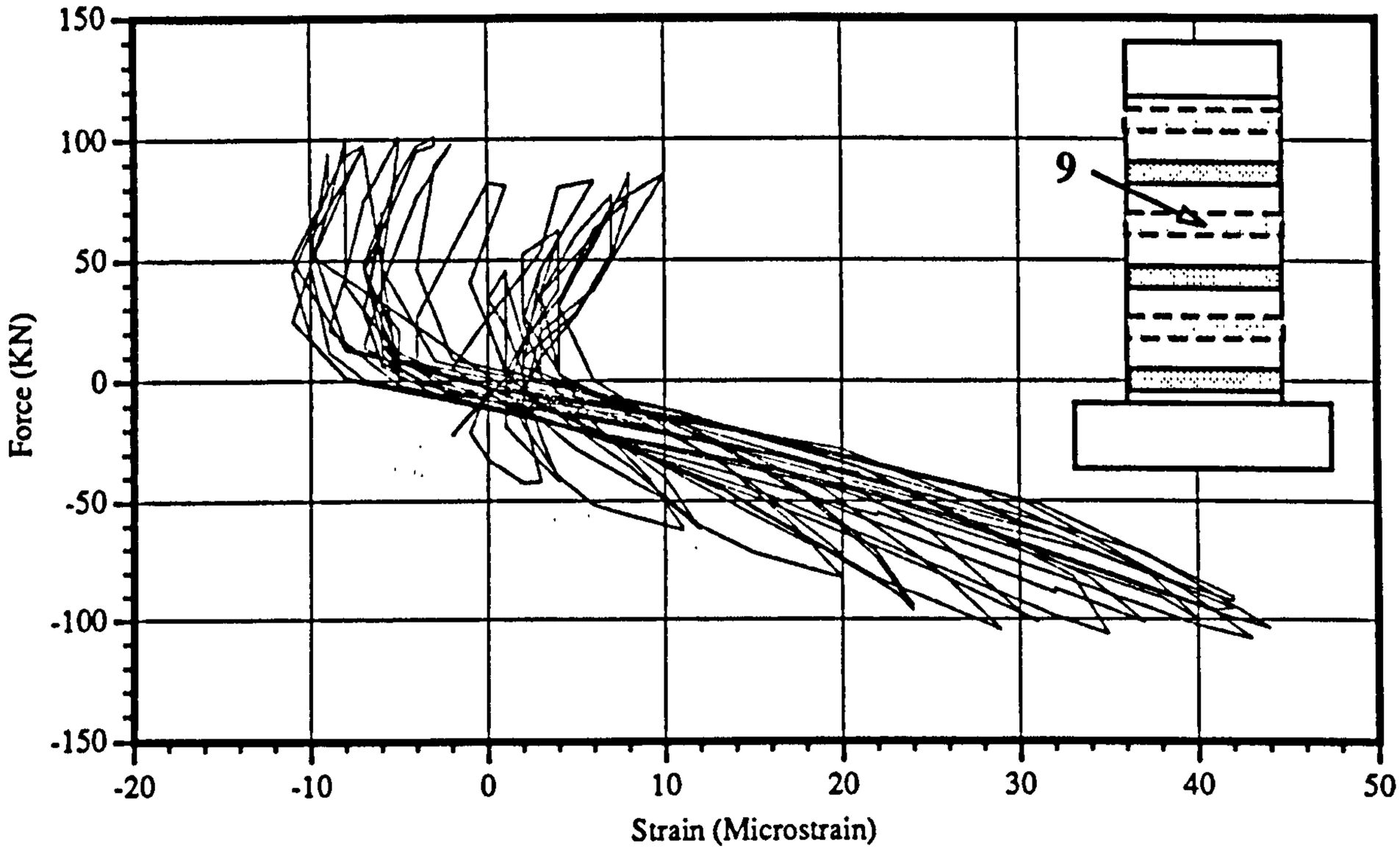


Fig. AII (R21) 9 Force - Steel Strain for SWR21 at Node 9

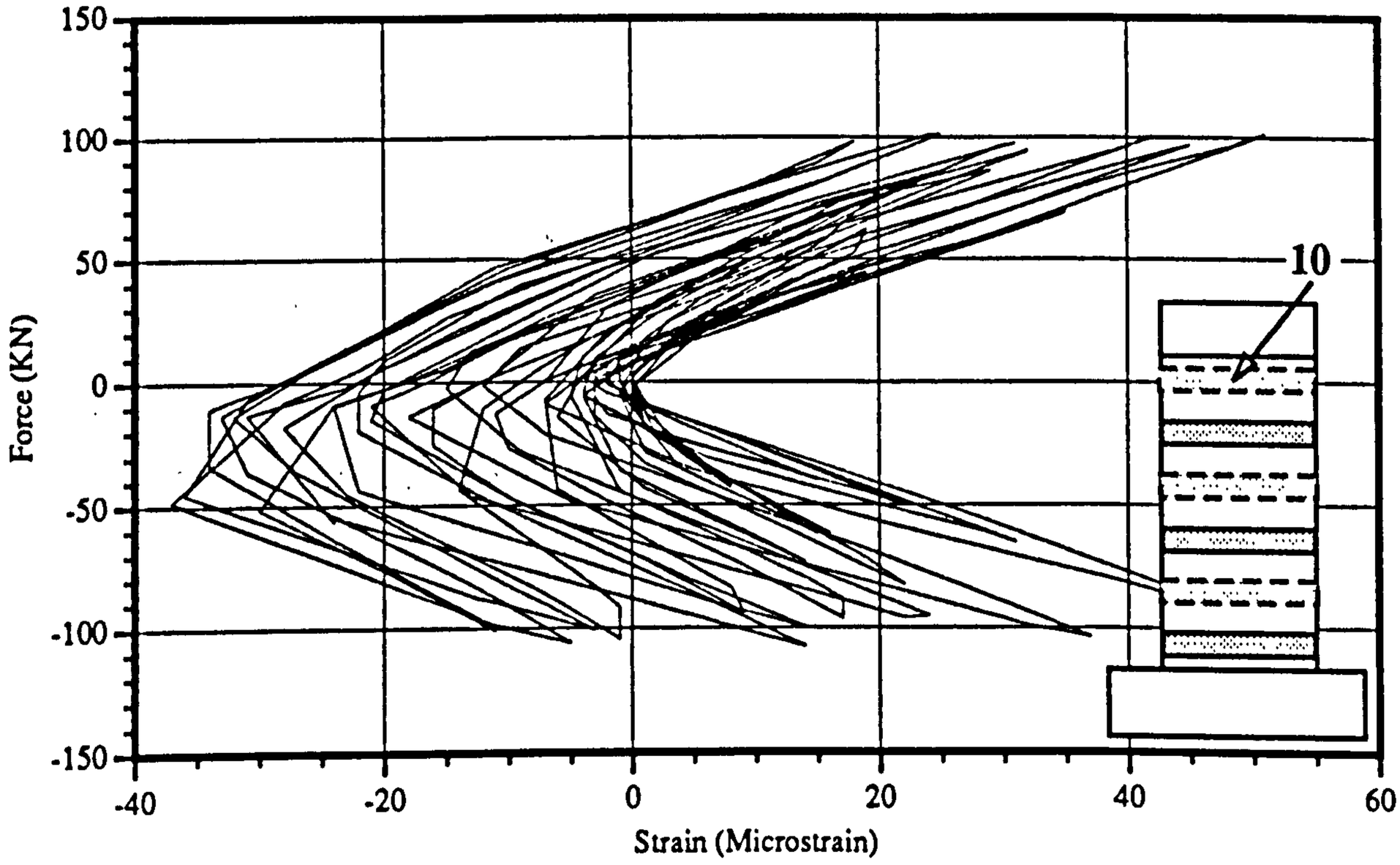


Fig. AII (R21) 10 Force - Steel Strain for SWR21 at Node 10

AII.6 Force-Steel Strain for SWR24

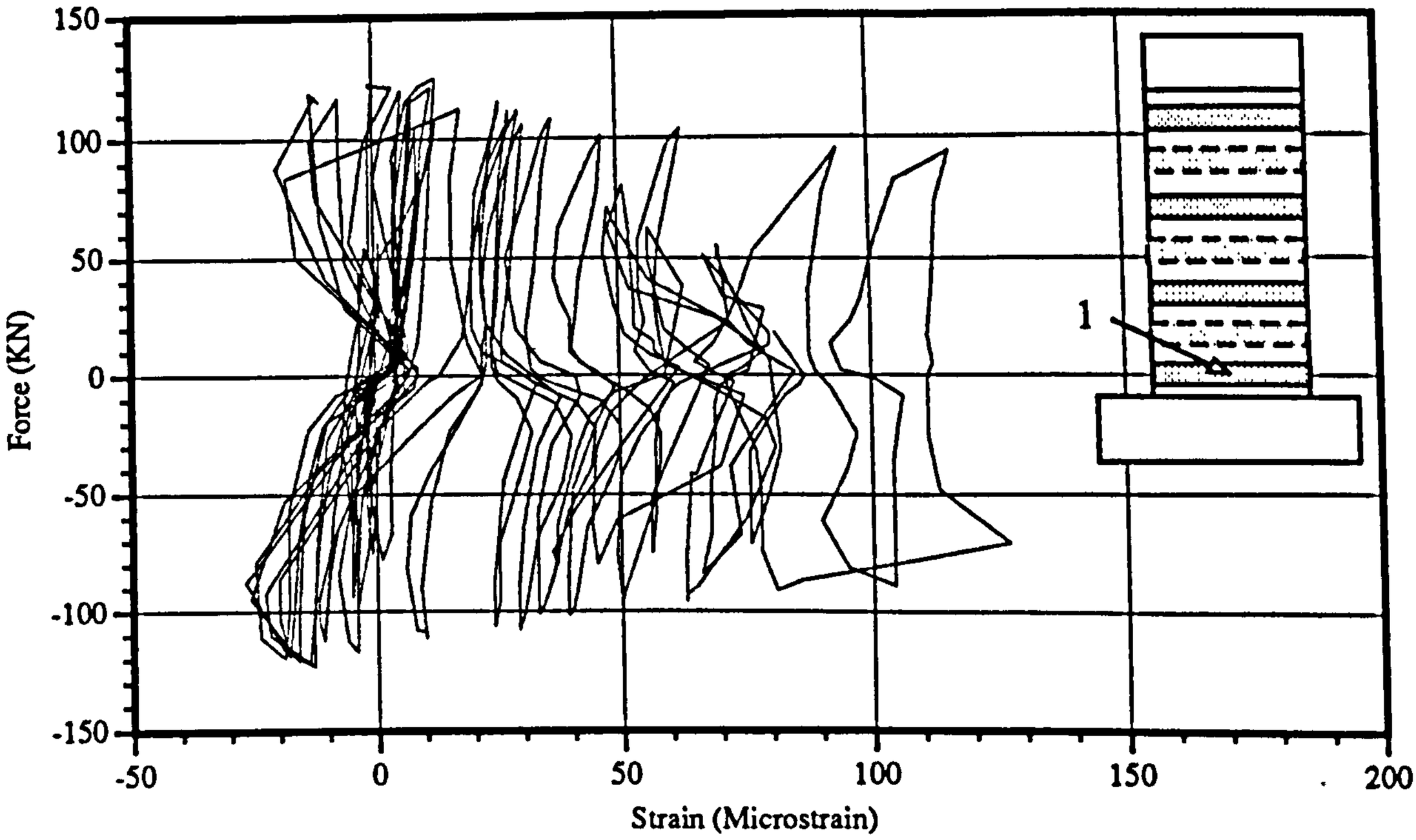


Fig. AII (R24) 1 Force - Steel Strain for SWR24 at Node 1

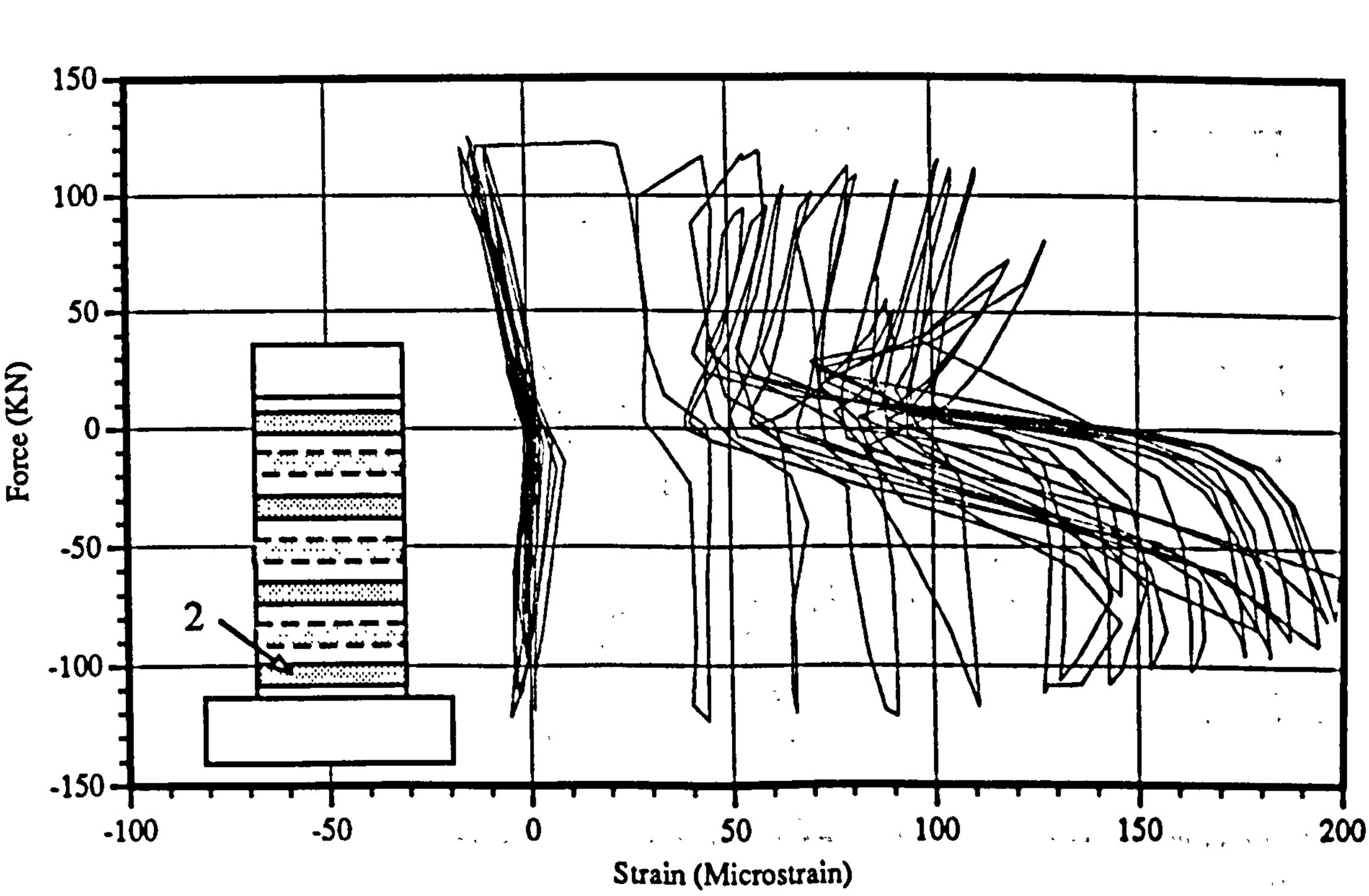


Fig. AII (R24) 2 Force - Steel Strain for SWR24 at Node 2

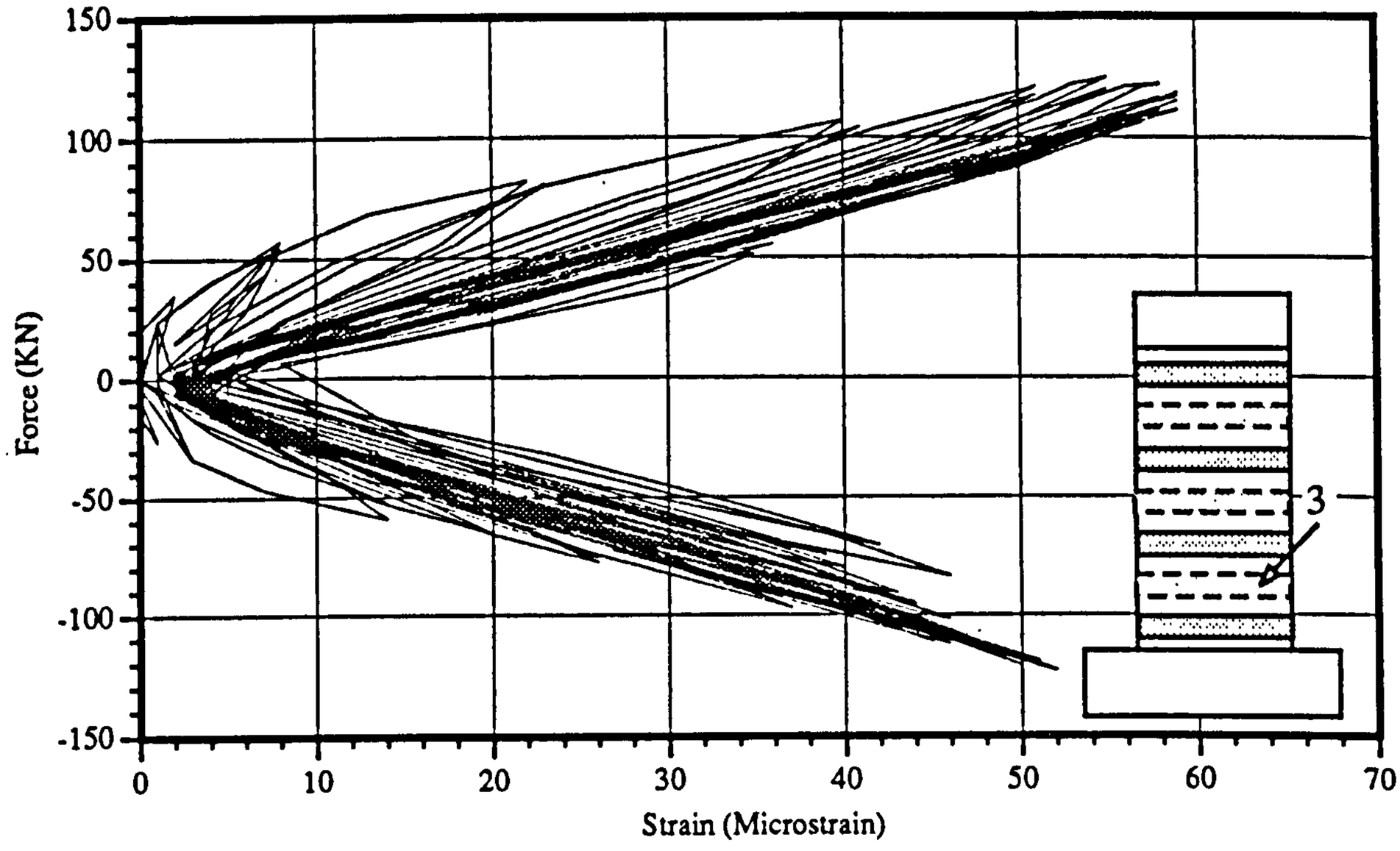


Fig. AII (R24) 3 Force - Steel Strain for SWR24 at Node 3

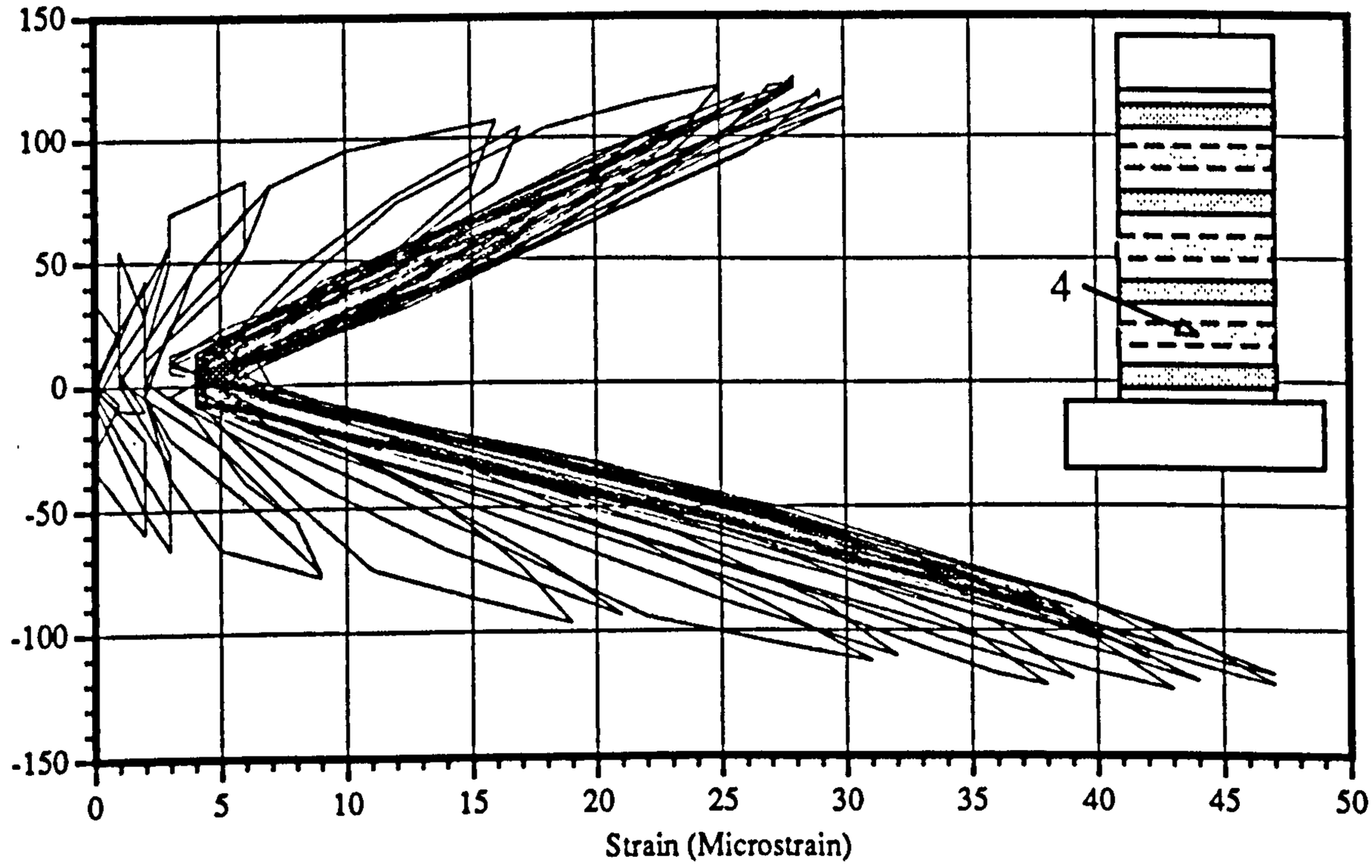


Fig. AII (R24) 4 Force - Steel Strain for SWR24 at Node 4

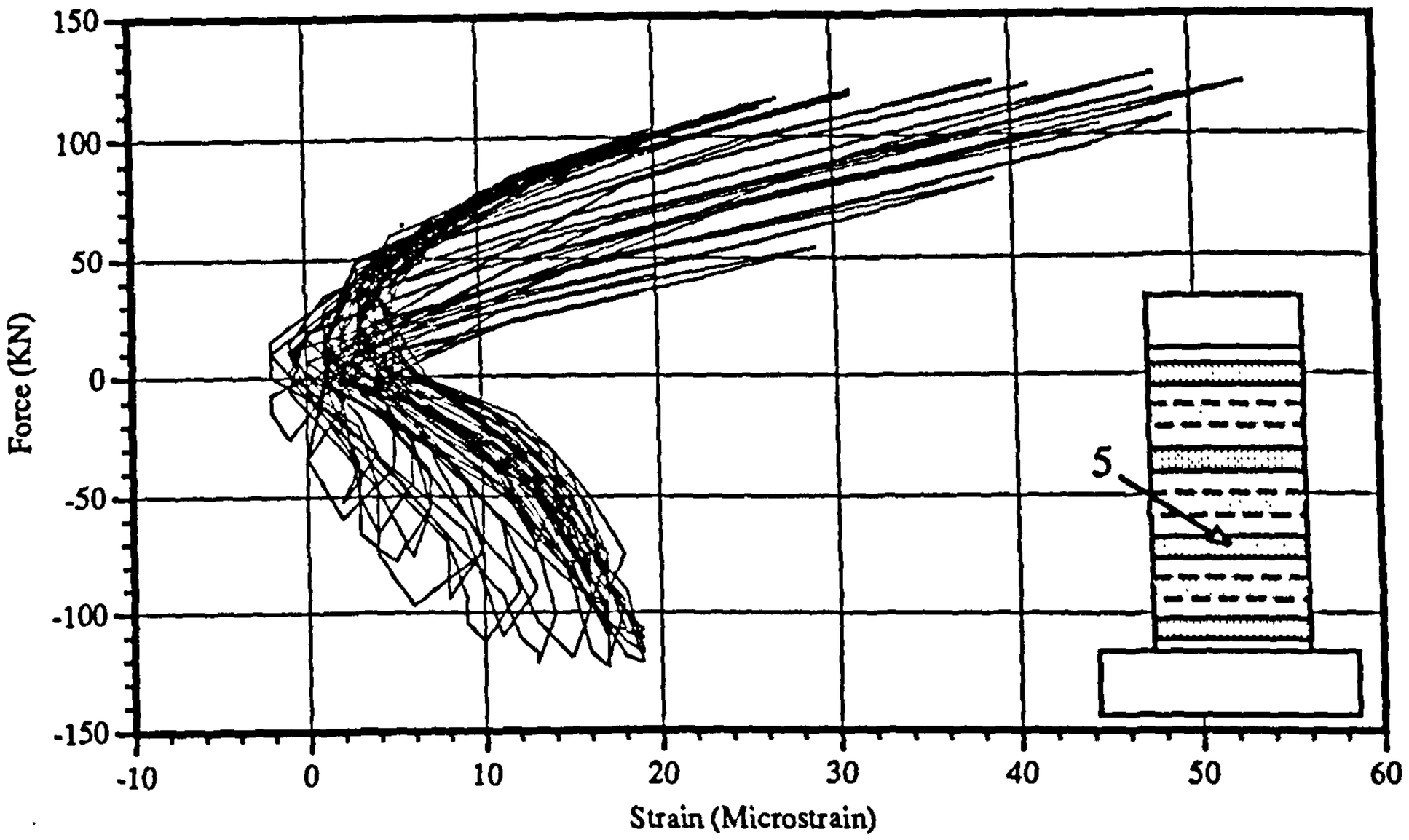


Fig. AII (R24) 5 Force - Steel Strain for SWR24 at Node 5

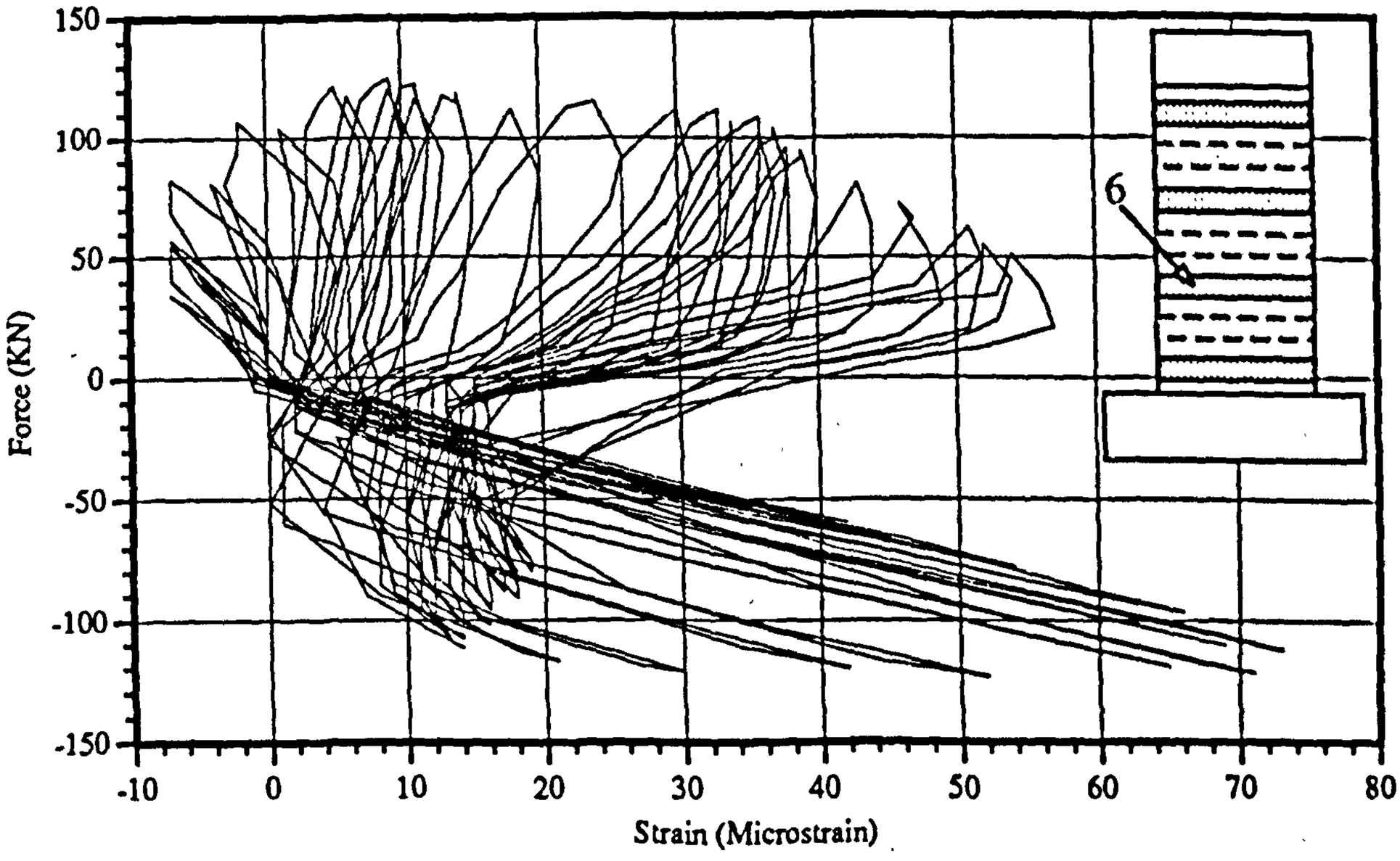


Fig. AII (R24) 6 Force - Steel Strain for SWR24 at Node 6

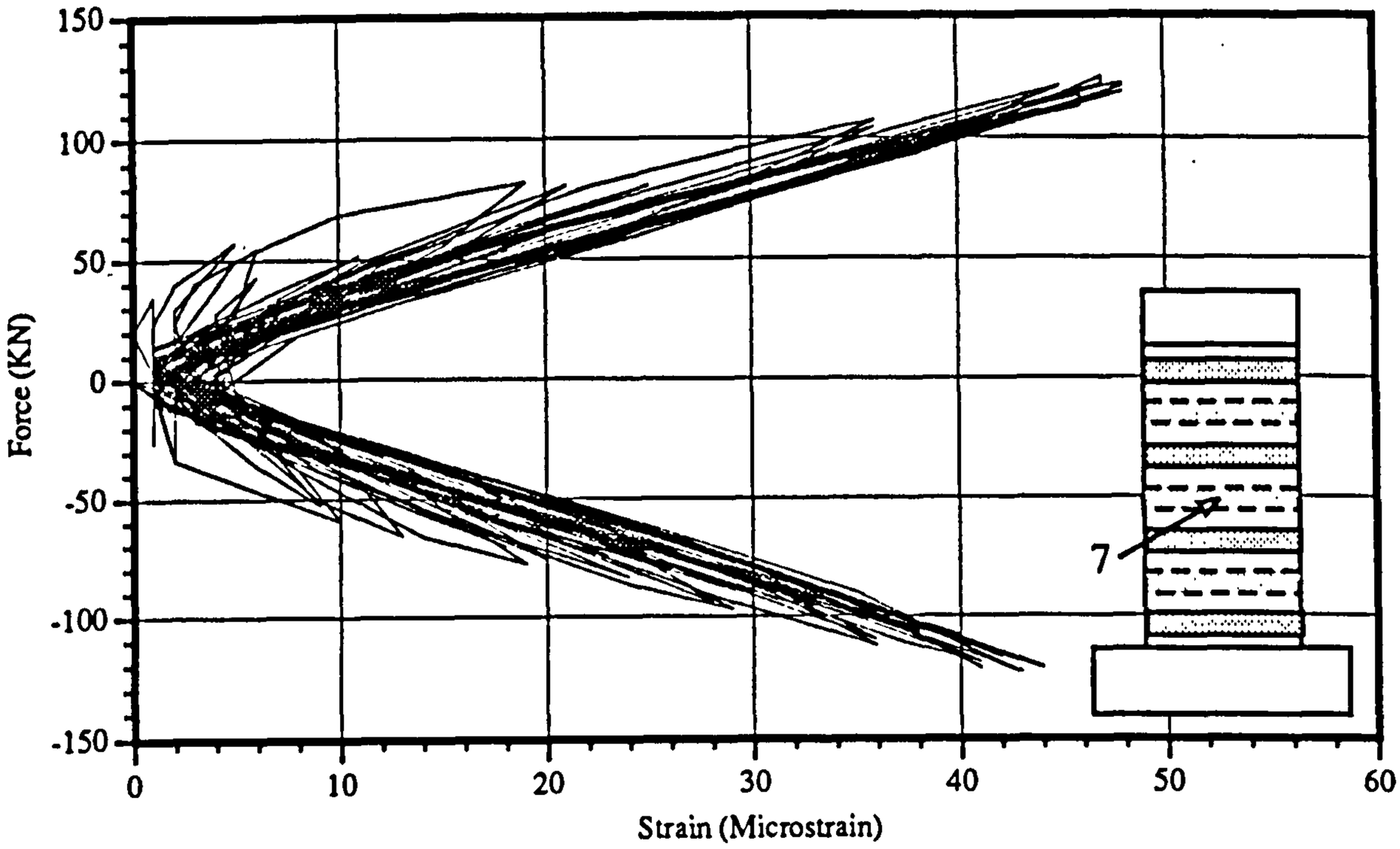


Fig. AII (R24) 7 Force - Steel Strain for SWR24 at Node 7

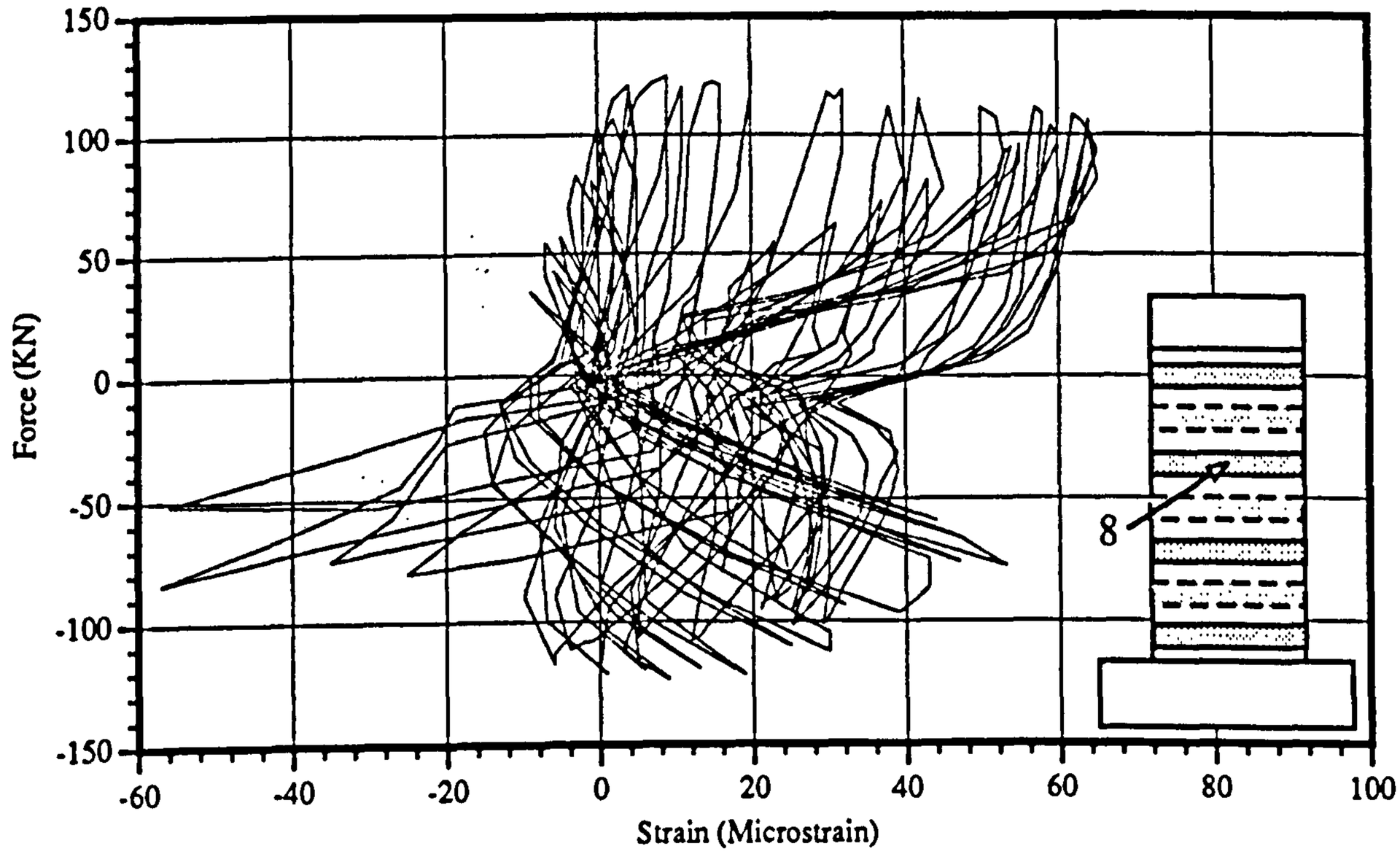


Fig. AII (R24) 8 Force - Steel Strain for SWR24 at Node 8

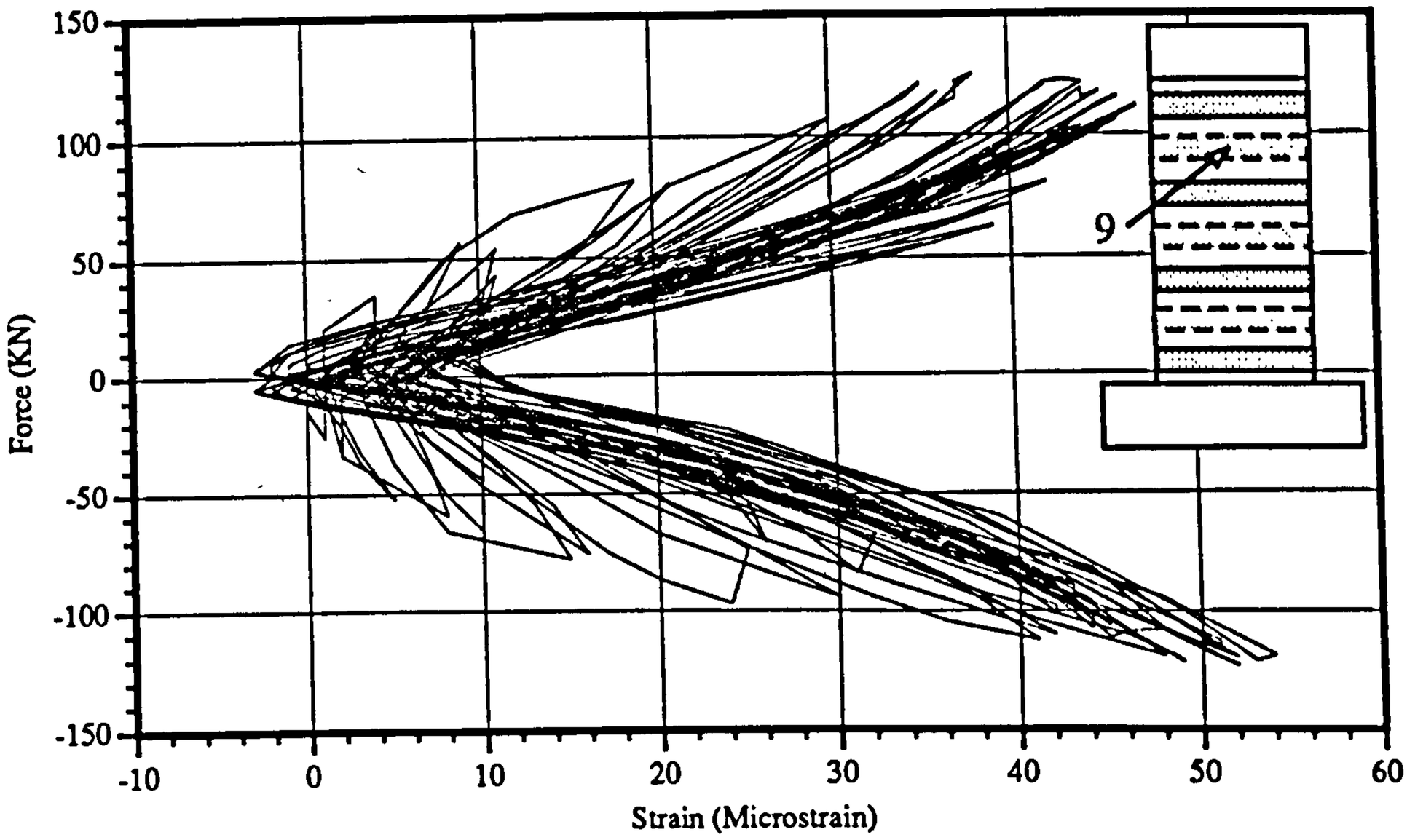


Fig. AII (R24) 9 Force - Steel Strain for SWR24 at Node 9

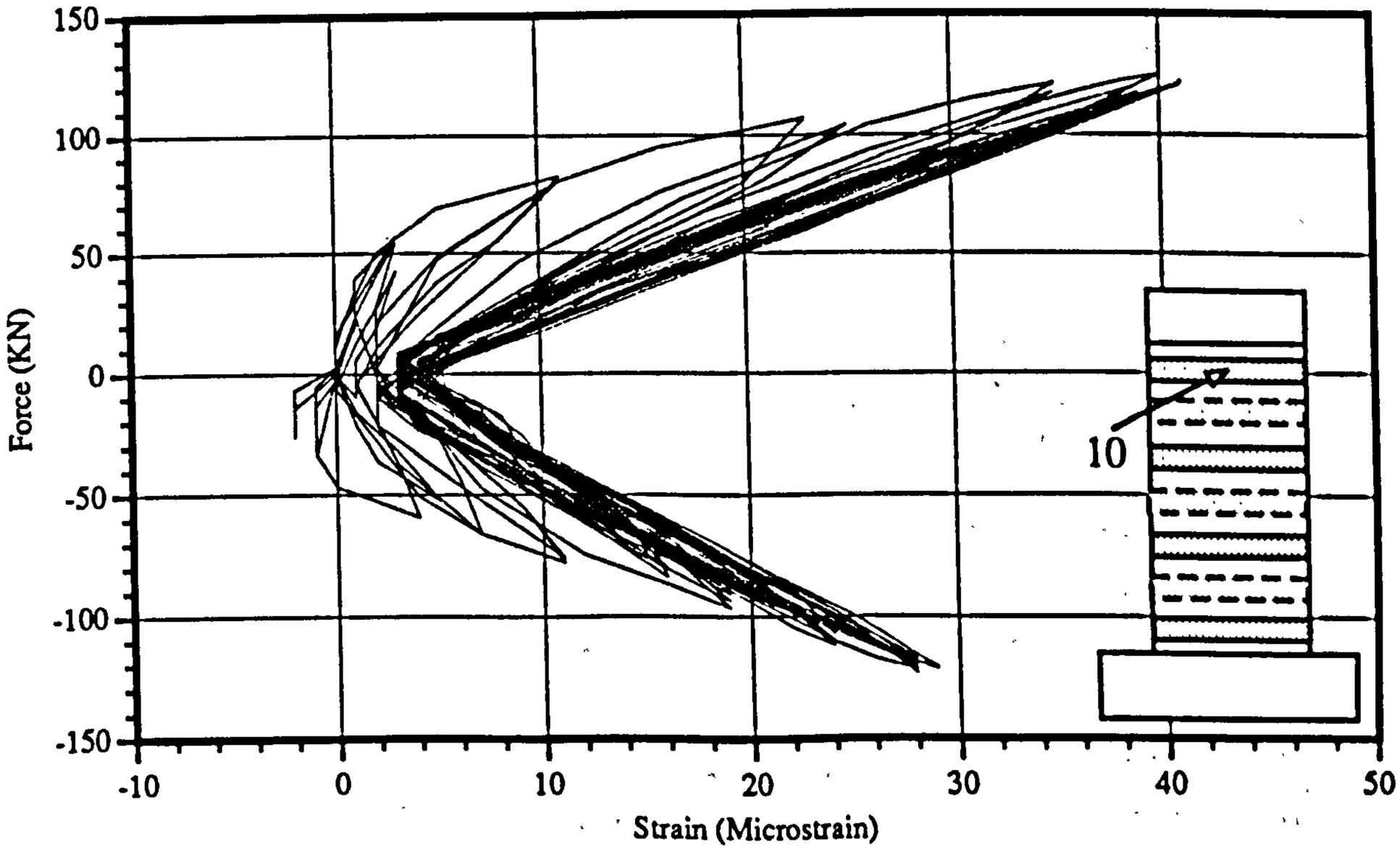


Fig. AII (R24) 10 Force - Steel Strain for SWR24 at Node 10

AII.7 : Force-Steel Strain for SW31

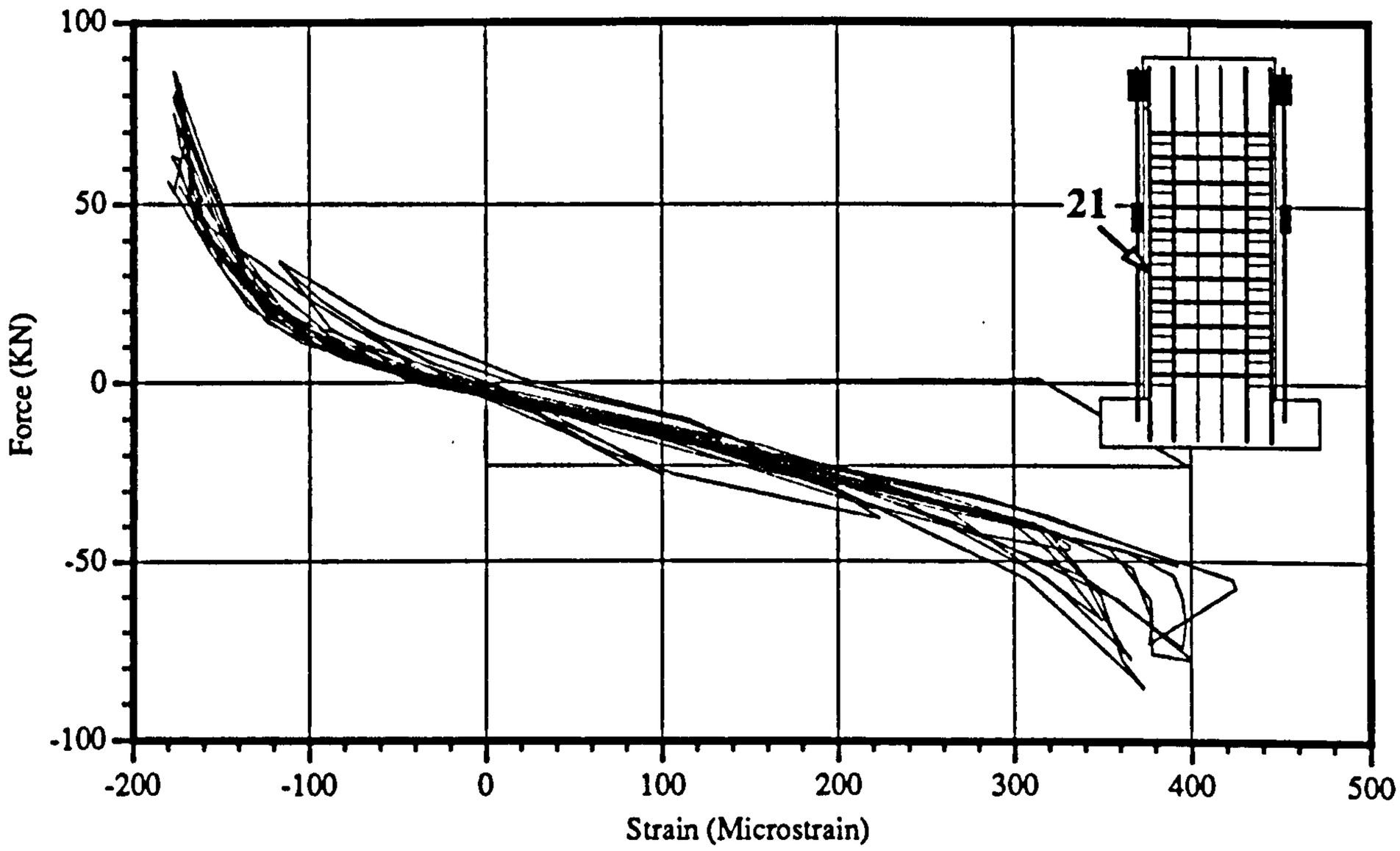


Fig. AII (31) 1 Force - Steel Strain for SW31 at Node 21

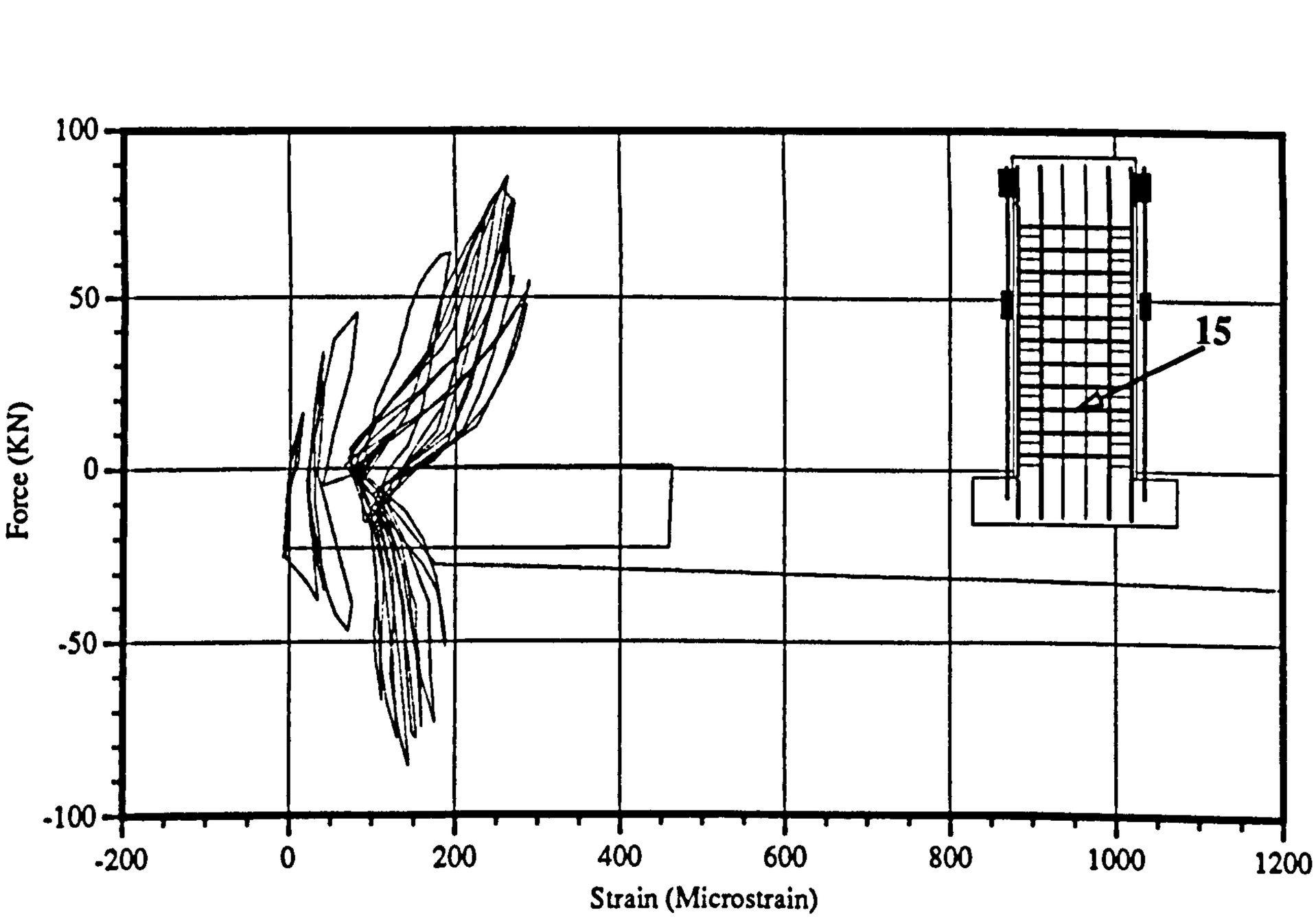


Fig. AII (31) 2 Force - Steel Strain for SW31 at Node 15

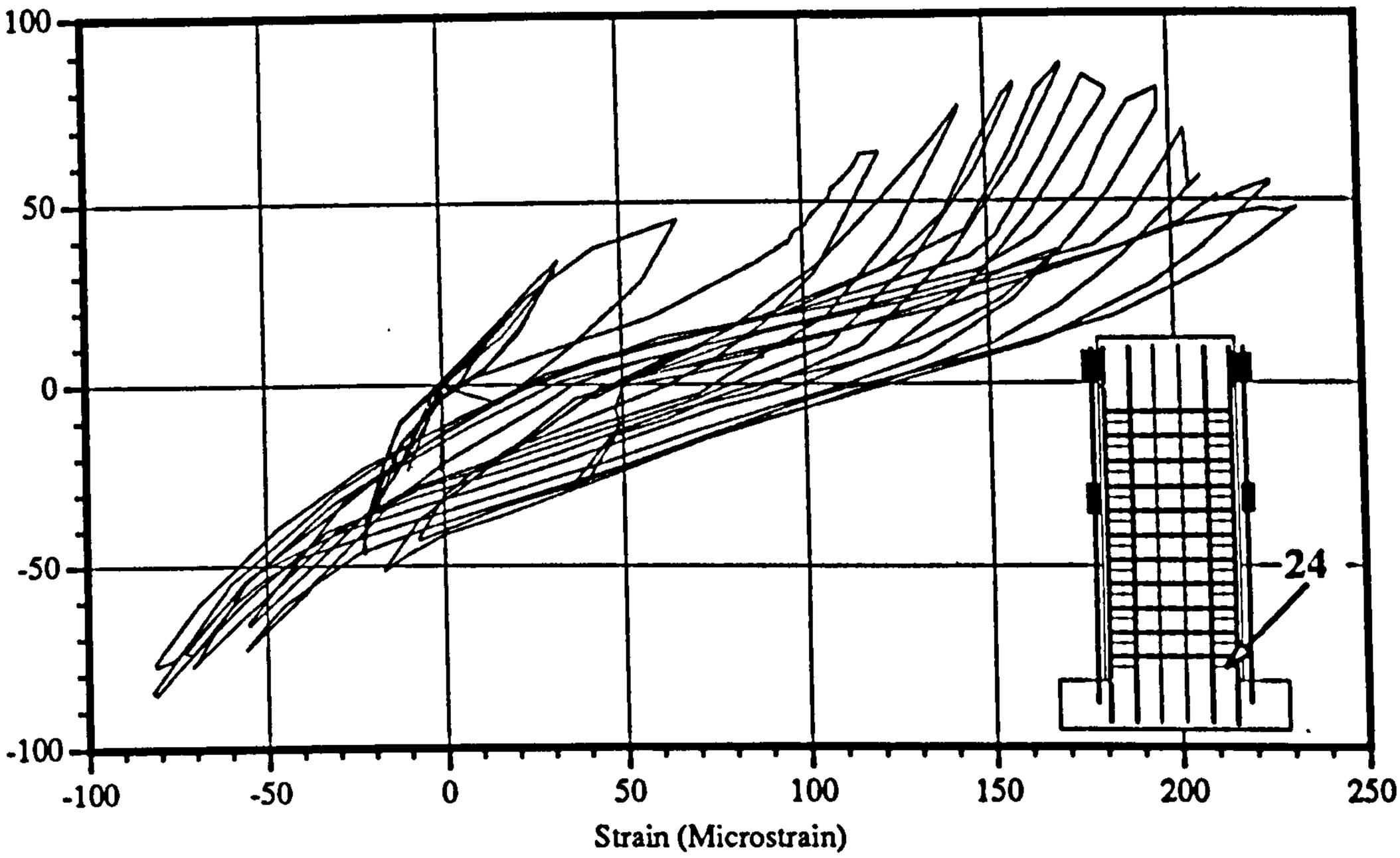


Fig. AII (31) 3 Force - Steel Strain for SW31 at Node 24

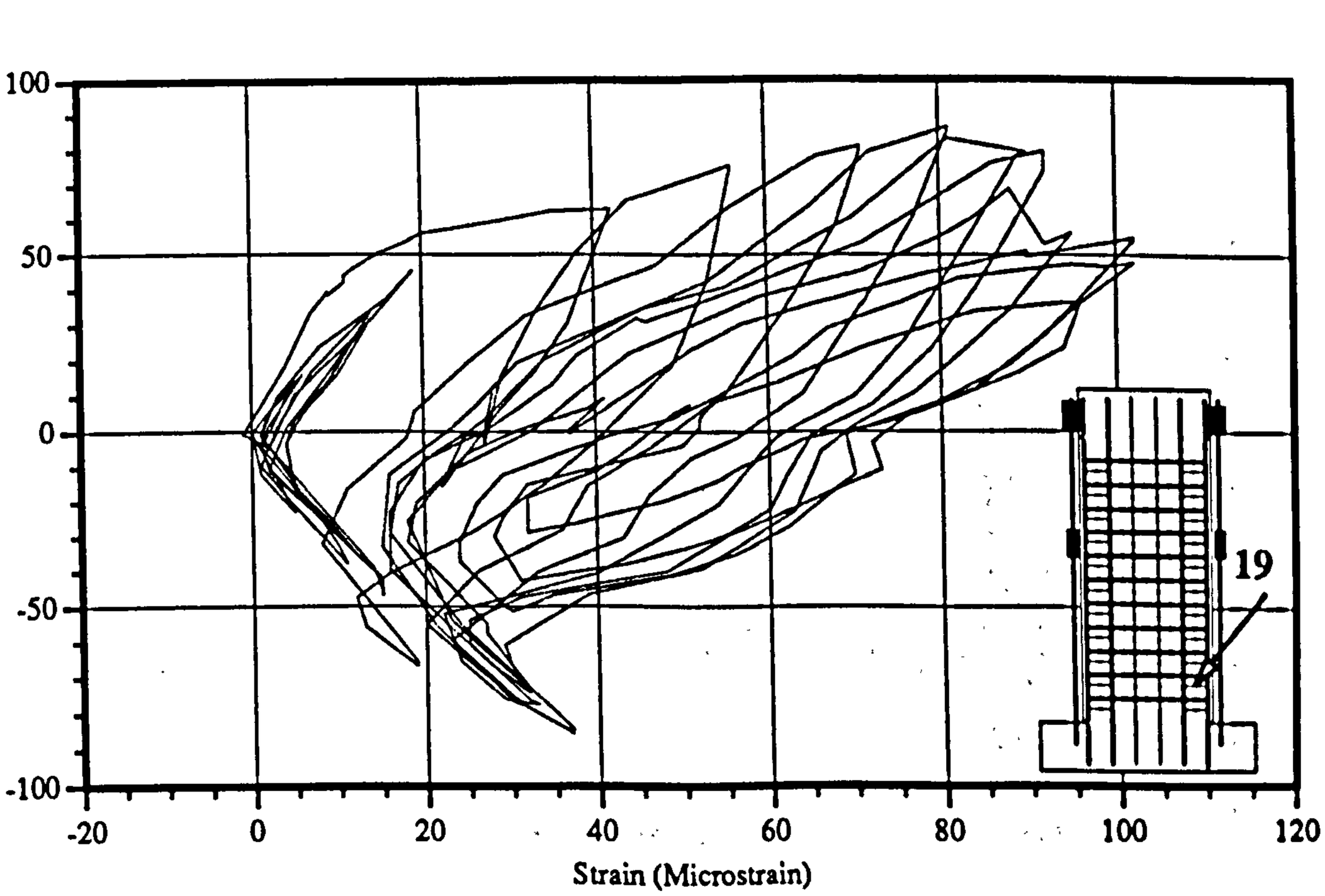


Fig. AII (31) 4. Force - Steel Strain for SW31 at Node 19

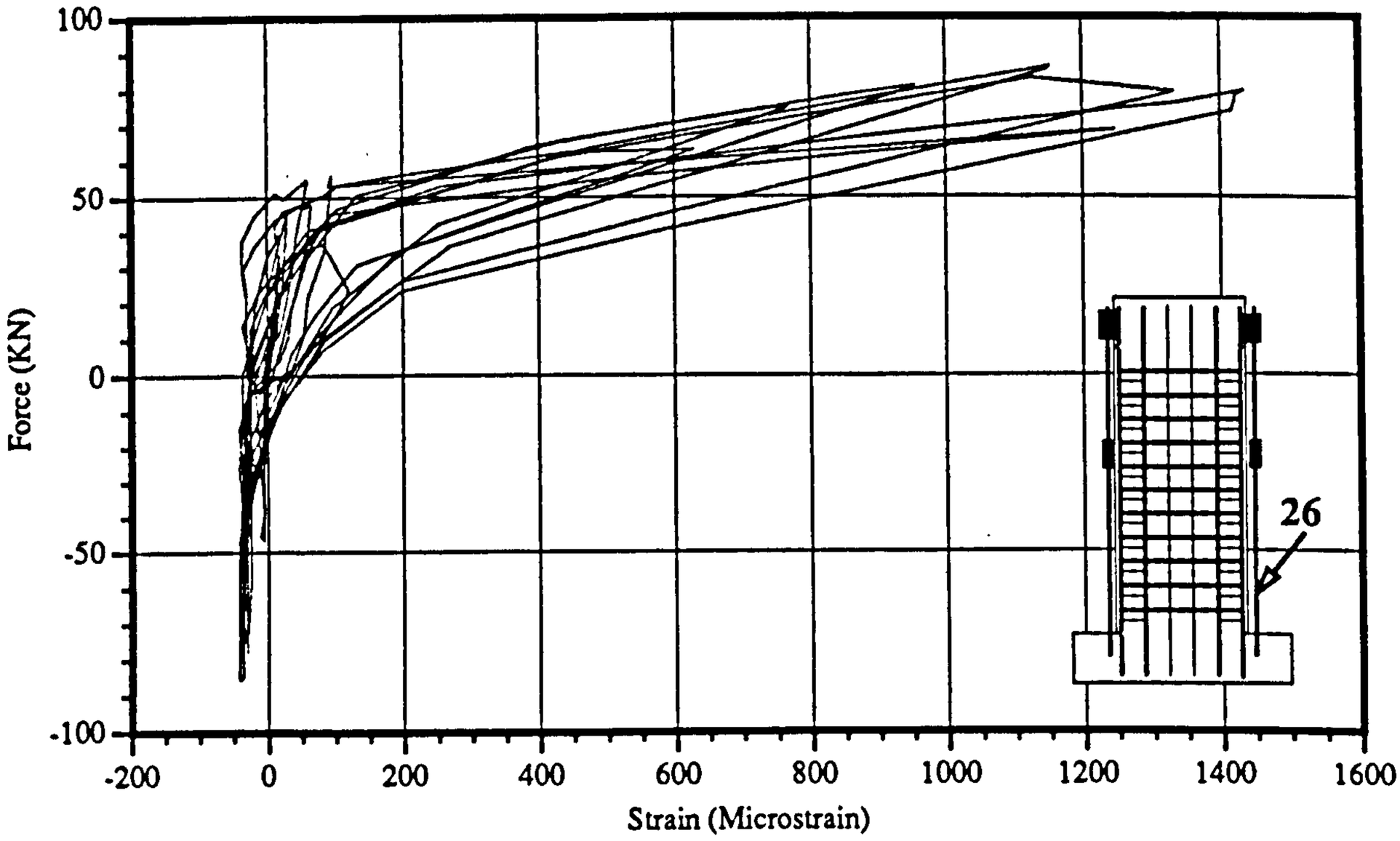


Fig. AII (31) 5 Force - Steel Strain for SW31 at Node 26

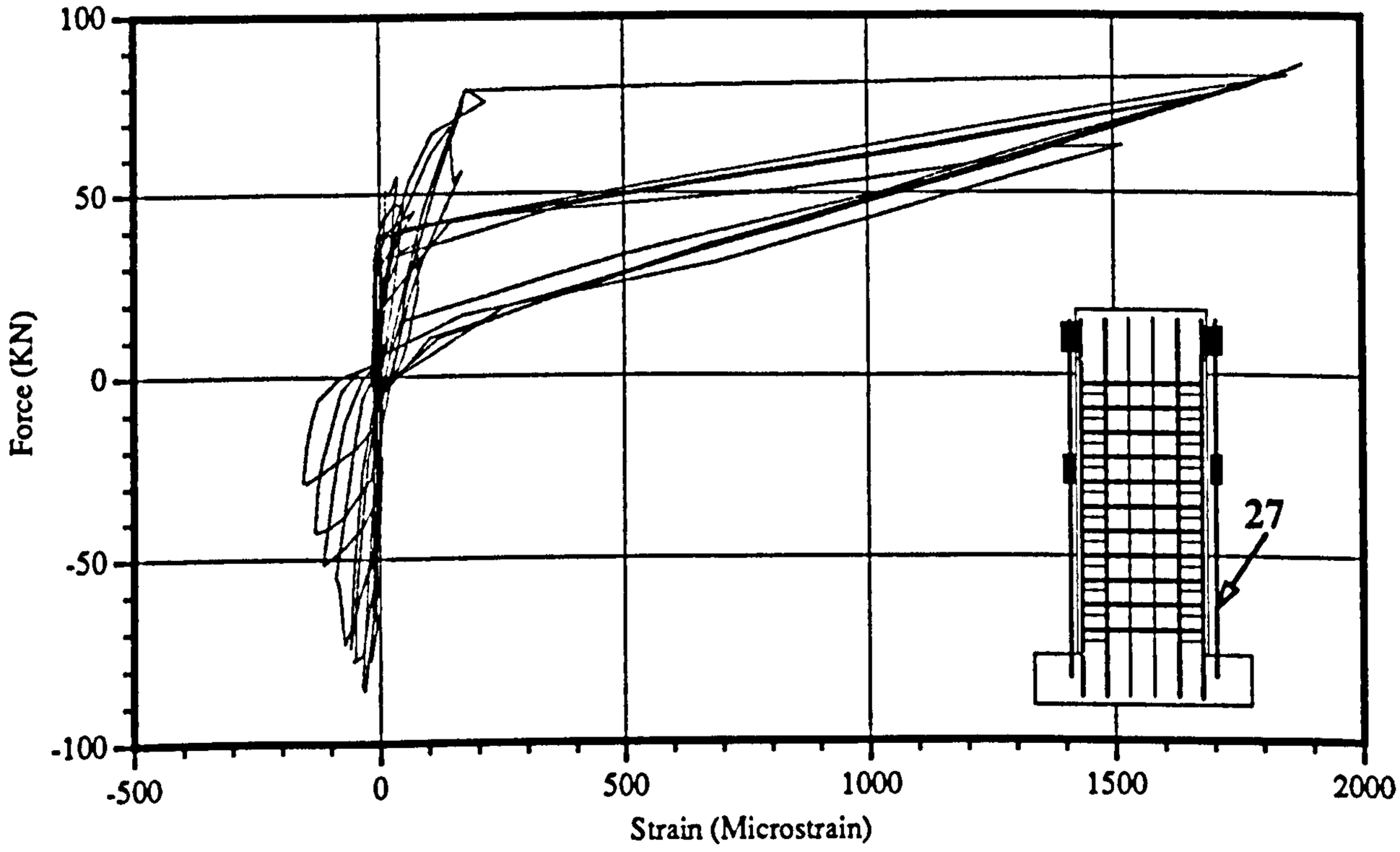


Fig. AII (31) 6 Force - Steel Strain for SW31 at Node 27

AII.8. Force-Steel Strain for SW32

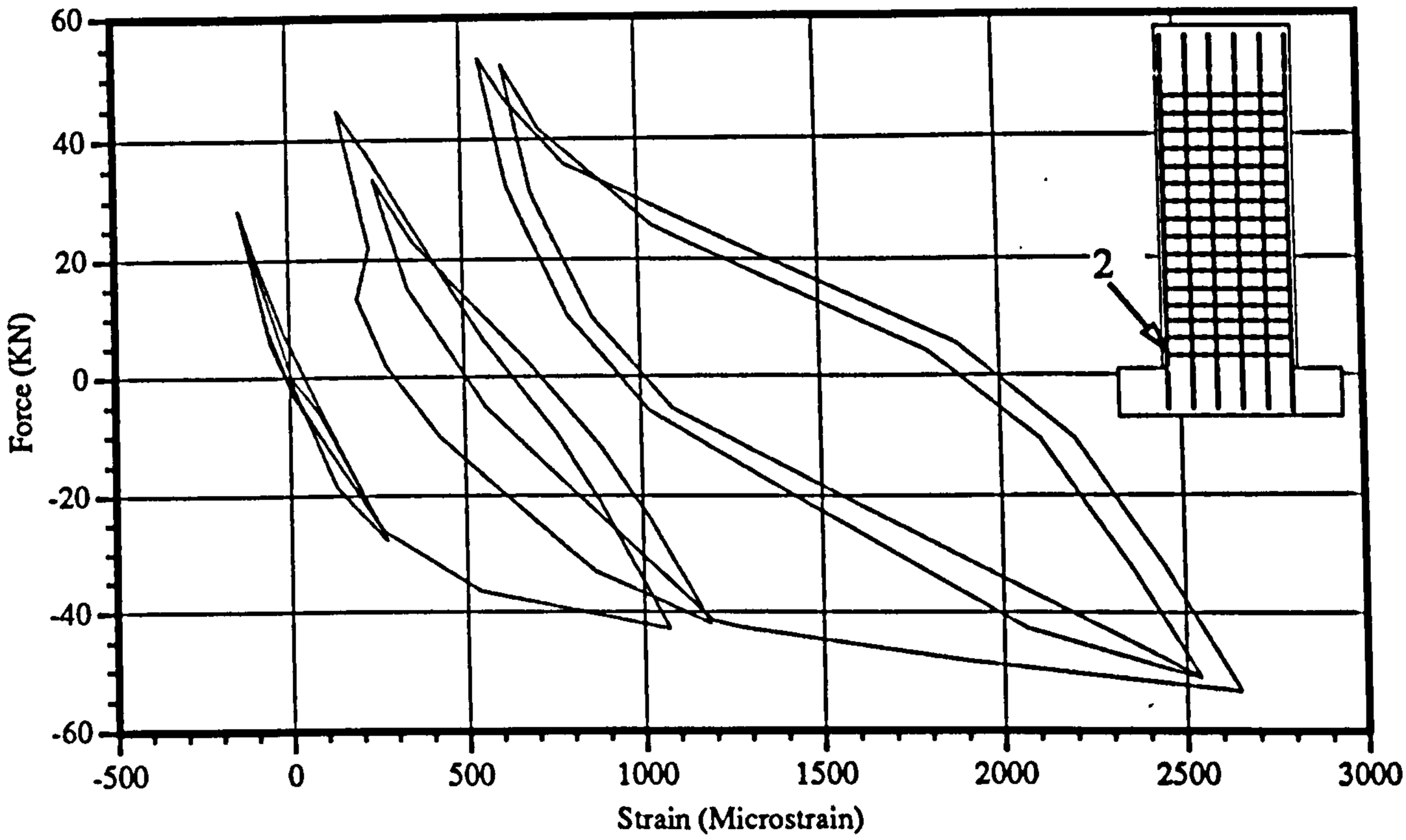


Fig. AII (32) 1 Force - Steel Strain for SW32 at Node 2

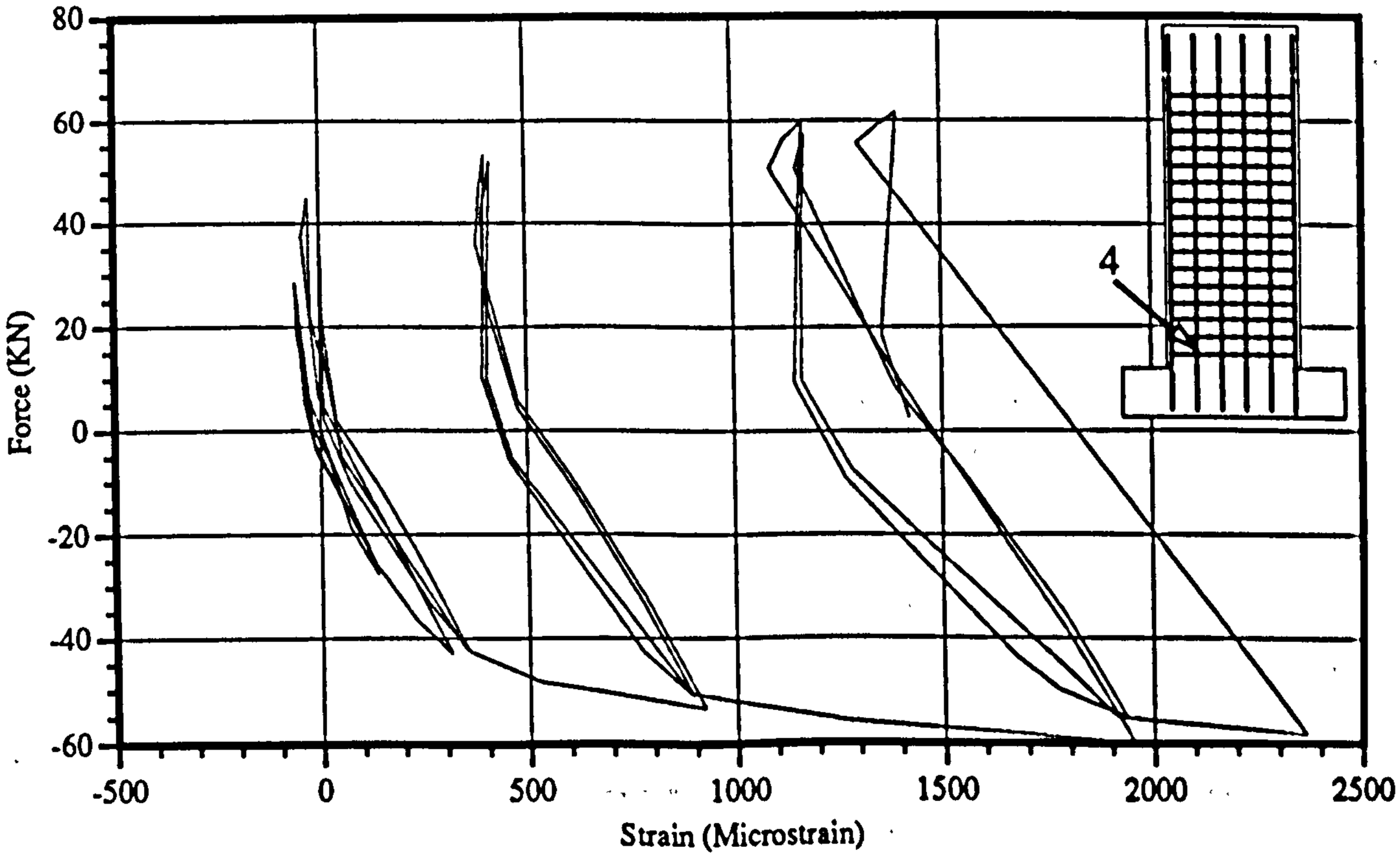


Fig. AII (32) 2 Force - Steel Strain for SW32 at Node 4

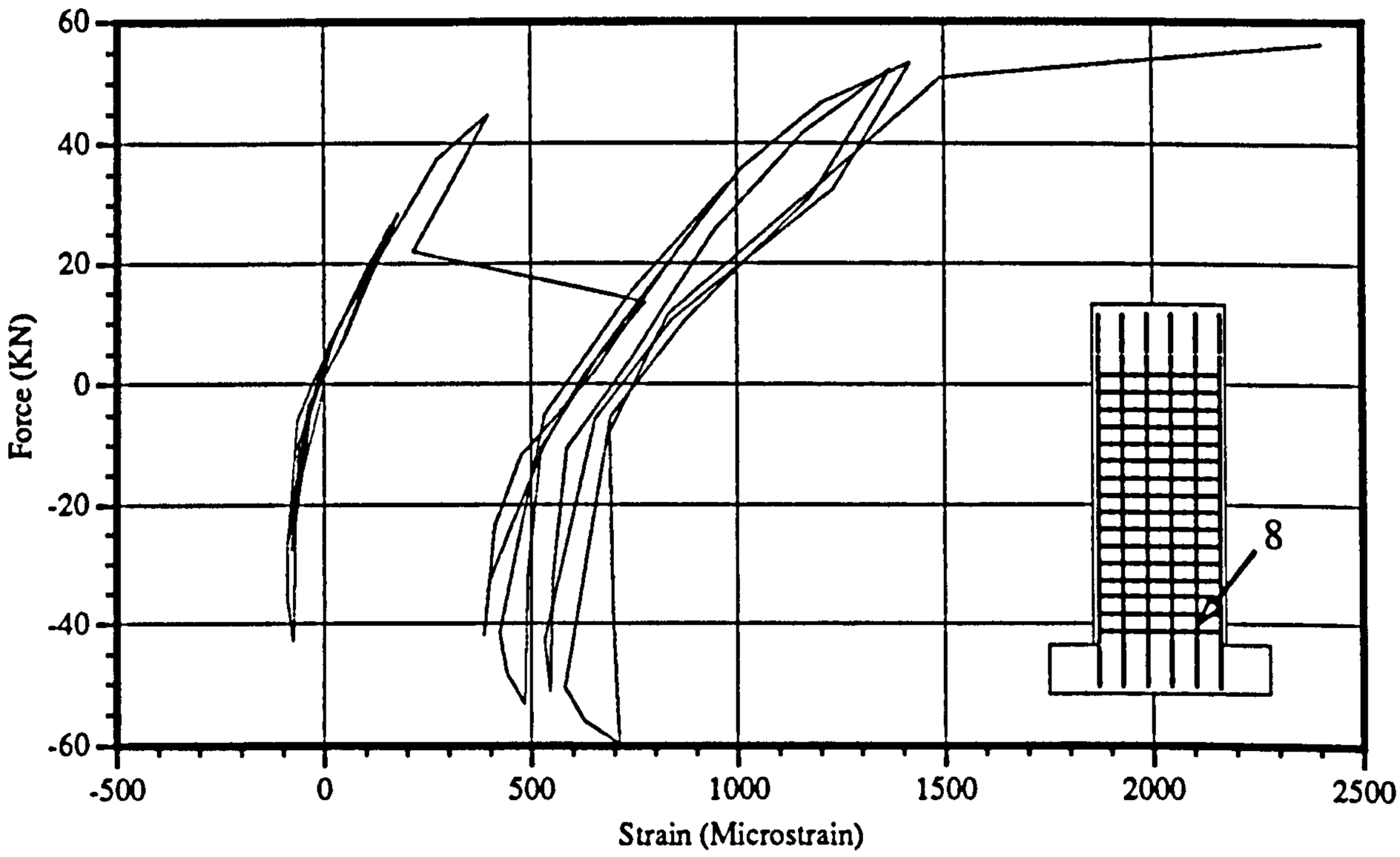


Fig. AII (32) 3 Force - Steel Strain for SW32 at Node 8

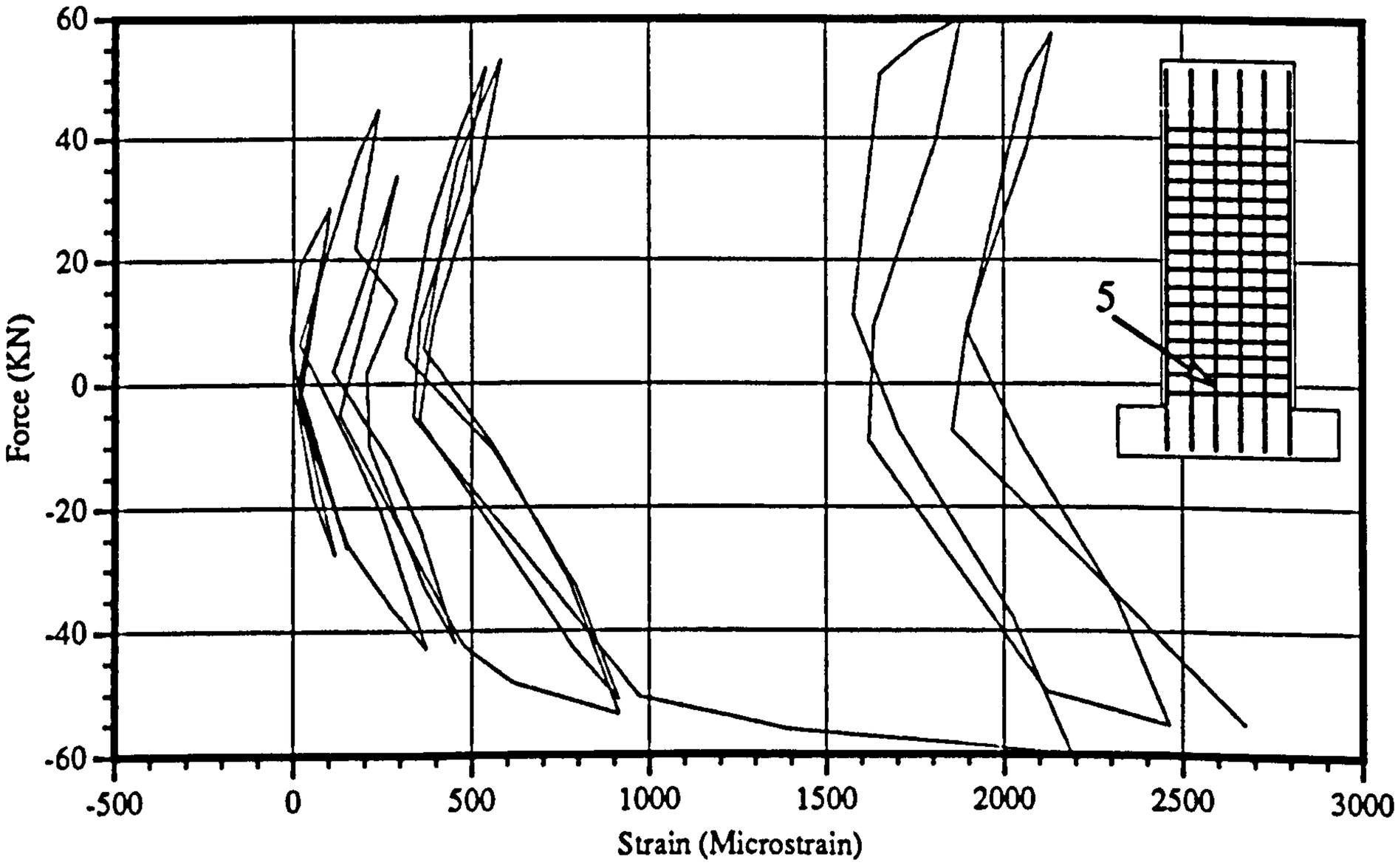


Fig. AII (32) 4 Force - Steel Strain for SW32 at Node 5

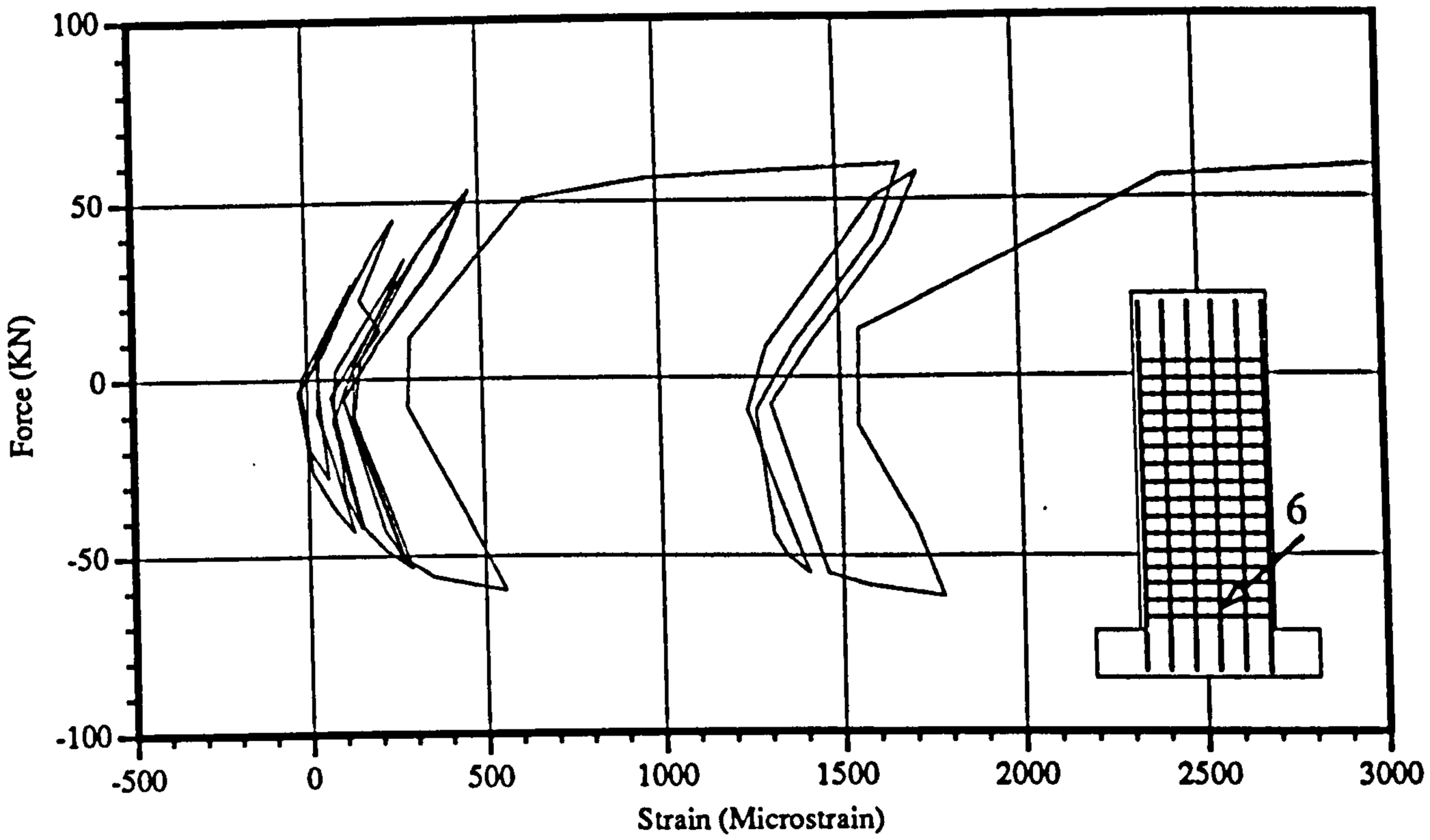


Fig. AII (32) 5 Force - Steel Strain for SW32 at Node 6

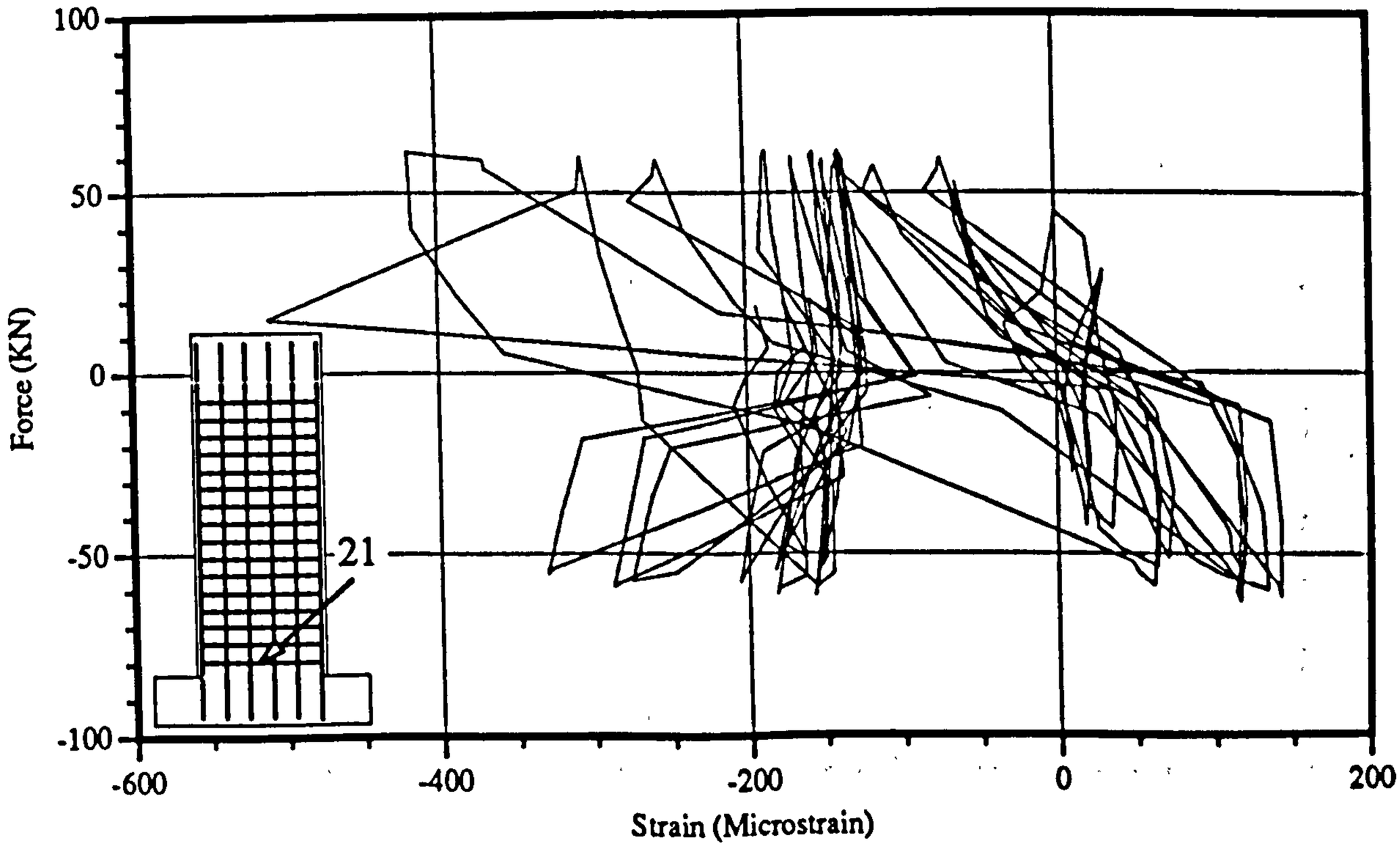


Fig. AII (32) 6 Force - Steel Strain for SW32 at Node 21

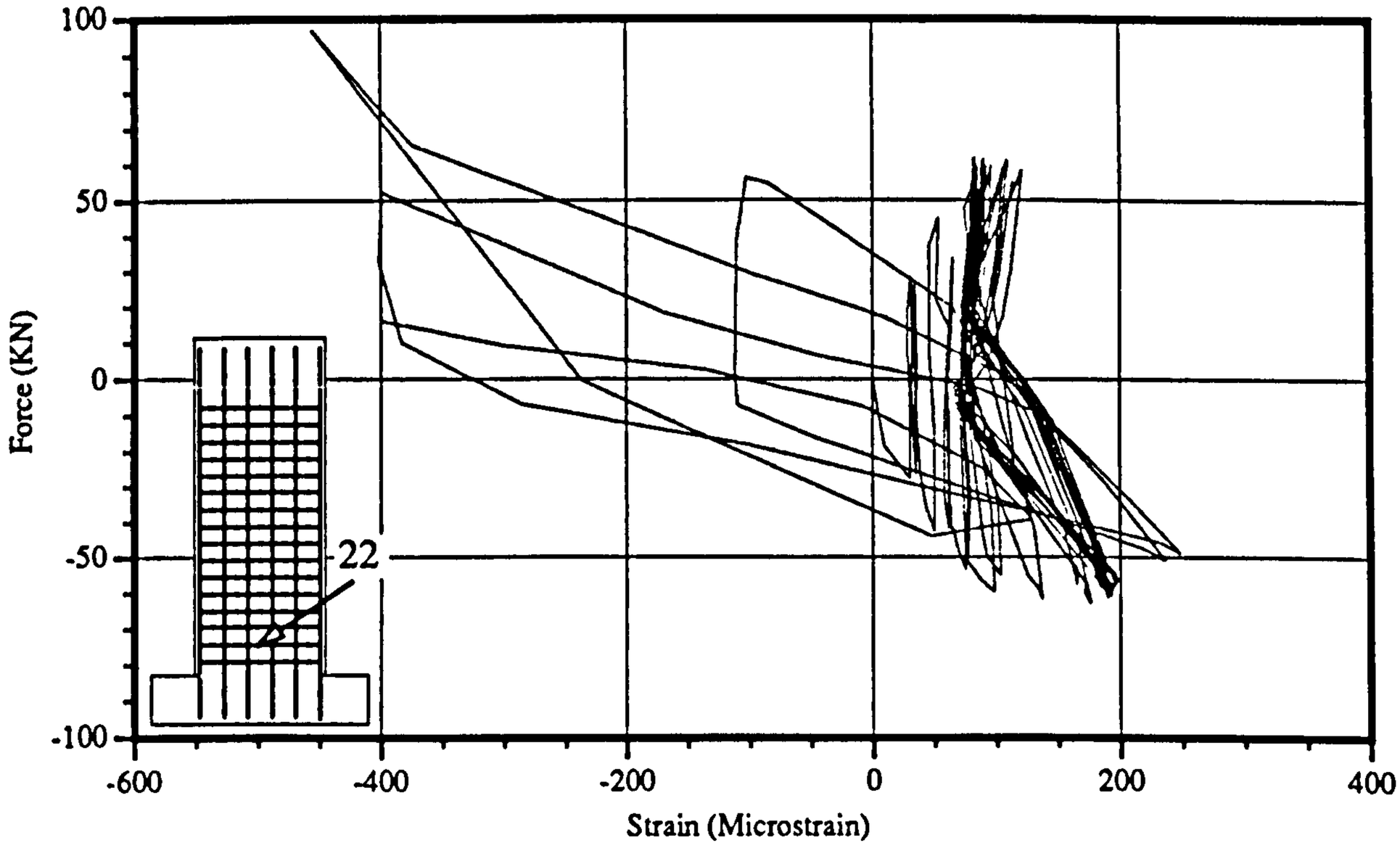


Fig. AII (32) 7 Force - Steel Strain for SW32 at Node 22

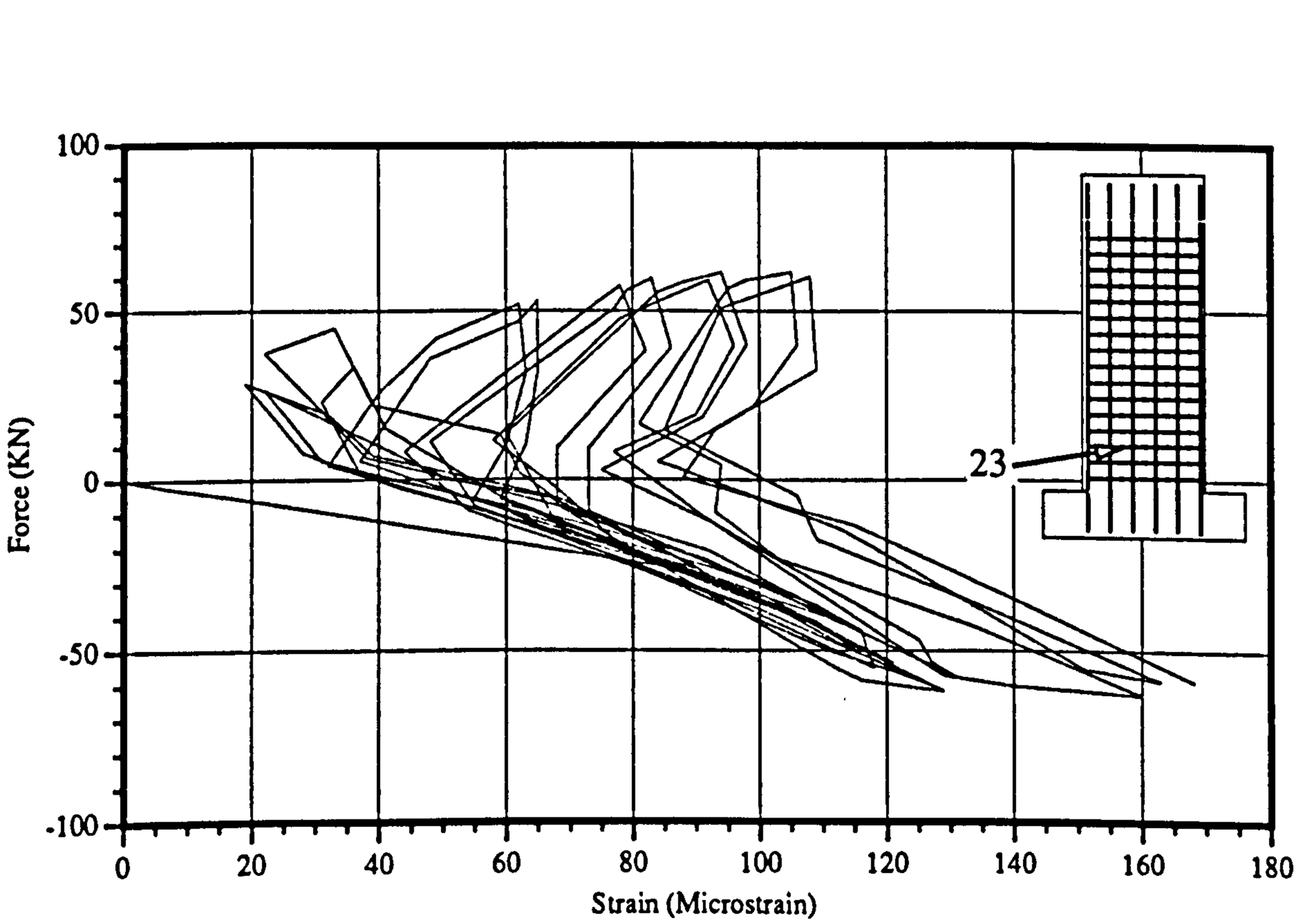


Fig. AII (32) 8 Force - Steel Strain for SW32 at Node 23

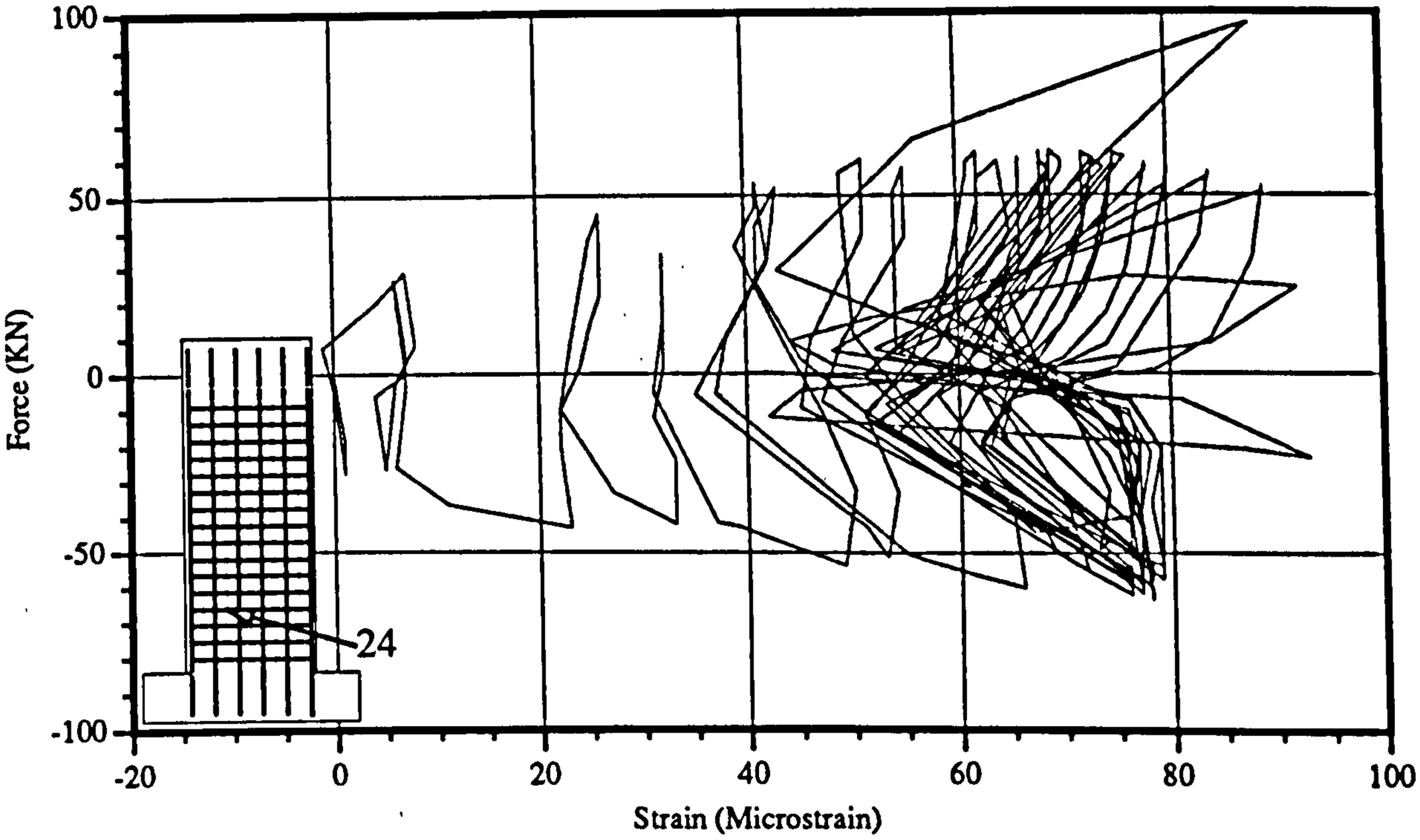


Fig. AII (32) 9 Force - Steel Strain for SW32 at Node 24

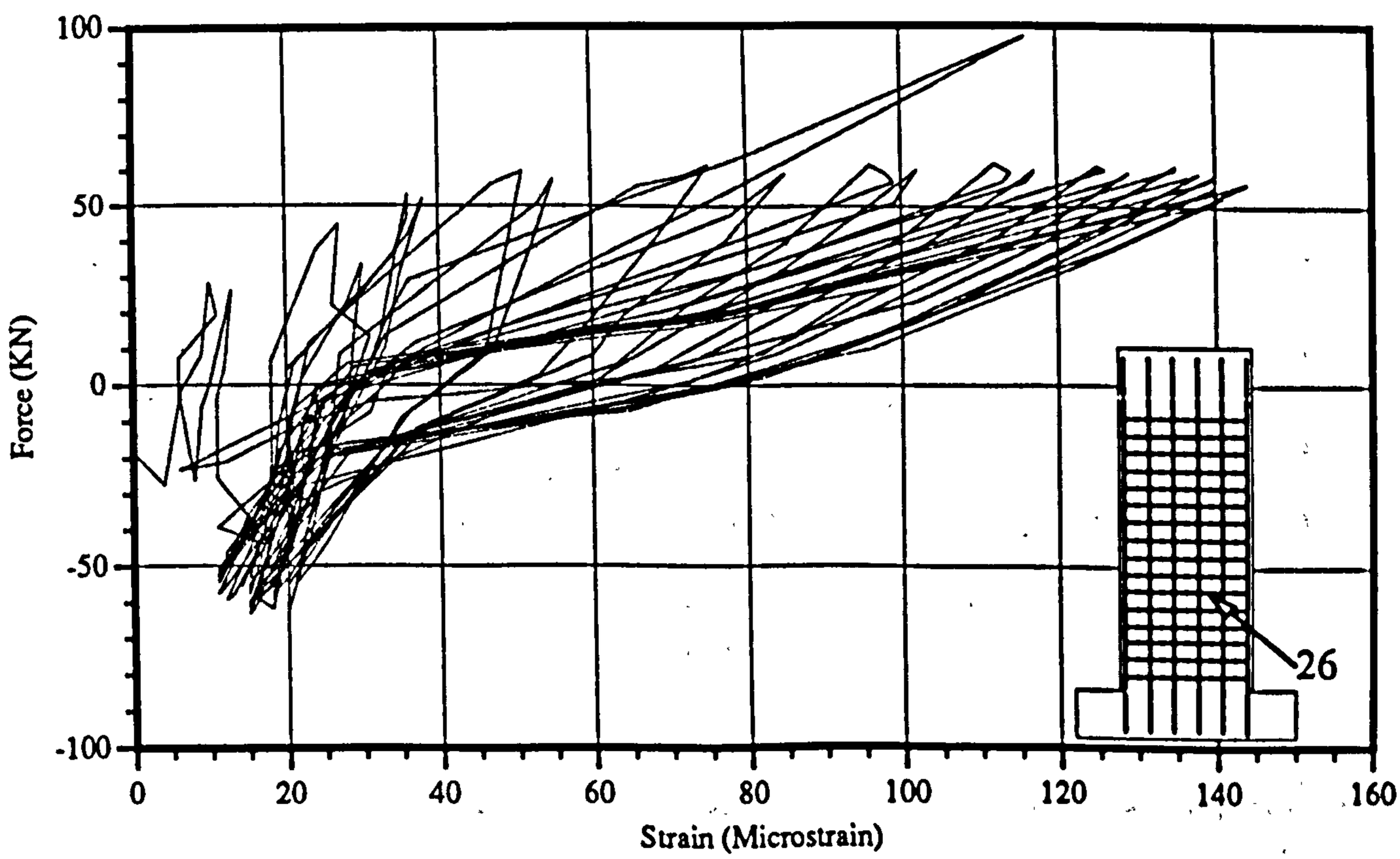


Fig. AII (32) 10 Force - Steel Strain for SW32 at Node 26

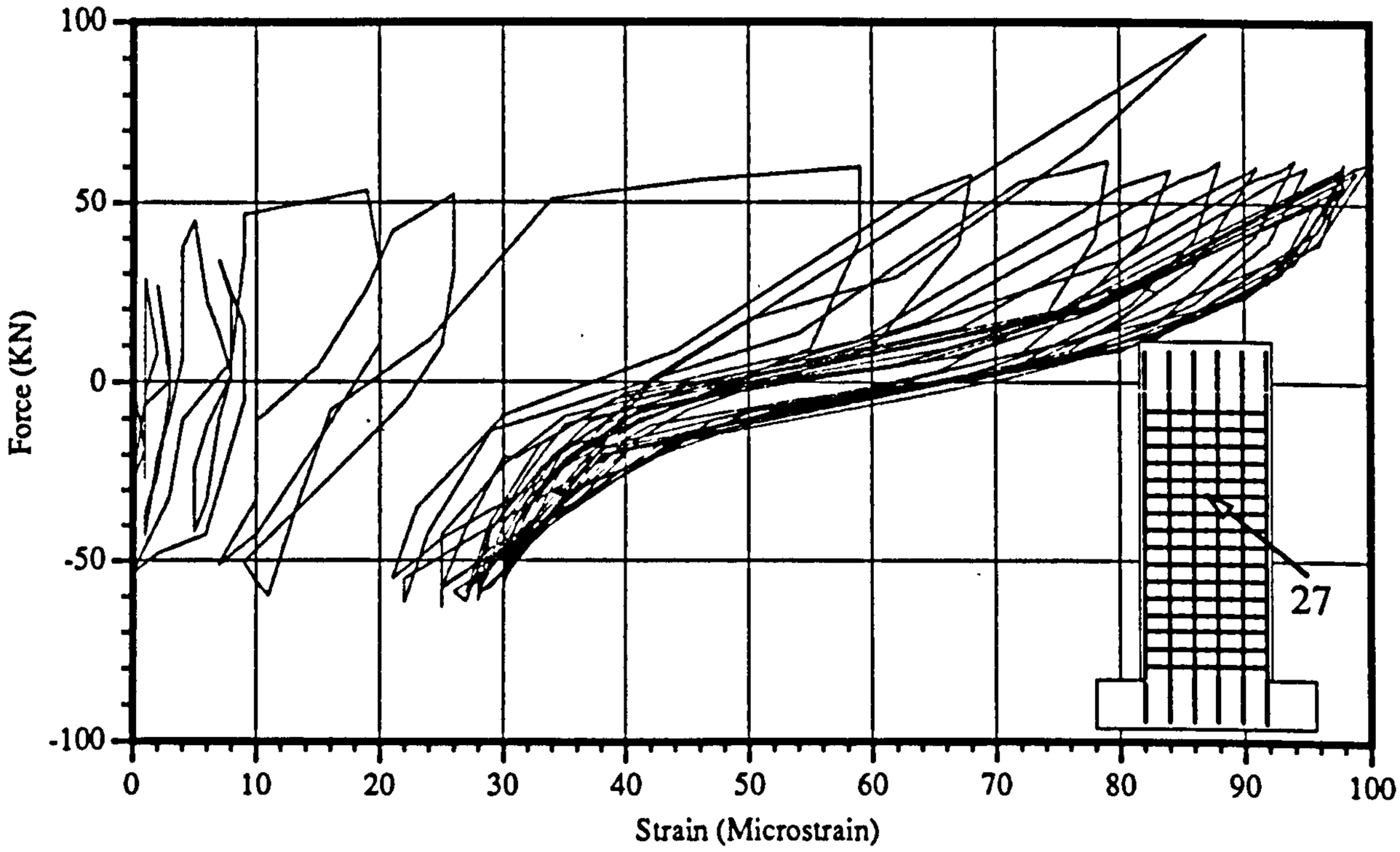


Fig. AII (32) 11 Force - Steel Strain for SW32 at Node 27

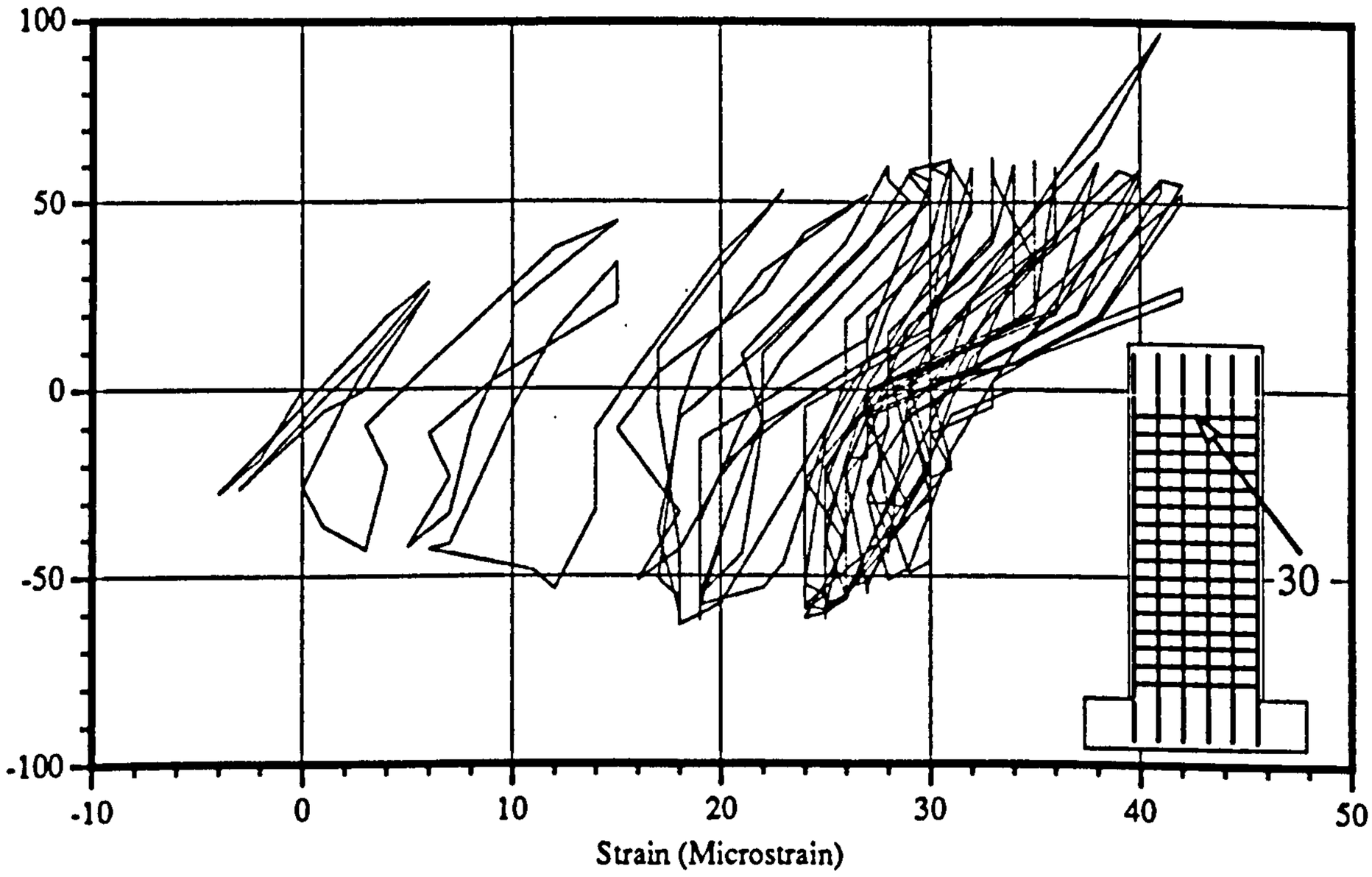


Fig. AII (32) 12 Force - Steel Strain for SW32 at Node 30

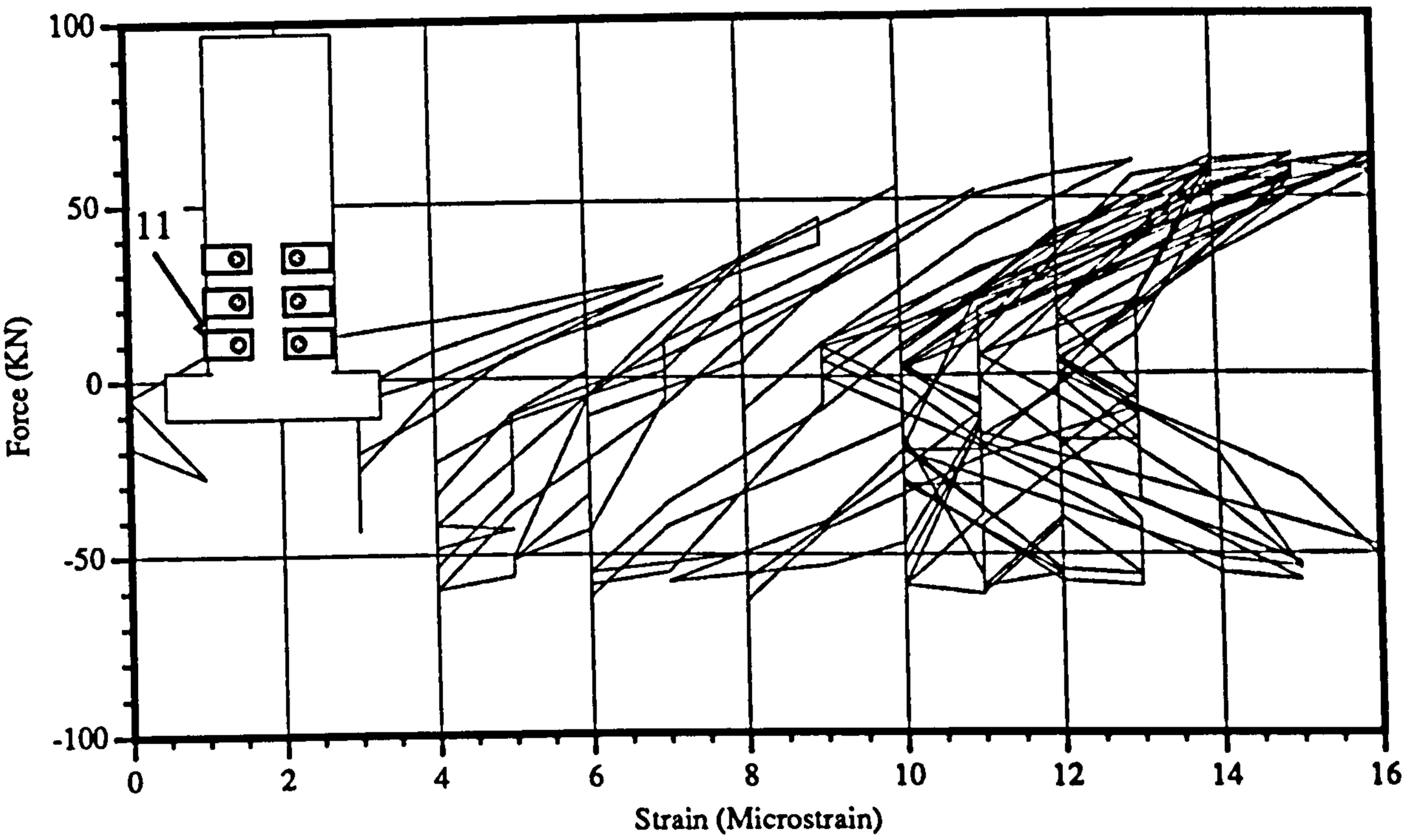


Fig. AII (32) 13 Force - Steel Strain for SW32 at Node 11

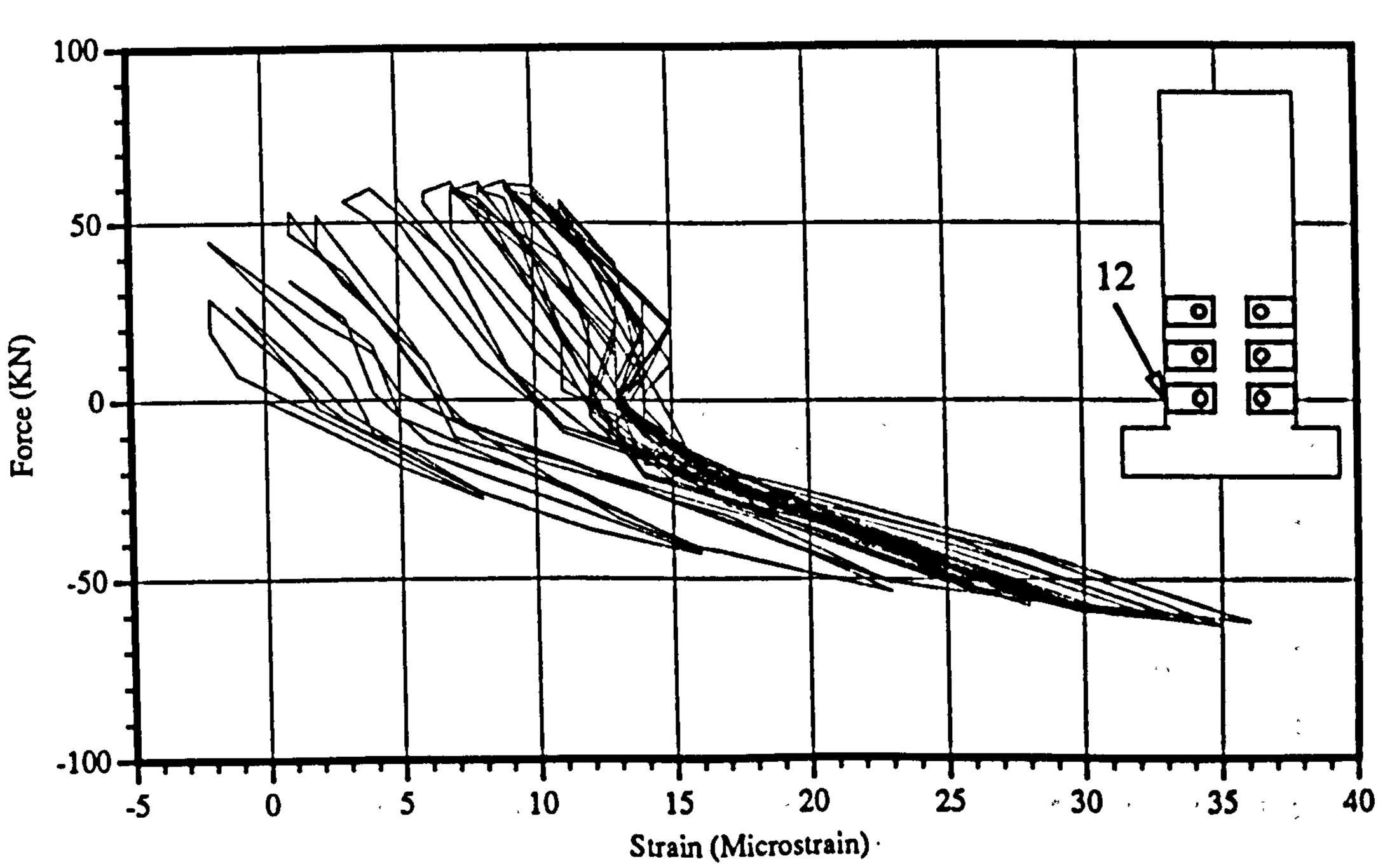


Fig. AII (32) 14 Force - Steel Strain for SW32 at Node 12

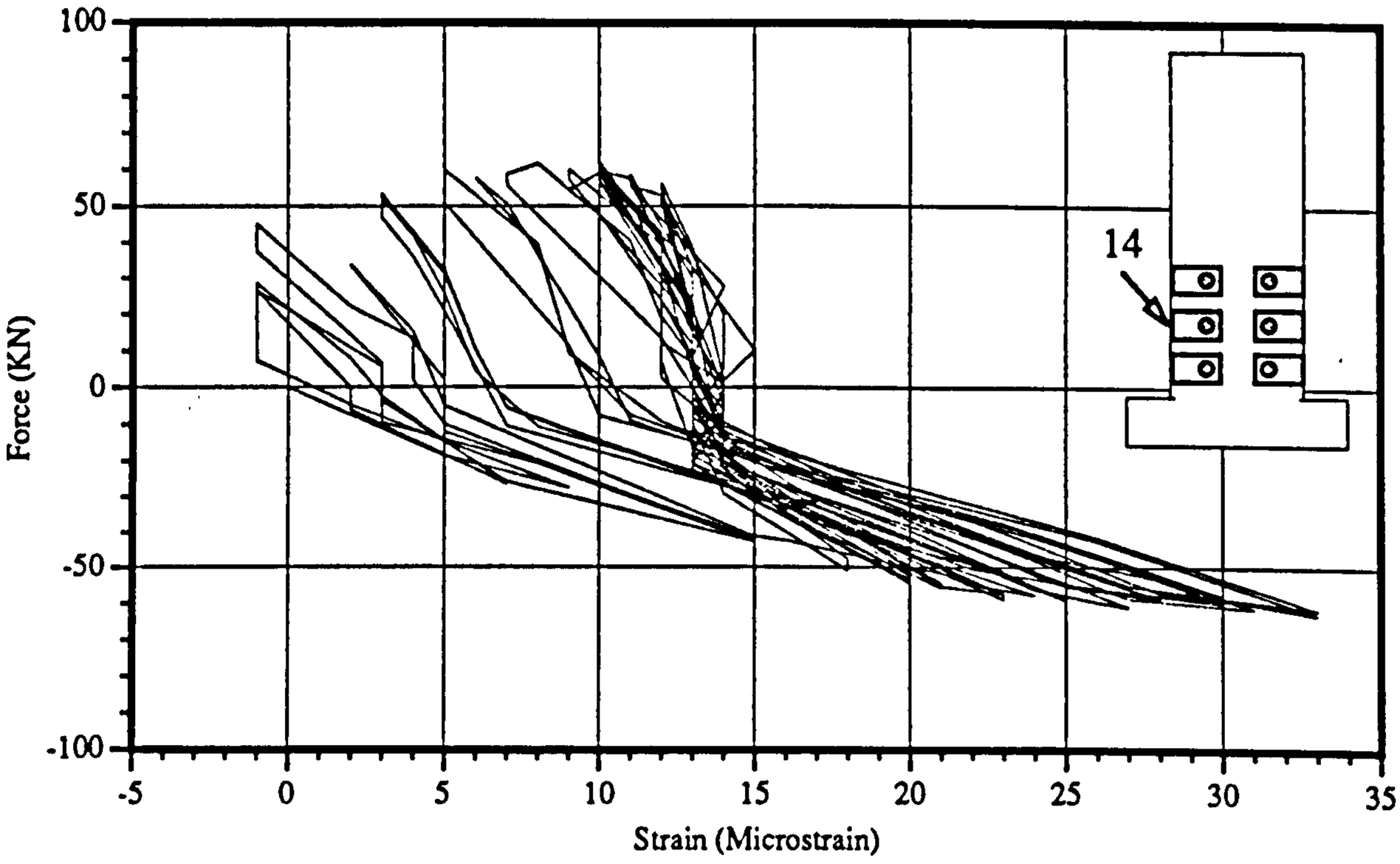


Fig. AII (32) 15 Force - Steel Strain for SW32 at Node 14

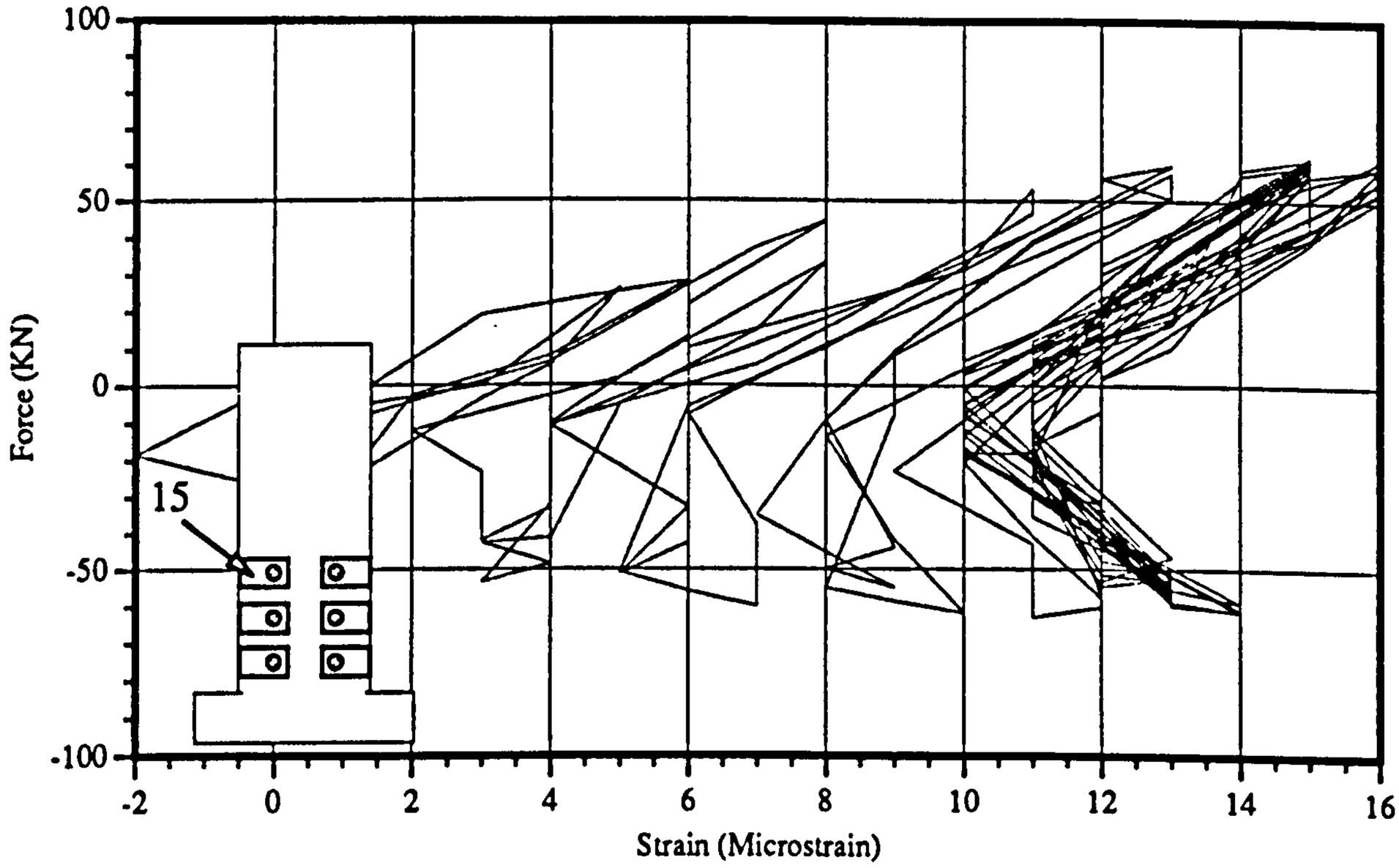


Fig. AII (32) 16 Force - Steel Strain for SW32 at Node 15

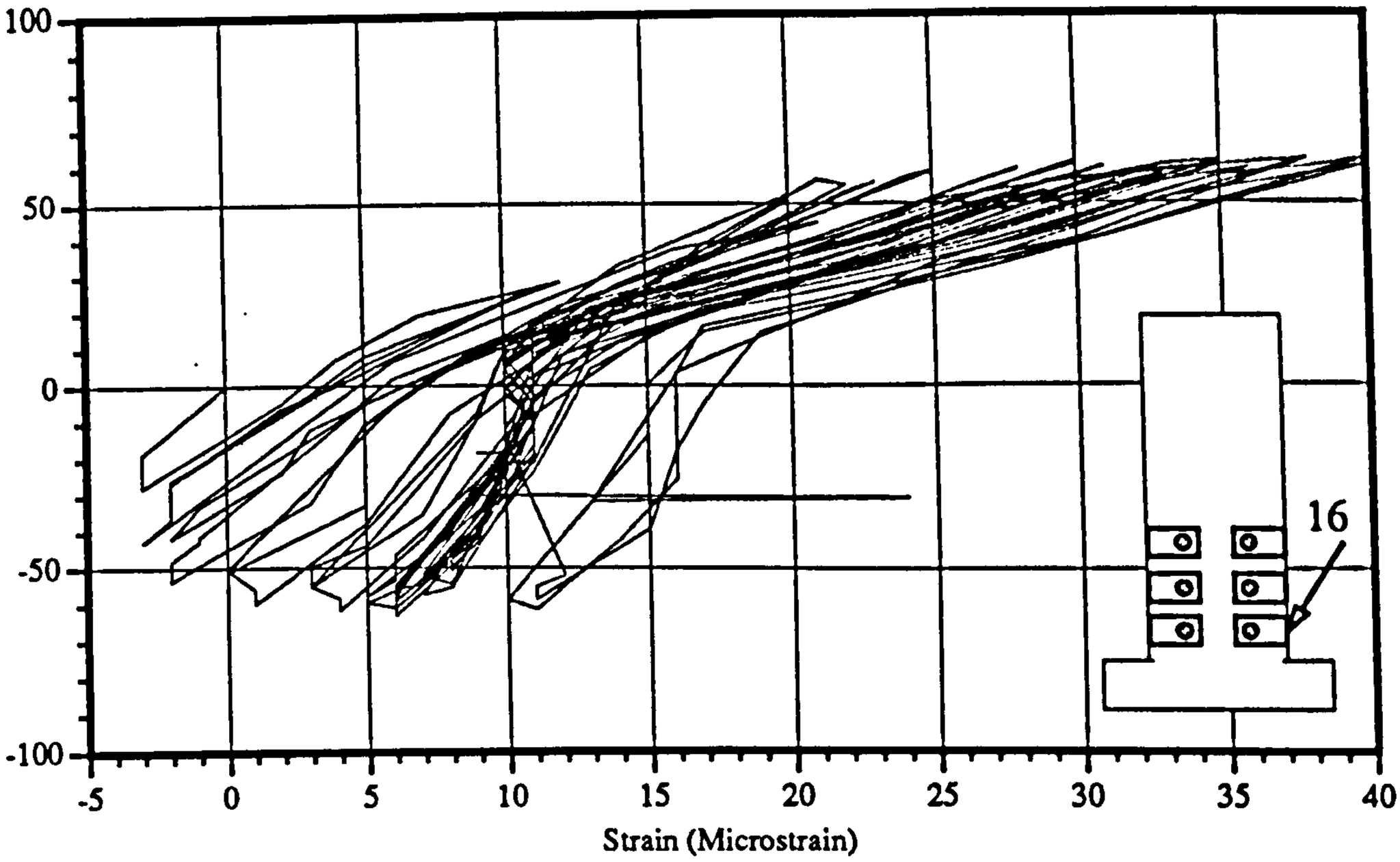


Fig. AII (32) 17 Force - Steel Strain for SW32 at Node 16

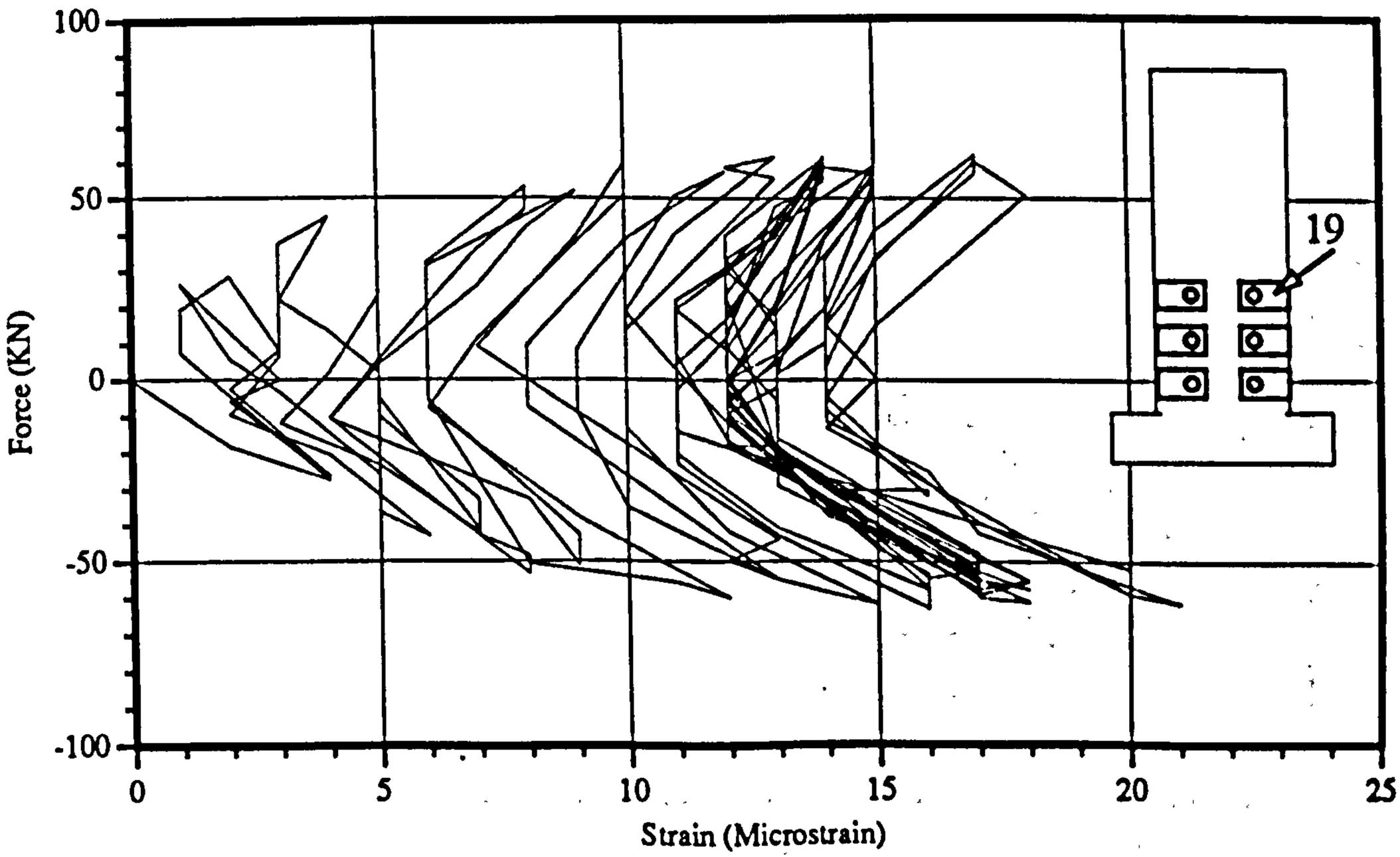


Fig. AII (32) 18 Force - Steel Strain for SW32 at Node 19

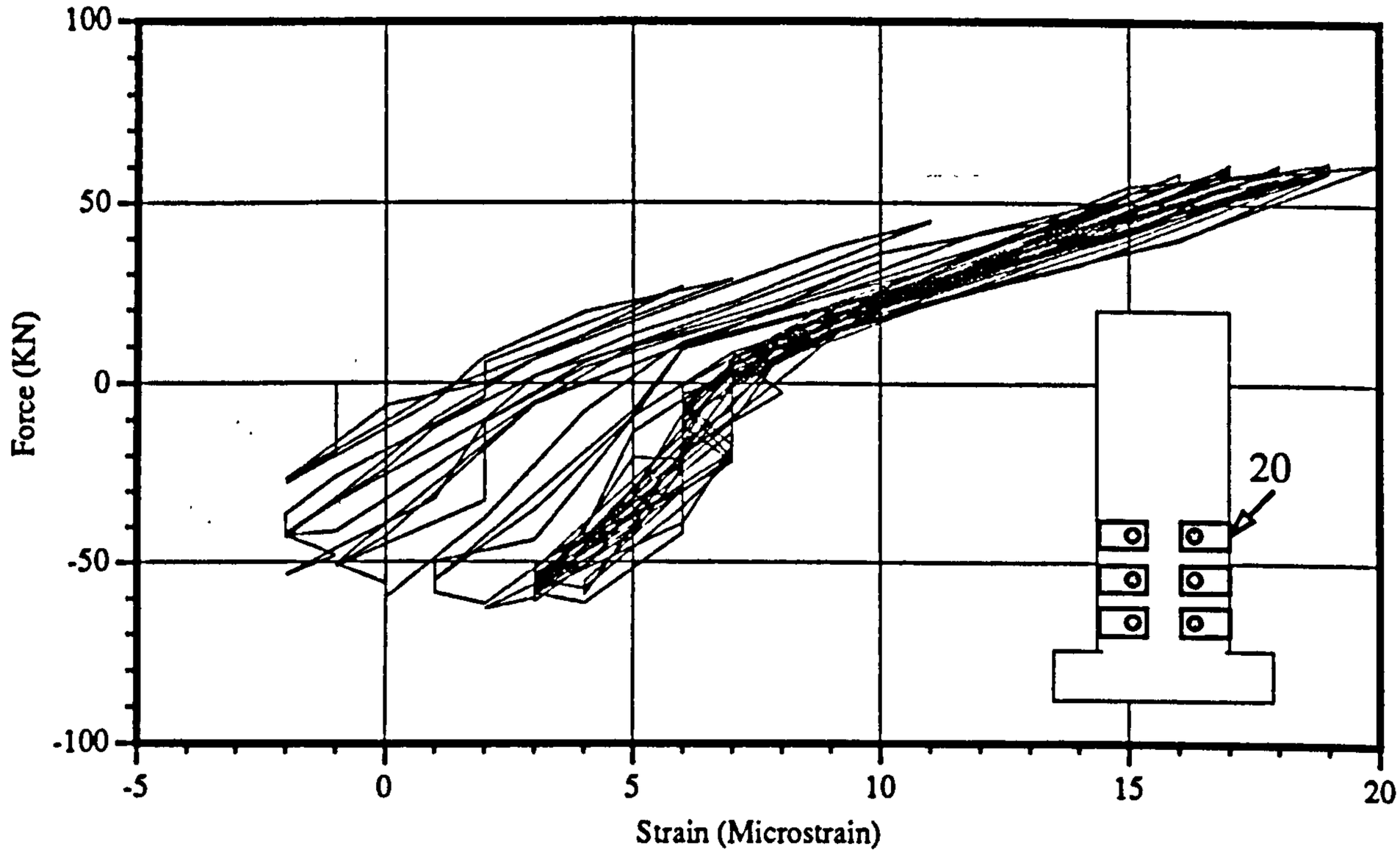


Fig. AII (32) 19 Force - Steel Strain for SW32 at Node 20

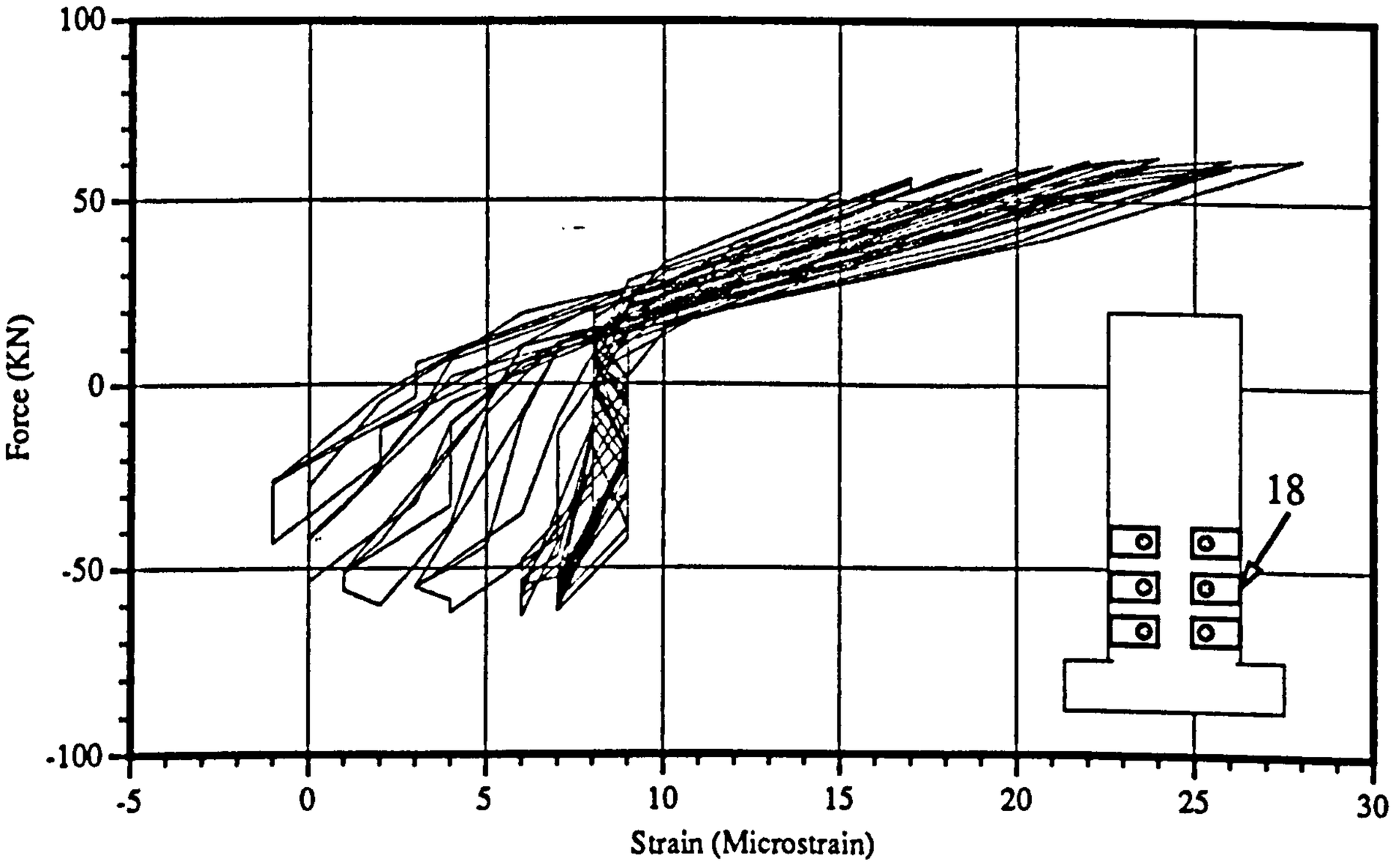


Fig. AII (32) 20 Force - Steel Strain for SW32 at Node 18

AII.9. Force-Steel Strain for SW33

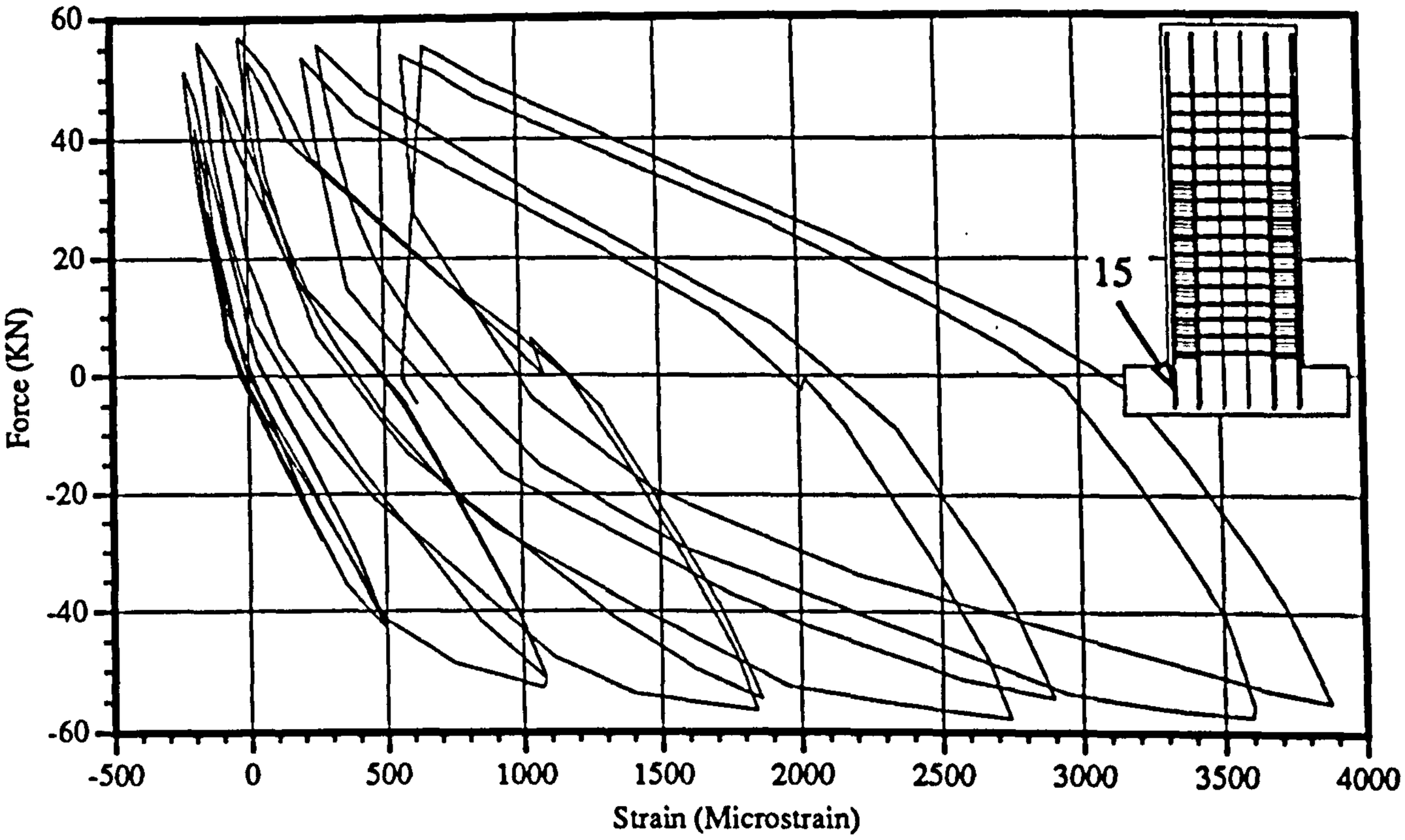


Fig. AII (33) 1 Force - Steel Strain for SW33 at Node 15

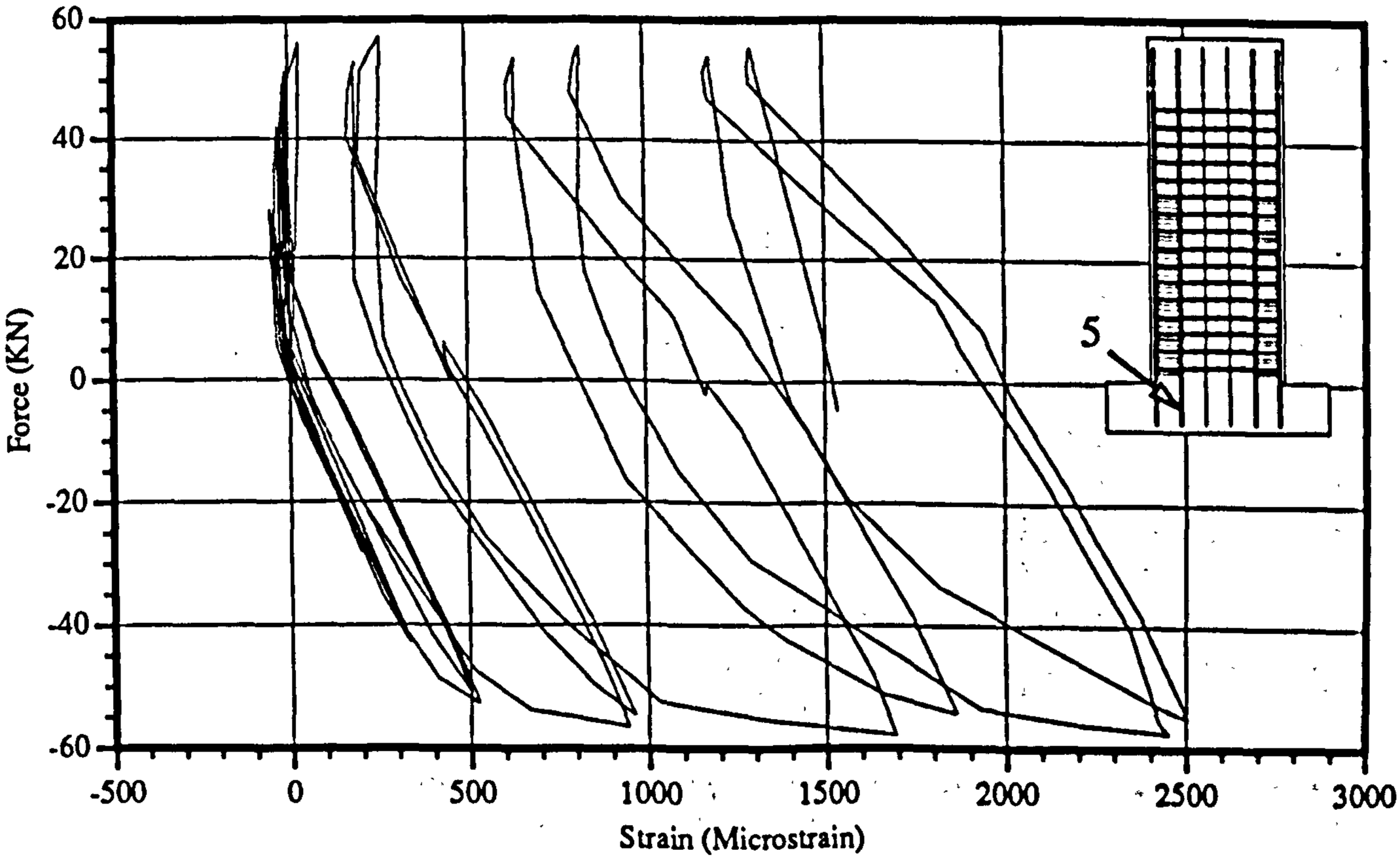


Fig. AII (33) 2 Force - Steel Strain for SW33 at Node 5

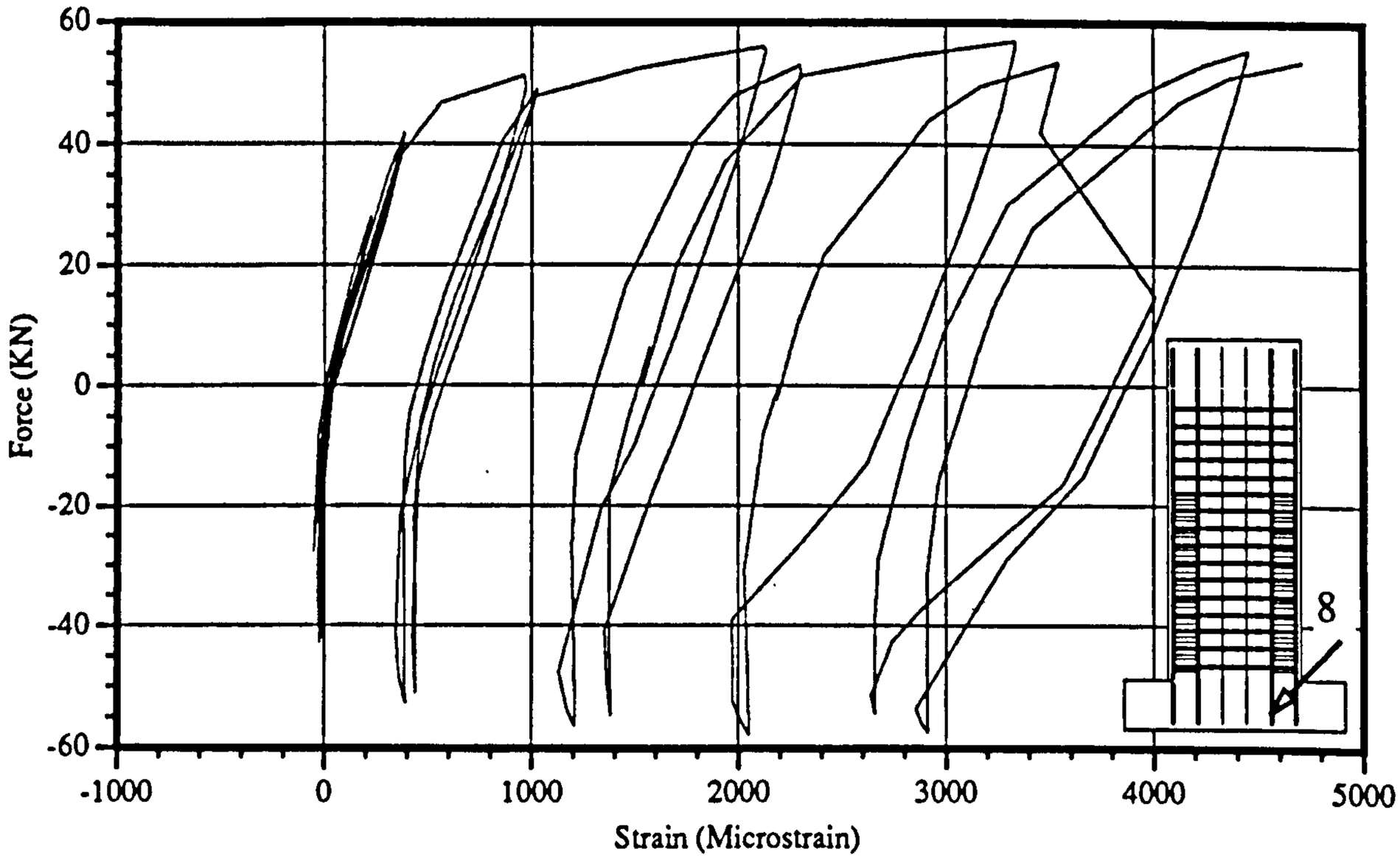


Fig. AII (33) 3 Force - Steel Strain for SW33 at Node 8

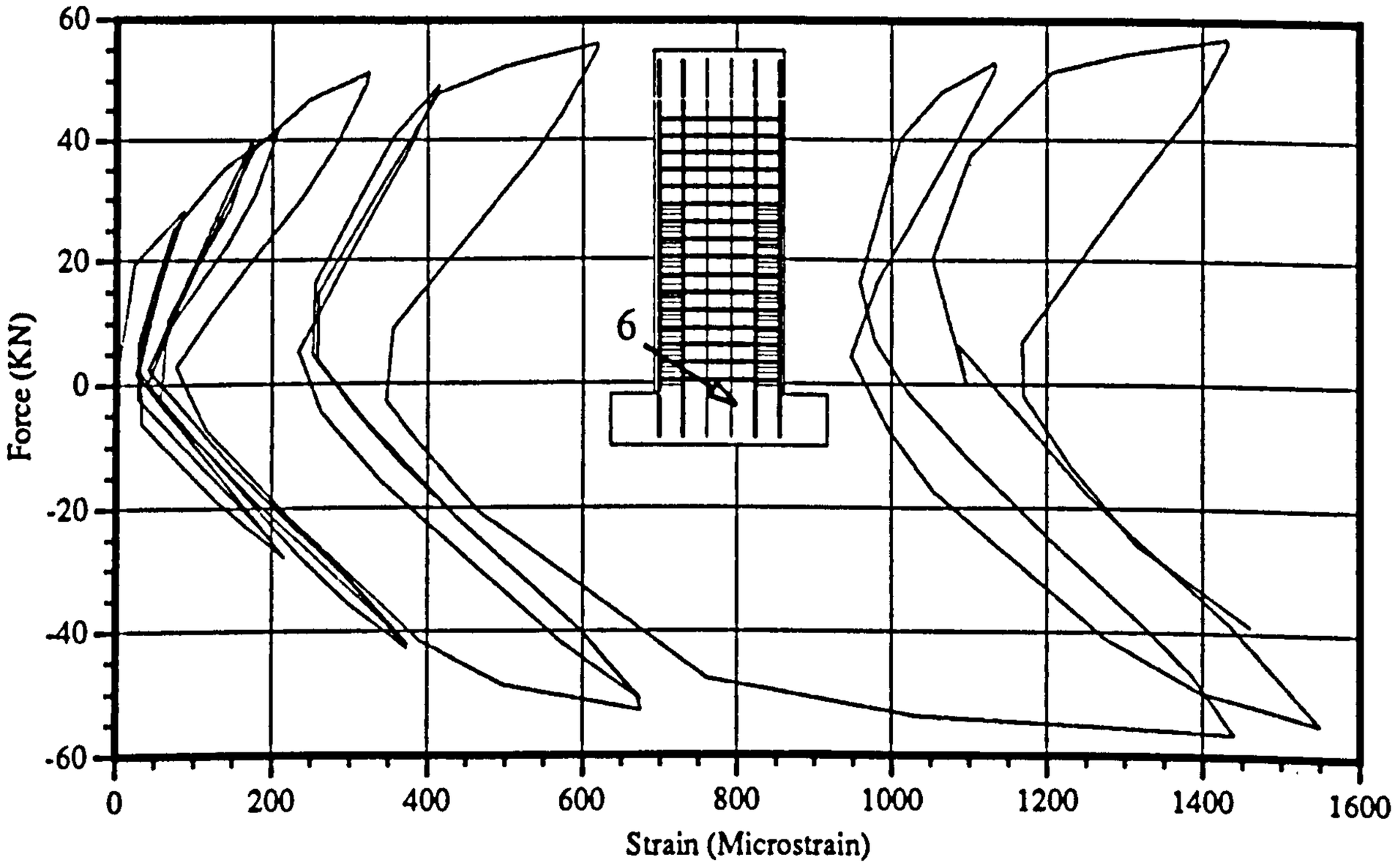


Fig. AII (33) 4 Force - Steel Strain for SW33 at Node 6

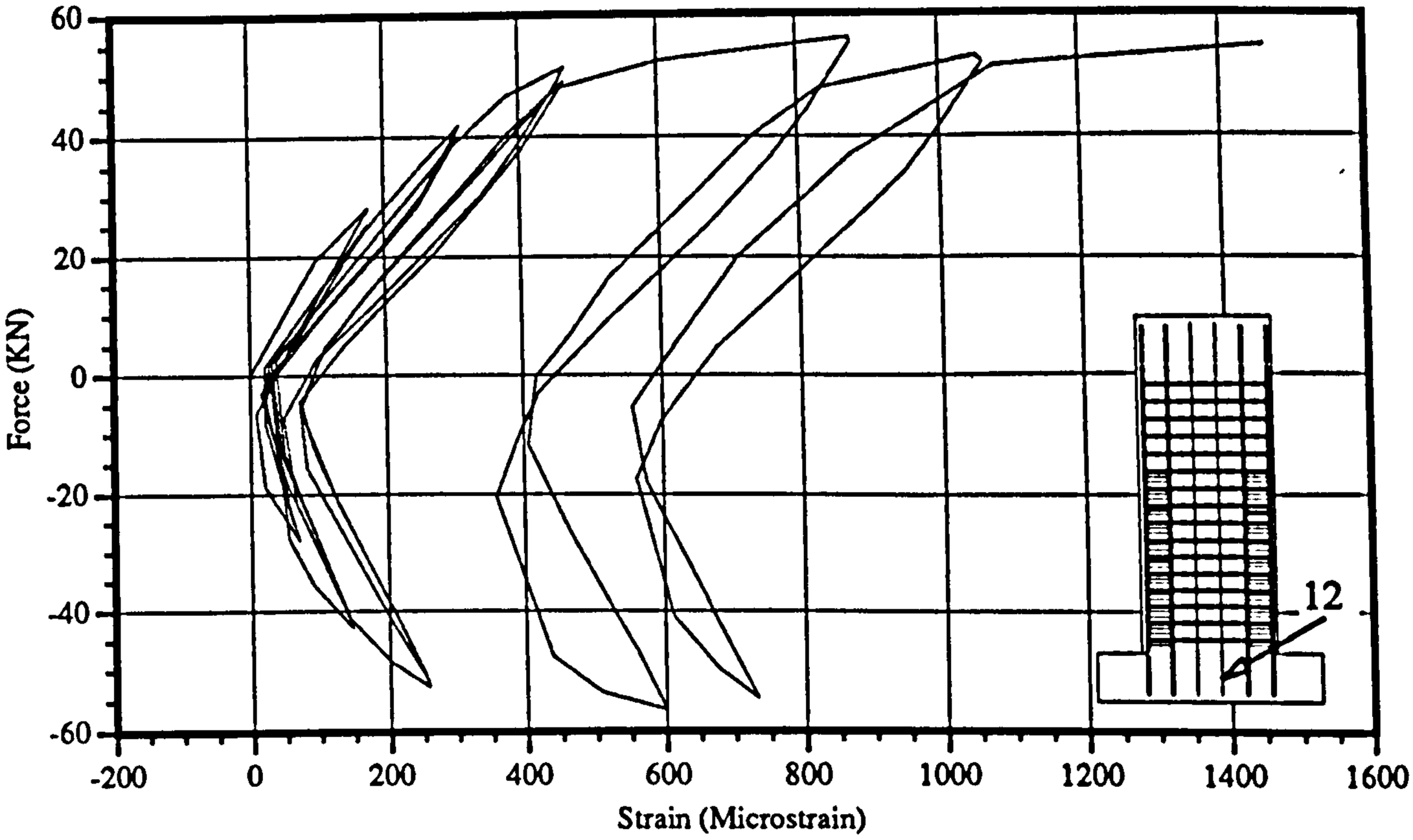


Fig. AII (33) 5 Force - Steel Strain for SW33 at Node 12

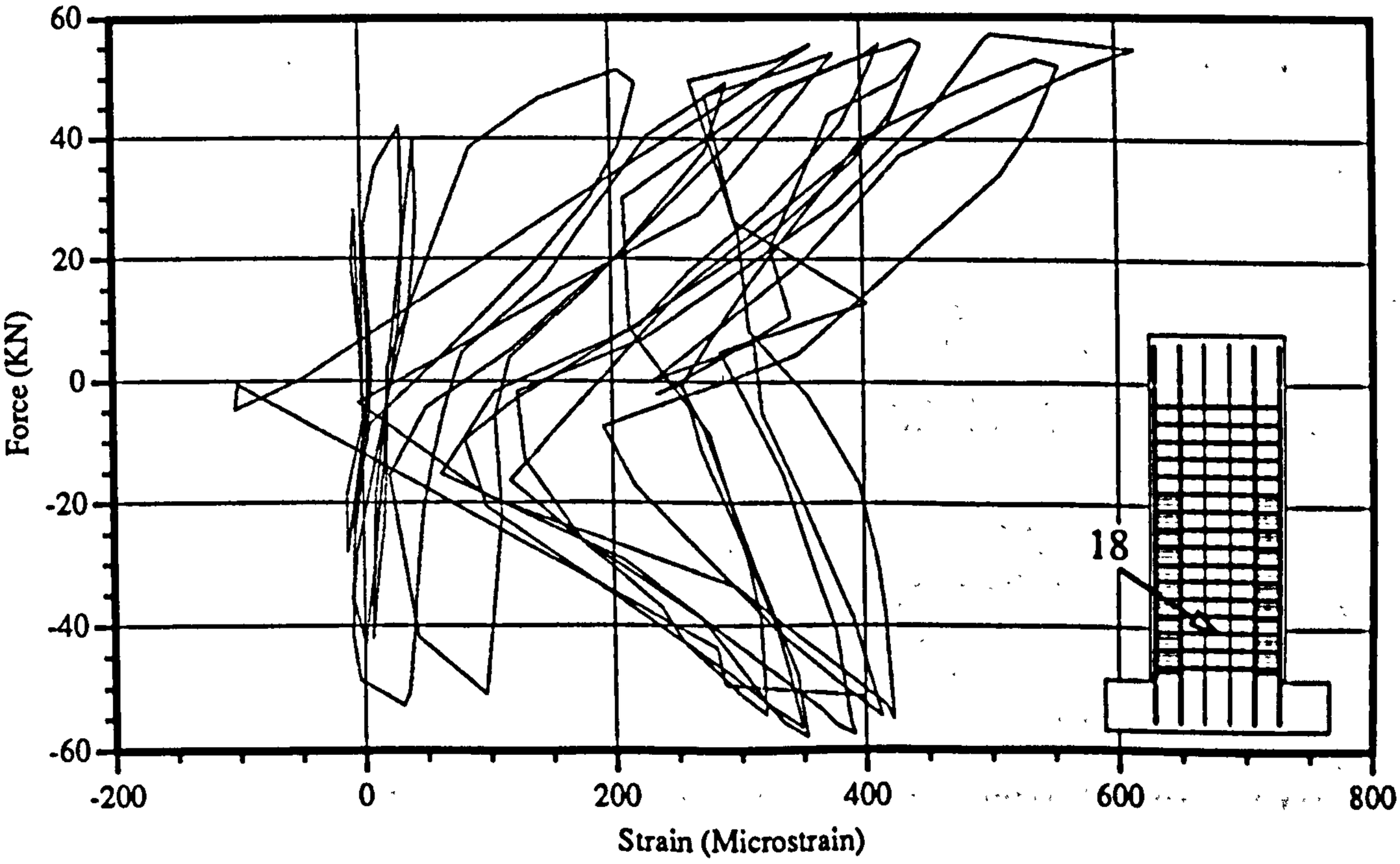


Fig. AII (33) 6 Force - Steel Strain for SW33 at Node 18

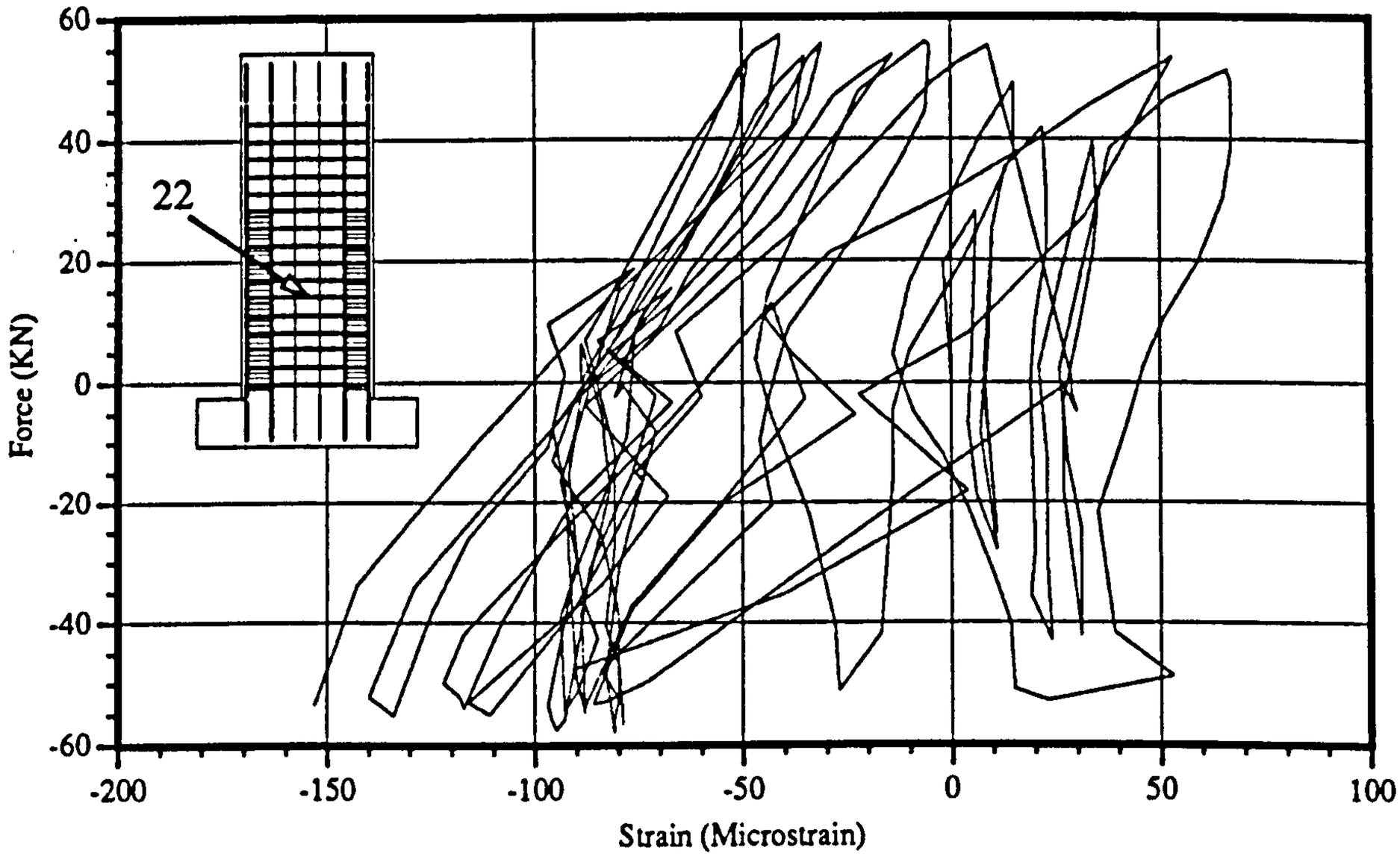


Fig. AII (33) 7 Force - Steel Strain for SW33 at Node 22

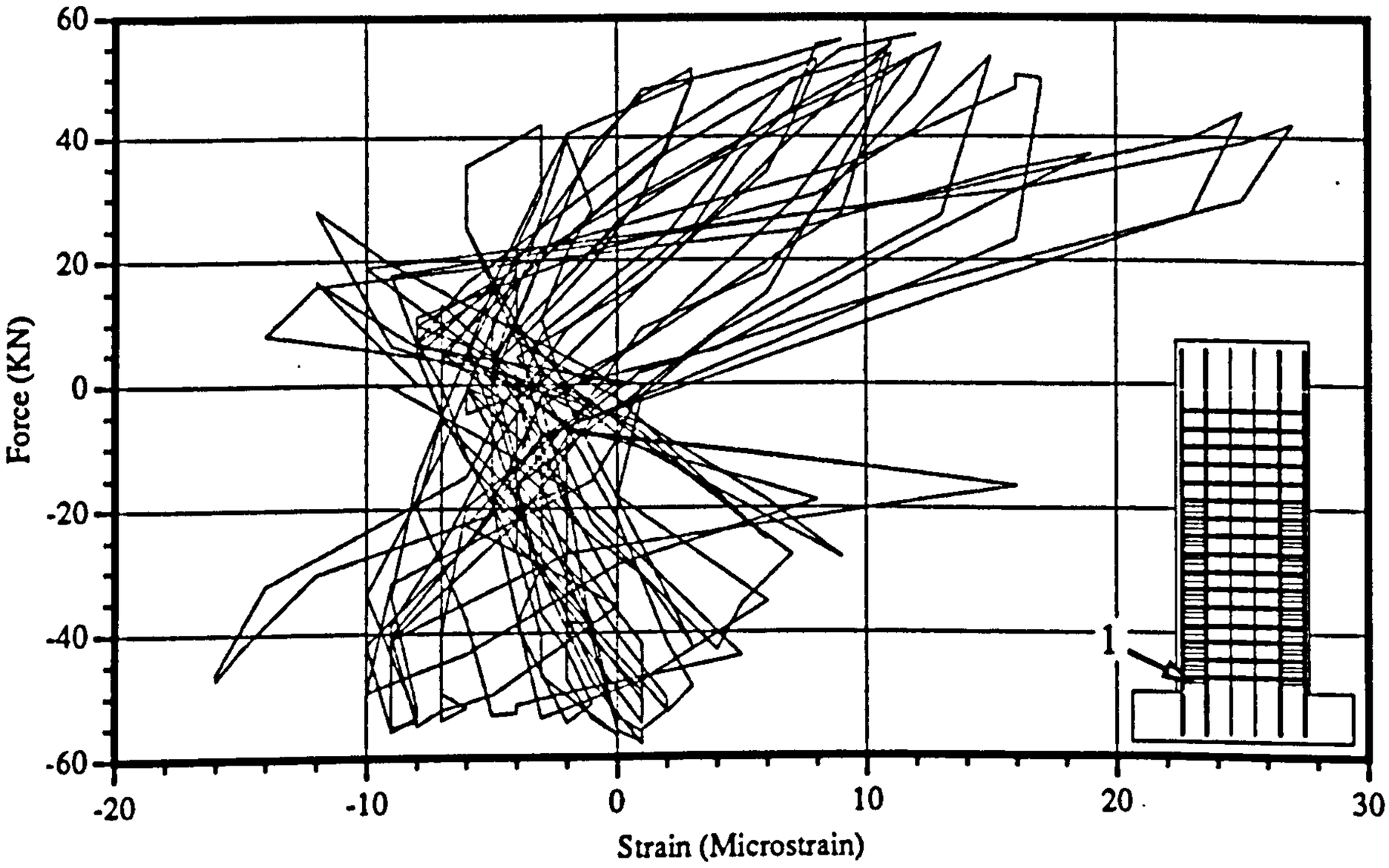


Fig. AII (33) 8 Force - Steel Strain for SW33 at Node 1

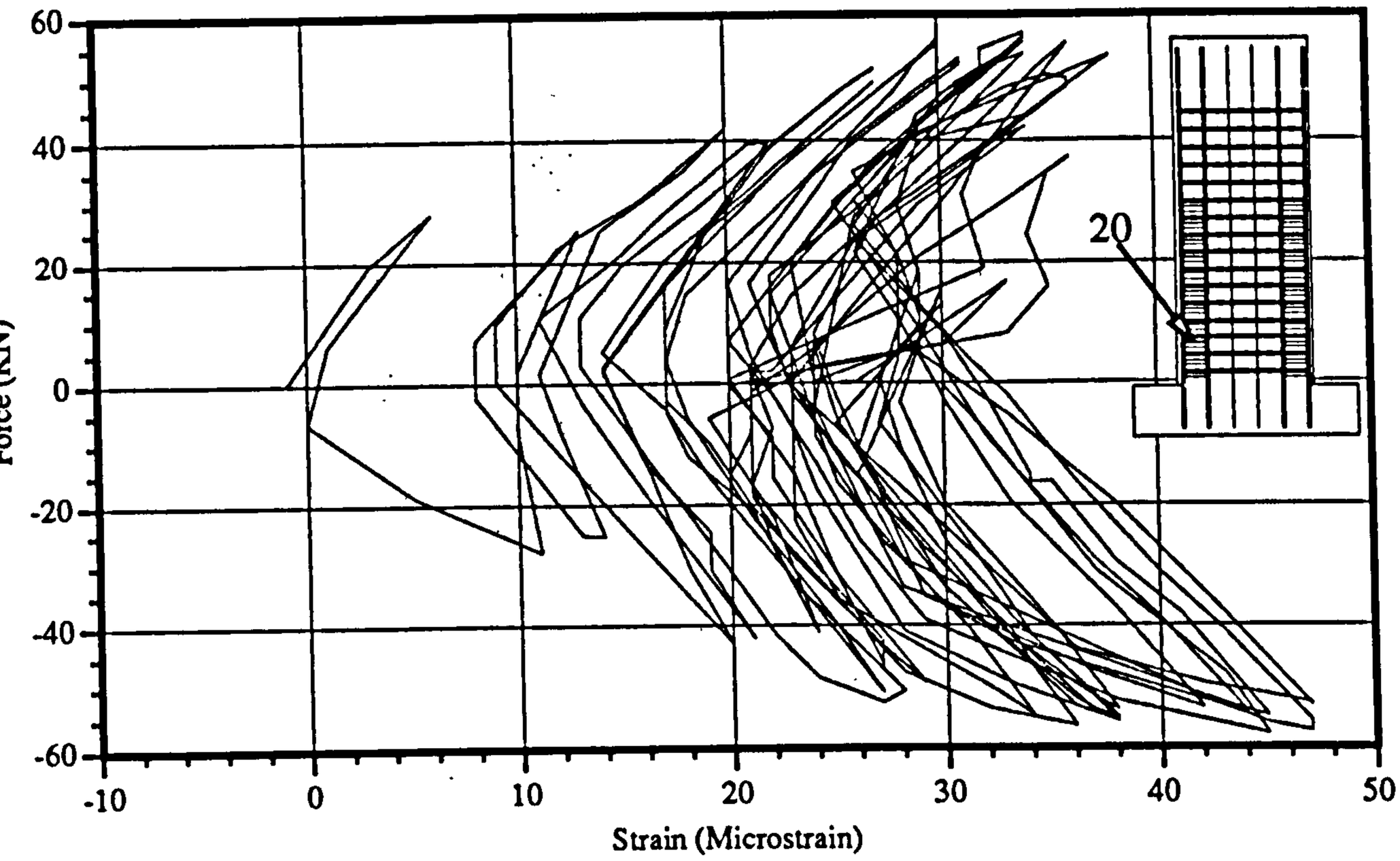


Fig. AII (33) 9 Force - Steel Strain for SW33 at Node 20

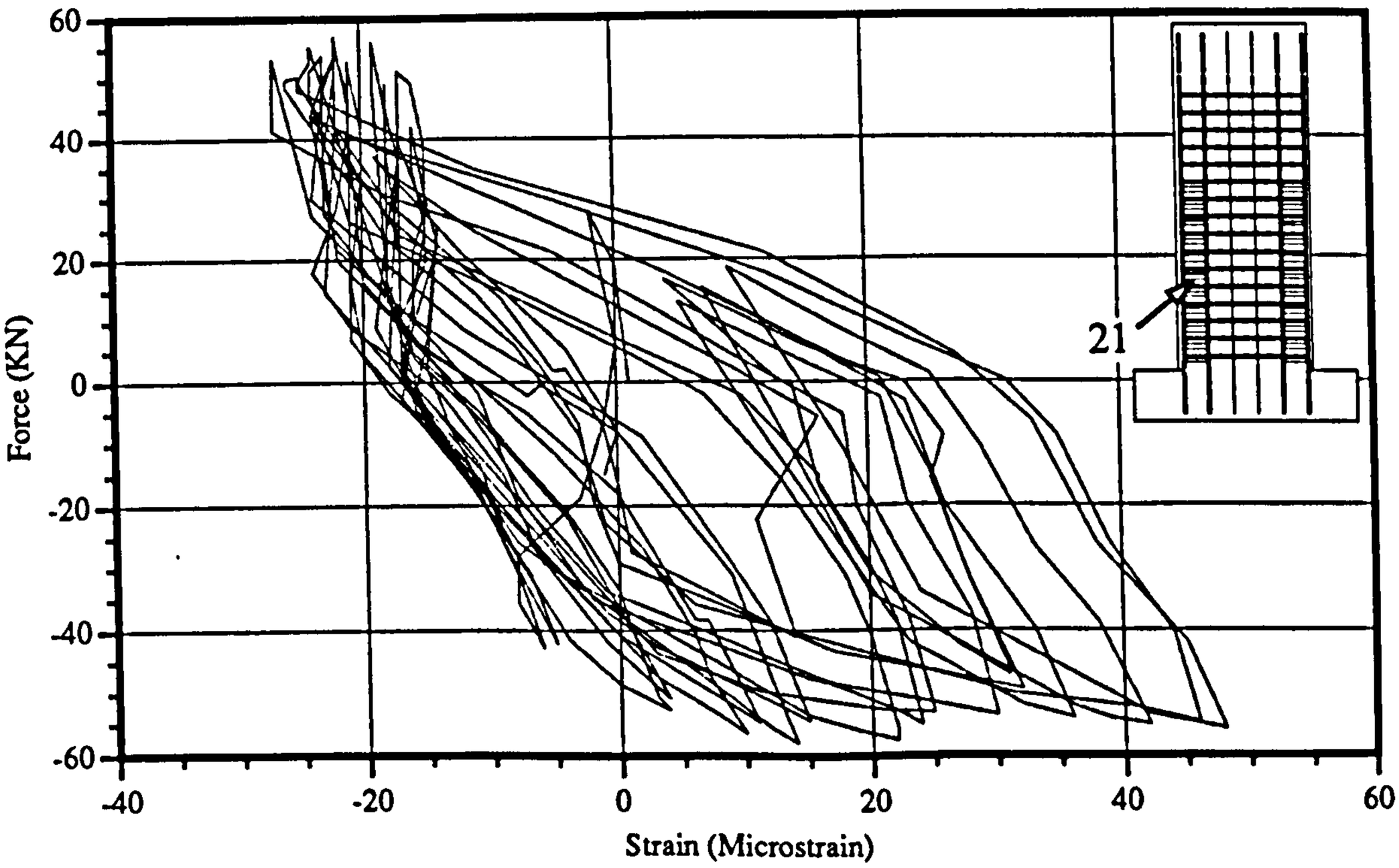


Fig. AII (33) 10 Force - Steel Strain for SW33 at Node 21

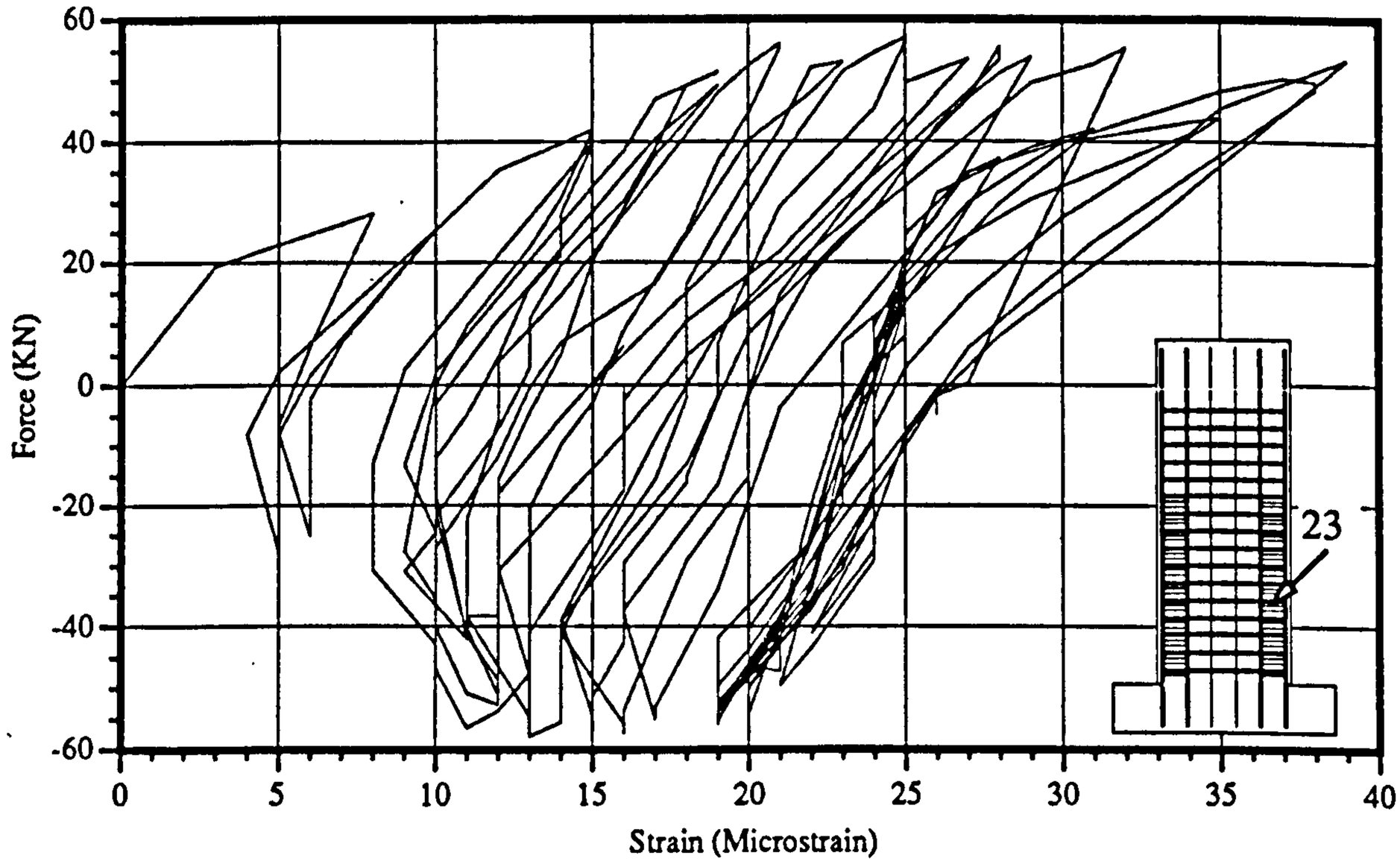


Fig. AII (33) 11 Force - Steel Strain for SW33 at Node 23

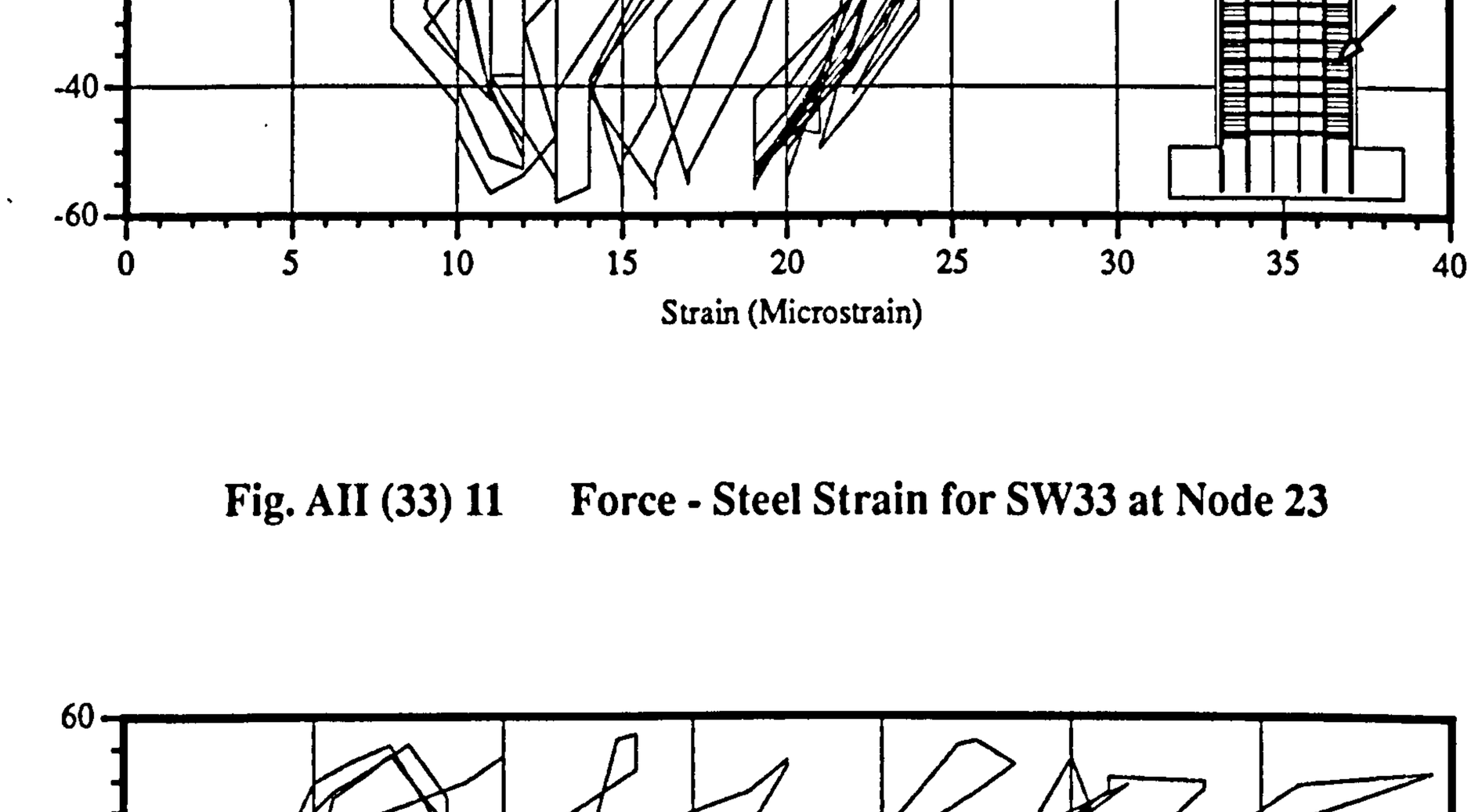


Fig. AII (33) 12 Force - Steel Strain for SW33 at Node 24

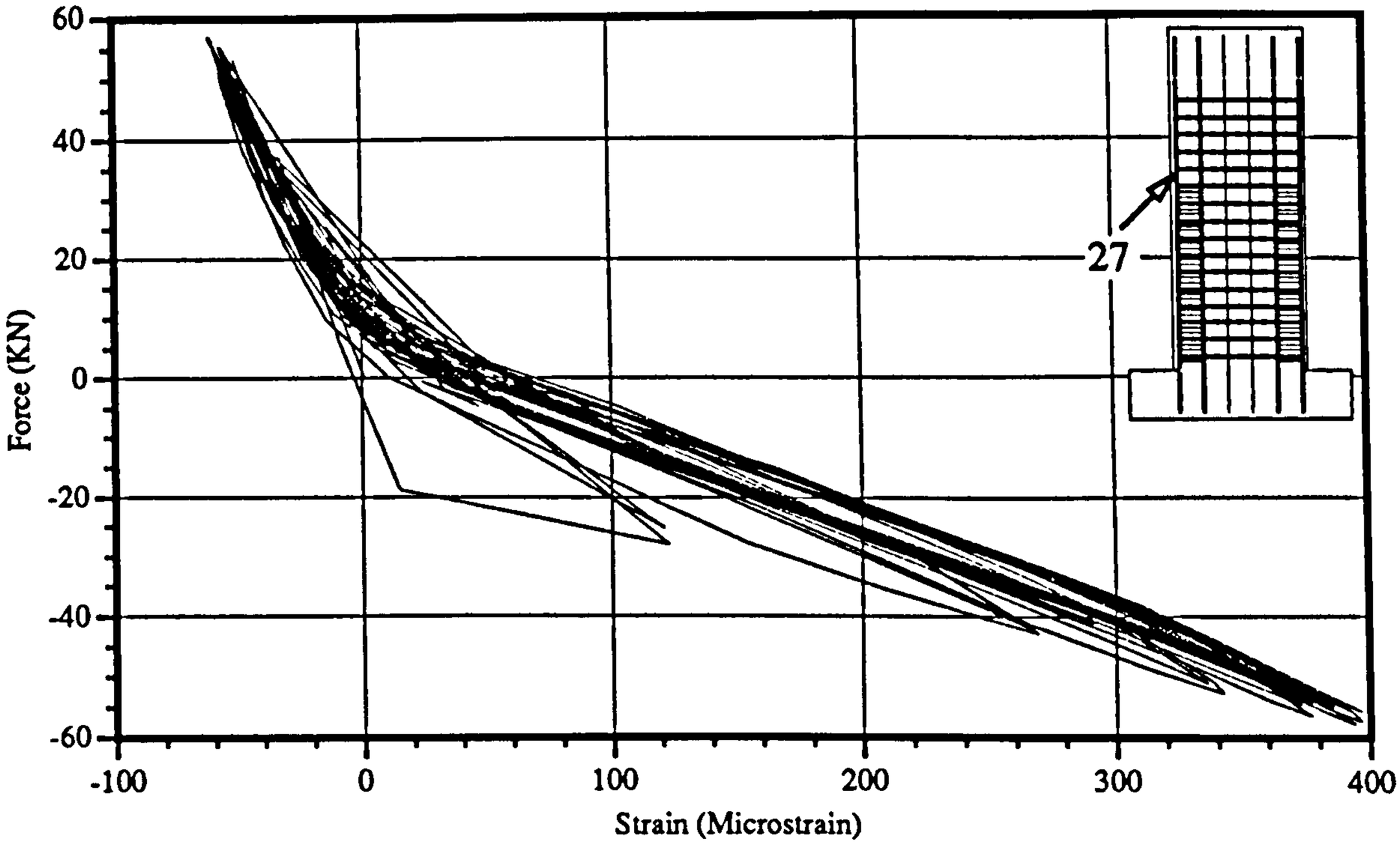


Fig. AII (33) 13 Force - Steel Strain for SW33 at Node 27

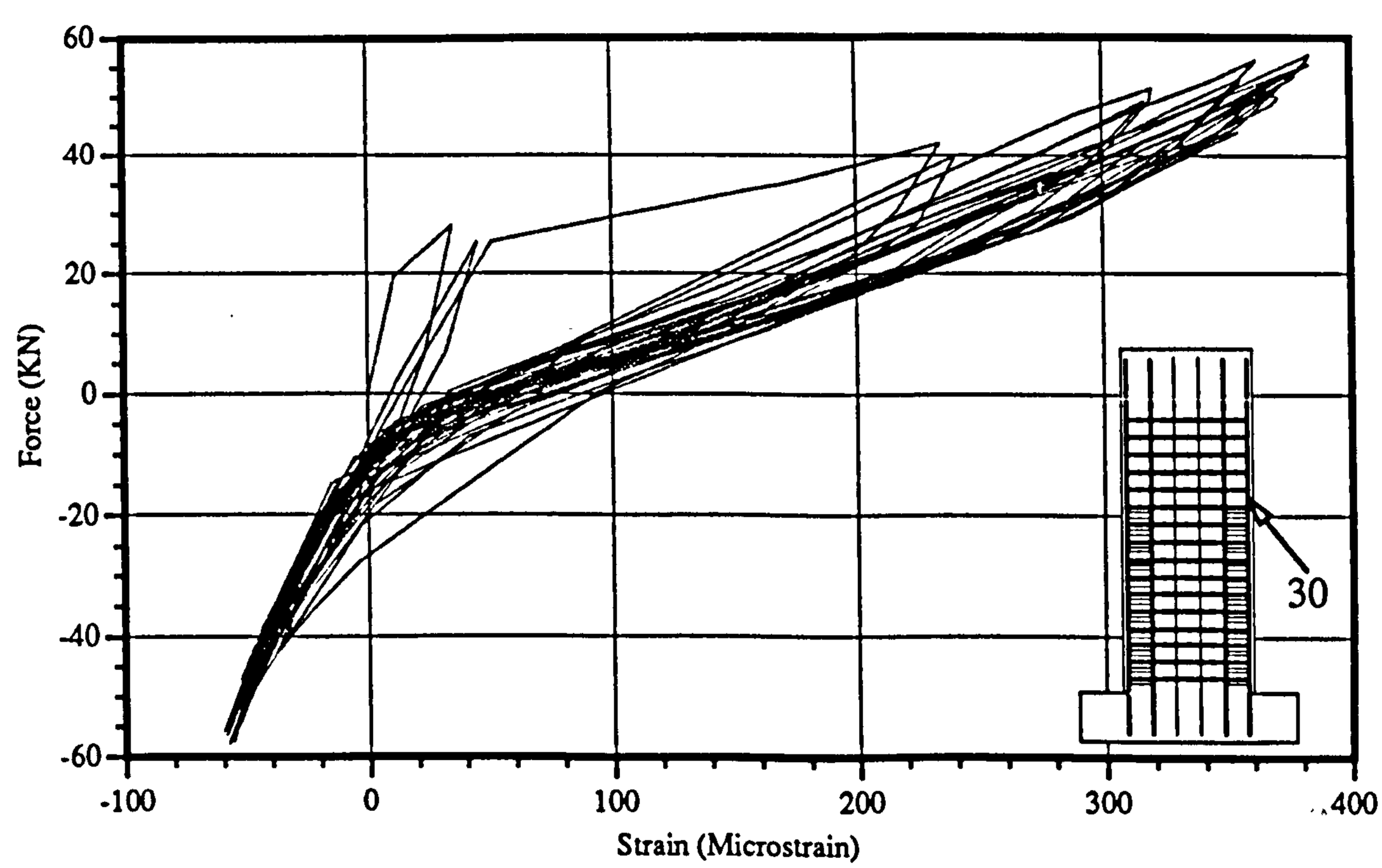


Fig. AII (33) 14 Force - Steel Strain for SW33 at Node 30

AII. 10. Force-Steel Strain for SW34

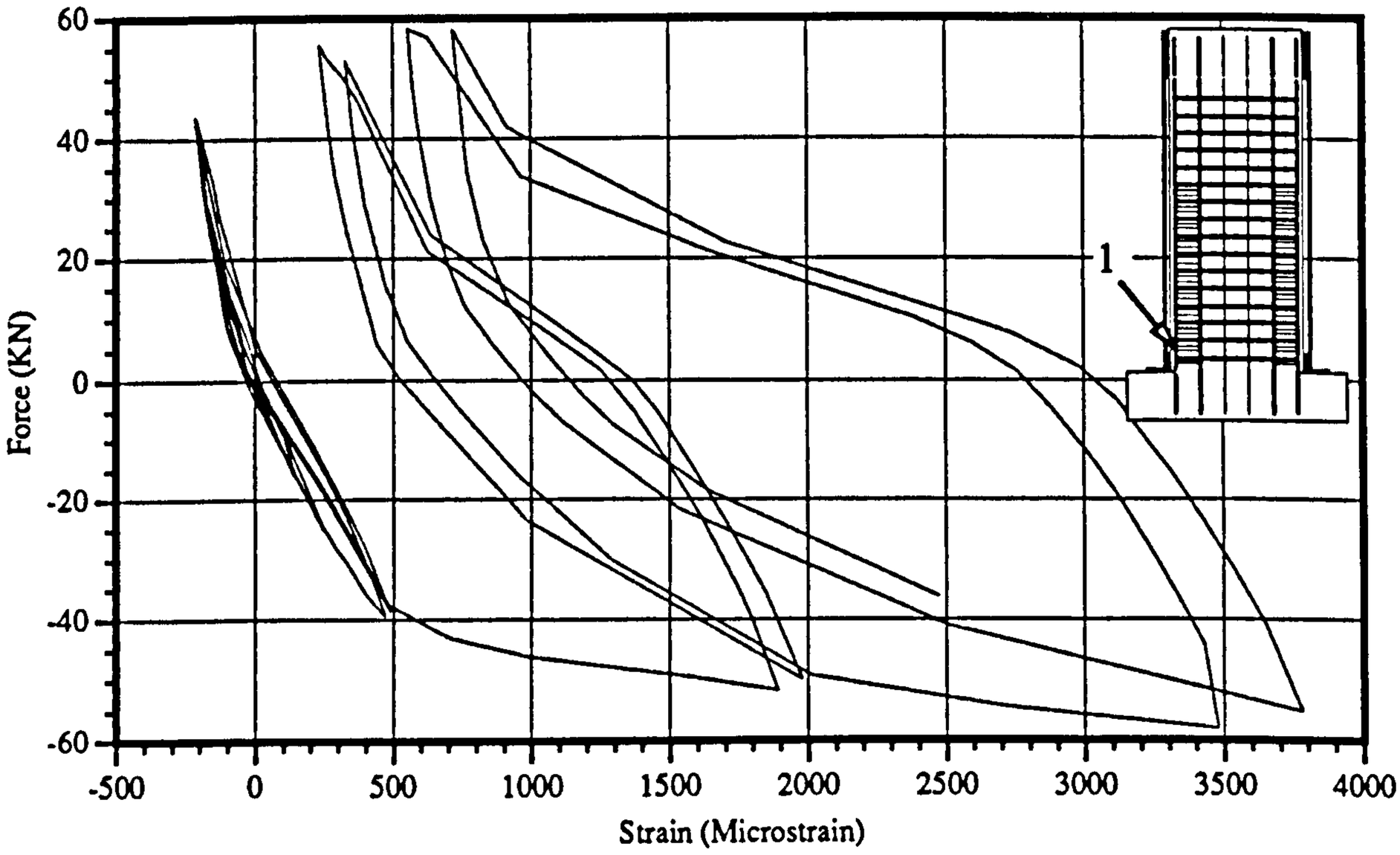


Fig. AII (34) 1 Force - Steel Strain for SW34 at Node 1

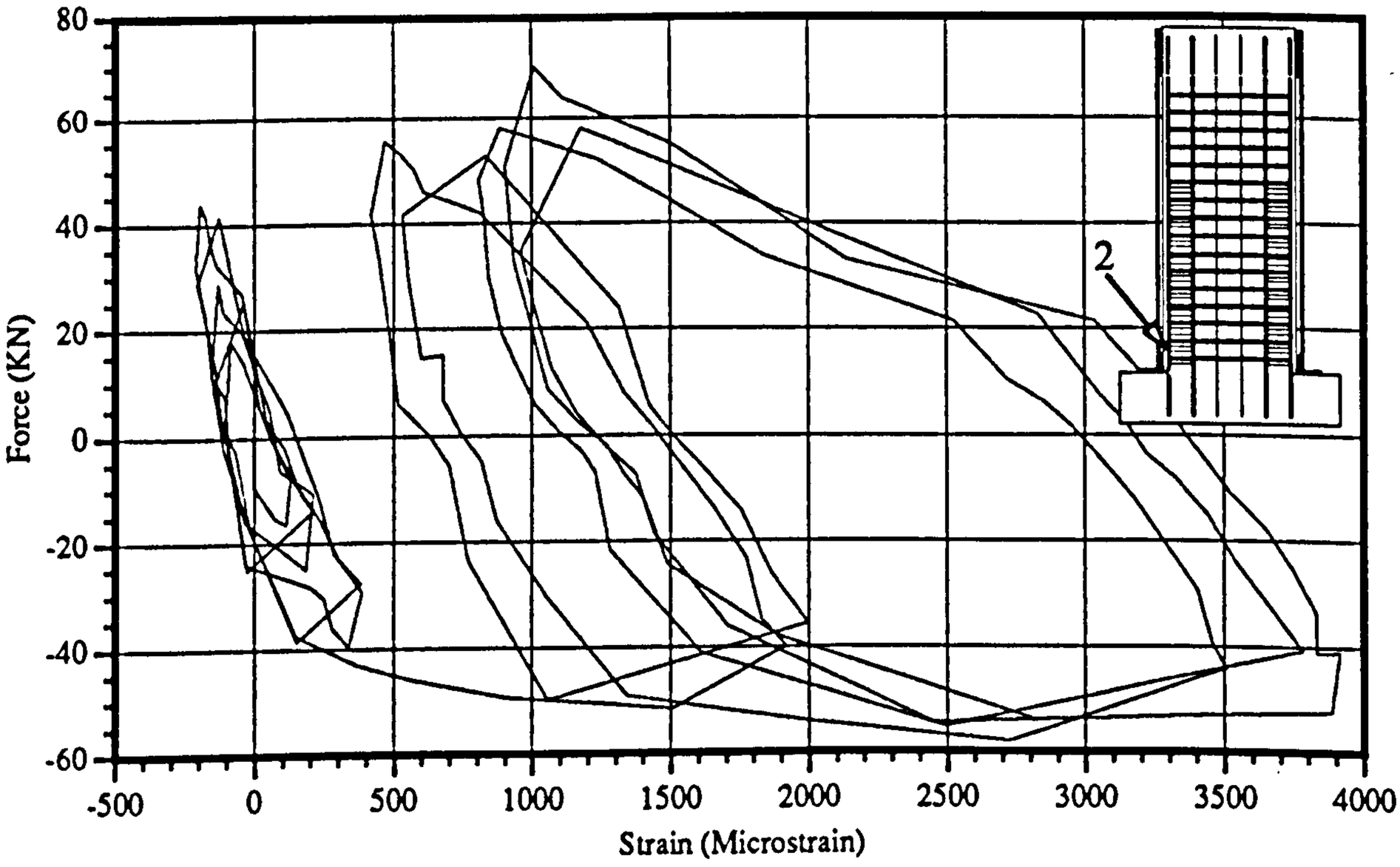


Fig. AII (34) 2 Force - Steel Strain for SW34 at Node 2

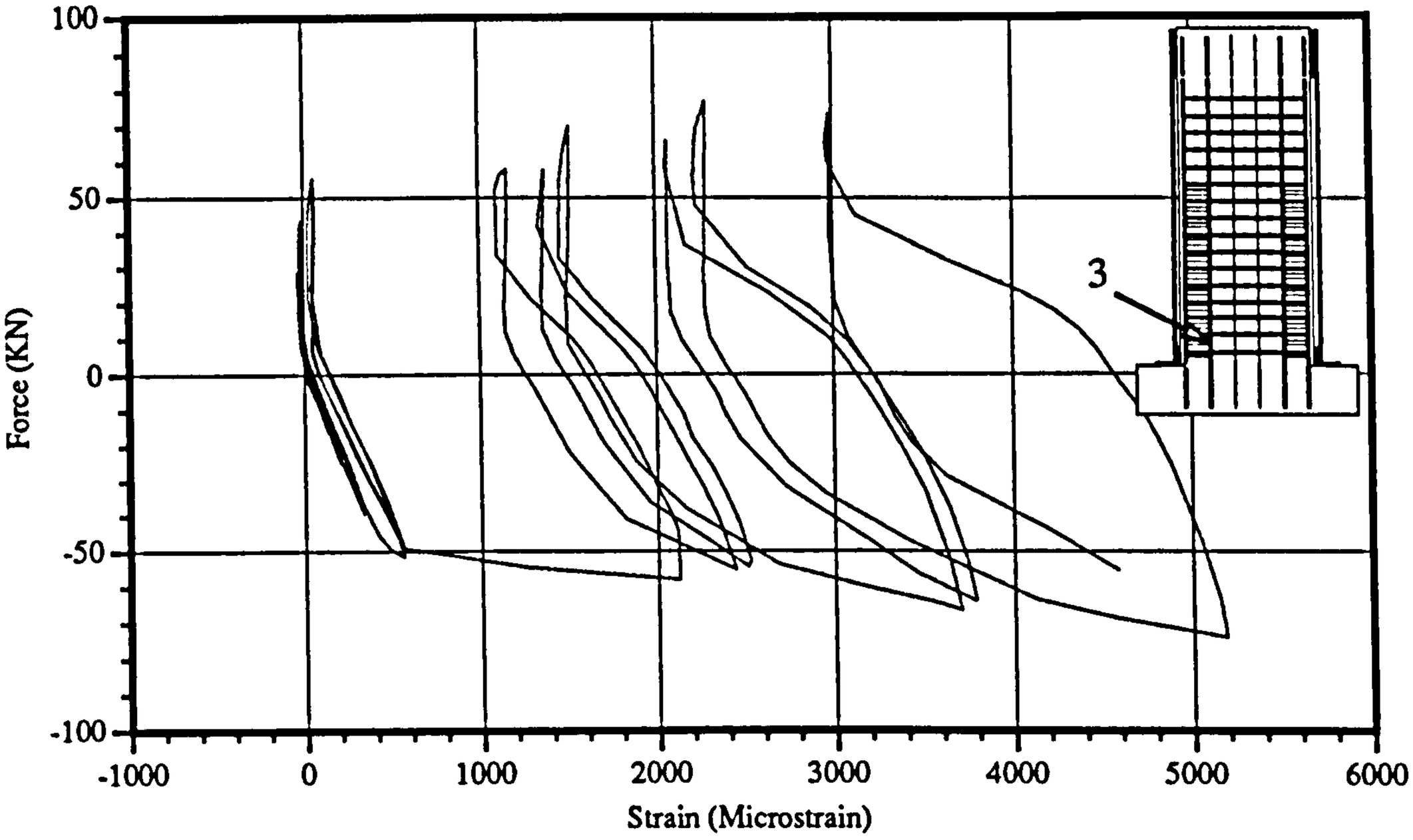


Fig. AII (34) 3 Force - Steel Strain for SW34 at Node 3

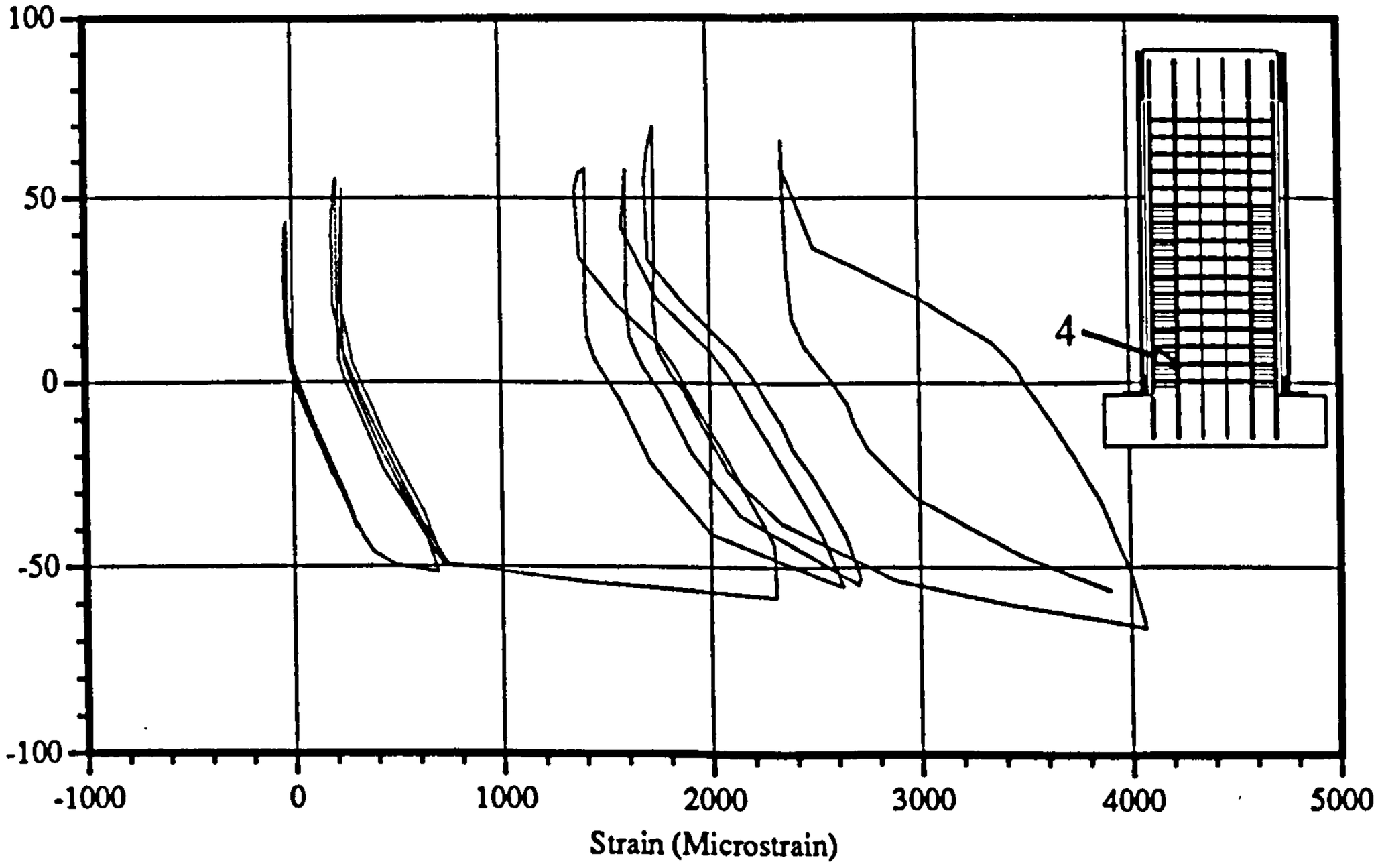


Fig. AII (34) 4 Force - Steel Strain for SW34 at Node 4

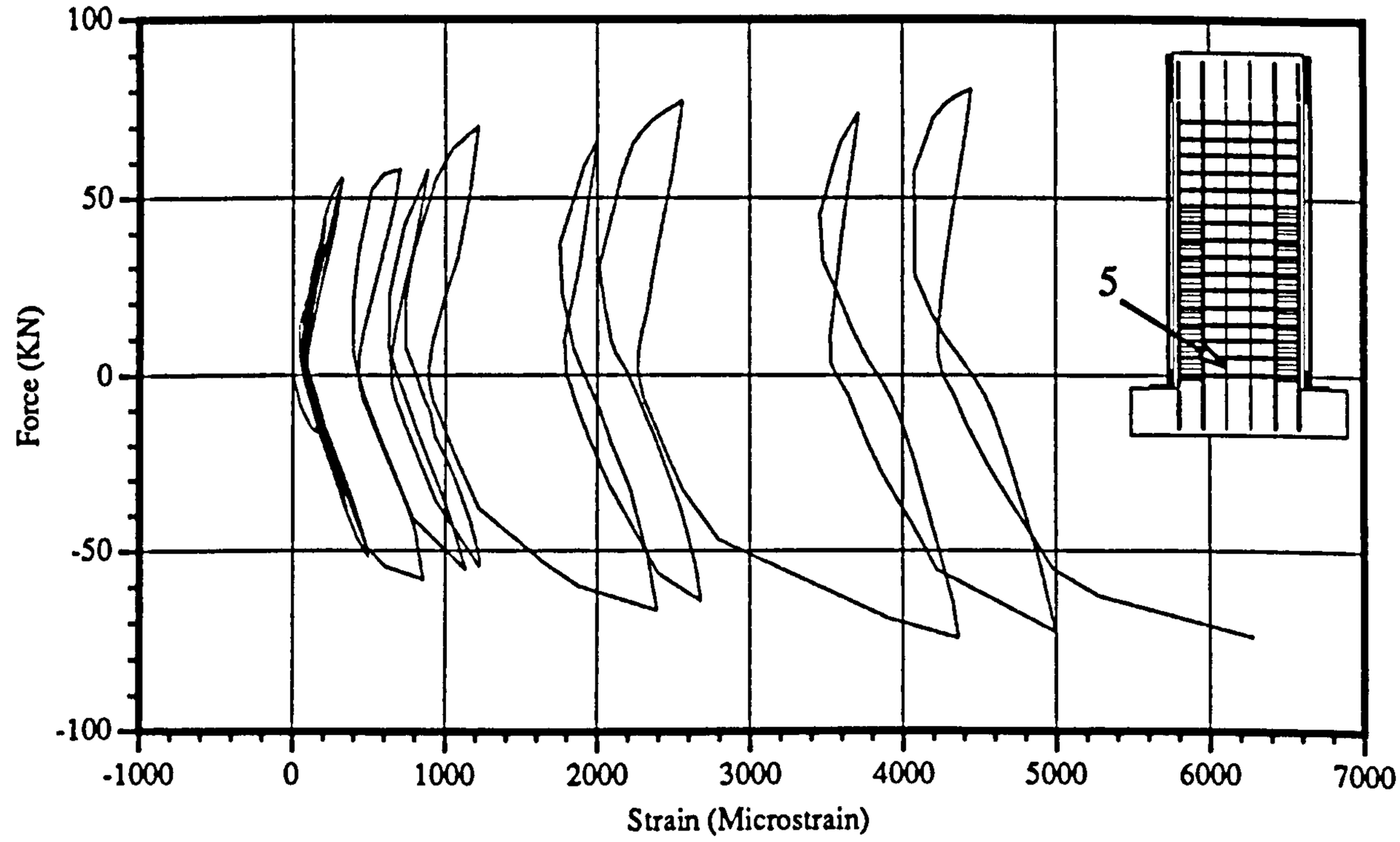


Fig. AII (34) 5 Force - Steel Strain for SW34 at Node 5

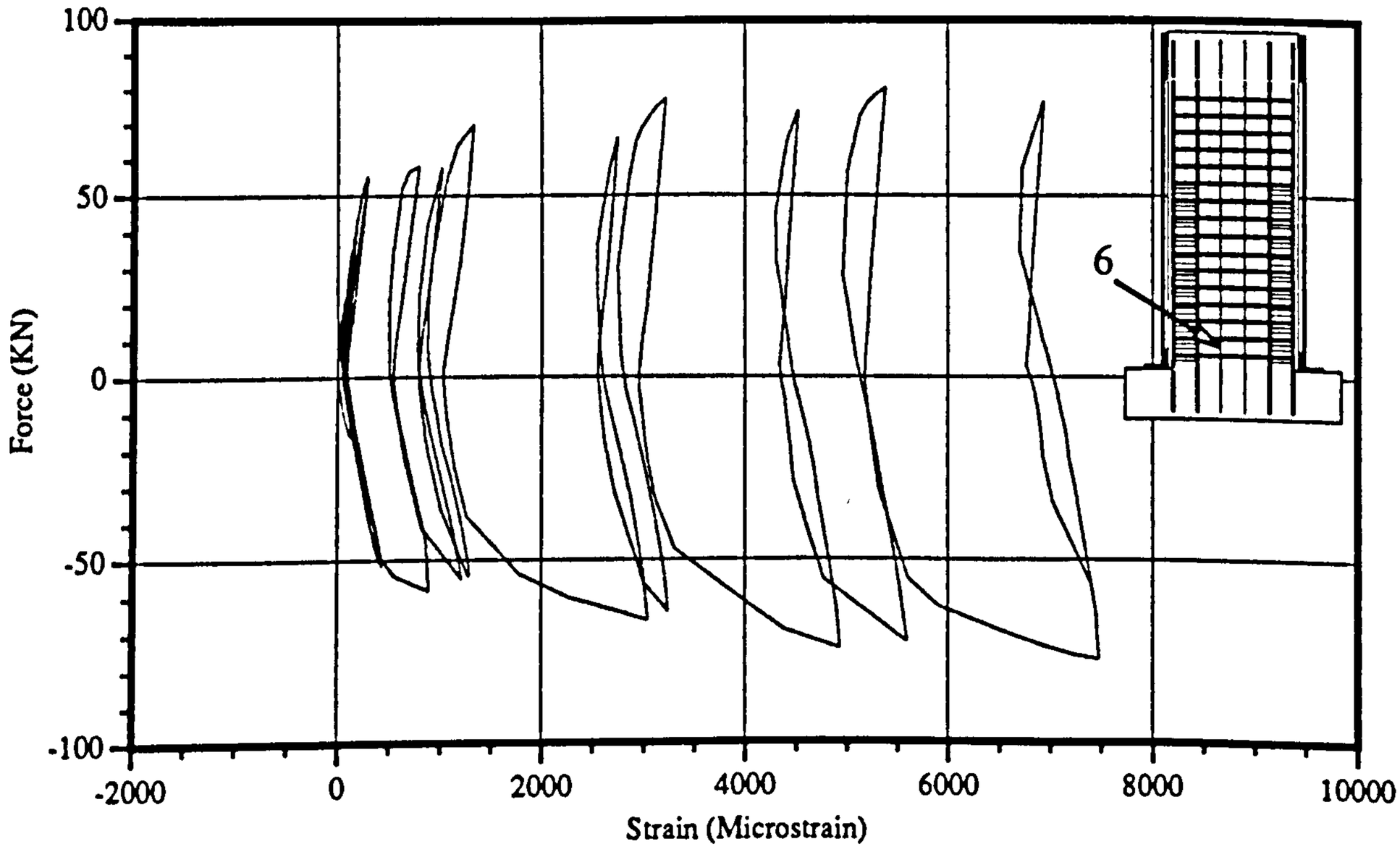


Fig. AII (34) 6 Force - Steel Strain for SW34 at Node 6

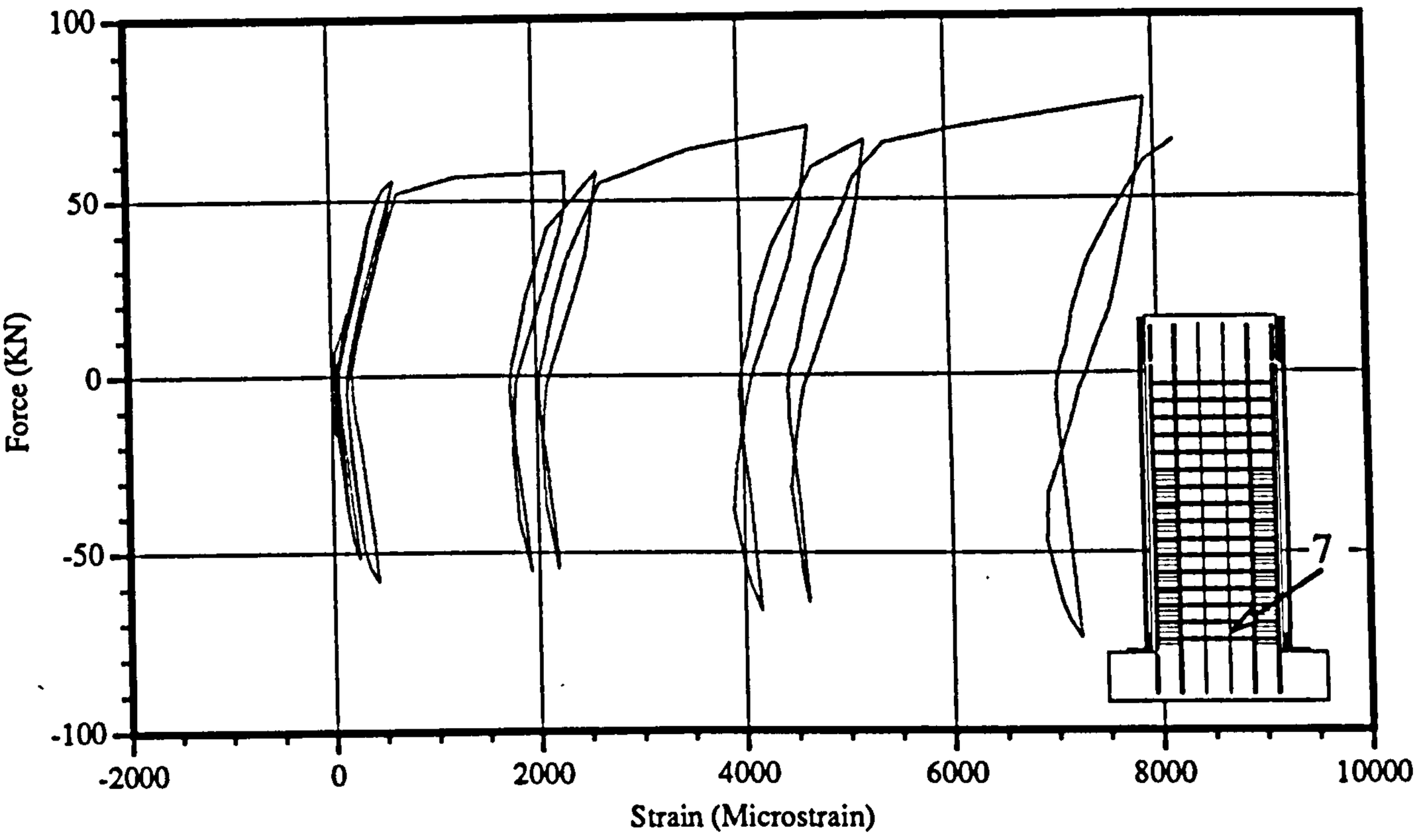


Fig. AII (34) 7 Force - Steel Strain for SW34 at Node 7

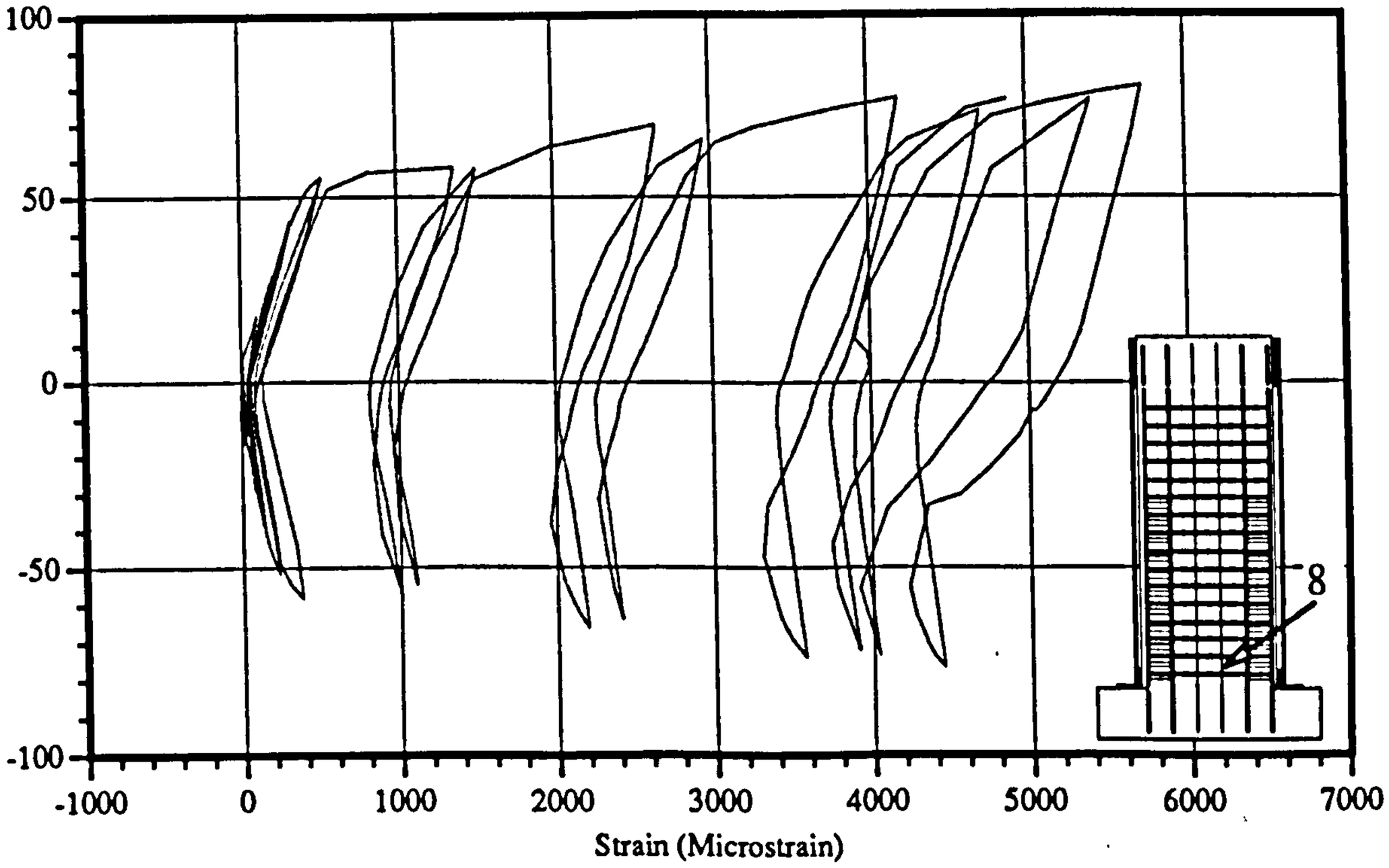


Fig. AII (34) 8 Force - Steel Strain for SW34 at Node 8

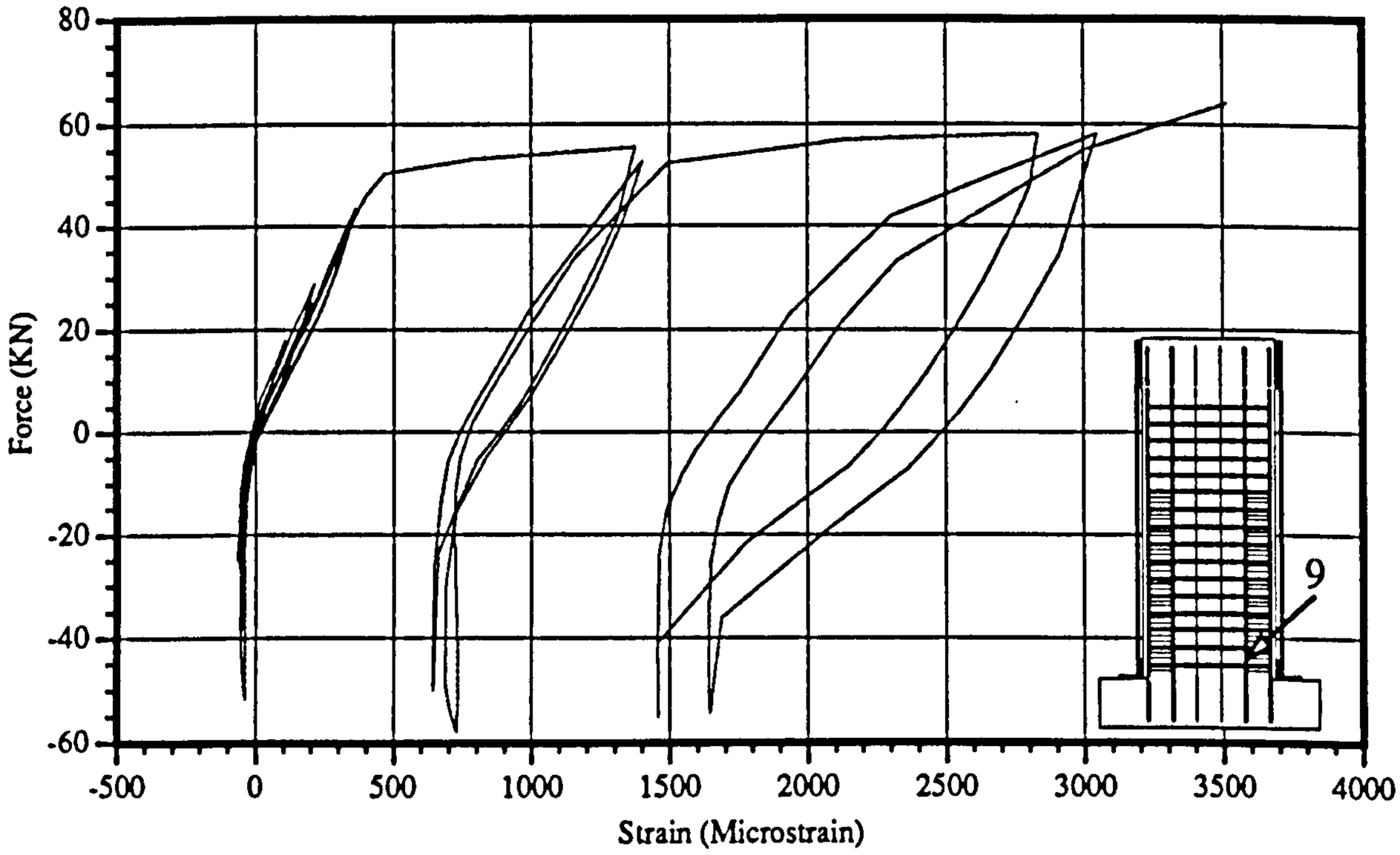


Fig. AII (34) 9 Force - Steel Strain for SW34 at Node 9

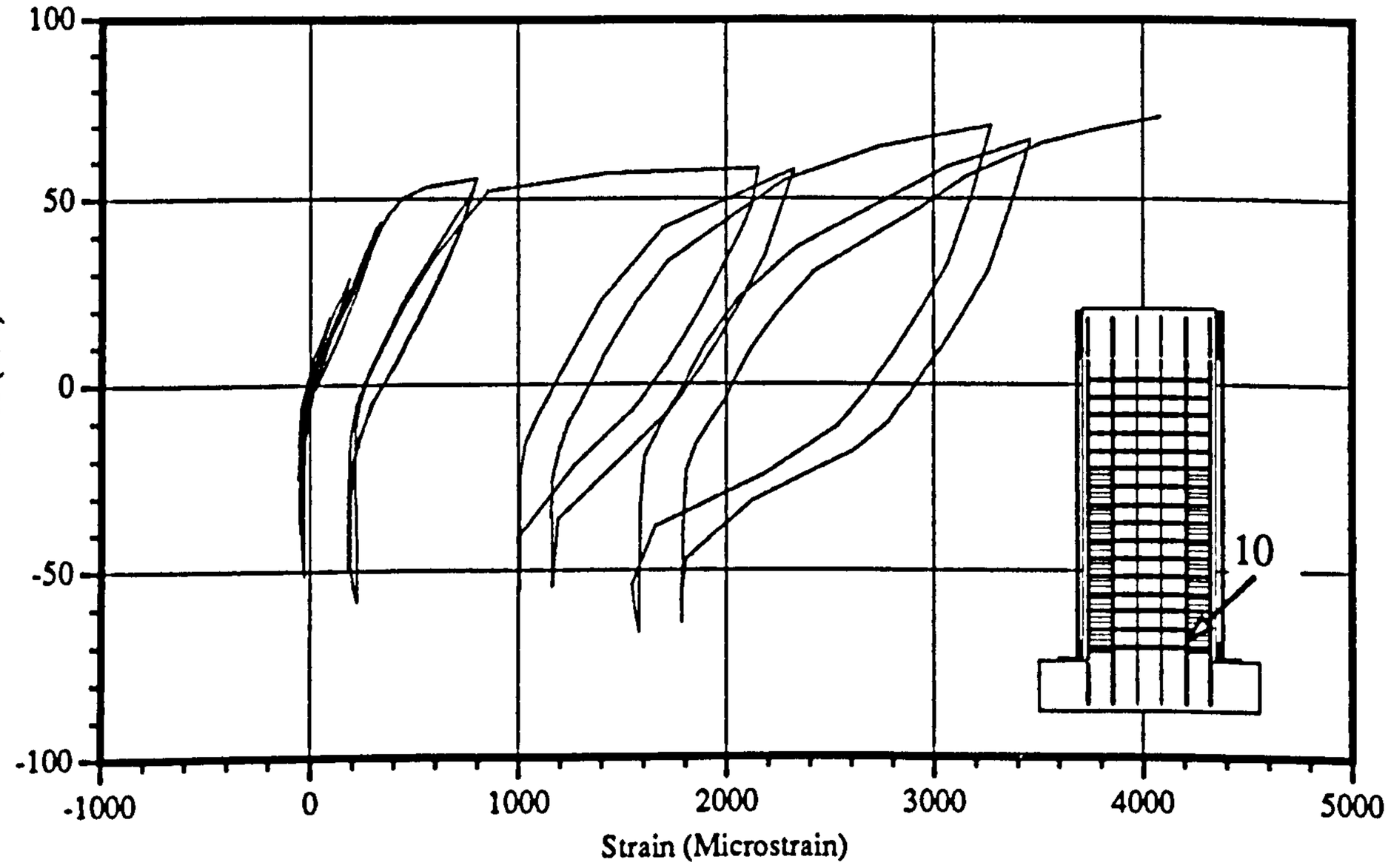


Fig. AII (34) 10 Force - Steel Strain for SW34 at Node 10

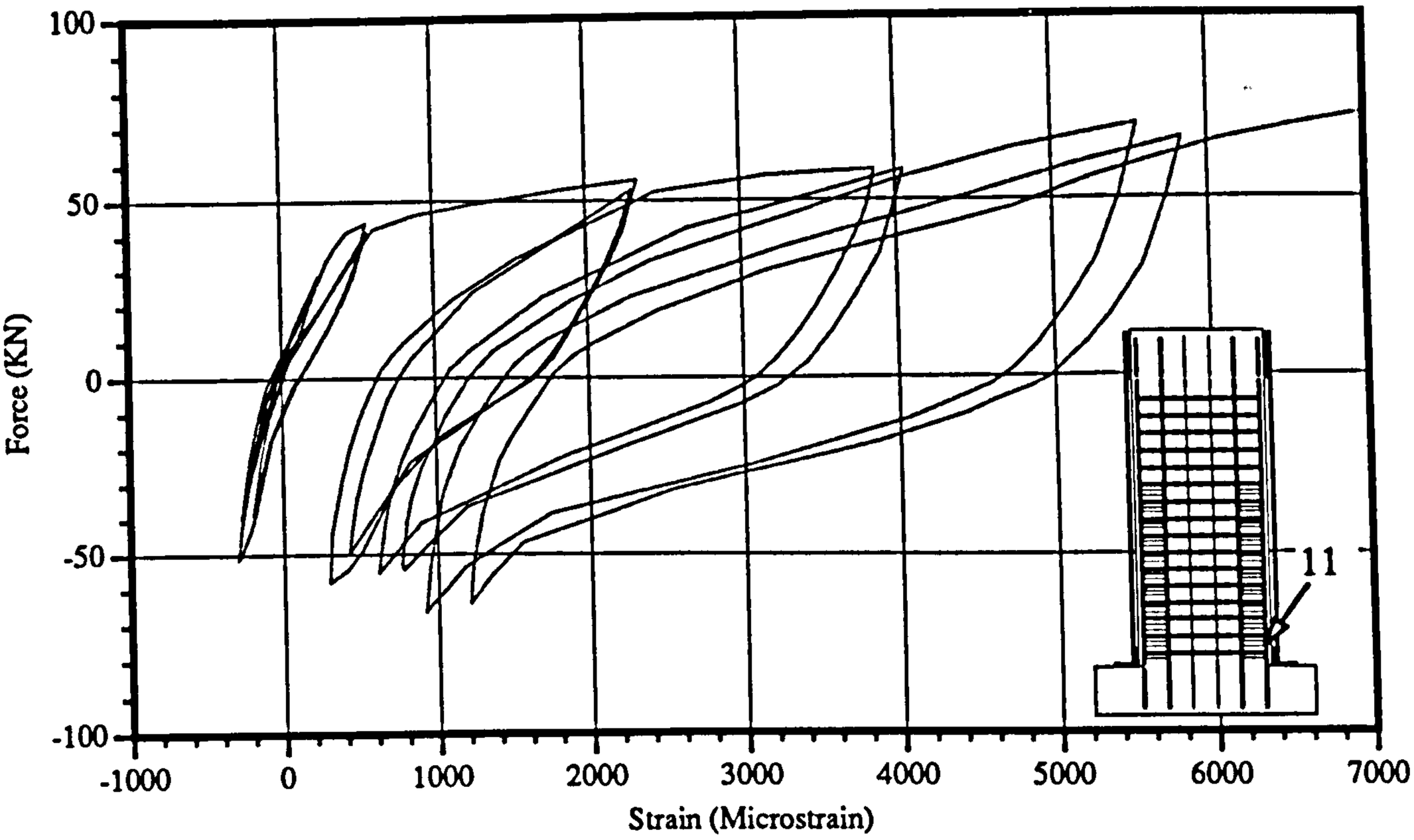


Fig. AII (34) 11 Force - Steel Strain for SW34 at Node 11

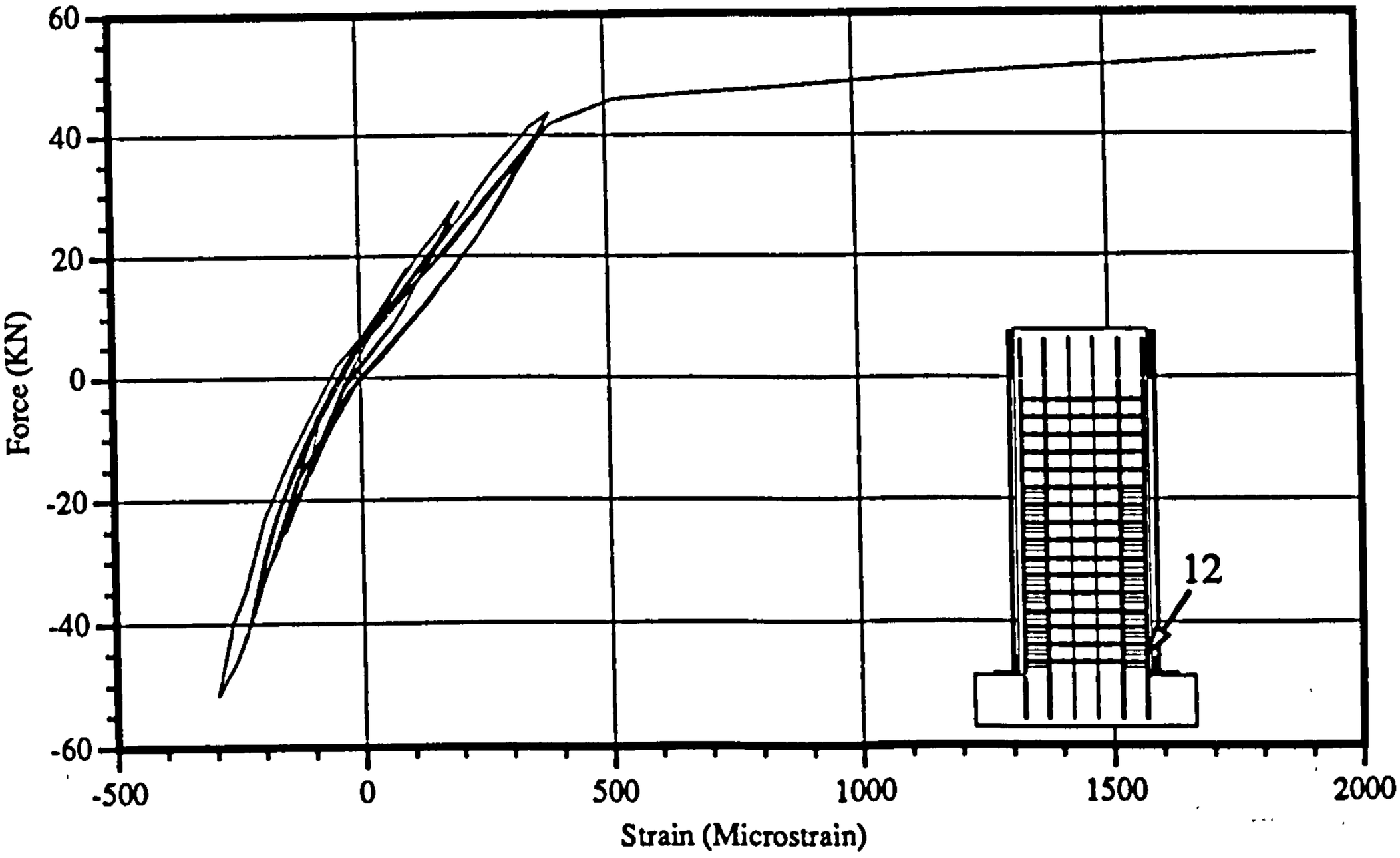


Fig. AII (34) 12 Force - Steel Strain for SW34 at Node 12

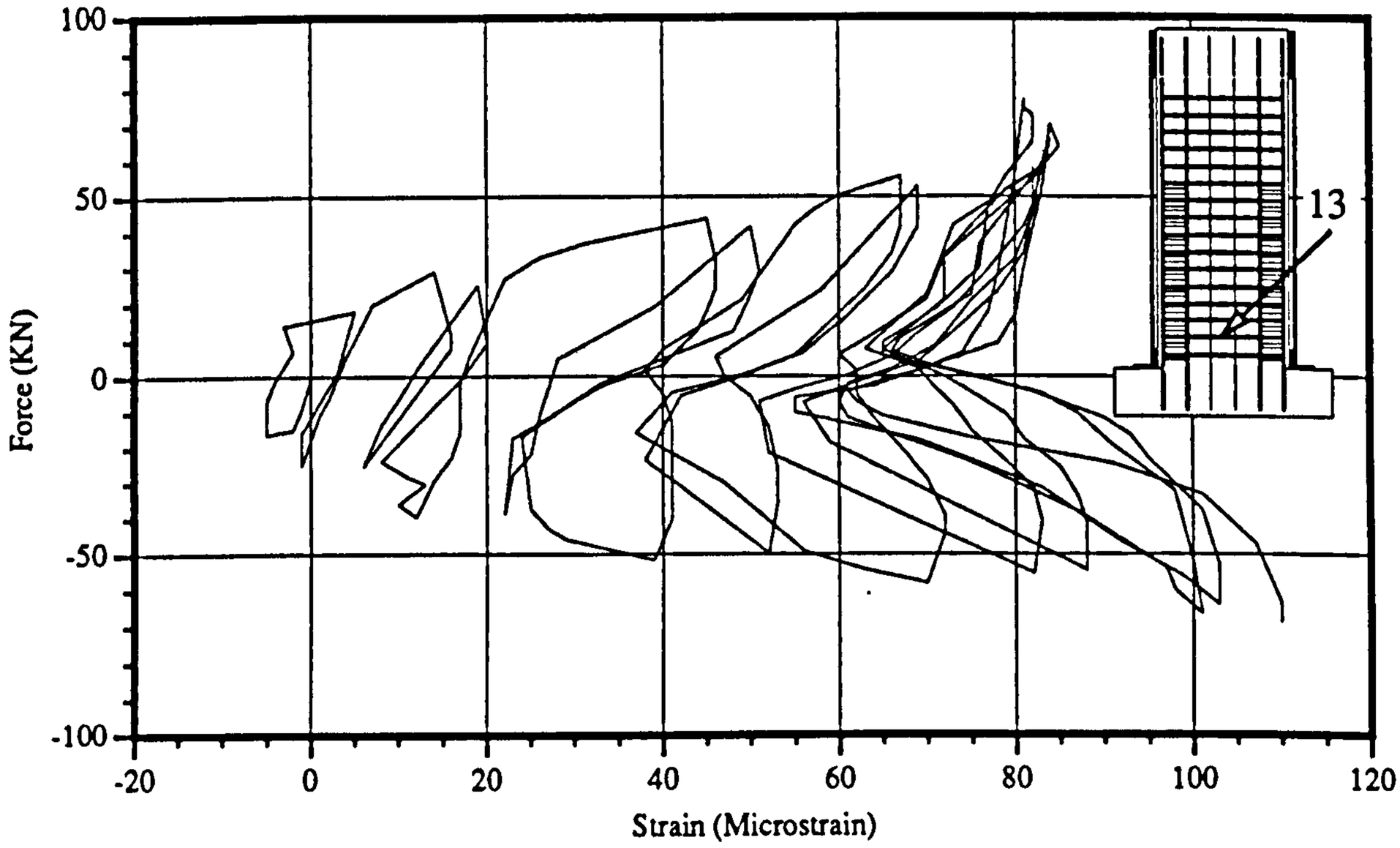


Fig. AII (34) 13 Force - Steel Strain for SW34 at Node 13

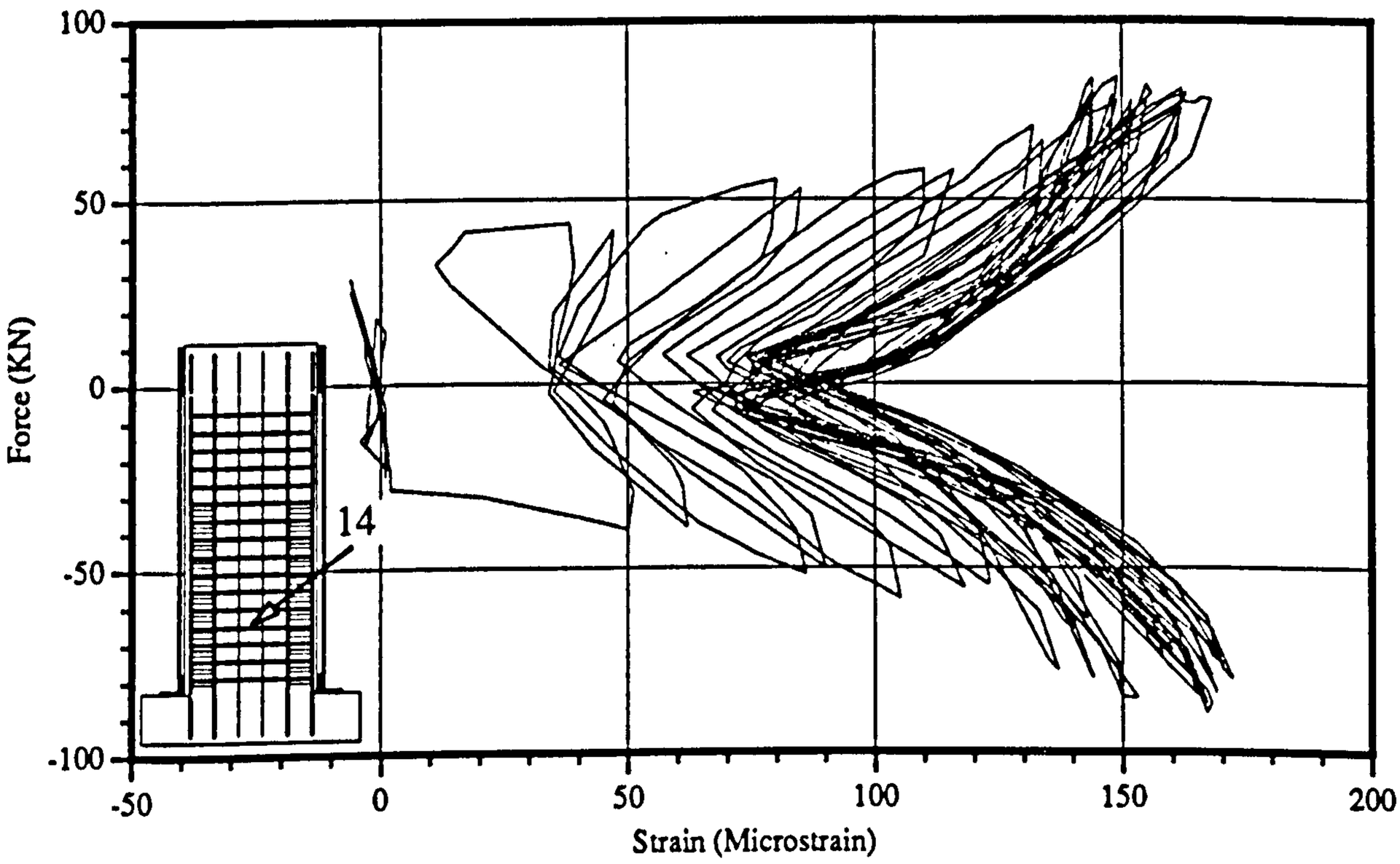


Fig. AII (34) 14 Force - Steel Strain for SW34 at Node 14

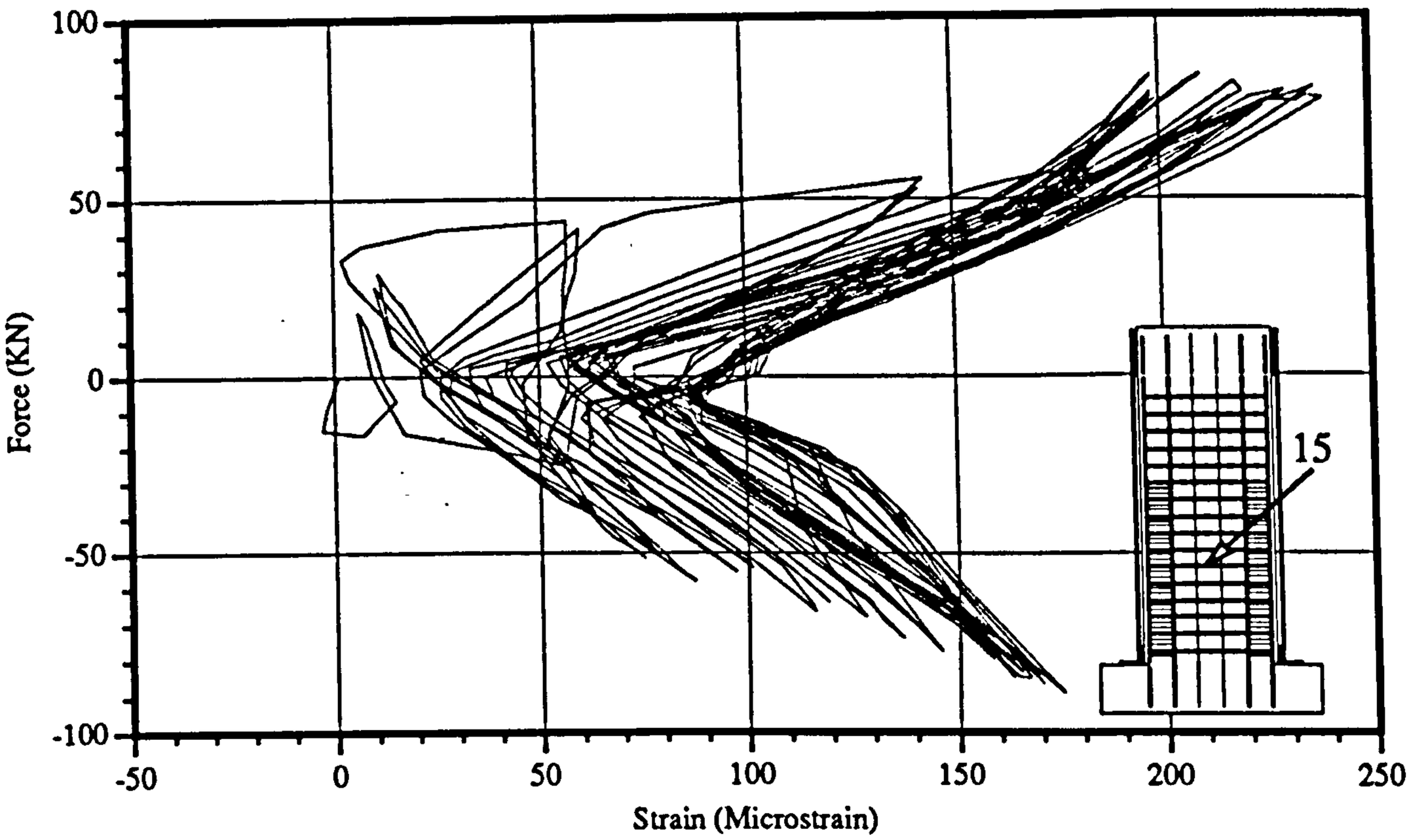


Fig. AII (34) 15 Force - Steel Strain for SW34 at Node 15

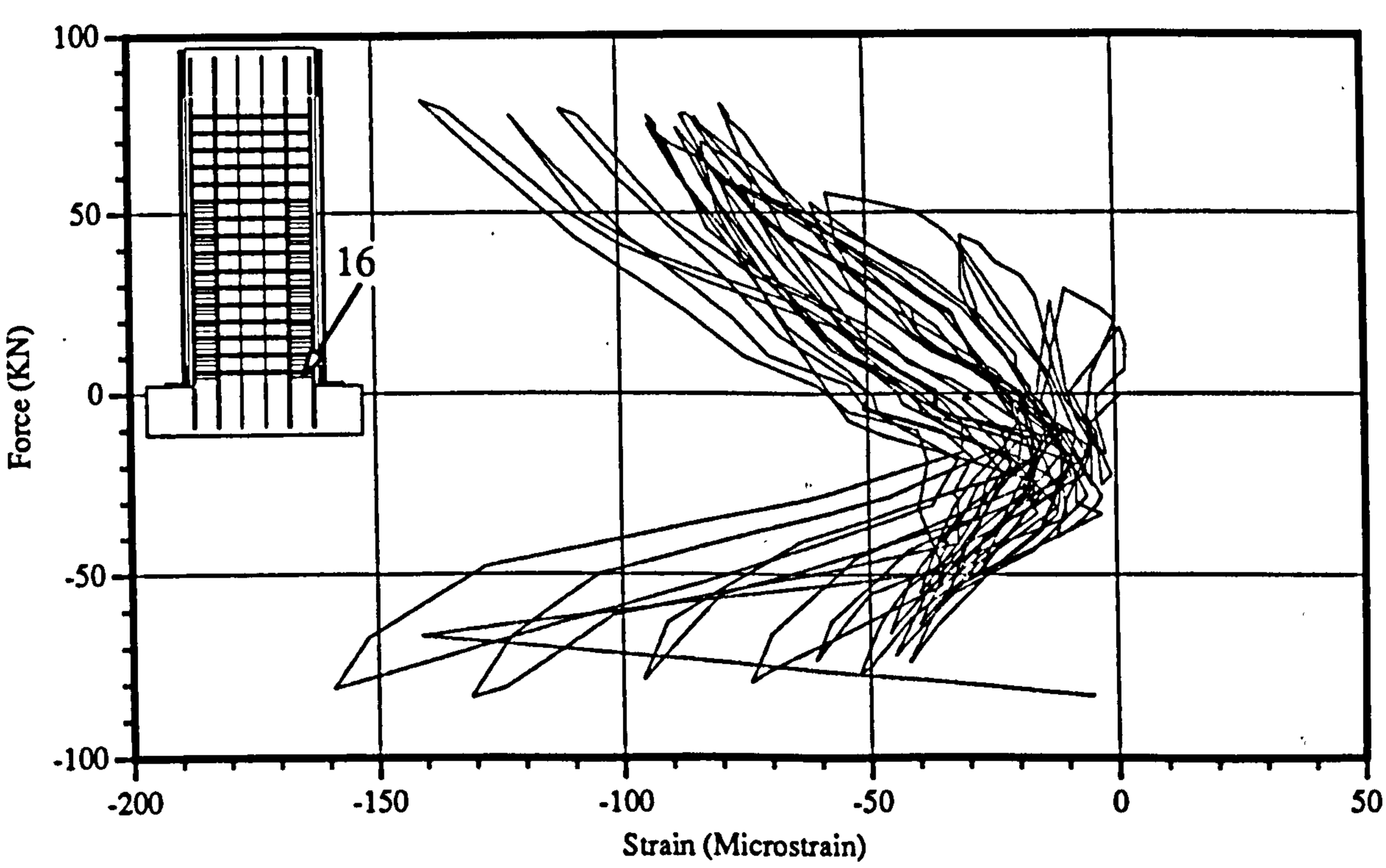


Fig. AII (34) 16 Force - Steel Strain for SW34 at Node 16

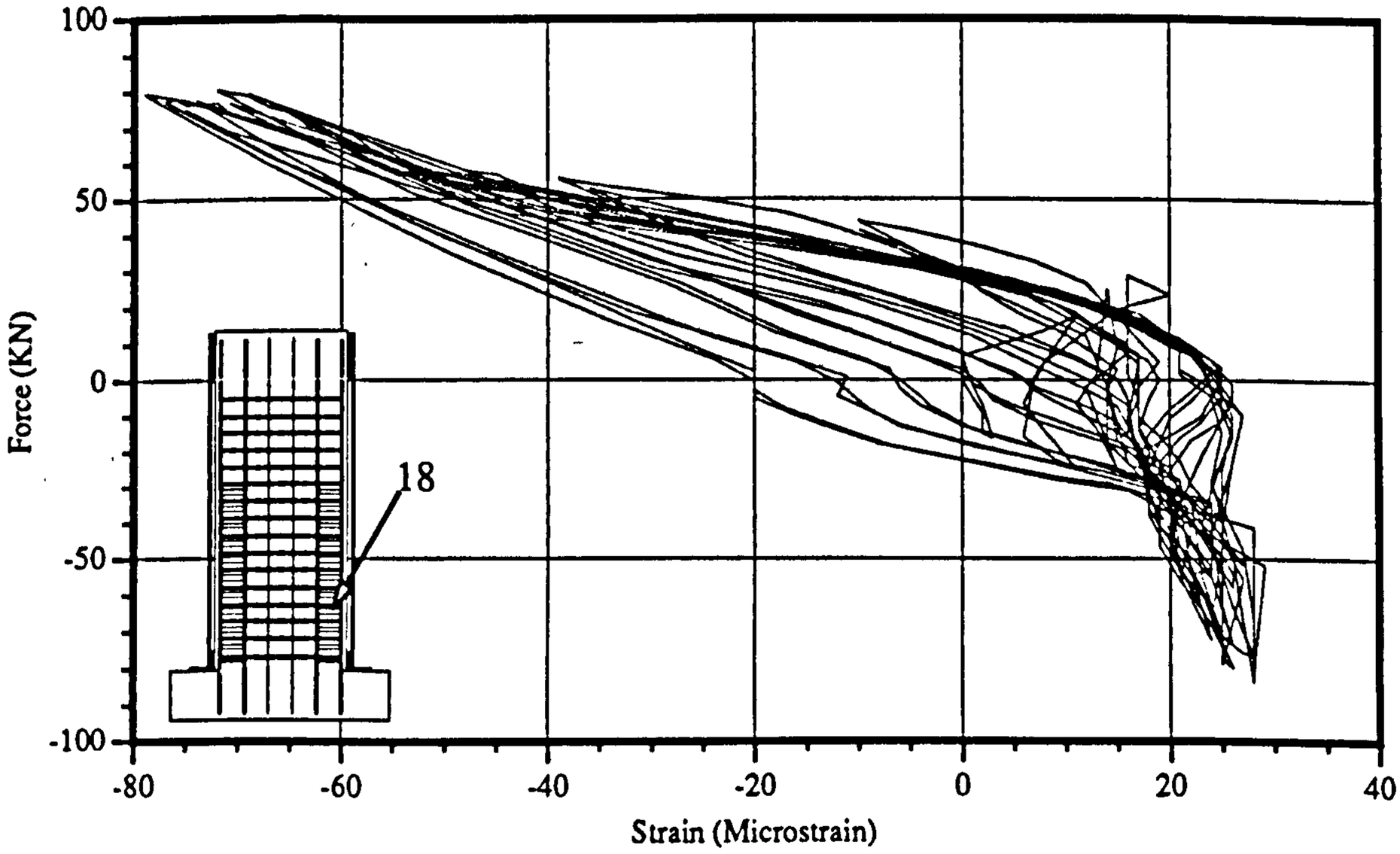


Fig. AII (34) 17 Force - Steel Strain for SW34 at Node 18

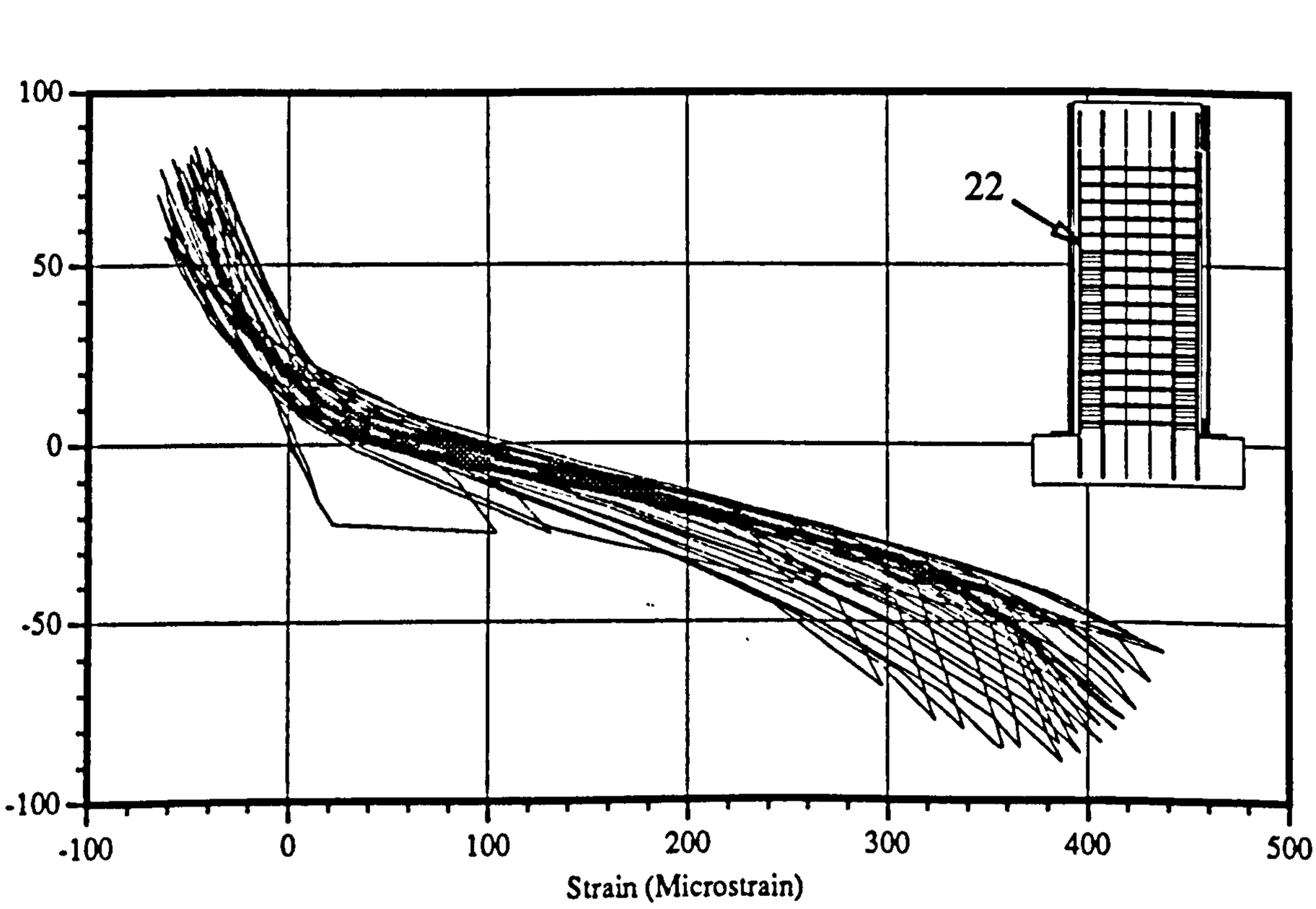


Fig. AII (34) 18 Force - Steel Strain for SW34 at Node 22

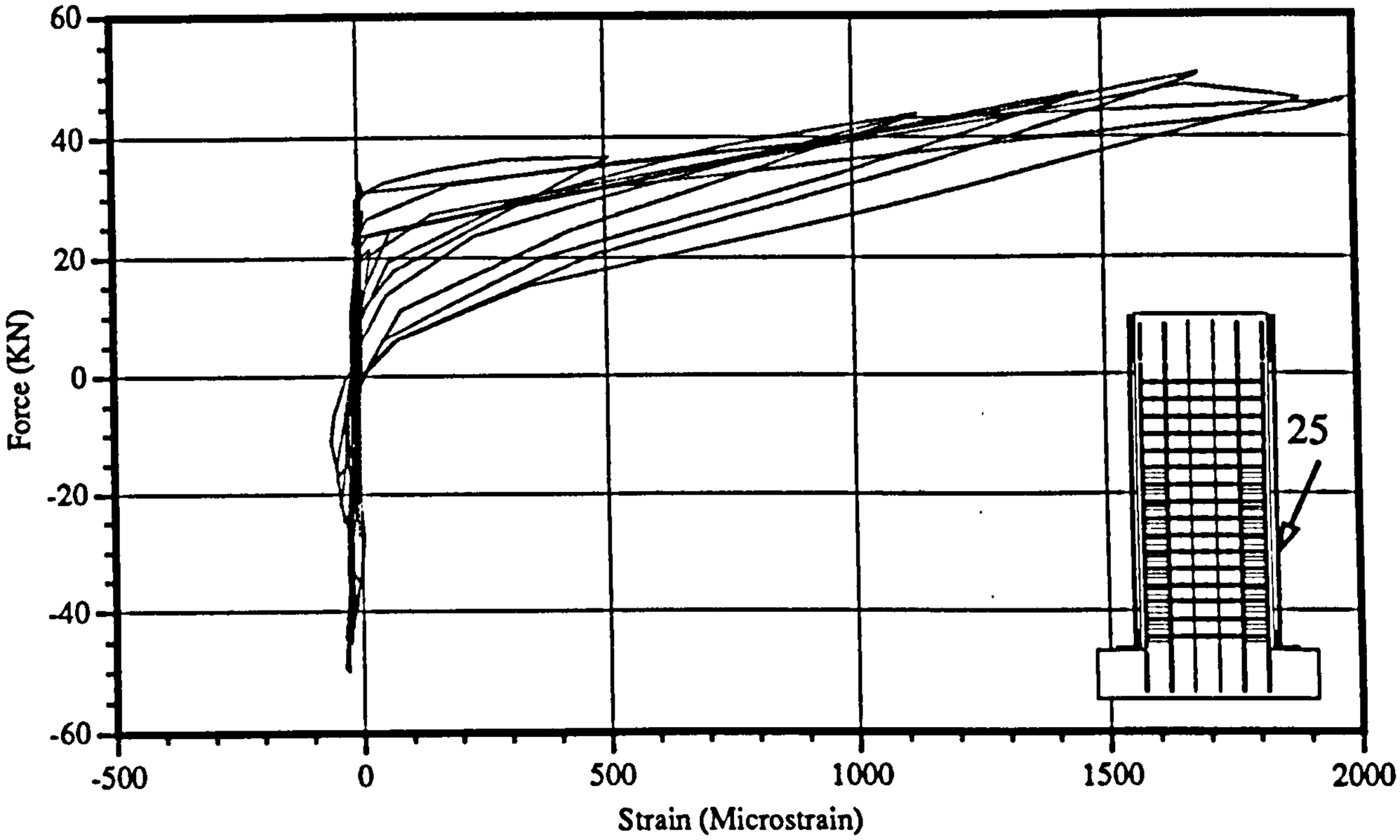


Fig. AII (34) 19 Force - Steel Strain for SW34 at Node 25

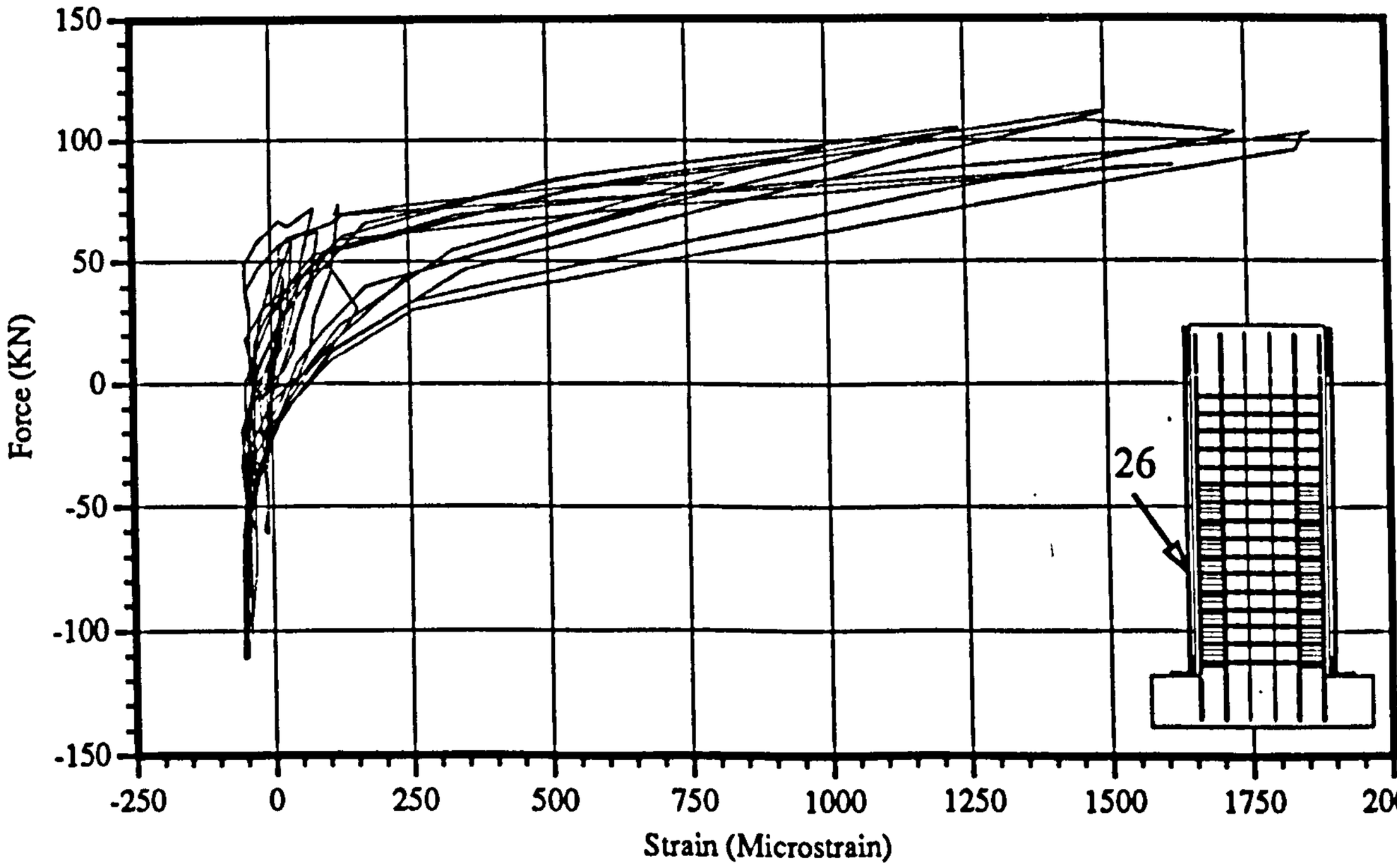


Fig. AII (34) 20 Force - Steel Strain for SW34 at Node 26

AII. 11 Force-Steel Strain for SW35

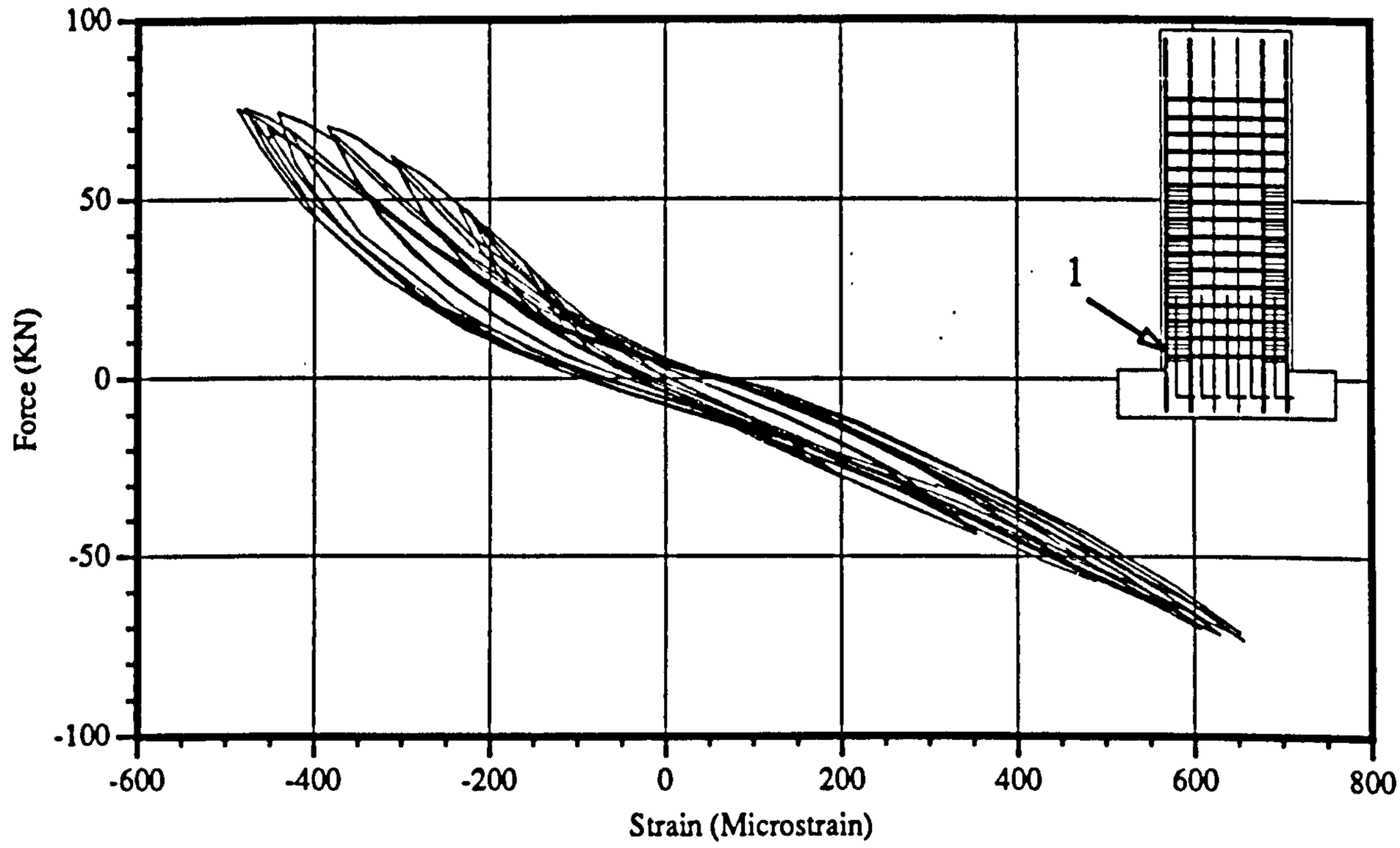


Fig. AII (35) 1 Force - Steel Strain for SW35 at Node 1

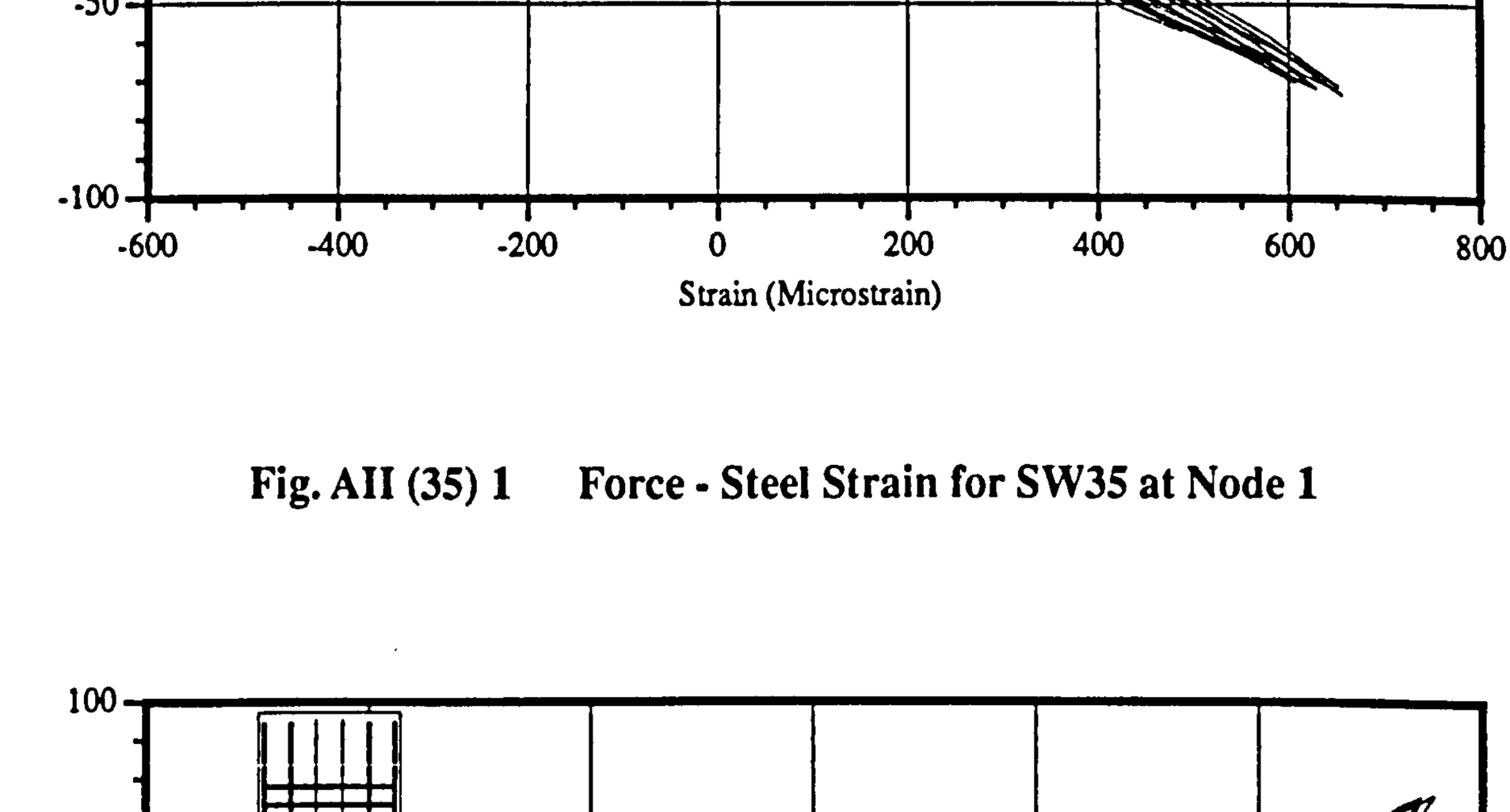


Fig. AII (35) 2 Force - Steel Strain for SW35 at Node 2

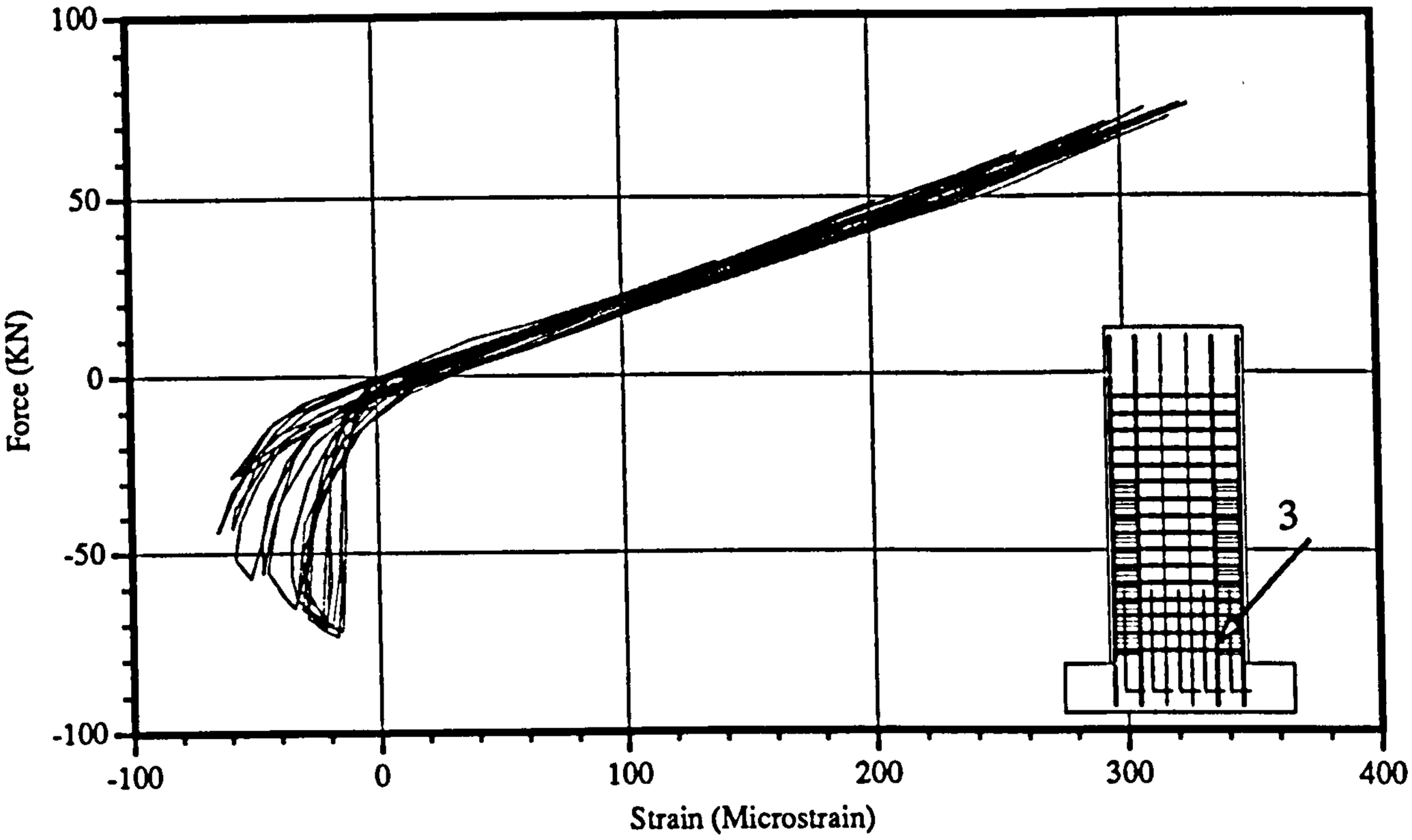


Fig. AII (35) 3 Force - Steel Strain for SW35 at Node 3

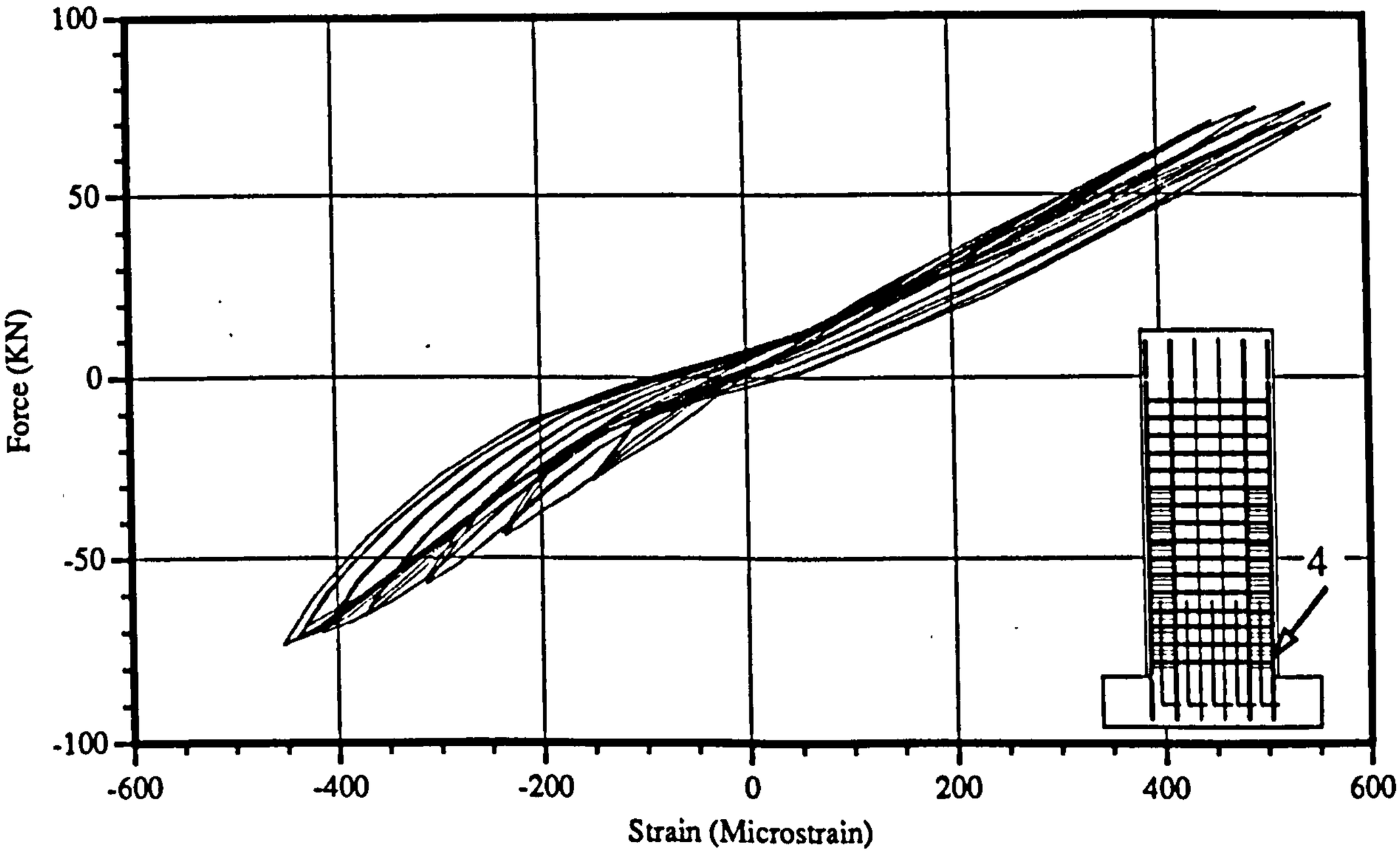


Fig. AII (35) 4 Force - Steel Strain for SW35 at Node 4

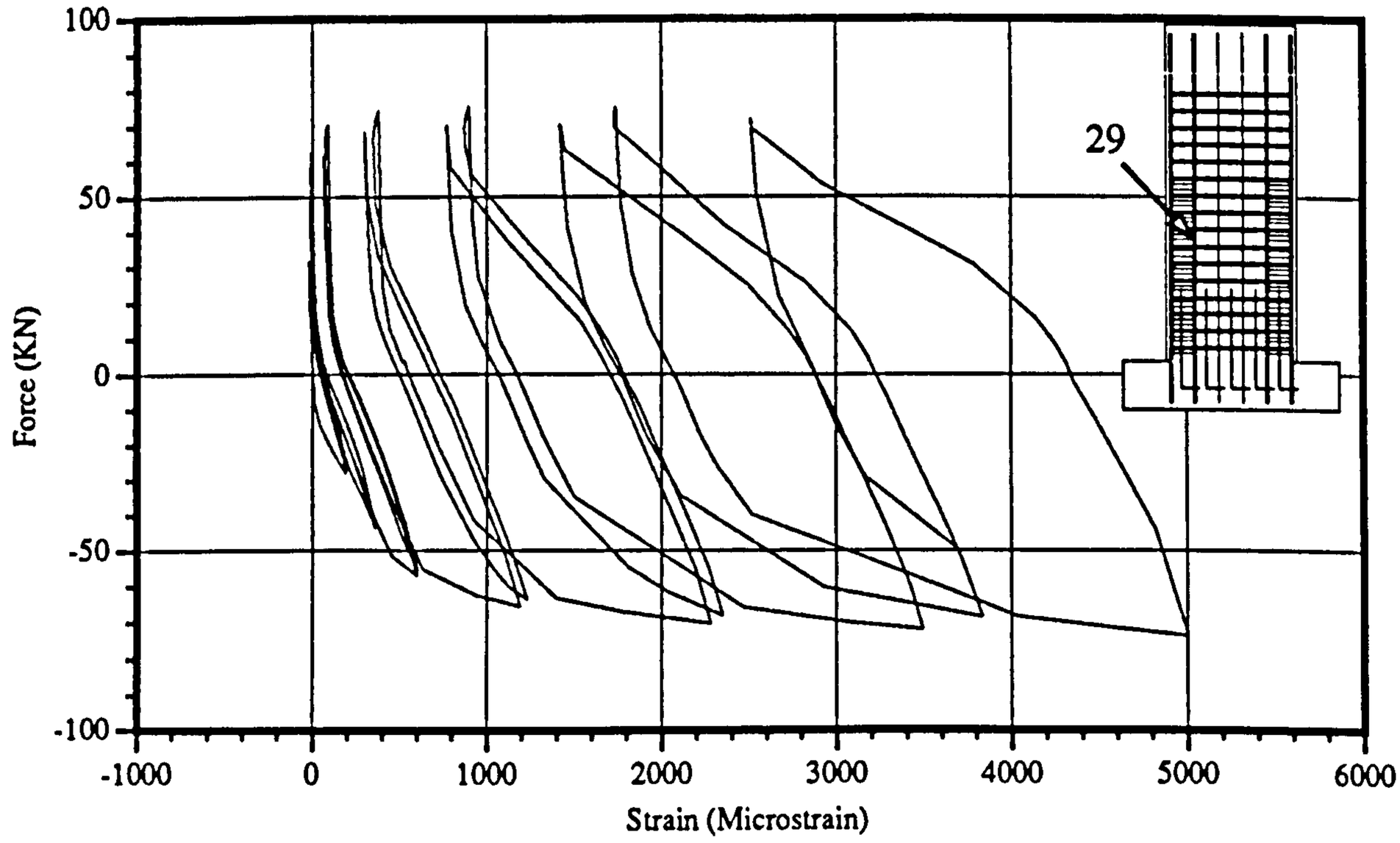


Fig. AII (35) 5 Force - Steel Strain for SW35 at Node 5

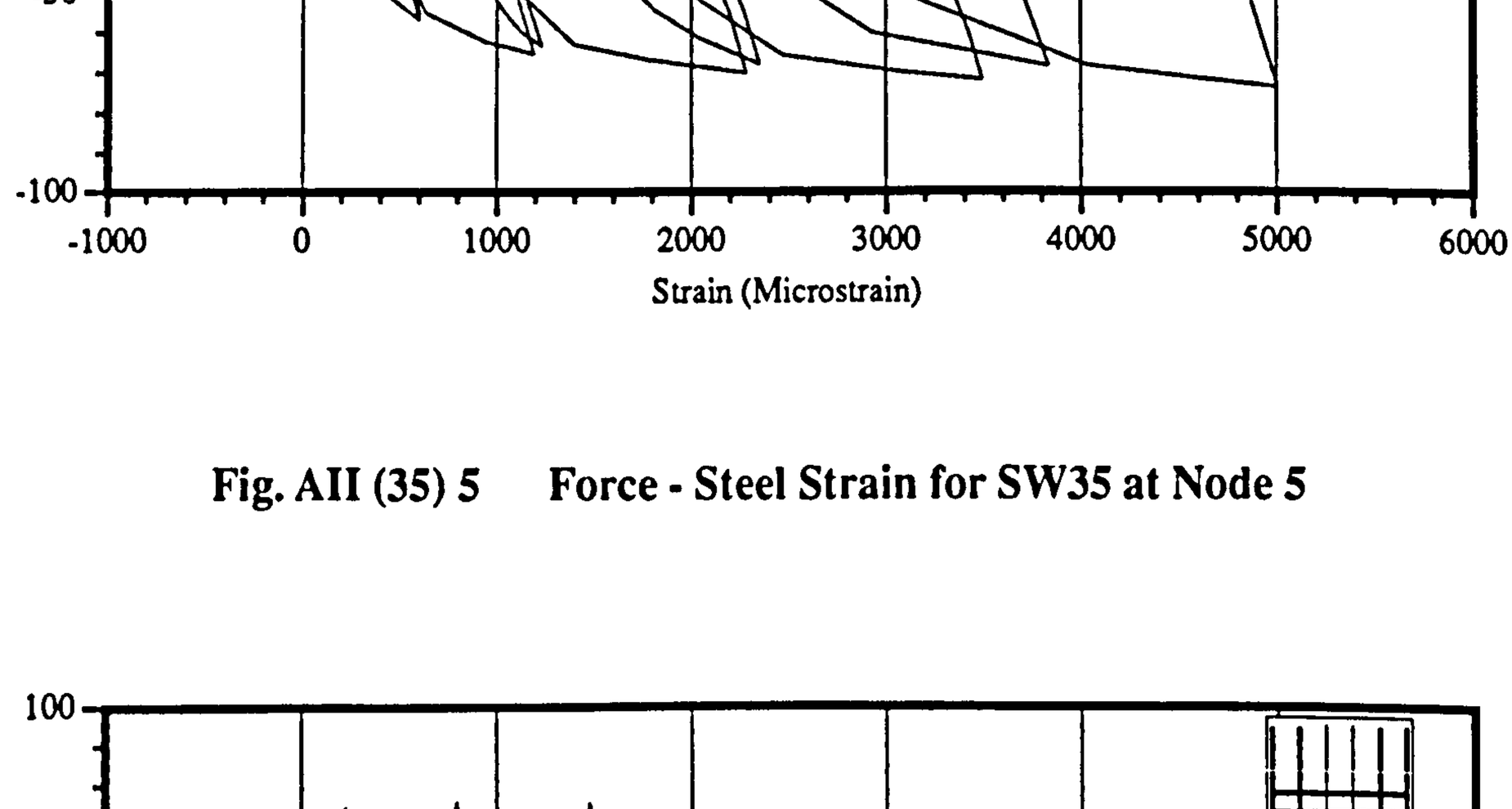


Fig. AII (35) 6 Force - Steel Strain for SW35 at Node 6

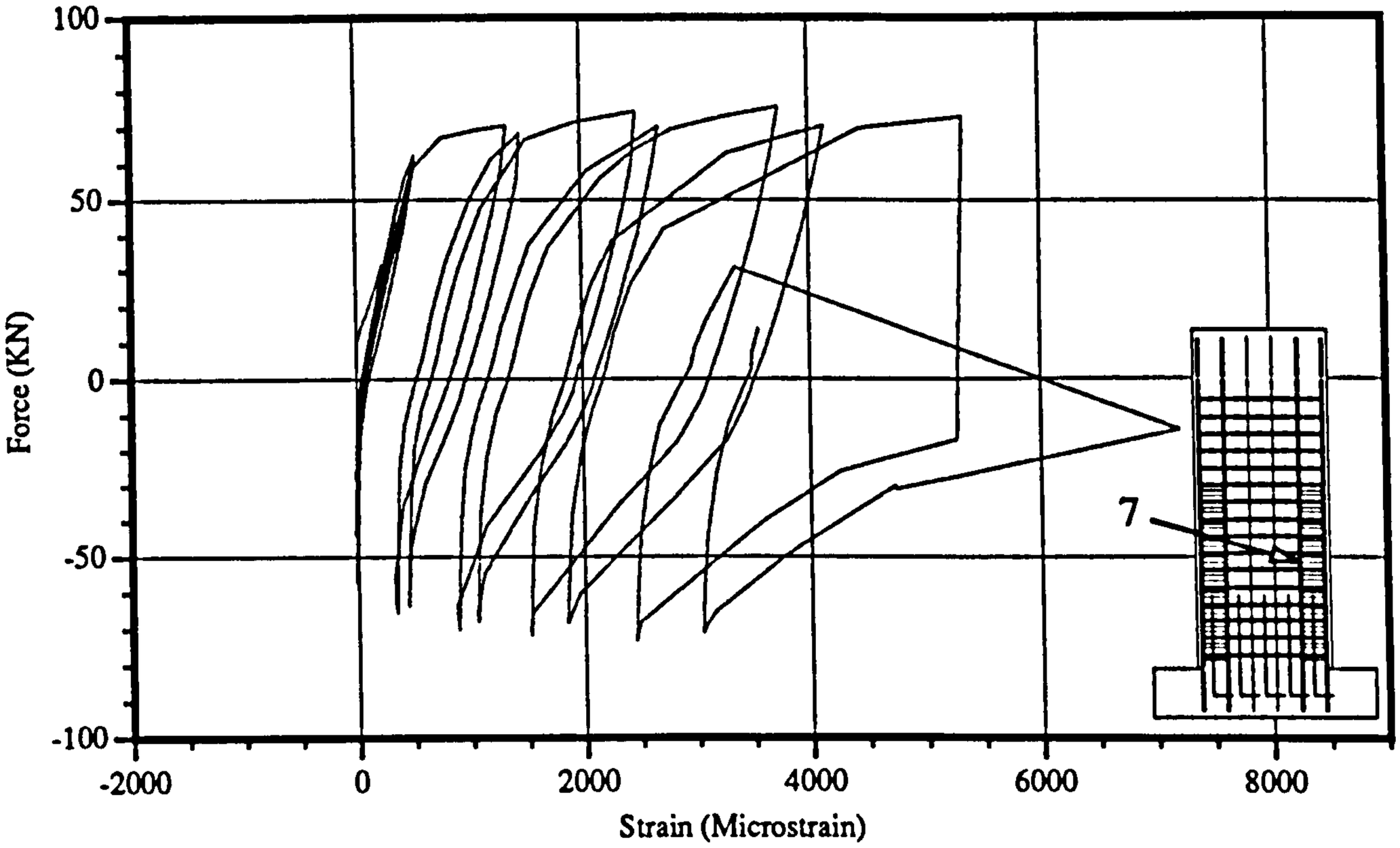


Fig. AII (35) 7 Force - Steel Strain for SW35 at Node 7

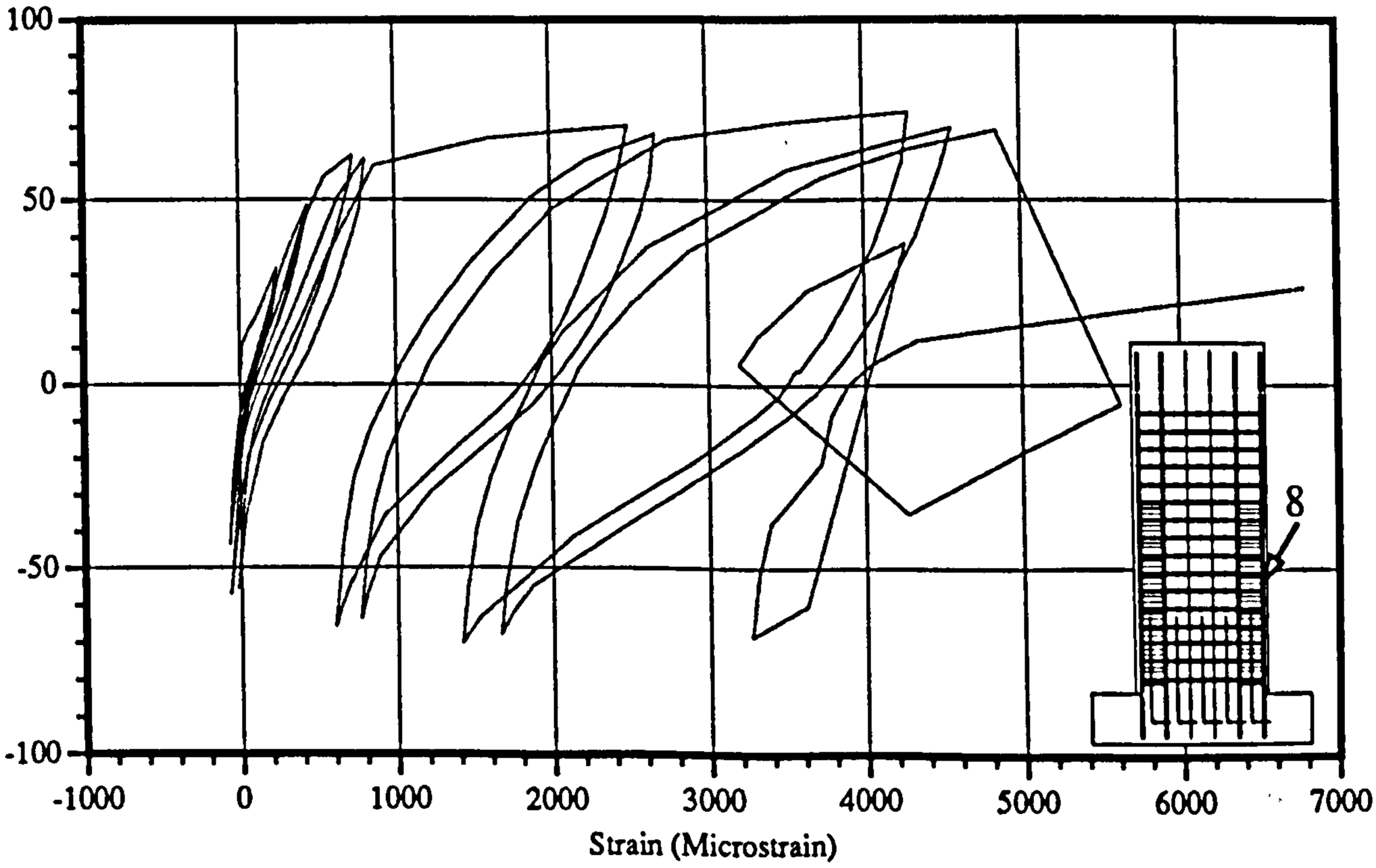


Fig. AII (35) 8 Force - Steel Strain for SW35 at Node 8

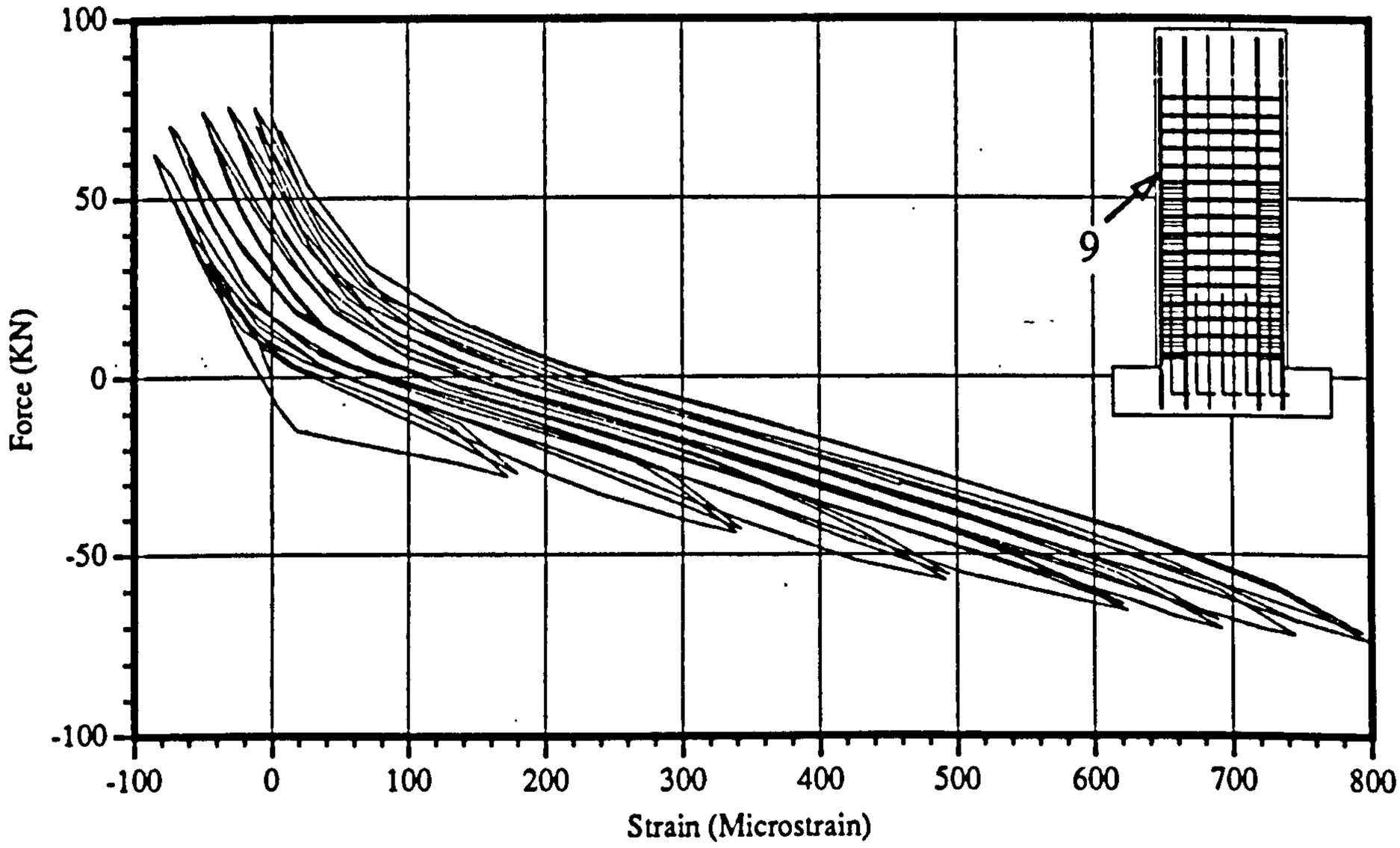


Fig. AII (35) 9 Force - Steel Strain for SW35 at Node 9

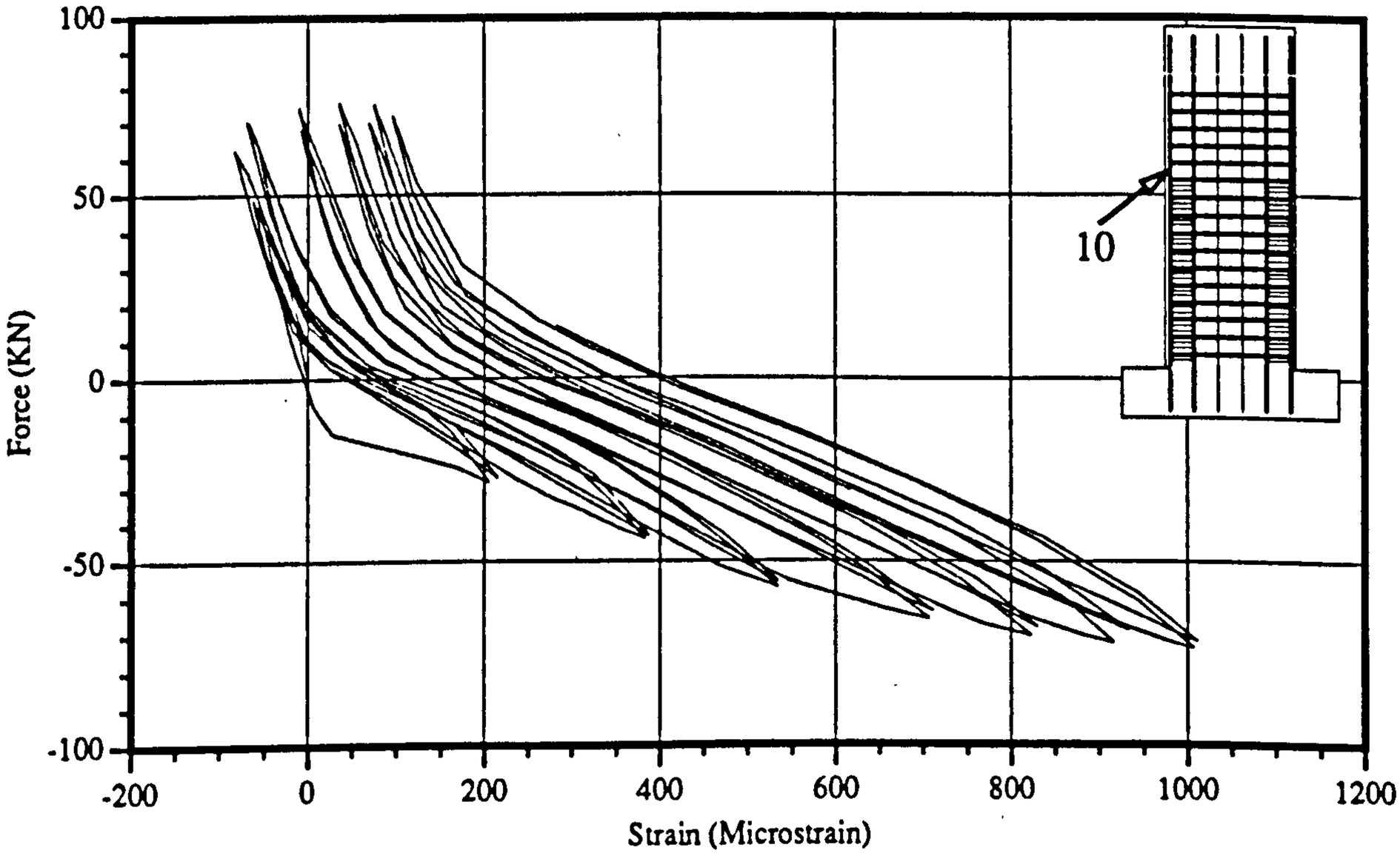


Fig. AII (35) 10 Force - Steel Strain for SW35 at Node 10

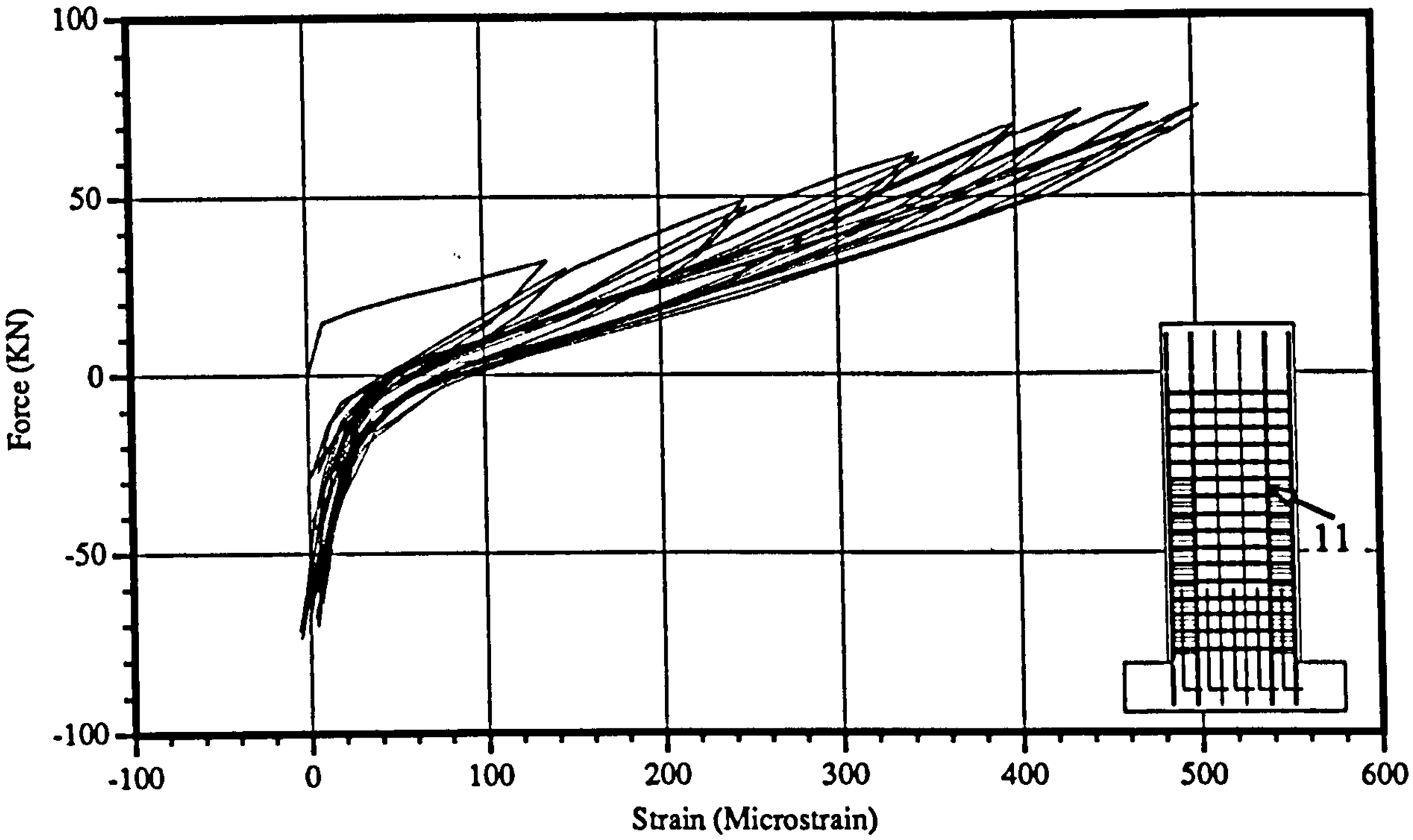


Fig. AII (35) 11 Force - Steel Strain for SW35 at Node 11

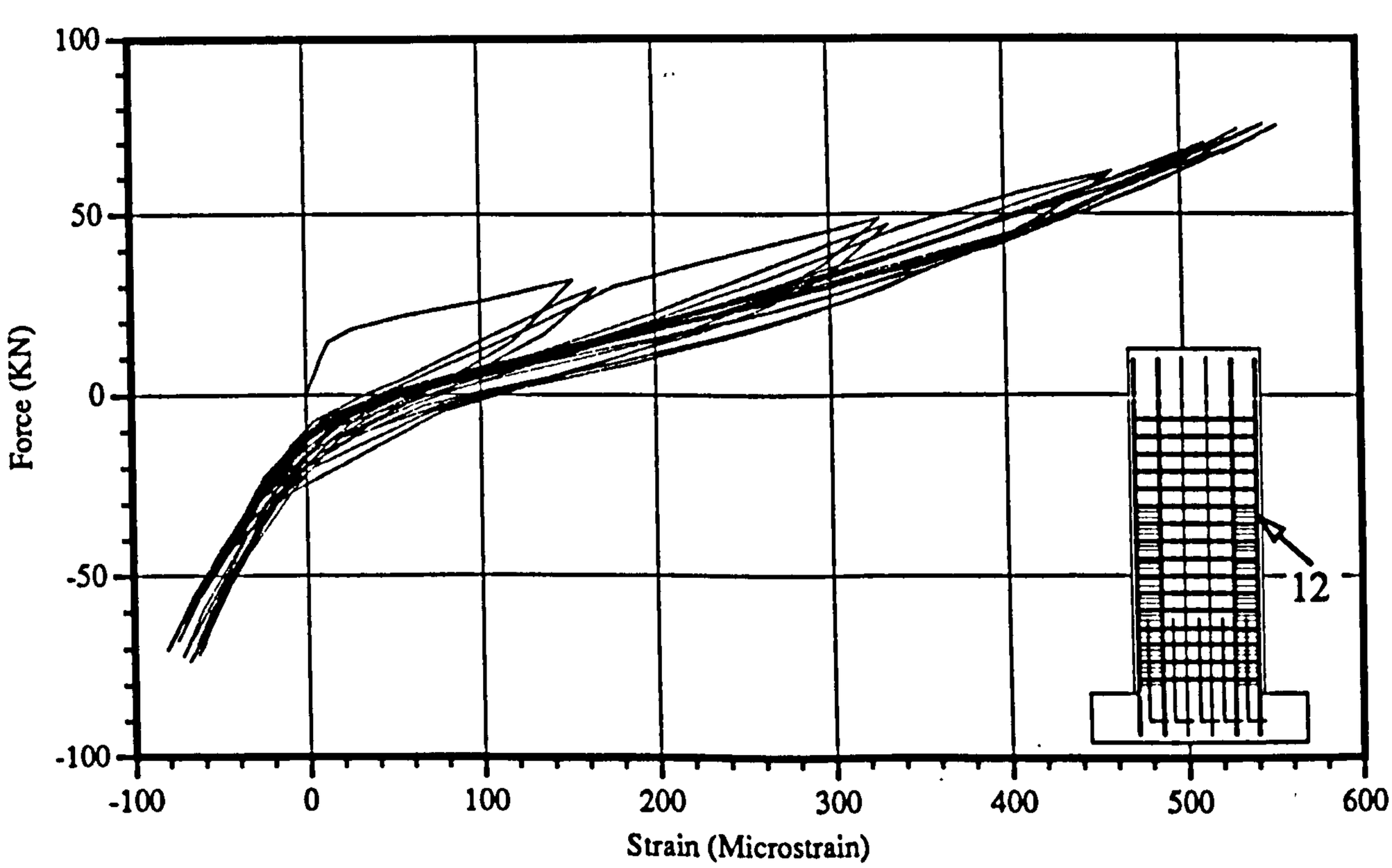


Fig. AII (35) 12 Force - Steel Strain for SW35 at Node 12

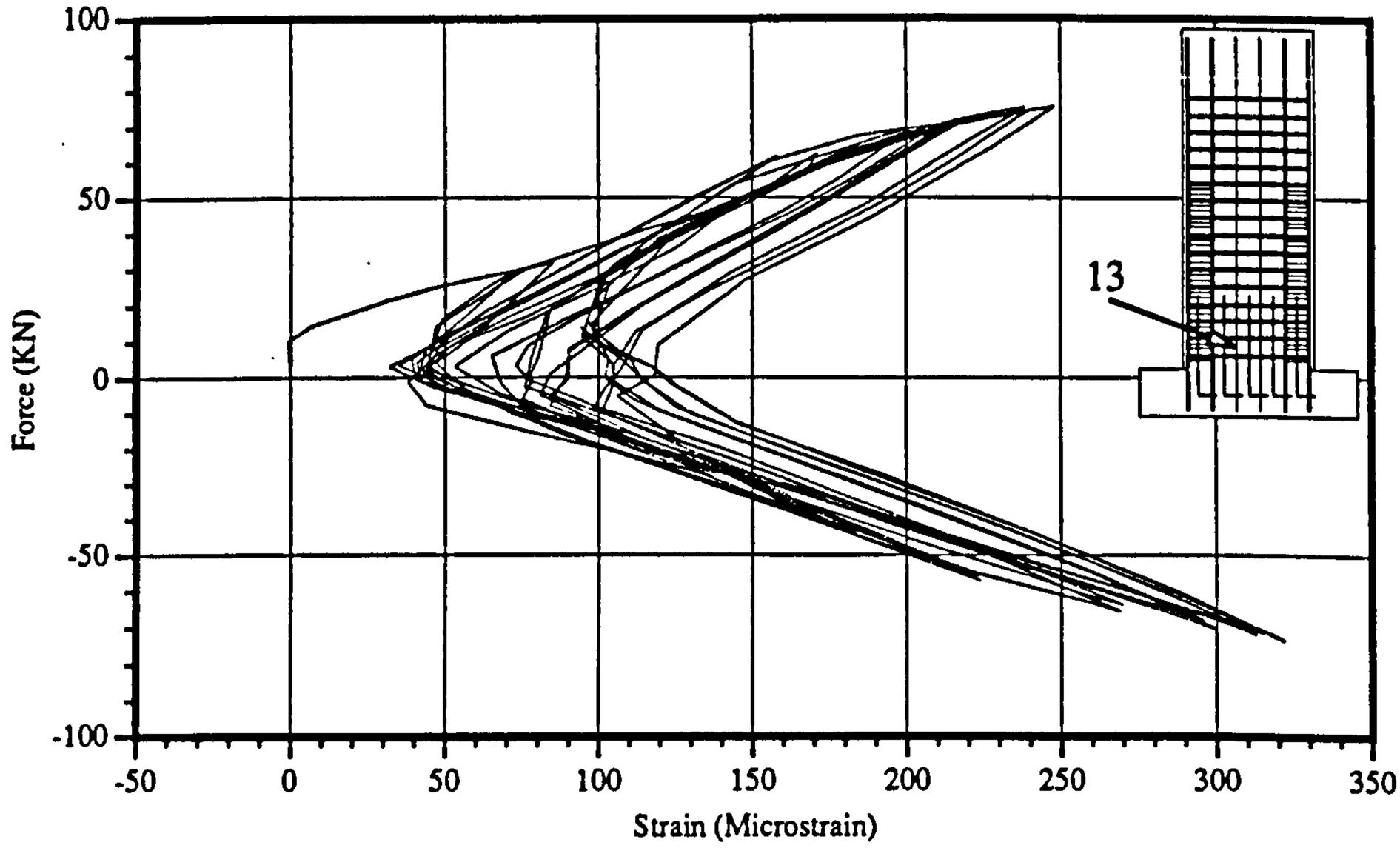


Fig. AII (35) 13 Force - Steel Strain for SW35 at Node 13

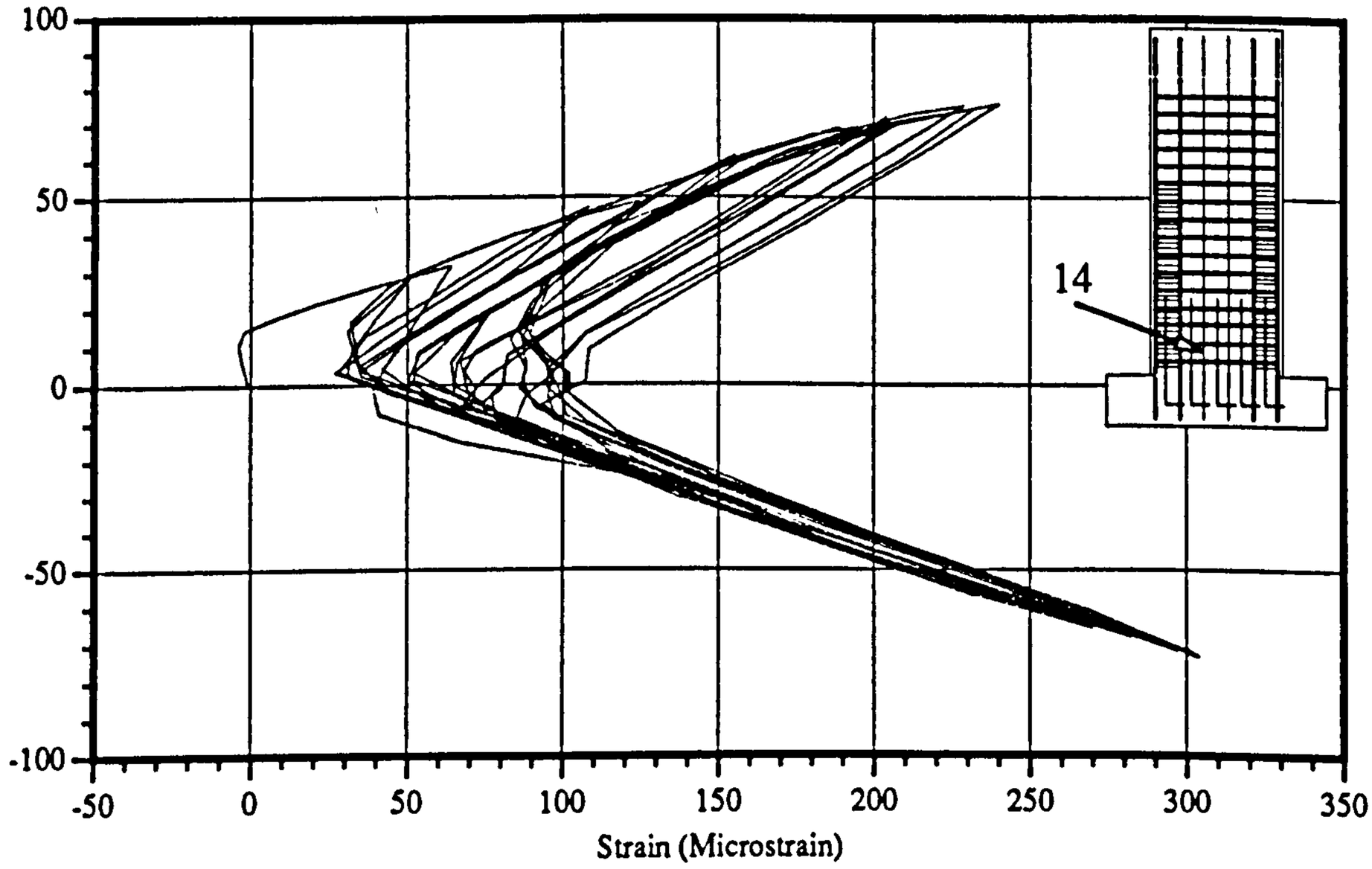


Fig. AII (35) 14 Force - Steel Strain for SW35 at Node 14

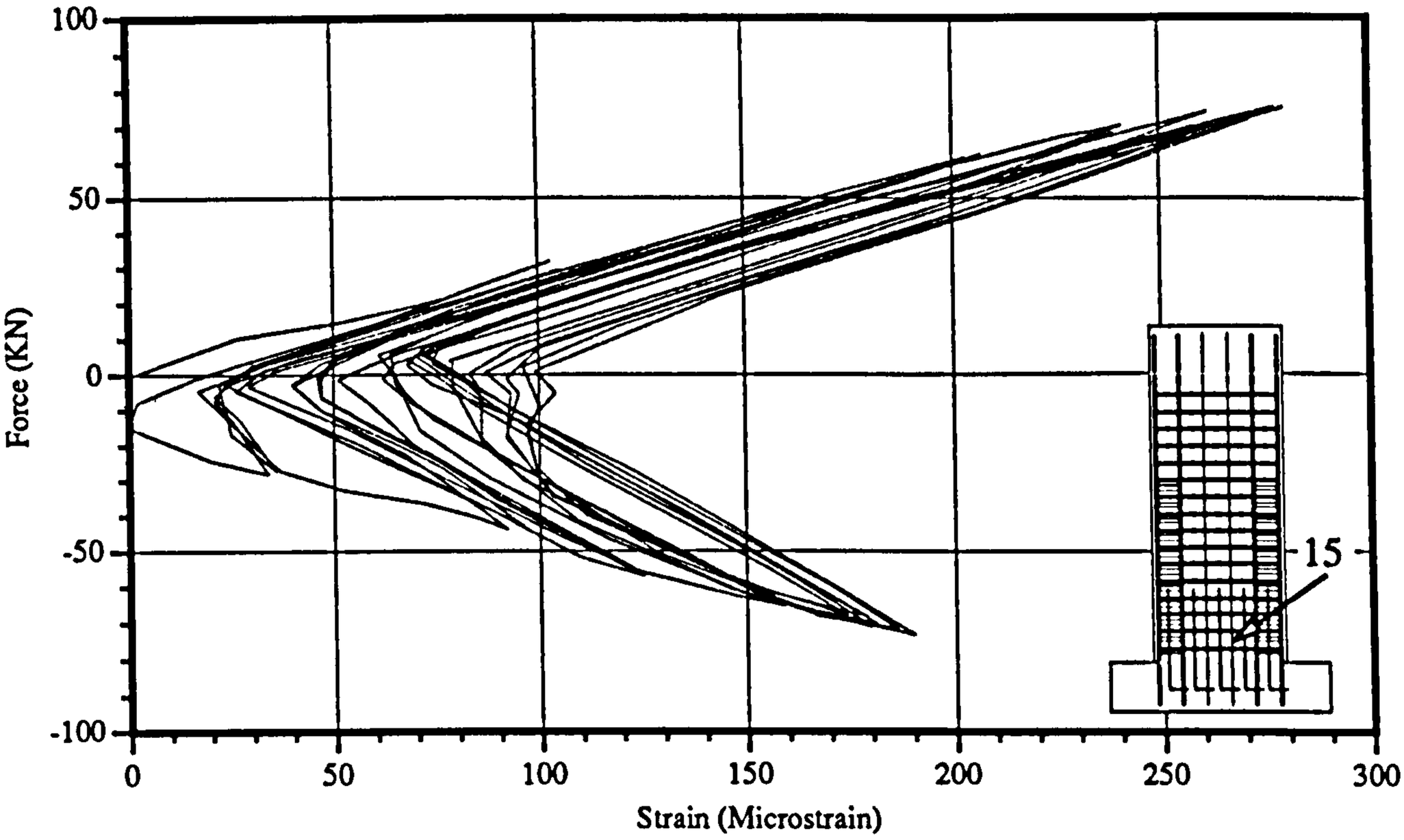


Fig. AII (35) 15 Force - Steel Strain for SW35 at Node 15

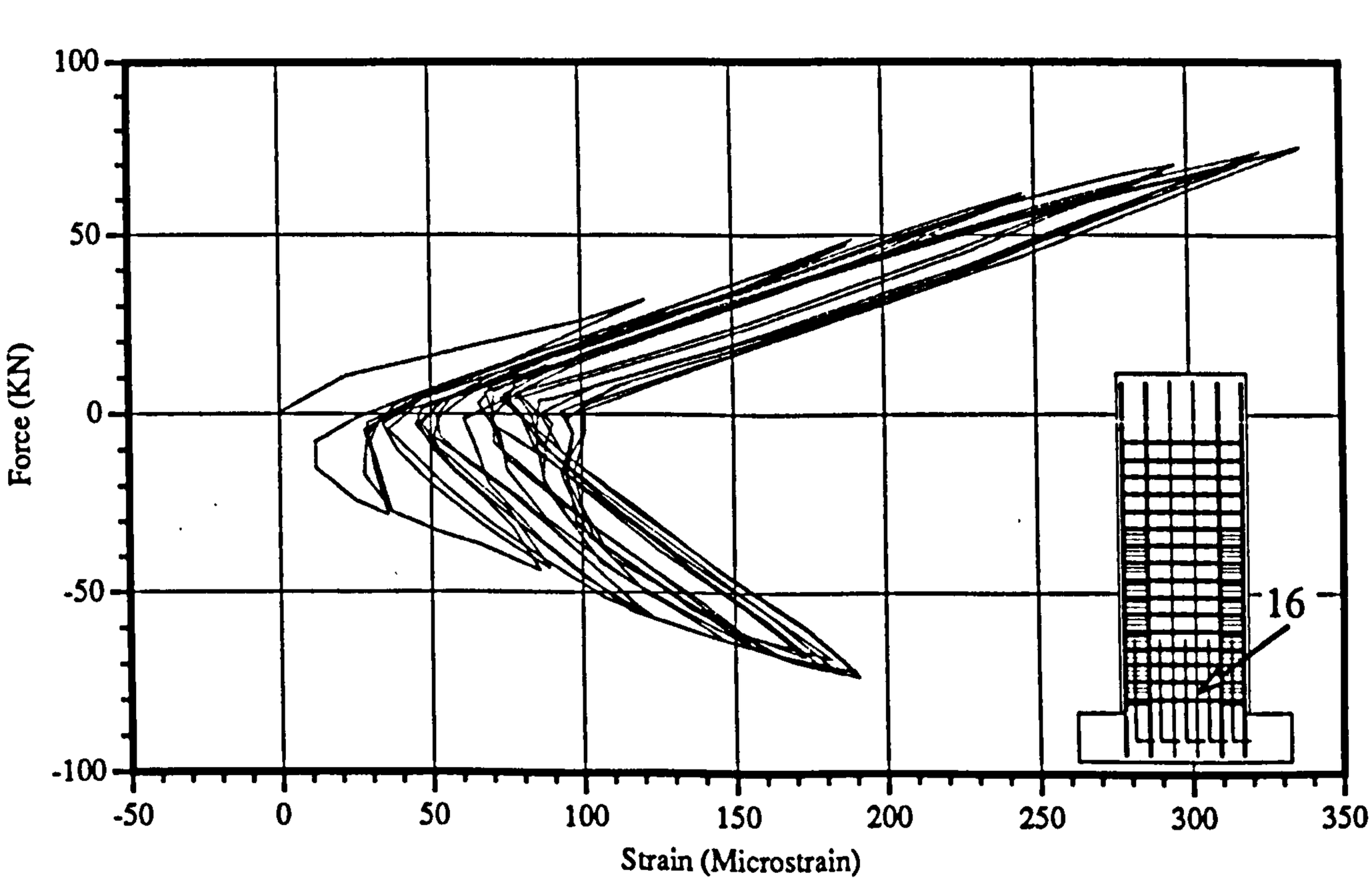


Fig. AII (35) 16 Force - Steel Strain for SW35 at Node 16

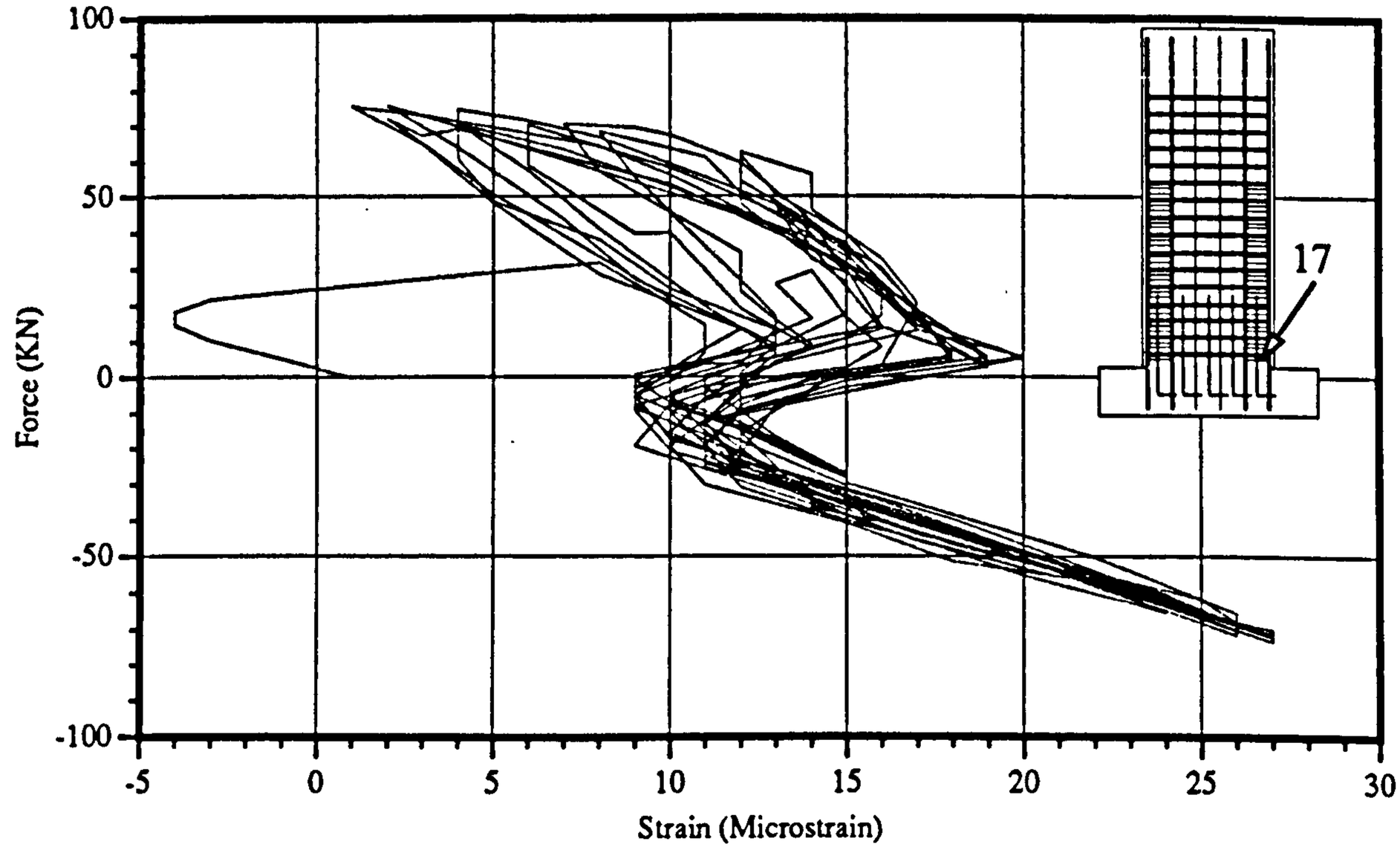


Fig. AII (35) 17 Force - Steel Strain for SW35 at Node 17

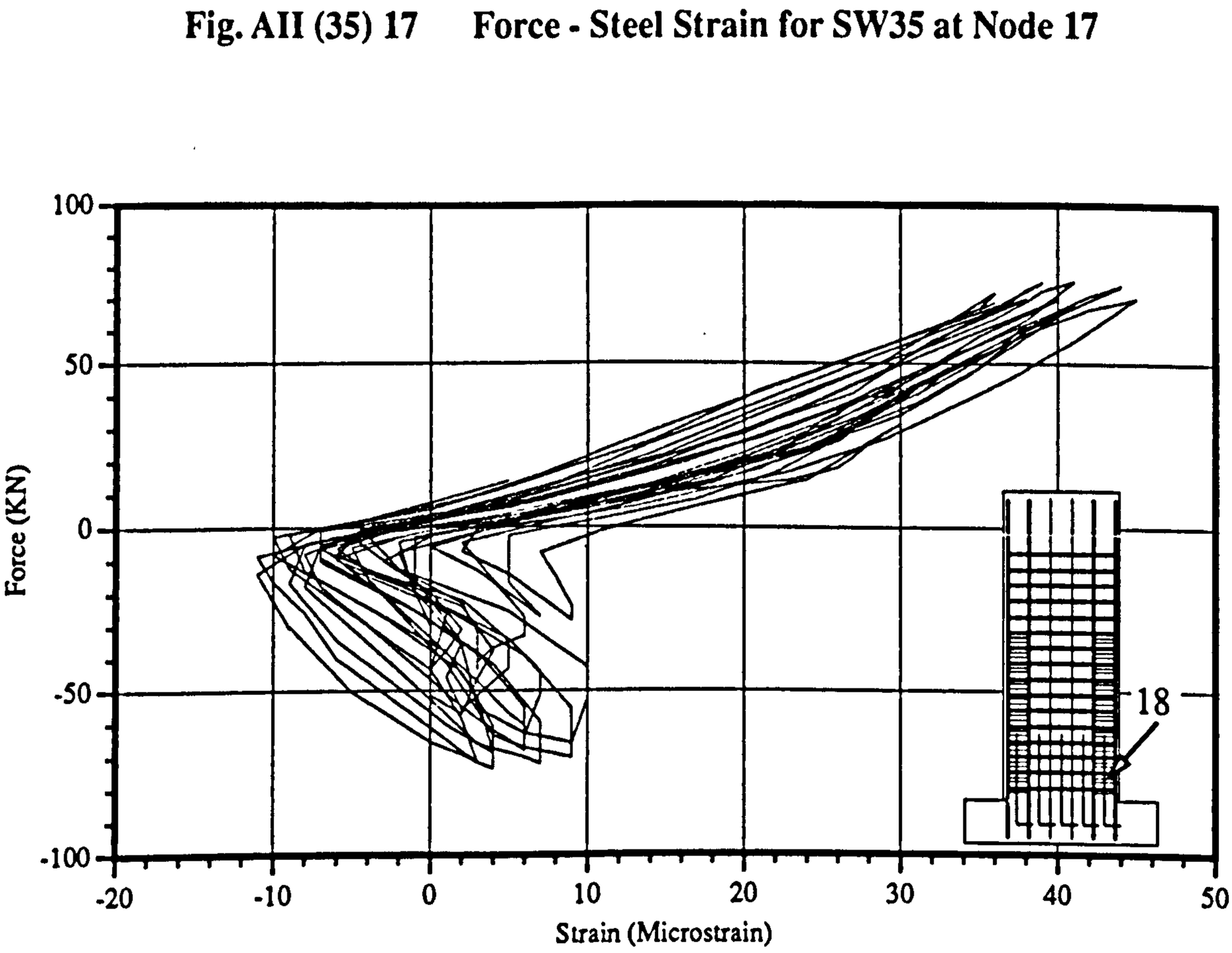


Fig. AII (35) 18 Force - Steel Strain for SW35 at Node 18

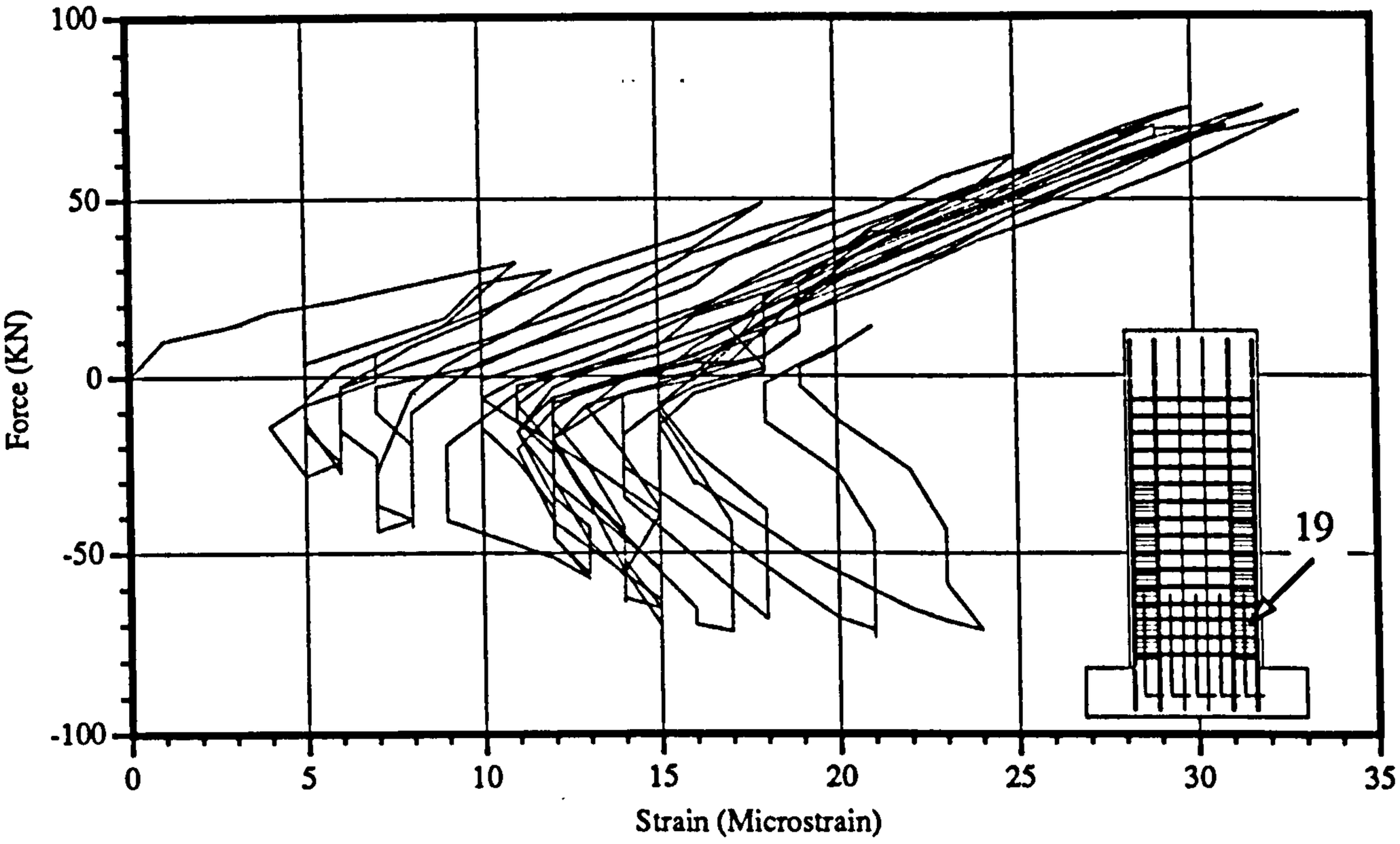


Fig. AII (35) 19 Force - Steel Strain for SW35 at Node 19

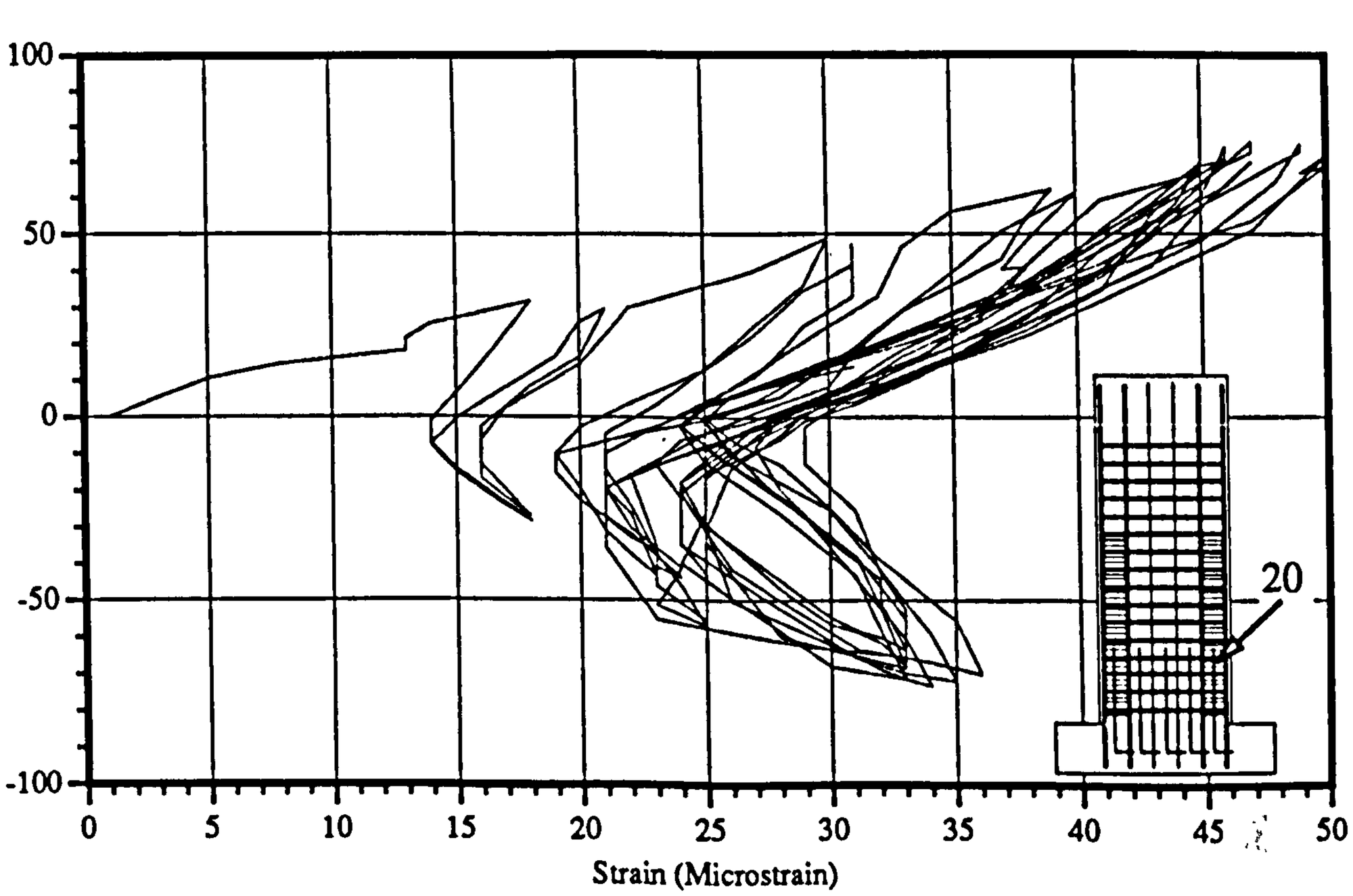


Fig. AII (35) 20 Force - Steel Strain for SW35 at Node 20

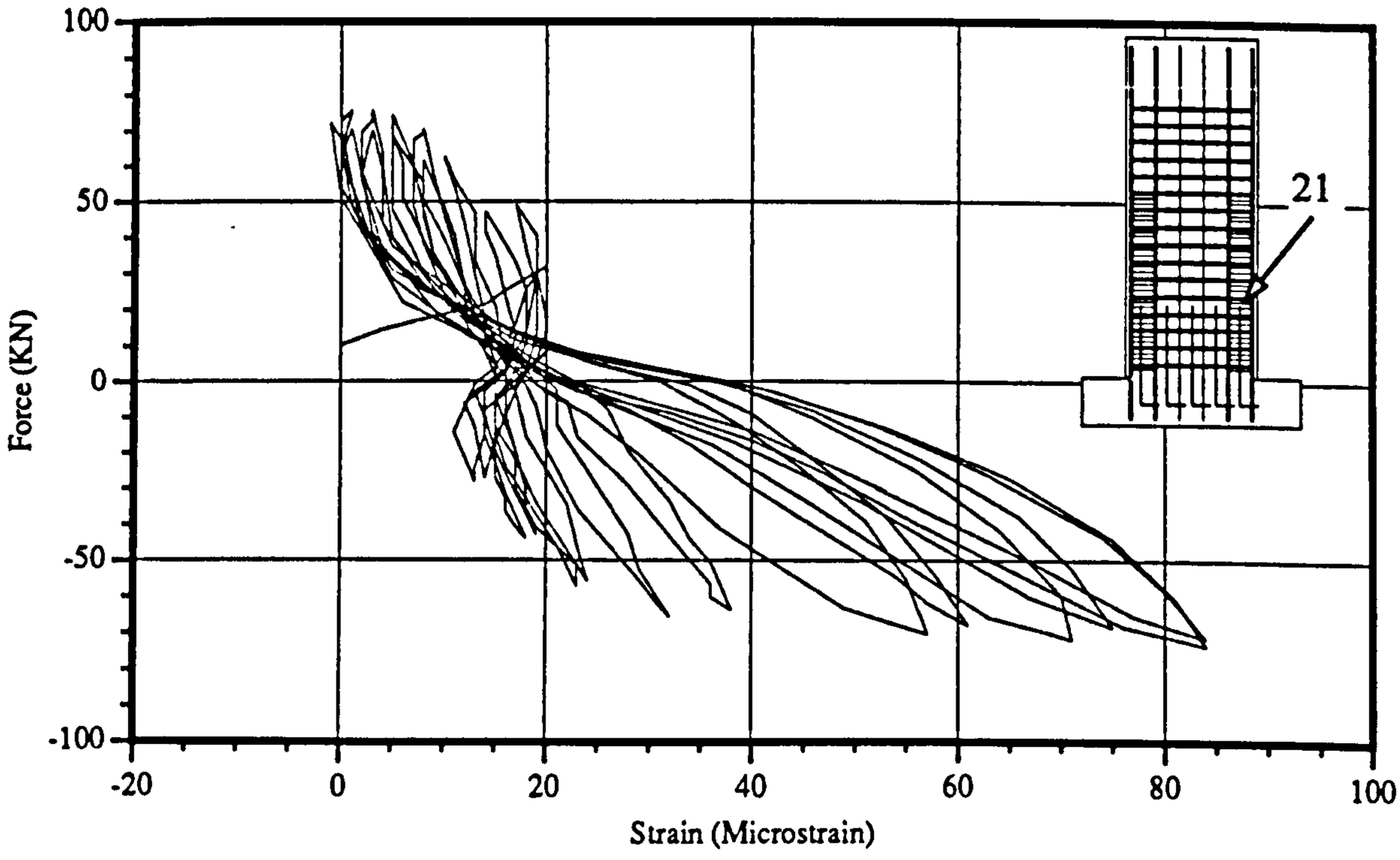


Fig. AII (35) 21 Force - Steel Strain for SW35 at Node 21

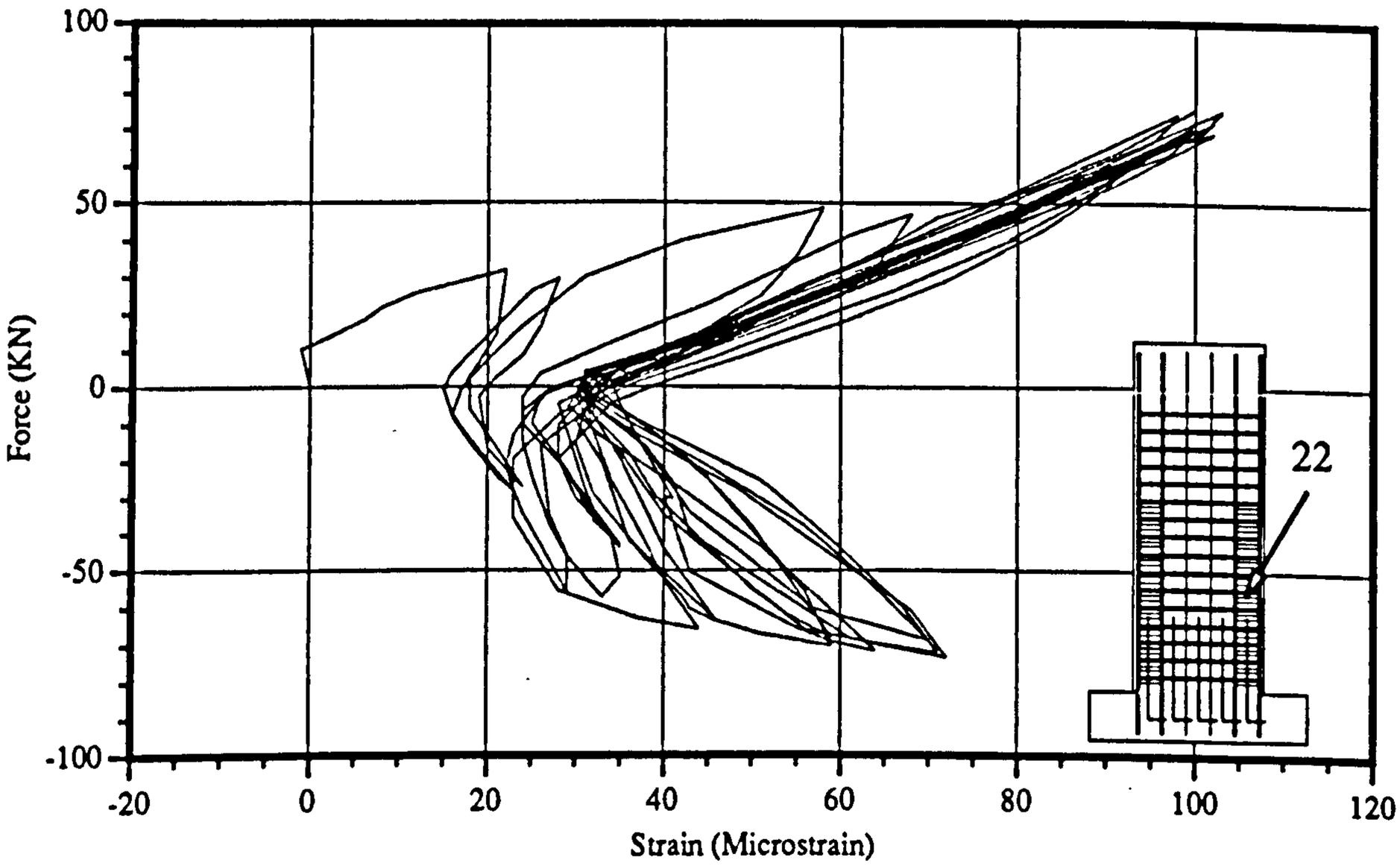


Fig. AII (35) 22 Force - Steel Strain for SW35 at Node 22

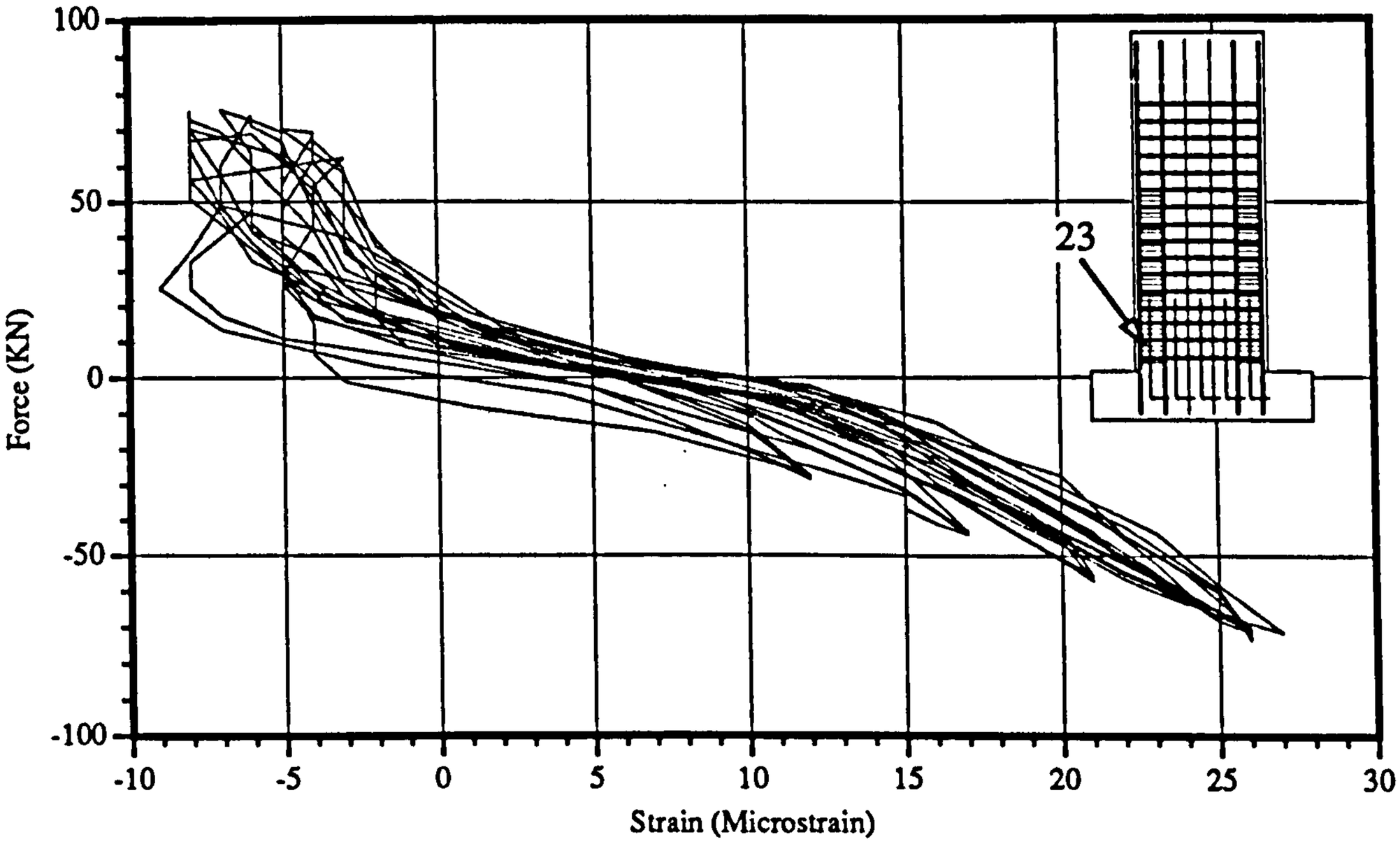


Fig. AII (35) 23 Force - Steel Strain for SW35 at Node 23

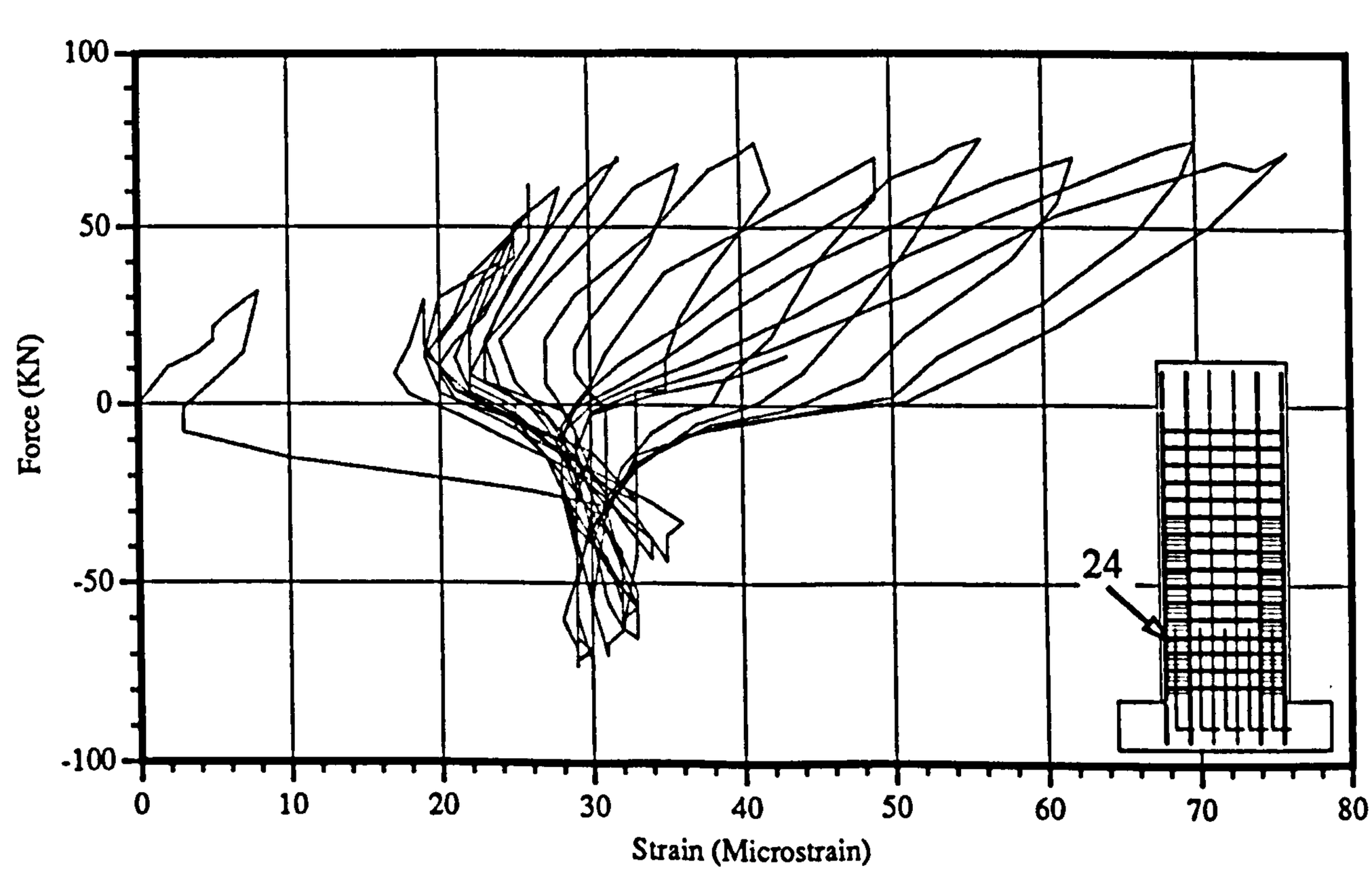


Fig. AII (35) 24 Force - Steel Strain for SW35 at Node 24

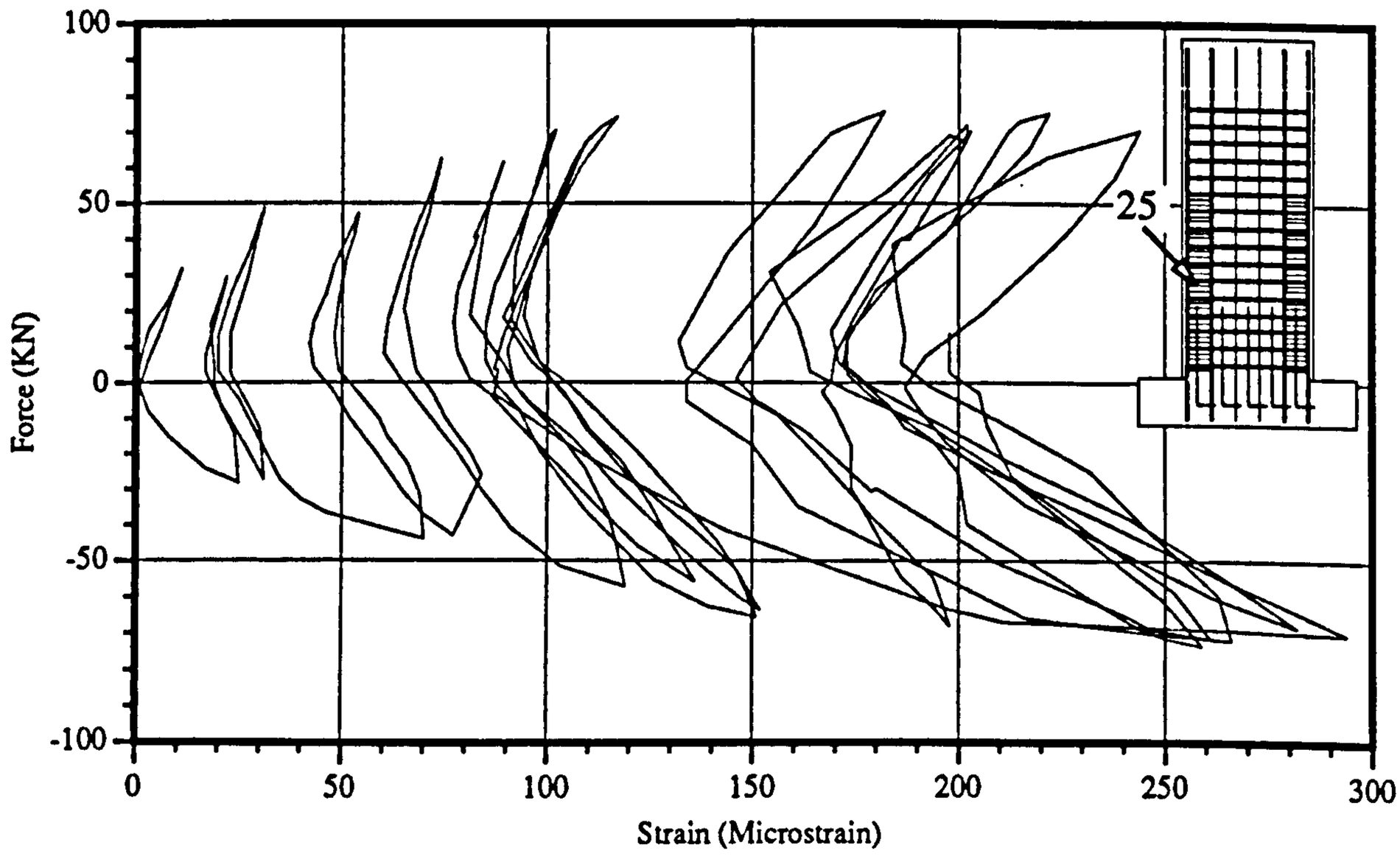


Fig. AII (35) 25 Force - Steel Strain for SW35 at Node 25

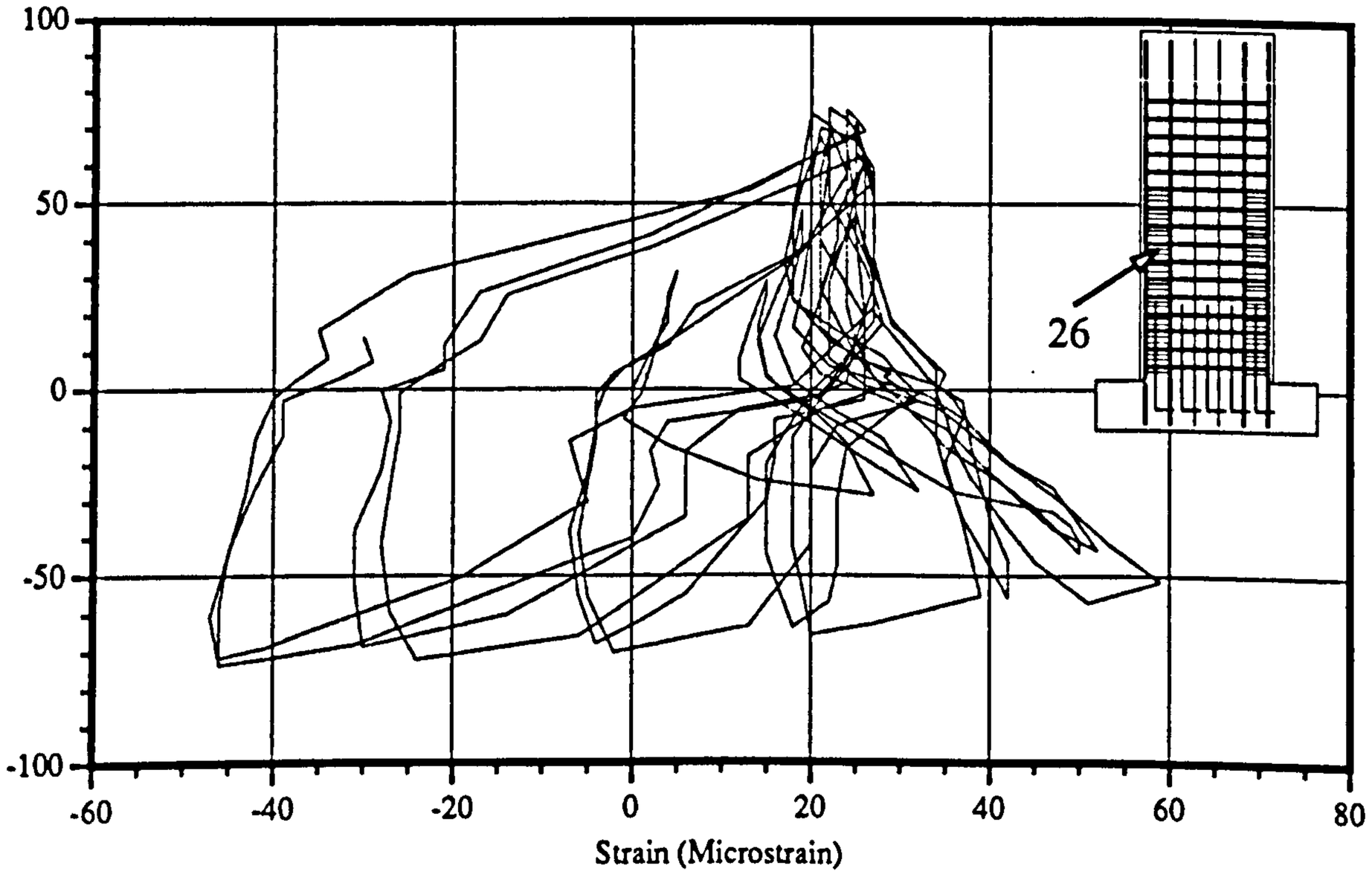


Fig. AII (35) 26 Force - Steel Strain for SW35 at Node 26

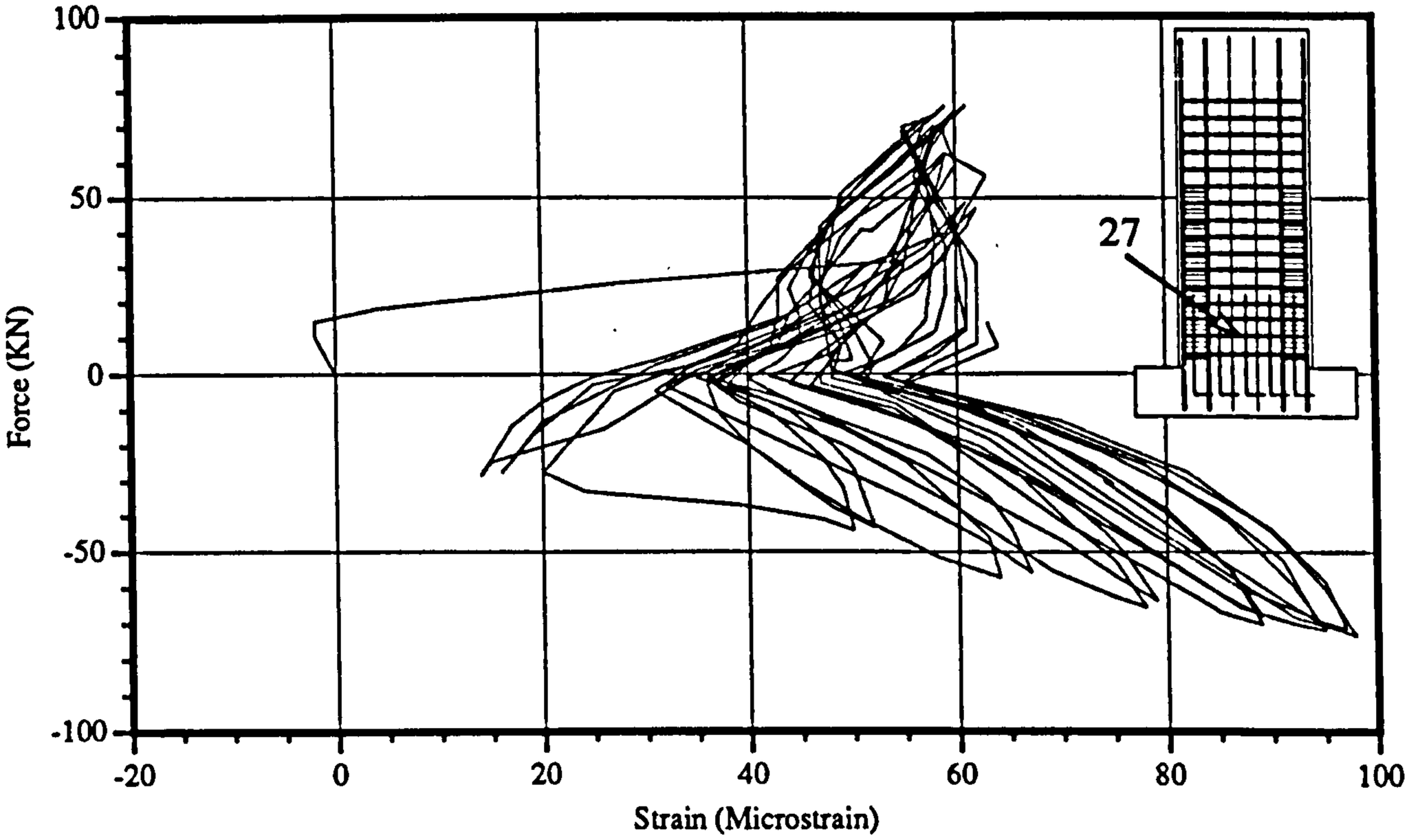


Fig. AII (35) 27 Force - Steel Strain for SW35 at Node 27

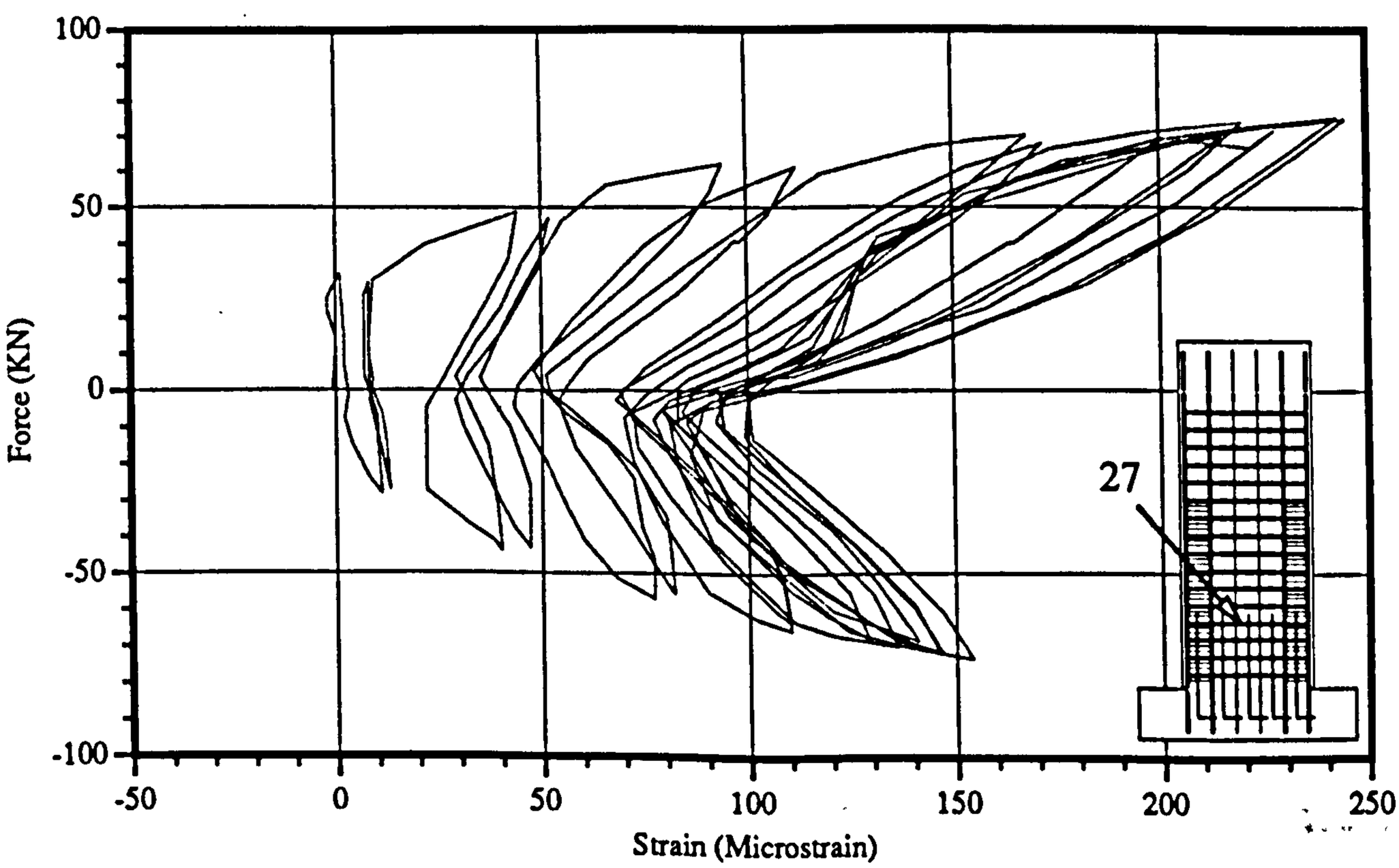


Fig. AII (35) 28 Force - Steel Strain for SW35 at Node 28

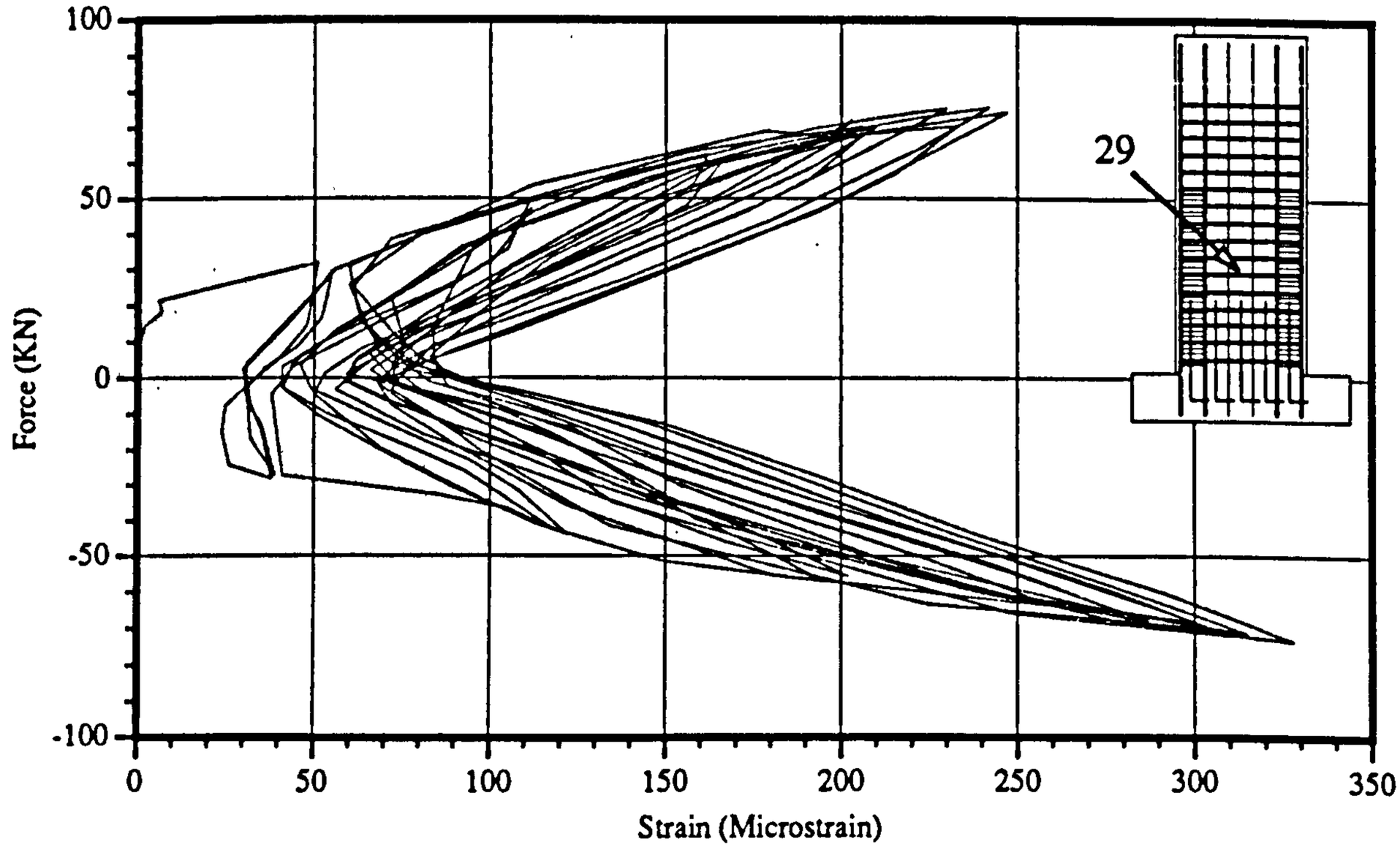


Fig. AII (35) 29 Force - Steel Strain for SW35 at Node 29

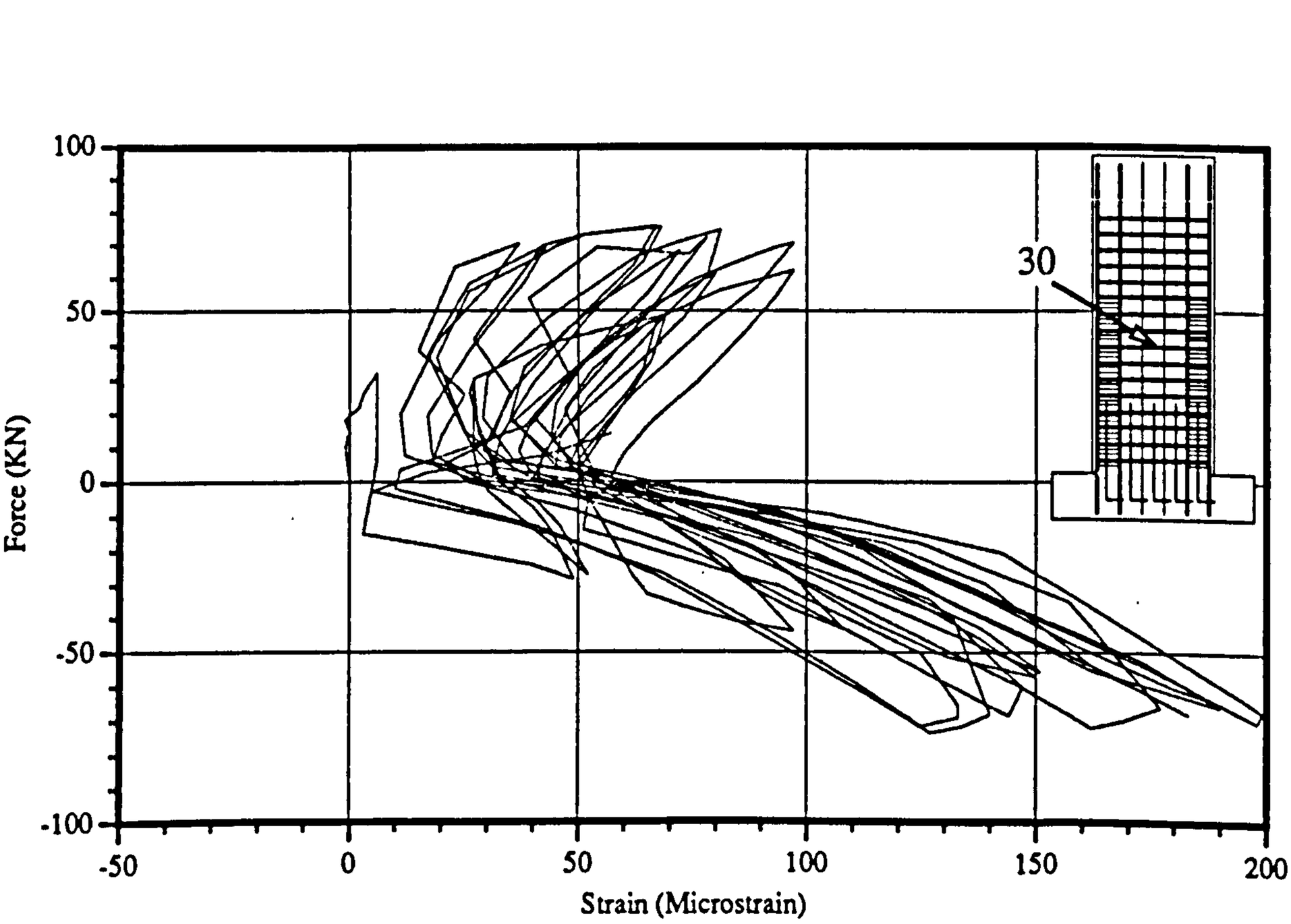


Fig. AII (35) 30 Force - Steel Strain for SW35 at Node 30

AII. 12. Force-Steel Strain for SWR35

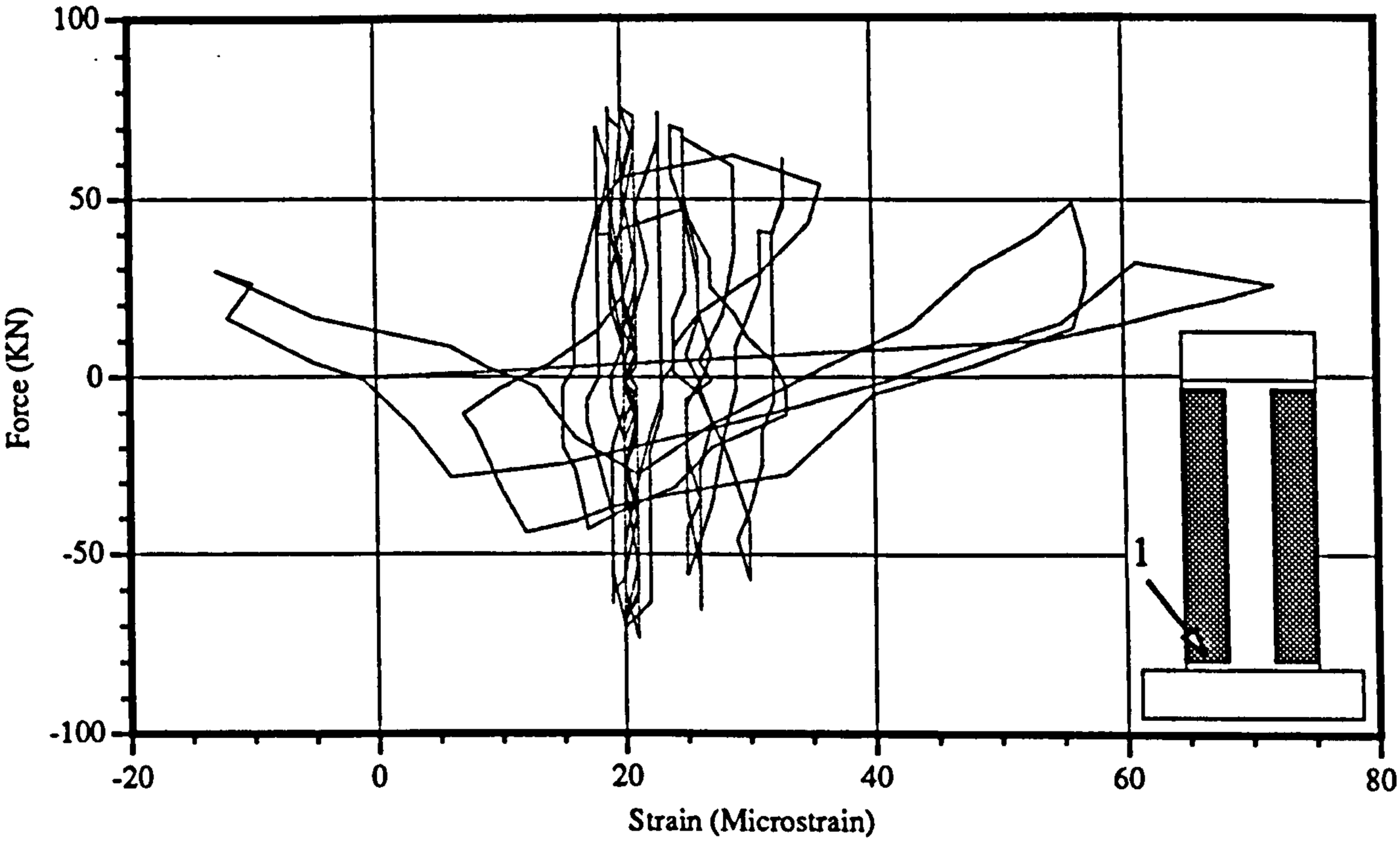


Fig. AII (R35) 1 Force - Steel Strain for SWR35 at Node 1

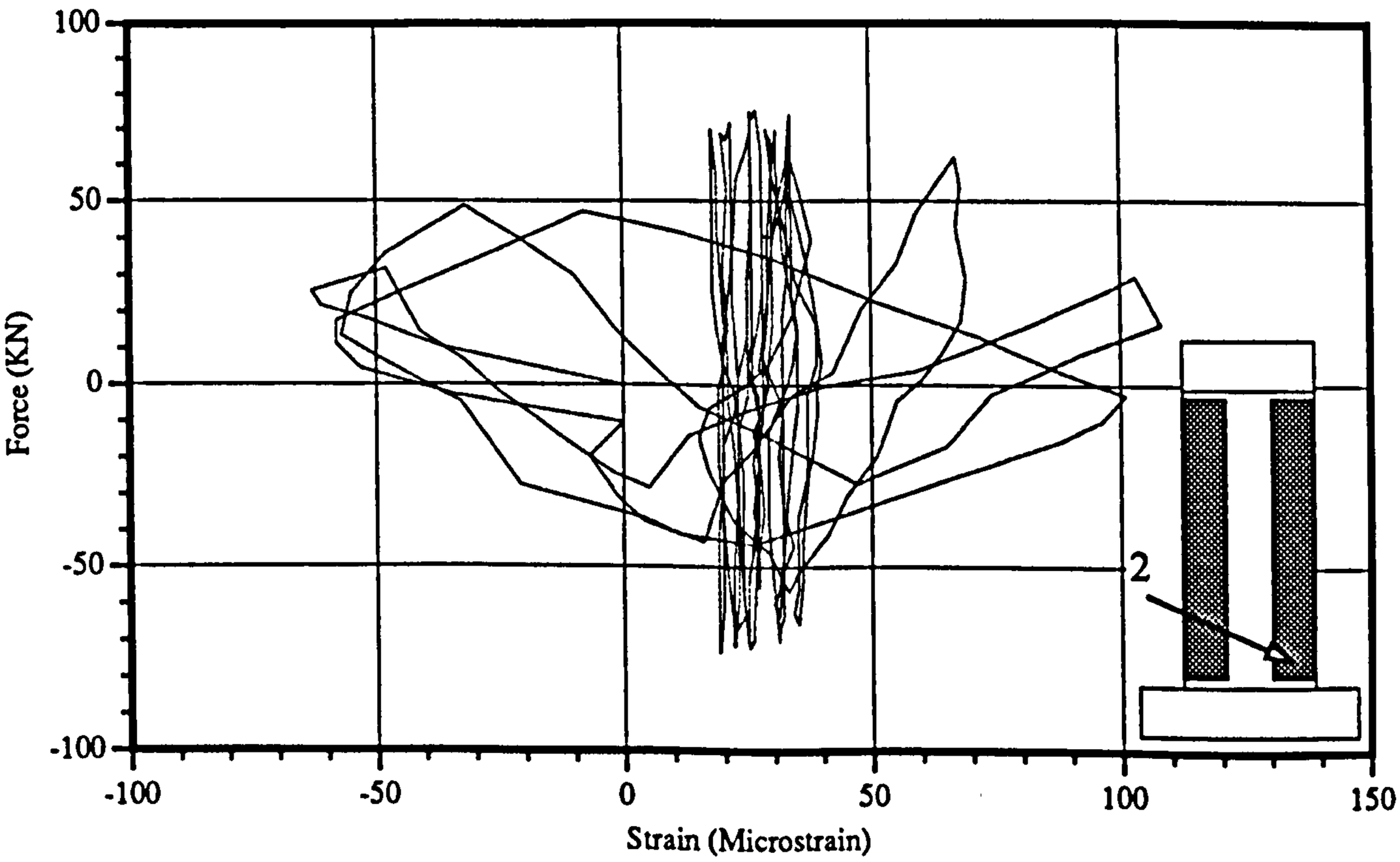


Fig. AII (R35) 2 Force - Steel Strain for SWR35 at Node 2

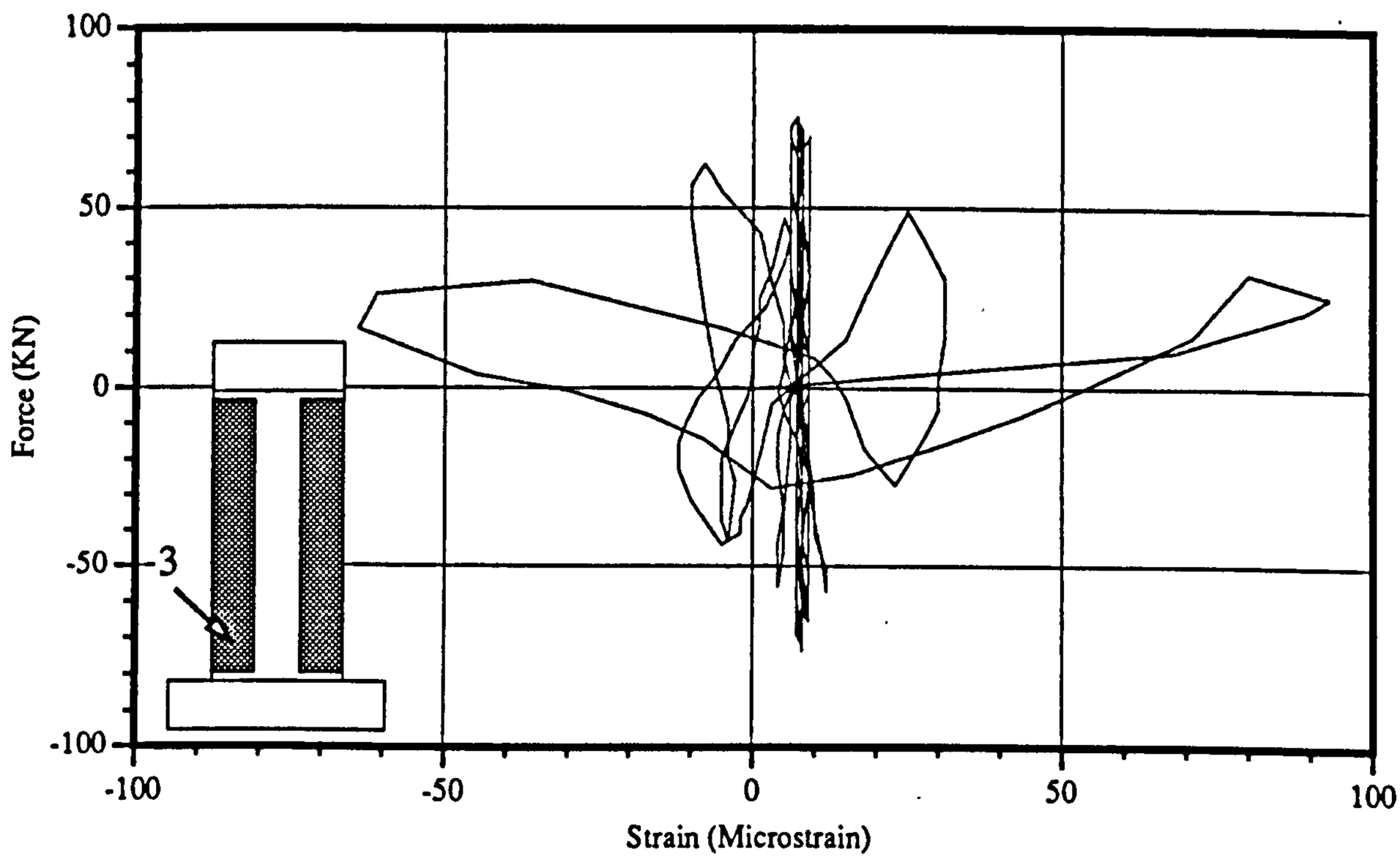


Fig. AII (R35) 3 Force - Steel Strain for SWR35 at Node 3

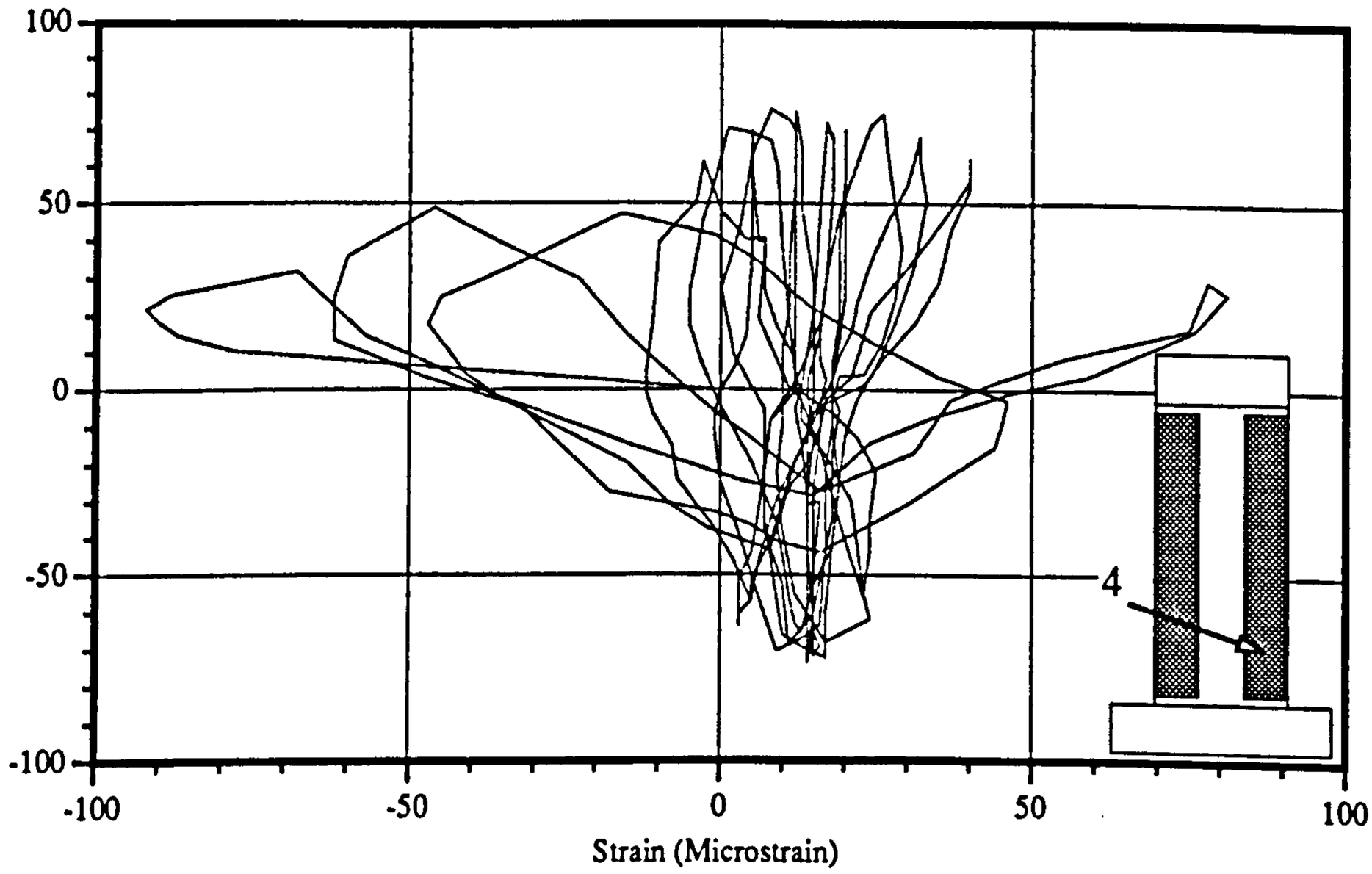


Fig. AII (R35) 4 Force - Steel Strain for SWR35 at Node 4

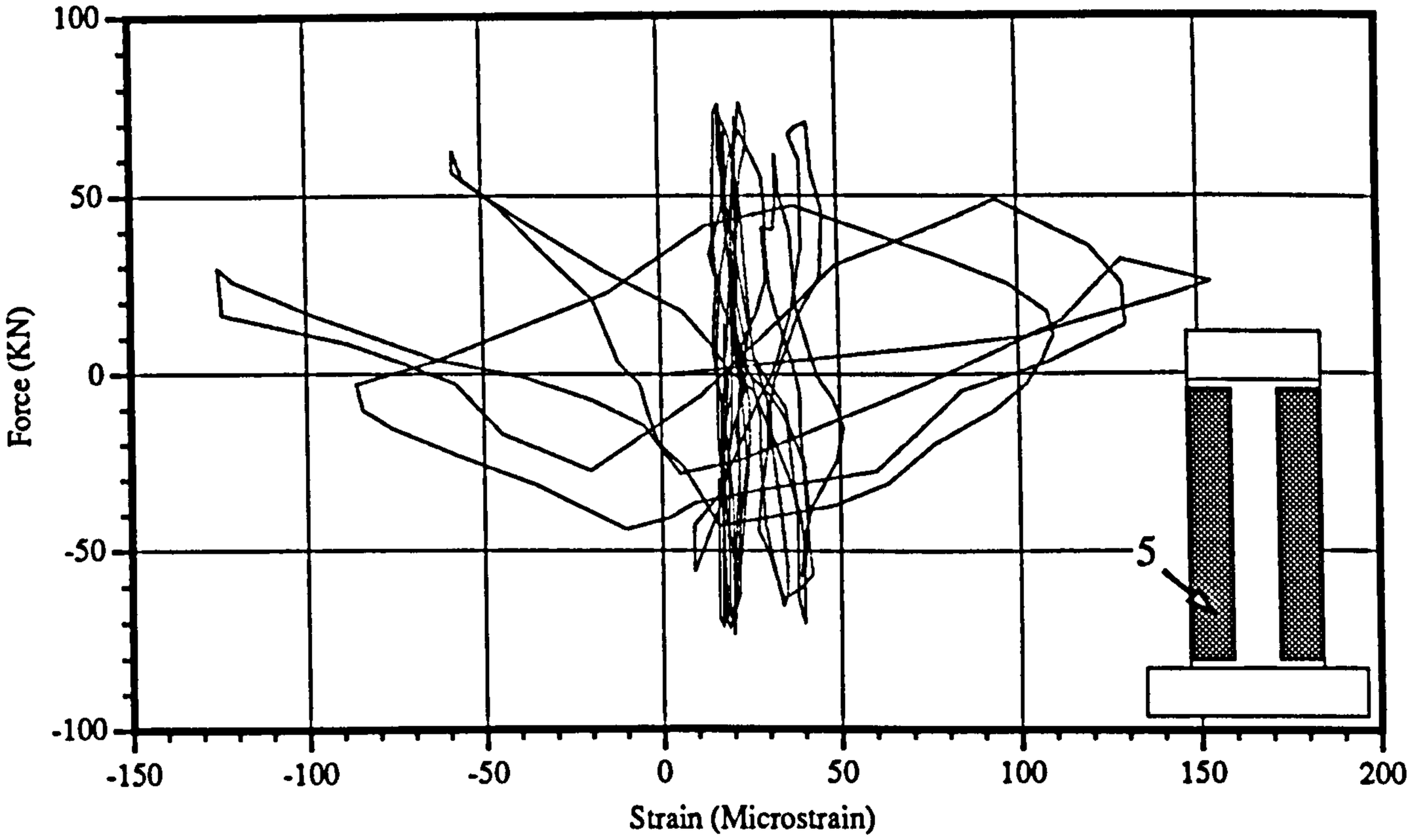


Fig. AII (R35) 5 Force - Steel Strain for SWR35 at Node 5

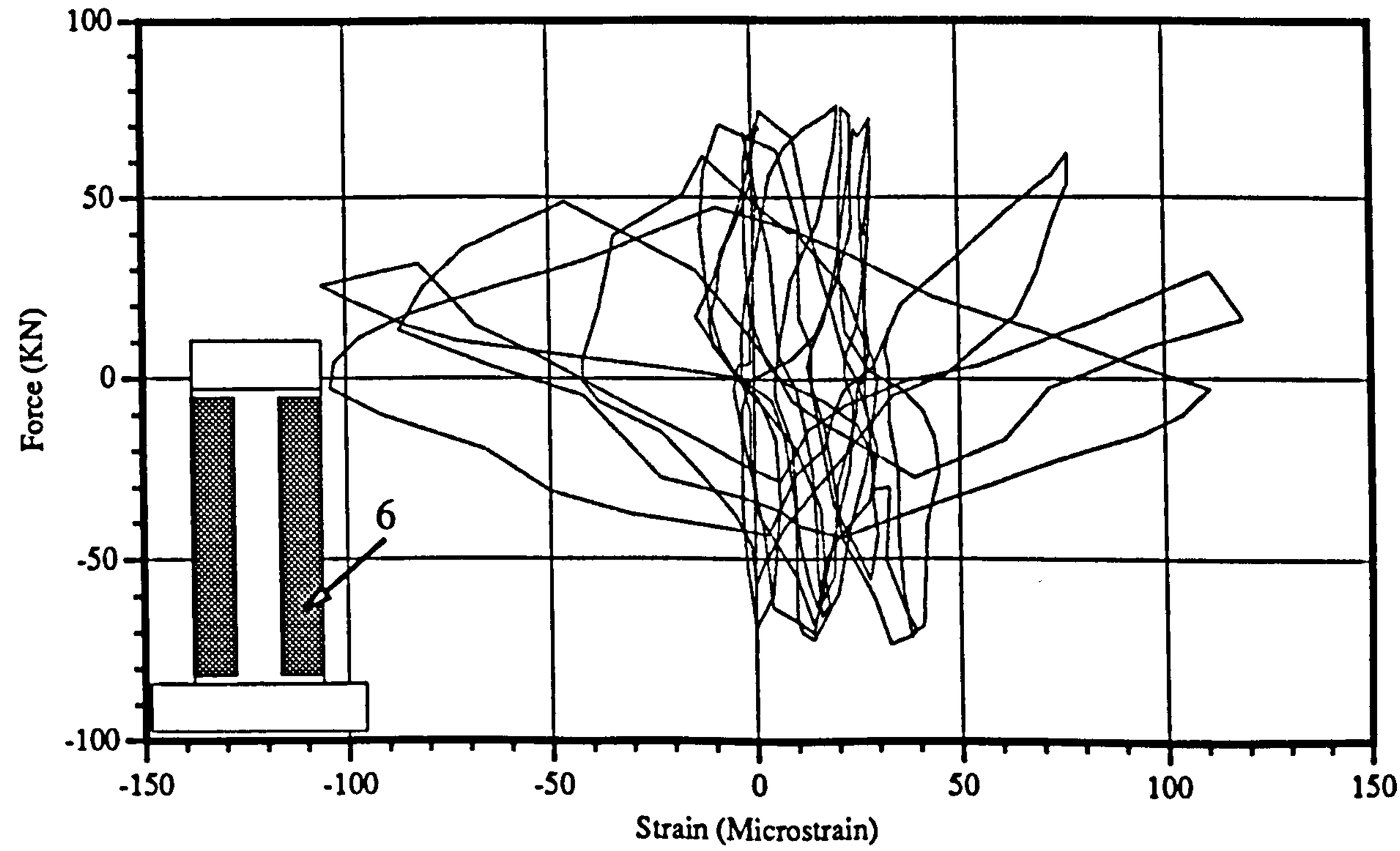


Fig. AII (R35) 6 Force - Steel Strain for SWR35 at Node 6

EARTHQUAKE DAMAGE INSPECTION FORM
No.1

GENERAL

1	Name of Cooperative	:	OZALTENKENT
2	List No	:	17
3	City	:	ERZINCAN
4	Town	:	ERZINCAN
5	District	:	ERZERUM
6	Lot No	:	2017
7	Drawing No	:	20815
8	Plot No	:	209
9	No of Units	:	24
10	No of Building Blocks	:	3
11	No of Floors	:	5
12	Basement		[X] Yes [ ] No
13	Inspection Team Code		[3]
14	Name of Cooperative Chairman		
15	Telephone No		
16	Address		
17	Building Use		[X] Residental [ ] Other.....
18	Occupied		[ ] Yes [X] No
19	Date of Construction	:.....	Started January 1991
20	Orientation of Facade		N X S E W
21	Architectural Drawings Available		[X] Yes [ ] No
22	Structural Drawings Available		[X] Yes [ ] No
23	Structural Calculations Available		[ ] Yes [X] No
24	Mechanical Drawings Available		[X] Yes [ ] No
25	Electrical Drawings Available		[X] Yes [ ] No
26	Sanitary Drawings Available		[X] Yes [ ] No
27	Permits Available		[X] Foundation [X] Superstructure [ ] Occupancy

Sheet: 1/16

TEAM NO : 3 BY : AIS SIGNATURE : [signature] DATE : 15 / 2 / 93

EARTHQUAKE DAMAGE INSPECTION FORM
No.2

BUILDING DETAILS - A

28 Identification Code : [2][0][1][7][1][7]

29 No of Units : 24

30 Area (m2) : 3000

31 Existing No of Floors: 4

32	Basement	[X] Yes	[ ] No	
33	Mezzanine	[ ] Yes	[X] No	
34	Penthouse	[ ] Yes	[X] No	
35	Roof Tank	[ ] Yes	[X] No	
36	Timber Roof Support Truss	[ ] Yes	[X] No	

Comments :

TEAM NO : 3 BY : AIS SIGNATURE : [signature] DATE : 15/2/93

EARTHQUAKE DAMAGE INSPECTION FORM
No.3

BUILDING DETAILS - B

37 Identification Code : [2][0][1][7][1][7]

38 Construction Material of Load-Bearing Elements
- [X] In-situ RC
- [ ] Pre-cast RC
- [ ] Block Masonry
- [ ] Brick Masonry

39 Stuructural System
- [ ] Wall-Bearing
- [X] RC Frame
- [ ] RC Frame/Wall
- [ ] RC Box
- [ ] RC Infilled Frame
- [ ] Mixed

40 Basement Peripheral Walls
- [ ] RC
- [ ] Brick
- [ ] Block
- [ ] Stone
- [X] None

Comments :

TEAM NO : 3 BY : AIS SIGNATURE : [signature] DATE : 15./2./93

EARTHQUAKE DAMAGE INSPECTION FORM
No.4

BUILDING DETAILS - C

42 Identification Code : [2][0][1][7][1][7]

43 Infill Panels [X] Yes [ ] No If No, skip section.

44 Material [X] Brick Masonry [ ] Block Masonry

[ ] Stone Masonry [ ] Other (Specify)

45 Reinf. In Masonry [ ] Yes [X] No

46 Conn. to Struct. Sys. [ ] Yes [X] No

47 Framing Action [ ] One Direction [X] Two Direction

48 Shear Walls [ ] One Direction [ ] Two Direction None

Comments :

TEAM NO : 3 BY : AIS SIGNATURE : DATE : 15/2/93

EARTHQUAKE DAMAGE INSPECTION FORM
No.5

PREVIOUS HISTORY

49 Identification Code : 2 0 1 7 1 7

50 Previous Damage to Building ☐ Yes ☒ No ☐ Unknown
(If Yes,give details)

51 Previous Damage to Adjacent Buildings ☐ Yes ☒ No ☐ Unknown
(If Yes,give details)

52 Previous Repair Measures ☐ Yes ☒ No ☐ Unknown
(If Yes,give details)

53 State of Repair ☐ Good ☐ Fair ☐ Poor

54 Construction Workmanship ☐ Good ☐ Fair ☒ Poor

Comments :

TEAM NO : 3 BY : AIS SIGNATURE : ..... DATE : 15/2../.93.

EARTHQUAKE DAMAGE INSPECTION FORM
No.6

MATERIALS

55 Identification Code : [2][0][1][7][1][7]

56 Visual Defects on Concrete [X] Yes [ ] No
(If No, skip section)

[ ] Segregation [ ] Low Cement Content [X] Spalling [ ] Others (specify)

[X] Cracking

57 Evidence of Steel Rusting
(If No, skip section)

[ ] Severe [ ] Serious [ ] Minor

58 Type of Main Steel Bars

[X] Plain [ ] Deformed

Comments : Two columns were totally ruptured in one of the blocks. Column cracking was observed in six other columns. Beam cracking spread throughout the buildings.

TEAM NO : 3 BY : AIS SIGNATURE : ... DATE : 15/.2/.93.

EARTHQUAKE DAMAGE INSPECTION FORM
No.7

SECTION DETAILS

59 Identification Code : 2 0 1 7 1 7

60 Concrete Cover (mm) : Slabs : 0-10 Beams : 0-20 Columns : 0-60

61 Stirrup Shape : ☒ ☐ ☐ ☐ Other (Sketch)

62 Stirrups : Avg. Diam.: 8 Avg. Spacing : 250

63 Tie Shape : ☒ ☐ ☐ ☐ Other (Sketch)

64 Ties : Avg. Diam.: 8 Avg. Spacing : 200

65 Average Percentage Reinforcement

Slabs : 0.3% Beams : 1% Columns : 1.5% Walls : -

Comments :

TEAM NO : 3 BY : AIS SIGNATURE [signature] DATE : 15/2/93

EARTHQUAKE DAMAGE INSPECTION FORM
No.8

MEMBER DETAILS

66 Identification Code : [2][0][1][7][1][7]

67	Slender Columns (b/h < 0.09)	☐ Yes	☒ No	
68	Short Columns (b/h < 0.3)	☐ Yes	☒ No	
69	Non-aligned Beams in Plan	☒ Yes	☐ No	
70	Non-aligned Beams in Elevation	☐ Yes	☒ No	
71	Non-aligned Columns in Elevation	☐ Yes	☒ No	

Comments :

TEAM NO : 3 BY : AIS SIGNATURE : [signature] DATE : 15/2/93

EARTHQUAKE DAMAGE INSPECTION FORM
No.9

SUB-ASSEMBLY DETAILS

72 Identification Code : [2][0][1][7][1][7]

73	Shear Reinforcement in Beam–Column Connection	☐ Yes	☒ No	
74	Strong–Beam/Weak–Column Design	☒ Yes	☐ No	

Comments :

TEAM NO : 3 BY : AIS SIGNATURE : [signature] DATE : 15/2/93

EARTHQUAKE DAMAGE INSPECTION FORM
No.10

STRUCTURAL IRREGULARITIES

75 Identification Code : [2][0][1][7][1][7]

76	Elevation Stiffness Irregularities (If Yes, give location)	[X]	Yes	[ ]	No
77	Discontinuous Infill Panels (If Yes, give location)	[X]	Yes	[ ]	No Basement level
78	Plan Asymmetry–Longitudinal (more than ~5%)	[X]	Yes	[ ]	No
79	Plan Asymmetry–Transverse (more than ~5%)	[ ]	Yes	[X]	No
80	Plan Reentrant Corners	[ ]	Yes	[X]	No
81	Elevation Set-Backs	[ ]	Yes	[X]	No

Comments :

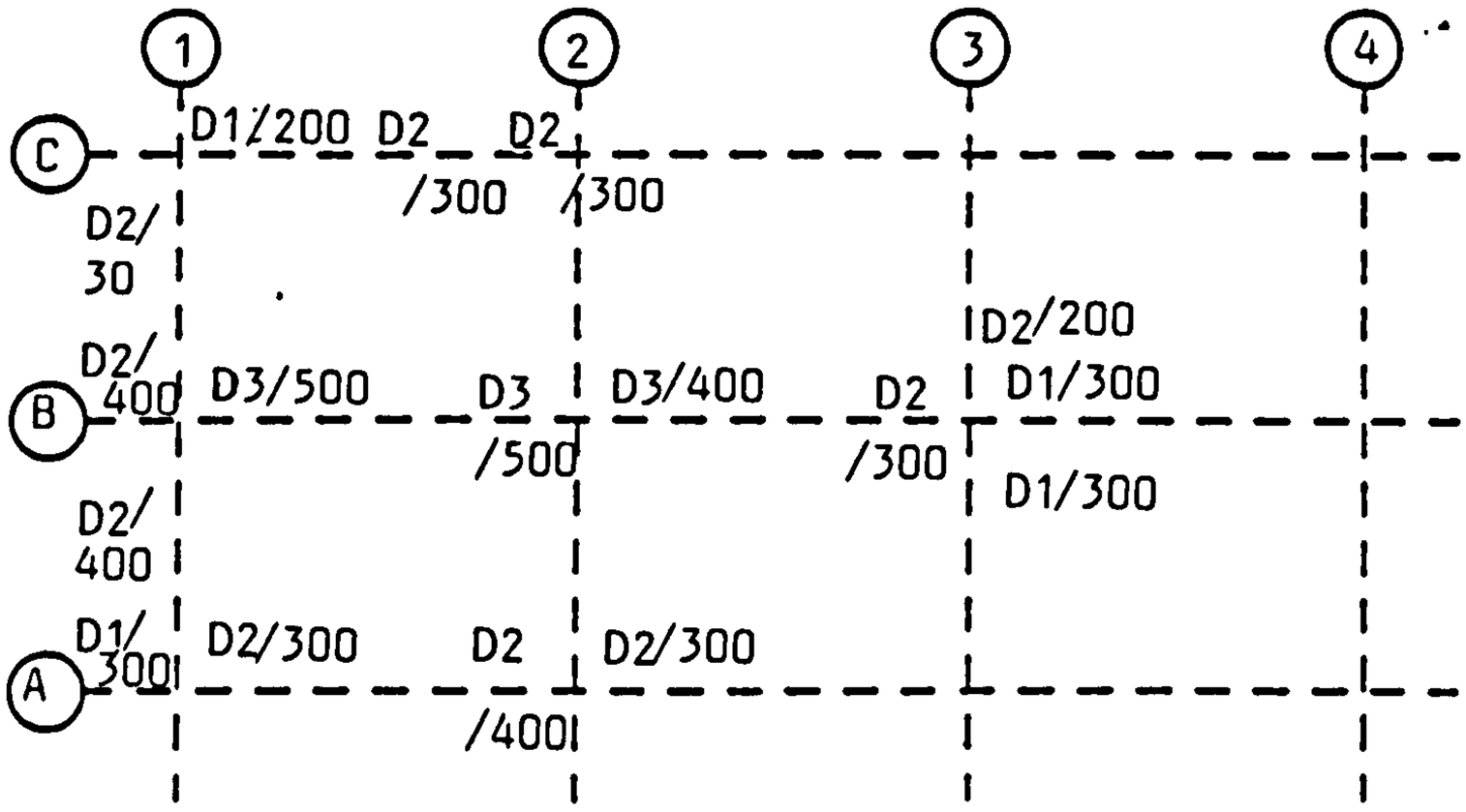
TEAM NO : 3 BY : AIS SIGNATURE : Asraad DATE : 15/2/93

EARTHQUAKE DAMAGE INSPECTION FORM
No.11

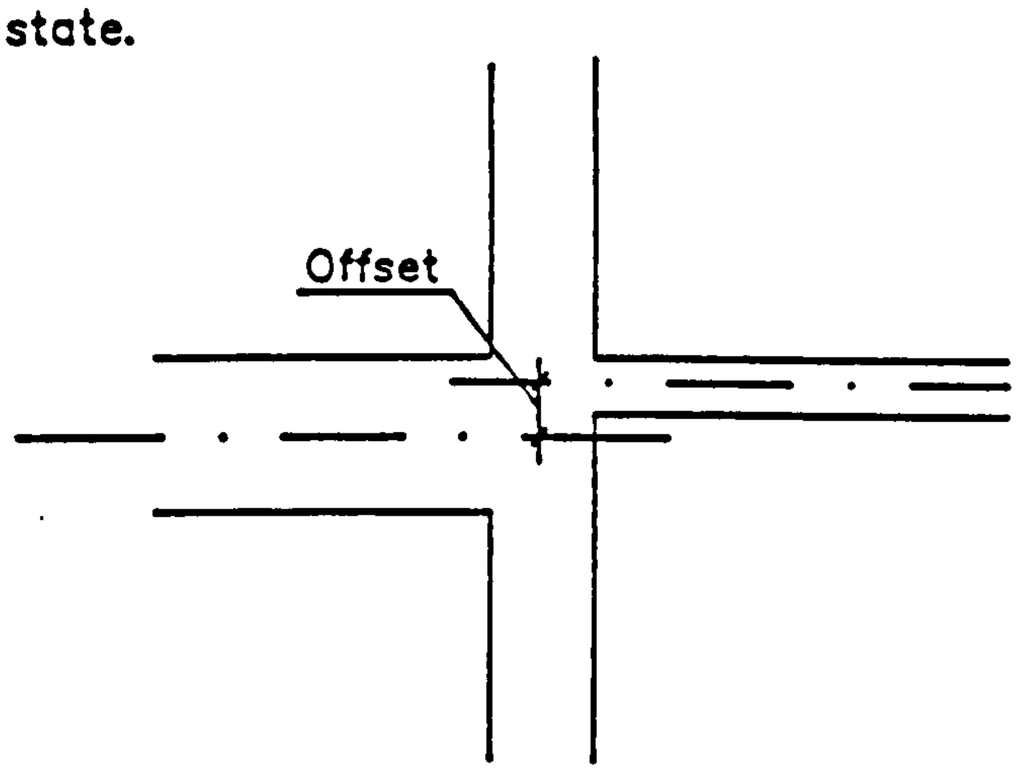
DEFECTS AND DAMAGE STATE OF SLABS AND BEAMS

82 Identification Code : 2 0 1 7 1 7

83 Floor Number : First



84 Note : Show offsets in plan and indicate offsets in elevation
Show crack state.



Elevation

Sheet: 11/16

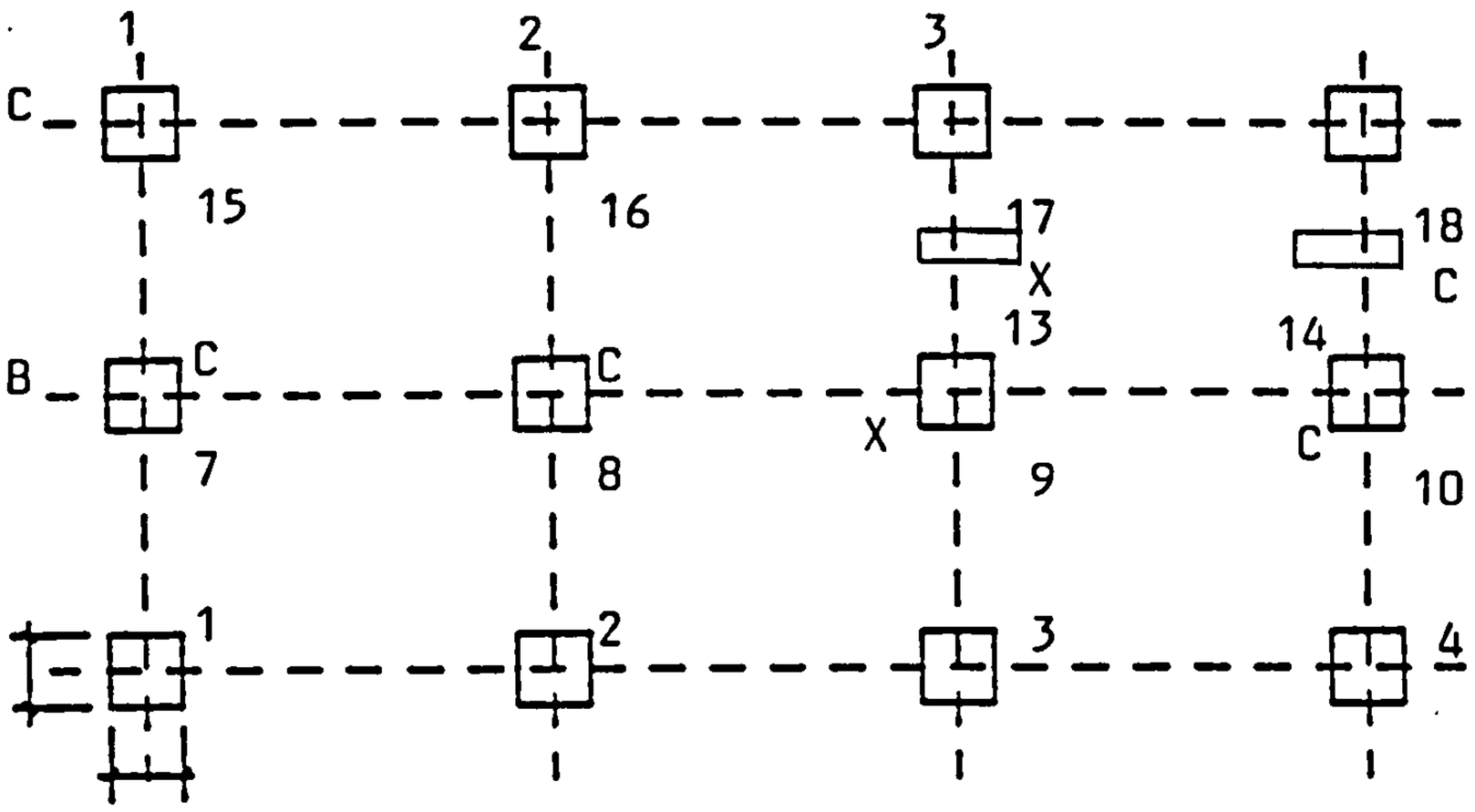
TEAM NO : 3 BY : AIS SIGNATURE : DATE : 15/2/93

EARTHQUAKE DAMAGE INSPECTION FORM
No.12

DEFECTS AND DAMAGE STATE OF COLUMNS

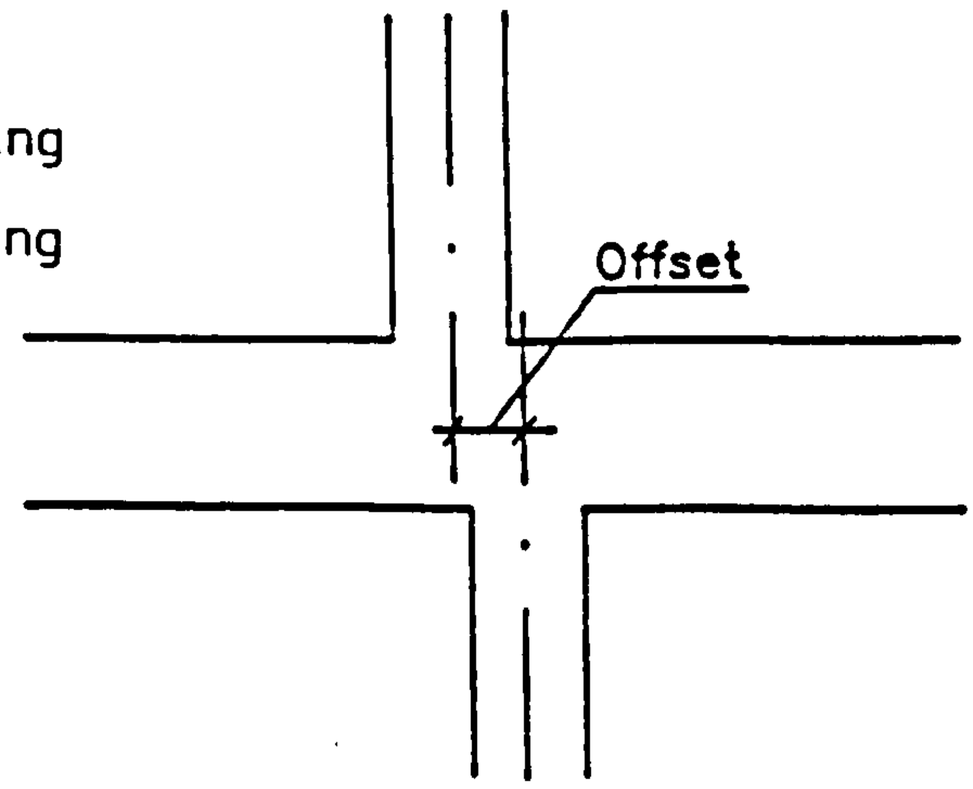
85 Identification Code : 2 0 1 7 1 7

86 Floor Number : 1



87 Note : Indicate offsets in elevation
Show crack/crush/buckling states
Columns shown are above the floor indicated.

Legend: C for Cracking
X for Crushing



Elevation

TEAM NO : 3 BY : AIS SIGNATURE : DATE : 15/2/93

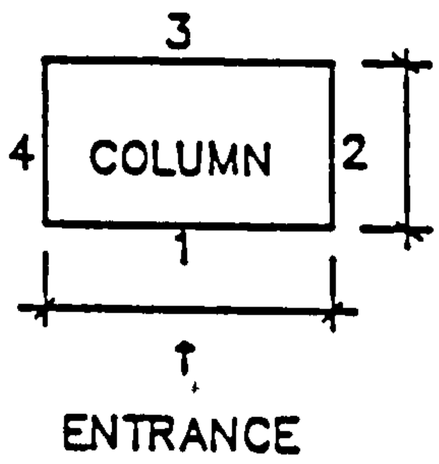
EARTHQUAKE DAMAGE INSPECTION FORM
No.13

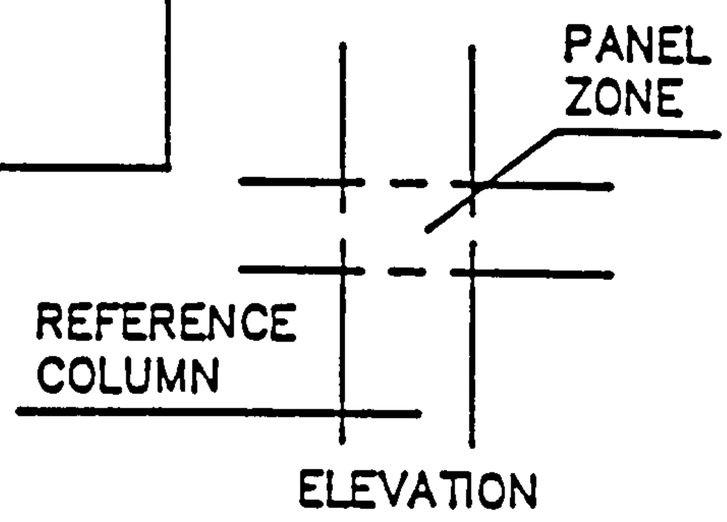
DAMAGE DESCRIPTION ON BEAM-COLUMN CONNECTION

88 Identification Code : 2 0 1 7 1 7

89 Floor Number :.....

Col. No	Exist. of Shear Reinf.	Construction Joints	Damage Code for Faces				Comments
			1	2	3	4	





DAMAGE DESCRIPTION ON COLUMNS AND WALLS

90 Identification Code : □□□□□□

91 Floor Number :.....

Col. No	% Steel in Sect.	Stirrup Spacing (mm)	Damage Code for Faces				Comments
			1	2	3	4	
17	2%	R8 @200		E2 E2 E1		E2 E2 E1	

92 Note : Enter short-columns code (SC) under comments.
Enter openning or drainage pipes code (OC) under comments.

93 DAMAGE CODES (See Annex A)

Sheet: 13/16

TEAM NO : 3 BY : AIS SIGNATURE : DATE : 15/2/93

EARTHQUAKE DAMAGE INSPECTION FORM
No.14

SOIL CONDITION

94 Identification Code : [2][0][1][7][1][7]

95 Level of Confidence in Information ☐ High ☒ Medium ☐ Low

96 Depth to Bedrock (m) : 3000 ☐ Unknown

97 Depth to Water Table (m): max : 30 ☐ Unknown
min : 20

98 Cohesive Soil ☒ Yes ☐ No
(if No, skip section)

☐ V.Soft ☐ Soft ☒ Stiff ☐ V.Stiff ☐ Hard

99 Undranied Shear Strength t/m2 : 20 ☐ Unknown

100 Non-Cohesive Soil ☐ Yes ☒ No
(if No, skip section)

☐ V.Loose ☐ Loose ☐ Medium ☐ Dense ☐ V.Dense

101 Stratified Soil ☐ Yes ☒ No
(if No, skip section)

102 Give details on layers below.

103 Estimated Avarage Shear Wave Velocity (mm/sec) : 3.5 e+5

104 Soil Problems ☐ Yes ☒ No
(if No, skip section)

☐ Liquefaction ☐ Stability ☐ Rockfalls

☐ Bulging ☐ Ground Cracks ☐ Other
(Specify below)

Sheet: 14/16

TEAM NO : 3 BY : AIS SIGNATURE : [illegible] DATE : 15/2/93

EARTHQUAKE DAMAGE INSPECTION FORM
No.15

FOUNDATION CONDITION

105 Identification Code : [2][0][1][7][1][7]

106 Foundation Depth (m) : 2

107 Foundation System

- ☐ Isolated Footings
- ☒ Footings & Beams
- ☐ Combined Footings
- ☐ Strip Footings
- ☐ Raft Foundation
- ☐ Others (specify below)

108 Foundation Problems (if No, skip section)

- ☐ Yes
- ☒ No

- ☐ Settlement (more than 2.5 cm)
- ☐ Differential Settlement (more than 2.0 cm)

Bearing Capacity : 10t/m2

Subgrade Modulus : .....

- ☐ Others (specify below)

Comments : An out of plumb of 10 cm was observed in a 15 m high. This is attributed most probably to a construction defect rather than a foundation problems.

Sheet: 15/16

TEAM NO : 3 BY : AIS SIGNATURE : [signature] DATE : 15./2./93

EARTHQUAKE DAMAGE INSPECTION FORM
No.16

RECOMMENDED FURTHER INVESTIGATION

109 Identification Code : 2 0 1 7 1 7

110 Concrete Cores (Specify Location)	[X]	First and second Floor Columns
111 Soil Tests (Specify Type)	[X]	Static penetration test to confirm allowable bearing Capacity
112 Plumb Checks (Specify Plane)	[X]	Western facade
113 Steel Tension Tests	[X]	Top Floor Columns and beams at beam-column Connections

ANY FURTHER COMMENTS

TEAM NO :..3.. BY :.....AIS..... SIGNATURE :.....DATE :15/.2/.93.

ANNEX A: DAMAGE IDENTIFICATION CODES TO BE USED IN STRUCTURAL DAMAGE SURVEY

1. Damage Identification Code for Beams

Vertical Cracks

1.1. D0: <0.2 mm
1.2. D1: 0.2-1 mm
1.3. D2: 1-2 mm
1.4. D3: 2-5 mm

Diagonal Cracks

1.5. E0: <0.2 mm
1.6. E1: 0.2-1 mm
1.7. E2: 1-2 mm
1.8. E3: 2-5 mm

Separation Cracks

1.9. AC: Spalling

2. Damage Identification Codes for Columns

Vertical Cracks

2.1. D0: <0.2 mm
2.2. D1: 0.2-1 mm
2.3. D2: 1-2 mm
2.4. D3: 2-5 mm

Diagonal Cracks

2.5. E0: < 0.2 mm
2.6. E1: 0.2-1 mm
2.7. E2: 1-2 mm
2.8. E3: 2-5 mm

Horizontal Cracks

2.9. Y0: < 0.2 mm
2.10. Y1: 0.2-1 mm
2.11. Y2: 1-2 mm
2.12. Y3: 2-5 mm
2.13. C0: Partial Compressive Crushing
2.14. C1: Total Compression Crusing
2.15. B0: One-side Reinforcement Buckling
2.16. B1: Two-side Reinforcement Buckling

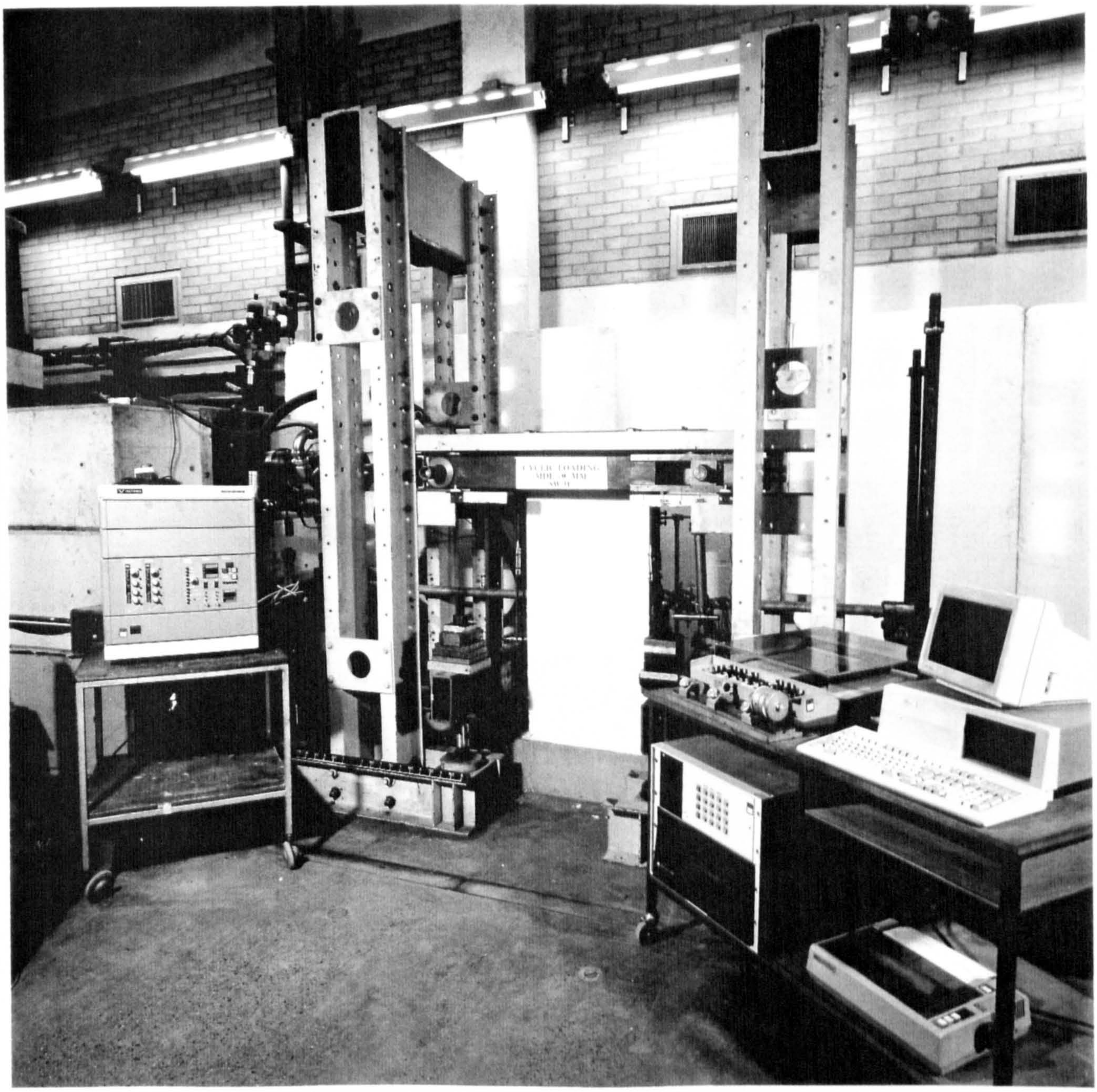


Plate 1: Test Set-up

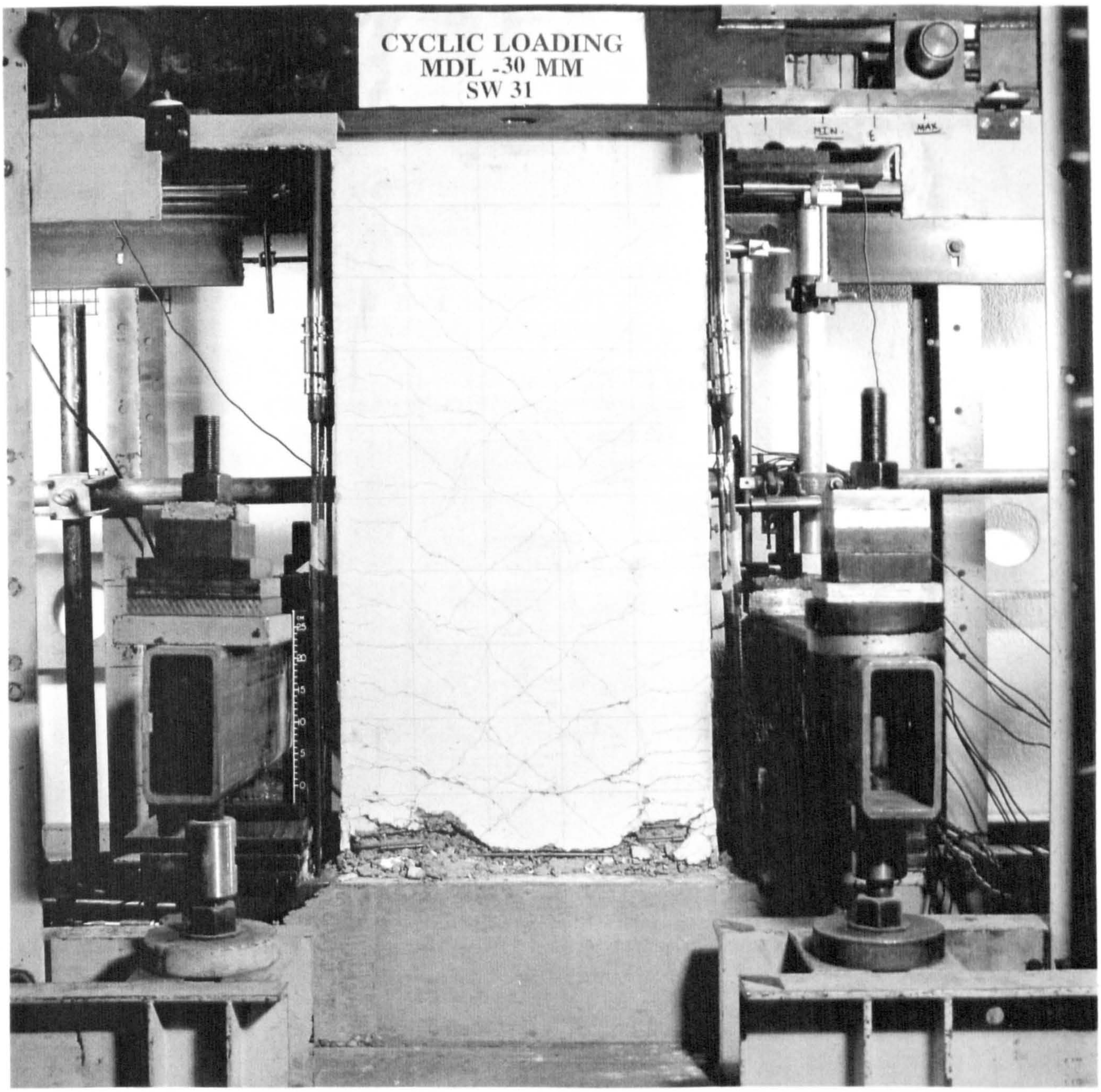


Plate 2: Failure Mode for SW31

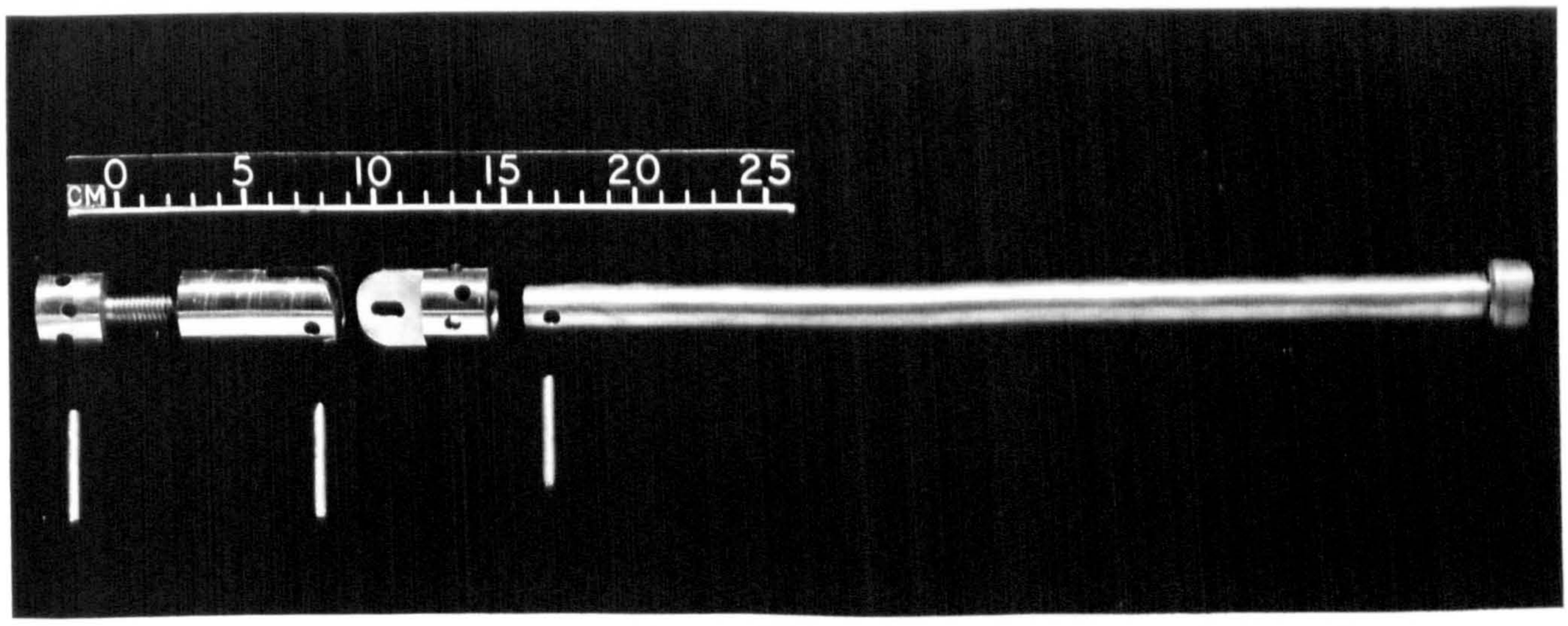
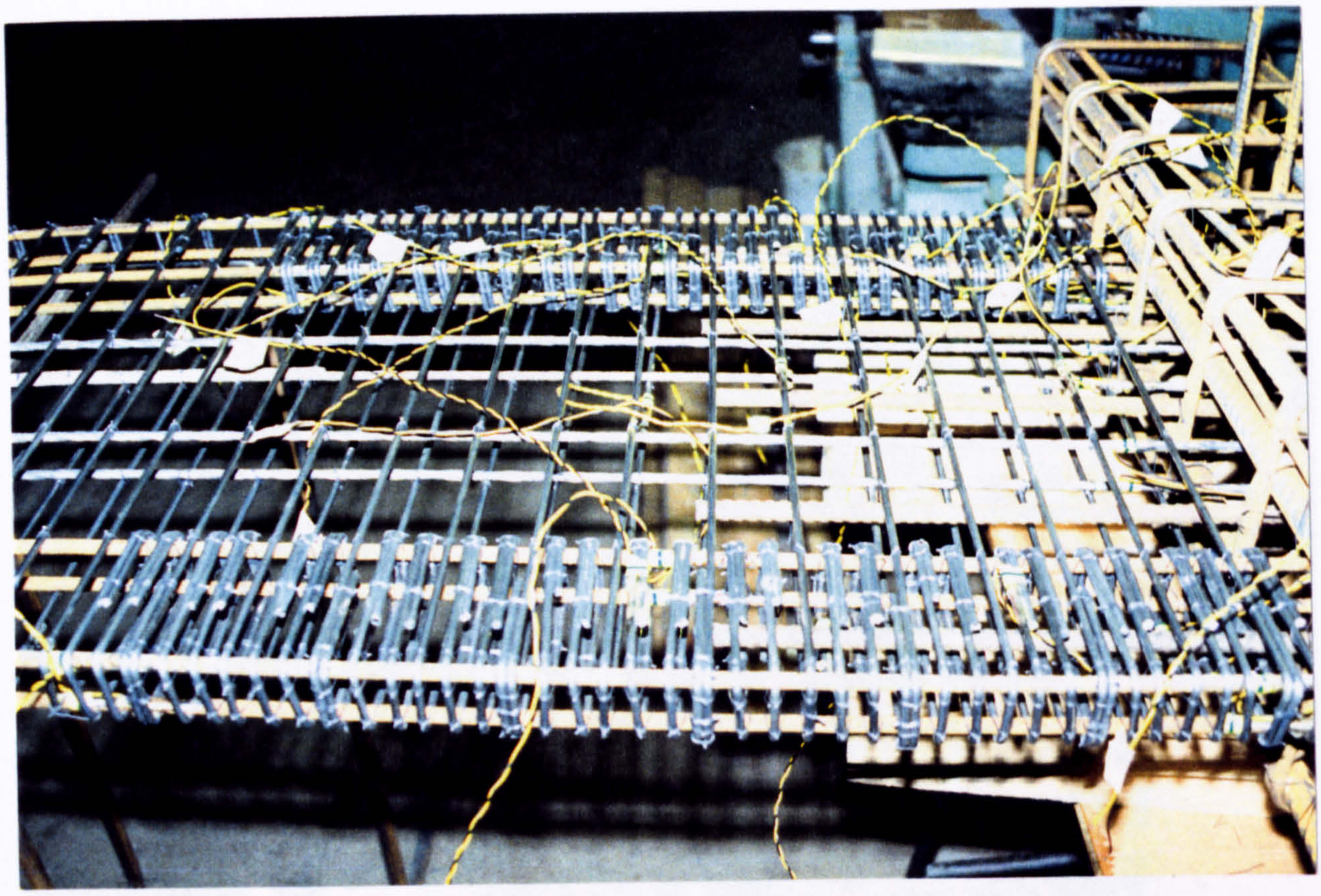


Plate 3: Details of Interaction Delay Mechanism



(a)



(b)

Plate 4 (a) & (b): Reinforcement Cage for SW31



Plate 5: Preparation of Reinforcement Cage for SW34



Plate 6: Mr. Tabor (Fosroc Technical Manager) Repairing SW22

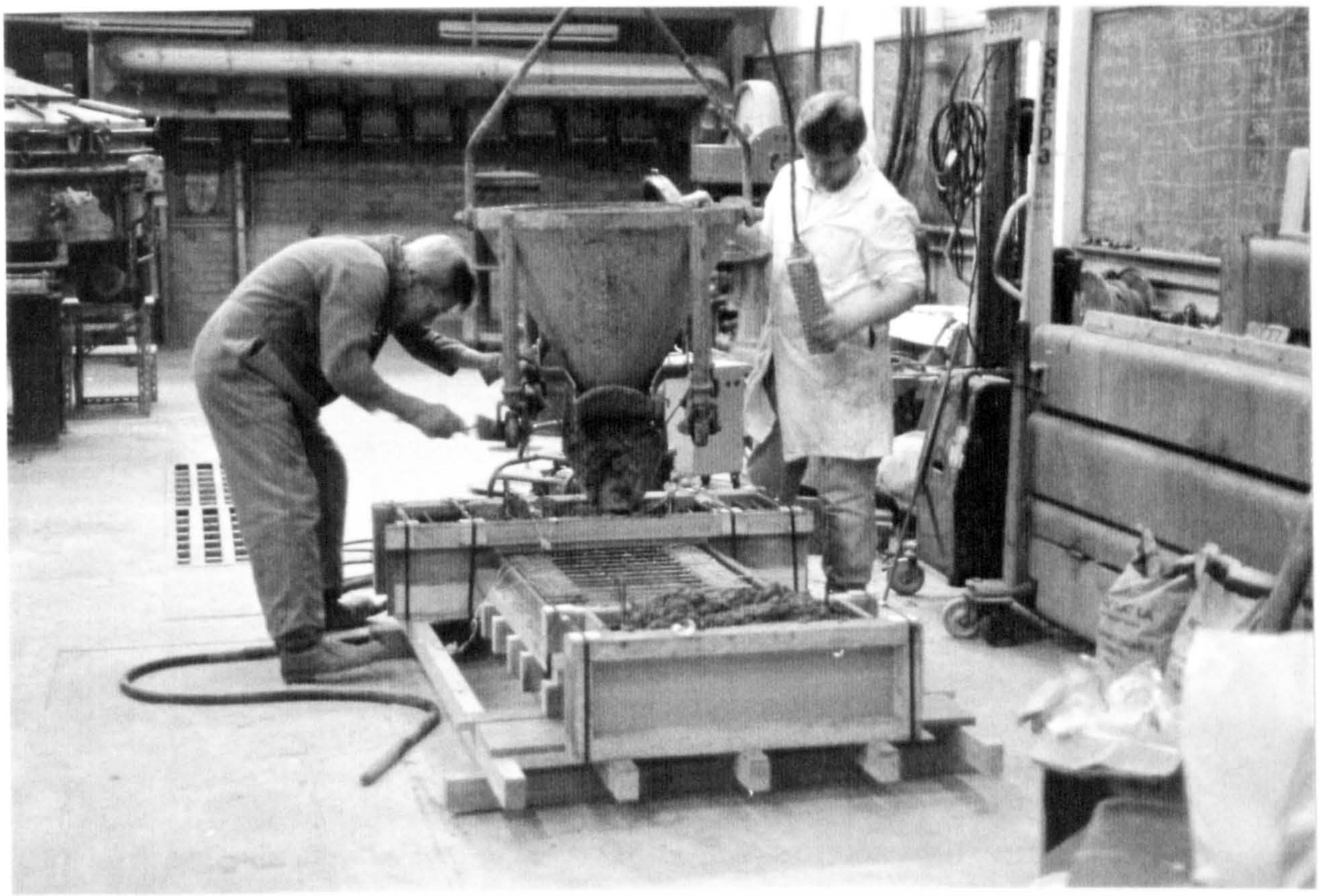


Plate 7: Casting Model SW34

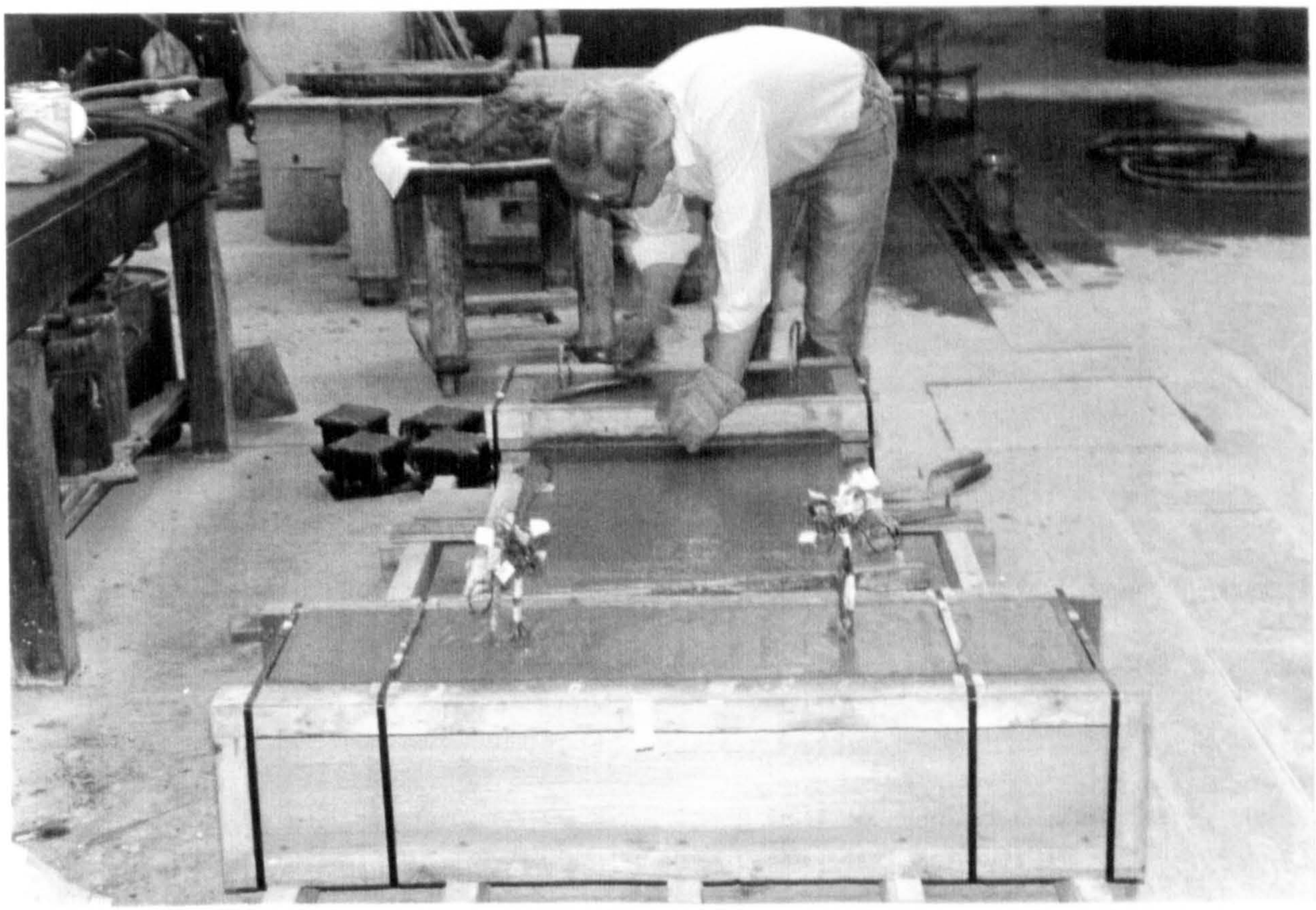


Plate 8: Finishing SW35

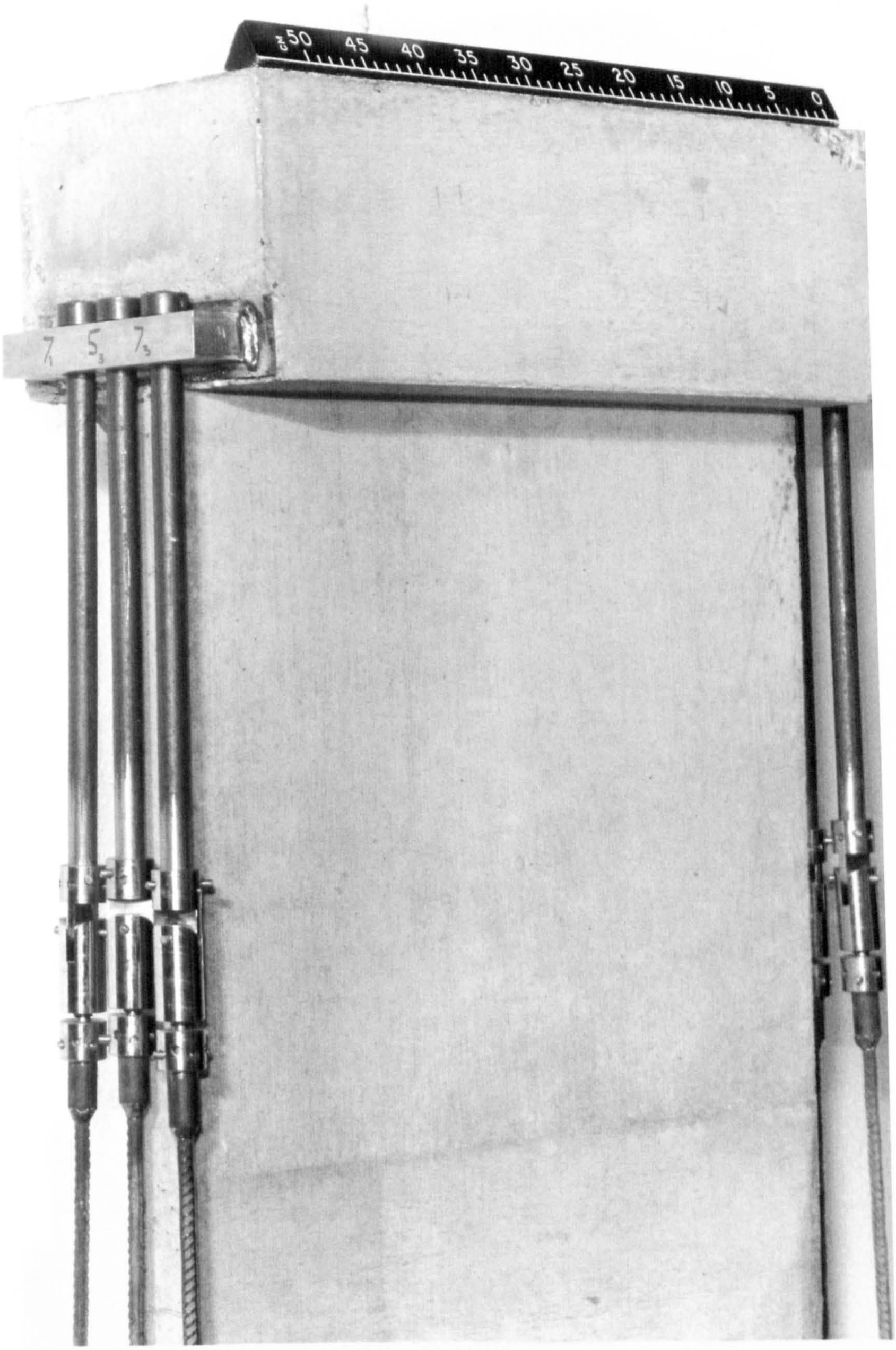


Plate 9: Strength-Only Intervention, Note Interaction Delay Mechanism

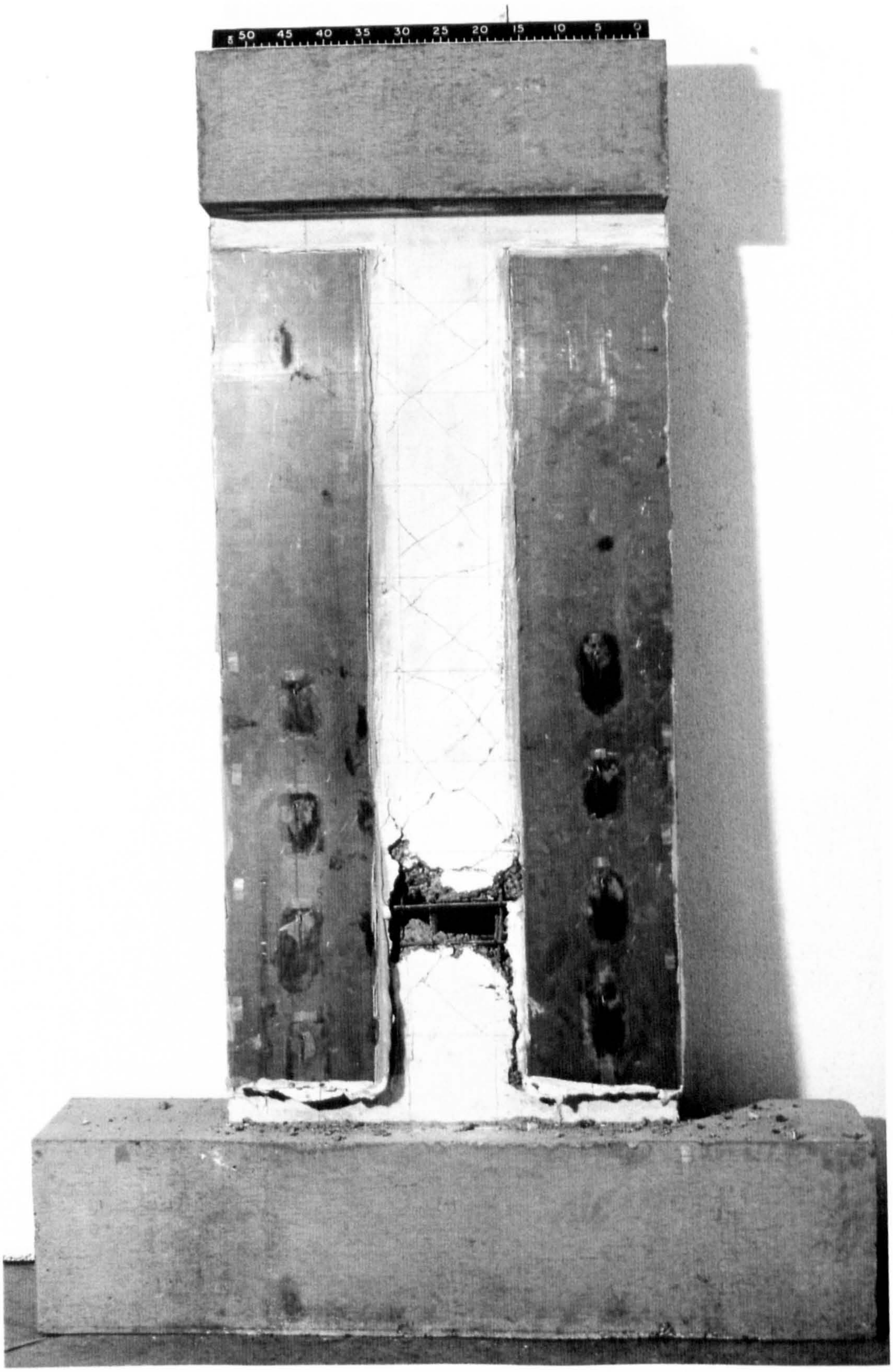


Plate 10: Model SWR9, Stiffness-Only Intervention



Plate 11: Model SWR21, Note Diagonal Shear Cracks



Plate 12: Model SWR24, Note Diagonal Shear Cracks

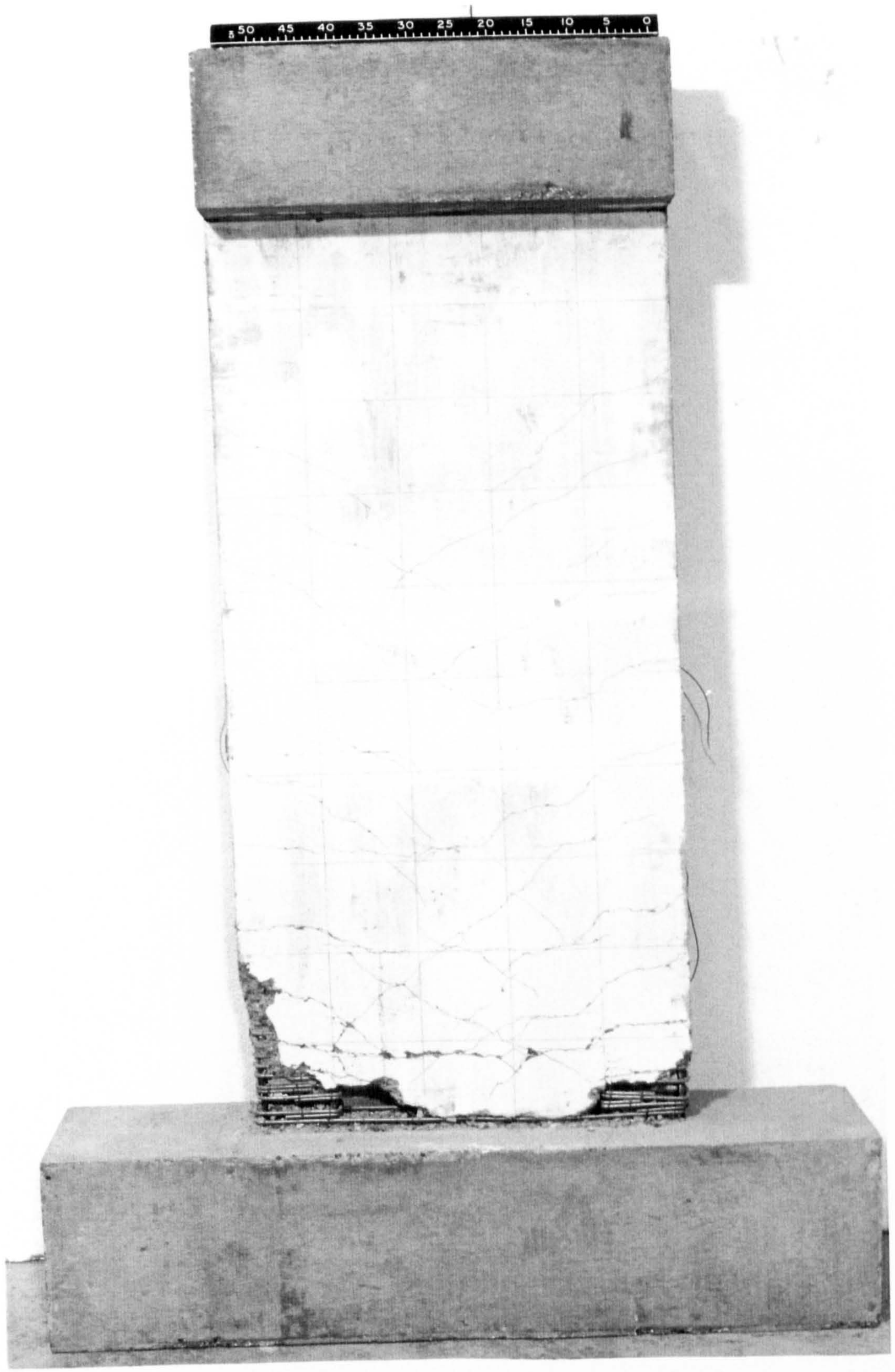


Plate 13: Model SW33, Control Model

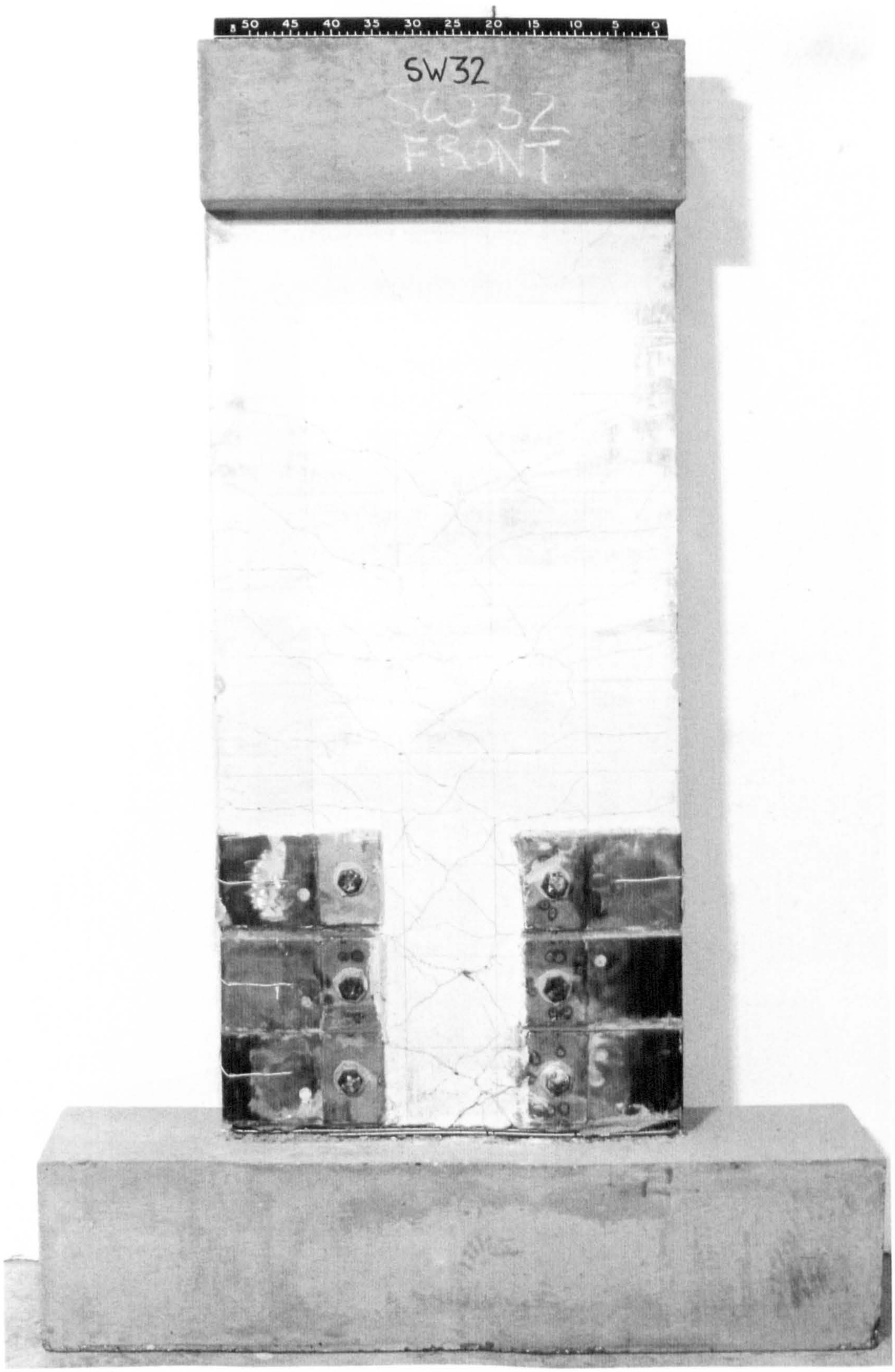


Plate 14: Model SW32, Ductility-Only Intervention

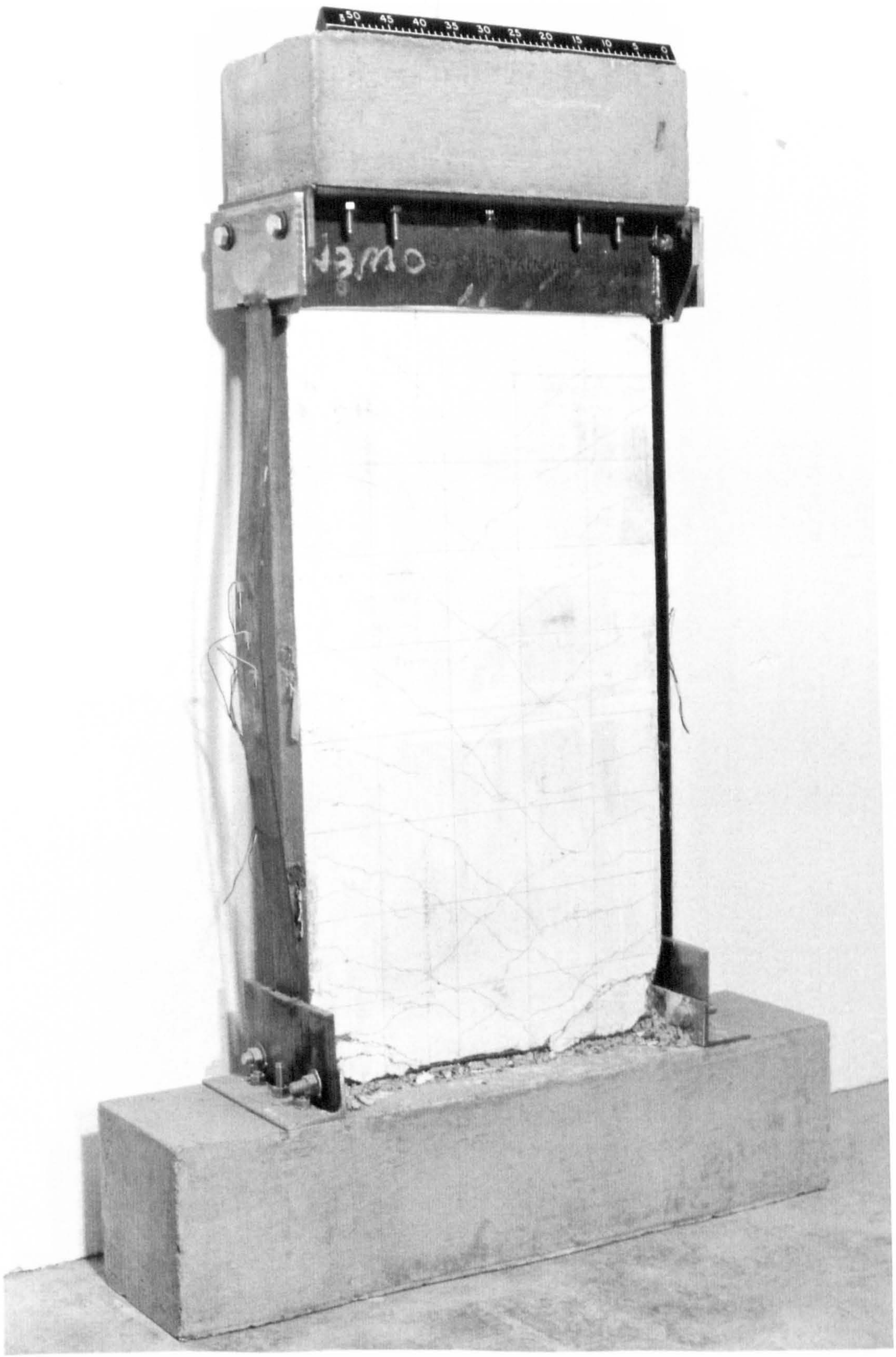


Plate 15: Model SW34, Strength-Only Intervention



Plate 16: Model SWR22, Note Shear Failure Mode



Pate 17: Typical Shear Failure in Shear Walls, Erzincan, Turkey



Plate 18: Typical Shear Failure in Columns, Erzincan, Turkey



Plate 19: Column Shear Failure in Typical Building, Erzincan, Turkey



Plate 20: Imperial College MSc. Field Mission, Erzincan, Turkey, May 1993

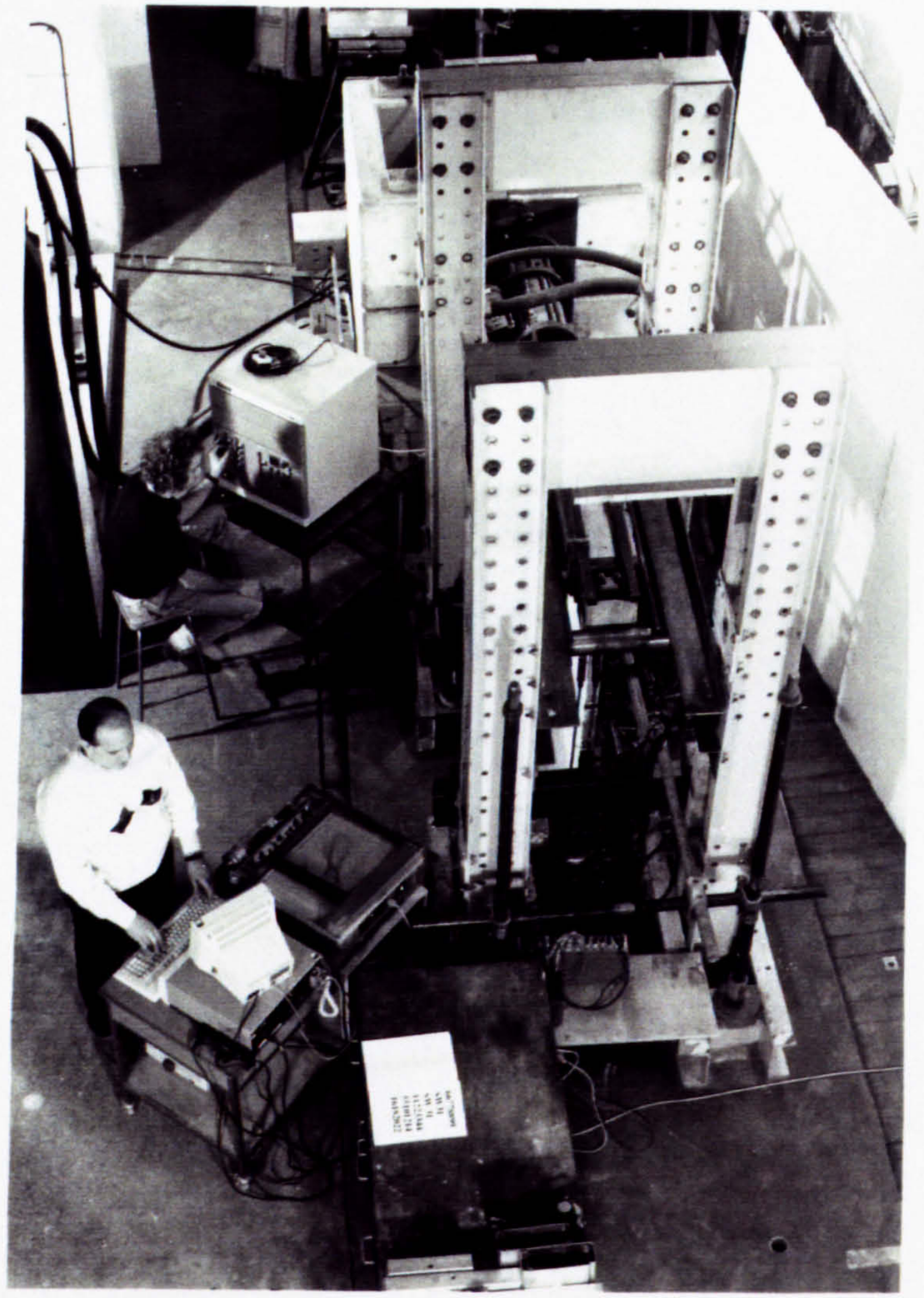


Plate 21: The writer Testing RC Walls at IC Lab.



Plate 22: The Writer Inspecting Typical Damage at Erzincan, Turkey